RESPONSE OF SOIL DEPOSITS ON THE DEFORMABLE BED-ROCK DURING EARTHQUAKES AND THE CONSEQUENT PORE-WATER PRESSURE DISSIPATION

by

EDWARD MARDIROSS, B.Sc.(Eng.), A.C.G.I.

a thesis submitted for the degree of

Doctor of Philosophy

in the Faculty of Engineering

of the University of London

Department of Civil Engineering

Imperial College of Science and Technology

London

February 1978

ABSTRACT

This thesis describes a theoretical investigation of the influence of ground conditions on ground response during earthquakes. It also includes a method for stabilizing potentially unstable deposits.

To widen the scope of knowledge, a method of analysis is presented for the seismic response of foundations underlain by deformable bedrock. The design method developed, being a closed form convergent solution, is based on real earthquake bedrock motions, real properties of foundation materials and takes into account the energy radiation from overburden into the underlying bedrock. Its application to predict the ground motion is demonstrated by comparing the computed response with that obtained by numerical solution. Good agreement between the two procedures indicate that the developed procedure, although not representing an exact solution to the problem, is sufficient for engineering purposes. The values for the average ratio of maximum velocity/maximum acceleration and predominant period for deep cohesionless soil condition computed by this method are shown to be in good agreement with field recorded data from previous earthquakes.

A computer program based on the proposed method has been developed. The program was used to study the influence of "radiation damping", duration of bedrock motion and softness of ground on foundation response. It was found that the "old-fashioned" way of treatment of the effect of radiation damping by the introduction of some additional

damping in each mode of rigid base solution, where the fundamental period of the overburden is not equal to the predominant period of the bedrock motion, may lead to misleading results. Under these conditions the "up-to-date" method, which is the proposed method, should be used.

A procedure for stabilizing unstable saturated sand deposits has been developed. Closed form solutions are given for expressing the rate of pore pressure dissipation after earthquakes for several cases: vertical dissipation, radial dissipation, and three-dimensional dissipation associated with foundations of engineering structures.

A new method for assessment of design data for aseismic design is proposed.

ACKNOWLEDGEMENTS

This thesis evaluates the results of a four and a quarter year research conducted by the author in the Civil Engineering Department of Imperial College of Science and Technology, University of London. The author wishes to express his great appreciation to the following scientists who helped in carrying out this project:

Professor A.W. Bishop, who reviewed the draft, offered many helpful suggestions and supervised the final stages of the project.

Dr. P.R. Vaughan, for support, encouragement, and comments on the work reported in Chapter 9.

Dr. D.J. Papastamatiou, who provided the author with some of his numerical results for the purpose of comparisons.

To all those who helped the author in his work by constructive criticism and comments.

The computations were performed at computer centres of Imperial College and University of London, using the CDC 6400, CDC 6600 and CDC 7600 computers.

The supervision of Dr. N. Aambraseys is also acknowledged.

The author is indebted to Prof. B.G. Neal and Mrs. Wyatt for their generous help. E. Mardiross

CONTENTS

ABSTRACT 1

ACKNOWLEDGEMENTS 3

CONTENTS 4

LIST OF TABLES 15

NOTATION 16

CHAPTER 1 : INTRODUCTION

1.1. Introduction 18

1.2. Object and scope of present investigation 29

CHAPTER 2 : CRITICAL REVIEW OF PREVIOUS WORK ON FOUNDATION RESPONSE TO SEISMIC LOADING

2.1. Introduction 31

2.1.1. Continum models 32

2.1.2. Lumped mass models 33

2.2. Finite element method 36

2.3. Concluding remarks 38

CHAPTER 3 : BEDROCK MOTION

3.1. Introduction 39

3.1.1. Use of previous earthquake strong motion records 39

3.1.2. Adjustment of the records 40

3.1.3. Response spectrum of bedrock motions 42

3.2. Motion characteristics by studying stable strong motion bedrock parameters 87

3.2.1. Size of an earthquake 87

3.2.2. Relationship between magnitude and effective duration of bedrock shaking 88

3.2.3. Relationship between magnitude and predominent period of bedrock motion 89

3.2.4. Correlations relating magnitude distance from causative fault, and bedrock maximum acceleration or velocity 89

3.3. Concluding remarks 92

CHAPTER 4 : A NEW METHOD FOR ANALIZING THE EFFECT OF FOUNDATION CONDITIONS ON FOUNDATION RESPONSE

4.1. Introduction 95

4.2. Observed facts 95

4.3. Theory 1oo

4.3.1. Formulation of the mathematical model . . . .

4.3.2. Propagation of vertical shear waves in one dimensional system 1oo

4.3.3. Transmitting boundary condition 1o1

4.4. Solution of the governing differential equation . . . 1o2

4.4.1. Introduction of boundary conditions 1o3

4.4.1.1. Initial conditions 1o5

4.4.1.2. Evaluation of the inversion integral 107

4.4.1.3. Sum of the residues 108

4.4.1.4. Roots of the transcendental equation (4.26) 111

4.4.1.5. Absolute displacement of the system 116

4.4.1.6. Free vibration response 117

4.4.1.7. Absolute velocity of the system . . . 118

4.4.1.8. Absolute acceleration of the system 119

4.4.2. Evaluation of integrals $S_{dnc}(t)$ and $S_{dns}(t)$ 120

4.5. Undamped natural frequencies of the system 121

4.6. Convergence and numerical results 122

4.7. Shear strain and shear stress 148

4.8. Overburden properties 149

4.8.1. Soil stress-strain relationship used 149

4.8.2. Damping and shear modulus 150

4.9. Special cases of interest 152

4.9.1. Radiation damping ratio assigned to zero and hysteretic damping ratio not zero 152

4.9.2. Radiation and hysteretic damping ratios assigned to zero 154

4.9.3. Radiation damping ratio tending to one when hysteretic damping ratio assigned to zero . . . 156

4.10. Developed solution compared with modified lumped mass model results 159

4.11. Concluding remarks 163

CHAPTER 5 : DESCRIPTION OF COMPUTER PROGRAM, SOIL PROPERTIES IN SEISMIC RESPONSE ANALYSIS AND EVALUATION OF PORE WATER PRESSURE DISSIPATION

5.1. Introduction 164

5.2. Description of the computer program named "EARTHQUAKE" 165

5.2.1. Structure of program 166

5.2.1.1. Concluding statements 168

5.3. Soil properties in seismic response analysis 17o

5.3.1. Introduction 17o

5.3.2. Damping characteristics and shear wave velocity of soil deposits 17o

5.3.2.1. Damping characteristics 17o

5.3.2.2. Shear wave velocity 171

5.3.3. Depth to bedrock 171

5.3.4. Shear wave velocity of bedrock formation . . . 173

5.3.5. Concluding remarks 174

5.3.6. Selection of soil properties for evaluation of pore water pressure dissipation after earthquake shaking 174

5.3.6.1. Coefficient of permeability of sand deposits 175

5.3.6.2. Coefficient of volume compressibility 175

CHAPTER 6 : INFLUENCE OF BEDROCK CHARACTERISTICS ON SEISMIC RESPONSE OF SOIL DEPOSITS

6.1. Introduction 176

6.2. Radiation damping ratio 176

6.3. Bedrock motion considered 177

6.4. Sites studied 178

6.5. Acceleration, velocity and displacement time histories 178

6.6. Response spectra 179

6.7. Site amplification 180

6.8. Influence of bedrock characteristics on seismic response of soil deposits 181

6.8.1. Influence of radiation and hysteretic damping ratios on ground response and their comparison 182

6.8.1.1. Fundamental period of the overburden is equal to the predominent period of the bedrock motion 182

6.8.1.2. Fundamental period of the overburden is not equal to the predominent period of the bedrock motion 261

6.8.1.3. Final comments 283

6.8.2. Influence of stiffness characteristics of bedrock formation on the seismic response of soil deposits 284

6.8.2.1. Results of case 1 284

6.8.2.2. Results of case 2 324

6.9. Evaluation of the response of a soil deposit with flexible bedrock by means of rigid base solution . . . 365

6.9.1. Concluding remarks 387

6.10. Influence of stiffness characteristics of bedrock formation on subsurface response of soil deposits . . . 388

6.10.1. Concluding remarks 411

CHAPTER 7 : INFLUENCE OF GROUND SOFTNESS, BEDROCK MOTION AND DEPTH TO BEDROCK ON GROUND RESPONSE

7.1. Introduction 413

7.2. Influence of ground softness on ground response 413

7.2.1. Soil properties for the sites 414

7.2.2. Bedrock motion for this study 414

7.2.3. Results of the study 414

7.2.4. Concluding statement 467

7.3. Investigation of influence of fundamental period on response of soil deposits and a new measure of the destructiveness of ground motion 468

7.3.1. A parameter as a measure of severity of ground shaking 469

7.4. Influence of base motion on ground response and comparison of computed and recorded values 508

7.4.1. Influence of frequency characteristics of bedrock motion on ground response 508

7.4.2. Influence of amplitude of base motion on ground response 509

7.5. Concluding remarks 517

7.6. Comparison between recorded and computed values of ratios of maximum surface velocity/maximum surface acceleration and predominent period for deep cohesionless soil condition 543

7.6.1. Input records 545

7.6.2. Results of the analysis 545

7.7. Influence of configuration of deposit on ground response 561

7.7.1. Concluding remarks 582

7.8. Influence of duration of bedrock motion on ground response 586

7.8.1. Concluding remarks 587

7.9. Engineering significant of the proposed design method o$ sample design problem 594

7.9.1. Basic requirements 594

7.9.1.1. Motion at depth 594

CHAPTER 8 : PORE WATER PRESSURE DISSIPATION ASSOCIATED WITH FOUNDATION SHAKING AFTER EARTHQUAKES

8.1. Introduction 603

8.2. Previous study 603

8.3. Scope and objective of present study 604

8.4. Role of weak thin trapped deposit 604

8.5. Theory 605

8.5.1. Formulation of the governing differential equation 605

8.5.2. Solution of the governing differential equation 606

8.6. Soil properties for use in numerical analysis 606

8.7. Computer program 607

8.7.1. Data preparation 607

8.7.2. Output 607

8.8. Numerical results 607

8.9. Sensitivity analysis 609

8.9.1. Investigation of influence of height of the deposit on excess pore water pressure dissipation 609

8.10. Investigation of influence of coefficient of consolidation on excess pore water pressure dissipation 621

8.11. Concluding remarks 621

CHAPTER 9 : USE OF VERTICAL SAND FILTERS AS A NEW MEANS OF STABLIZING UNSTABLE SATURATED SAND DEPOSITS AGAINST EARTHQUAKES

9.1. Introduction 626

9.2. Previous remedial measures 627

9.2.1. Increasing overburden pressure by a pervious fill 627

9.2.2. Densification of soil by means of compaction piles 627

9.2.3. Densification of soil by means of vibroflotation 628

9.3. Previous work 628

9.4. Scope and objective of present study 629

9.5. Effect of trapped weak layer on the system shown by fig. 9.1.D. 629

9.6. Purpose of sand filters 632

9.6.1. Statement of the problem 632

9.7. Theory 632

9.7.1. Dissipation of excess pore water pressure after earthquake shaking in the two layer system 632

9.7.1.1. Governing differential equation in the upper layer 633

9.7.1.2. Boundary conditions for equation 9.2 634

9.7.1.3. Boundary conditions for equation (9.3) 635

9.7.1.4. Solution of differential equation (9.2) 635

9.7.1.5. Solution of differential equation (9.3) 636

9.7.1.6. Excess pore water dissipation for the combined flow in the top layer 636

9.7.2. Governing differential equation in the lower layer 636
9.7.2.1. Boundary conditions for equation (9.8) 637
9.7.2.2. Solution of differential equation (9.8) 637
9.8. Computer program 637
9.9. Influence of sand filters on post earthquake dissipation of excess pore water pressure 638
9.10. Influence of layout and spacing of sand filters on dissipation of excess pore water pressure 651
9.10.1. Layout of sand filters 651
9.10.2. Spacing of sand filters 651
9.11. Influence of diameter of sand filters on dissipation characteristics of excess pore pressure 662
9.12. Influence of horizontal coefficient of consolidation on dissipation characteristics of excess pore pressure 667
9.13. Design of vertical sand filters and methods of installation 682
9.14. Design procedure and design example 682
9.14.1. Case study 695
9.14.1.1. Effect of installation of vertical sand filters at the Nigata site . . . 695
9.15. Concluding remarks 697

CHAPTER 10 : SUMMARY OF NEW DEVELOPMENTS, MAIN CONCLUSIONS OF PRESENT INVESTIGATION AND SUGGESTIONS FOR FUTURE RESEARCH

10.1. Summary of new developments 698

10.2. Main conclusions of present investigation 701

10.3. Suggestions for future research 705

CHAPTER 11 : THE RECOMMENDED APPROACH FOR ASSESSMENT OF SEISMIC DESIGN SPECTRA : ACCOUNTING FOR THE LOCAL SITE CONDITIONS

11.1 Introduction..... 707

11.2 Basic information..... 708

11.2.1. The potential earthquake magnitude..... 708

11.2.2. Predominant period of the bedrock motion.... 708

11.2.3. Prediction of maximum bedrock velocity..... 709

11.2.4. Assessment of duration of bedrock motion.... 711

11.3. Method of analysis..... 711

11.4. Design spectrum or time histories and seismic microzoning..... 713

11.5. Evaluation of effect of post earthquake rates of pore pressure dissipation..... 720

11.6. Conclusions..... 720

APPENDICES..... 722

REFERENCES..... 778

This thesis contains 782 pages.

LIST OF TABLES

3.1	Recorded data on shale-like or sounder rock	90
6.1	Site data for investigation of influence of radiation and hysteretic damping ratios on response	184
6.2	Data on the influence of bedrock characteristics on response of soil deposits	297
6.3	Data on the influence of bedrock characteristics on response of soil deposits	316
6.4	Data on the influence of bedrock characteristics on response of soil deposits	343
6.5	Data on the influence of bedrock characteristics on response of soil deposits	360
6.6	Data on the influence of bedrock characteristics on subsurface and surface response	410
7.1	Results of the influence of ground softness on computed ground response	444
7.2	Values of VEL_{max}/ACC_{max} for deep soil conditions	559
7.3	Results of increasing thickness of overburden	583
9.1	Effect of filter diameter on the dissipation rate in the top layer	668
9.2	Effect of filter diameter on the dissipation rate in the lower layer	669

NOTATION

The following list contains symbols used in the ground response theory and evaluation of pore water pressure dissipation. Any other symbol used than those below are defined where they appear in the text:

A.1. LIST OF SYMBOLS RELATED TO GROUND RESPONSE THEORY

A.1.1. General

H	:	Depth to bedrock.
$C1$	:	Coefficient of viscosity in shear of the layer.
G_s	:	Shear modulus of the layer.
$g_o(t)$	:	Horizontal bedrock displacement.
$\dot{g}_o(t)$	:	" " velocity.
$\ddot{g}_o(t)$	:	" " acceleration.
RAD	:	Radiation damping ratio.
S_s	:	Shear wave velocity of the layer.
S_r	:	Shear wave velocity of the bedrock.
$U_{abs}(y,t)$	:	Absolute displacement at depth "y" at time "t".
$\dot{U}_{abs}(y,t)$	:	Absolute velocity at depth "y" at time "t".
$\ddot{U}_{abs}(y,t)$	:	Absolute acceleration at depth "y" at time "t".
ρ_s	:	mass density of the layer.
ρ_r	:	mass density of the bedrock.
ε	:	hysteretic damping ratio.

A.1.2. Evaluation of Pore water Pressure

H : Total thickness of the deposit located above the weak layer or impermeable formation.

C_h : Coefficient of consolidation for horizontal drainage.

ζ : Radial coordinate.

R : Effective radius of filters.

S : Spacing of filters.

t : Time

U(z,t) : Excess pore water pressure in the deposit at time "t" at depth $(H - z)$.

U(r,t) : Excess pore water pressure in the deposit at time "t" at radial coordinate "r".

U(r, ,t) : Excess pore water pressure in the deposit at time "t" at depth $(z - H)$ at radial coordinate "r".

CHAPTER 1

INTRODUCTION

1.1. INTRODUCTION

For dynamic analysis of engineering structures the first thing required is; what ground motion is. It is now clear that local site conditions have an important influence on the local seismic motions that must be considered in design. Considerable research has been done on the subject in the past decade; however, there still remains a great deal to be learned about this branch of soil mechanics.

Modern analytical techniques in most cases, based on convenient assumption that the bedrocks underlain by soil deposits are infinitely rigid, have helped to a better understanding of the influence of ground conditions on ground response. The present work is an attempt to improve the methods for ground response analysis for earthquake motions. The developed design method takes into account real earthquake motions, real material properties of the overburden and the elasticity of the bedrock.

Figs. 1.1. through 1.8 illustrate that an overburden having different bedrock characteristics will respond differently to the same earthquake. In the first case, where the overburden is underlain by weathered rock as shown in figs. 1.1 to 1.4, maximum surface acceleration has been amplified by about one-fifth and maximum surface velocity by about one-fourth. Frequency characteristics of bedrock

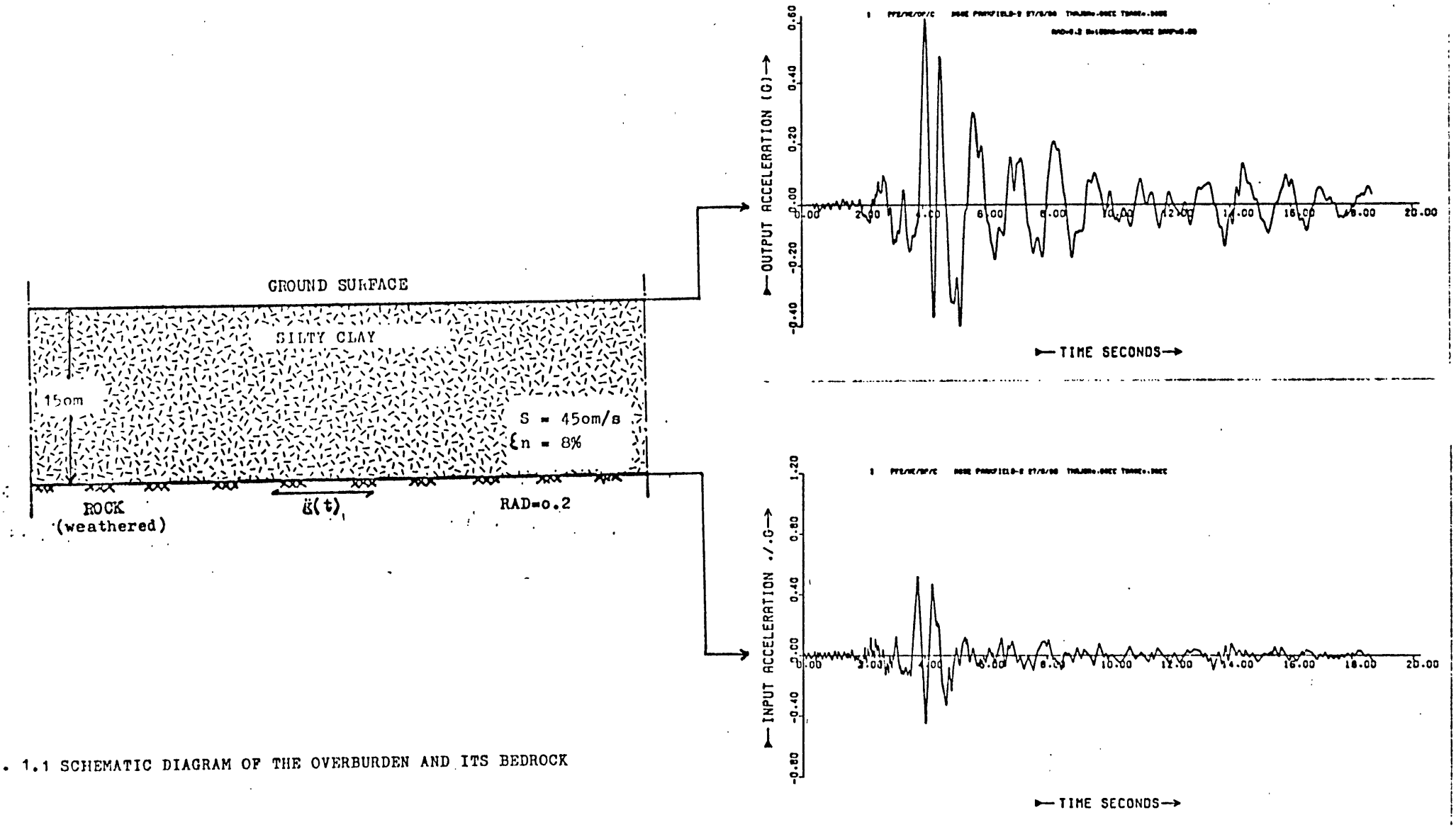


FIG. 1.1 SCHEMATIC DIAGRAM OF THE OVERBURDEN AND ITS BEDROCK

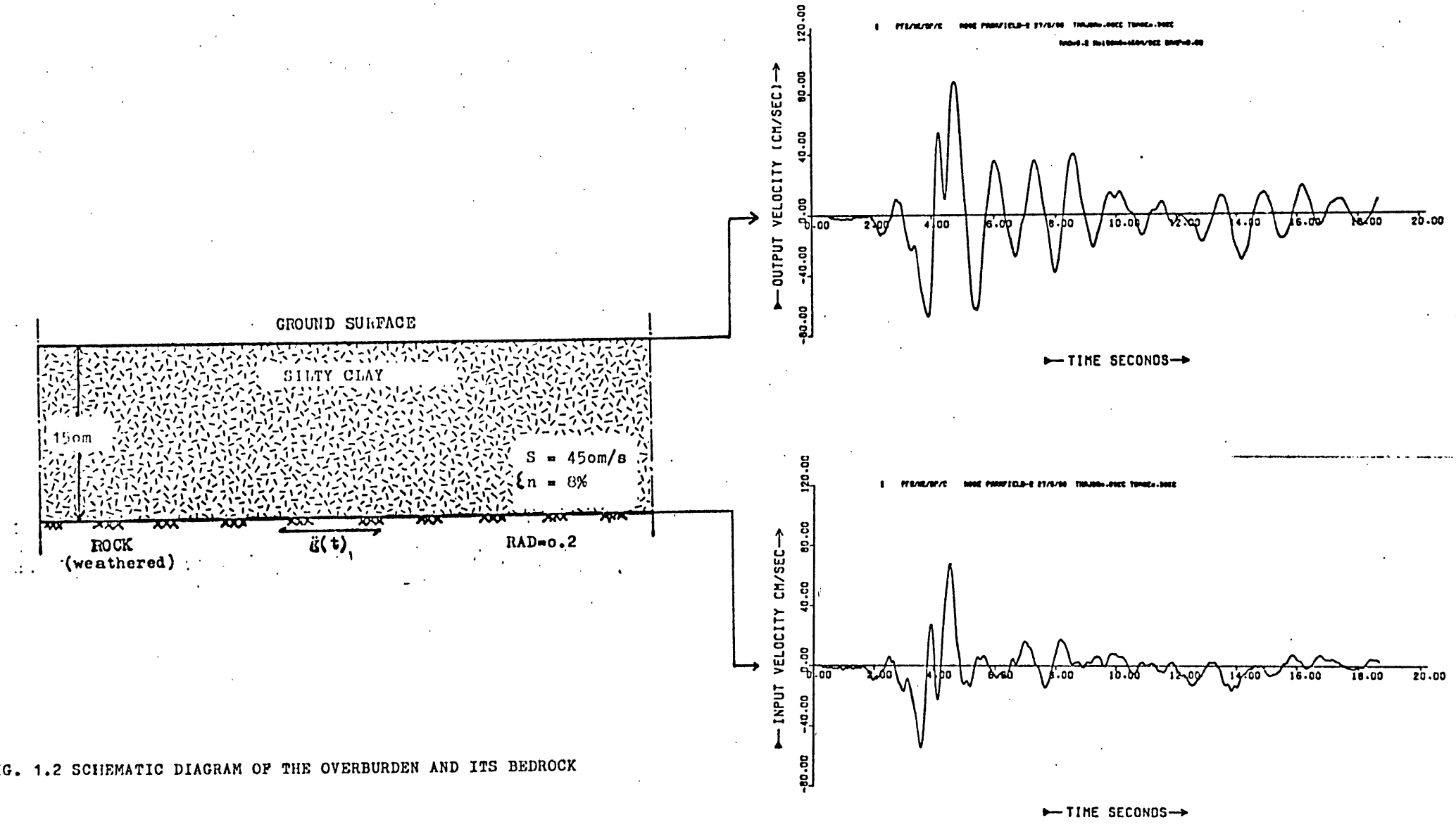
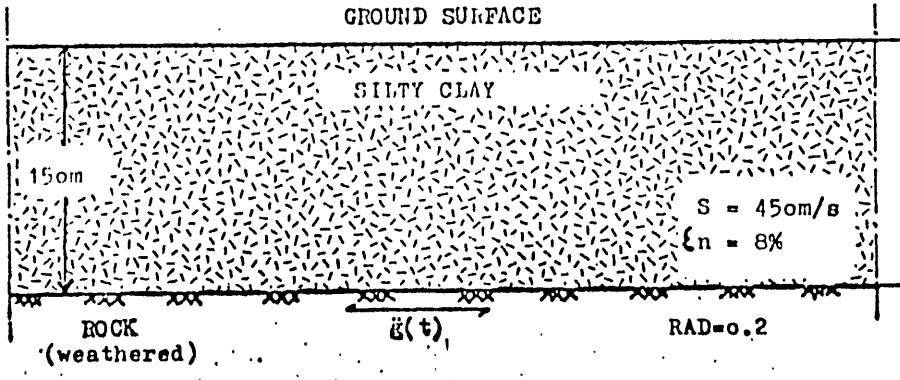
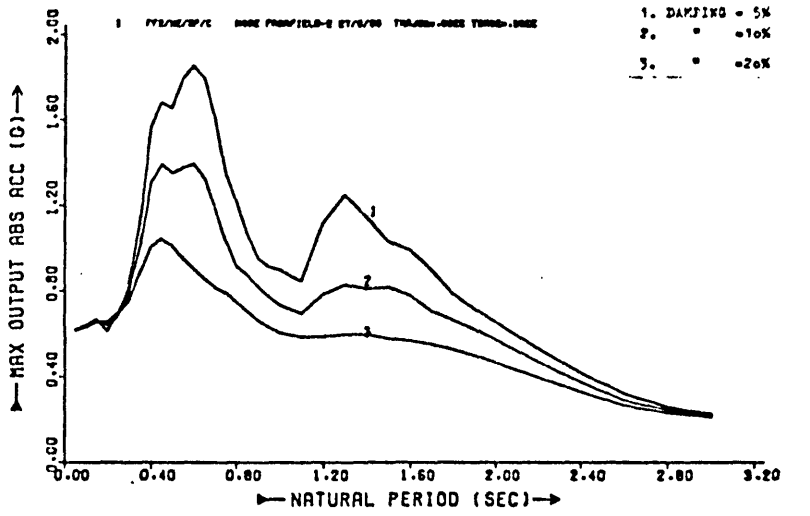


FIG. 1.2 SCHEMATIC DIAGRAM OF THE OVERBURDEN AND ITS BEDROCK





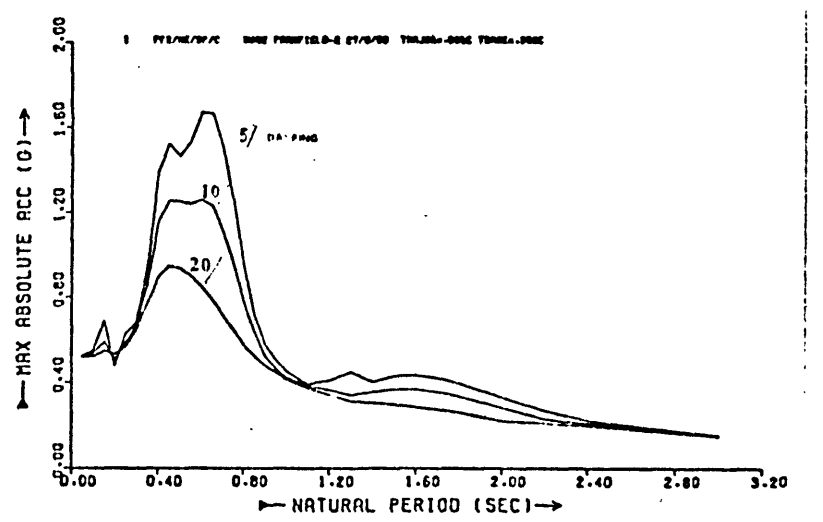
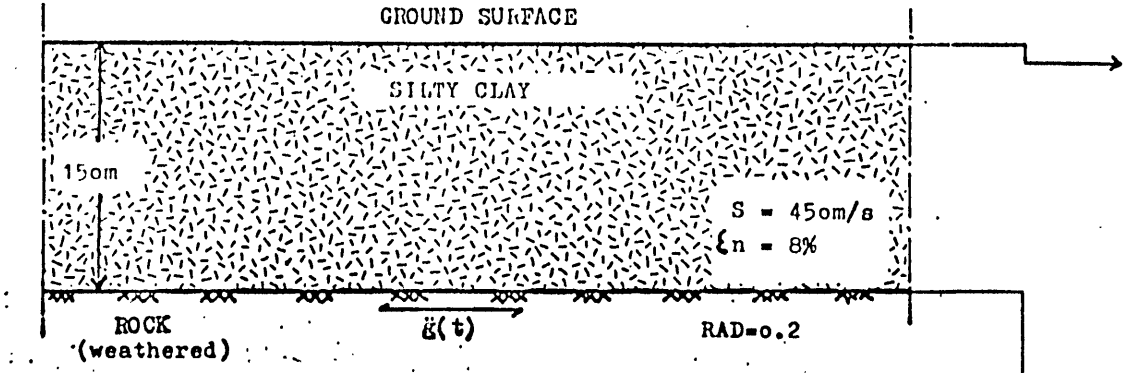
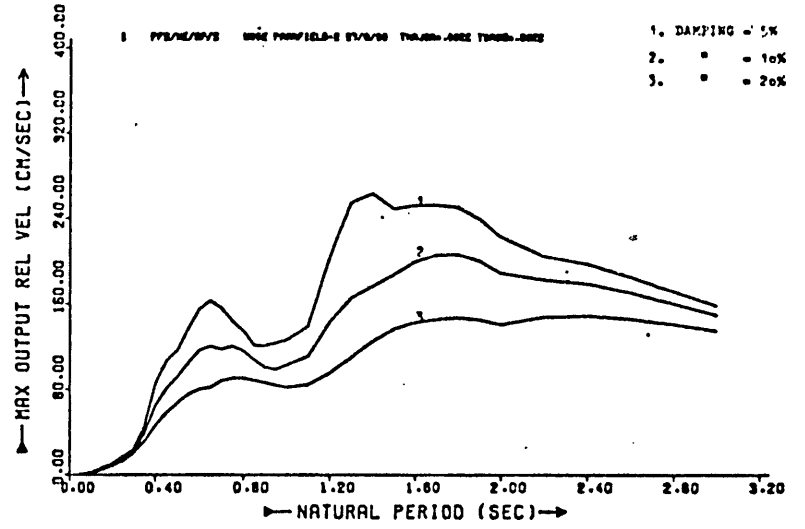


FIG. 1.3 SCHEMATIC DIAGRAM OF THE OVERBURDEN AND ITS BEDROCK





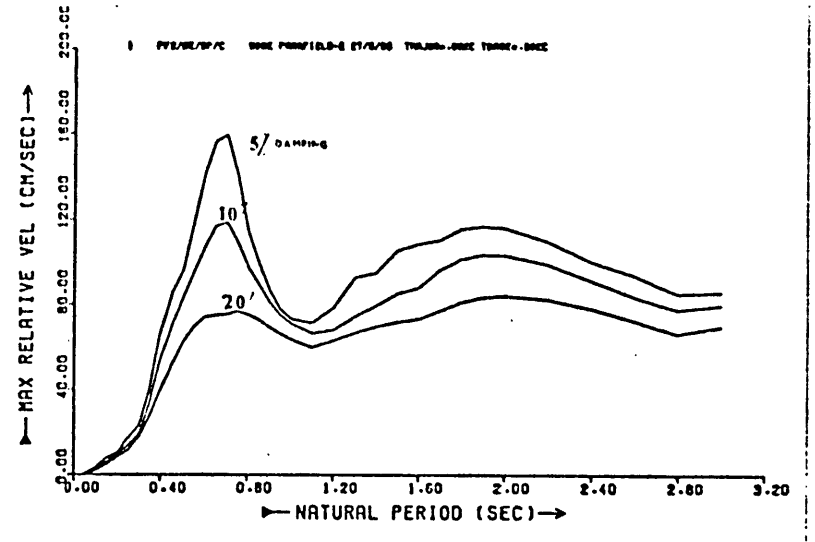


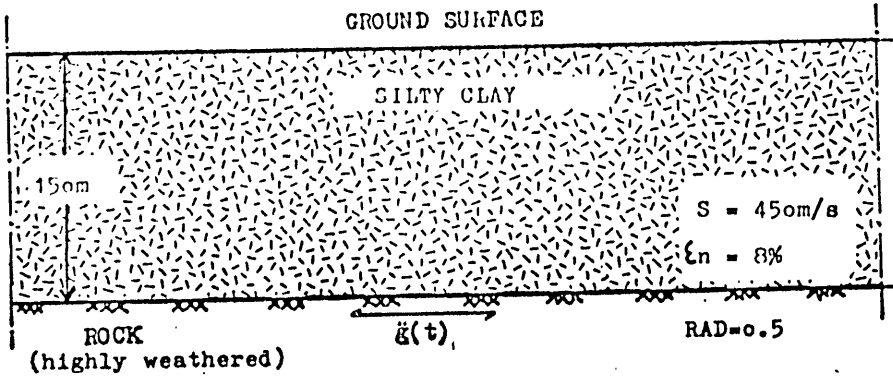
FIG. 1.4 SCHEMATIC DIAGRAM OF THE OVERBURDEN AND ITS BEDROCK

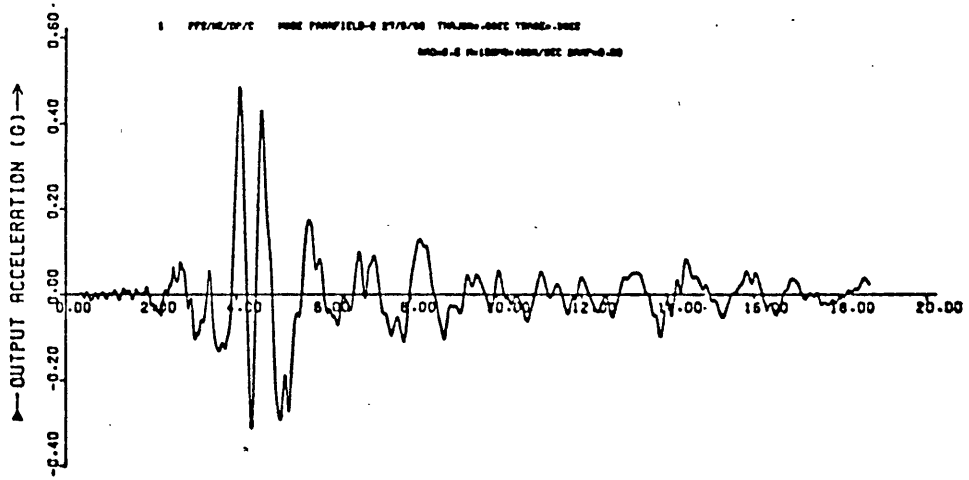
motion have also been modified especially in the intermediate range of frequencies.

Figs. 1.5 to 1.8 illustrate the results of the second case where the deposit of silty clay is underlain by a highly weathered rock. Maximum surface acceleration has hardly been amplified and maximum surface velocity has been amplified by about one-tenth, the frequency characteristics of bedrock motion have changed to a lesser degree compared with the first case. The increase in spectral velocity of bedrock motion in the intermediate frequency range differ considerably in both cases.

A schematic diagram of the problem, for which an approximate closed form solution is given in this thesis, is shown in fig. 1.9. An exact closed form solution of the problem is virtually out of the question, because of the mathematical difficulties associated with the solution. The importance of the developed design method lies in the fact that, without it, no understanding of the phenomenon known as "Radiation Damping" can be achieved. This is also the first study of its type which illustrates in detail the effect of radiation damping on ground response.

During earthquake loading instability due to shear failure might occur. Such aspect of the problem is not dealt with in this study. The instability due to increase in pore water pressure has been dealt with in this thesis and a means of stabilizing potentially unstable deposits has been suggested.





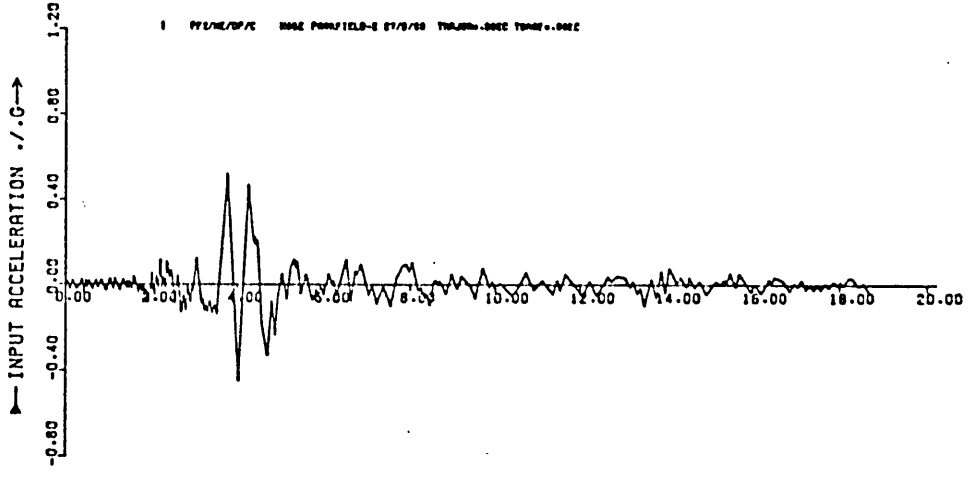


FIG. 1.5 SCHEMATIC DIAGRAM OF THE OVERBURDEN AND ITS BEDROCK

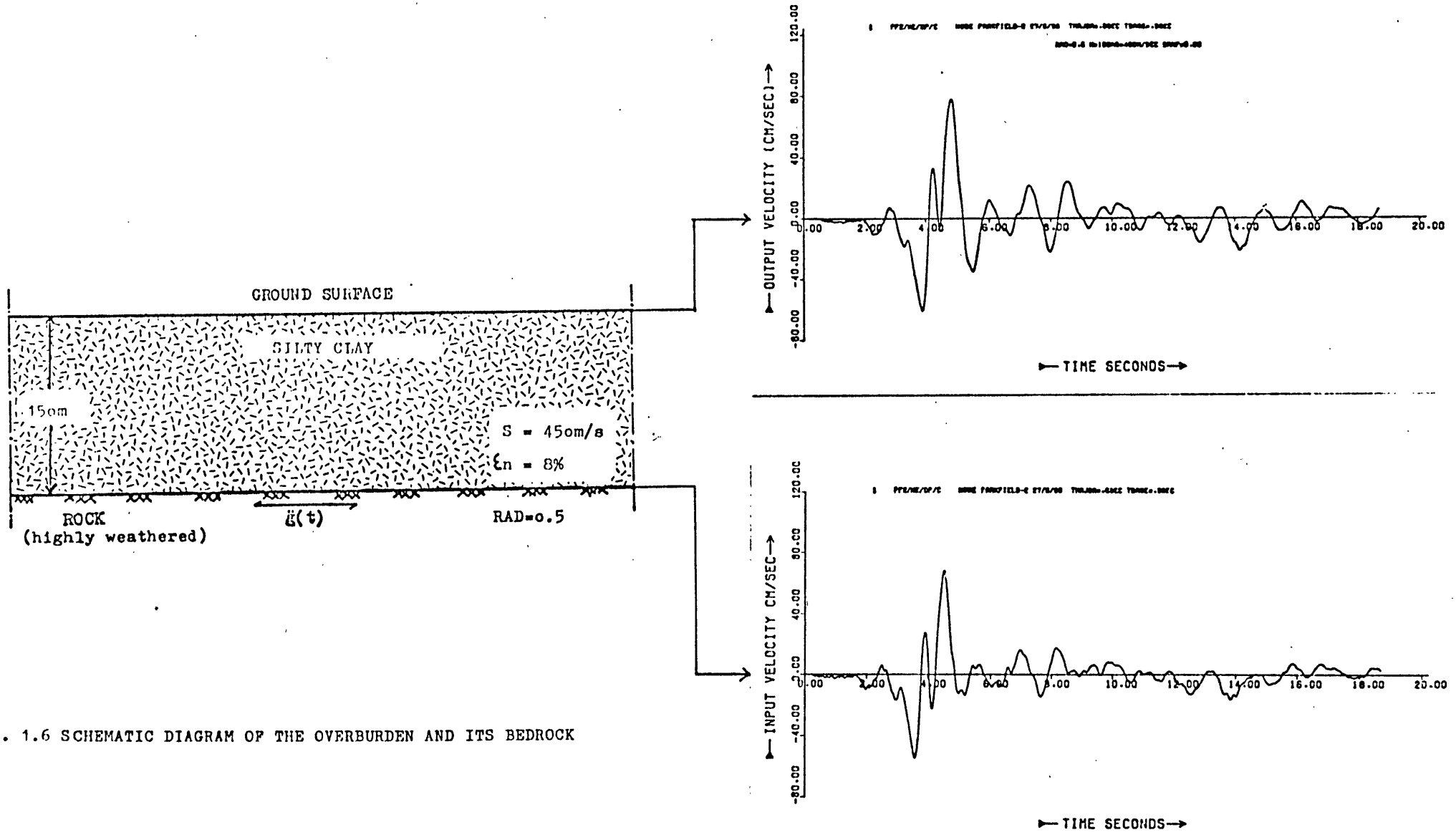
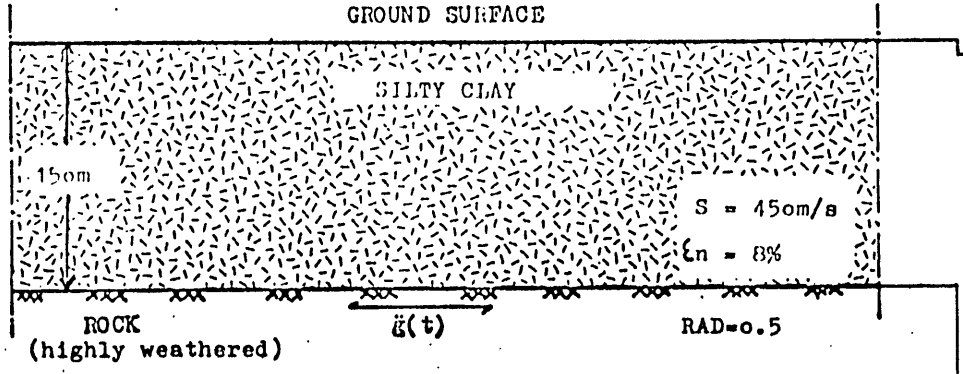
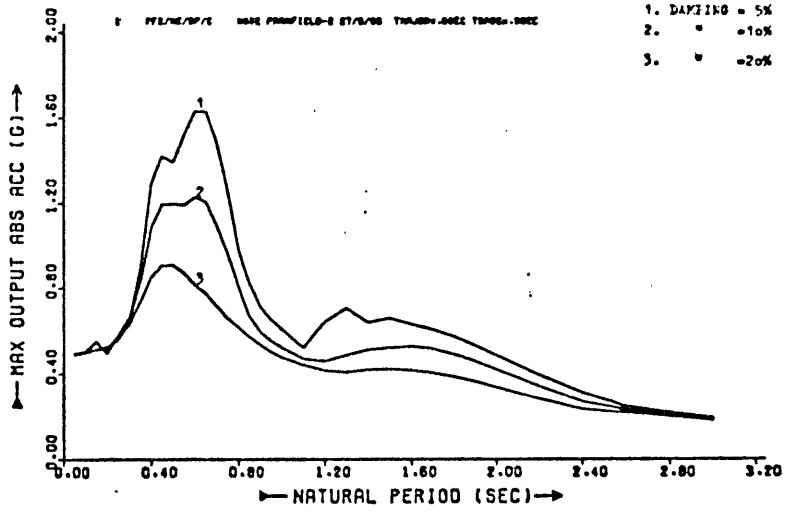


FIG. 1.6 SCHEMATIC DIAGRAM OF THE OVERBURDEN AND ITS BEDROCK





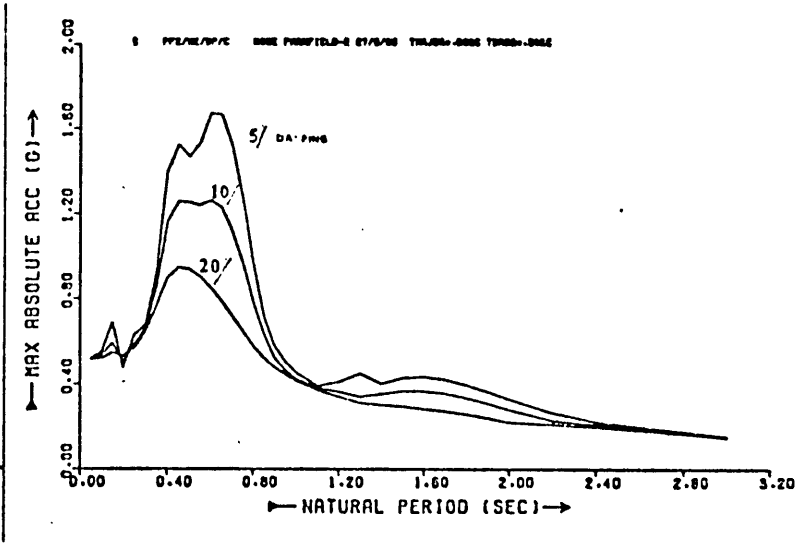
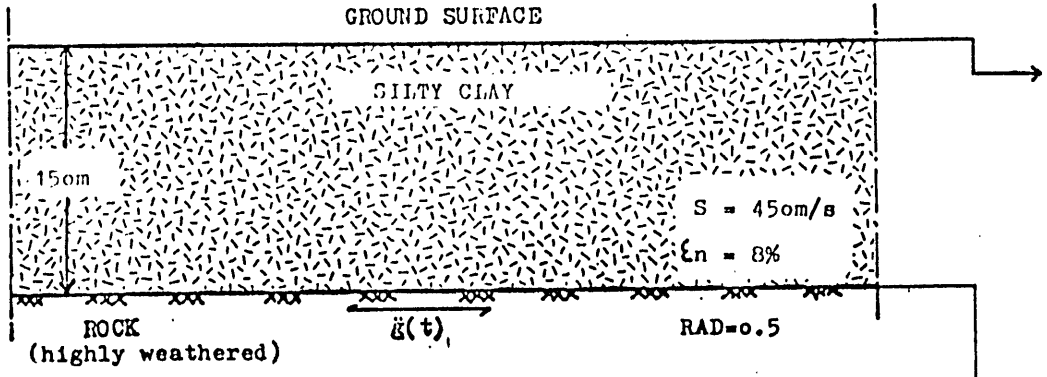
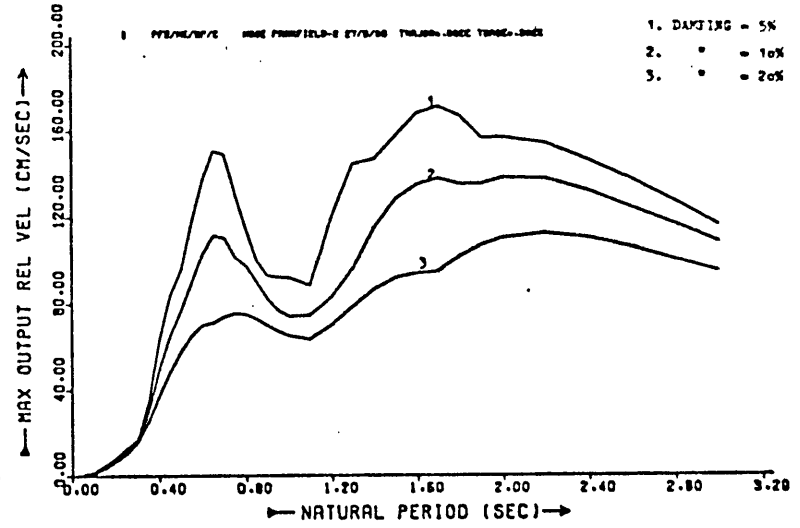


FIG. 1.7 SCHEMATIC DIAGRAM OF THE OVERBURDEN AND ITS BEDROCK





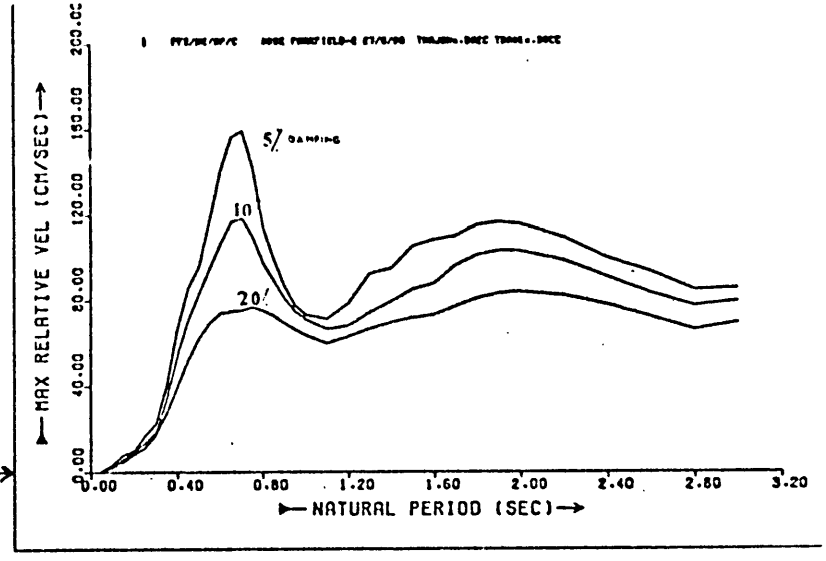


FIG. 1.8 SCHEMATIC DIAGRAM OF THE OVERBURDEN AND ITS BEDROCK

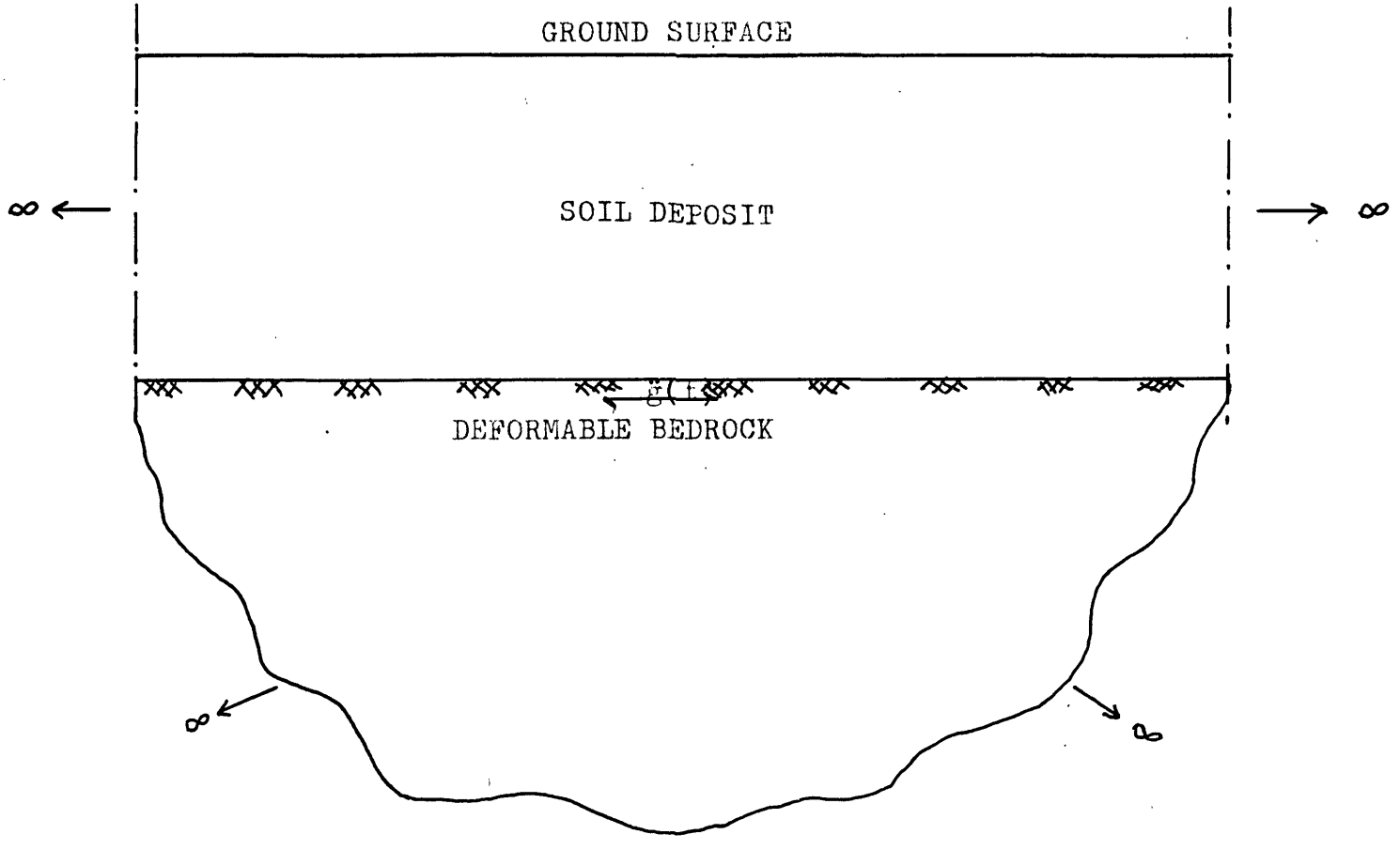


FIG. 1.9 SCHEMATIC DIAGRAM OF SOIL DEPOSIT UNDERLAIN BY DEFORMABLE BEDROCK

$\ddot{g}(t)$ = bed rock acceleration

1.2. OBJECT AND SCOPE OF PRESENT INVESTIGATION

The research reported in this thesis was undertaken in order to study foundation response underlain by deformable bedrock to seismic loading. The main objectives of the study are:

1. To develop a new mathematical model for investigation of the influence of ground conditions on ground response, taking into account deformability of bedrock.
2. To determine the influence of radiation damping, soil properties and bedrock motion on foundation response.
3. To investigate differences on computed response between rigid base solution and deformable base solution.
4. To compare the results with real field behaviour.
5. To develop a computer program for the proposed mathematical model by which records obtained from strong ground motion instruments could be used as bedrock motion to compute the motion in the overlying soil deposit.
6. To investigate pore pressure redistribution associated with ground shaking after earthquakes in deposits of sand located above a weak layer or an impervious bedrock.
7. To suggest a procedure for stabilizing potentially unstable deposits and provide some theory for the proposed procedure.
8. To summarize major findings of this investigation in the light of recommendations for design.

All of the objectives noted above have been accomplished. However, after undertaking a comprehensive study of all numerical techniques and deriving the relevant expressions, it was decided to change point one from "to develop suitable numerical techniques for

the prediction of strong ground motions in elasto-plastic foundation materials" to that noted above. This was done because it was felt that it would be very difficult to make an original contribution to knowledge for the following reasons:

i) Elasto-plastic model suffers from limitations of wave front formations. [62]

ii) Numerical models suffer from inadequate transmission capability. [16]

iii) The problem had already been solved in the case of constant shear modulus by a former student. [46]

iv) Owing to lack of quantative data on variation of shear modulus with depth, one is unable to take this effect into account.

v) Even though the true variation of shear modulus with depth in soil deposits were known, it could only be incorporated in numerical models based on the assumption of a constant shear modulus within each individual sub-layer. [38]

The thesis that follows includes: chapter 2, critical review of previous work. Chapter 3, character of bedrock motion. Chapter 4 through 9 represent results and discussions relevant to the above objectives. A summary of the major findings of this research, together with the most important conclusions, are included in chapter 10. Chapter 11 discusses the recommended approach for assessment of design data for earthquake resistant design.

CHAPTER 2

CRITICAL REVIEW OF PREVIOUS WORK ON FOUNDATION RESPONSE TO SEISMIC LOADING

2.1 INTRODUCTION

In recent years, there has been a remarkable interest in foundation response to seismic loading. However, the number of basic contributions to the topic are limited. Some effort has been put by seismologists into the formulation of analytical models for this purpose, which are of very little use to practising engineers because they are either based on far-field observations or consider highly idealized topographical features. These studies are not included here. The following is a brief review of the most important studies which are of great value to practising engineers.

Analysis of response of foundation materials to seismic loading is a three-dimensional anisotropic, non-homogenous, non-linear, with complicated geometry (not often), complex problem, for which practical solutions are expensive or impossible to obtain. Conventially, to make the mathematics tractable, the analysis is carried out in one dimension with restrictive assumptions. The overburden is assumed to be semi-infinite (i.e. constant depth, infinite in the horizontal plane), the boundaries of the overburden as well as the bedrock are horizontal and the medium undergoes shear deformation caused by

vertically travelling shear waves. It has been assumed that instabilities, due to liquifaction and extensive settlement would not occur during earthquake. The most important one-dimensional mathematical models, can be grouped as follows:

a) Continum models.

b) Lumped mass models.

2.1.1. CONTINUM MODELS

This group of models is very popular with practising engineers; they produce accurate results, are easy to use, offer a fundamental insight into the influence of ground conditions on ground response, do not require large computers, and allow a considerable amount of parametric study at very little cost.

Kanai(1950)[36] studied response of a visco-elastic foundation system underlain by elastic bedrock, subjected to harmonic excitation at bedrock level of the overburden. The author obtained amplification spectrum equation, which is a function of incident wave periods and layer thickness, for small values of viscosity of the overburden and zero for the underlying bedrock. The author concludes that his results clearly resemble the features of ground movements which were obtained by the accelerometers at several places in Tokyo and Yakahama. The analysis presented by the author assumes that earthquake motion is harmonic; this assumption has been widely reported to be untrue.[20]

Matthiesen, Duke and Leeds (1964)[44] extend Kanai's work to "n" layer case. They applied their method to 66 strong ground motion sites in California, U.S.A. Solutions up to n = 3 had already been

obtained by Kanai[37]

Schnabel, Seed and Lysmer (1972)[41] have incorporated some new features into the work already developed by Matthiesen et. al. The authors have assumed that the earthquake motion was represented by a series of sinusoidal motions of different frequencies. This was done by the introduction of Fourier transform techniques. They have also incorporated strain dependent material properties by a special iterative procedure. Both of these new features merit criticism. It has already been shown by[24] that earthquake motion can only be approximately represented by a series of sinusoidal motions of different frequencies. The strain dependent hysteretic damping and shear modulus used by the authors are non-standard. Aramaki and Kaga[7] have found that, for poor soil, both damping and shear modulus decrease with increasing strain levels.

Herrera and Rosenblueth (1965)[30] have presented a method in which the soil medium has been assumed to be visco-elastic, consisting of "n" layer system subjected at its base to stationary Gaussian process type earthquake motion. A matrix form solution has been presented by the authors. The assumption that earthquakes are stationary Gaussian processes merits discussion.

The criticisms given in this section emphasize the need to develop a new model equally simple but more accurate, efficient, and closer to reality. The new mathematical model developed in this thesis, together with its accompanying computer program, has increased the horizon of knowledge of engineers in the specialised field of Eng. Seismology for the following reasons:

i) It takes into account real earthquake loading recorded by strong ground motion instruments.

ii) Real properties of soil and deformability of the bedrock. The assumption, of small value, of damping in the overburden, as made by the author, has also been made by Kanai [36]

iii) The model is relatively cheaper, in respect of comparison of the cost and time involved, than the usual models.

iv) It has thrown light on the phenomenon known as "radiation damping".

2.1.2. LUMPED MASS MODELS

This group of models, which emerged in the 1960's, became very popular among engineers, because they were an extension of the classical theories regarding structural dynamics. Non-linearity could easily be incorporated in them, as well as variation of soil properties with depth, in an approximate manner.

It is today agreed that all lumped mass solutions have inadequate transmission capability. Maximum frequency transmitted through the system is given by:

$$f_m = \frac{S}{\pi . \Delta y}$$

where:

f_m = maximum frequency (c.p.s).

S = shear wave velocity of the overburden.

Δy = spacing between masses.

Sinusoidal signals whose frequencies are greater than f_m cannot propagate through the system. Signals with frequencies less than "f_m" propagate with shear wave velocity less than "S". It is this defect in lumped mass solutions which can cause large errors in computed response. Shallow soil deposits cannot be modelled because of numerical instability in the time history calculating schemes.

Penzien, Scheffery and Parmelee (1964)[47] introduced the lumped mass solution approach for evaluating the seismic response of semi-infinite soil layers, having hysteretic bilinear stress-strain characteristics. How far the use of bilinear stress-strain relationship is justified to represent behaviour of clays under earthquake loading is questionable. In the paper there is no mention of radiation damping.

Idriss and Seed (1968)[34] obtained linear lumped mass solutions and have shown that an equivalent linear analysis could be used to obtain results of a bilinear analysis. This recommendation does not permit one to calculate the value of permanent displacement, which is also of importance to practising engineers.

Rosset and Whitman (1969)[48] in their study have developed a formula by which influence of bedrock characteristics is incorporated in the lumped mass solution as an additional damping in each mode according to the following formula:

$$\beta_{equ} = \frac{2}{\pi} \cdot \frac{\gamma_{soil} \cdot S_{soil}}{\gamma_{rock} \cdot S_{rock}} \cdot \frac{1}{2n - 1}$$

where γ = unit weight.

S = shear wave velocity.

β_{equ} = equivalent hysteretic damping ratio

n = number of modes

The validity of the authors' statement has been fully investigated in chapter 6. The authors have also emphasized that no prediction of ground response is complete without consideration of characteristics of bedrock in the analysis.

Tsai and Housner (1970)[60] extended the classical lumped mass

approach to include the elasticity of the bedrock. This was done by means of coupling a dashpot to the base of the lumped mass model to account for half-space bedrock. The bedrock motion was represented approximately by a series of sinisoidal motions of different frequencies. To illustrate the use of their model, the authors have compared their results with that recorded in the field at Union Bay site and have concluded:

i) "Although the general agreement between computed and recorded clay motion is reasonably good .... the large discrepancy observed for the first 0.25 seconds results from the fact that in the calculation the system started from rest at t = 0 but this transient error was rapidly attenuated by the damping."

ii) "The discrepancies,we think, result from the fact that waves are not ideal vertically travelling, planar , shear waves and that clay and till are not exactly planar.

Papastamatiou(1971)[46] extends the work of Penzien, Scheffery and Parmelee to the case of elasto-plastic model and follows the approach developed by Tsai and Housner to include the elasticity of the bedrock. The author also emphasizes the importance of radiation damping. The model used by the author to represent behaviour of soils under earthquake loading merits discussion.

2.2. FINITE ELEMENT METHOD

The finite element method is mainly used for problems for which neither closed form solutions nor lumped mass solutions can be found. The method allows much flexibility in the variations of soil properties and configurations of foundation materials. The main disadvantages of the finite element method when used for investigation of influence of foundation conditions on foundation response are:

i) Cannot take into account the relevant physical characteristics

of the interface between the foundation and its underlying bedrock. The transparent boundary techniques are insufficient for representation of radiating boundary conditions.

ii) Does not correctly account for the infinite extent of boundaries.

iii) Suffers from inadequate transmission capability; a relatively coarse mesh has to be chosen in the foundation to keep the problem within computability limits.

iv) Deep soil deposits cannot be modelled because of computer memory limitations.

v) Paramatic analysis cannot be performed by finite element methods because of cost of computer time.

For all these reasons the finite element method has not been employed very effectively in the study of foundation response to seismic loading. More research is required in this direction.

Idriss and Seed (1967)[33] adopted the finite element method to study response of earth banks to seismic loading. They have concluded that:

"vertical component of base motion has little effect on the horizontal components of the response values of the bank or the shear stresses developed, but may influence the vertical response values considerably".

Deyfulian and Seed (1970, 1971)[21,22] extended Idriss and Seed's analysis to include a wider variety of soil configurations with sloping bedrocks for out of phase bedrock earthquake excitation, as a time dependent phenomenon approaching or moving away from the inclined bedrock. They found that for the excitation travelling in either direction, the location of points of peak response are shifted with respect to the corresponding stationary excitation solution in the direction of propagation. As the velocity of the travelling wave increases, the peaks approach more closely to the position of the peak for the stationary excitation solution. Spacial variation of the base motion is very important in ground response analysis for earthquake motion. It is my

recommendation that until more is known about spacial variations in (weathered, highly weathered, etc.) rock motions, due to wave propagation effects, these effects should not be included in ground response analysis, in order to minimize the resulting errors.

2.3. CONCLUDING REMARKS

In preparing this critical review, the method known as Method of Characteristics [57] was excluded. This was done because the length of the article describing the method is not sufficient for the author fully to appreciate the method.

The number of previous studies on chapter 8 are very limited; a brief review is included in the chapter. Previous work on chapter 9 is non-existent. However, certain suggestions have been of great value in the development of the work reported in chapter 9 , which are quoted in the relevant sections.

CHAPTER 3

BEDROCK MOTION

3.1. INTRODUCTION

For design of engineering structures on specified sites, engineers need to know about the character of bedrock motion that can be expected during future earthquakes. There are three general approaches to the problem. Firstly, to ask experienced seismologists to develop an entirely new theory for earthquakes, so that engineers could use this to calculate the bedrock shaking. Secondly, to use previous earthquake instrumental, strong motion accelerograph, data. Thirdly, to gain a fair degree of understanding of future bedrock motion characteristics* by studying stable strong motion bedrock parameters. The first approach is beyond reach of present day seismologists. It is the objective of this chapter to provide a brief discussion of the last two approaches.

3.1.1. USE OF PREVIOUS EARTHQUAKE STRONG MOTION RECORDS

There are now about 4000 accelerographs distributed all over the world, from which a few thousand records have been obtained. Since 1933 the U.S. network has produced about 350 good accelerograms of engineering interest. Among these accelerograms fourteen recorded in the

---

* predominant period, maximum acceleration, velocity, duration of shaking, etc.

near-field (i.e. source distance $\lesssim$ 12 Km) were used in this study. The records considered are:

1. Parkfield (cholame Shandon No 2) 27/6/66
2. San Fernando (Pacoima Dam S16E) 9/2/71
3. San Fernando (Pacoima Dam S74W) 9/2/71
4. Parkfield (cholame Shandon No 5 N65E) 27/6/66
5. Parkfield (cholame Shandon No 5 N5W) 27/6/66
6. Parkfield (cholame Shandon No 8 N50E) 27/6/66
7. Parkfield (cholame Shandon No 8 N40W) 27/6/66
8. Parkfield (TEMBLOR S25W) 27/6/66
9. Parkfield (TEMBLOR N65W) 27/6/66
10. El Centro (El Centro E-W) 18/5/40
11. San Francisco (Golden Gate Park N10E) 22/3/57
12. San Francisco (Golden Gate Park S80E) 22/3/57
13. Port Hueneme (Port Hueneme E-W) 18/3/57
14. Port Hueneme (Port Hueneme N-S) 18/3/57

The accelerograms used are available in the uncorrected digitized form in the Department of Civil Engineering of Imperial College of Science and Technology.

3.1.2. ADJUSTMENT OF THE RECORDS

Each of the fourteen bedrock motions considered in this study was adjusted in a form that the velocity has a minimum mean square value. The procedure assumes that the new base line is in the form of a parabola:

$$\underset{\text{(corrected)}}{\text{acceleration (t)}} = \underset{\text{(uncorrected)}}{\text{acceleration (t)}} - C_1 - C_2 t - C_3 t^2 \qquad (3.1)$$

For the velocity to have a minimum mean square value, we must have

$$\frac{\delta}{\delta c_j} \int_0^{\text{Total duration}} \text{velocity (t)}^2_{\text{(corrected)}}\, dt = 0 \quad (j = 1,2,3) \qquad (3.2)$$

where: t = time; c_j are constants.

Integrating equation (3.1) to obtain bedrock velocity in order to substitute in (3.2) a knowledge of initial uncorrected velocity (at t=0) is required. If the instrument did not require a certain level of acceleration to initiate recording, a proper base line correction could be done; however, because of starting delay error, the beginning of the earthquake acceleration is not recorded. Therefore, the true value of initial velocity is not known and, to minimize the resulting error, its value is assigned to zero.

The baseline error results from the fact that the instrument does not mark the axis of reference which would pass through the position of zero acceleration from which accelerations could be read. When a reference axis is drawn, its position does not coincide with the position of zero baseline. It is beyond the purpose of this chapter to discuss other sources of errors, such as instrument sensitivity error, mounting error, etc.

The procedure discussed in this section was incorporated in a computer program named ADJUST. The program applies a parabolic base-line correction to the accelerogram and integrates resulting acceleration time history, to obtain velocity and displacement time histories. "ADJUST" is dimensioned to handle 5000 output values (acceleration, velocity and displacement) per accelerogram.

Data Preparation: Input data include one or more acceleration time histories digitized at any interval of time in terms of gravity "g". Output: Output includes (a) input data and printed out ground acceleration, velocity and displacement time histories with relevant plots plotted directly on KINGMATIC Plotter.

The program is written in FORTRAN iv and was run on CDC 6400 of Imperial College. Method of integration of the corrected time history to obtain ground velocity and displacement time history is given in appendix A.

Figs 3.1(a),(b),(c) through 3.14(a),(b),(c) show plots of corrected acceleration, velocity and displacement time histories used as bedrock motion in this study. These time histories were computed to gain some depth of insight into the behaviour of overburden, by comparing computed bedrock time histories with that of ground surface.

3.1.3. RESPONSE SPECTRUM OF BEDROCK MOTIONS

After obtaining corrected time histories for each bedrock motion, the time history was used to compute response spectra (see section 6.6) for the following reasons:

a) Frequency characteristics of each motion is represented by its predominant period, period at which maximum spectral acceleration develops.

b) To compute acceleration and velocity amplification spectra (see section 6.7)

c) To investigate how shape of bedrock spectra influences shape of the corresponding ground surface response spectra.

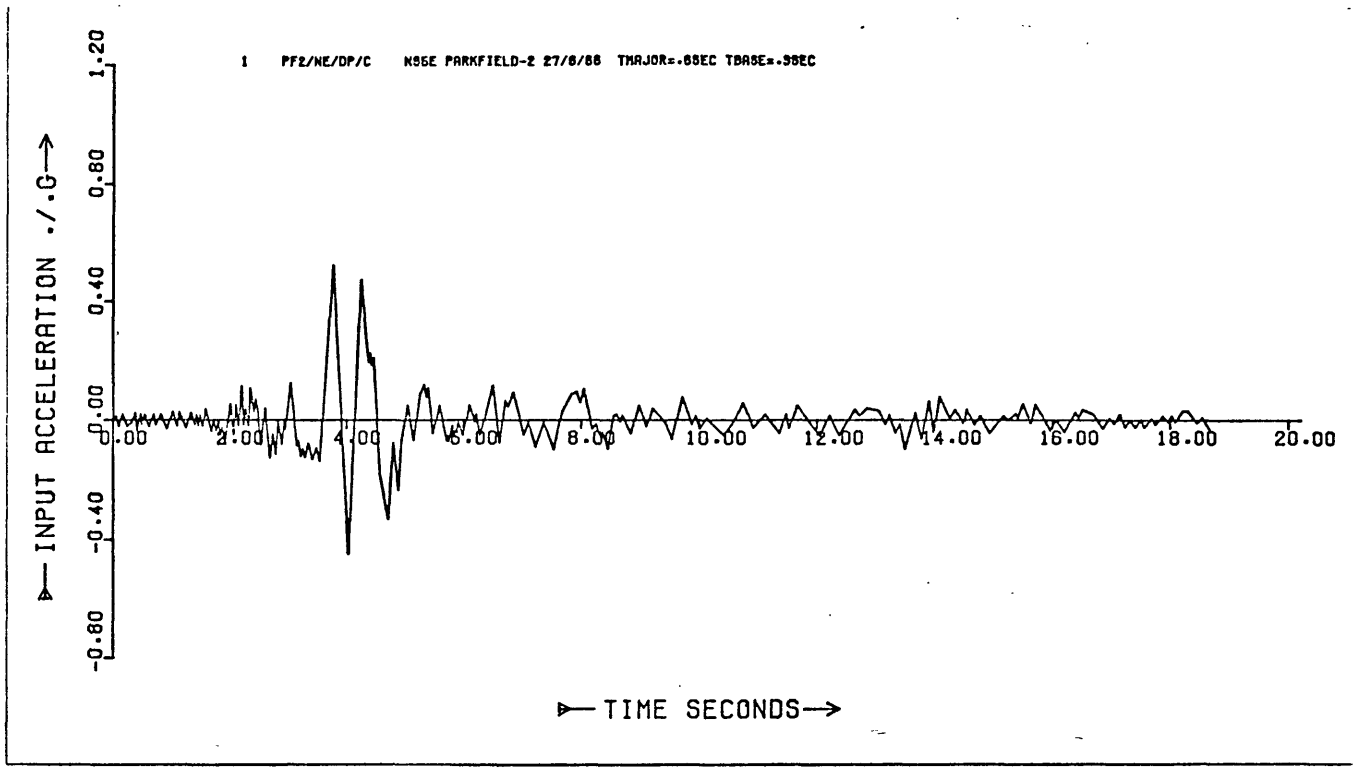


FIG. 3.1a SUBSURFACE BEDROCK MOTION USED AS INPUT MOTION IN CALCULATIONS

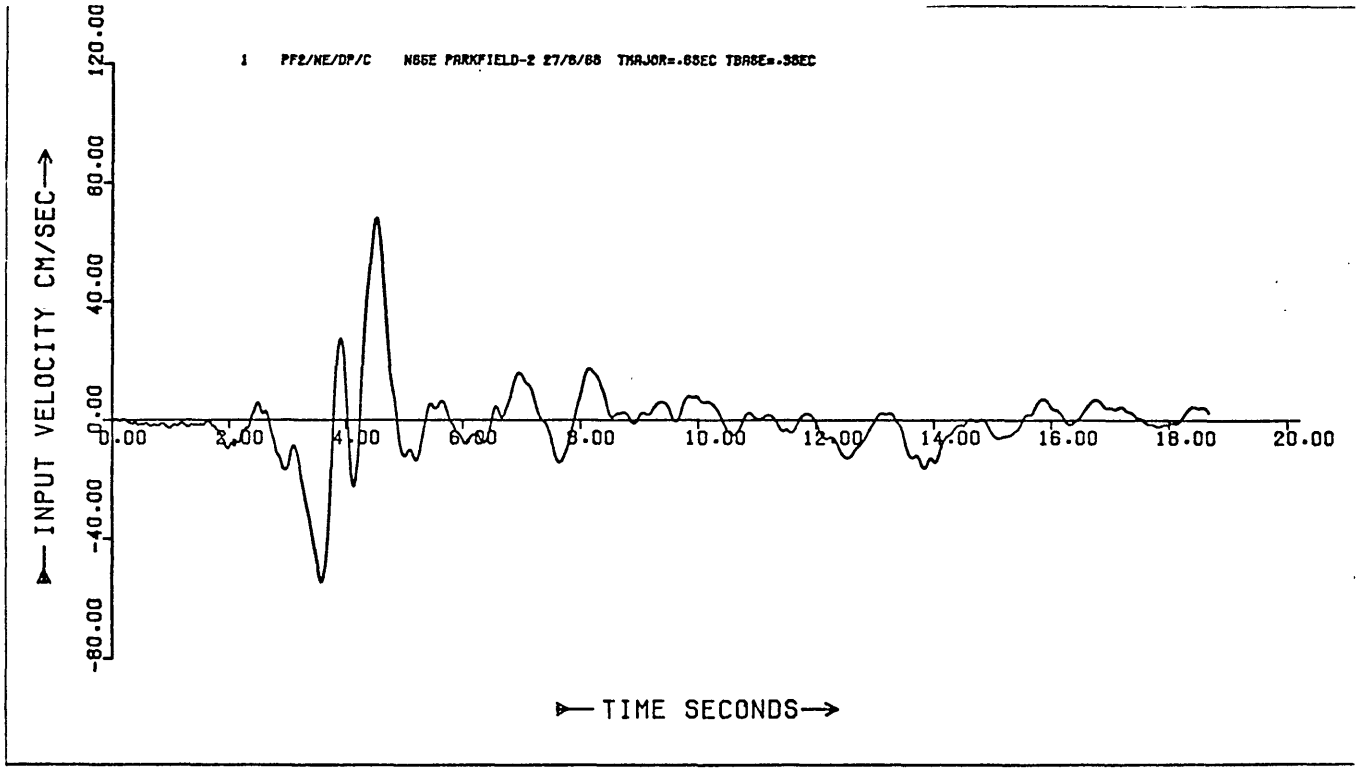


FIG. 3.1b COMPUTED SUBSURFACE BEDROCK VELOCITY TIME HISTORY

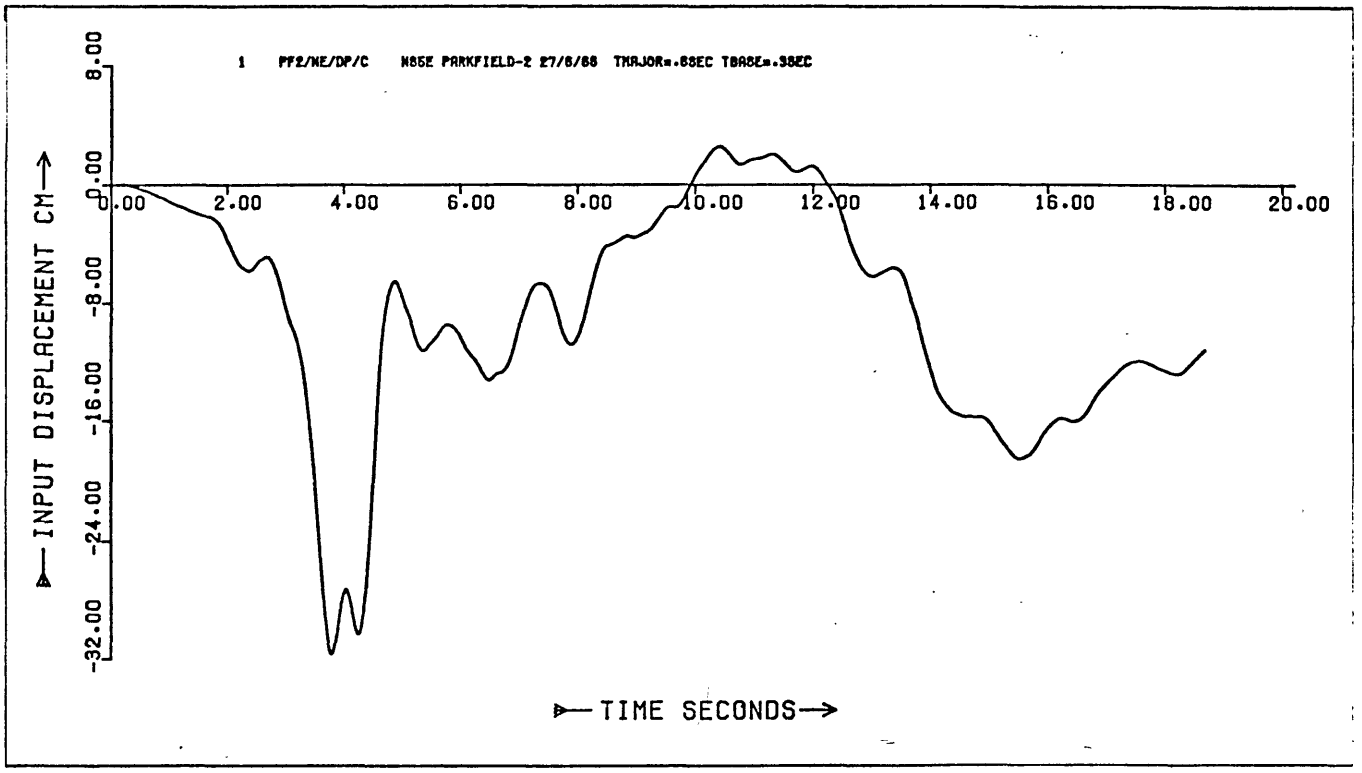


FIG. 3.1c COMPUTED SUBSURFACE BEDROCK DISPLACEMENT TIME HISTORY

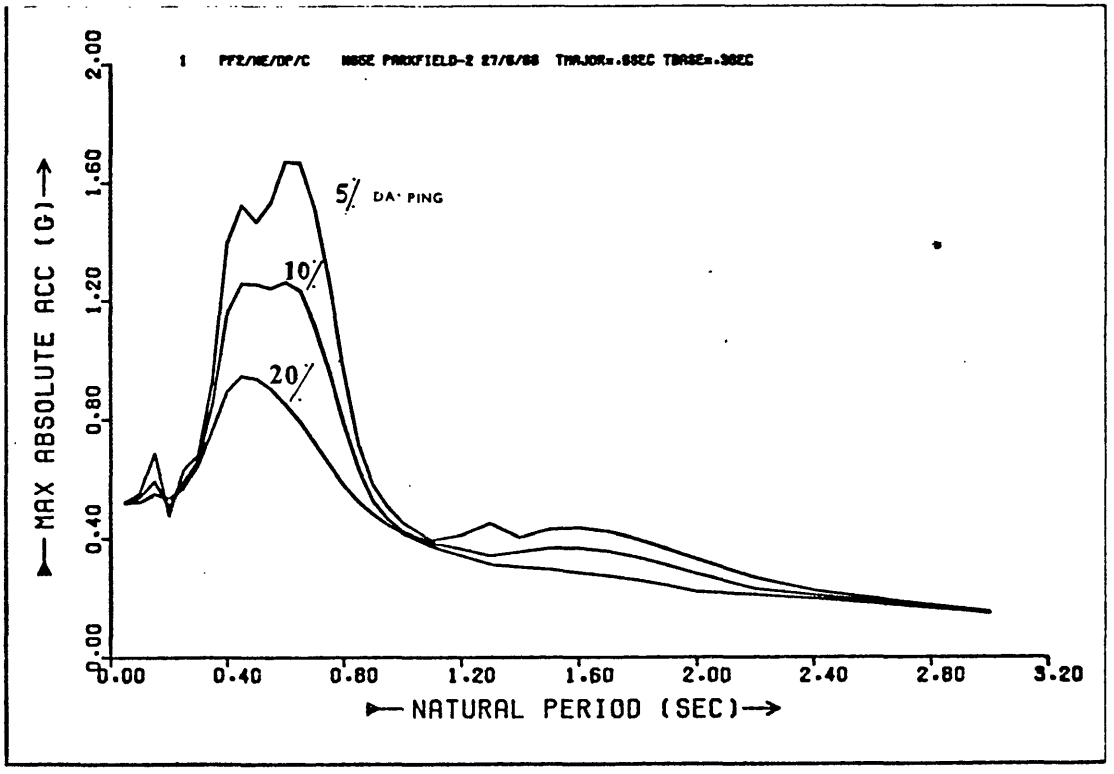


FIG. 3.1d COMPUTED SUBSURFACE BEDROCK ACCELERATION RESPONSE SPECTRA

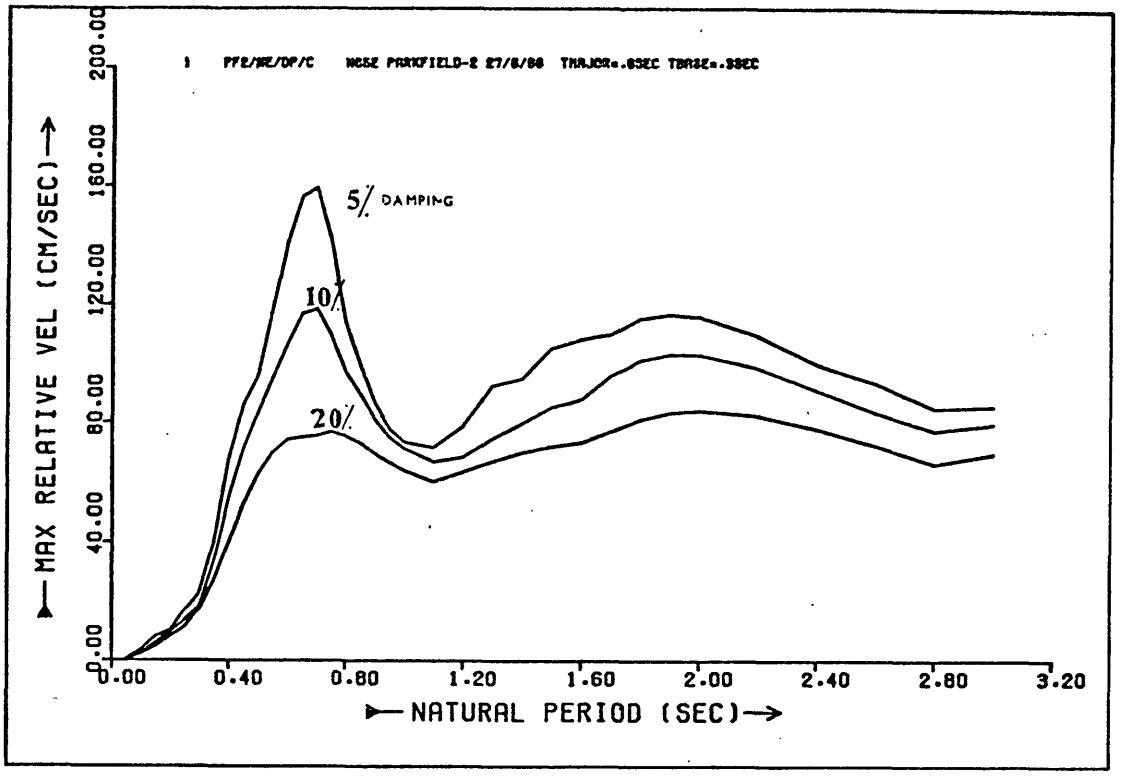


FIG. 3.1e COMPUTED SUBSURFACE BEDROCK VELOCITY RESPONSE SPECTRA

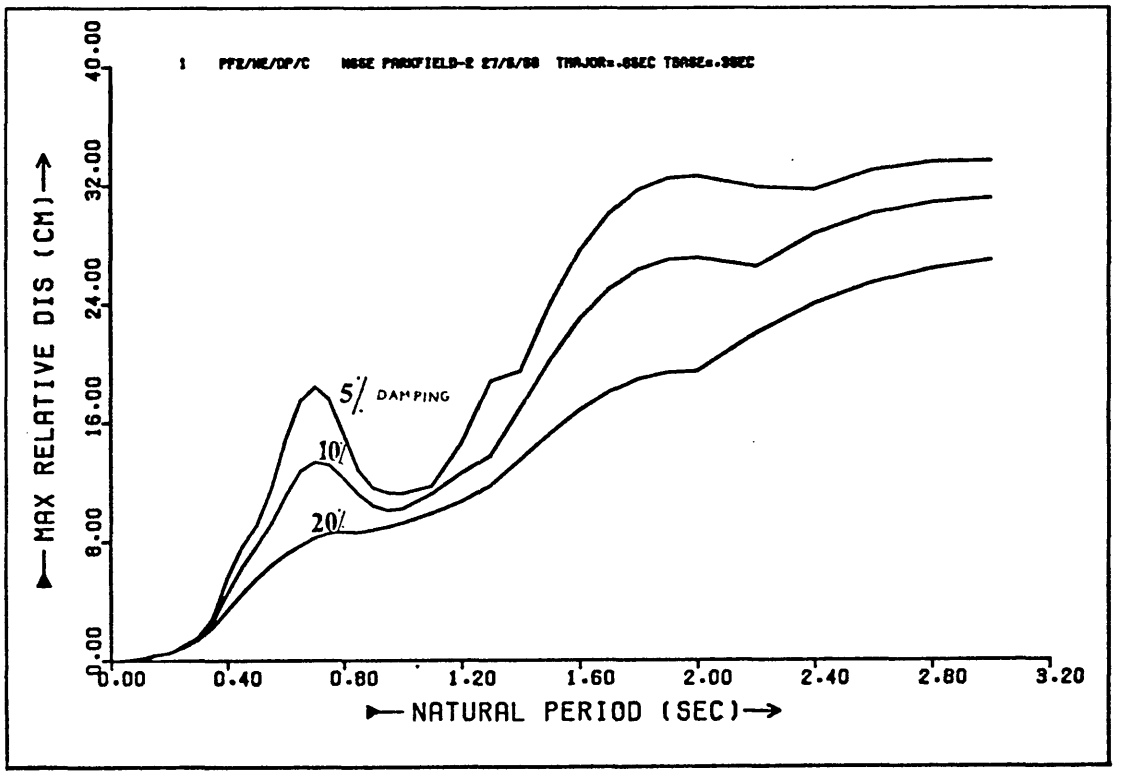


FIG. 3.1f COMPUTED SUBSURFACE BEDROCK DISPLACEMENT RESPONSE SPECTRA

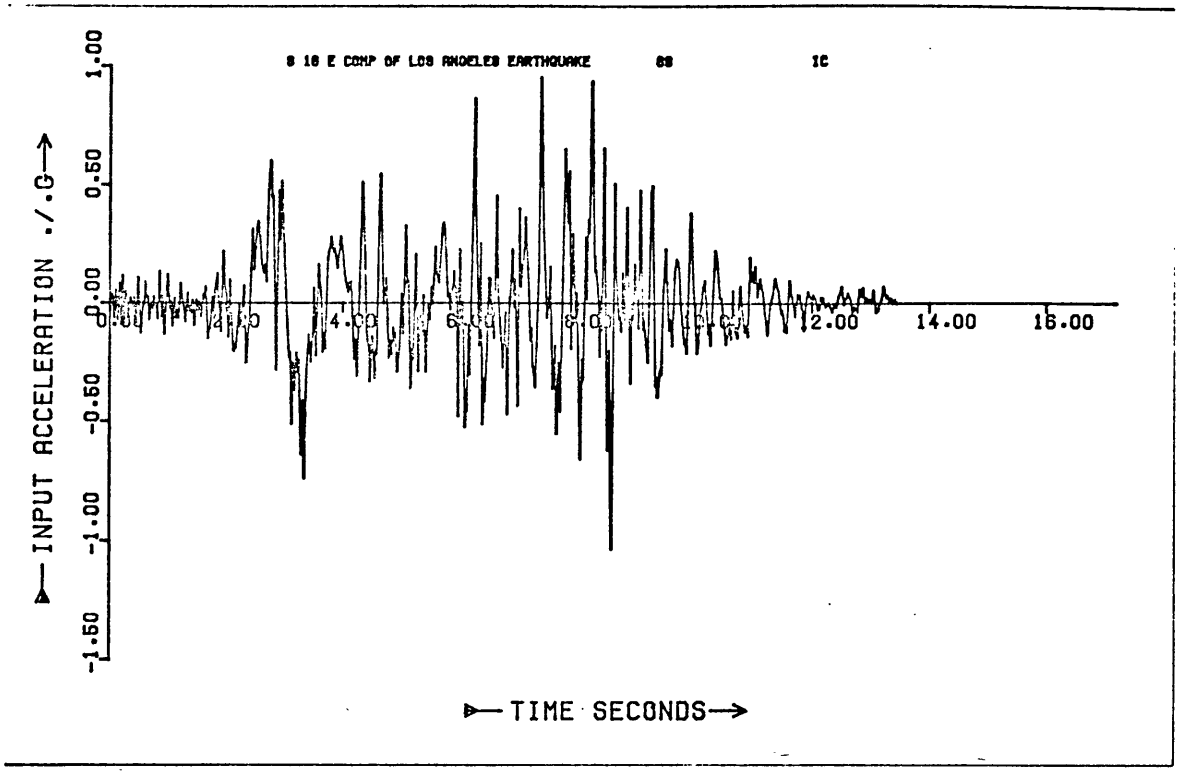


FIG. 3.2a SUBSURFACE BEDROCK MOTION USED AS INPUT MOTION IN CALCULATIONS

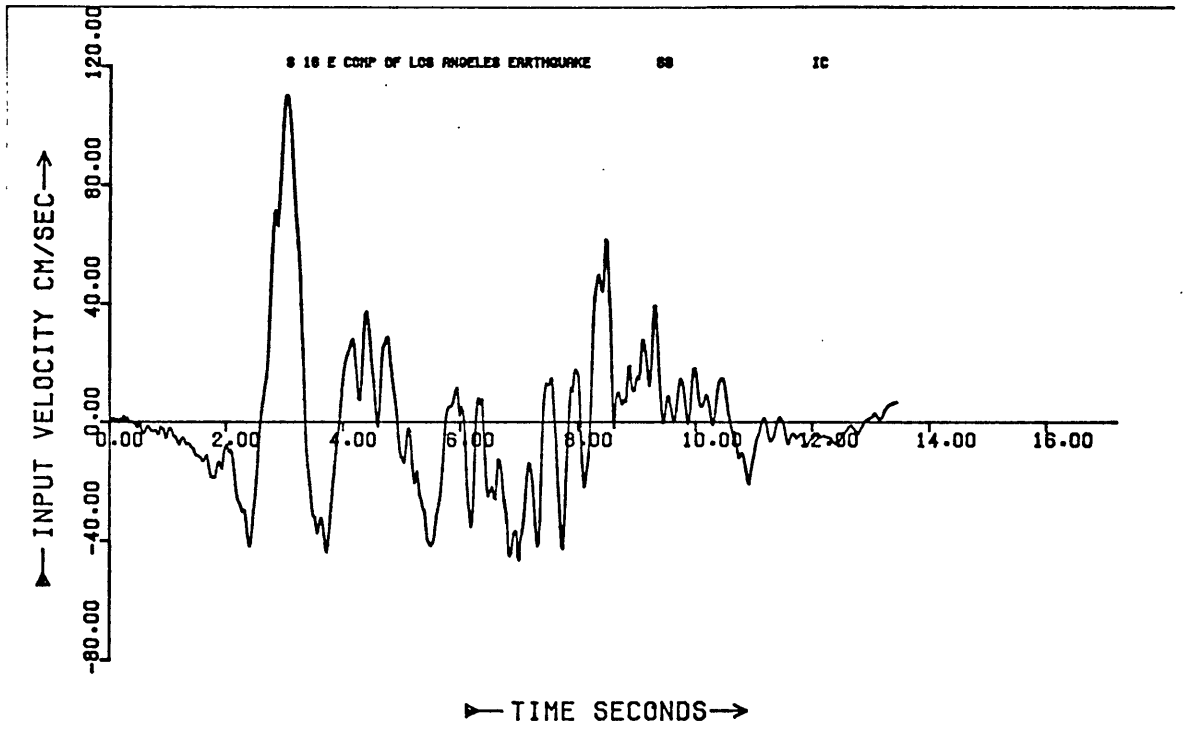


FIG. 3.2b COMPUTED SUBSURFACE BEDROCK VELOCITY TIME HISTORY

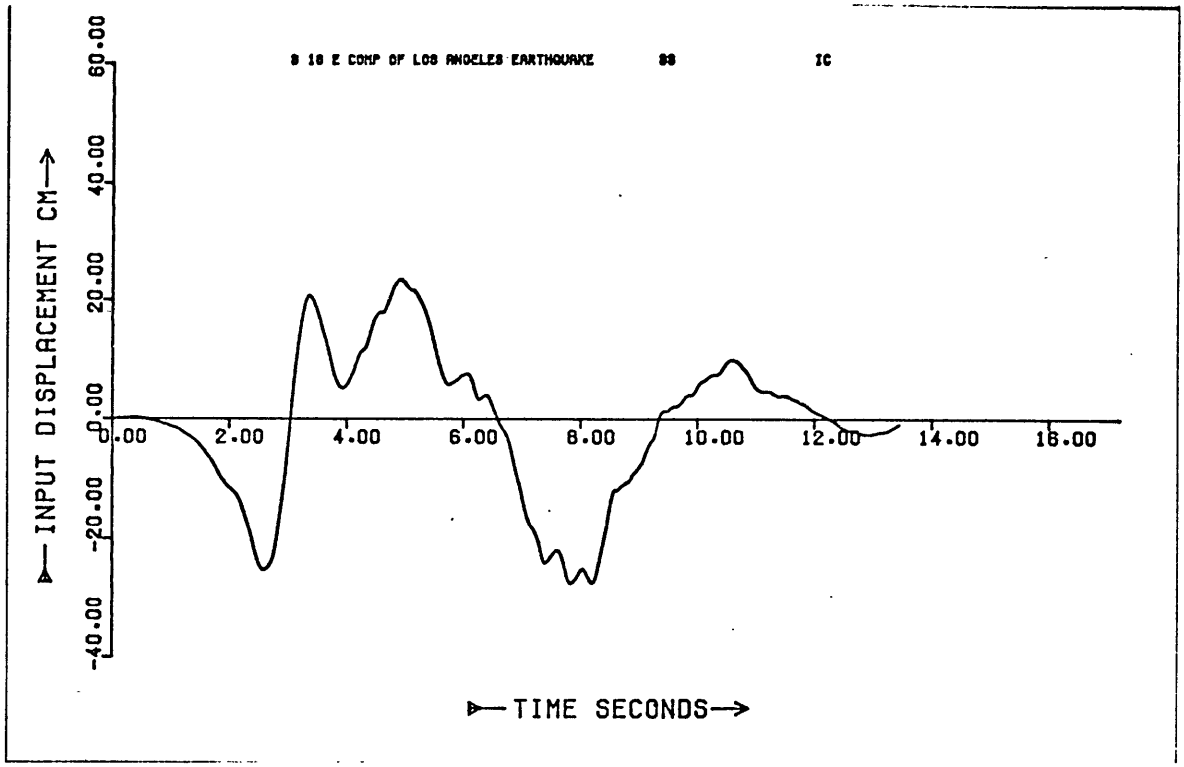


FIG. 3.2c COMPUTED SUBSURFACE BEDROCK DISPLACEMENT TIME HISTORY

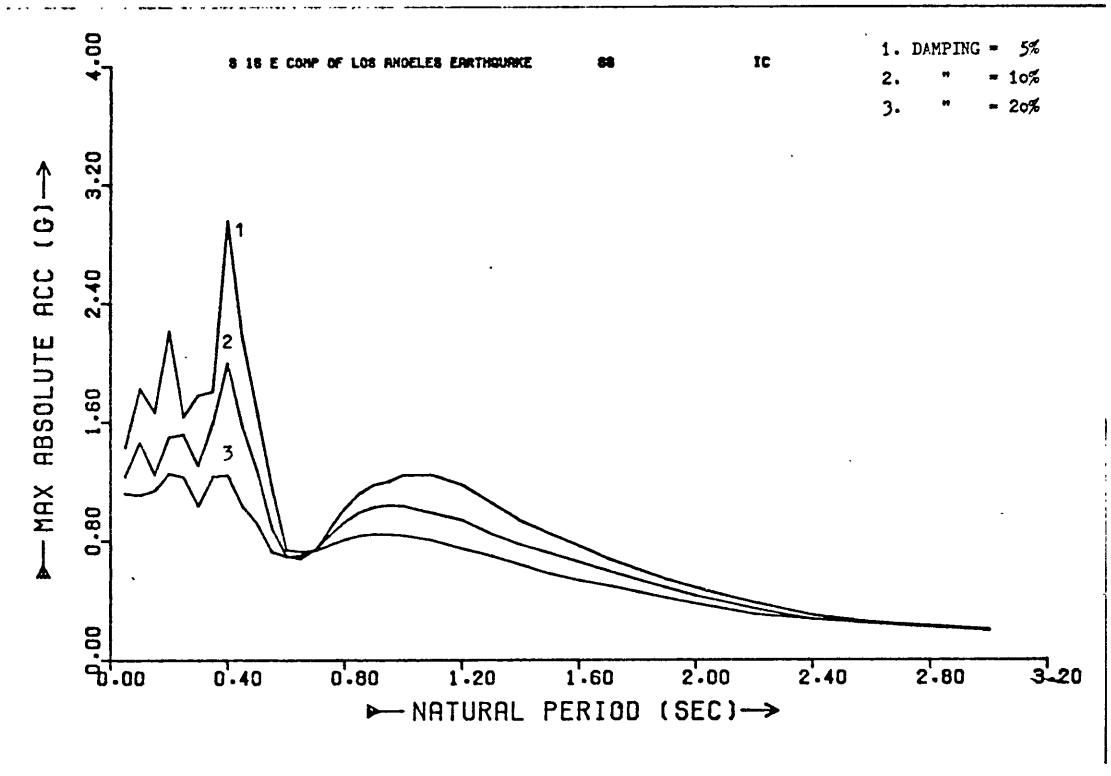


FIG. 3.2d COMPUTED SUBSURFACE BEDROCK ACCELERATION RESPONSE SPECTRA

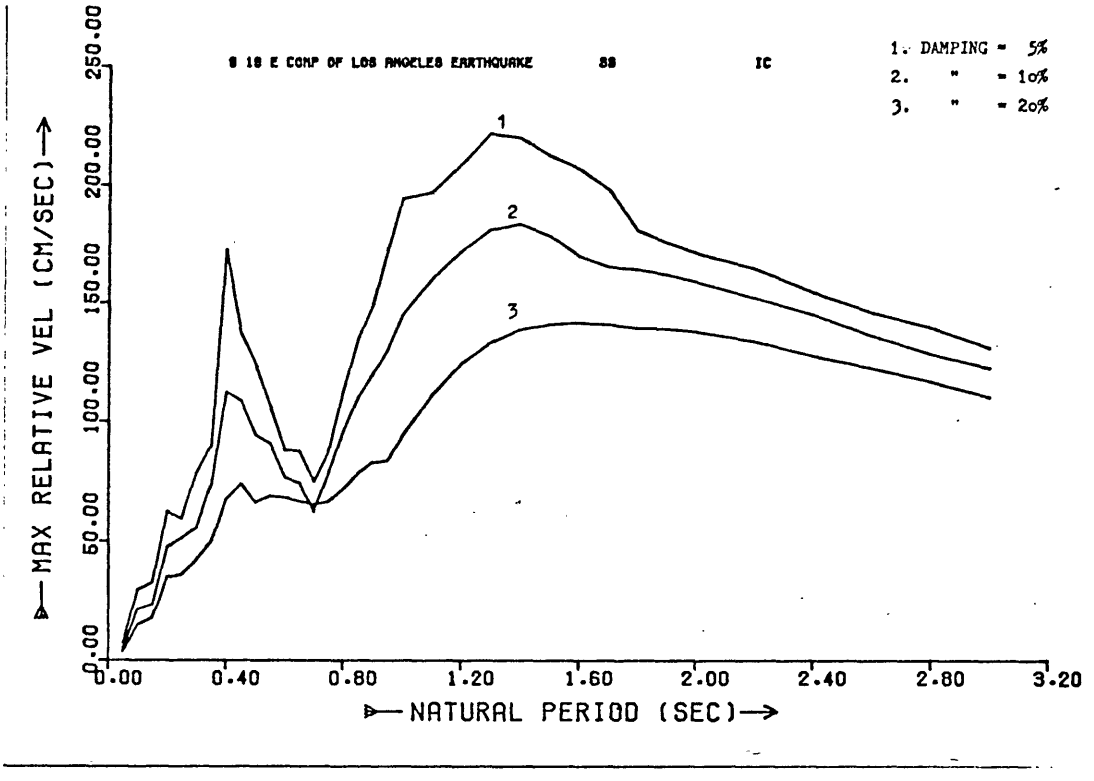


FIG. 3.2e COMPUTED SUBSURFACE BEDROCK VELOCITY RESPONSE SPECTRA

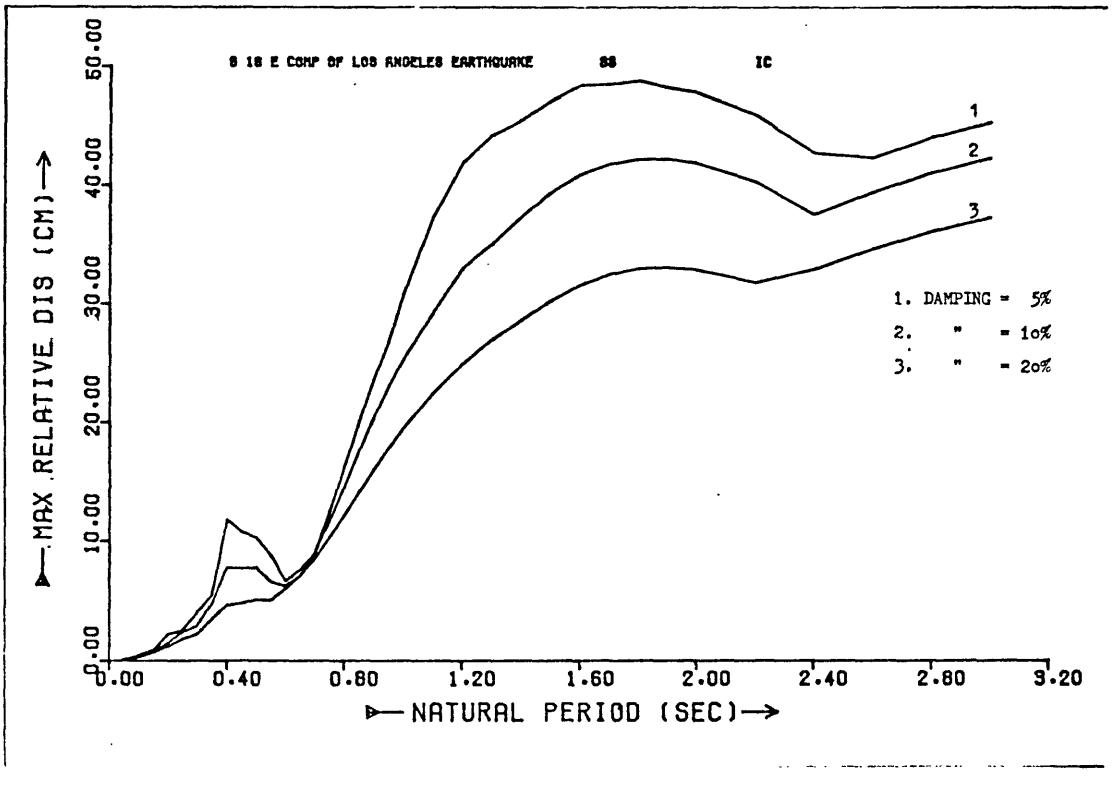


FIG. 3.2f COMPUTED SUBSURFACE BEDROCK DISPLACEMENT RESPONSE SPECTRA

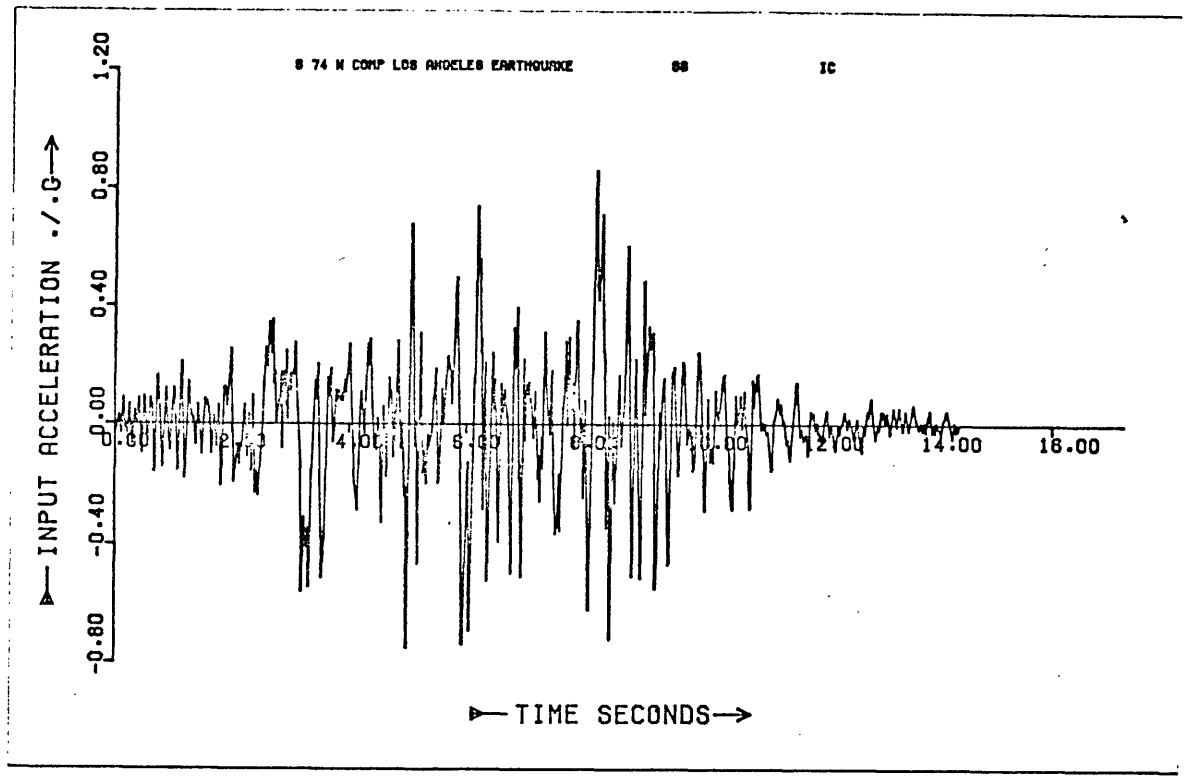


FIG.3.3a SUBSURFACE BEDROCK MOTION USED AS INPUT MOTION IN CALCULATIONS

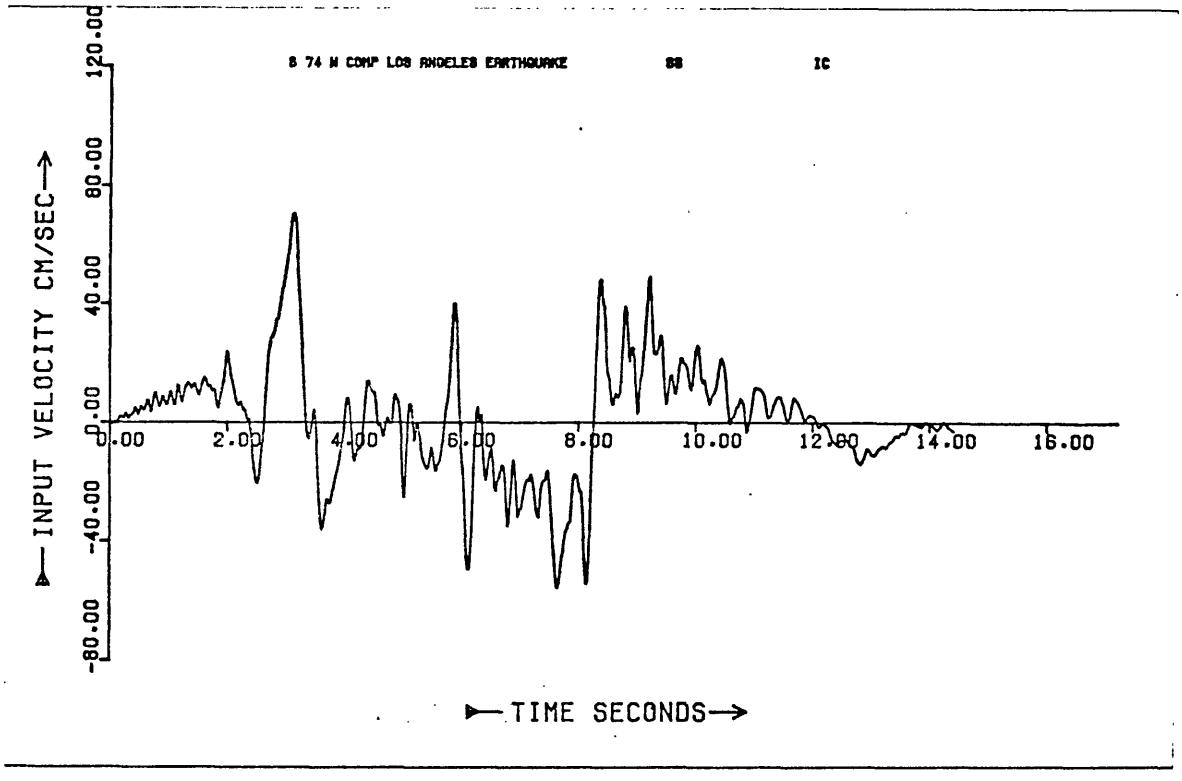


FIG.3.3b COMPUTED SUBSURFACE BEDROCK VELOCITY TIME HISTORY

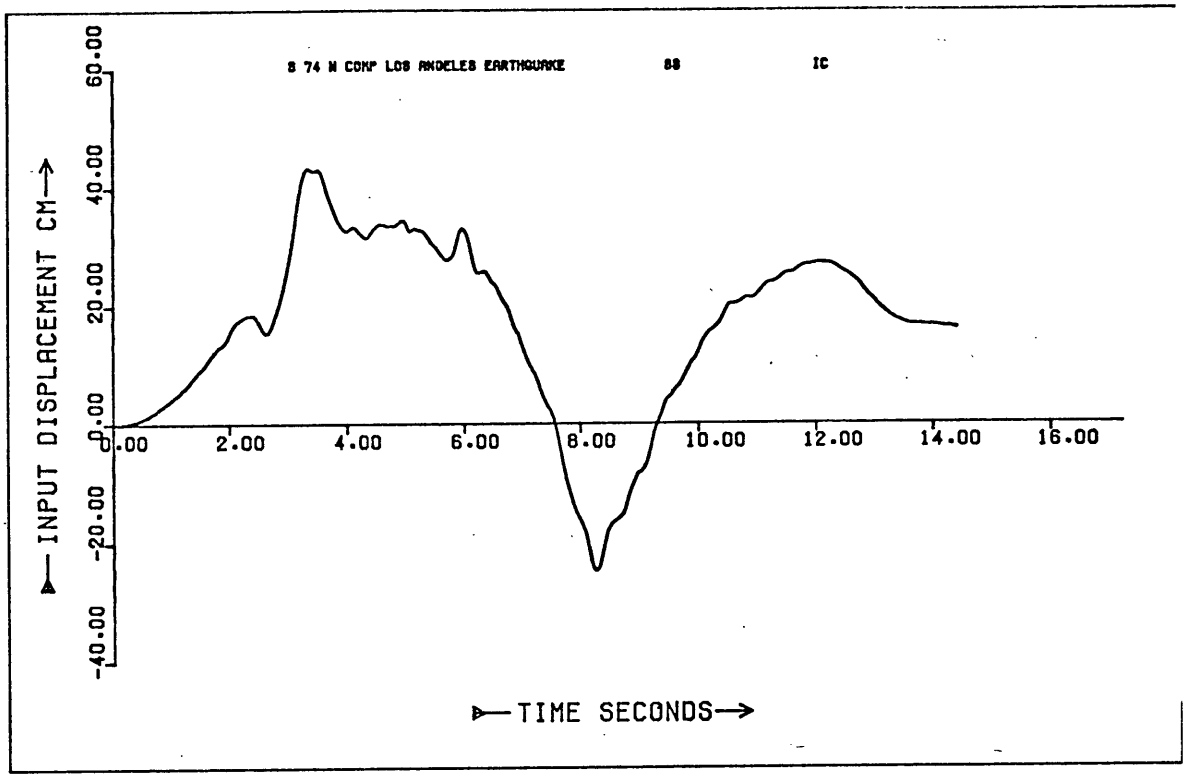


FIG.3.3c COMPUTED SUBSURFACE BEDROCK DISPLACEMENT TIME HISTORY

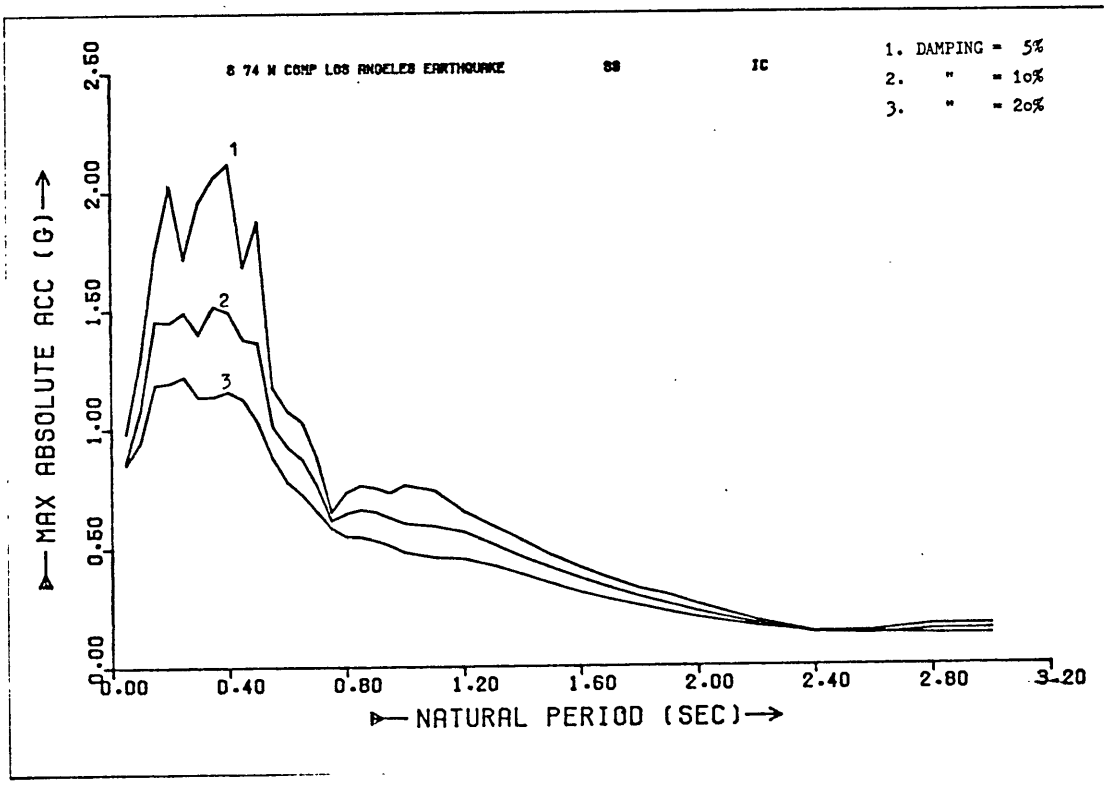


FIG.3.3d COMPUTED SUBSURFACE BEDROCK ACCELERATION RESPONSE SPECTRA

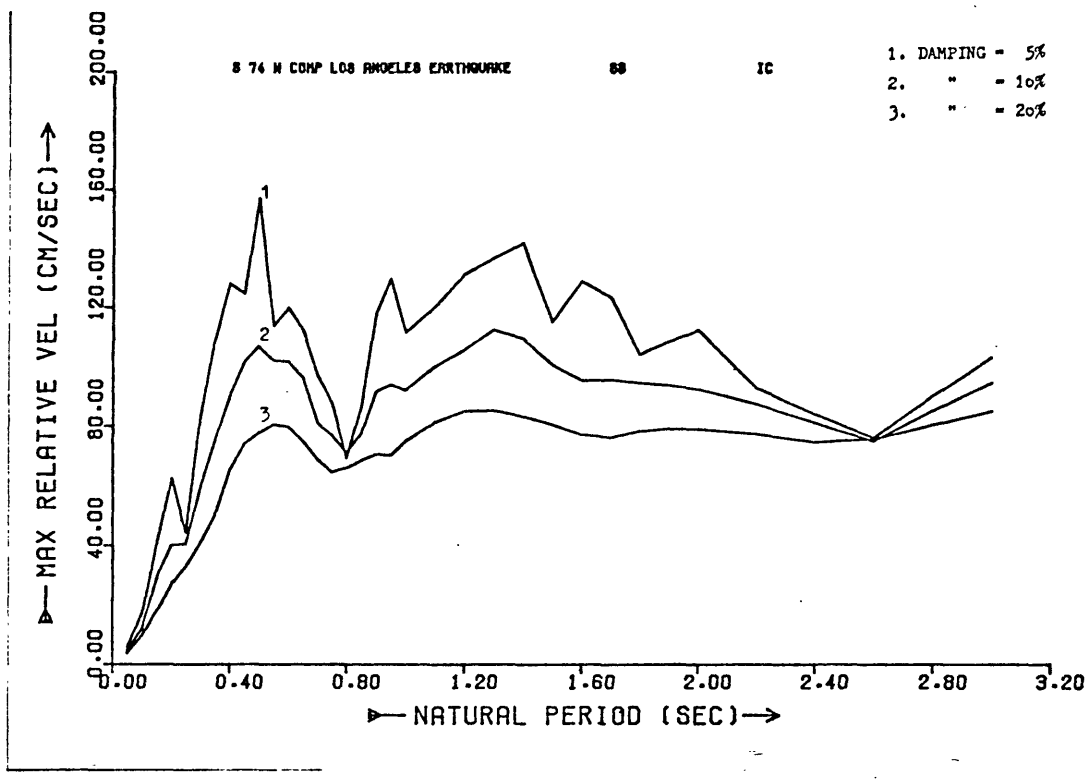


FIG. 3.3e COMPUTED SUBSURFACE BEDROCK VELOCITY RESPONSE SPECTRA

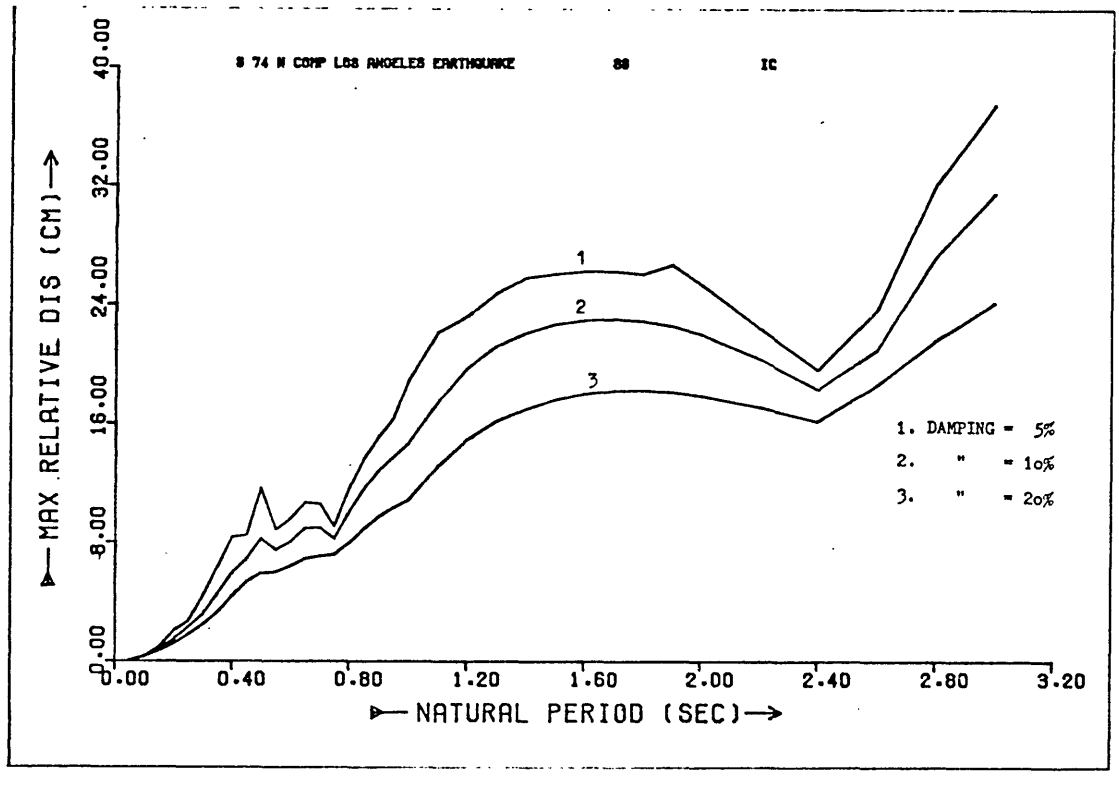


FIG. 3.3f COMPUTED SUBSURFACE BEDROCK DISPLACEMENT RESPONSE SPECTRA

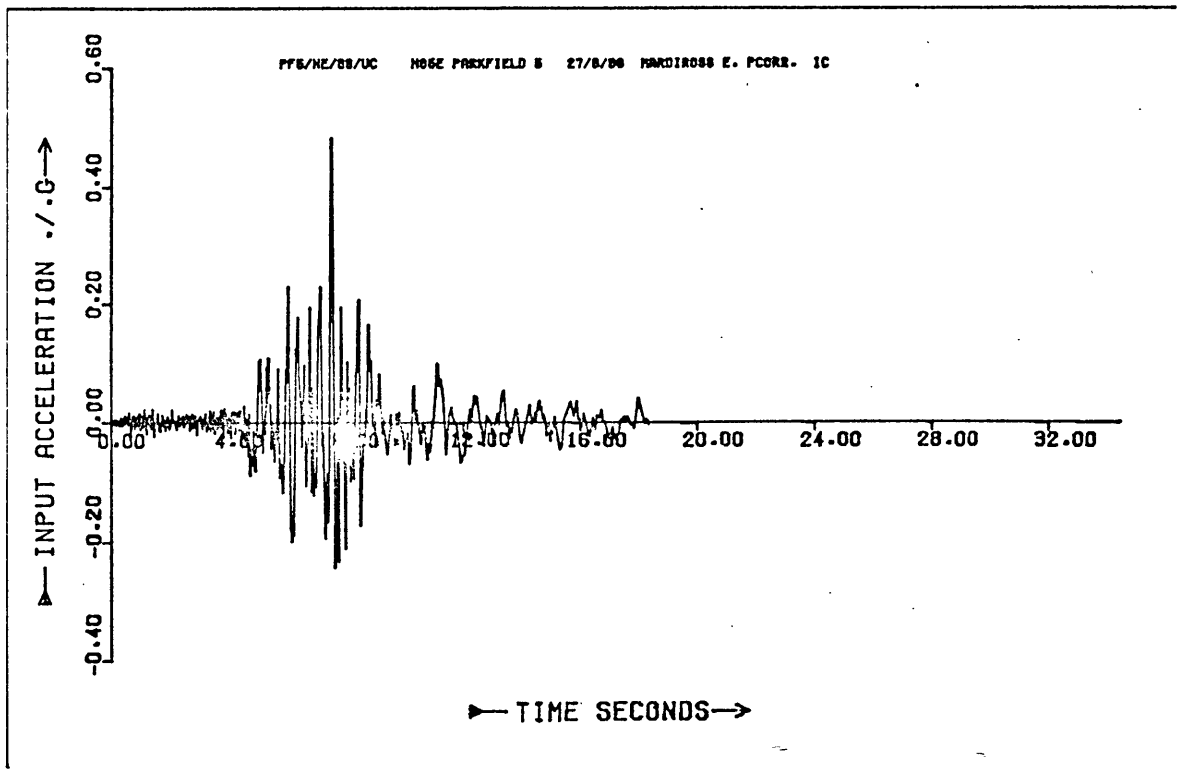


FIG. 3.4a SUBSURFACE BEDROCK MOTION USED AS INPUT MOTION IN CALCULATIONS

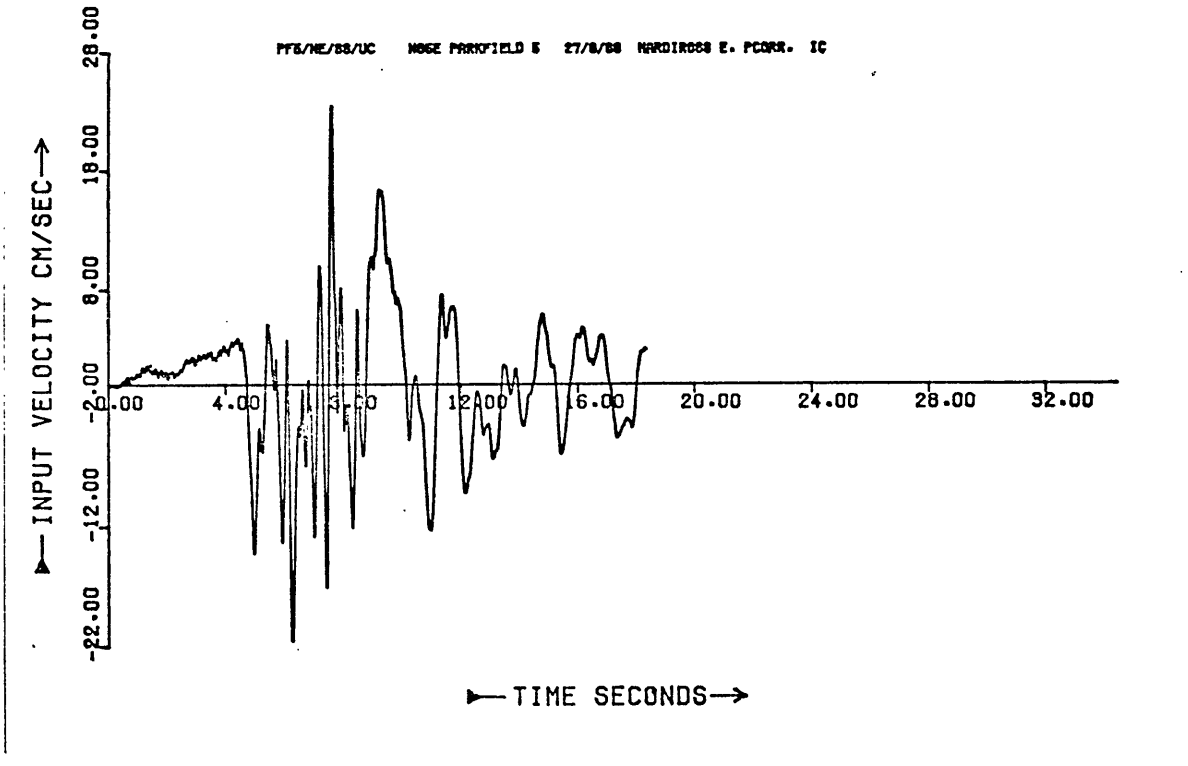


FIG. 3.4b COMPUTED SUBSURFACE BEDROCK VELOCITY TIME HISTORY

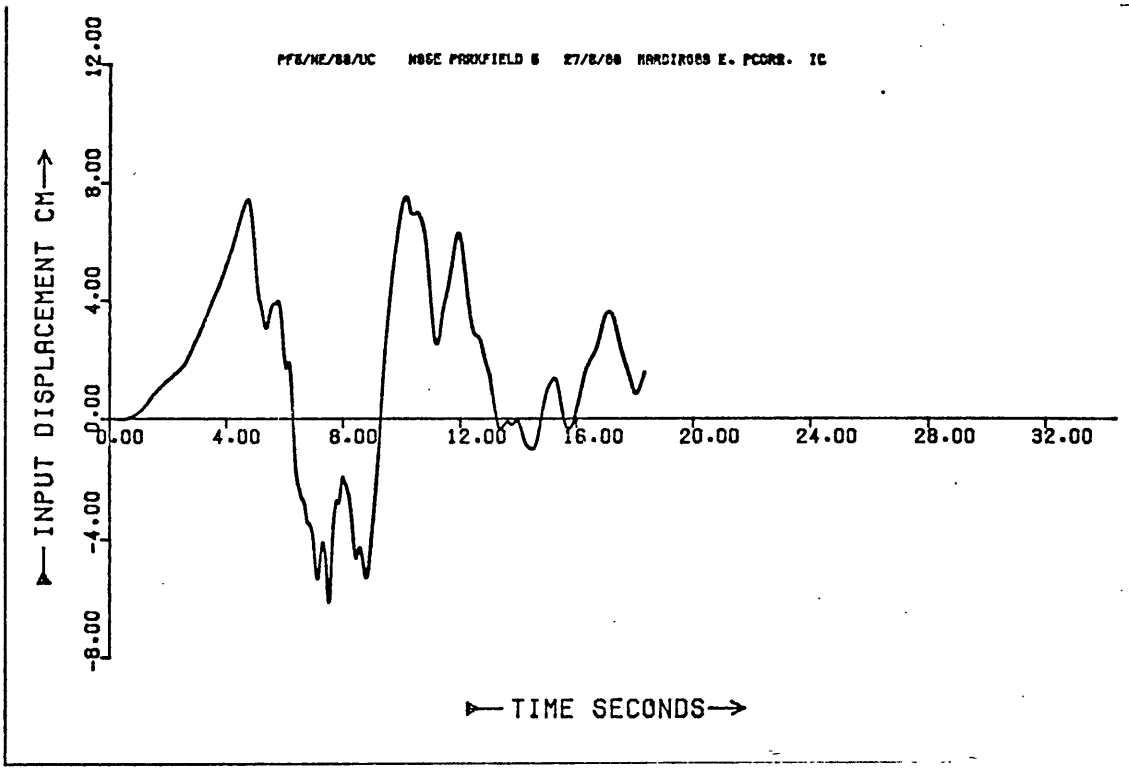


FIG.3.4c COMPUTED SUBSURFACE BEDROCK DISPLACEMENT TIME HISTORY

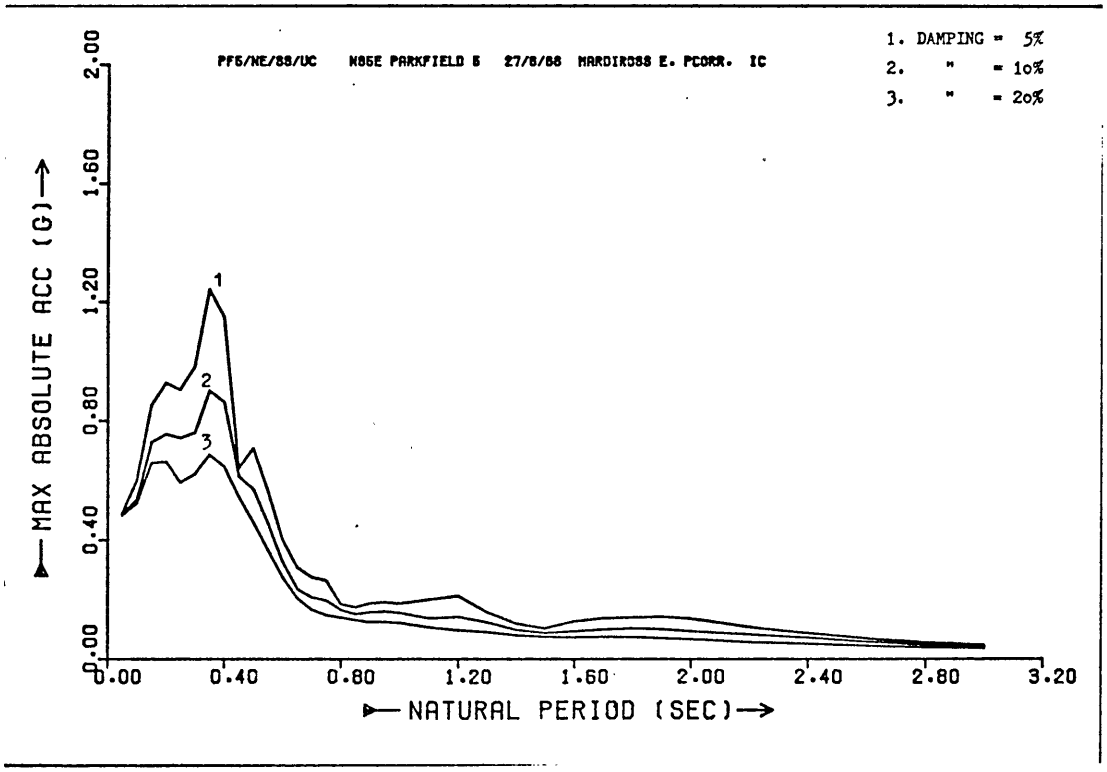


FIG.3.4d COMPUTED SUBSURFACE BEDROCK ACCELERATION RESPONSE SPECTRA

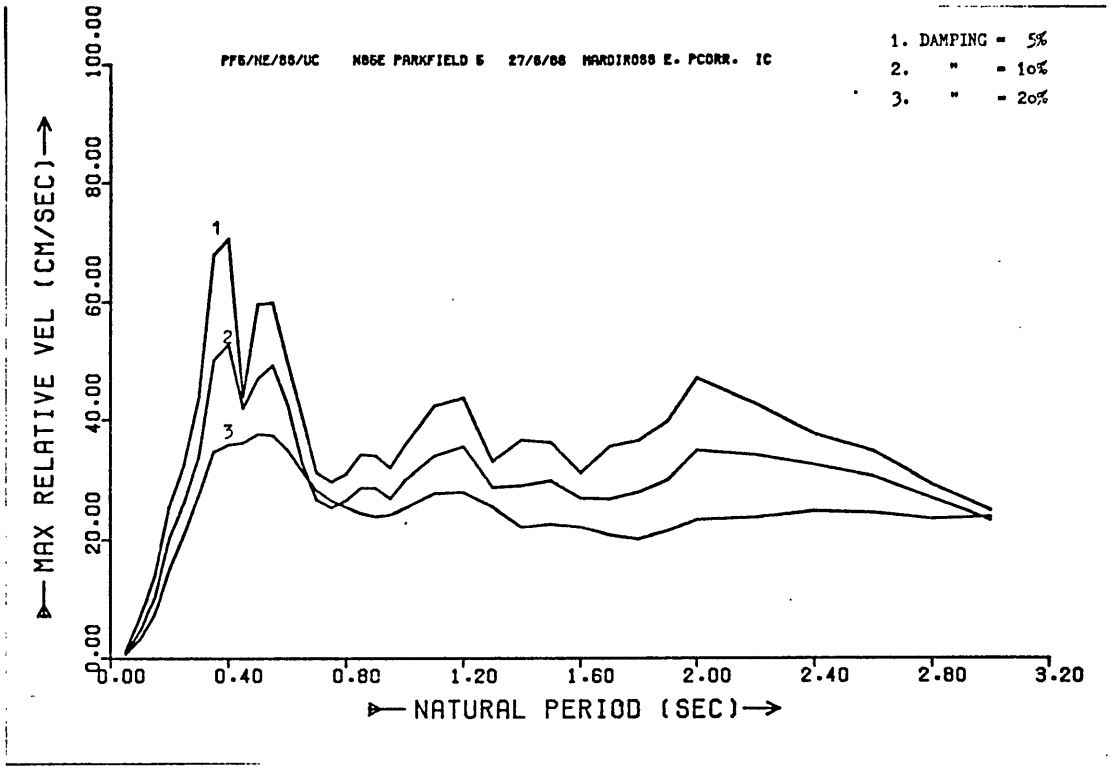


FIG.3.4e COMPUTED SUBSURFACE BEDROCK VELOCITY RESPONSE SPECTRA

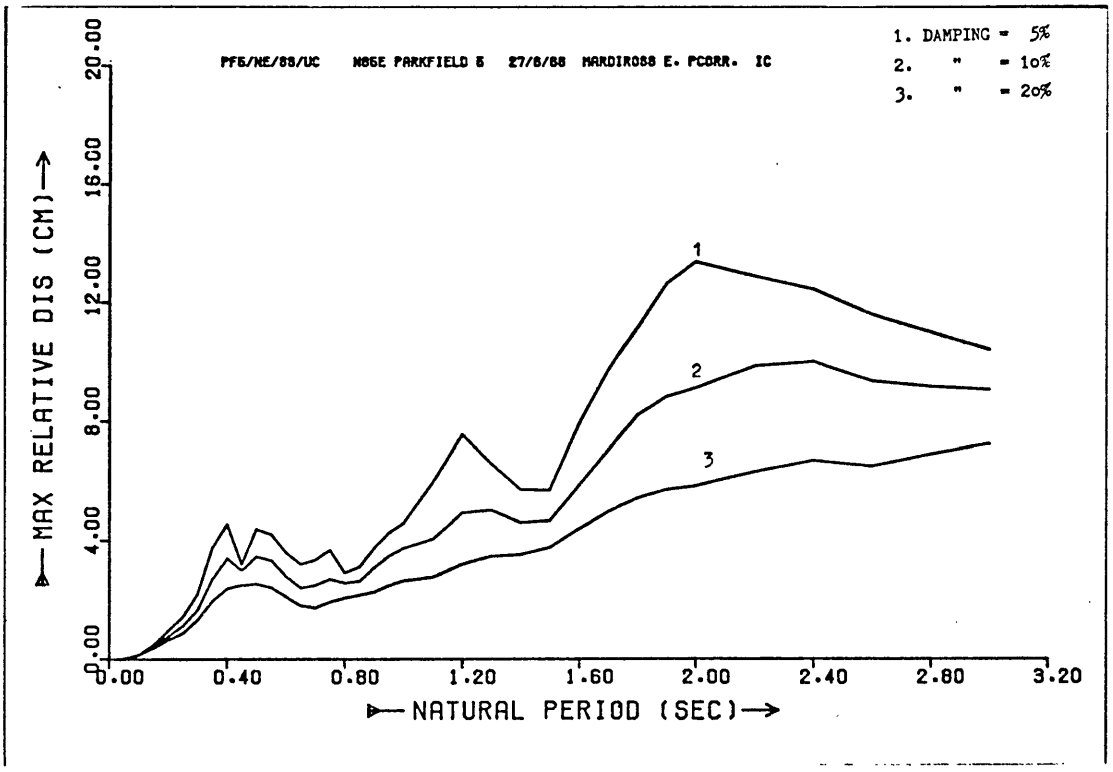


FIG.3.4f COMPUTED SUBSURFACE BEDROCK DISPLACEMENT RESPONSE SPECTRA

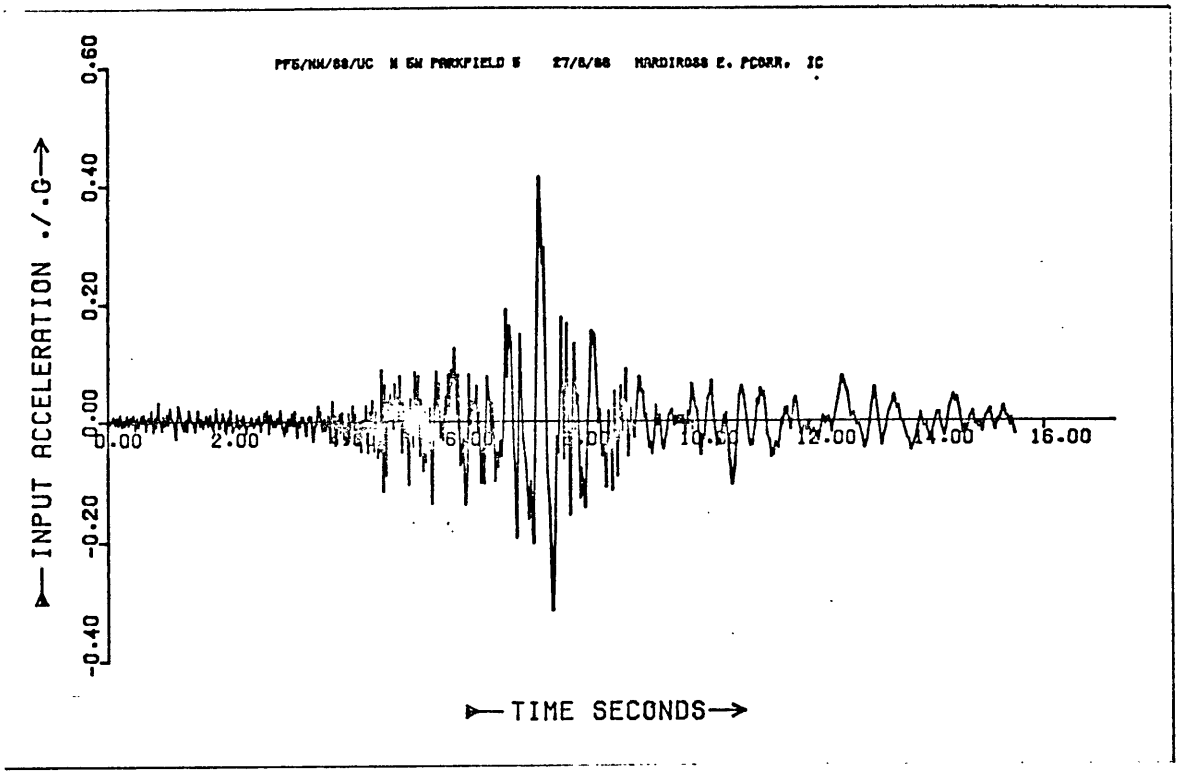


FIG. 3.5a SUBSURFACE BEDROCK MOTION USED AS INPUT MOTION IN CALCULATIONS

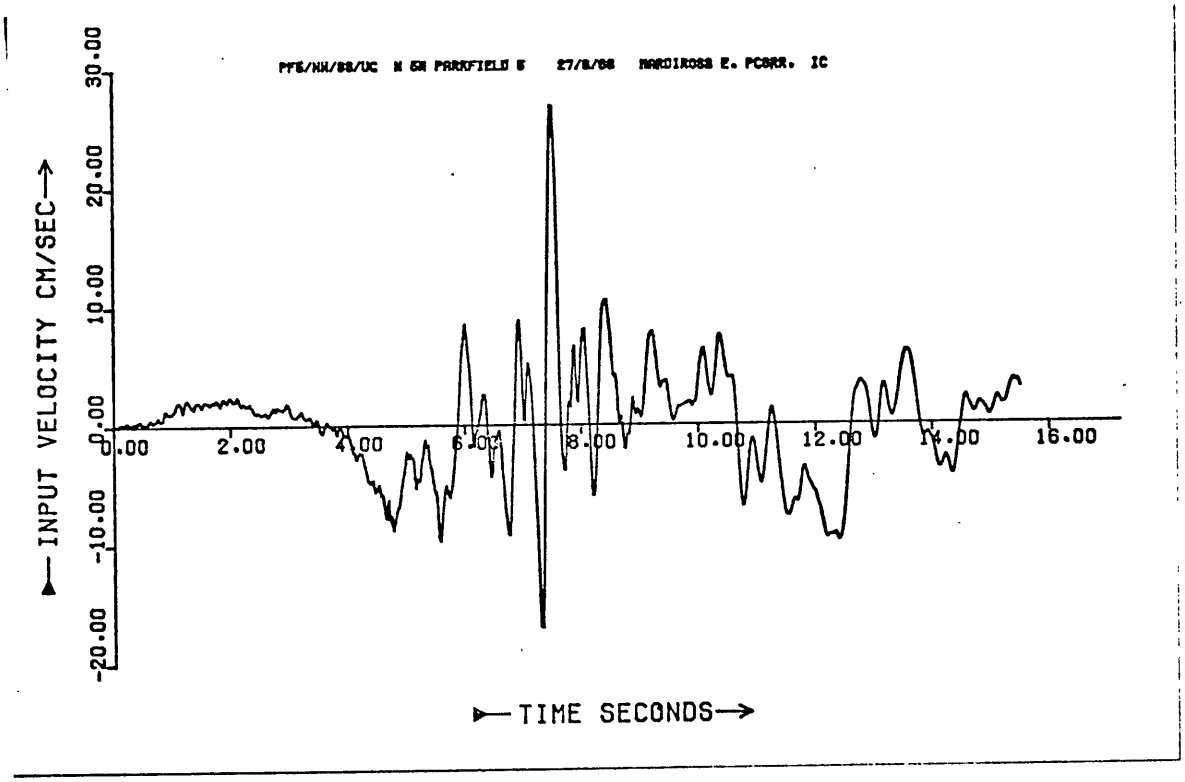


FIG. 3.5b COMPUTED SUBSURFACE BEDROCK VELOCITY TIME HISTORY

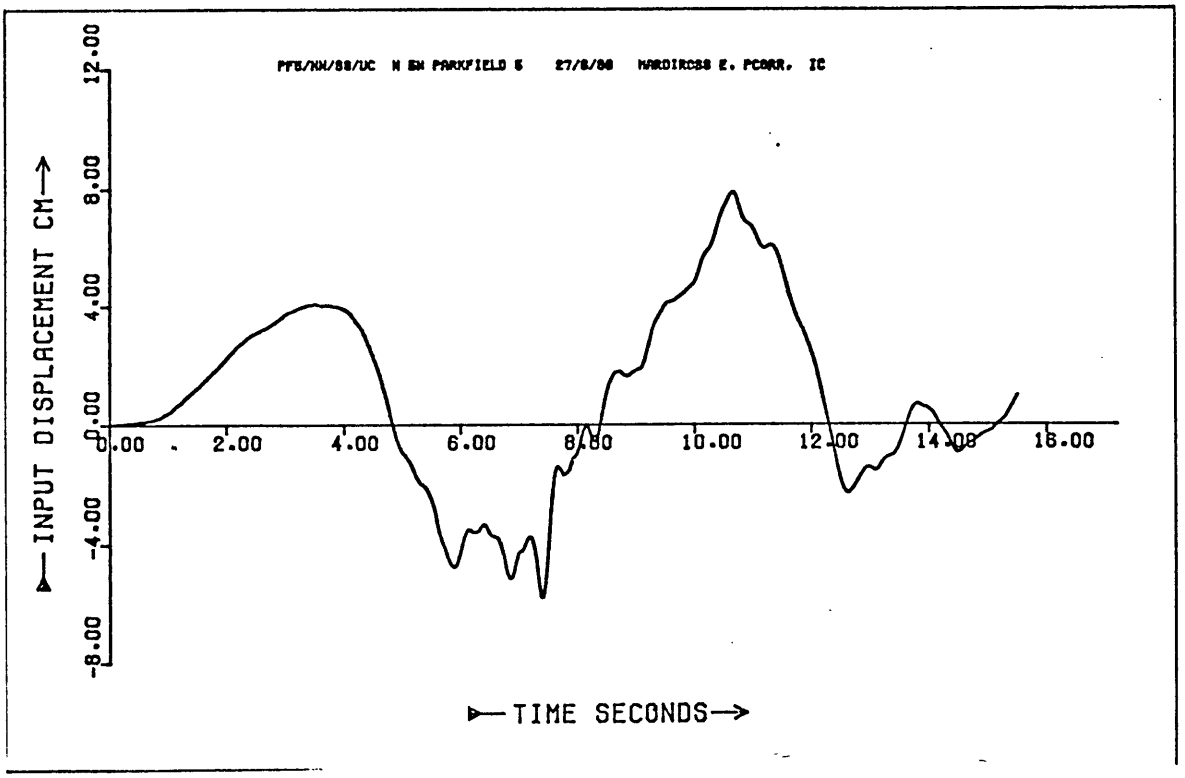


FIG. 3.5c COMPUTED SUBSURFACE BEDROCK DISPLACEMENT TIME HISTORY

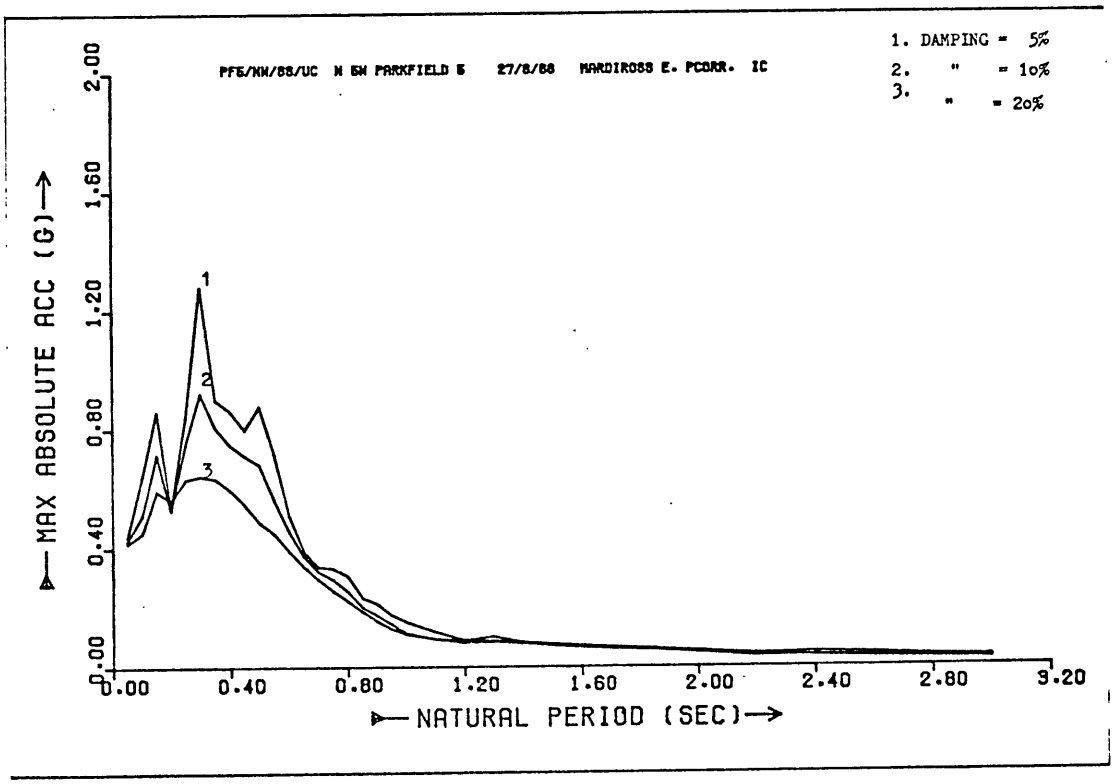


FIG. 3.5d COMPUTED SUBSURFACE BEDROCK ACCELERATION RESPONSE SPECTRA

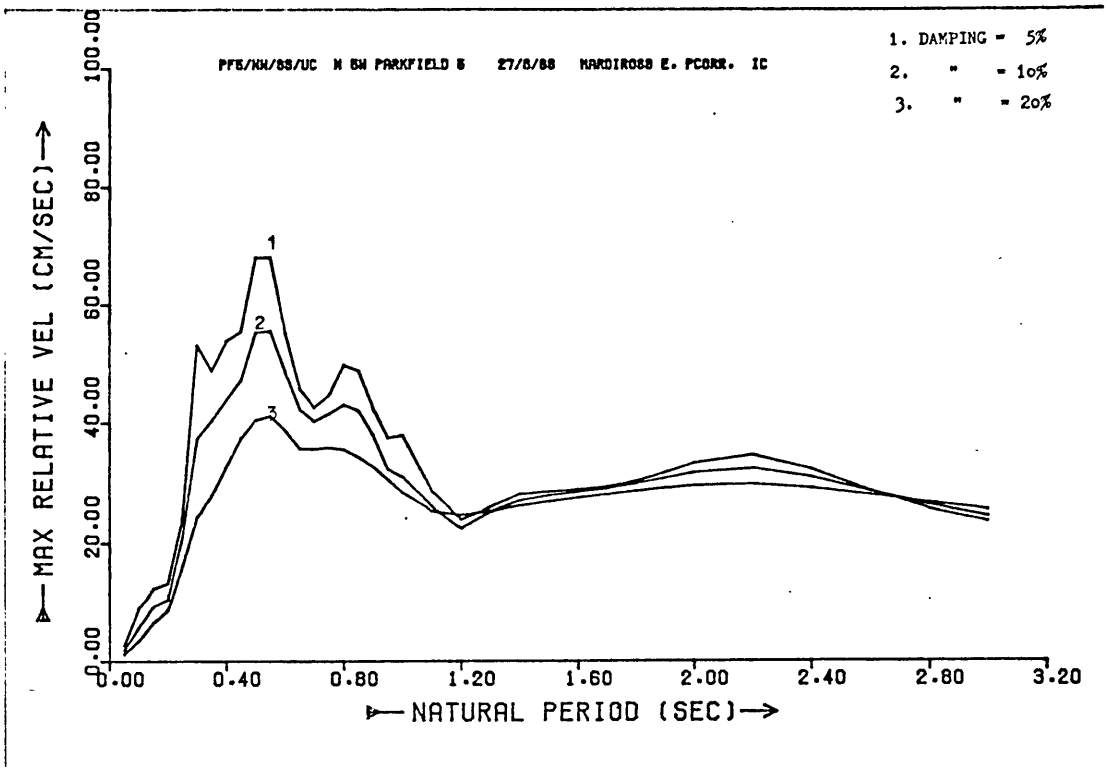


FIG. 3.5e COMPUTED SUBSURFACE BEDROCK VELOCITY RESPONSE SPECTRA

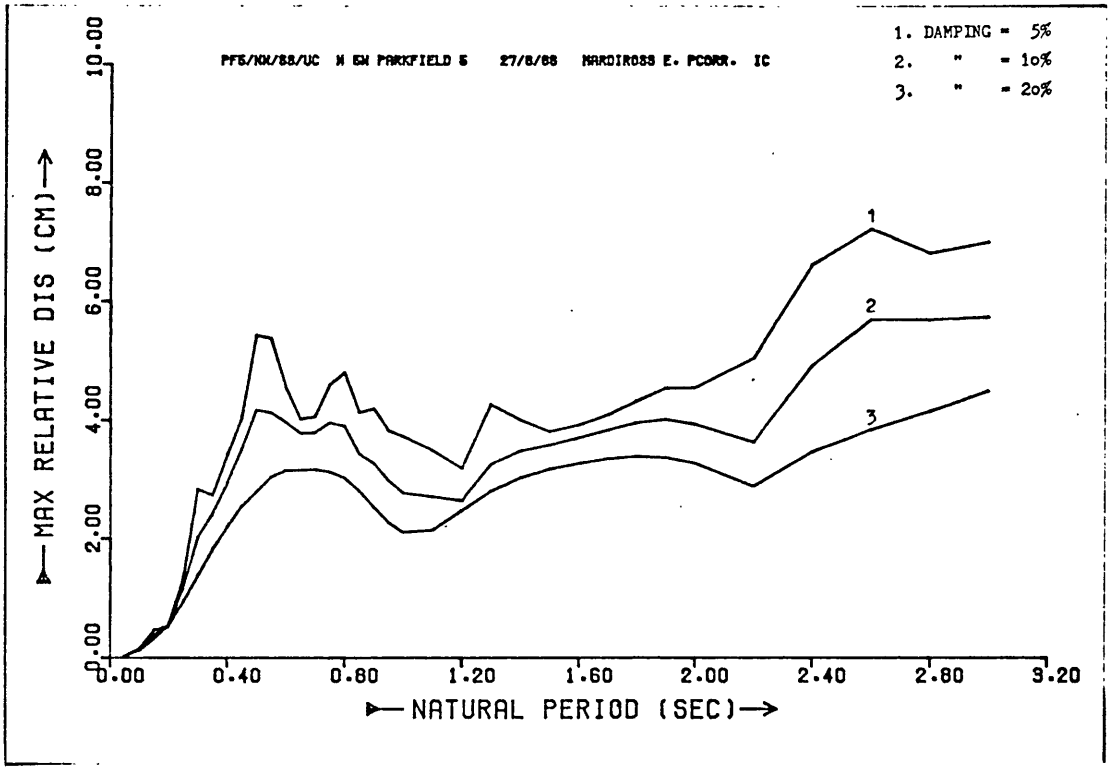


FIG. 3.5f COMPUTED SUBSURFACE BEDROCK DISPLACEMENT RESPONSE SPECTRA

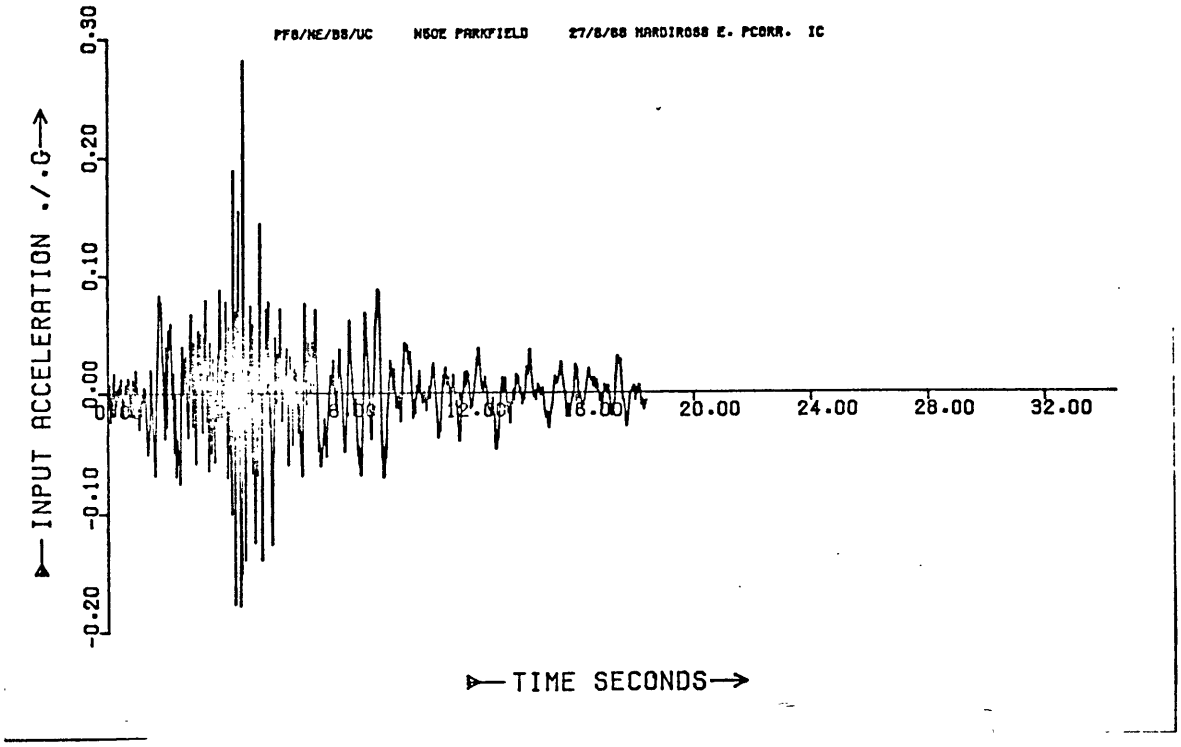


FIG 3.6a SUBSURFACE BEDROCK MOTION USED AS INPUT MOTION IN CALCULATIONS

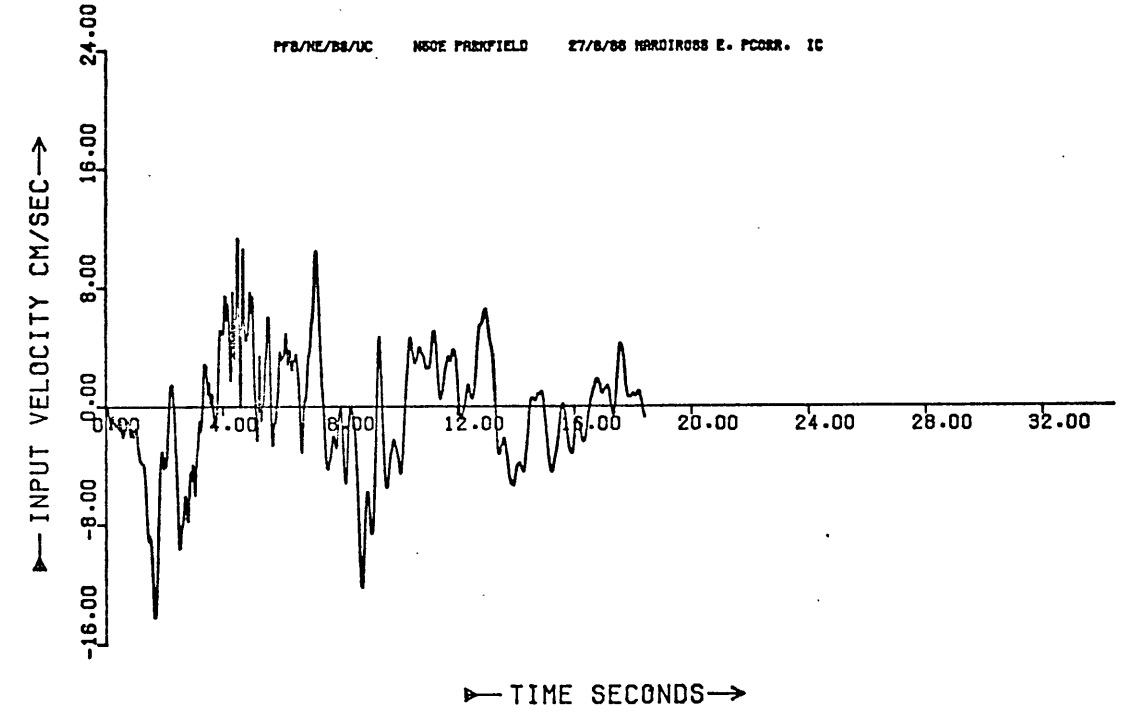


FIG.3.6b COMPUTED SUBSURFACE BEDROCK VELOCITY TIME HISTORY

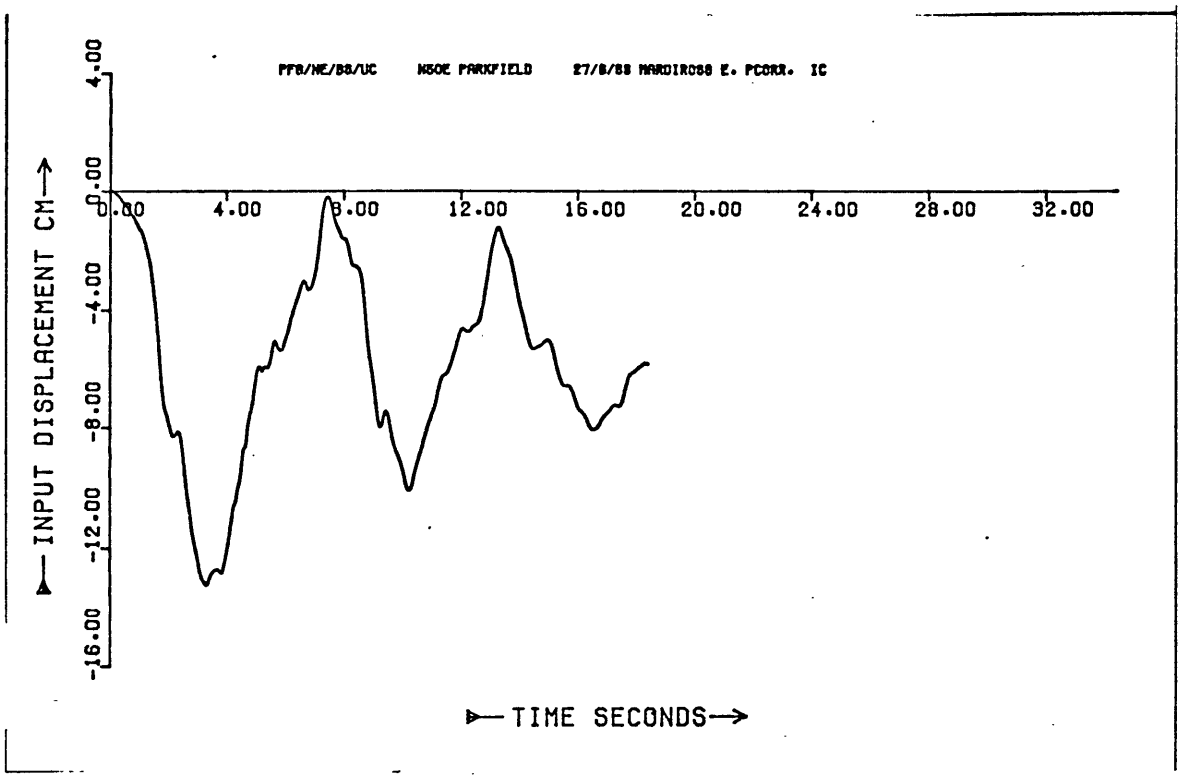


FIG.3.6c COMPUTED SUBSURFACE BEDROCK DISPLACEMENT TIME HISTORY

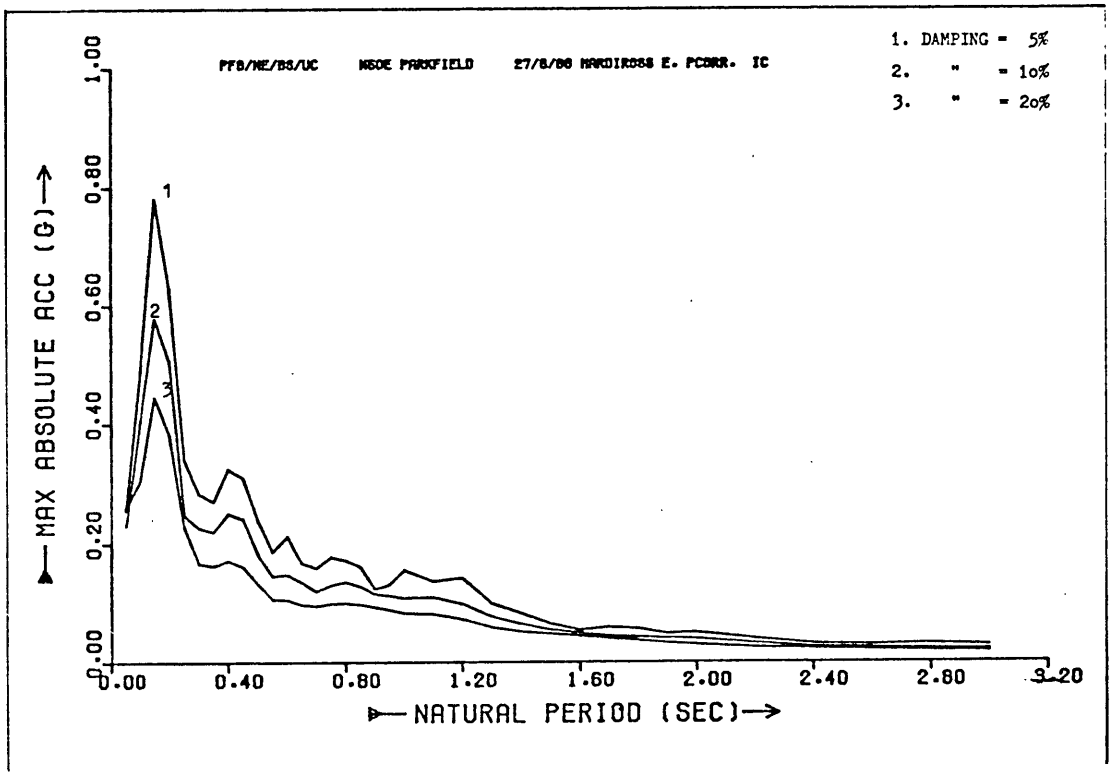


FIG.3.6d COMPUTED SUBSURFACE BEDROCK ACCELERATION RESPONSE SPECTRA

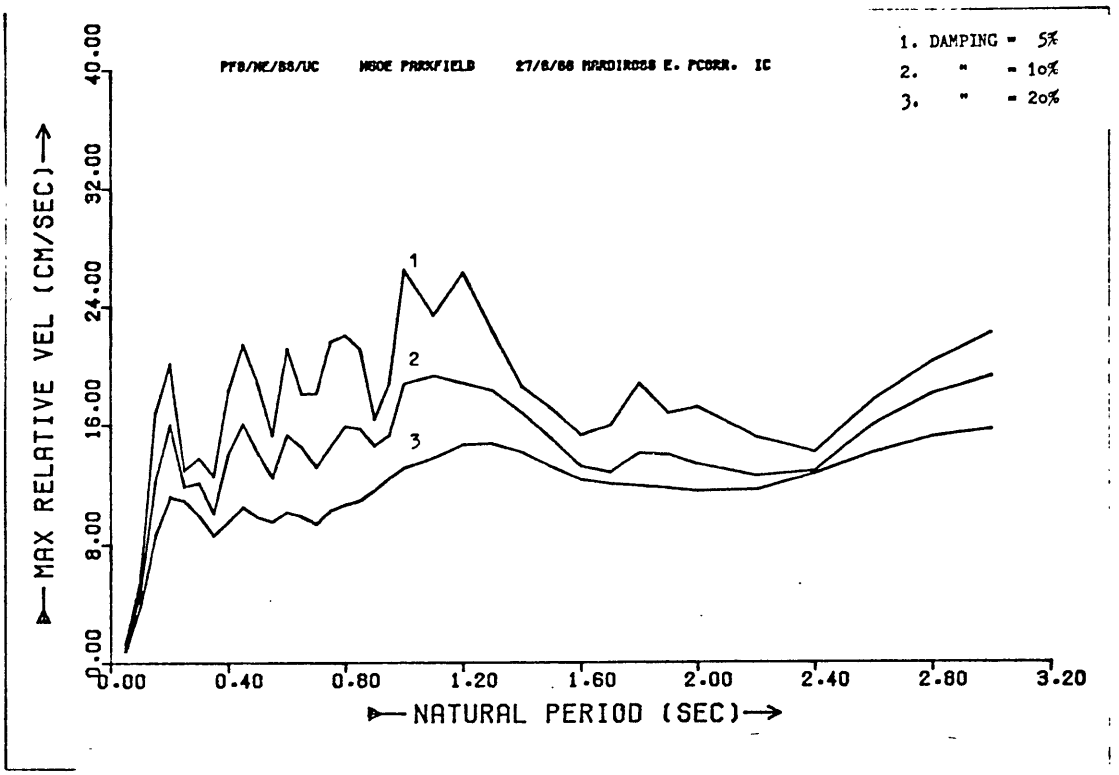


FIG.3.6e COMPUTED SUBSURFACE BEDROCK VELOCITY RESPONSE SPECTRA

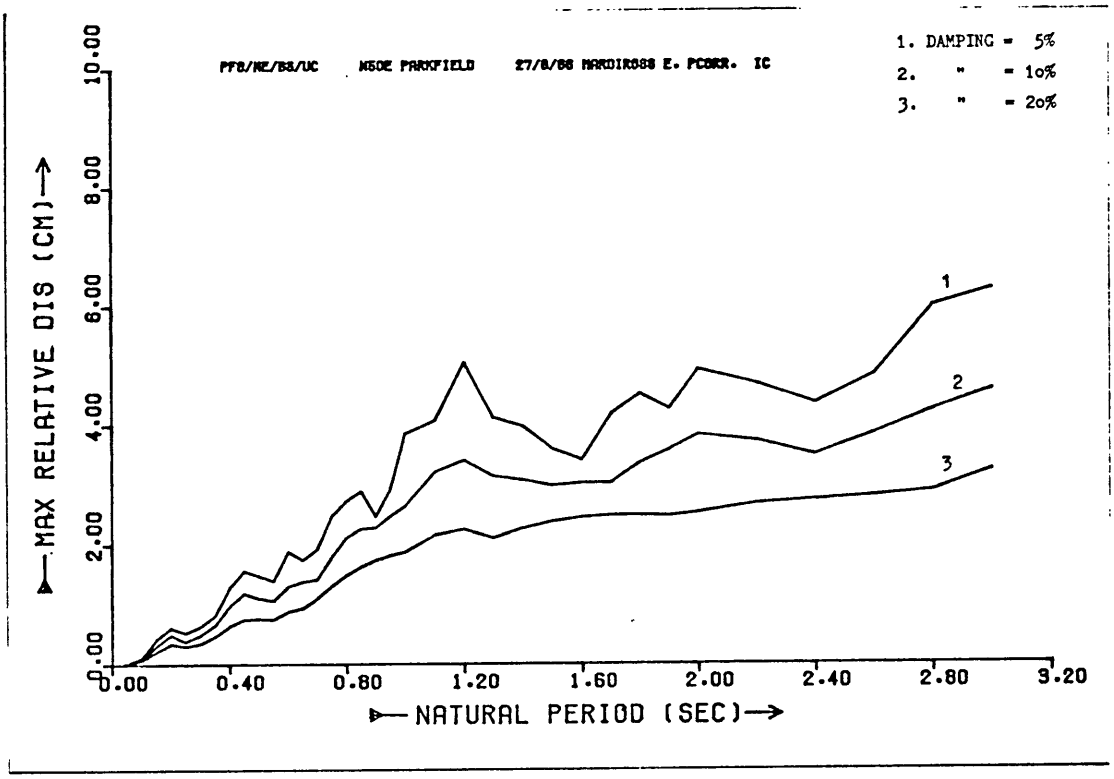


FIG 3.6f COMPUTED SUBSURFACE BEDROCK DISPLACEMENT RESPONSE SPECTRA

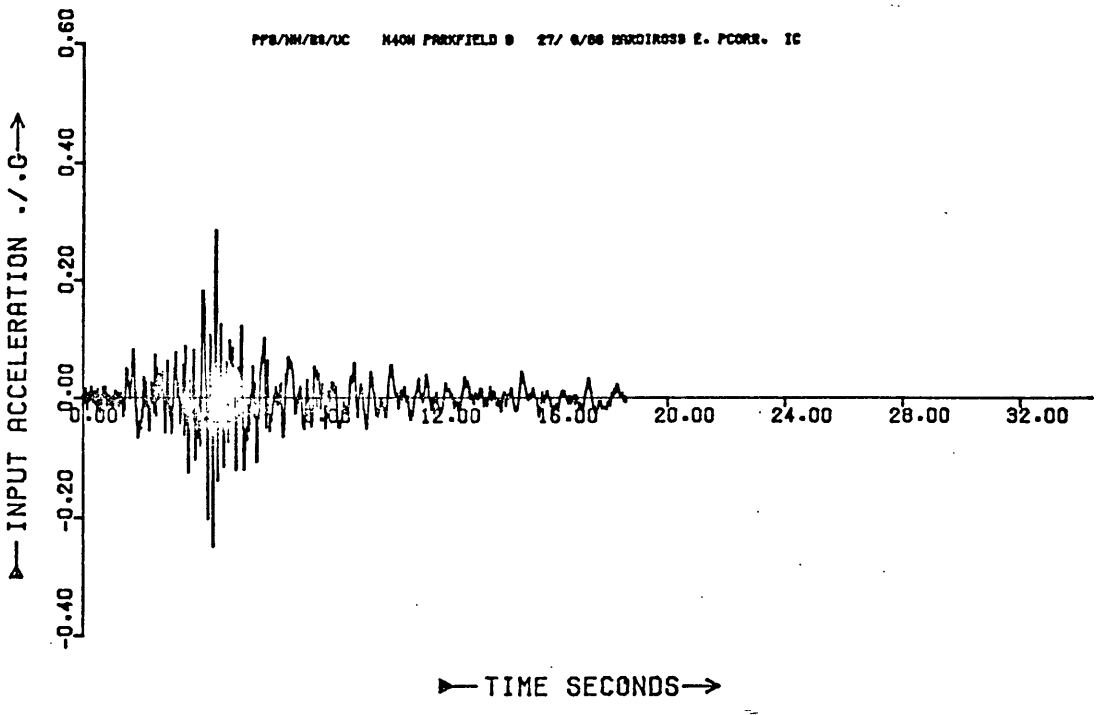


FIG3.7a SUBSURFACE BEDROCK MOTION USED AS INPUT MOTION IN CALCULATIONS

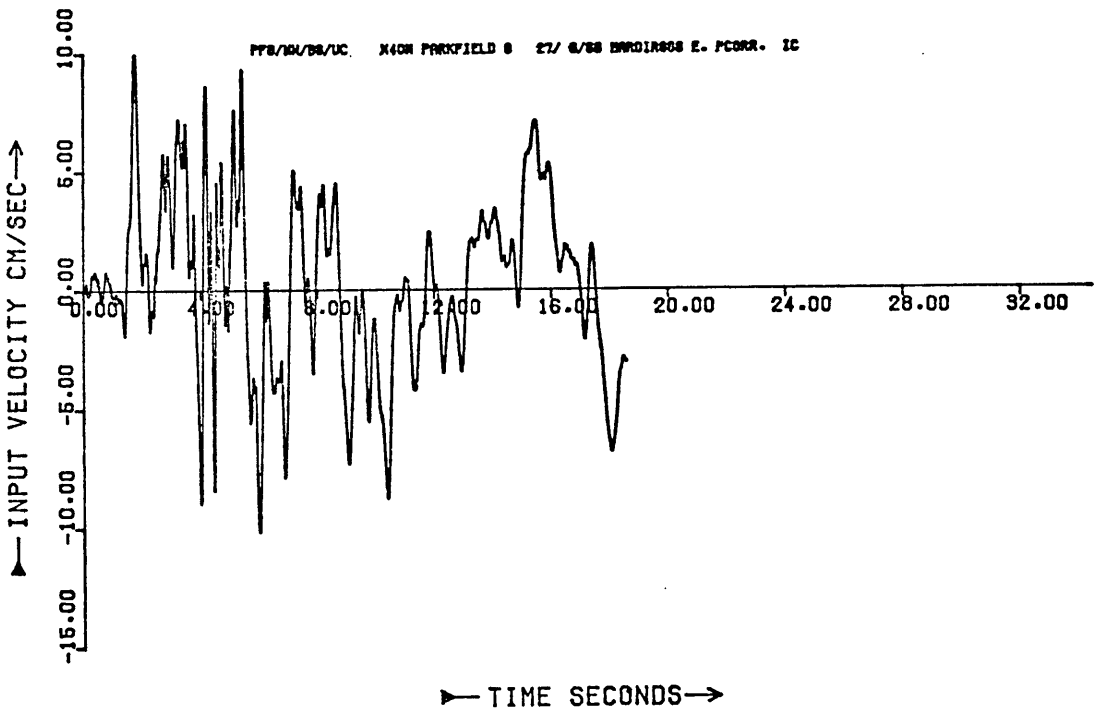


FIG. 3.7b COMPUTED SUBSURFACE BEDROCK VELOCITY TIME HISTORY

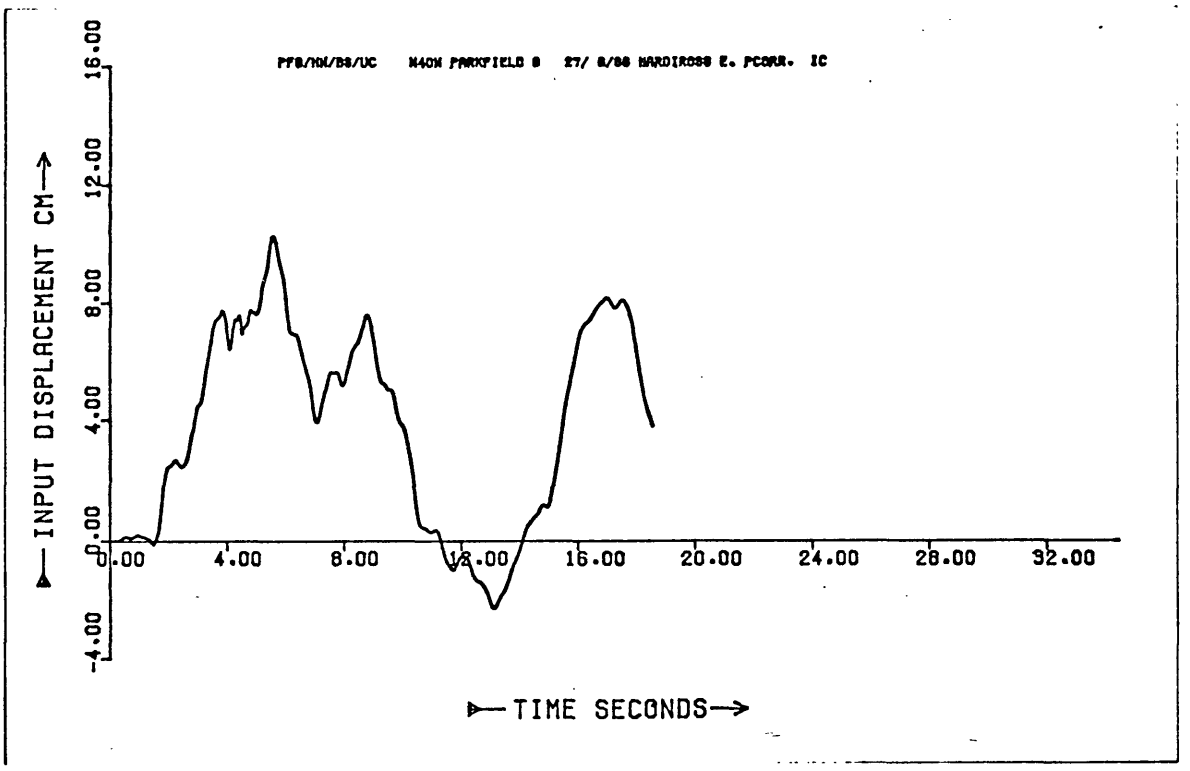


FIG. 3.7c COMPUTED SUBSURFACE BEDROCK DISPLACEMENT TIME HISTORY

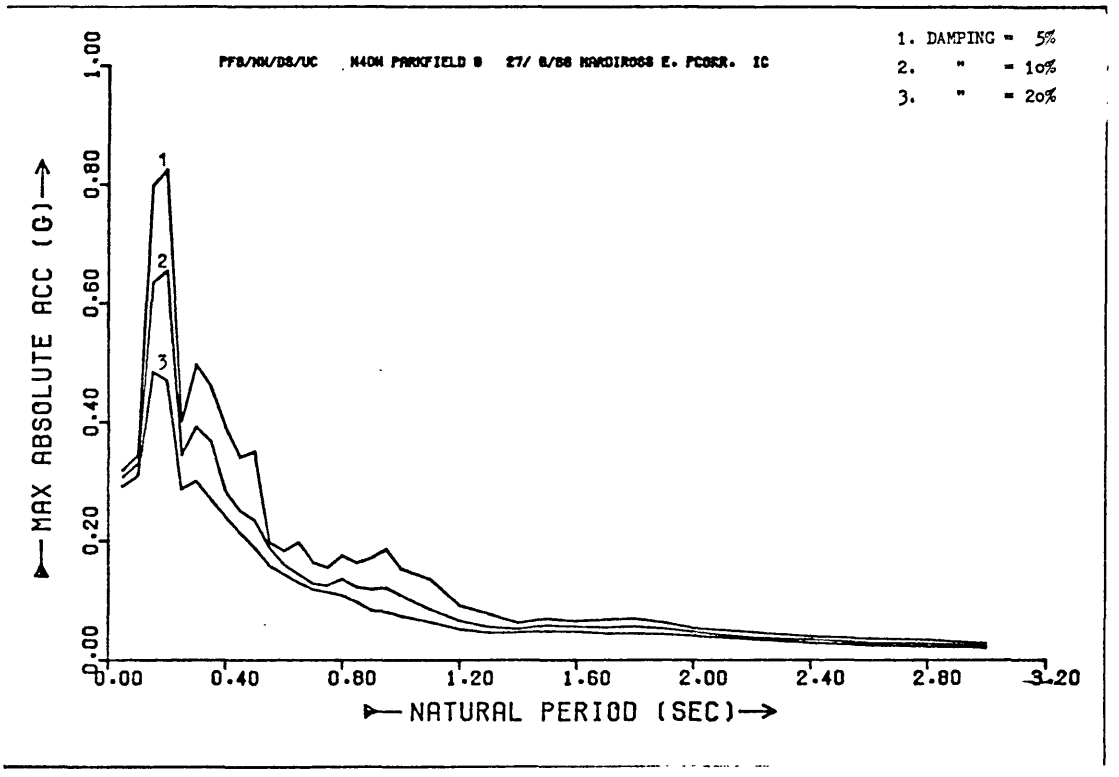


FIG. 3.7d COMPUTED SUBSURFACE BEDROCK ACCELERATION RESPONSE SPECTRA

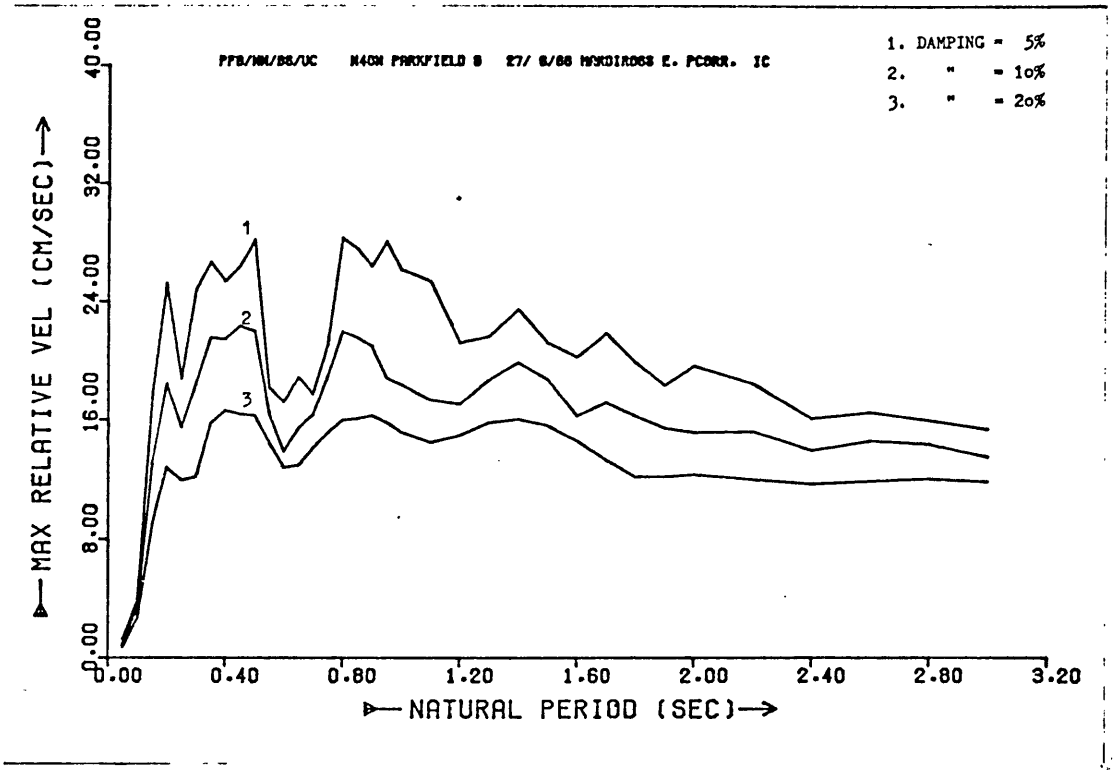


FIG. 3.7e COMPUTED SUBSURFACE BEDROCK VELOCITY RESPONSE SPECTRA

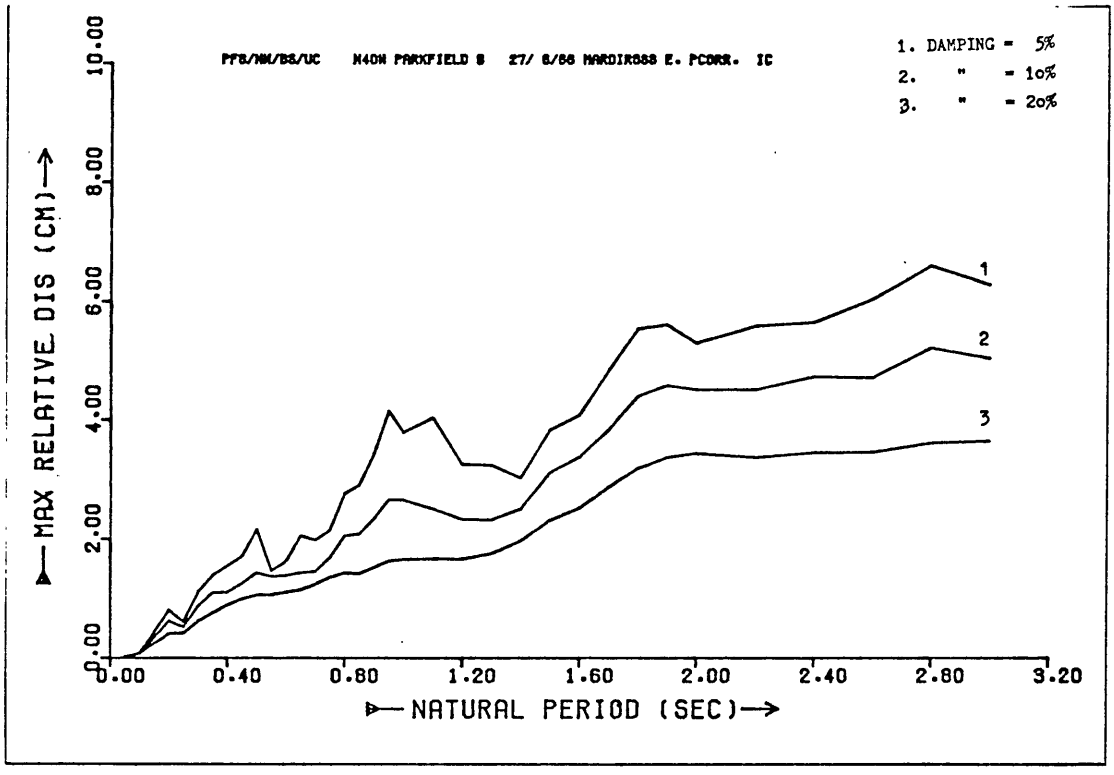


FIG. 3.7f COMPUTED SUBSURFACE BEDROCK DISPLACEMENT RESPONSE SPECTRA

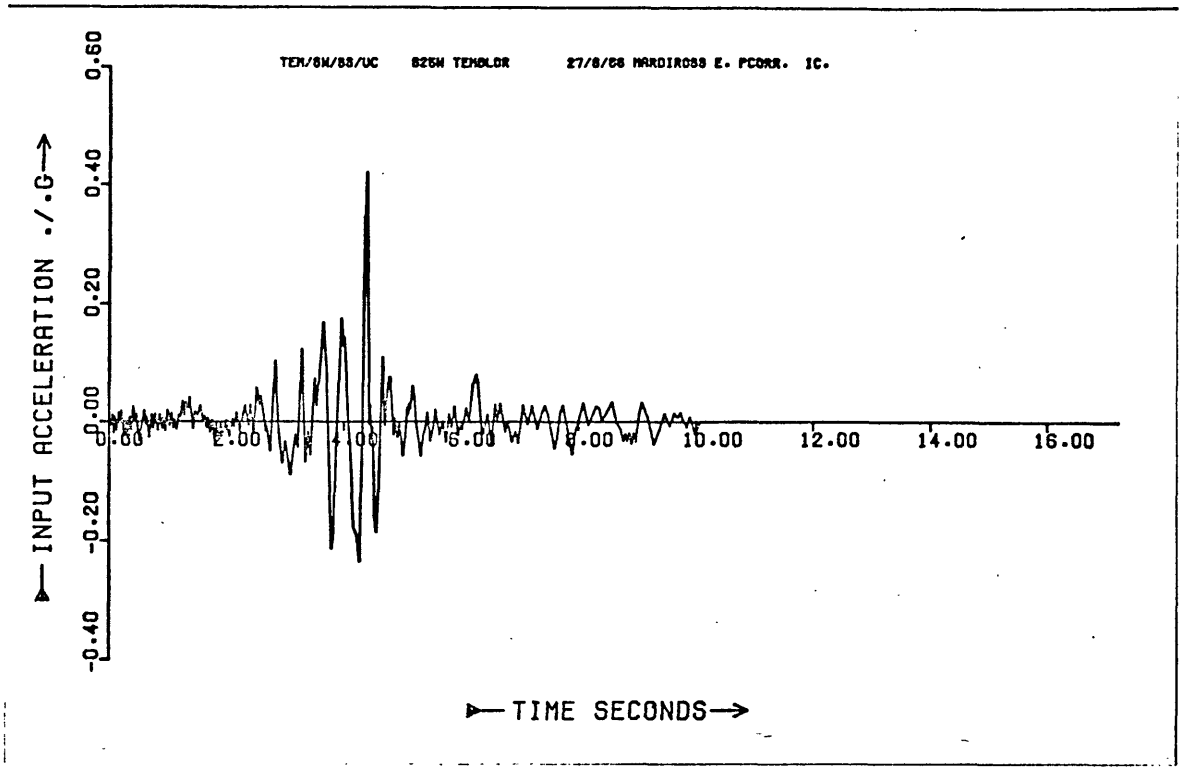


FIG.3.8a SUBSURFACE BEDROCK MOTION USED AS INPUT MOTION IN CALCULATIONS

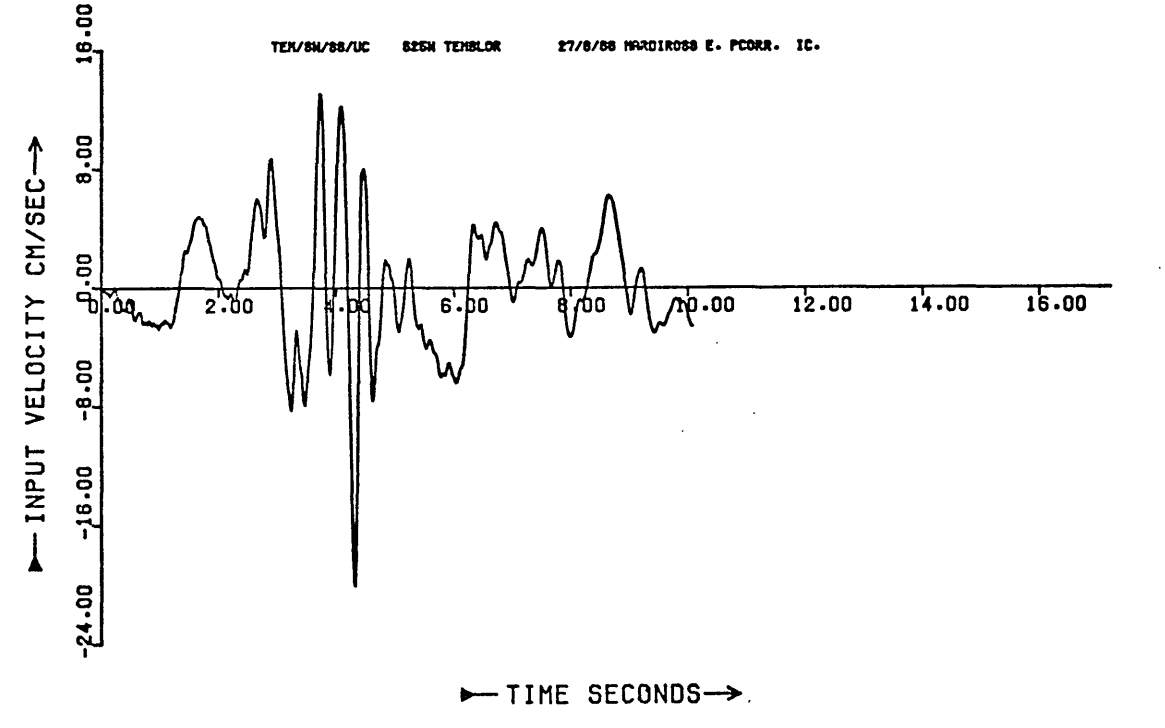


FIG.3.8b COMPUTED SUBSURFACE BEDROCK VELOCITY TIME HISTORY

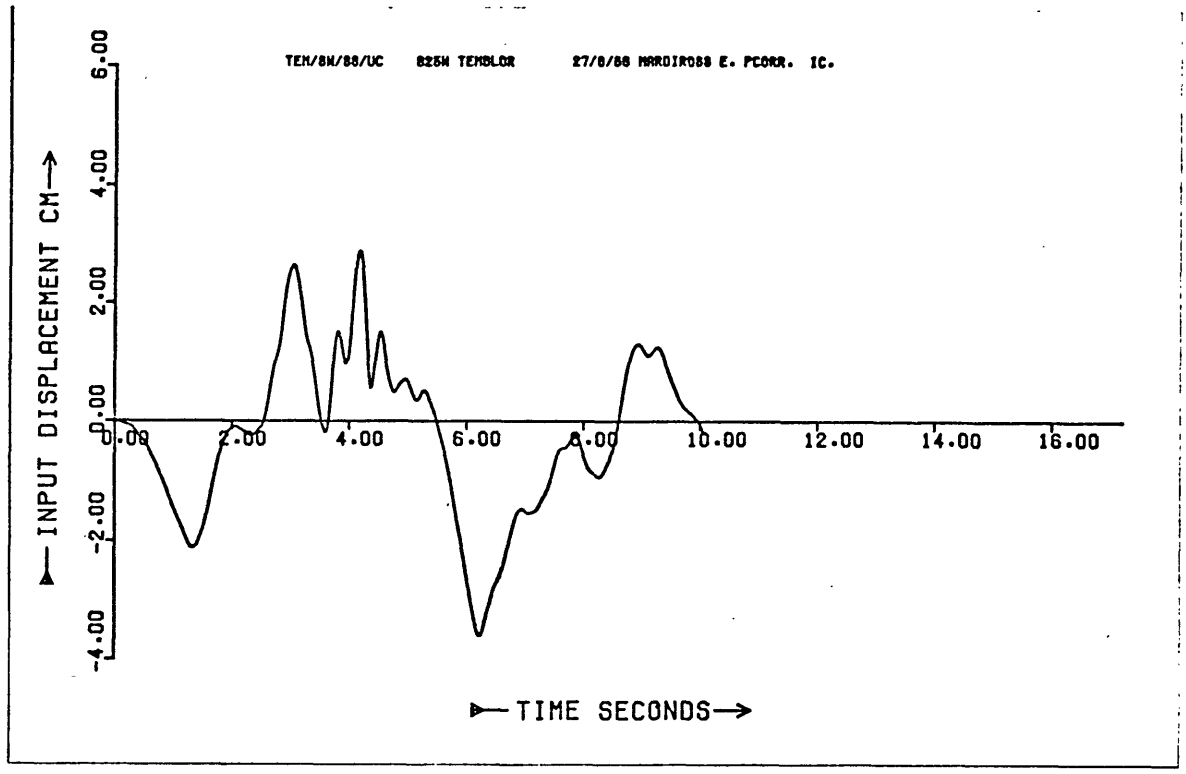


FIG.3.8c COMPUTED SUBSURFACE BEDROCK DISPLACEMENT TIME HISTORY

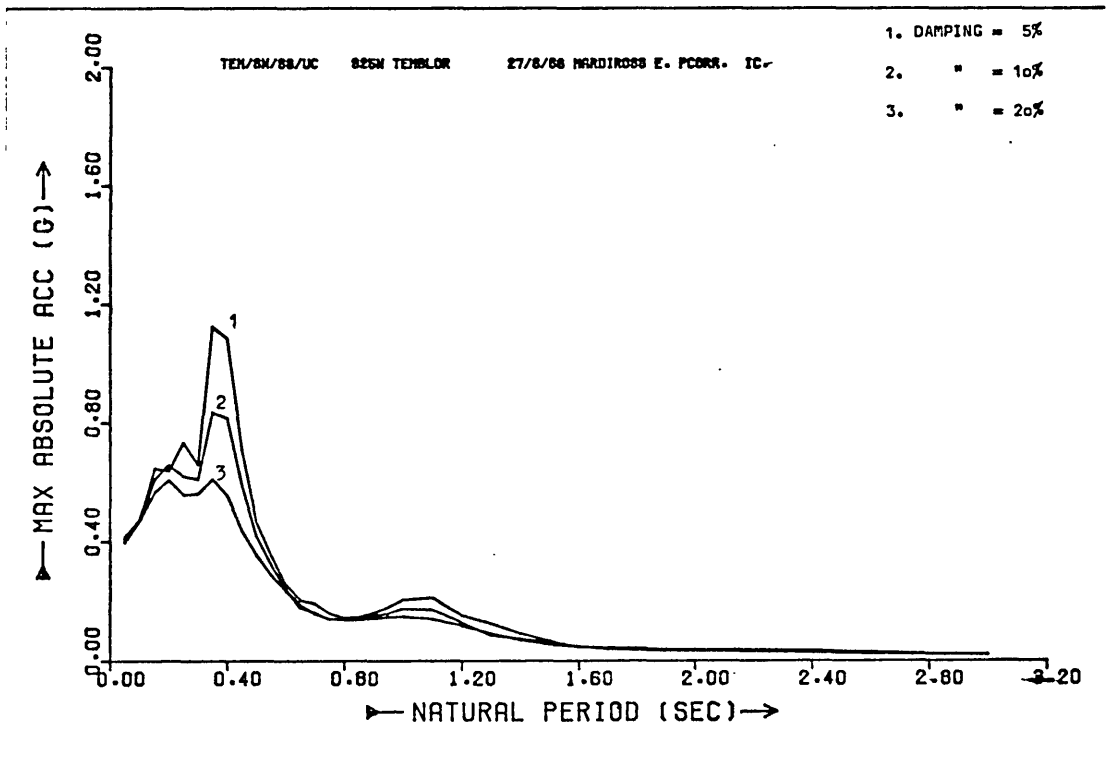


FIG.3.8d COMPUTED SUBSURFACE BEDROCK ACCELERATION RESPONSE SPECTRA

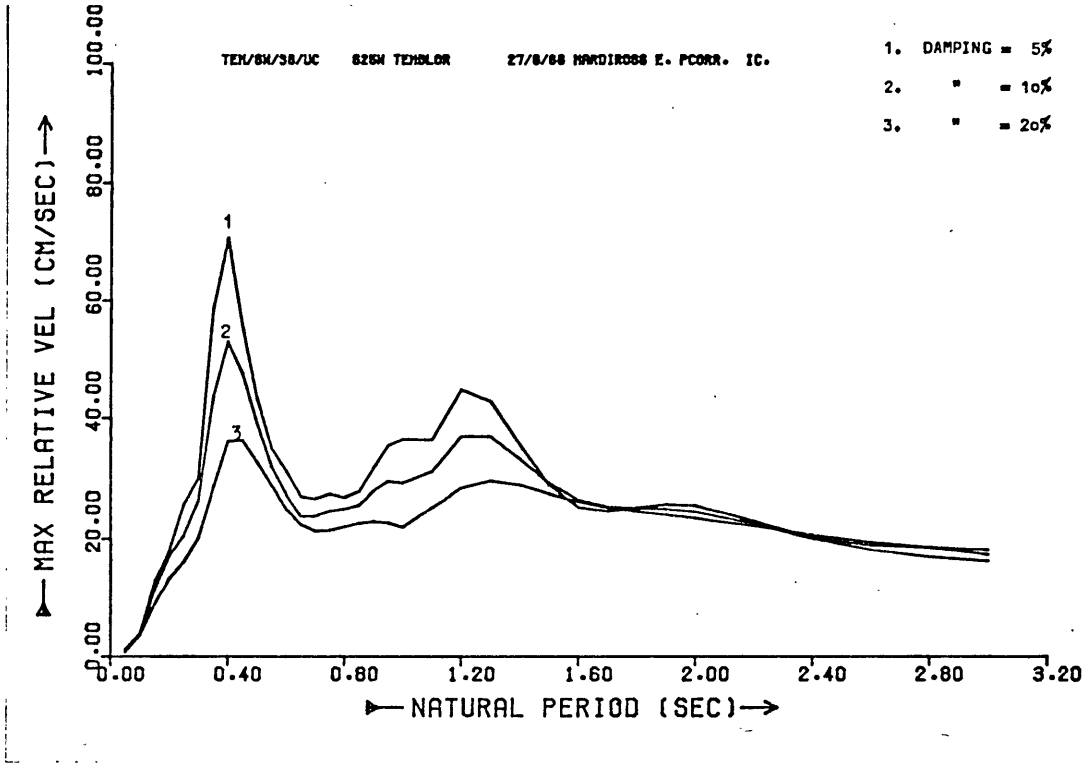


FIG. 3.8e COMPUTED SUBSURFACE BEDROCK VELOCITY RESPONSE SPECTRA

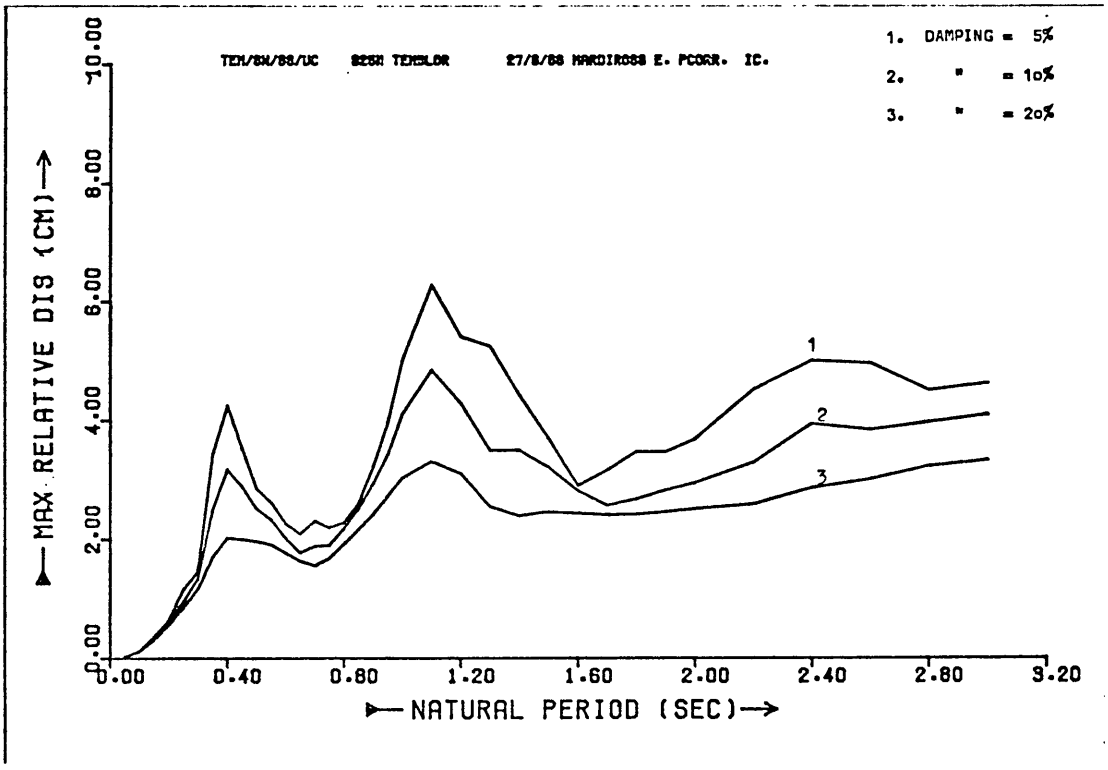


FIG.3.8f COMPUTED SUBSURFACE BEDROCK DISPLACEMENT RESPONSE SPECTRA.

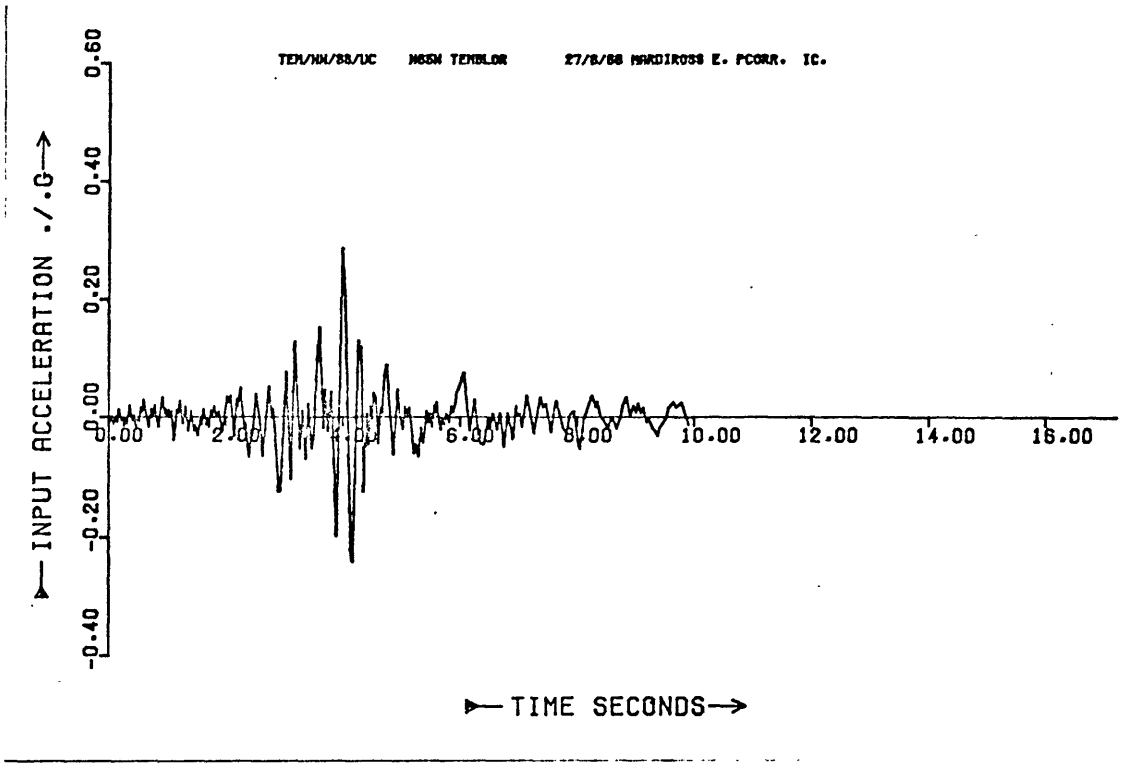


FIG.3.9a SUBSURFACE BEDROCK MOTION USED AS INPUT MOTION IN CALCULATIONS

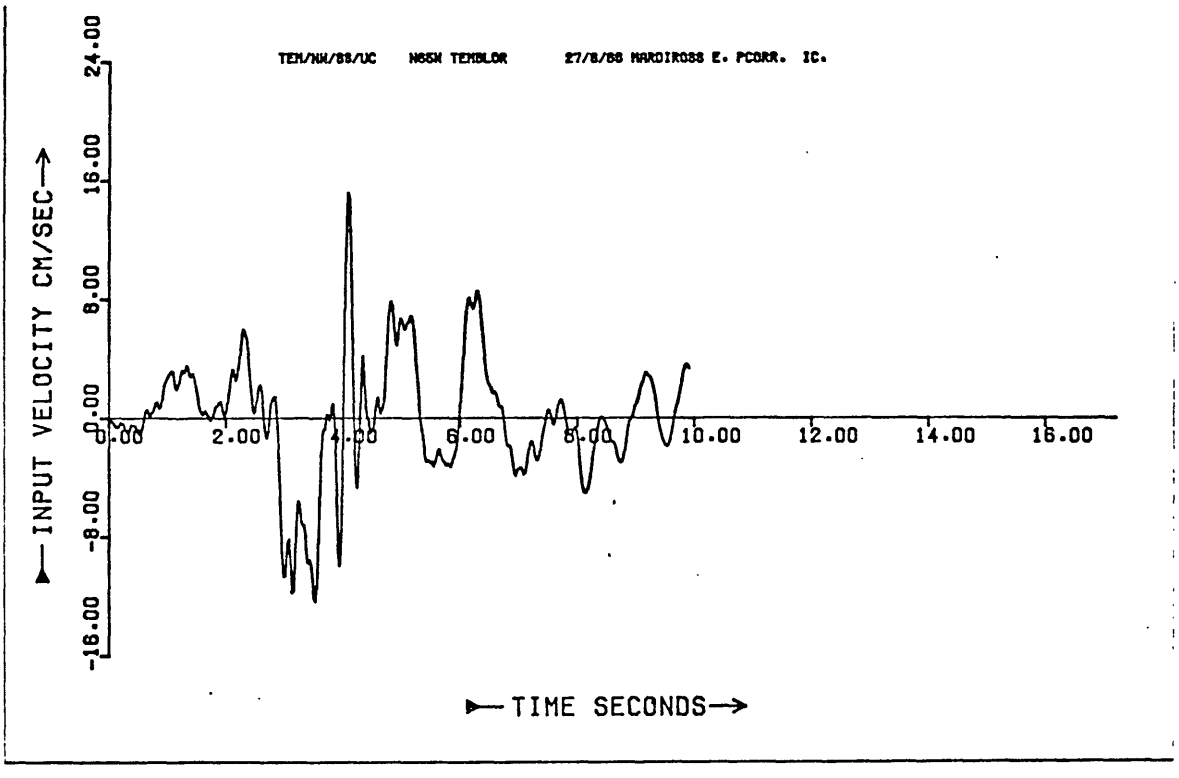


FIG. 3.9b COMPUTED SUBSURFACE BEDROCK VELOCITY TIME HISTORY

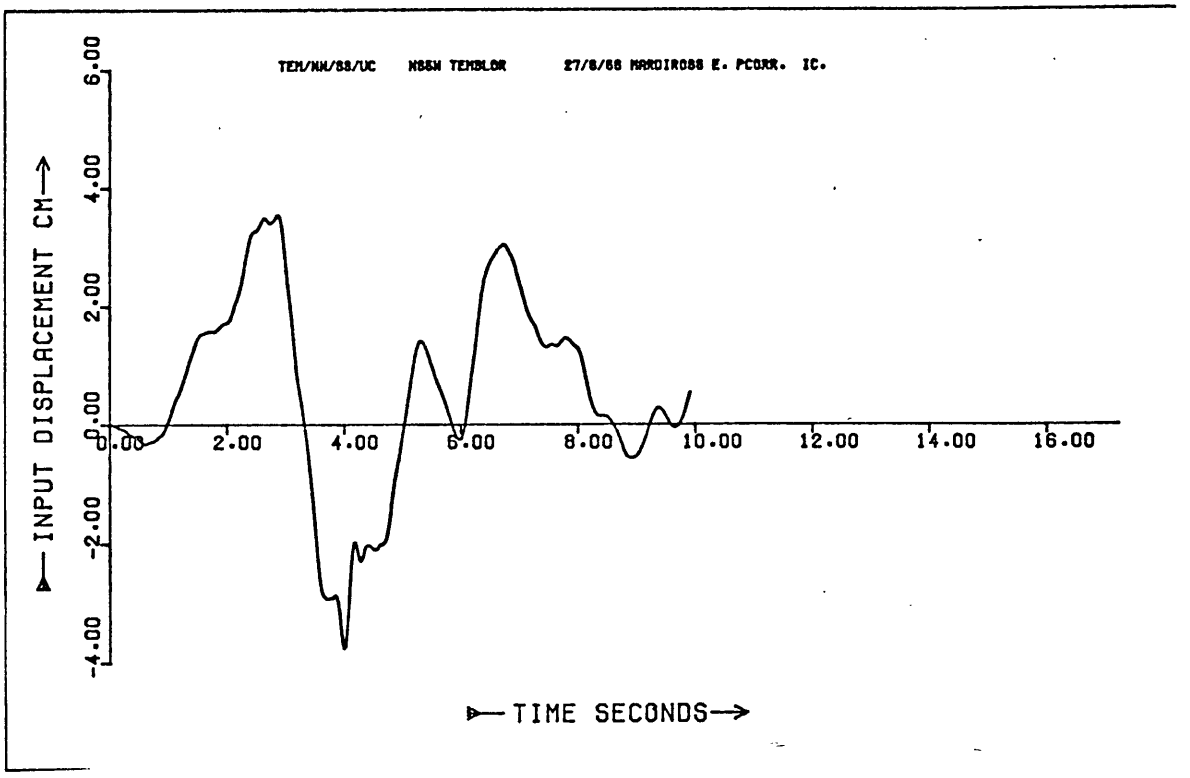


FIG. 3.9c COMPUTED SUBSURFACE BEDROCK DISPLACEMENT TIME HISTORY

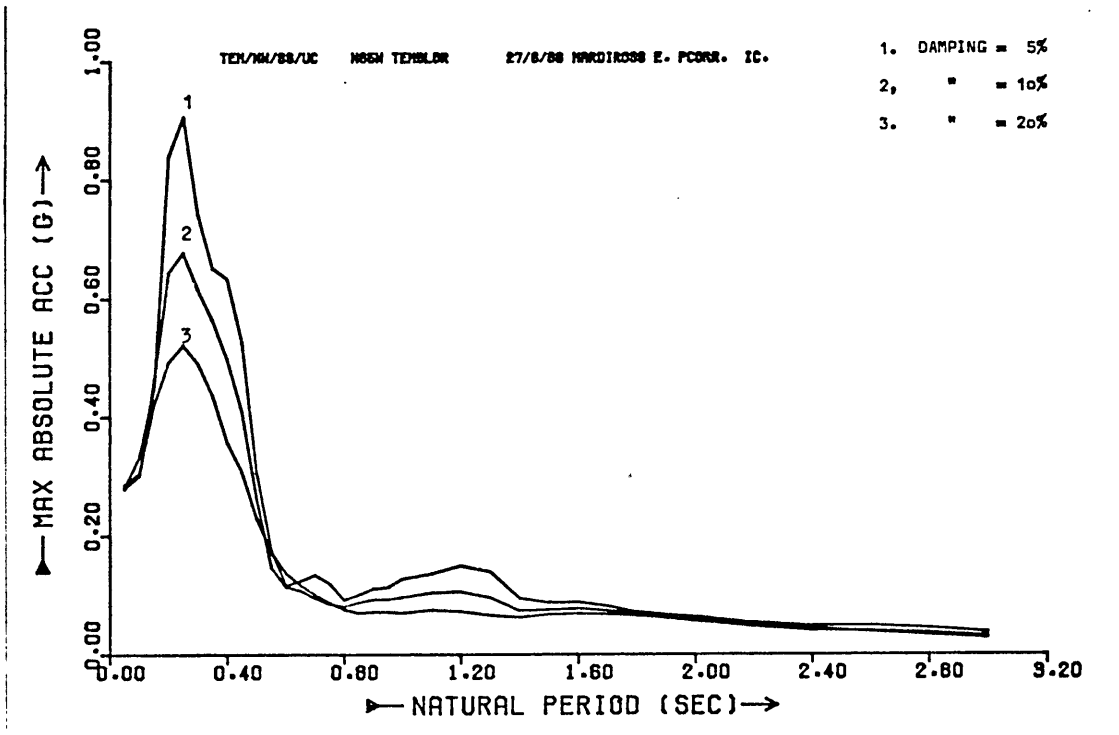


FIG. 3.9d COMPUTED SUBSURFACE BEDROCK ACCELERATION RESPONSE SPECTRA

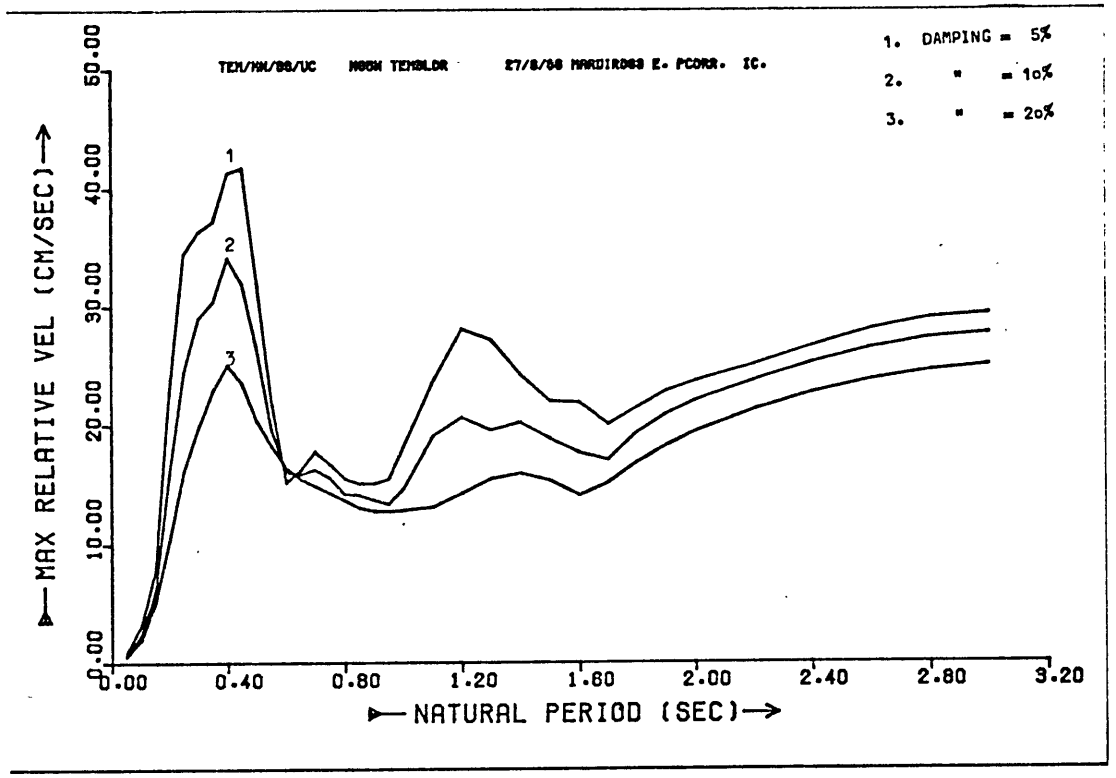


FIG. 3.9e COMPUTED SUBSURFACE BEDROCK VELOCITY RESPONSE SPECTRA

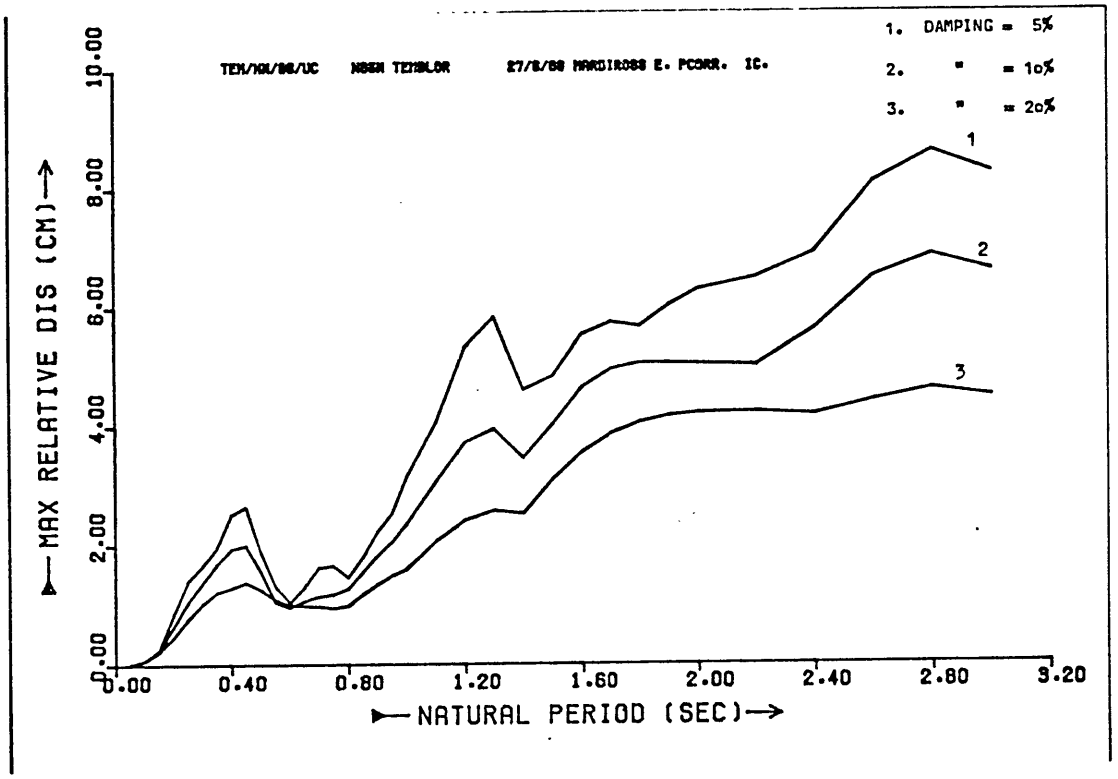


FIG. 3.9f COMPUTED SUBSURFACE BEDROCK DISPLACEMENT RESPONSE SPECTRA.

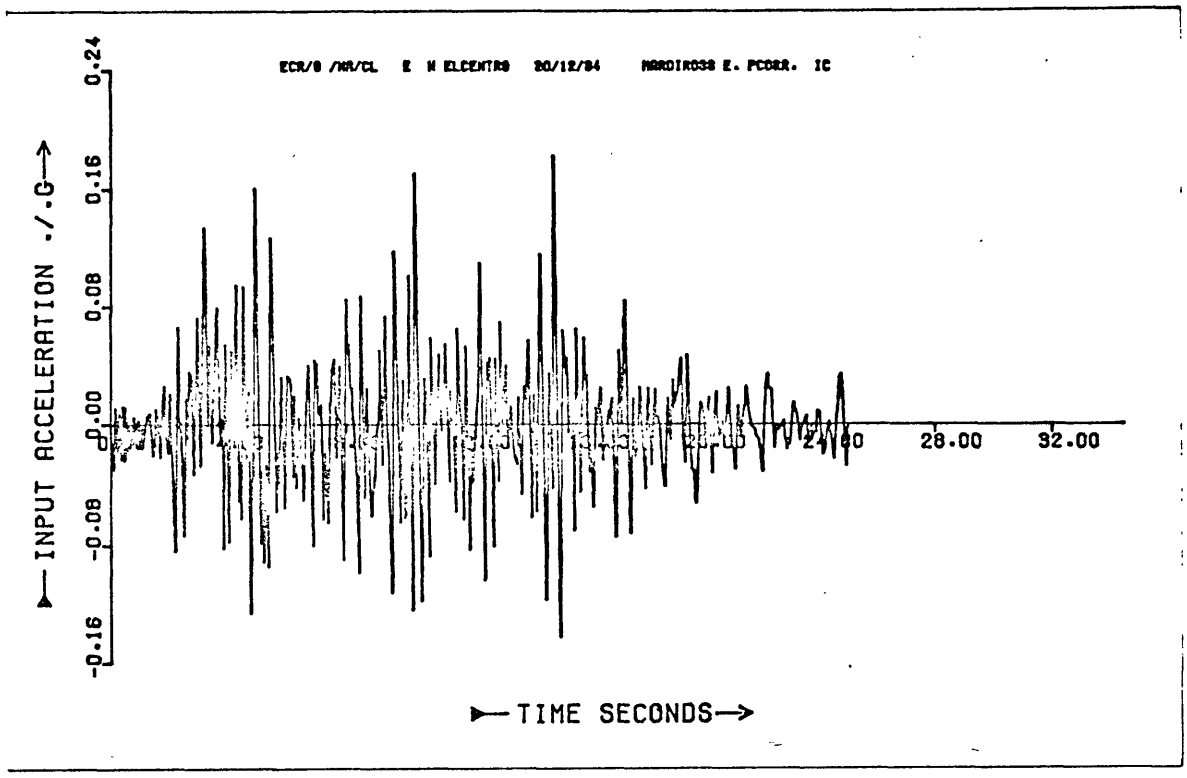


FIG 3.10a SUBSURFACE BEDROCK MOTION USED AS INPUT MOTION IN CALCULATIONS

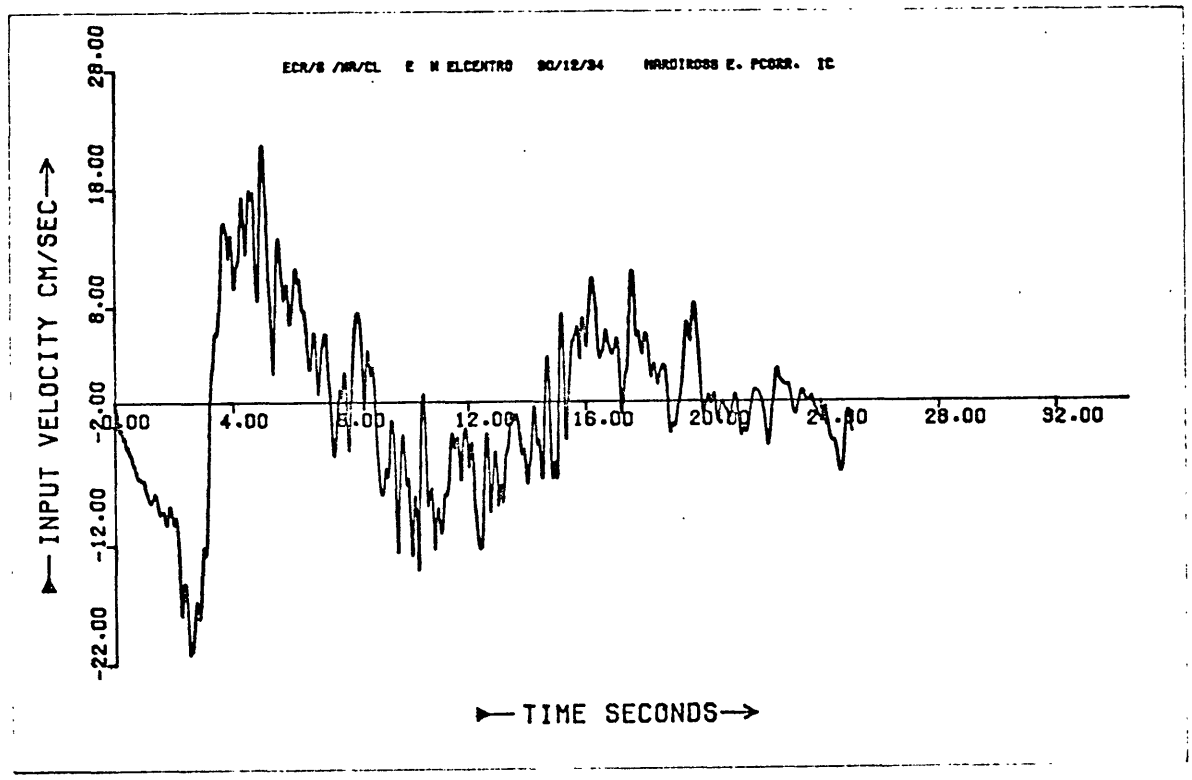


FIG .3.10b COMPUTED SUBSURFACE BEDROCK VELOCITY TIME HISTORY

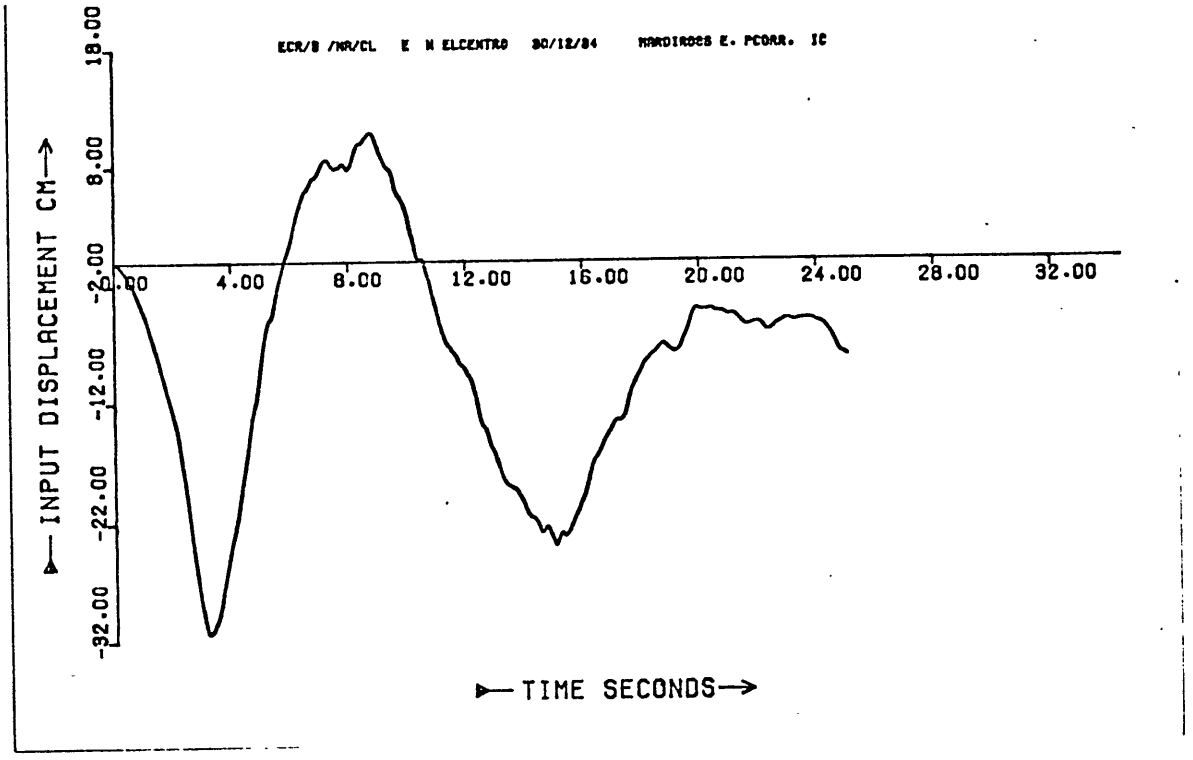


FIG. 3.10c COMPUTED SUBSURFACE BEDROCK DISPLACEMENT TIME HISTORY

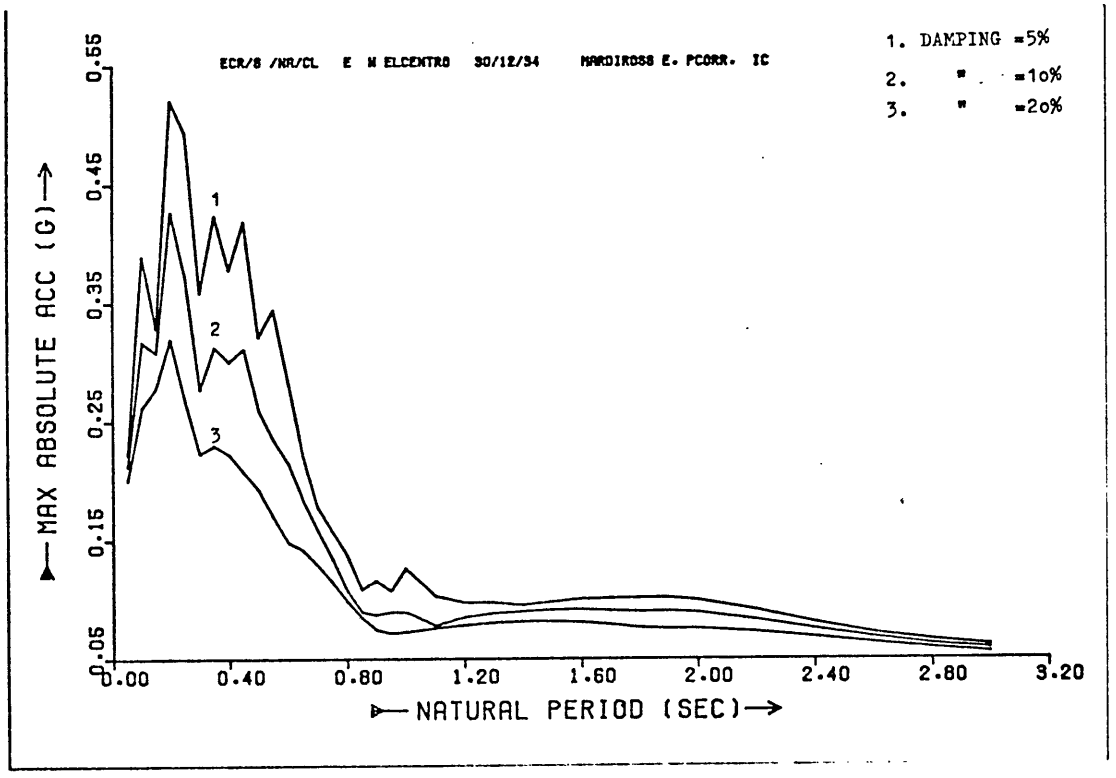


FIG3. 10d COMPUTED SUBSURFACE BEDROCK ACCELERATION RESPONSE SPECTRA

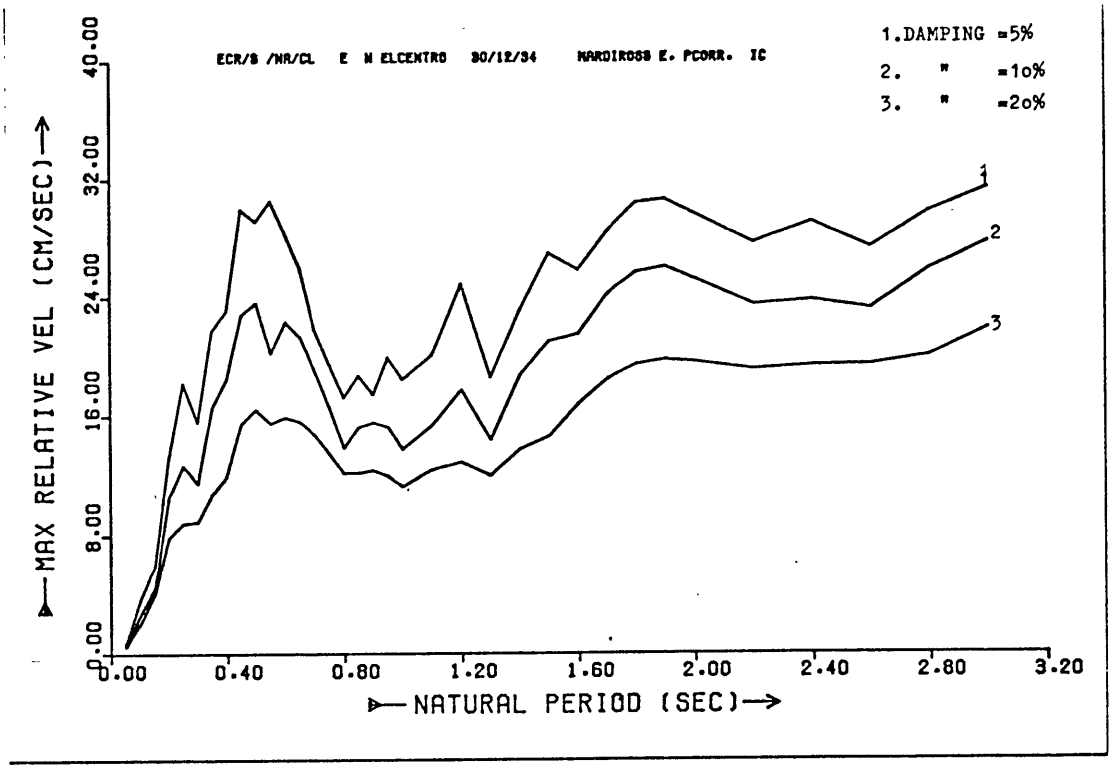


FIG 3.1oe COMPUTED SUBSURFACE BEDROCK VELOCITY RESPONSE SPECTRA

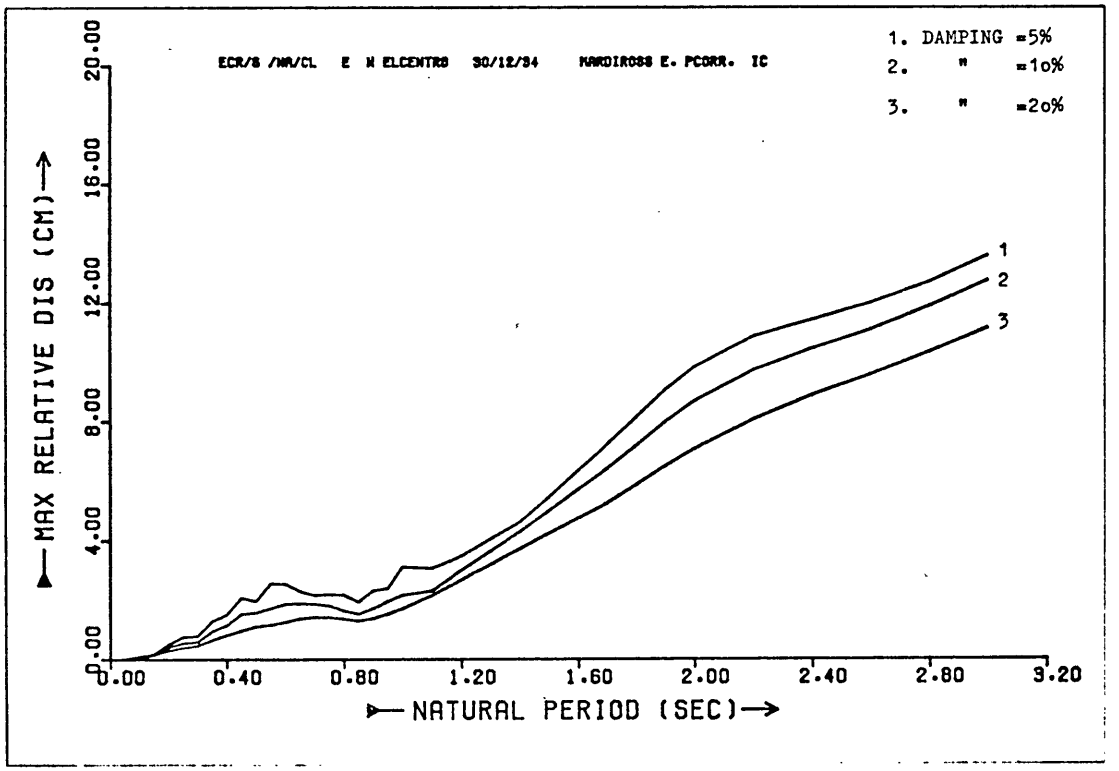


FIG. 3.1of COMPUTED SUBSURFACE BEDROCK DISPLACEMENT RESPONSE SPECTRA

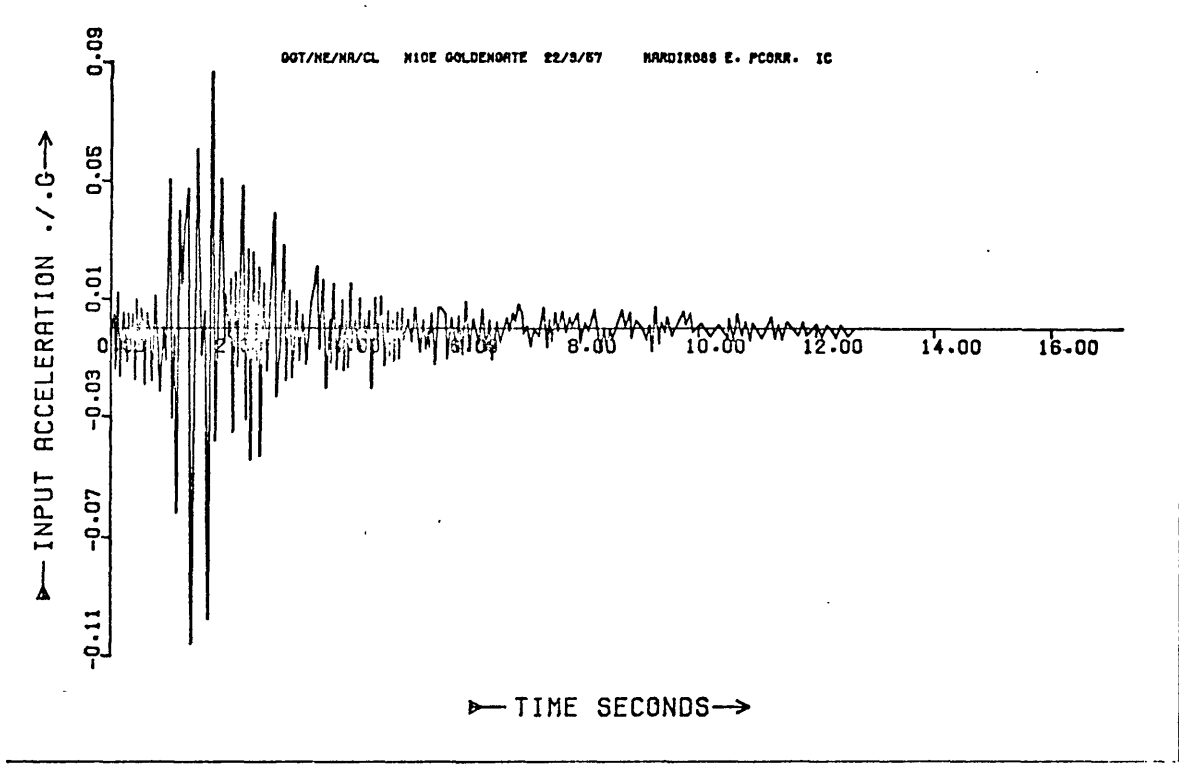


FIG.3.11a SUBSURFACE BEDROCK MOTION USED AS INPUT MOTION IN CALCULATIONS

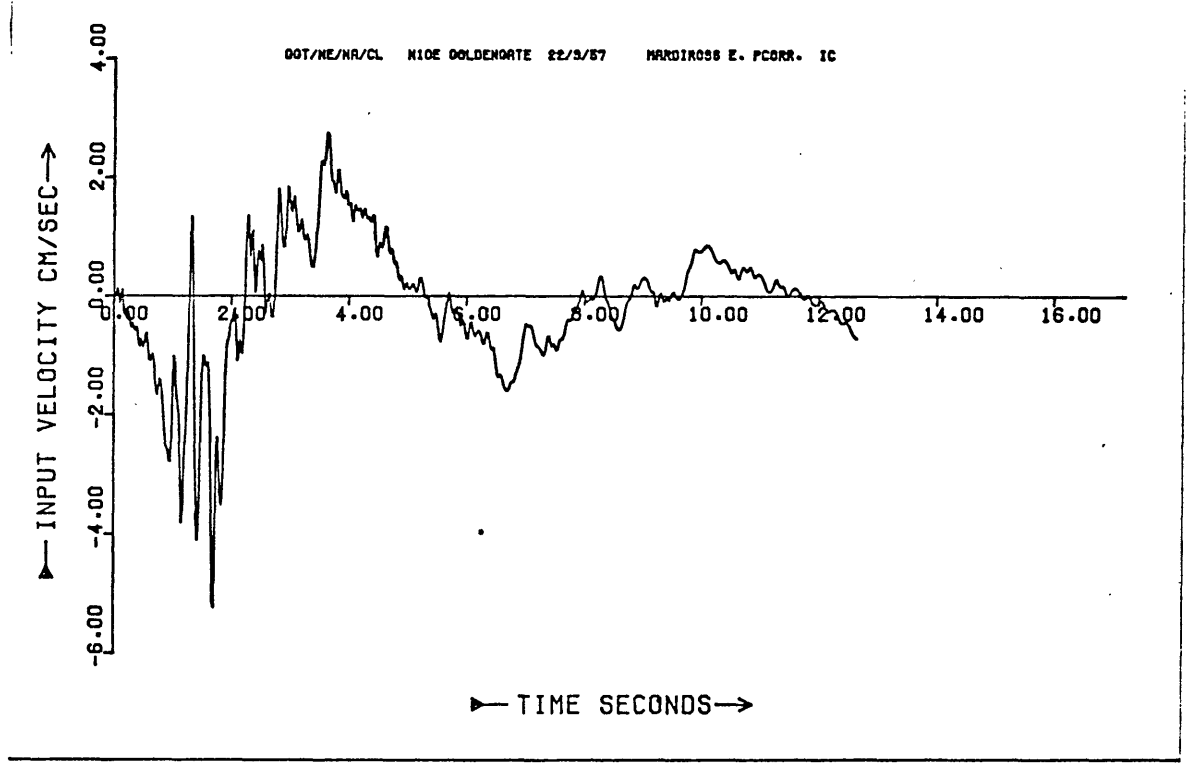


FIG.3.11b COMPUTED SUBSURFACE BEDROCK VELOCITY TIME HISTORY

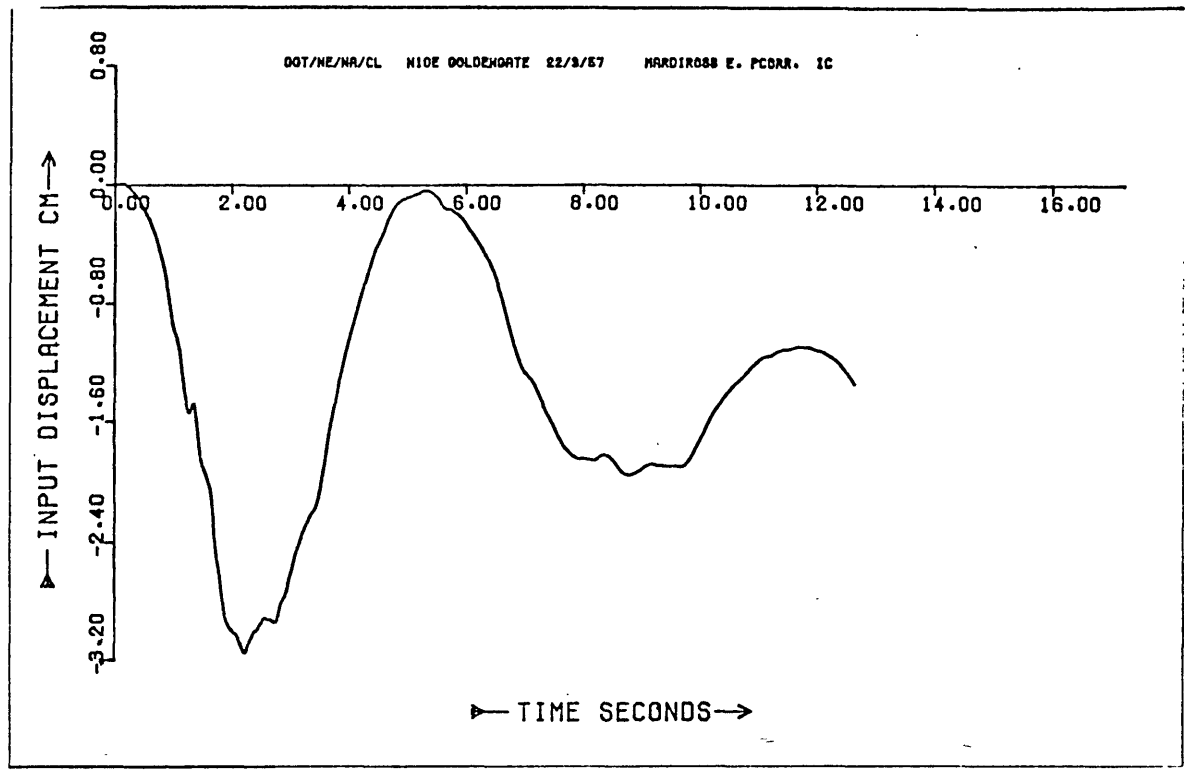


FIG. 3.11c COMPUTED SUBSURFACE BEDROCK DISPLACEMENT TIME HISTORY

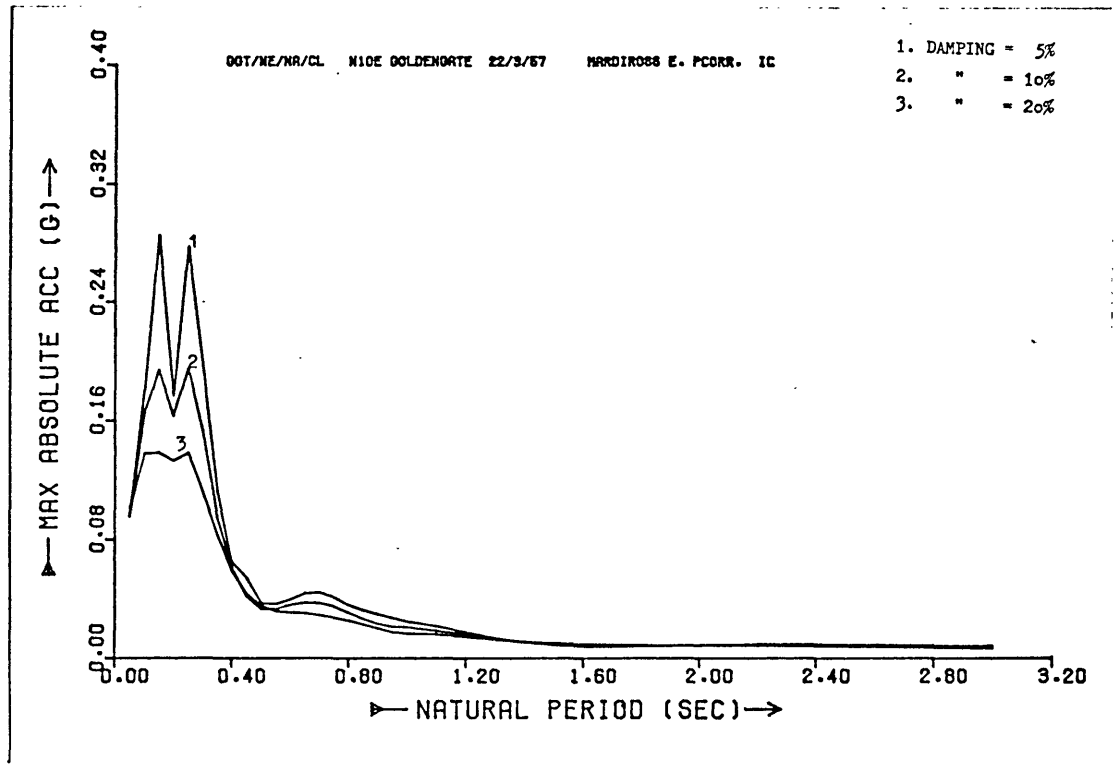


FIG.3.11d COMPUTED SUBSURFACE BEDROCK ACCELERATION RESPONSE SPECTRA

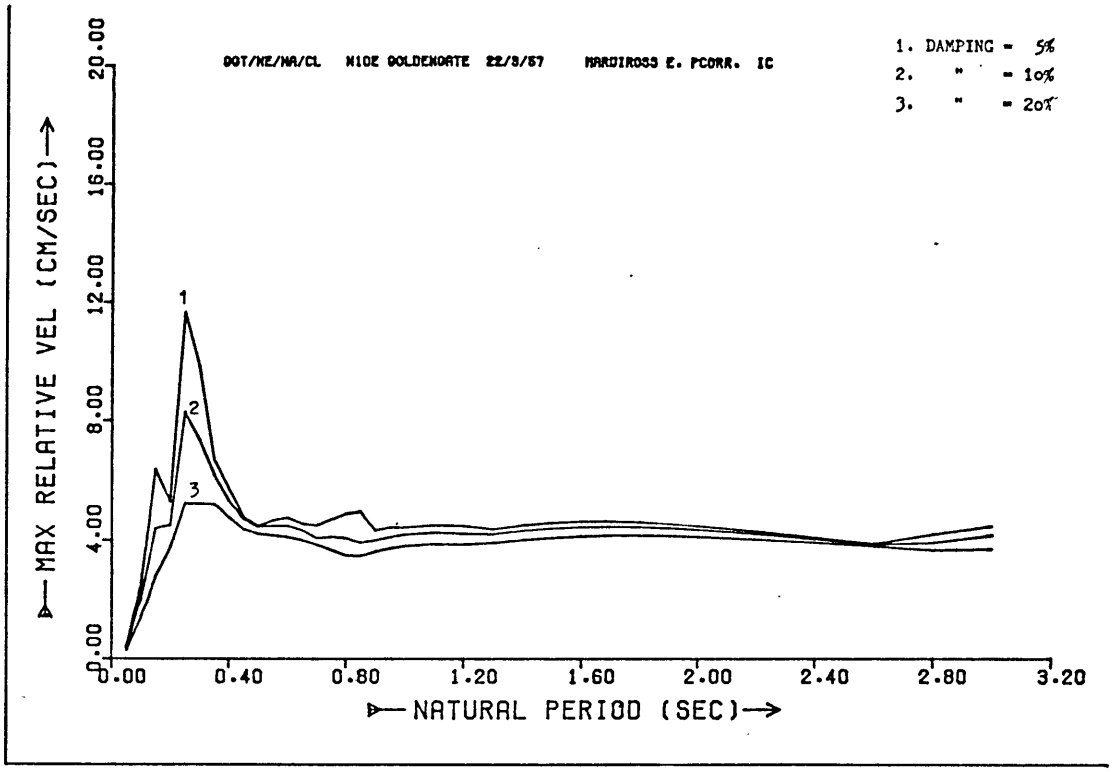


FIG.3.11e COMPUTED SUBSURFACE BEDROCK VELOCITY RESPONSE SPECTRA

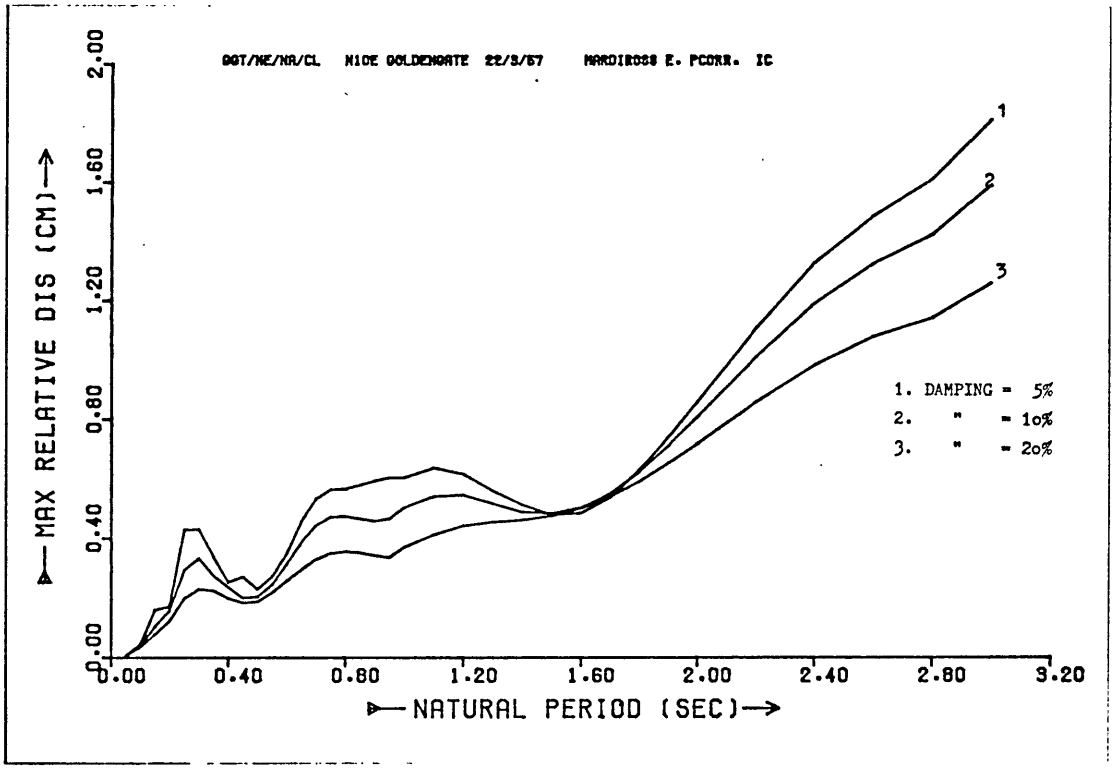


FIG.3.11f COMPUTED SUBSURFACE DISPLACEMENT RESPONSE SPECTRA

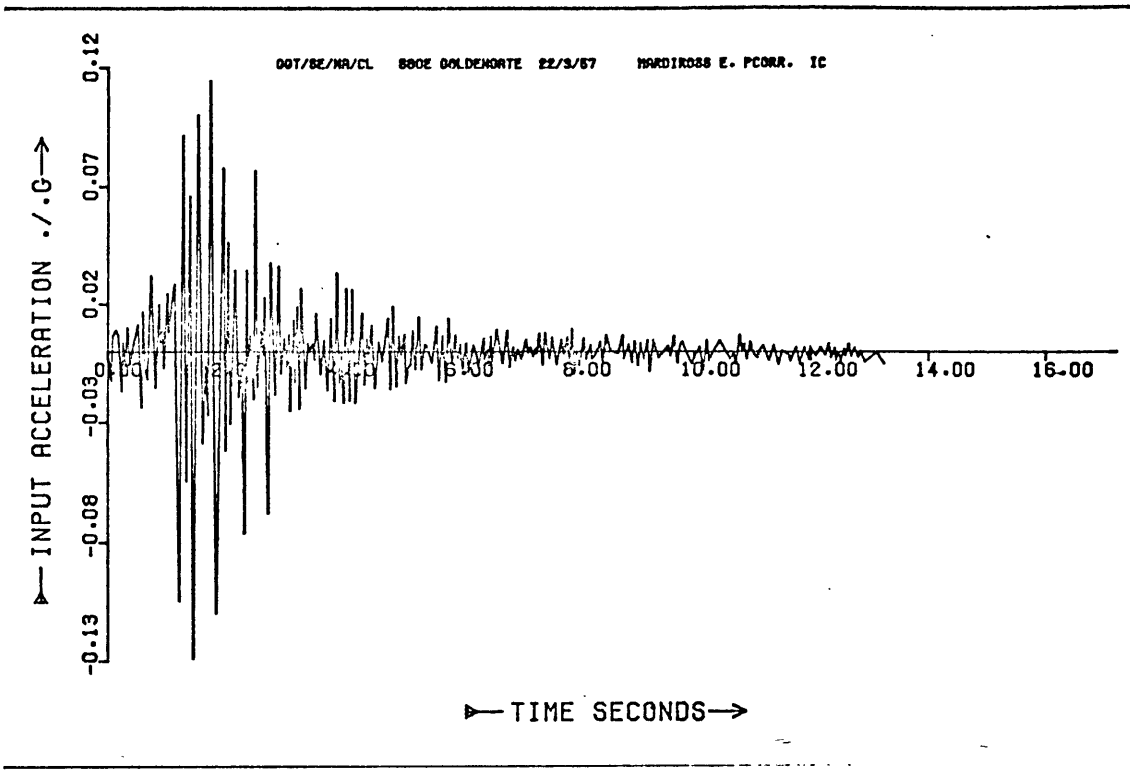


FIG. 3.12a SUBSURFACE BEDROCK MOTION USED AS INPUT MOTION IN CALCULATIONS

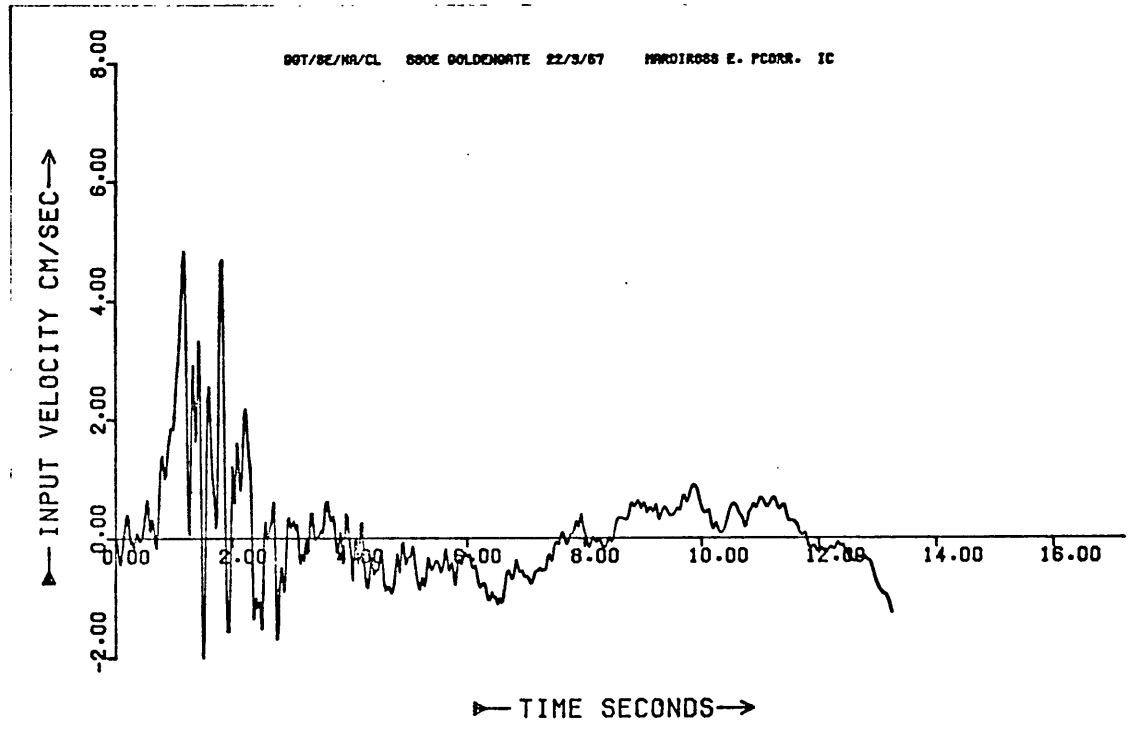


FIG. 12b COMPUTED SUBSURFACE BEDROCK VELOCITY TIME HISTORY

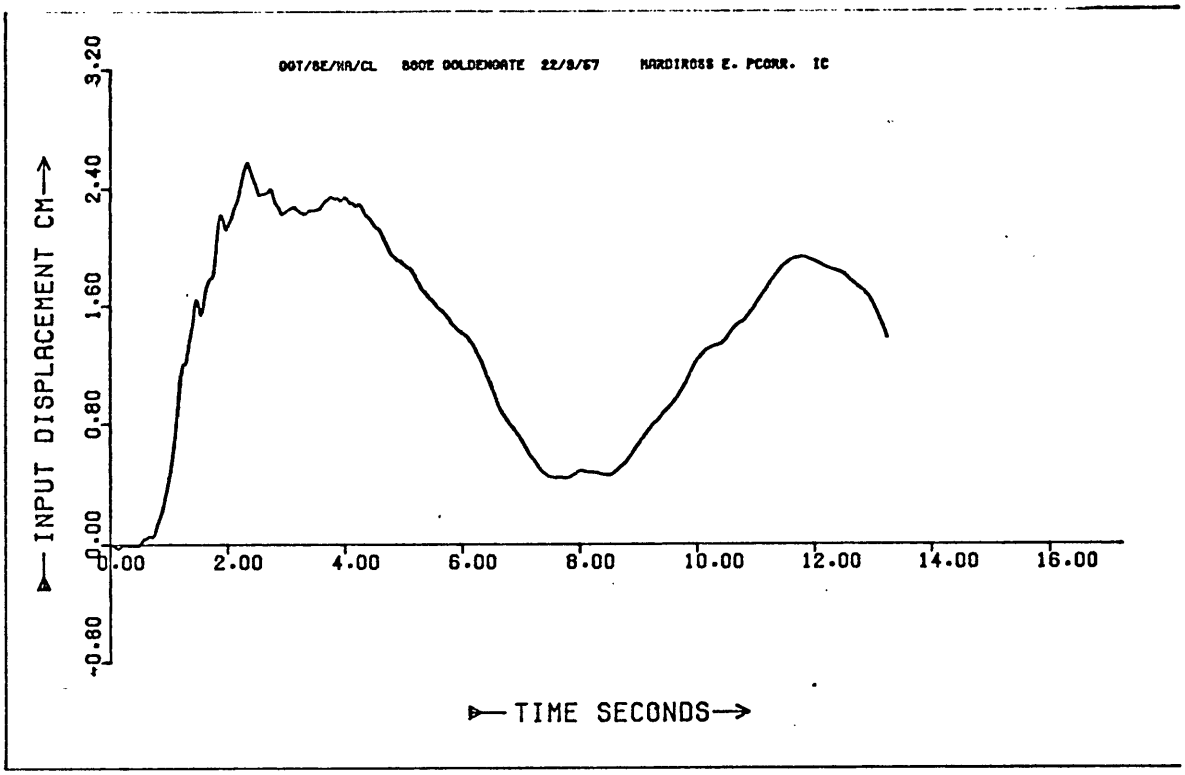


FIG. 3.12c COMPUTED SUBSURFACE BEDROCK DISPLACEMENT TIME HISTORY.

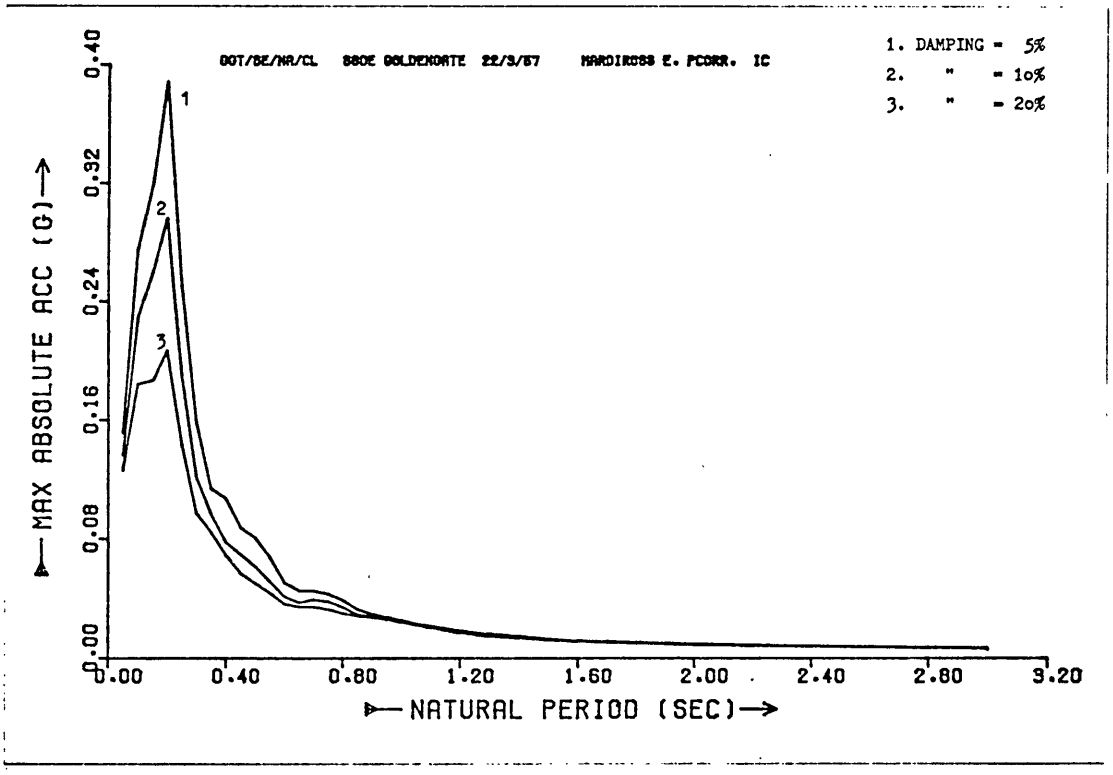


FIG. 3.12d COMPUTED SUBSURFACE BEDROCK ACCELERATION RESPONSE SPECTRA

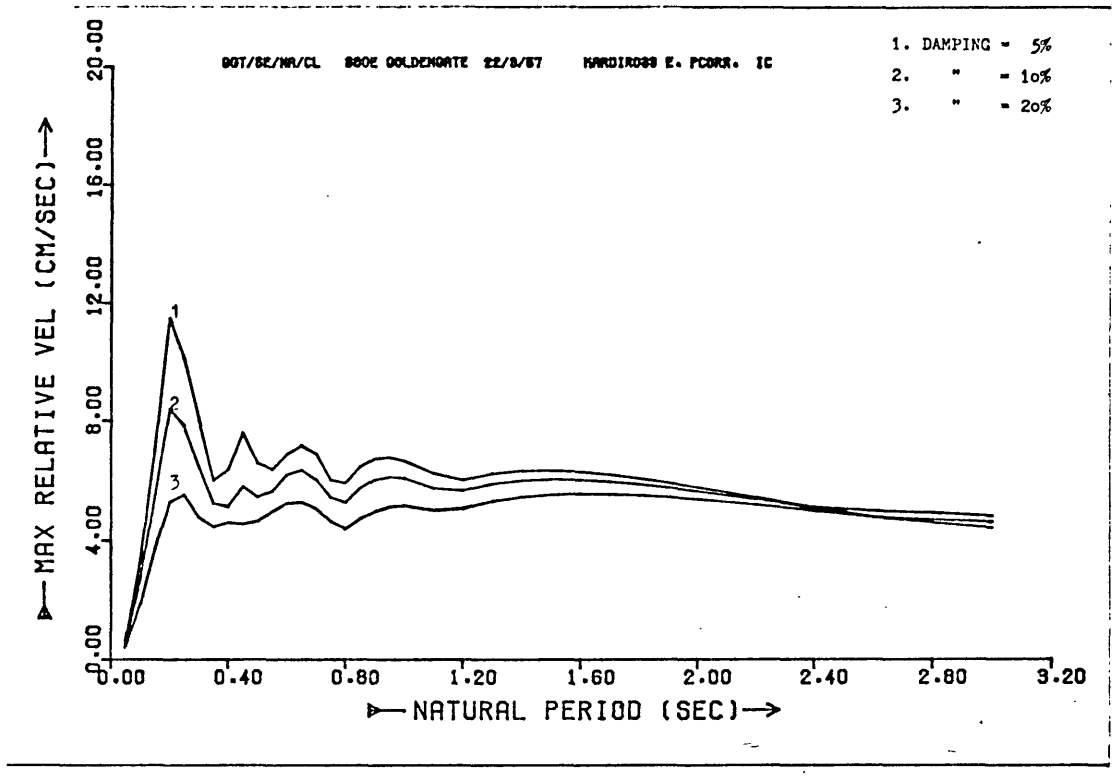


FIG.3.12e COMPUTED SUBSURFACE BEDROCK VELOCITY RESPONSE SPECTRA

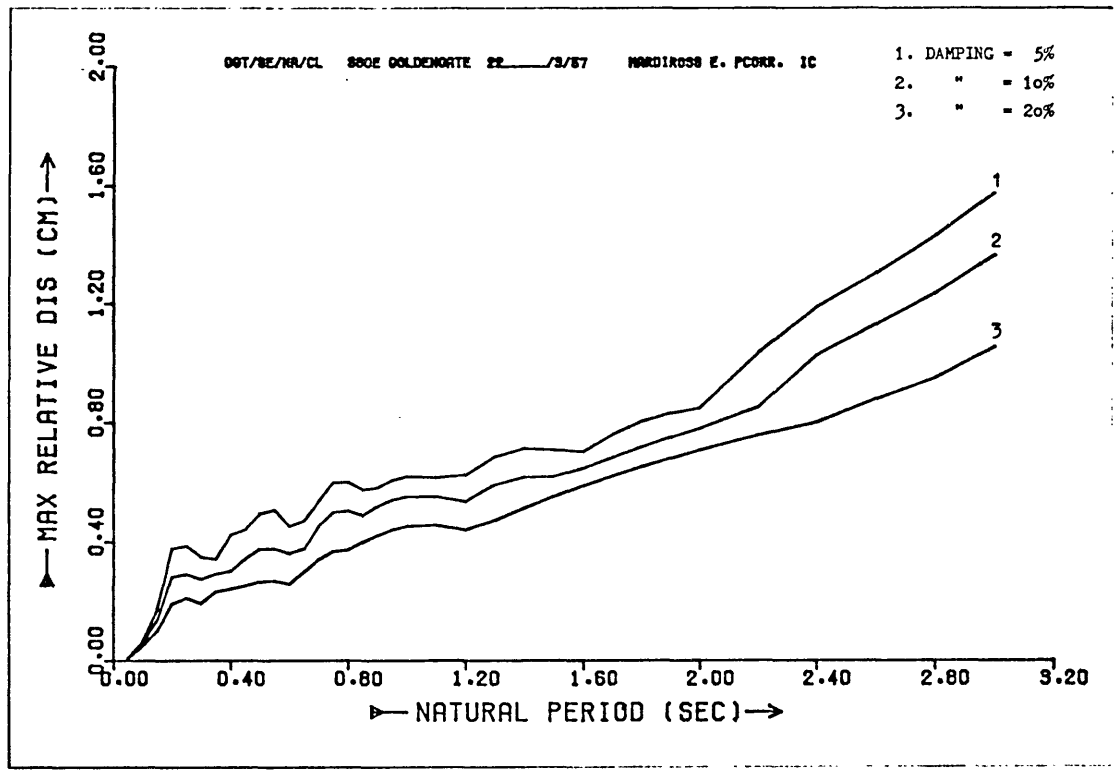


FIG.3.12f COMPUTED SUBSURFACE BEDROCK DISPLACEMENT RESPONSE SPECTRA.

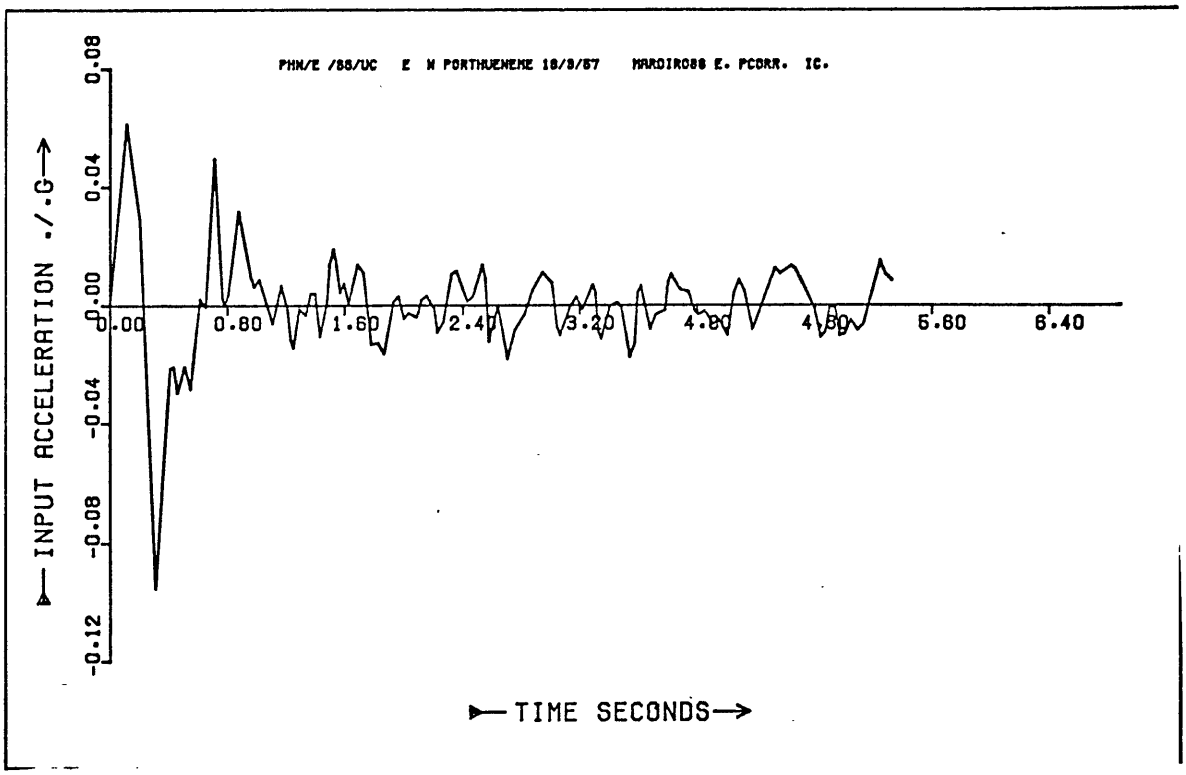


FIG.3.13a SUBSURFACE BEDROCK MOTION USED AS INPUT MOTION IN CALCULATIONS

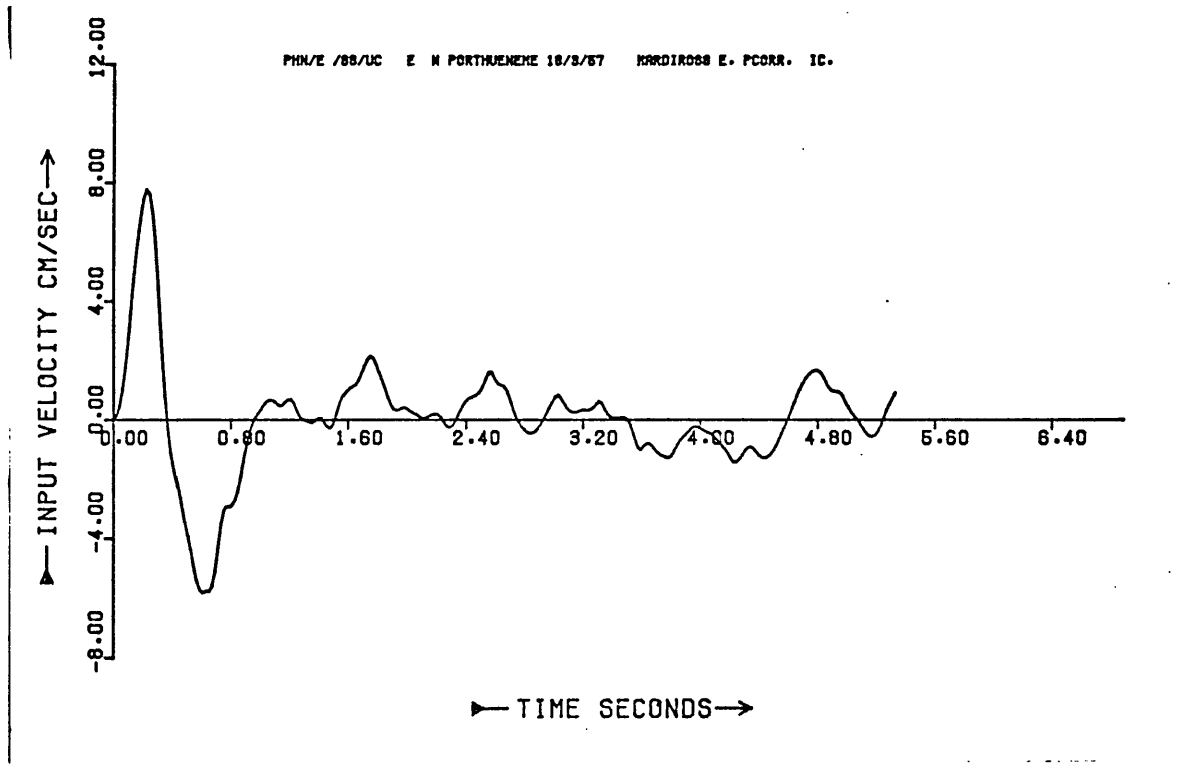


FIG.3.13b COMPUTED SUBSURFACE BEDROCK VELOCITY TIME HISTORY

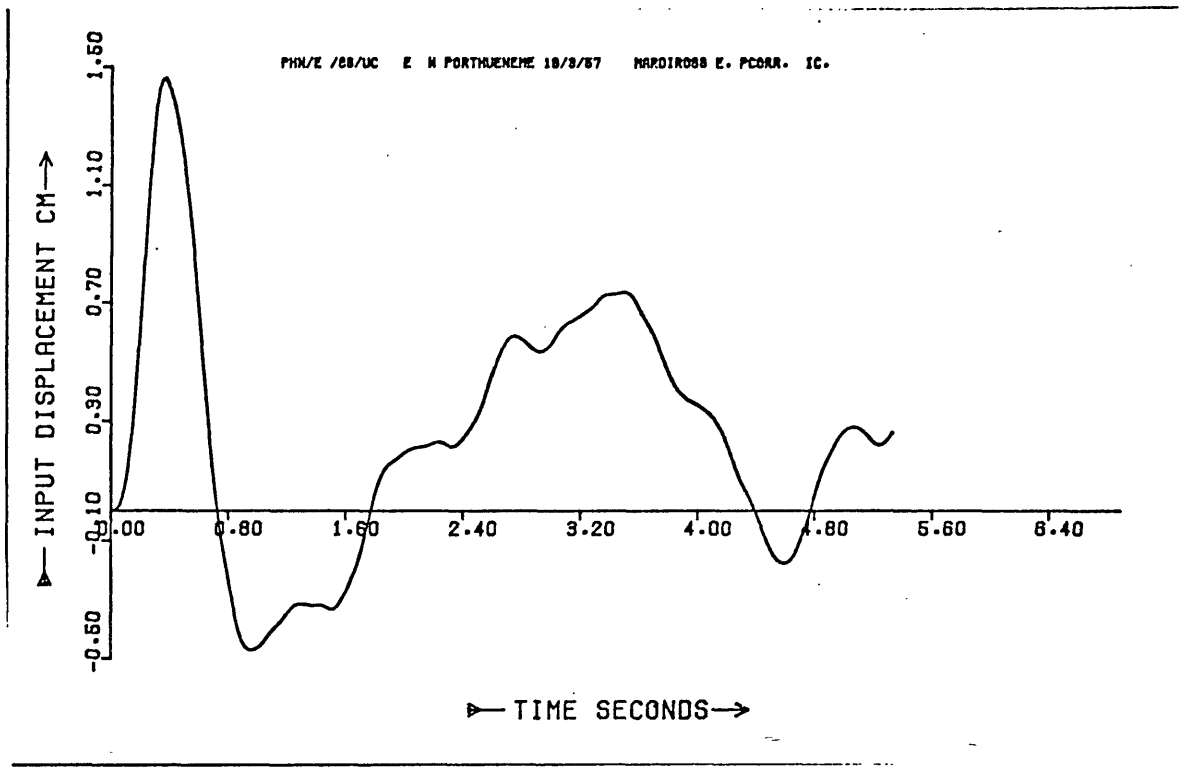


FIG.3.13c. COMPUTED SUBSURFACE BEDROCK DISPLACEMENT TIME HISTORY

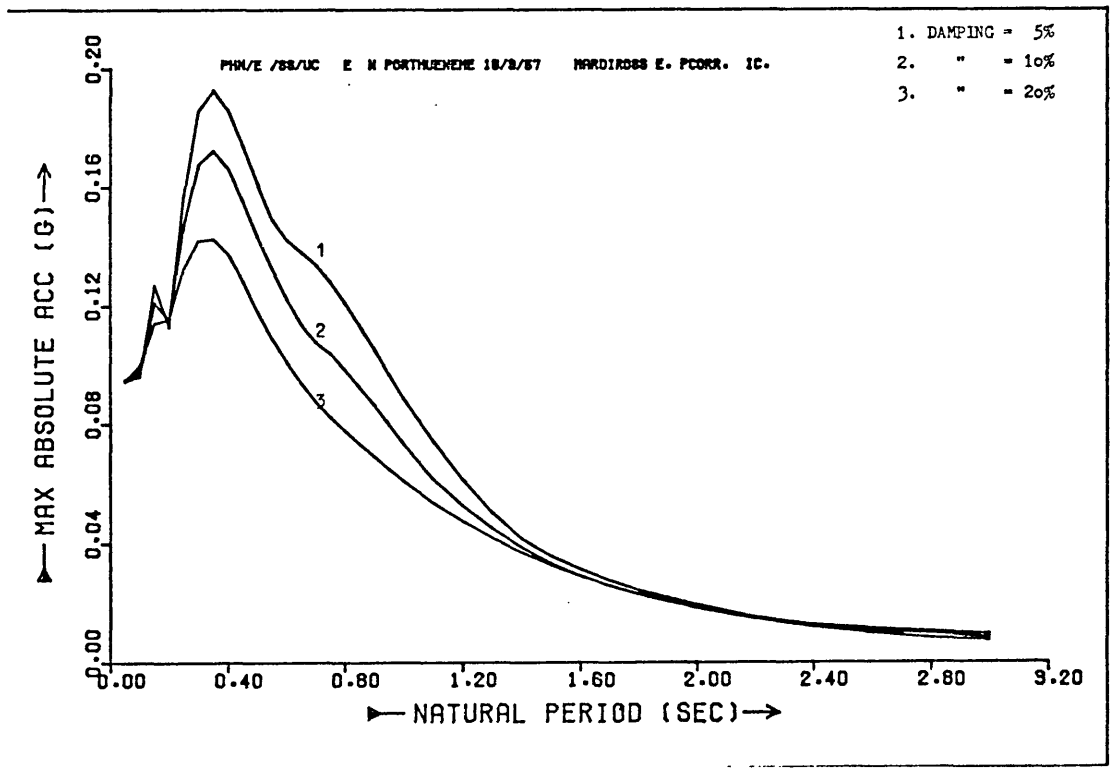


FIG.3.13d COMPUTED SUBSURFACE BEDROCK ACCELERATION RESPONSE SPECTRA

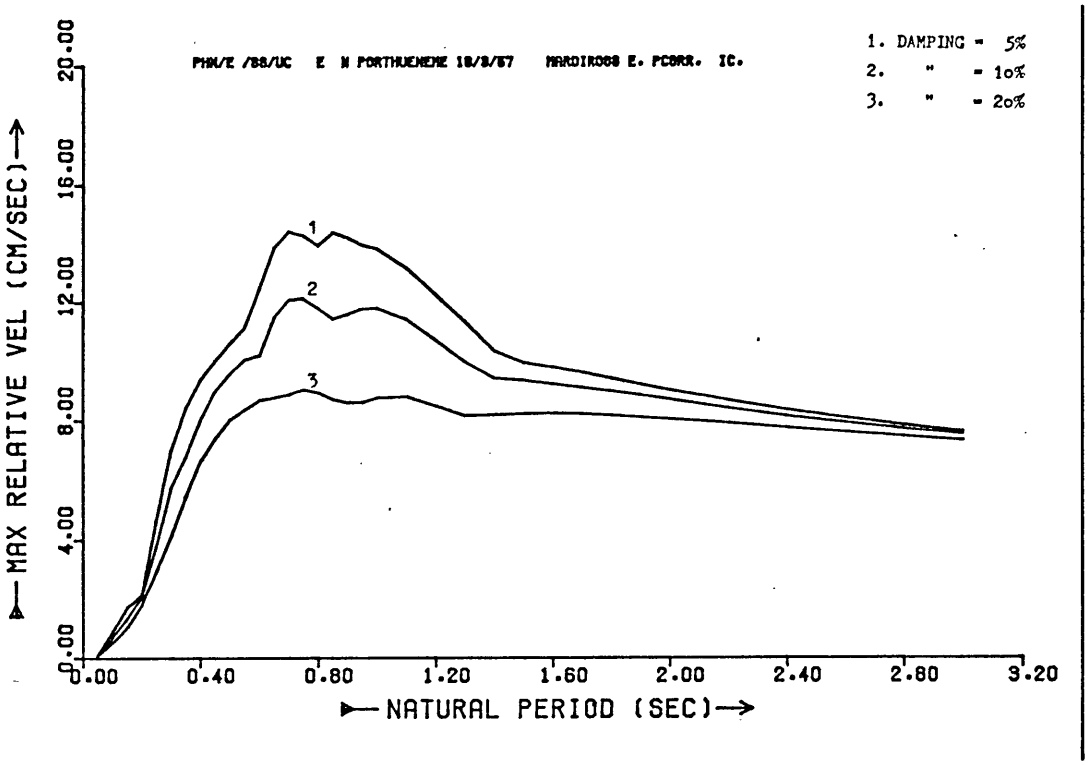


FIG.3.13e COMPUTED SUBSURFACE BEDROCK VELOCITY RESPONSE SPECTRA

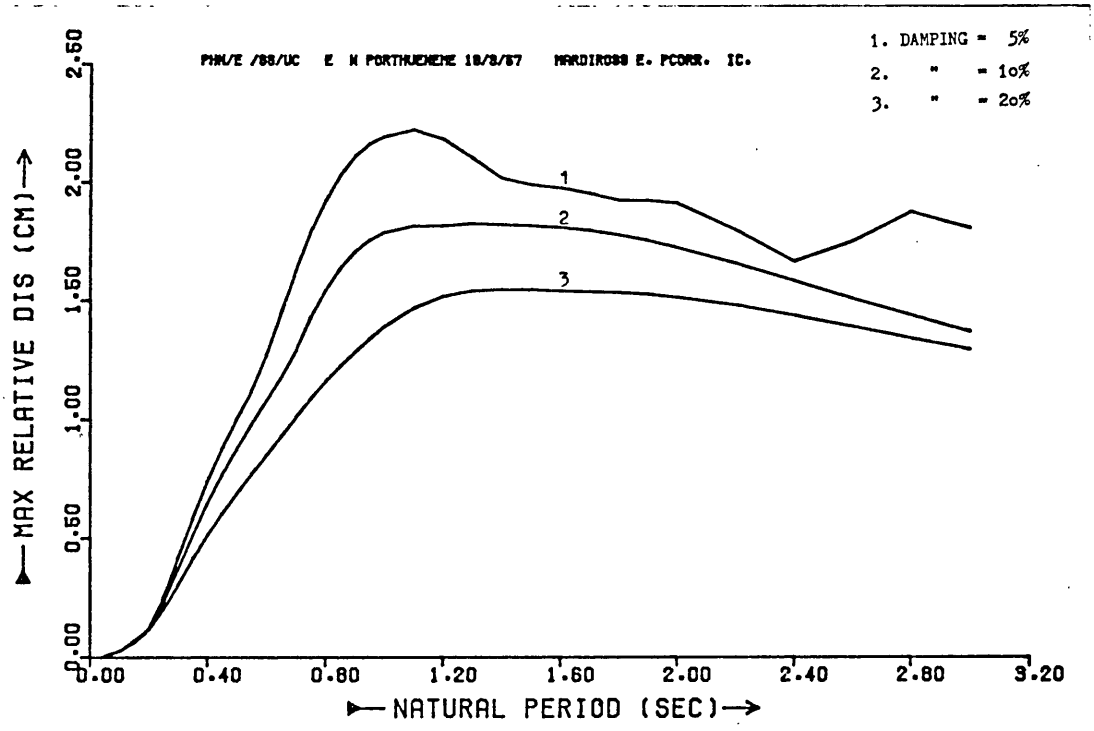


FIG. 3.13f COMPUTED SUBSURFACE BEDROCK DISPLACEMENT RESPONSE SPECTRA

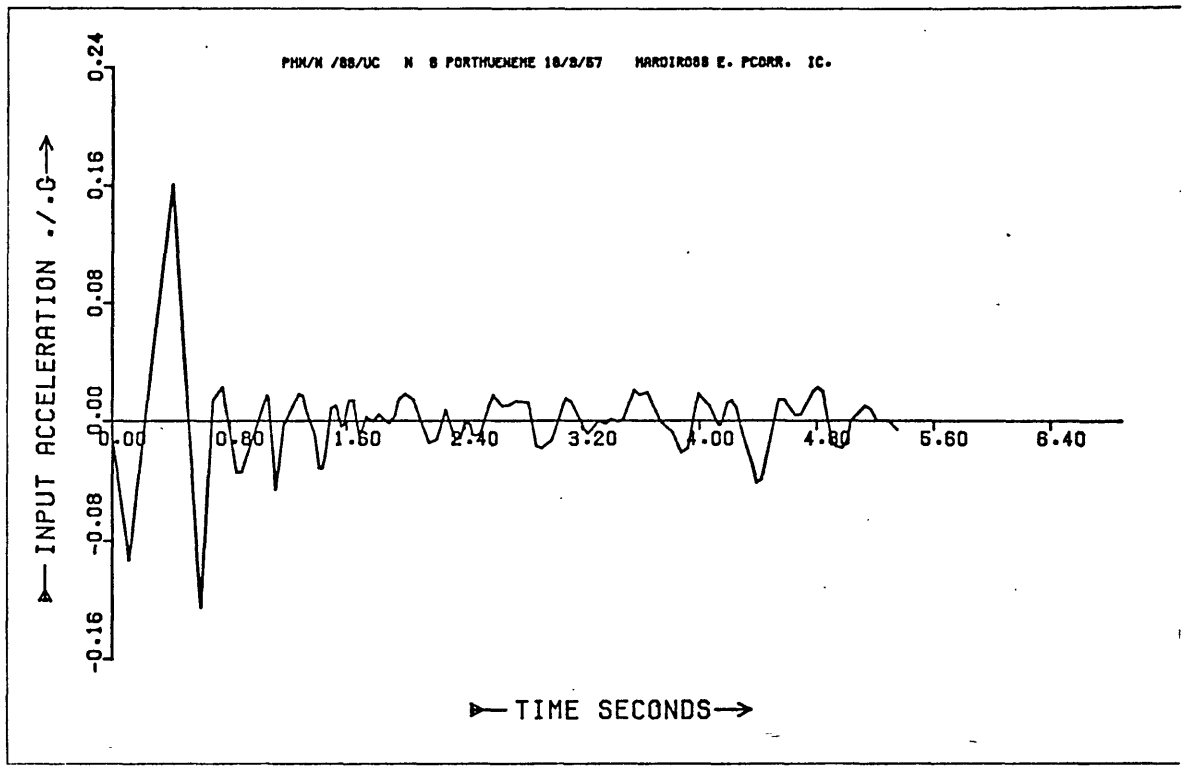


FIG. 3.14a SUBSURFACE BEDROCK MOTION USED AS INTUT MOTION IN CALCULATIONS

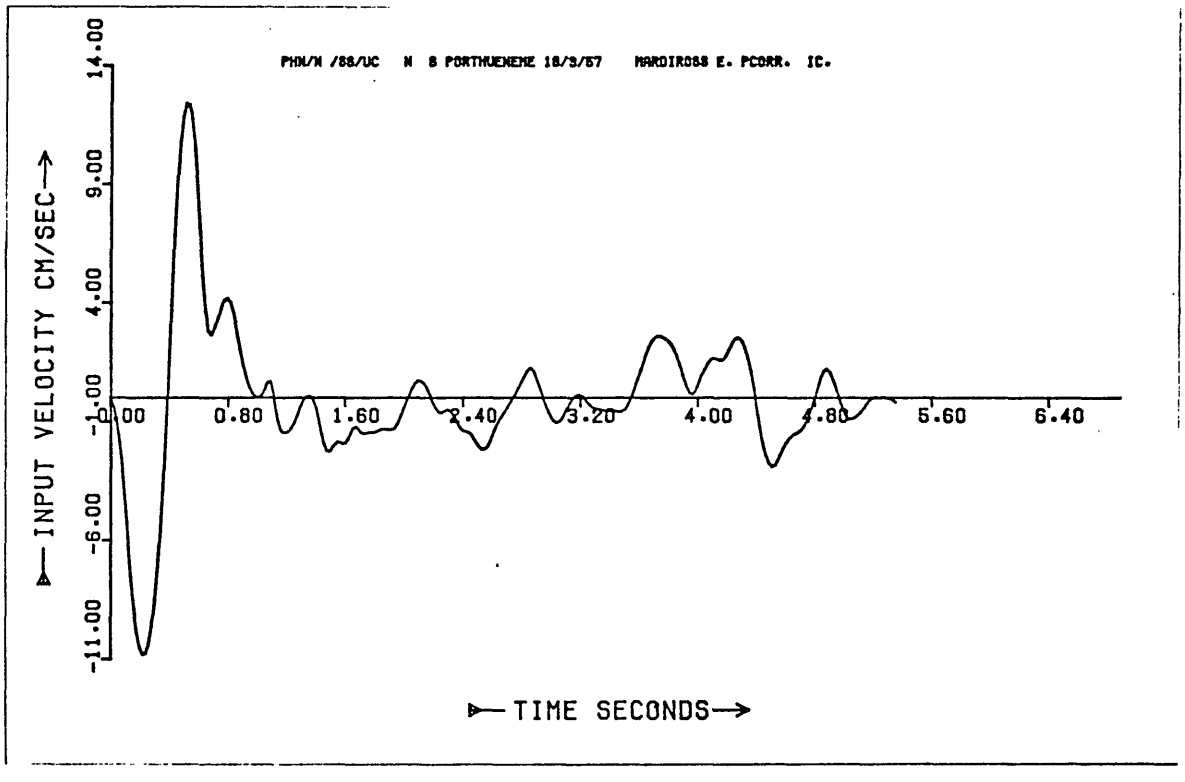


FIG. 3.14b COMPUTED SUBSURFACE BEDROCK VELOCITY TIME HISTORY

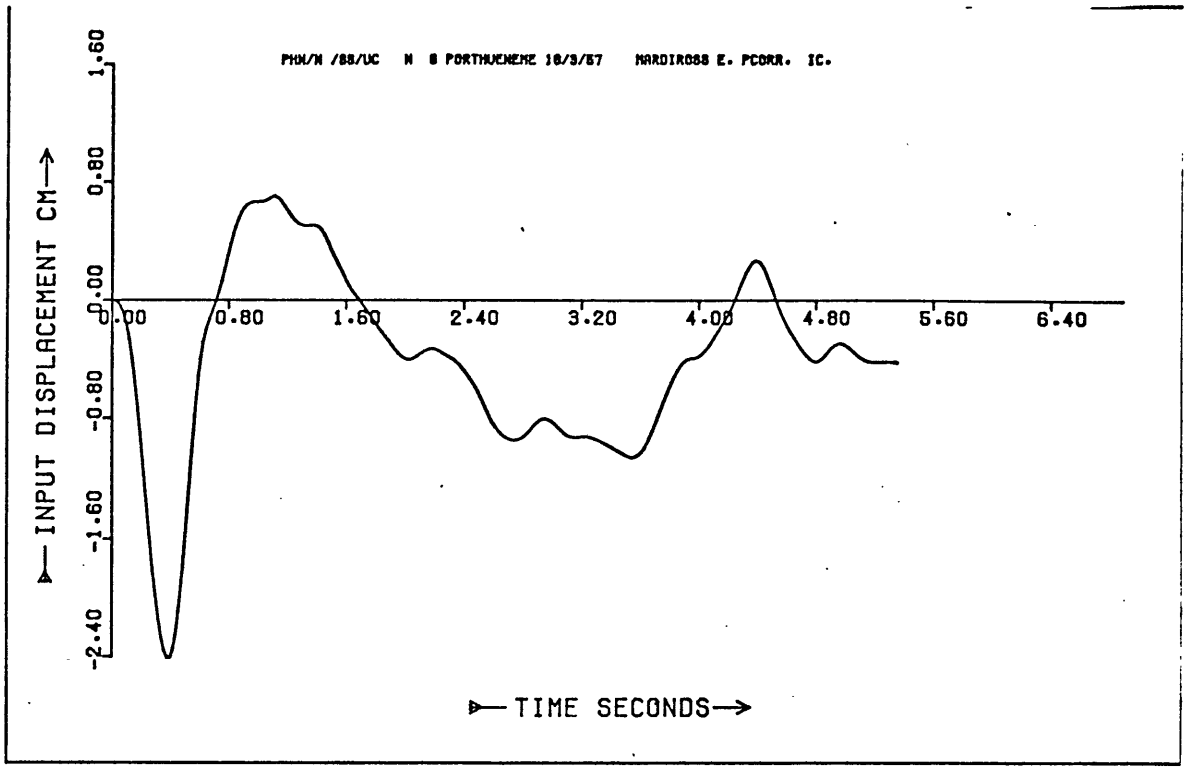


FIG. 3.14c COMPUTED SUBSURFACE BEDROCK DISPLACEMENT TIME HISTORY

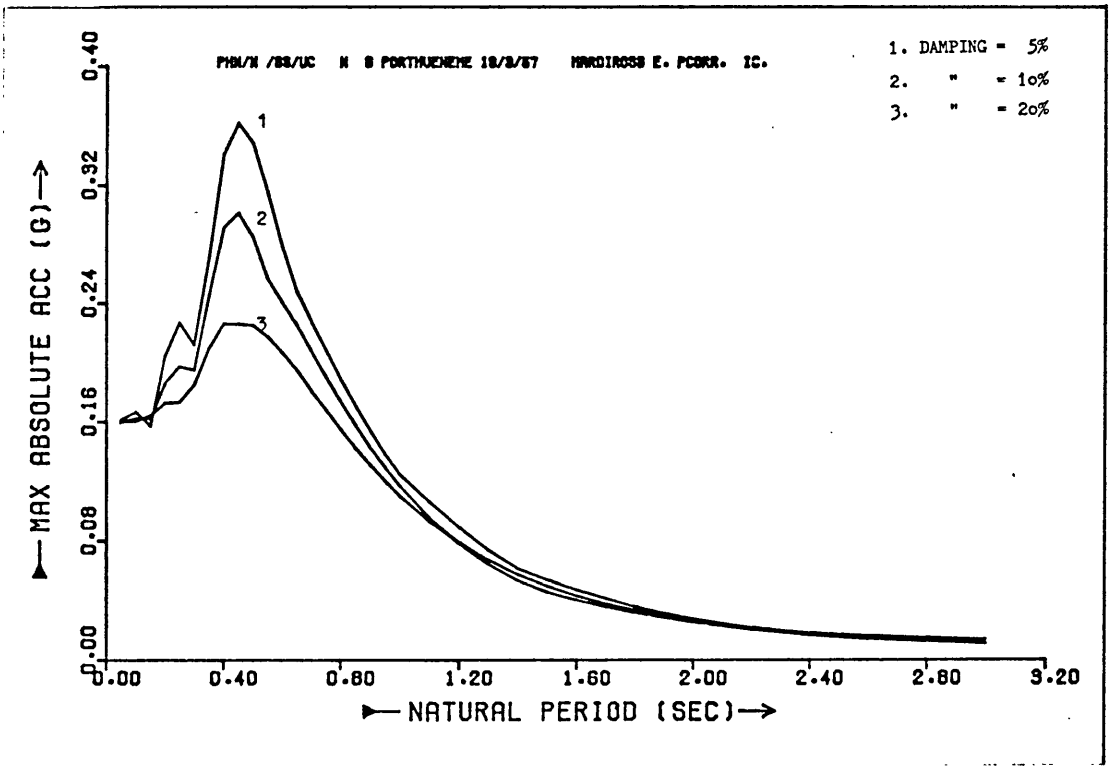


FIG. 3.14d COMPUTED SUBSURFACE BEDROCK ACCELERATION RESPONSE SPECTRA

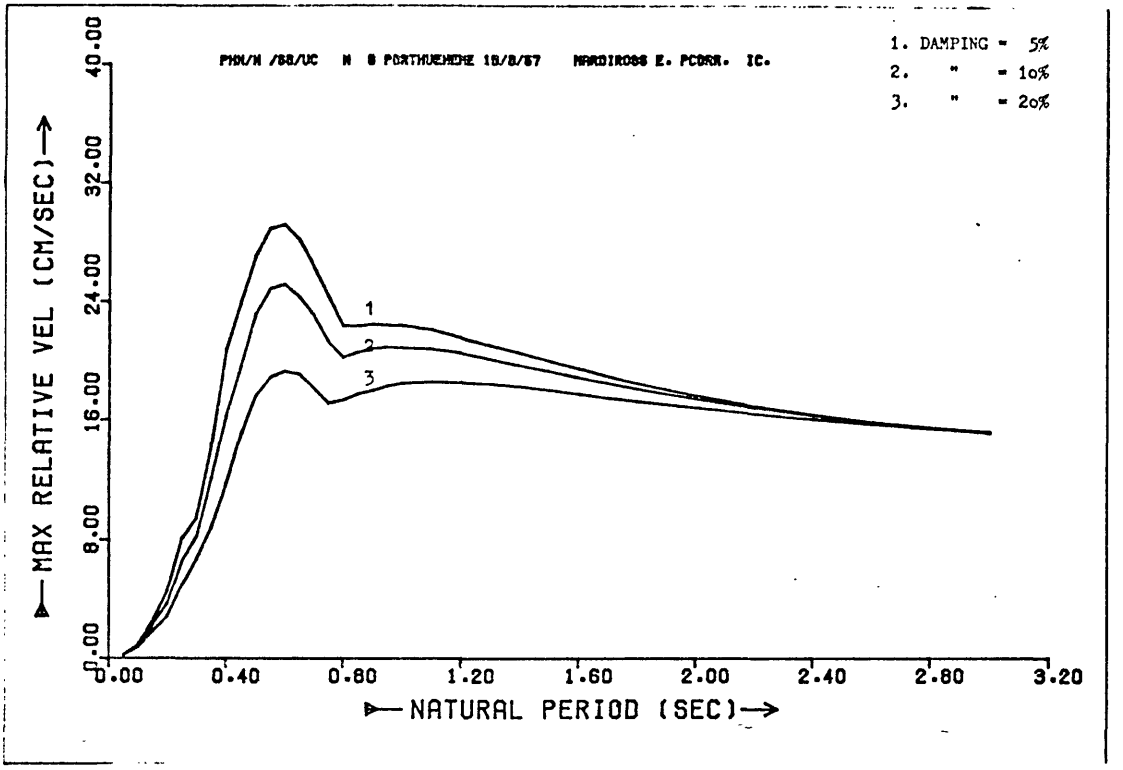


FIG. 3.14e COMPUTED SUBSURFACE BEDROCK VELOCITY RESPONSE SPECTRA

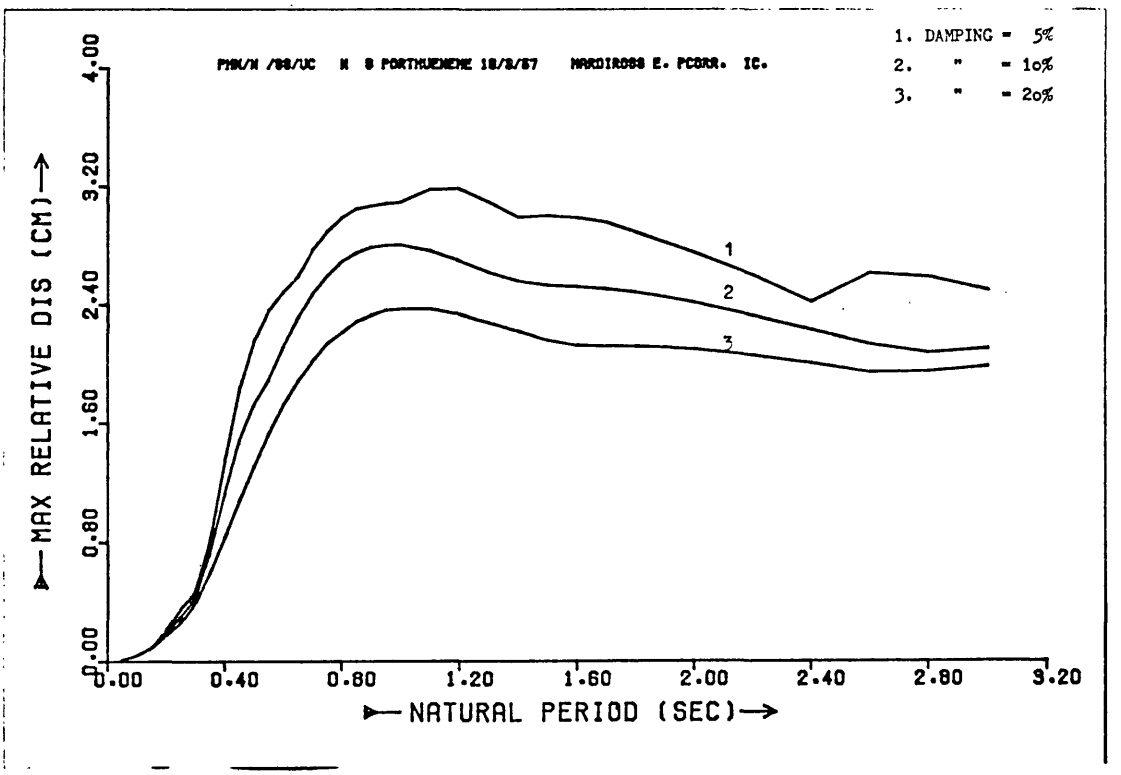


FIG.3.14f COMPUTED SUBSURFACE BEDROCK DISPLACEMENT RESPONSE SPECTRA

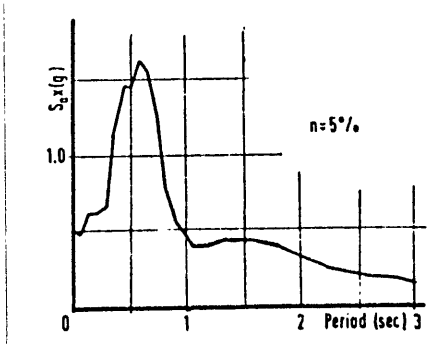
Method of computation of response spectra is given in appendix B . The method was incorporated in a computer program named SPECTRA. The program computes response spectra from accelerograms digitized at unequal time intervals. The program is written in FORTRAN iv and is capable of handling up to 3 damping values, 50 period values and 4000 ground acceleration values.

Data Preparation: Input data include periods and damping values for which spectras are required and digitized and corrected strong motion accelerograph data.

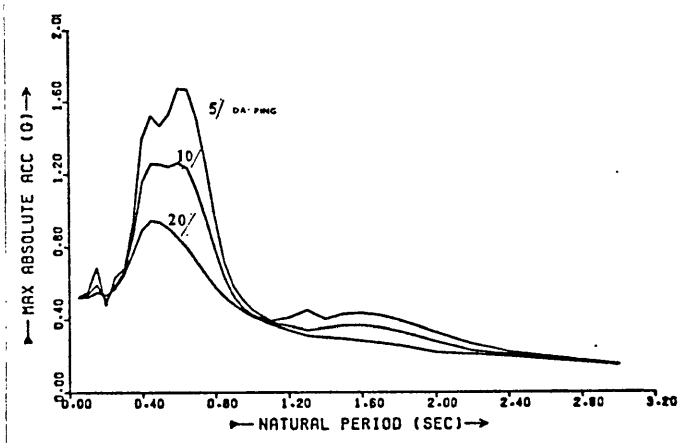
Output: In addition to printout of all input data, the following output is given by the program: acceleration velocity and displacement response spectra. Plots of these values versus period on KINGMATIC plotter.

The bedrock motion response spectra computations were made by means of "SPECTRA" for 5%,10% and 20% critical damping for 35 periods with a range of periods from 0.05 to 3.0 secs. Figs 3.1(d),(e),(f) through 3.14(d),(e),(f) show plots of computed acceleration velocity and displacement spectrum. To test the correctness of plotted graphs, a comparison was made between two spectrum for Parkfield 2, one computed by Professor N. Ambraseys[6] and the other by the author, and is shown in fig 3.15 The agreement between the two spectrum is very good. The minor differences between the two spectrum are due to different procedures used for computations, different number of periods used and different steps of integration.

The selected accelerograms are representative of near-field "rock" motions as well as "hard ground" or "weathered rock". The records provide valuable information about the character of bedrock motion, but



From Ref. 6



COMPUTED

FIG.3.15 COMPARISON OF ACCELERATION RESPONSE SPECTRAS COMPUTED BY AMBRASEYS, N.N.[6] AND THE AUTHOR

the number of available records in the nearfield are insufficient* to provide a basis for general conclusions to be drawn.

3.2. MOTION CHARACTERISTICS BY STUDYING STABLE STRONG MOTION BEDROCK PARAMETERS

The characterization of bedrock motion for engineering purposes during earthquakes requires defining, a parameter to indicate the size of an earthquake and the following three parameters to define bedrock motion:

a) Duration of shaking of bedrock motion.

b) Predominant period of bedrock motion.

c) Peak bedrock horizontal acceleration or velocity.

The objective of this section is to obtain new curves showing decrease in maximum bedrock acceleration and velocity with increasing distance from causative fault for San Fernando 9/2/1971 earthquake, and to discuss validity of these curves and existing corelations between earthquake magnitude and above parameters.

3.2.1. SIZE OF AN EARTHQUAKE

The measure of earthquake size, using instruments, is MAGNITUDE. The Richter magnitude, defined by Richter in the 1930's, is the logarithm of the amplitude of the largest wave recorded on a Wood Anderson seismograph located at a distance of 100 km from the epicentre. The magnitude

---

* Total of 17 near-field records are available in the U.S., fourteen of which are included in this study. Helena, Federal Building 31/10/1935 was excluded because it is too old to have enough accuracy.

is a measure of the energy released in an earthquake in the form of elastic waves and is logarithmic, meaning that a one-unit increase on the scale corresponds to a 25-fold increase in real energy released. An earthquake registering 6.0 on the scale is 25 times stronger than one registering 5.0, one registering 7.0 is 25 x 25 = 625 times stronger than the one measuring 5.0 and finally one registering 8.0 is 25 x 25 x 25 = 15625 times stronger than the one registering 5.0.

3.2.2. RELATIONSHIP BETWEEN MAGNITUDE AND EFFECTIVE DURATION OF BEDROCK SHAKING

Dobry et. al.,[18] using data from recorded events on rock in the near-field (approximate source distance $<$ 16 km) show variations of duration of shaking v.s. magnitude, which is expressed by the equation

$$D = 10^{(0.435M - 1.85)}$$

The effective duration of shaking "D" is expressed in seconds and is defined as the time needed to develop between 5% and 95% of $\frac{\int_0^t a^2(t)}{\int_0^\infty a^2(t)}$ for the entire record, a(t) being ground acceleration. "M" is the Richter magnitude scale. "t" is time.

The above formula can only produce realistic results if "M" is restricted to lie in between 5.1 and 6.8. Effective duration of shaking as used by the authors has no clear physical meaning. A better definition for effective duration of shaking would be the interval of time needed to develop 90% - 95% of the total energy of the entire record or the interval of time between the first and last velocity excursions greater than a given level(5 cm/sec.).

3.2.3. RELATIONSHIP BETWEEN MAGNITUDE AND PREDOMINENT PERIOD OF BEDROCK MOTION

Reliable relationships between magnitude and predominant period of bedrock motions are non-existent. The available relationships are summarized by Seed, et.al.[52]

3.2.4. CORELATIONS RELATING MAGNITUDE DISTANCE FROM CAUSATIVE FAULT, AND BEDROCK MAXIMUM ACCELERATION OR VELOCITY

For economic design of engineering structures on soil deposits, it is desirable to estimate maximum acceleration or velocity which is likely to develop on bedrock formations of these deposits. Several relationships are available which are given in standard text books on Earthquake Engineering.[40,45]

The San Fernando 9/2/1971 earthquake provided 9 very good rock (shale-like or sounder, shear wave velocity greater than 760/sec, whose reliability was confirmed by means of borings) accelerograms at sites within 4 to 42 km of the fault.[54] Values of maximum acceleration and velocity computed by the California Institute of Technology for the above 9 sites are given in table 3.1. The variations of maximum acceleration and velocity with approximate source distance are shown in figs. 3.16 - 3.17

Fig.3.16 shows a distinct attenuation of maximum acceleration with source distance. This is expected because, as the waves propagate outwards from causative fault, they occupy a larger volume, hence a gradual decrease in energy per unit volume takes place with increasing source distance. This is known as geometric attenuation. The

TABLE 3.1

RECORDED DATA ON SHALE-LIKE OR SOUNDER ROCK

(Shear wave velocity > 2500 f.p.s) during
San Fernando 9/2/71 EARTHQUAKE)
M = 6.6

Record No.	Approximate Source Distance (km)	Component	Max acc (g)	Max vel cm/sec	SITE	Source of Information
1	4	-	1.240	115.0	Pacoima Dam	Cal. Tech
2	24	N-S	0.180	12.3	3838 Lankershim	"
3	26	S-69-E	0.172	5.3	Lake Hughes	"
4	29	S-08-E	0.217	9.9	Santa Felicia Dam(outlet works)	"
5	33	N-37-W	0.100	8.3	Fairmont Reservoir	"
6	37	E-W	0.192	11.6	Cal Tech. Seism. Lab.	"
7	39	S-40-W	0.173	16.1	Water & Power Bldg.	"
8	41	-	0.150	17.4	445 S. Figueroa	"
9	42	S-28-W	0.08	11.5	2011 Zonall	"

Ref.54

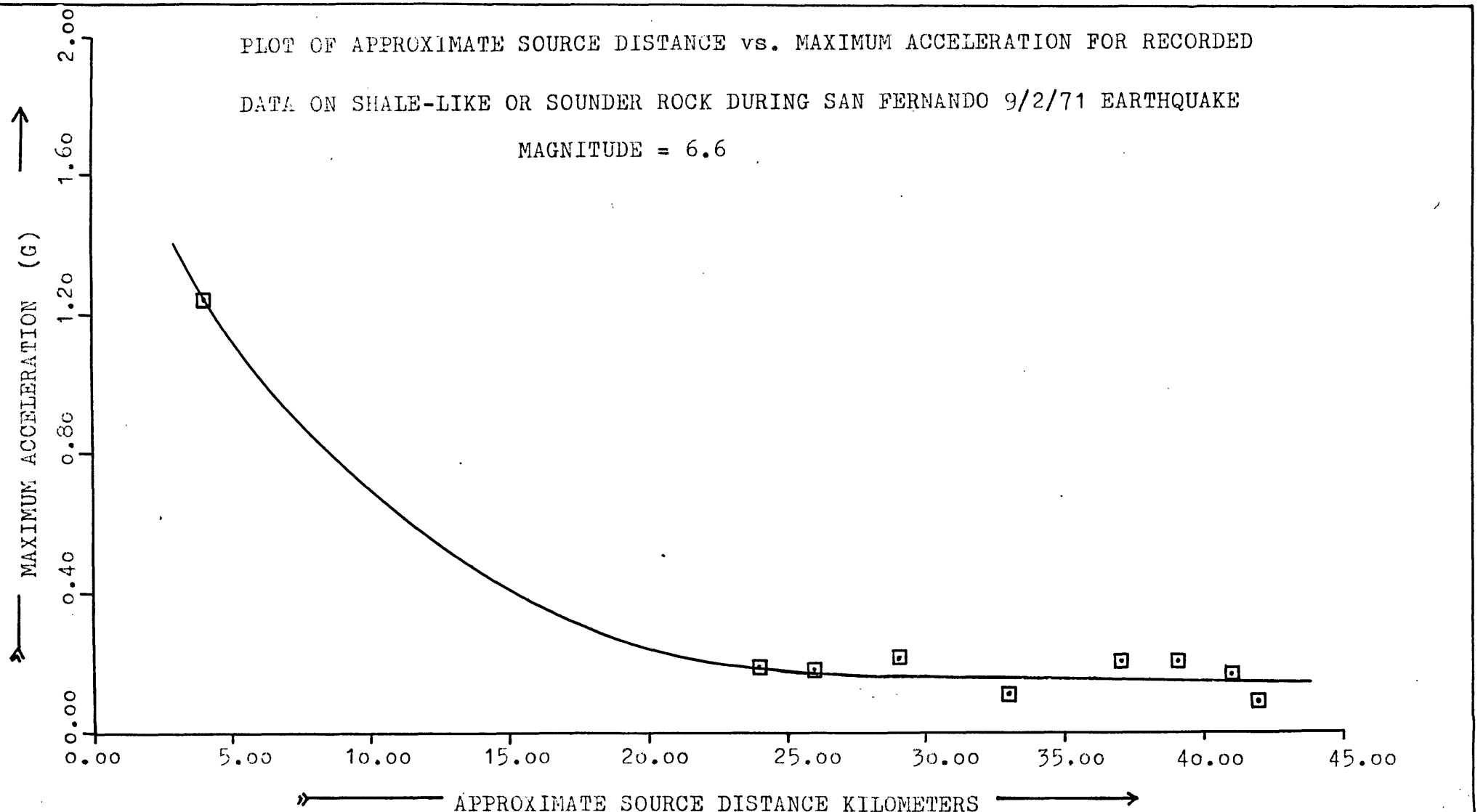


FIG.3.16 ATTENUATION OF MAXIMUM ROCK ACCELERATION WITH SOURCE DISTANCE

attenuation is also due to internal damping in rocks attenuating high frequency components more rapidly.[12] These results also indicate that maximum acceleration very close to causative fault could have been in the order of 200%g or more. Confirming Professor Ambraseys'[6] conclusion: "Maximum acceleration may reach values well in excess of 200%g".

Fig.3.17 shows attenuation of maximum velocity with source distance. The results show that maximum bedrock velocity near causative fault of this earthquake could have been in the order of 160 cm/sec. Confirming the general conclusions reached by Professor Ambraseys[6] based on different grounds.

The above results emphasize the need for development of new attenuation laws based on the latest recorded data on regional basis; to reduce scatter due to different transmission paths, different faulting mechanisms, etc. The effect of fault rupture on results, if they are used for assessing the maximum acceleration or velocity likely to develop in future earthquakes in the area are discussed by Savage.[49] It is beyond the purpose of this section to go into the details of fault rupture mechanism.

3.3. CONCLUDING REMARKS

a) None of the three approaches discussed in this chapter are sufficient for prediction of bedrock time histories. Substitution of simple mathematical models for approach,one backed with the results of approaches two and three,will considerably increase the confidence limit and would provide a fair insight into the future bedrock motion at a particular site and source area. Reliability of approaches two and

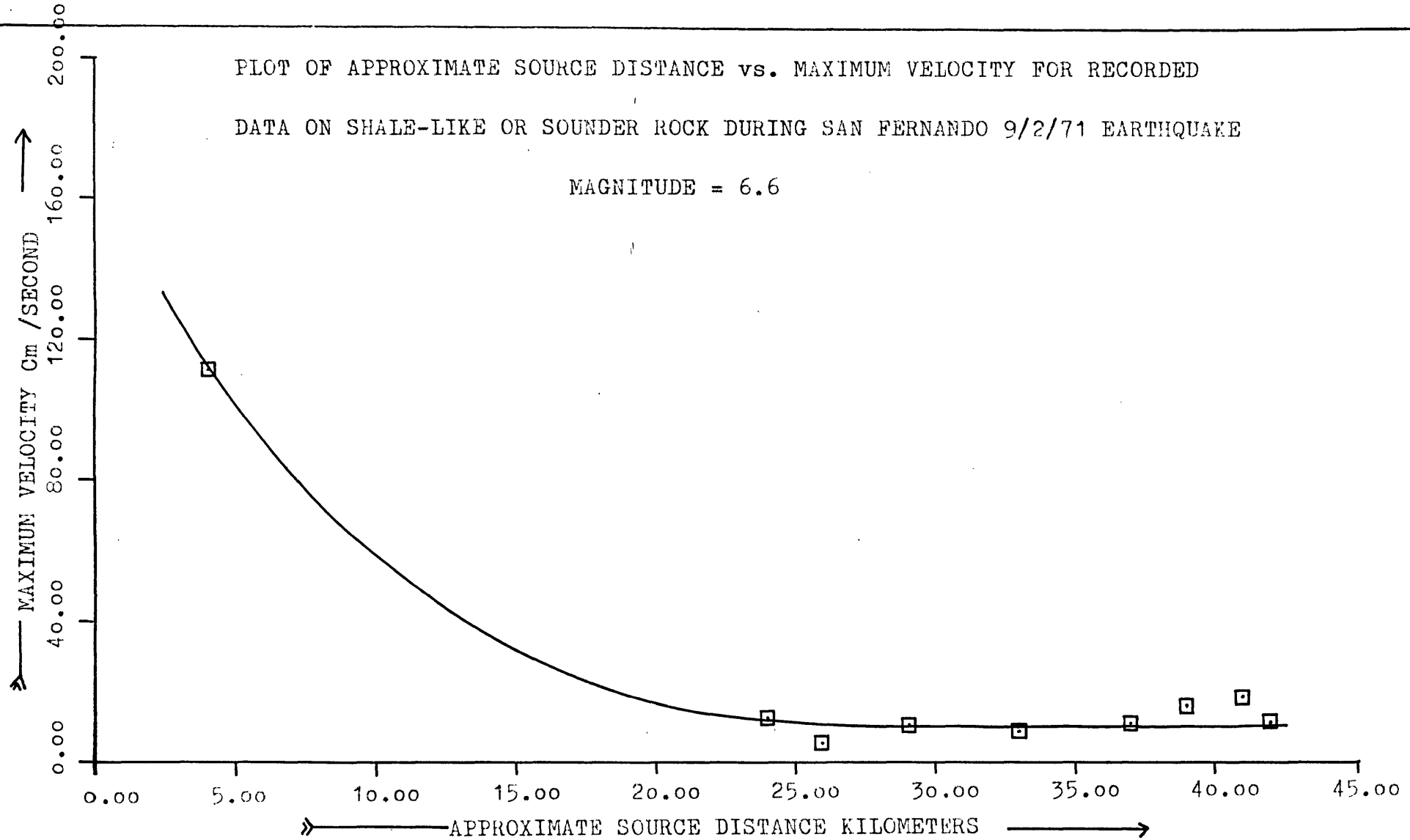


FIG.3.17 ATTENUATION OF MAXIMUM ROCK VELOCITY WITH SOURCE DISTANCE

three can also be considerably improved by incorporation of data from small events.

b) The amplitude of maximum acceleration and velocity decrease with increasing source distance. Existing field data, although not sufficient, especially within 5 to 20 km of the fault, indicate that very close to the causative fault maximum bedrock acceleration and velocity could have been as high as 200% g and 160 cm/sec, respectively.

CHAPTER 4

A NEW METHOD FOR ANALYZING THE EFFECT OF FOUNDATION CONDITIONS ON FOUNDATION RESPONSE.

4.1. INTRODUCTION.

The current research has led to a new design method based on actual earthquake bedrock movements, recorded by strong ground motion instruments, real foundation materials and a new procedure for modeling a transmitting boundary. The original solution of this new theory, which takes into account radiation effects as well as internal absorption effects, being a closed form solution, gives very accurate response values for small values of damping ratios,as exhibited by all soils when deformed elastically. The method can be used for design of foundations of dams, nuclear power plants, etc. in seismic countries.

Under earthquake loading, the developed strains may be large to cause the foundation materials to have inelastic behaviour. In such cases, the response may be calculated by numerical techniques. The method developed has been used to obtain the results presented in chapters 6 and 7. In chapter 5 the developed computer program, which incorporates the solution developed, is described.

4.2. OBSERVED FACTS.

A shallow depth earthquake may be assumed to result from a sudden

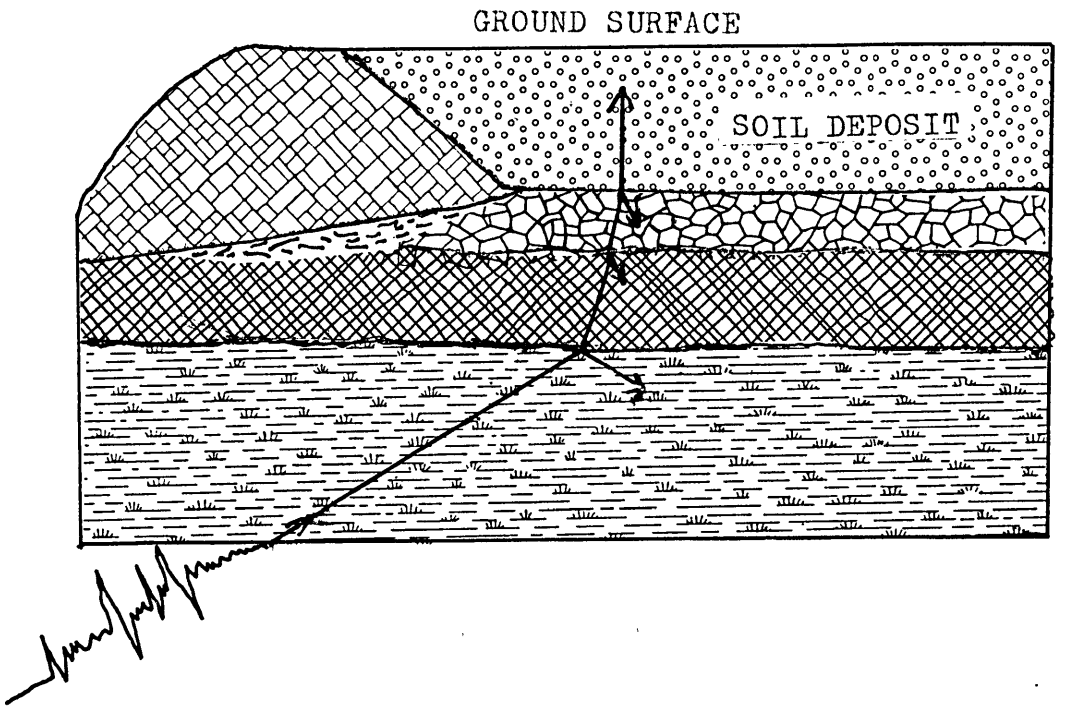
release of strain energy due to rupture or slip along a fault surface. The stress and strains build up slowly as a consequence of geological processes in certain parts of the earth's crust. When the stresses at any one point become larger than the existing frictional force at that point, rupture is initiated. The release of stress at one point increases stress at the next point and, as a result, rupture progresses along a certain length of the fault, depending upon the magnitude of the energy released. As the rupture advances along the fault, energy is released and propagates away from the fault in the form of p-waves (longitudinal waves) and S-waves (shear waves). P-waves are longitudinal, meaning that particles hit by this wave oscillate back and forth with respect to their equilibrium position in the direction of propagation. S-waves are transverse, meaning that particle motion is in a plane perpendicular to the direction of propagation. For convenience, shear wave motion is split into a horizontal component (SH) and a vertical component (SV). Within a distance of about 80 km from source, body waves are the most important carriers of energy.[12] The mechanism of faulting controls the relative proportion of wave types generated. In general, a strike slip fault generates more energy in the form of SH waves and a dip-slip fault generates more energy in the form of p and SV waves.[12,42] The horizontal components of accelerations of interest to Engineers, in the near field, result mainly from SH-waves, whereas the vertical acceleration components are caused primarily by p and SV waves.

Due to the fact that shear modules of the earth's crust decreases as the distance to bedrock level of an overburden decreases, the waves having shorter wave lengths are almost reflected to vertical path as

they approach the bedrock level of an overburden, as shown in fig. 4.1. Therefore, one could conclude that, in cases where soil deposits have essentially horizontal boundaries and extend to infinity in horizontal directions, one-dimensional models, as shown in fig. 4.2, are often sufficient for evaluation of effect of ground conditions on ground response.

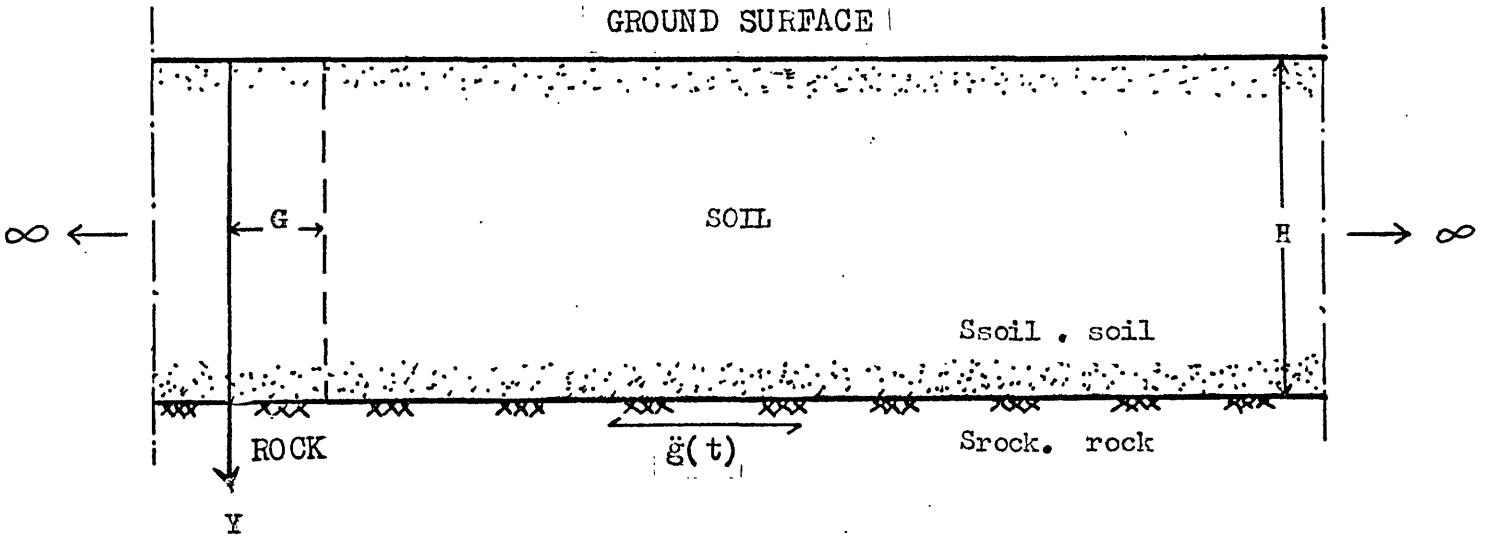
The second type of seismic waves are surface waves, which propagate along the surface. These waves are of two types: Love-waves and Rayligh-waves. Love-waves have no vertical or longitudinal components; they have a particle motion which agrees with SH-waves, i.e. transverse horizontal. Rayligh waves have particle motion, which is elliptic, with the plane of the ellipse vertical lying in the plane of propagation (the particles are displaced vertically and in the direction of propagation with no transverse motion). The particles' motion in the ellipse describe retrograde elliptical orbits. In the near field, the region of interest to engineers, surface waves do not carry much energy, it is only at large distances (greater than 80 km. from the fault or 5X focal depth), that they become the most important carriers of energy, especially low frequency waves which alternate more rapidly due to the presence of damping effects.

However, in shallow earthquakes, there are cases when a significant amount of energy is trapped in the overburden as surface waves, which could significantly contribute to ground motion in the near field. In such cases, the response can be calculated by means of transfer functions.[42]



TRANSMISSION PATH OF BODY WAVES FROM AN EARTHQUAKE

FIG. 4.1



$$RAD = \frac{Ssoil.\rho soil}{Srock.\rho rock}$$

RESPONSE OF HYSTERETIC DEPOSITS WITH RADIATION.

SCHEMATIC SOIL PROFILE FOR SITE

FIG. 4 .2

4.3. THEORY

4.3.1. FORMULATION OF THE MATHEMATICAL MODEL

The developed theory considers response due to vertical shear waves through a semi-infinite*** overburden of hysteretic nature underlain by a half-space. The overburden was considered to be homogenous and iso tropic with depth to half-space "H" shear modulus "G" and mass density "P" and hysteretic damping ratio "ζ". The half space is characterized by shear modulus "G" and mass density "P". Determination of all these parameters under seismic loading conditions is discussed in chapter 5.

4.3.2. PROPAGATION OF VERTICAL SHEAR WAVES IN ONE DIMENSIONAL SYSTEM

The differential equation governing the motion of the uniform deposit excited by vertically-travelling, shear waves is: (see appendix C)

$$\frac{\delta^2 u_{abs}}{\delta t^2}(y,t) = S_s^2 \cdot \frac{\delta^2 u_{abs}}{\delta y^2}(y,t) + C \frac{\delta^3 u_{abs}}{\delta t \, \delta y^2}(y,t) \qquad (4.1)$$

where

$$S_s^2 = \frac{G_s}{\rho_s} \qquad (4.2)$$

$$C = \frac{C1}{\rho_s} \qquad (4.3)$$

*** A horizontal overburden having a constant finite thickness and extending to infinite in a horizontal direction is called a "SEMI-INFINITE" overburden.

ρ_s = mass density of the layer

G_s = shear modulus of the layer

C1 = coefficient of viscosity in shear of the layer

$u_{abs}(y,t)$ = absolute displacement at a depth "y" at time "t".

4.3.3. TRANSMITING BOUNDARY CONDITION

The mathematical equation governing the strain at the bedrock level of the overburden is as follows:

$$\text{RAD.}\ \frac{\delta u_{abs}}{\delta y}(y,t) = \frac{1}{S_s}\left[2\dot{g}_o(t) - \dot{u}_{abs}(y,t)\right]\Bigg|_{y=H} \qquad (4.4)$$

where

$$\text{RAD} = \frac{S_s \cdot \rho_s}{S_r \cdot \rho_r} \qquad (4.5)$$

S_s = shear wave velocity of the layer.

S_r = " " " " " half-space.

ρ_s = mass density of the layer.

ρ_r = mass density of the half-space.

$\dot{g}_o(t)$ = horizontal base velocity at time "t" from t=0 position.

$u_{abs}(y,t)$ = absolute displacement at a depth "y" at time "t".

$\dot{u}_{abs}(y,t)$ = absolute velocity at a depth "y" at time "t".

The proof of equation (4.4) is given in appendix D

The surface is free from stresses:

$$\left.\frac{\delta u_{abs}\,(y,t)}{\delta y}\right|_{y=o} = 0 \qquad (4.6)$$

Assuming the motion does not start from rest

$$u_{abs}(y,0) \neq 0 \qquad (4.7)$$

$$\dot{u}_{abs}(y,0) \neq 0 \qquad (4.8)$$

4.4 SOLUTION OF THE GOVERNING DIFFERENTIAL EQUATION

To solve equation (4.1) $u_{abs}(y,t)$ is replaced by a new dependent variable

$$\bar{u}(y,p) = \int_o^\infty \bar{e}^{pt}.u_{abs}(y,t).dt \qquad (4.9)$$

equation (4.1) becomes

$$\frac{d^2\bar{u}}{dy^2}\,(y,p) - \lambda^2\bar{u}(y,p) = -\frac{p}{s^2 + Cp}\,u(y,0) - \frac{1}{s^2 + Cp}\,\dot{u}(y,0) \qquad (4.10)$$

where:

$$\lambda^2 = \frac{p^2}{s_s^2 + CP} \tag{4.11}$$

solution of equation (4.10) is as follows:

$$\bar{u}(y,p) = A\cosh \lambda y + B\sinh \lambda y + \frac{1}{p} u(y,0) + \frac{1}{p^2} \dot{u}(y,0) \tag{4.12}$$

where A and B are constants to be determined from boundary conditions (4.4) and (4.6)

4.4.1. INTRODUCTION OF BOUNDARY CONDITIONS

Boundary condition given by equation (4.6) is introduced first.

$$\frac{\delta \bar{u}}{\delta y}(y,p) = A\lambda \sinh \lambda y + B\lambda \cosh \lambda y \tag{4.13}$$

Boundary condition (4.6) implies at $y = 0$, $\frac{\delta \bar{u}}{\delta y}(y,p) = 0$

therefore

$$B = 0 \tag{4.14}$$

combining (4.12) and 4.14)

$$\bar{u}(y,p) = A\cosh \lambda y + \frac{1}{p} u(y,0) + \frac{1}{p^2} \dot{u}(y,0) \tag{4.15}$$

Imposing boundary condition (4.4) on (4.15)

$$A = \frac{2\bar{\dot{g}}_o(P)}{(RAD \cdot \lambda \cdot S_s \cdot \sinh \lambda H + P \cdot \cosh \lambda H)} -$$

$$- \frac{\dot{u}(H,0)}{P\,(RAD \cdot \lambda \cdot S_s \cdot \sinh \lambda H + P \cosh \lambda H)} \qquad (4.16)$$

where

$$\bar{\dot{g}}_o(P) = \int_o^\infty \dot{g}(t) \cdot \quad e^{-pt} dt \qquad (4.17)$$

combining (4.15) and (4.16) and calling $\underline{S_s = S}$

$$\bar{u}(y,P) = \frac{2\cosh \lambda y}{P\left(\frac{RAD \cdot S}{\sqrt{S^2 + CP}} \sinh \lambda H + \cosh \lambda H\right)} \cdot \bar{\dot{g}}_o(P) -$$

$$- \frac{\cosh \lambda y}{P^2\left(\frac{RAD \cdot S}{\sqrt{S^2 + CP}} \sinh \lambda H + \cosh \lambda H\right)} \dot{u}(H,0) +$$

$$+ \frac{1}{P} u(y,0) + \frac{1}{P^2} \dot{u}(y,0) \qquad (4.18)$$

4.4.1.1. INITIAL CONDITIONS

For computation of complete response of the overburden, a knowledge of initial conditions of the system is required. The true value of these initial conditions is not known. In order to minimize the resulting error in response calculations, zero initial conditions were assumed. For any other specified initial conditions, the free vibration response given by equation 4.61 must be added to 4.59, and its first and second derivatives to 4.64 and 4.66, respectively.

Assuming the motion starts from rest, 4.18 becomes

$$\frac{\bar{u}(y,p)}{2} = \frac{\cosh \lambda y}{p\left(\frac{RAD.S}{\sqrt{S^2 + CP}} \sinh \lambda H + \cosh \lambda H\right)} \cdot \bar{g}_o(p) \qquad (4.19)$$

INVERSION OF EQUATION (4.19)

To invert equation (4.19) use of convolution theorem was made

$$\mathcal{L}^{-1}\left[\bar{f}(p).\bar{g}(p)\right] = \int_o^t G(\tau)F(t-\tau)d\tau \qquad (4.20)$$

where $G(t) = \mathcal{L}^{-1}\left[\bar{g}(p)\right]$ & $F(t) = \mathcal{L}^{-1}\left[\bar{f}(p)\right]$

To use Convolution Theorem we call:

$$G(t) = \mathcal{L}^{-1}\left[\bar{\dot{g}}_0(P)\right] \tag{4.21}$$

$$F(t) = \mathcal{L}^{-1}\left\{\frac{1}{P}\left[\frac{\cosh \lambda y}{\frac{RAD.S}{\sqrt{S^2 + CP}} \sinh \lambda H + \cosh \lambda H}\right]\right\} \tag{4.22}$$

The legitimate use of the convolution theorem requires the absolute existence of the Laplace integrals of the function G(t) and F(t). This is shown in appendix E .

Therefore, the problem now reduces to inversion of (4.21) and (4.22).

From (4.17) the value of (4.21) is as follows

$$G(t) = \dot{g}_0(t) \tag{4.23}$$

To evaluate (4.22) we make use of Fourier-Mellin inversion integral.

$$F(t) = \frac{1}{2\pi\lambda} \cdot \int_{\gamma - \lambda\infty}^{\gamma + \lambda\infty} \frac{e^{Mt}}{M}\left[\frac{\cosh Ry}{\frac{Rad.S}{\sqrt{S^2+CM}} \sinh RH + \cosh RH}\right] dM \tag{4.24}$$

where from (4.11)

$$R^2 = \frac{M^2}{S^2 + CM} \tag{4.25}$$

4.4.1.2. EVALUATION OF THE INVERSION INTEGRAL (4.24)

The integrand of (4.24) is a single-valued* function of M with a simple pole at M = 0 and simple poles obtained from the roots of the transcendental equation:

$$\frac{RAD.S}{\sqrt{S^2 + CM}} \sinh RH + \cosh RH = 0 \qquad (4.26)$$

where from (5.25)

$$R = \frac{M}{\sqrt{S^2 + CM}} \qquad (4.27)$$

Remembering the poles "M_n" n = 1,2,3 ... are the roots of the above equation

RESIDUE AT M = 0

Evaluating the residue at M = 0 we have:

$$\left[\frac{e^{Mt}.\cosh Ry}{\frac{RAD.S}{\sqrt{S^2 + CM}} . \sinh RH + \cosh RH} \right]_{M=0} = 1 \qquad (4.28)$$

---

* since

$$\left[\frac{\cosh Ry}{\frac{RAD.S}{S^2 + CM} \sinh RH + \cosh RH} \right] =$$

$$= \frac{1 + \frac{y^2}{2!}.\frac{M^2}{(S^2 + CM)} + \frac{y^4}{4!}.\frac{M^4}{(S^2 + CM)^2} + \ldots.}{\frac{RAD.S}{\sqrt{S^2 + CM}} \left[\frac{M.H}{\sqrt{S^2 + CM}} + \frac{1}{3!} . \left(\frac{MH}{\sqrt{S^2 + CM}} \right)^3 + \ldots \right] + \left[1 + \frac{1}{2!}. \frac{M^2H^2}{(S^2 + CM)} + \ldots \right]}$$

and thus contains only integral powers of M

since:

$\sinh(0) = 0$ & $\cosh(0) = 1$ and from (4.25)

$$R^2 = \frac{M^2}{S^2 + CM} \tag{4.29}$$

4.4.1.3. SUM OF ALL THE RESIDUES

Thus, using Fig*4.3, it follows by the theory of residues, that the line integral in (5.19) equals $2\pi\dot{\lambda}$ times the sum of the residues at the poles of its integrand, i.e.

$$F(t) = \sum_{n=1}^{\infty} Res_n \tag{4.30}$$

or

$$F(t) = 1 + \sum_{n=1}^{\infty} \left[\frac{e^{Mt}}{M} \cdot \frac{\cosh Ry}{\frac{d}{dM}\left(\frac{RAD.S}{\sqrt{S^2 + CM}} \cdot \sinh RH + \cosh RH \right)} \right]_{M=M_n} \tag{4.31}$$

where from (4.27)

$$R = \frac{M}{\sqrt{S^2 + CM}} \tag{4.32}$$

---

* Mathematical proof of why contour of integration is in the form shown by Fig4.3 is given in appendix .

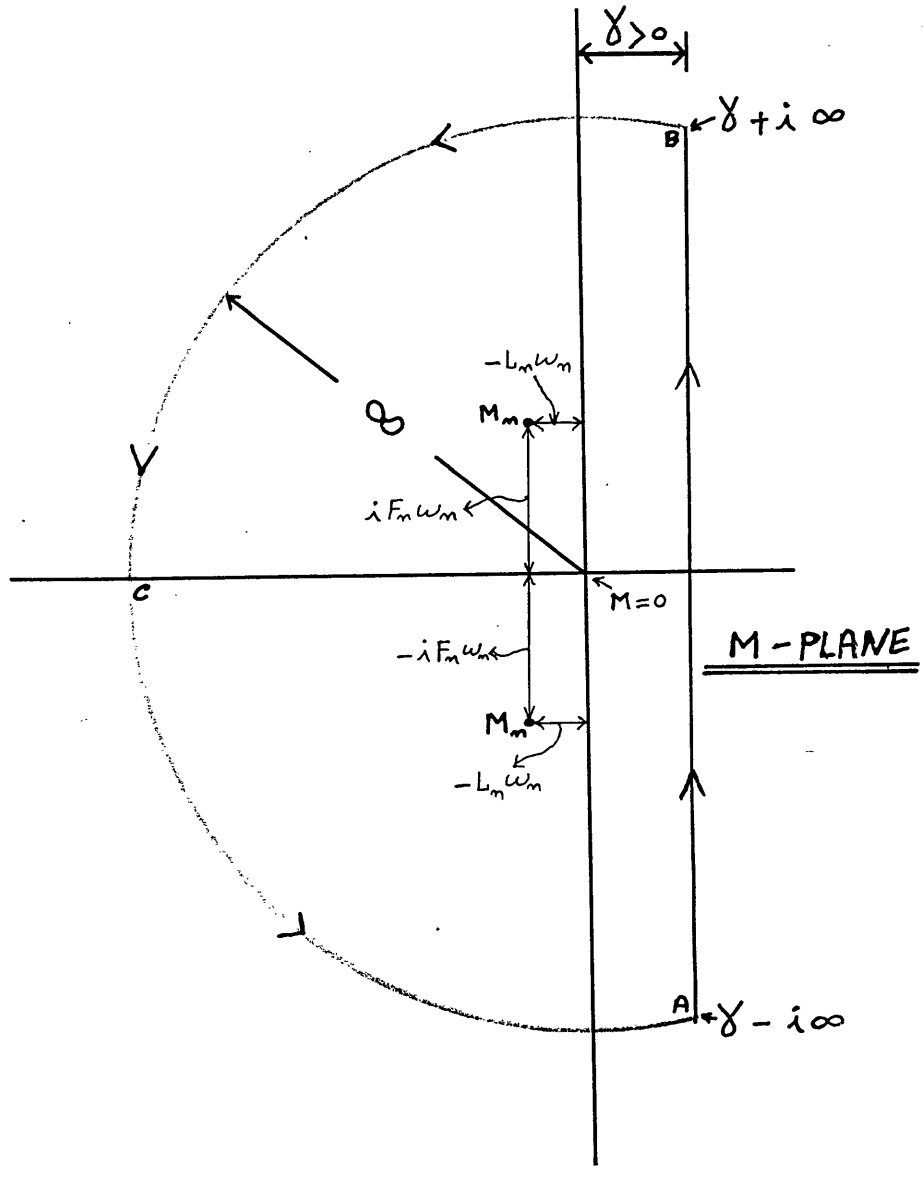


FIG. 4.3 CONTOUR OF INTEGRATION

Equation(4.31) is insoluble. Over four years ago, Professor N.N. Ambraseys attempted to solve this problem and concluded that "For real deposits, the analytical solution to this problem is virtually out of the question."* [6] This is because the transcendental equation (4.26) cannot be solved analytically.

However, a standard procedure is to truncate the series given by (4.31) and consider only a finite number of terms. [15] Physically speaking, this is justified due to the fact that strong motion recordings are not sensitive to wave components with frequencies higher than a fixed value (10 c.p.s in most cases) [13]; therefore, the recordings obtained from these instruments are weak in high frequency components.

The use of the above recordings in design of structures, dams, etc. is justified on the basis that missing high frequency components (e.g. greater than 10 c.p.s) have very little influence on the response of these structures. Therefore, the actual number of modes to be calculated for practical purposes do not exceed 5 or 6. [15]

In discrete form (4.31) becomes:

$$F(t) \doteq 1 + \sum_{n=1}^{N} \left[\frac{e^{Mt}}{M} \cdot \frac{\cosh Ry}{\frac{d}{dM}\left(\frac{RAD.S}{S^2+CM} \cdot \sinh RH + \cosh RH\right)} \right]_{M=M_n} \qquad (4.33)$$

---

* See next page.

FIFTH WORLD CONFERENCE ON EARTHQUAKE ENGINEERING
ROME 1973

DYNAMICS AND RESPONSE OF FOUNDATION MATERIALS IN EPICENTRAL REGIONS OF STRONG EARTHQUAKES

Prof. N. N. AMBRASEYS

6. Let us now discuss the problem of the application of a ground motion input to an engineering structure or to soil deposits.

So far, most studies of the response of soil deposits and structures to strong ground motions consider an infinitely rigid bedrock which supplies the motion. Thus, the input motion is applied at the foundation of an arch or earth dam, at the basement level of a building or at bedrock level for an overburden. It is not difficult to see that this type of input implies a "powerful engine" supplying an ever increasing amount of energy onto a structure that has to absorb it internally. This invariably results in an over-estimation of stresses or displacements in the "insulated" structure. In reality the structure or the overburden interferes with the oncoming wave trains and refracts part of the energy back into the source.

For real deposits the analytical solution to this problem is virtually out of the question. Numerical models have been devised, however, which can take into account radiation effects but so far results from this type of study are limited, (21,25,31).

4.4.1.4. ROOTS OF THE TRANSCENDENTAL EQUATION (4.26)

Values of "M_n" n=1,2,....N are the roots of the transcendental equation (5.21) which, after rearrangement, can be written as:

$$\coth RH = -\frac{RAD}{\sqrt{1 + \frac{C}{S^2}.M}} \qquad (4.34)$$

where from (4.32)

$$R = \frac{M}{\sqrt{S^2 + CM}}$$

After substituting value of "C" from (4.3) in (4.34) and calling $\beta = \frac{C1}{S^2.\rho}$ equation (4.34) becomes

$$\coth RH = -\frac{RAD}{\sqrt{1 + \beta M}} \qquad (4.35)$$

The general solution of equation (4.35) is very complicated indeed, if not impossible analytically, because of its transcendental nature. However, "during earthquakes of moderate or small intensities, the subsoil may behave linearly with very small damping"[59] and for typical strains induced in the overburden equivalent hysteretic damping ratio " ξ_n " is typically $\ll$ o.o1~o.1o[61] (see chapter 5)

The constant " β " defined above can be written as:

$$\beta = \frac{C1}{S^2.\rho} = \frac{2.S^2.\rho.\xi_n/\omega_n}{S^2.\rho} = \frac{2\,\xi_n}{\omega_n} \qquad (5.31)$$

For relatively small values of ξ_n, as met in most layer problems, "β" has a small value. Hence the only alternative is to exploit this fact and solve (4.35) for the case where

$$\left| \beta . M_N \right| \ll 1 \qquad (4.36)$$

The advantage of this method lies in the fact that the right hand side of equation (4.35) can be written as

$$\text{cothRH} = - \text{RAD} \left[1 + 0(\beta \, M_N) \right] \qquad (4.37)$$

To solve (4.37) the asymptotic approximation (which is the leading term) only is used.[29] As shown in section 4.10, the error estimated for frequencies and damping has of engineering interest is extremely small. Therefore equation (4.37) becomes:

$$\text{cothRH} \doteq - \text{RAD} \qquad (4.38)$$

General solution of (4.38) is given in appendix G. The final results are only mentioned here, which are:

$$M_n = \omega_n(- L_n \pm \lambda F_n) \qquad (4.39)$$

where

$$L_n = \xi_n + \frac{K}{\alpha_m} E_n - \frac{\xi_n K^2}{\alpha_m^2} - D_n \qquad (4.40)$$

$$F_n = \frac{K}{a_m} D_n + E_n - \frac{2\,\xi_m K}{a_n} \tag{4.41}$$

$$K = \frac{1}{2} \log_e \frac{1 + RAD}{1 - RAD} \tag{4.42}$$

$$a_n = n\Pi - \frac{\Pi}{2} \text{ where } n = 1,2,3,4,\ldots N \tag{4.43}$$

$$\omega_n = a_n \cdot \frac{S}{H} \tag{4.44}$$

$$\xi_n = \frac{C1 \cdot \omega_n}{2G} \tag{4.45}$$

$$E_n = \left[\frac{d_n + \sqrt{d_n^2 + f_n^2}}{2} \right]^{\frac{1}{2}} \tag{4.46}$$

$$D_n = \left[\frac{-d_n + \sqrt{d_n^2 + f_n^2}}{2} \right]^{\frac{1}{2}} \tag{4.47}$$

$$d_n = 1 - \xi_n^2 + \frac{\xi_n^2 K^2}{a_n} \tag{4.48}$$

$$f_n = \frac{2\,\xi_n^2 K}{a_n} \tag{4.49}$$

We need next the term

$$M.\frac{d}{dM}\left(\frac{RAD.S}{\sqrt{S^2 + CM}}.\sinh RH + \cosh RH\right) = \qquad (4.50)$$

$$= \frac{RAD.S.H.(2M - CR^2)}{2.(S^2 + CM)}\cosh RH +$$

$$+ \frac{S.(H.S - C.RAD).R}{2.(S^2 + CM)}\sinh RH + \frac{R.H}{2}\sinh RH \qquad (4.51)$$

The value of (4.51) at $M_n = \omega_n(-L_n \pm \lambda F_n)$ is thus evaluated to be

$$A_n \pm \lambda B_n$$

where:

$$A_n = \frac{RAD.a_n}{(1 - 2\,\xi_n L_n)^2 + 4\,\xi_n^2 F_n^2}\sinh K.\sin a_n \;X$$

$$X\left[(F_n + \frac{2\,\xi_n K}{a_n})(1 - 2\,\xi_n L_n) - 2\,\xi_n F_n(-L_n - \frac{\xi_n K^2}{a_n^2} + \xi_n)\right] -$$

$$-\frac{(1 - \frac{2\,\xi_n}{a_n}.RAD)(2K\,\xi_n F_n + a_n(1 - 2\,\xi_n L_n))}{2((1 - 2\,\xi_n L_n)^2 + 4\,\xi_n^2 F_n^2)}\sin a_n.\cosh K -$$

$$- \frac{a_n}{2} \sin a_n \cdot \cosh K \qquad (4.52)$$

and

$$B_n = - \frac{RAD.a_n}{(1 - 2\,\varepsilon_n L_n)^2 + 4\,\varepsilon_n^2 F_n^2} \sinh K.\sin a_n X$$

$$X \left[(- L_n - \frac{\varepsilon_n K^2}{a_n^2} + \varepsilon_n)(1 - 2\,\varepsilon_n L_n) + 2\,\varepsilon_n F_n (F_n + \frac{2\,\varepsilon_m K}{a_n}) \right] +$$

$$+ \frac{(1 - \frac{2\,\varepsilon_m}{a_n} RAD)(2\,\varepsilon_n F_n a_n - K.(1 - 2\,\varepsilon_n L_n))}{2((1 - 2\,\varepsilon_n L_n)^2 + 4\,\varepsilon_n^2 F_n^2)} \sin a_n.\cosh K -$$

$$- \frac{K}{2} \sin a_n.\cosh K \qquad (4.53)$$

Now equation (4.33) becomes:

$$F(t) = 1 + \sum_{n=1}^{N} \frac{e^{\omega_n(- L_n + \lambda F_n)t} \cosh(-K + \lambda a_n)^{y/H}}{(A_n + \lambda B_n)} +$$

$$+ \sum_{n=1}^{N} \frac{e^{\omega_n(- L_n - \lambda F_n)t} \cosh(-K - \lambda a_n)^{y/H}}{(A_n - \lambda B_n)} \qquad (4.54)$$

After some algebraic manipulations

$$F(t) = 1 + \sum_{n=1}^{N} C_{nc} . e^{-\omega_n L_n t} . \cos \omega_n F_n t + \sum_{n=1}^{N} C_{ns} . e^{-\omega_n L_n t} \sin \omega_n F_n t \quad (4.55)$$

where

$$C_{nc} = \frac{2(A_n . \cosh K\frac{y}{H} . \cos a_n \frac{y}{H} - B_n . \sinh K\frac{y}{H} . \sin a_n \frac{y}{H})}{(A_n^2 + B_n^2)} \quad (4.56)$$

$$C_{ns} = \frac{2(A_n . \sinh K\frac{y}{H} . \sin a_n \frac{y}{H} + B_n \cosh K\frac{y}{H} . \cos a_n \frac{y}{H})}{(A_n^2 + B_n^2)} \quad (4.57)$$

4.4.1.5. ABSOLUTE DISPLACEMENT OF THE SYSTEM

The final solution of (4.19), in terms of absolute displacement at any time "t" and any point "y" in the overburden, is obtained by combining (4.23) and (4.55) by means of convolution theorem of (4.20). This is legitimate because, in appendix E, it is shown that the absolute values of the Laplace integrals of G(t) and F(t) given by (4.23) and (4.55) exist ; therefore, the final solution given by

$$u(y,t) = \int_0^t G(\tau) . F(t-\tau) d\tau \quad (4.58)$$

exists. A simple proof of this has been given by [19]

Notice here that $g_o(t)$ and $\dot{g}_o(t)$ are the half-space displacements and velocities if this surface were free.

$$u_{abs}(y,t) = g_o(t) + \sum_{n=1}^{N} C_{nc} \cdot \int_o^t \dot{g}_o(\tau).e^{-\omega_n L_n(t-\tau)} \cos \omega_n F_n(t-\tau) d\tau +$$

$$+ \sum_{n=1}^{N} C_{ns} \cdot \int_o^t \dot{g}_o(\tau).e^{-\omega_n L_n(t-\tau)} \sin \omega_n F_n(t-\tau) d\tau \quad (4.59)$$

where: ω_n is the undamped frequency for the nth mode. Relative displacement at any point "y" and any time "t" is given by:

$$u_{rel}(y,t) = u_{abs}(y,t) - g_o(t) \quad (4.60)$$

4.4.1.6 FREE VIBRATION RESPONSE

In deriving equation (4.59), it was assumed that the system was at rest at t = 0. For any other specified initial conditions, the free vibration response given by (4.61) must be added to (4.59) and its first and second derivatives to 4.59 and 4.68.

$$u_{abs}(y,t) = u(y,0) + \frac{RAD.H}{S} .\dot{u}(H,0) + (\dot{u}(y,0) - u(H,0))t +$$

$$+ \dot{u}(H,0) \sum_{n=1}^{n=N} \frac{2.\cos\omega_n F_n t}{\omega_n(L_n^2 + F_n^2)(A_n^2 + B_n^2)} \times e^{-\omega_n L_n t} \times$$

$$X(P_n.\cosh K\tfrac{y}{H}.\cos a_n\tfrac{y}{H} + Q_n \sinh K\tfrac{y}{H}.\sin a_n\tfrac{y}{H}) +$$

$$+ \dot{u}(H,0) \sum_{n=1}^{n=N} \frac{2.\sin\omega_n F_n t}{\omega_n(L_n^2 + F_n^2)(A_n^2 + B_n^2)} \times e^{-\omega_n L_n t} \times$$

$$X(P_n.\sinh K\tfrac{y}{H}.\sin a_n\tfrac{y}{H} - Q_n \cosh K\tfrac{y}{H}.\cos a_n\tfrac{y}{H}) \qquad (4.61)$$

where:

$$P_n = L_n A_n + F_n B_n \qquad (4.62) \qquad Q_n = F_n A_n - L_n B_n \qquad (4.63)$$

The rest of the symbols are defined previously.

4.4.1.7. ABSOLUTE VELOCITY OF THE SYSTEM.

Absolute velocity at any point "y" and at any time "t" is obtained be differentiating (4.59) w.r.t. "t"

$$\dot{u}_{abs}(y,t) = \dot{g}_o(t) + \sum_{n=1}^{n=N} C_{nc}.S_{vnc}(t) +$$

$$+ \sum_{n=1}^{n=N} C_{ns}.S_{vns}(t) \qquad (4.64)$$

where:

$$S_{vnc}(t) = -\omega_n L_n . S_{dnc}(t) - \omega_n F_n S_{dns}(t) + \dot{g}_o(t) \qquad (4.65)$$

$$S_{vns}(t) = -\omega_n . L_n . S_{dns}(t) + \omega_n F_n S_{dnc}(t) \qquad (4.66)$$

$$S_{dnc}(t) = \int_o^t \dot{g}_o(\tau) . e^{-\omega_n L_n (t-\tau)} \cos \omega_n F_n (t-\tau) d\tau \qquad (4.66)$$

$$S_{dns}(t) = \int_o^t \dot{g}_o(\tau) . e^{-\omega_n L_n (t-\tau)} \sin \omega_n F_n (t-\tau) d\tau \qquad (4.67)$$

$$\dot{} = \frac{d}{dt}$$

4.4.1.8. ABSOLUTE ACCELERATION OF THE SYSTEM.

Absolute acceleration at any point "y" and at any time "t" is obtained by differentiating (4.64) w.r.t. "t"

$$\ddot{u}_{abs}(y,t) = \ddot{g}_o(t) + \sum_{n=1}^{n=N} C_{nc} . S_{anc}(t) + \sum_{n=1}^{n=N} C_{ns} . S_{ans}(t) \qquad (4.68)$$

where:

$$S_{anc}(t) = \omega_n^2(\Lambda_n^2 - F_n^2).S_{dnc}(t) +$$

$$+ 2\omega_n^2 \Lambda_n.F_n.S_{dns}(t) - \omega_n.\Lambda_n.\dot{g}_o(t) + \ddot{g}_o(t) \qquad (4.69)$$

$$S_{ans}(t) = \omega_n^2(\Lambda_n^2 - F_n^2).S_{dns}(t) -$$

$$- 2\omega_n^2 F_n.\Lambda_n.S_{dnc}(t) + \omega_n.F_n.\dot{g}_o(t) \qquad (4.70)$$

$$\cdot\cdot = \frac{d^2}{dt^2}$$

4.4.2. EVALUATION OF INTEGRALS, $S_{anc}(t)$ AND $S_{dns}(t)$

There are many schemes for numerical evaluation of integrals (4.66) and (4.67). The scheme used is new and it was developed by the author and is an exact way for evaluation of following integrals. From (5.49)

$$S_{dnc}(t) = \int_0^t \dot{g}_o(\tau).e^{-\omega_n \Lambda_n (t-\tau)} \cos\omega_n F_n(t-\tau)d\tau \qquad (4.71)$$

from (5.50)

$$S_{dns}(t) = \int_0^t \dot{g}_o(\tau).e^{-\omega_n L_n(t-\tau)} \sin \omega_n F_n(t-\tau)d\tau \qquad (4.72)$$

The details of the scheme are given in appendix H . A computer program in FORTRAN IV was developed for the above scheme and was tested on CDC 6400 computer of Imperial College. The time taken for approximately 1000 points of $\ddot{g}_o(t)$ distributed at intervals of o.o2 sec.is almost the same when a numerical technique involving Trapezoidal Rule, is used. The developed scheme is an accurate scheme and gives very accurate values of response, whereas the numerical scheme in the same computational time provides only approximate values of response.

4.5. UNDAMPED NATURAL FREQUENCIES OF THE SYSTEM.

The undamped natural frequencies of the overburden " ω_n" in different modes is given by:

$$\omega_n = a_n \cdot \frac{S}{H} \qquad (4.73)$$

where:

$a_n = (2n - 1)\frac{\pi}{2}$ $\quad n = 1,2,3 \ldots.$

S_s = shear wave velocity of the layer

H = thickness of the layer.

$_n$ = the natural frequency of the layer in the "n"th mode (radians per second).

The mode having the lowest frequency is called the first mode or fundamental mode. The second mode is that associated with the second lowest frequency and so on. More energy is required to excite higher modes to appreciable amplitude; higher modes have more nodal points, i.e. points of zero displacement, than lower modes. However, if the frequencies of earthquake wave components having the greatest acceleration are available at frequencies close to the higher mode frequencies, then knowledge of these frequencies becomes essential. In general, earthquakes excite only the lowest mode of the system and a few higher modes (this is shown in section 4.6)

4.6. CONVERGENCE AND NUMERICAL RESULTS.

To evaluate the convergence of the solution developed and the effectiveness of the first few modes of the system to represent the dynamic response, solutions for two cases of interest were evaluated. In the first case, the deposit had a fundamental period of 0.4 seconds (H = 40m, S = 250m/sec), which is very close to the predominant period of the bedrock motion (0.6 seconds, Parkfield-2). Solutions with one, three, six and nine modes were evaluated. The results are shown in figs. 4.4a,b,c,e,f through 4.7a,b,c,d,e,f. There are no numerical results for comparison, but, from the figures, it is obvious that the solution converges to a constant value. It is clear that very few modes, three in this case, are enough accurately to represent the response of the system. In fact, it can be seen that one mode also gives good values for the computed response.

In the second case considered, the deposit has a fundamental period of 2.0 seconds, which is far from the predominant period of the

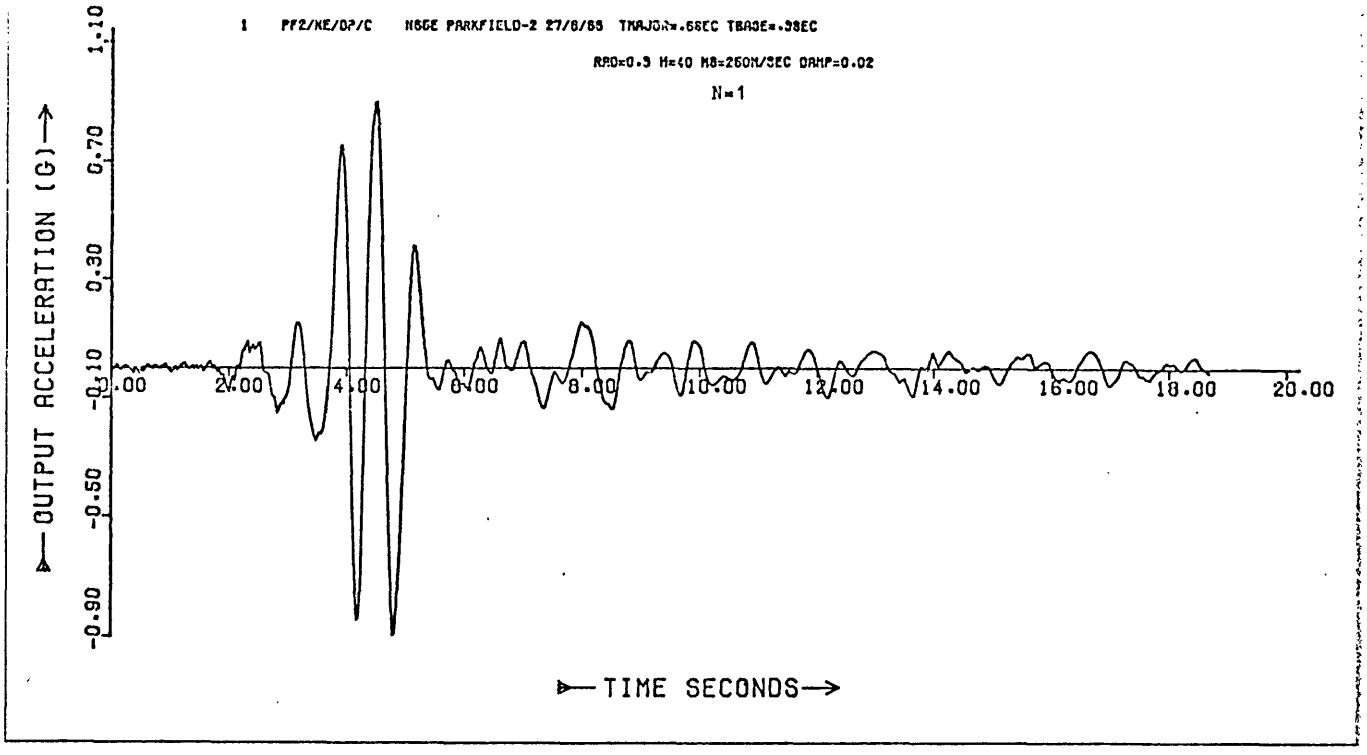


FIG. 4.4a COMPUTED GROUND SURFACE ACCELERATION TIME HISTORY

NUMBER OF MODES INCLUDED = 1

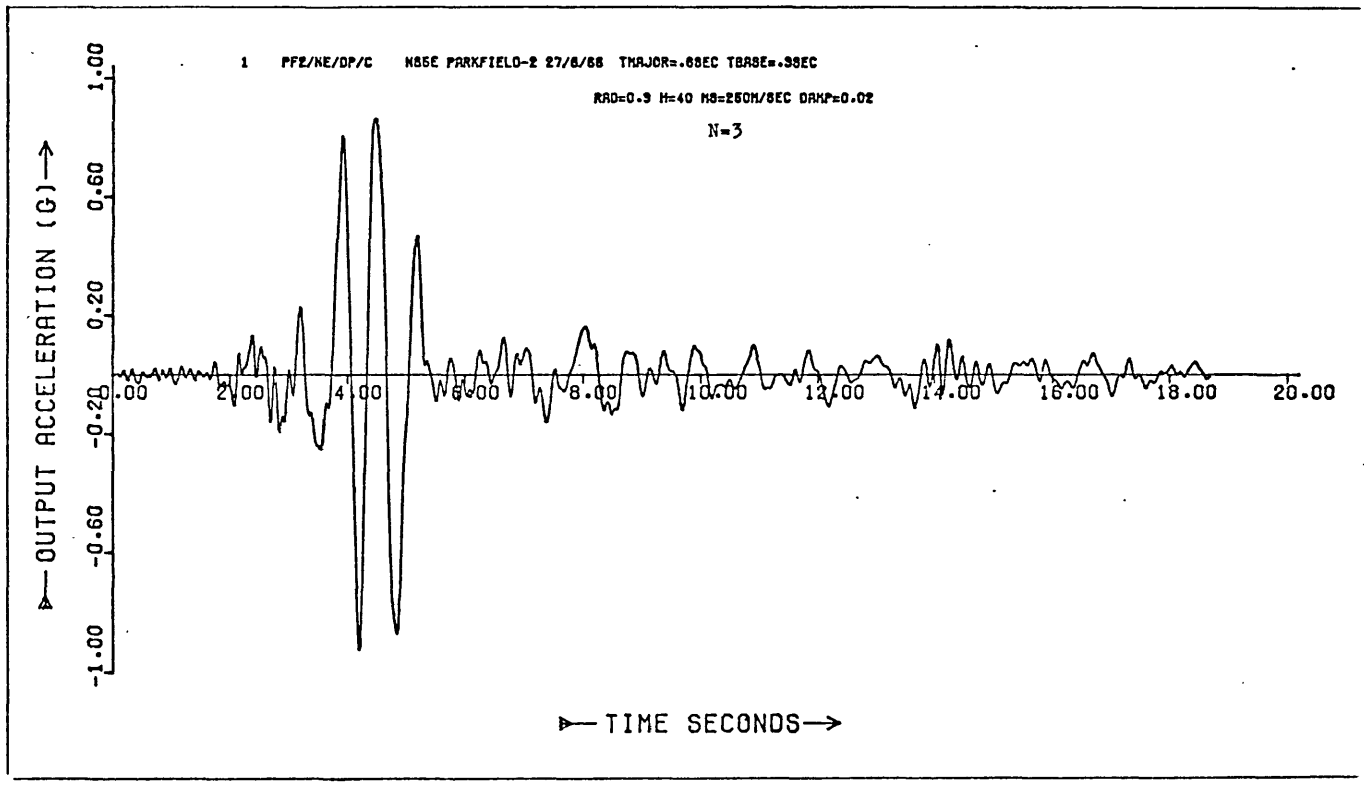


FIG. 4.5a COMPUTED GROUND SURFACE ACCELERATION TIME HISTORY

NUMBER OF MODES INCLUDED = 3

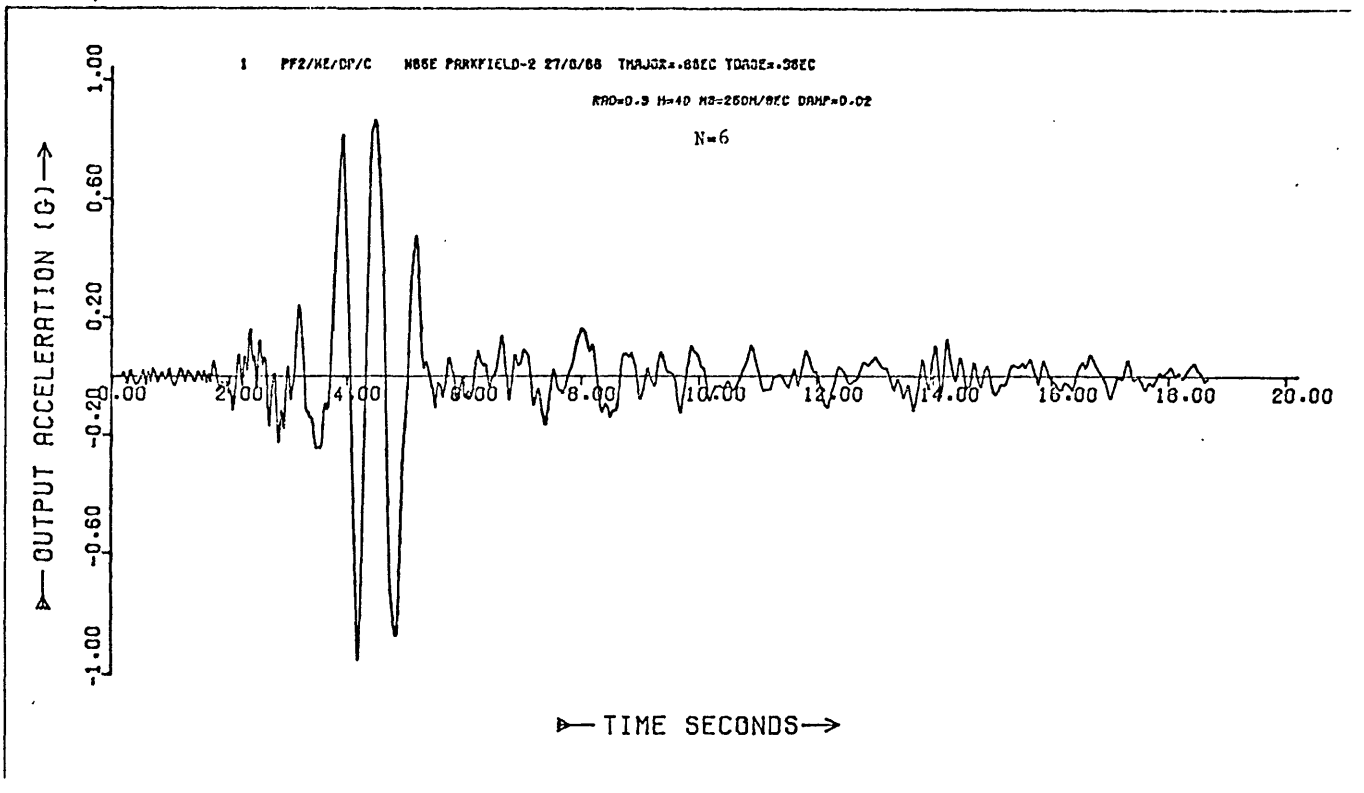


FIG.4.6a COMPUTED GROUND SURFACE ACCELERATION TIME HISTORY

NUMBER OF MODES INCLUDED = 6

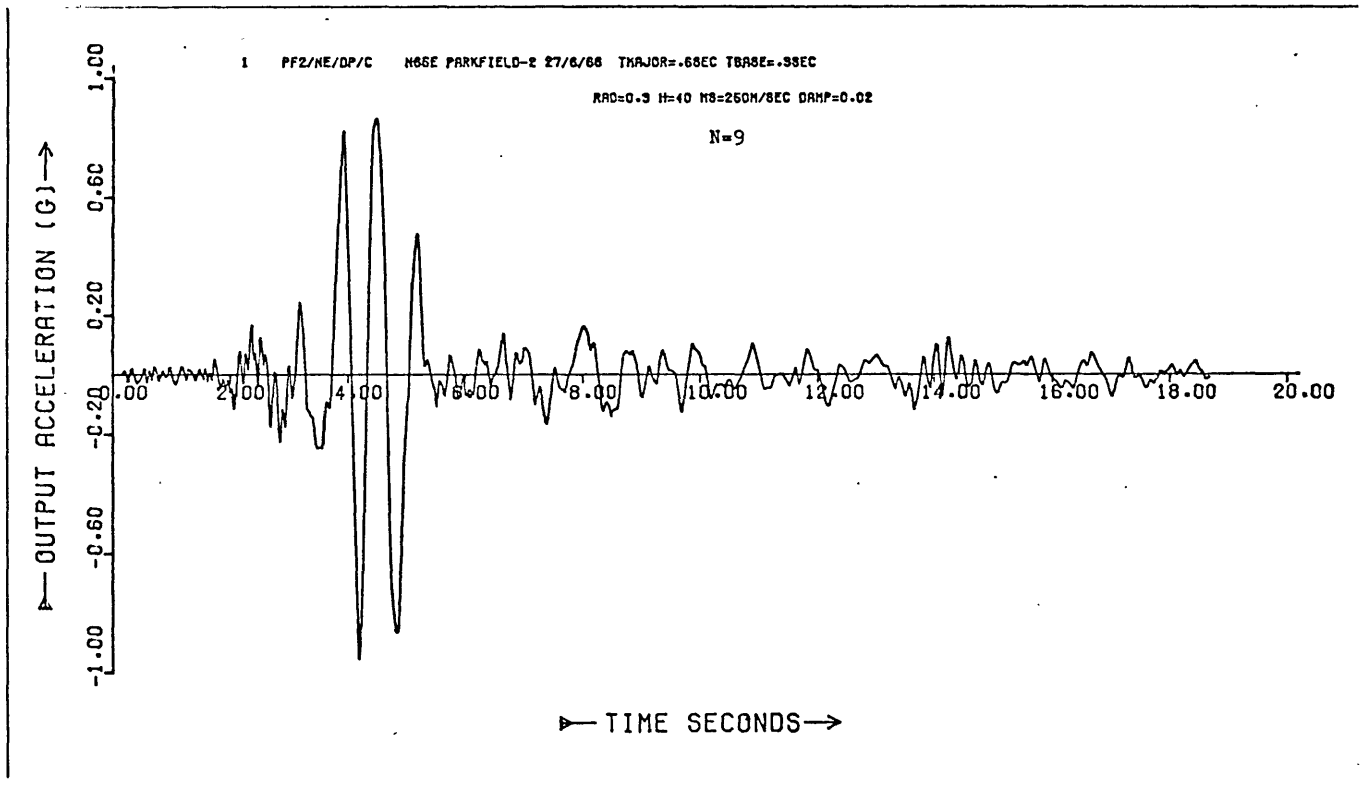


FIG. 4.7a COMPUTED GROUND SURFACE ACCELERATION TIME HISTORY

NUMBER OF MODES INCLUDED = 9

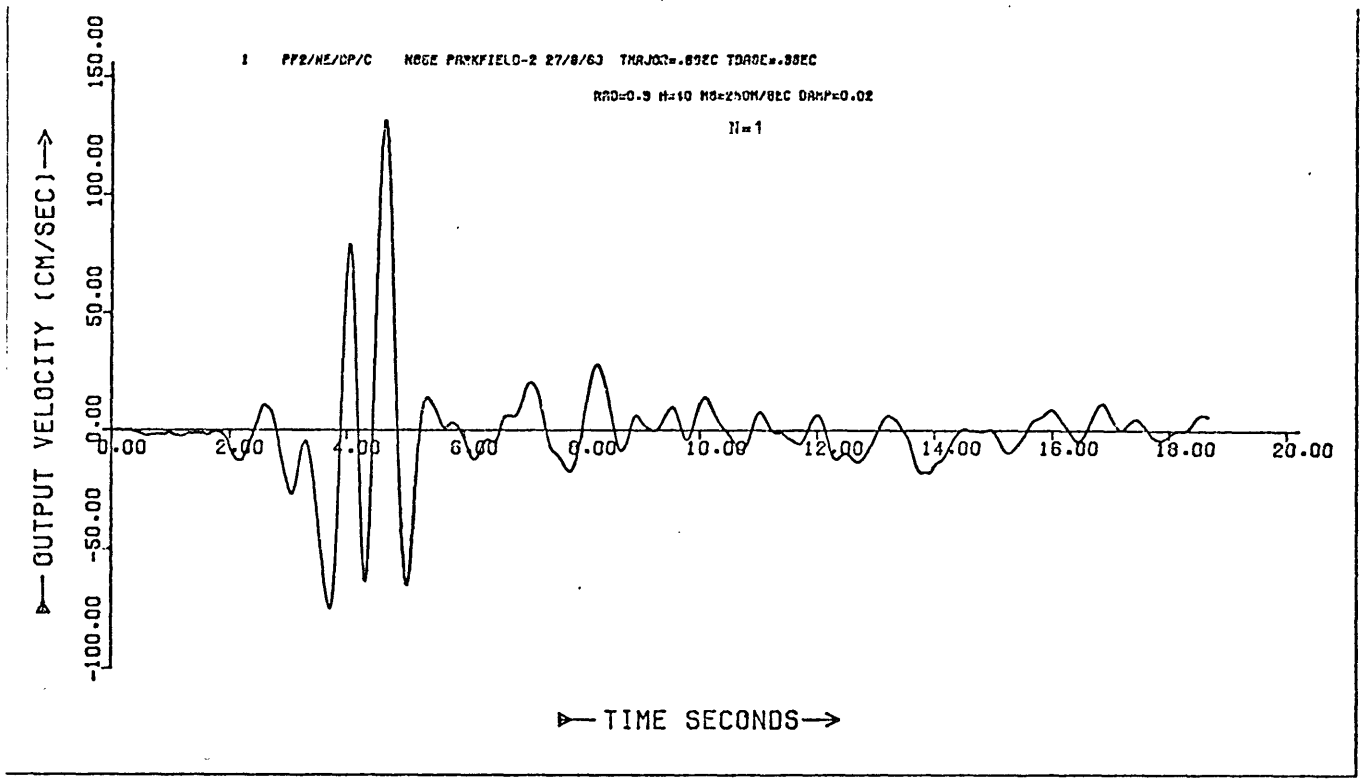


FIG.4.4b COMPUTED GROUND SURFACE VELOCITY TIME HISTORY

NUMBER OF MODES INCLUDED = 1

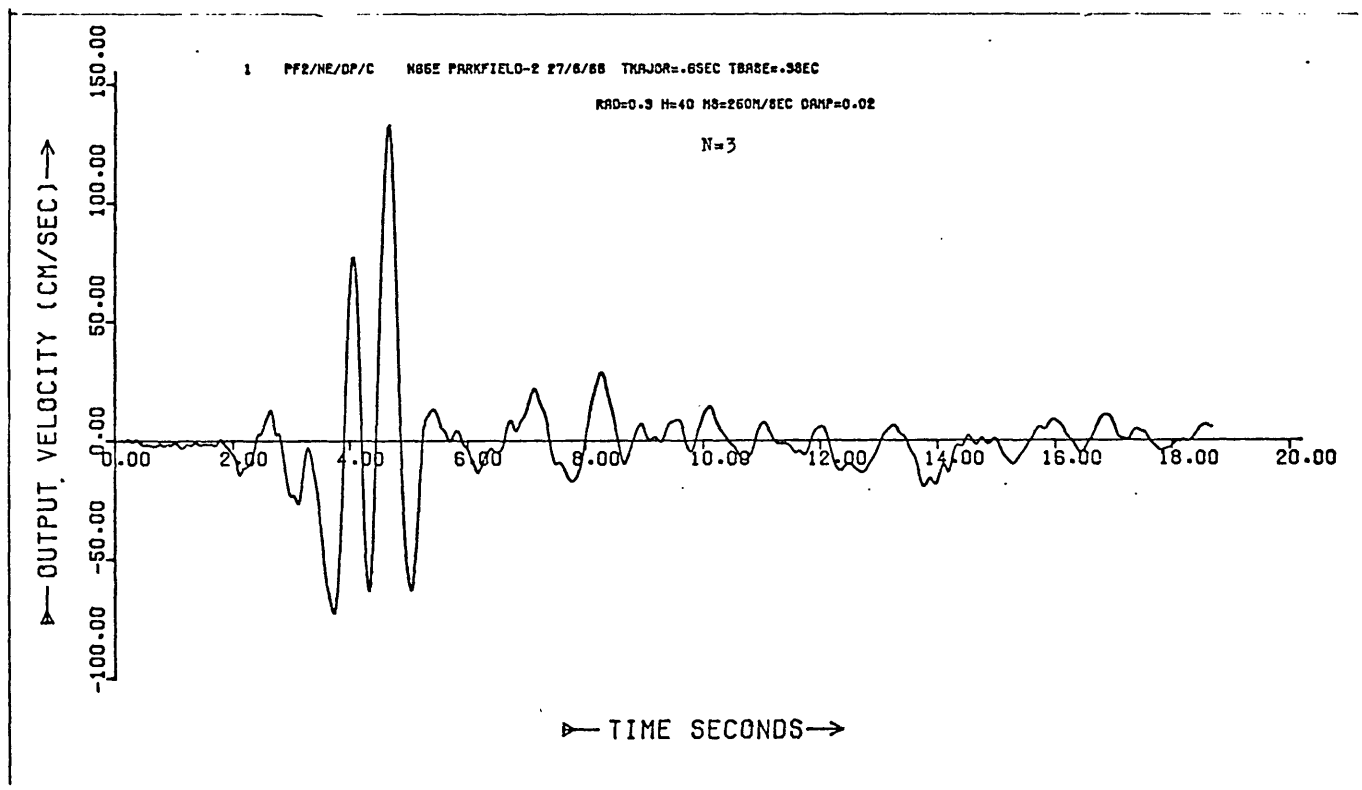


FIG. 4.5bCOMPUTED GROUND SURFACE VELOCITY TIME HISTORY

NUMBER OF MODES INCLUDED = 3

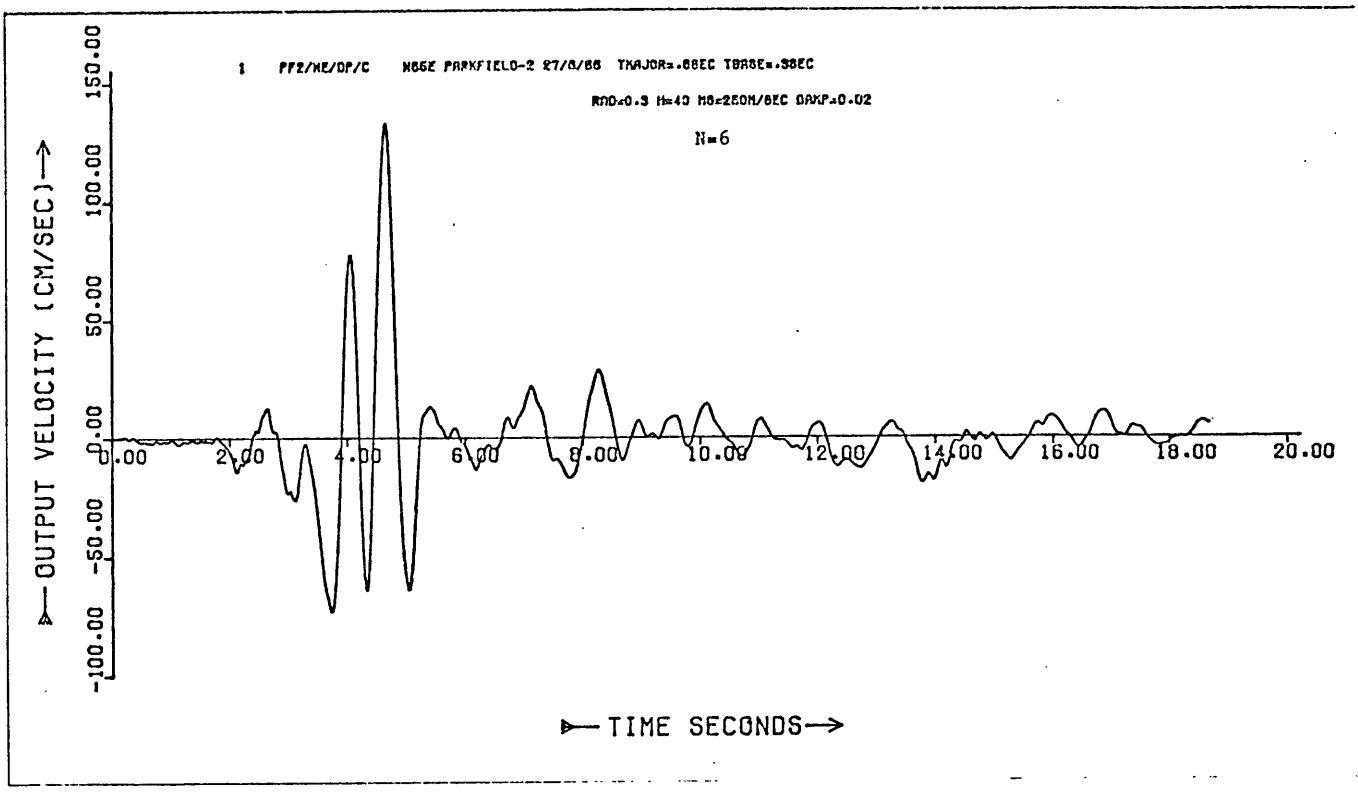


FIG. 4.6b COMPUTED GROUND SURFACE VELOCITY TIME HISTORY

NUMBER OF MODES INCLUDED = 6

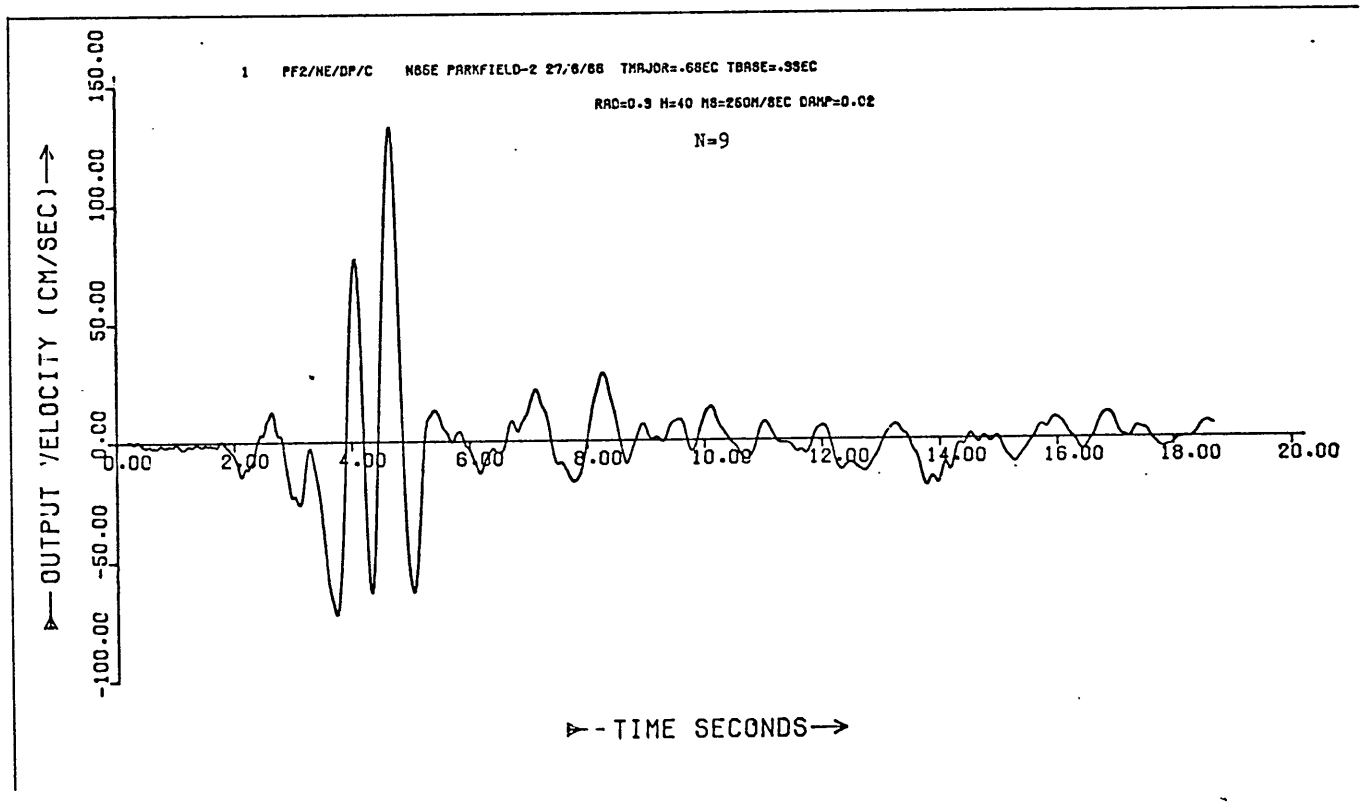


FIG.4.7b COMPUTED GROUND SURFACE VELOCITY TIME HISTORY

NUMBER OF MODES INCLUDED = 9

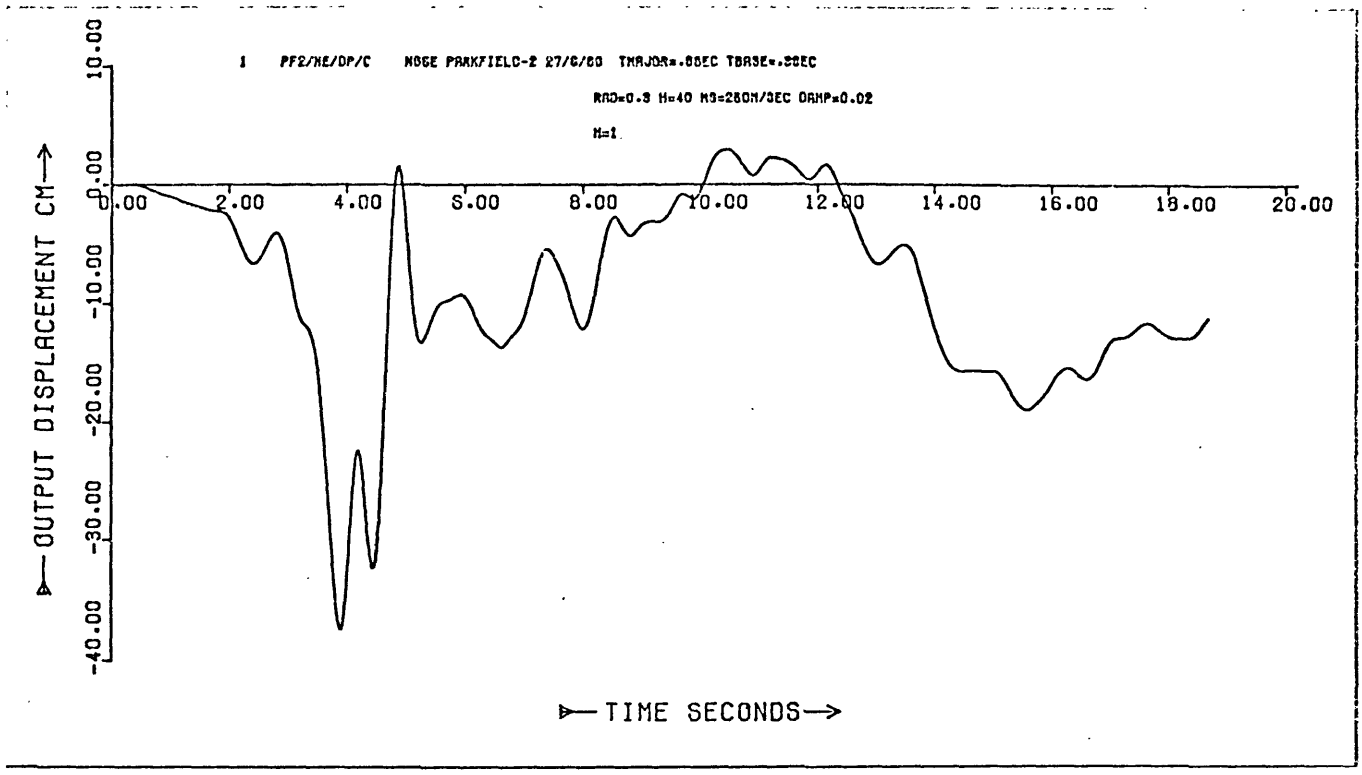


FIG.4.4c COMPUTED GROUND SURFACE DISPLACEMENT TIME HISTORY

NUMBER OF MODES INCLUDED = 1

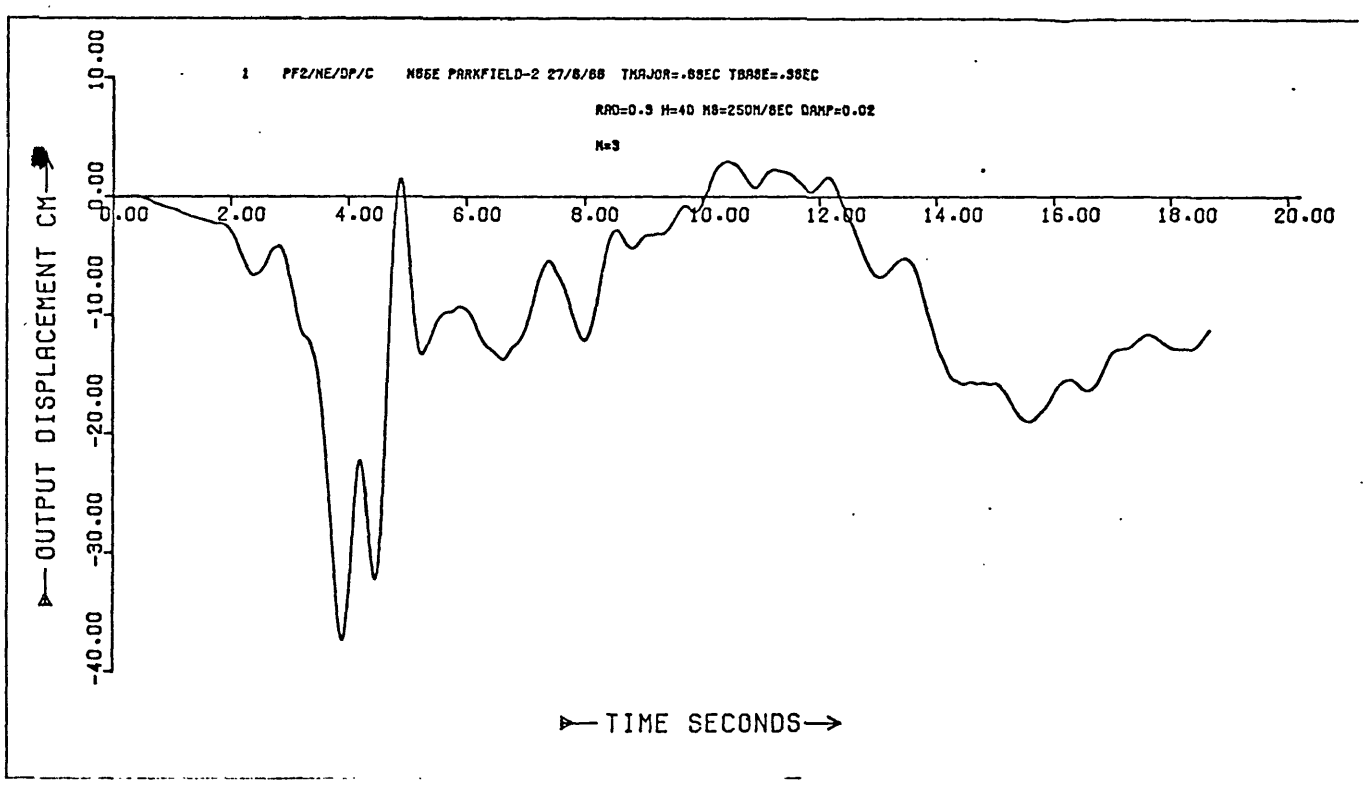


FIG. 4.5c COMPUTED GROUND SURFACE DISPLACEMENT TIME HISTORY

NUMBER OF MODES INCLUDED = 3

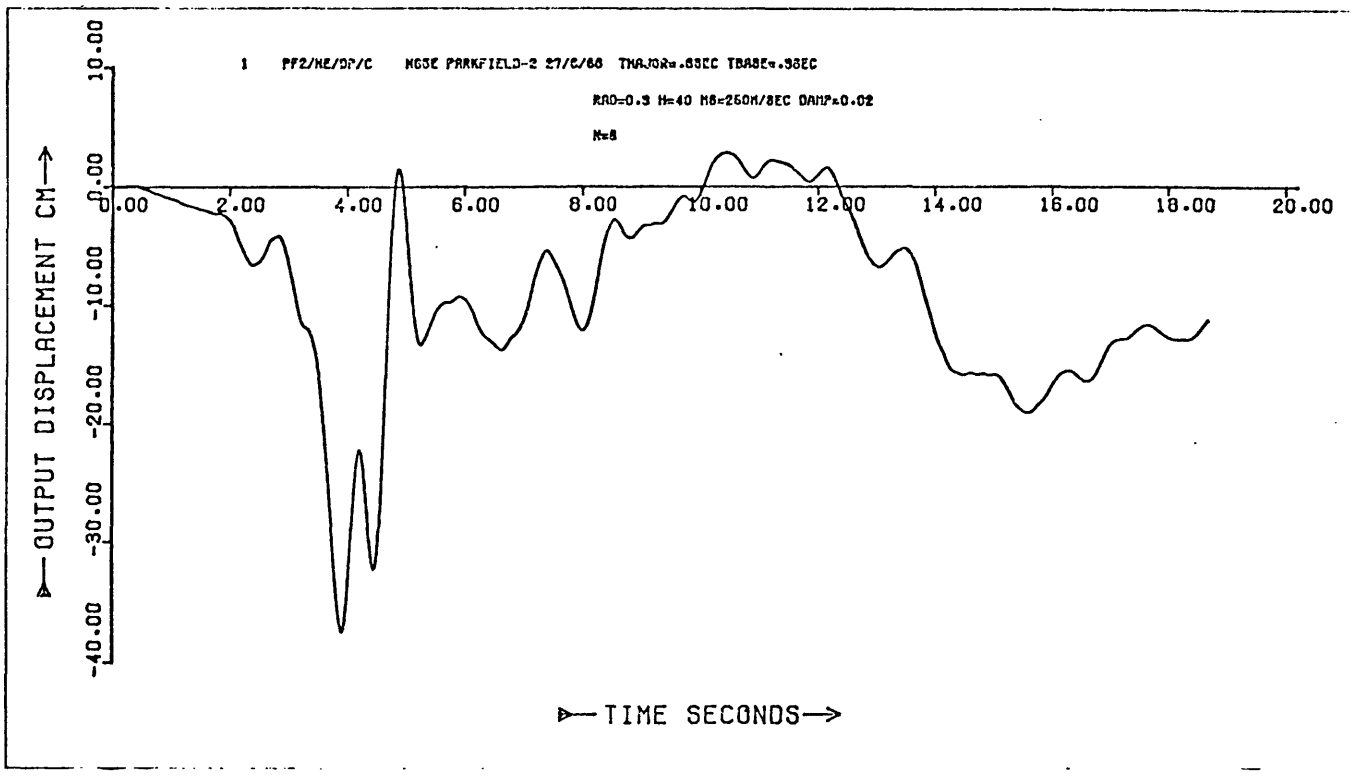


FIG. 4.6c COMPUTED GROUND SURFACE DISPLACEMENT TIME HISTORY

NUMBER OF MODES INCLUDED = 6

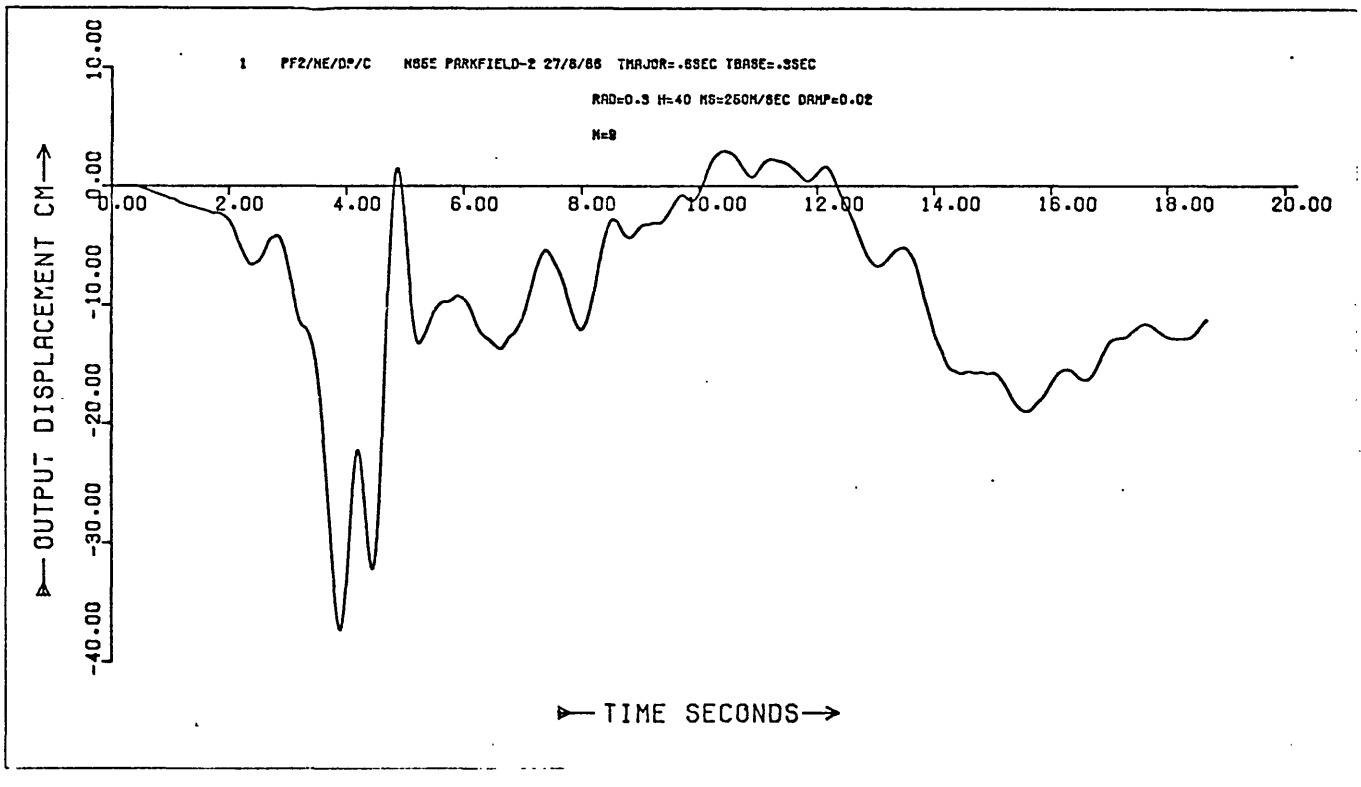


FIG. 4.7c COMPUTED GROUND SURFACE DISPLACEMENT TIME HISTORY

NUMBER OF MODES INCLUDED = 9

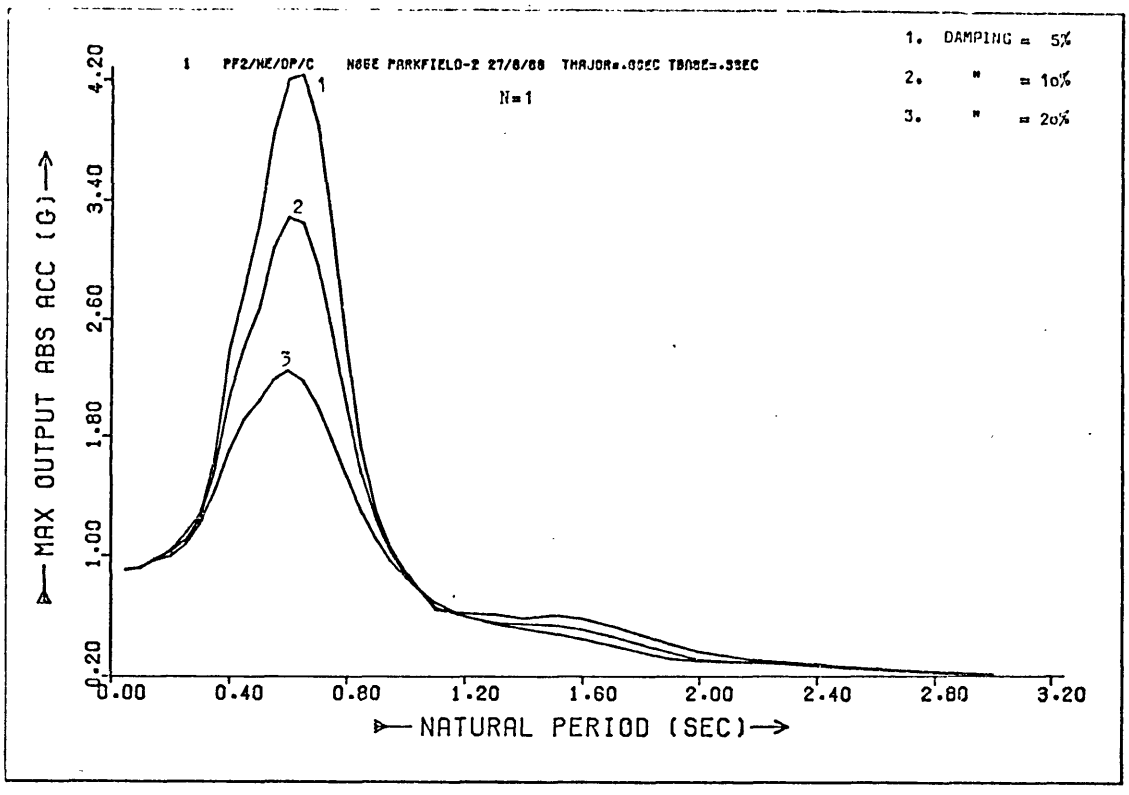


FIG.4.4d COMPUTED GROUND SURFACE ACCELERATION RESPONSE SPECTRA

NUMBER OF MODES INCLUDED = 1

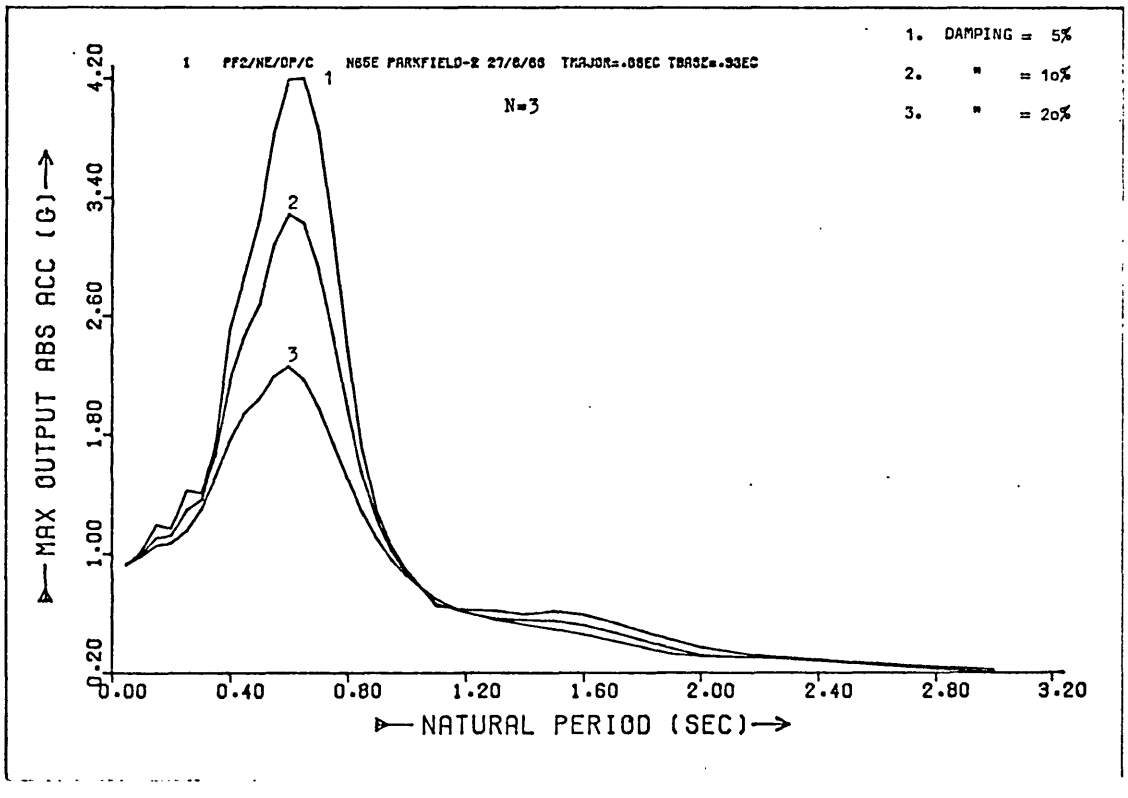


FIG. 4.5d COMPUTED GROUND SURFACE ACCELERATION RESPONSE SPECTRA

NUMBER OF MODES INCLUDED = 3

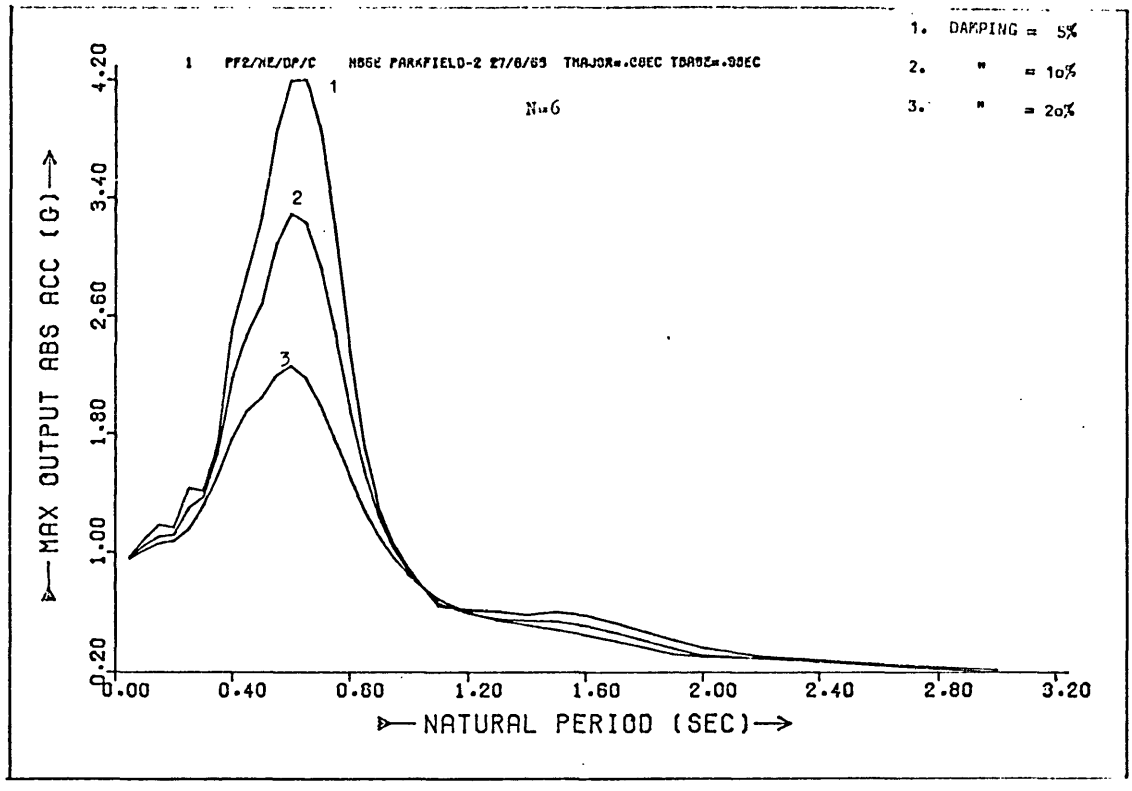


FIG.4.6d COMPUTED GROUND SURFACE ACCELERATION RESPONSE SPECTRA

NUMBER OF MODES INCLUDED = 6

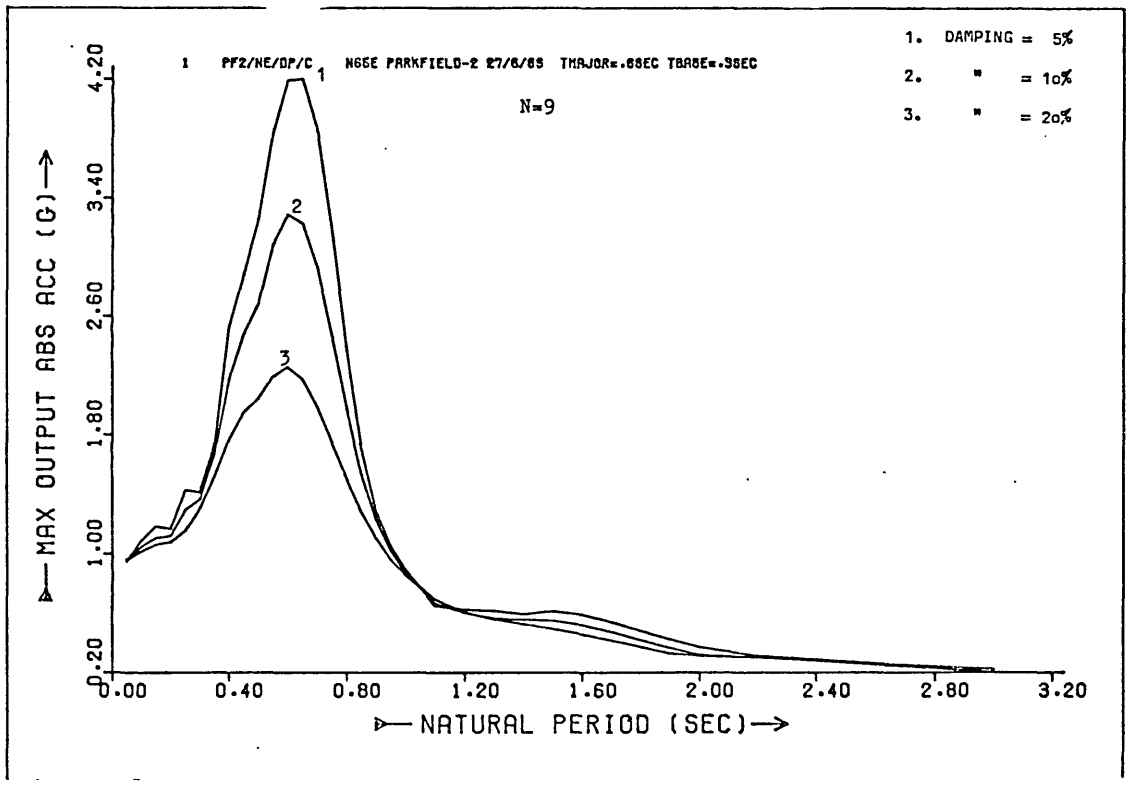


FIG. 4.7d COMPUTED GROUND SURFACE ACCELERATION RESPONSE SPECTRA

NUMBER OF MODES INCLUDED = 9

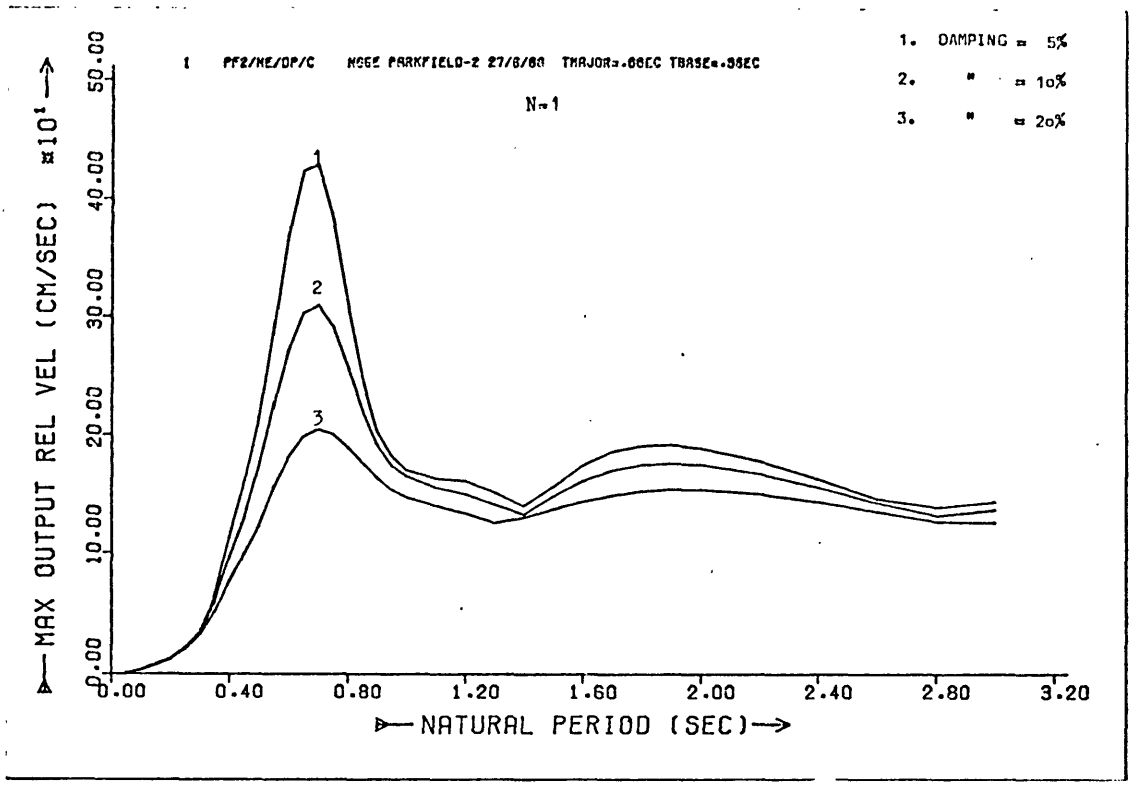


FIG.4.4e COMPUTED GROUND SURFACE VELOCITY RESPONSE SPECTRA

NUMBER OF MODES INCLUDED = 1

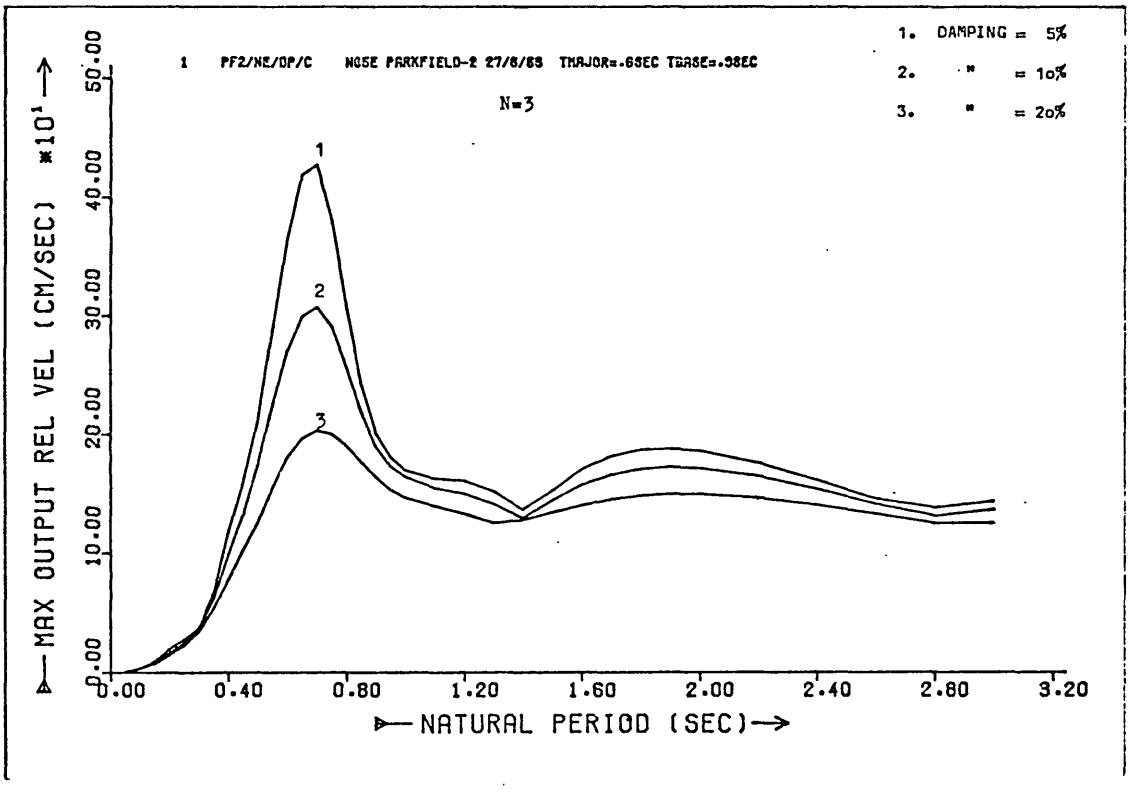


FIG. 4.5e COMPUTED GROUND SURFACE VELOCITY RESPONSE SPECTRA

NUMBER OF MODES INCLUDED = 3

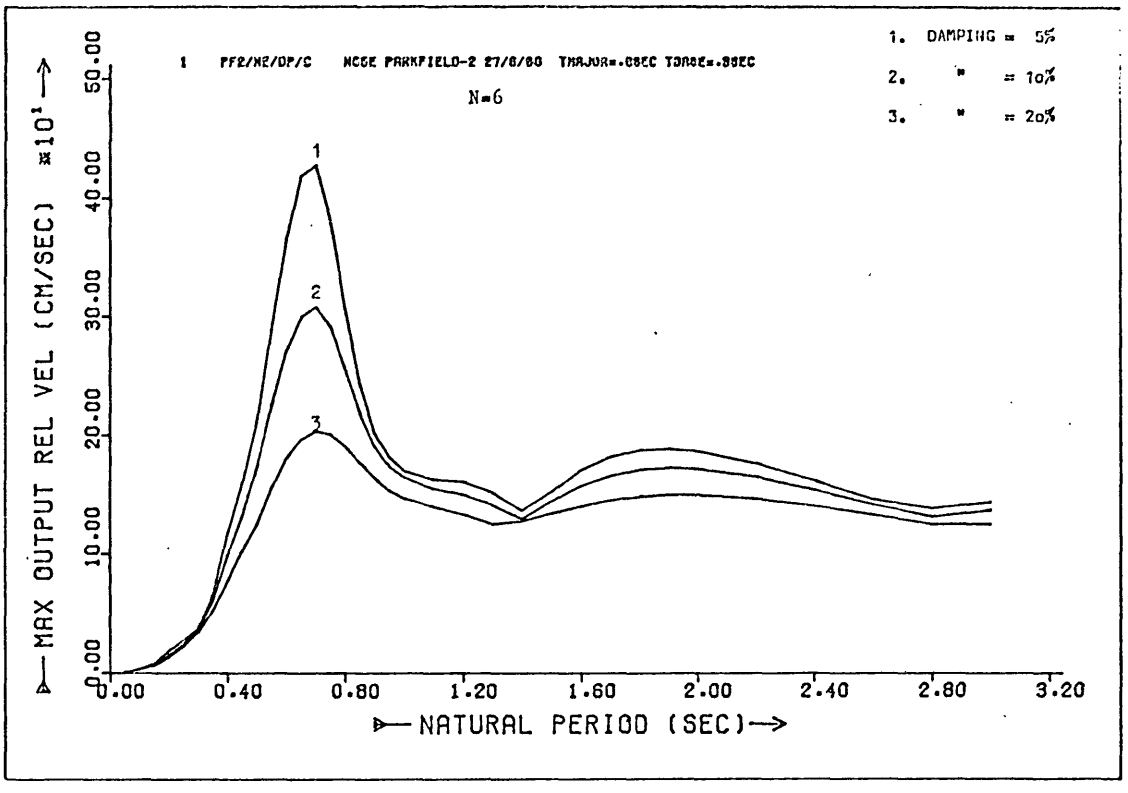


FIG.4.6e COMPUTED GROUND SURFACE VELOCITY RESPONSE SPECTRA

NUMBER OF MODES INCLUDED = 6

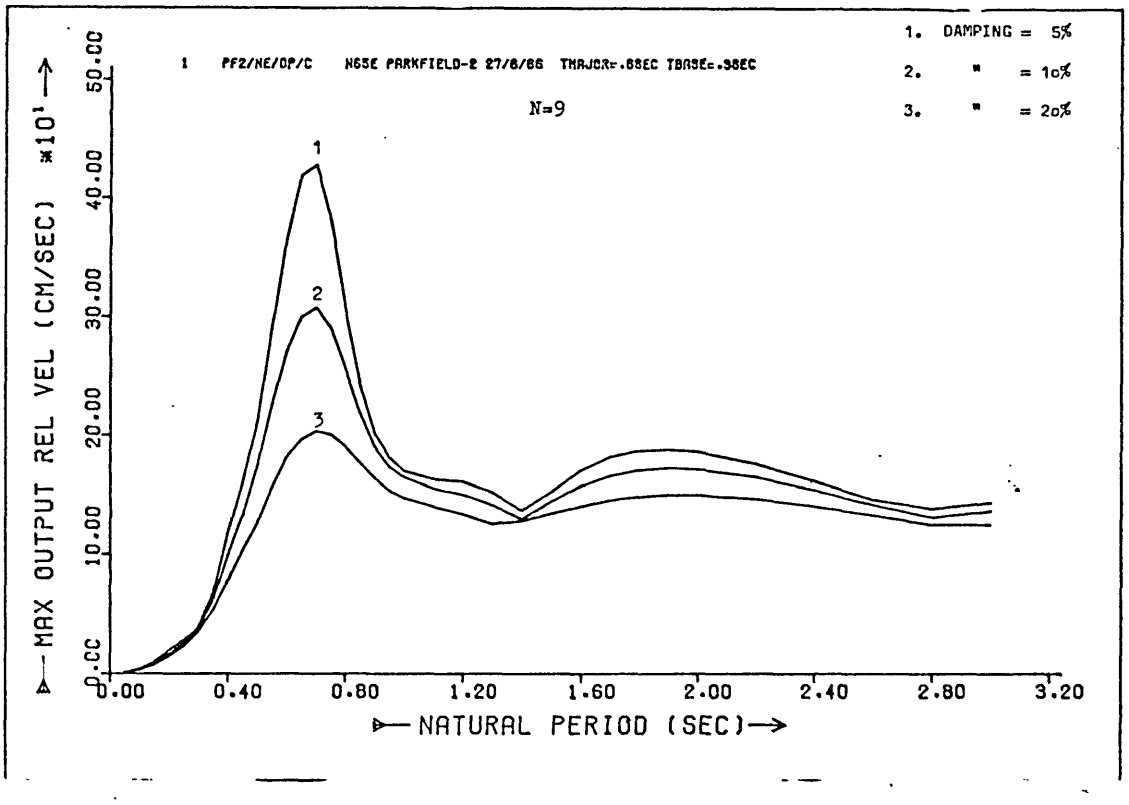


FIG.4.7e COMPUTED GROUND SURFACE VELOCITY RESPONSE SPECTRA

NUMBER OF MODES INCLUDED = 9

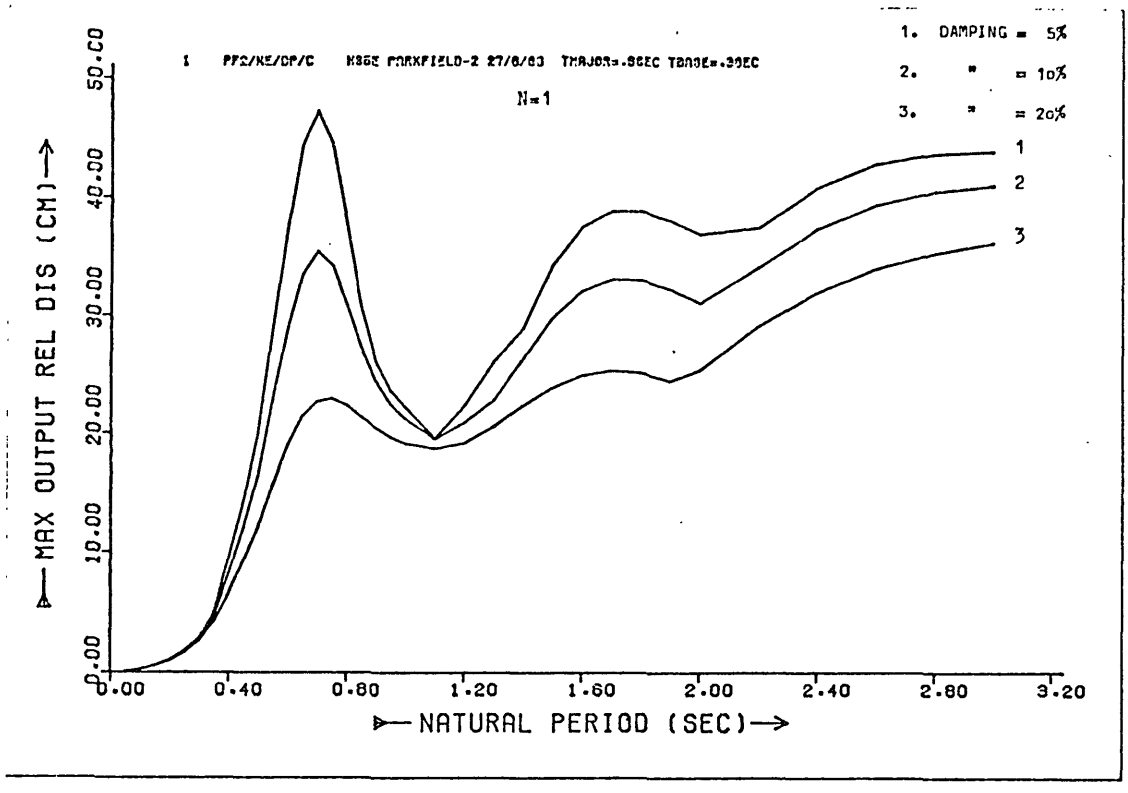


FIG. 4.4f COMPUTED GROUND SURFACE DISPLACEMENT RESPONSE SPECTRA

NUMBER OF MODES INCLUDED = 1

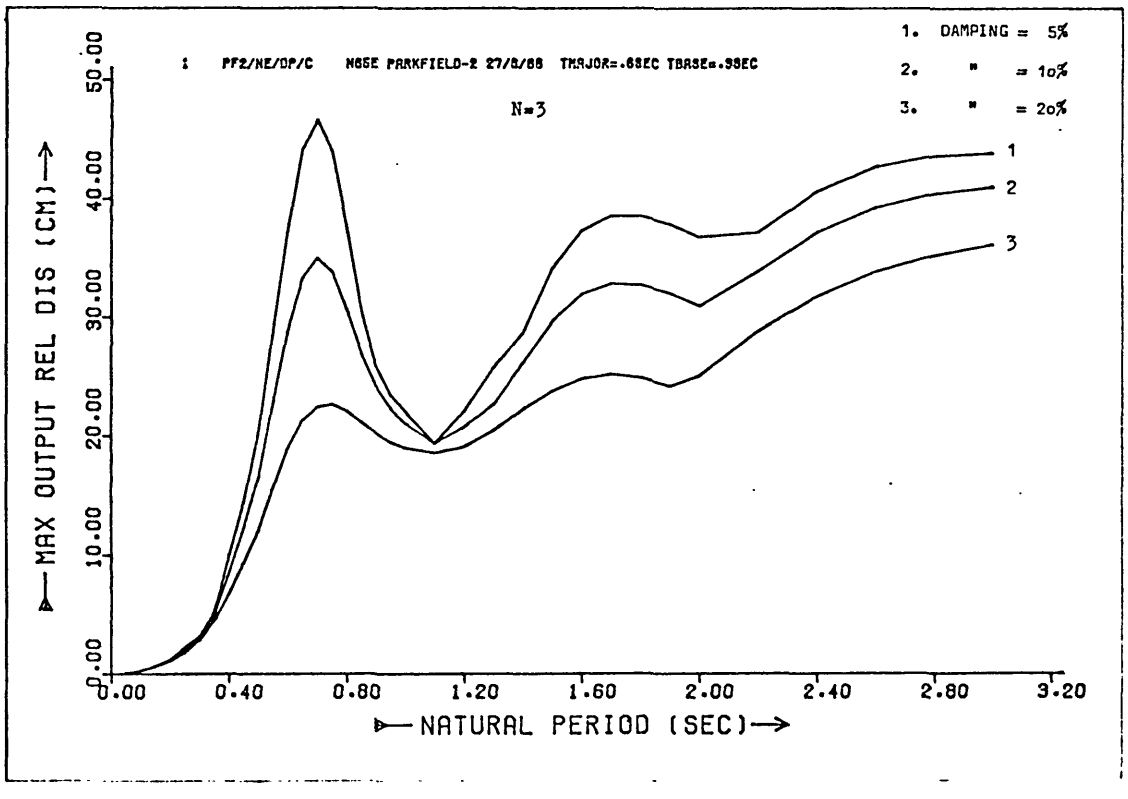


FIG. 4.5f COMPUTED GROUND SURFACE DISPLACEMENT RESPONSE SPECTRA

NUMBER OF MODES INCLUDED = 3

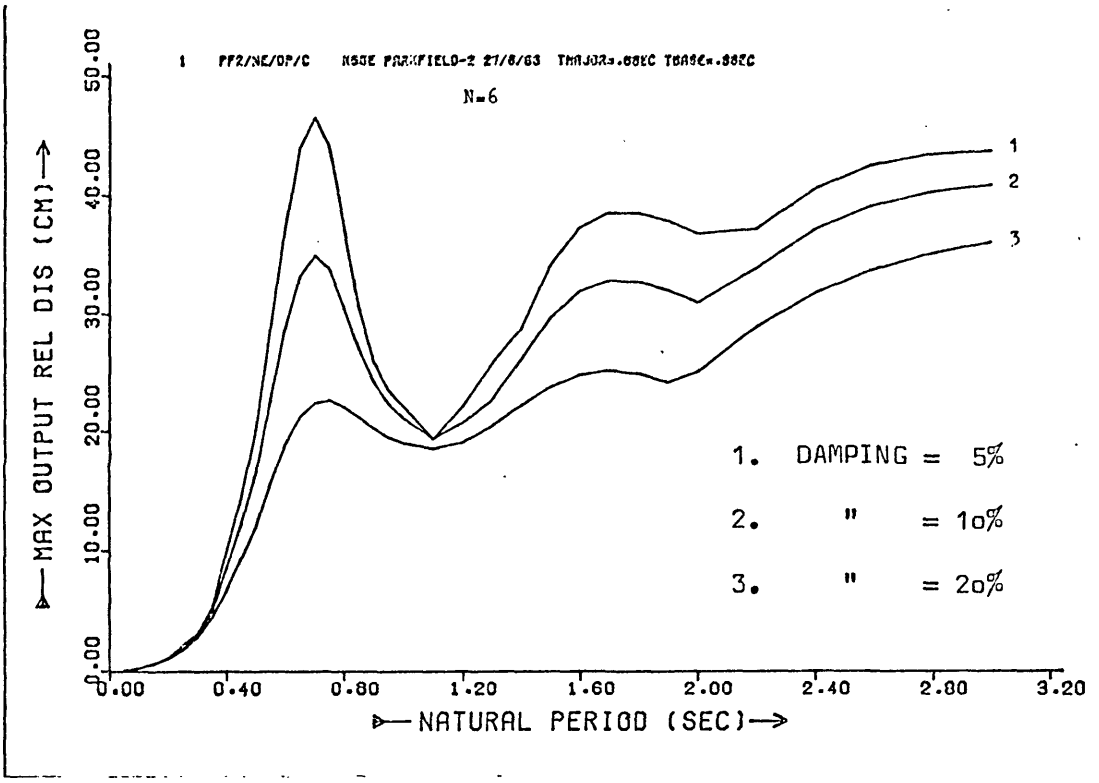


FIG. 4.6f COMPUTED GROUND SURFACE DISPLACEMENT RESPONSE SPECTRA

NUMBER OF MODES INCLUDED = 6.

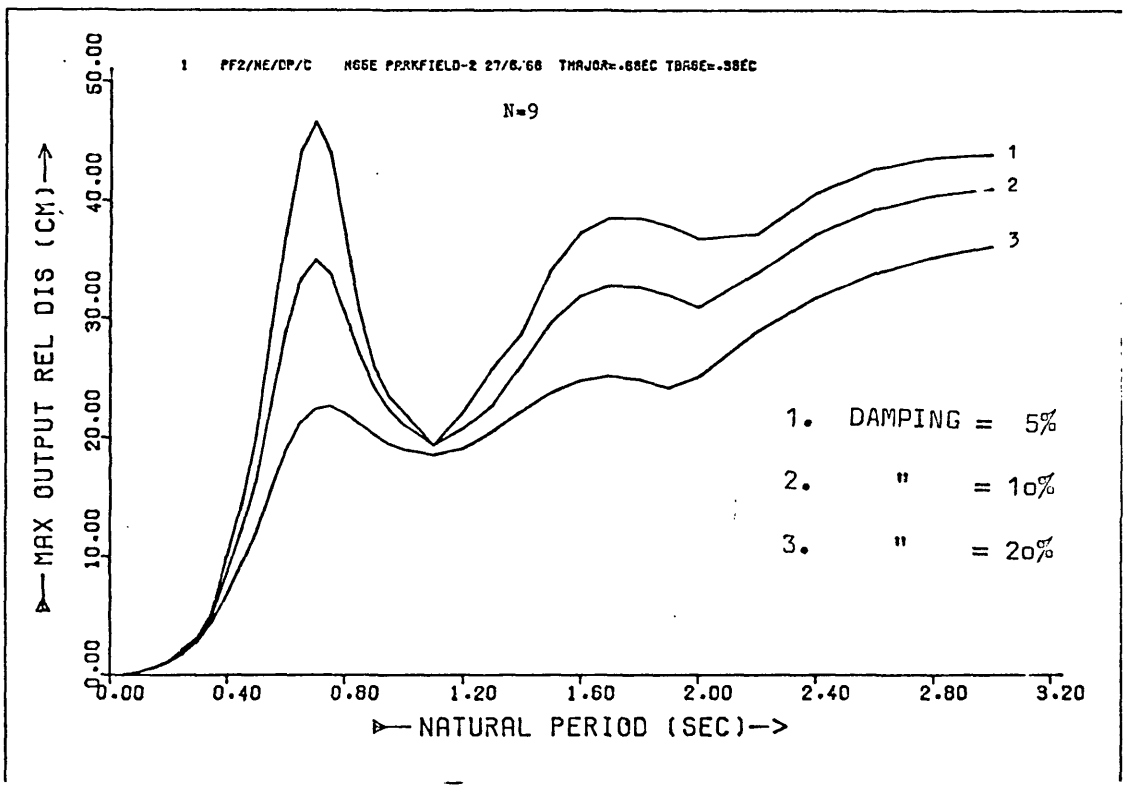


FIG. 4.7f COMPUTED GROUND SURFACE DISPLACEMENT RESPONSE SPECTRA

NUMBER OF MODES INCLUDED = 9

bedrock motion. Solutions as above were evaluated. The results are shown in figs. 4.8a,b,c,d,e,f to 4.11a,b,c,d,e,f. As expected, the results are similar to the previous case; six modes are enough accurately to represent the response of the system, but three modes also give good results for the computed response. Thus, accurate solutions are obtained by including those modes with natural periods within or slightly beyond the period range of interest. In this study, an average of 9 modes were taken to represent the foundation response. Solutions with nine modes were compared with a "numerical solution" in section 4.10. From the results, it is clear that the solution developed gives a very fast convergence and, in general, the response to earthquake bedrock motion is primarily due to the frequencies associated with the first mode and a few higher modes. However, there may well be very rare cases when a very deep deposit with a large fundamental period, e.g. 4 seconds (H = 500m, S = 500m/sec) is subjected to a base motion with a small predominant period, e.g. 0.1 seconds. In such cases, the present solution procedure may break down, since the number of modes needed may violate the approximation made in section 4.4.1. However, this does not represent a serious limitation in the analysis because these cases are very rare: it should be noted that depth to bedrock for cases such as the one mentioned above of $\frac{1}{2}$Km. deep deposit can be determined with an accuracy of 60m (see 5.3.3). In view of such large errors any attempt to compute the response of these deposits may be expected to produce unrealistic results.

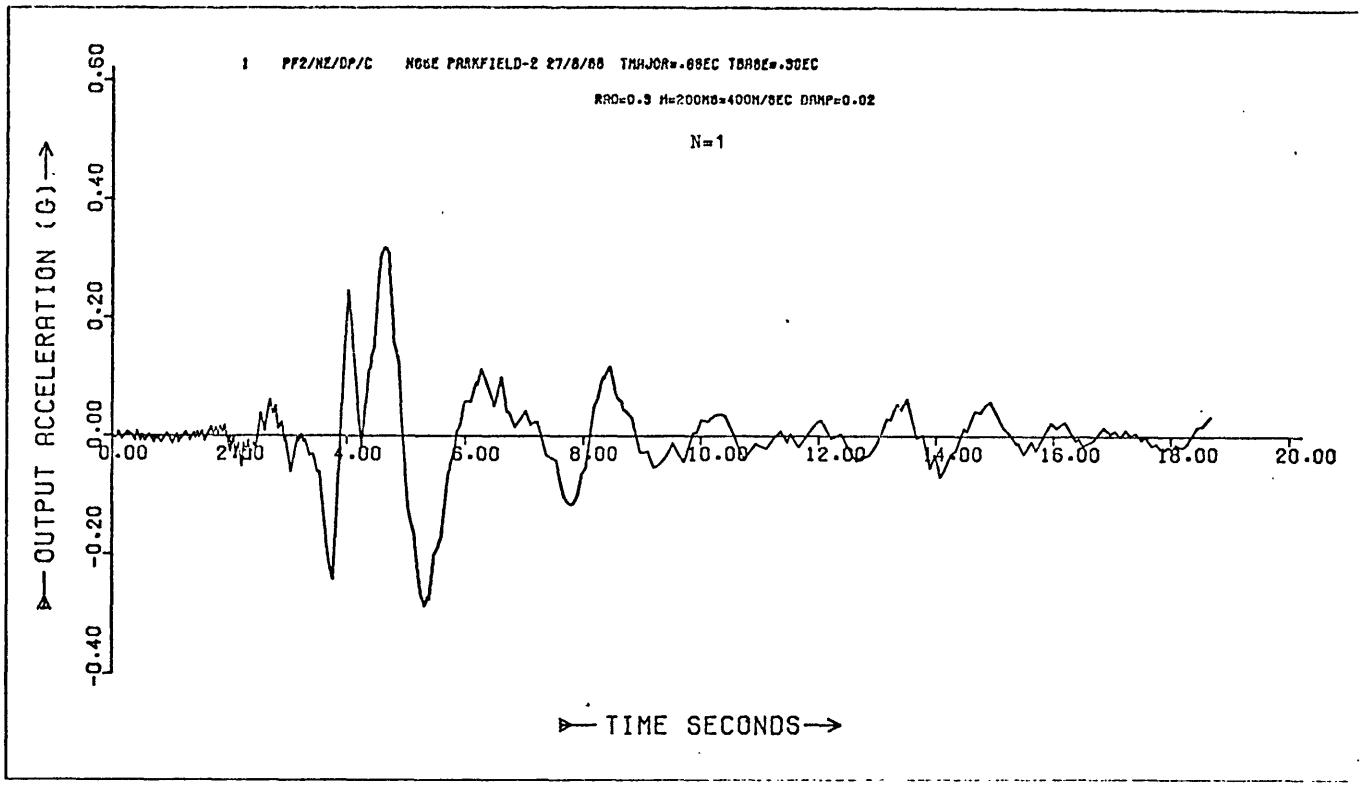


FIG. 4.8a COMPUTED GROUND SURFACE ACCELERATION TIME HISTORY

NUMBER OF MODES INCLUDED = 1

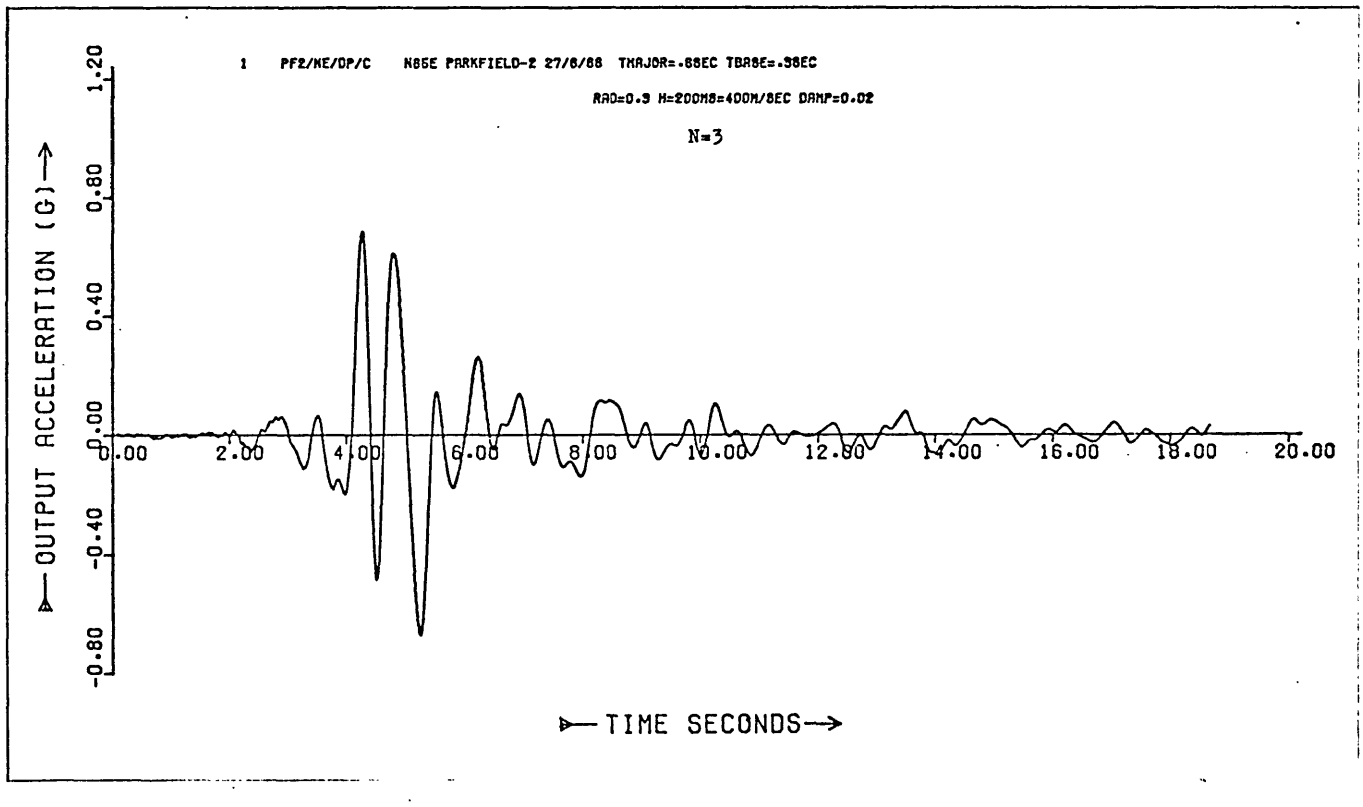


FIG.4.9a COMPUTED GROUND SURFACE ACCELERATION TIME HISTORY

NUMBER OF MODES INCLUDED = 3

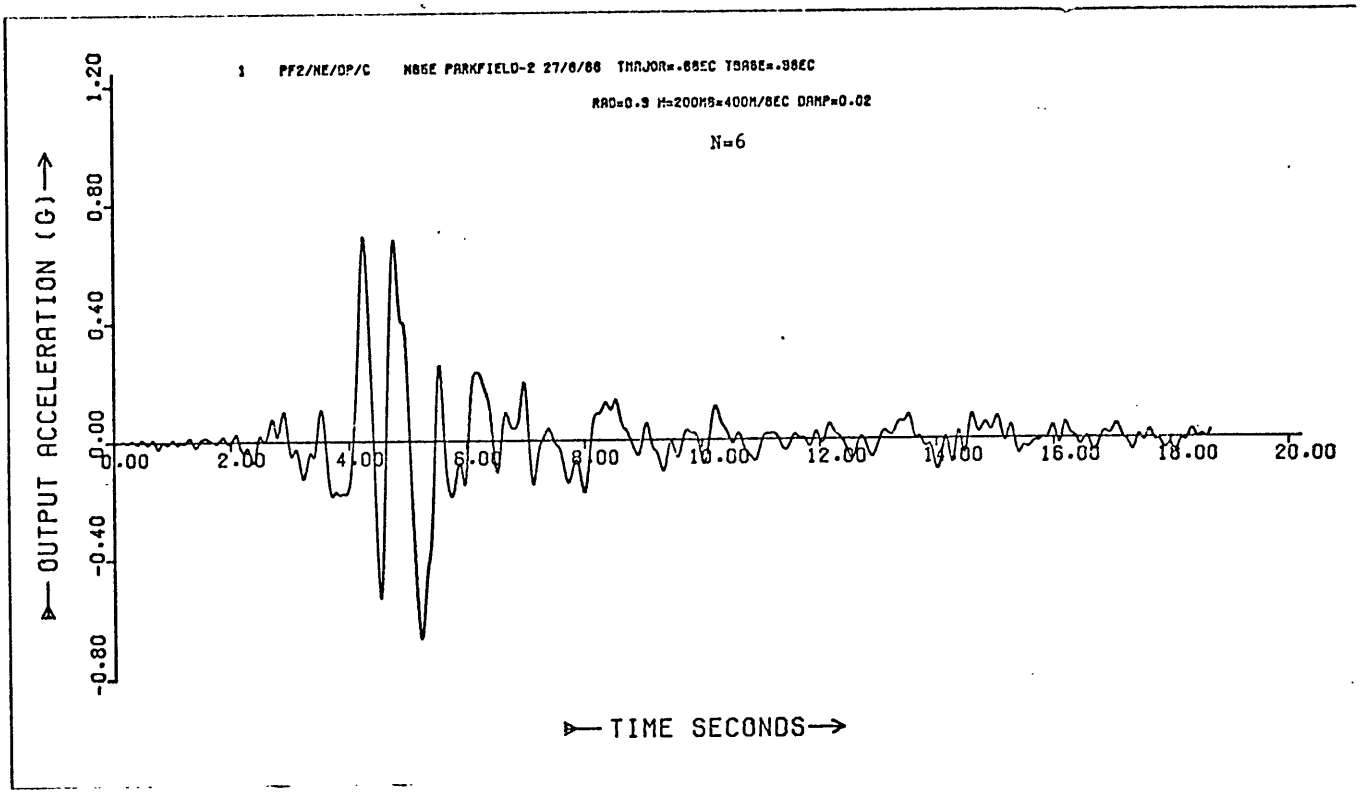


FIG. 4.10a COMPUTED GROUND SURFACE ACCELERATION TIME HISTORY

NUMBER OF MODES INCLUDED =6

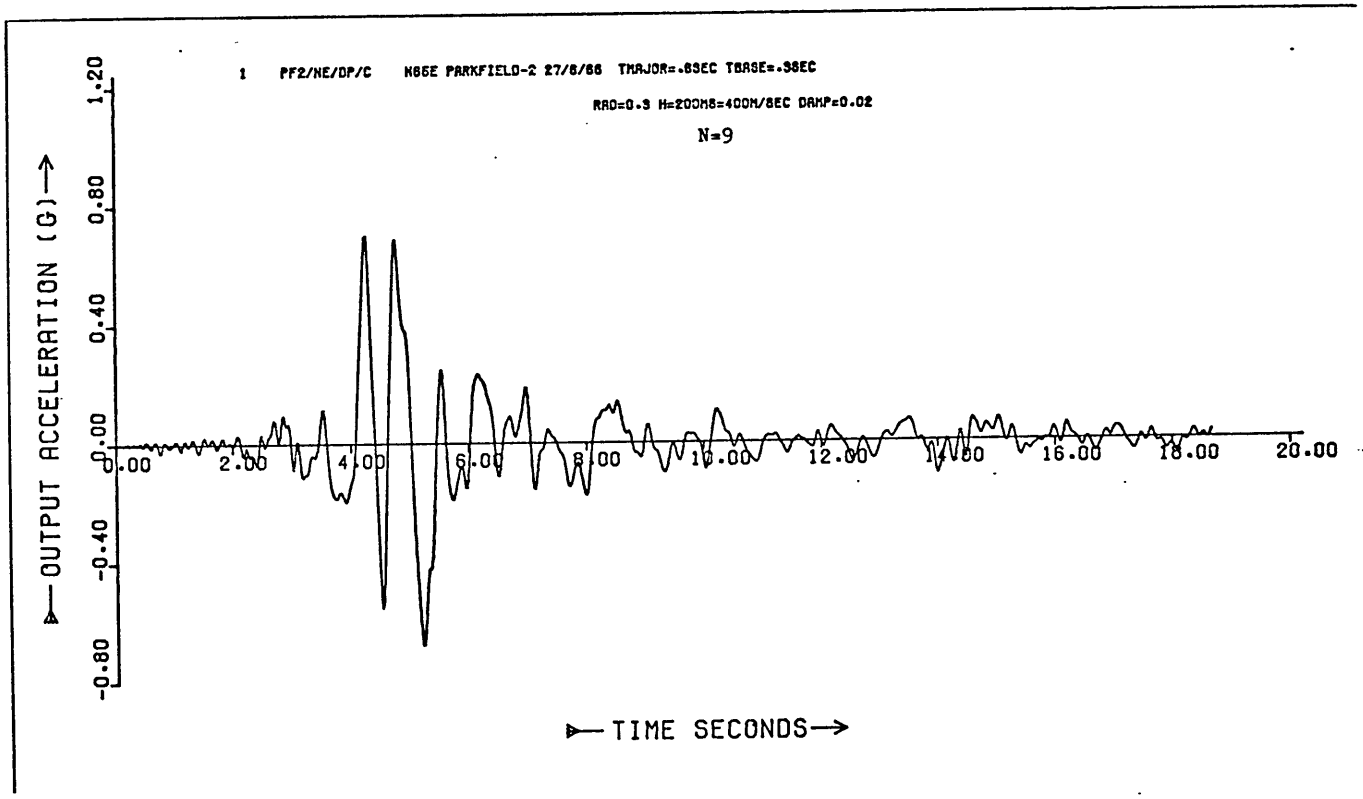


FIG. 4.11a COMPUTED GROUND SURFACE ACCELERATION TIME HISTORY

NUMBER OF MODES INCLUDED =9

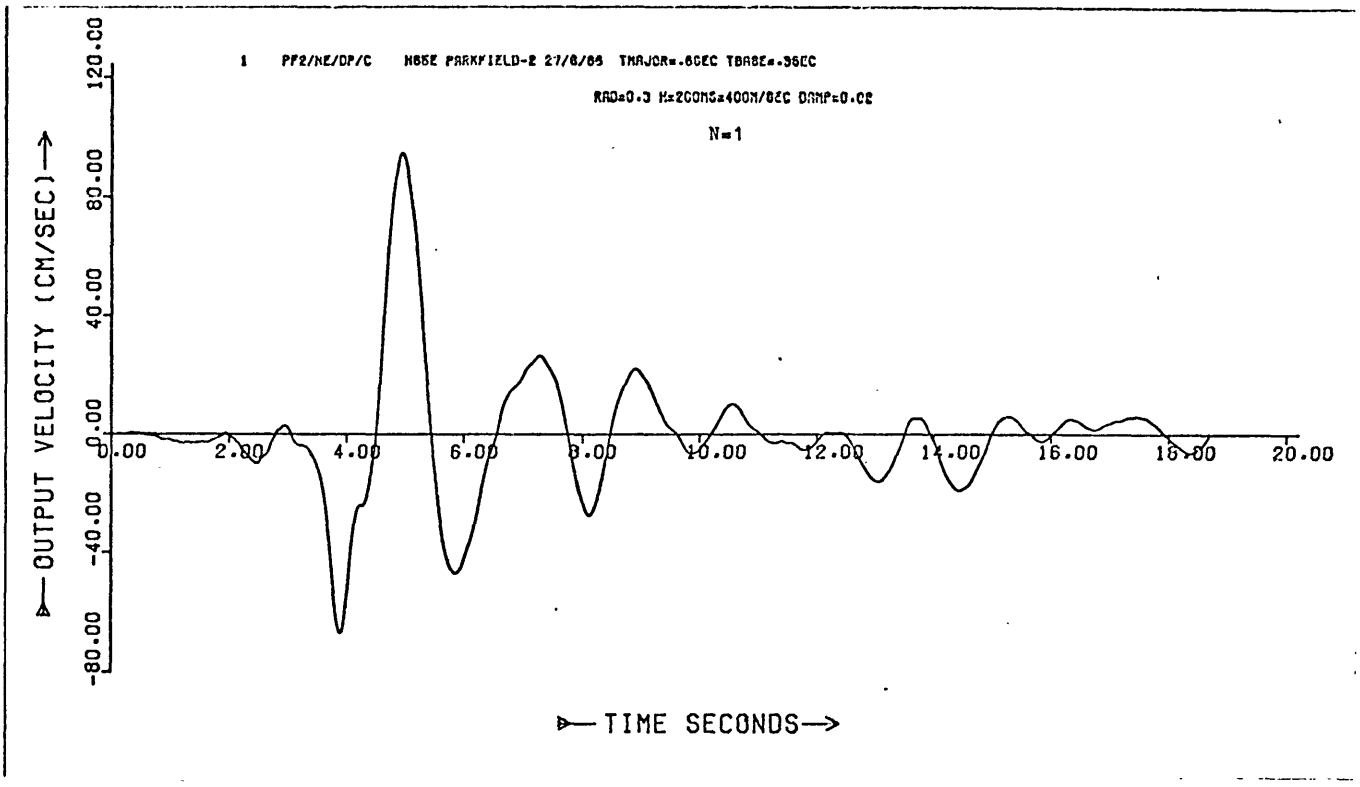


FIG A.8b COMPUTED GROUND SURFACE VELOCITY TIME HISTORY

NUMBER OF MODES INCLUDED = 1

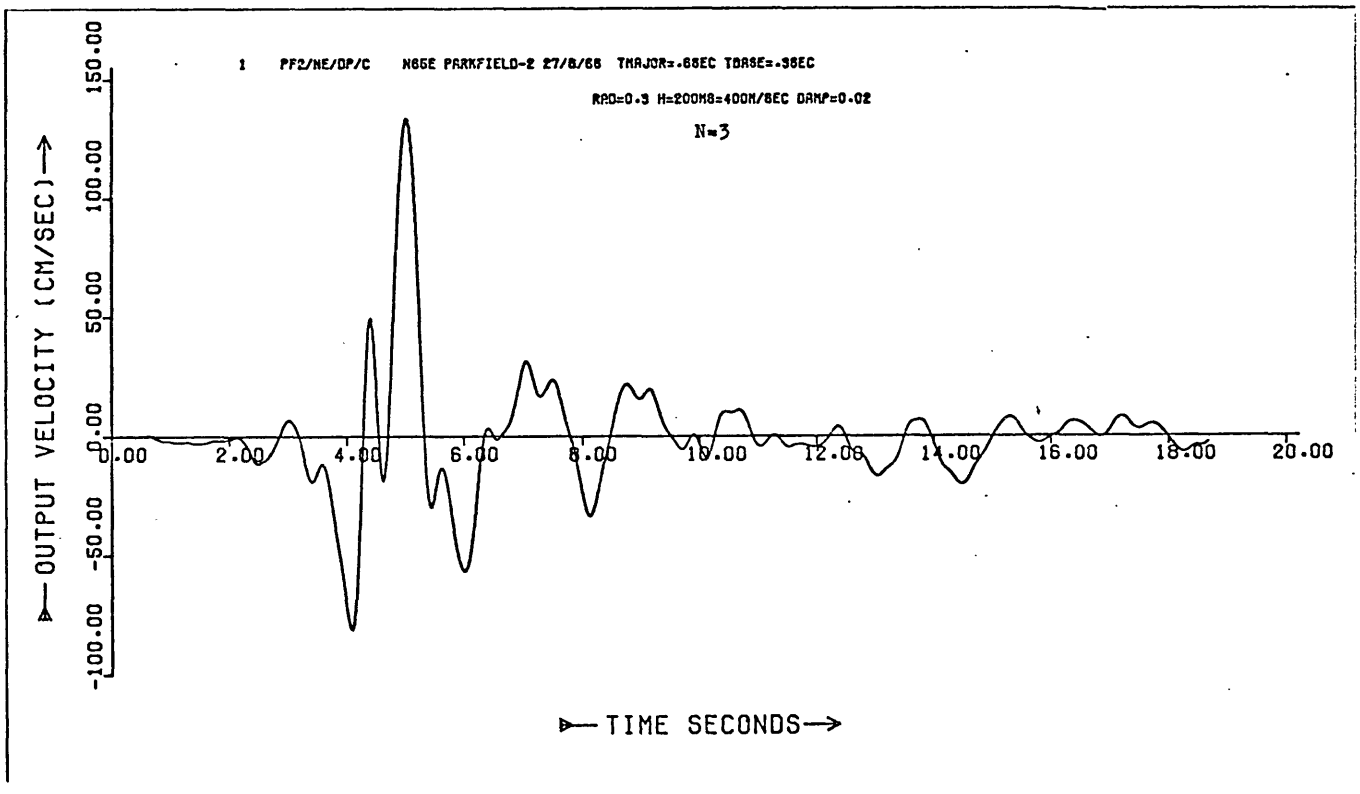


FIG. 4.9b COMPUTED GROUND SURFACE VELOCITY TIME HISTORY

NUMBER OF MODES INCLUDED = 3

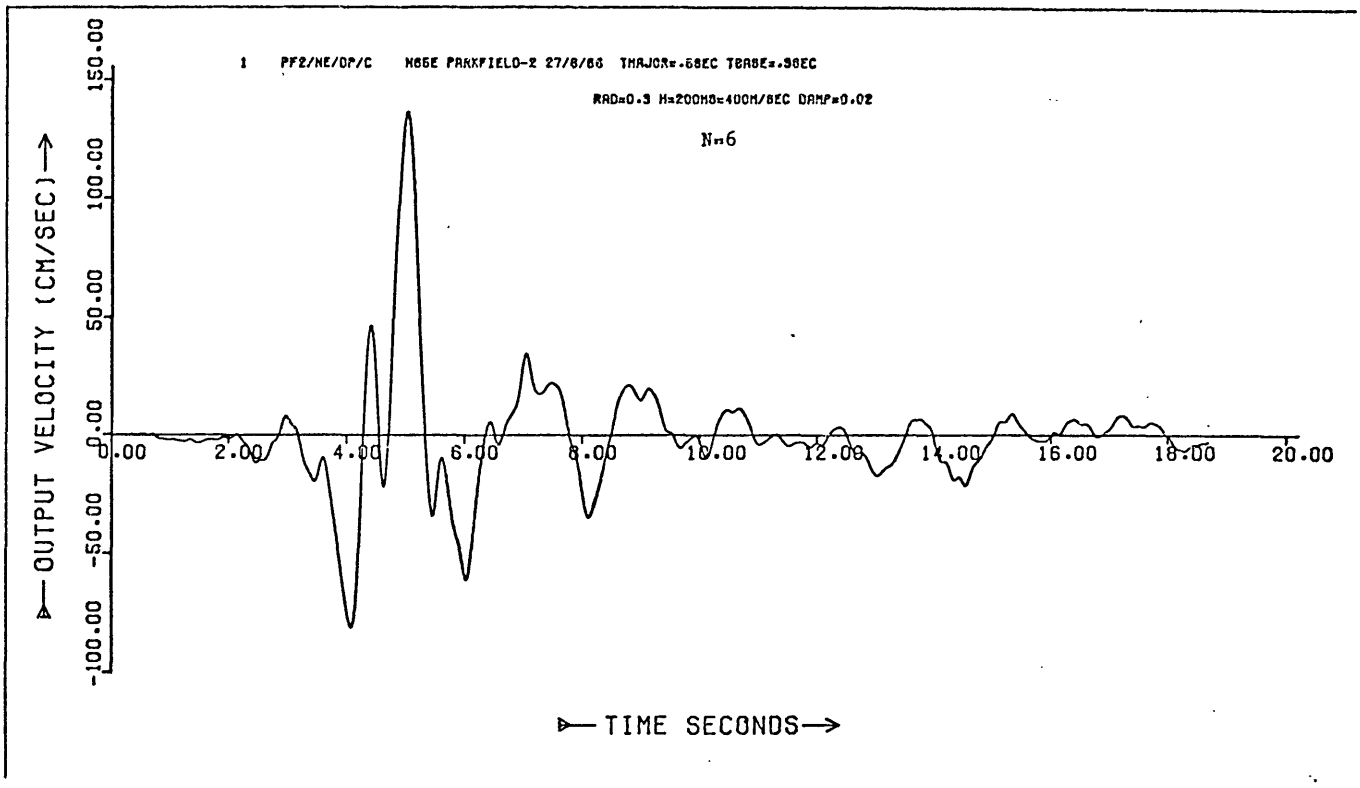


FIG. 4.10 COMPUTED GROUND SURFACE VELOCITY TIME HISTORY

NUMBER OF MODES INCLUDED = 6

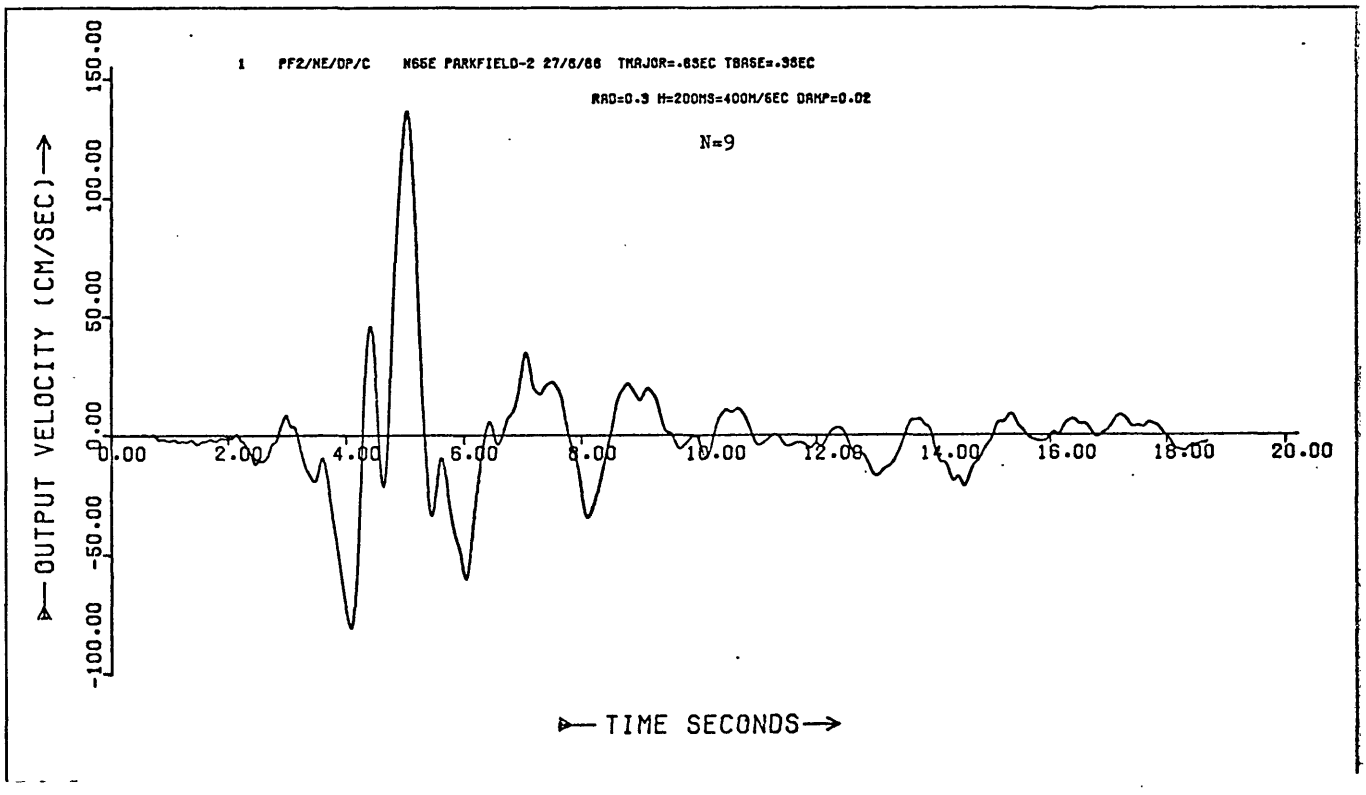


FIG. 4.11 COMPUTED GROUND SURFACE VELOCITY TIME HISTORY

NUMBER OF MODES INCLUDED = 9

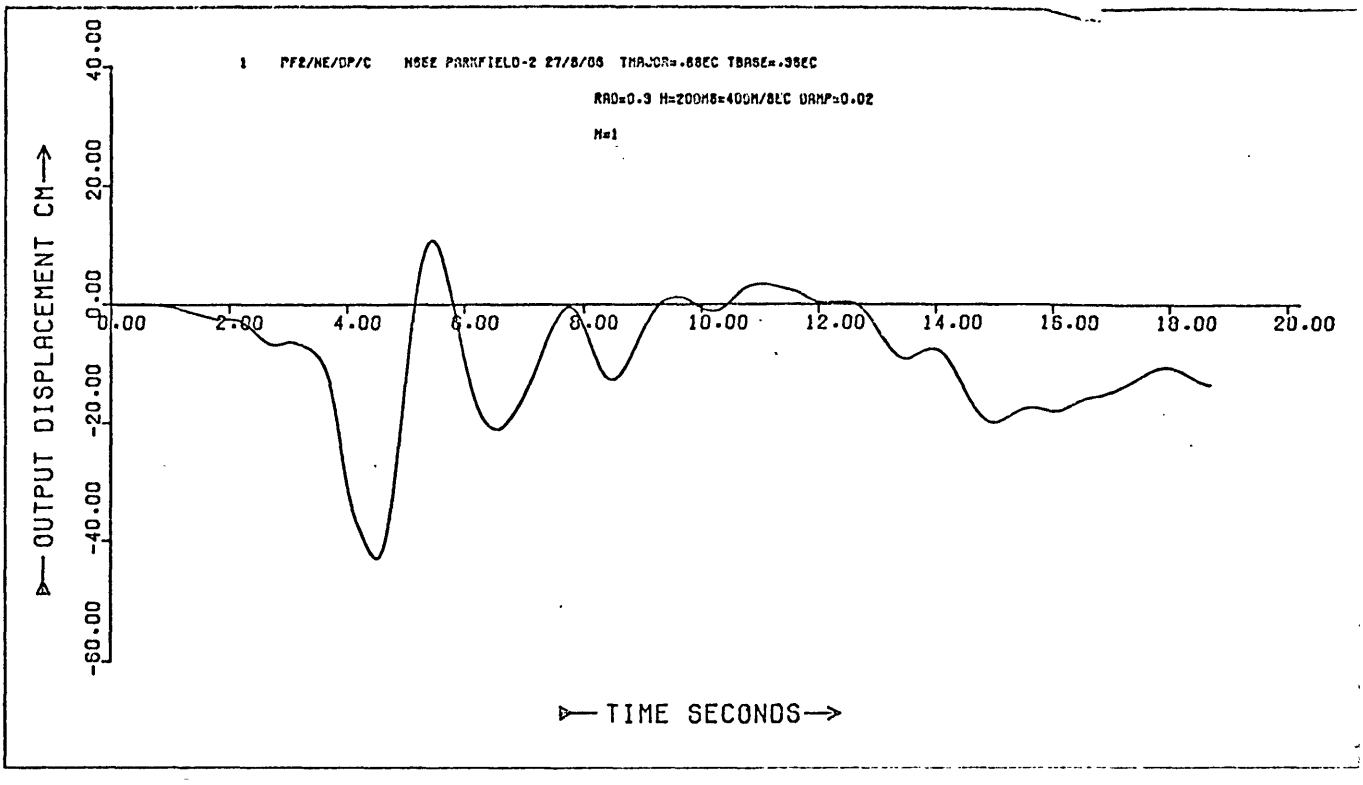


FIG 4.8c COMPUTED GROUND SURFACE DISPLACEMENT TIME HISTORY

NUMBER OF MODES INCLUDED = 1

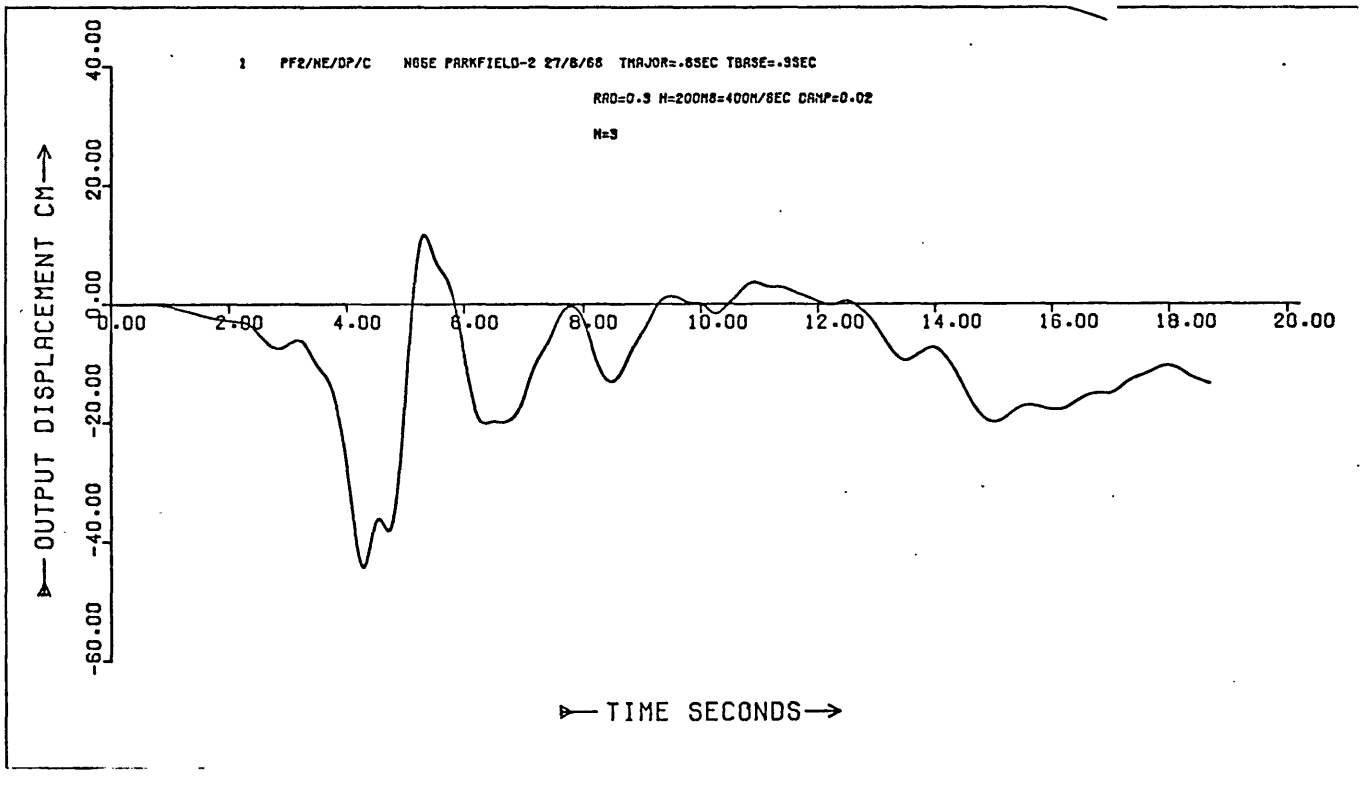


FIG.4.9c COMPUTED GROUND SURFACE DISPLACEMENT TIME HISTORY

NUMBER OF MODES INCLUDED = 3

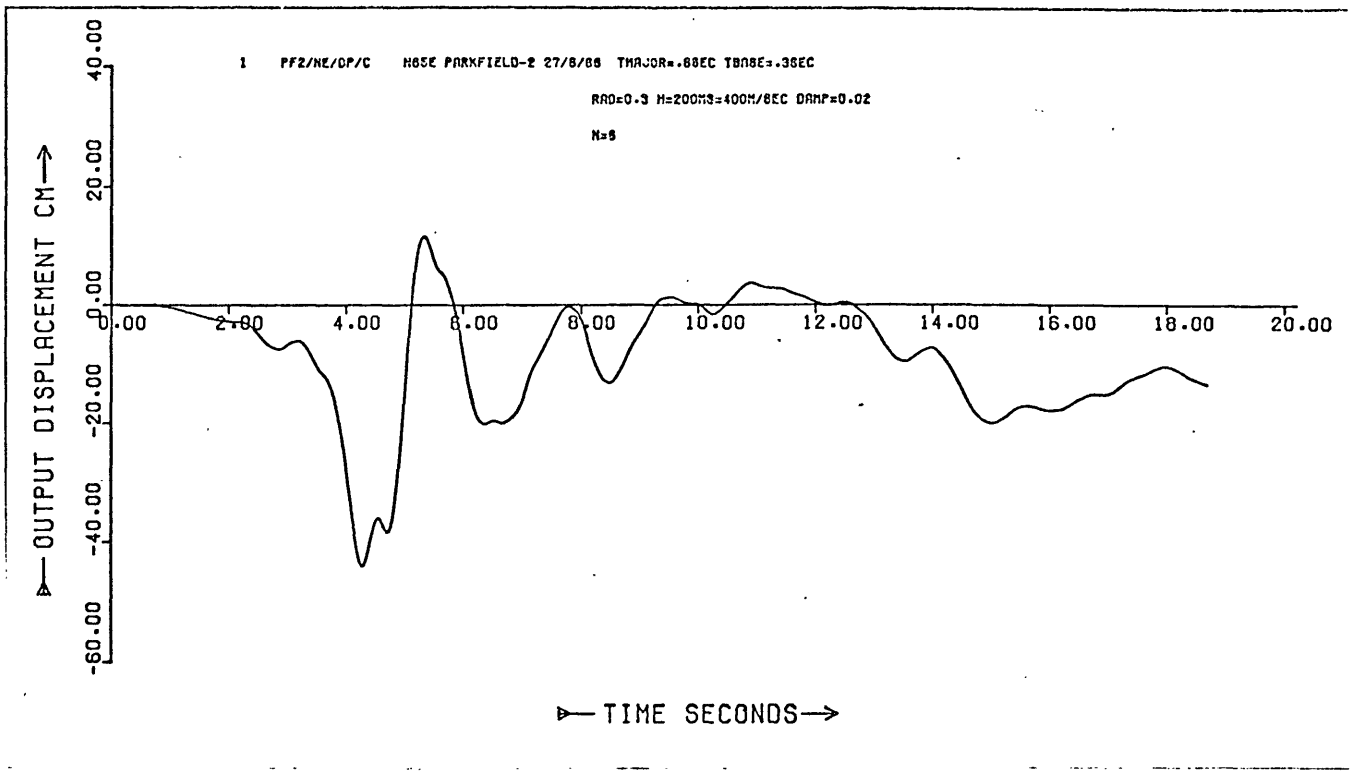


FIG.4.1oc COMPUTED GROUND SURFACE DISPLACEMENT TIME HISTORY

NUMBER OF MODES INCLUDED = 6

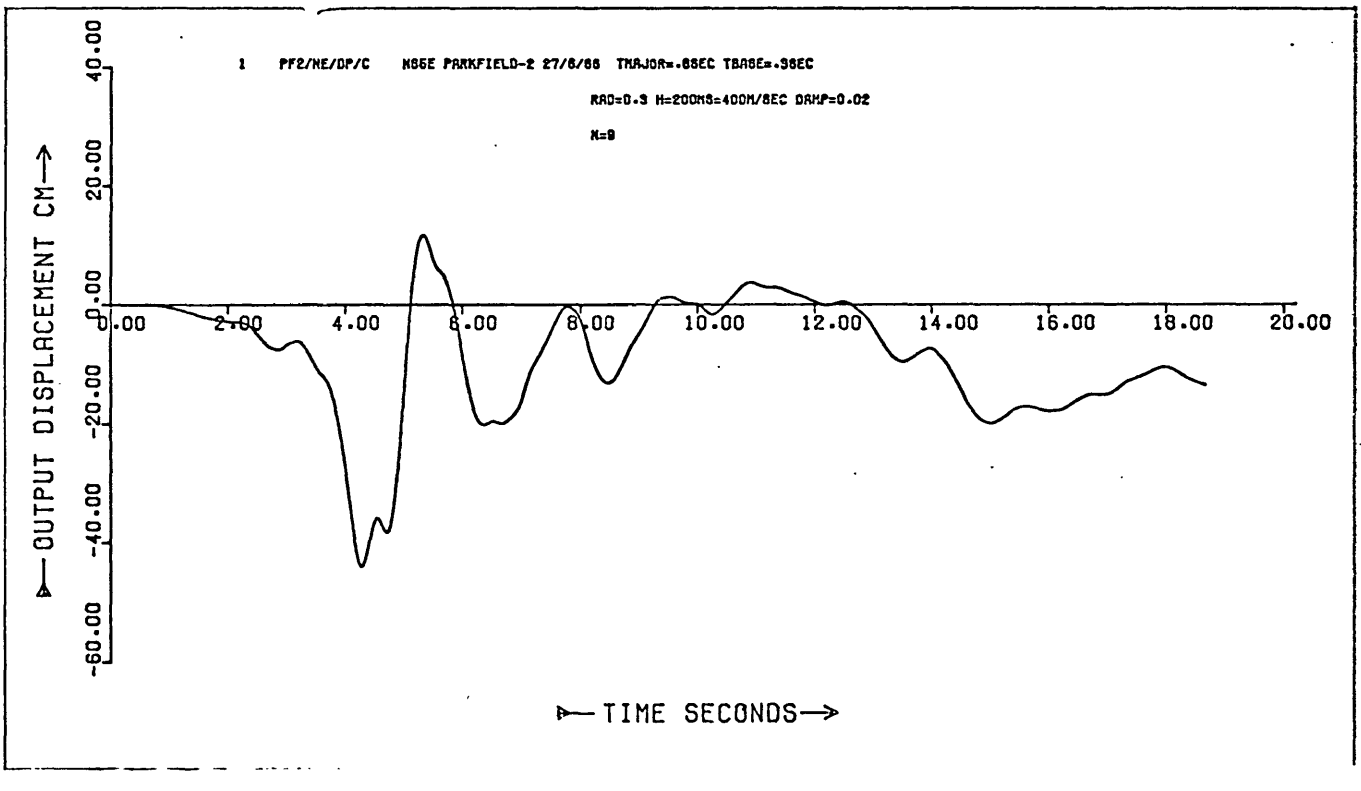


FIG.4.11cCOMPUTED GROUND SURFACE DISPLACEMENT TIME HISTORY

NUMBER OF MODES INCLUDED = 9

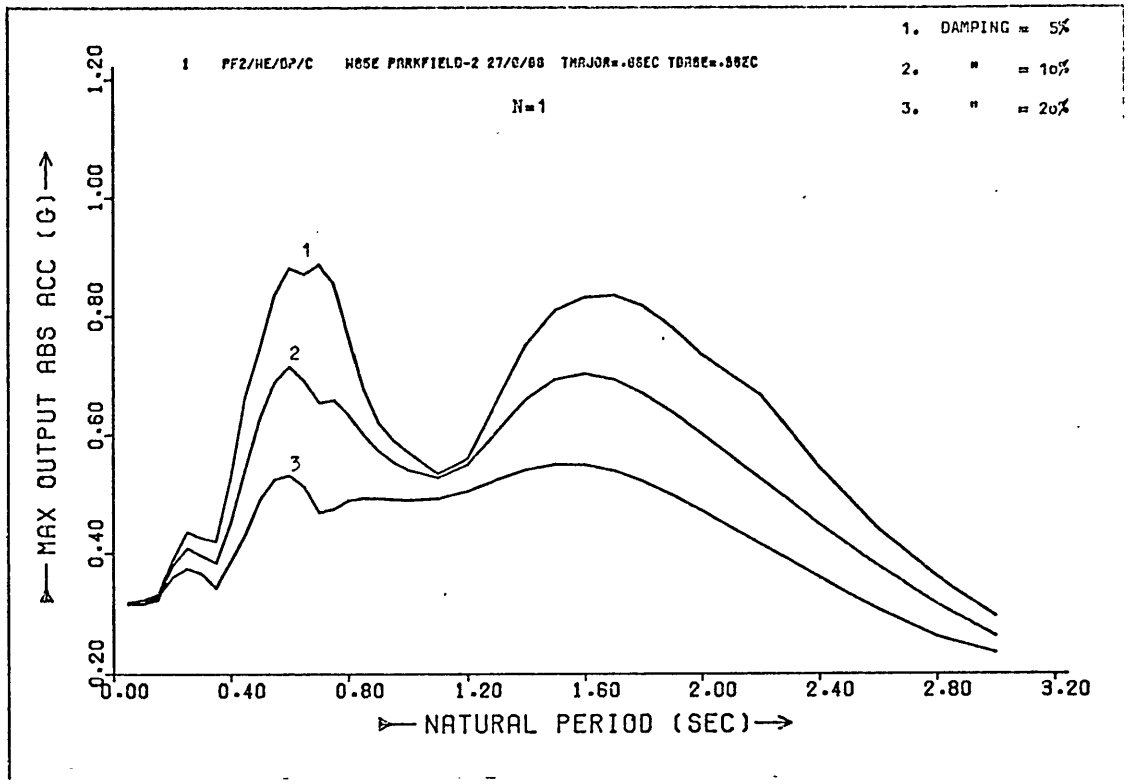


FIG.4.8d COMPUTED GROUND SURFACE ACCELERATION RESPONSE SPECTRA

NUMBER OF MODES INCLUDED = 1

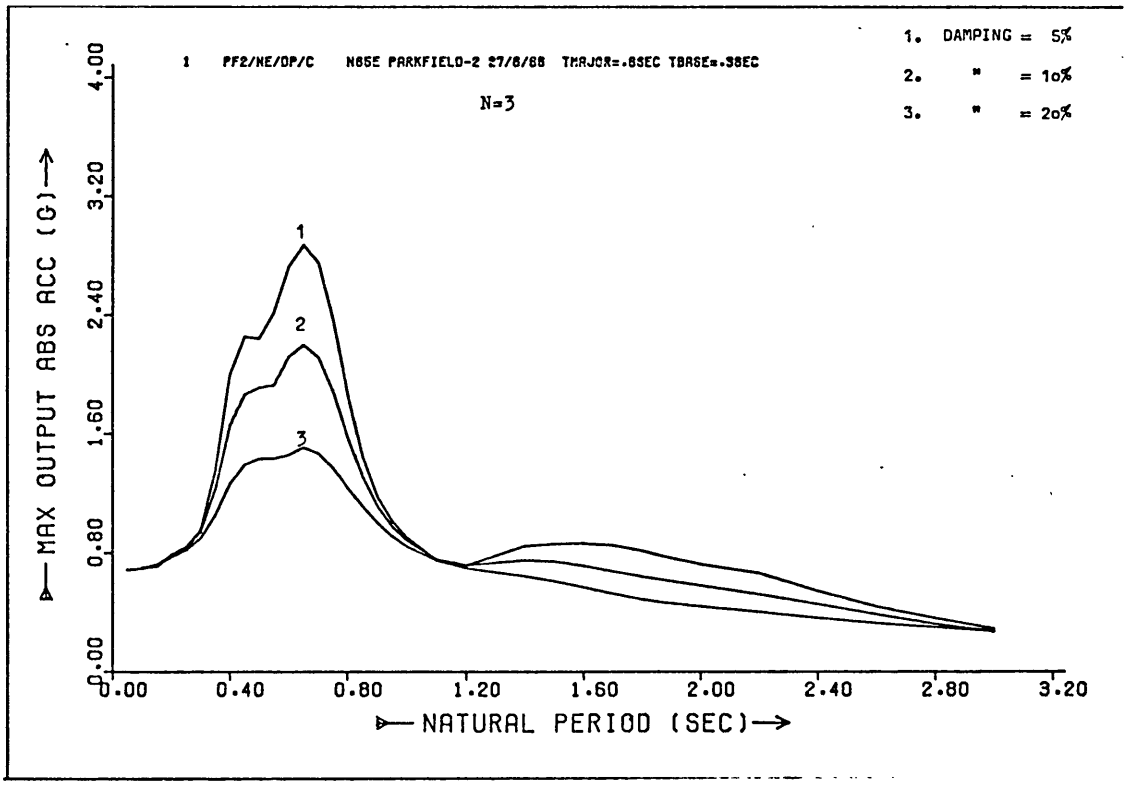


FIG. 4.9d COMPUTED GROUND SURFACE ACCELERATION RESPONSE SPECTRA

NUMBER OF MODES INCLUDED = 3

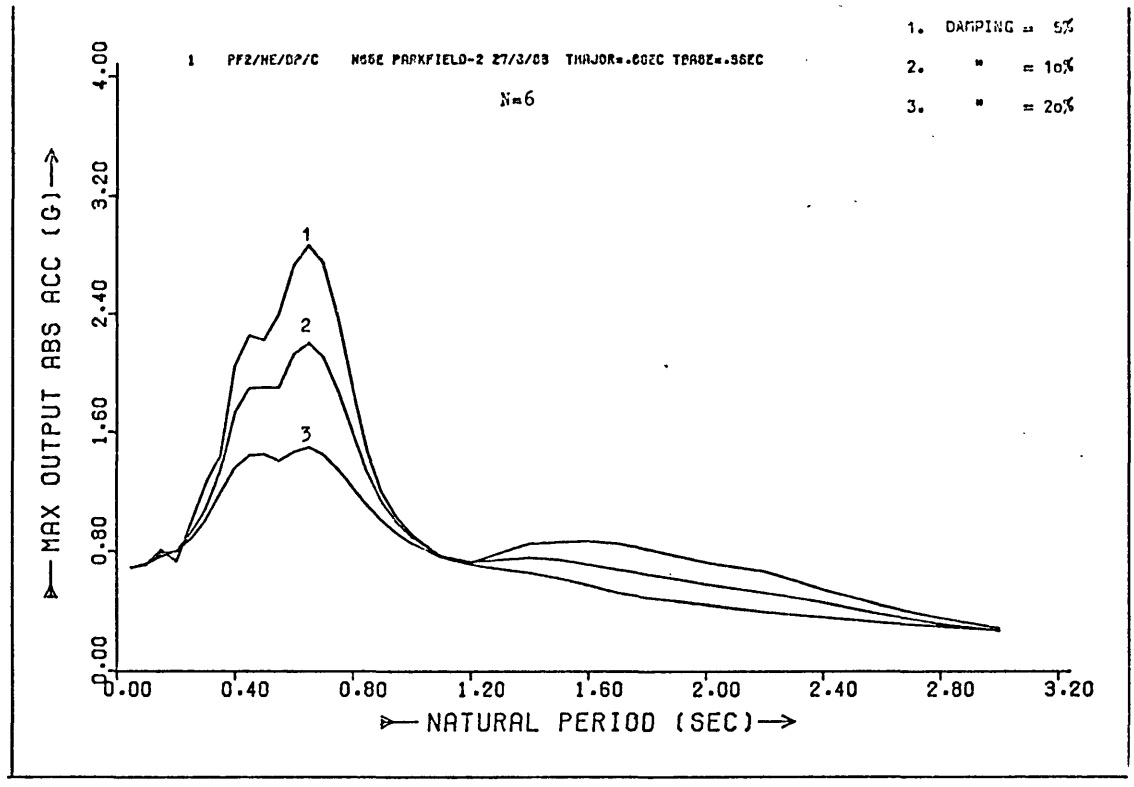


FIG.4.10d COMPUTED GROUND SURFACE ACCELERATION RESPONSE SPECTRA

NUMBER OF MODES INCLUDED = 6

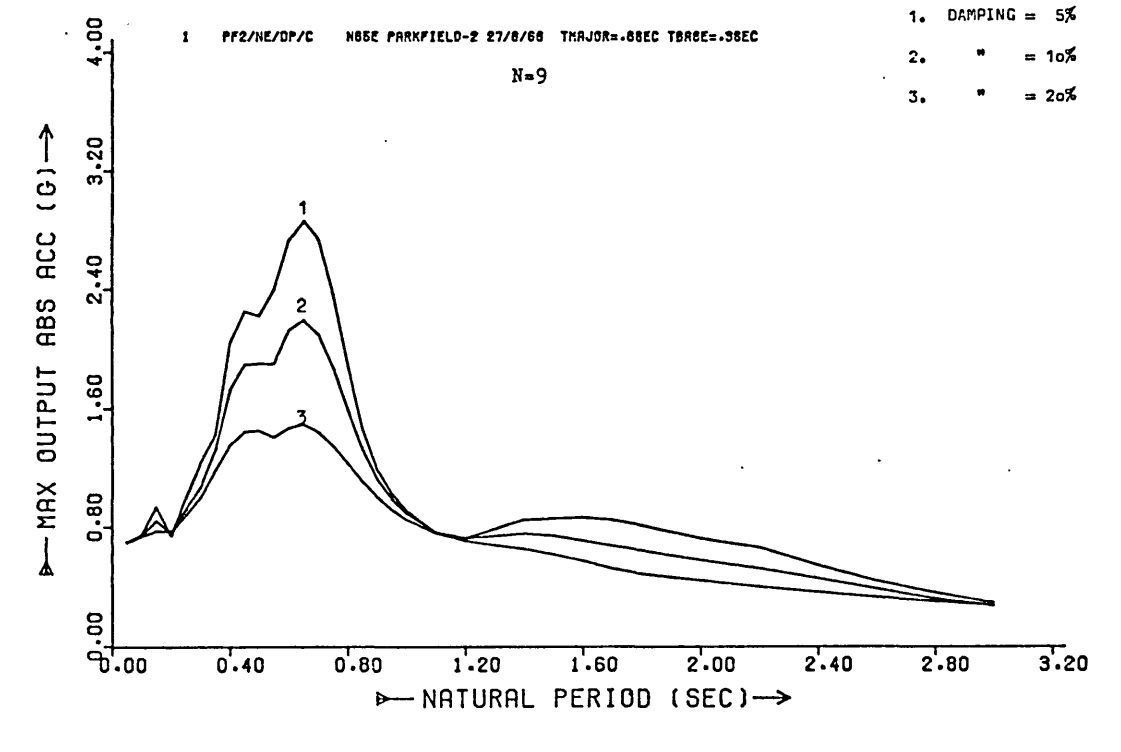


FIG.4.11d COMPUTED GROUND SURFACE ACCELERATION RESPONSE SPECTRA

NUMBER OF MODES INCLUDED = 9

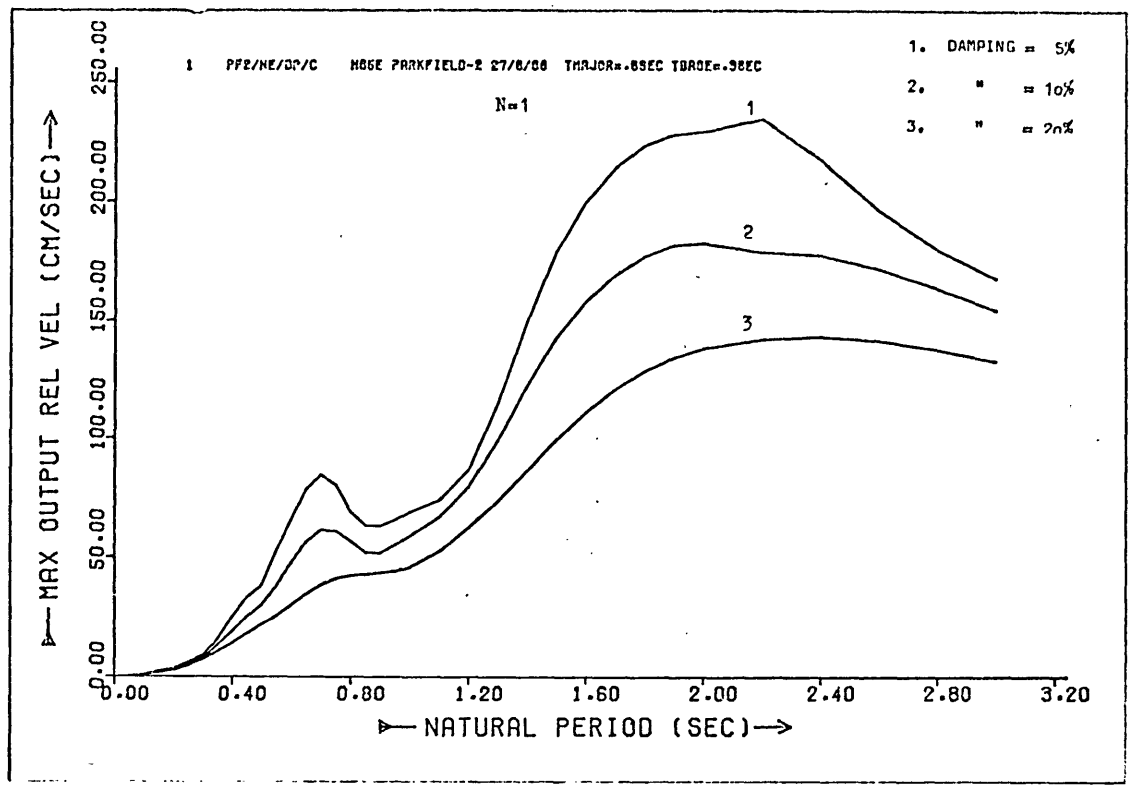


FIG.4.8e COMPUTED GROUND SURFACE VELOCITY RESPONSE SPECTRA

NUMBER OF MODES INCLUDED = 1

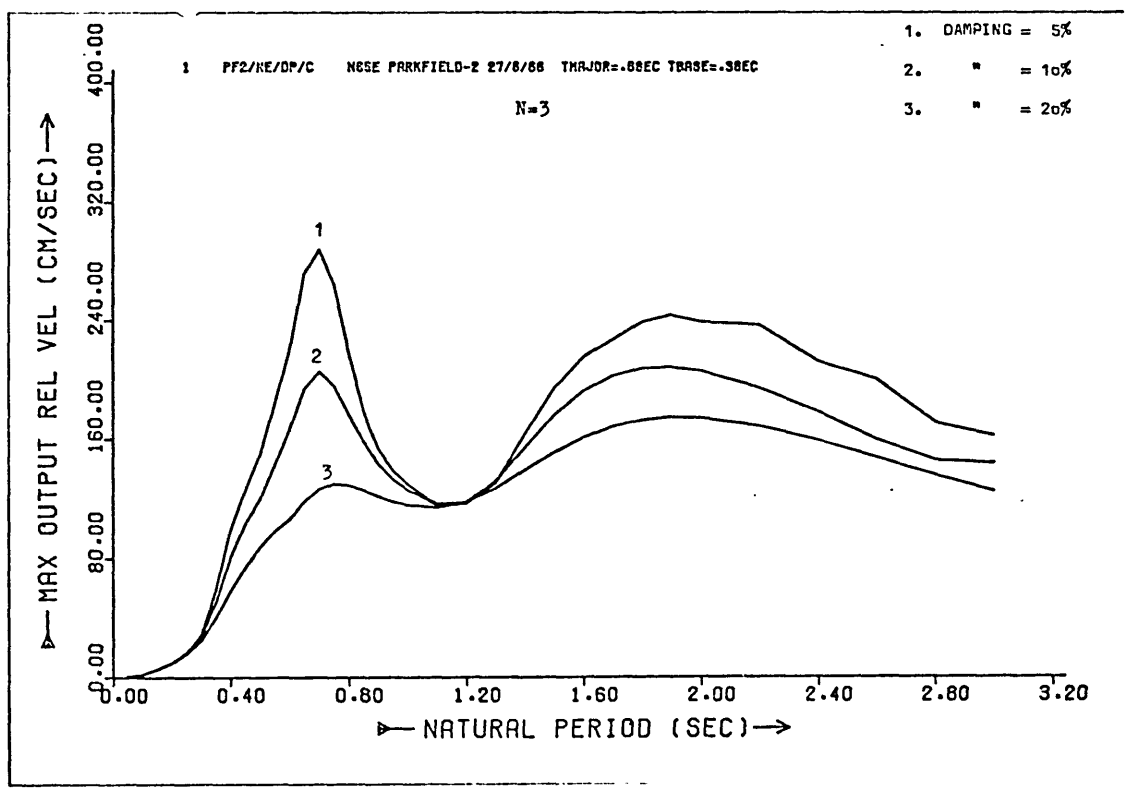


FIG.4.9e COMPUTED GROUND SURFACE VELOCITY RESPONSE SPECTRA

NUMBER OF MODES INCLUDED = 3

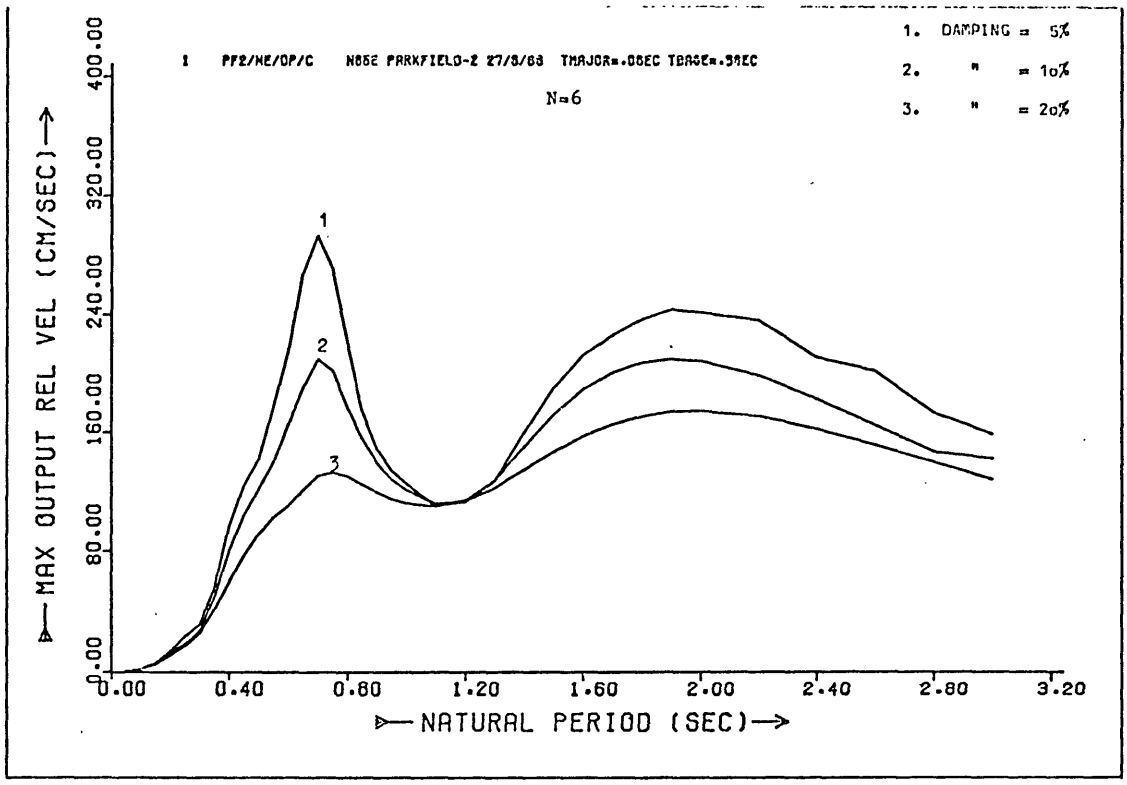


FIG. 4.1oeCOMPUTED GROUND SURFACE VELOCITY RESPONSE SPECTRA

NUMBER OF MODES INCLUDED = 6

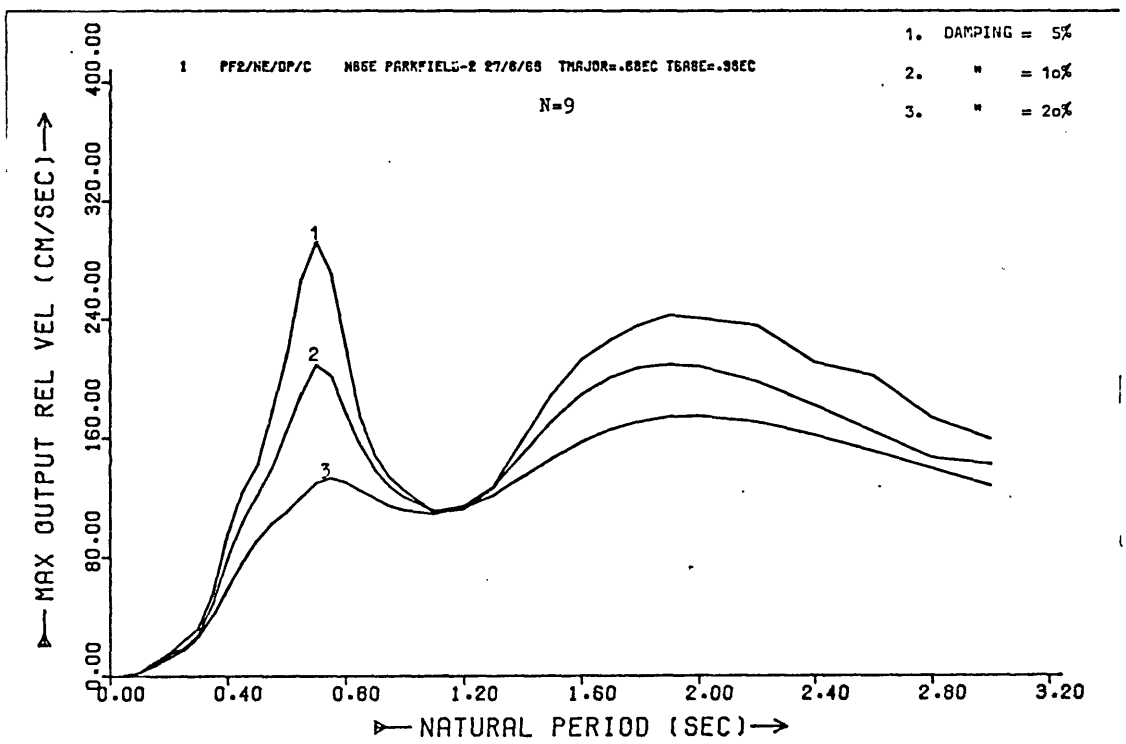


FIG.4.11eCOMPUTED GROUND SURFACE VELOCITY RESPONSE SPECTRA

NUMBER OF MODES INCLUDED = 9

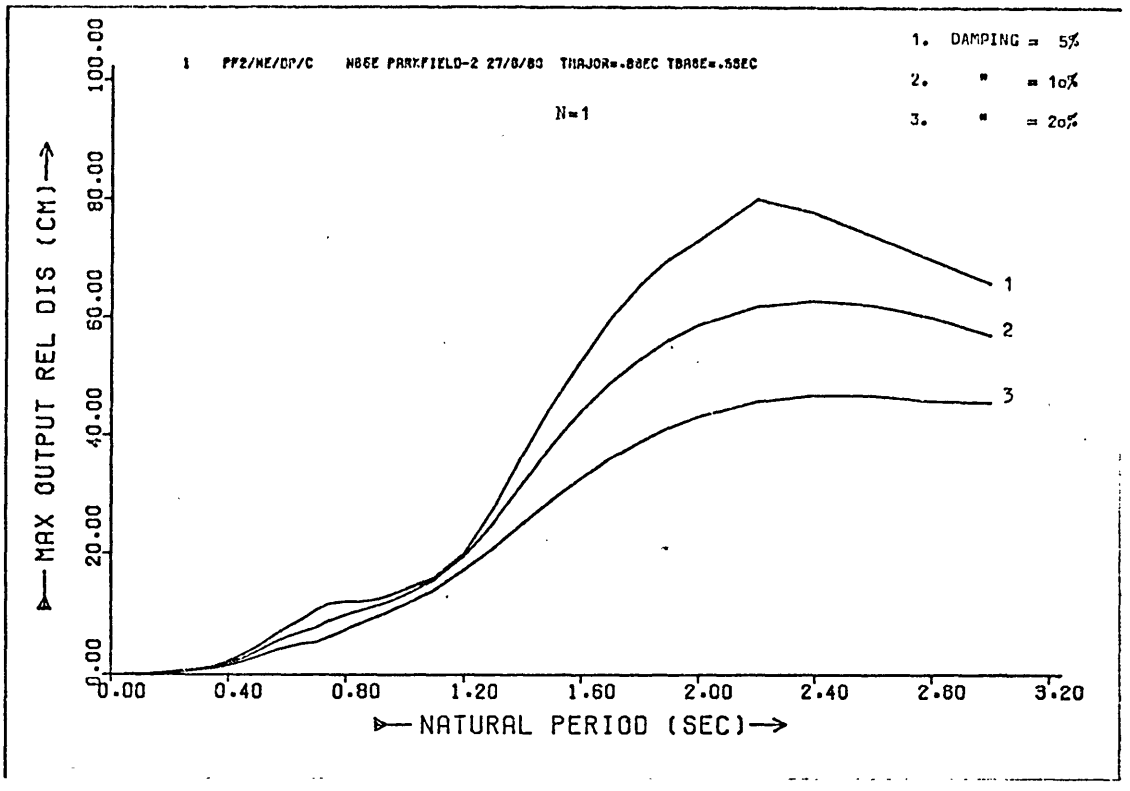


FIG. 4.8f COMPUTED GROUND SURFACE DISPLACEMENT RESPONSE SPECTRA

NUMBER OF MODES INCLUDED = 1

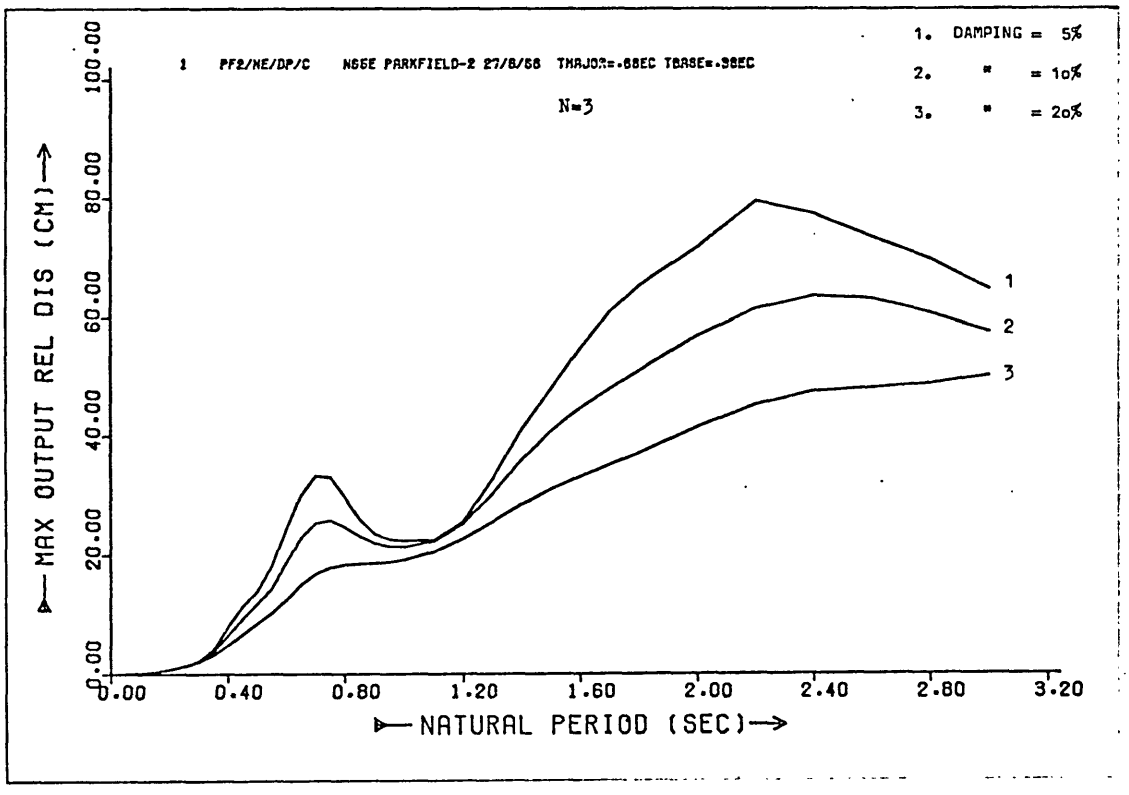


FIG. 4.9f COMPUTED GROUND SURFACE DISPLACEMENT RESPONSE SPECTRA

NUMBER OF MODES INCLUDED = 3

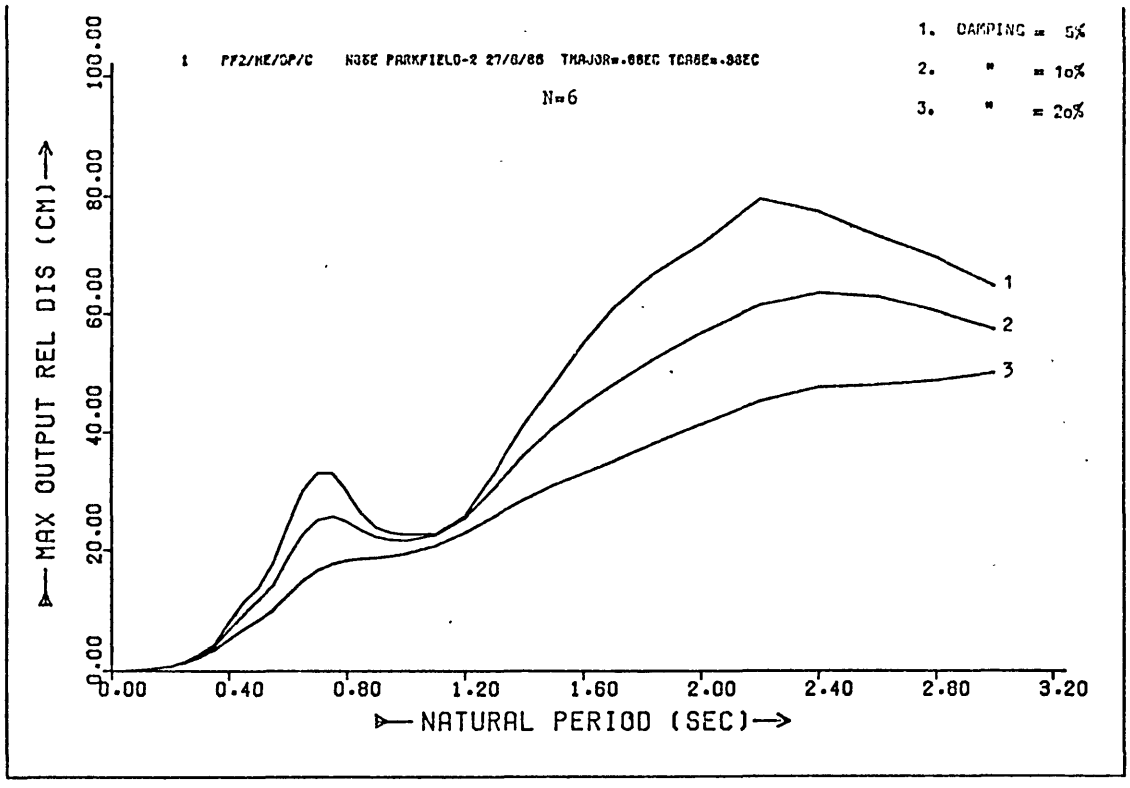


FIG.4.10 COMPUTED GROUND SURFACE DISPLACEMENT RESPONSE SPECTRA

NUMBER OF MODES INCLUDED = 6

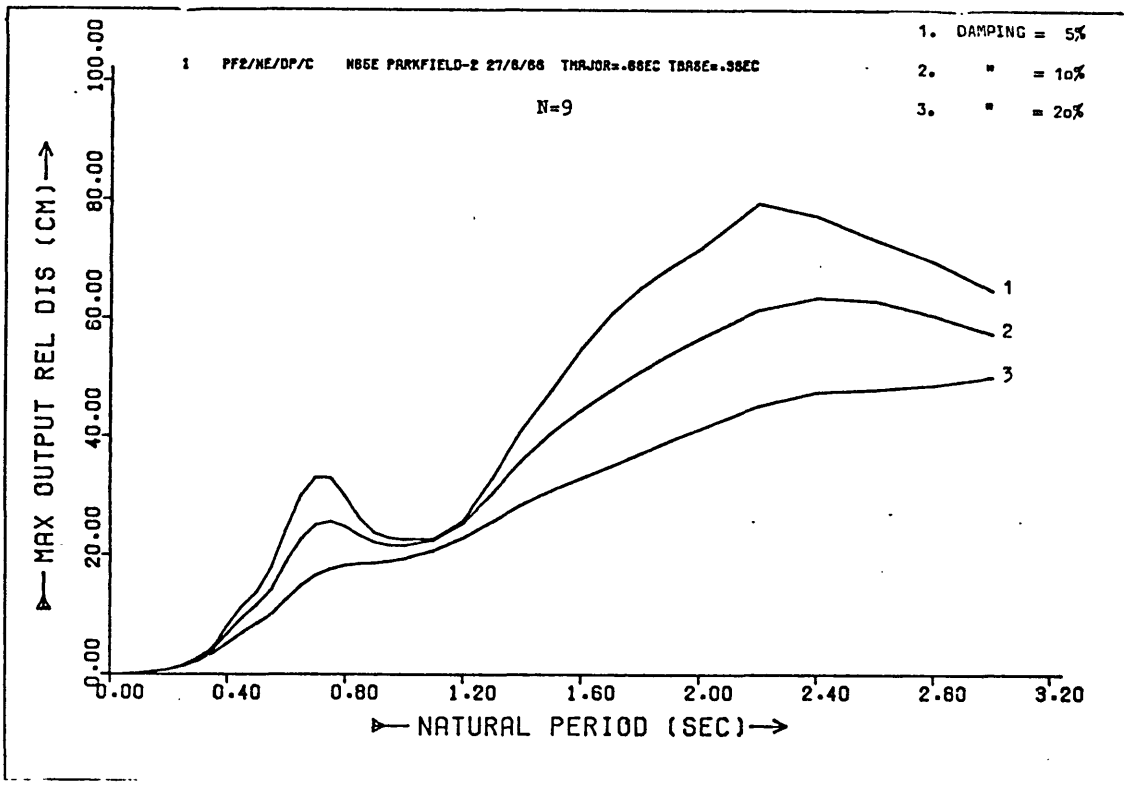


FIG.4.11 COMPUTED GROUND SURFACE DISPLACEMENT RESPONSE SPECTRA

NUMBER OF MODES INCLUDED = 9

4.7. SHEAR STRAIN AND SHEAR STRESS.

The distribution of shear strain throughout the height of the layer is calculated by differentiating (4.59) w.r.t. the depth "y":

$$\frac{\delta u\ (y,t)}{\delta y} = + \sum_{n=1}^{N} C_{nc\varepsilon} \cdot \int_{o}^{t} \dot{g}_o(\tau).e^{-\omega_n \mu_n (t-\tau)} \cos {}_nF_n(t-\tau)d\tau \ +$$

$$+ \sum_{n=1}^{N} C_{ns\varepsilon} \cdot \int_{o}^{t} \dot{g}_o(\tau).e^{-\omega_n \mu_n (t-\tau)} \sin {}_nF_n(t-\tau)d\tau \qquad (4.74)$$

and thus the distribution of shear stress $\tau(y,t)$ is expressed by

$$\tau(y,t) = G_s \frac{\delta u}{\delta y}(y,t) \qquad (4.75)$$

where:

G_s = shear modulus of the layer

$$C_{nc\varepsilon} = \frac{2(KA_n - B_n.a_n)}{H.(A_n^2 + B_n^2)} \sinh K\tfrac{y}{H}.\ \cos a_n\tfrac{y}{H} \ -$$

$$- \frac{2(A_n.a_n + B_nK)}{H.(A_n^2 + B_n^2)} \cosh K\tfrac{y}{H}.\sin a_n\tfrac{y}{H} \qquad (4.76)$$

$$C_{ns\ell} = \frac{2(K.A_n - B_n.a_n)}{H.(A_n^2 + B_n^2)} \cosh K\frac{y}{H} \sin a_n\frac{y}{H} +$$

$$+ \frac{2(A_n.a_n + B_n.K)}{H.(A_n^2 + B_n^2)} \sinh K\frac{y}{H} \cos a_n\frac{y}{H} \qquad (4.77)$$

4.8. OVERBURDEN PROPERTIES.

4.8.1. SOIL STRESS - STRAIN RELATIONSHIP USED.

When stress waves pass through soils, an apparent energy dissipation is observed. The elastic material relationship connecting the state of stress to the state of deformation has built into it the assumption that stresses are independent of the rate of deformation, i.e.

$$\tau = G.\gamma \qquad (4.78)$$

This would lead to unacceptable conclusions. To remedy the situation, a time dependence factor is introduced in (4.78) in the form

$$\tau = G.\gamma + C1.\frac{\delta\gamma}{\delta t} \qquad (4.79)$$

This means that the state of stress does not only depend on the state of deformation, but also on the rate at which strain changes. Use of this relationship does not imply that soil is thought to be visco-elastic, Kelvin type material. Rather, this relationship is used because the coefficients appearing in the relation regarded as parameters characterizing the properties of the material can be made to fit the key

features of the response of hysteretic material. In the present study, equation (4.79) was used in deriving basic one-dimensional wave equation given by 4.1. The relationship between the coefficient of viscosity in shear "C1" of the overburden and hysteretic damping ratio "ξ" is given by equation 4.81.

4.8.2. DAMPING AND SHEAR MODULUS

The hysteretic damping ratio defined in fig. 4.12 provides a measure of energy absorbing characteristics of a deposit. Under earthquake loading, damping arises mainly from non-linear, frictional effects, known as hysteresis, caused by slipage among soil particles; therefore, the degree of slipage will affect the amount of energy absorbed.

From fig. 4.12 the hysteretic damping ratio

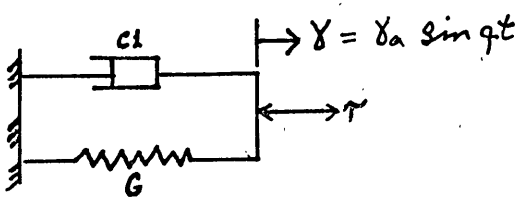
$$\xi = \frac{C1 \cdot P}{2 \cdot G} \qquad (4.80)$$

at resonance $P = \omega$ where "ω" is undamped natural frequency of the deposit, then:

$$\xi = \frac{C1 \cdot \omega}{2 \cdot G} \qquad (4.81)$$

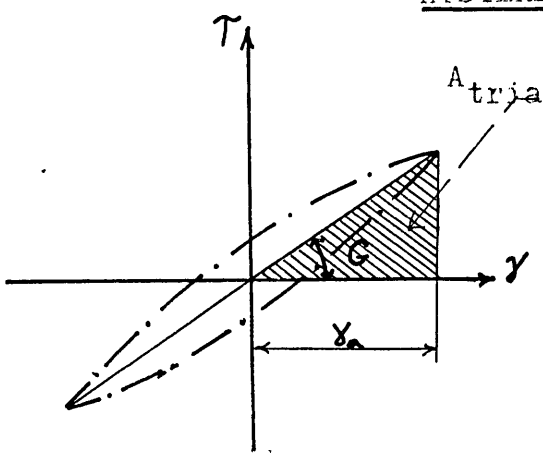
equation (4.81) has been employed in this study.

As indicated above and in chapter 5, there is a growing awareness that hysteretic damping ratio "ξ" is frequency independent but dependent on strains greater than $10^{-3}\%$ developed during earthquakes. Lack of information on the quantitative strain dependence enables one



$$\tau = G \cdot \gamma + c1 \cdot \frac{\delta \gamma}{\delta t}$$

HYSTERETIC DAMPING RATIO "ξ"



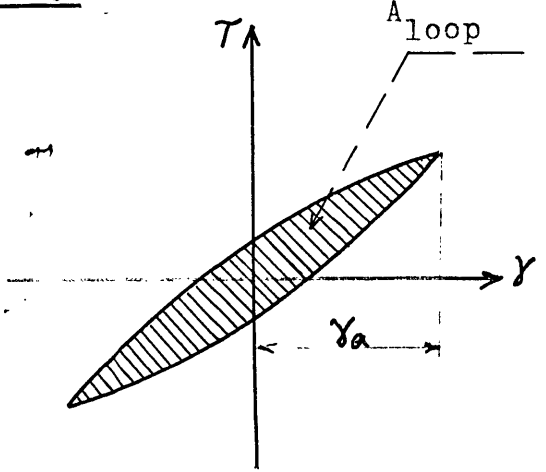
q=circular frequency of applied motion

γ_a=shear strain amplitude

A=area

Maximum strain energy stored during cycle of loading $= A_{triangle} =$

$$= \frac{1}{2} \cdot G \cdot \gamma_a^2$$



q=cilcular frequency of applied motion

γ_a=shear strain amplitude

A=area

Energy lost during cycle of loading $= A_{Loop} = \int_0^{\frac{2\pi}{q}} \left(c1 \cdot \frac{\delta \gamma}{\delta t} \right) d\gamma$

$$= c1 \cdot \int_0^{\frac{2\pi}{q}} \left(\frac{\delta \gamma}{\delta t} \right)^2 \cdot \delta t = \underline{\underline{\pi \cdot c1 \cdot q \cdot \gamma_a^2}}$$

$$\xi = \frac{A_{loop}}{4\pi \cdot A_{triangle}} = \frac{c1 \cdot q}{2G}$$

FIG. 4.12 HYSTERETIC STRESS - STRAIN RELATIONSHIP

to take this effect into account. Similar arguments apply to shear modulus "G", determined from the slope of the line joining the picks of the hysteresis loops.

Variation of shear modulus with depth has been observed in the field for soil deposits. The true variation is not known. Using numerical techniques and rigid bedrock, Kiefer[38] has studied how the response of a deposit with constant modulus differs from that of a variable modulus. He concluded that maximum accelerations are slightly higher throughout of the deposit with a constant modulus. Computed acceleration spectrum at the surface of both deposits shown in fig.4.13 illustrate almost identical shapes, except constant modulus site having slightly higher peak. (fig.4.13 show results from one of the 3 sites studied by him; the other 2 sites also show similar results).

In this study the shear modulus of the overburden was taken to be uniform throughout the depth of the overburden, since the main objective of the study was to investigate the influence of bedrock characteristics on ground response.

4.9. SPECIAL CASES OF INTEREST.

The complexity of the developed solution makes it unrewarding to try to test its special cases analytically. The solution has, therefore, been evaluated numerically for special cases of interest. The results are as follows:

4.9.1. RADIATION DAMPING RATIO ASSIGNED TO ZERO AND HYSTERETIC DAMPING RATIO NOT ZERO

Radiation damping ratio assigned to zero (RAD = 0) means that

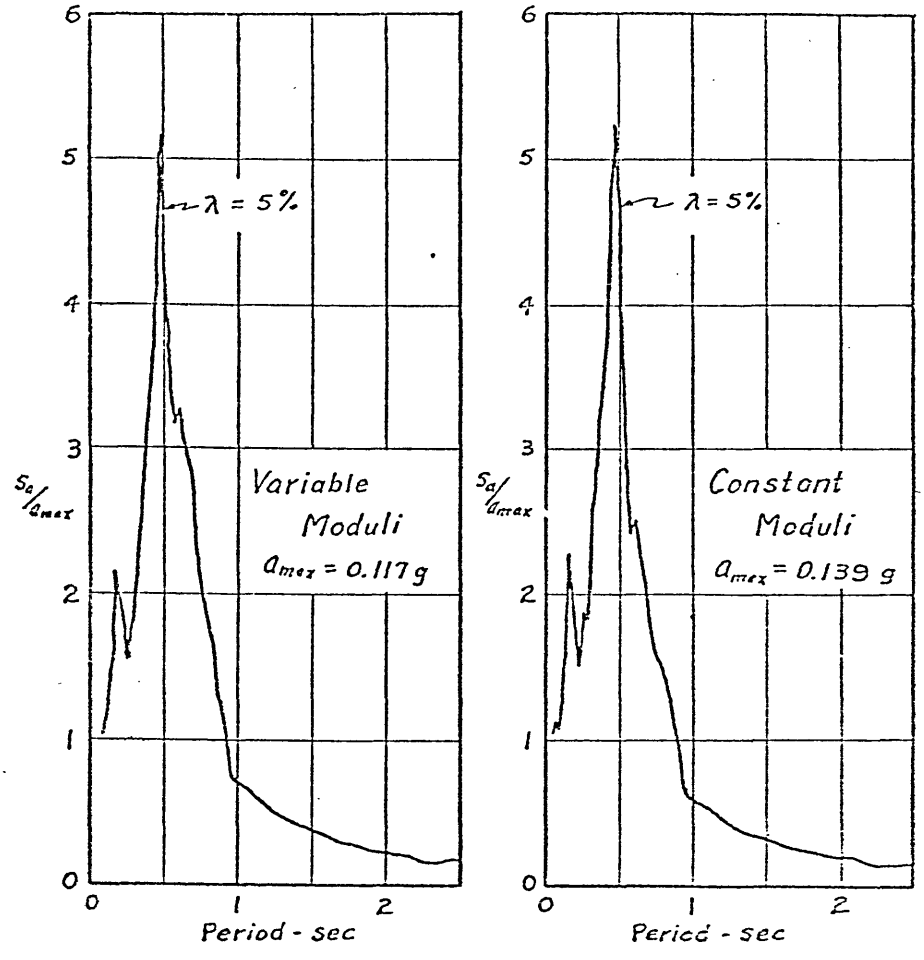


FIG. 4.13 COMPARISON OF NORMALIZED ACCELERATION RESPONSE SPECTRAS FOR A SITE , H=5o ft. SHEAR STRENGTH S_u=96op.s.f., ξ=o.o7 INPUT TAFT S21W 21 JULY 1952 * o.3. USING A LUMPED MASS SOLUTION Ref. 38

underlying half-space becomes infinitely rigid. The transmitting boundary ceases to allow waves to pass out to underlying half-space and spurious reflections occur. The developed ground motion at the surface of the overburden can be considered to be an upper bound on the actual ground motion.

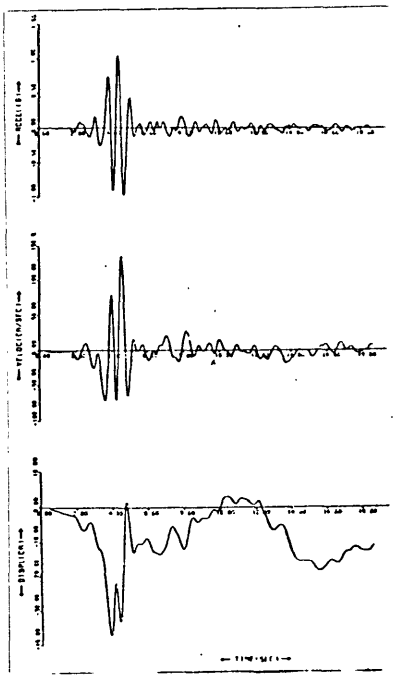
To test this special case of interest, a site consisting of loose gravel with a shear wave velocity of 500 m/sec., depth to bedrock of 75 m, zero radiation damping ratio and 20% hysteretic damping ratio was analysed. The input motion at bedrock level used was that of D. Papastamatiou,[46] a copy of which is available at Imperial College, Parkfield 2 recorded at Parkfield, California on 27/6/1963, with a maximum velocity of 67.89 cm/sec. and a predominant period of 0.6 secs.

Results of the calculations from developed solution and lumped mass solution are compared on the basis of absolute surface acceleration, velocity and displacement time histories. The computed time histories compare very well.

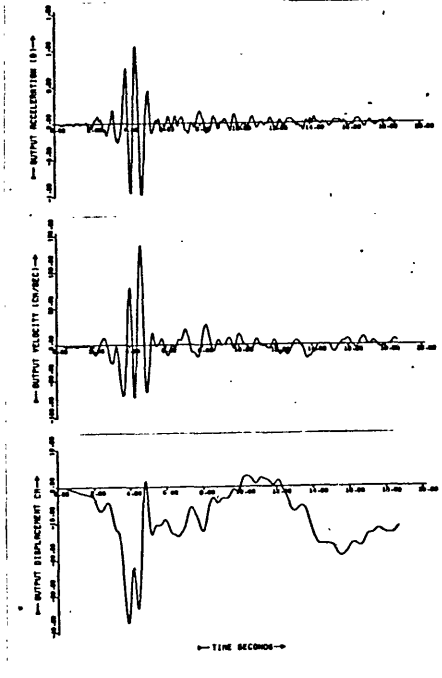
Fig.4.14(a) and (b) show computed time histories at the surface, the deposit from lumped mass and the developed model. The agreement between the lumped mass and closed form solution is good.

4.9.2. RADIATION AND HYSTERETIC DAMPING RATIOS ASSIGNED TO ZERO

To test this special case of interest, a site similar to that described in section 4.9.1, with the same bedrock motion, was chosen. Hysteretic damping ratio was assigned to zero. Computed response in



(a) COMPUTED BY LUMPED MASS SOLUTION



(b) COMPUTED BY THE DEVELOPED METHOD

FIG. 4.14(a) and (b) TIME HISTORIES FOR A SURFACE POINT OF A SOIL DEPOSIT WITH H=75m. S=500m. ξ=0.2 RAD=0.0

the form of absolute surface acceleration, velocity and displacement time histories from developed solution and lumped mass model were compared. Excellent agreement between the computed time histories were obtained.

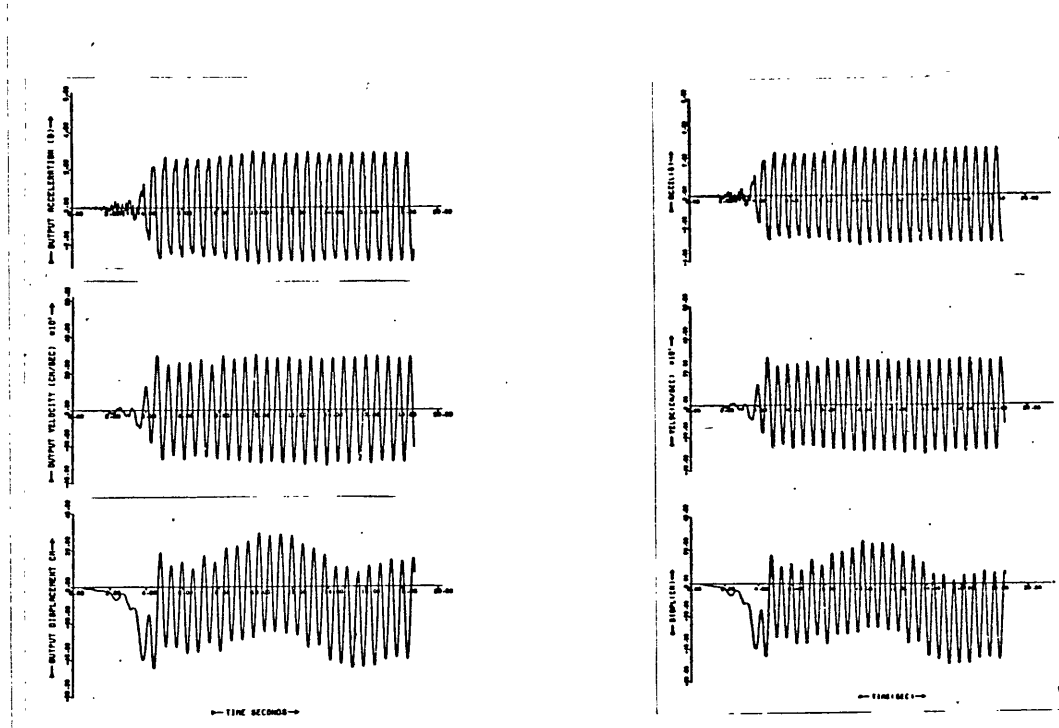
Figs.4.15 (a) and (b) show these results. The results are in good agreement.

4.9.3. RADIATION DAMPING RATIO TENDING TO ONE WHEN HYSTERETIC DAMPING RATIO ASSIGNED TO ZERO

Radiation damping ratio tending to one when hysteretic damping ratio assigned to zero implies that material of the overburden approaches to that of underlying half-space. The input disturbance $0.5\ddot{g}_o(t)$ reaches to the free surface without knowing that it has travelled through the overburden. Since the air at free surface absorbs practically negligible energy, total reflection occurs at free surface and the input disturbance becomes $\dot{g}_o(t)$. The disturbance at the surface is conceived of superposition of the incident wave and its mirror image that moves in the opposite direction. The free surface acts as a mirror.

To investigate this special case of interest a site similar to that described in section 4.9.2 was chosen. The radiation damping ratio was assigned to 0.98, (RAD must be less than one, see appendix G), which is very close to one.

Figs.4.16a,b show comparisons of bedrock acceleration time histories if this surface were free with computed surface motions. They are in good agreement. As expected, there is a minor shift in the

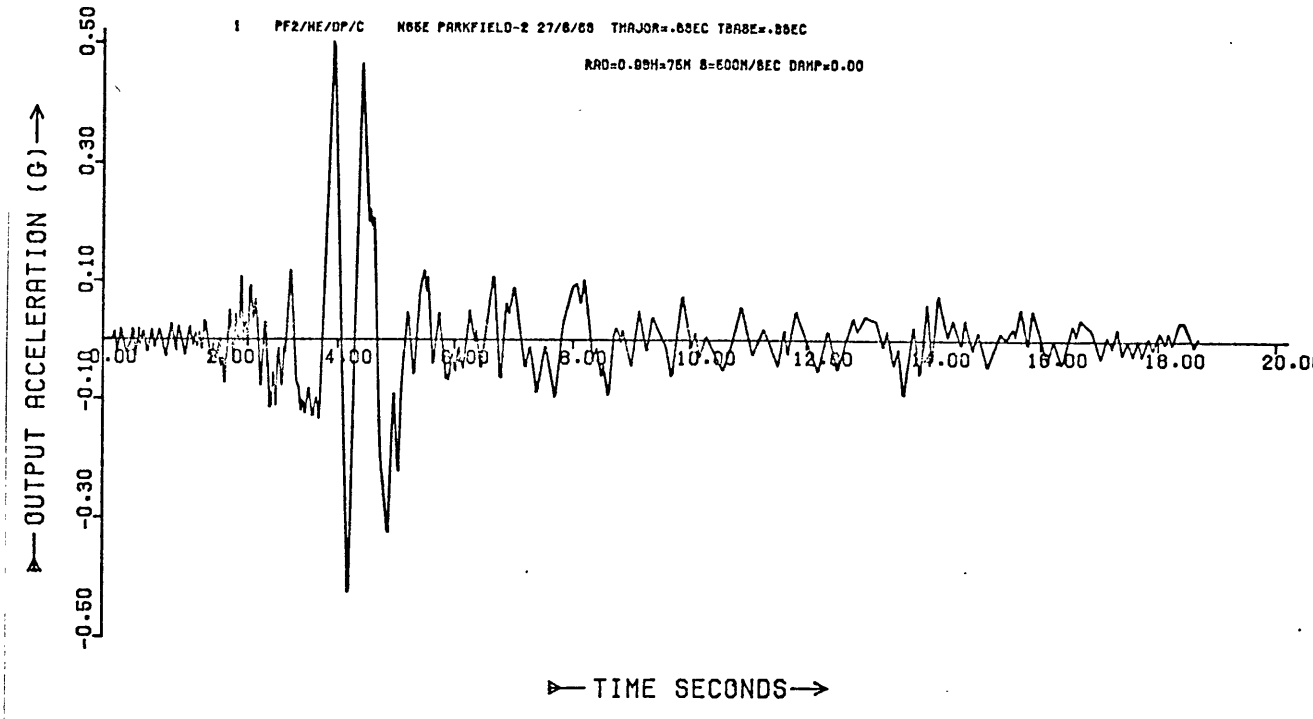


(a) COMPUTED BY THE DEVELOPED METHOD

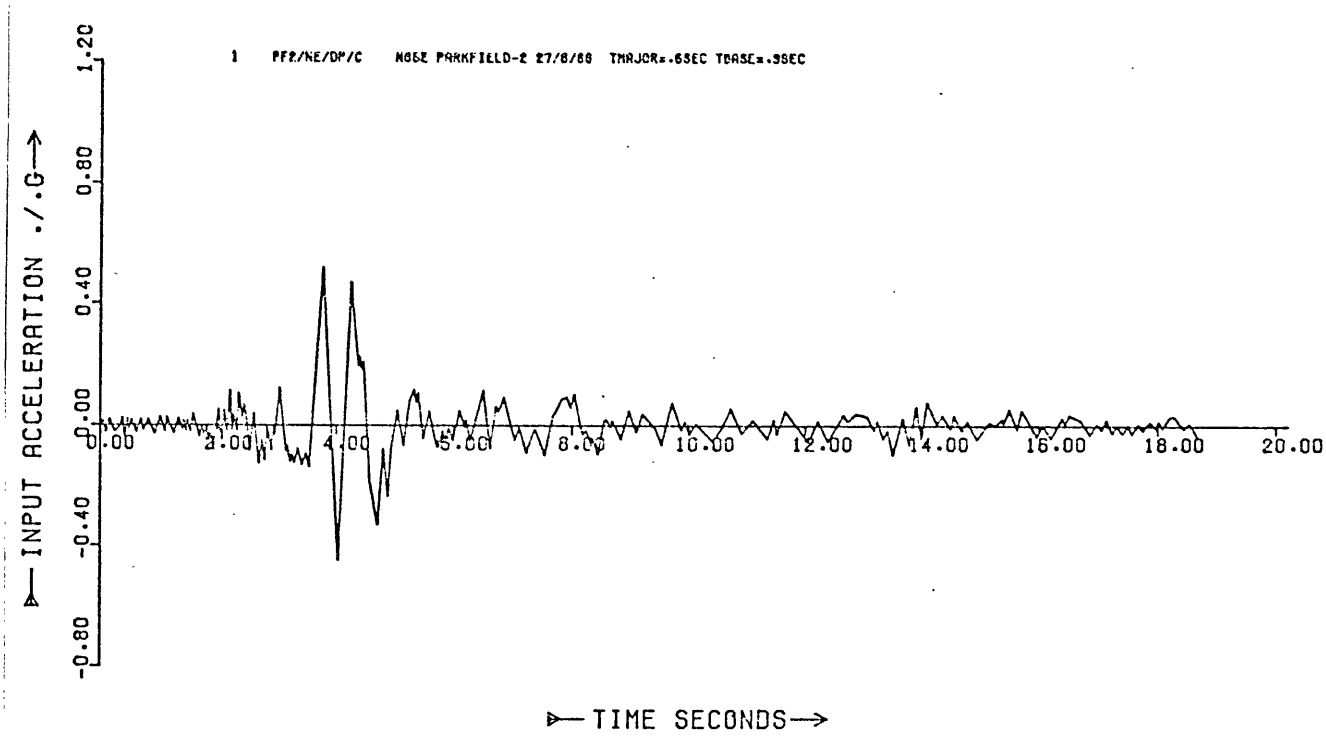
(b) COMPUTED BY LUMPED MASS SOLUTION

FIG. 4.15 (a) and (b) TIME HISTORIES OF A SURFACE POINT OF A SOIL DEPOSIT H=75m .S=500m. ξ =0.0 RAD= 0.0

NOTE SCALES ARE DIFFERENT



(a) SURFACE



(b) BEDROCK

FIG. 4.16 SUBSURFACE AND BEDROCK ACCELERATION TIME HISTORIES FOR A SITE, H=75m, S=500m/sec, ξ=0.0, RAD=0.98

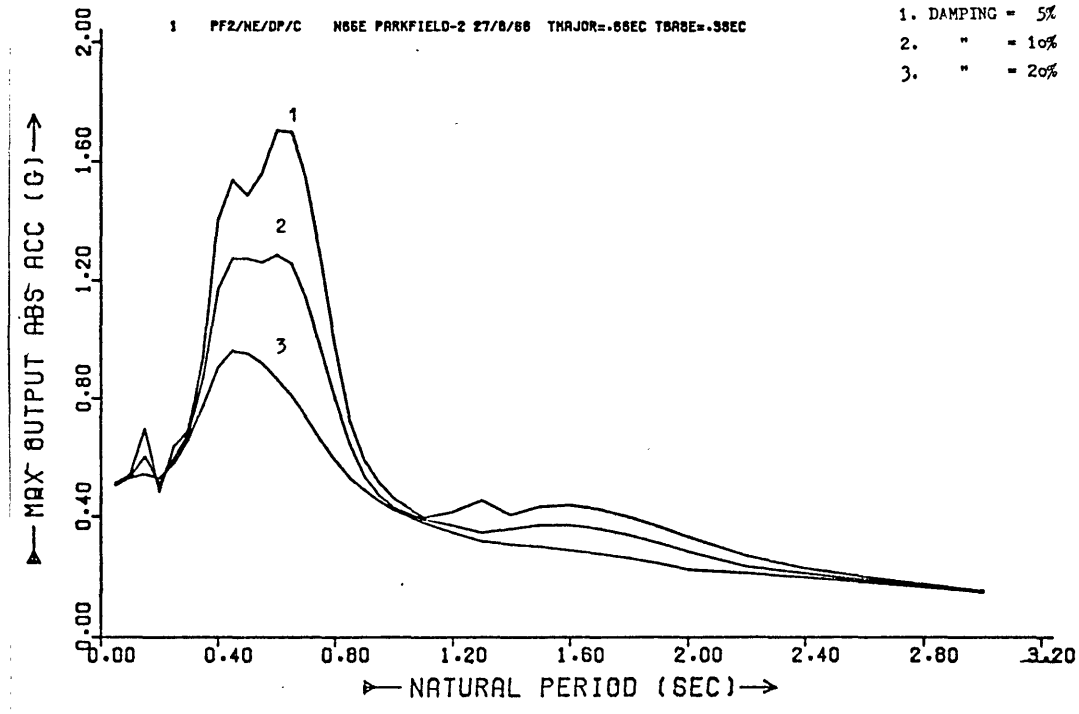
time co-ordinates of computed ground motion equal to 0.15 secs. This is the time taken for the motion to travel from bedrock to surface.

Acceleration and velocity response spectrum for bedrock motion and for ground surface motion obtained are shown in figs. 4.17&4.18 The good agreement between the spectrum over the period range considered indicate that the objective noted in the first paragraph has been accomplished.

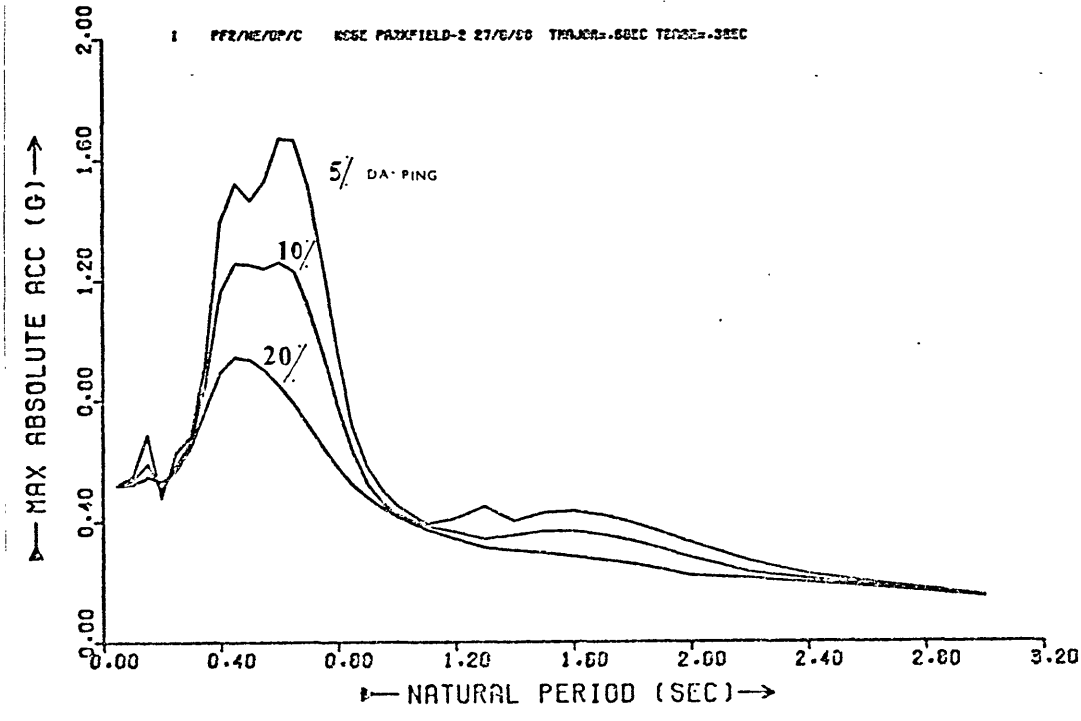
4.10. DEVELOPED SOLUTION COMPARED WITH MODIFIED LUMPED MASS MODEL RESULTS

In order to investigate how results of the developed solution compares with that of modified lumped mass model for real sites with real material properties, a site consisting of dense sand with shear wave velocity of 450 m/sec., depth to bedrock of 150 m., radiation damping ratio of 0.32, and 1% hysteretic damping ratio was adopted. The input motion at bedrock level was the one described in section 4.9.1.

In order to assess impact of model difference on the output response for the specific input considered, results of the calculations were compared on the basis of surface acceleration, velocity and displacement time histories. The results which are of great importance to earthquake engineers are given in figs. 4.19(a) & (b). Fig 4.19 (a) was produced from Dr. Papastamatios Ph.D. thesis with his special permission. Good agreement between the results gives one confidence that both the developed solution and the computer program described in chapter five are correct and reliable in the ranges of damping and frequencies of interest to earthquake and geotechnical engineers at the present time and provide a realistic basis for assessing the influence of local soil conditions on ground response during earthquakes.

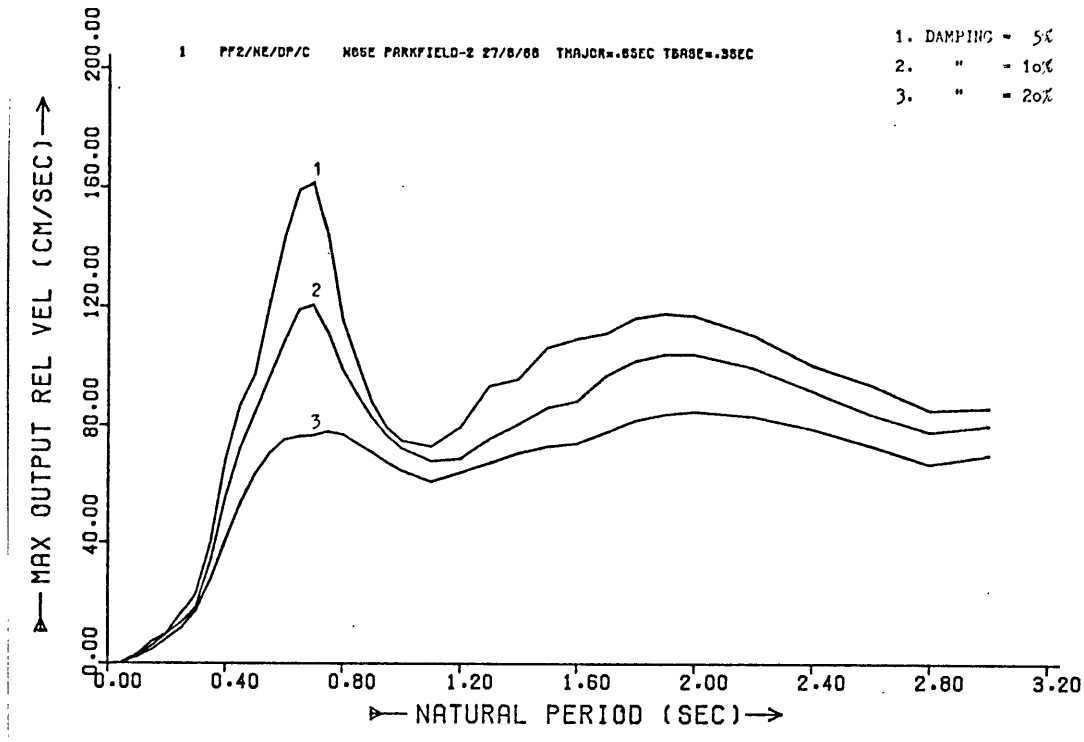


(a) SURFACE

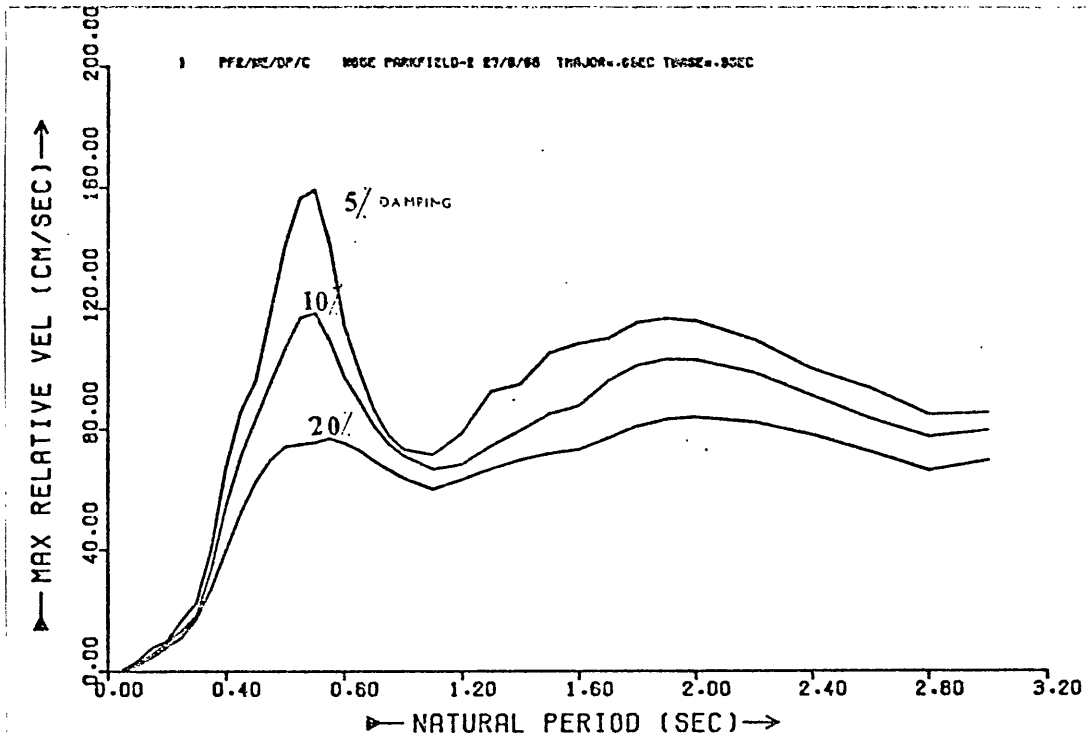


(b) BEDROCK

FIG. 4.17 SURFACE AND BEDROCK ACCELERATION RESPONSE SPECTRAS FOR A SITE , H=75m, S=500m/sec. ξ=0.0,RAD=0.98

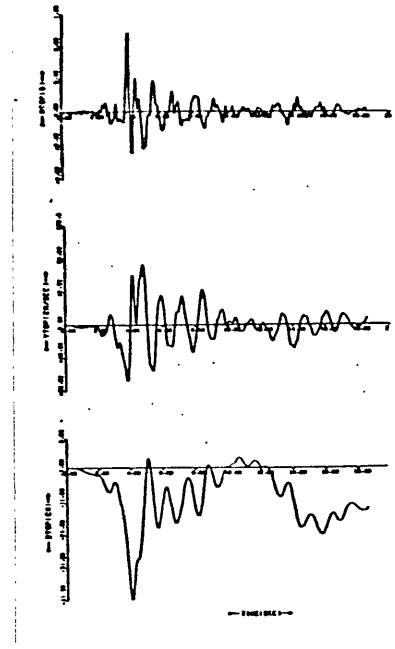


(a) SURFACE

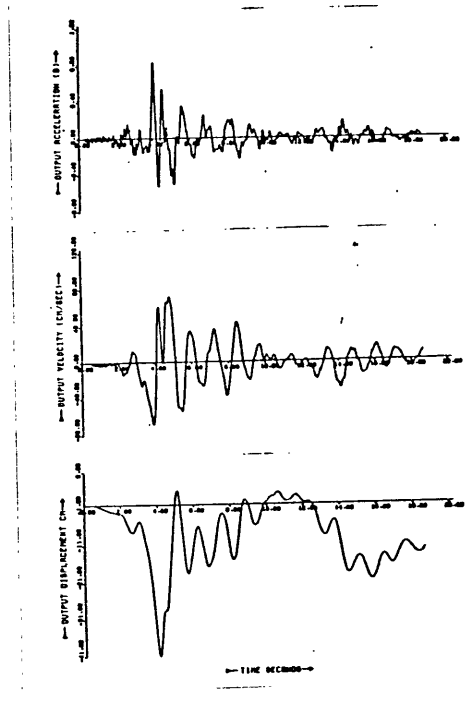


(b) BEDROCK

FIG. 4.18 SURFACE AND BEDROCK VELOCITY RESPONSE SPECTRAS FOR A SITE H=75m, s=500m/sec, ξ=0.0,RAD=0.98



(a) CALCULATED BY MODIFIED LUMPED MASS METHOD



(b) CALCULATED BY THE DEVELOPED METHOD

FIG. 4.19(a)and (b) TIME HISTORIES FOR A SURFACE POINT OF A DEPOSIT WITH H=75m. S=45om. ξ=o.o1 RAD =0.32

4.11. CONCLUDING REMARKS

a) In developing this new theory described in this chapter, use of some mathematical principles were made, which are not original, to be described in detail, but the developed design method is invaluable to practising earthquake and geotechnical engineers.

b) "In the absence of a complete solution of the problem, the best approximation must be accepted, if it appears to be reasonably adequate."[2] This is true in this case.

c) The approach seems to be compatible with the accuracy with which the data on material properties and bedrock motion in seismic response analysis can be obtained. Although further refinements in the theory are undoubtedly possible it is believed that the design method developed in this chapter can provide enough insight to guide practising earthquake and geotechnical engineers to evaluate the effect of ground conditions on ground response for practical purposes at the present time.

d) The method can also be used in developing countries by soil engineers, who may be handicapped by lack of large modern computers and have access only to small computers.

CHAPTER 5

DESCRIPTION OF COMPUTER PROGRAM, SOIL PROPERTIES IN SEISMIC RESPONSE ANALYSIS AND EVALUATION OF PORE WATER PRESSURE DISSIPATION

5.1. INTRODUCTION

In this chapter a description is given of the main features of the computer program named "EARTHQUAKE," consisting of 1200 cards, which was developed during the course of this work, to solve the earthquake response of soil deposits underlain by deformable bedrock by the developed method described in chapter 4.

EARTHQUAKE, represents the practical implementation of the theoretical modelling of horizontal soil deposits resting on flexible bedrock during earthquakes.

The second part of this chapter deals with soil properties in earthquake response analysis and dissipation of pore water pressures after earthquake excitation, as employed in the present study.

5.2. DESCRIPTION OF THE COMPUTER PROGRAM NAMED "EARTHQUAKE"

EARTHQUAKE, computes the response in a horizontal soil layer system, resting on flexible bedrock formation and subjected at the bedrock level to an earthquake excitation. The following set of operations can be performed by the program:

a) read the bedrock input motion in the form of time history of accelerations obtained from a strong-motion record.

b) read data for the soil deposit and its underlying bedrock formation.

c) compute new motions at the top of the layer or inside the layer.

d) print (or punch) and plot the motions at the top of the layer or inside the layer.

e) compute, print and plot acceleration, velocity and displacement response spectrum for the motion.

f) compute, print and plot the acceleration velocity and displacement amplification spectra for the layer.

g)* compute, print and plot stress or strain time-history at any point in the layer.

h) compute and print strength (see section 7.1) of the earthquake at the surface of the deposit.

The program was developed on the CDC6400 computer of Imperial College using FORTRAN IV. It has been run on CDC6600 and 7600 of University of London. The program requires a core storage of 50K to analyse a layer system, subjected at its flexible base to an accelergram consisting of 2000 points.

---

* can easily be included.

A description of the program sequence of operation and the functions of various modules and subroutines are as follows:

5.2.1. STRUCTURE OF PROGRAM

The program consists of six modules, each with a distinct operational function. Each module is composed of one or more subroutines. The modules are controlled by the main program, a description of which, as well as the program sequence of operations, is briefly given below:

MAIN PROGRAM, the main program calculates the sine and cosine integrals (given by 4.67 and 4.66) and multiplies these integrals to their corresponding coefficients, which have been calculated and stored by the previous call of COEF, and adds these separate contributions for the specified number of modes to give the combined response at the specified time. It also writes the response values in the form of absolute acceleration, velocity and displacement time histories, with their maximum values, separately.

1. BEDROCK MOTION MODULE, this is the first module called by the main program and is composed of two subroutines called READ and INTERP. READ, handles the input bedrock motion, i.e. reads the digitized time history, which is available in the form of decks of punched cards. The accelerations are normally specified at an arbitrary interval, which are not often good to be used as integration interval in computing the base velocity time history which serves as input to the analysis. Thus it is necessary to interpolate the earthquake record to intervals of 0.01 or 0.02 seconds. Both time

intervals are often good values to be used in computing the response. A time interval of 0.02 second was used throughout the analyses in this thesis. The small time interval is also necessary to ensure stability of the developed solution. The control of calculations of interpolation is done by means of subroutine INTERP, which is controlled by READ, and is capable of interpolating the acceleration time history record to any specified time interval. The subroutine READ, also computes bedrock displacement time history and the maximum values of bedrock acceleration, velocity and displacement time histories.

2. COEFFICIENT AND MATERIAL MODULE, this is the second module called by the main program and is composed of one subroutine called COEF. It handles input data describing the material properties of the overburden, its underlying bedrock (i.e. hysteretic and radiation damping ratios and shear wave velocity of the overburden) and depth to bedrock. The subroutine computes also the coefficient of the sine and cosine integrals given by 4.57 and 4. 56 , for any specified number of modes of vibrations and depth from surface and stores these values for use in the main program.

3. SPECTRA MODULE, this module consists of the subroutines SPECT, MAXVAL and is entered after the response time histories are calculated. The module evaluates dynamic response spectra at various periods, writes and plots the results. On the basis of computed acceleration time histories, the routine integrates the convolution integral for various damping ratios. Absolute accelerations, relative velocities and displacements are computed for natural periods from 0.05 seconds

to 3.0 seconds. The routine MAXVAL, which is controlled by SPECT, finds the absolute maximum value of the calculated response.

4. AMPLIFICATION MODULE, this module consists of the subroutine AMP. It computes acceleration and velocity amplification spectrum, for the natural periods and damping values for which input and output spectrum have been evaluated. It writes and plots the results.

5. STRENGTH MODULE, this module calculates the new measure of severity of ground shaking named "Strength" (see 7.3.1). It consists of one subroutine STRNGT.

6. PLOTTING MODULE, this is the last module entered and is composed of several plotting routines, which plot the dynamic response of the overburden in the form of acceleration, velocity and displacement time histories vs. time, using either KINGMATIC or CALCOMP plotters of computer centre of Imperial College.

The schematic diagram of the modules is shown in fig. 5.1.

5.2.1.1. CONCLUDING STATEMENT

Besides the main program EARTHQUAKE, four other programs namely:

1. FILTER (350 cards)
2. PORE PRESSURE (250 cards)
3. ADJUST (250 cards)
4. SPECTRA (300 cards)

were developed. These programs are explained in chapters 9, 8 and 3, respectively. The average time taken for development of these programs as well as EARTHQUAKE, is four to five cards per day.

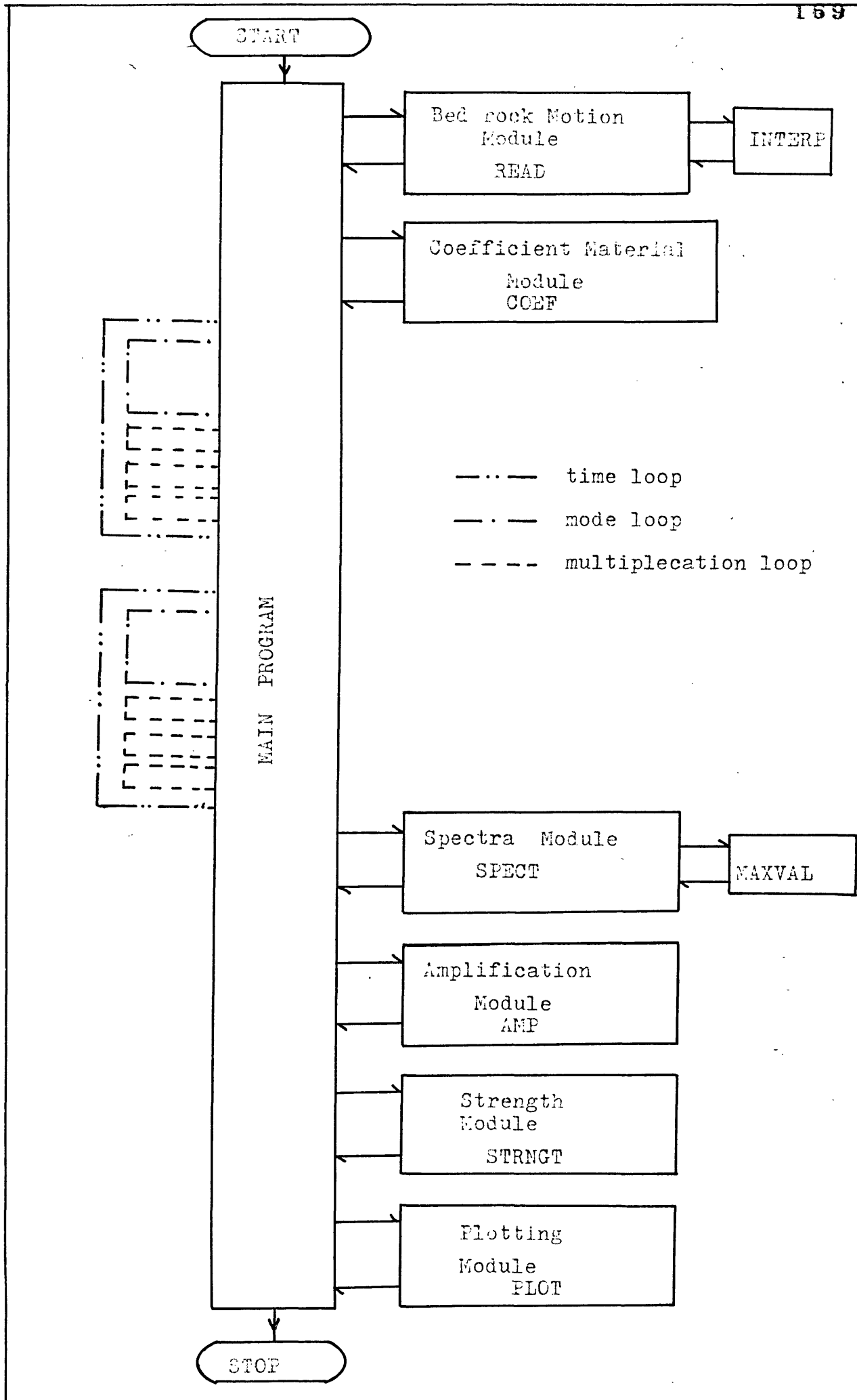


FIG. 5.1 MAIN PROGRAM AND ITS MODULES

5.3. SOIL PROPERTIES IN SEISMIC RESPONSE ANALYSIS

5.3.1. INTRODUCTION

In the ground response theory developed in chapter 4, the overburden has been characterized by depth to bedrock, shear wave velocity (or shear modulus), mass density and hysteretic damping ratio and the half-space by shear wave velocity (or shear modulus) and mass density. It is only through accurate determination of these constants that realistic results can be obtained by the method developed. Considerable effort has been put into the development or improvement of methods for determining the dynamic soil properties; but still the present knowledge of the dynamic properties of soils is still inadequate. This is because stress-strain-time relations for soils are complex and, as Finn[23] put it early in 1977, "our analytical capability far outstrips our ability to describe the stress-strain-time behaviour of the soils."

5.3.2. DAMPING CHARACTERISTICS AND SHEAR WAVE VELOCITY OF SOIL DEPOSITS

5.3.2.1. DAMPING CHARACTERISTICS

As stated in section 4.8.2, the energy loss in soils under earthquake loading is caused mainly by internal friction resulting in a damping ratio which is independent of frequency for the range from 0.1 c.p.s to 200 c.p.s, at low strains of 10^{-5} to 10^{-3} per cent. This is proof that damping is caused primarily by non-linear rather than viscous effects.[62]

A survey of the factors affecting the damping factor of soils have been presented by Hardin and Drnevich.[27] The authors suggest that the energy dissipation characteristics of soils are expressed as a percentage of critical damping, referred to as the hysteretic damping ratio, which is found to be dependent upon many factors, such as strain amplitude, effective overburden pressure, void ratio, degree of saturation, etc.. Measured average values of hysteretic damping ratio for sands and saturated clays are shown in figs. 5.2 and 5.3.

Figs. 5.2 and 5.3 clearly illustrate that at small strains, as occur in small and moderate earthquakes, the hysteretic damping ratio is very small and tends to zero at very low strains, which further consolidates the assumption made in section 4.4.1.5. The values of the hysteretic damping ratio used in the present study for different soils were determined on the basis of the results reported by[53,61] [35,20] and, in some cases, on the basis of values used by different investigators, reported in chapter 2.

5.3.2.2. SHEAR WAVE VELOCITY

The shear wave velocity of soil deposits is determined by either field geophysical methods or tests on the soil samples in the laboratory. Good experimental and field data on shear wave velocity are relatively scarce. The values for this parameter used in the present study were determined on the basis of results reported in[53, 63,5,20]

5.3.3. DEPTH TO BEDROCK

If a reasonable degree of success is to be attained in the

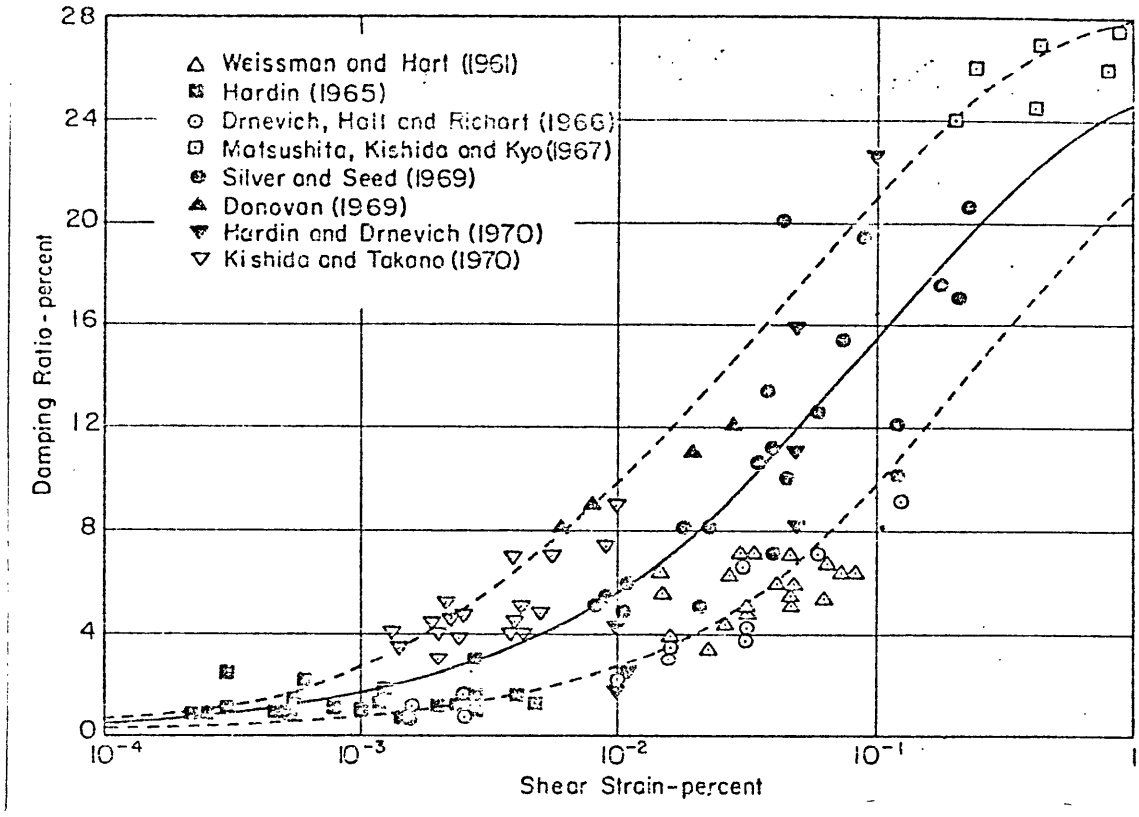


FIG. 5.2 DAMPING RATIOS FOR SANDS
Ref. 53

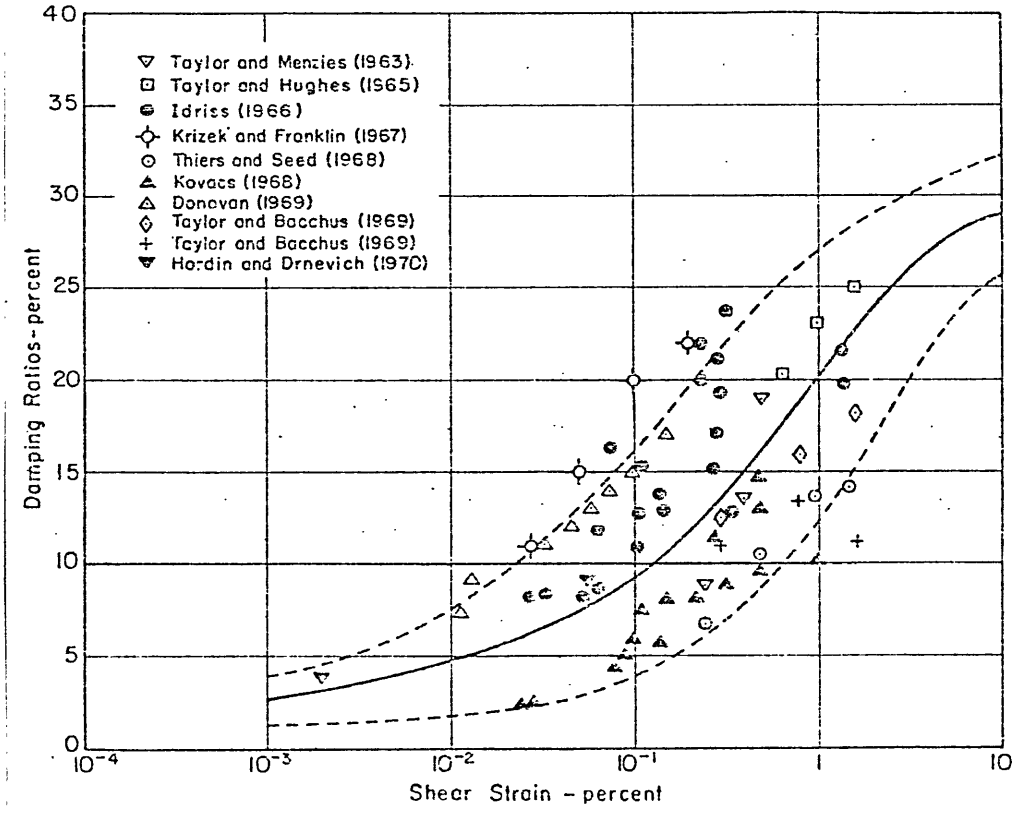


FIG. 5.3 DAMPING RATIOS FOR SATURATED CLAYS
Ref. 53

prediction of the influence of local soil conditions on bedrock motion, a good determination of the depth to bedrock would be necessary. Depth to bedrock of foundations is determined by means of borings and by taking continuous samples. The number of borings and the interval at which samples are taken would depend on the importance of the project. Making holes in ground below a depth of 100m is uneconomical. Below this depth, geophysical refraction surveys are used to determine depth to bedrock. The results are then backed with any available information in the area (geological maps, water well drill logs, etc.). The order of error involved in depth to bedrock determination is as follows: [20]

Bedrock depth (m)	Approximate accuracy (m)
0 - 30	1.5
30 - 60	1.5 - 3.0
60 - 150	6.0 - 15.0
150 - 300	15.0 - 30.0
> 300	60.0

5.3.4. SHEAR WAVE VELOCITY OF BEDROCK FORMATION

An assessment of the shear wave velocity of bedrock formation is necessary if computation of the ground motion is made according to the method developed in chapter 4. The shear wave velocity of rock formations can be determined either from core samples, geophysical methods or both. The main advantage of the field seismic technique is that it produces a much better picture of the number and character of discontinuities present.

In the present study, the term "bedrock" has been used to denote

a material for which the shear wave velocity at low strains is greater or equal to 600 m/sec. Typical values for shear wave velocity of different rocks are given by [26,63,5] which were used in this study.

5.3.5. CONCLUDING REMARKS

From the foregoing discussion one may conclude that:

a) The hysteretic damping ratio for soil deposits at small strains, as met with in small and moderate earthquakes, is very small and tends to zero at very low strains.

b) There is a huge gap in the data available; therefore,it is the more necessary to know the engineering properties of the materials in seismic response analysis before a satisfactory analysis can be made. There is no point in using a sophisticated analysis with poor material properties.

c) At the present time, shear wave velocity seems to be one of the most reliable parameters for classification of soil and rock materials under earthquake loading.

5.3.6. SELECTION OF SOIL PROPERTIES FOR EVALUATION OF PORE WATER PRESSURE DISSIPATION AFTER EARTHQUAKE SHAKING

Application of the developed theories in chapters 8 and 9 requires accurate determination of:

i) permeability of the sand deposit.

ii) compressibility of sand deposit.

The coefficient of consolidation for vertical drainage is calculated from

$$C_v = K/(m_v \cdot \gamma_w)$$

where:

K = coefficient of permeability for vertical drainage.

m_v = coefficient of volume compressibility.

γ_w = unit weight of water.

5.3.6.1. COEFFICIENT OF PERMEABILITY OF SAND DEPOSITS

The coefficient of permeability "K" of a soil is defined as the ratio of average percolation velocity to hydraulic gradient in the soil at that particular point. In general, a qualitative approximation of the permeability of the sand deposits can be made on the basis of grain size. Typical average values for the coefficient of permeability for different sand deposits has been given by Seed et al,[55] which have been used in this study.

5.3.6.2. COEFFICIENT OF VOLUME COMPRESSIBILITY

The coefficient of volume compressibility is defined as the change in volumetric strain corresponding to a small change in effective pressure. ($m_v = \frac{d\varepsilon_v}{d\sigma'}$). The values used in this study are those published by Seed et. al,[55] for different saturated sand deposits.

CHAPTER 6

INFLUENCE OF BEDROCK CHARACTERISTICS ON SEISMIC RESPONSE OF SOIL DEPOSITS

6.1. INTRODUCTION

Seismic response of soil deposits resting upon a rock formation depends on the engineering characteristics of the underlying materials. In nature, bedrock materials are to some extent weathered, due to the chemical processes which take place between ground water and these materials. The extent of deformability of these materials depends on the degree of weathering. Response study of these deposits is of great importance in seismic design. Therefore, it is essential to investigate the influence of bedrock characteristics on response of such deposits.

This chapter is concerned with the influence of bedrock characteristics on ground response. The bedrock characteristics are discussed in terms of the radiation damping ratio defined in section 6.2. In the first section of this chapter the influence of radiation damping ratio on ground surface response and its comparison with hysteretic damping ratio is discussed. This section is then followed by an investigation of evaluation of the response of soil deposits with elastic bases by means of rigid base solution. The third and final section of this chapter describes the influence of bedrock characteristics on sub-surface response.

6.2. RADIATION DAMPING RATIO

The deformability of the bedrock of an overburden causes loss of some incoming seismic energy back into the bedrock. As shown in appendix D

Radiation Damping Ratio "RAD" defined as follows:

$$RAD = \frac{S_{soil} \times \rho_{soil}}{S_{rock} \times \rho_{rock}}$$

where:

S_{soil} and S_{rock}: are the shear wave velocities of the overburden and the bedrock.

ρ_{soil} and ρ_{rock}: are the mass density of the soil and the bedrock controls the energy loss.

The term "Radiation Damping Ratio" is directly analogous to "Radiation Damping Coefficient", "Geometrical Damping" and "Impedence Ratio". The author prefers to use the first one because it indicates the phenomenon involved very clearly.

6.3. BEDROCK MOTIONS CONSIDERED

The bedrock motions considered in this chapter are:

1. Parkfield (Cholame Shandon No. 2, N65W) 27/6/66
2. San Fernando (Pacoima Dam S16E) 9/2/71
3. San Fernando (Pacoima Dam S74W) 9/2/71
4. Parkfield (Cholame Shandon No. 5, N5W) 27/6/66
5. Parkfield (Cholame Shandon No. 8, N50E) 27/6/66
6. Parkfield (Temblar S25W) 27/6/66
7. San Francisco (Golden Gate Park S60E) 22/3/57
8. San Francisco (Golden Gate Park N10E) 22/3/57

The records were recorded in the epicentral region of the above earthquakes and are representative of a stiff soil, weathered rock and rock

motions in their specific events. None of the records in this study were scaled because, from studying existing strong ground motion records, it was found that scaling of the records should be based on correlations between amplitude of pulses and their frequencies. In the absence of such correlations, scaling of the records which are representative of a specific event might lead to completely unrealistic results.

6.4. SITES STUDIED

A total of 94 sites, consisting of coarse gravel, loose gravel, cemented sand, dense sand, saturated silt, sandy clay, medium clay, sandy clay, clay with high water content, soft to medium clay and soft clay, were studied. 39 of these sites are reported in this chapter and the rest 55 - in chapter 7. The assumed shear wave velocity for each material is marked on the corresponding site.

6.5. ACCELERATION, VELOCITY AND DISPLACEMENT TIME HISTORIES

The response of foundations to seismic loading may be expressed by acceleration, velocity and displacement time histories. At present, it is most common to use horizontal acceleration time histories for the design of engineering structures; this is a measure of forces that structures may undergo during earthquakes. Acceleration time history is also used for computation of response spectra (see section 6.6).

There is a general trend towards the use of velocity time history for earthquake resistant design purposes; there is a better correlation between period of peak velocity and response predominant period of most structures. Velocity time history is also used for computation of strength defined in section 7.3.1.

Displacement time history is sometimes used to compute the strains that large structures, such as dams, etc., may be subjected to during an earthquake.

In this study all the three response parameters were computed.

6.6. RESPONSE SPECTRA

Motion of a soil deposit at the surface or at some depth is described by parameters such as:

a) Maximum acceleration.

b) Frequency content.

c) Duration of shaking.

(a) and (b) plus to some extent (c) are summarized in a response spectrum. It should be pointed out that response spectrum is weak in illustrating point (c). Two sites might have almost the same response spectrum but completely different damaging potentials. Response spectrum, which was first introduced by Benioff[9], today has become a standard technique for dynamic analysis of group 2 and 3 structures.*[14]

For the purpose of this study, acceleration, velocity and displacement response spectrum(which are plots of maximum response of absolute acceleration), relative velocity and displacement of a family of single degree of freedom linear viscously damped systems to a specified ground motion versus the natural period of the systems for various fractions of critical damping, were calculated for the following reason:

---

* Group 2 structures are: Schools, Colleges, Shopping centers, Offices, Apartments, Hotels, etc.

Group 3 structures are: dwellings, town houses, factories, service stations, etc.

To find the period at which a motion develops its maximum spectral acceleration known as predominant period. The predominant period of base motion is very important in the response analysis of soil deposits; the bedrock acceleration is most amplified when the fundamental period of a deposit is equal to the predominant period of the bedrock motion. Variation of the predominant period with damping values used in the spectral analysis is generally small for the ranges of damping values met in engineering practice. This variation may be neglected for general discussions. In this chapter and the next the predominant periods quoted correspond to 5% spectral damping values as met in design of engineering structures.

The computation of response spectra is given in appendix B . Acceleration, velocity and displacement response spectrum for 5%, 10% and 20% critical damping for 35 periods with a range of periods from 0.05 to 3.0 secs. for both input and output motion were computed. Input motion spectrum are given in chapter 3.

6.7. SITE AMPLIFICATION

To show precisely the amplifying or de-amplifying effect of a deposit, the spectral ratio between output and input spectrum for 5% critical damping was calculated. A plot of this ratio versus the corresponding period for which the ratio was calculated is referred to Amplification Spectra. The amplification spectra clearly illustrates for which period of structures the amplification of the deposit may be significant.

6.8. INFLUENCE OF BEDROCK CHARACTERISTICS ON SEISMIC RESPONSE OF SOIL DEPOSITS

As stated in the introduction, the bedrock characteristics of a deposit is discussed in terms of the radiation damping ratio defined in section 6.2. The influence of radiation damping ratio on ground response has been studied by Lysmer et. al.[41] based on a mathematical model, which assumes earthquake motion was represented by a series of sinisoidal motions of different frequencies and strain dependent material properties, have concluded that: "The computed spectra for the surface accelerations are virtually independent of the properties of the base rock provided the latter is homogeneous." Papastamatio[46] in his study, based on a modified lumped mass model which suffers from inadequate transmission capability, having only dealt with the first stage of the problem (i.e. predominant period of bedrock motion equal to fundamental period of the overburden, considering only one site and one bedrock motion), has made the generalized conclusion that "the use of hysteretic damping ratio gives almost identical results with the radiation mechanism ...".

In recognition of these problems, investigations were performed to study the influence of radiation damping ratio on ground response, based on a much more realistic mathematical model, real earthquake motions and real material properties. A total of 39 sites with six different bedrock motions were analysed. It is believed that the cases analysed in this study are of sufficient extent and variety to simulate actual field conditions and provide solid bases to derived conclusions.

6.8.1. INFLUENCE OF RADIATION AND HYSTERETIC DAMPING RATIOS ON GROUND RESPONSE AND THEIR COMPARISON

The influence of radiation damping ratio on ground response and its comparison with hysteretic damping ratio was studied through analysing a number of idealized layers for the following cases:

a) Fundamental period of the overburden is equal to the predominant period of the bedrock motion (i.e. first mode of vibration dominating the response).

b) Fundamental period of the overburden is different from the predominant period of the bedrock motion (first few higher modes dominating the response).

It is believed that it is only through the following analysis, helped by efficient monitoring, that a better insight into the "radiation damping" phenomenon, which would be of interest to practising engineers, could be achieved. A number of other approaches to the problem are also possible; one which can be adopted by the geophysicists is called "wave analysis". A third approach is to substitute the real earthquake excitation by a simple harmonic motion; this approach, which might provide a very rough guide under certain conditions, might be completely misleading under others. This point is clearly illustrated when a comparison is made between computed spectrum, using earthquake (see chapter 3) and harmonic excitation.[20] In what follows the recommended approach is described.

6.8.1.1. FUNDAMENTAL PERIOD OF THE OVERBURDEN IS EQUAL TO THE PREDOMINANT PERIOD OF THE BEDROCK MOTION

To investigate this case of interest a number of analyses were made, using the developed mathematical model, to determine the effect of radiation damping ratio on ground response. The effect of hysteretic damping ratio

on ground response is also investigated. Comparisons have been made between these two types of damping under this special condition.

Radiation and hysteretic damping ratios appear in the developed solution in the forms:

$$RAD = \frac{s_{soil} \cdot \rho_{soil}}{s_{rock} \cdot \rho_{rock}} \quad ; \qquad \xi = \frac{C1 \cdot P}{2 \cdot G}$$

where: RAD and ξ are the radiation and hysteretic damping ratios, respectively. " P " is circular frequency of the applied load, " $_G$ " is shear modulus of the overburden, " $_{C1}$ " is the coefficient of viscosity of the overburden in shear, "s " is the shear wave velocity and " ρ" the mass density. A total of twenty-one different sites were analysed which are included in table 6.1. All the sites were subjected to the full length of the bedrock motions. The number of modes considered for each site was nine, with an integration time step of 0.02 second. In each case, all parameters, other than the parameter studied, were kept constant.

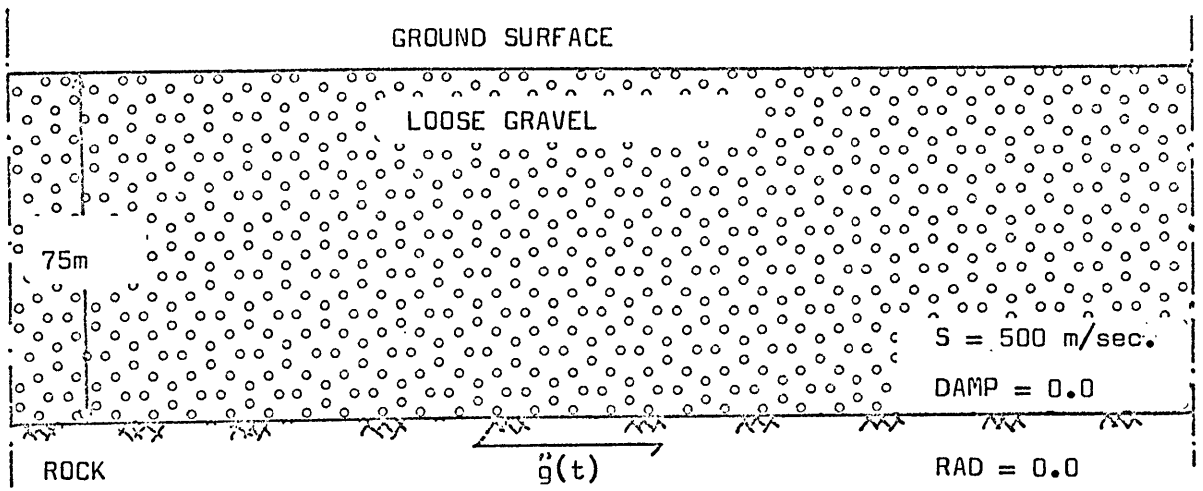
Figs. 6.1a,b,c,d,e,f show the response of a 75-m. deposit of loose gravel subjected to Parkfield-2 at the bedrock level. Both radiation and hysteretic damping ratios were assigned to zero (case 1). The fundamental period of the soil deposit shown in fig. 6.1 is 0.6 second, the predominant period of the bedrock motion is 0.6 second. The two periods are equal, therefore a condition of resonance exists, this is clearly demonstrated by a single narrow peak at the period of 0.6 second on acceleration response spectra shown in fig. 6.1d. A sharp peak is also observed around the fundamental period of the deposit on velocity and displacement response spectra shown in figs. 6.1e and f.

Results of case 2 (hysteretic damping ratio assigned to zero, radiation

SITE DATA FOR INVESTIGATION OF INFLUENCE OF RADIATION AND HYSTERETIC DAMPING RATIOS ON RESPONSE

CASE NO.	BEDROCK MOTION	MATERIAL OF THE DEPOSIT	HYSTERETIC DAMPING RATIO	RADIATION DAMPING RATIO	SHEAR WAVE VELOCITY m/sec.	DEPTH TO BEDROCK (m)
1	Parkfield-2	Loose Gravel	0.0	0.0	500	75
2	Parkfield-2	Loose Gravel	0.0	0.05, 0.1 0.15, 0.2 0.3, 0.4 0.5, 0.9 0.98	500	75
3	Parkfield-2	Loose Gravel	0.05 0.10 0.15 0.20	0.0	500	75
4	SAN FERNANDO S16E & S79W	Soft Clay	0.0 0.08	0.12 0.0	200	20
5	Temblor S25W	Soft Clay	0.0 0.08	0.12 0.0	200	22

TABLE 6.1



RESPONSE OF HYSTERETIC DEPOSIT UNDERLAIN BY DEFORMABLE BEDROCK

SCHEMATIC SOIL PROFILE FOR SITE NO. 6.1

FIG. 6.1

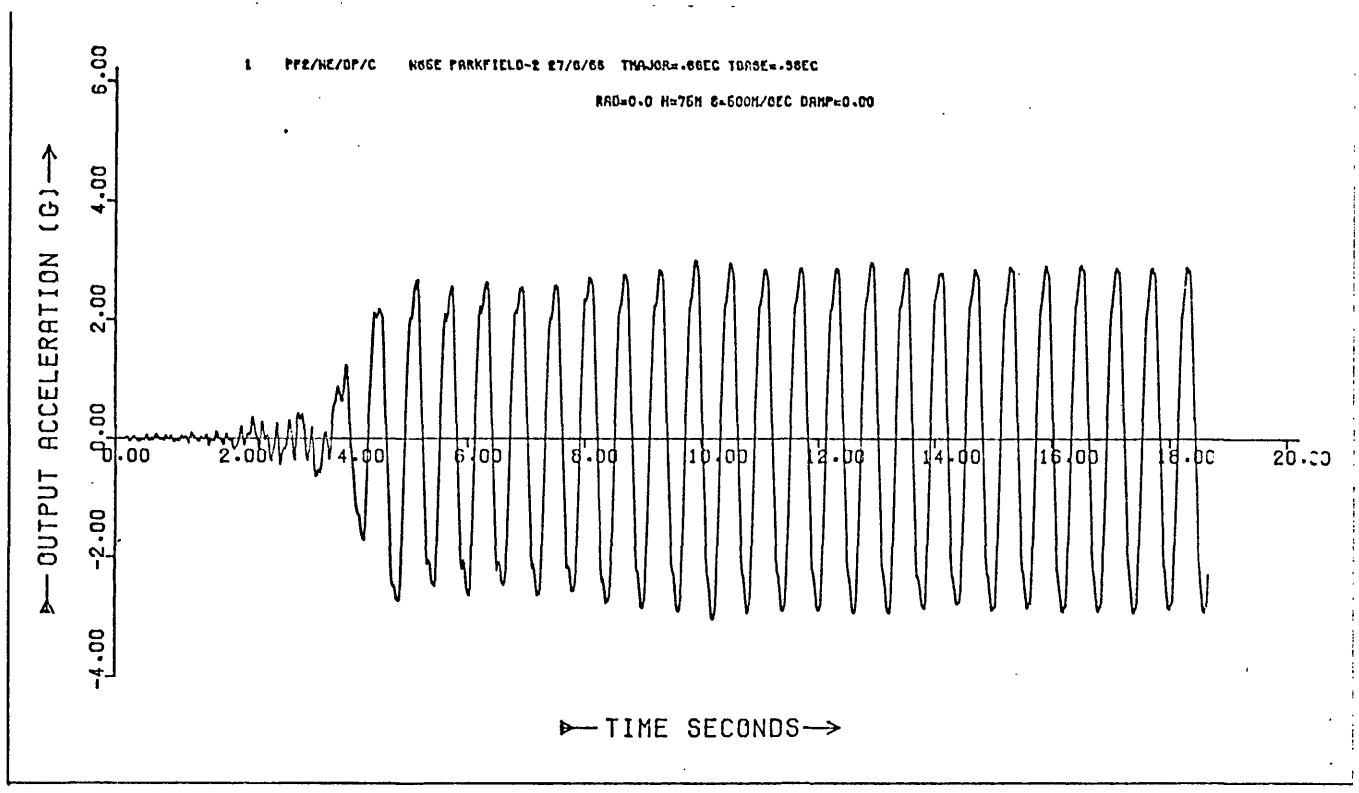


FIG. 6.1a COMPUTED GROUND SURFACE ACCELERATION TIME HISTORY AT SITE NO 6.1

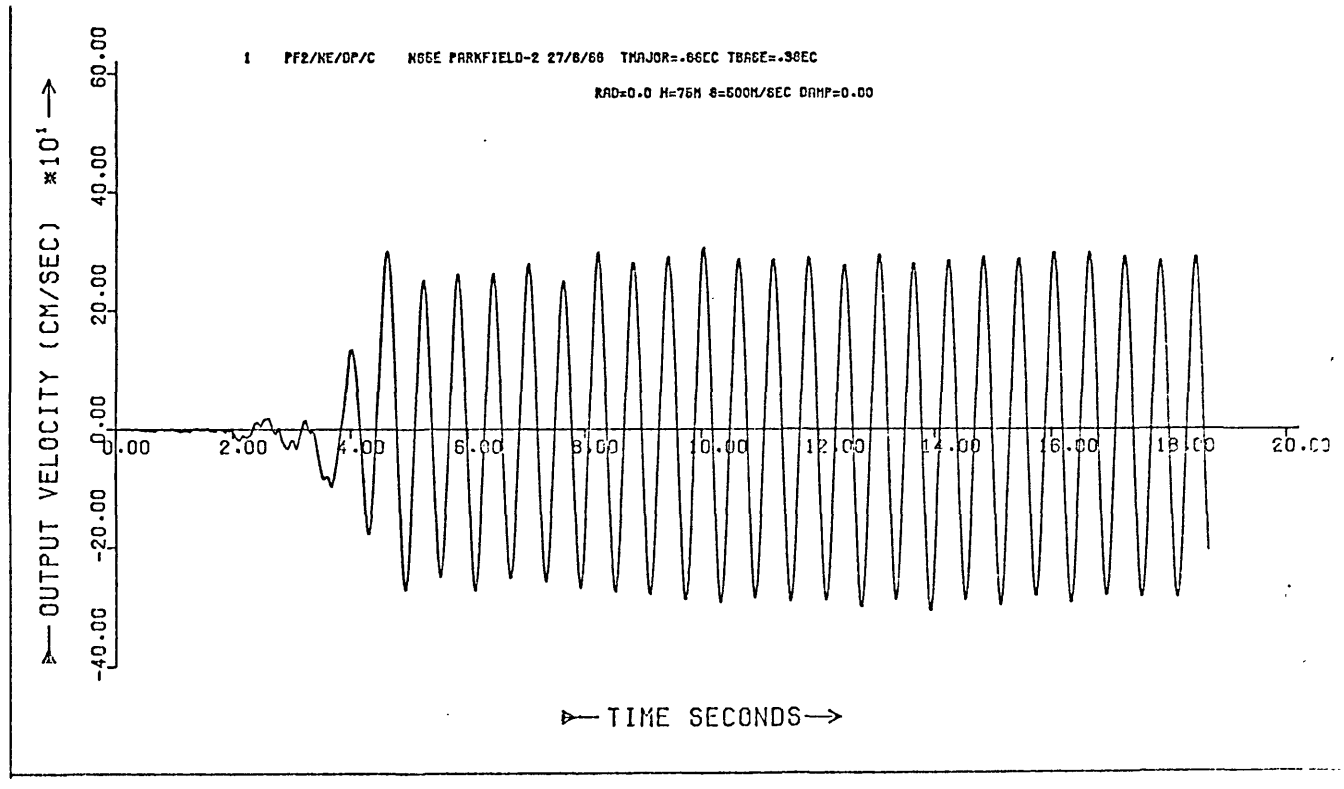


FIG. 6.1b COMPUTED GROUND SURFACE VELOCITY TIME HISTORY AT SITE NO 6.1

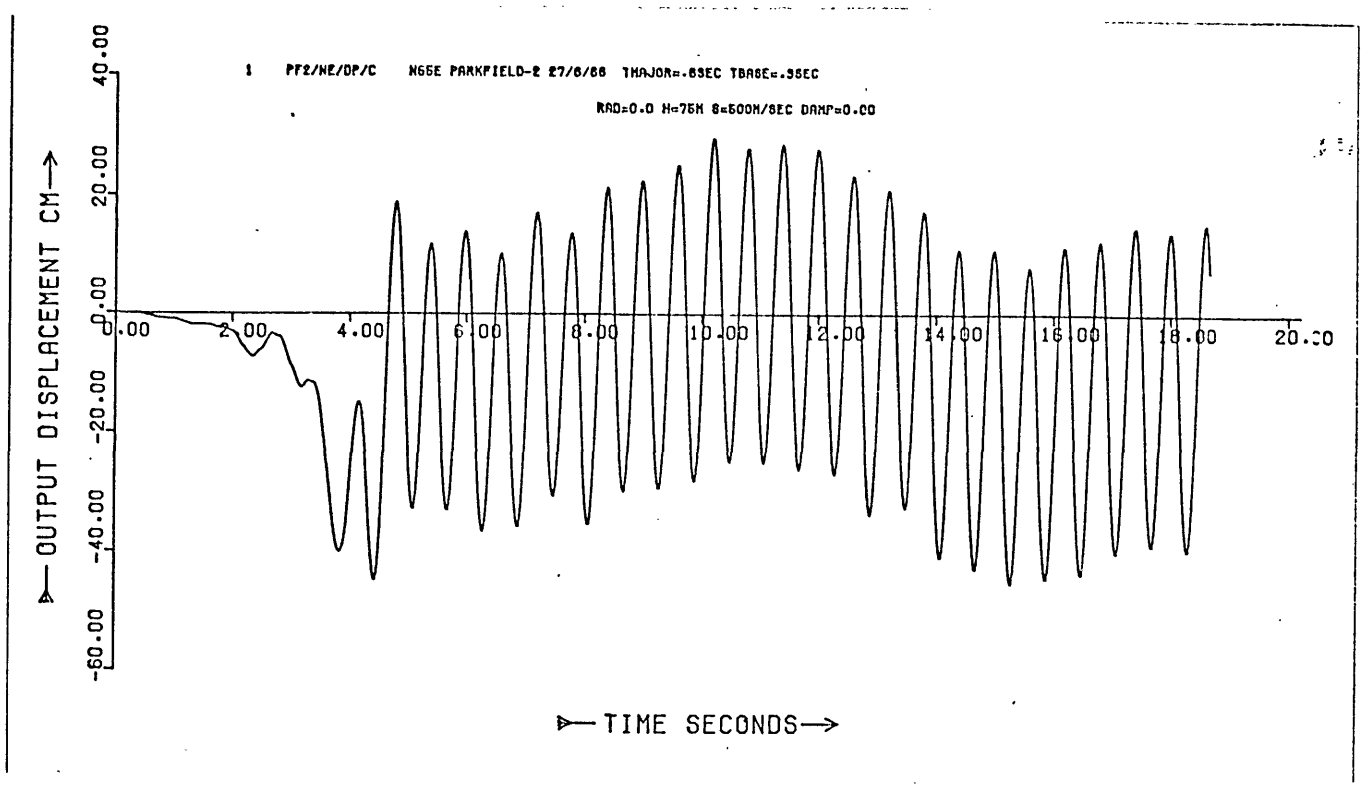


FIG. 6.1c COMPUTED GROUND SURFACE DISPLACEMENT TIME HISTORY AT SITE NO 6.1

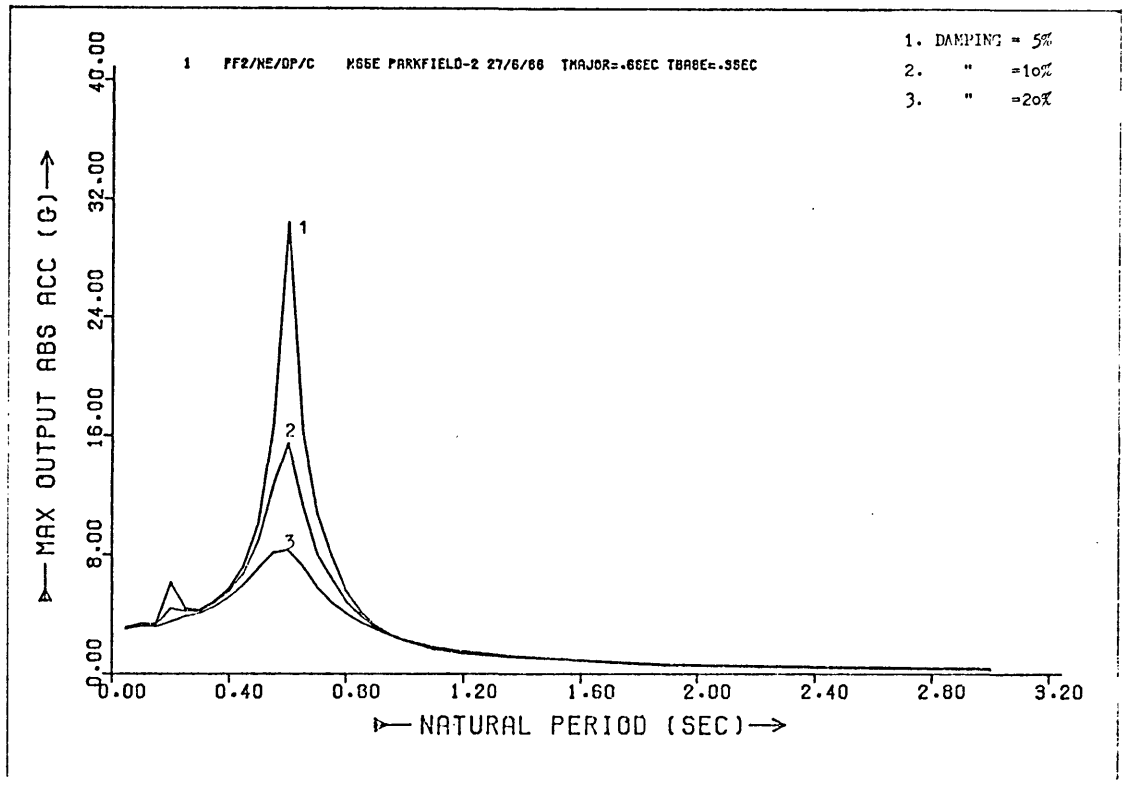


FIG.6.1d COMPUTED GROUND SURFACE ACCELERATION RESPONSE SPECTRA AT SITE NO 6.1

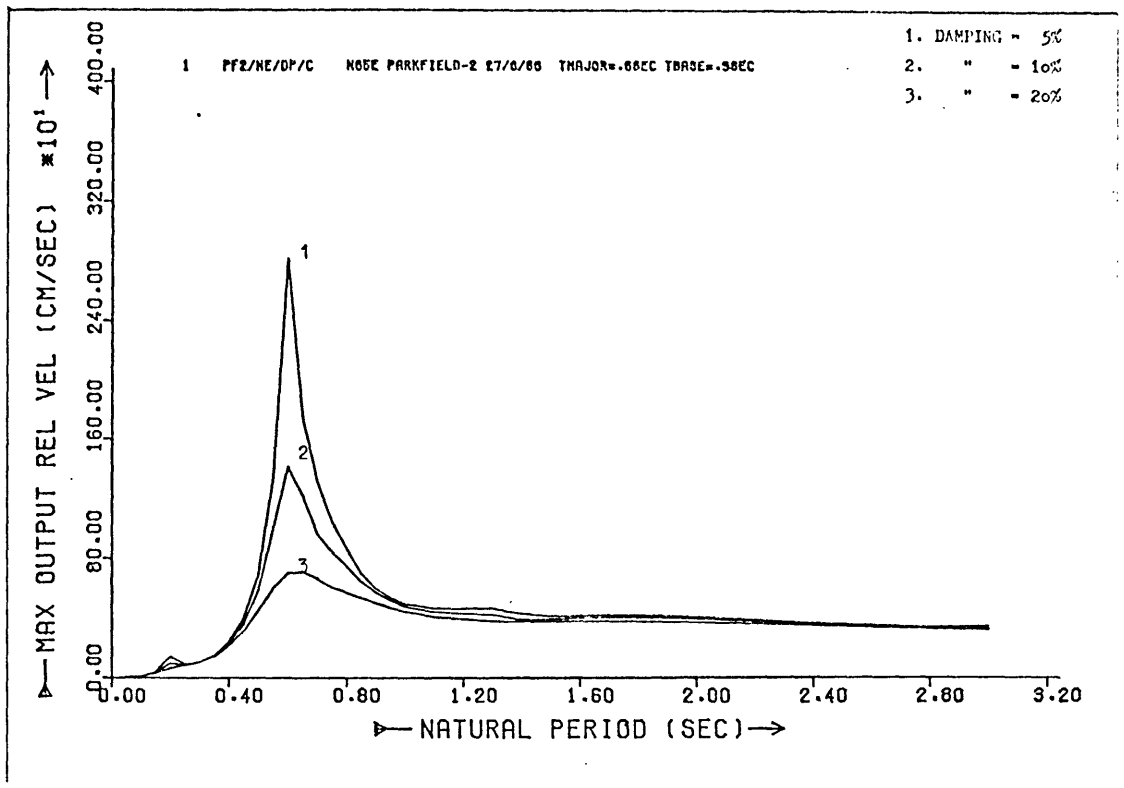


FIG.6.1e COMPUTED GROUND SURFACE VELOCITY RESPONSE SPECTRA AT SITE NO 6.1

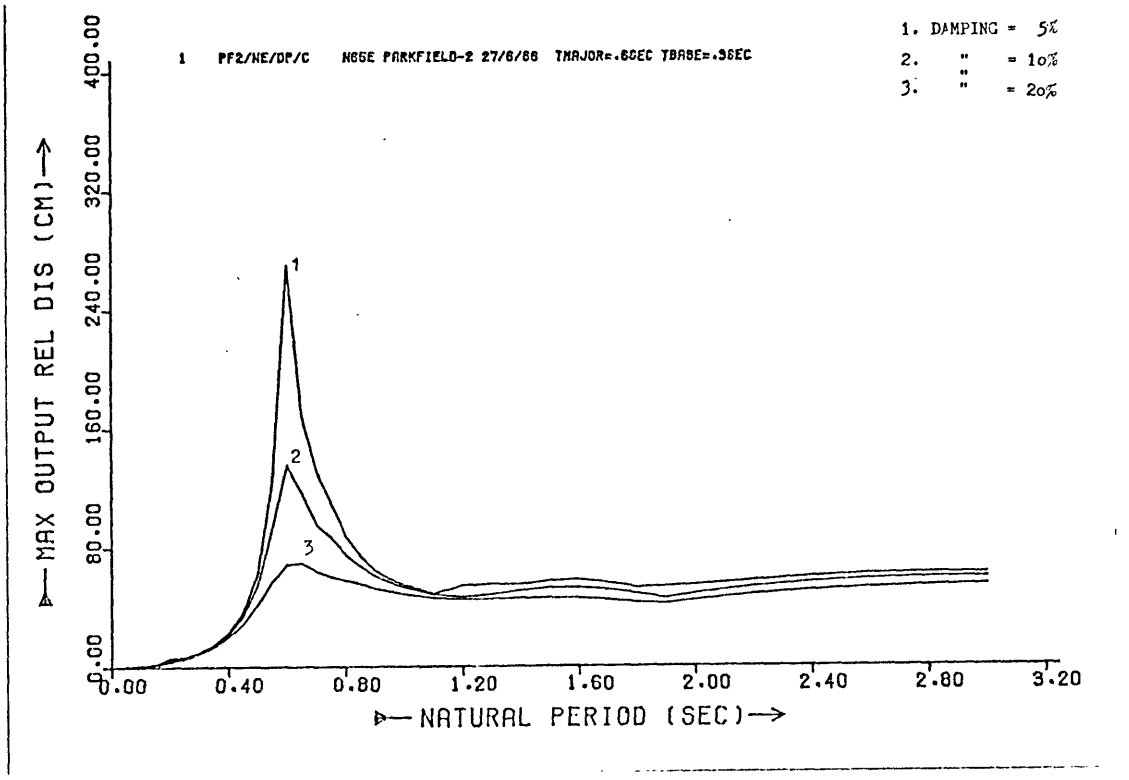
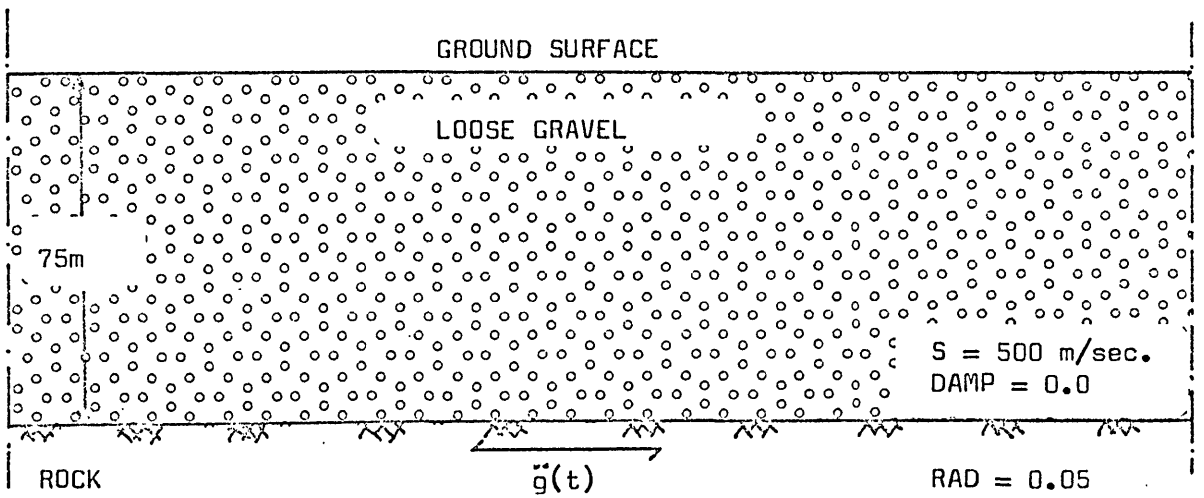


FIG.6.1f COMPUTED GROND SURFACE DISPLACEMENT RESPONSE SPECTRA AT SITE NO6.1

damping ratio not zero) are illustrated in figs. 6.2 through 6.10, which show the effect of radiation damping ratio on ground response when the fundamental period of the overburden is equal to the predominant period of the bedrock motion (Parkfield-2, 0.6 sec) for nine values of radiation damping ratio ranging from 0.05 corresponding to a very rigid bedrock to 0.98, representing a bedrock almost as soft as the deposit.

The influence of radiation damping ratio on the response values is described by surface acceleration, velocity and displacement time histories. These time histories for case 2 are shown in figs. 6.2a,b,c to 6.10a,b,c. In general, it is noticed that the computed surface acceleration, velocity and displacement time histories for the nine sites considered are quite similar except that they differ in the amplitude of the pulses. The peak surface acceleration and velocity for site No 6.2 (2.0g and 252. cm/sec) is considerably greater than site No. 6.8(0.71g and 100.6 cm/sec), the larger amplitude belonging to the smaller radiation damping ratio, illustrating the effect of radiation damping ratio on ground response. These results indicate that, in general, the greater the radiation damping ratio the smaller the peaks of the pulses. It is also noticed that the greater the radiation damping ratio the closer are the computed surface motions to that of bedrock motions if this surface were free. At the limit, when radiation damping ratio becomes close to one, site No. 6.10 computed surface motion, approach to the bedrock motions, as shown in figs. 6.10a,b,c,d,e,f. Acceleration, velocity and displacement response spectrum computed from surface motion time histories of the sites analysed are shown in figs. 6.2d,e,f to 6.10d,e,f.

Figs. 6.2d,e,f through 6.10d,e,f indicate that the shape of output spectras are influenced by the shape of input spectrum; if the deposits



RESPONSE OF HYSTERETIC DEPOSIT UNDERLAIN BY DEFORMABLE BEDROCK

SCHEMATIC SOIL PROFILE FOR SITE NO. 6.2

6.3,6.4,6.5,6.6,6.7,6.8,6.9, and 6.10

FIG. 6.2

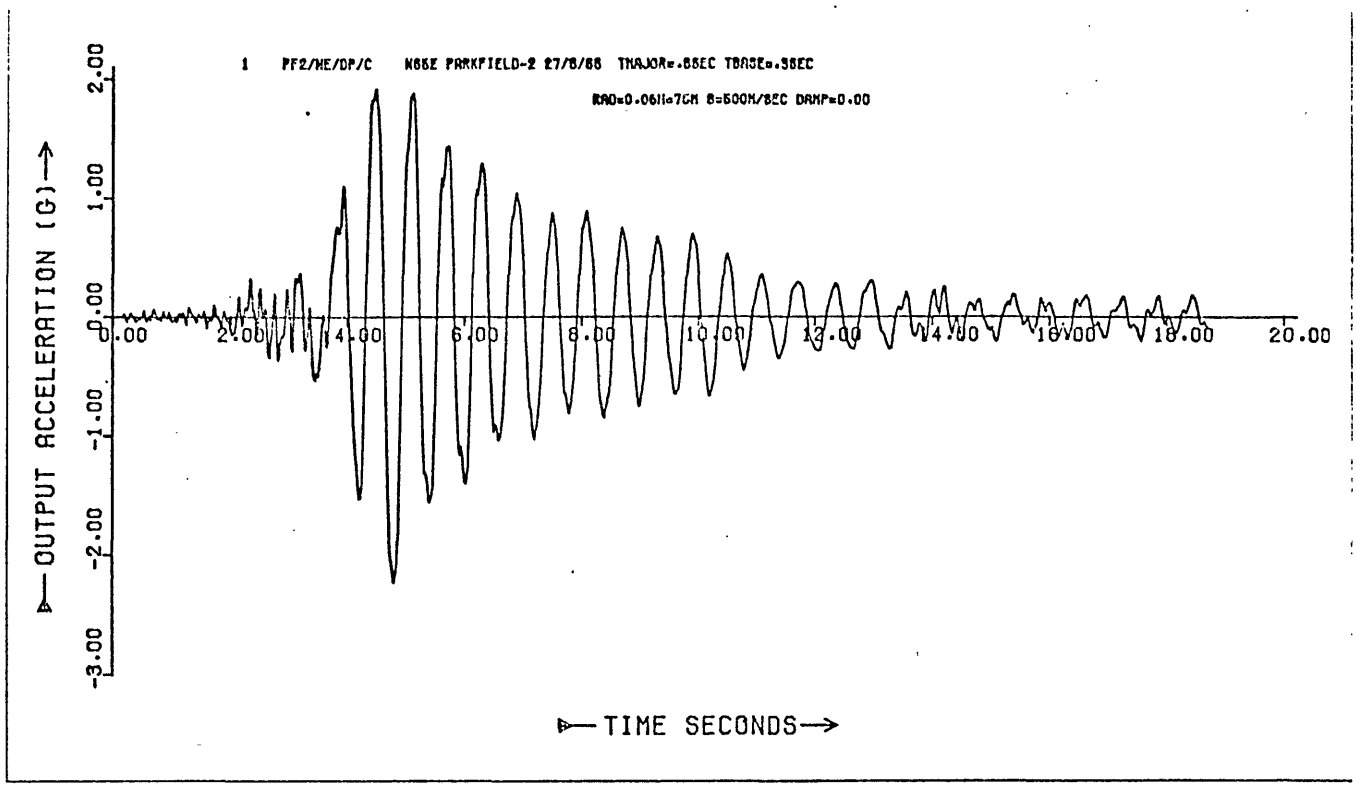


FIG.6.2a COMPUTED GROUND SURFACE ACCELERATION TIME HISTORY AT SITE NO 6.2

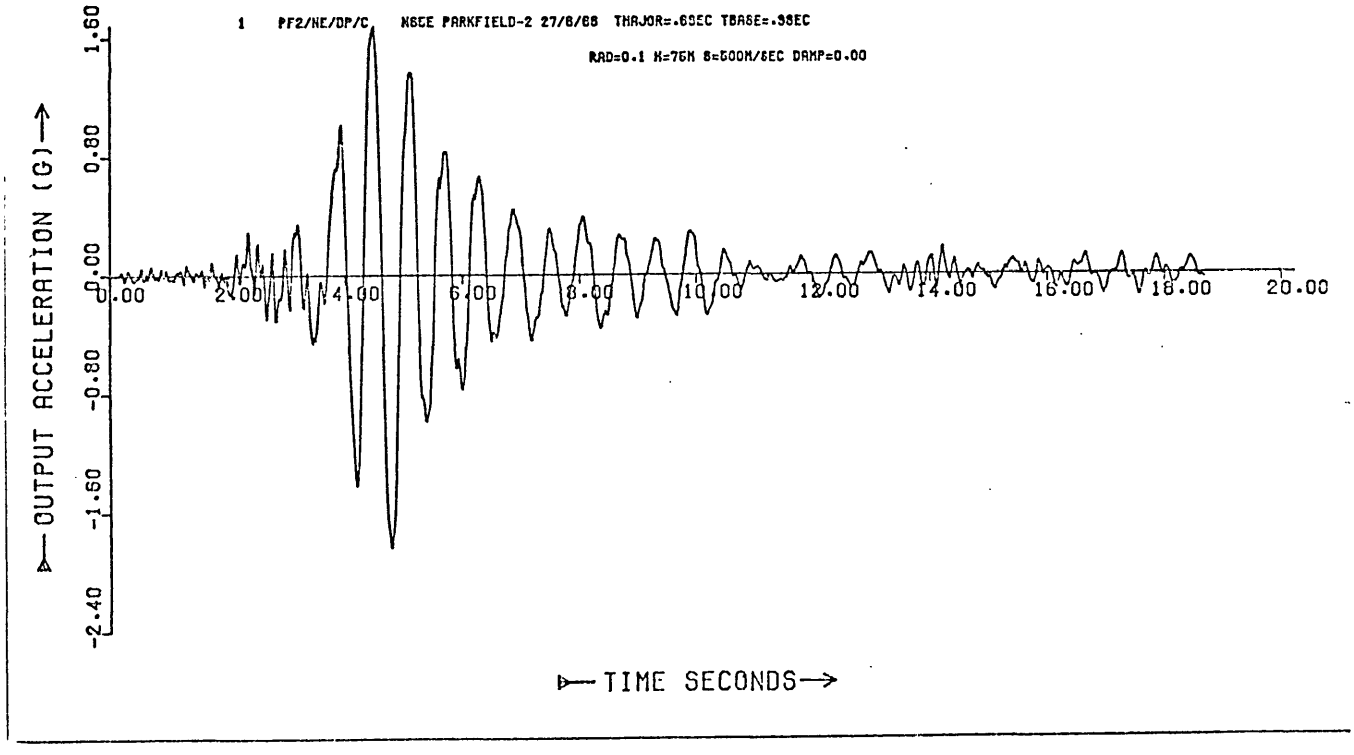


FIG. 6.3a COMPUTED GROUND SURFACE ACCELERATION TIME HISTORY AT SITE NO 6.3

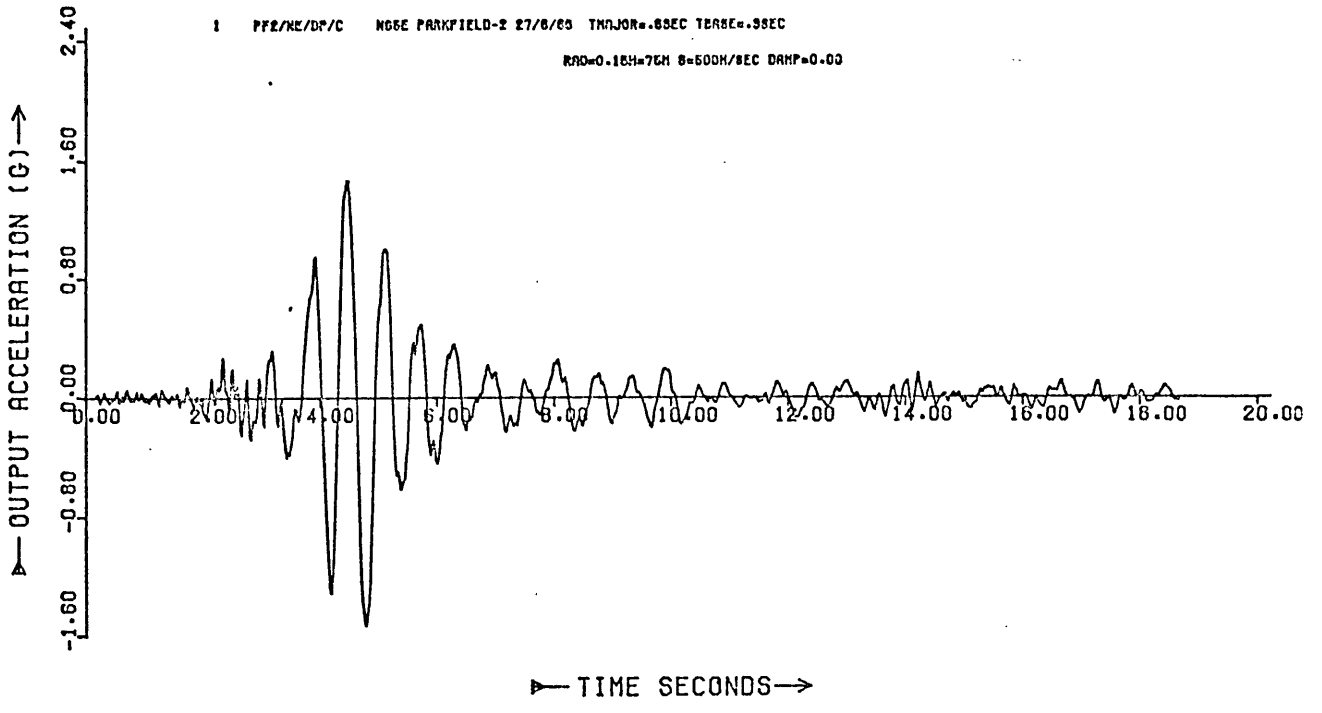


FIG. 6.4a COMPUTED GROUND SURFACE ACCELERATION TIME HISTORY AT SITE NO 6.4

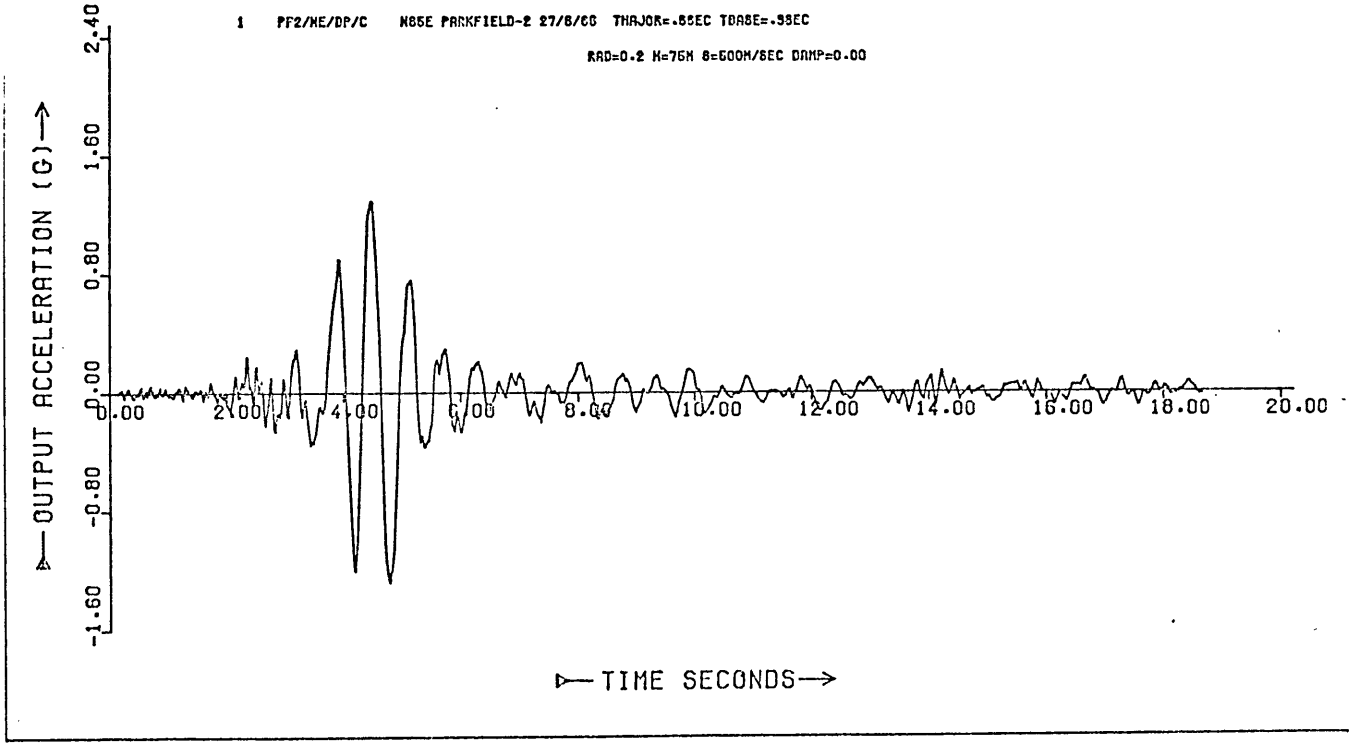


FIG. 6.5a COMPUTED GROUND SURFACE ACCELERATION TIME HISTORY AT SITE NO 6.5

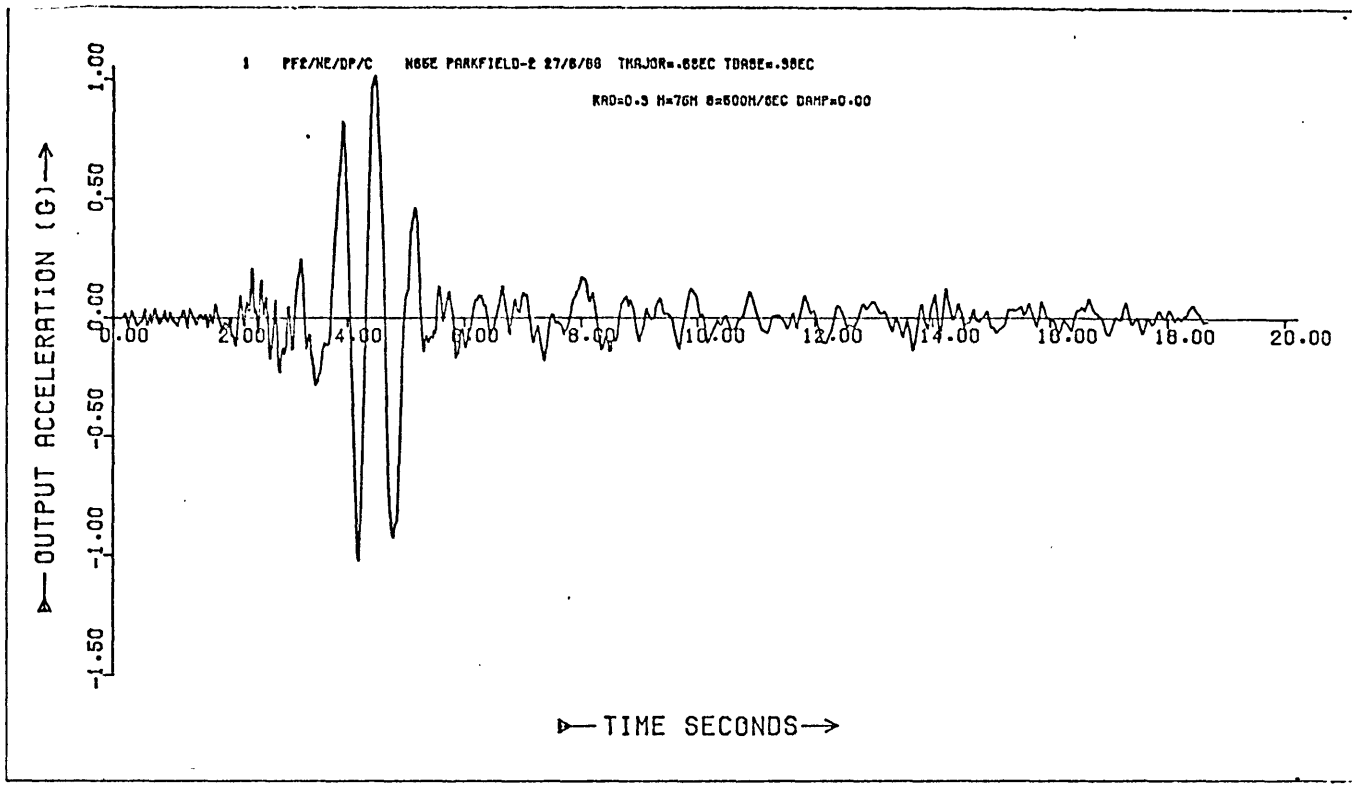


FIG. 6.6a COMPUTED GROUND SURFACE ACCELERATION TIME HISTORY AT SITE NO 6.6

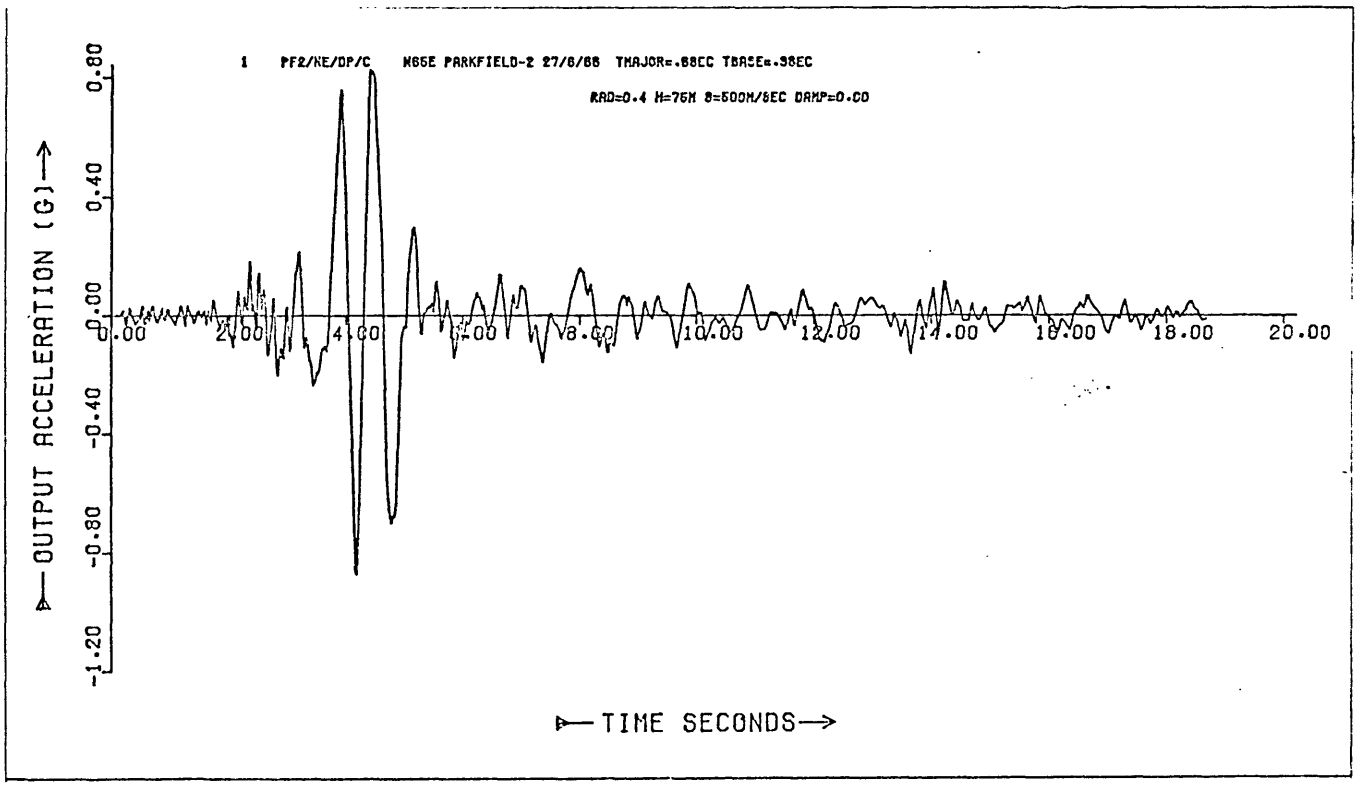


FIG. 6.7a COMPUTED GROUND SURFACE ACCELERATION TIME HISTORY AT SITE NO 6.7

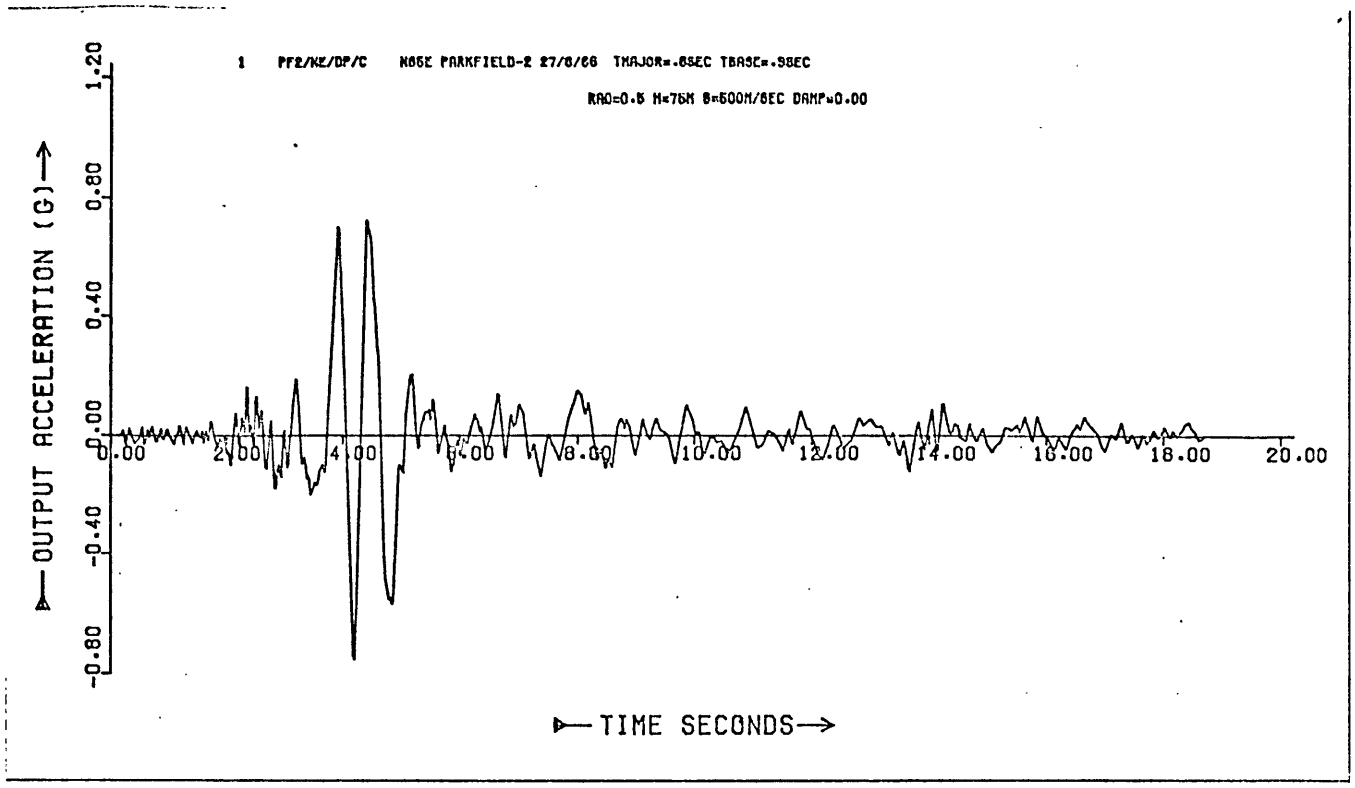


FIG. 6.8a COMPUTED GROUND SURFACE ACCELERATION TIME HISTORY AT SITE NO 6.8

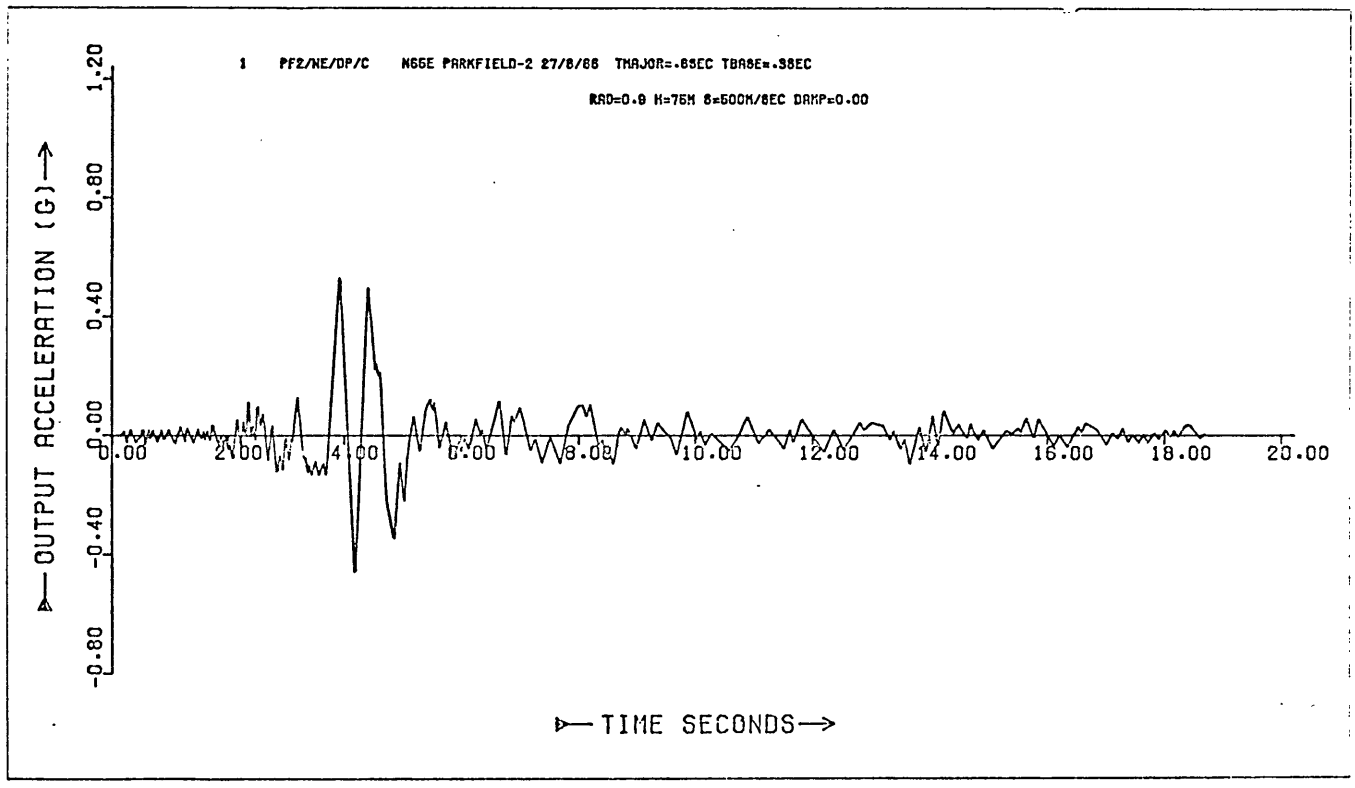


FIG. 6.9a COMPUTED GROUND SURFACE ACCELERATION TIME HISTORY AT SITE NO 6.9

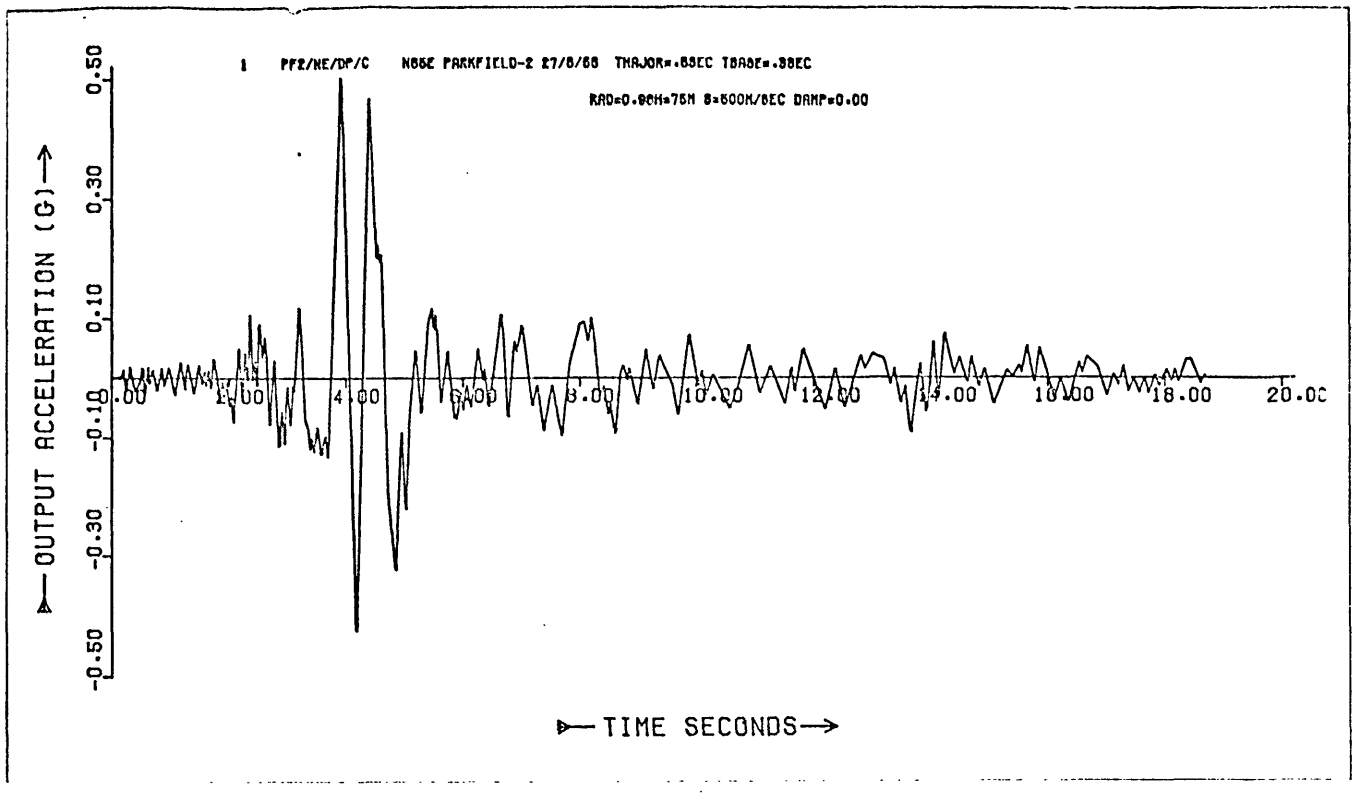


FIG. 6.1oa COMPUTED GROUND SURFACE ACCELERATION TIME HISTORY AT SITE NO 6.1o

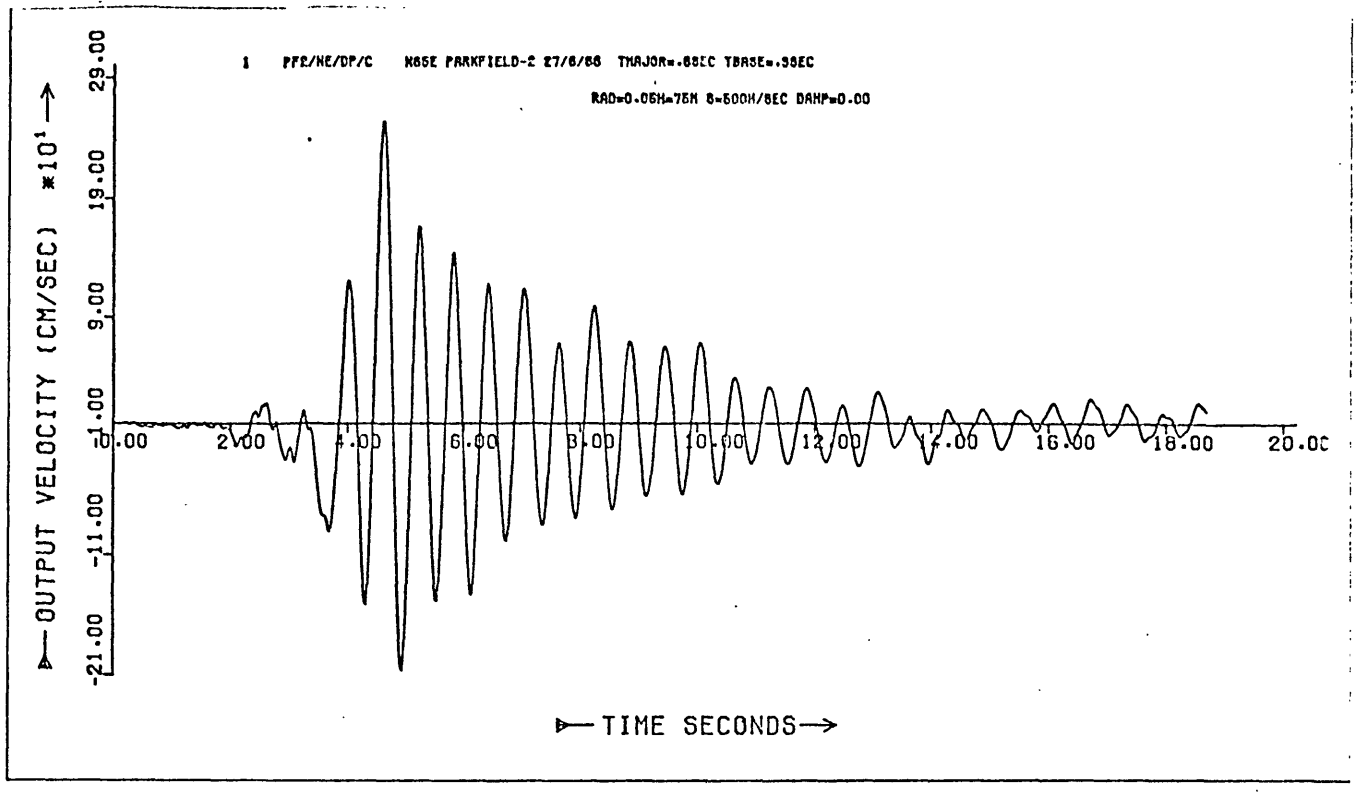


FIG. 6.2b COMPUTED GROUND SURFACE VELOCITY TIME HISTORY AT SITE NO 6.2

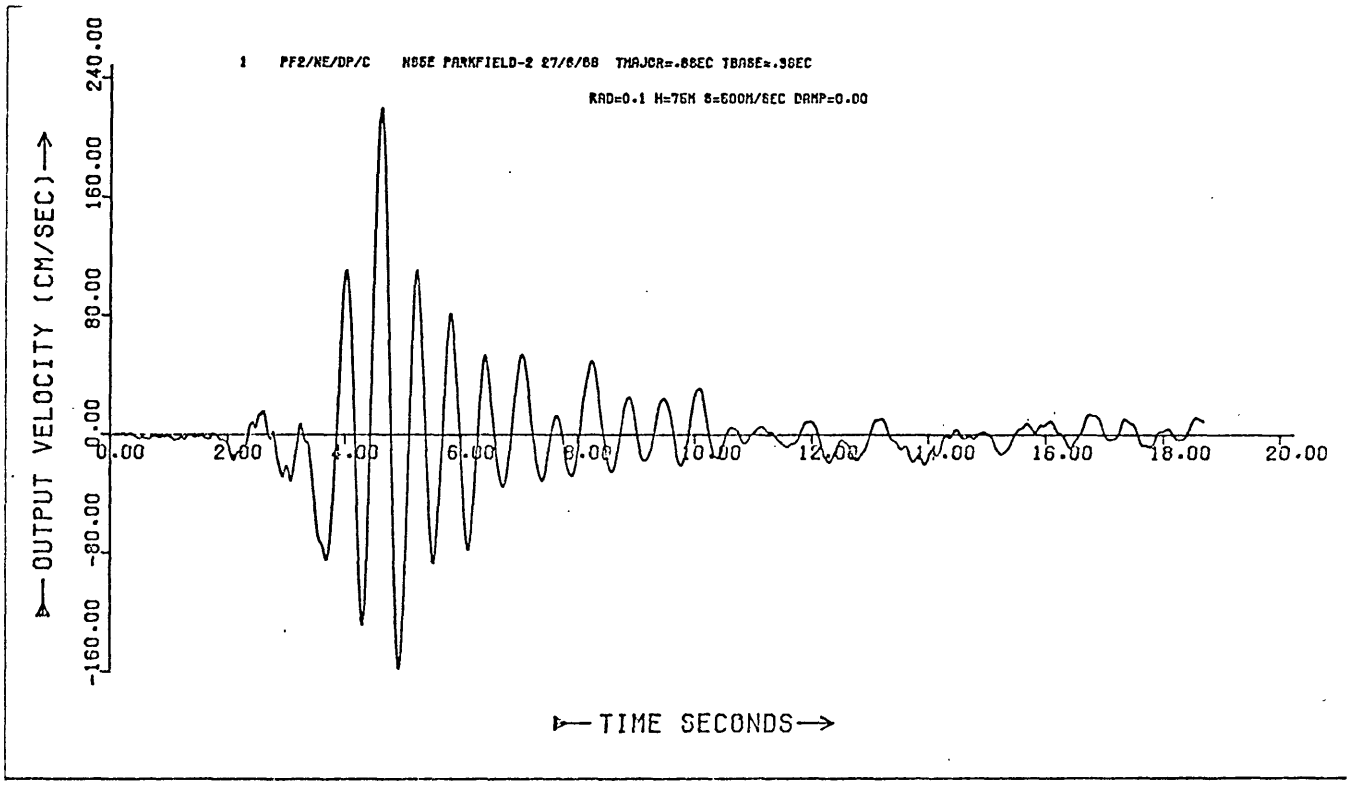


FIG. 6.3b COMPUTED GROUND SURFACE VELOCITY TIME HISTORY AT SITE NO 6.3

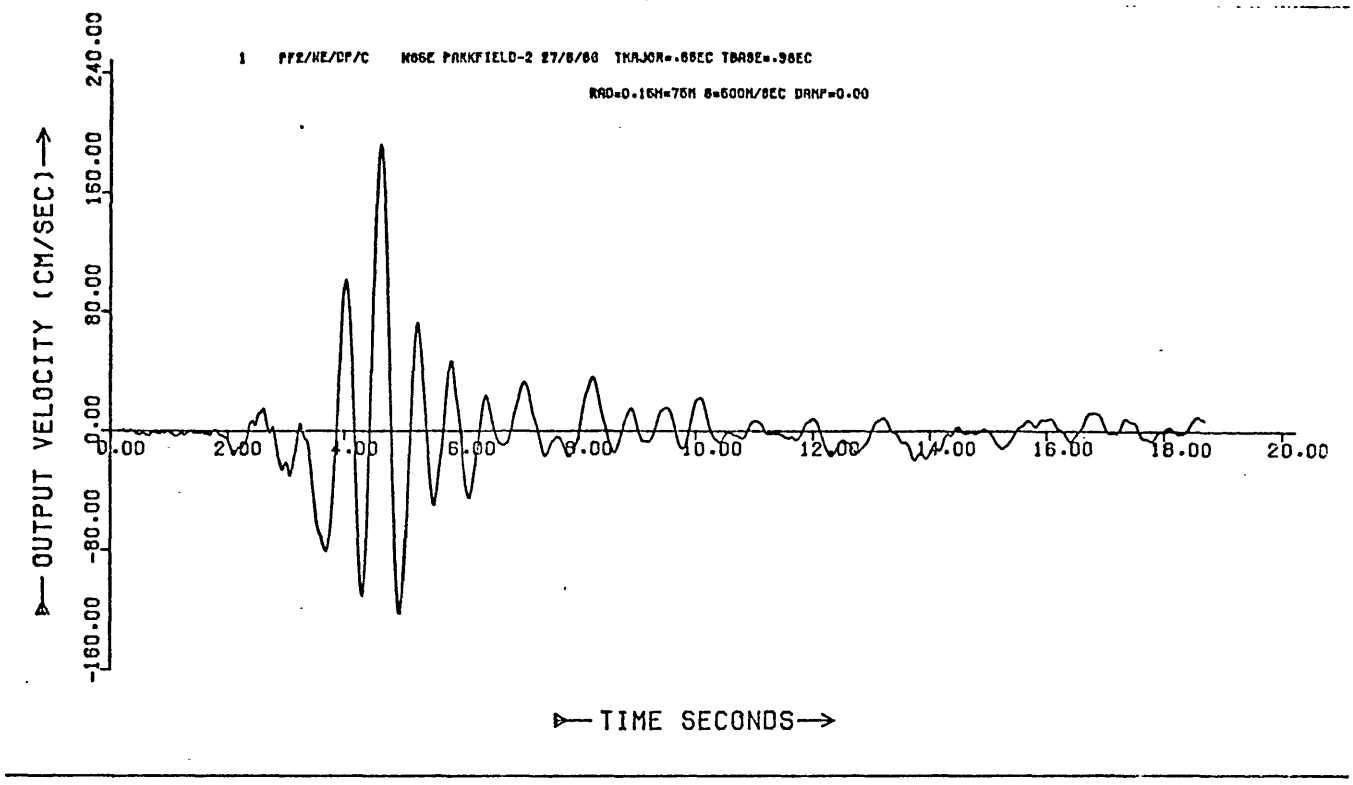


FIG. 6.4b COMPUTED GROUND SURFACE VELOCITY TIME HISTORY AT SITE NO 6.4

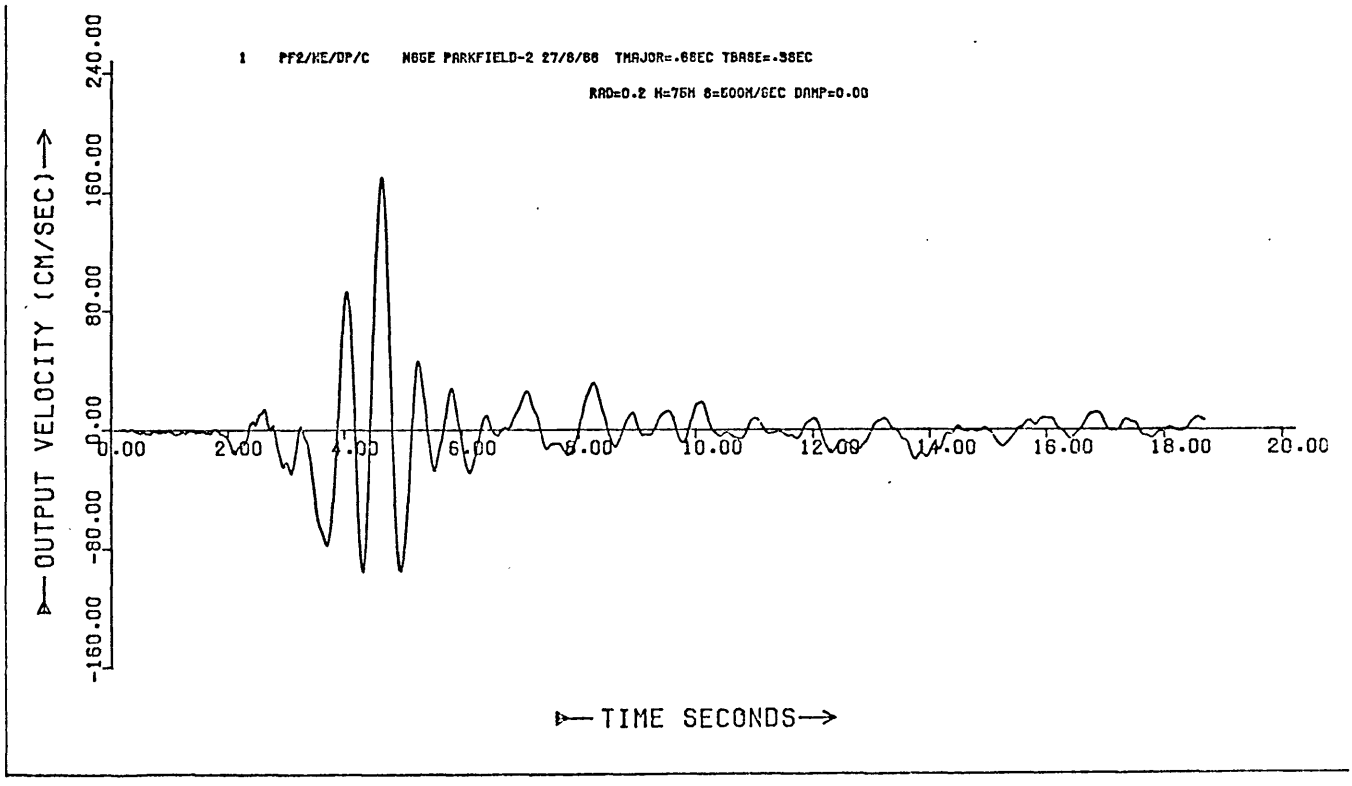


FIG. 6.5b COMPUTED GROUND SURFACE VELOCITY TIME HISTORY AT SITE NO 6.5

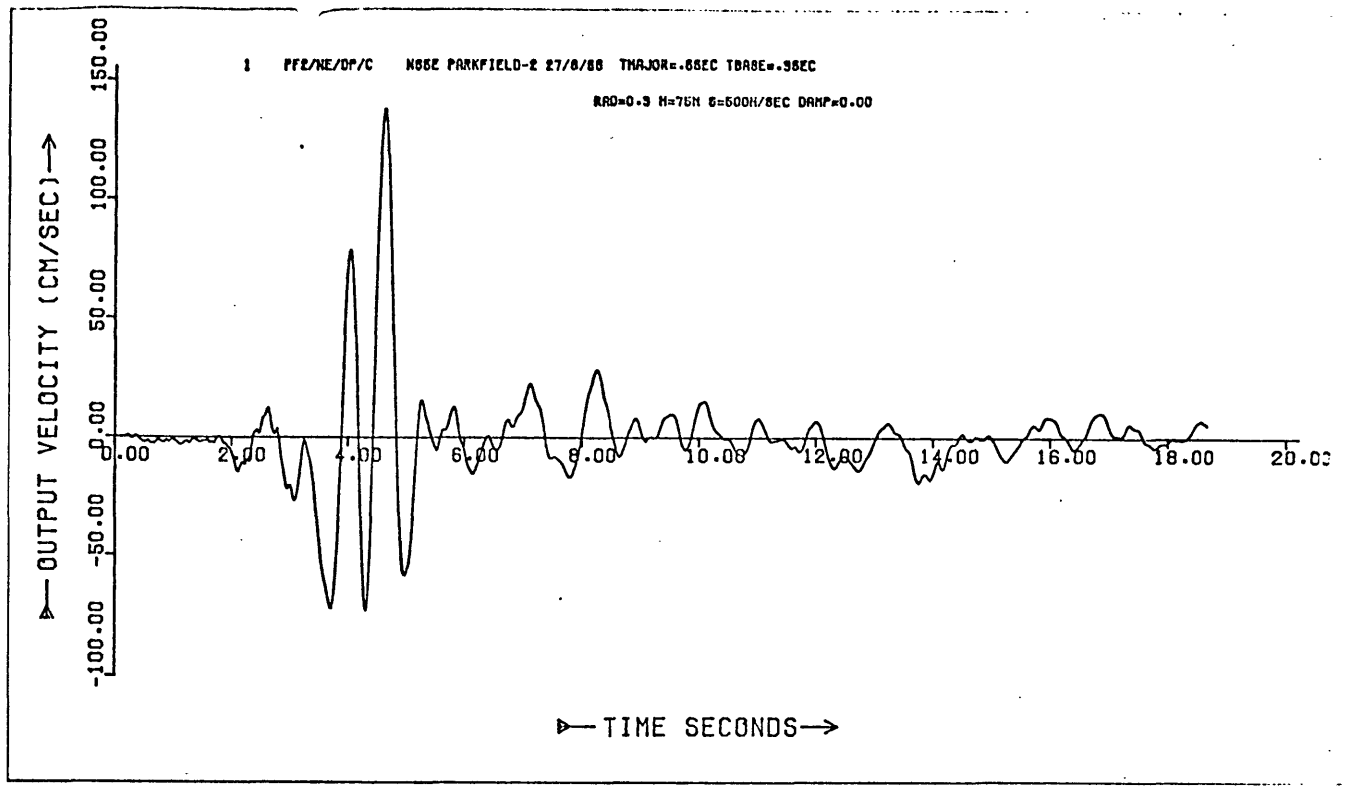


FIG. 6.6b COMPUTED GROUND SURFACE VELOCITY TIME HISTORY AT SITE NO 6.6

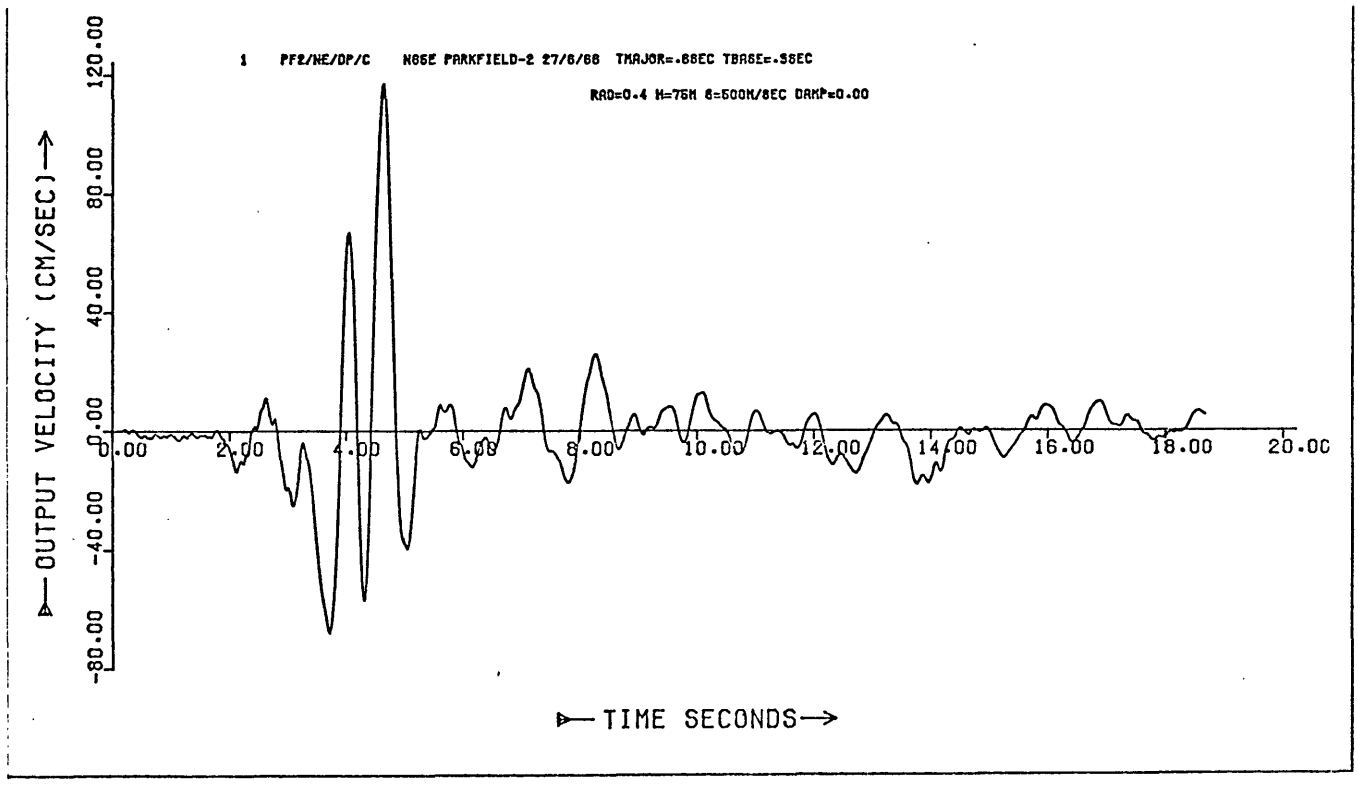


FIG. 6.7b COMPUTED GROUND SURFACE VELOCITY TIME HISTORY AT SITE NO 6.7

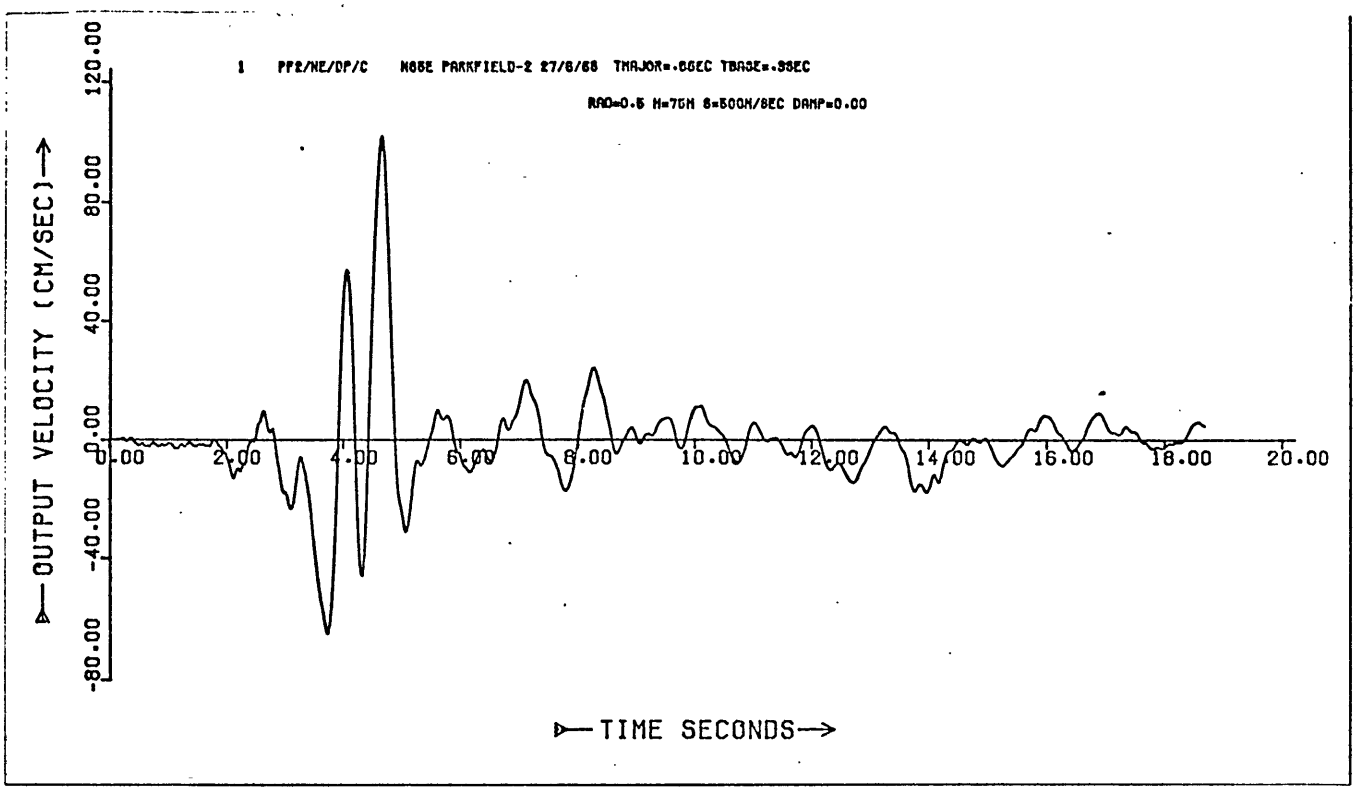


FIG. 6.8b COMPUTED GROUND SURFACE VELOCITY TIME HISTORY AT SITE NO 6.8

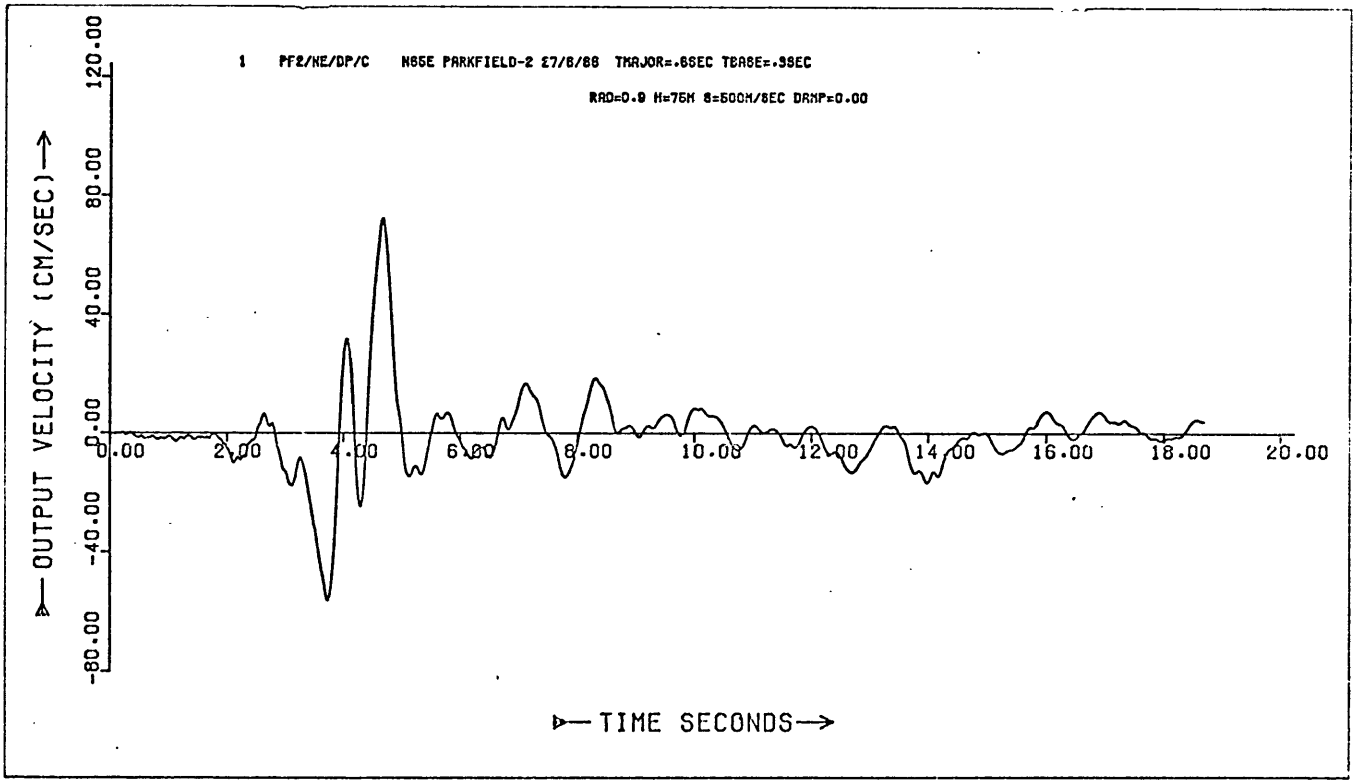


FIG. 6.9b COMPUTED GROUND SURFACE VELOCITY TIME HISTORY AT SITE NO 6.9

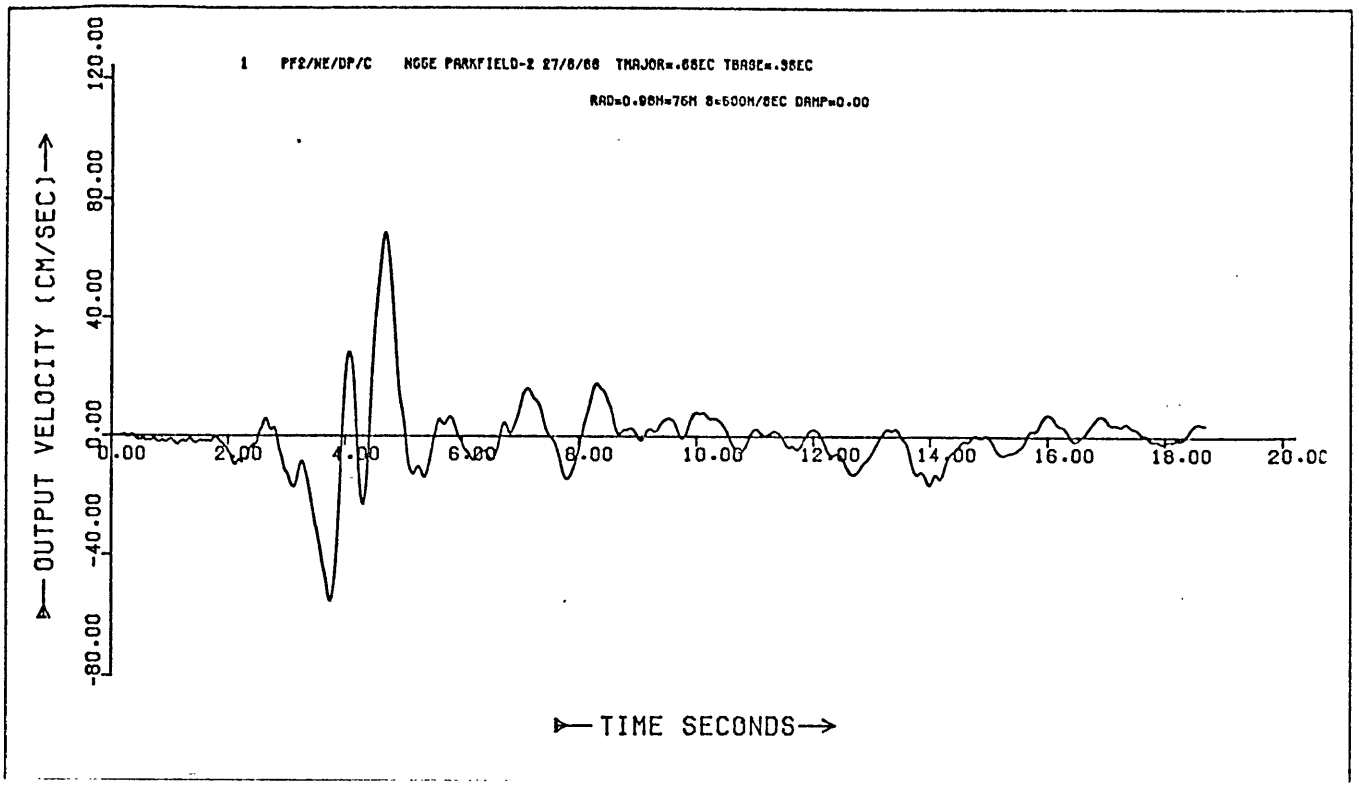


FIG. 6.1ob COMPUTED GROUND SURFACE VELOCITY TIME HISTORY AT SITE NO 6.1o

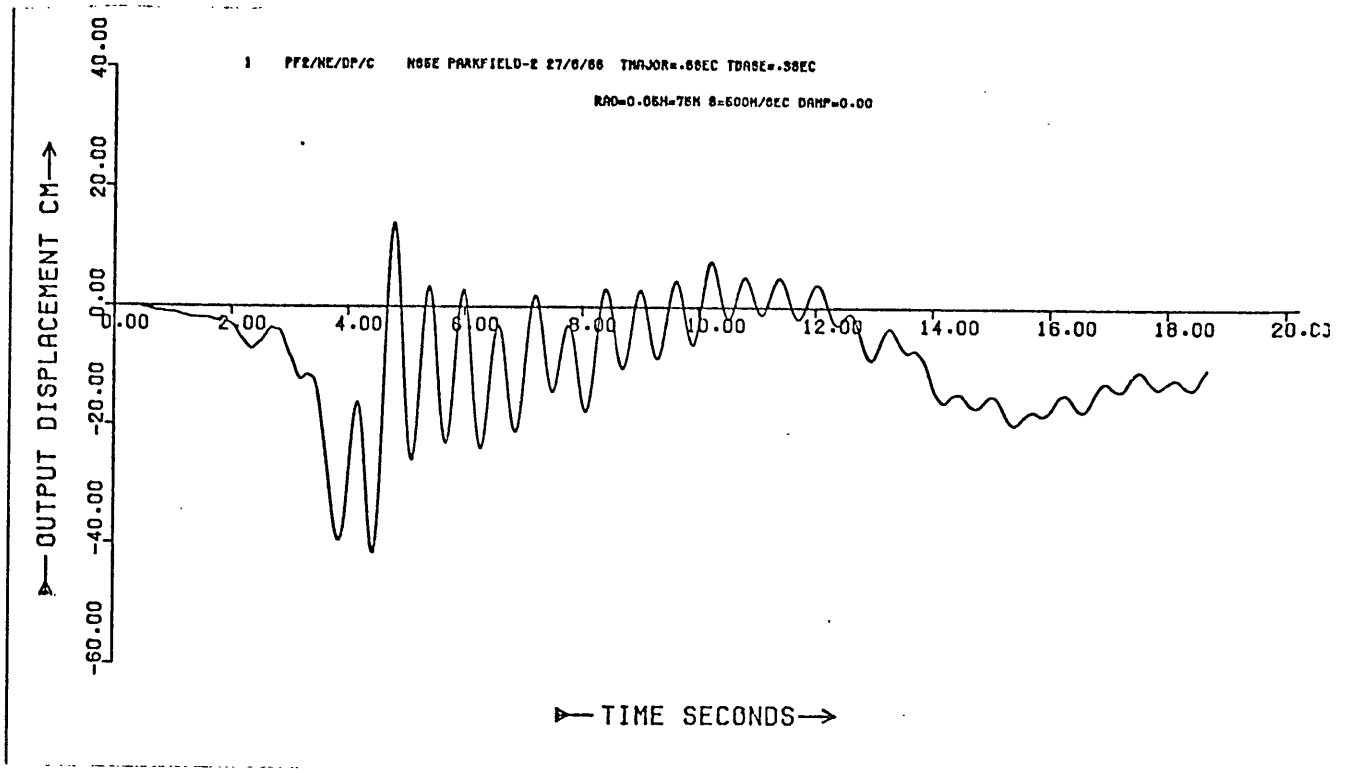


FIG.6..2c COMPUTED GROUND SURFACE DISPLACEMENT TIME HISTORY AT SITE NO 6.2

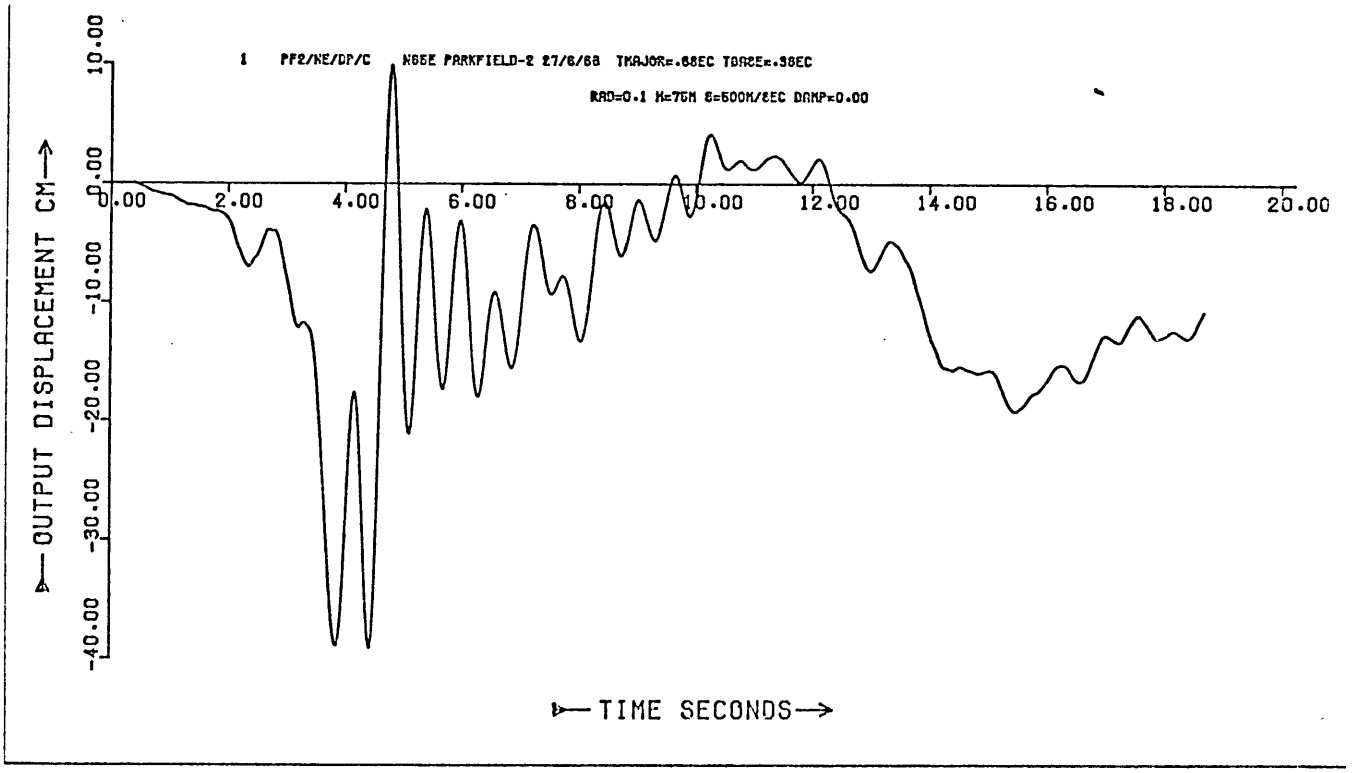


FIG. 6.3c COMPUTED GROUND SURFACE DISPLACEMENT TIME HISTORY AT SITE NO 6.3

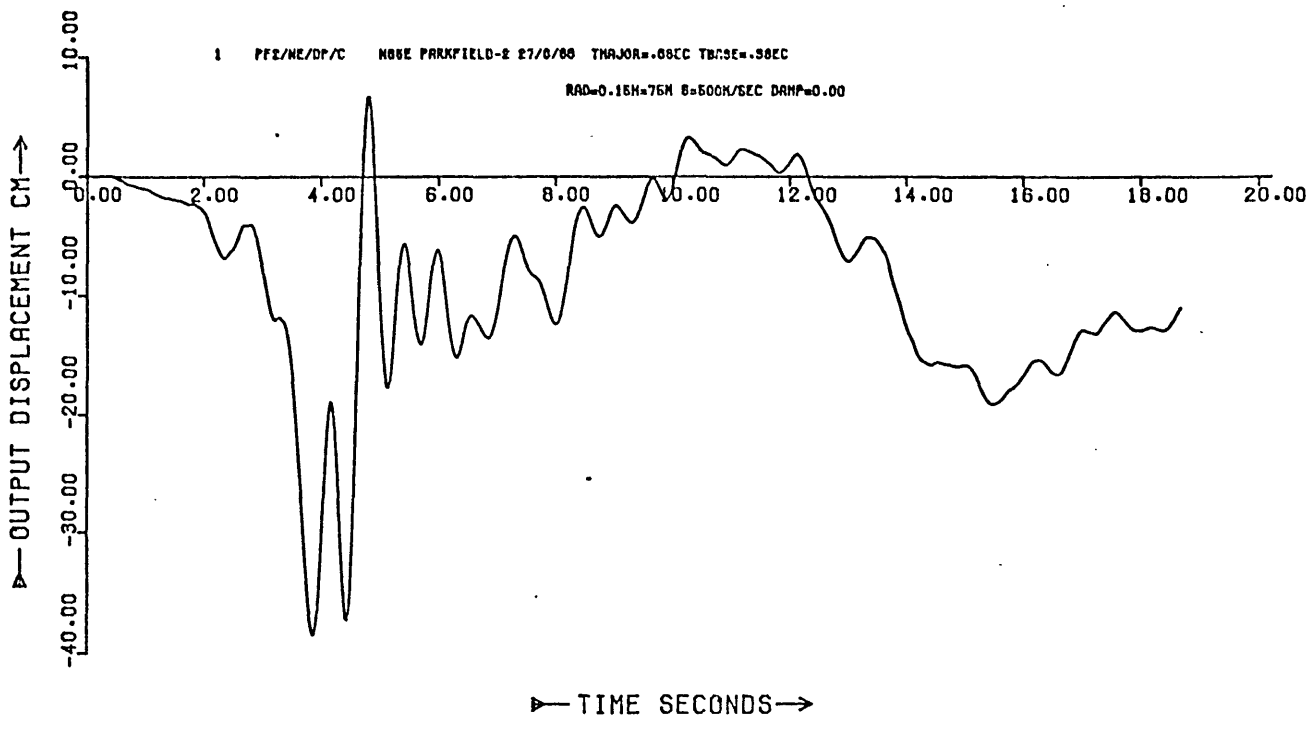


FIG 6.4c COMPUTED GROUND SURFACE DISPLACEMENT TIME HISTORY AT SITE NO 6.4

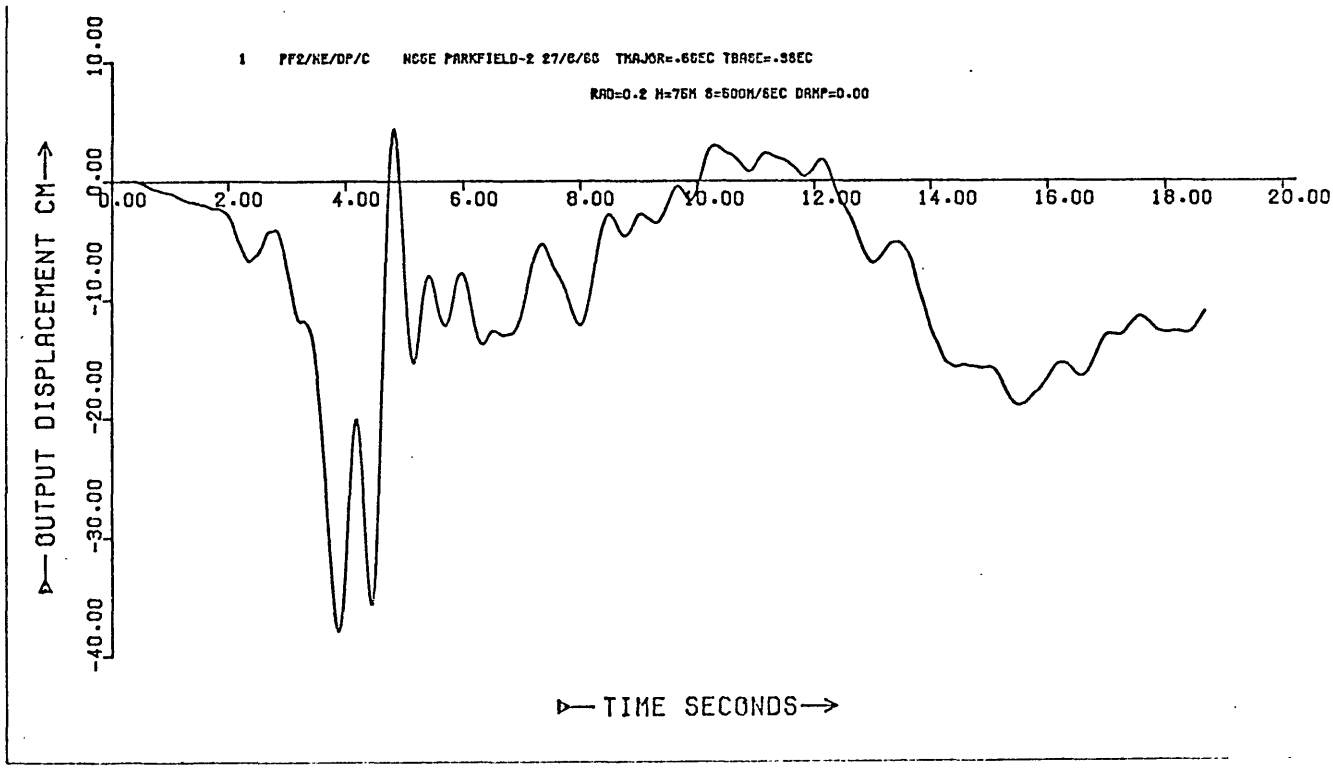


FIG. 6.5c COMPUTED GROUND SURFACE DISPLACEMENT TIME HISTORY AT SITE NO 6.5

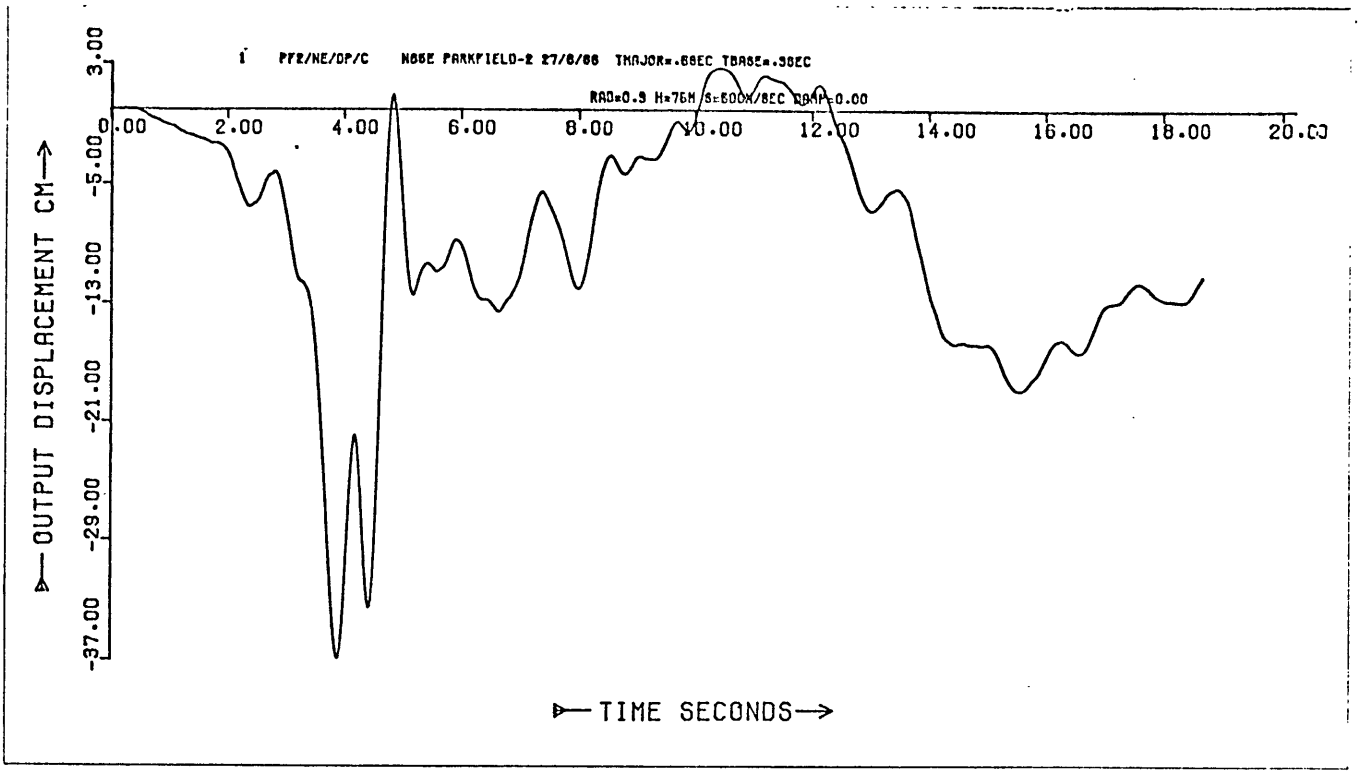


FIG.6.6c COMPUTED GROUND SURFACE DISPLACEMENT TIME HISTORY AT SITE NO6.6

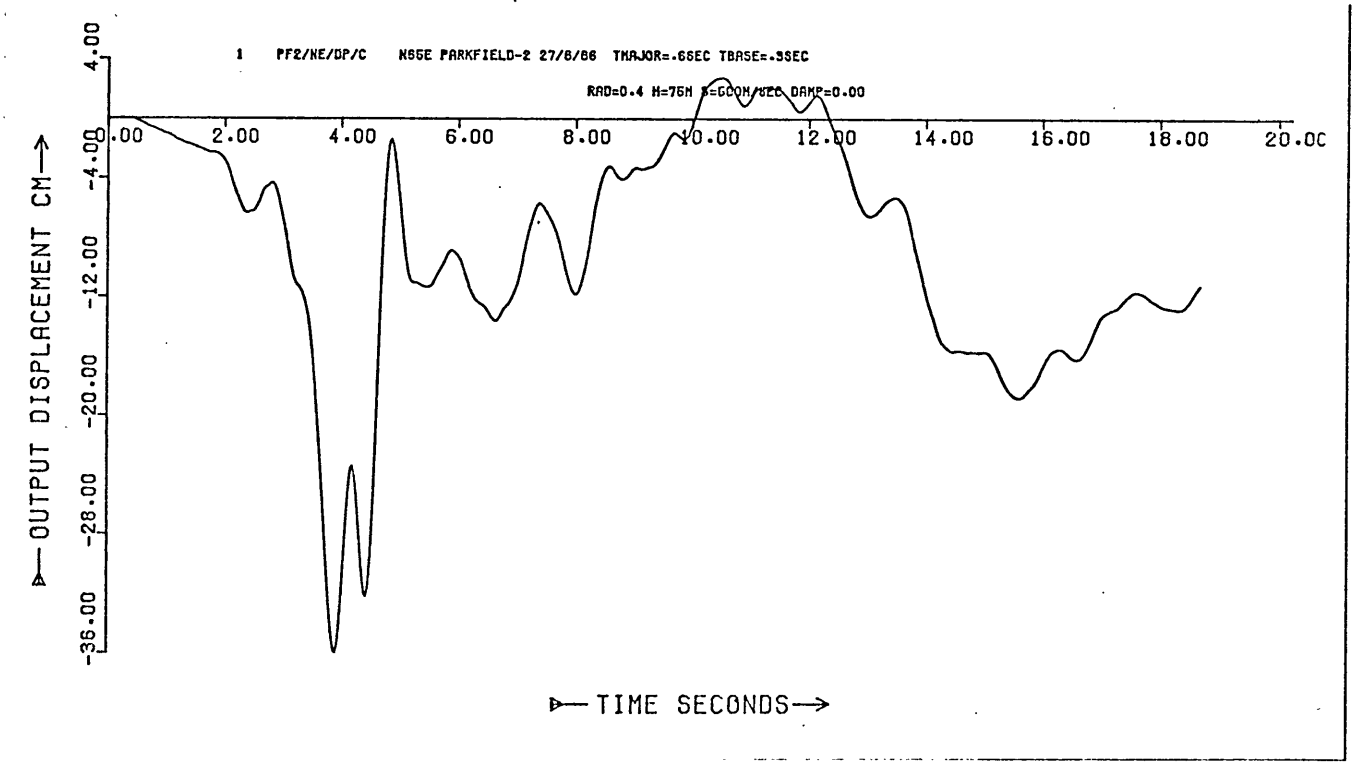


FIG. 6.7c COMPUTED GROUND SURFACE DISPLACEMENT TIME HISTORY AT SITE NO 6.7

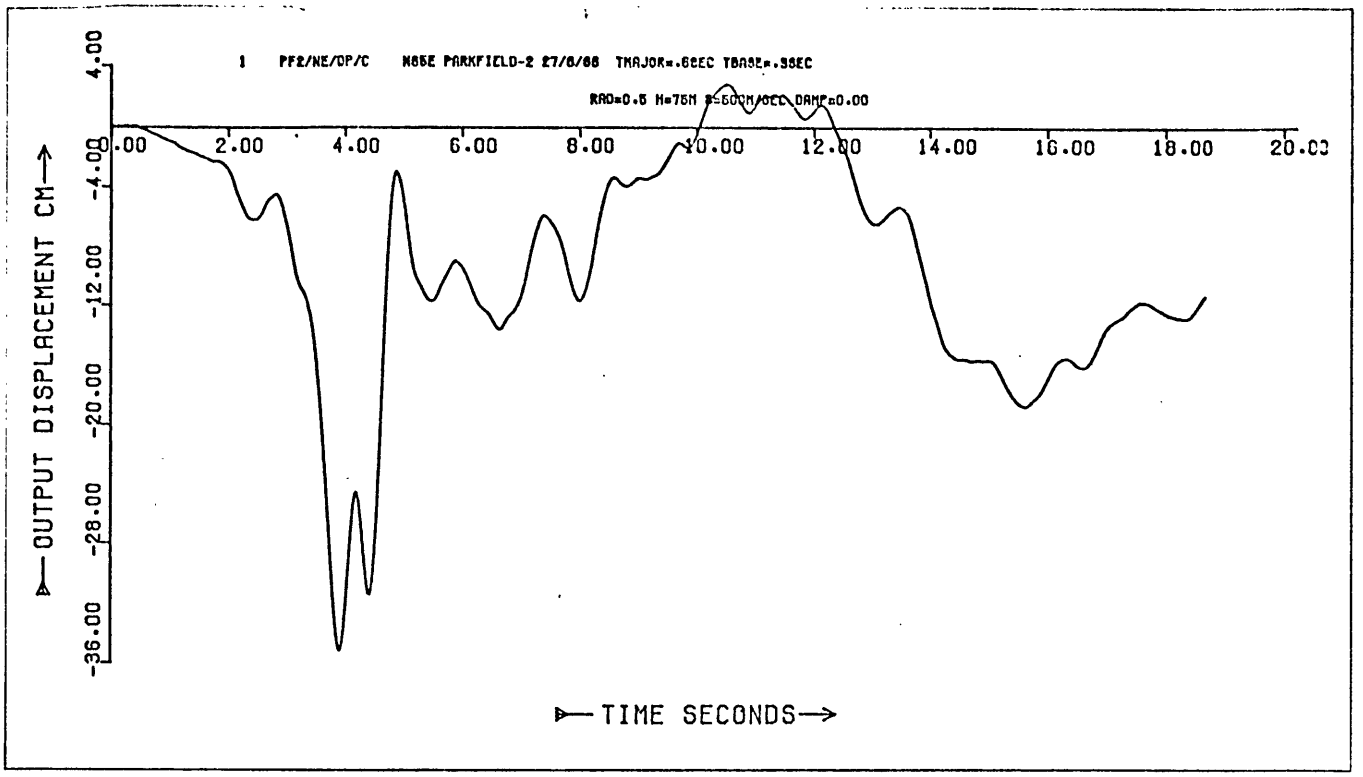


FIG. 6.8c COMPUTED GROUND SURFACE DISPLACEMENT TIME HISTORY AT SITE NO 6.8

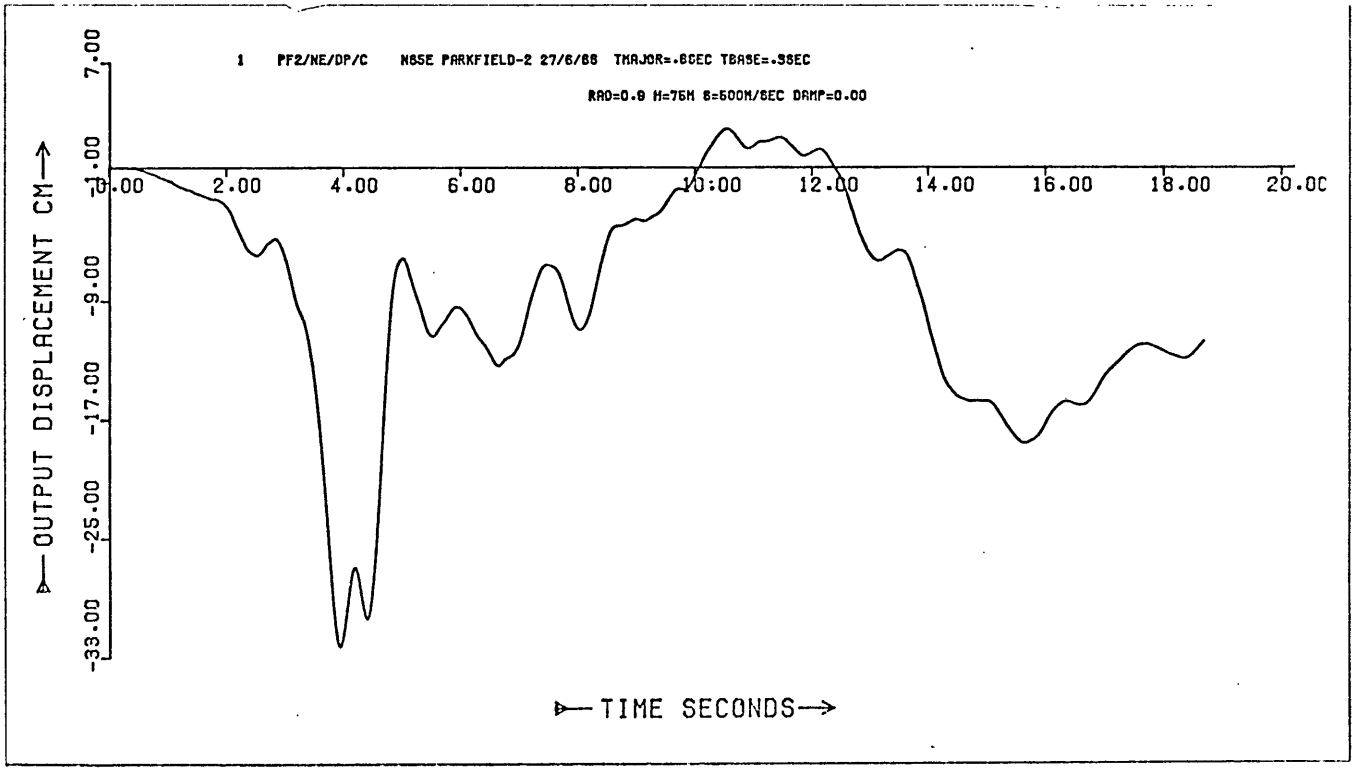


FIG. 6.9c COMPUTED GROUND SURFACE DISPLACEMENT TIME HISTORY AT SITE NO 6.9

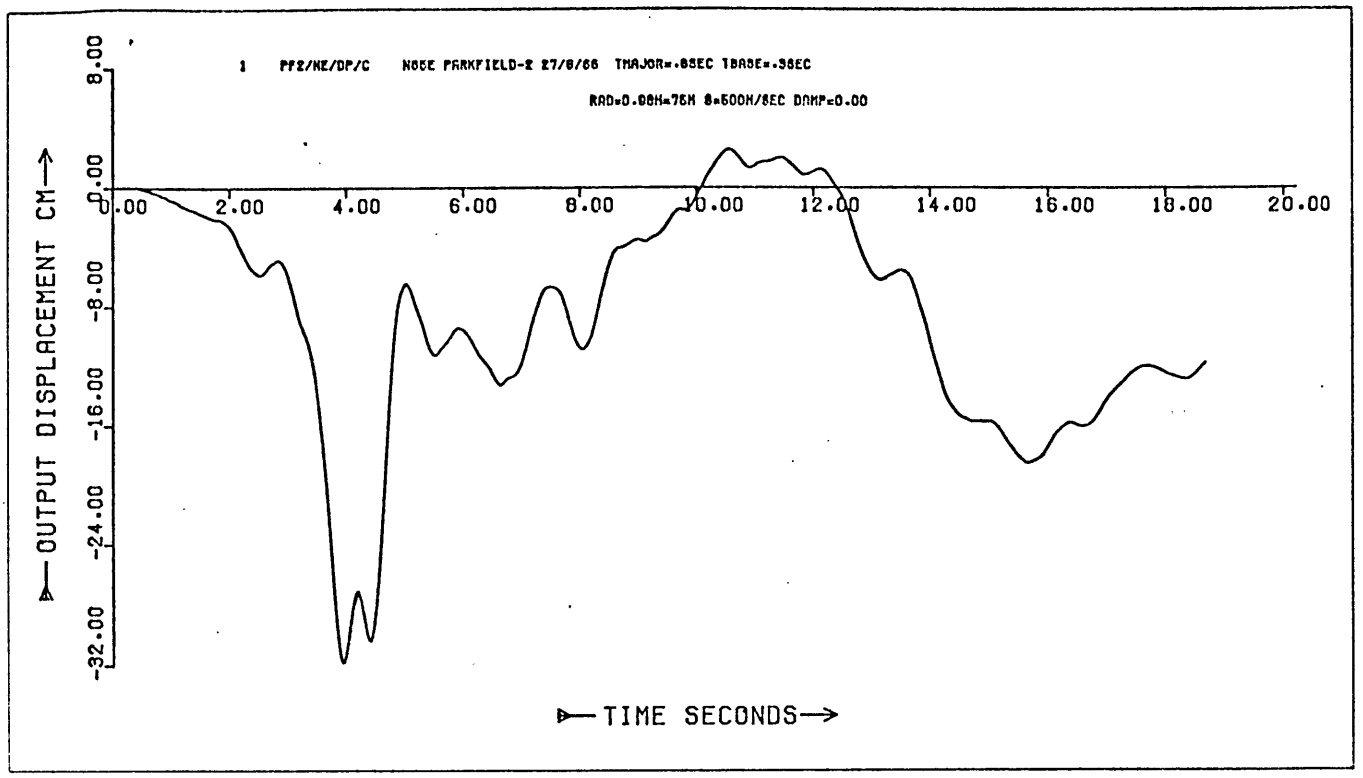


FIG. 6.1oc COMPUTED GROUND SURFACE DISPLACEMENT TIME HISTORY AT SITE NO 6.1o

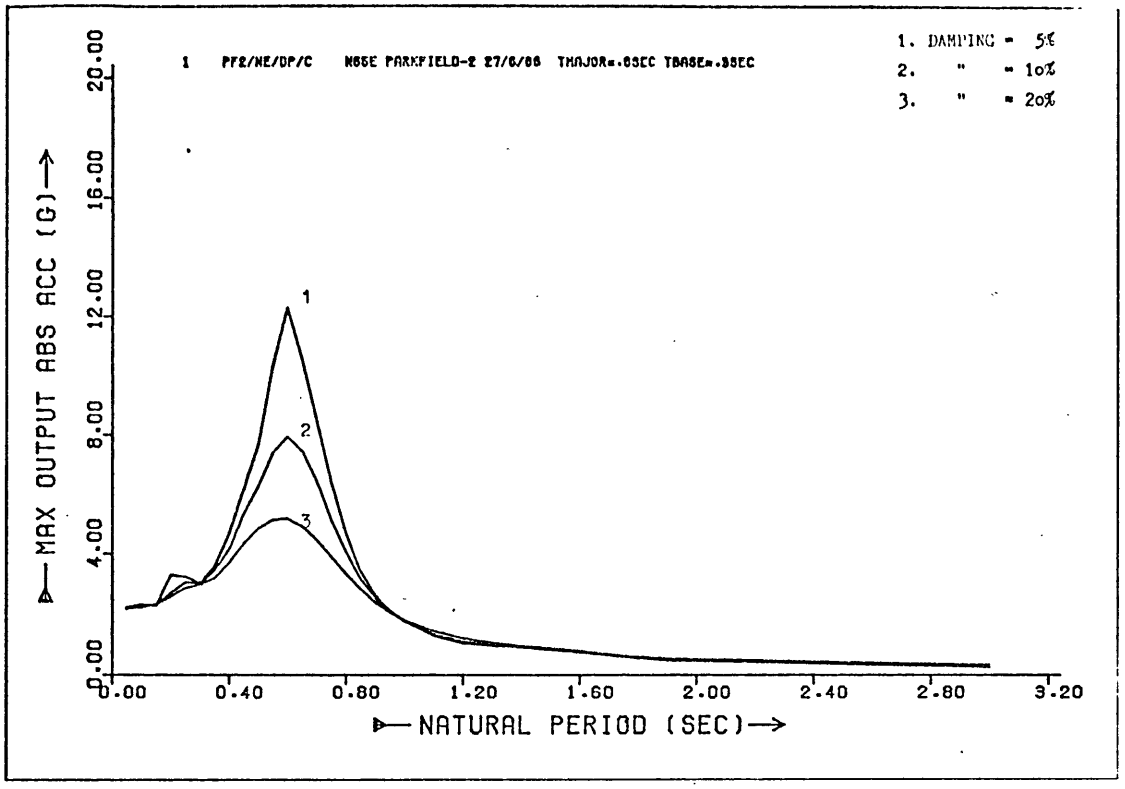


FIG. 6.2d COMPUTED GROUND SURFACE ACCELERATION RESPONSE SPECTRA AT SITE NO 6.2

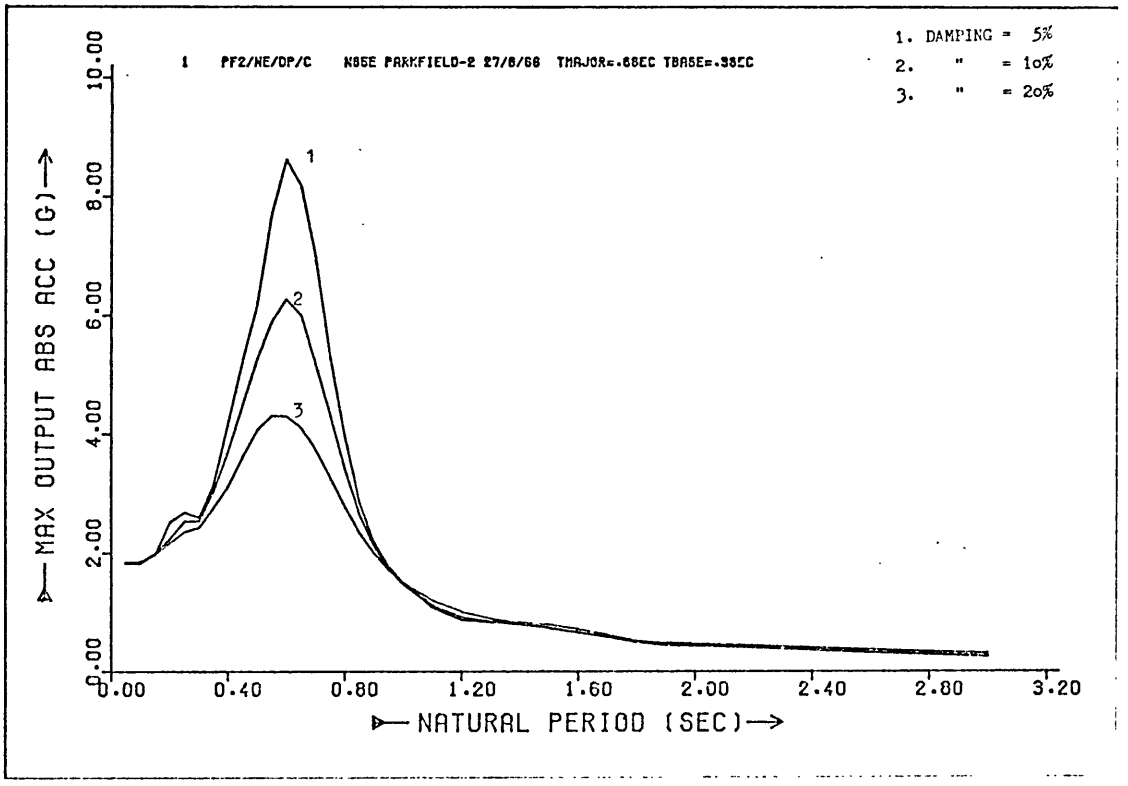


FIG. 6.3d COMPUTED GROUND SURFACE ACCELERATION RESPONSE SPECTRA AT SITE NO 6.3

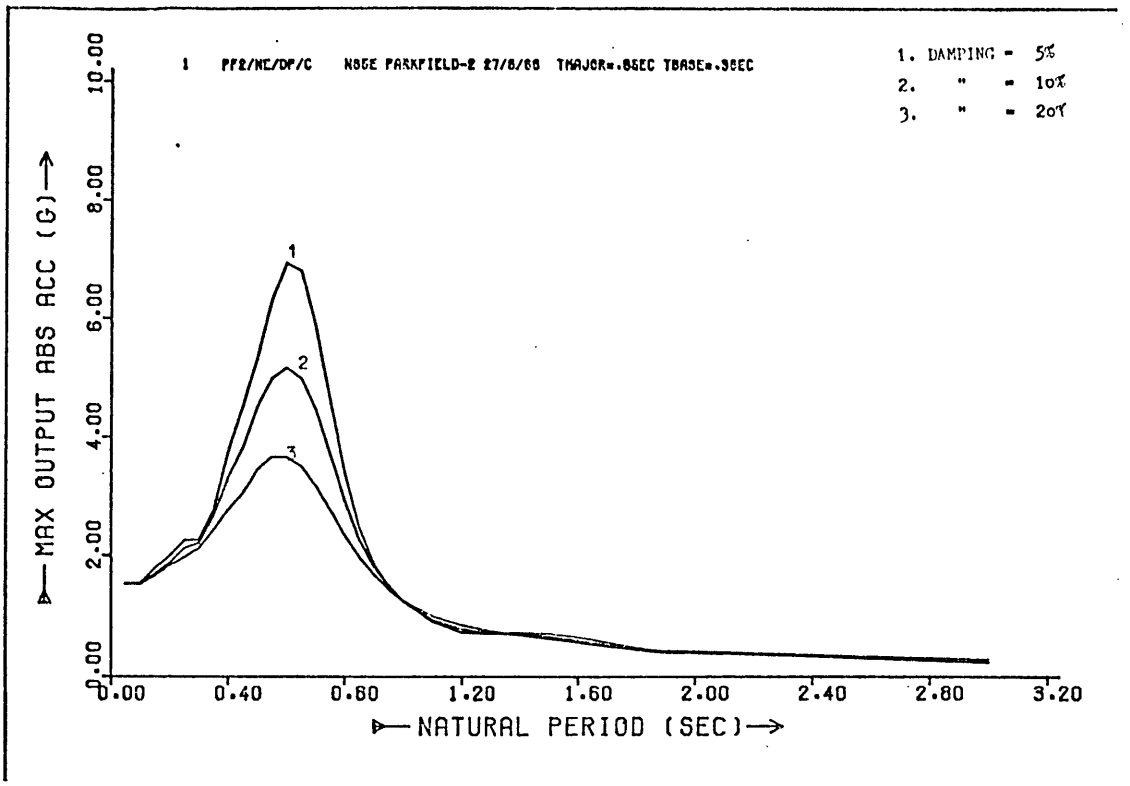


FIG. 6.4d COMPUTED GROUND SURFACE ACCELERATION RESPONSE SPECTRA AT SITE NO 6.4

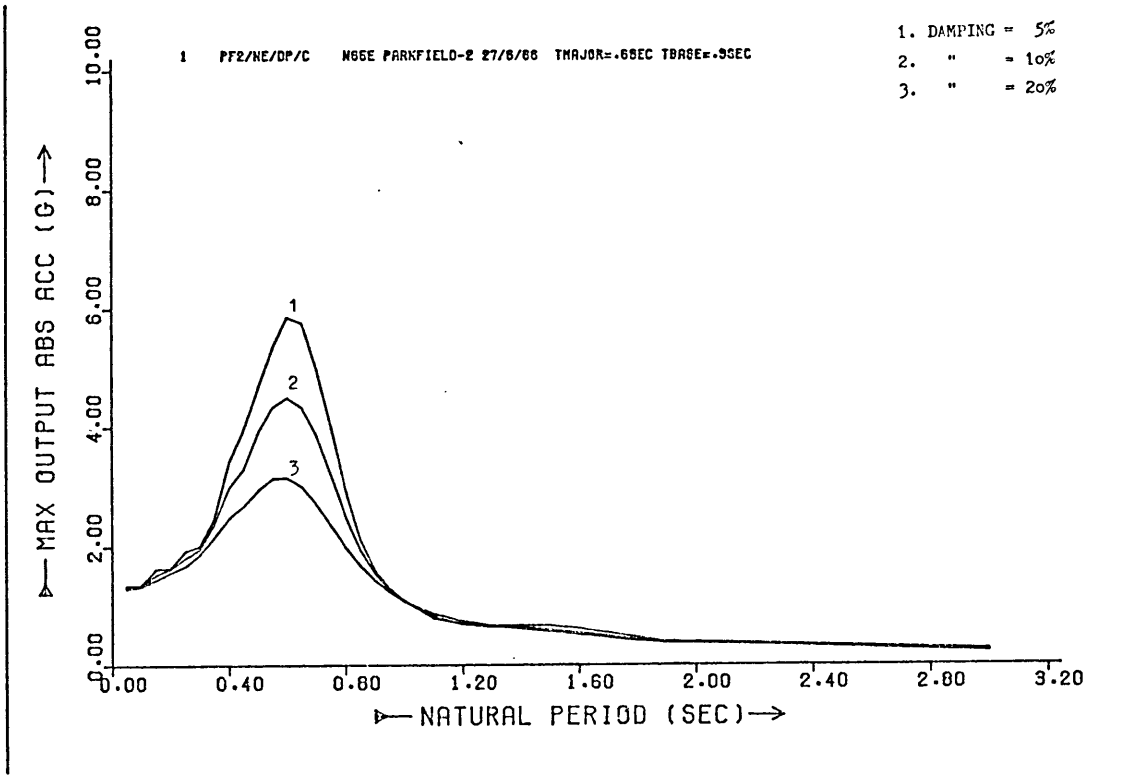


FIG. 6.5d COMPUTED GROUND SURFACE ACCELERATION RESPONSE SPECTRA AT SITE NO 6.5

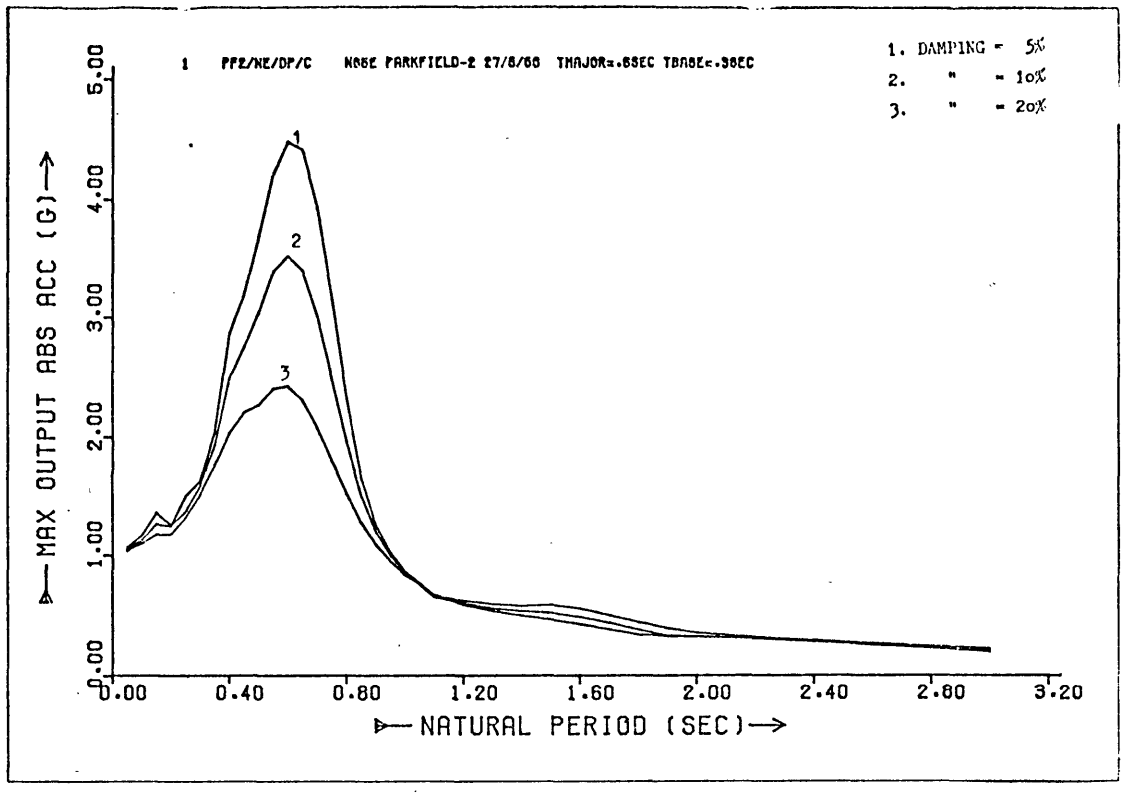


FIG. 6.6d COMPUTED GROUND SURFACE ACCELERATION RESPONSE SPECTRA AT SITE NO 6.6

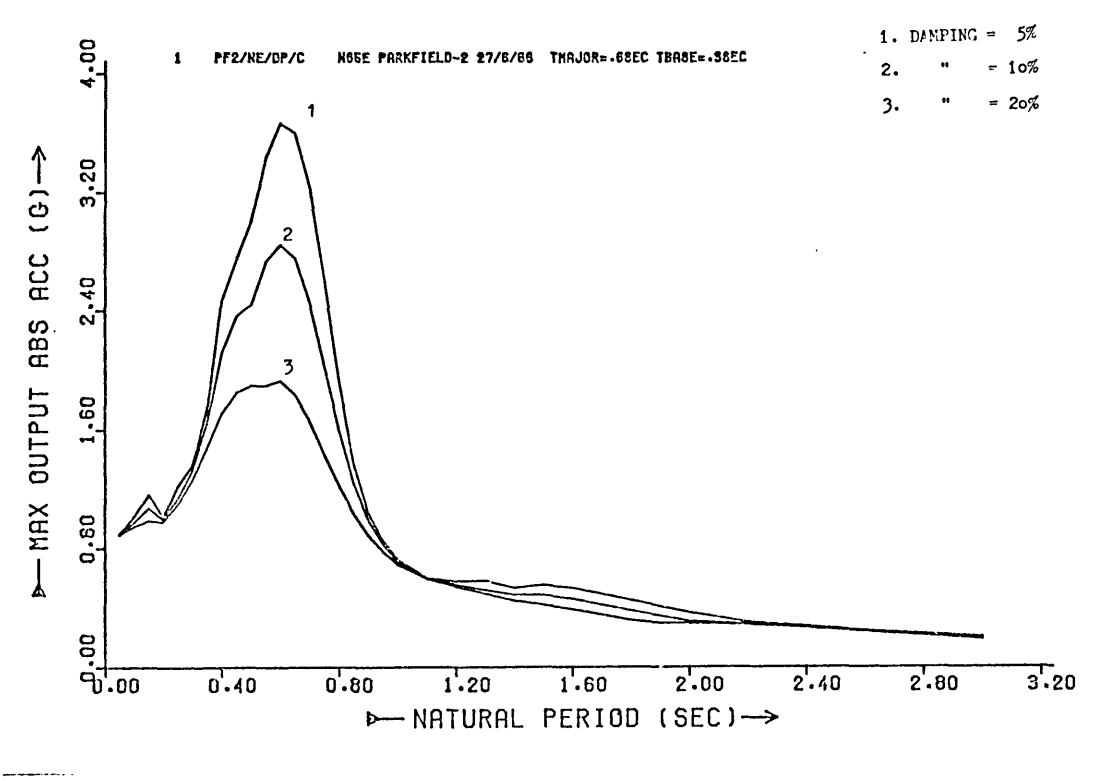


FIG. 6.7d COMPUTED GROUND SURFACE ACCELERATION RESPONSE SPECTRA AT SITE NO 6.7

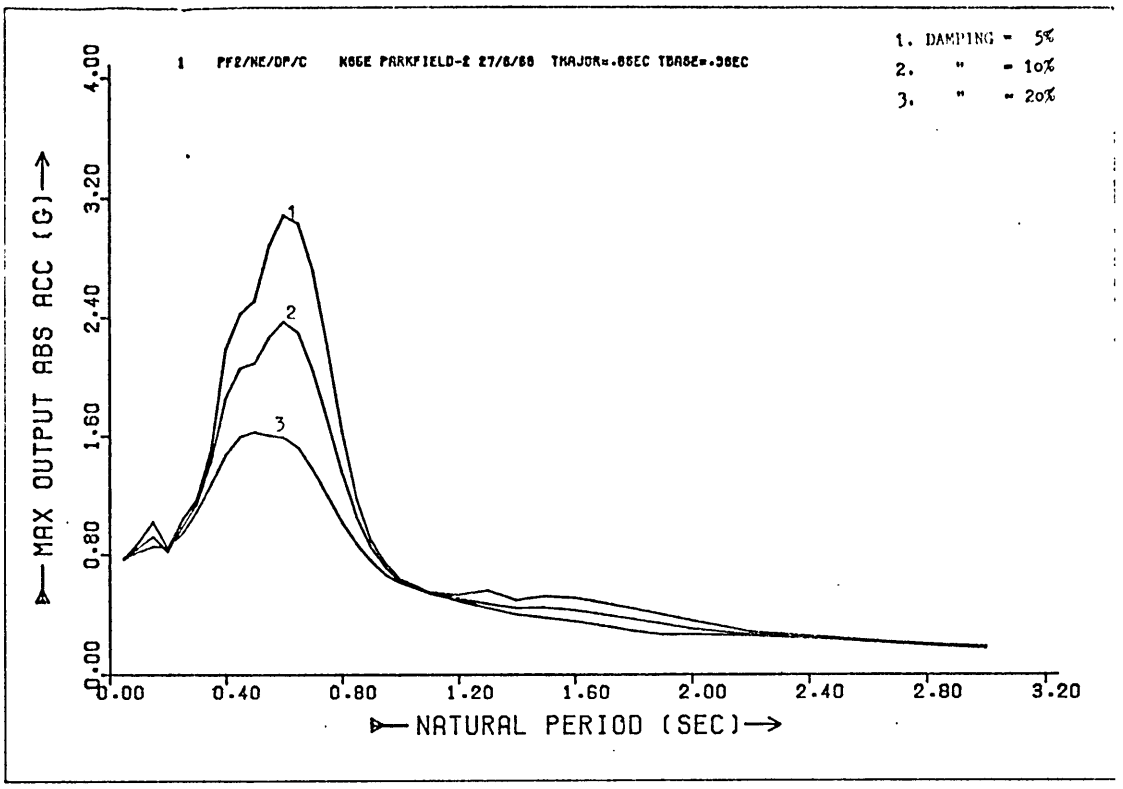


FIG. 6.8d COMPUTED GROUND SURFACE ACCELERATION RESPONSE SPECTRA AT SITE NO 6.8

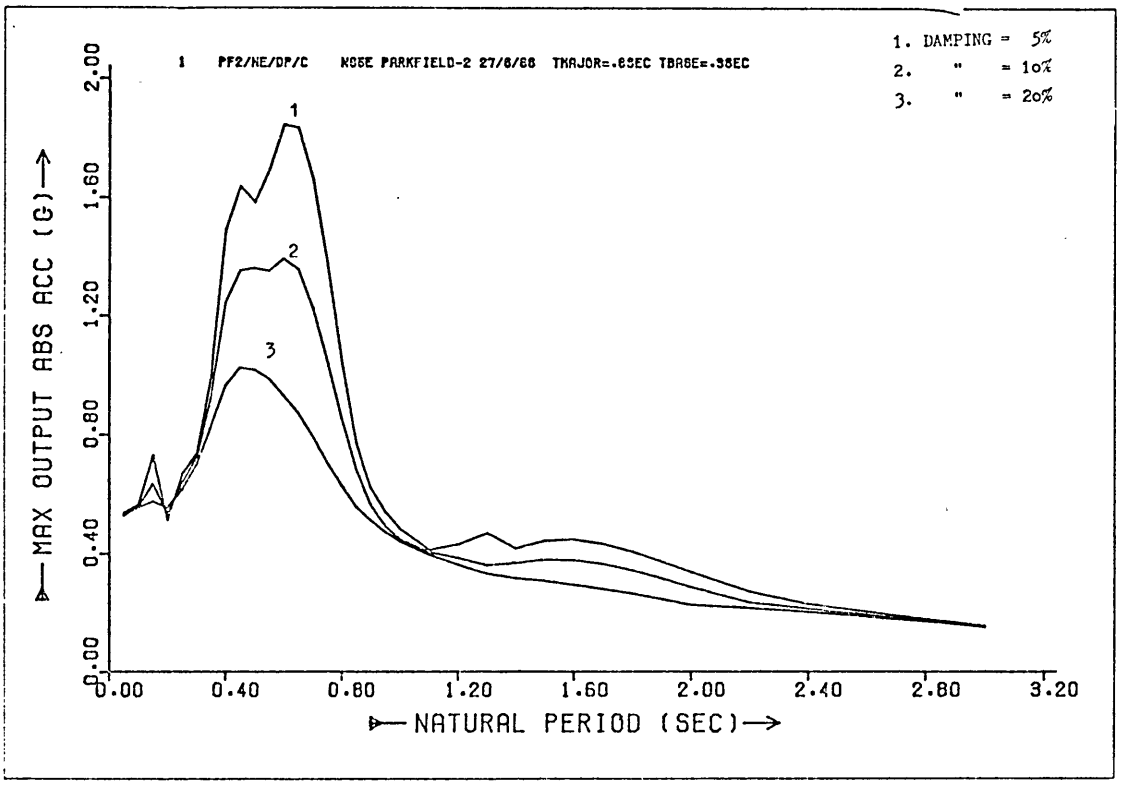


FIG. 6.9d COMPUTED GROUND SURFACE ACCELERATION RESPONSE SPECTRA AT SITE NO 6.9

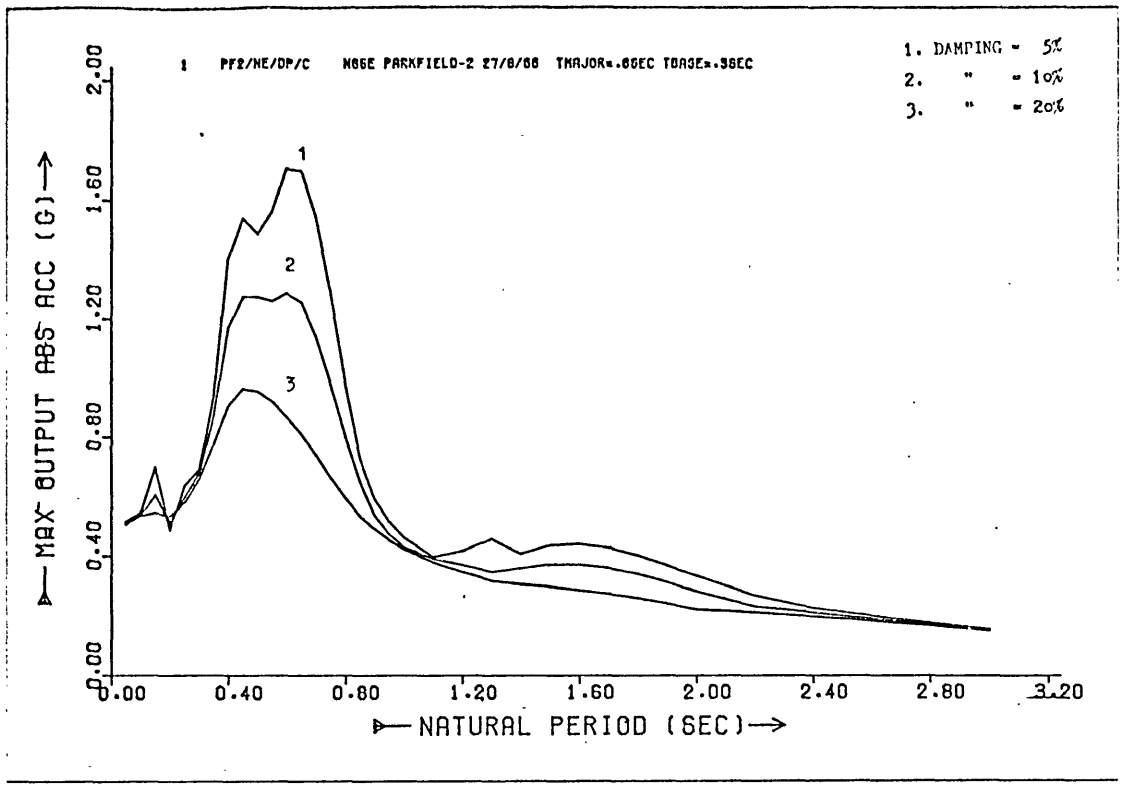


FIG. 6.1od COMPUTED GROUND SURFACE ACCELERATION RESPONSE SPECTRA AT SITE NO 6.1o

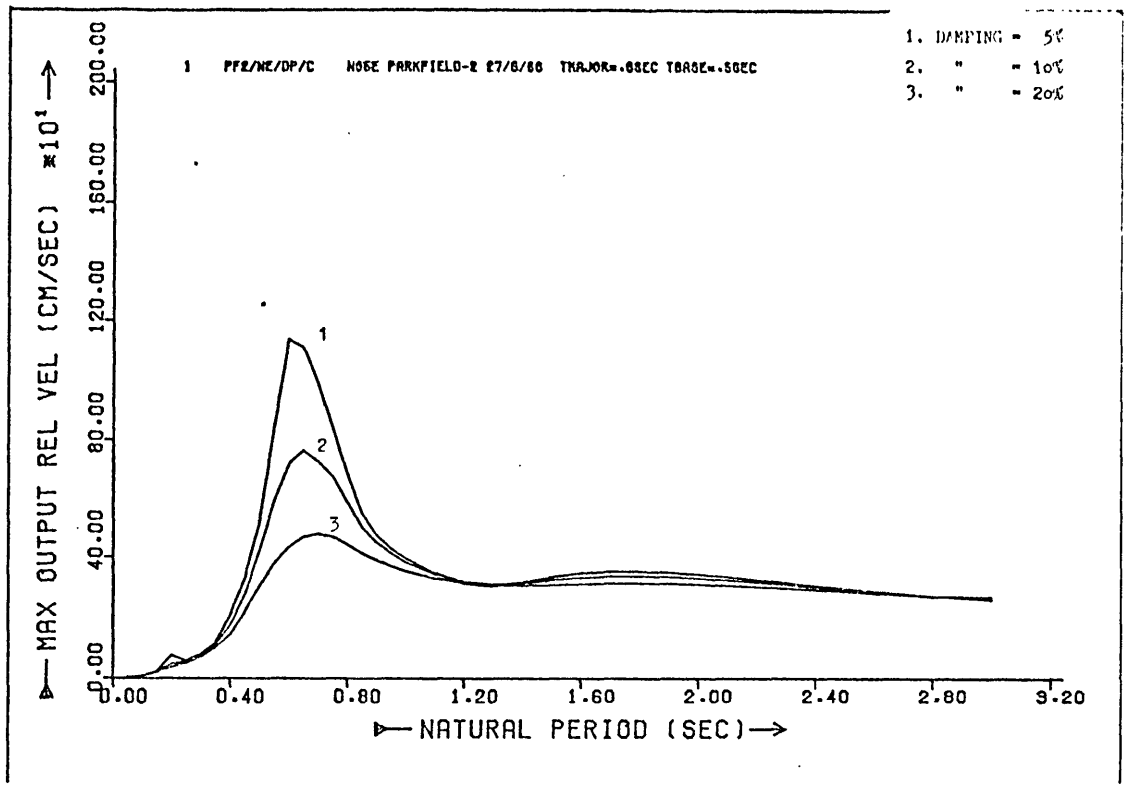


FIG. 6.2e COMPUTED GROUND SURFACE VELOCITY RESPONSE SPECTRA AT SITE NO 6.2

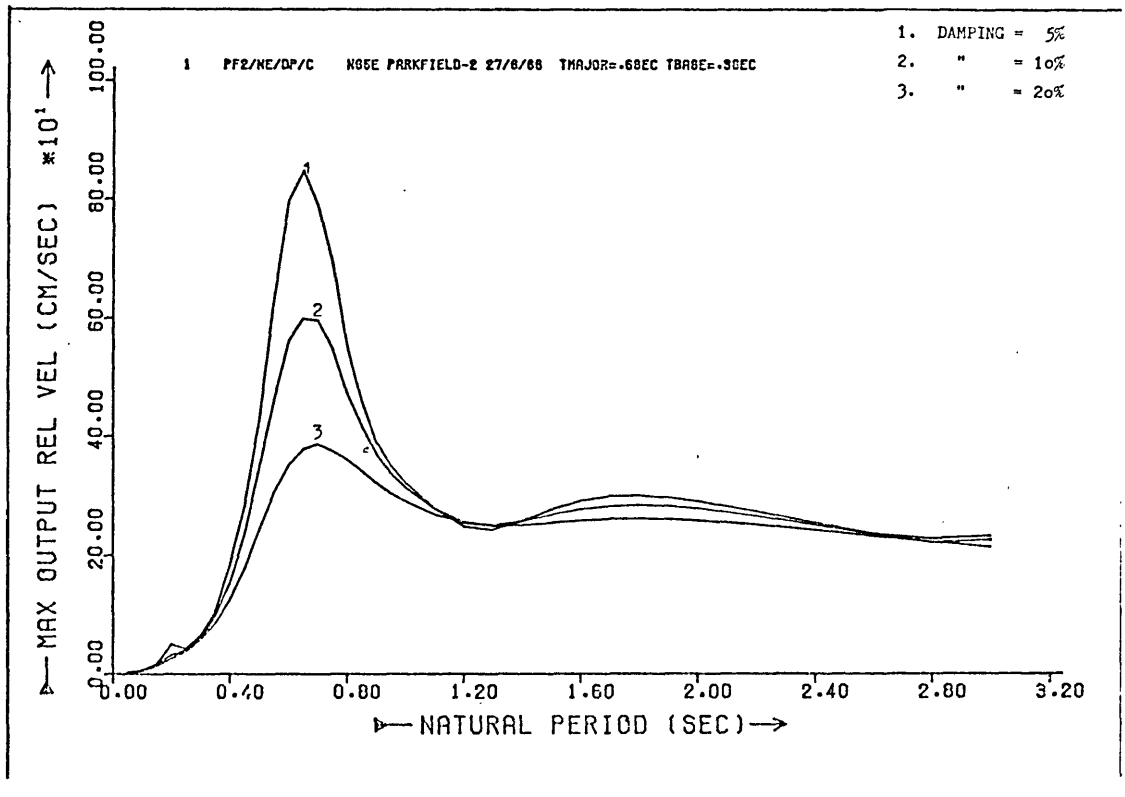


FIG. 6.3e COMPUTED GROUND SURFACE VELOCITY RESPONSE SPECTRA AT SITE NO 6.3

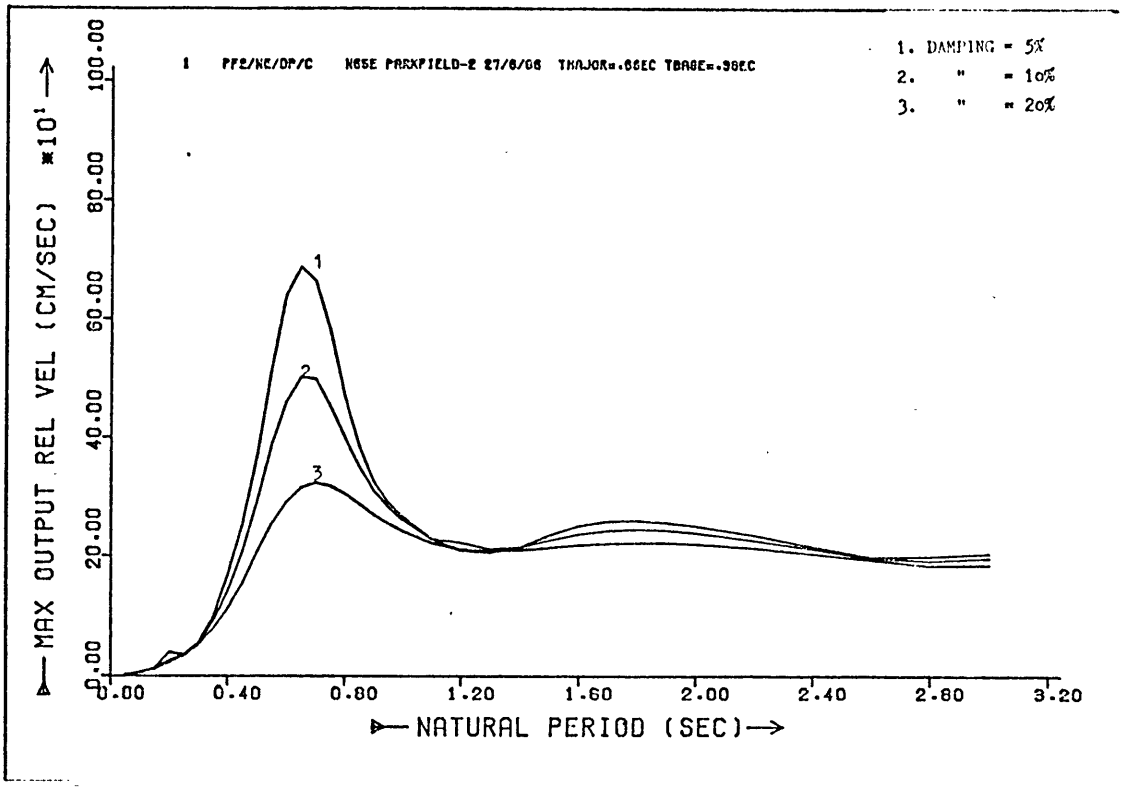


FIG. 6.4e COMPUTED GROUND SURFACE VELOCITY RESPONSE SPECTRA AT SITE NO 6.4

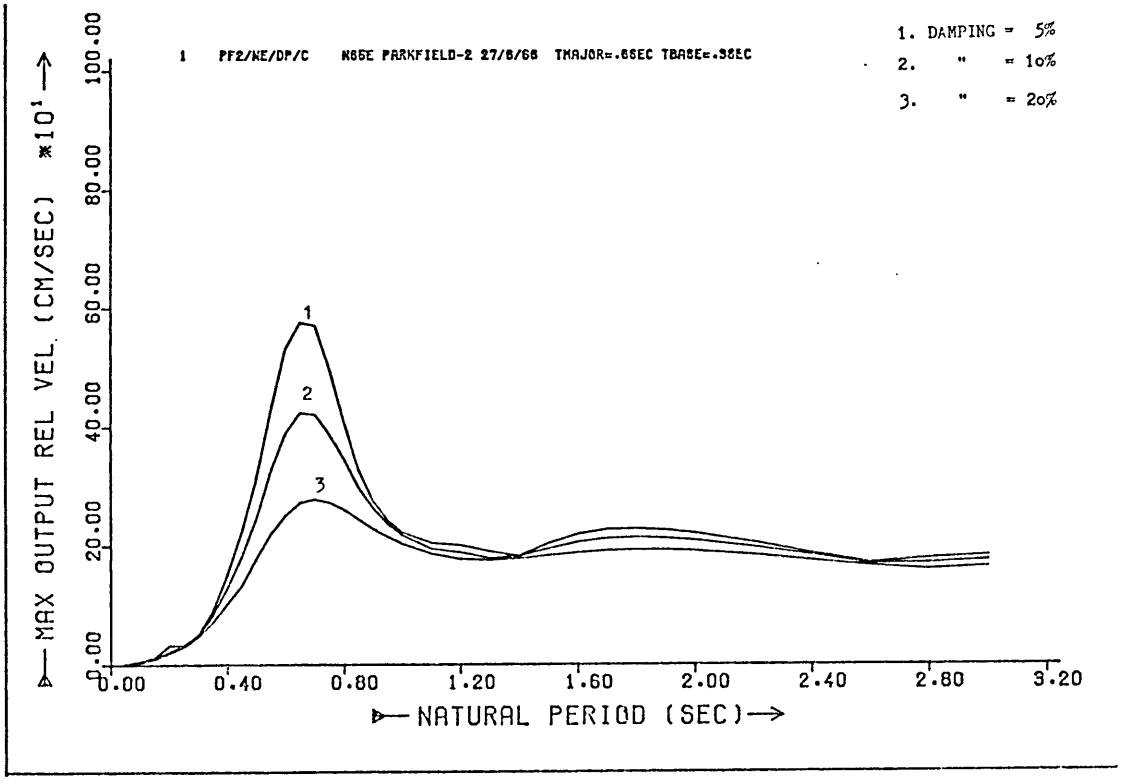


FIG. 6.5e COMPUTED GROUND SURFACE VELOCITY RESPONSE SPECTRA AT SITE NO 6.5

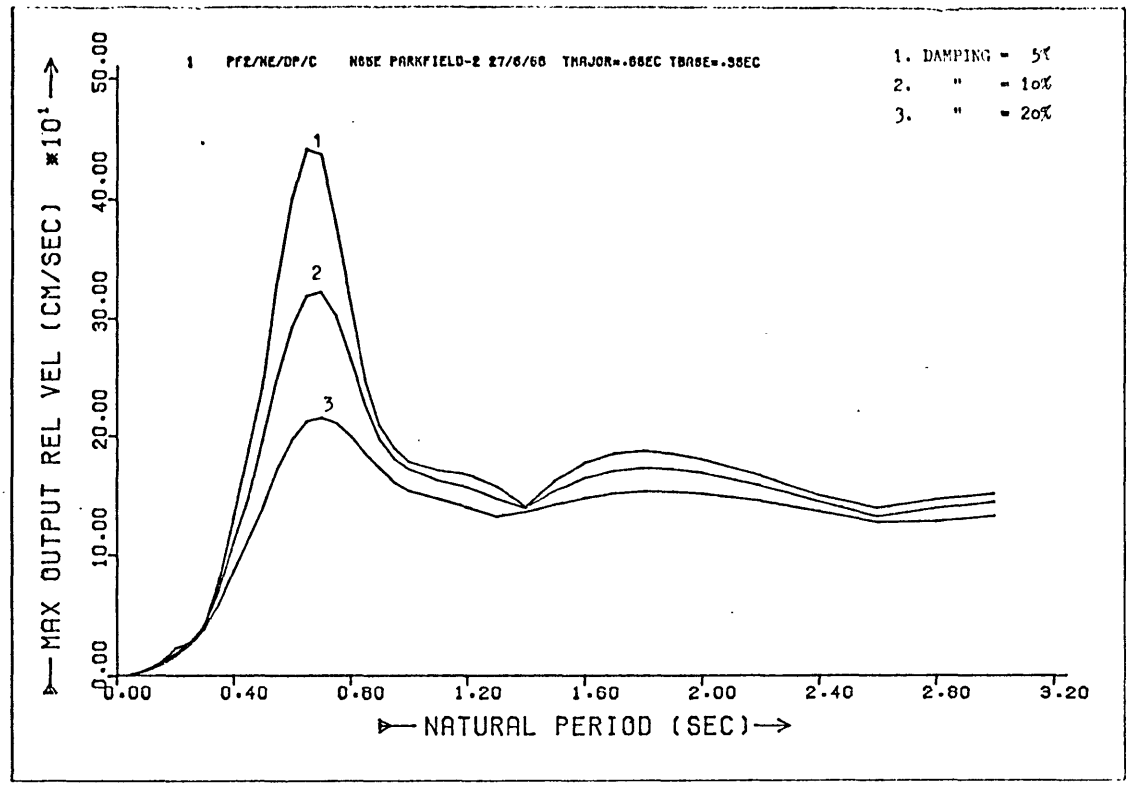


FIG. 6.6e COMPUTED GROUND SURFACE VELOCITY RESPONSE SPECTRA AT SITE NO 6.6

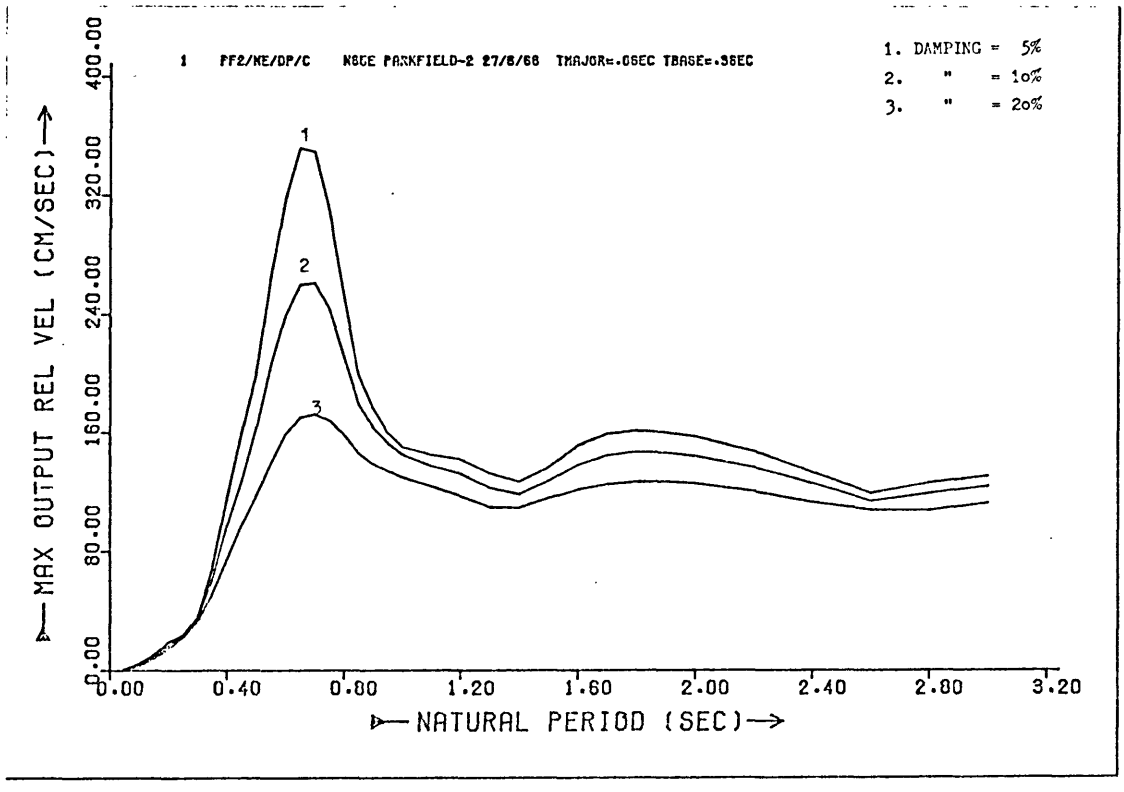


FIG. 6.7e COMPUTED GROUND SURFACE VELOCITY RESPONSE SPECTRA AT SITE NO 6.7

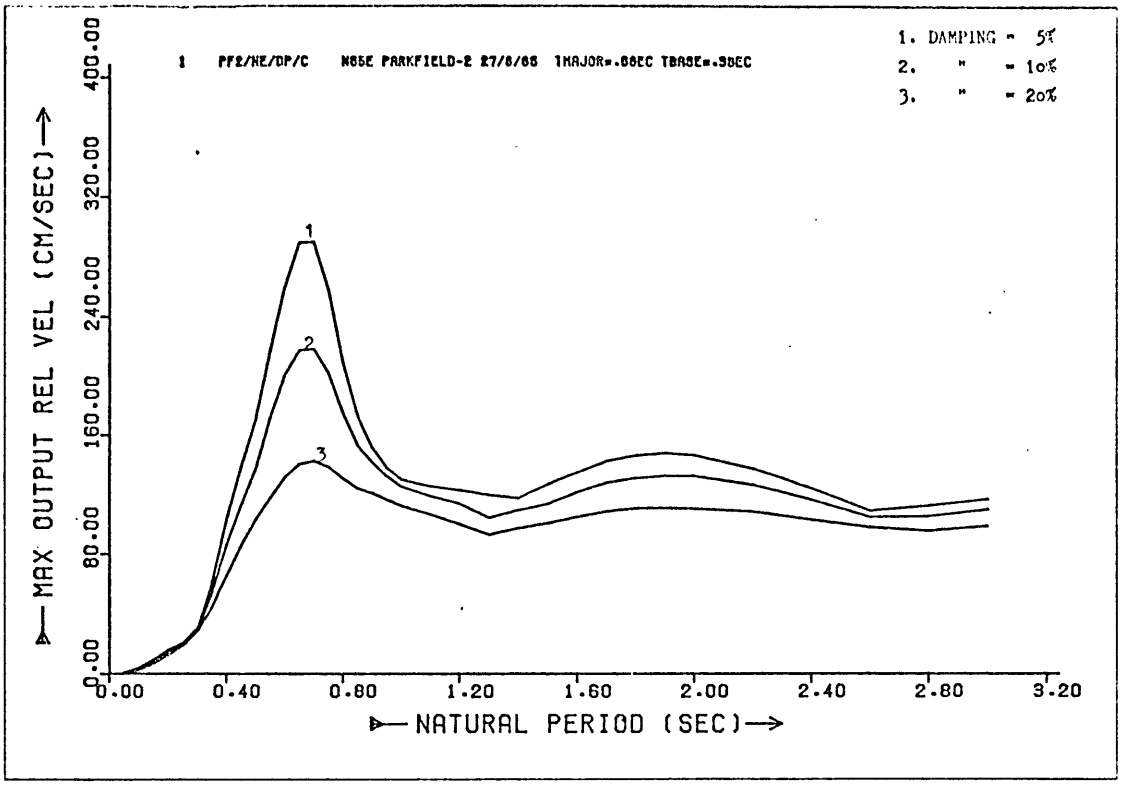


FIG. 6.8e COMPUTED GROUND SURFACE VELOCITY RESPONSE SPECTRA AT SITE NO 6.8

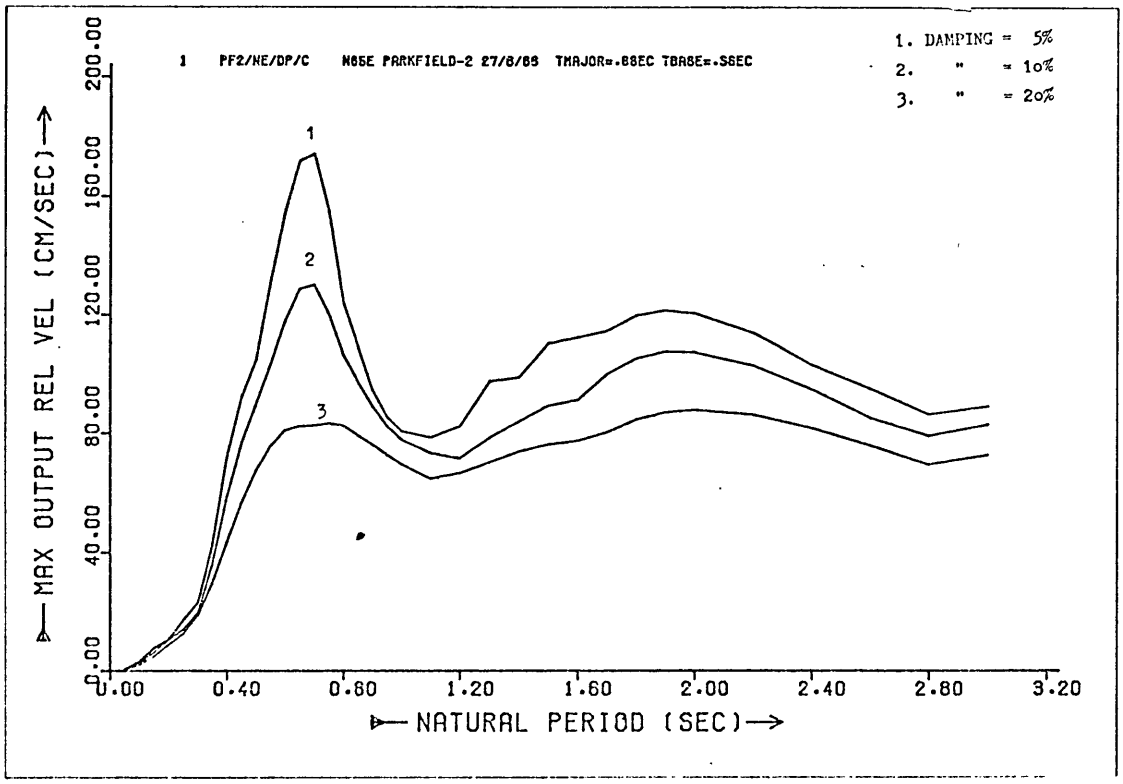


FIG. 6.9e COMPUTED GROUND SURFACE VELOCITY RESPONSE SPECTRA AT SITE NO 6.9

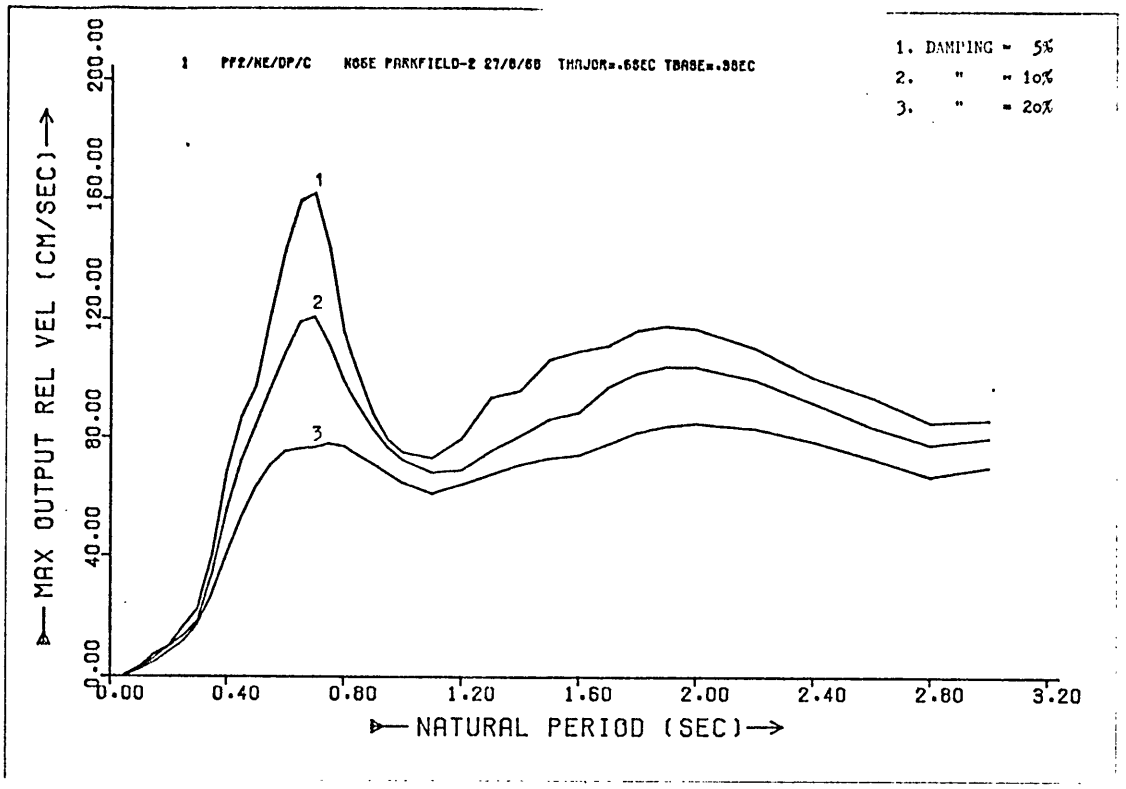


FIG. 6.1oe COMPUTED GROUND SURFACE VELOCITY RESPONSE SPECTRA AT SITE NO 6.1o

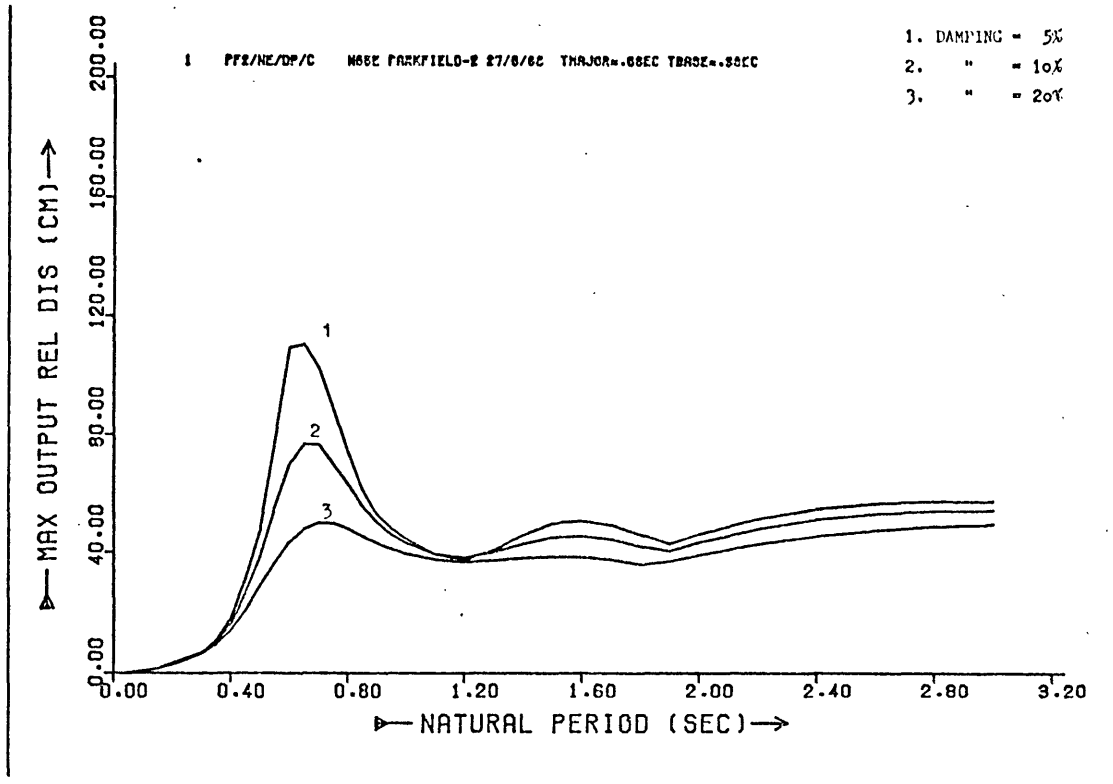


FIG. 6.2f COMPUTED GROUND SURFACE DISPLACEMENT RESPONSE SPECTRA AT SITE NO 6.2

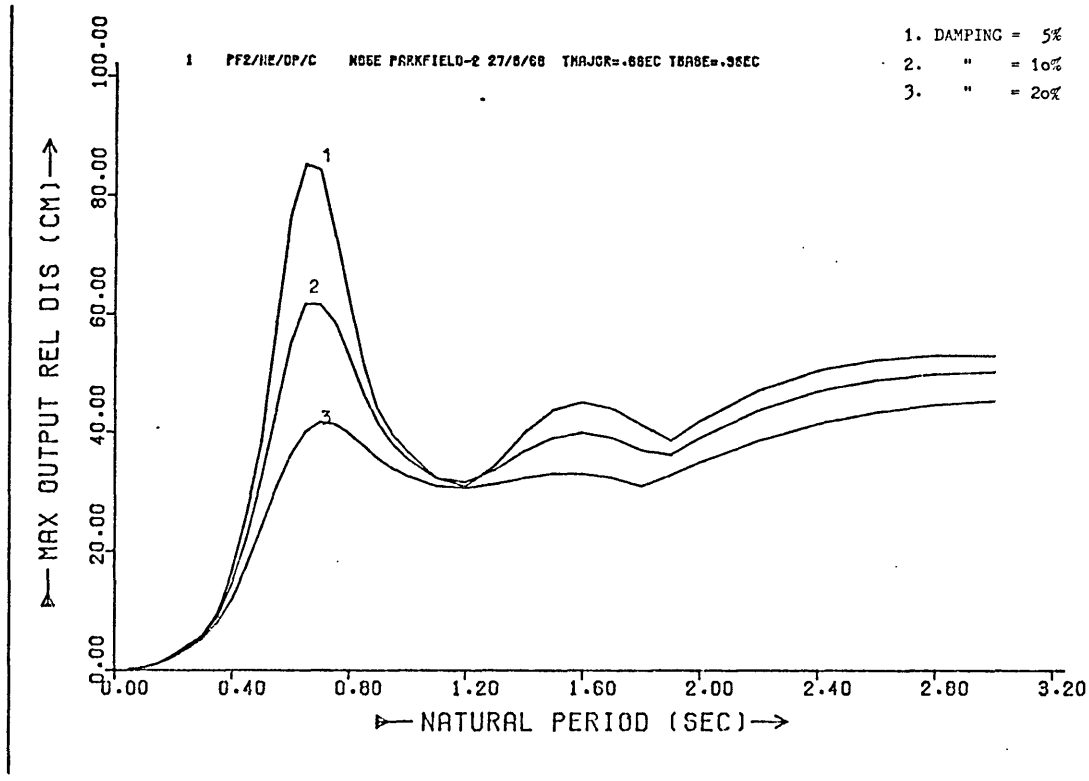


FIG. 6.3f COMPUTED GROUND SURFACE DISPLACEMENT RESPONSE SPECTRA AT SITE NO 6.3

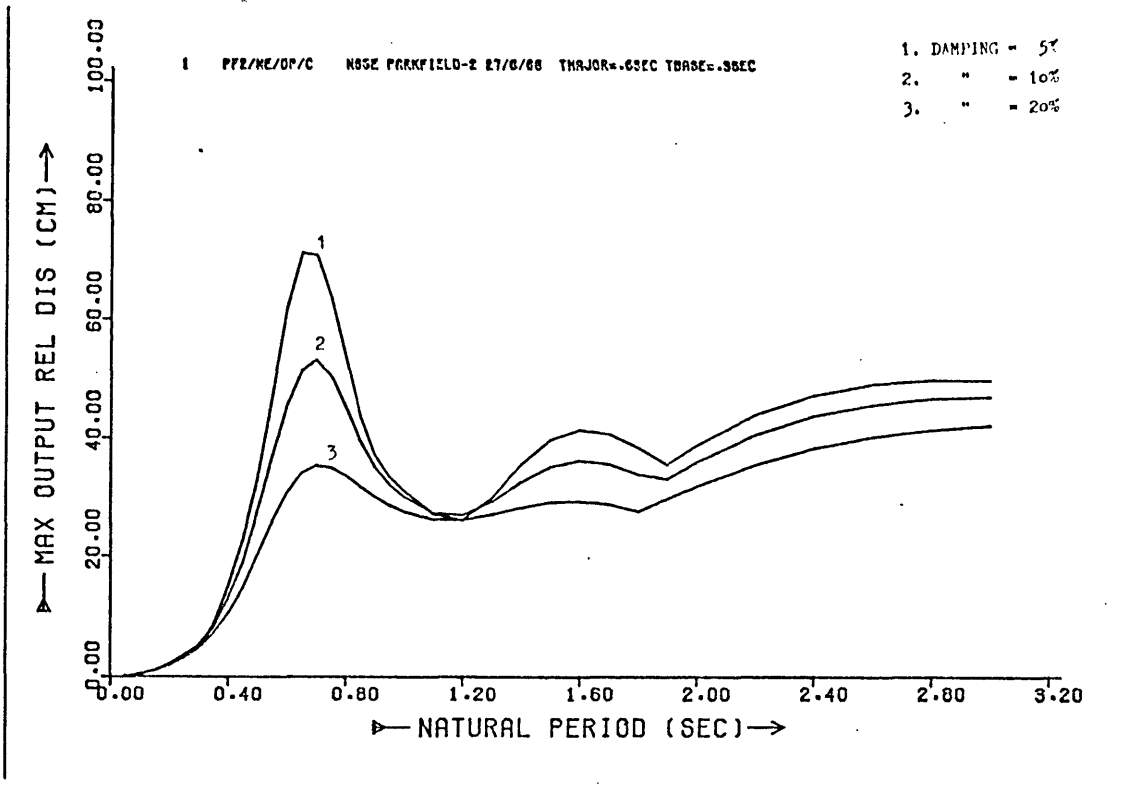


FIG. 6.4f COMPUTED GROUND SURFACE DISPLACEMENT RESPONSE SPECTRA AT SITE NO 6.4

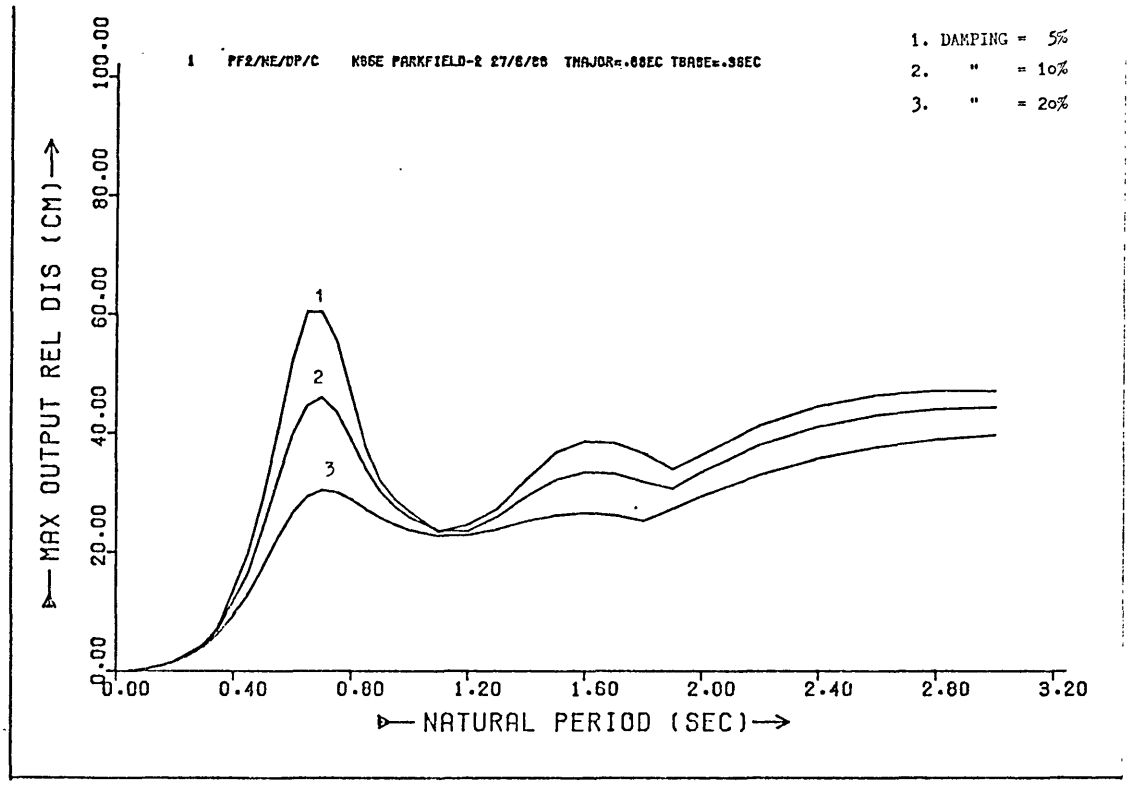


FIG. 6.5f COMPUTED GROUND SURFACE DISPLACEMENT RESPONSE SPECTRA AT SITE NO 6.5

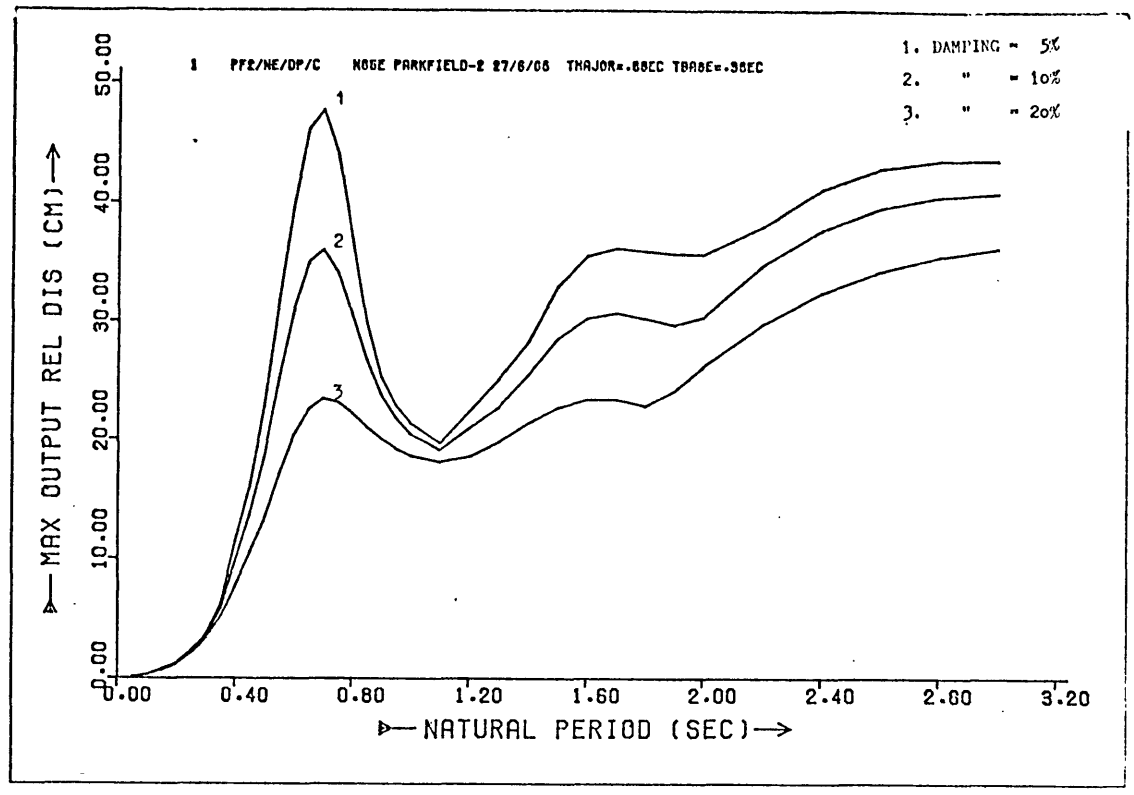


FIG. 6.6f COMPUTED GROUND SURFACE DISPLACEMENT RESPONSE SPECTRA AT SITE NO 6.6

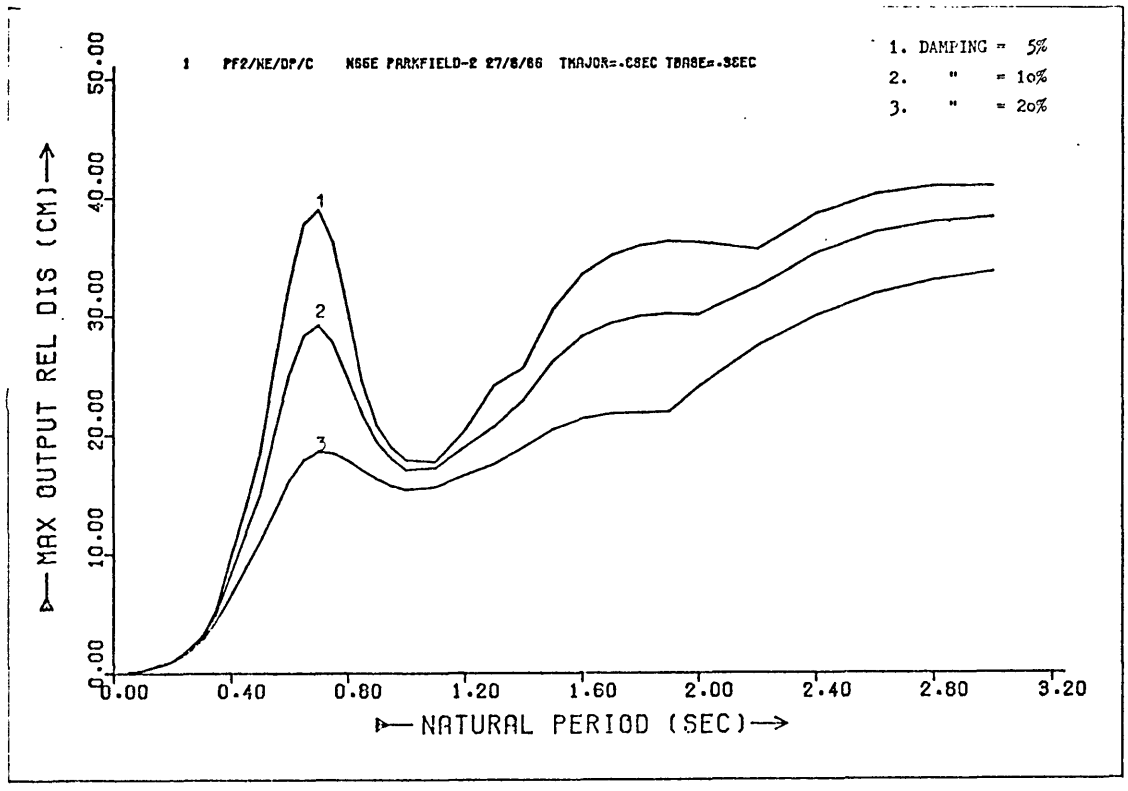


FIG. 6.7f COMPUTED GROUND SURFACE DISPLACEMENT RESPONSE SPECTRA AT SITE NO 6.7

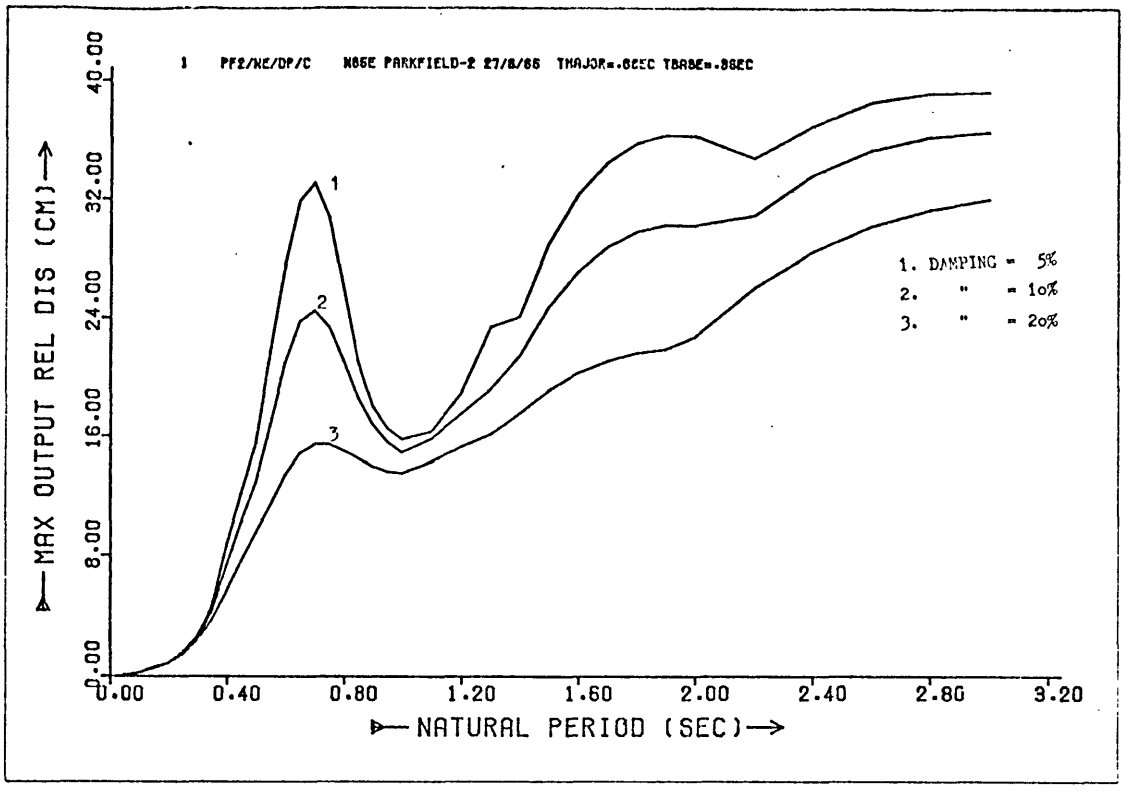


FIG. 6.8f COMPUTED GROUND SURFACE DISPLACEMENT RESPONSE SPECTRA AT SITE NO 6.8

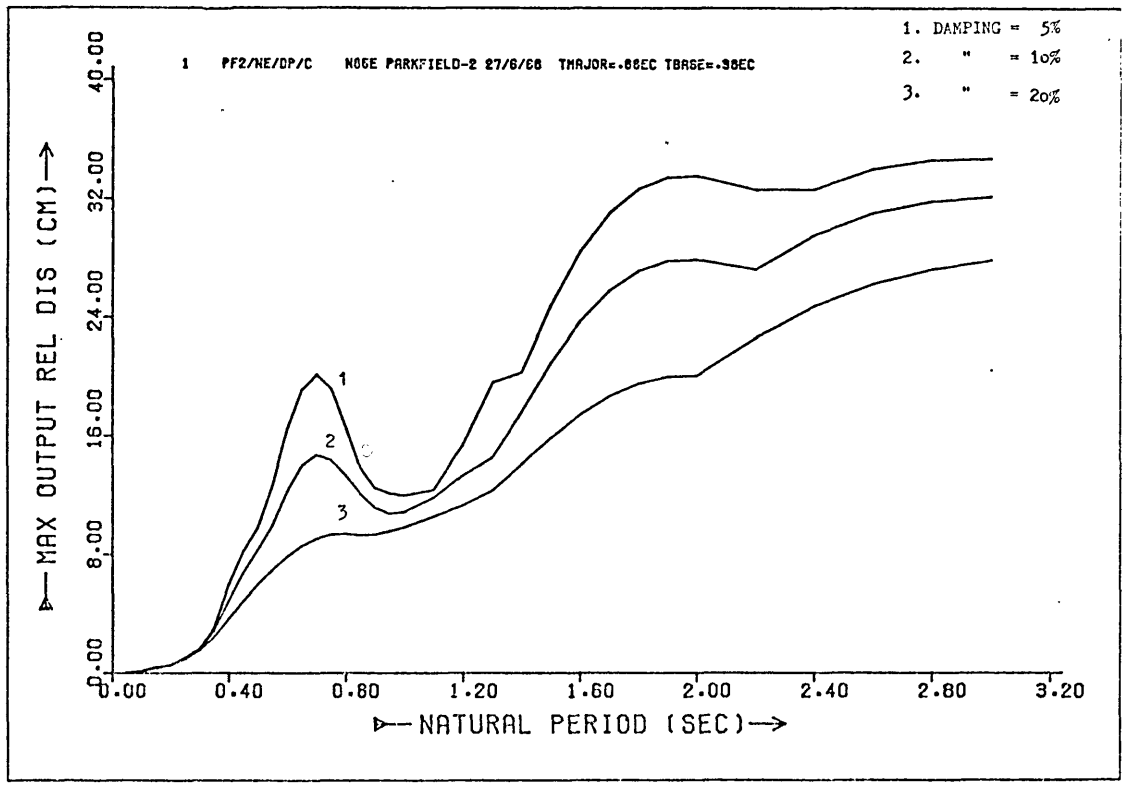


FIG. 6.9f COMPUTED GROUND SURFACE DISPLACEMENT RESPONSE SPECTRA AT SITE NO 6.9

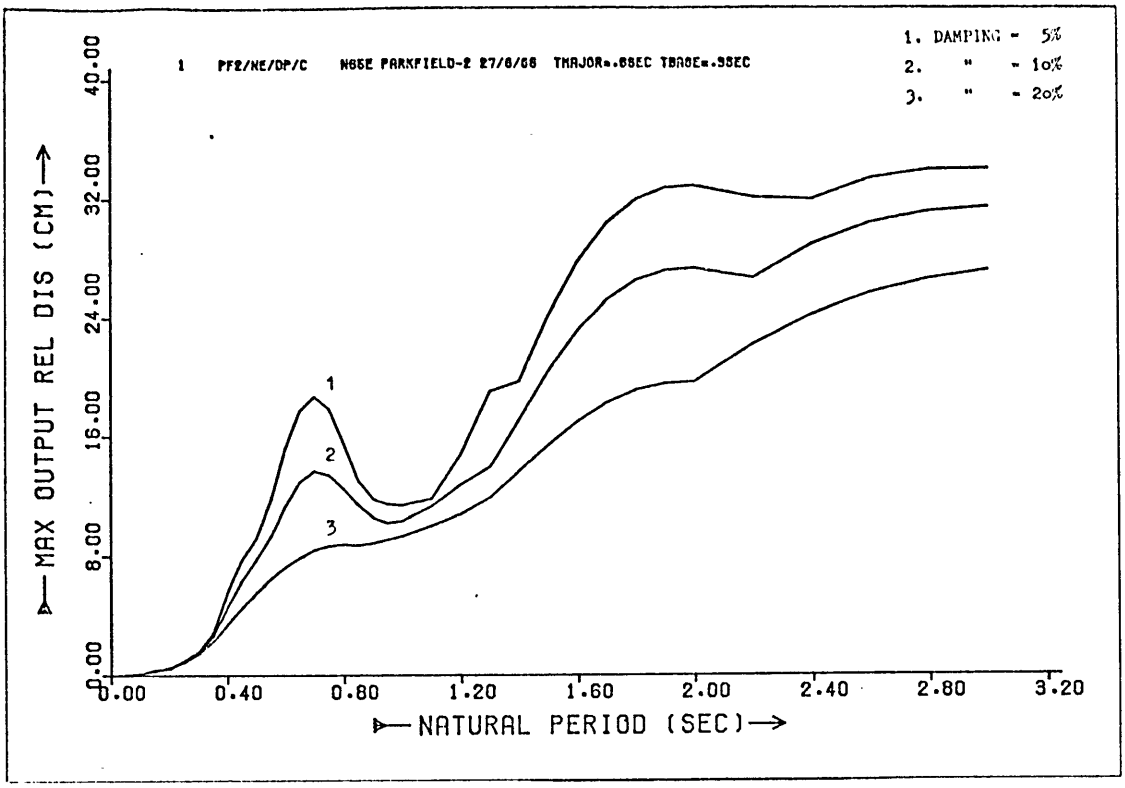


FIG. 6 .1of COMPUTED GROUND SURFACE DISPLACEMENT RESPONSE SPECTRA AT SITE NO 6.1o

behaved as single-degree of freedom systems, the shape of output spectrum would be very closely approximated by the bedrock spectrum; however, seismic response of a soil deposit is the combined action of many modes of vibration, therefore an exact agreement could never exist.

From figs. 6.2d to 6.10d, it is observed that the peak corresponding to the fundamental period of the deposit - 0.6 second is greatly excited, being equal to the predominant period of the bedrock motion - 0.6 second, simulating a condition of resonance. Radiation damping ratio has a pronounced effect on ground response at these resonance periods; this is expected from the transmitting boundary condition given by equation 4. 4 For further illustration of this point, acceleration and velocity amplification spectrum are calculated for eight different values of radiation damping ratios. The results of the analysis are shown in figs. 6.11 a and 6.11b.

Fig. 6.11 a clearly illustrates that radiation damping, as expected from the transmitting boundary condition, has considerable effect around the natural periods of the overburden, which govern the pattern of resonant peaks. The degree of suppression of these peaks depends on the value of radiation damping ratio and is not a linear function of this ratio. It is also observed that acceleration amplification spectra is highly dependent on radiation damping ratio throughout. The dependence at periods located between the two peaks and at longer periods is considerably less than that at resonance periods. Fig. 6.11 a also illustrates that frequency characteristics of output motion in this particular case (fundamental period of the overburden equal to the predominant period of bedrock motion) is not affected to an extent to be reflected on computed acceleration amplification spectra.

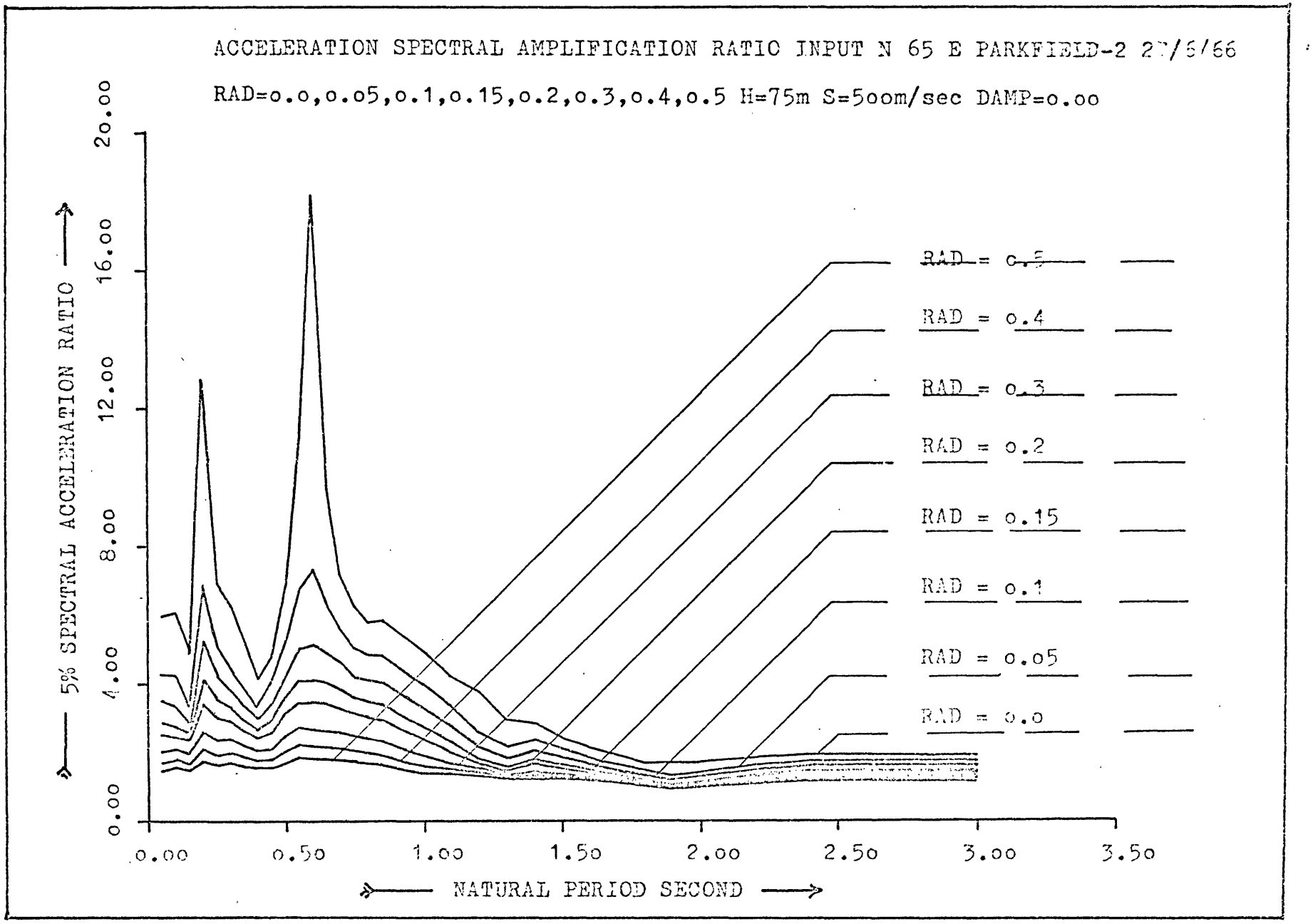

ACCELERATION SPECTRAL AMPLIFICATION RATIO INPUT N 65 E PARKFIELD-2 27/6/66
RAD=o.o,o.o5,o.1,o.15,o.2,o.3,o.4,o.5 H=75m S=5oom/sec DAMP=o.oo
5% SPECTRAL ACCELERATION RATIO
0.00
4.00
8.00
12.00
16.00
20.00
RAD = o.5
RAD = o.4
RAD = o.3
RAD = o.2
RAD = o.15
RAD = o.1
RAD = o.o5
RAD = o.o
0.00
0.5o
1.00
1.5o
2.00
2.5o
3.00
3.5o
NATURAL PERIOD SECOND

FIG. 6.11 a

Fig. 6.11b shows velocity amplification spectrum for eight different values of radiation damping, which illustrates a behaviour quite similar to that of acceleration amplification spectrum; which is just coincidence.

Case 3 (hysteretic damping ratio not zero and radiation damping ratio assigned to zero) demonstrates that the energy dissipation characteristics of the deposit are only of hysteresis. The responses of four 75m loose gravel materials for four different hysteretic damping ratios, subjected at their bedrock level to Parkfield-2, are shown in figs. 6.12a,b,c,d,e,f to 6.15a,b,c,d,e,f.

Figs. 7.12a,b,c,d,e,f through 7.15a,b,c,d,e,f show that the greater the hysteretic damping ratio the smaller are the calculated response values. From figs. 7.12d to 7.15d it is observed that a condition of resonance is simulated at period of 0.6 second, greatly exciting the particular peak. This point is clearly reflected in acceleration amplification spectrum for the four deposits shown in fig. 6.16. The peak at period of 0.6 second is followed by a second peak at 0.2 second, which corresponds to the periods at second modes of the deposits.

Comparison of computed surface acceleration, velocity and displacement response spectrum for site 6.5 (results of case 2) with that of site 6.13 (results of case 3) results give rise to the conclusion that,under certain condition ,i.e. the fundamental period of the overburden is equal to the predominant period of the bedrock motion, hysteretic and radiation damping ratios produce similar results. This observation gives rise to two very important conclusions:

a) Radiation damping ratio can be considered as a measure of energy lost into the bedrock formation, due to the deformability of the bedrock.

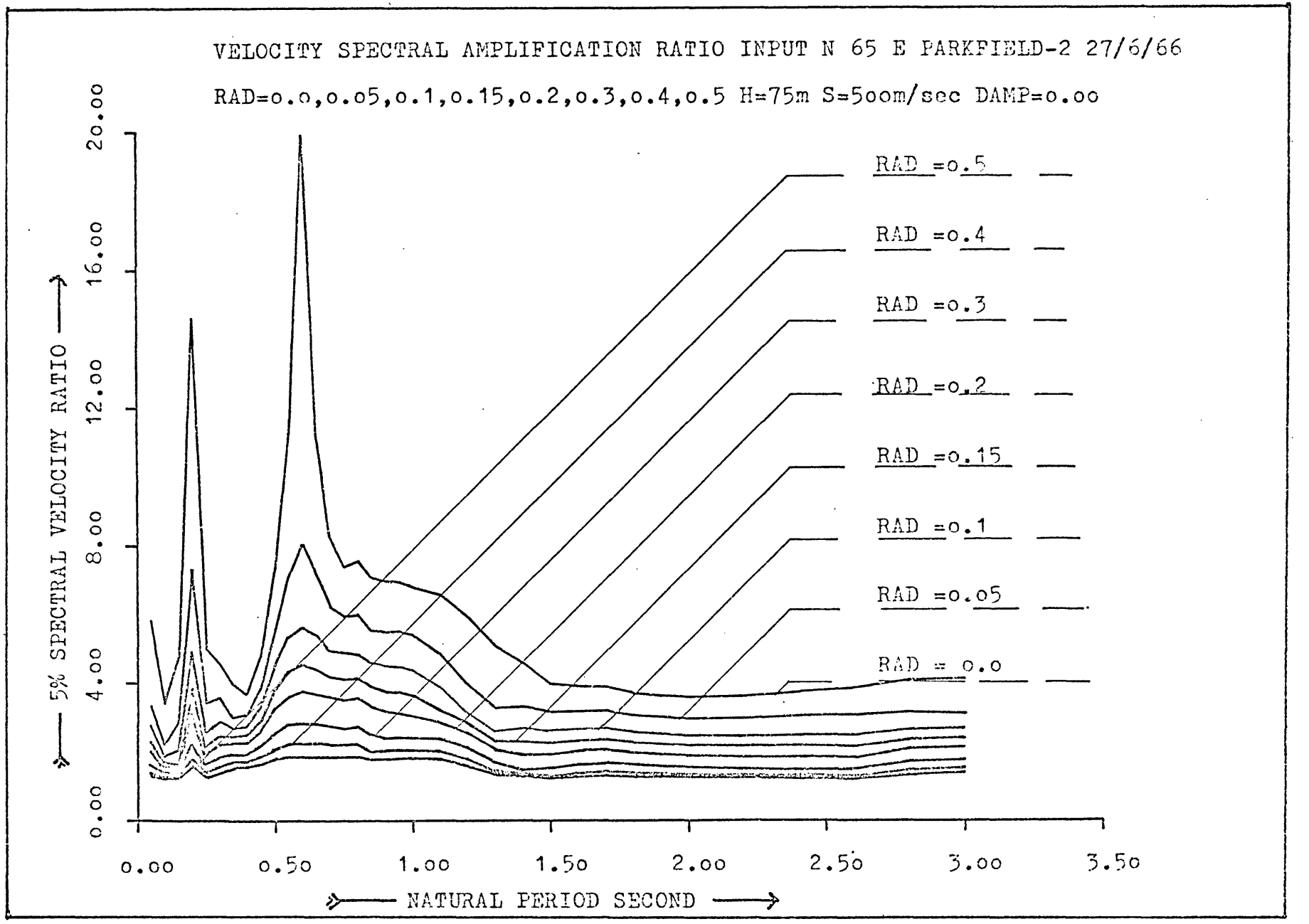
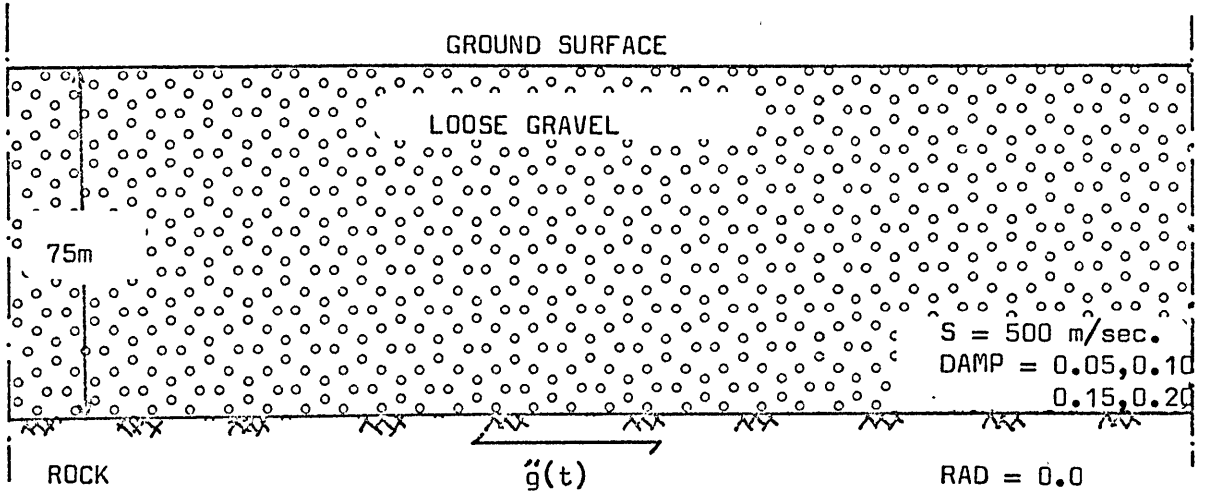

VELOCITY SPECTRAL AMPLIFICATION RATIO INPUT N 65 E PARKFIELD-2 27/6/66
RAD=o.o,o.o5,o.1,o.15,o.2,o.3,o.4,o.5 H=75m S=5oom/sec DAMP=o.oo
RAD =o.5
RAD =o.4
RAD =o.3
RAD =o.2
RAD =o.15
RAD =o.1
RAD =o.o5
RAD = o.o
5% SPECTRAL VELOCITY RATIO
0.00
4.00
8.00
12.00
16.00
20.00
0.00
0.5o
1.00
1.5o
2.00
2.5o
3.00
3.5o
NATURAL PERIOD SECOND

FIG. 7.11b



RESPONSE OF HYSTERETIC DEPOSIT UNDERLAIN BY DEFORMABLE BEDROCK

SCHEMATIC SOIL PROFILE FOR SITE NO. 6.11,

6.12, 6.13, and 6.14

FIG. 6.12

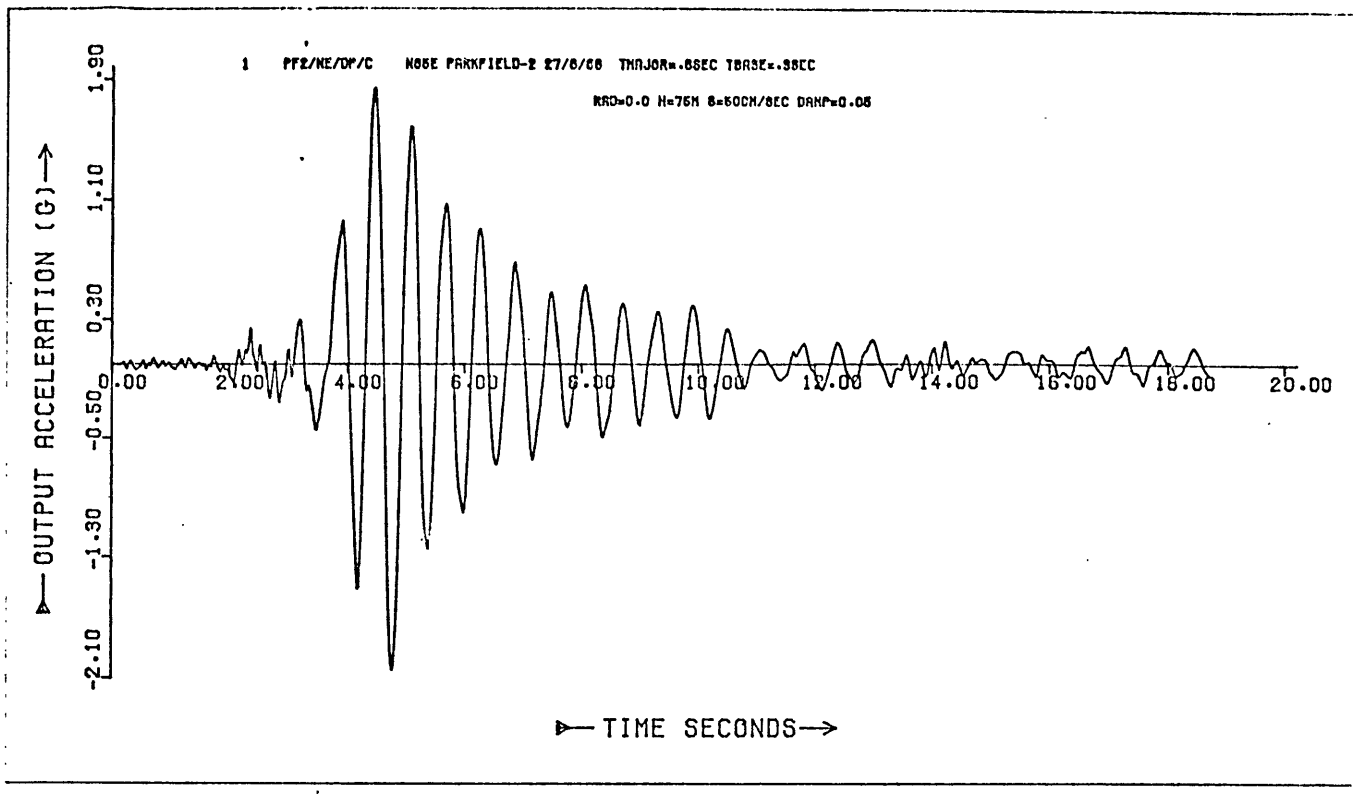


FIG.6.12a COMPUTED GROUND SURFACE ACCELERATION TIME HISTORY AT SITE NO 6.11

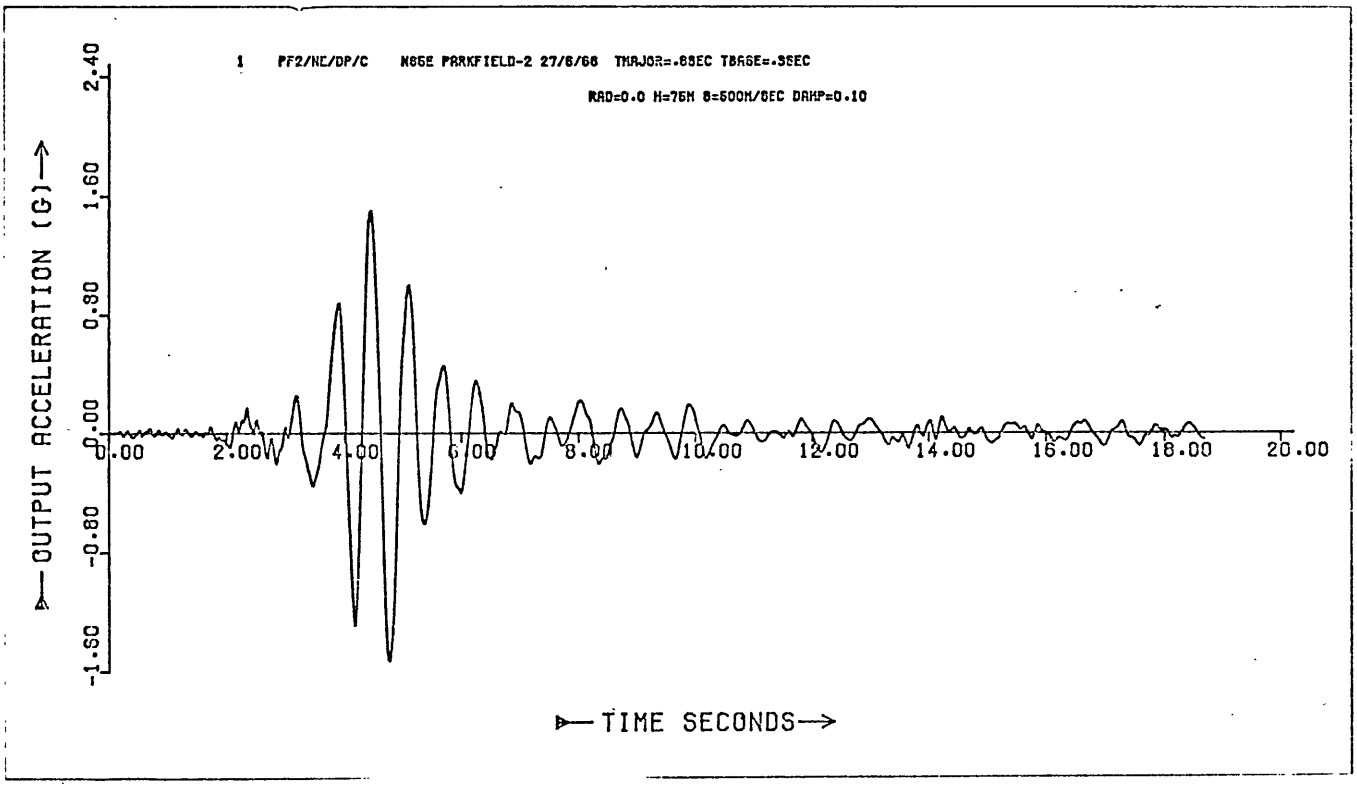


FIG.6.13a COMPUTED GROUND SURFACE ACCELERATION TIME HISTORY AT SITE NO 6.12

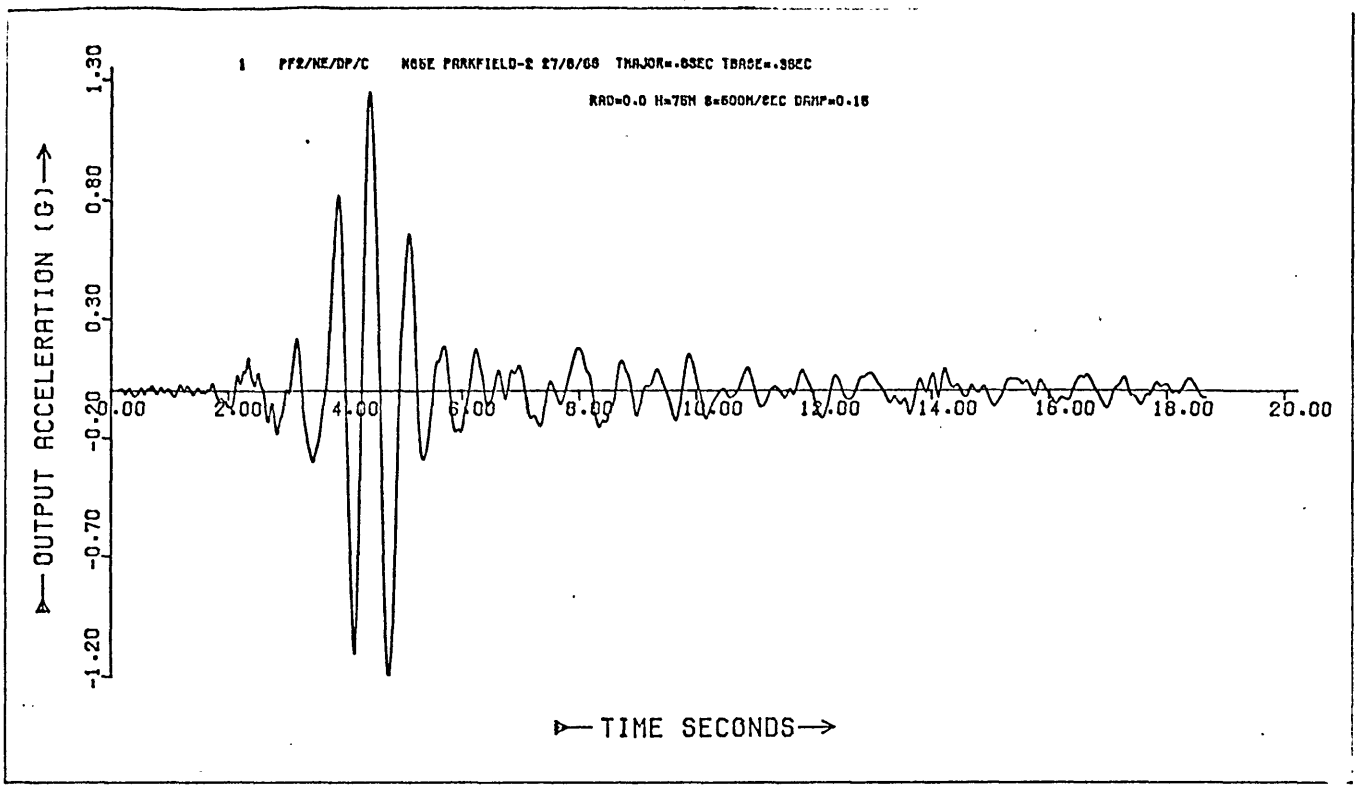


FIG. 6.14a COMPUTED GROUND SURFACE ACCELERATION TIME HISTORY AT SITE NO 6.13

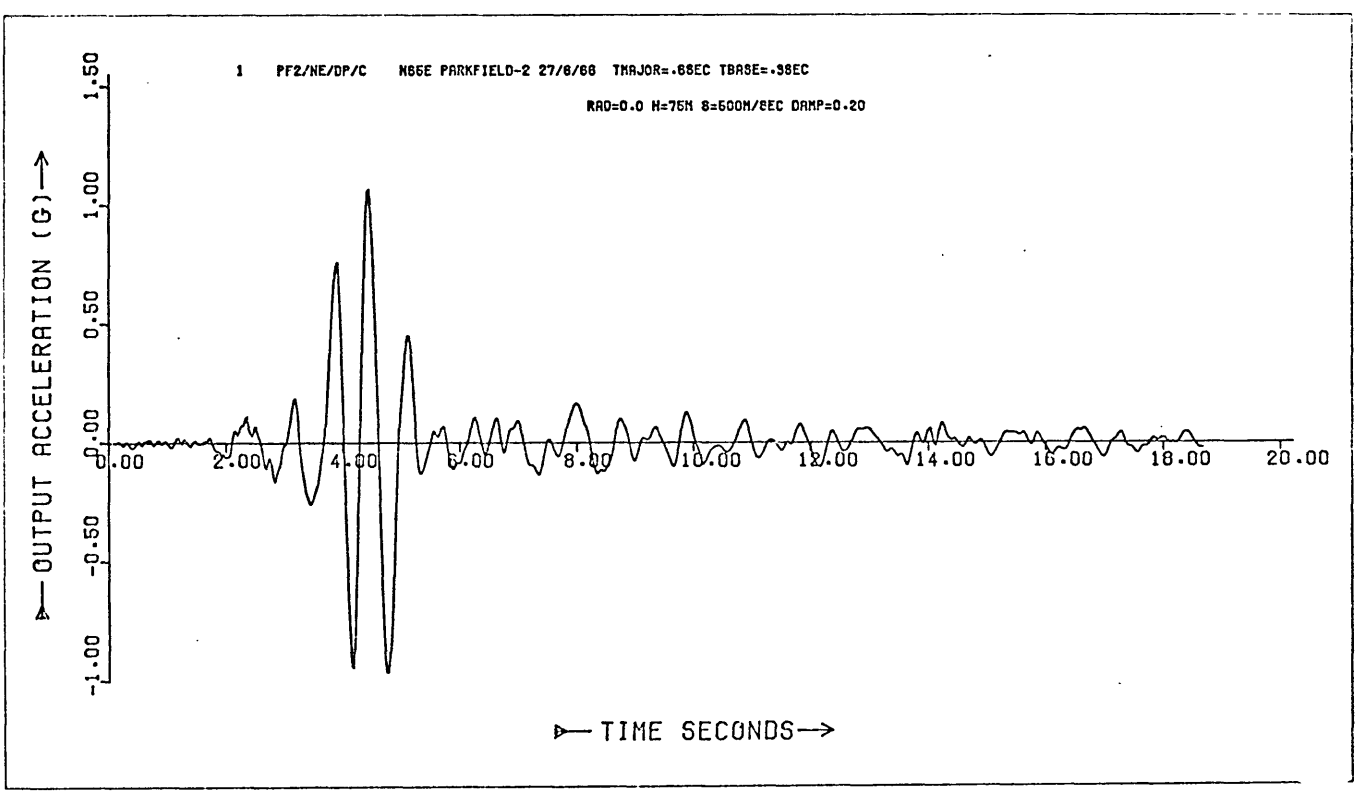


FIG. 6.15a COMPUTED GROUND SURFACE ACCELERATION TIME HISTORY AT SITE NO 6.14

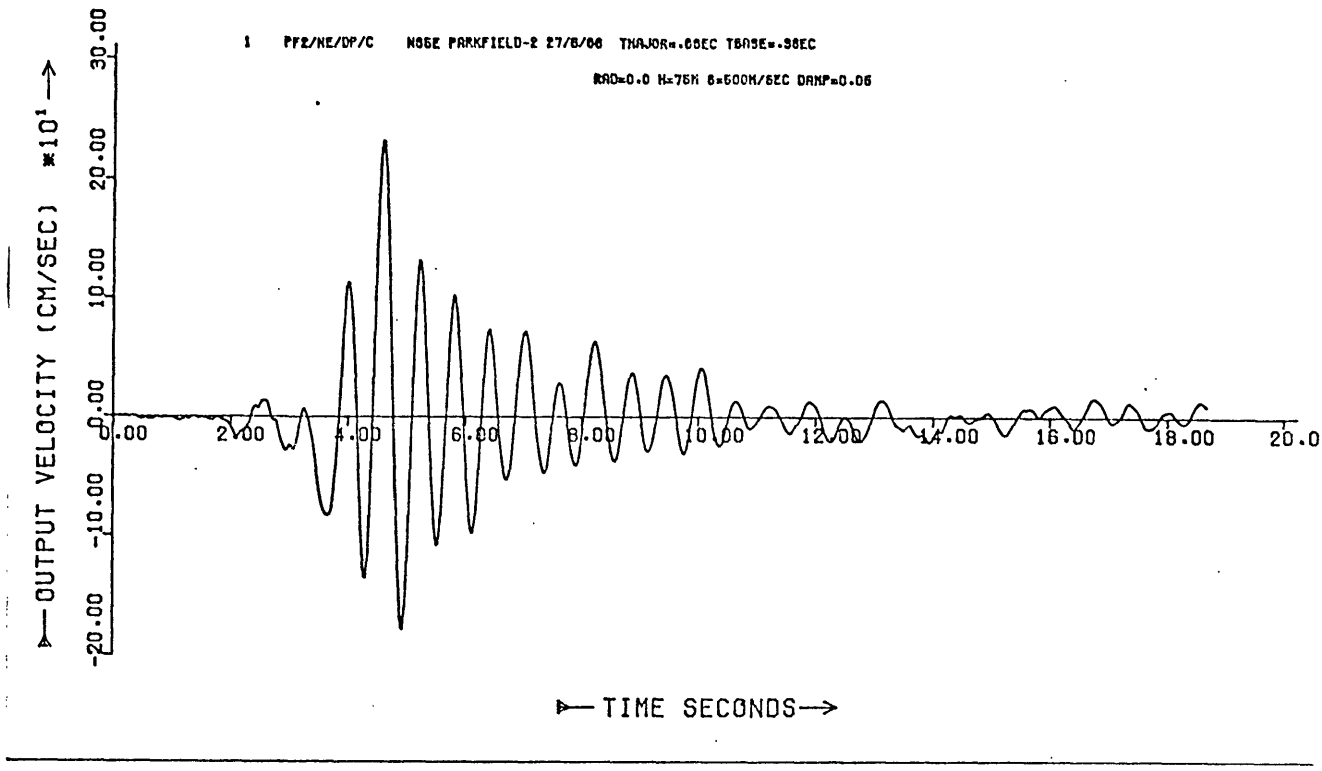


FIG. 6.12b COMPUTED GROUND SURFACE VELOCITY TIME HISTORY AT SITE NO 6.11

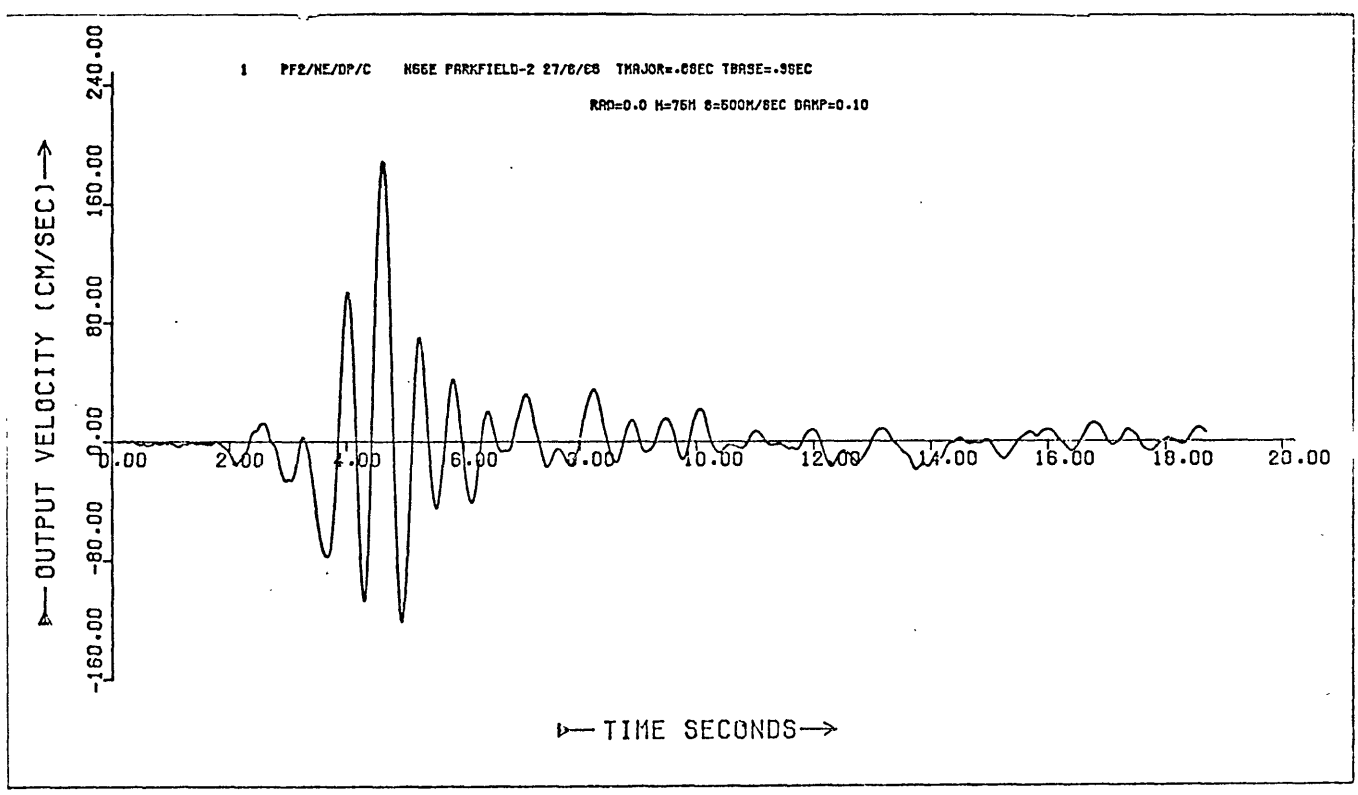


FIG. 6.13b COMPUTED GROUND SURFACE VELOCITY TIME HISTORY AT SITE NO 6.12

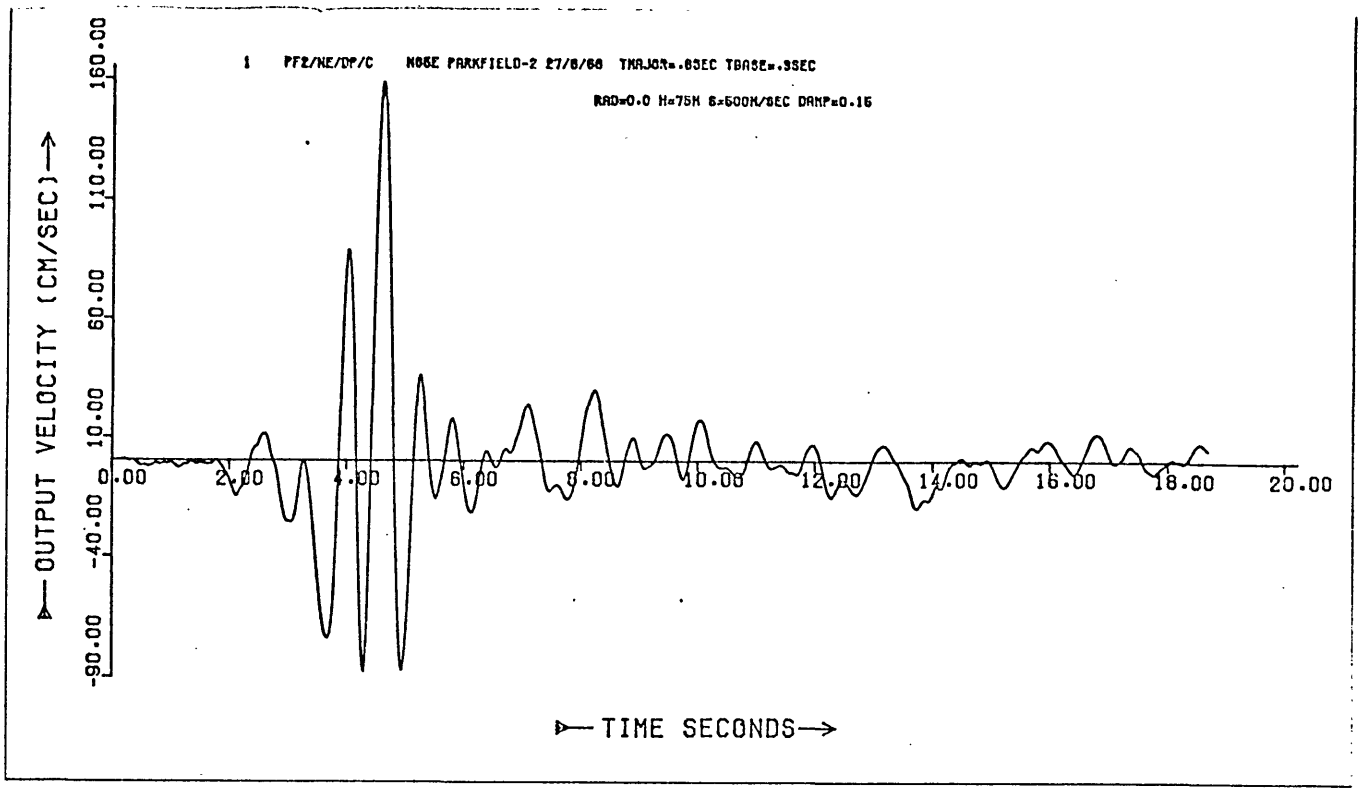


FIG. 6.14b COMPUTED GROUND SURFACE VELOCITY TIME HISTORY AT SITE NO 6.13

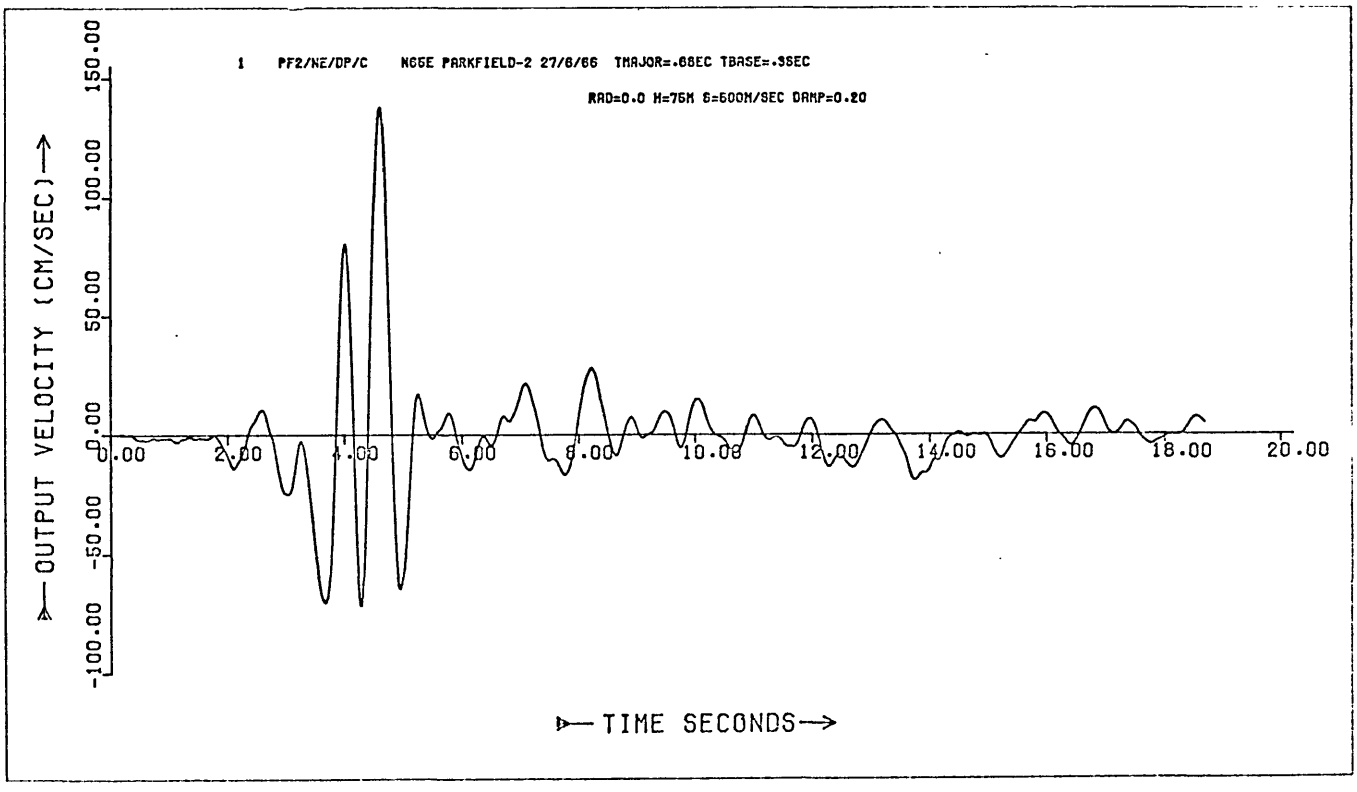


FIG.6.15b COMPUTED GROUND SURFACE VELOCITY TIME HISTORY AT SITE NO 6.14

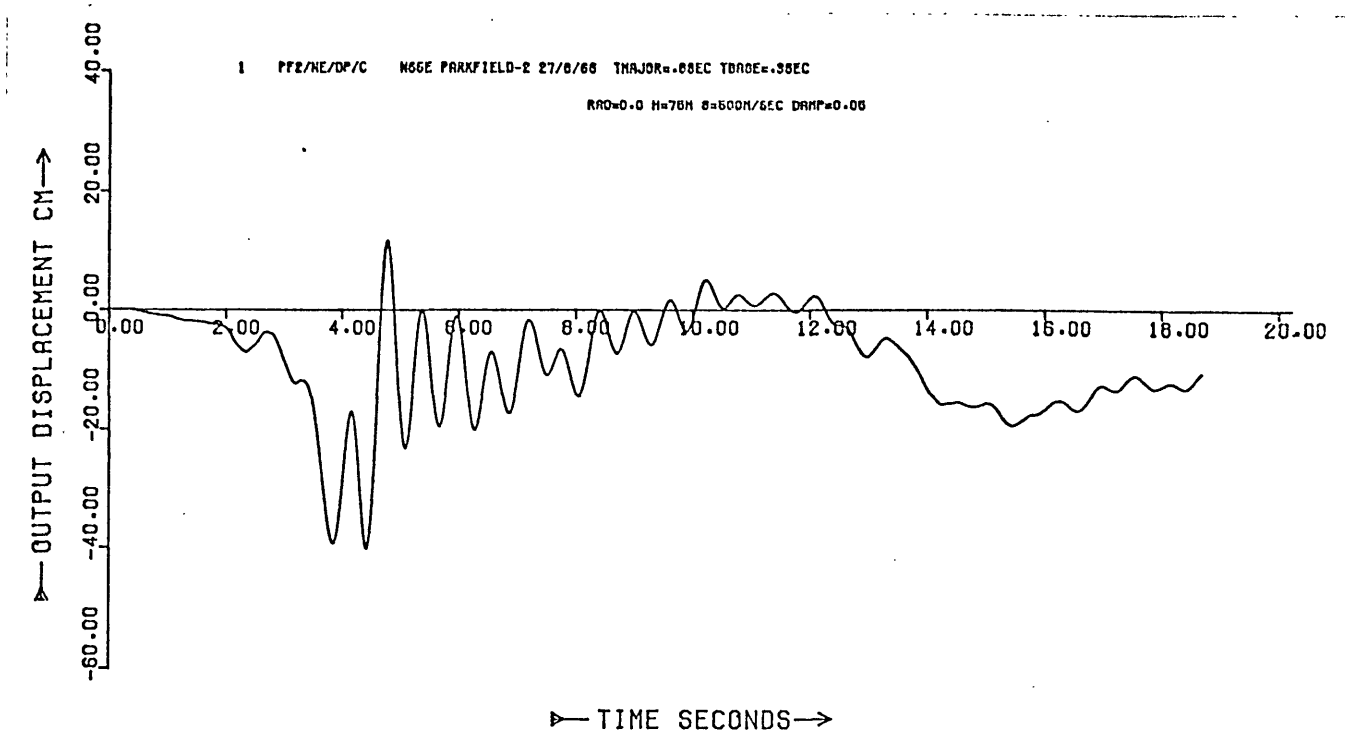


FIG. 6.12c COMPUTED GROUND SURFACE DISPLACEMENT TIME HISTORY AT SITE NO 6.11

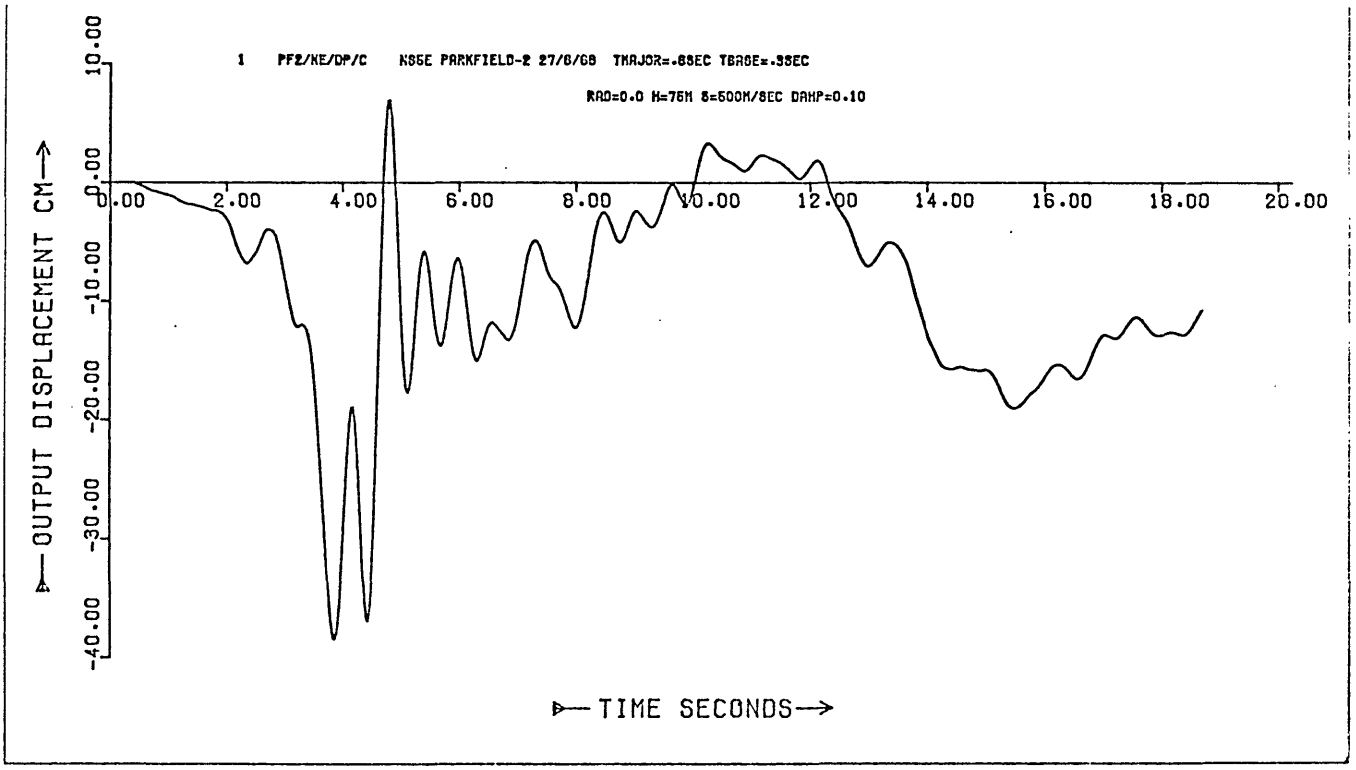


FIG. 6.13c COMPUTED GROUND SURFACE DISPLACEMENT TIME HISTORY AT SITE NO 6.12

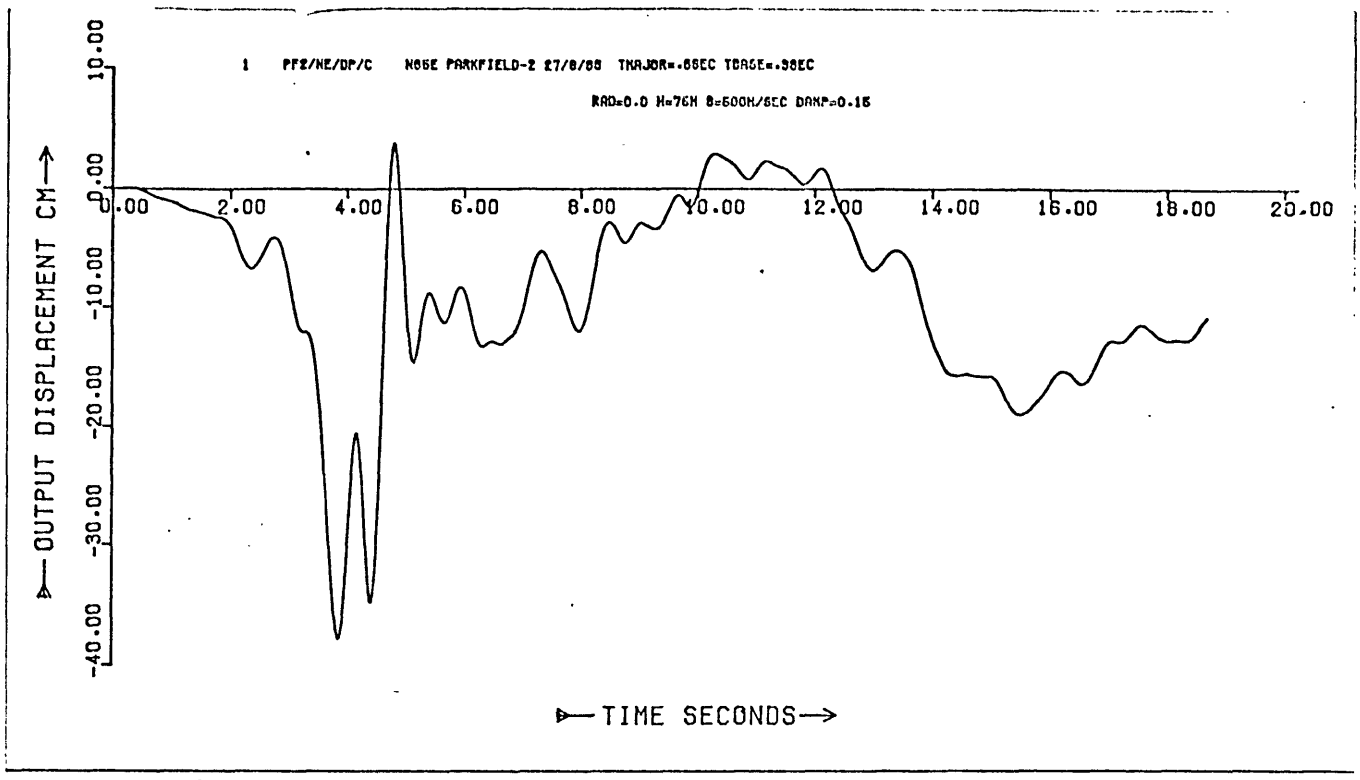


FIG.6.14c COMPUTED GROUND SURFACE DISPLACEMENT TIME HISTORY AT SITE NO 6.13

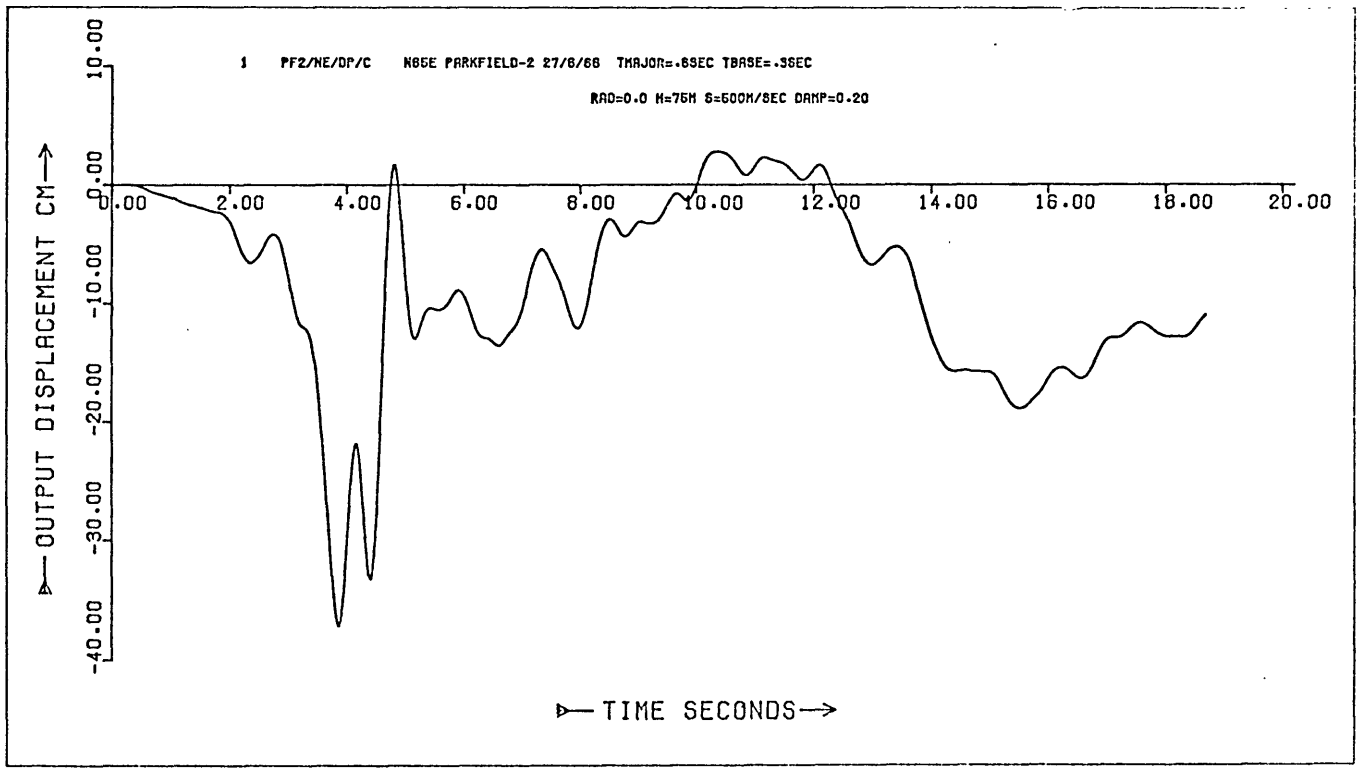


FIG. 6.15c COMPUTED GROUND SURFACE DISPLACEMENT TIME HISTORY AT SITE NO 6.14

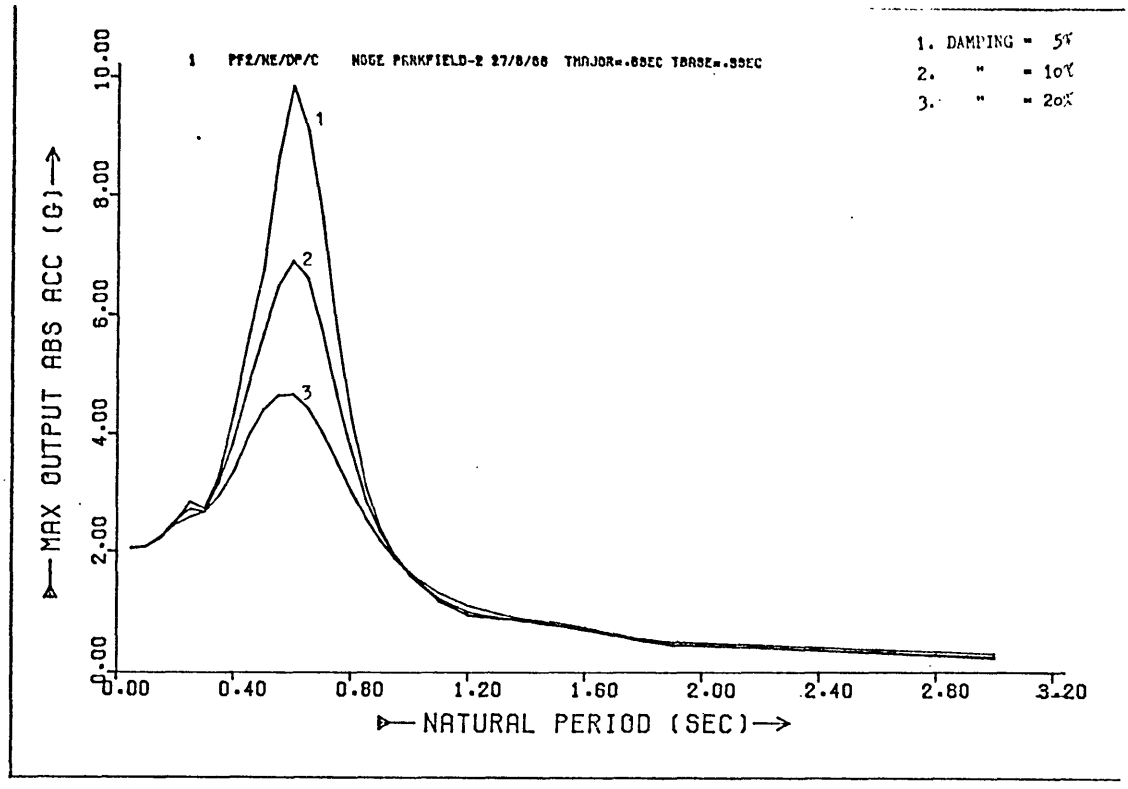


FIG. 6.12d COMPUTED GROUND SURFACE ACCELERATION RESPONSE SPECTRA AT SITE NO 6.11

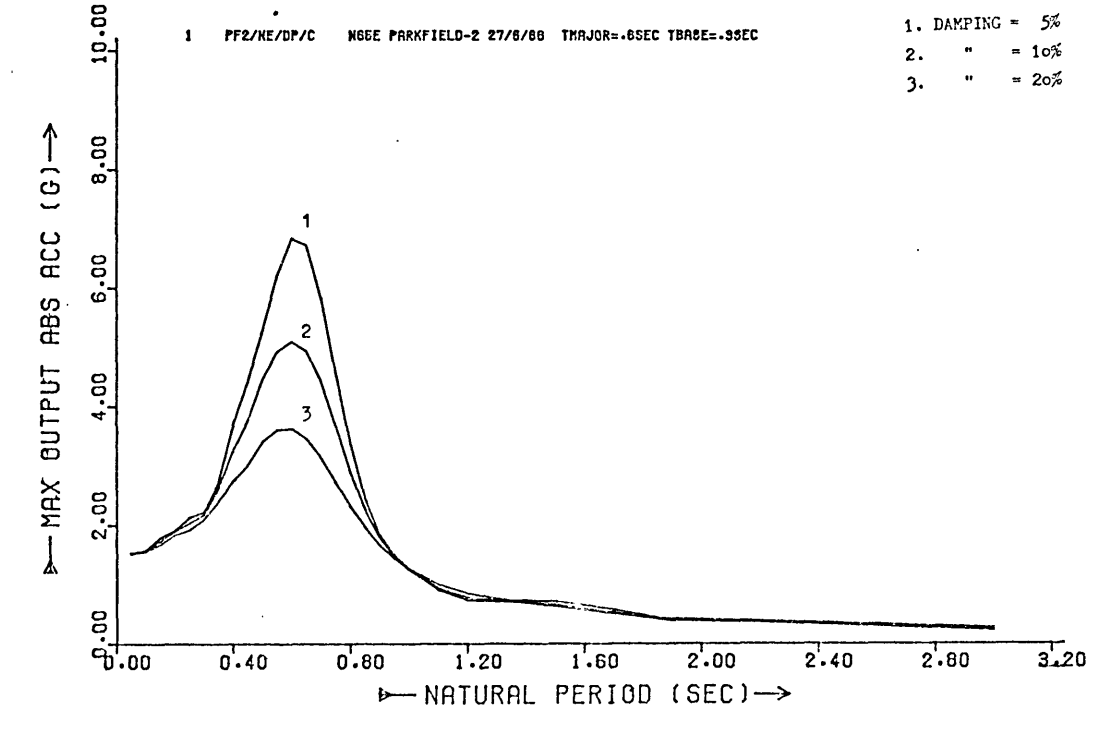


FIG.6.13d COMPUTED GROUND SURFACE ACCELERATION RESPONSE SPECTRA AT SITE NO6.12

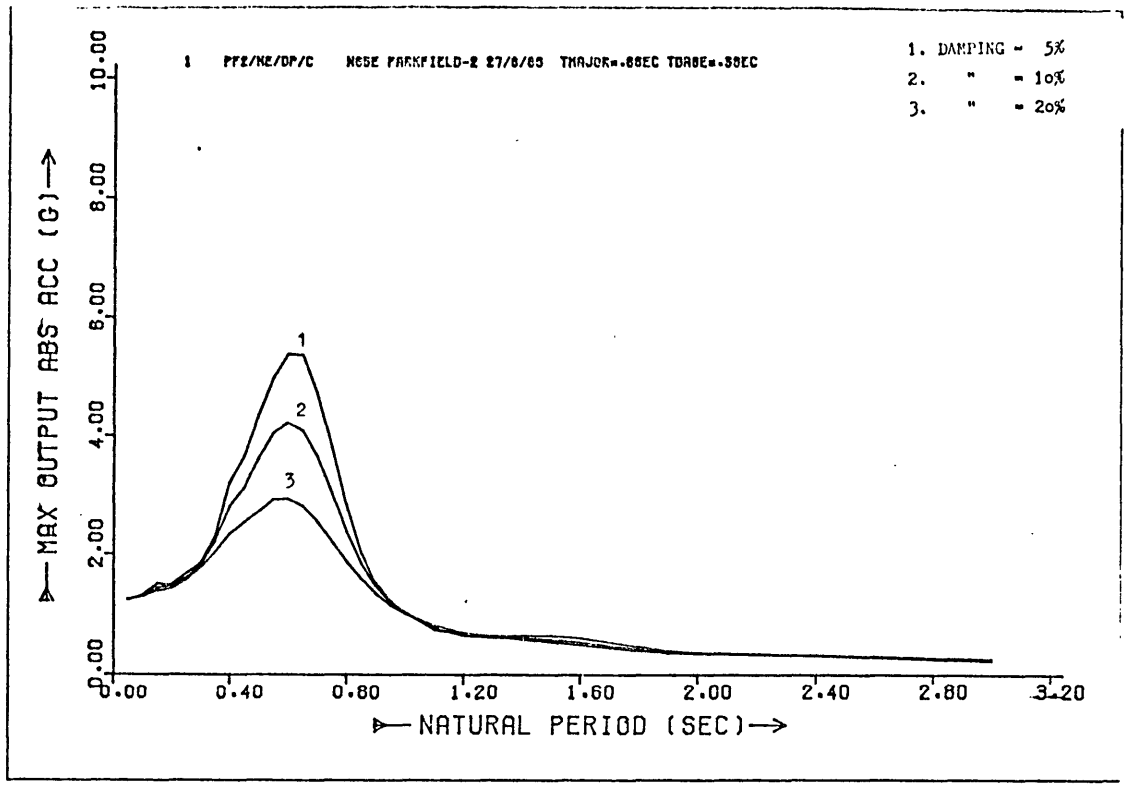


FIG.6.14d COMPUTED GROUND SURFACE ACCELERATION RESPONSE SPECTRA AT SITE NO 6.13

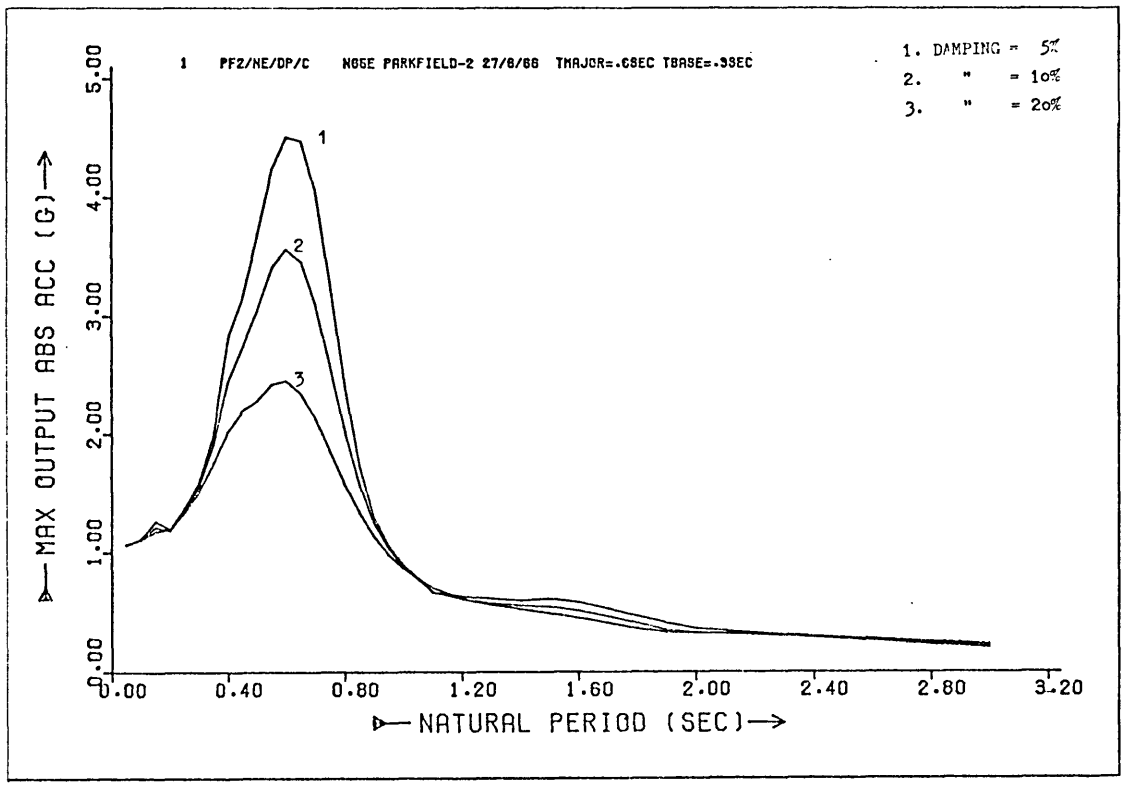


FIG.6.15d COMPUTED GROUND SURFACE ACCELERATION RESPONSE SPECTRA AT SITE NO 6.14

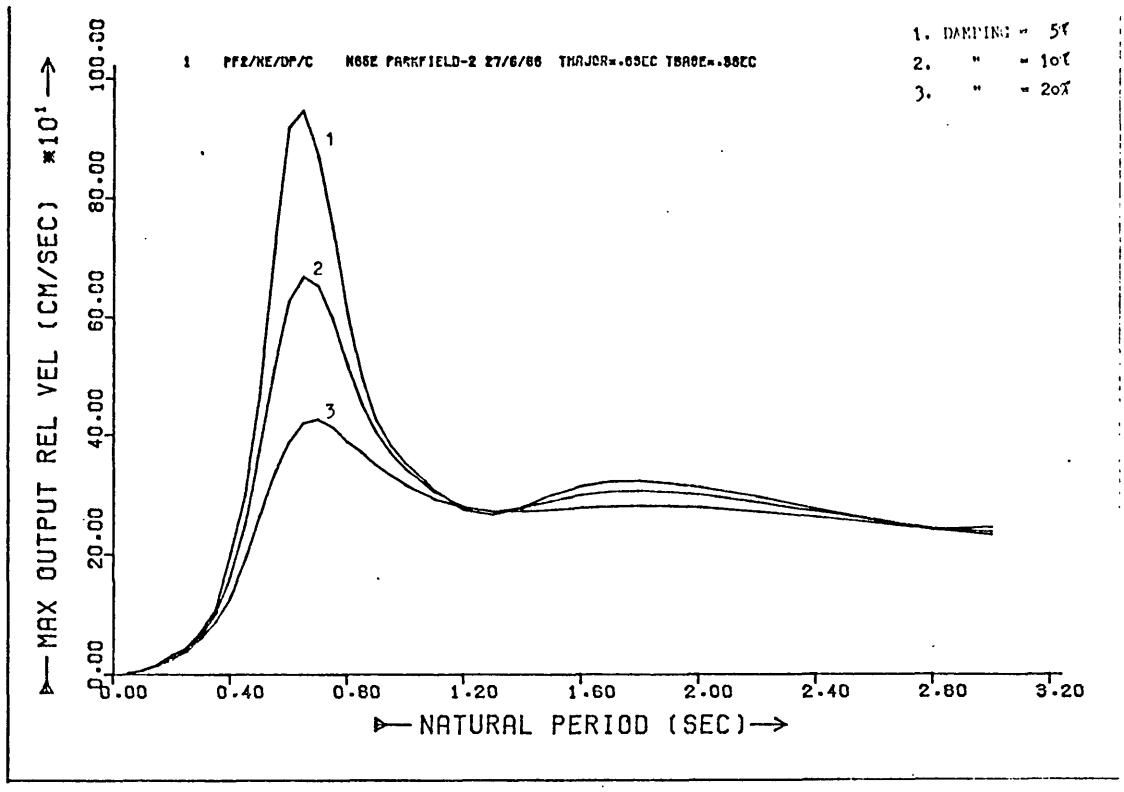


FIG.6.12e COMPUTED GROUND SURFACE VELOCITY RESPONSE SPECTRA AT SITE NO 6.11

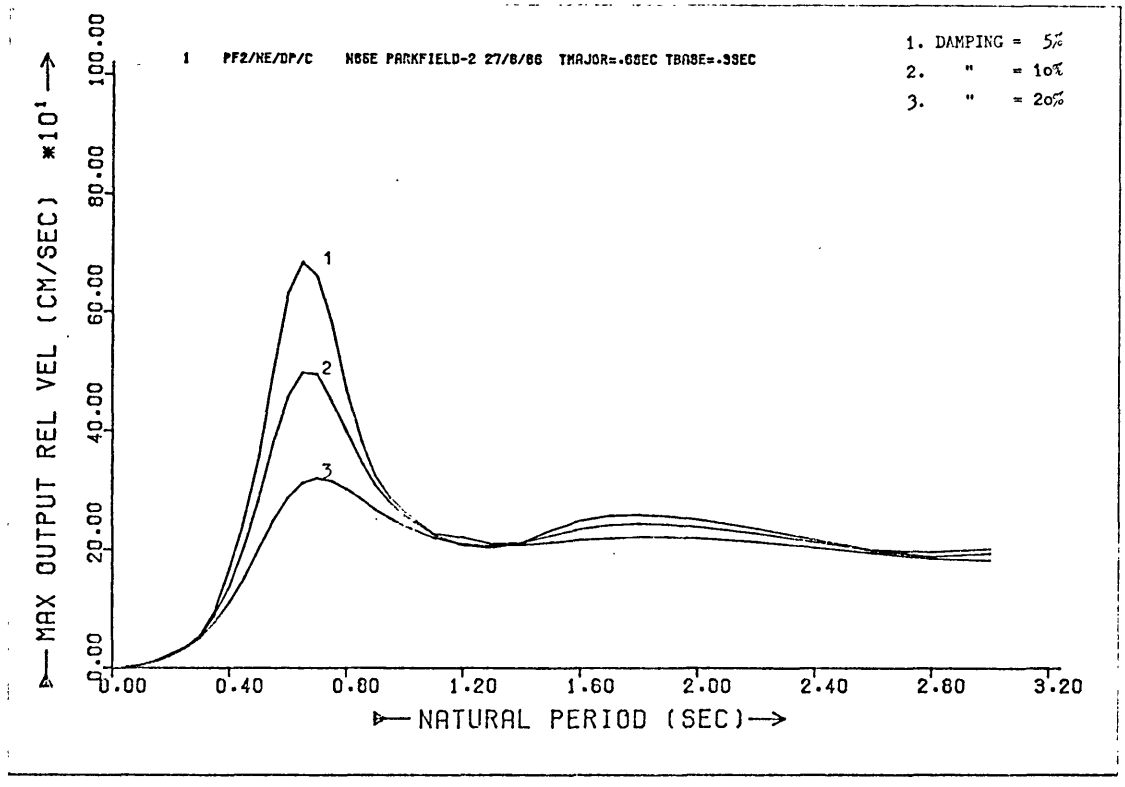


FIG. 6.13e COMPUTED GROUND SURFACE VELOCITY RESPONSE SPECTRA AT SITE NO 6.12

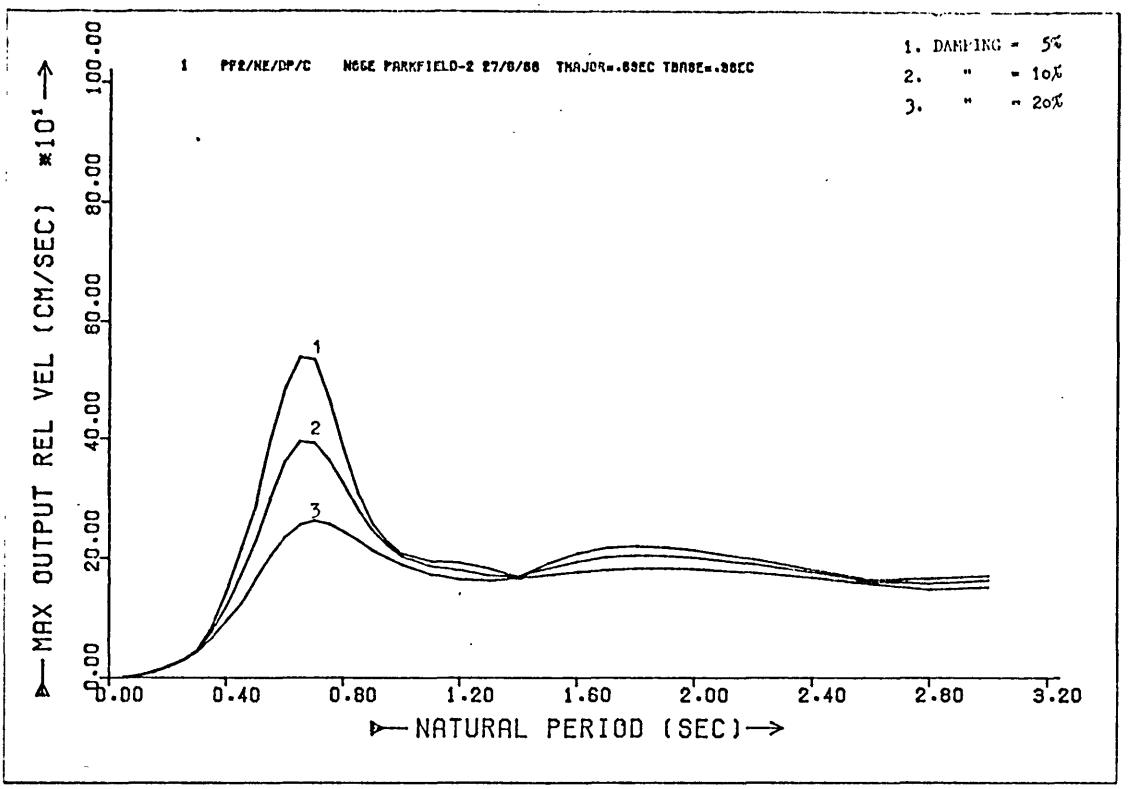


FIG. 6.14e COMPUTED GROUND SURFACE VELOCITY RESPONSE SPECTRA AT SITE NO6.13

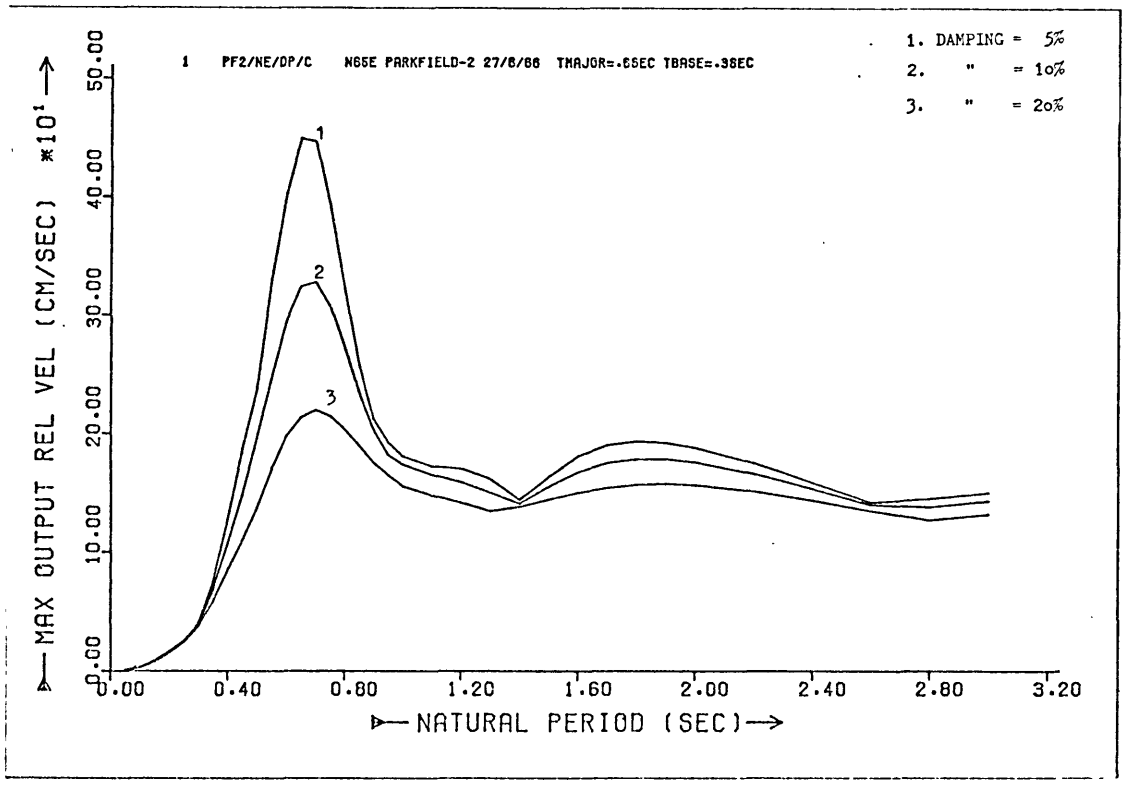


FIG.6.15e COMPUTED GROUND SURFACE VELOCITY RESPONSE SPECTRA AT SITE NO 6.14

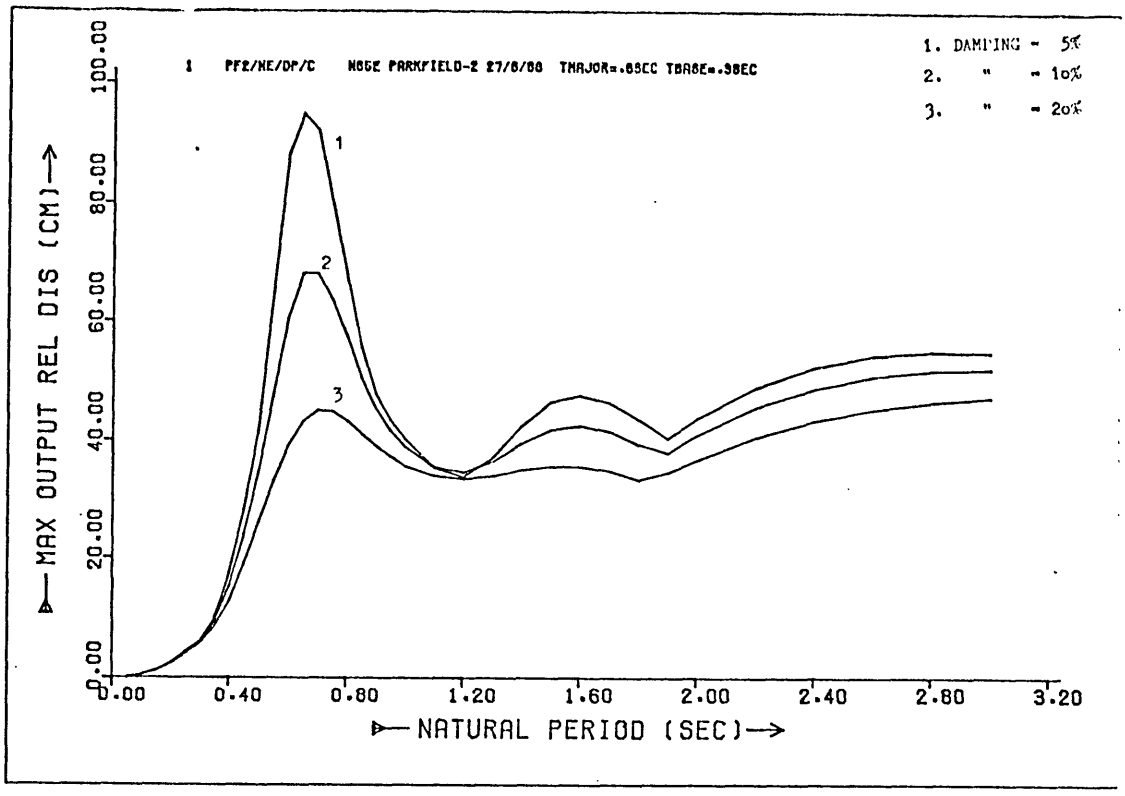


FIG.6.12f COMPUTED GROUND SURFACE DISPLACEMENT RESPONSE SPECTRA AT SITE NO 6.11

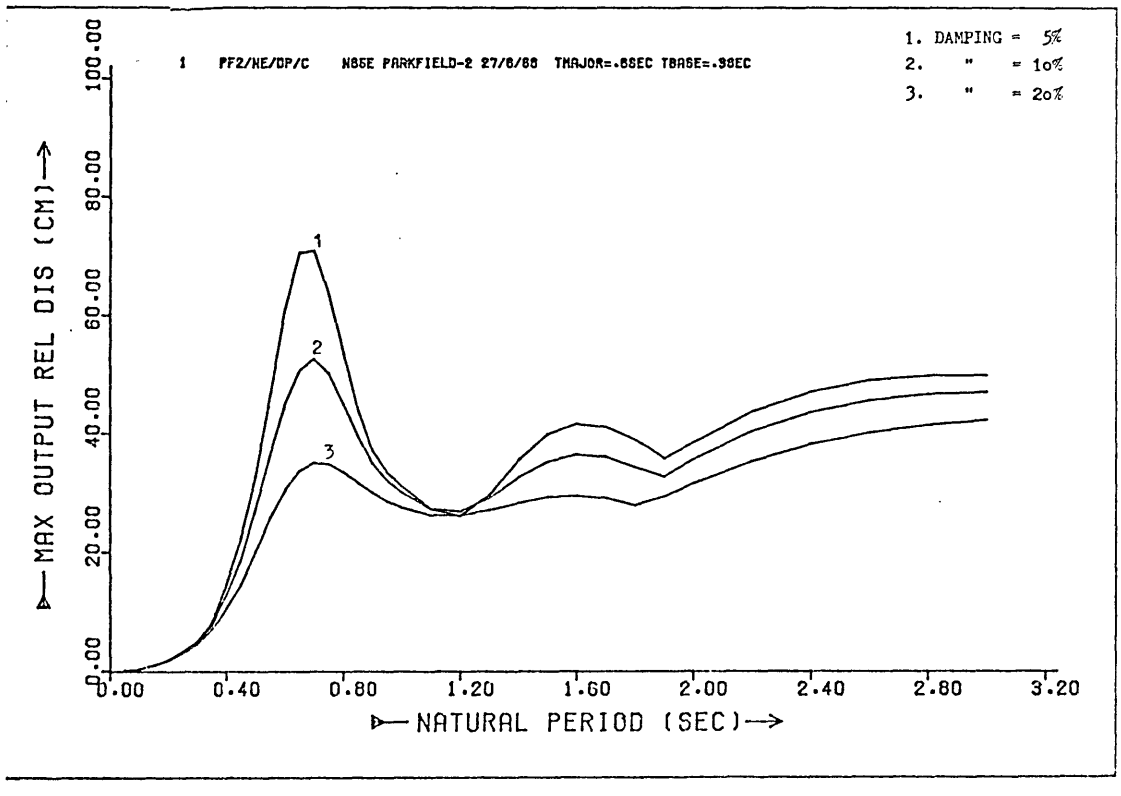


FIG. 6.13f COMPUTED GROUND SURFACE DISPLACEMENT RESPONSE SPECTRA AT SITE NO 6.12

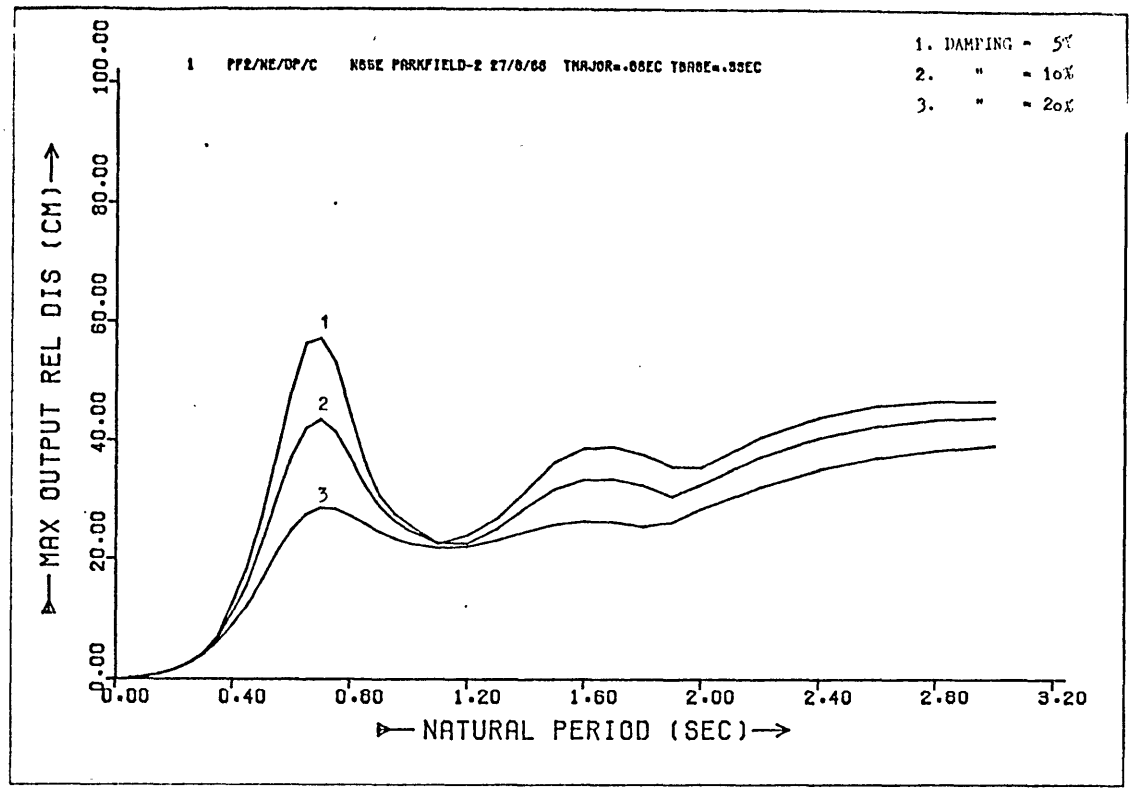


FIG. 6.14f COMPUTED GROUND SURFACE DISPLACEMENT RESPONSE SPECTRA AT SITE NO 6.13

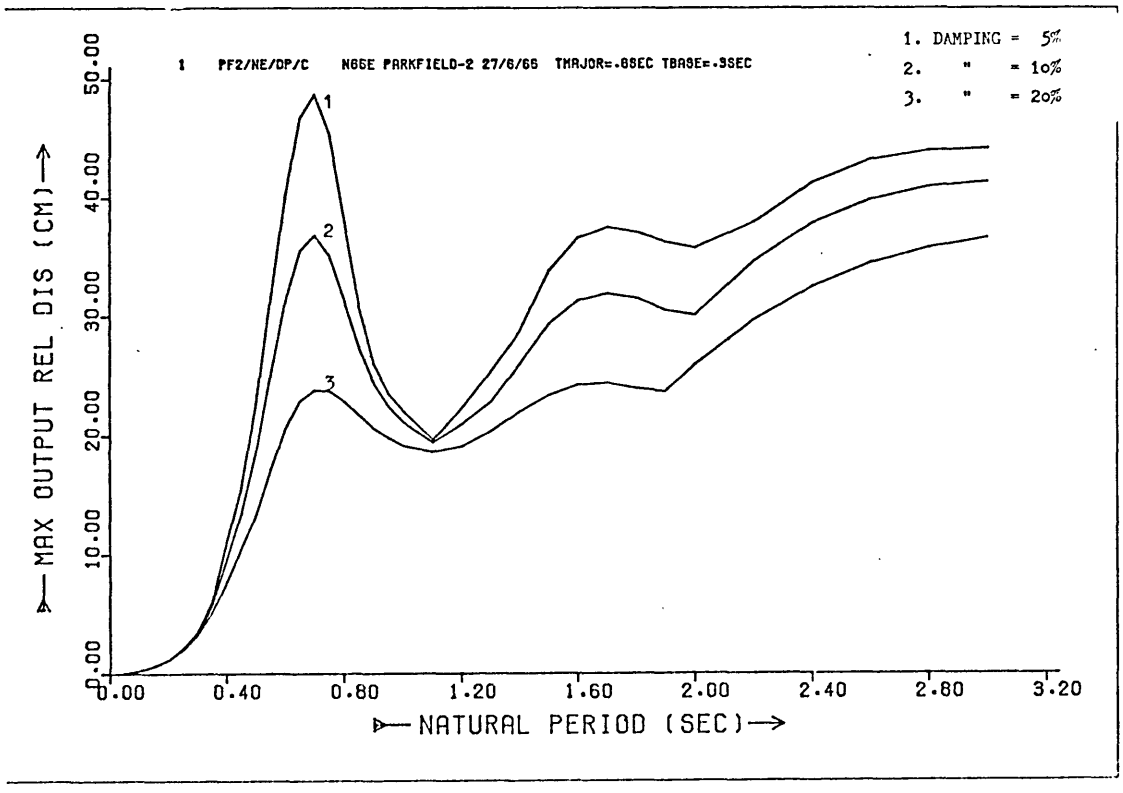


FIG. 6.15f COMPUTED GROUND SURFACE DISPLACEMENT RESPONSE SPECTRA AT SITE NO 6.14

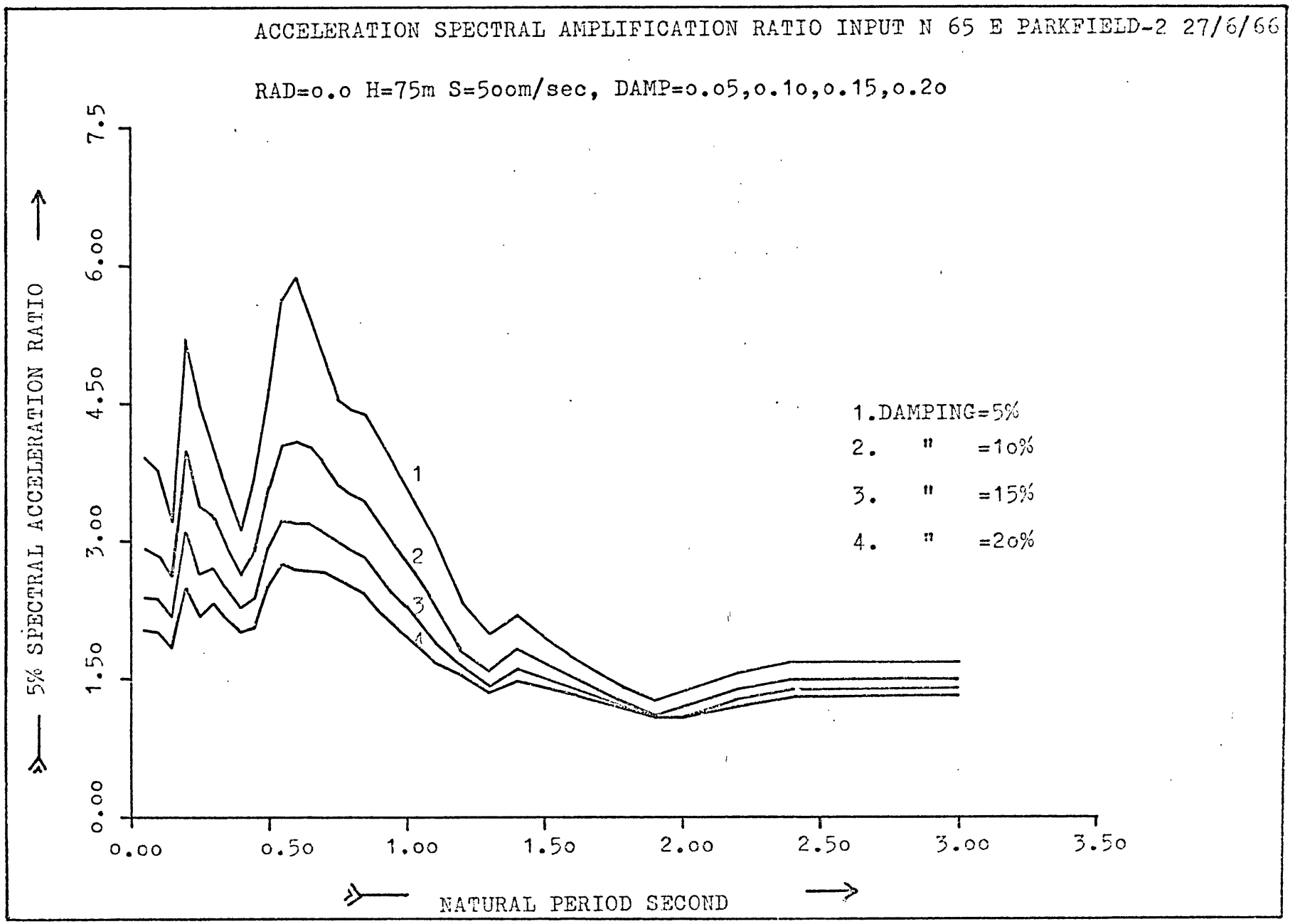
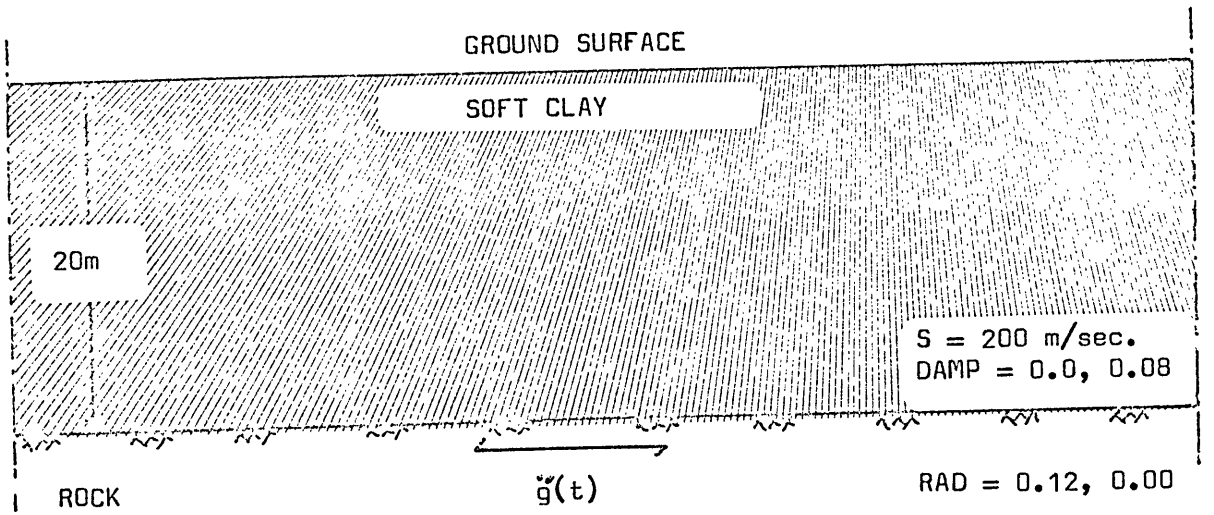

ACCELERATION SPECTRAL AMPLIFICATION RATIO INPUT N 65 E PARKFIELD-2 27/6/66
RAD=o.o H=75m S=5oom/sec, DAMP=o.o5,o.1o,o.15,o.2o
5% SPECTRAL ACCELERATION RATIO
0.00
1.5o
3.00
4.5o
6.00
7.5
0.00
0.5o
1.00
1.5o
2.00
2.5o
3.00
3.5o
NATURAL PERIOD SECOND
1.DAMPING=5%
2. " =1o%
3. " =15%
4. " =2o%
1
2
3
4

FIG. 6.16

b) Influence of radiation damping ratio in the fundamental mode of vibration which dominates in this case; its period, being equal to the predominant period of the bedrock motion, is the same as the hysteretic damping ratio. Under this condition, higher modes do not contribute to the response to an extent to influence the results.

To show that point (b) is a general rule, figs. 6.17a,b,c,d,e to 6.22a,b,c,d,e have been included, which show response of 20m and 22m deposits of soft clay and medium clay; the former subjected to San Fernando S16E & S74W, with predominant periods of 0.4 second, and the latter subjected to Temblar S25W, with a predominant period of 0.35 second, for two values of radiation and hysteretic damping ratios: RAD = 0.12, DAMP=0.0 and RAD = 0.0, DAMP = 0.08. All the three motions used are typical rock motions. The use of San Fernando S16E instead of El Centro 1940 N-S, which is widely used in earthquake engineering, is preferred because the former is a typical rock motion and possesses only one peak less than the latter in its acceleration response spectra.

The behaviour of the deposits under consideration could be best described by computed surface acceleration, velocity and displacement time histories shown in figs. 6.17a,b,c through 6.22a,b,c. Comparison of each pair of calculations illustrates that these time histories are similar in shape except that they differ in the amplitude of pulses; this is expected because the values of RAD =0.12 and DAMP = 0.08 were chosen based on engineering judgement from the results of sites 6.12 and 6.5; however, slight variations in either of these values or both would produce almost identical time histories.



RESPONSE OF HYSTERETIC DEPOSIT UNDERLAIN BY DEFORMABLE BEDROCK

SCHEMATIC SOIL PROFILE FOR SITE NO. 6.15 and 6.16

FIG. 6.17

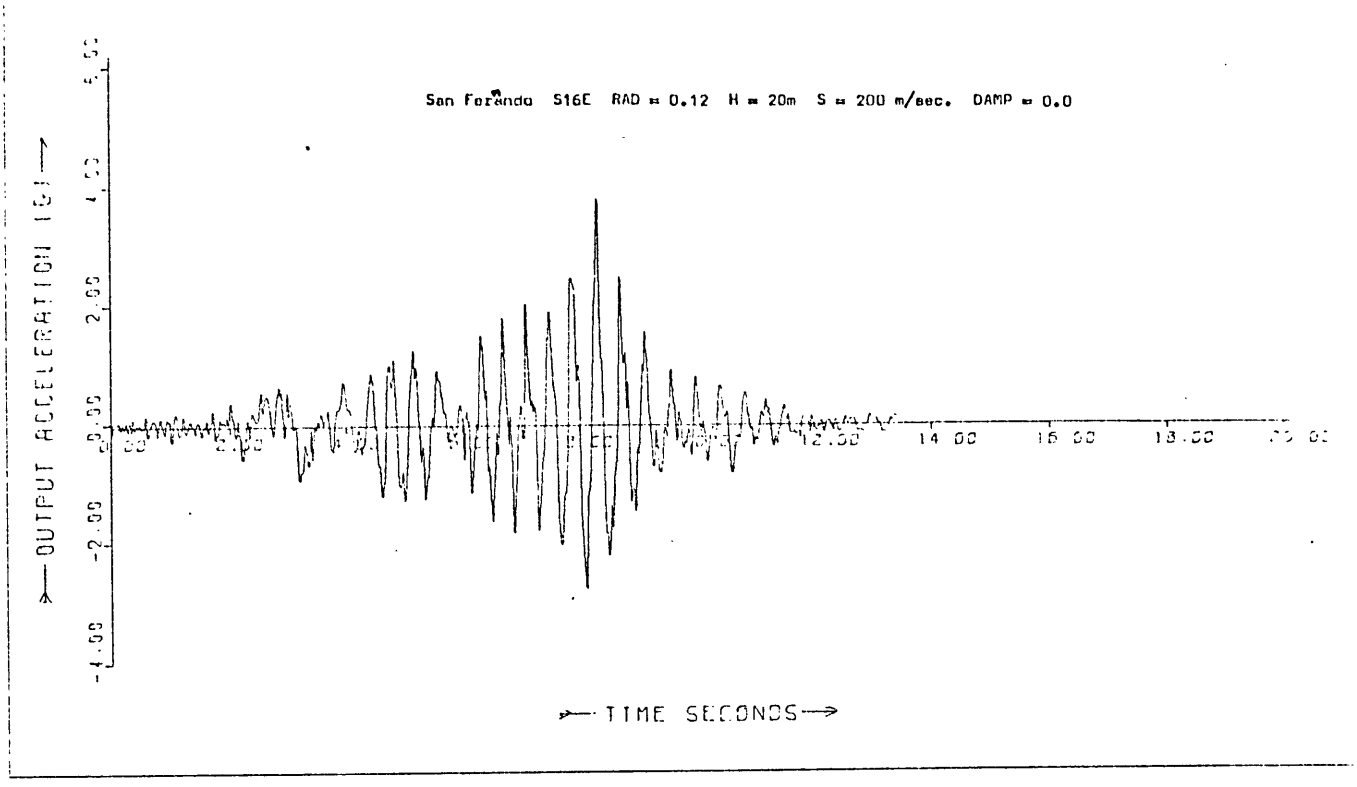


FIG 6.17a COMPUTED GROUND SURFACE ACCELERATION TIME HISTORY AT SITE NO. 6.15

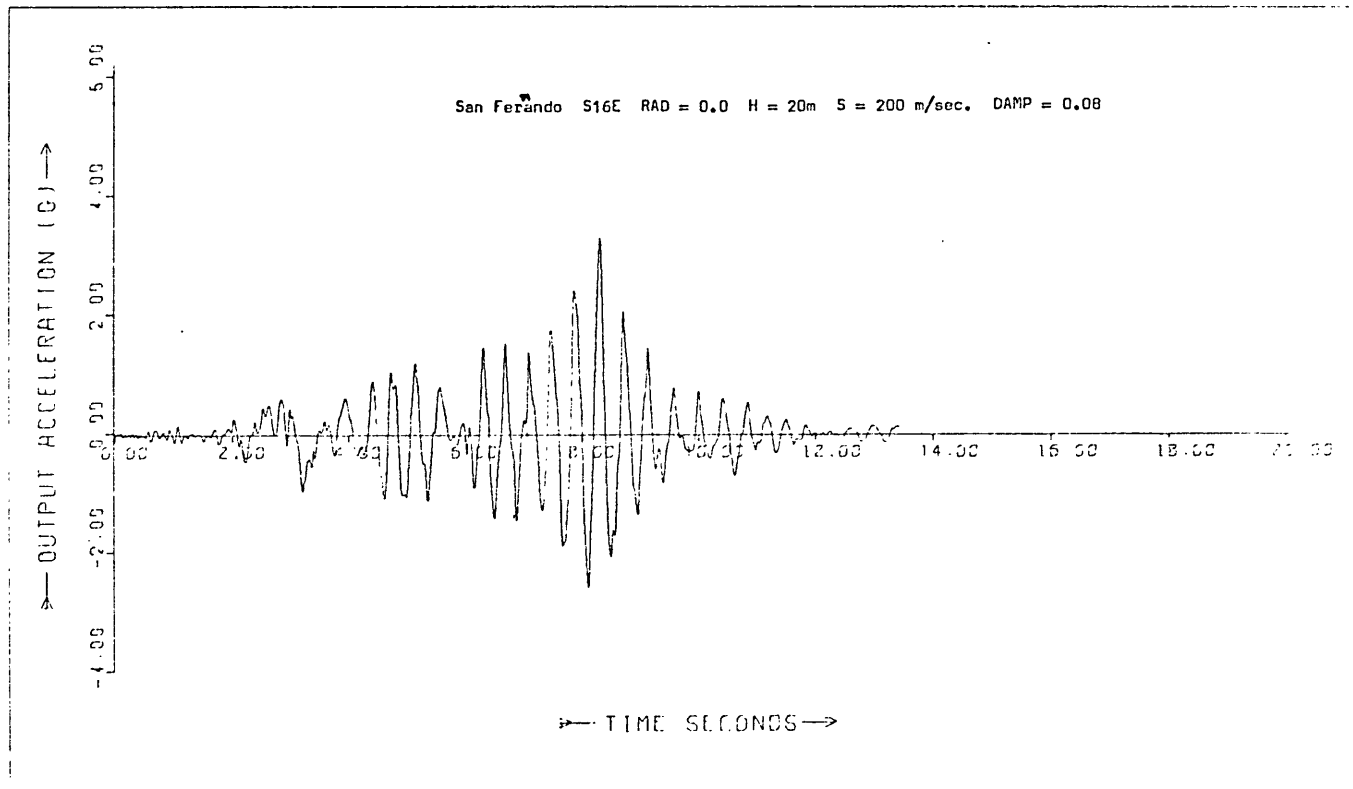


FIG. 6,18a COMPUTED GROUND SURFACE ACCELERATION TIME HISTORY AT SITE NO. 6.16

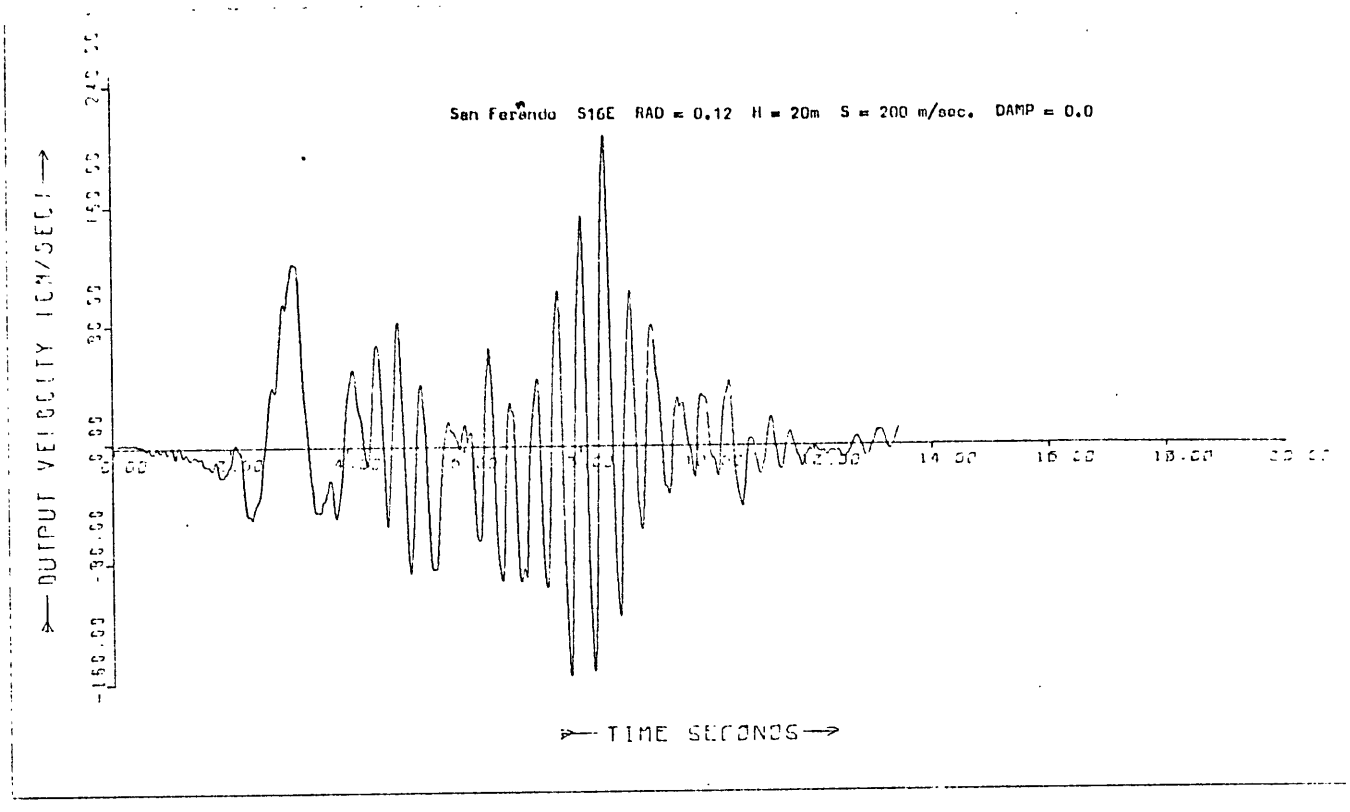


FIG. 6.17b COMPUTED GROUND SURFACE VELOCITY TIME HISTORY AT SITE NO. 6.15

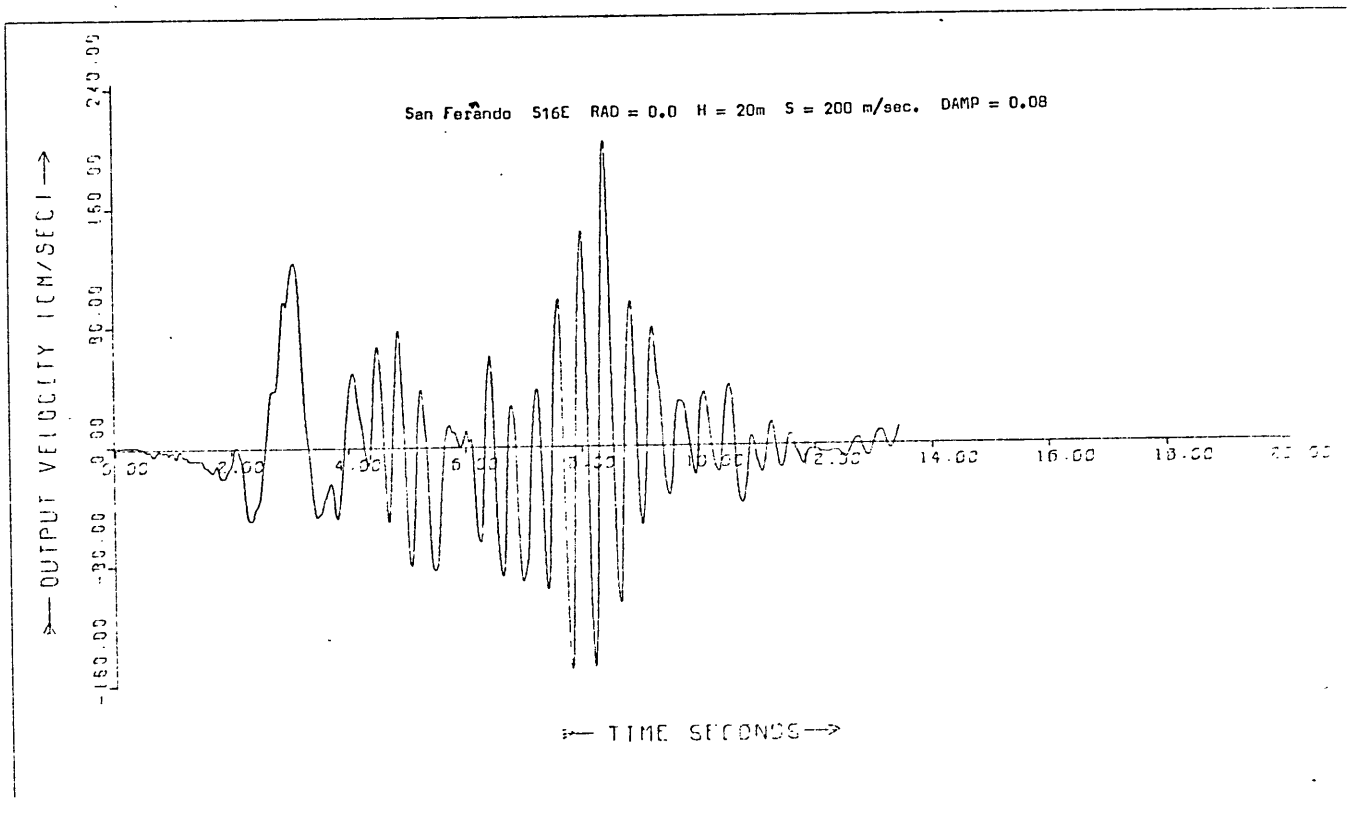


FIG.6.18b COMPUTED GROUND SURFACE VELOCITY TIME HISTORY AT SITE NO. 6.16

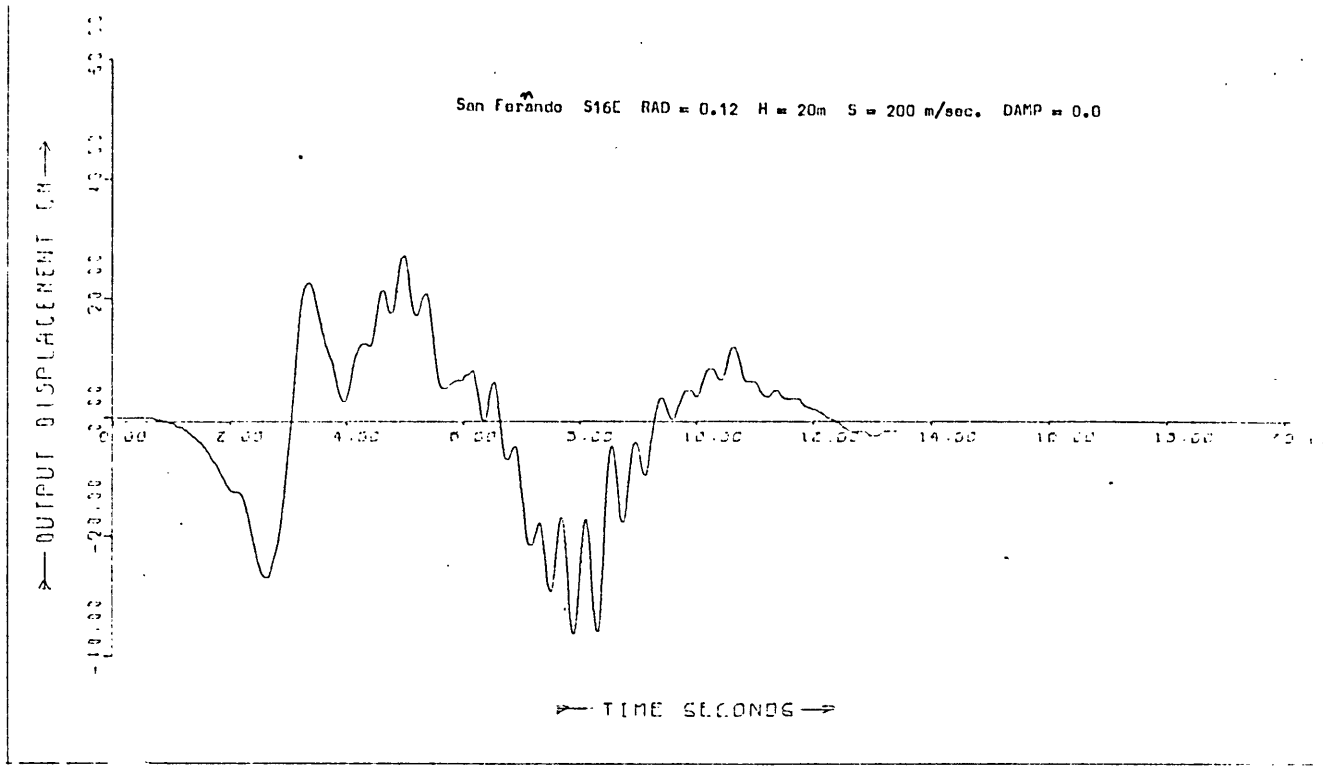


FIG.6.17c COMPUTED GROUND SURFACE DISPLACEMENT TIME HISTORY AT SITE NO. 6.15

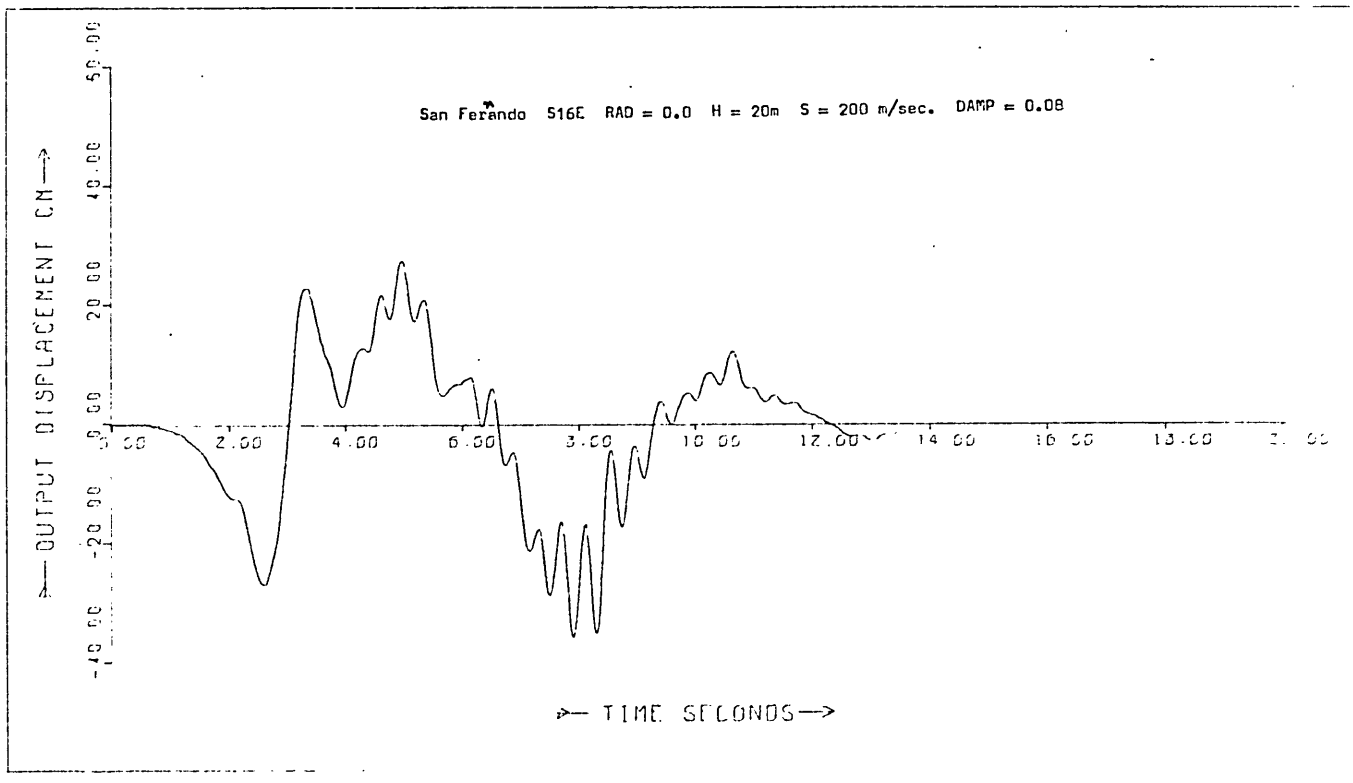


FIG.6.18c COMPUTED GROUND SURFACE DISPLACEMENT TIME HISTORY AT SITE NO. 6.16

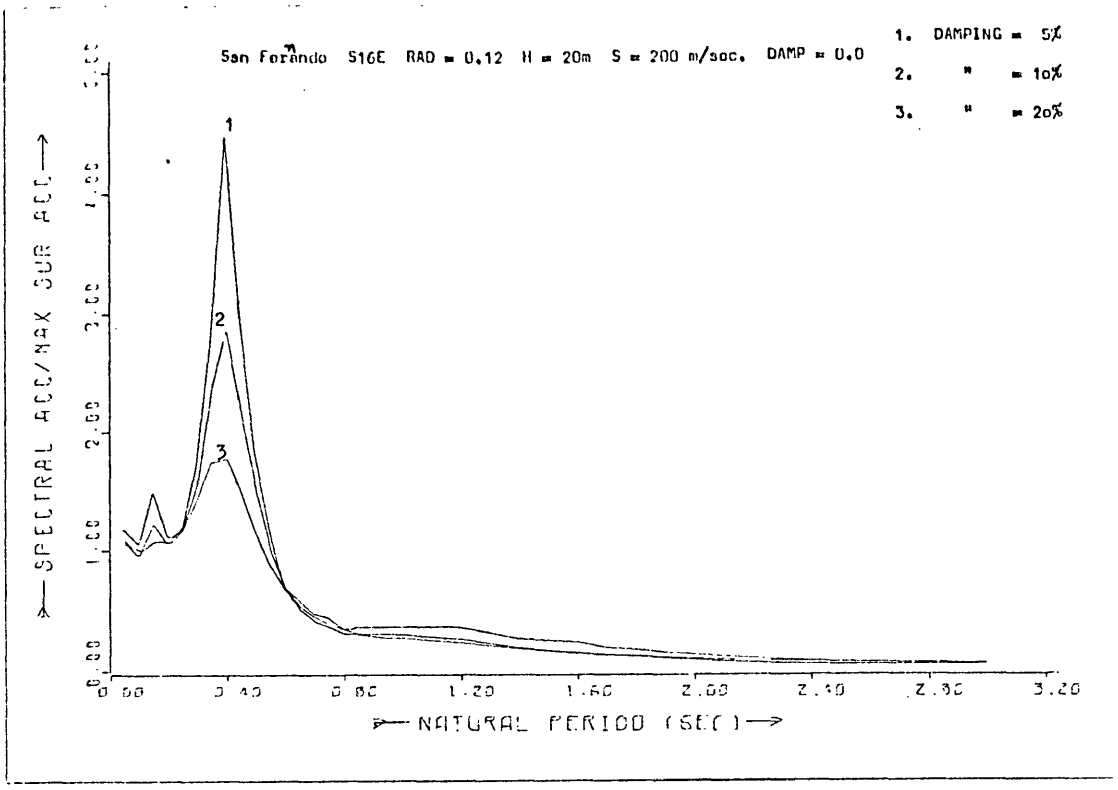


FIG. 6.17d COMPUTED GROUND SURFACE ACCELERATION RESPONSE SPECTRA AT SITE NO. 6.15 -

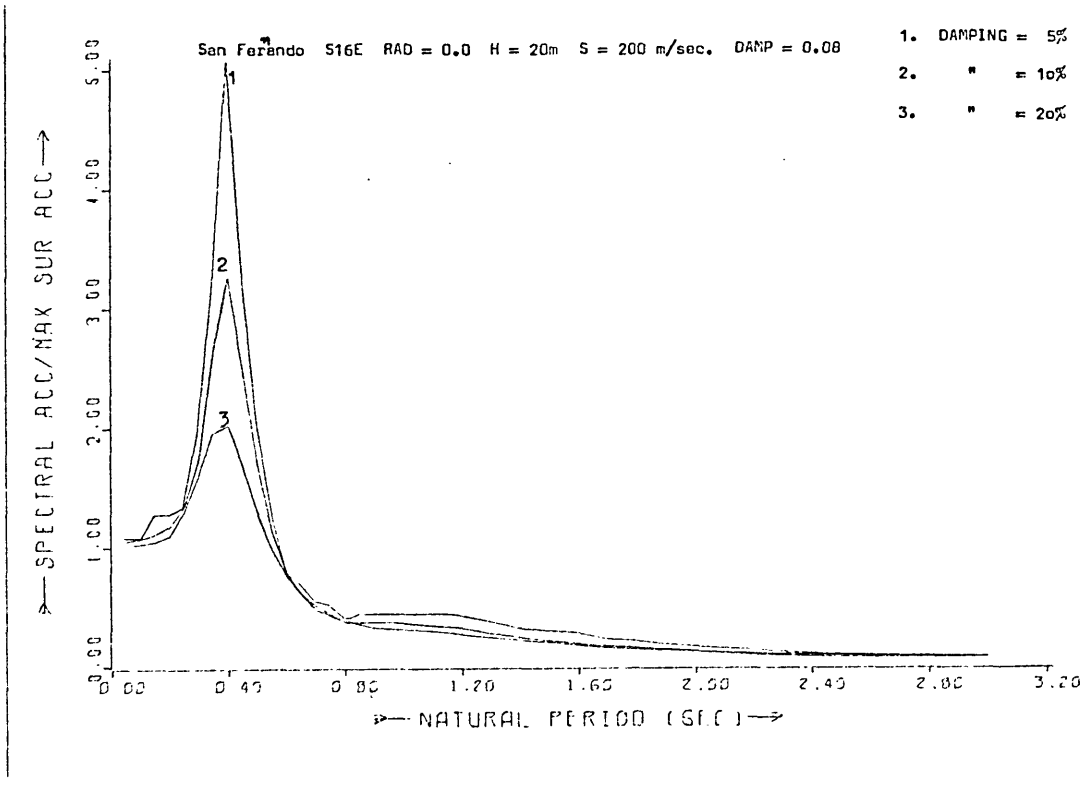


FIG. 6.18d COMPUTED GROUND SURFACE ACCELERATION RESPONSE SPECTRA AT SITE NO. 6.16

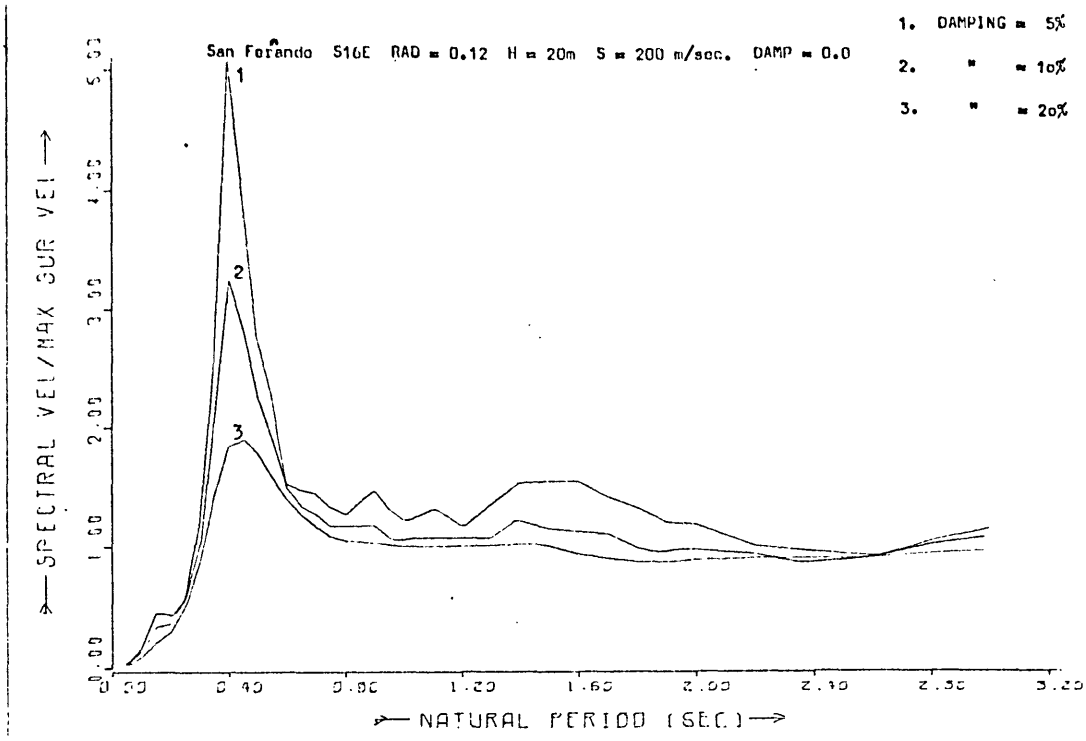


FIG. 6.17 COMPUTED GROUND SURFACE VELOCITY RESPONSE SPECTRA AT SITE NO. 6.15

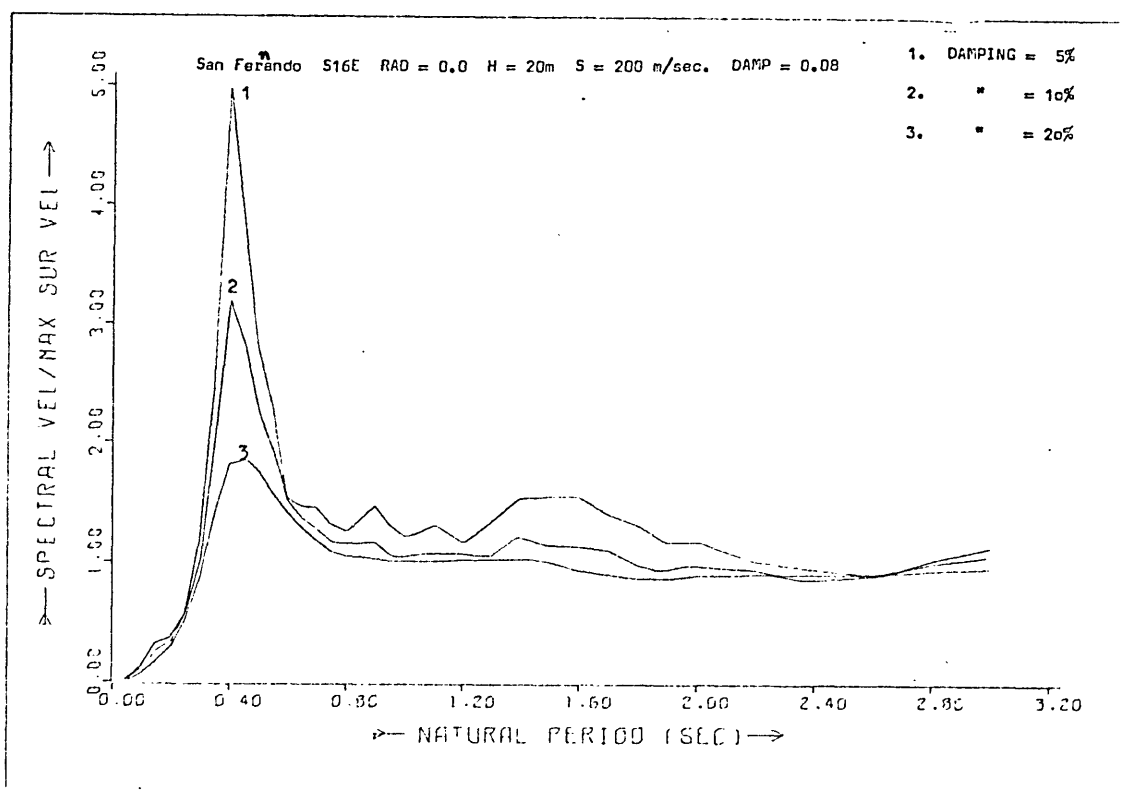


FIG. 6.18 COMPUTED GROUND SURFACE VELOCITY RESPONSE SPECTRA AT SITE NO. 6.16

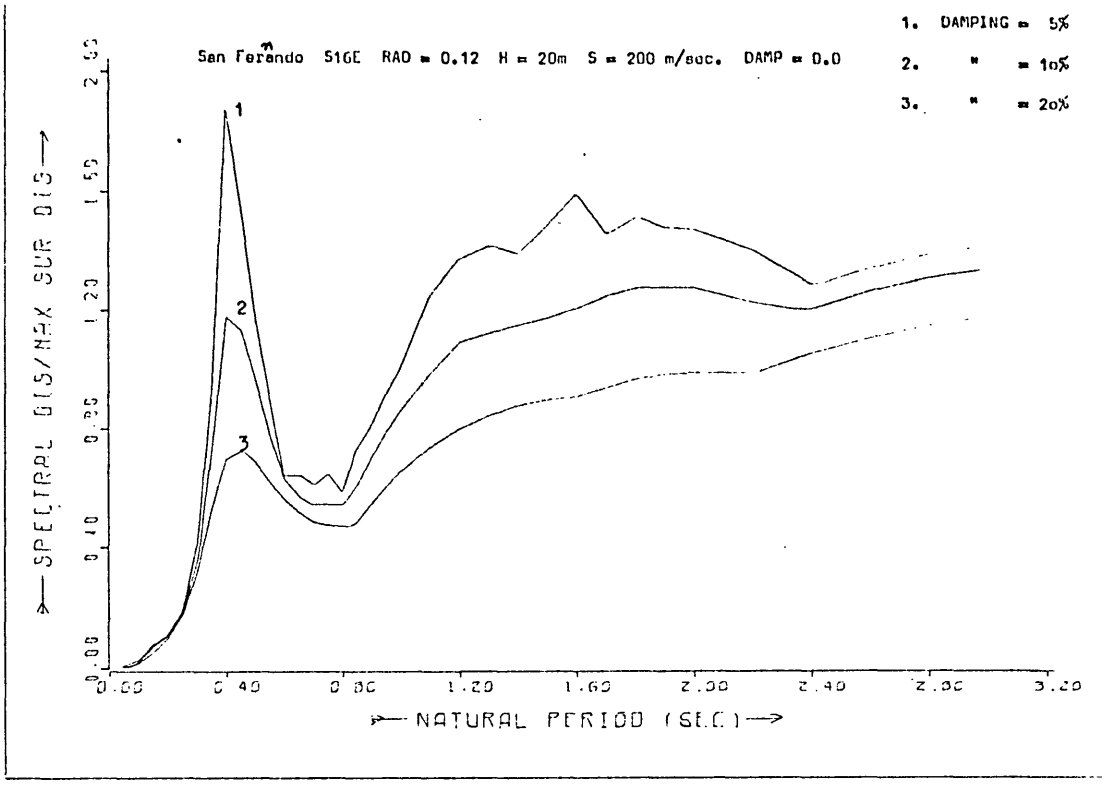


FIG.6.17f COMPUTED GROUND SURFACE DISPLACEMENT RESPONSE SPECTRA AT SITE NO. 6.15

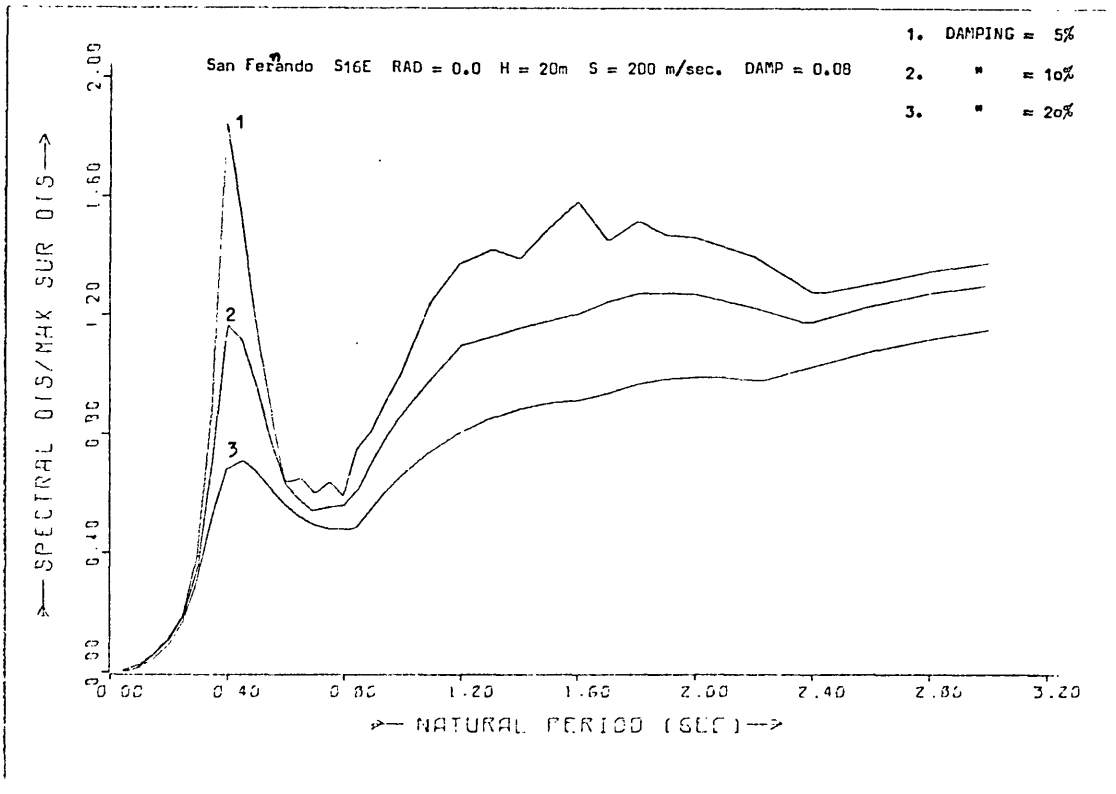


FIG. 6.18 COMPUTED GROUND SURFACE DISPLACEMENT RESPONSE SPECTRA AT SITE NO. 6.16

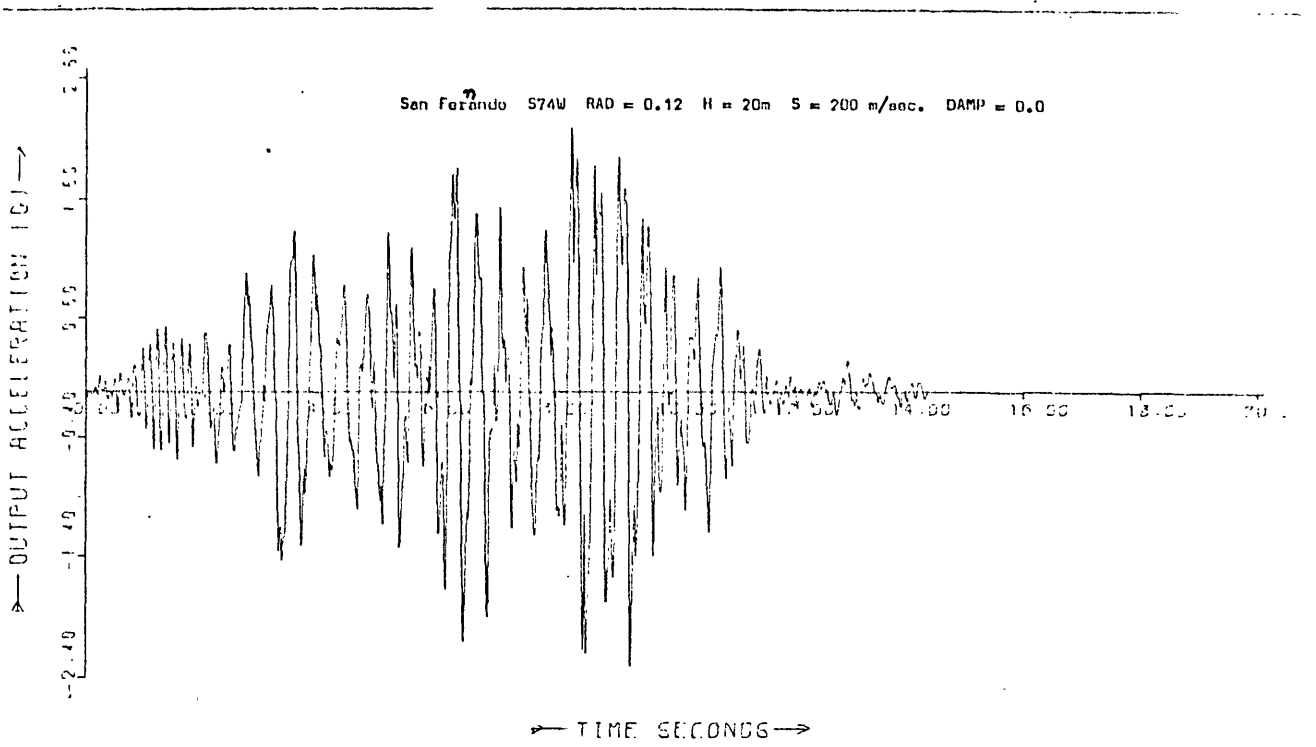


FIG.6.19a COMPUTED GROUND SURFACE ACCELERATION TIME HISTORY AT SITE NO. 6.15

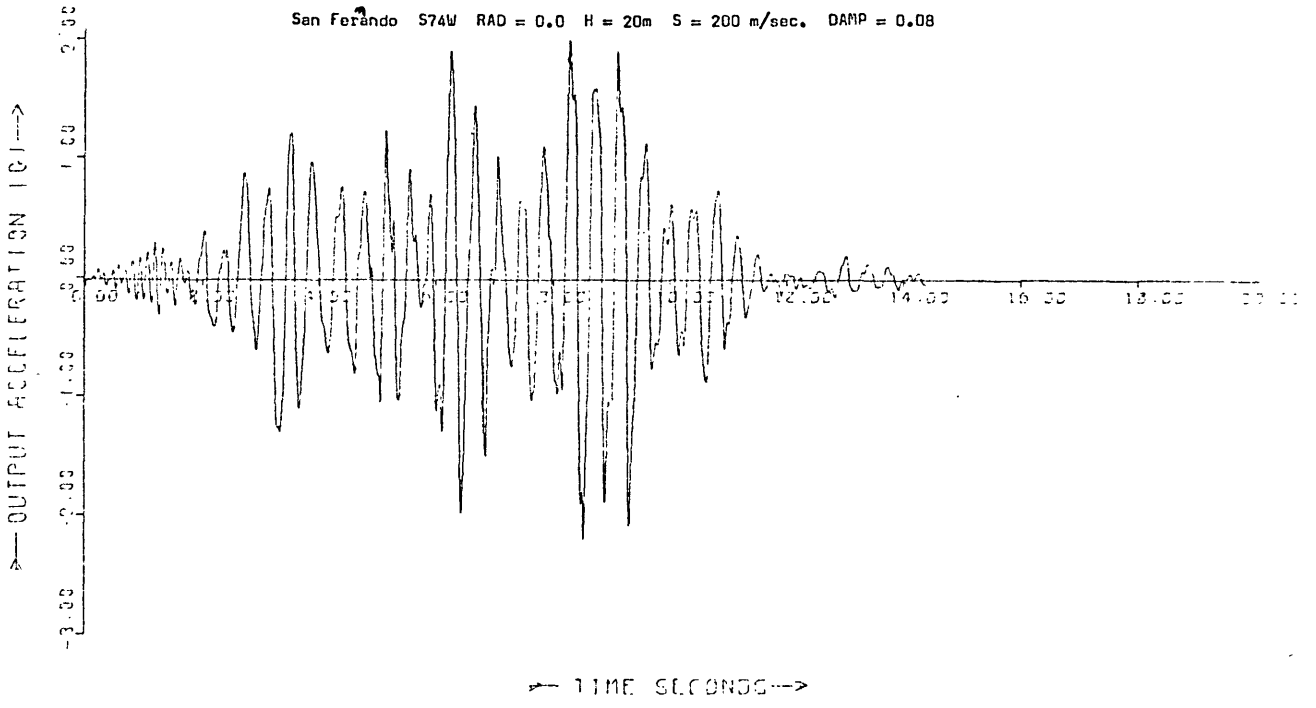


FIG.6.20a COMPUTED GROUND SURFACE ACCELERATION TIME HISTORY AT SITE NO. 6.16

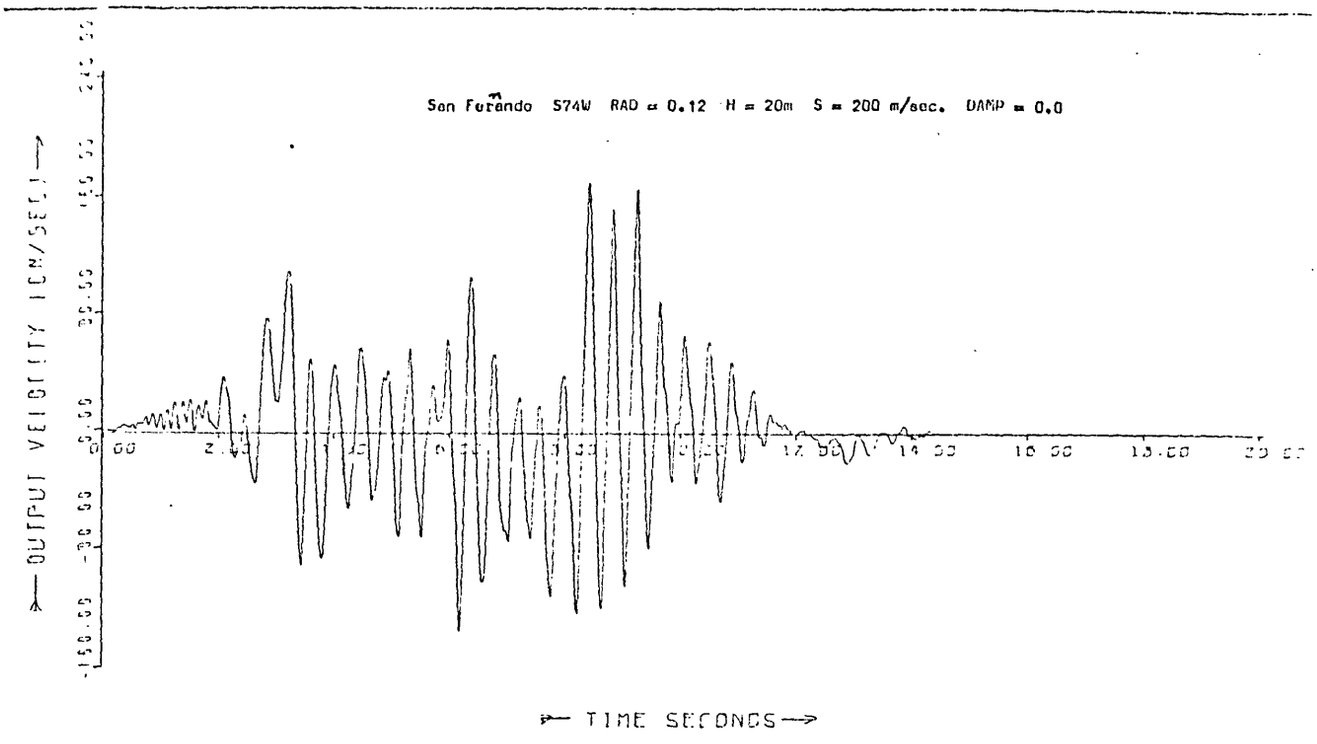


FIG.6.19b COMPUTED GROUND SURFACE VELOCITY TIME HISTORY AT SITE NO.6.15

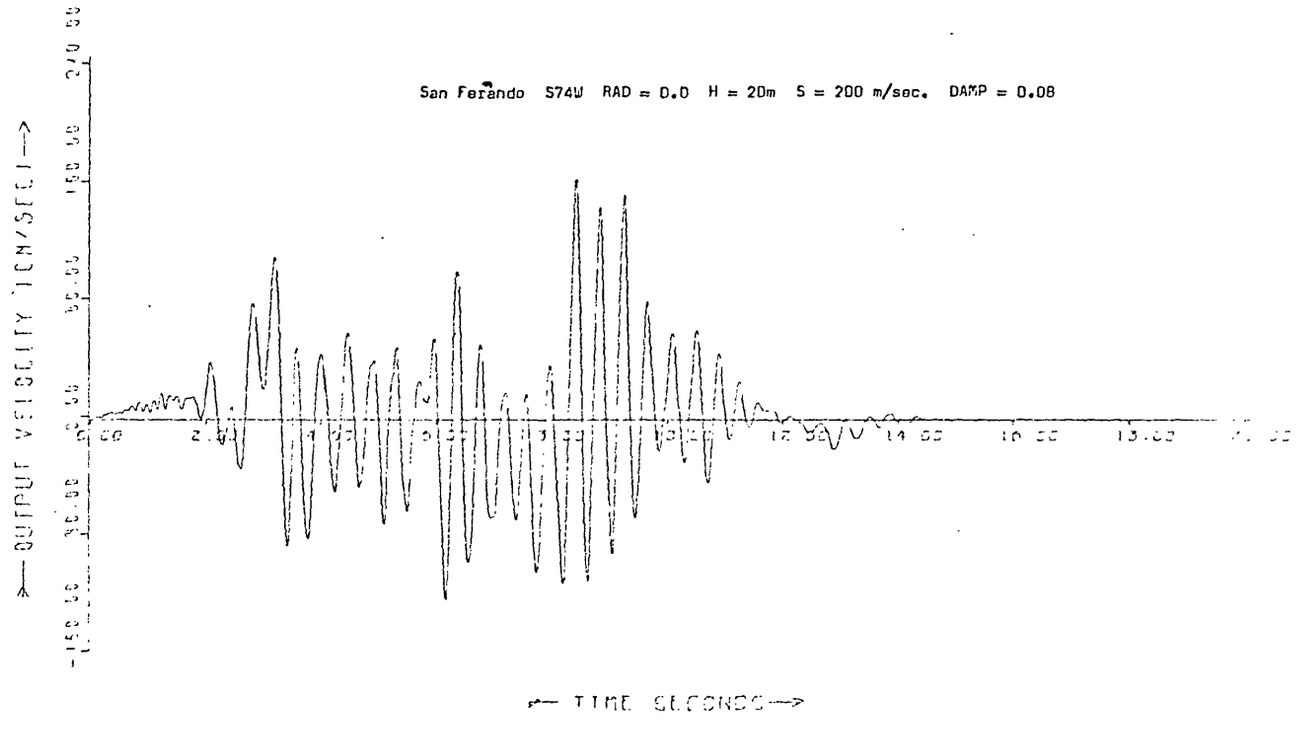


FIG.6.20b COMPUTED GROUND SURFACE VELOCITY TIME HISTORY AT SITE NO. 6.16

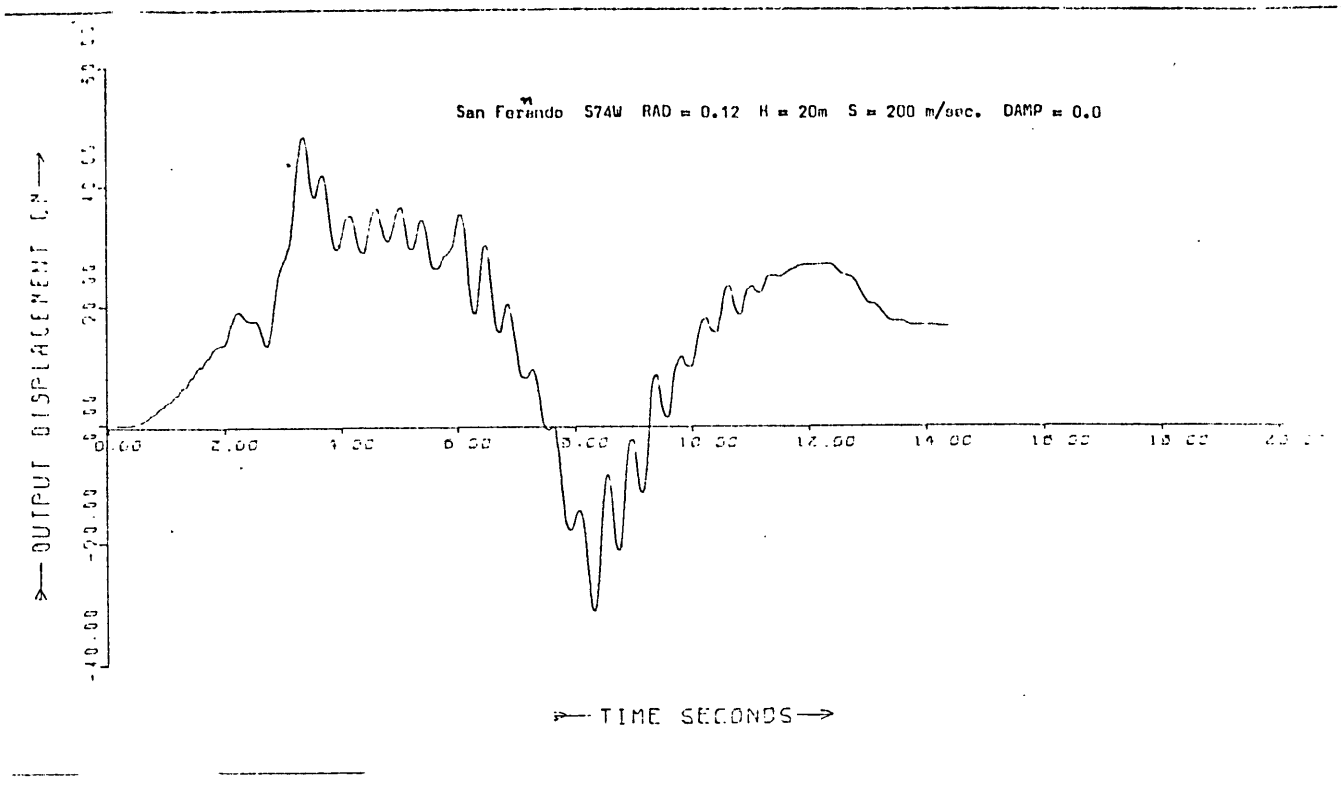


FIG 6.19c COMPUTED GROUND SURFACE DISPLACEMENT TIME HISTORY AT SITE NO. 6.15

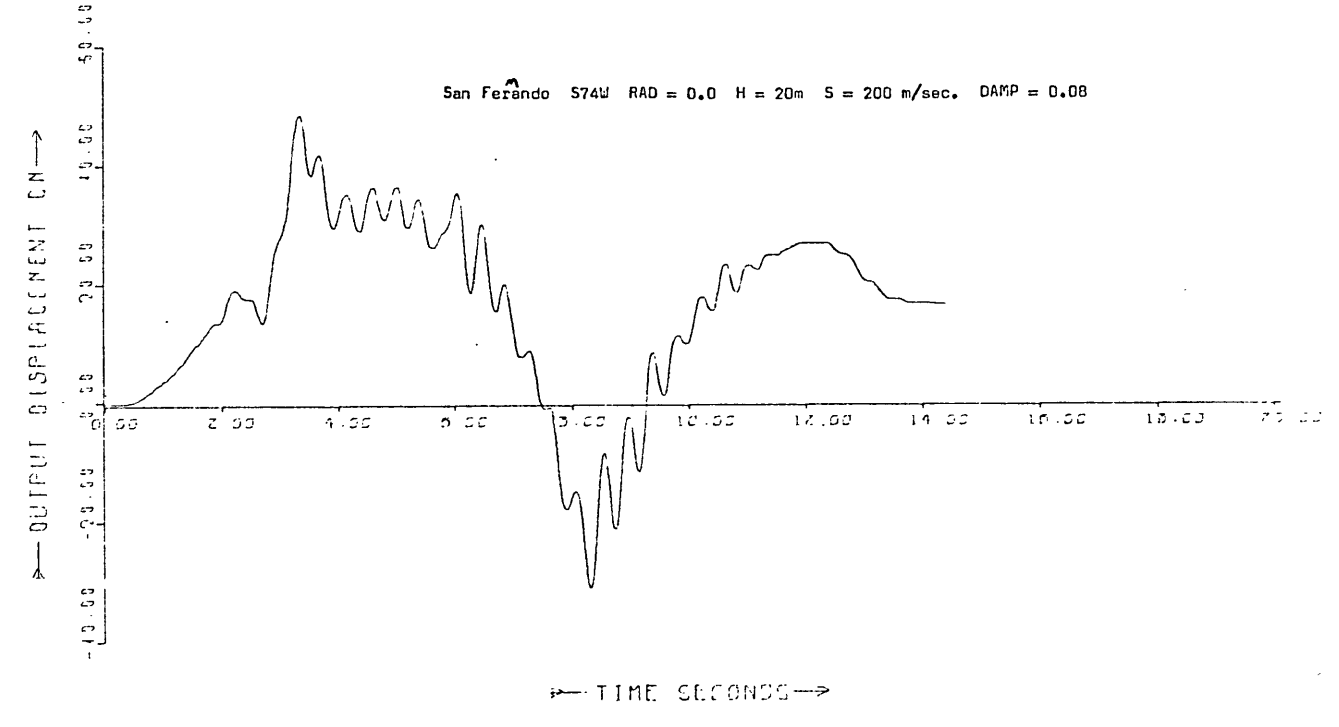


FIG 6.20c COMPUTED GROUND SURFACE DISPLACEMENT TIME HISTORY AT SITE NO. 6.16

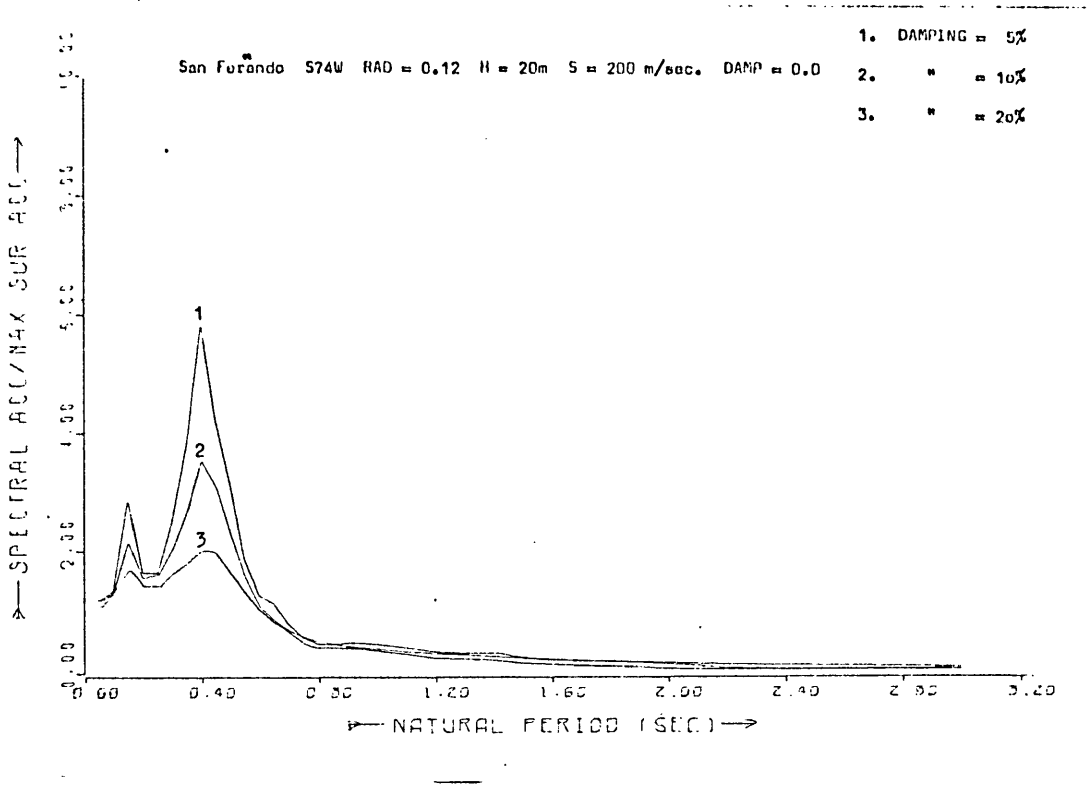


FIG. 6.19d COMPUTED GROUND SURFACE ACCELERATION RESPONSE SPECTRA AT SITE NO. 6.15

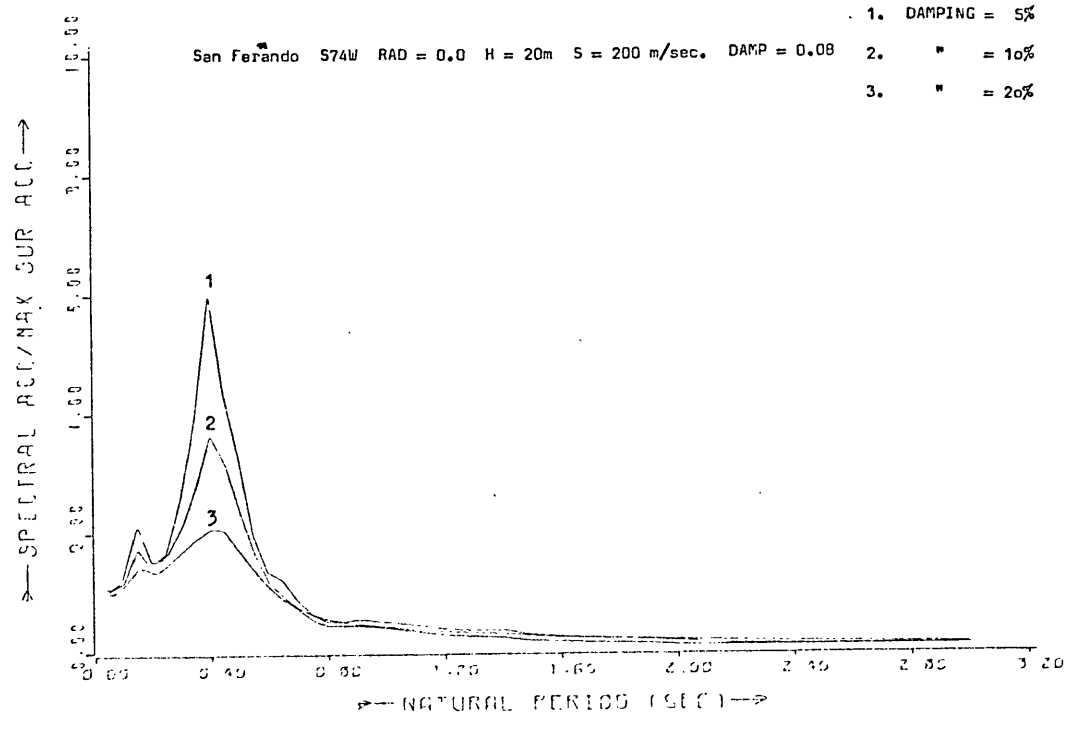


FIG. 6.20d COMPUTED GROUND SURFACE ACCELERATION RESPONSE SPECTRA AT SITE NO. 6.16

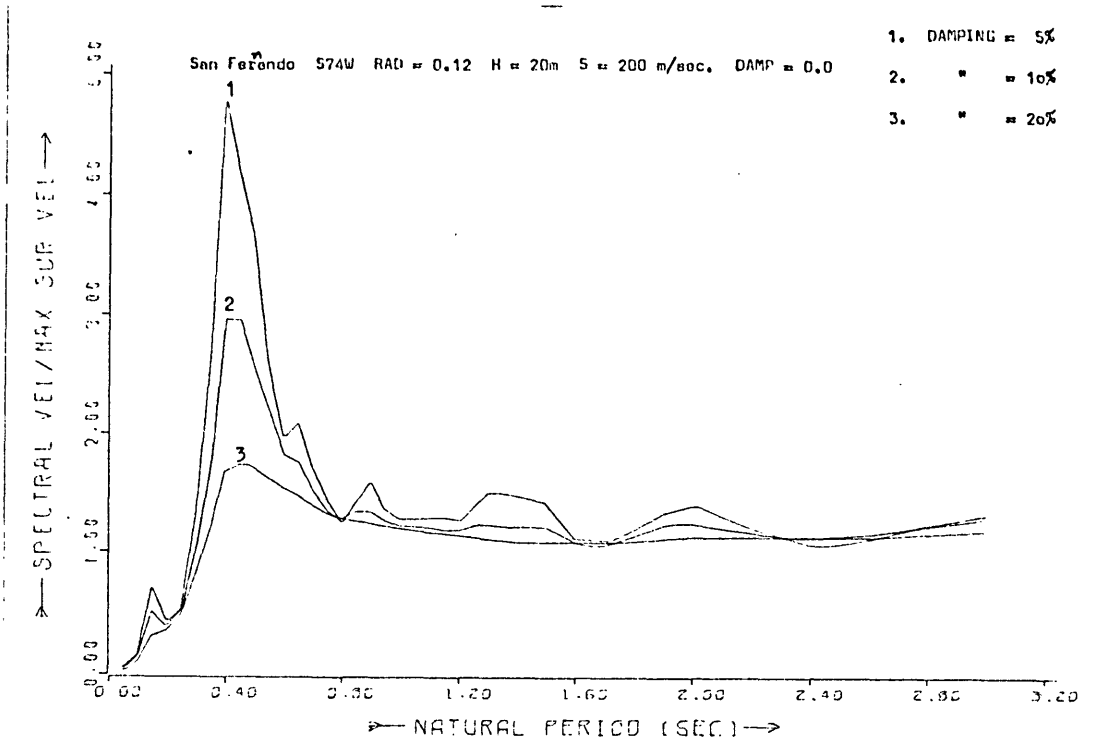


FIG.6.19 COMPUTED GROUND SURFACE VELOCITY RESPONSE SPECTRA AT SITE NO. 6.15

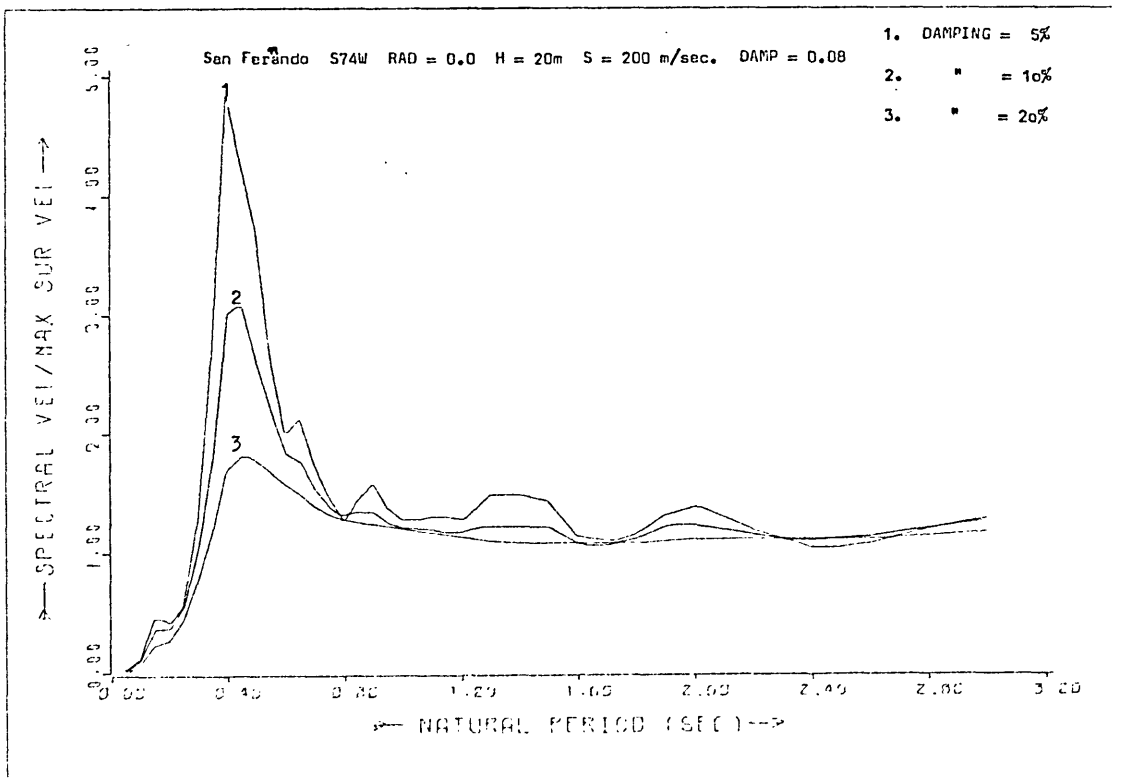


FIG.6.20 COMPUTED GROUND SURFACE VELOCITY RESPONSE SPECTRA AT SITE NO. 6.16

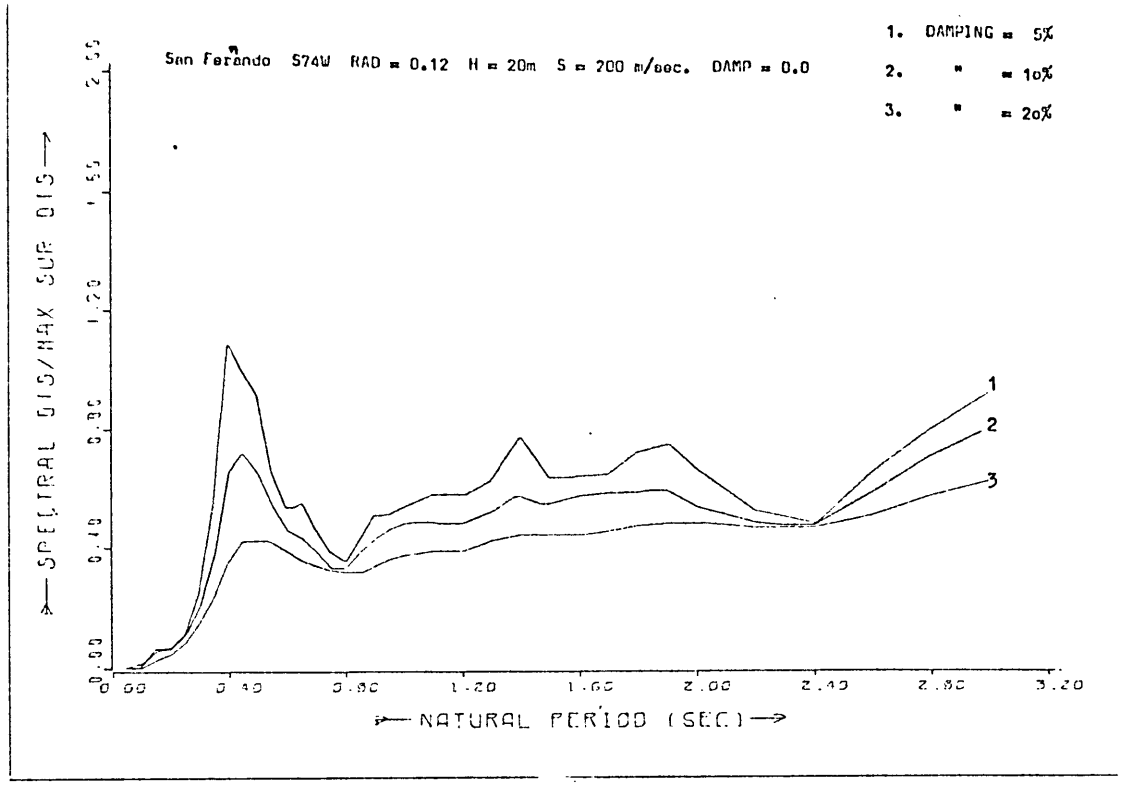


FIG. 6.19 COMPUTED GROUND SURFACE DISPLACEMENT RESPONSE SPECTRA AT SITE NO. 6.15

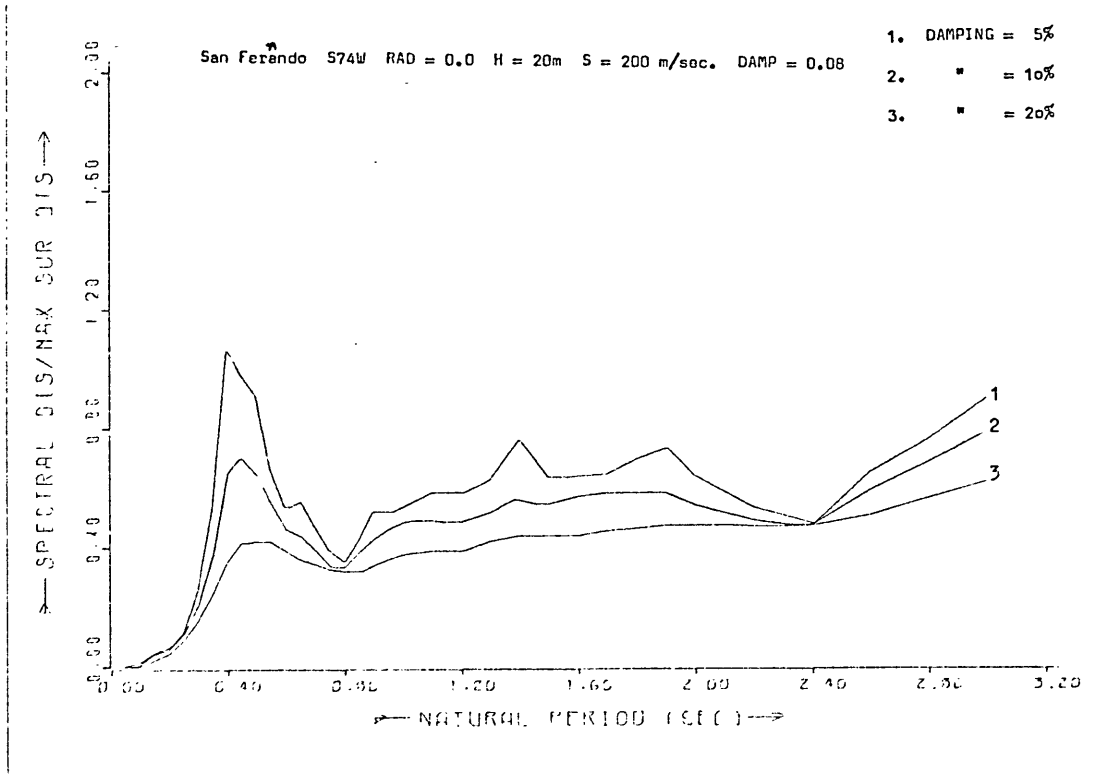
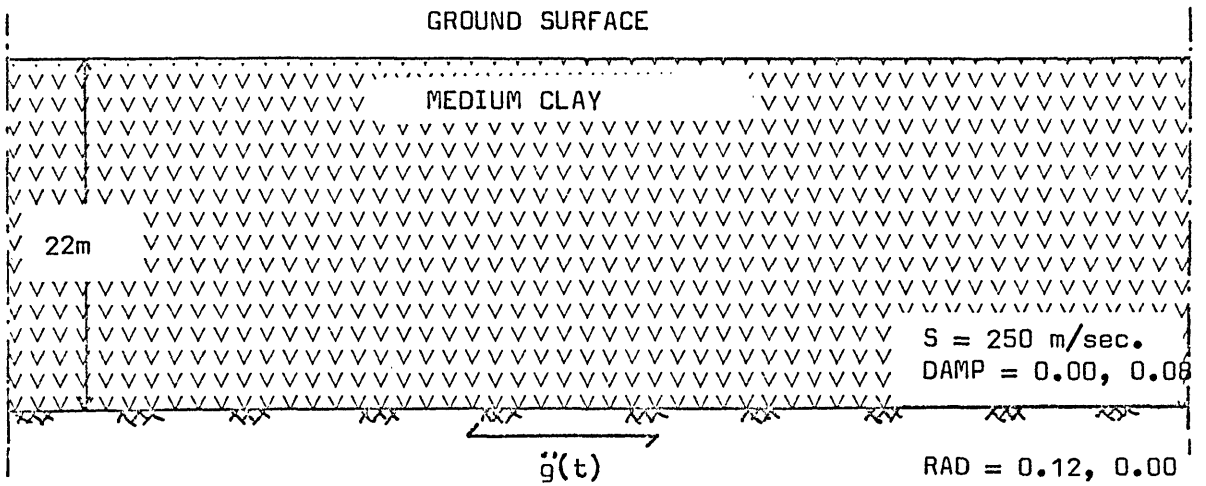


FIG. 6.20 COMPUTED GROUND SURFACE DISPLACEMENT RESPONSE SPECTRA AT SITE NO. 6.16



RESPONSE OF HYSTERETIC DEPOSIT UNDERLAIN BY DEFORMABLE BEDROCK

SCHEMATIC SOIL PROFILE FOR SITE NO. 6.17 and 6.18

FIG. 6.21

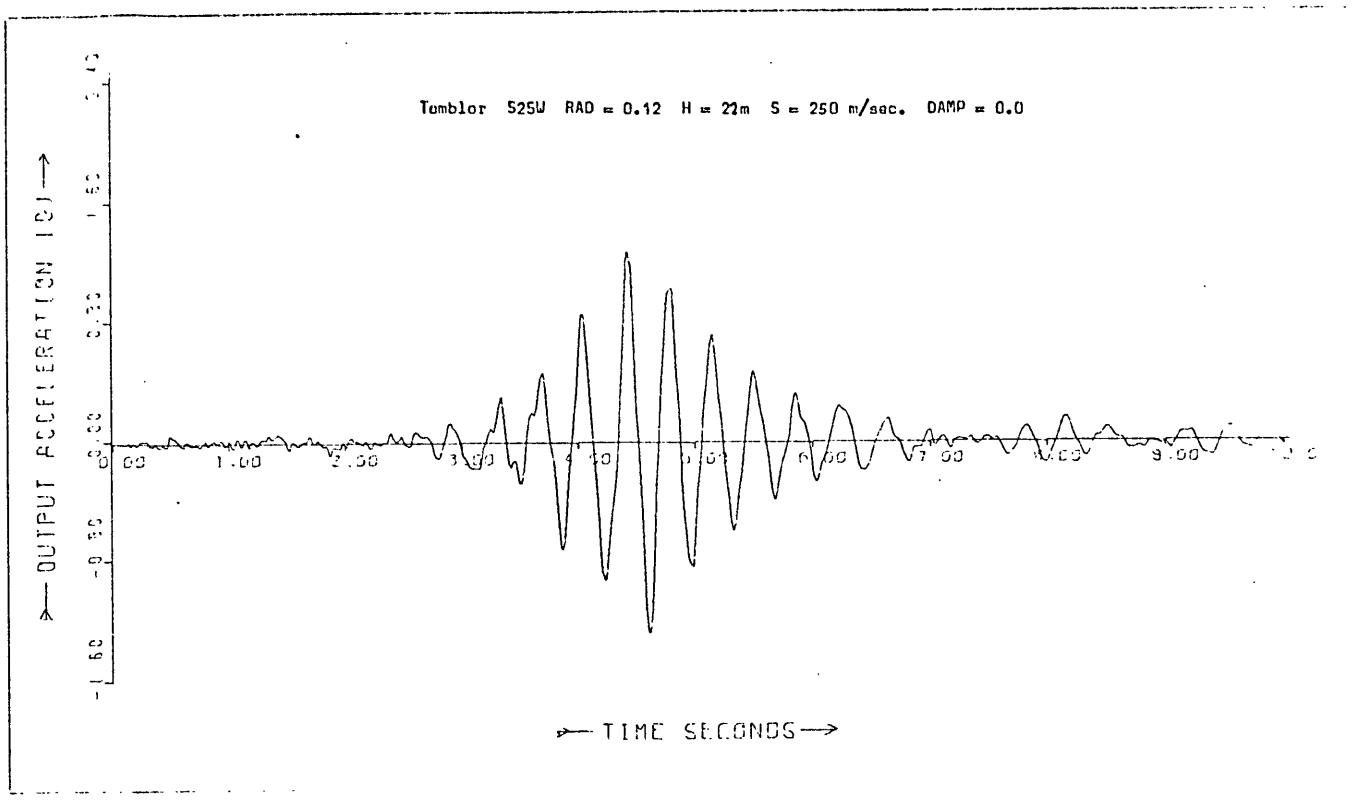


FIG.6.21a COMPUTED GROUND SURFACE ACCELERATION TIME HISTORY AT SITE NO. 6.17

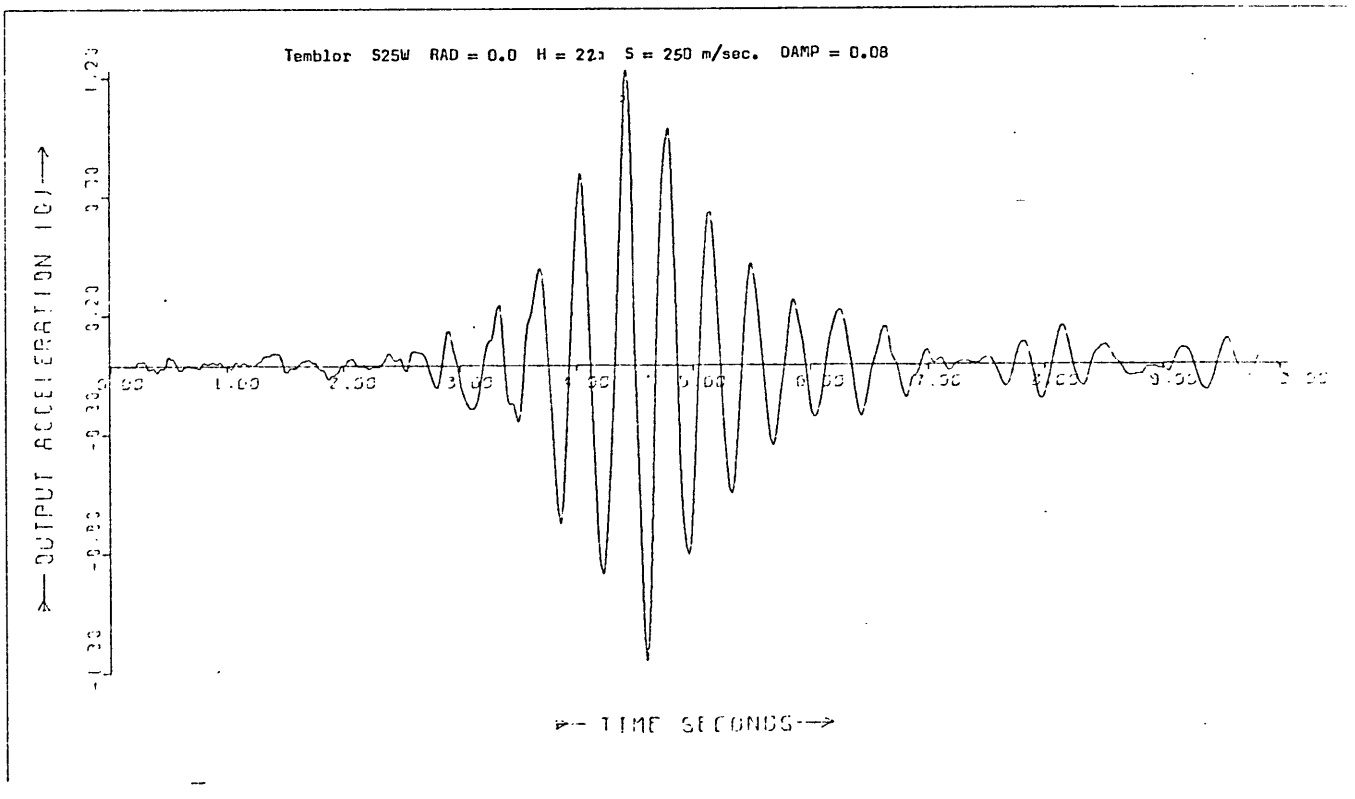


FIG.6.22a COMPUTED GROUND SURFACE ACCELERATION TIME HISTORY AT SITE NO. 6.18

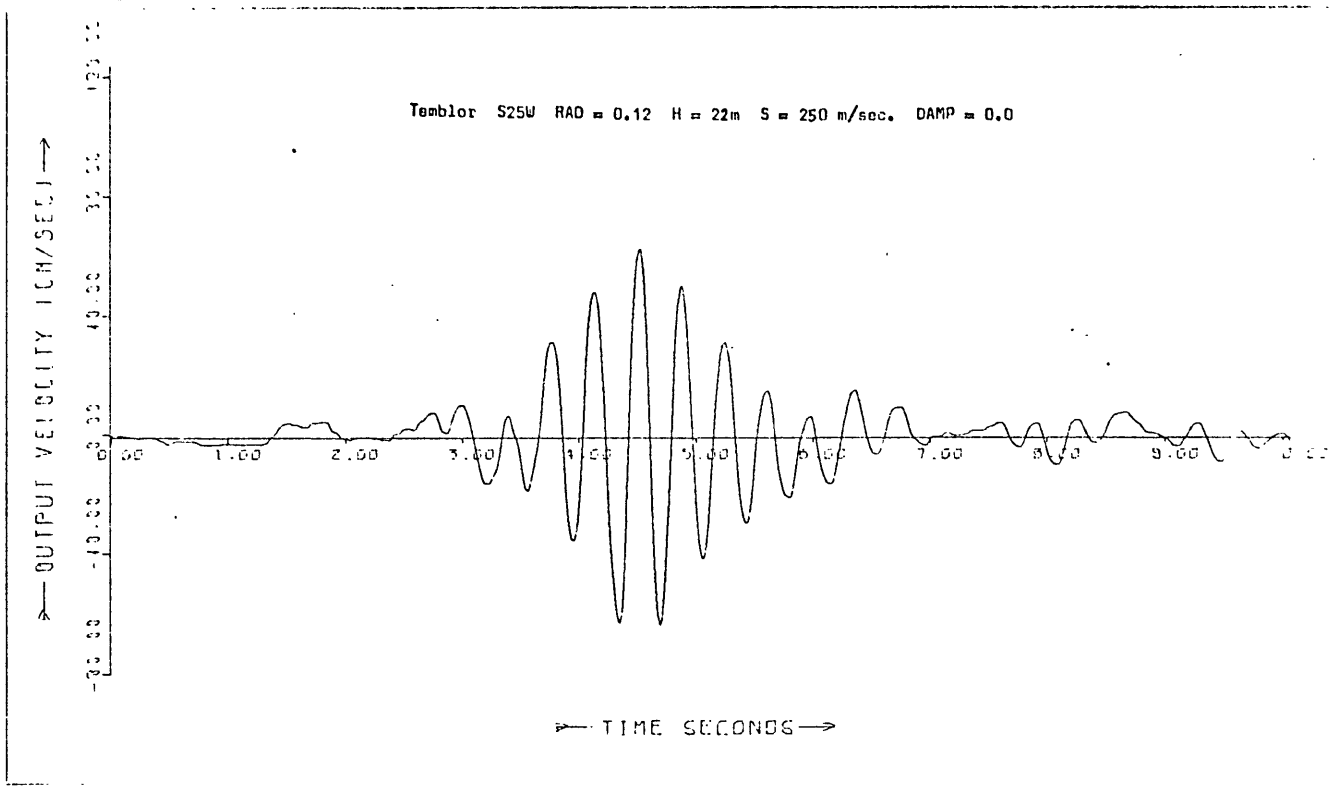


FIG. 6.21b COMPUTED GROUND SURFACE VELOCITY TIME HISTORY AT SITE NO. 6.17

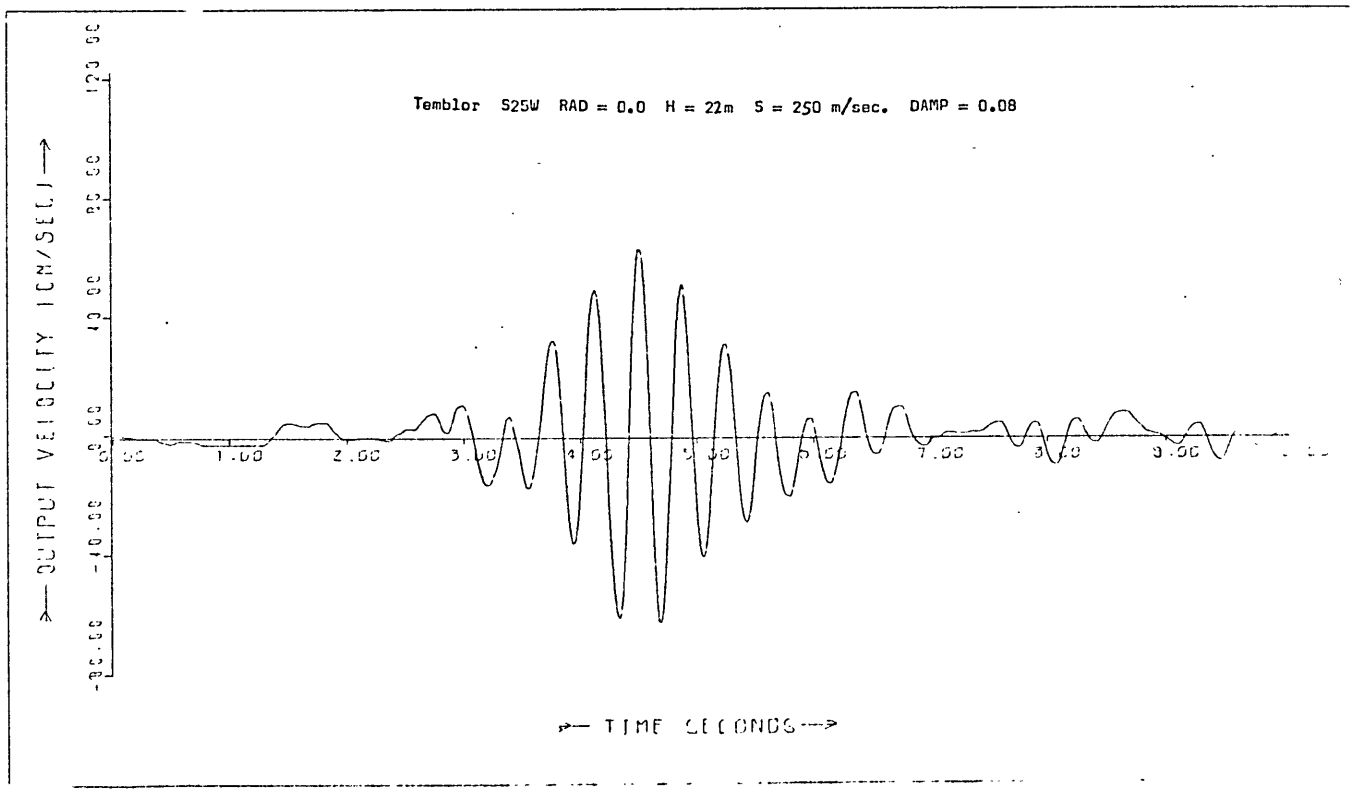


FIG. 6.22b COMPUTED GROUND SURFACE VELOCITY TIME HISTORY AT SITE NO. 6.18

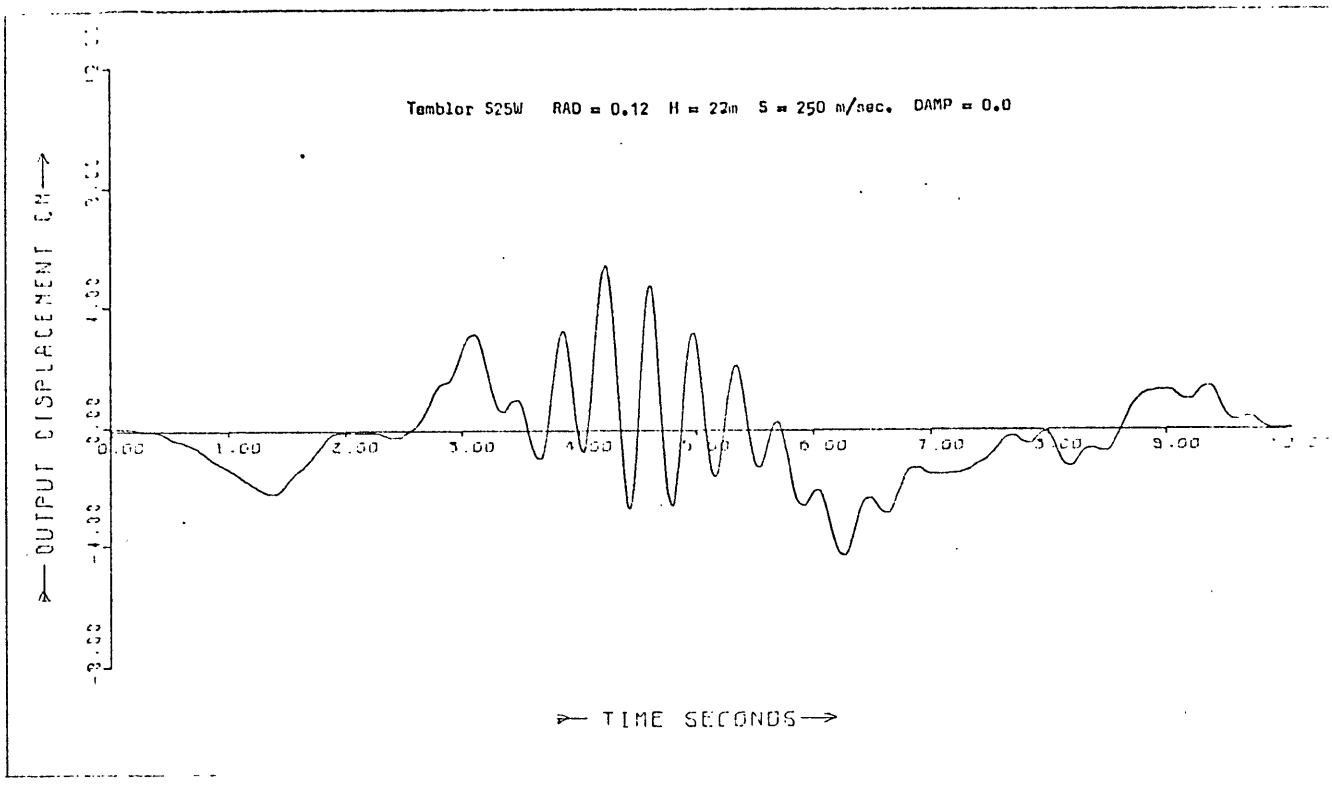


FIG.6.21c COMPUTED GROUND SURFACE DISPLACEMENT TIME HISTORY AT SITE NO. 6.17

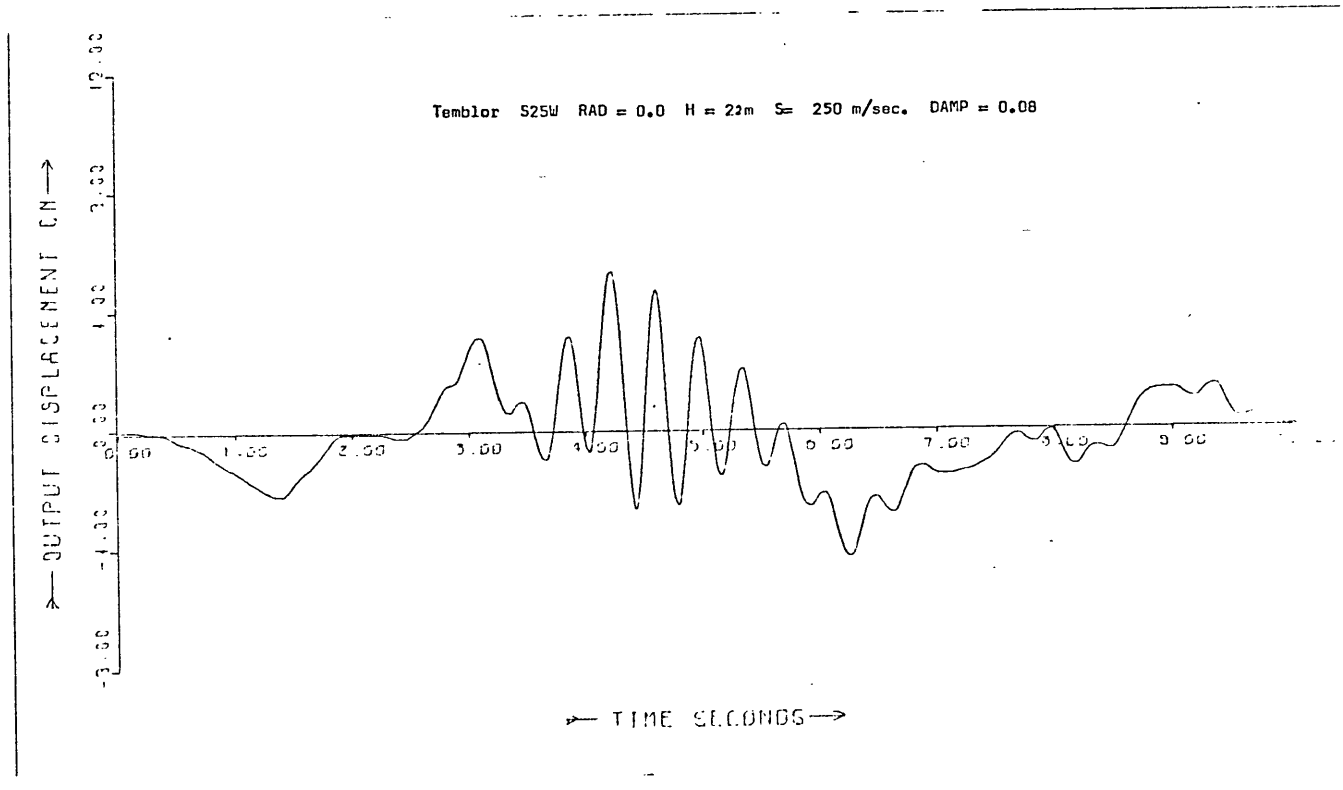


FIG.6.22c COMPUTED GROUND SURFACE DISPLACEMENT TIME HISTORY AT SITE NO. 6.18

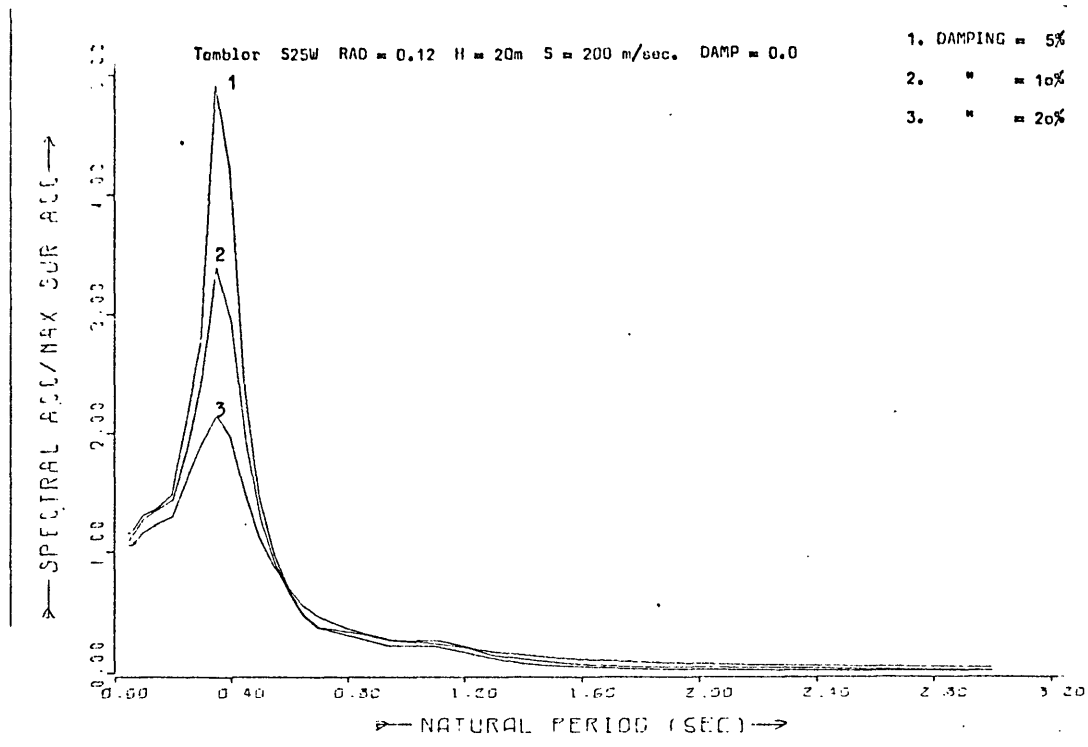


FIG.6.21d COMPUTED GROUND SURFACE ACCELERATION RESPONSE SPECTRA AT SITE NO.6.17

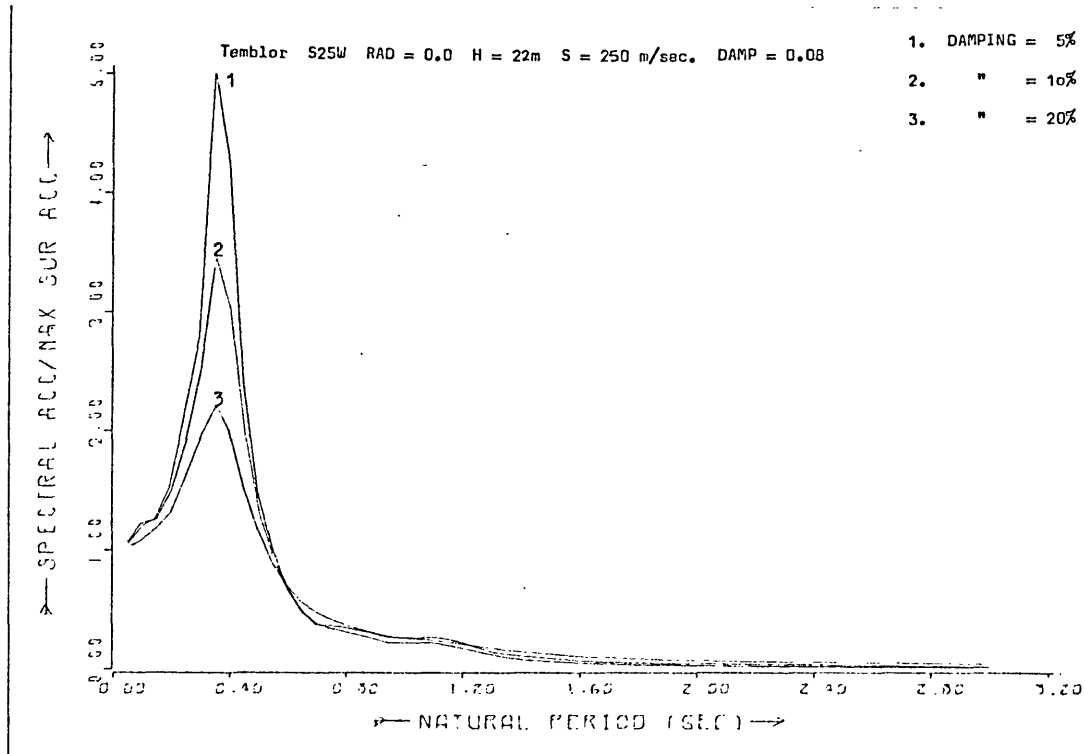


FIG.6.22d COMPUTED GROUND SURFACE ACCELERATION RESPONSE SPECTRA AT SITE NO.6.18

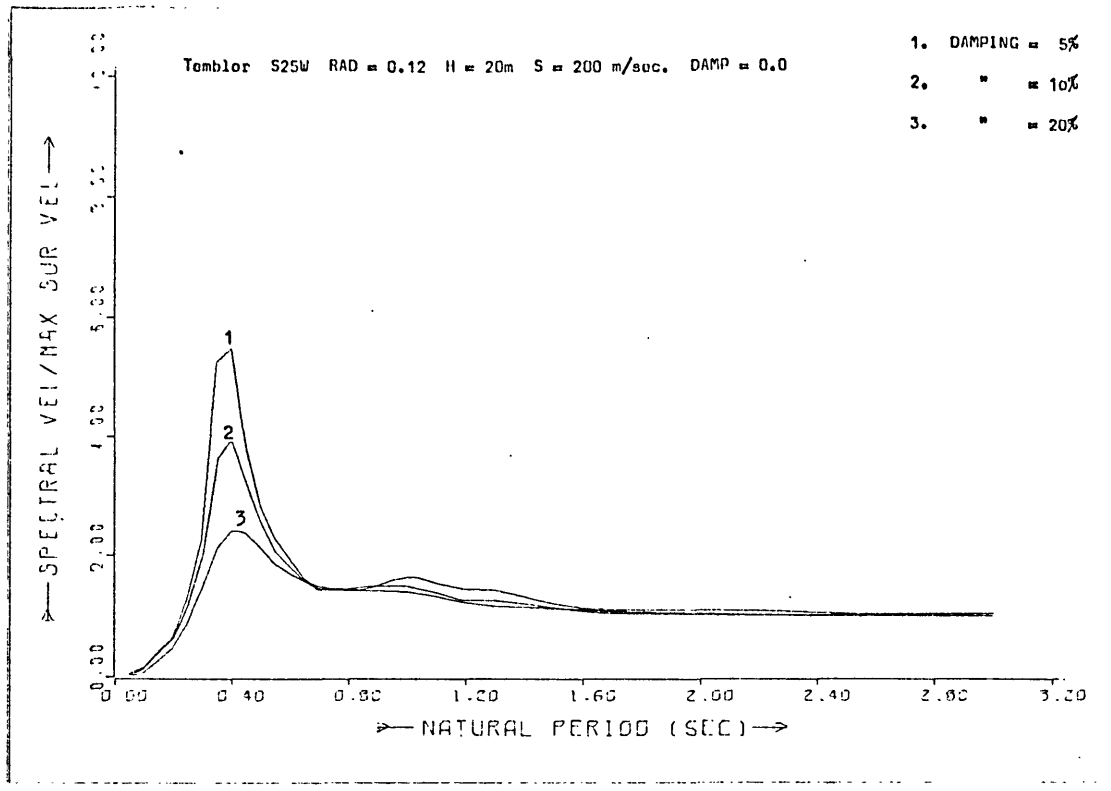


FIG 6.21e COMPUTED GROUND SURFACE VELOCITY RESPONSE SPECTRA AT SITE NO. 6.17

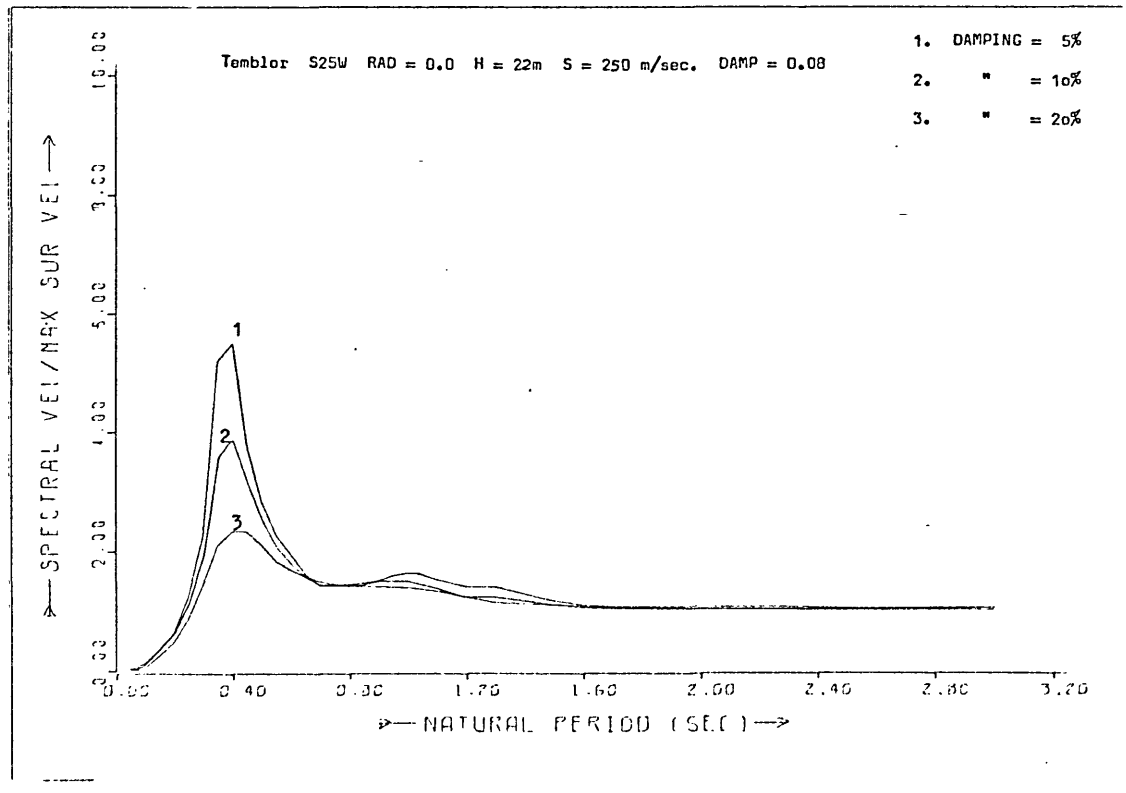


FIG.6.22eCOMPUTED GROUND SURFACE VELOCITY RESPONSE SPECTRA AT SITE NO.6.18

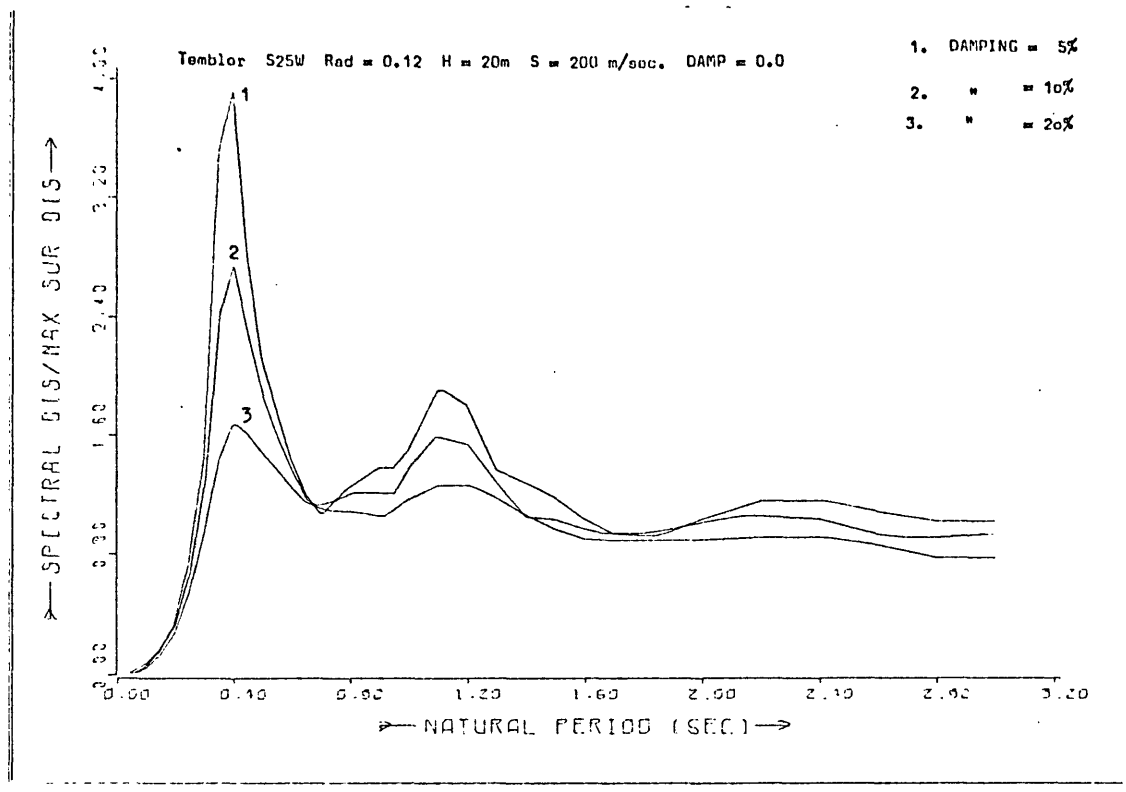


FIG. 6.21 COMPUTED GROUND SURFACE DISPLACEMENT RESPONSE SPECTRA AT SITE NO. 6.17

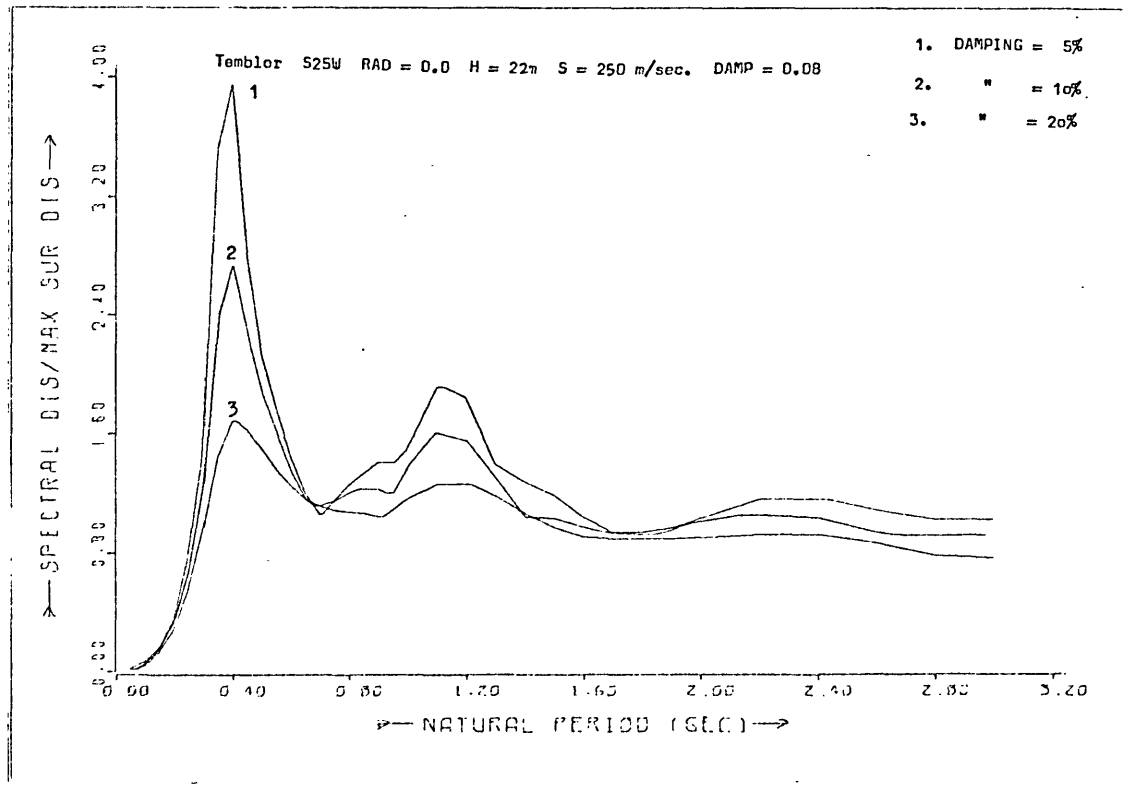


FIG. 6.22 COMPUTED GROUND SURFACE DISPLACEMENT RESPONSE SPECTRA AT SITE NO. 6.18

Figs. 6.17d,e,f to 6.22d,e,f show computed surface acceleration, velocity and displacement spectrum normalized with respect to maximum surface acceleration, velocity and displacement, respectively, to provide a common basis for comparison purposes. The results are almost identical, except that they differ slightly in the peaks. Frequency characteristics of output motions for all sets of calculations are clearly reflected in normalized acceleration response spectrum shown in figs. 6.17d to 6.22d, which indicate that frequency characteristics of output motions are almost identical. The sharp peaks at periods of 0.4 second in figs. 6.17d to 6.20d, which correspond to the fundamental period of the first deposit, and at period of 0.35 second, corresponding to the fundamental period of the second deposit on figs. 6.21d and 6.22d, are noteworthy. These comparisons clearly confirm the fact that radiation and hysteretic damping ratios have the same effect in the first mode of vibrations, which dominates in this case.

CONCLUSIONS

From the results presented, it appears that:

a) In general, under the special condition, i.e. fundamental period of the overburden equal to the predominant period of the bedrock motion (first mode of vibration dominating the response), radiation and hysteretic damping ratios produce almost identical response values and equivalence between the two dissipative mechanisms under this special condition can be established.

b) Radiation damping ratio is less effective in supressing the response than the hysteretic damping ratio; therefore, establishing any equivalence should include more radiation

damping than hysteretic damping.

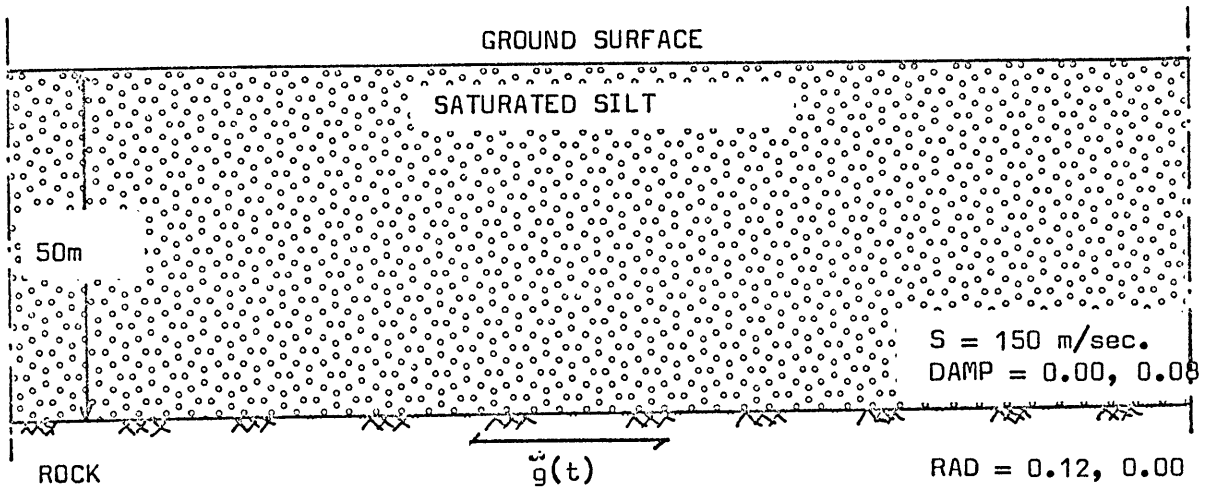
c) Frequency characteristics of output motions are unaffected by increasing radiation damping ratio.

6.8.1.2. FUNDAMENTAL PERIOD OF THE OVERBURDEN IS NOT EQUAL TO THE PREDOMINANT PERIOD OF THE BEDROCK MOTION

The influence of radiation damping ratio on ground response and its comparison with hysteretic damping ratio for the case when the fundamental period of the overburden is not equal to the predominant period of the bedrock motion is studied by making four different comparisons among the eight cases shown in figs. 6.23a,b,c,d,e through 6.30a,b,c,d,e.

Figs. 6.23a,b,c,d,e to 6.30a,b,c,d,e show response of a 50m deposit of saturated silt for two damping types (RAD = 0.12, DAMP = 0.0 and RAD = 0.0, DAMP = 0.08) subjected to four different bedrock motions: Parkfield-8 N50E, Golden Gate N10E, San Ferando S74W, Parkfield-5 N5W, with different frequency characteristics.

Figs. 6.23a,b,c to 6.30 a,b,c show computed surface acceleration, velocity and displacement time histories for four different pairs of comparisons. The results clearly illustrate the substantial differences in each comparison. The differences are more substantial in acceleration and velocity time histories than in displacement time histories, indicating that acceleration and velocity time histories are more sensitive to the changes in the parameters studied than the displacement time histories. These substantial differences are clearly reflected in the normalized acceleration response spectrum shown in figs. 6.23d to 6.30d, illustrating the fact that frequency characteristics of output motions for each pair of calculations differ considerably. Major differences are observed near the



RESPONSE OF HYSTERETIC DEPOSIT UNDERLAIN BY DEFORMABLE BEDROCK

SCHEMATIC SOIL PROFILE FOR SITE NO. 6.19 and 6.20

FIG. 6.23

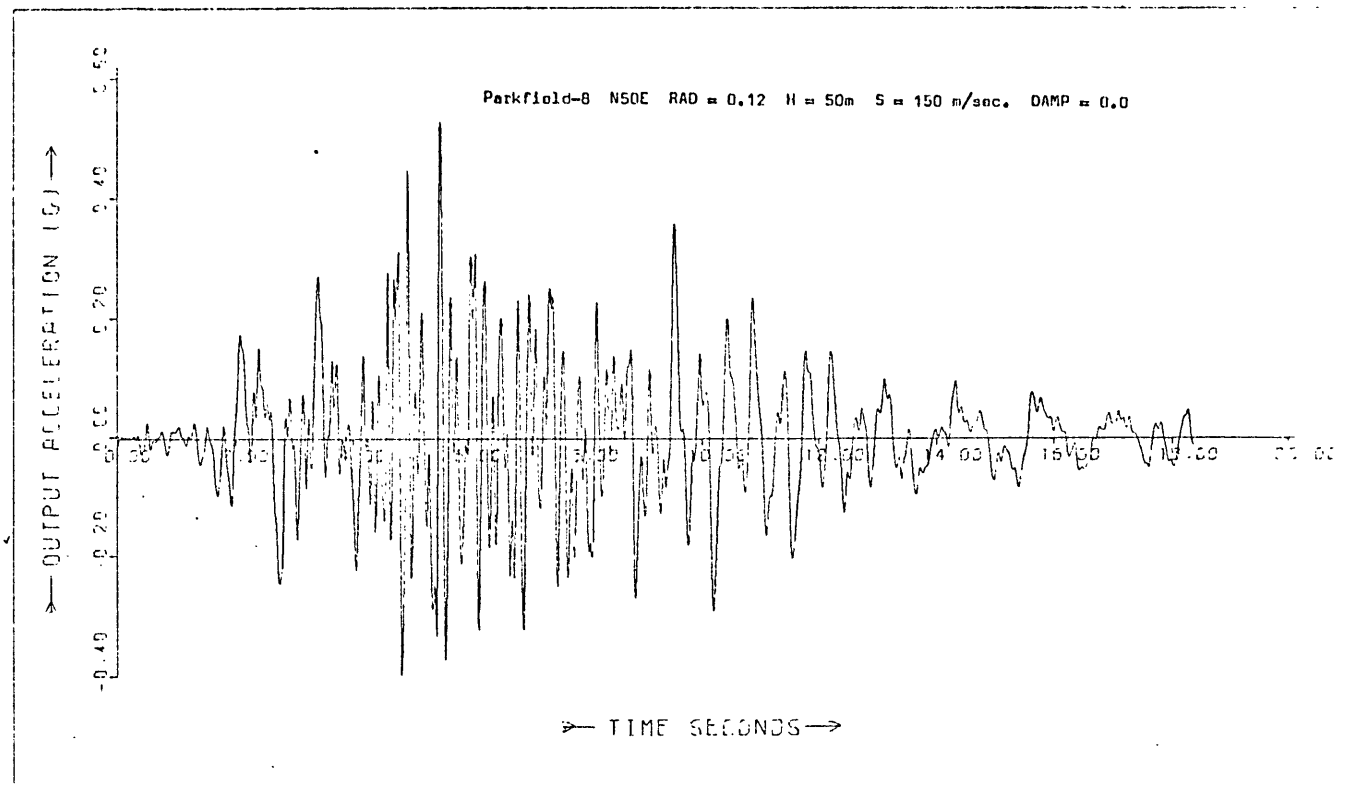


FIG.6.23 COMPUTED GROUND SURFACE ACCELERATION TIME HISTORY AT SITE NO. 6.19

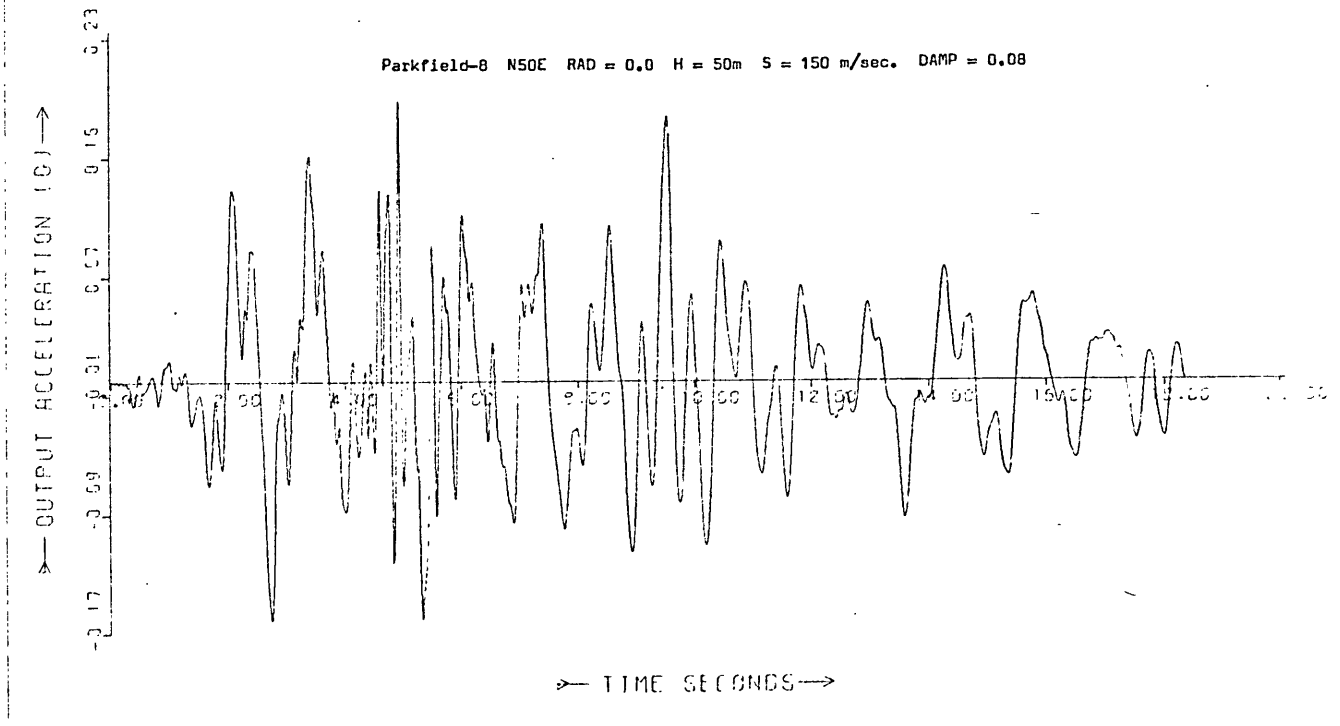


FIG.6.24a COMPUTED GROUND SURFACE ACCELERATION TIME HISTORY AT SITE NO. 6.20

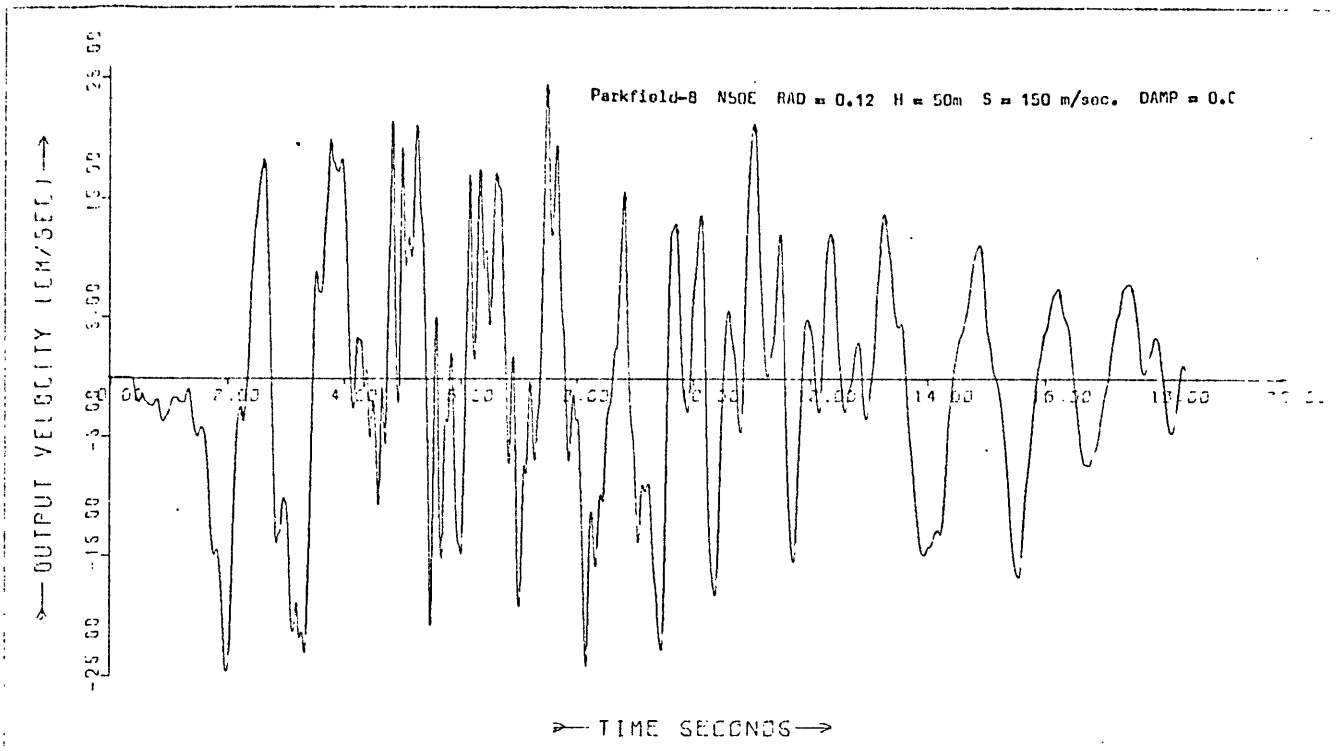


FIG.6.23b COMPUTED GROUND SURFACE VELOCITY TIME HISTORY AT SITE NO. 6.19

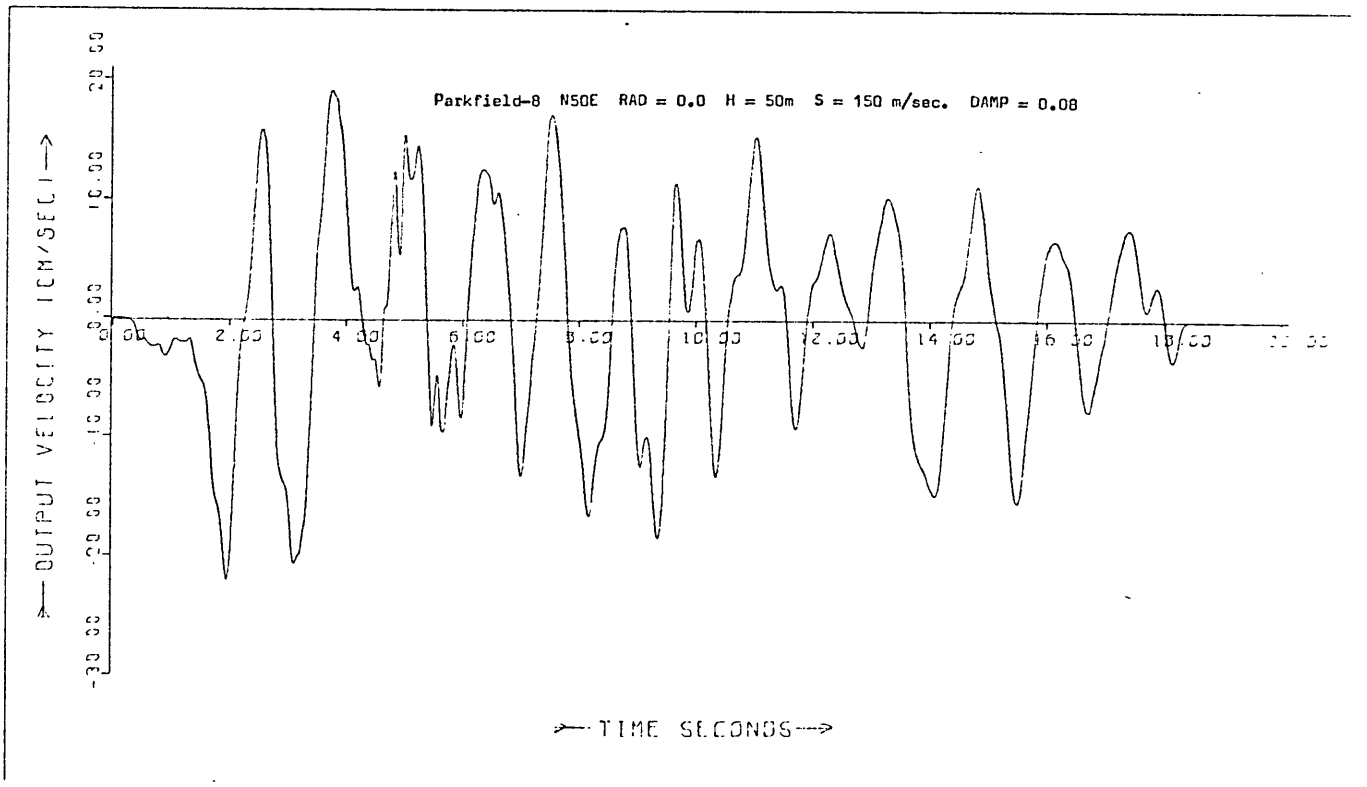


FIG.6.24b COMPUTED GROUND SURFACE VELOCITY TIME HISTORY AT SITE NO. 6.20

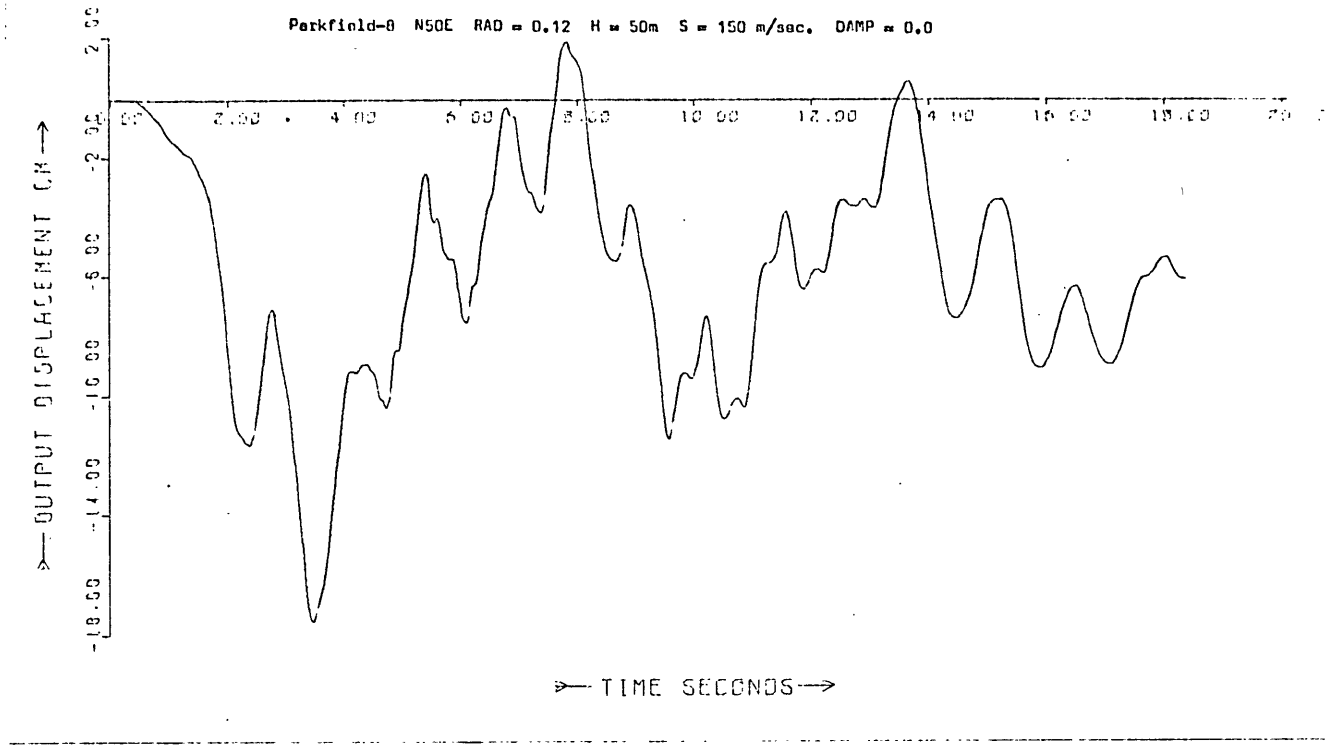


FIG. 6.23c COMPUTED GROUND SURFACE DISPLACEMENT TIME HISTORY AT SITE NO. 6.19

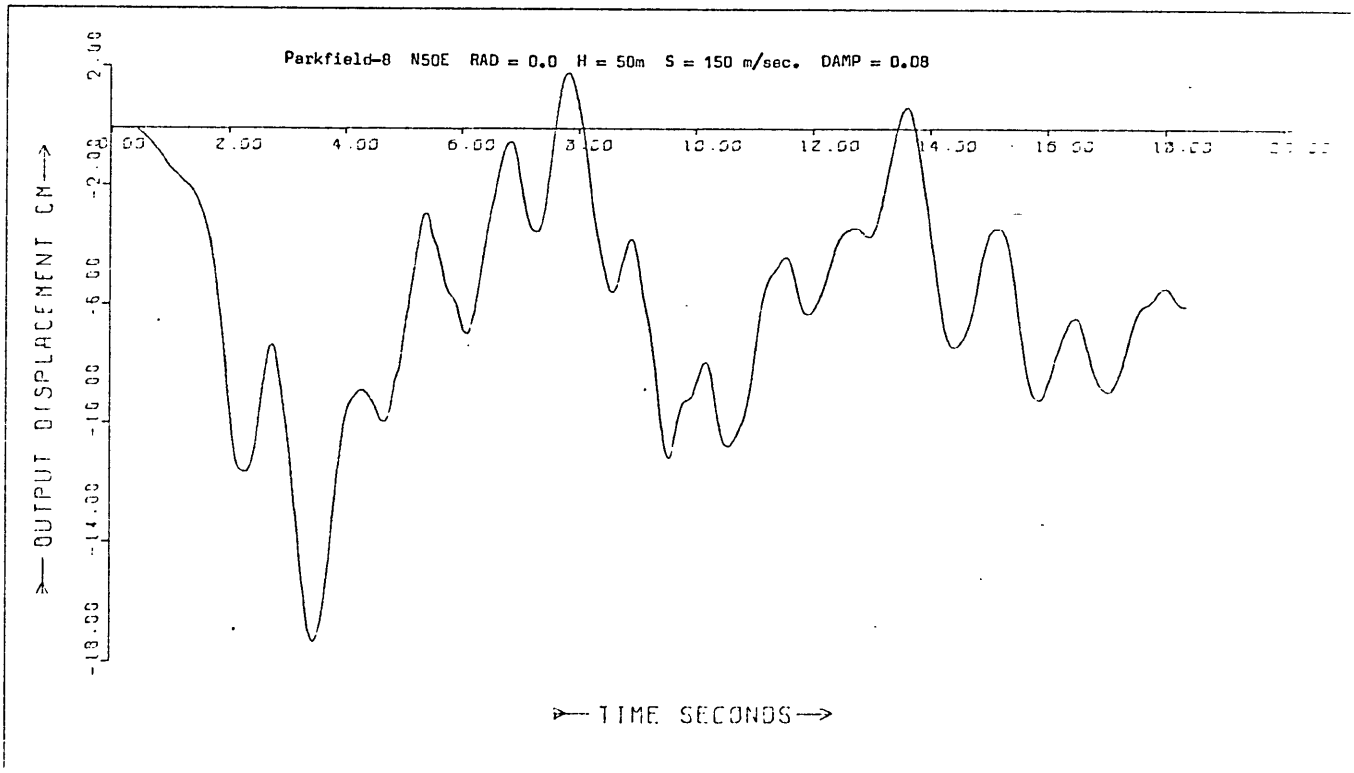


FIG. 6.24c COMPUTED GROUND SURFACE DISPLACEMENT TIME HISTORY AT SITE NO. 6.20

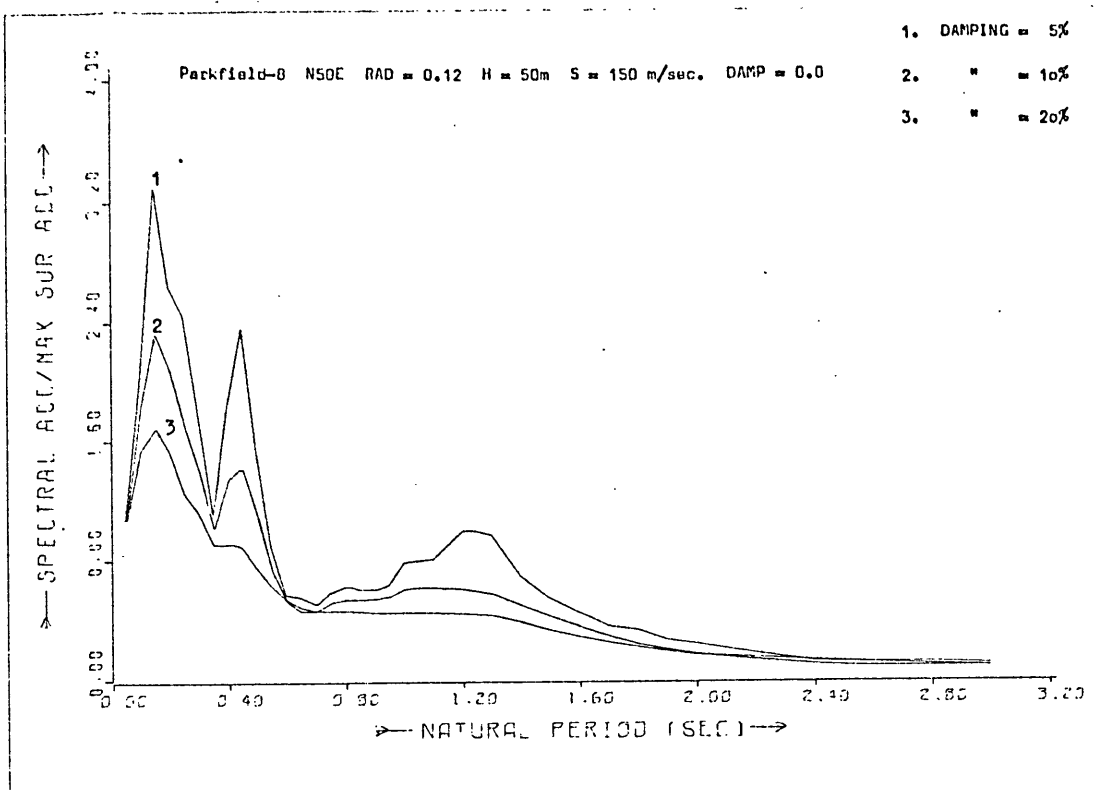


FIG.6.23d COMPUTED GROUND SURFACE ACCELERATION RESPONSE SPECTRA AT SITE NO. 6.19

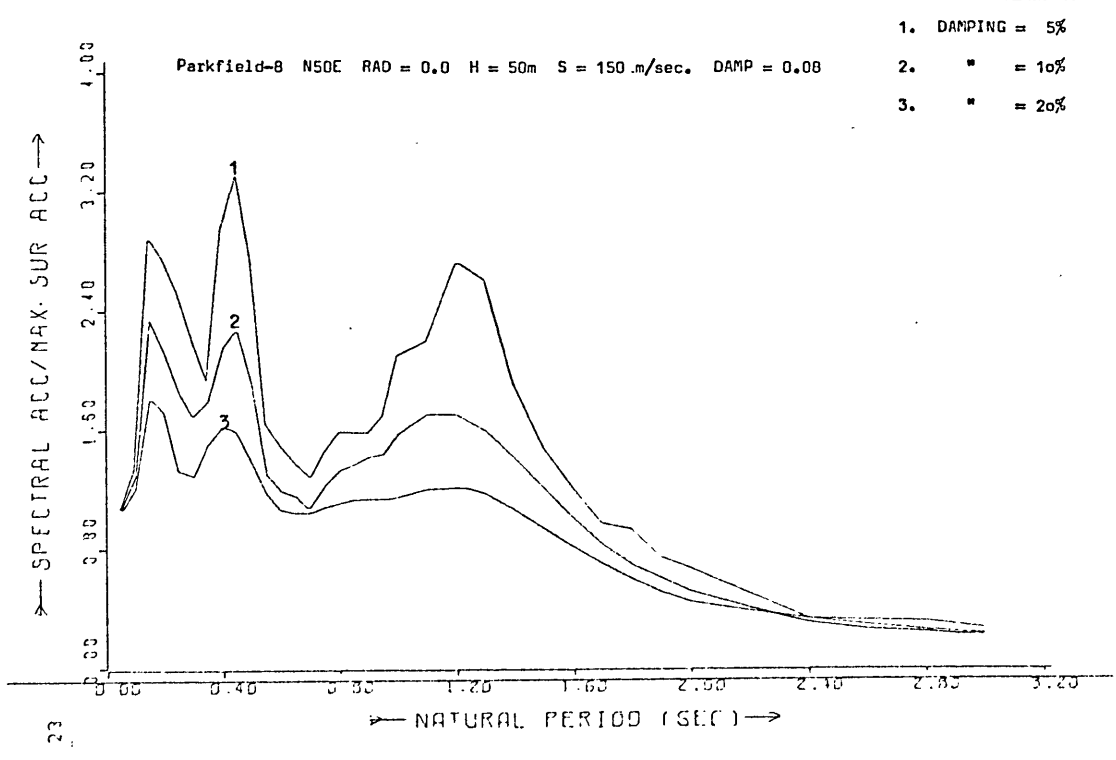


FIG.6.24d COMPUTED GROUND SURFACE ACCELERATION RESPONSE SPECTRA AT SITE NO.6.20

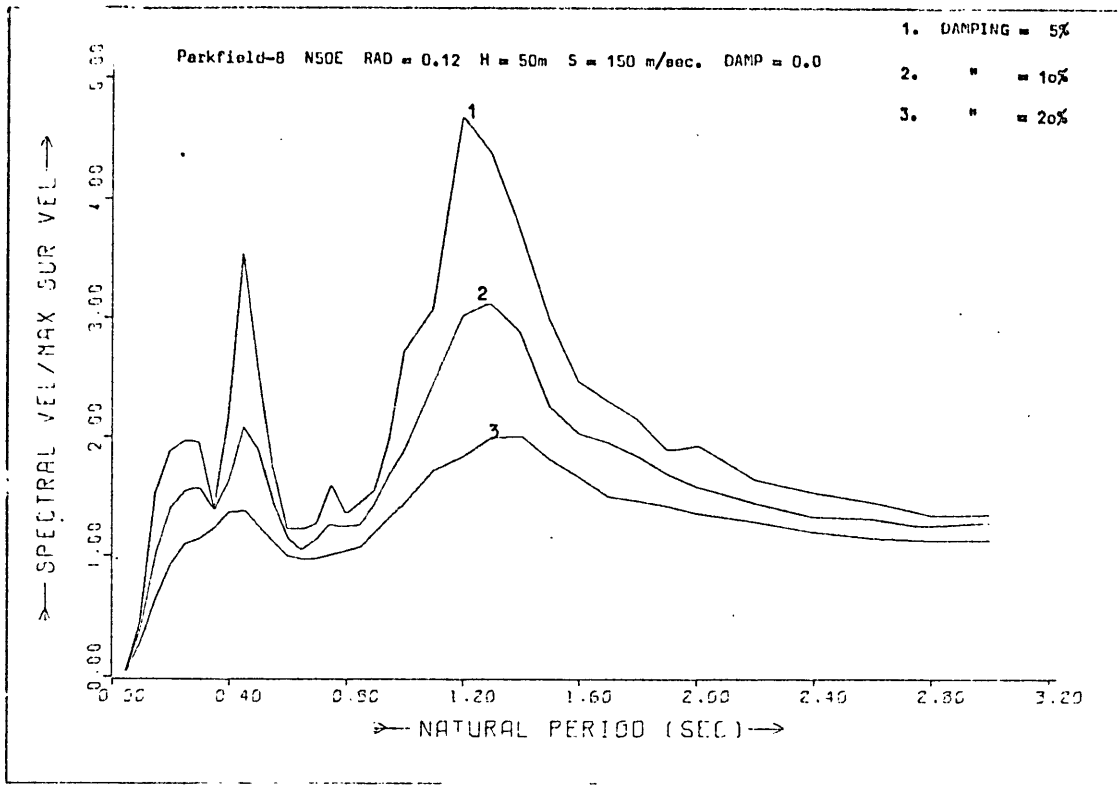


FIG.6.23e COMPUTED GROUND SURFACE VELOCITY RESPONSE SPECTRA AT SITE NO. 6.19

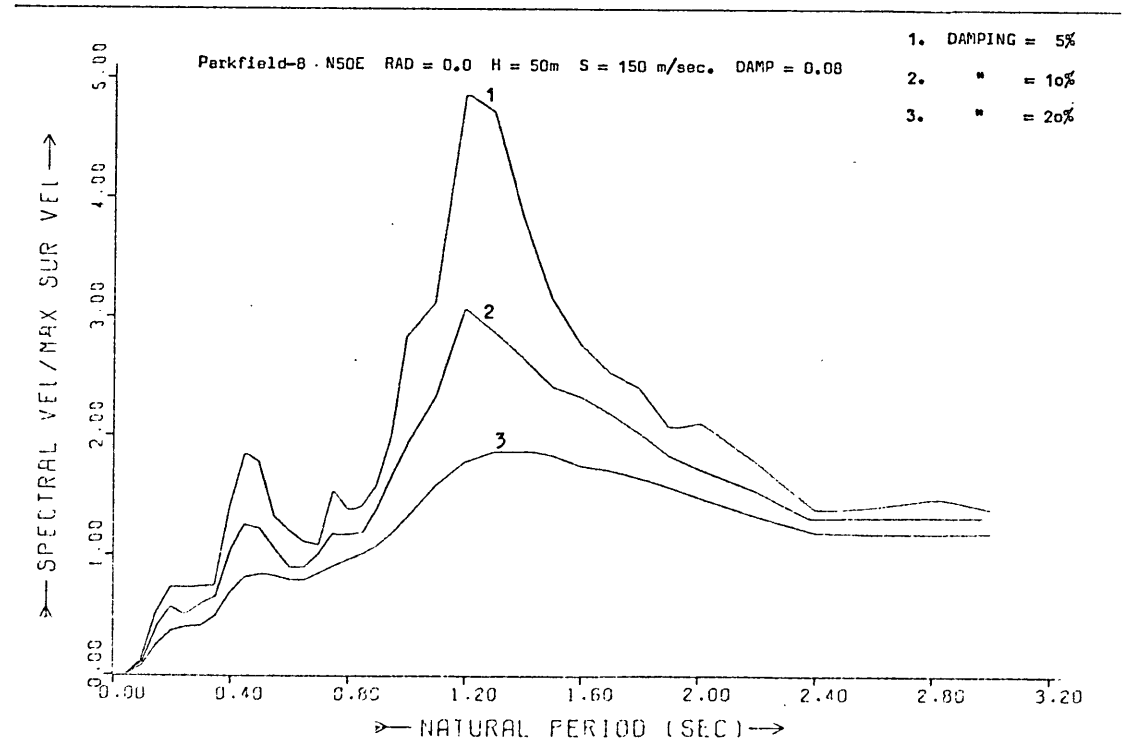


FIG6.24e COMPUTED GROUND SURFACE VELOCITY RESPONSE SPECTRA AT SITE NO.6.20

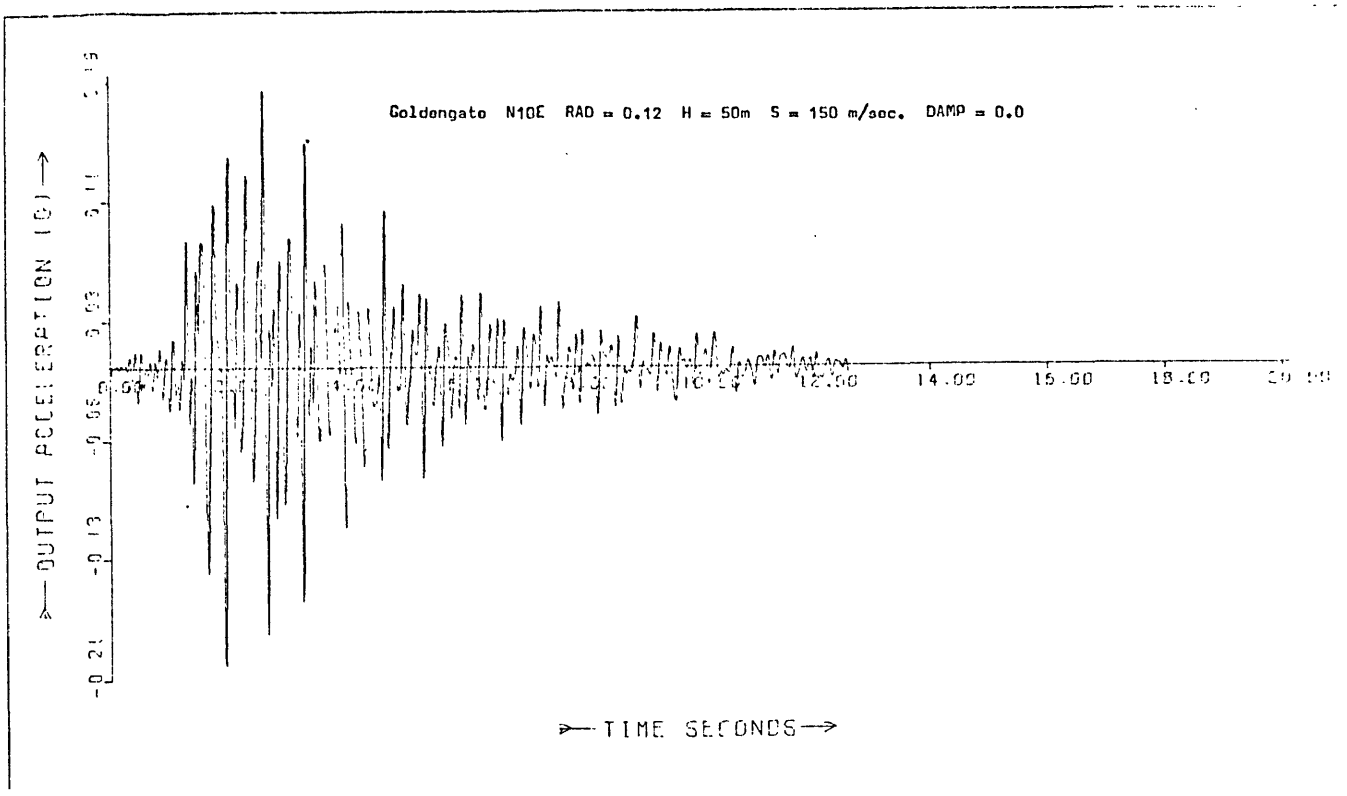


FIG6.25a COMPUTED GROUND SURFACE ACCELERATION TIME HISTORY AT SITE NO. 6.19

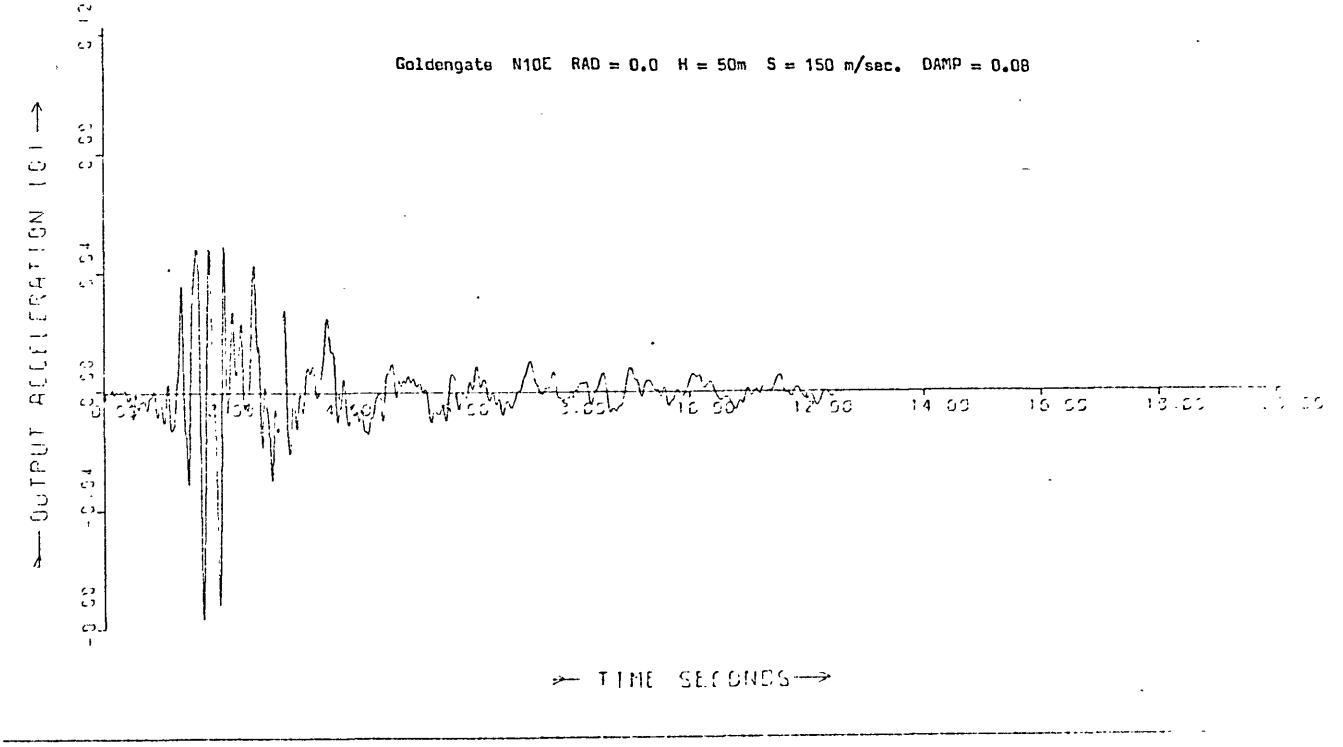


FIG.6.26a COMPUTED GROUND SURFACE ACCELERATION TIME HISTORY AT SITE NO. 6.20

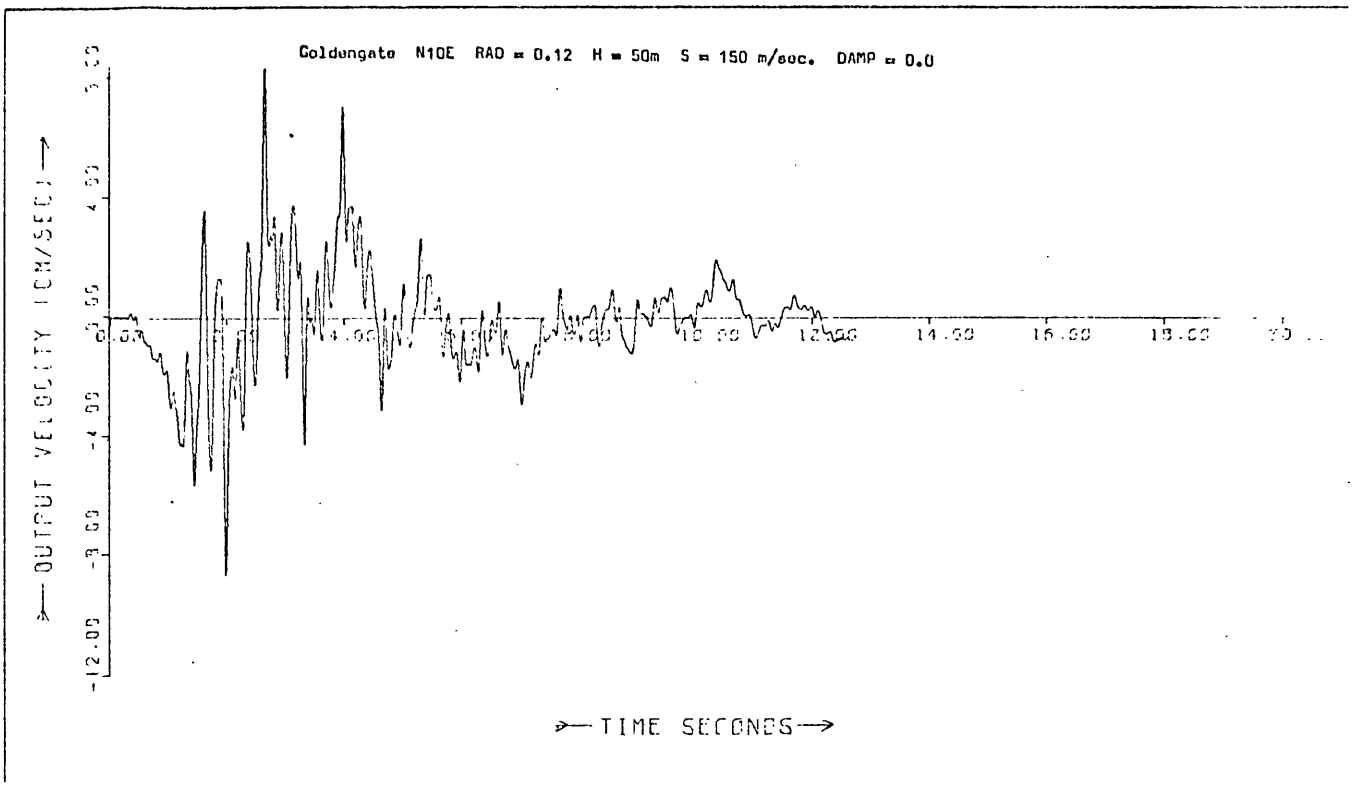


FIG6.25b COMPUTED GROUND SURFACE VELOCITY TIME HISTORY AT SITE NO. 6.19

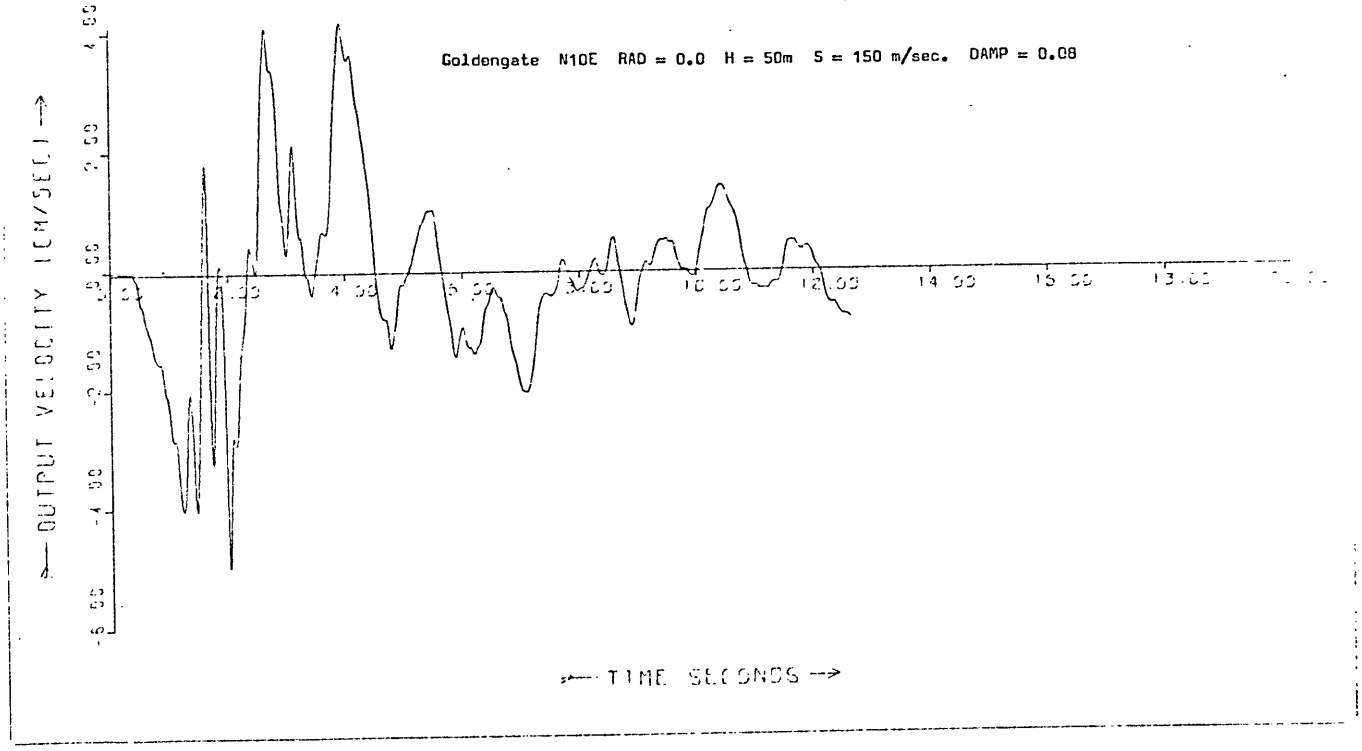


FIG.6.26b COMPUTED GROUND SURFACE VELOCITY TIME HISTORY AT SITE NO. 6.20

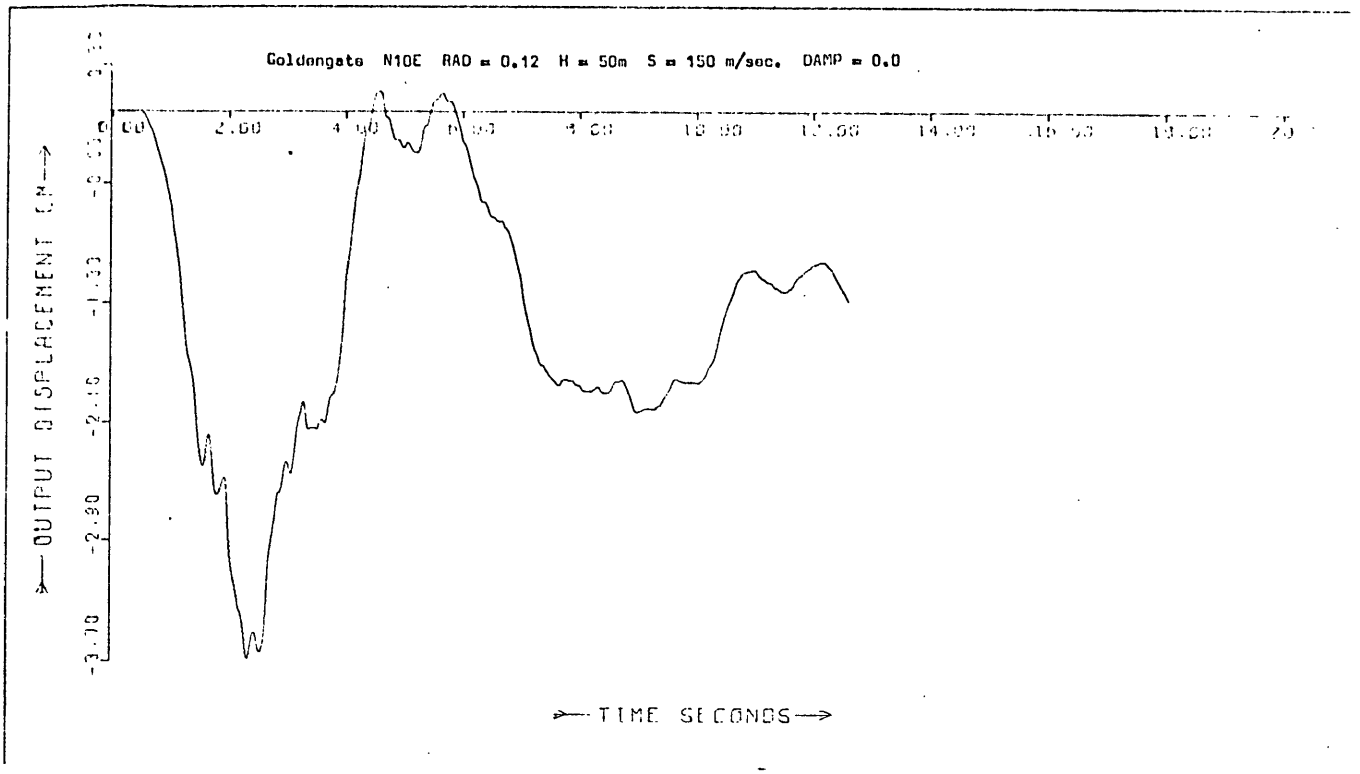


FIG. 6.25 COMPUTED GROUND SURFACE DISPLACEMENT TIME HISTORY AT SITE NO. 6.19

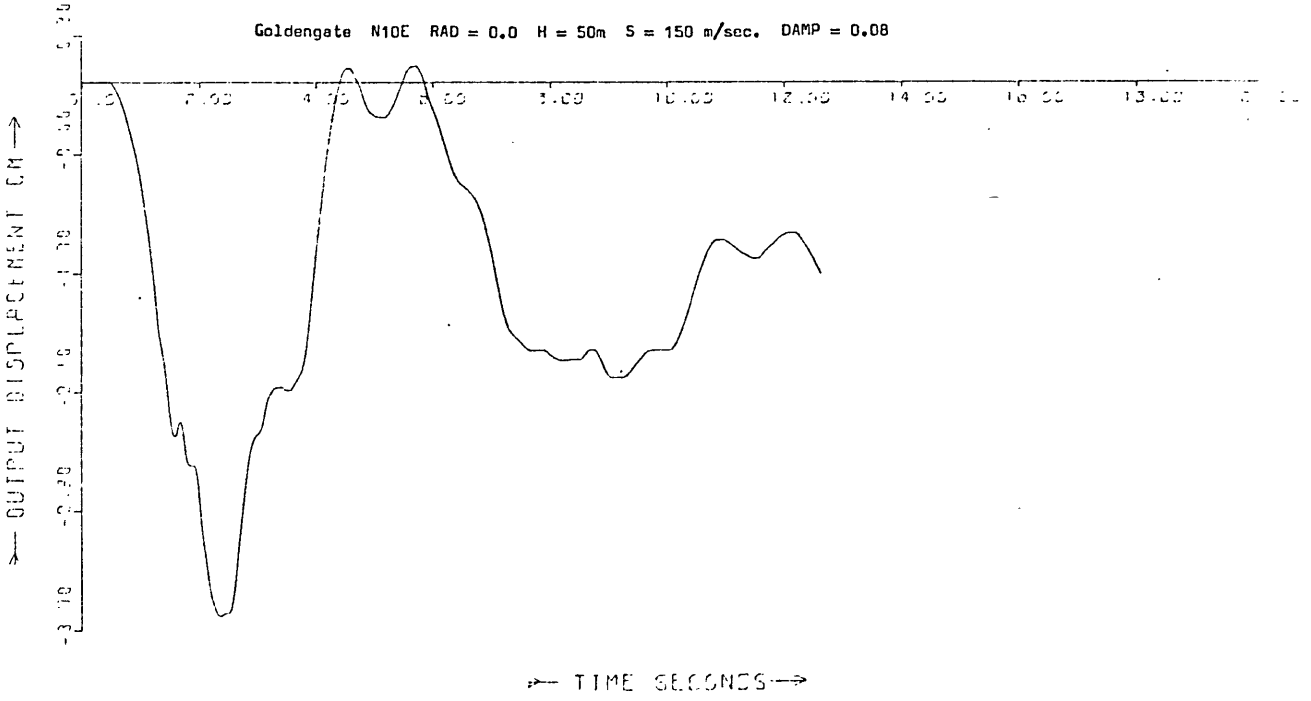


FIG. 6.26 COMPUTED GROUND SURFACE DISPLACEMENT TIME HISTORY AT SITE NO. 6.20

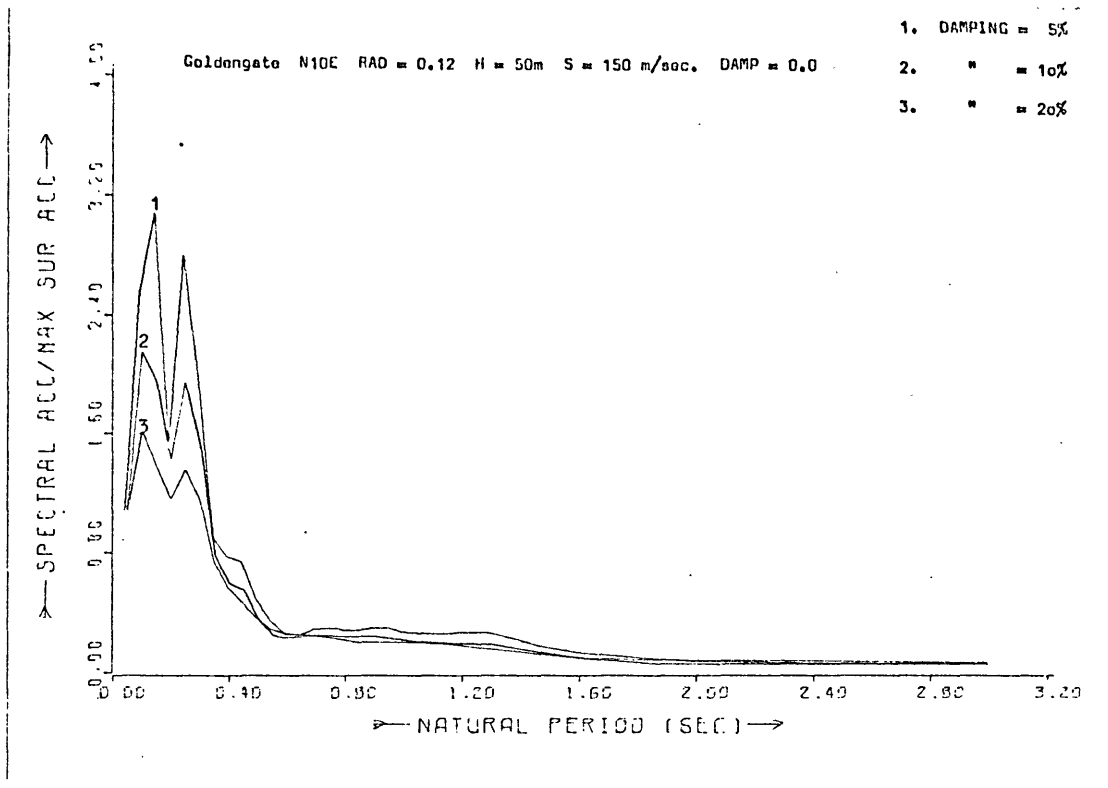


FIG 6.25d COMPUTED GROUND SURFACE ACCELERATION RESPONSE SPECTRA AT SITE NO. 6.19

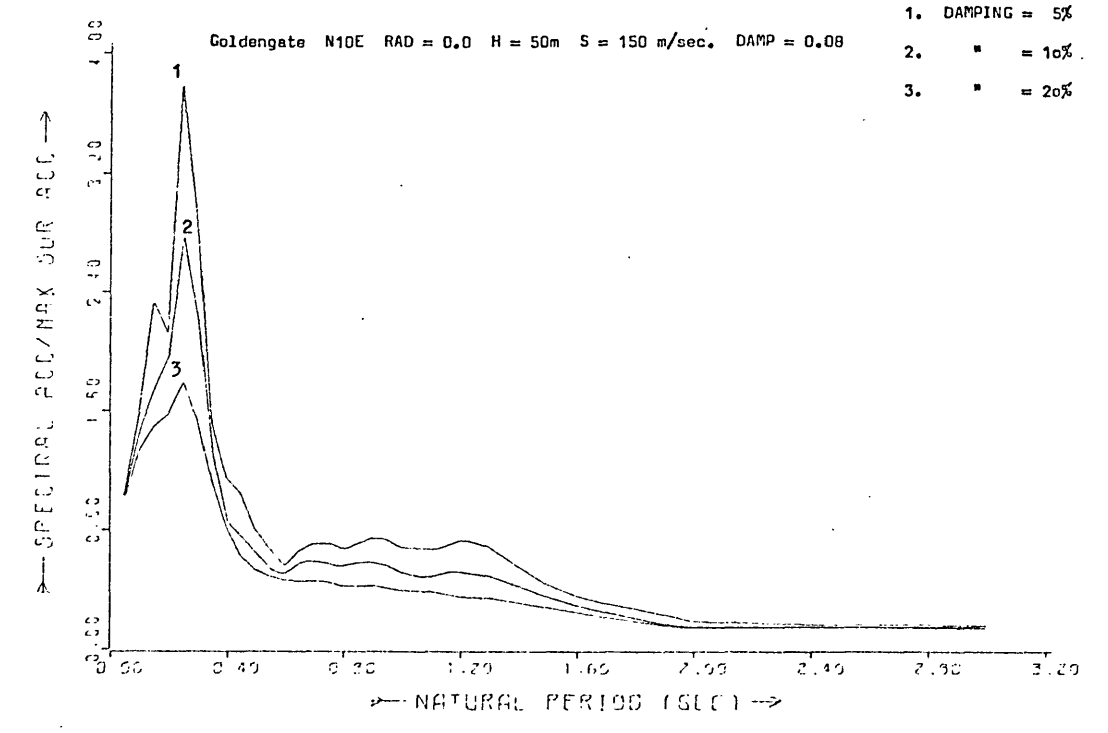


FIG.6.26d COMPUTED GROUND SURFACE ACCELERATION RESPONSE SPECTRA AT SITE NO. 6.20

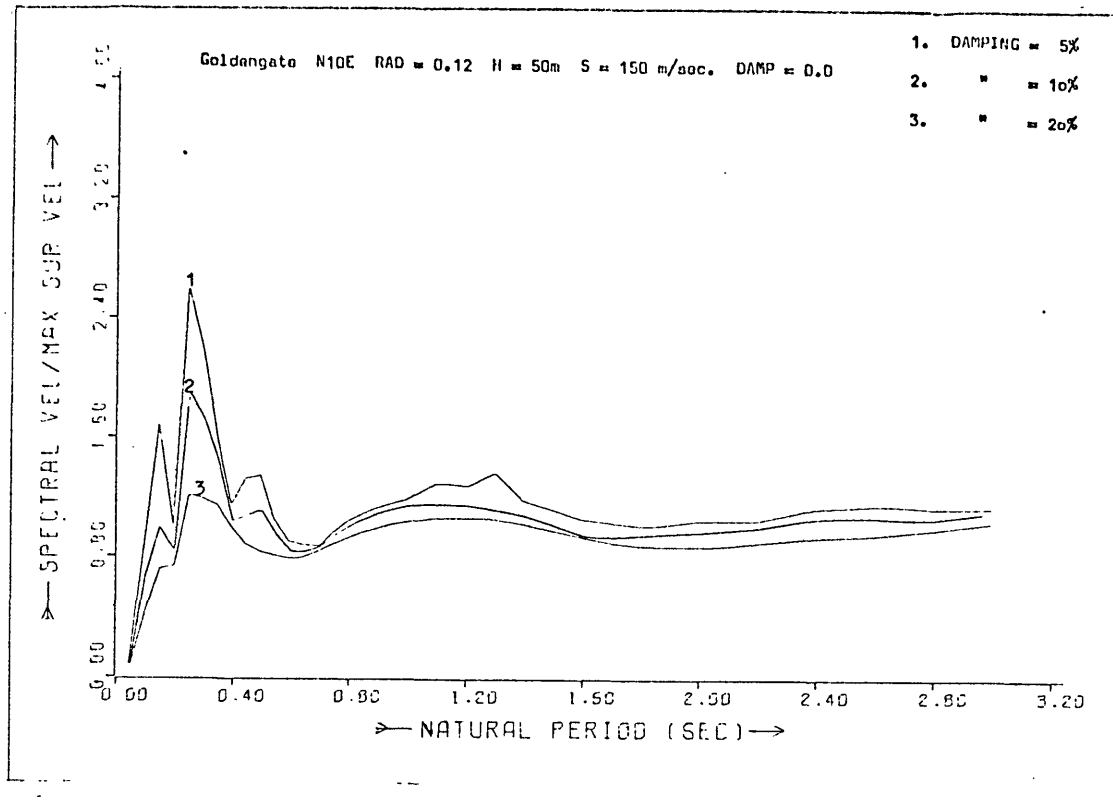


FIG.6.25eCOMPUTED GROUND SURFACE DISPLACEMENT RESPONSE SPECTRA AT SITE NO. 6.19

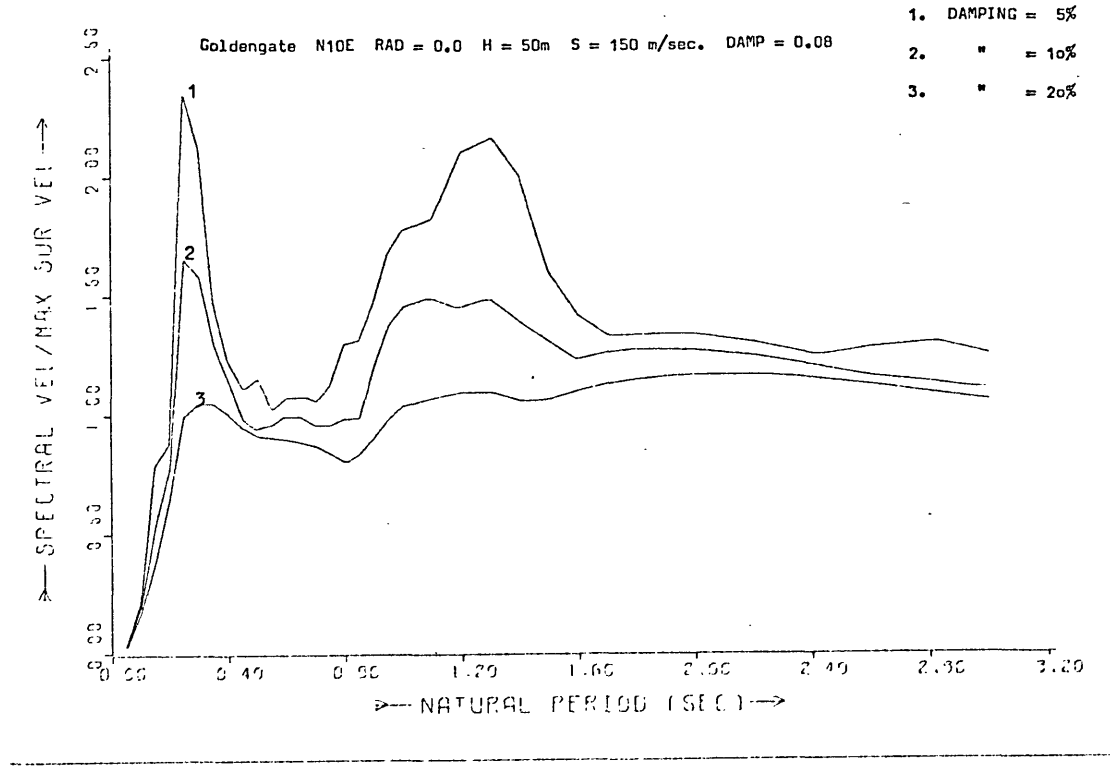


FIG.6.26eCOMPUTED GROUND SURFACE VELOCITY RESPONSE SPECTRA AT SITE NO. 6.2o

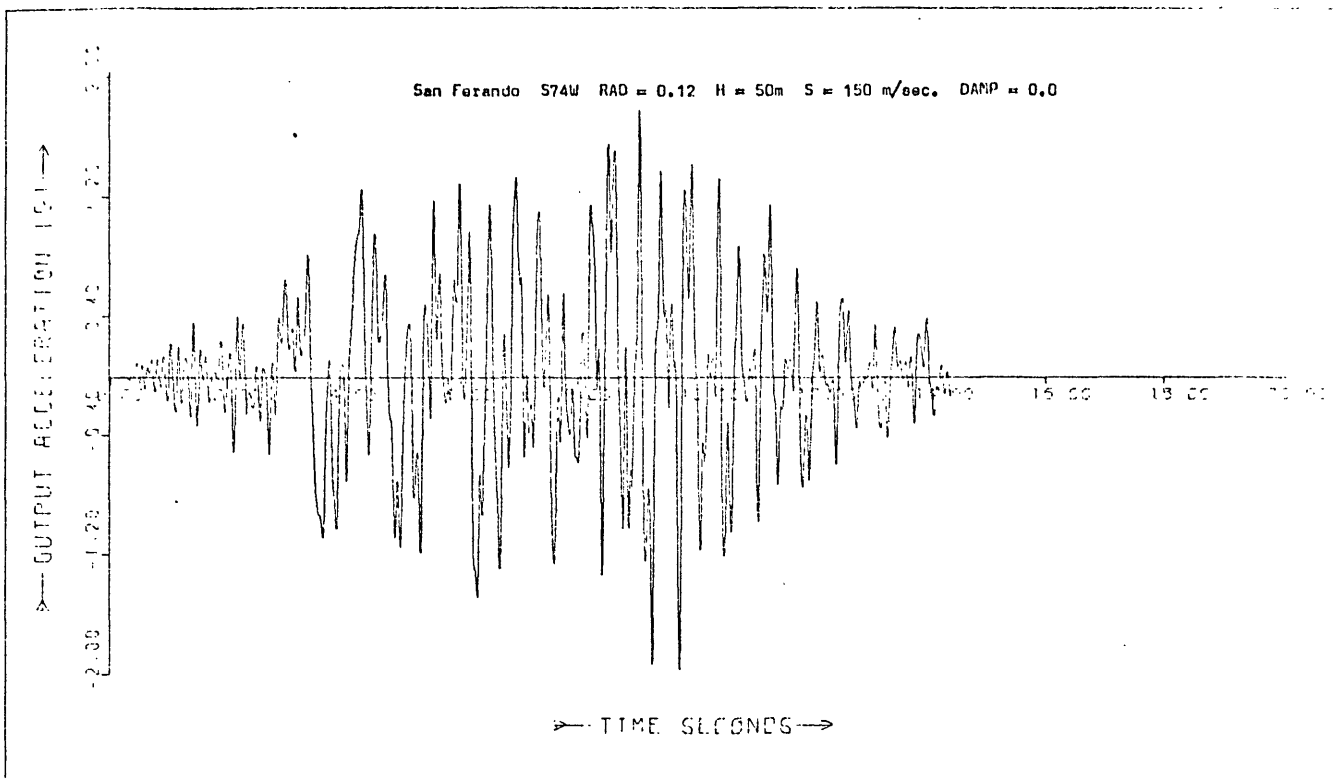


FIG. 6.27 COMPUTED GROUND SURFACE ACCELERATION TIME HISTORY AT SITE NO. 6.19

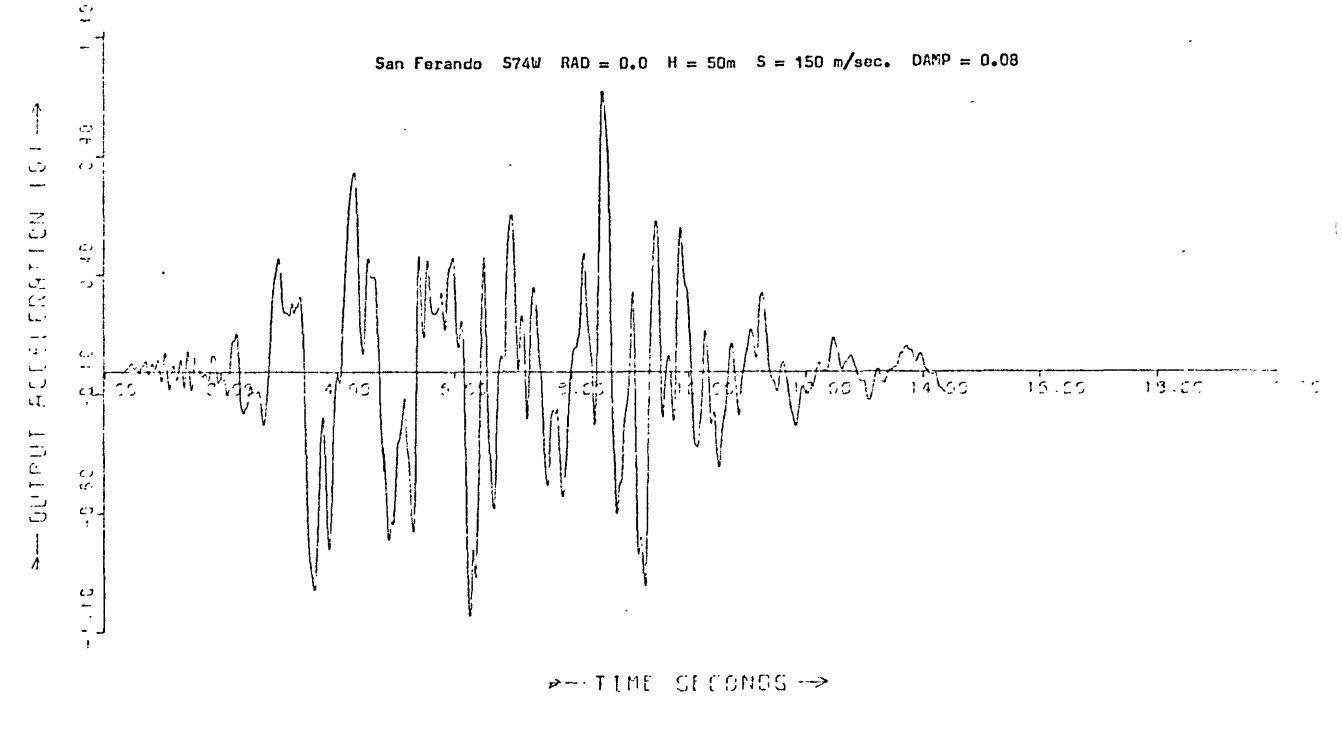


FIG. 6.28 COMPUTED GROUND SURFACE ACCELERATION TIME HISTORY AT SITE NO. 6.20

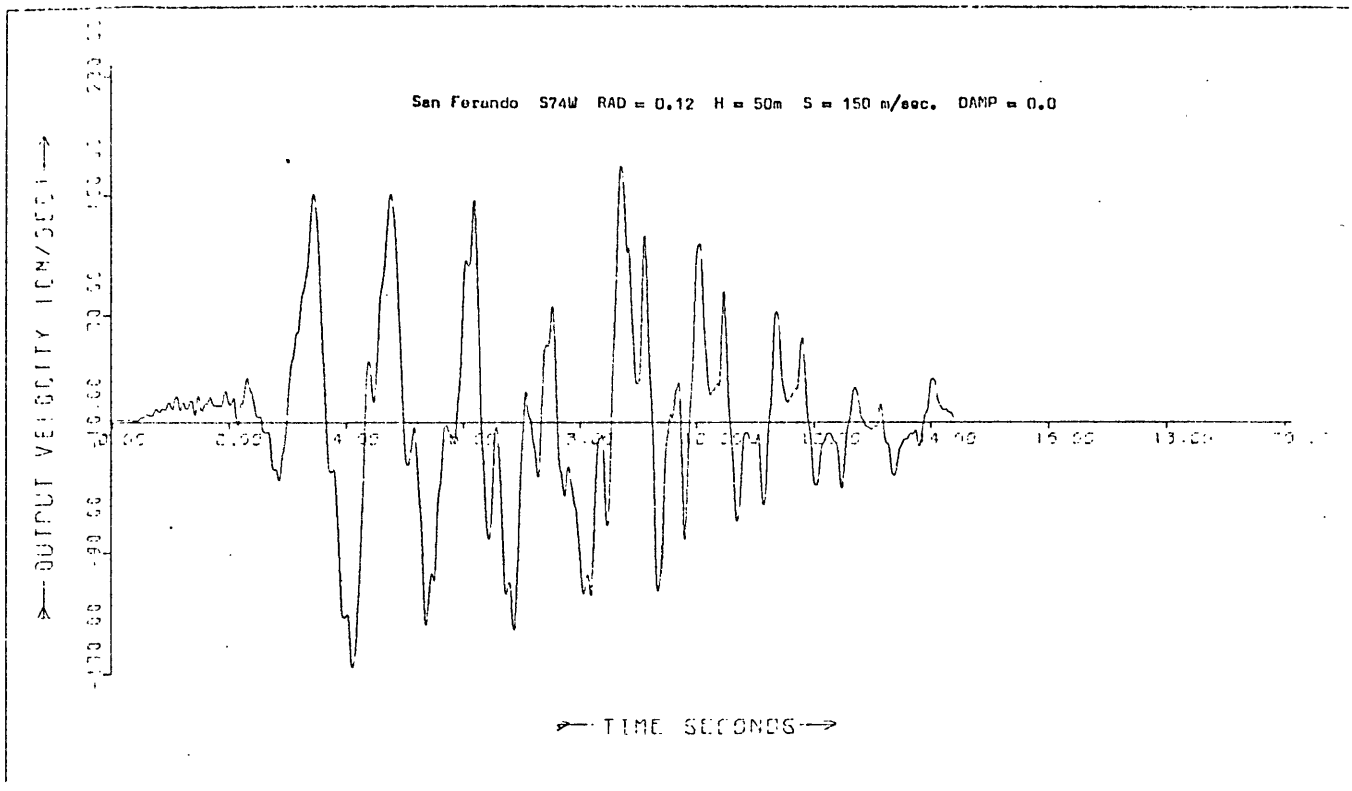


FIG 6.27b COMPUTED GROUND SURFACE VELOCITY TIME HISTORY AT SITE NO. 6.19

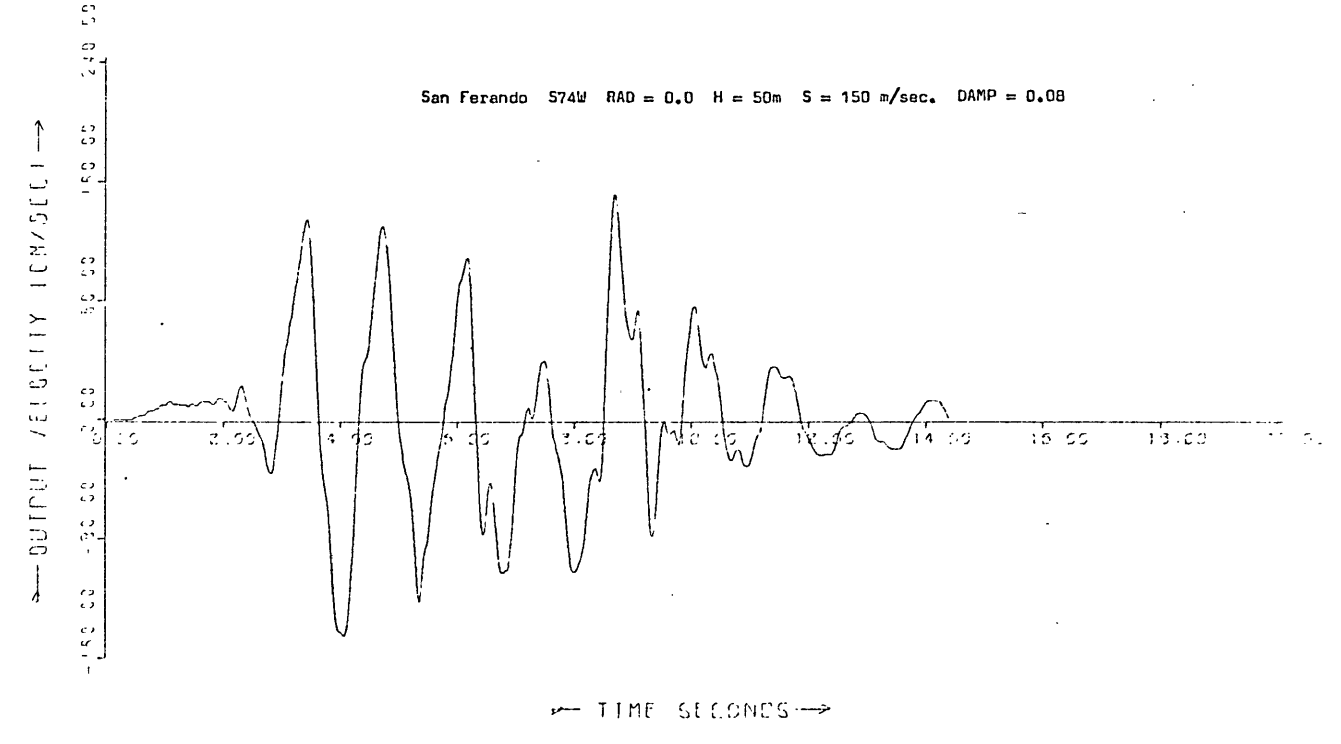


FIG 6.28b COMPUTED GROUND SURFACE VELOCITY TIME HISTORY AT SITE NO. 6.20

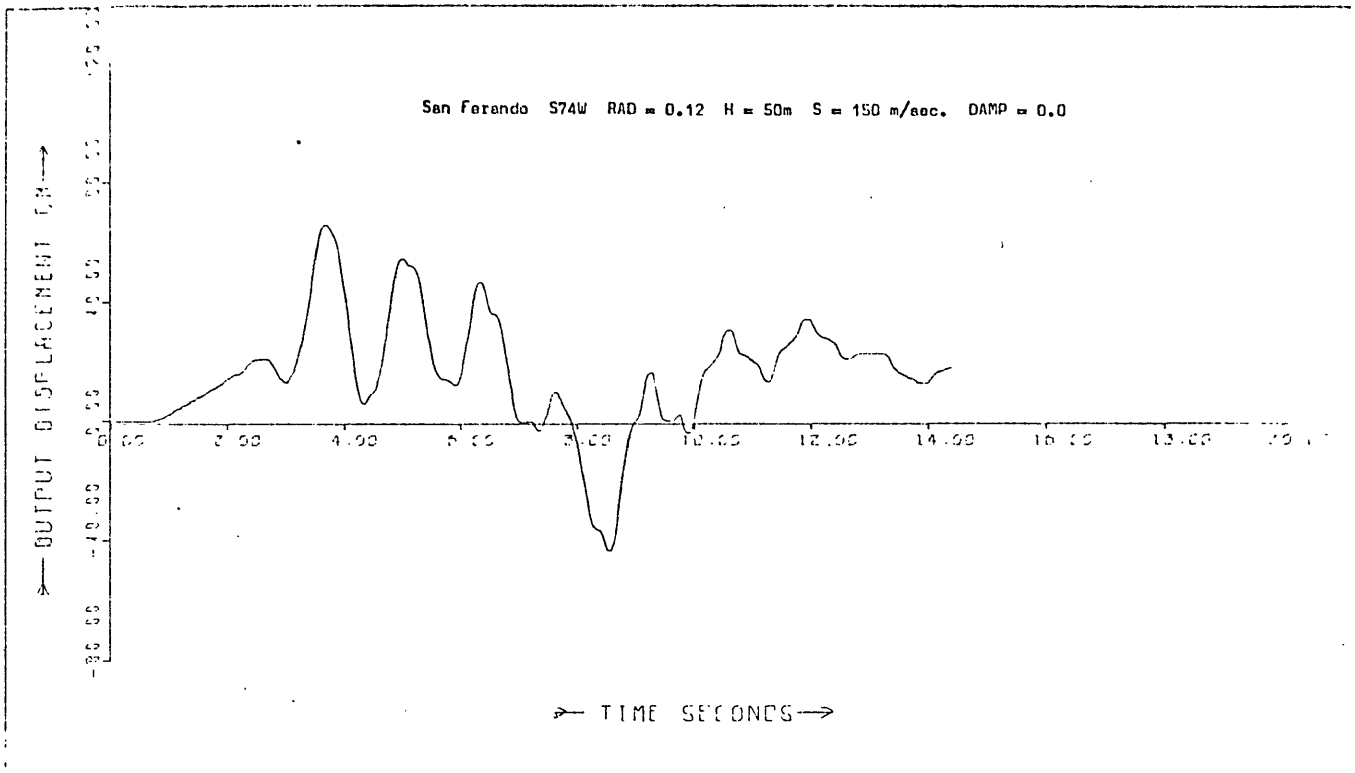


FIG 6.27c COMPUTED GROUND SURFACE DISPLACEMENT TIME HISTORY AT SITE NO. 6.19

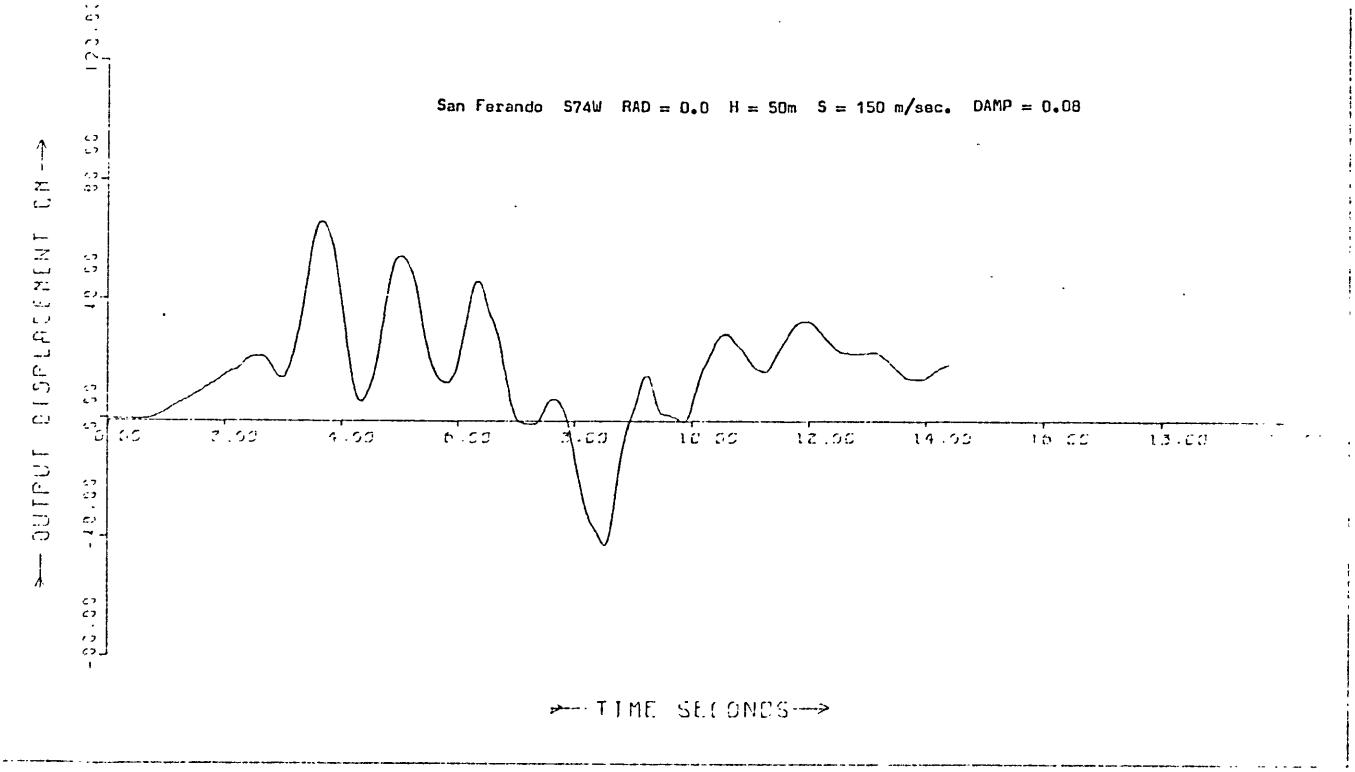


FIG.6.28c COMPUTED GROUND SURFACE DISPLACEMENT TIME HISTORY AT SITE NO. 6.20

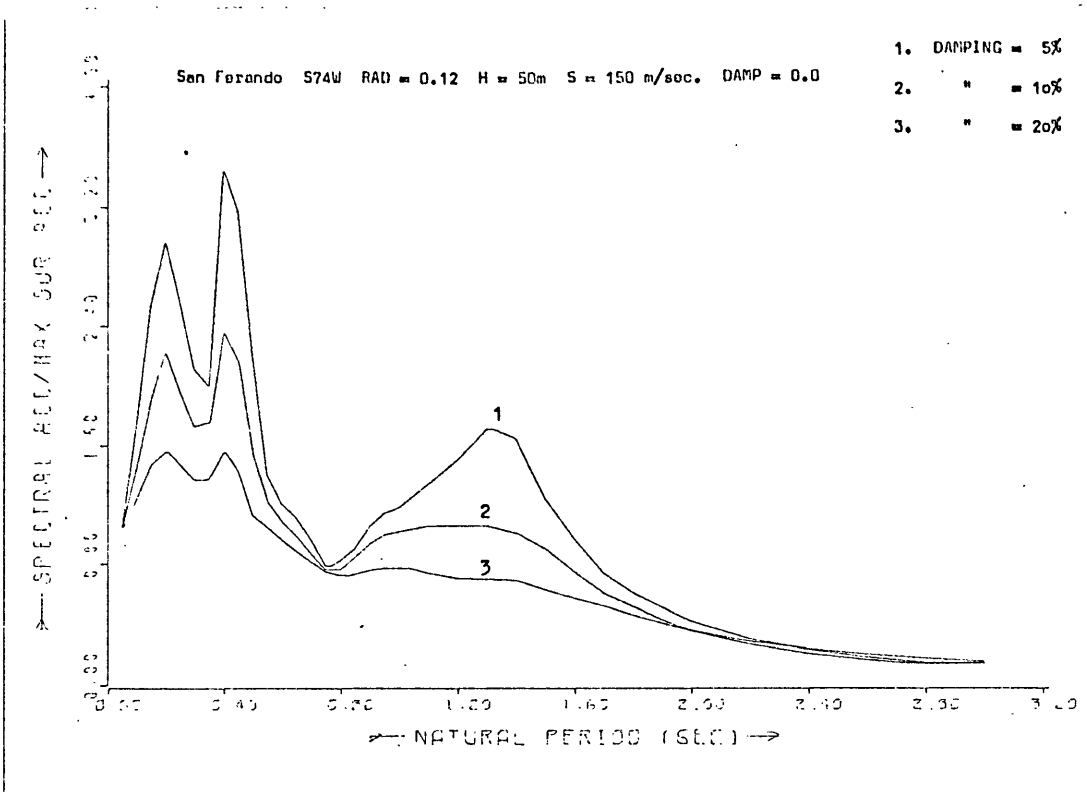


FIG.6.27dCOMPUTED GROUND SURFACE ACCELERATION RESPONSE SPECTRA AT SITE NO.6.19

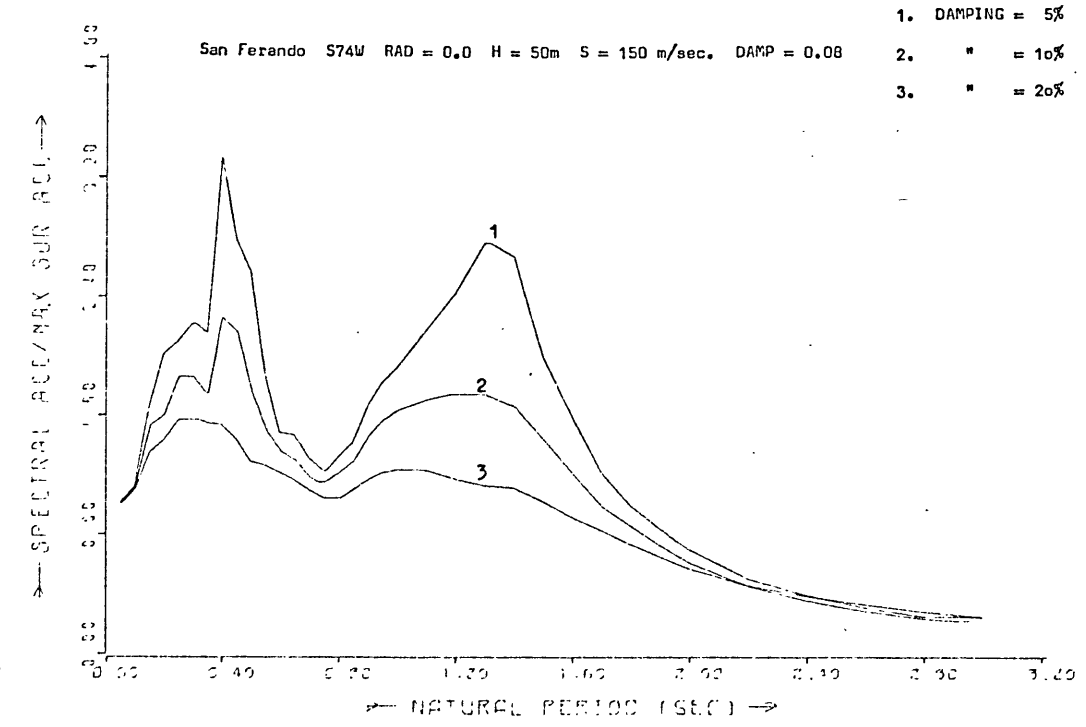


FIG.6.28dCOMPUTED GROUND SURFACE ACCELERATION RESPONSE SPECTRA AT SITE NO.6.20

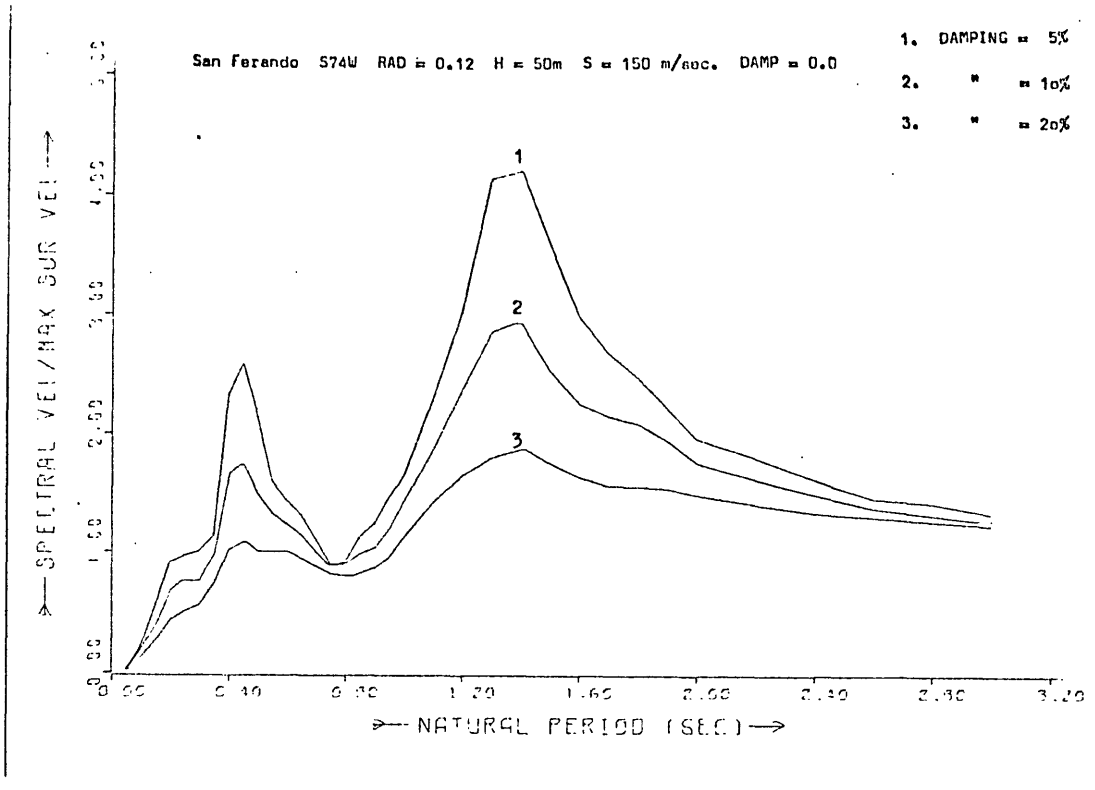


FIG.6.27e COMPUTED GROUND SURFACE VELOCITY RESPONSE SPECTRA AT SITE NO. 6.19

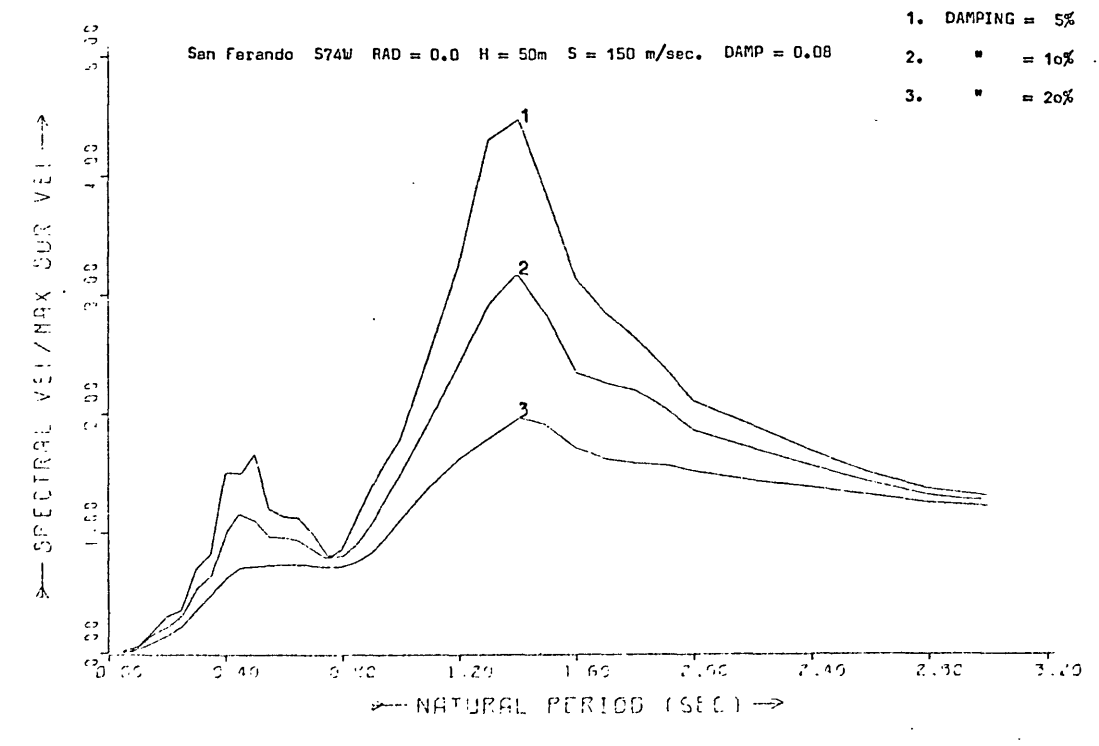


FIG.6.28e COMPUTED GROUND SURFACE VELOCITY RESPONSE SPECTRA AT SITE NO.6.20

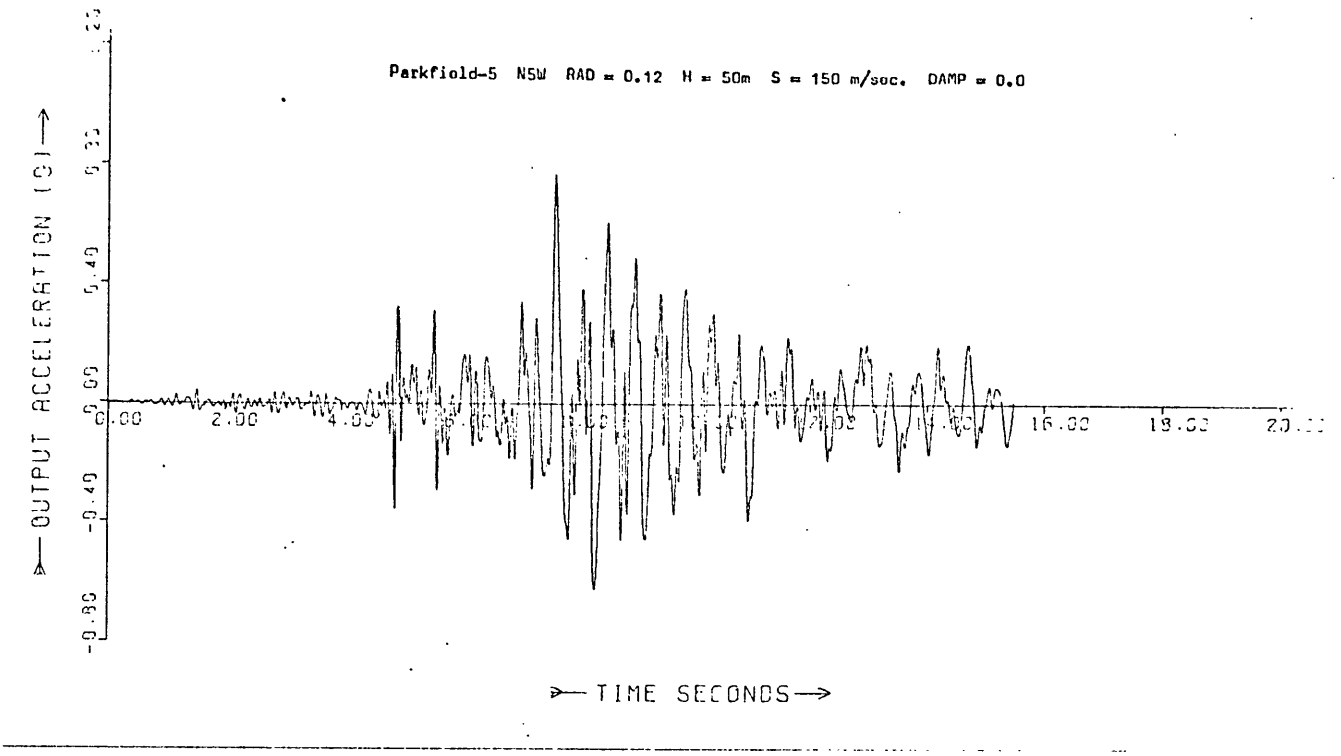


FIG.6.29a COMPUTED GROUND SURFACE ACCELERATION TIME HISTORY AT SITE NO. 6.19

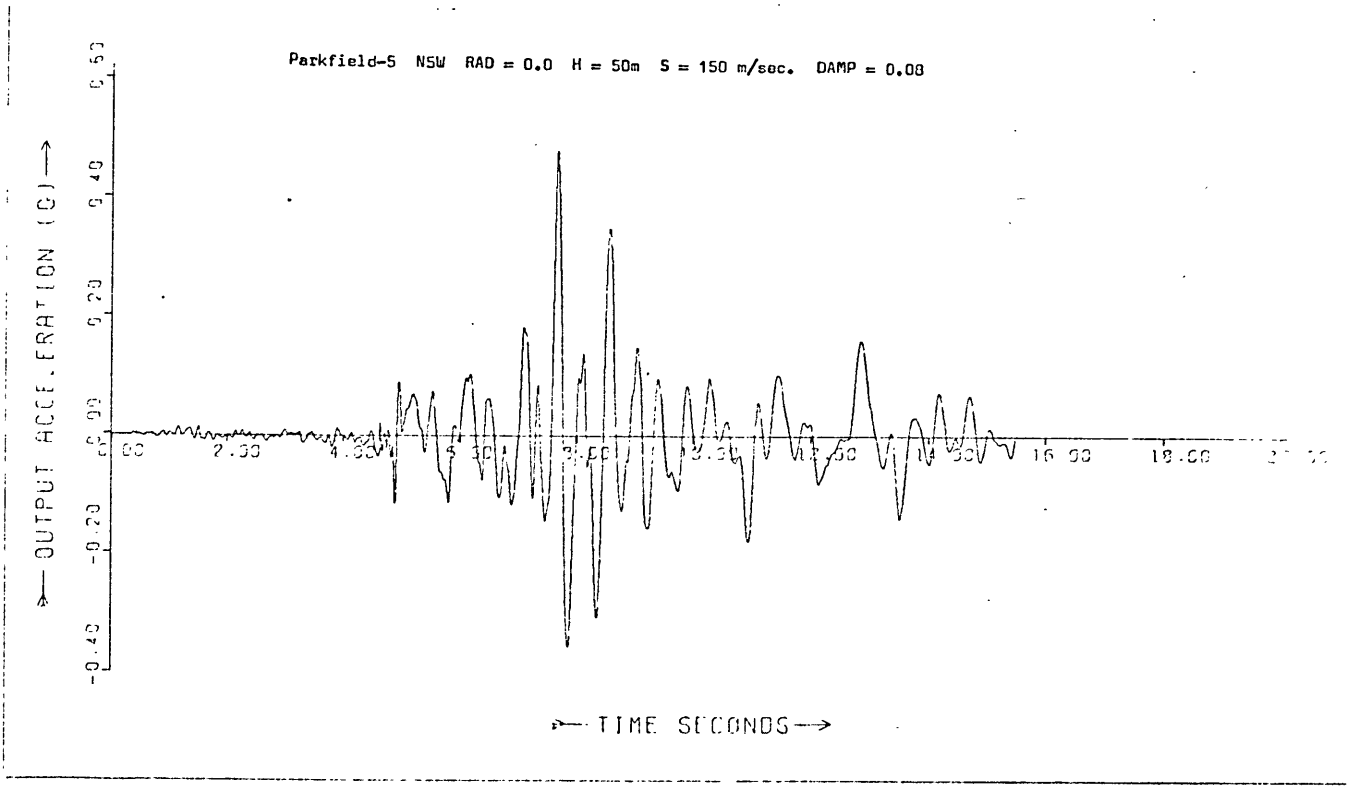


FIG.6.30a COMPUTED GROUND SURFACE ACCELERATION TIME HISTORY AT SITE NO. 6.20

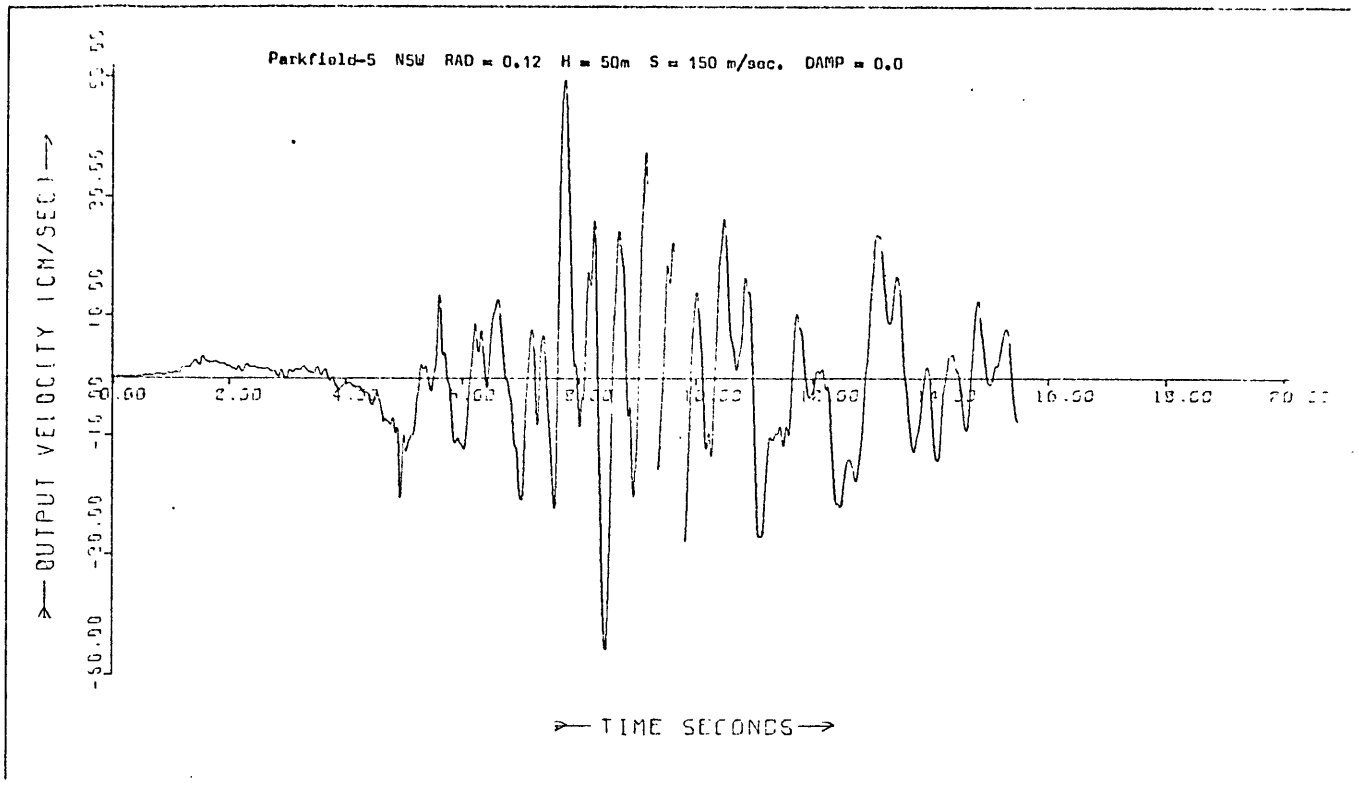


FIG.6.29b COMPUTED GROUND SURFACE VELOCITY TIME HISTORY AT SITE NO. 6.19

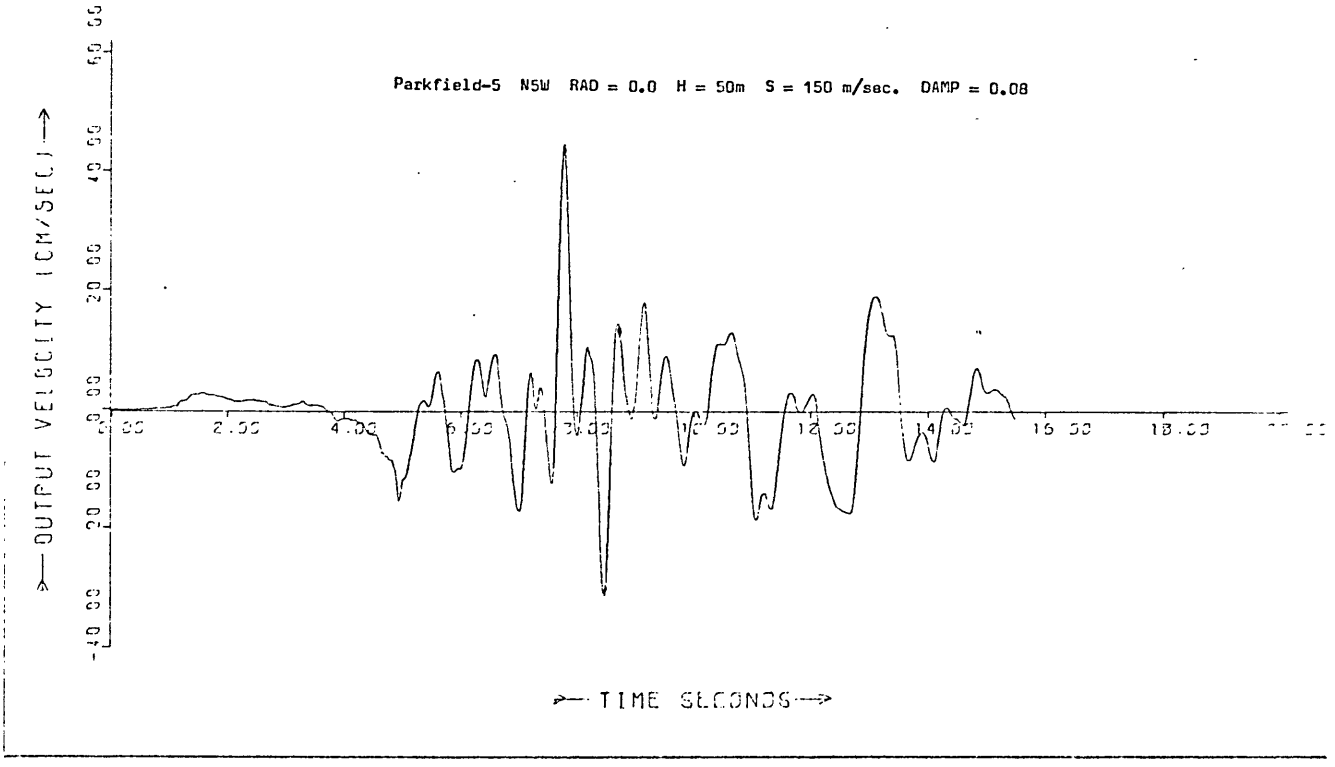


FIG.6.30b COMPUTED GROUND SURFACE VELOCITY TIME HISTORY AT SITE NO. 6.20

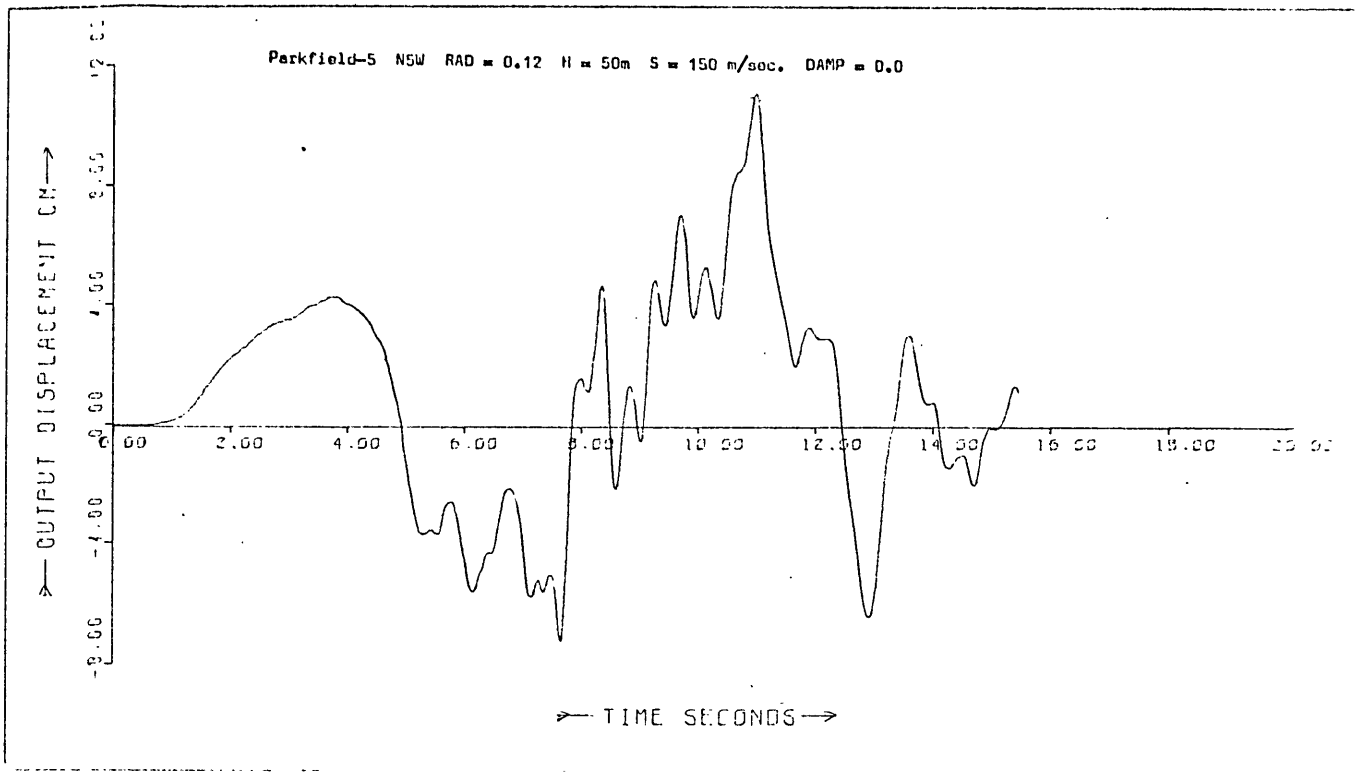


FIG. 6.29c COMPUTED GROUND SURFACE DISPLACEMENT TIME HISTORY AT SITE NO. 6.19

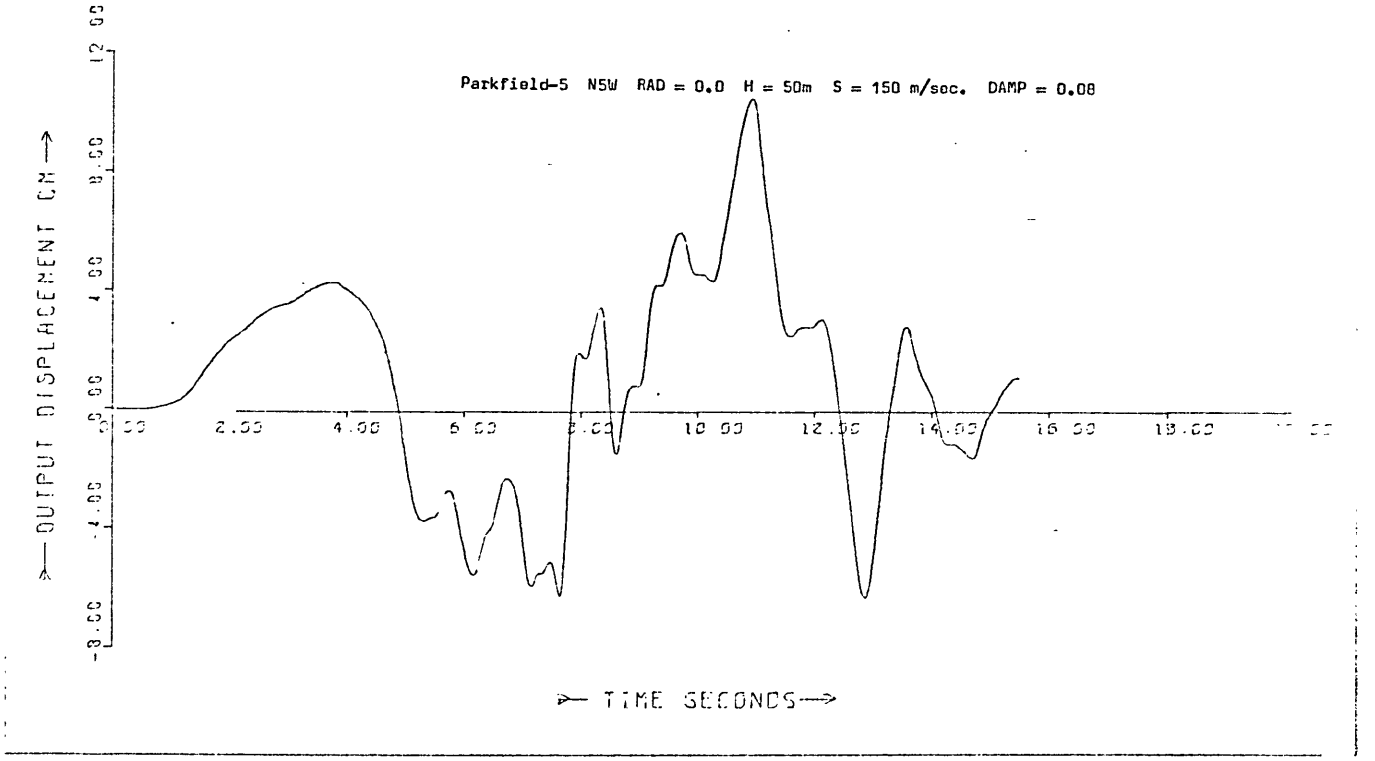


FIG 6.30c COMPUTED GROUND SURFACE DISPLACEMENT TIME HISTORY AT SITE NO. 6.20

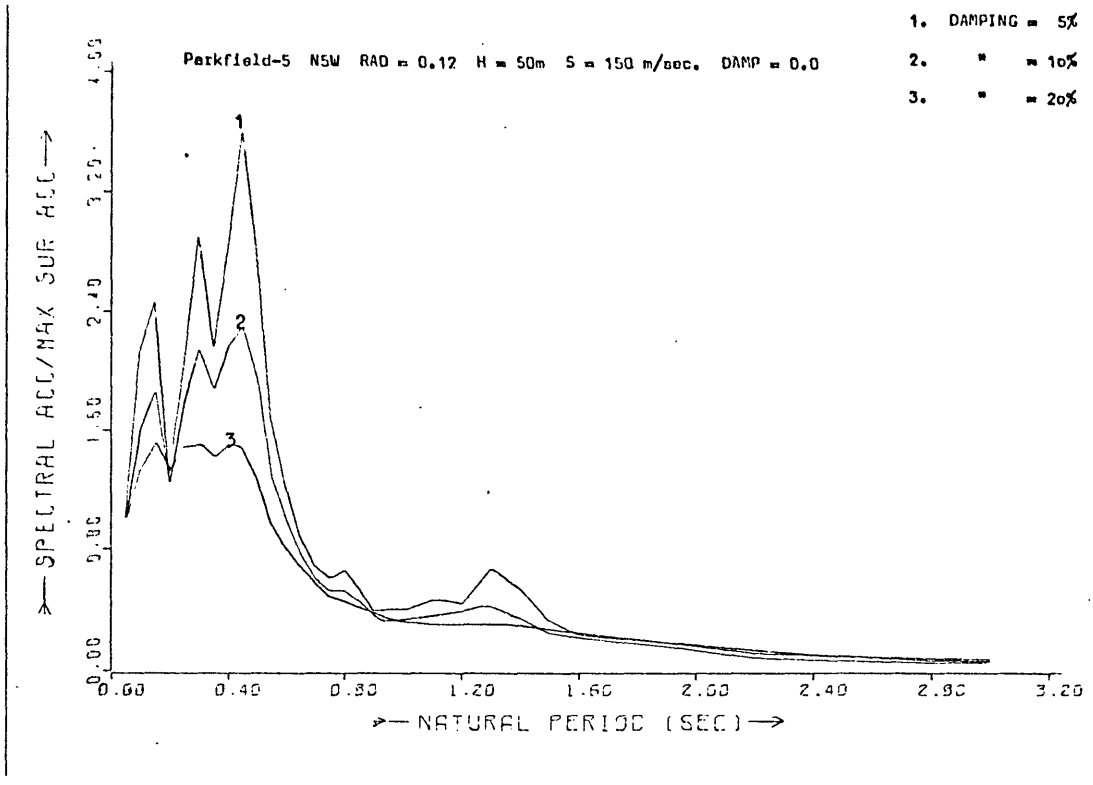


FIG.6.29d COMPUTED GROUND SURFACE ACCELERATION RESPONSE SPECTRA AT SITE NO.6.19

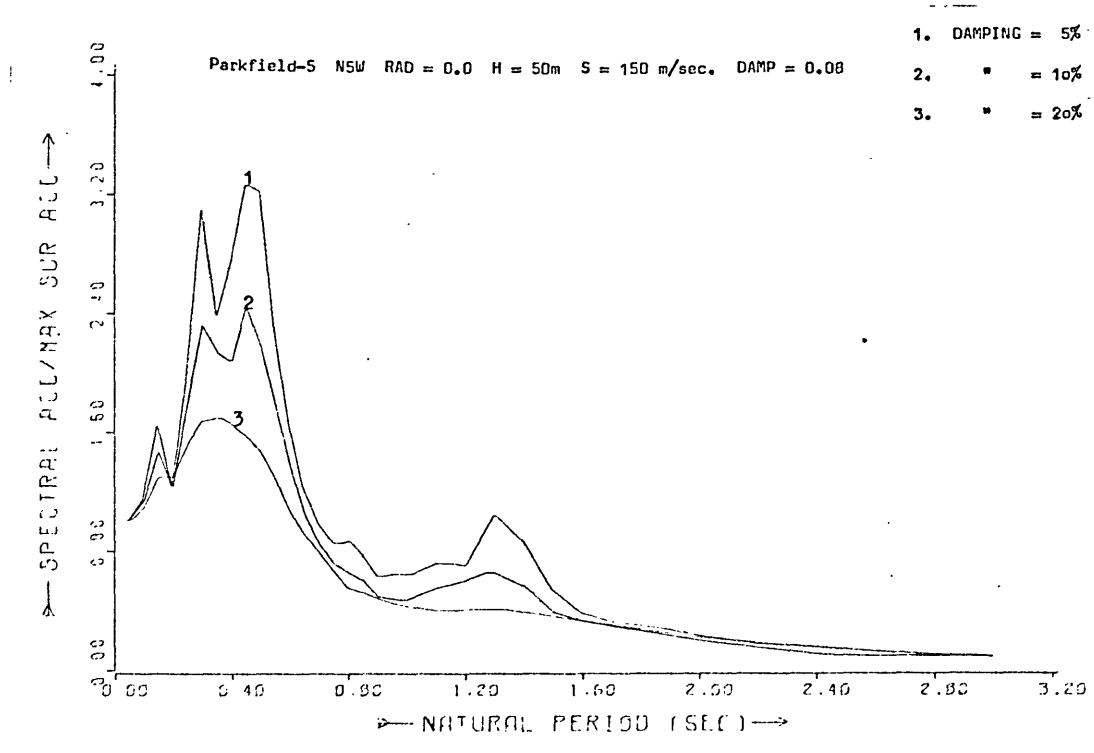


FIG.6.30d COMPUTED GROUND SURFACE ACCELERATION RESPONSE SPECTRA AT SITE NO.6.20

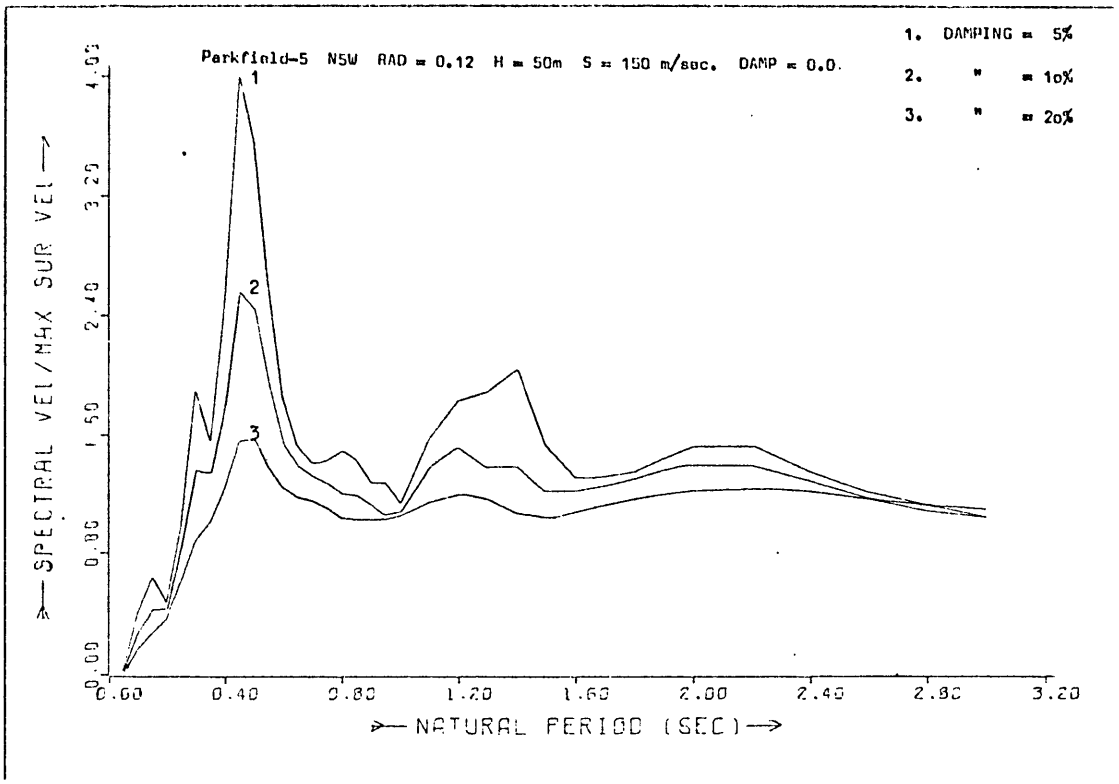


FIG.6.29eCOMPUTED GROUND SURFACE VELOCITY RESPONSE SPECTRA AT SITE NO. 6.19

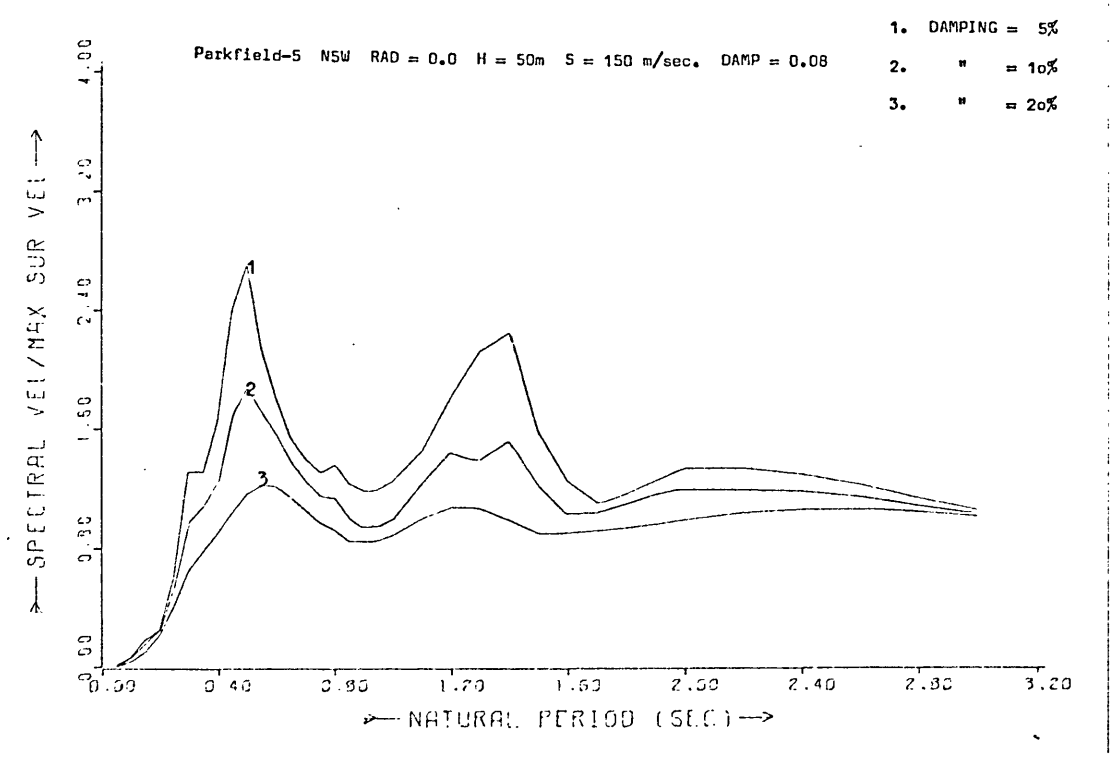


FIG.6.3oeCOMPUTED GROUND SURFACE VELOCITY RESPONSE SPECTRA AT SITE NO. 6.2o

higher resonant periods of the overburden.

The observations noted above give rise to two very important conclusions:

a) The influence of radiation damping ratio on higher modes of vibrations is not the same as hysteretic damping ratio.

b) No equivalence between the two dissipative mechanisms can be established under this condition.

However, the above results are not surprising. This behaviour was expected from the transmitting boundary condition given by equation 4. 4 , which clearly illustrates that the transmitting boundary condition is not only a function of radiation damping ratio but also a function of frequency distribution of bedrock motion relative to the natural periods of the overburden.

It should also be noted that such a condition (fundamental period of the overburden is not equal to the predominant period of the bedrock motion) will be truly realized in nature in most of the cases; therefore, the following conclusions are of great importance to practising engineers:

a) Hysteretic and radiation damping ratios, when the fundamental period of the overburden is not equal to the predominant period of the bedrock motion, produce quite different response values.

b) The major disagreement is exhibited in acceleration and velocity time histories.

6.8.1.3. FINAL COMMENTS

The results reported in sections 6.8.1.1 and 6.8.1.2 clearly indicate that radiation damping ratio plays an important role in determining the

seismic response characteristics of soil deposits. Radiation and hysteretic damping ratios have the same effect on the first mode of vibration and under the condition when the fundamental period of the deposit is equal to the predominant period of the bedrock motion, i.e. first mode of vibrations dominating the response, the two dissipative mechanisms produce results which are almost identical. However, the effect of the two dissipative mechanisms on higher modes of vibration are quite different, giving rise to computed response values which differ considerably both in frequency characteristics and amplitude of the pulses.

6.8.2. INFLUENCE OF STIFFNESS CHARACTERISTICS OF BEDROCK FORMATION ON THE SEISMIC RESPONSE OF SOIL DEPOSITS

The influence of stiffness characteristics of bedrock formation on the seismic response of soil deposits was assessed by analysing four different deposits, each having several different bedrock characteristics - completely rigid to very soft. As before, the following two cases were considered:

CASE 1: Fundamental period of the deposit is equal to the predominant period of the bedrock motion.

CASE 2: Fundamental period of the deposit is different from the predominant period of the bedrock motion.

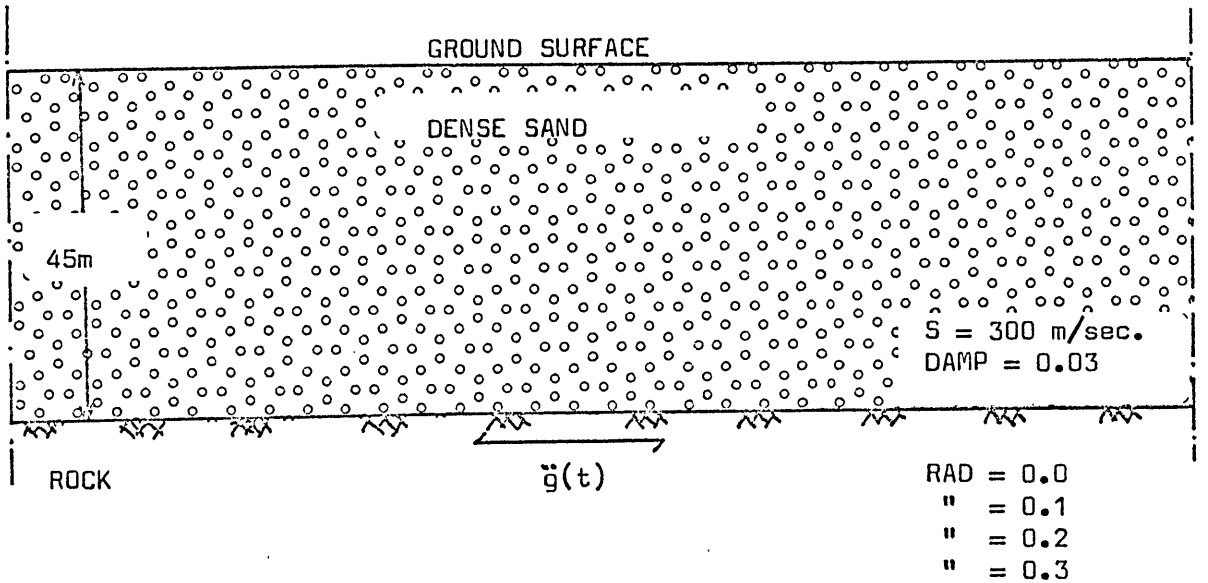
6.8.2.1. RESULTS OF CASE 1

To show the influence of bedrock characteristics on response of soil deposits to earthquake shocks, for this particular case, analyses were performed on a 45m. thick deposit of dense sand underlain by bedrock with shear wave velocities of ∞ (completely rigid), 3000, 1500 and 1000 m/sec., subjected at the bedrock level to Parkfield-2 with predominent period of 0.6 second, which corresponds to fundamental period of the deposit 0.6 second.

A hysteretic damping ratio of 0.02 was assigned to all modes of the deposit. The results of the calculation are shown in figs. 6.31a,b,c,d,e through 6.34a,b,c,d,e.

Figs. 6.31a,b,c through 6.34a,b,c show computed surface acceleration, velocity and displacement time histories for four radiation damping ratios 0.0, 0.1, 0.2 and 0.3. The radiation damping ratios were calculated based on the assumption described in section 7.2.1. In general, it is observed that the pattern of acceleration, velocity and displacement time histories remain quite similar with increasing radiation damping ratio, except that they differ in amplitudes of the pulses. Comparison of maximum acceleration, velocity and displacement developed at the surface of the deposit underlain by rock with shear wave velocities of 3000, 1500, 1000 and ∞ m/sec. are listed in table 62. In each comparison as stated above, all parameters other than radiation damping ratio, which reflects the bedrock characteristics, were kept constant. Based on the results obtained for soil deposits having rock formations with shear wave velocities of 3000, 1500 and 1000 m/sec., maximum surface accelerations vary by 32.6%, 50% and 59.6%, respectively, compared to that of the deposit on infinitely rigid base. Similar conclusions may be drawn concerning the maximum amplitude of ground surface velocities and displacements with variations of 23.81%, 39.44%, 49.72% and 7.56%, 10.03%, 12.24%, respectively. The results clearly indicate that amplitude of maximum accelerations are more sensitive to changes in bedrock formation characteristics than the peak velocities and displacements. In order to study the influence of bedrock characteristics on frequency characteristics of surface motions figs. 6.31d to 6.34d have been included.

Figs. 6.31d through 6.34d show computed surface acceleration spectras



RESPONSE OF HYSTERETIC DEPOSIT UNDERLAIN BY DEFORMABLE BEDROCK

SCHEMATIC SOIL PROFILE FOR SITE NO. 6.21,

6.22, 6.23, and 6.24.

FIG. 6.31

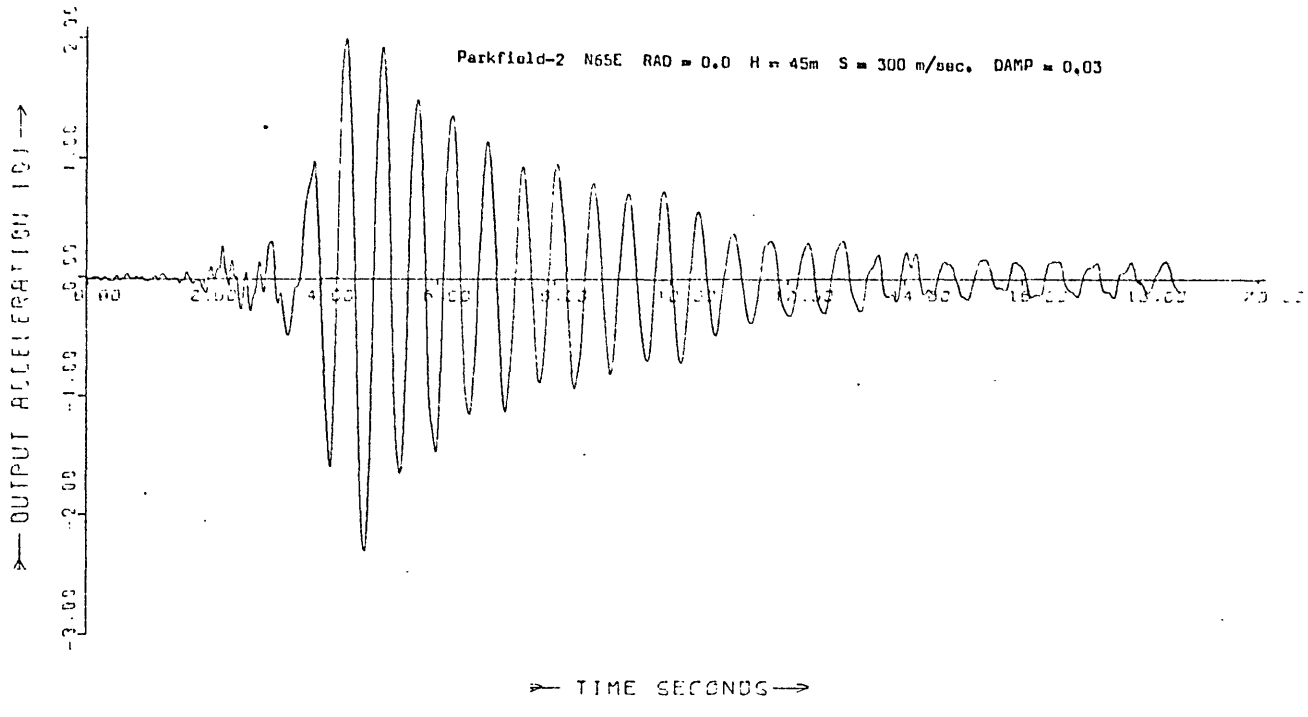


FIG.6.31a COMPUTED GROUND SURFACE ACCELERATION TIME HISTORY AT SITE NO. 6.21

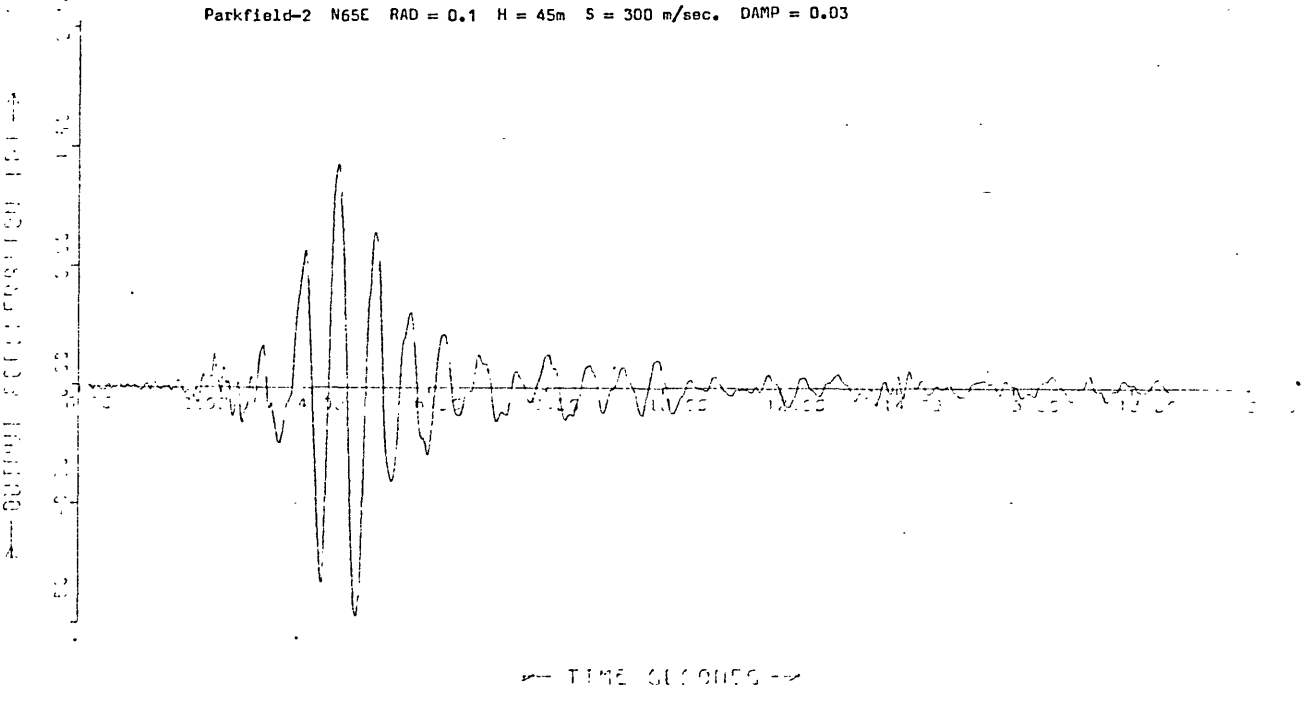


FIG. 6.32a COMPUTED GROUND SURFACE ACCELERATION TIME HISTORY AT SITE NO. 6.22

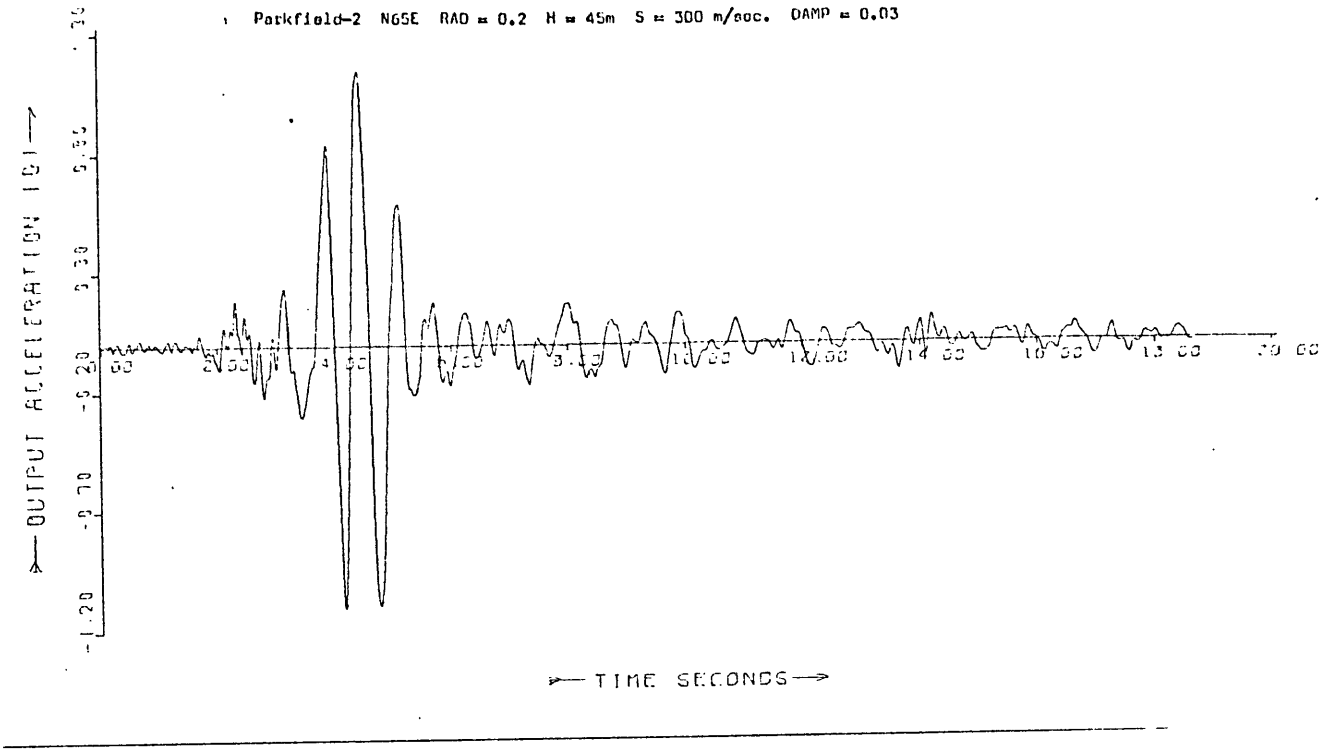


FIG.6.33a COMPUTED GROUND SURFACE ACCELERATION TIME HISTORY AT SITE NO. 6.23

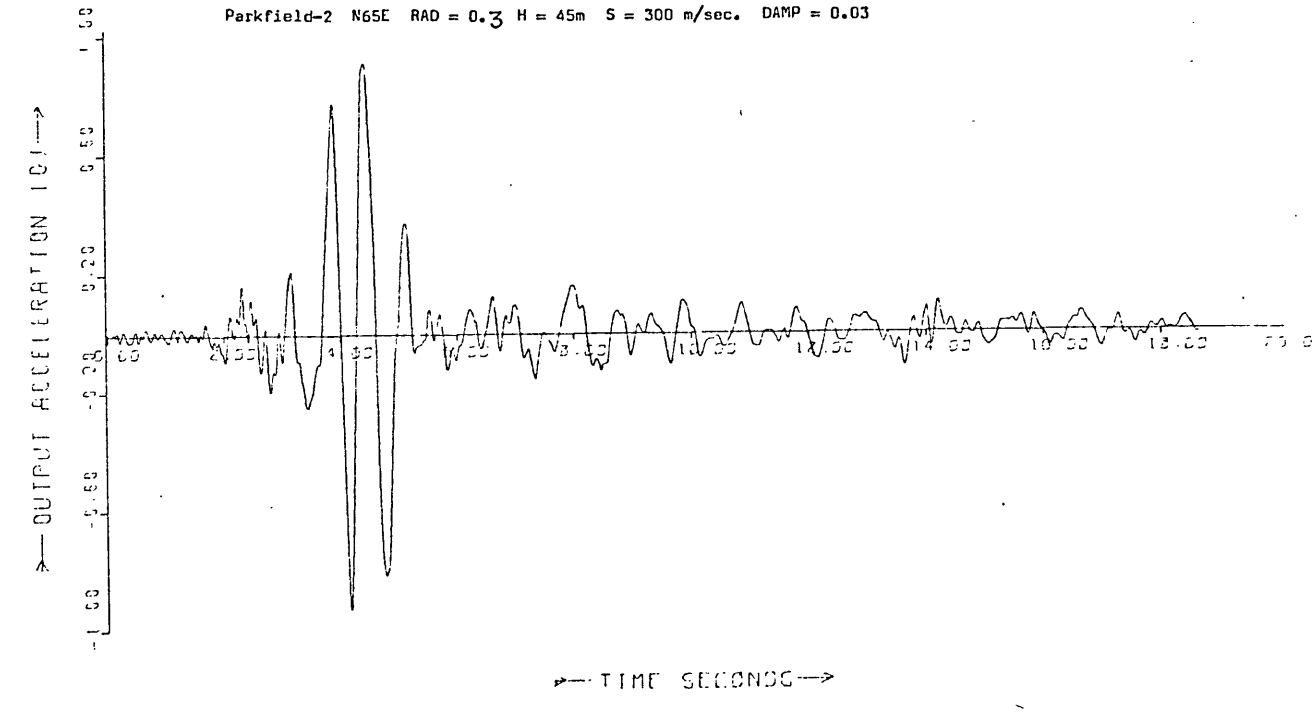


FIG6.34a COMPUTED GROUND SURFACE ACCELERATION TIME HISTORY AT SITE NO.6.24

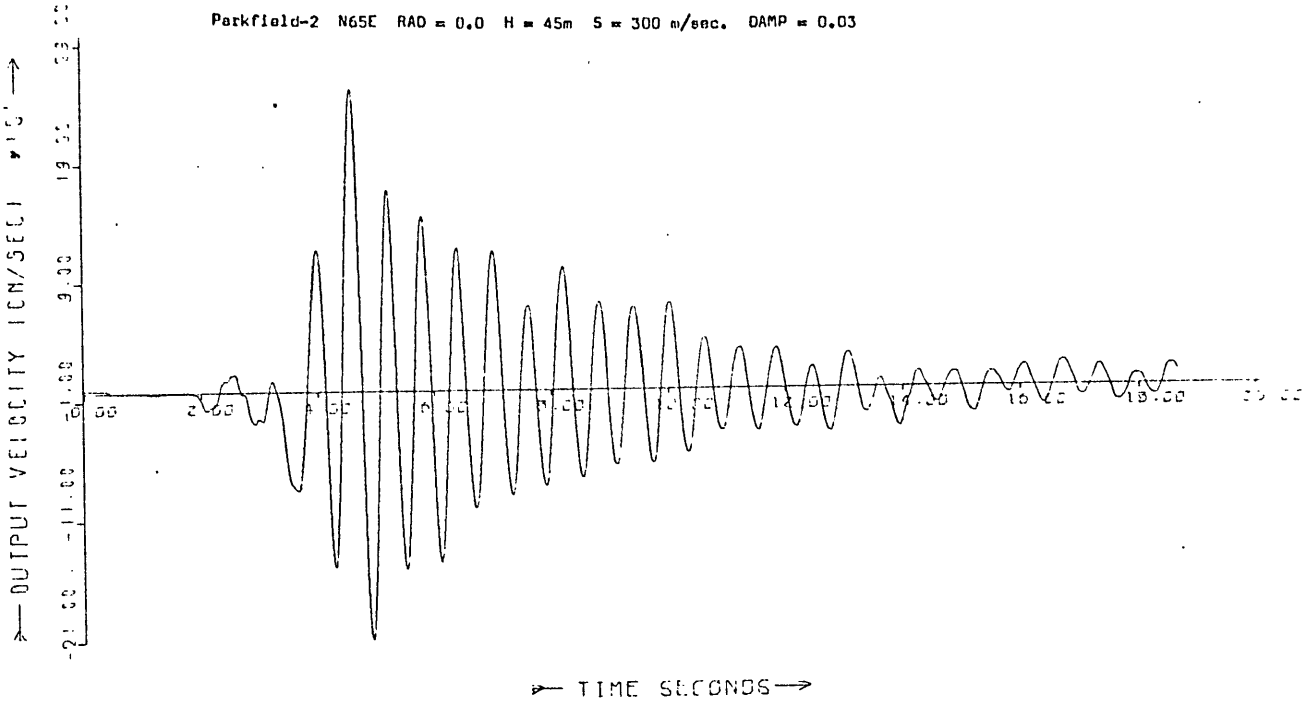


FIG.6.31b COMPUTED GROUND SURFACE VELOCITY TIME HISTORY AT SITE NO. 6.21

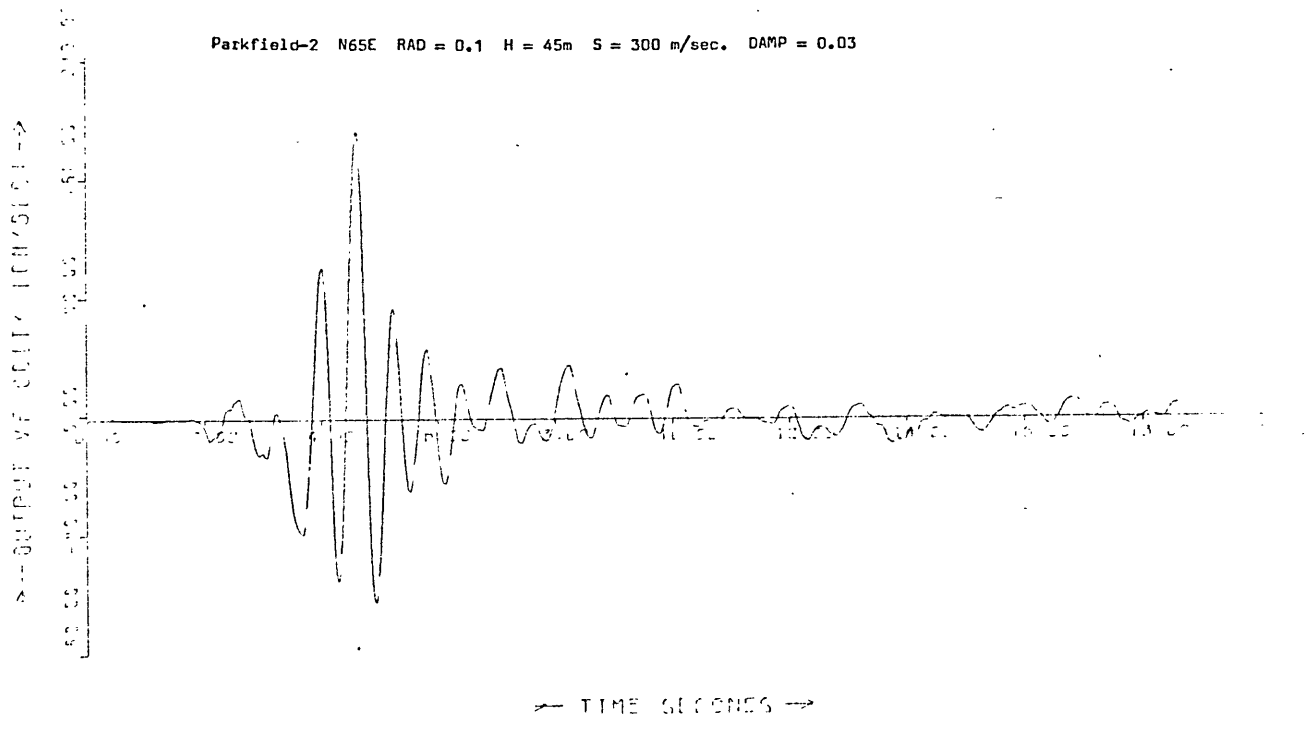


FIG.6.32b COMPUTED GROUND SURFACE VELOCITY TIME HISTORY AT SITE NO. 6.22

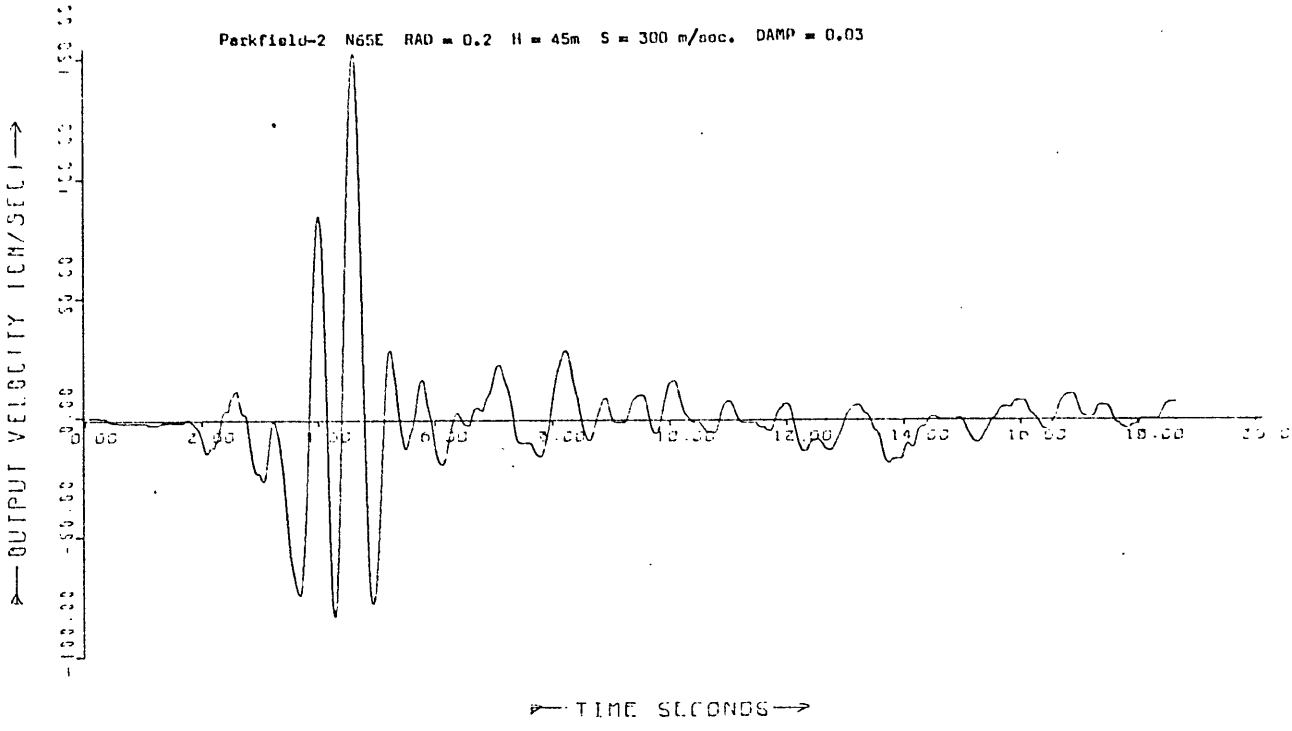


FIG.6.33b COMPUTED GROUND SURFACE VELOCITY TIME HISTORY AT SITE NO. 6.23

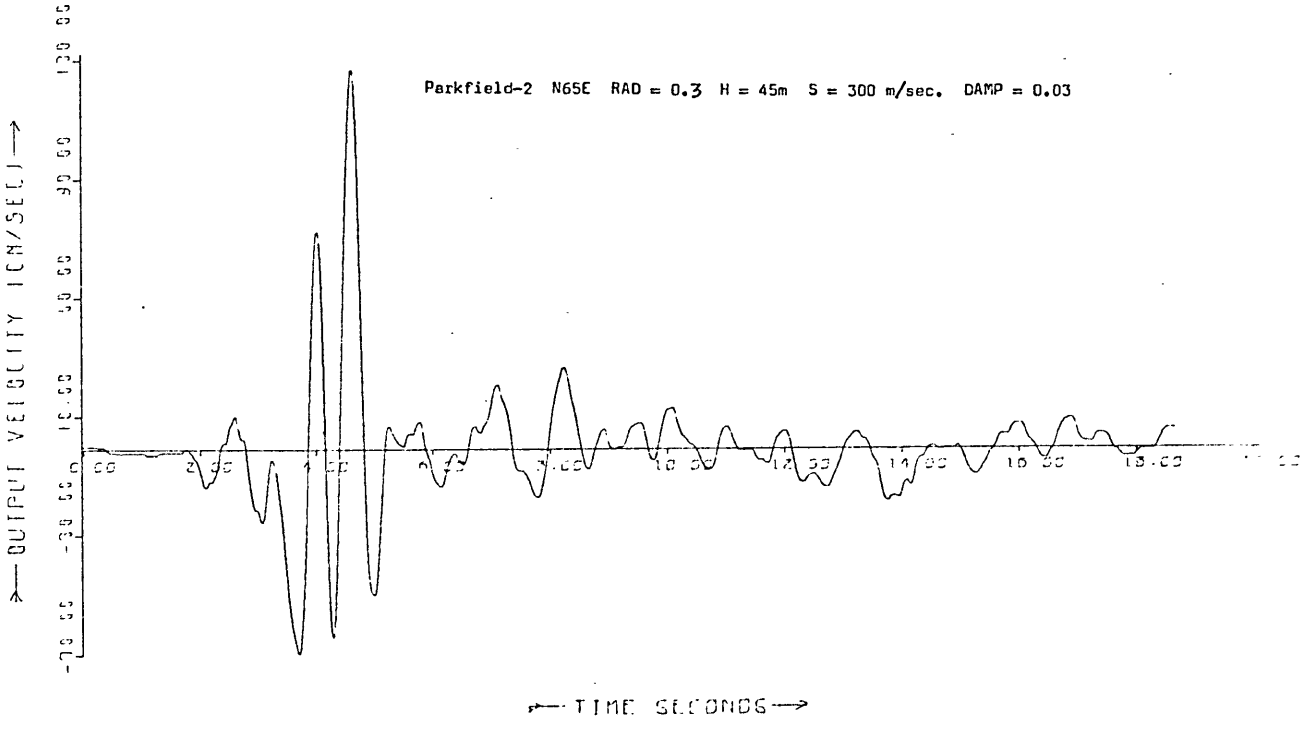


FIG.6.34b COMPUTED GROUND SURFACE VELOCITY TIME HISTORY AT SITE NO. 6.24

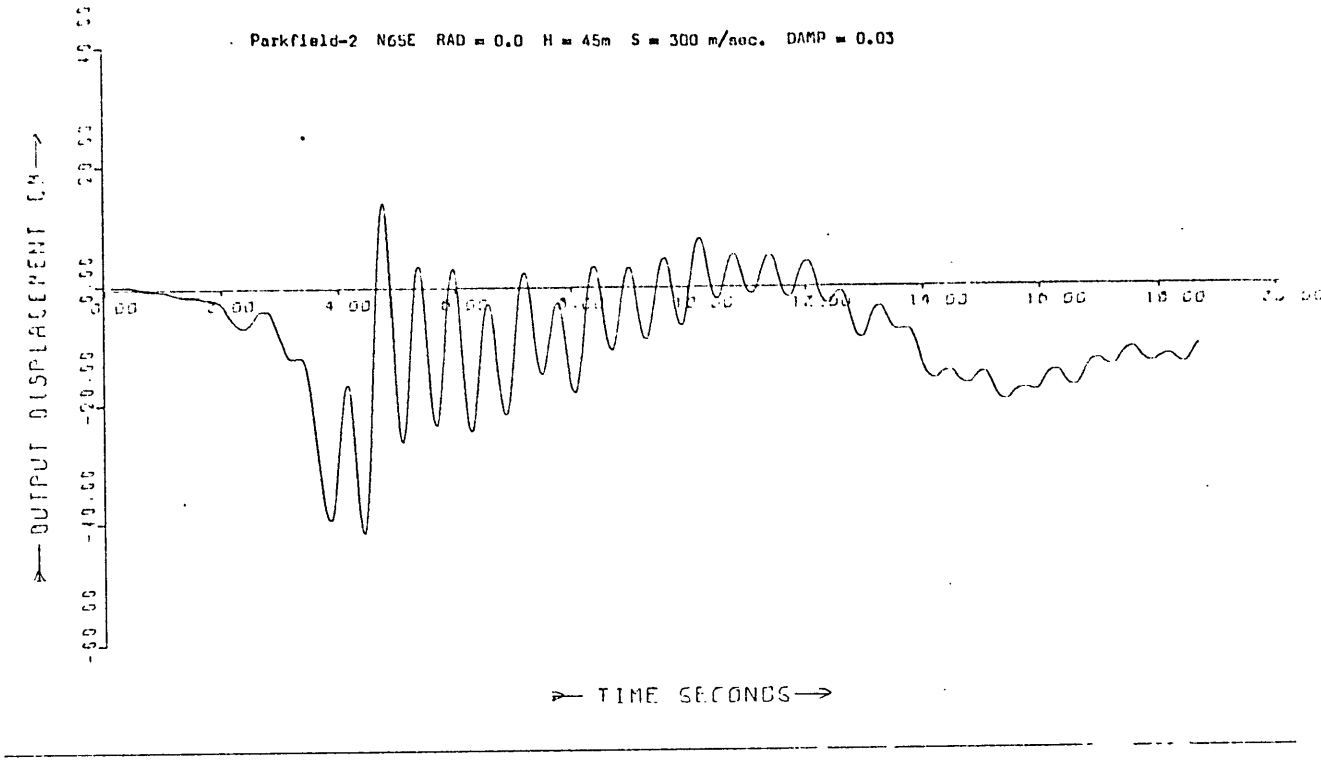


FIG.6.31cCOMPUTED GROUND SURFACE DISPLACEMENT TIME HISTORY AT SITE NO. 6.21

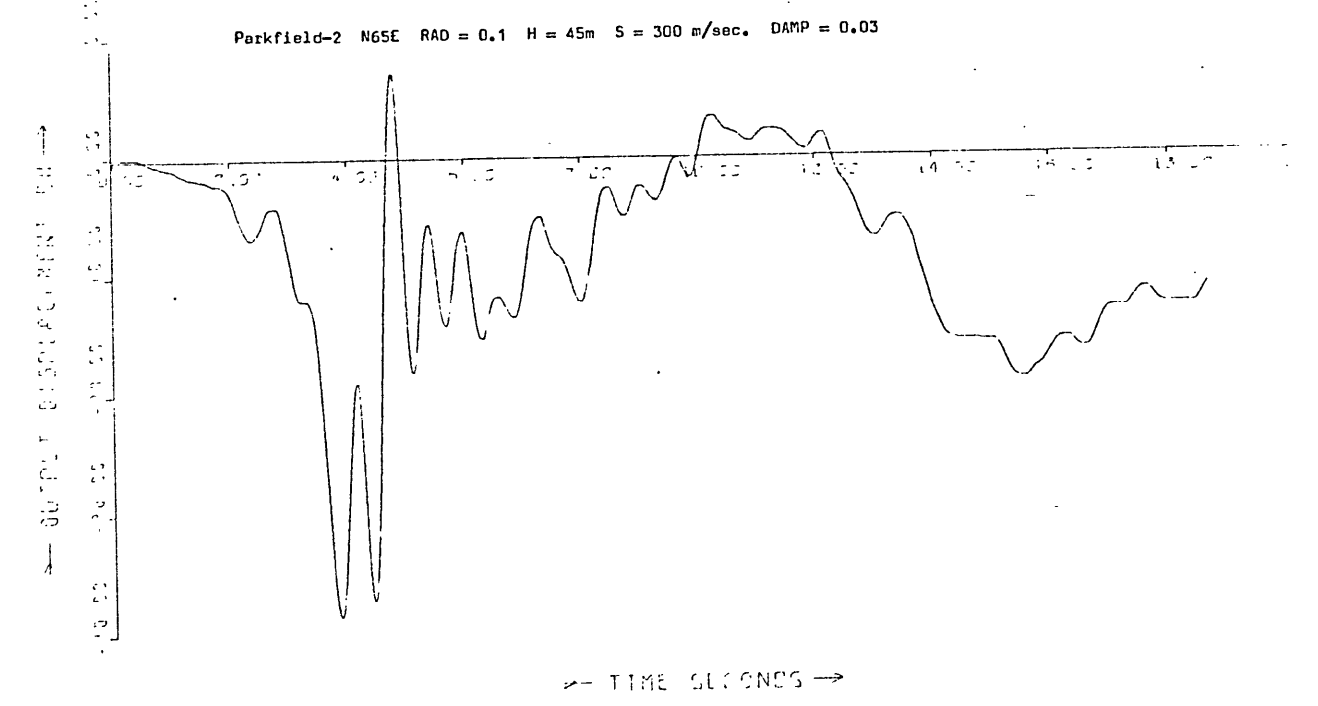


FIG6.32c COMPUTED GROUND SURFACE DISPLACEMENT TIME HISTORY AT SITE NO.6.22

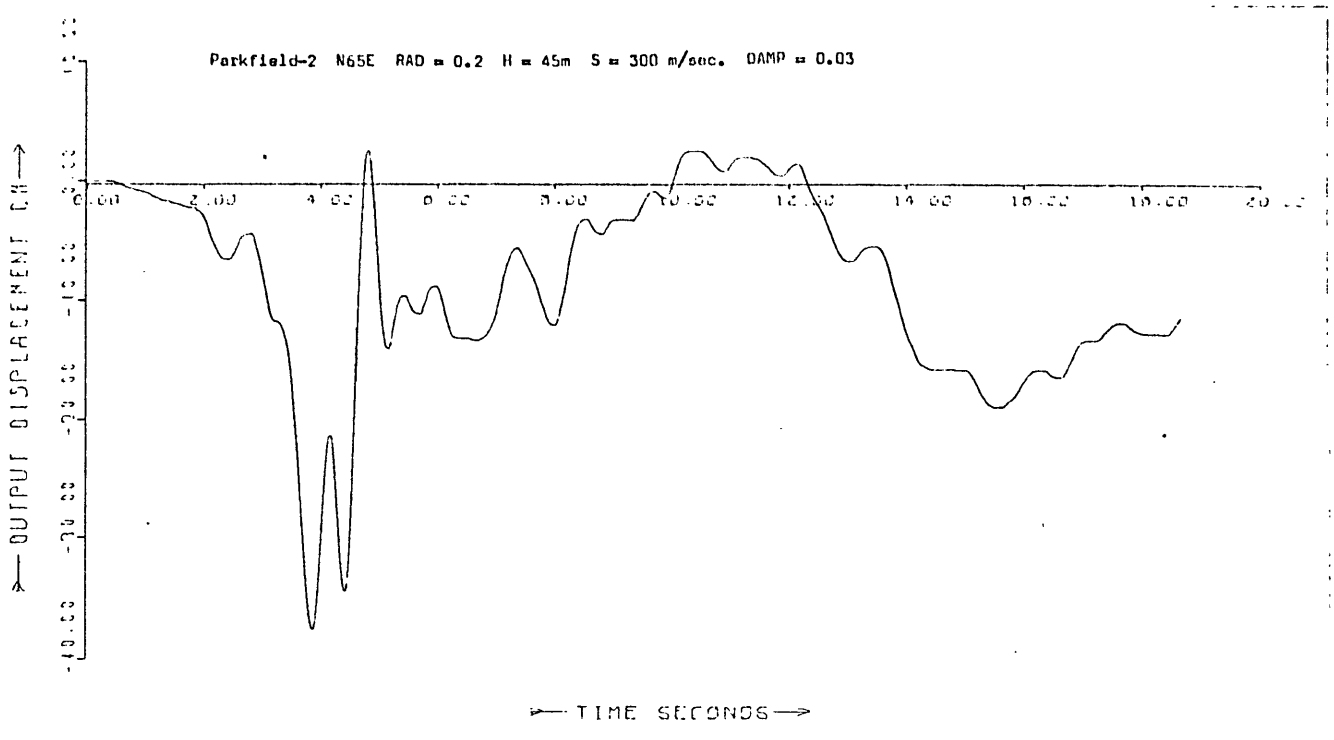


FIG.6.33c COMPUTED GROUND SURFACE DISPLACEMENT TIME HISTORY AT SITE NO. 6.23

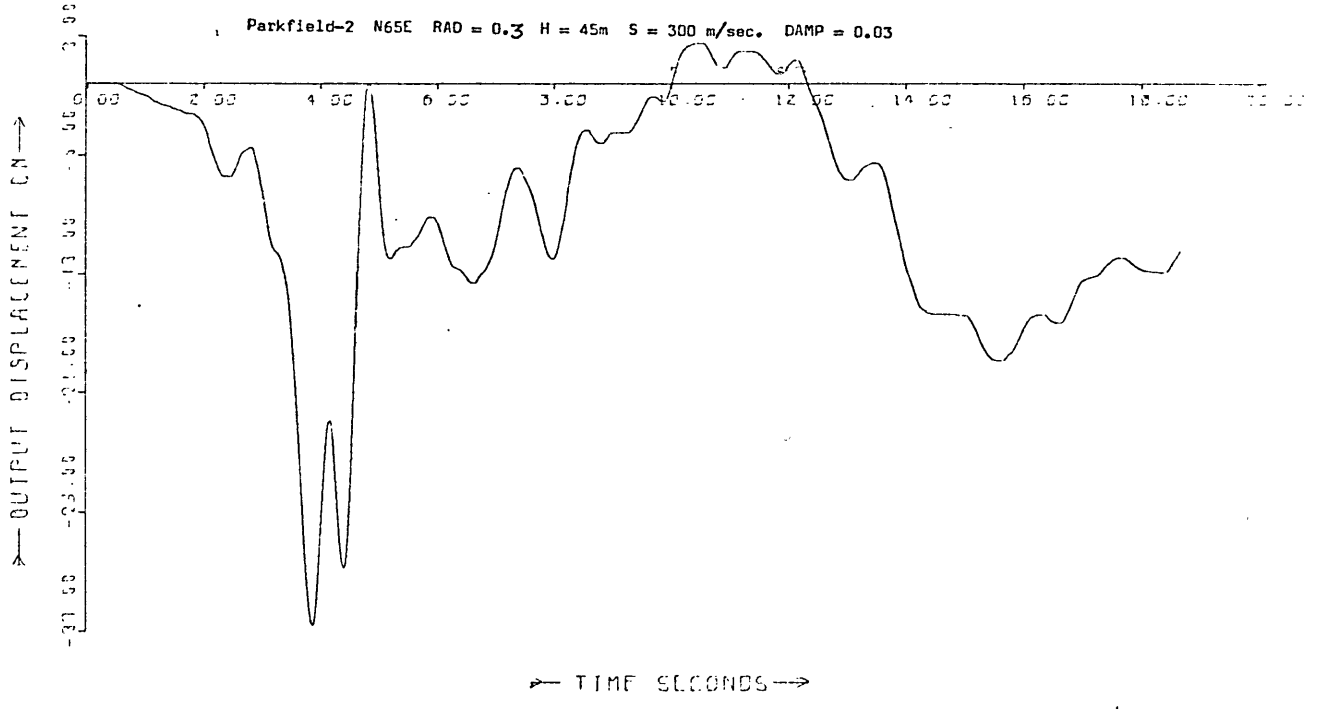


FIG.6.34c COMPUTED GROUND SURFACE DISPLACEMENT TIME HISTORY AT SITE NO. 6.24

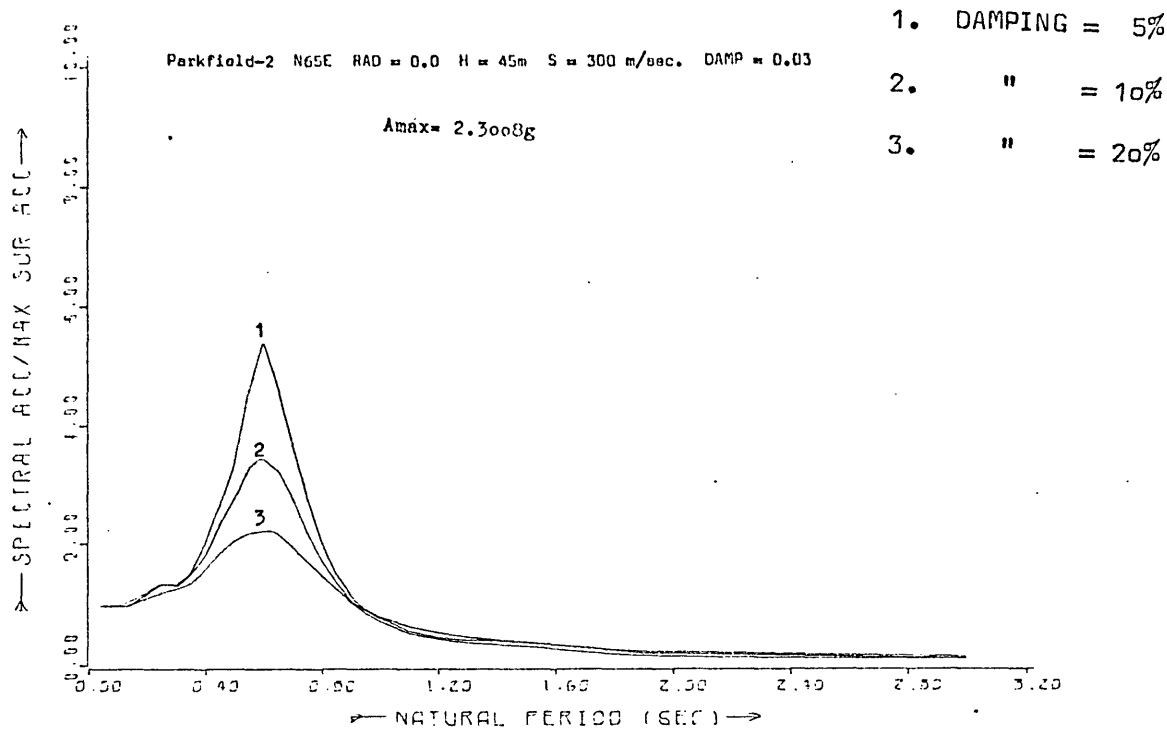


FIG.6.31d COMPUTED GROUND SURFACE ACCELERATION RESPONSE SPECTRA AT SITE NO. 6.21

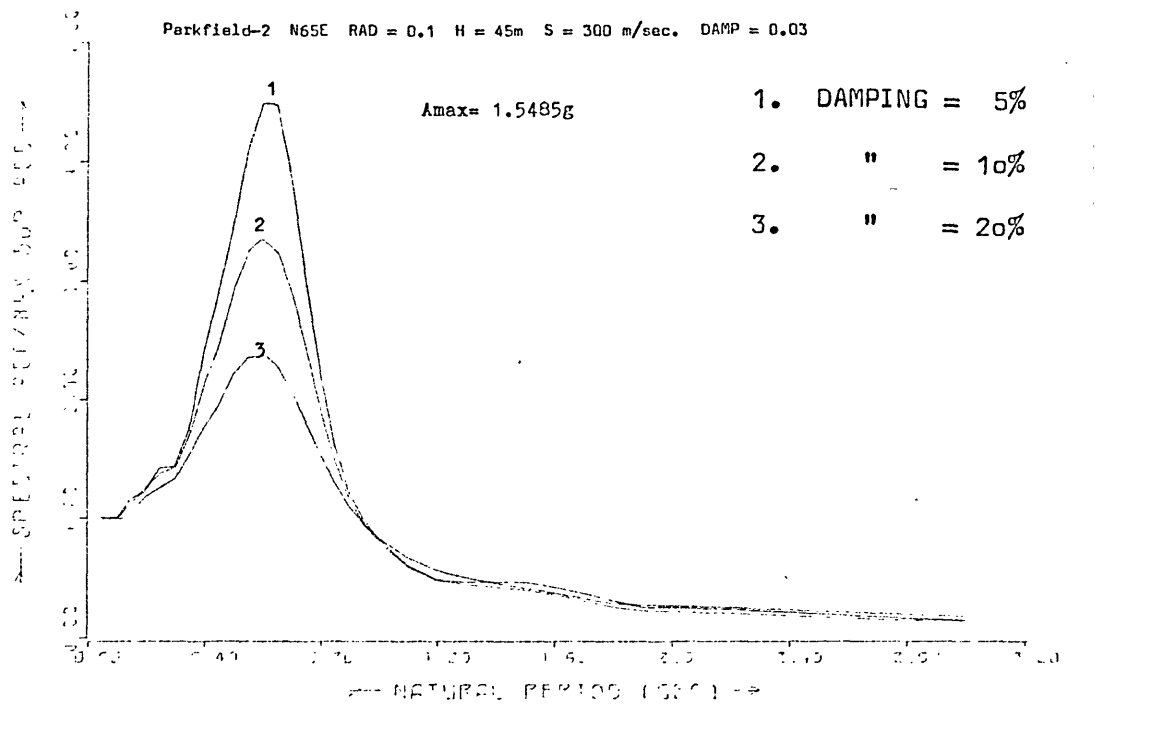


FIG.6.32d COMPUTED GROUND SURFACE ACCELERATION RESPONSE SPECTRA AT SITE NO. 6.22

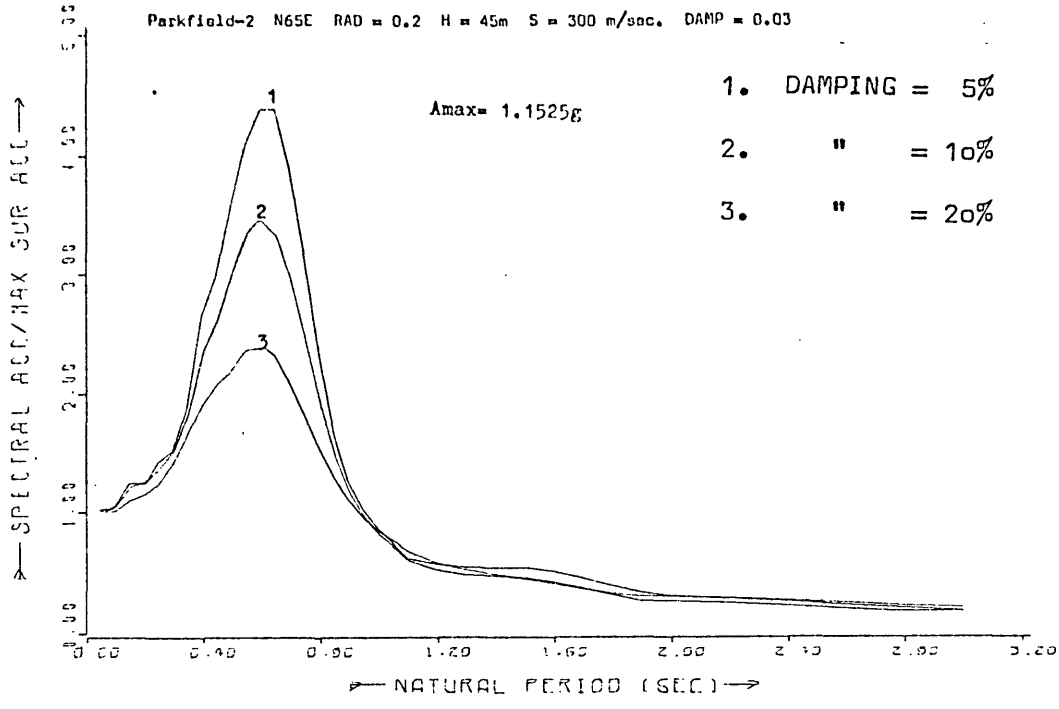


FIG 6.33d COMPUTED GROUND SURFACE ACCELERATION RESPONSE SPECTRA AT SITE NO. 6.23

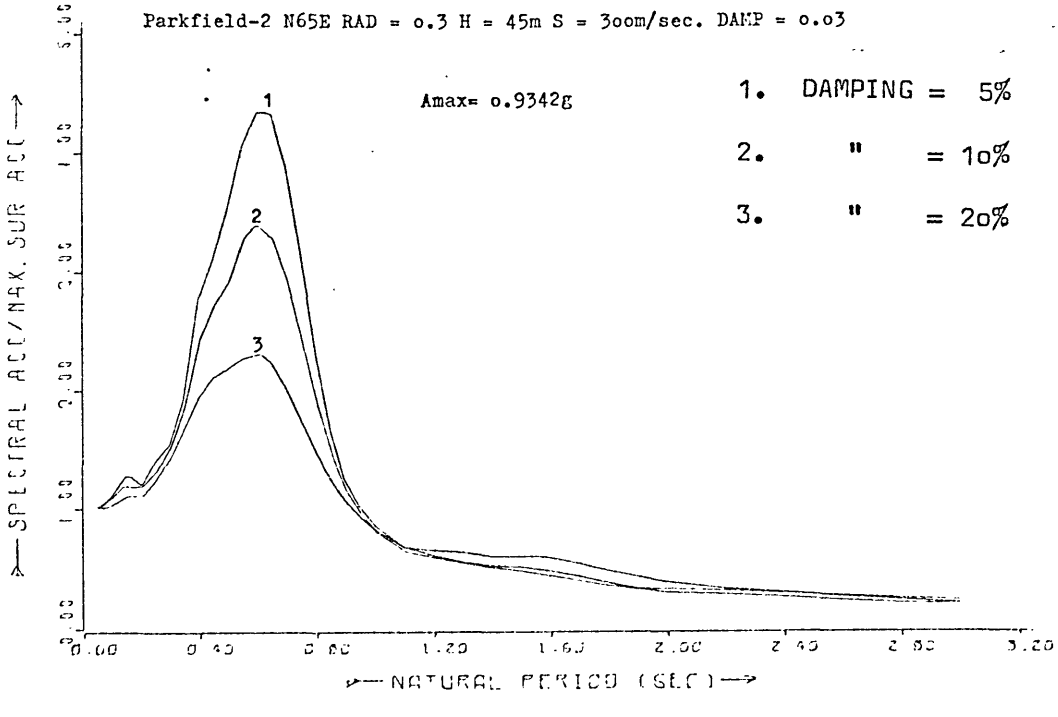


FIG. 6.34d COMPUTED GROUND SURFACE ACCELERATION RESPONSE SPECTRA AT SITE NO. 6.24

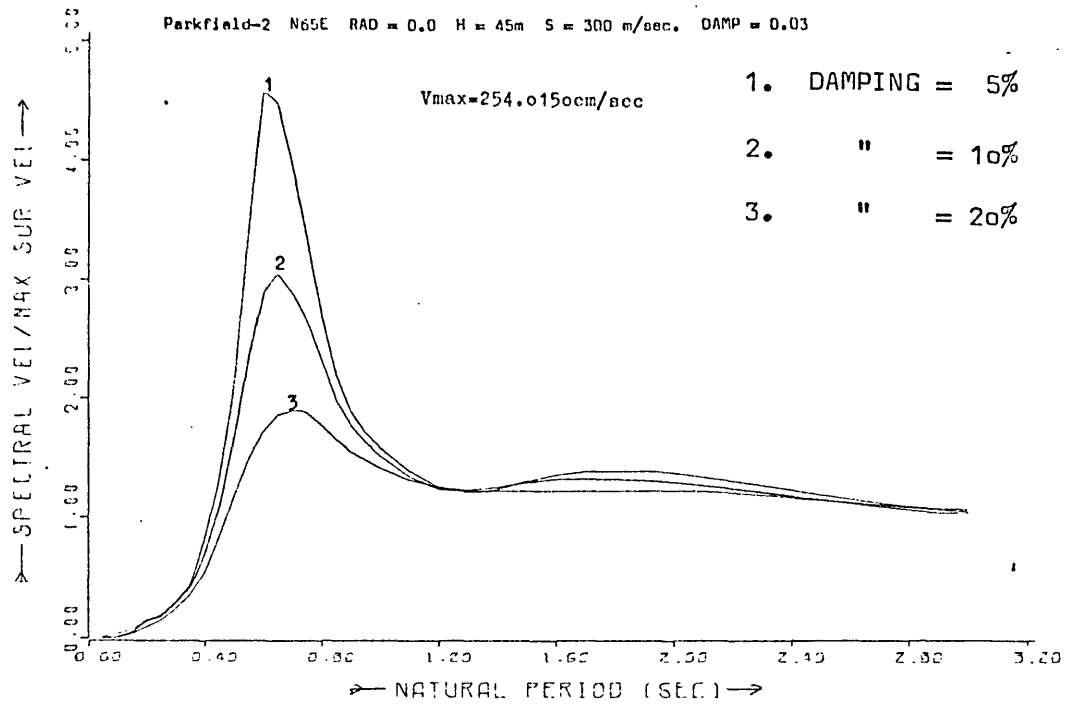


FIG 6.31e COMPUTED GROUND SURFACE VELOCITY RESPONSE SPECTRA AT SITE NO. 6.21

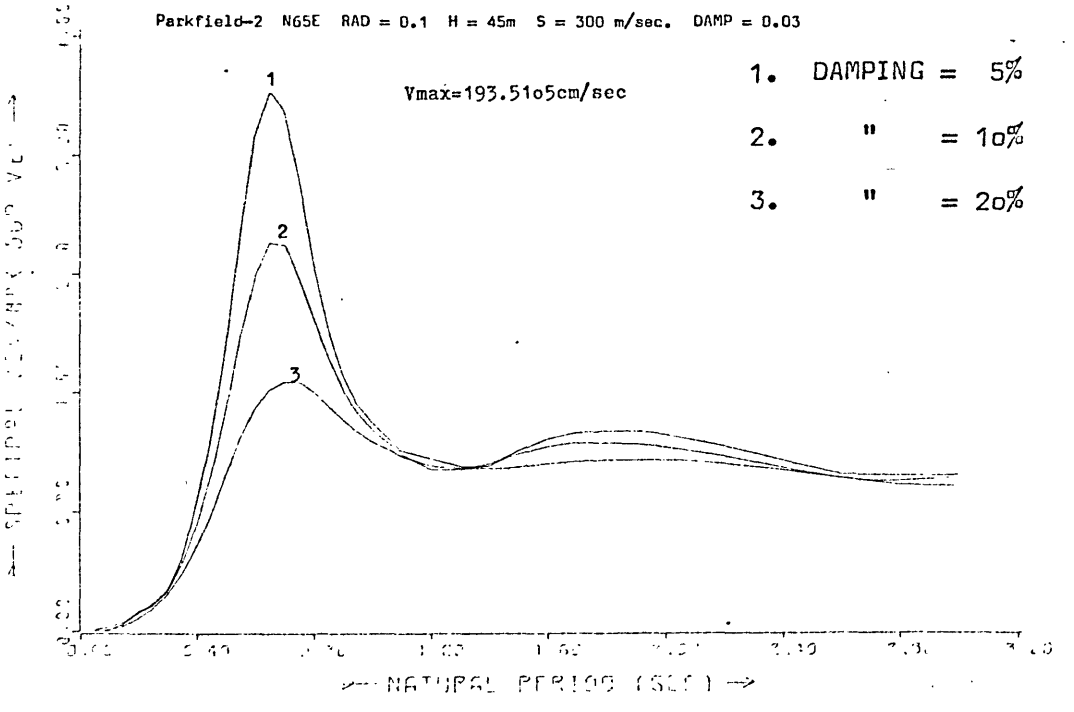


FIG 6.32e COMPUTED GROUND SURFACE VELOCITY RESPONSE SPECTRA AT SITE NO. 6.22

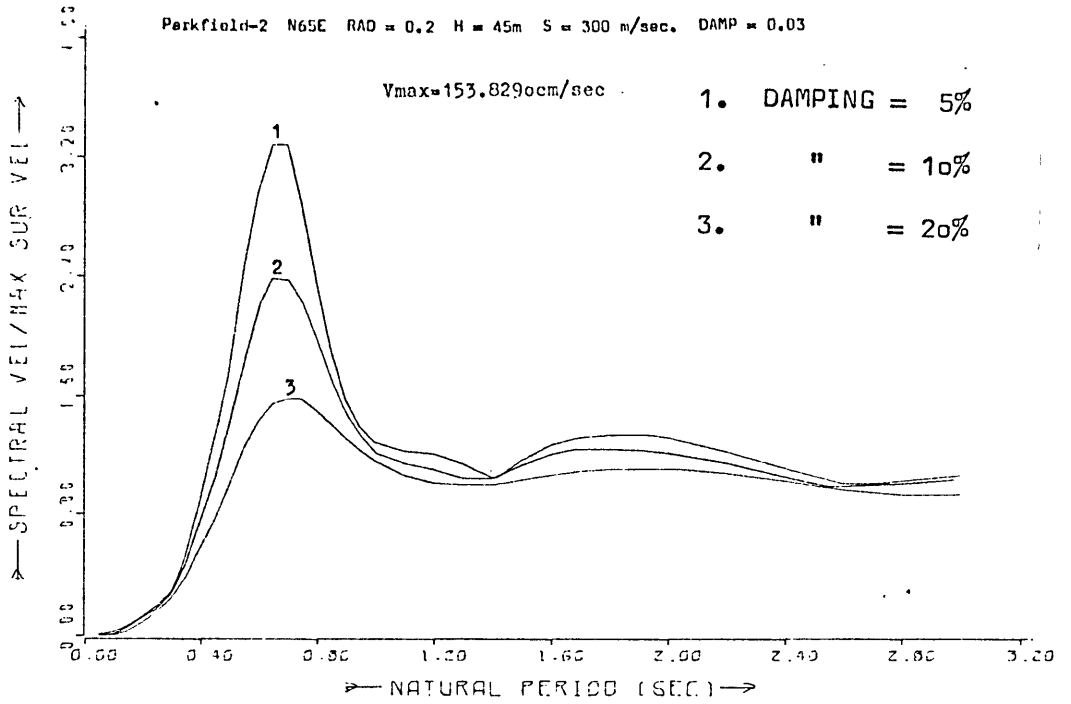


FIG.6.33e COMPUTED GROUND SURFACE VELOCITY RESPONSE SPECTRA AT SITE NO. 6.23

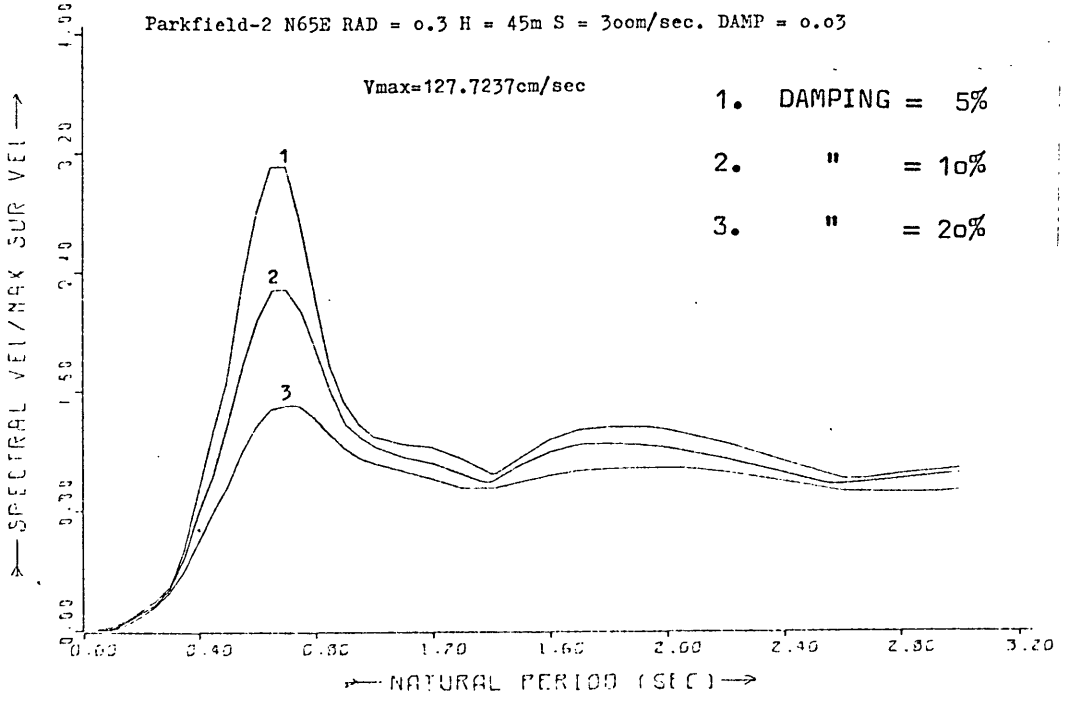


FIG 6.34e COMPUTED GROUND SURFACE VELOCITY RESPONSE SPECTRA AT SITE NO. 6.24

DATA ON THE INFLUENCE OF BEDROCK CHARACTERISTICS ON RESPONSE OF SOIL DEPOSITS

RADIATION DAMPING RATIO	MAX. SUR. ABS. ACC. (g)	$\frac{ACC_{RAD}}{1 - ACC_{0.0}} \times 100\%$	MAX. SUR. ABS. VEL. (cm/sec)	$\frac{VEL_{RAD}}{1 - VEL_{0.0}} \times 100\%$	MAX. SUR. ABS. DIS. (cm)	$\frac{DIS_{RAD}}{1 - DIS_{0.0}} \times 100\%$	STRENGTH $(cm/sec)^2$
0.0	2.30	0.00	254.01	0.00	41.68	0.00	28172
0.1	1.55	32.6	193.51	23.81	38.53	7.56	8613
0.2	1.15	50.0	153.83	39.44	37.50	10.03	5134
0.3	0.93	59.6	127.72	49.72	36.58	12.24	3697

TABLE 6.2

for the four sites in normalized form. The advantages of normalized acceleration spectra over that of the ordinary spectra are the following:

i) Frequency characteristics of different motions can be studied by superposition of normalized acceleration spectrum of these motions.

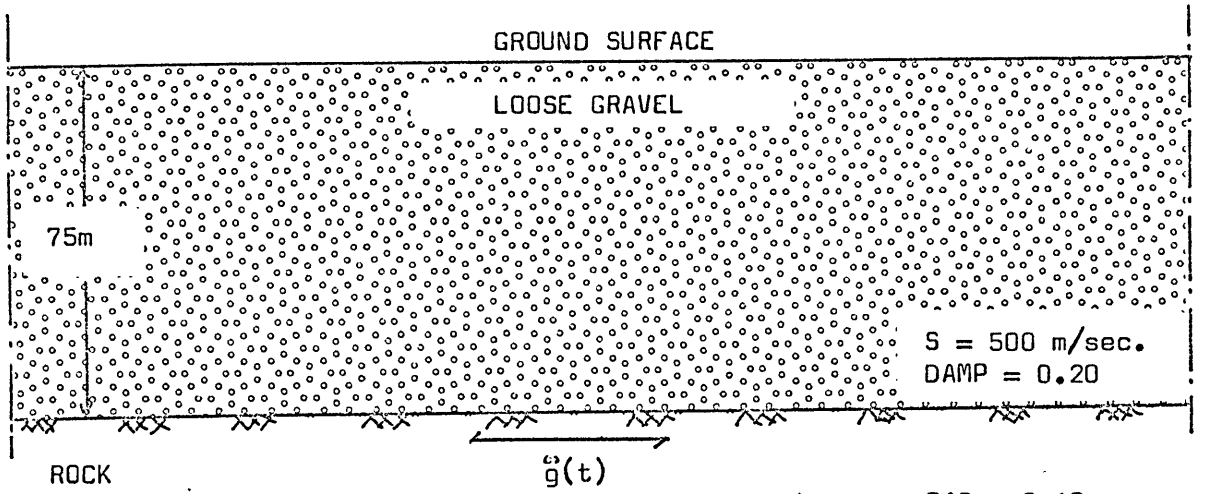
ii) Every ordinate on the spectra can be multiplied by any peak ground acceleration assessed by the designer.

The results clearly indicate that, under the especial case, i.e. fundamental period of the overburden equal to the predominant period of the bedrock motion, frequency characteristics of output motion, are not affected to the extent to be reflected in acceleration response spectra, whether the shear wave velocity of the underlying bedrock is 3000, 1500, 1000 or ∞ m/sec. A similar behaviour is also exhibited by normalized velocity spectrum shown in figs. 6.31e to 6.34e.

The computed values for strength of earthquake motion "S" (see section 7.3.1 for the four sites) are given in the last column of table 6.2. The results illustrate that the energy available for damage to buildings located on the deposit whose underlying rock formation has a shear wave velocity of ∞ is 7.6 times more than that of 1000 m/sec., 5.4 times more than that having a shear wave velocity of 1500 m/sec., and, finally, 3.2 times more than that having a shear wave velocity of 3000 m/sec.

In order further to consolidate the above conclusions and investigate the manner in which the amplification spectrum of the surface motions are affected by the stiffness characteristics of underlying bedrock, figs. 6.35a,b,c,d,e to 6.39a,b,c,d,e are included.

Figs. 6.35a,b,c,d,e to 6.39a,b,c,d,e show response of a 75m deposit of loose gravel with bedrock shear wave velocities of 5000, 2500, 1666, 1250



RAD = 0.10
" = 0.20
" = 0.30
" = 0.40
" = 0.50

RESPONSE OF HYSTERETIC DEPOSIT UNDERLAIN BY DEFORMABLE BEDROCK

SCHEMATIC SOIL PROFILE FOR SITE NO. 6.25,

6.26, 6.27, 6.28, 6.29.

FIG.6.35

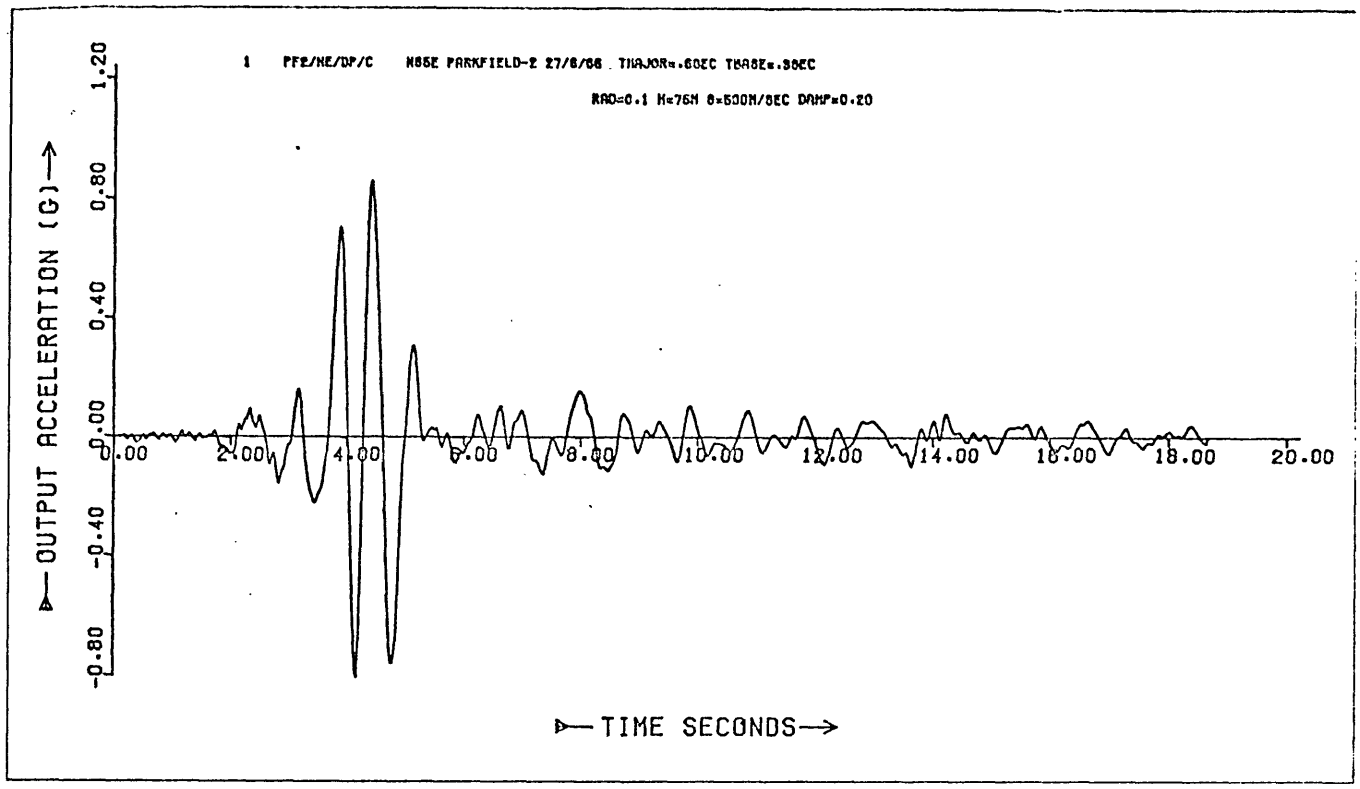


FIG. 6.35a COMPUTED GROUND SURFACE ACCELERATION TIME HISTORY AT SITE NO 6.25

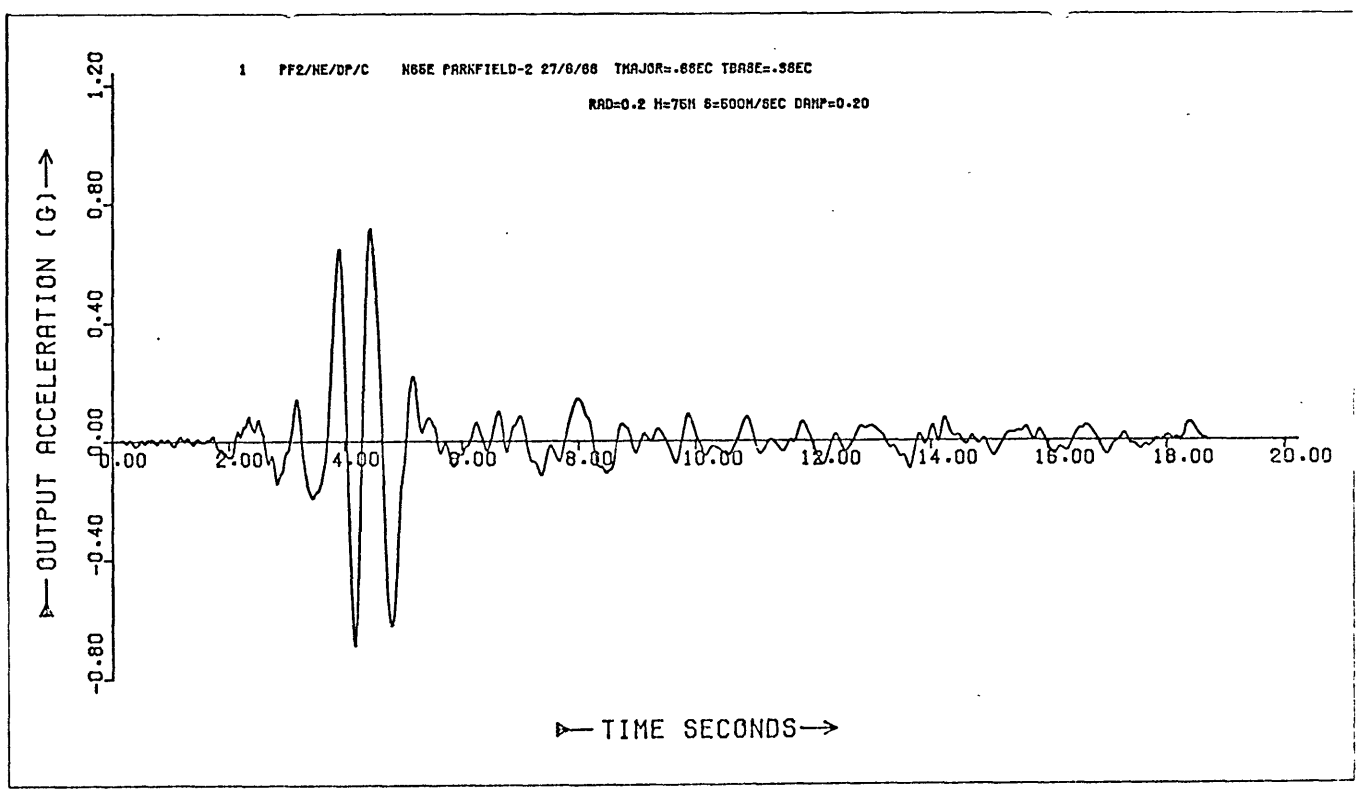


FIG. 6.36a COMPUTED GROUND SURFACE ACCELERATION TIME HISTORY AT SITE NO 6.26

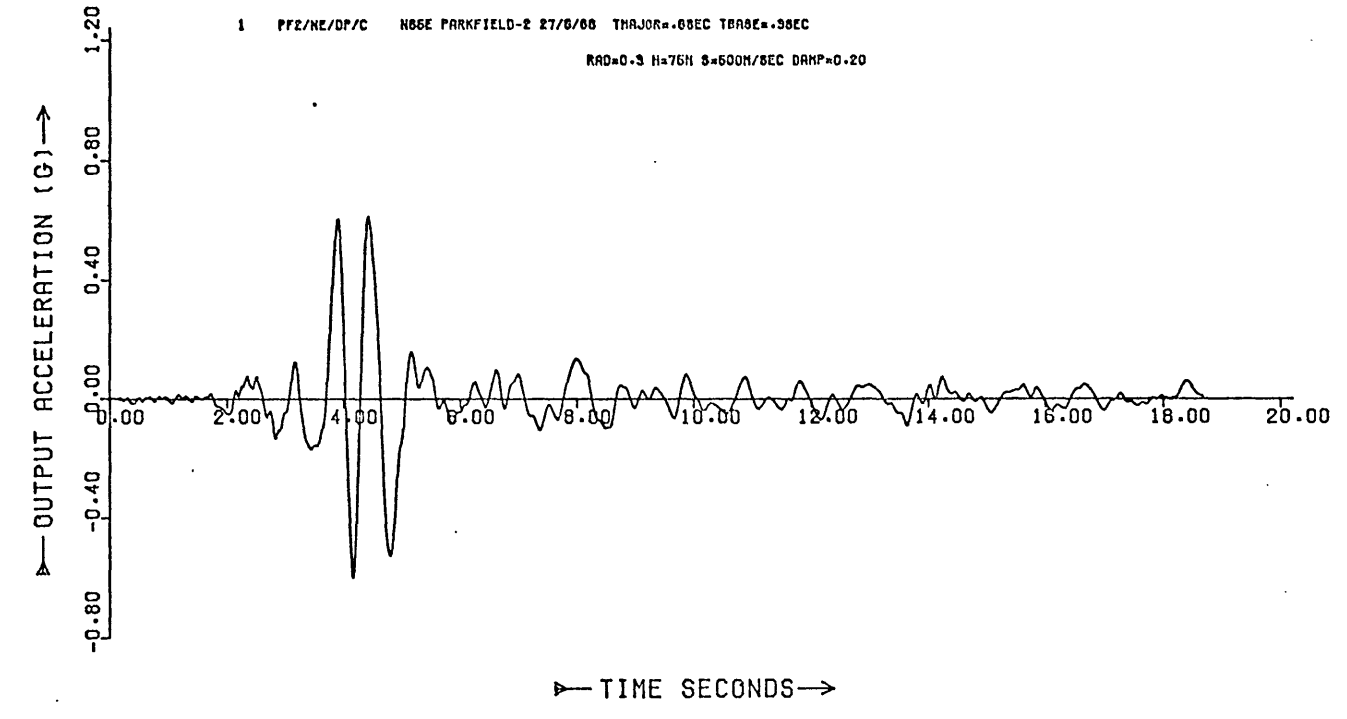


FIG. 6.37a COMPUTED GROUND SURFACE ACCELERATION TIME HISTORY AT SITE NO 6.27

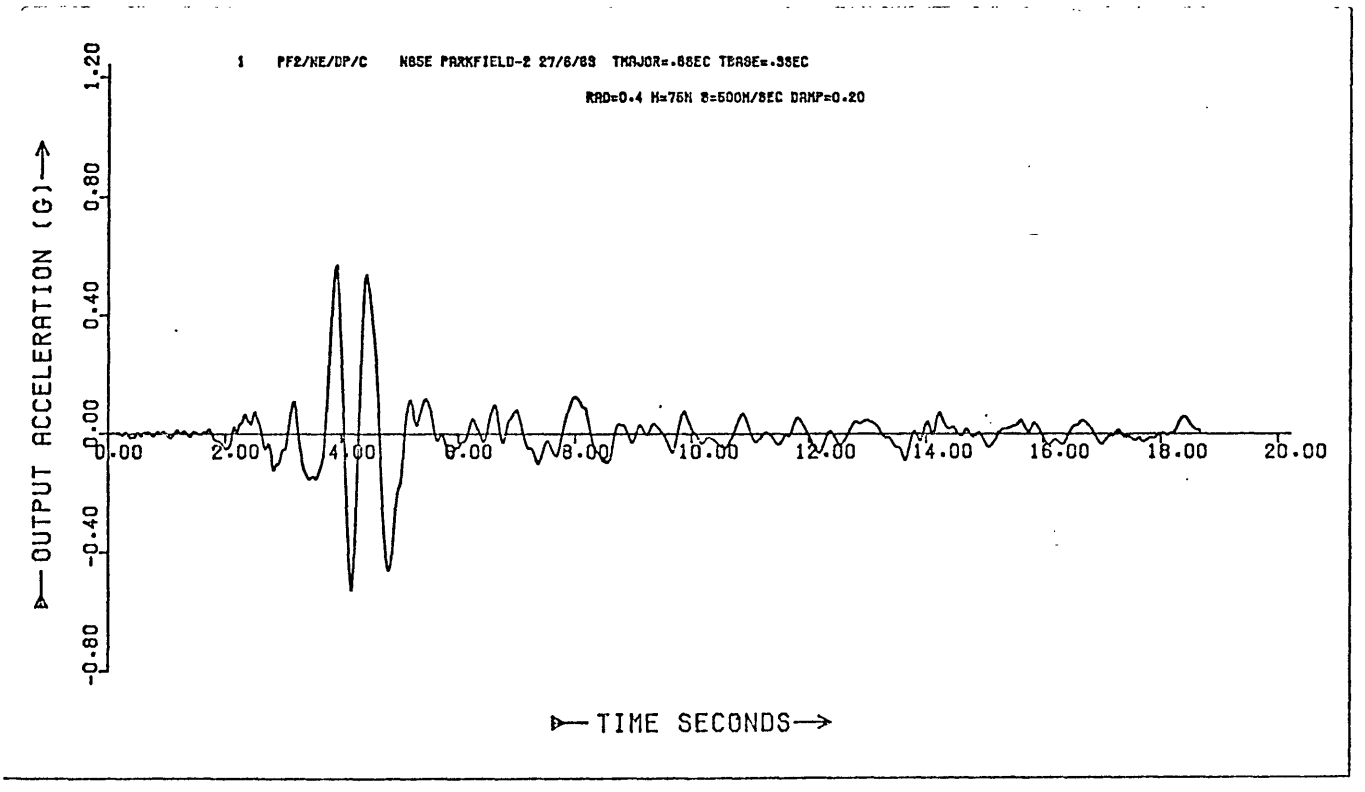


FIG.6.38a COMPUTED GROUND SURFACE ACCELERATION TIME HISTORY AT SITE NO 6.28

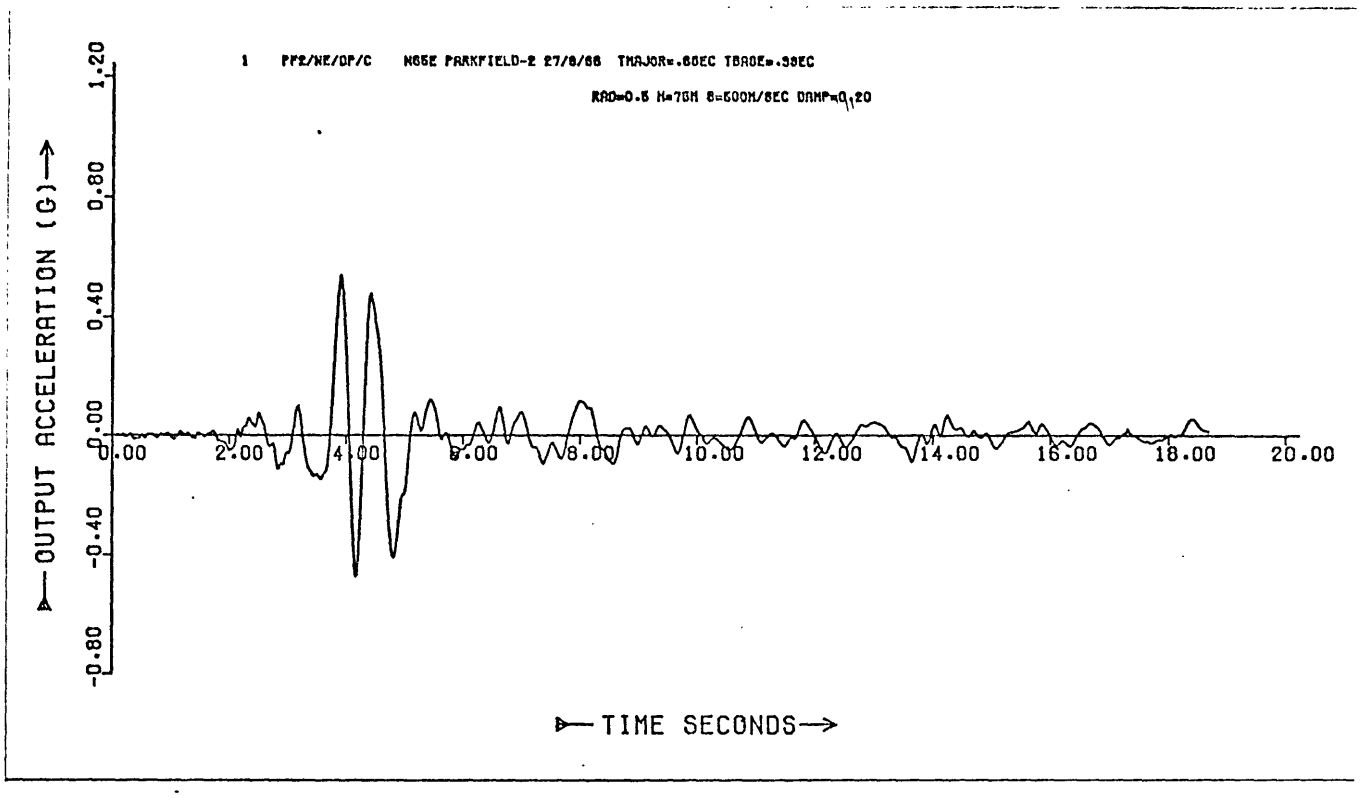


FIG. 6.39a COMPUTED GROUND SURFACE ACCELERATION TIME HISTORY AT SITE NO 6.29

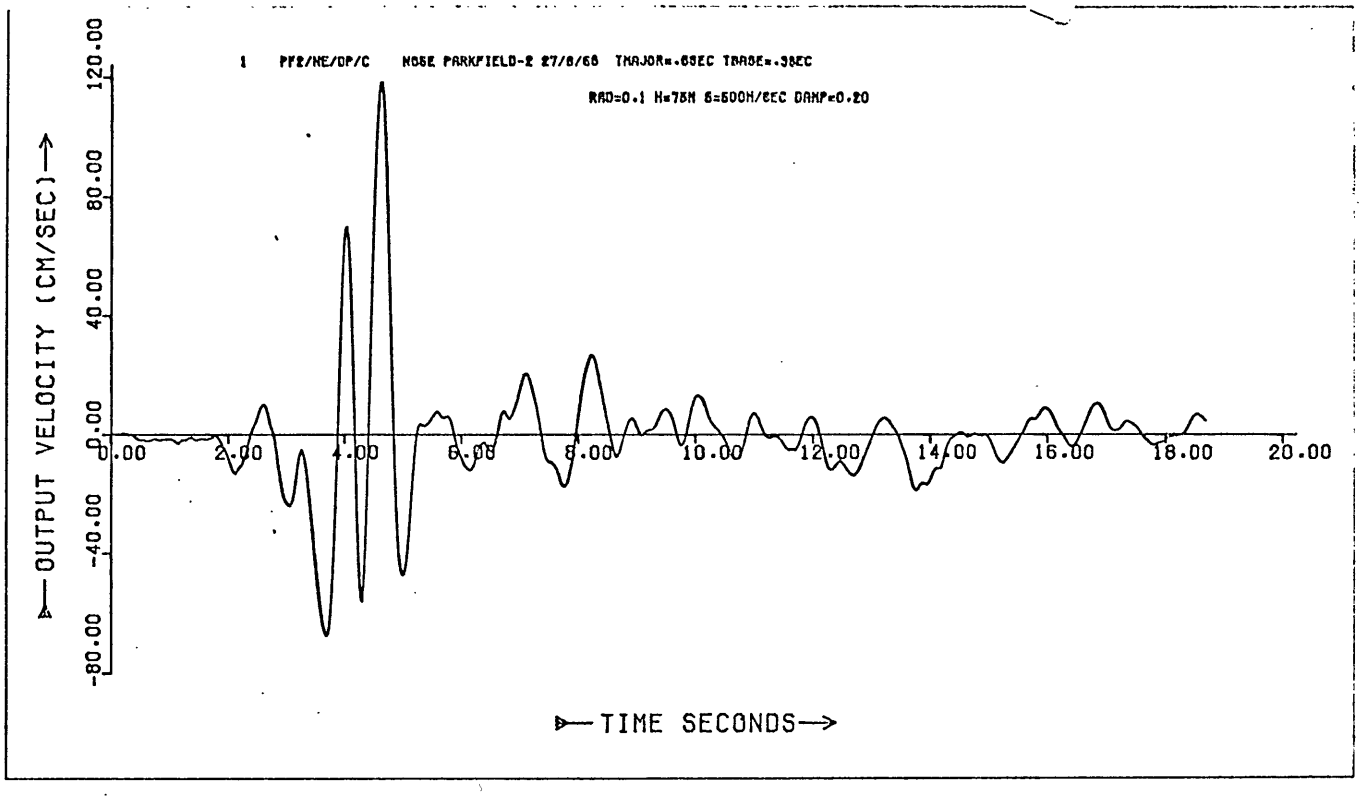


FIG. 6.35b COMPUTED GROUND SURFACE VELOCITY TIME HISTORY AT SITE NO 6.25

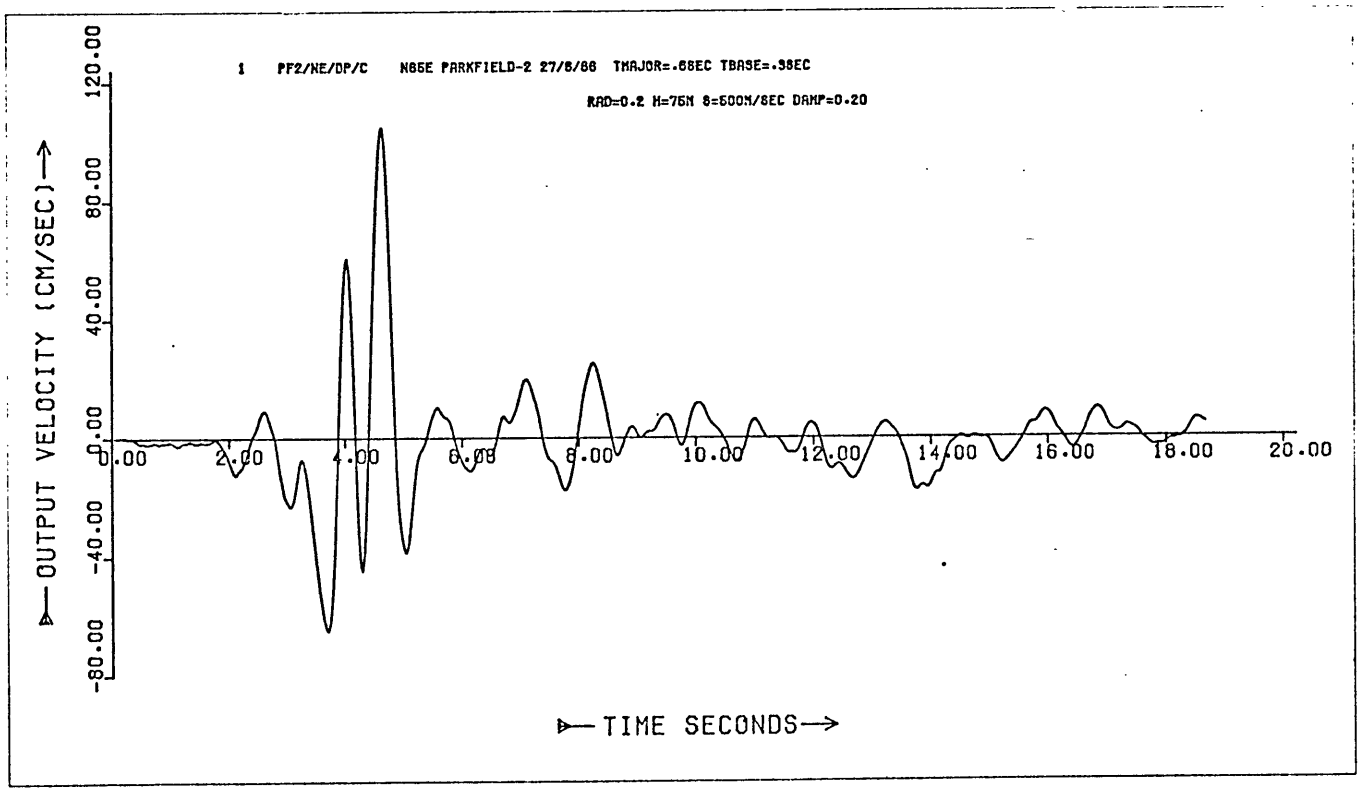


FIG. 6.36b COMPUTED GROUND SURFACE VELOCITY TIME HISTORY AT SITE NO 6.26

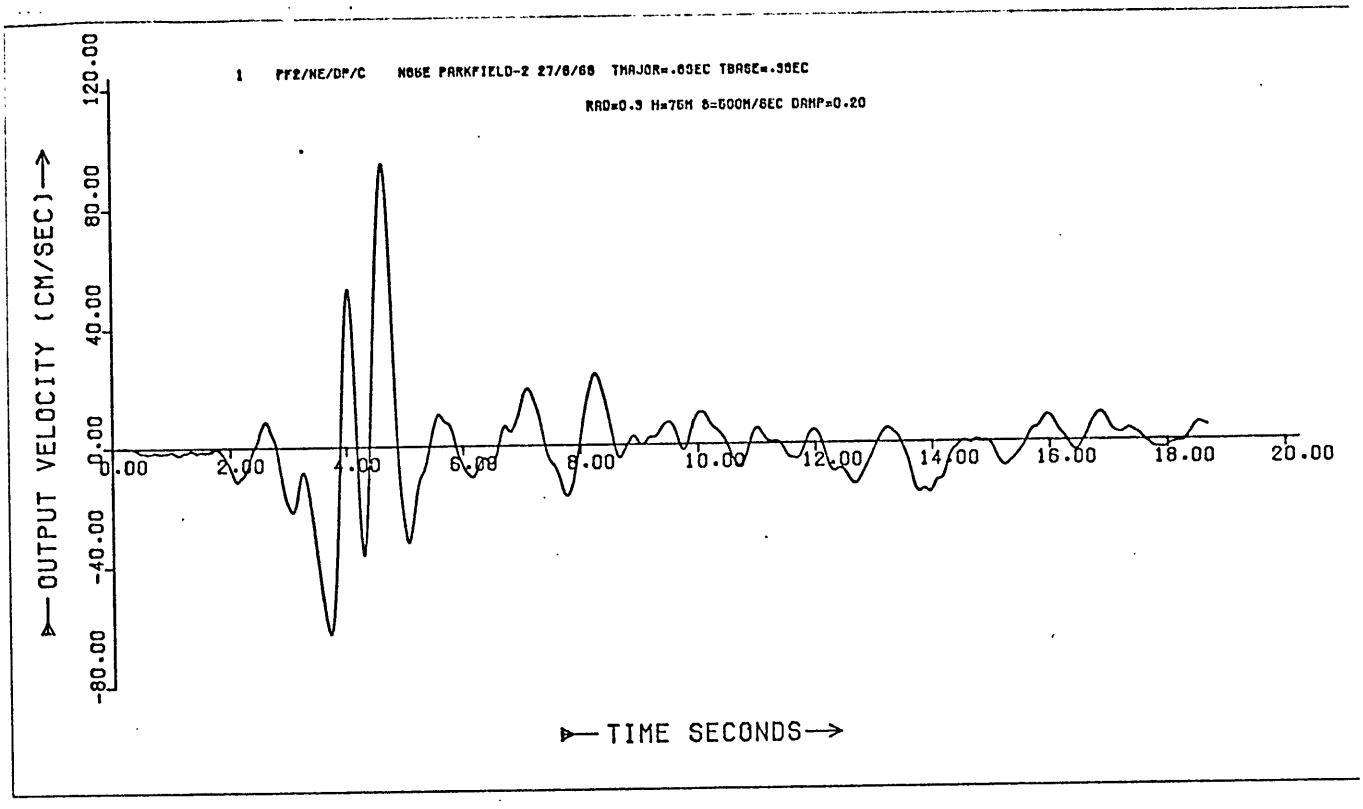


FIG.6.37 b COMPUTED GROUND SURFACE VELOCITY TIME HISTORY AT SITE NO 6.27

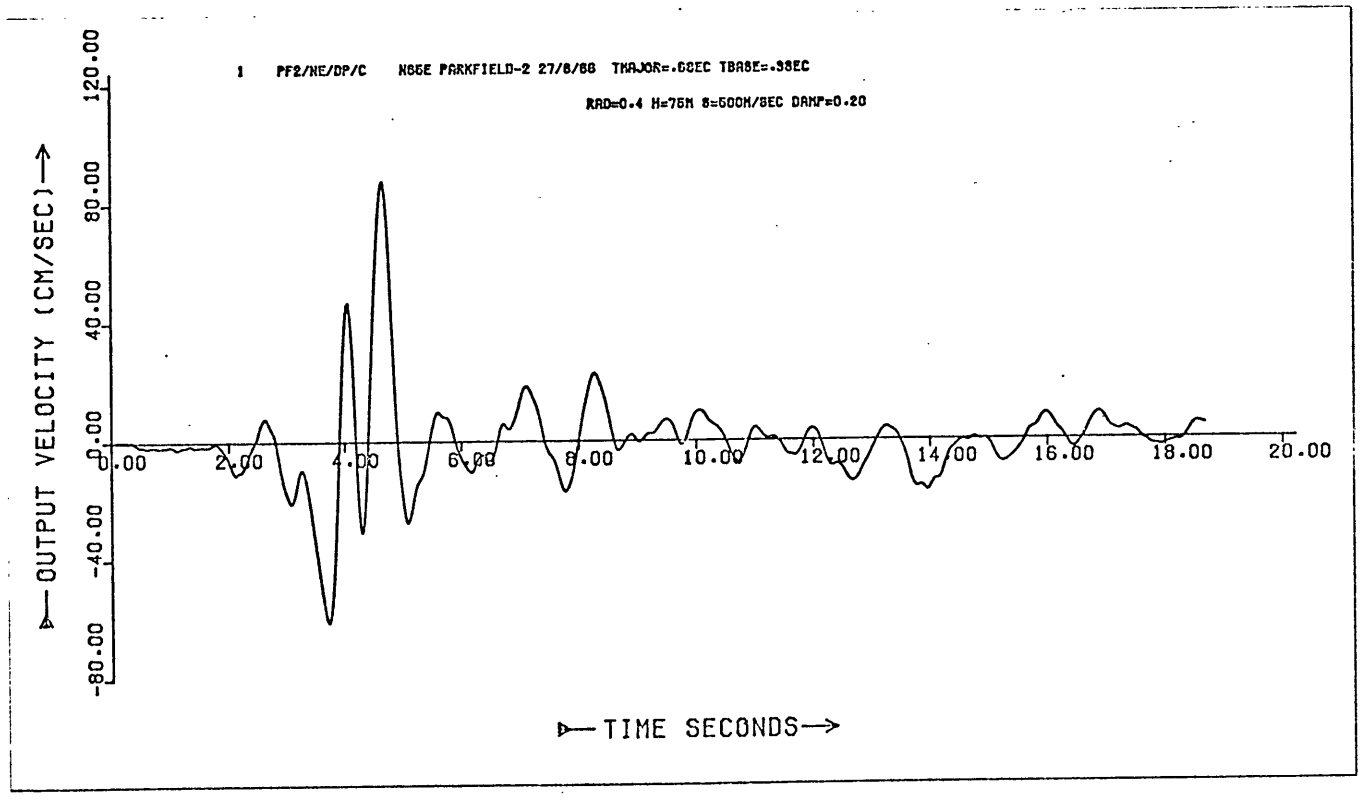


FIG. 6.38 bCOMPUTED GROUND SURFACE VELOCITY TIME HISTORY AT SITE NO 6.28

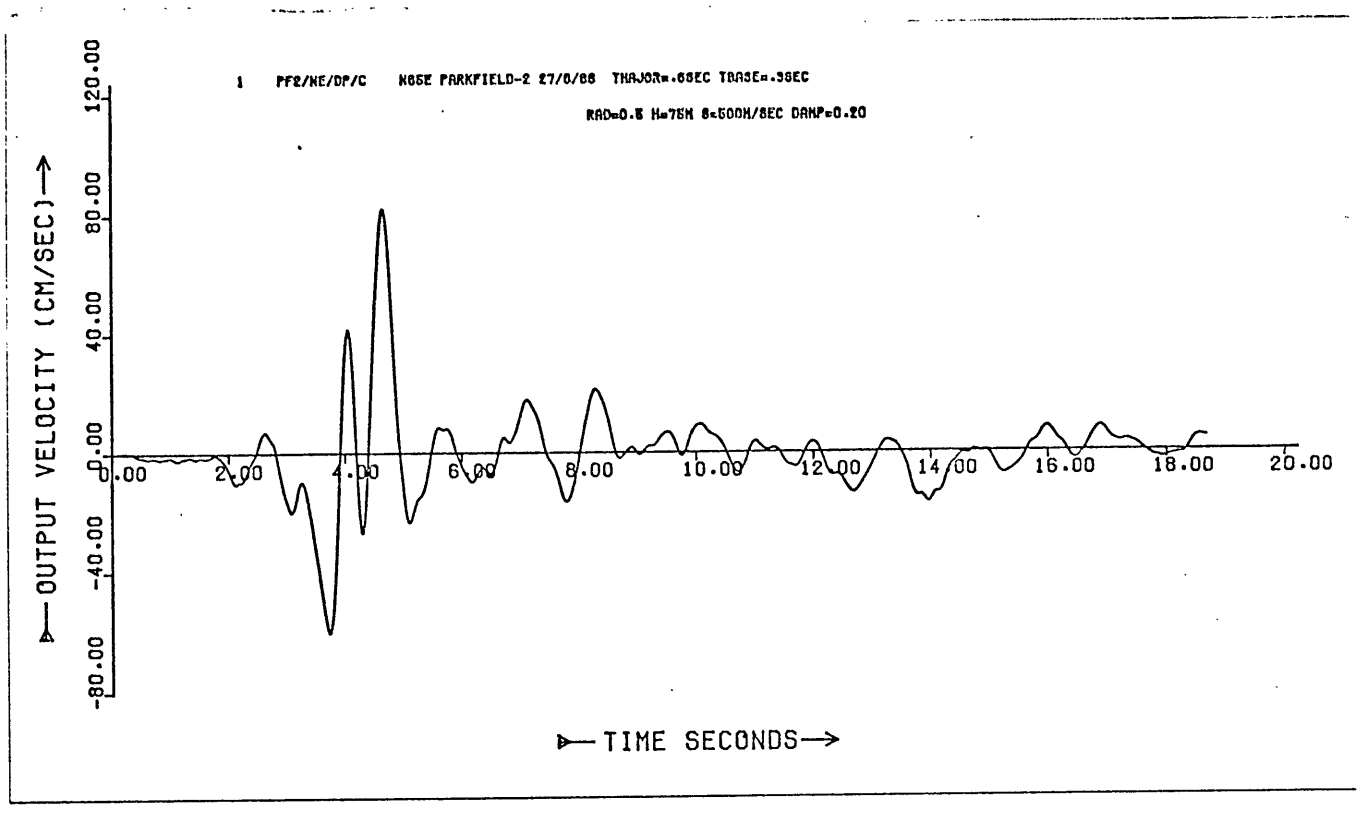


FIG. 6.39b COMPUTED GROUND SURFACE VELOCITY TIME HISTORY AT SITE NO 6.29

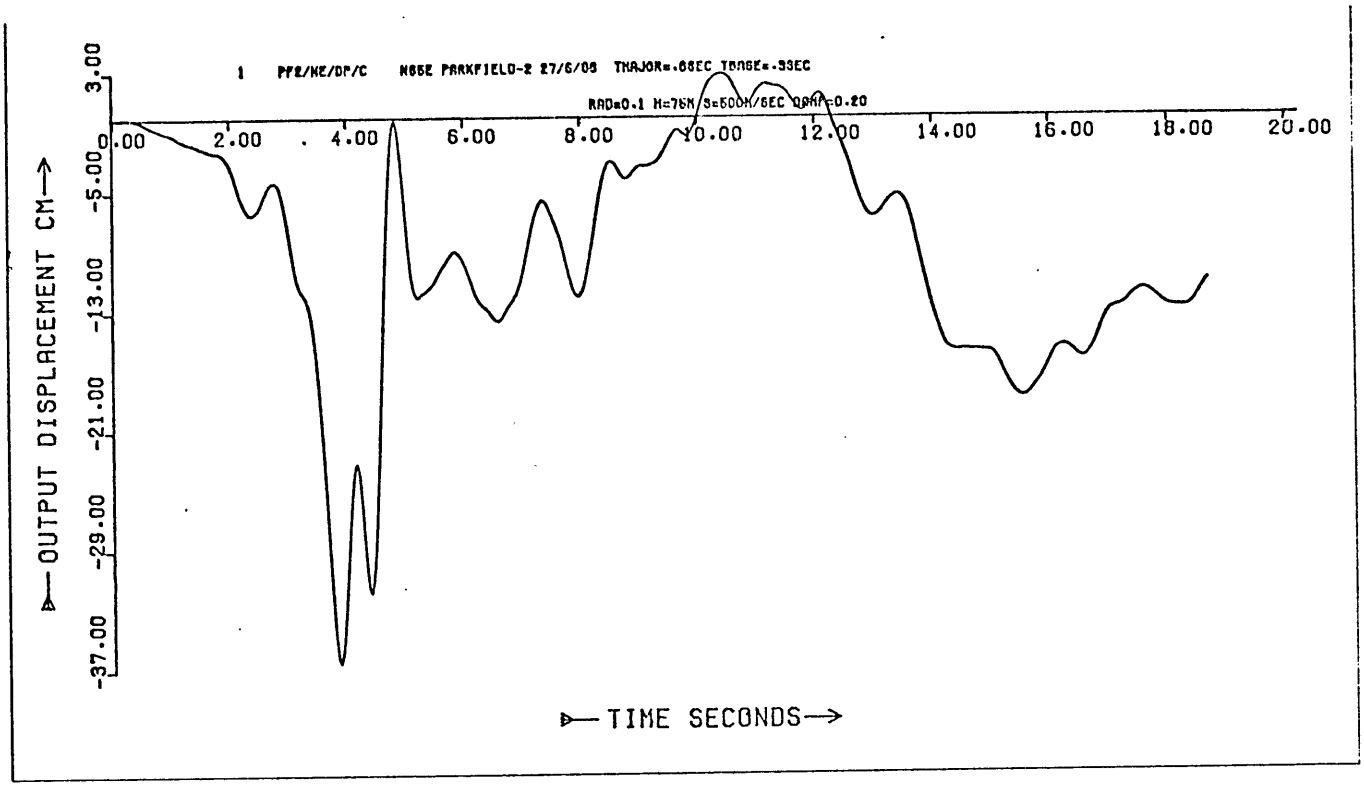


FIG.6.35c COMPUTED GROUND SURFACE DISPLACEMENT TIME HISTORY AT SITE NO 6.25

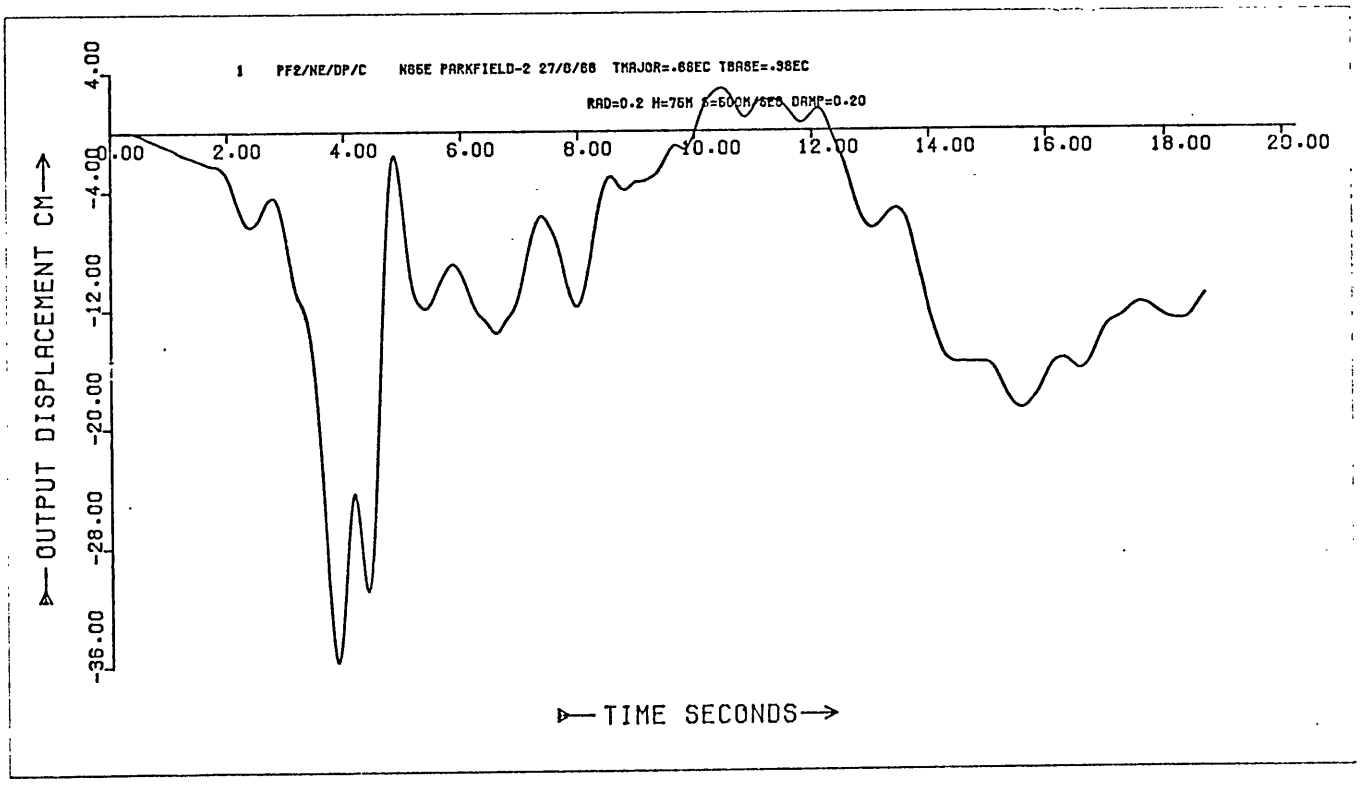


FIG.6.36c COMPUTED GROUND SURFACE DISPLACEMENT TIME HISTORY AT SITE NO 6.26

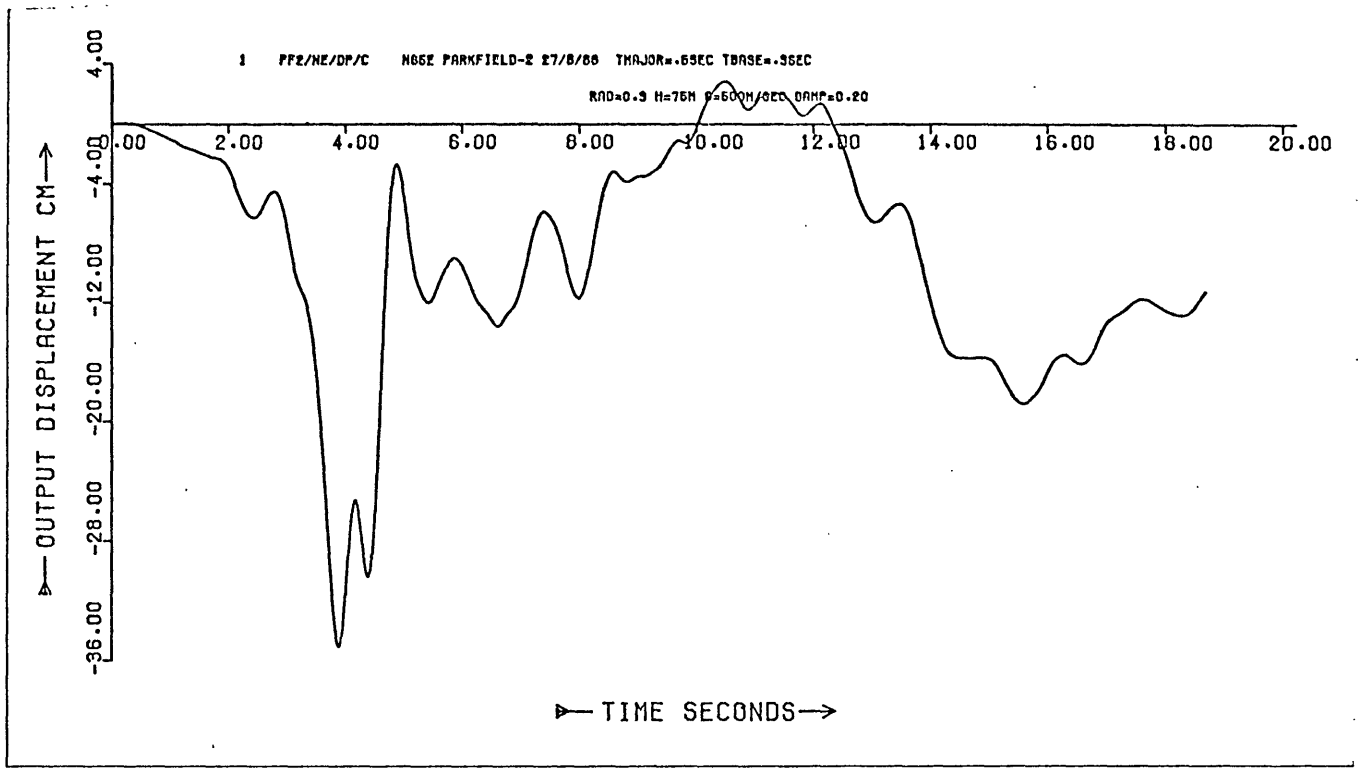


FIG. 6.37c COMPUTED GROUND SURFACE DISPLACEMENT TIME HISTORY AT SITE NO 6.27

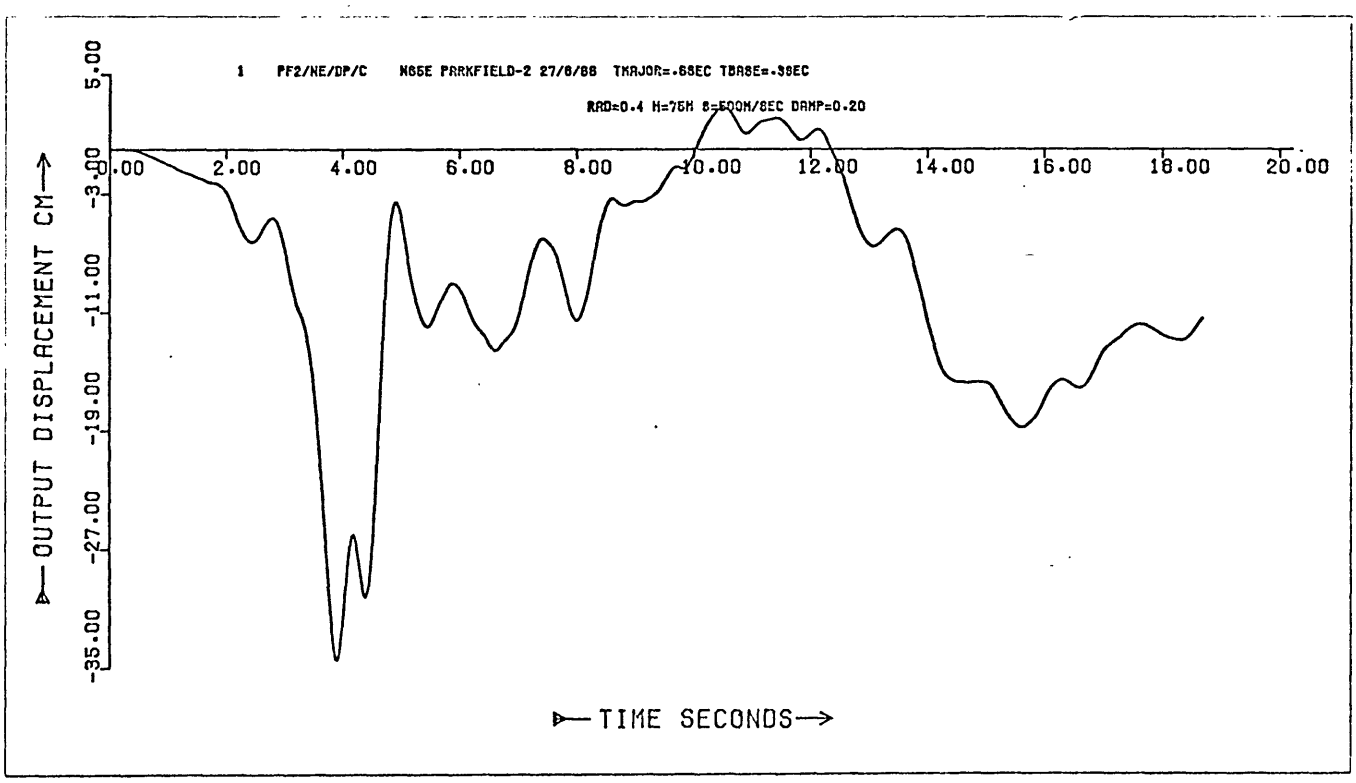


FIG. 6.38c COMPUTED GROUND SURFACE DISPLACEMENT TIME HISTORY AT SITE NO 6.28

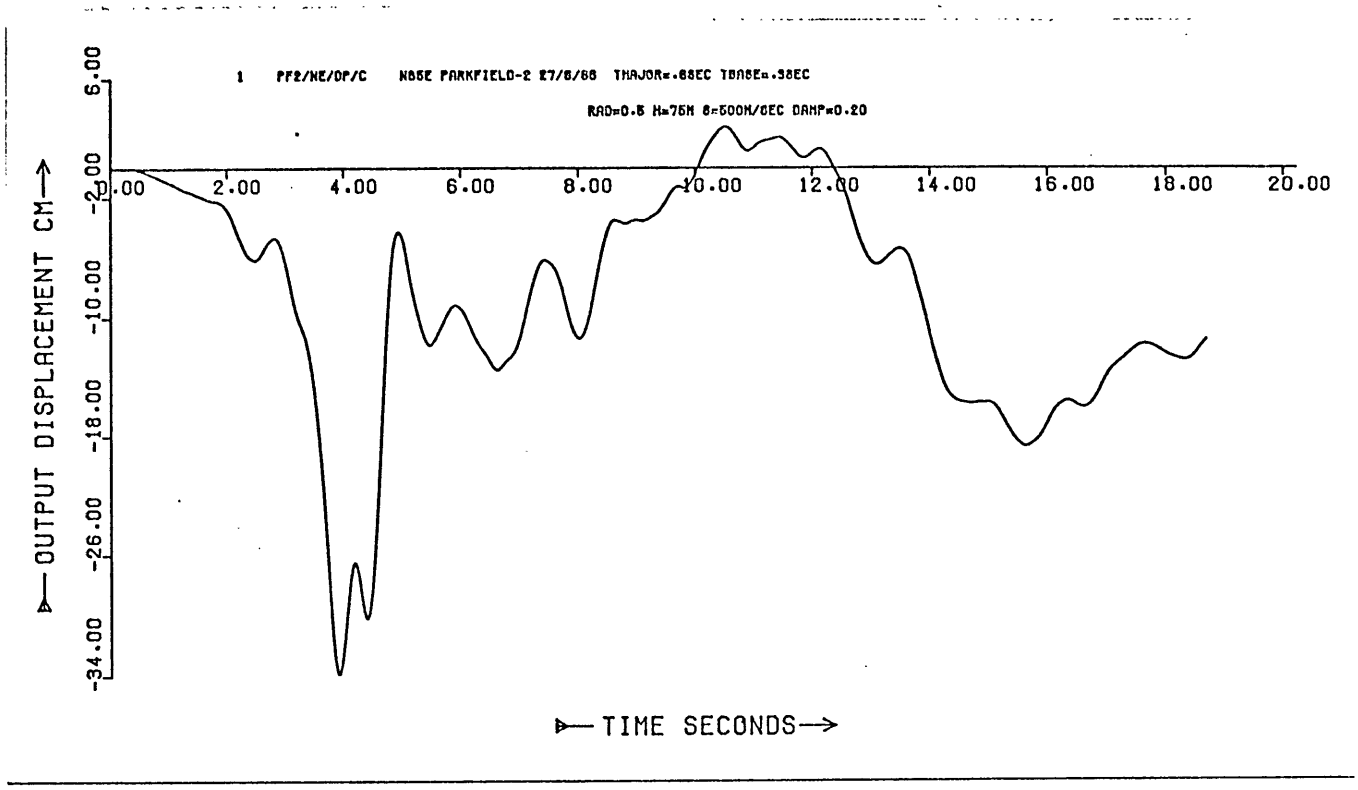


FIG.6.39c COMPUTED GROUND SURFACE DISPLACEMENT TIME HISTORY AT SITE NO 6.29

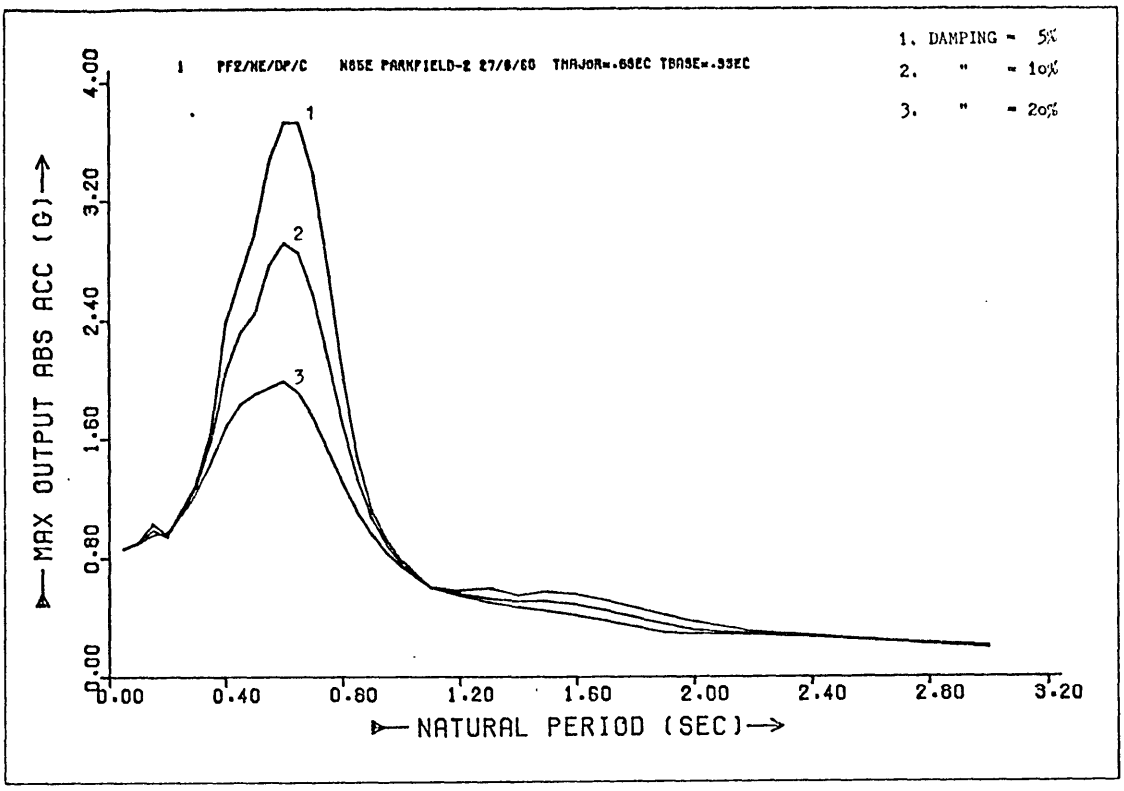


FIG.6.35d COMPUTED GROUND SURFACE ACCELERATION RESPONSE SPECTRA AT SITE NO 6.25

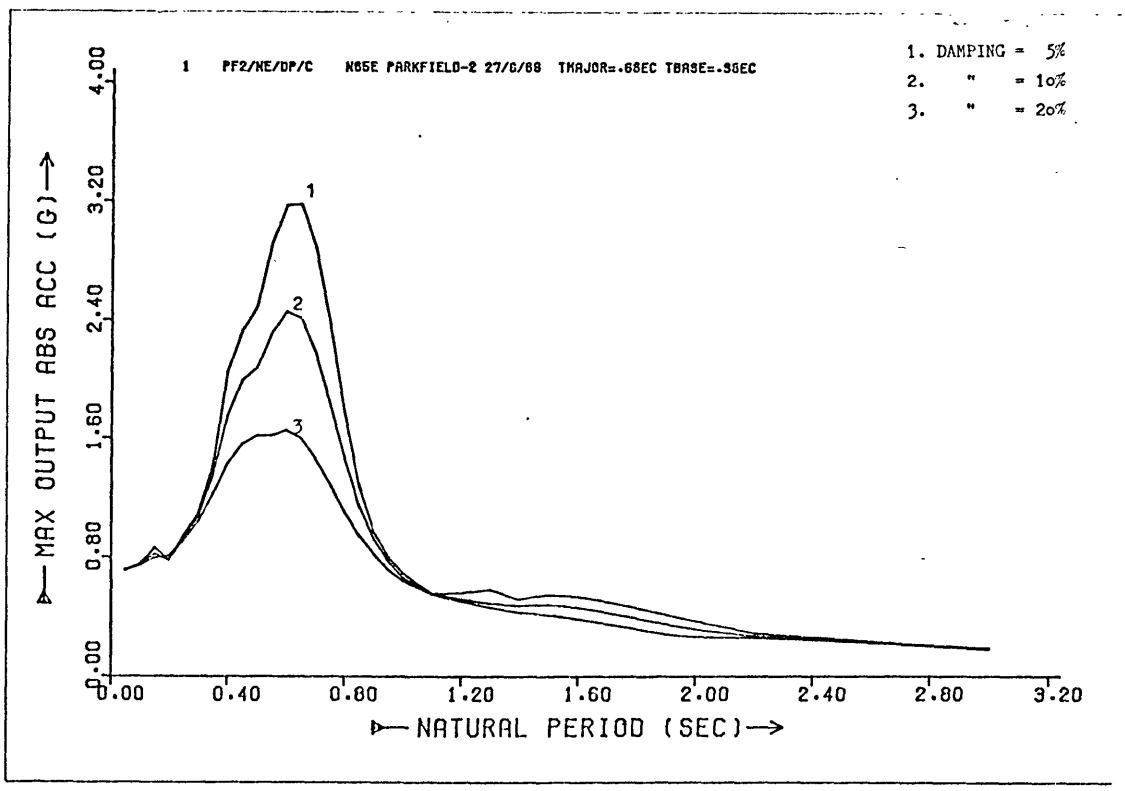


FIG. 6.36d COMPUTED GROUND SURFACE ACCELERATION RESPONSE SPECTRA AT SITE NO 6.26

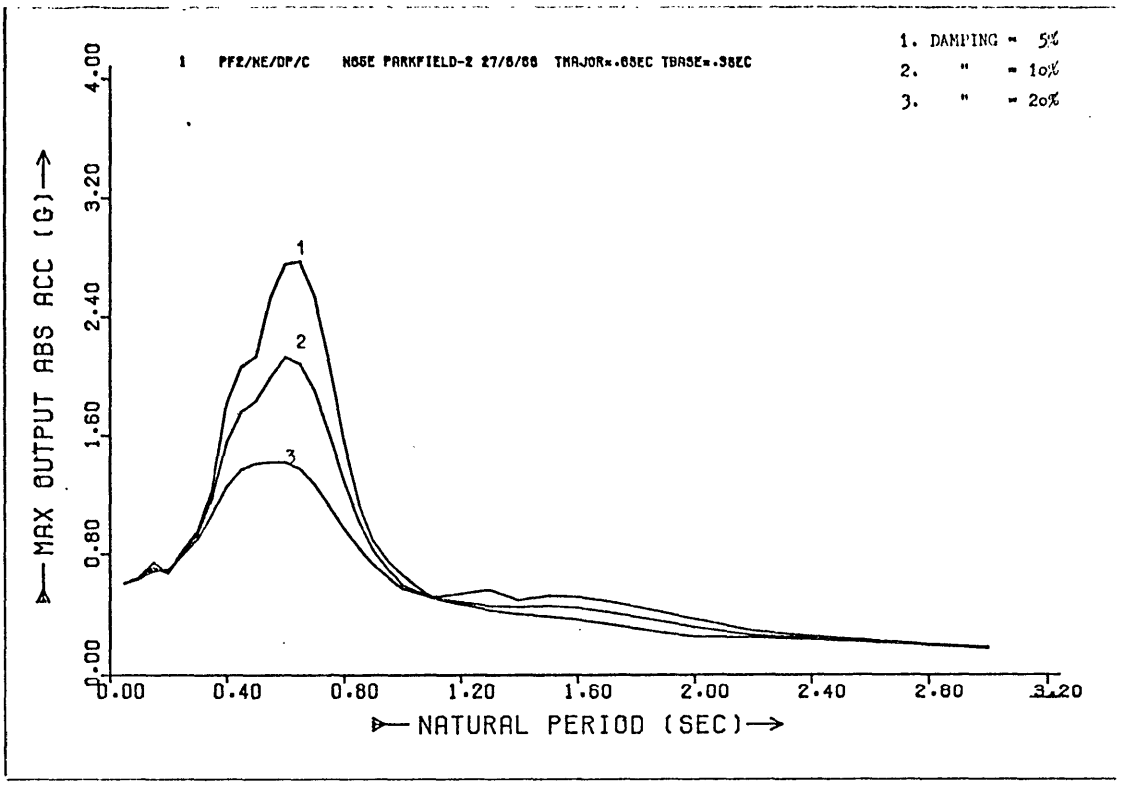


FIG. 6.37d COMPUTED GROUND SURFACE ACCELERATION RESPONSE SPECTRA AT SITE NO 6.27

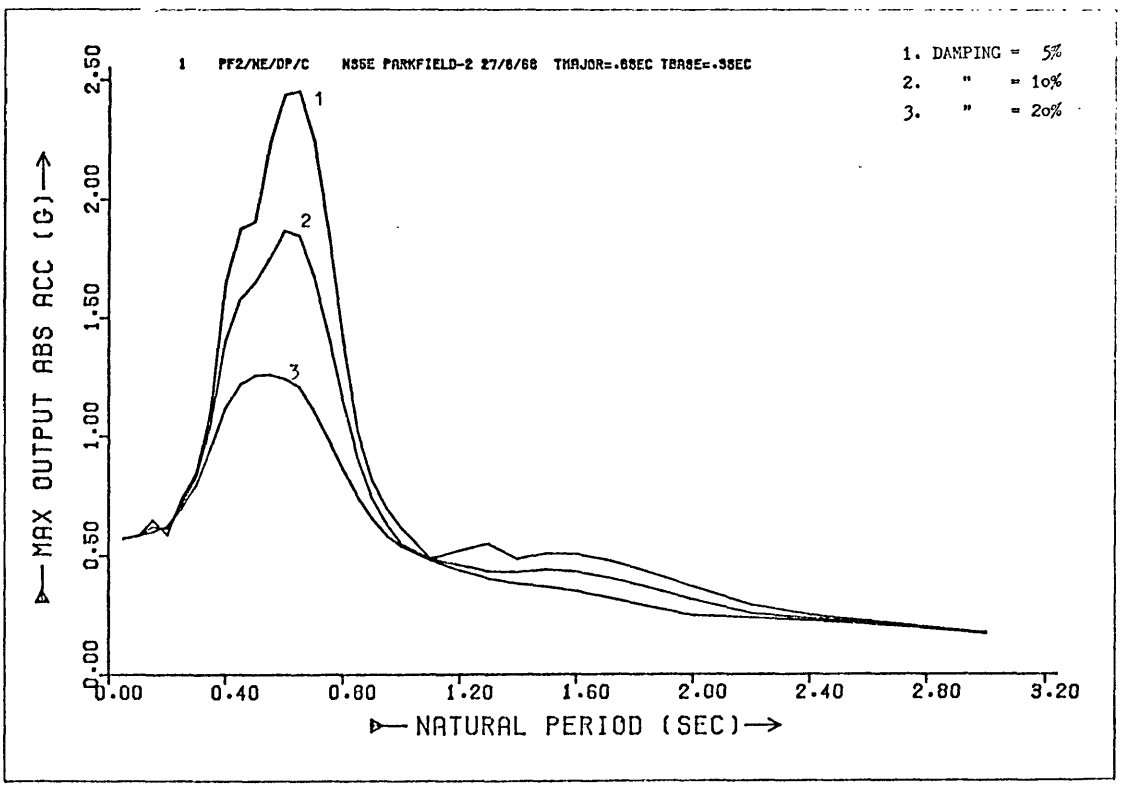


FIG. 6.38d COMPUTED GROUND SURFACE ACCELERATION RESPONSE SPECTRA AT SITE NO 6.28

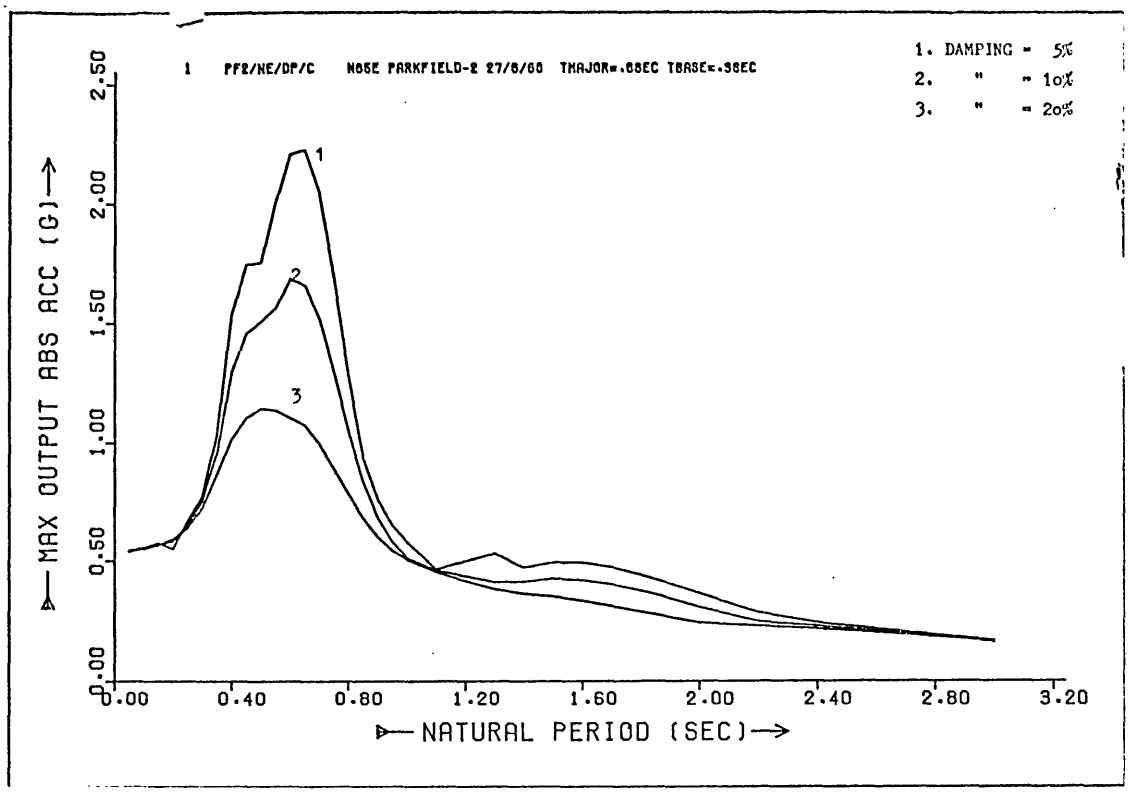


FIG.6.39d COMPUTED GROUND SURFACE ACCELERATION RESPONSE SPECTRA AT SITE NO 6.29

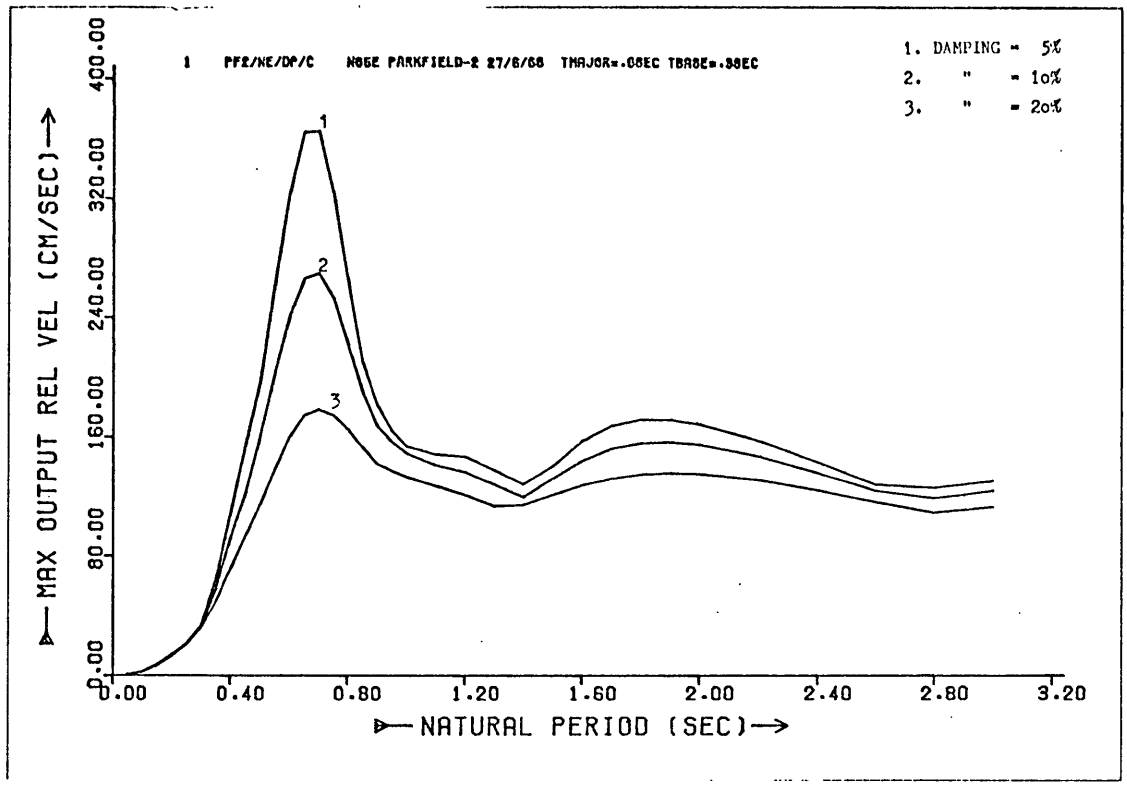


FIG.6.35e COMPUTED GROUND SURFACE VELOCITY RESPONSE SPECTRA AT SITE NO 6.25

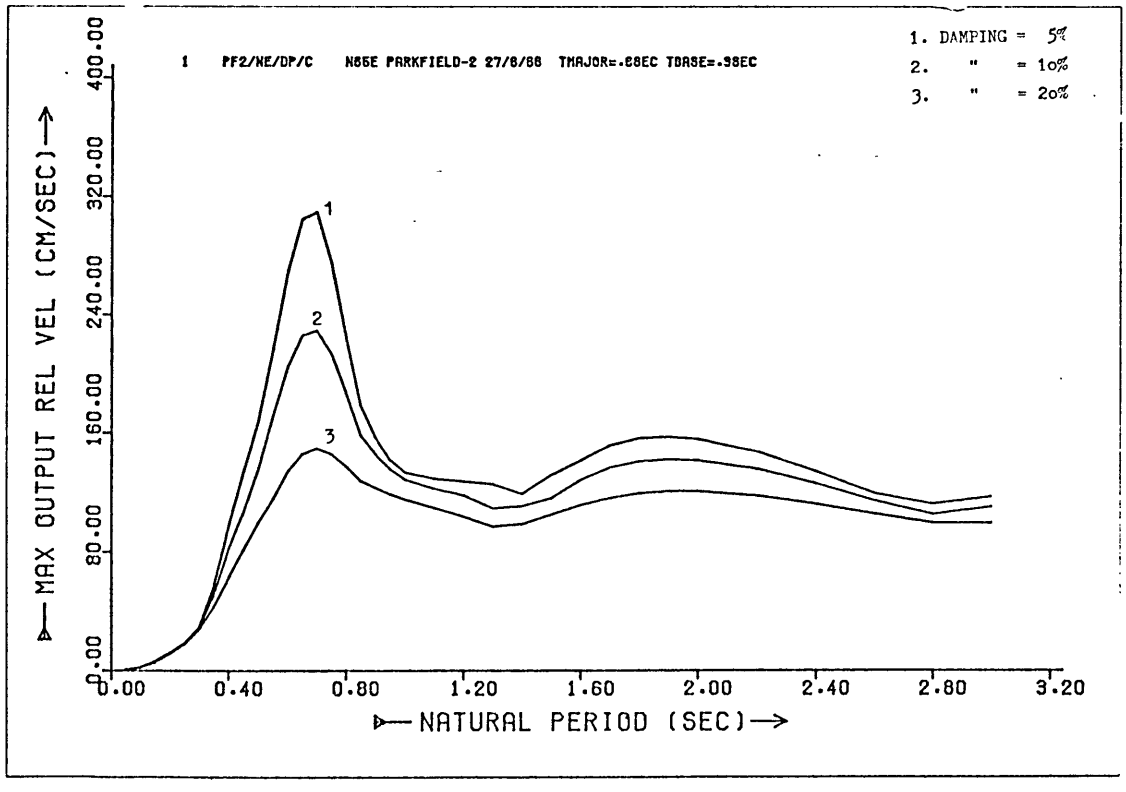


FIG. 6.36e COMPUTED GROUND SURFACE VELOCITY RESPONSE SPECTRA AT SITE NO 6.26

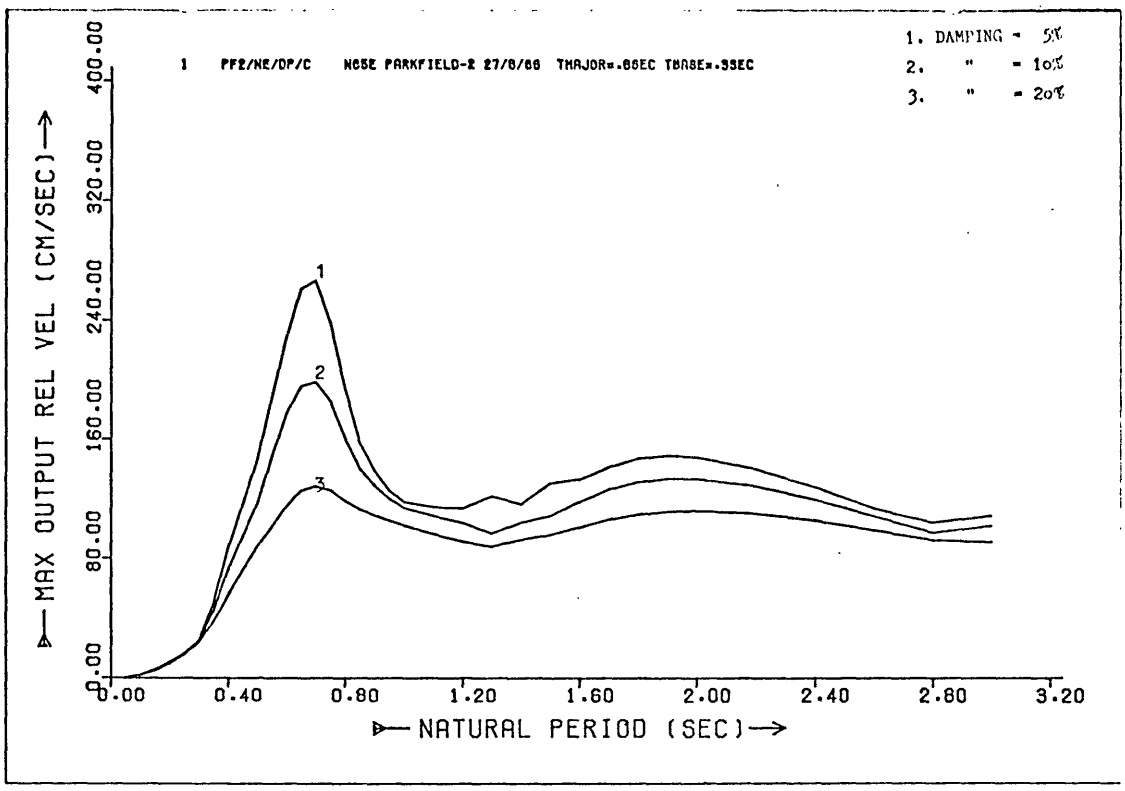


FIG. 6.37e COMPUTED GROUND SURFACE VELOCITY RESPONSE SPECTRA AT SITE NO 6.27

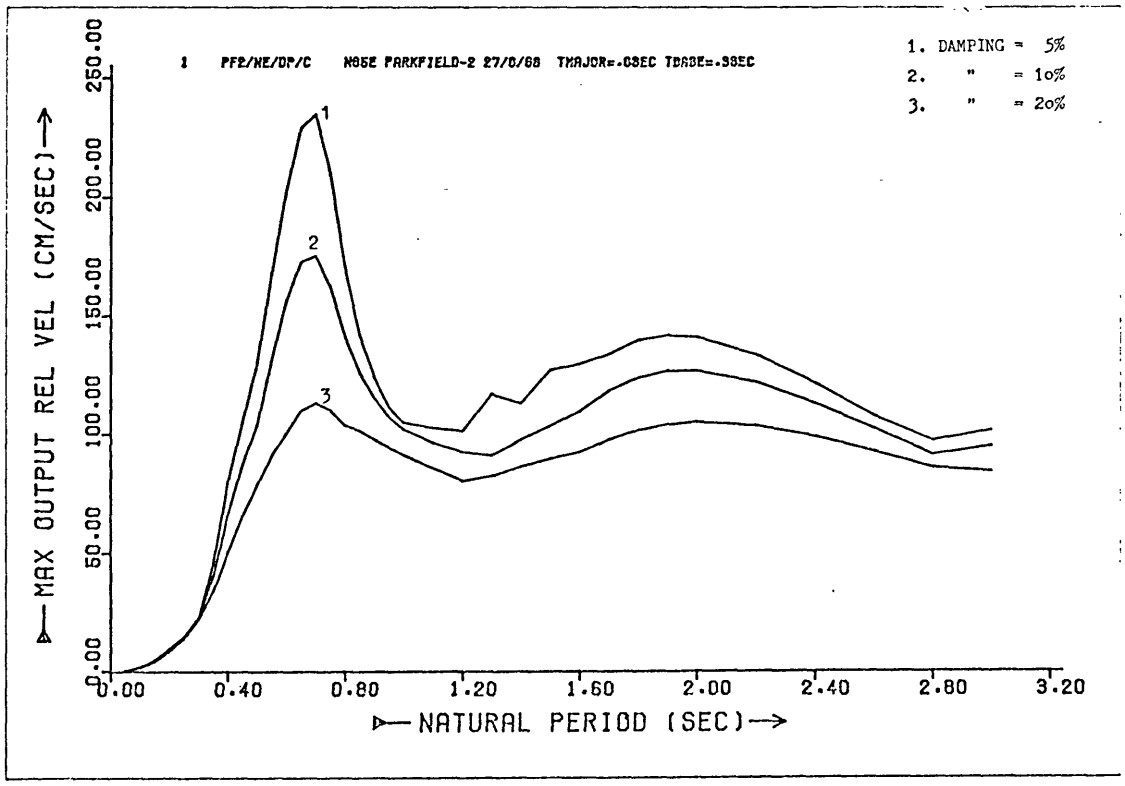


FIG. 6.38e COMPUTED GROUND SURFACE VELOCITY RESPONSE SPECTRA AT SITE NO 6.28

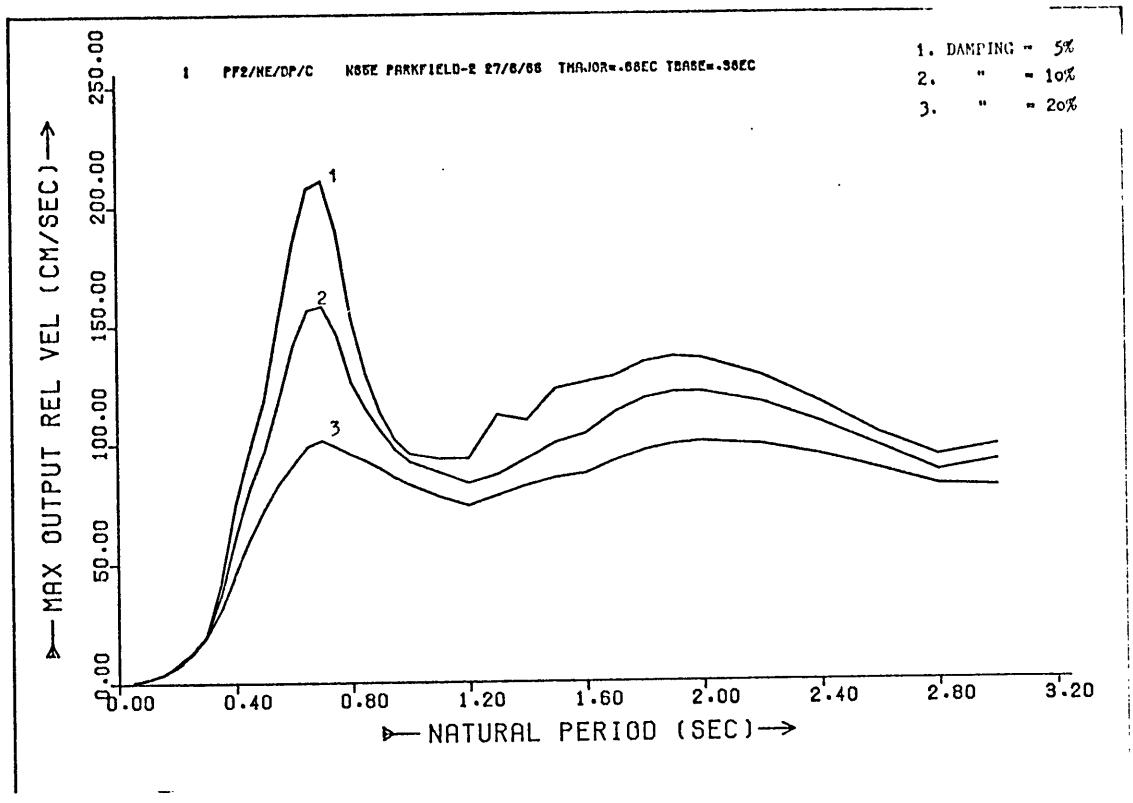


FIG. 6.39e COMPUTED GROUND SURFACE VELOCITY RESPONSE SPECTRA AT SITE NO 6.29

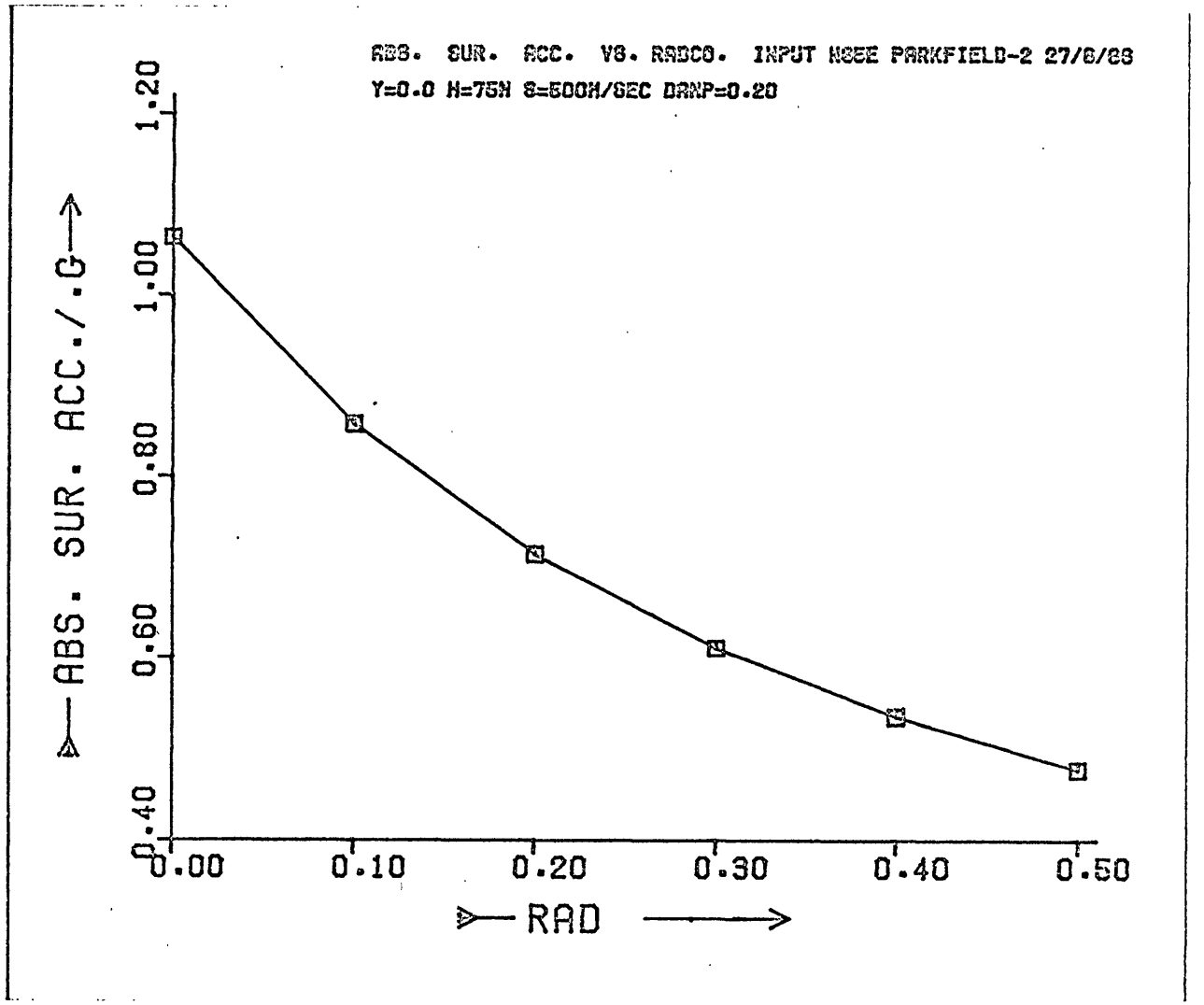
and 1000 m/sec. subjected to Parkfield-2 at the bedrock level. The maximum acceleration, velocity and displacement produced at the surface of the deposits and their comparisons with the values obtained when underlying rock formation has shear wave velocity of infinity as shown in fig. 6.15a,b,c are shown in table 6.3. The results of this set of calculations clearly confirm the observed features reported in the previous set of calculations.

Figs. 6.40 and 6.41 show variation of maximum absolute surface acceleration and 5% spectral acceleration with radiation damping ratio for the six sites considered. Figs. 6.42 to 6.43 summarize the results for maximum absolute velocity and maximum 5% spectral velocity. It is apparent that radiation damping ratio has a significant effect on response characteristics; however, such pronounced differences are expected from the transmitting boundary condition reported in chapter 4. The ten sites reported under case 1 each possess a fundamental period of 0.6 second, which corresponds to the predominant period of the bedrock motion used, thus maximizing the effect of the bedrock characteristics; the bedrock characteristics which were introduced into the solution by transmitting boundary condition given by equation 4.4 to be a substitute for the half-space bedrock formation is not only a function of radiation damping ratio, but also depends on the frequency characteristics of bedrock motion relative to the natural frequencies of the overburden. In this thesis it has been assumed that the effect of the frequency characteristics of the bedrock motion is reflected only through its predominant period. Since the bedrock accelerations are most amplified when the fundamental period of a deposit is equal to the predominant period of the bedrock motion, simulating a condition of resonance, consequent as one expects from equation 4.4 influence of constant "RAD" (radiation damping ratio) on the

DATA ON INFLUENCE OF BEDROCK CHARACTERISTICS ON RESPONSE OF SOIL DEPOSITS

RADIATION DAMPING RATIO	MAX. SUR. ABS. ACC. (%g)	$1 - \frac{ACC._{RAD}}{ACC._{0.0}} \times 100\%$	MAX. SUR. ABS. VEL. (cm/sec)	$1 - \frac{VEL._{RAD}}{VEL._{0.0}} \times 100\%$	MAX. SUR. ABS. DIS. (cm)	$1 - \frac{DIS._{RAD}}{DIS._{0.0}} \times 100\%$
0.0	1.063	00.00%	137.758	00.00%	37.155	00.00%
0.1	0.857	19.48%	117.968	14.36%	36.446	1.90%
0.2	0.714	32.83%	104.702	23.99%	35.720	3.86%
0.3	0.611	42.52%	94.663	31.28%	35.055	5.65%
0.4	0.535	49.67%	87.656	36.37%	34.425	7.35%
0.5	0.478	55.03%	82.014	40.46%	33.815	8.98%

TABLE 6.3



INFLUENCE OF BEDROCK CHARACTERISTICS ON MAXIMUM SURFACE ACCELERATION

FIG. 6.40

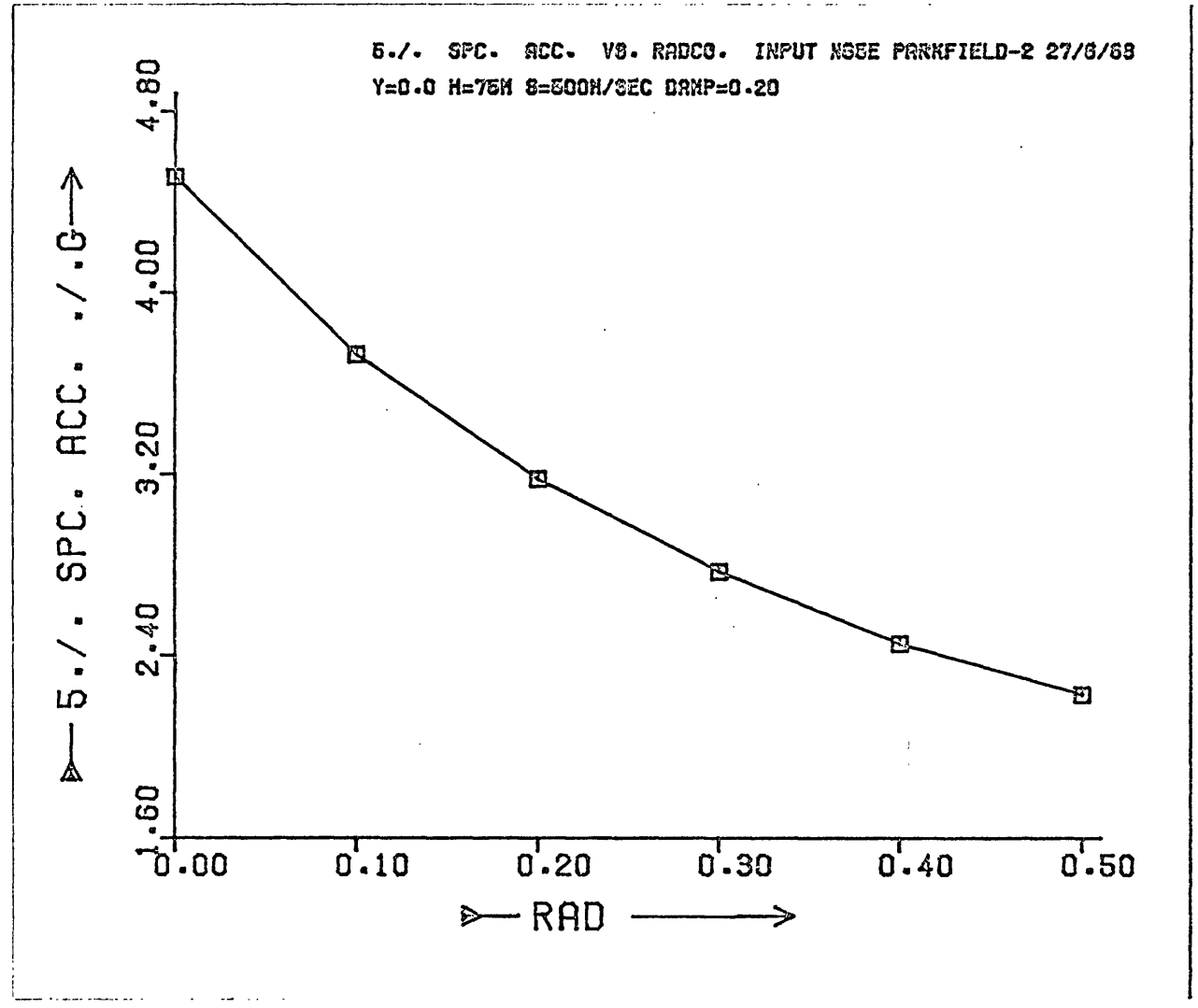


FIG. 6.41

INFLUENCE OF BEDROCK CHARACTERISTICS ON MAXIMUM 5% SPECTRAL ACCELERATION

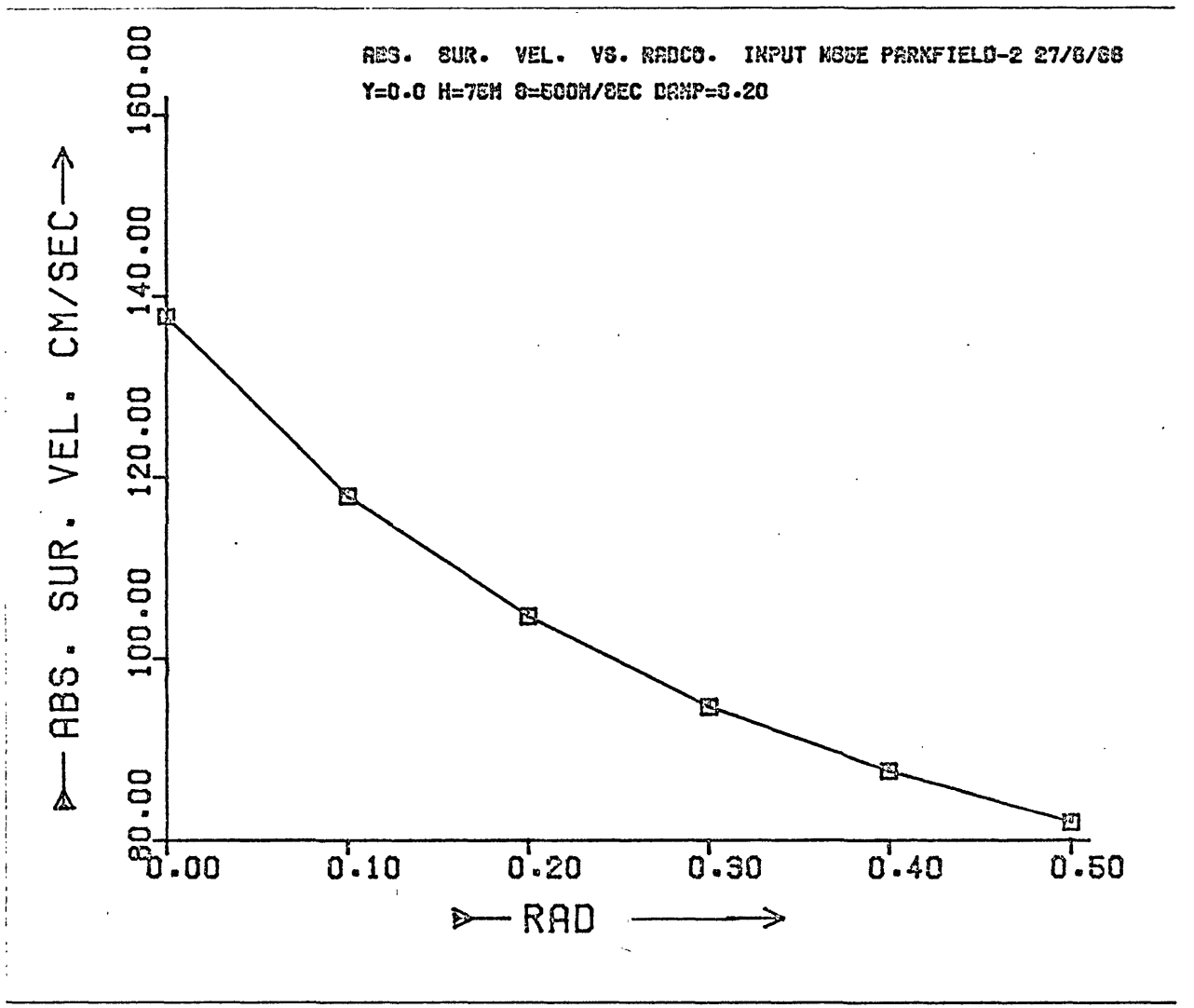
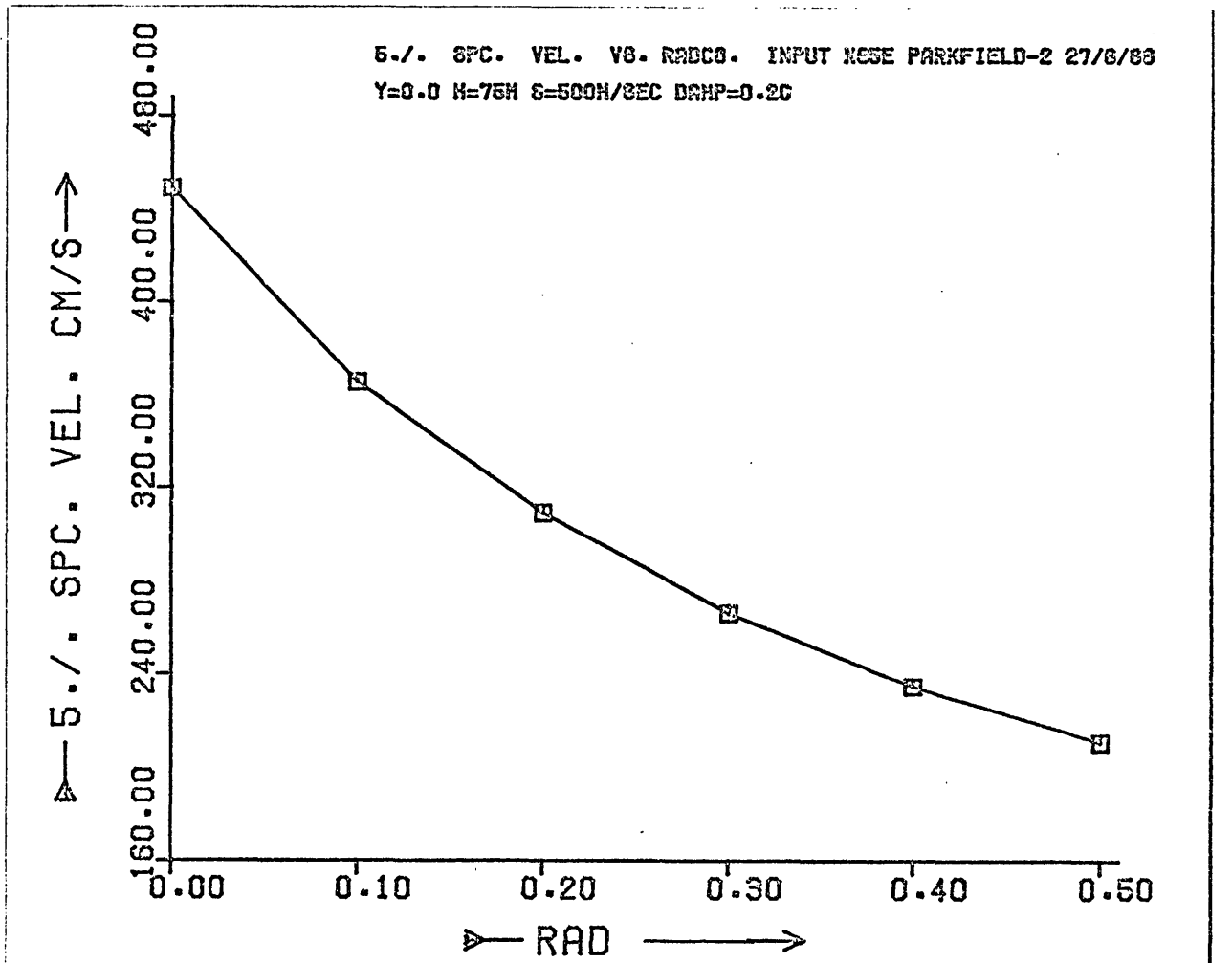


FIG. 6.42

INFLUENCE OF BEDROCK CHARACTERISTICS ON MAXIMUM SURFACE VELOCITY



INFLUENCE OF BEDROCK CHARACTERISTICS ON MAXIMUM 5% SPECTRAL VELOCITY

FIG. 6.43

system under resonance condition is maximized, hence influence of stiffness characteristics of bedrock formation is maximized. From figs. 6.40, 6.41 and 6.42, 6.43 it may be seen that the variation of maximum surface acceleration and velocity are approximately proportional to the values of maximum spectral acceleration and velocity, respectively. Thus it may be concluded that the ratios of maximum spectral acceleration/maximum ground acceleration and maximum spectral velocity/maximum ground velocity are constant; a point which will also be stressed in chapter 7.

To illustrate the influence of stiffness of the bedrock on acceleration amplification spectra fig. 6.44 has been included. Fig. 6.44 shows a family of acceleration amplification spectrum for different values of radiation damping ratios. It is observed that the softer the bedrock, the smaller is the amplification, especially at short and intermediate periods. It is also observed that the reduction in amplitudes of amplification spectra at resonance periods are not a linear function of radiation damping ratio.

Fig. 6.45 shows a family of velocity amplification spectrum for the five sites considered. It is observed that the stiffer the bedrock the higher is the amplification for short, intermediate and long periods.

CONCLUSIONS

Based on the results presented, the following conclusions are reached:

a) The frequency characteristics of surface motions are very slightly influenced by the bedrock characteristics.

b) The amplitude of pulses of surface motions are considerably affected by the characteristics of bedrock. In general, a stiffer bedrock develops higher peaks in acceleration,

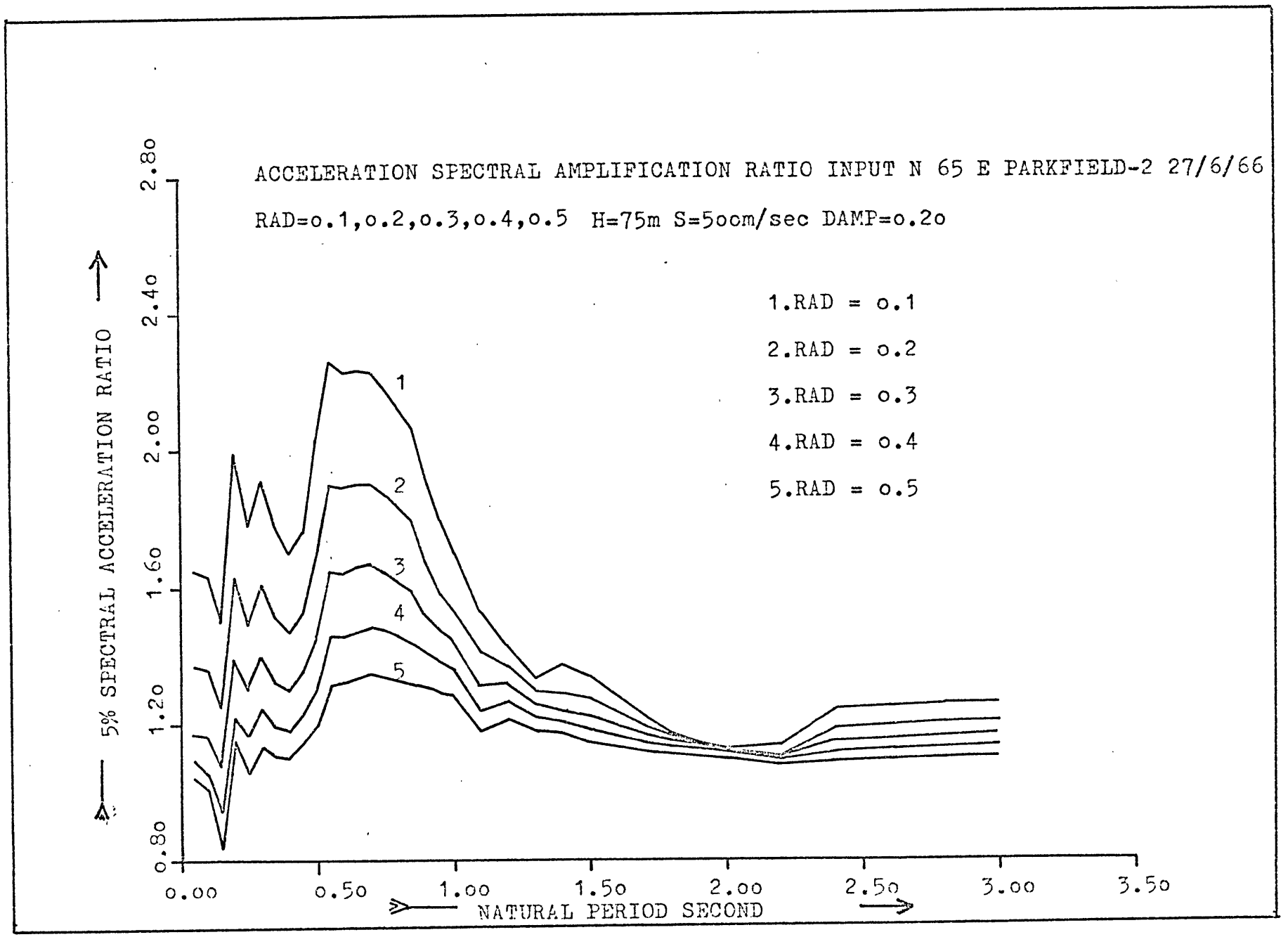

ACCELERATION SPECTRAL AMPLIFICATION RATIO INPUT N 65 E PARKFIELD-2 27/6/66
RAD=o.1,o.2,o.3,o.4,o.5 H=75m S=5oom/sec DAMP=o.2o
1.RAD = o.1
2.RAD = o.2
3.RAD = o.3
4.RAD = o.4
5.RAD = o.5
5% SPECTRAL ACCELERATION RATIO
2.8o
2.4o
2.oo
1.6o
1.2o
o.8o
0.00
0.5o
1.oo
1.5o
2.oo
2.5o
3.oo
3.5o
NATURAL PERIOD SECOND

FIG.6.44

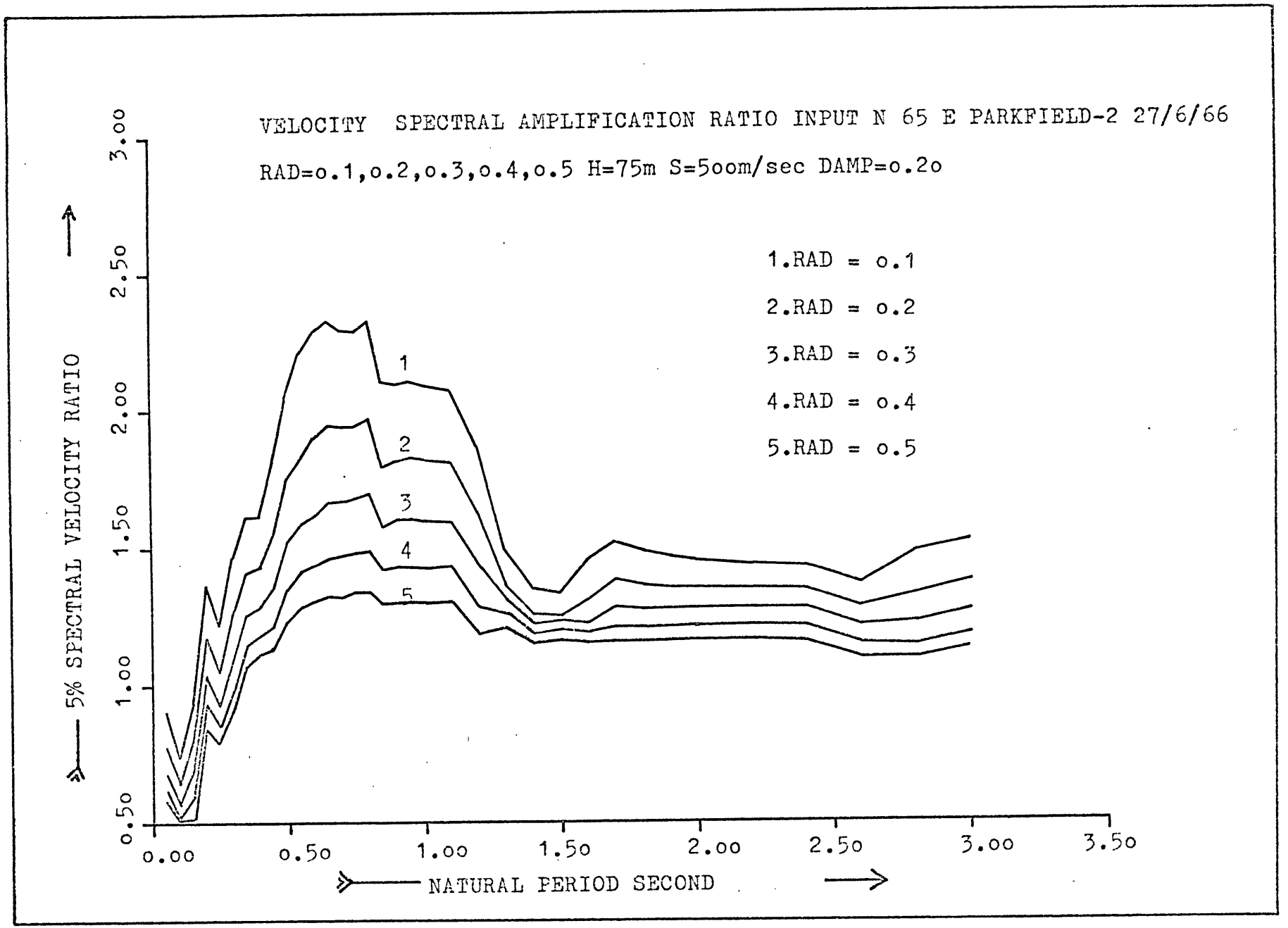

VELOCITY SPECTRAL AMPLIFICATION RATIO INPUT N 65 E PARKFIELD-2 27/6/66
RAD=o.1,o.2,o.3,o.4,o.5 H=75m S=5oom/sec DAMP=o.2o
1.RAD = o.1
2.RAD = o.2
3.RAD = o.3
4.RAD = o.4
5.RAD = o.5
5% SPECTRAL VELOCITY RATIO
NATURAL PERIOD SECOND
0.50
1.00
1.50
2.00
2.50
3.00
0.00
0.50
1.00
1.50
2.00
2.50
3.00
3.50
1
2
3
4
5

FIG. 6.45

velocity and displacement distribution pattern. The magnitude of the influence on maximum ground surface acceleration is maximized in the case considered (i.e. predominant period of bedrock motion equal to the fundamental period of the overburden).

c) The energy available for damage is highly dependent on the characteristics of bedrock formation.

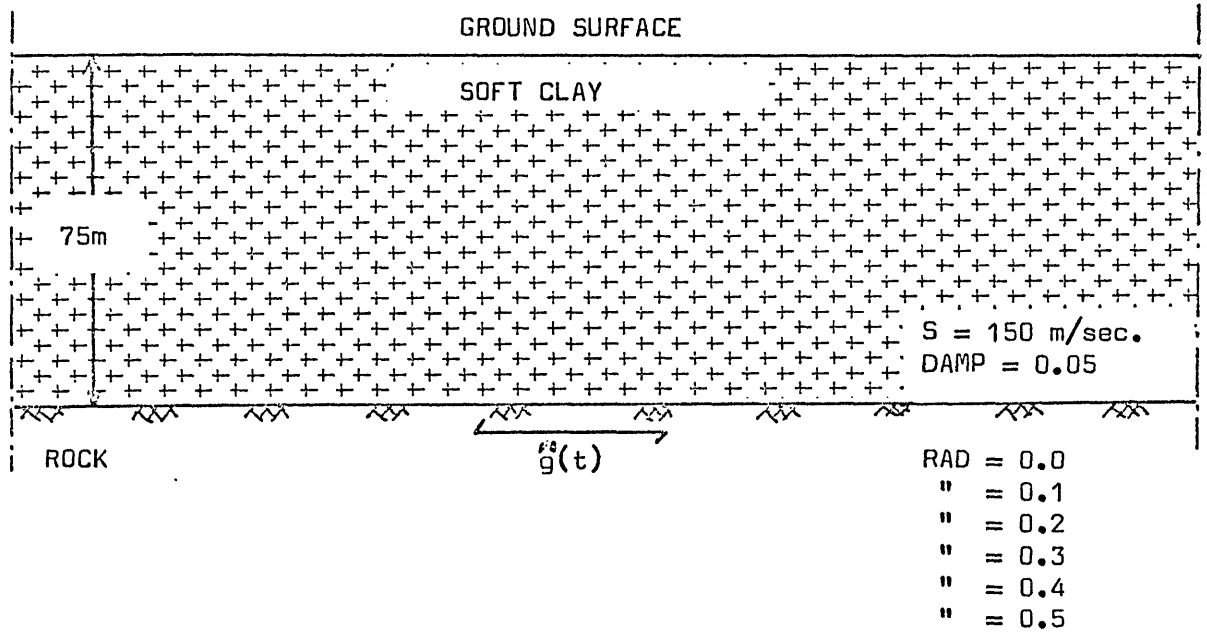
d) The softer the bedrock the smaller is the acceleration amplification, especially near the natural periods of the overburden.

6.8.2.2. RESULTS OF CASE 2

In most cases, the predominant period of bedrock motion is not equal to the fundamental period of the soil deposit . This section provides further comparisons between frequency distribution and amplitudes of surface motions of a semi-infinite layer, having six different bedrock characteristics subjected at its bedrock level to two different motions. In each comparison, all parameters other than the radiation damping ratio, were kept constant. Based on the results obtained, it will be shown that stiffness characteristics of the bedrock may have a considerable influence on frequency distribution of output motions and amplitude of the pulses.

Figs. 6.46a,b,c,d,e through 6.51a,b,c,d,e show response of six 50m. deposit of soft clay with fundamental periods of 1.33 second underlain by bedrock having different stiffness characteristics, as shown in fig. 6.46. The deposits were subjected at their bedrock level to Parkfield-8 N50E, with a predominant period of 0.15 second and maximum acceleration of 0.28g.

The time histories of computed surface motions are shown in figs.



RESPONSE OF HYSTERETIC DEPOSIT UNDERLAIN BY DEFORMABLE BEDROCK

SCHEMATIC SOIL PROFILE FOR SITE NO. 6.30.

6.31, 6.32, 6.33, 6.34, 6.35

FIG. 6.46

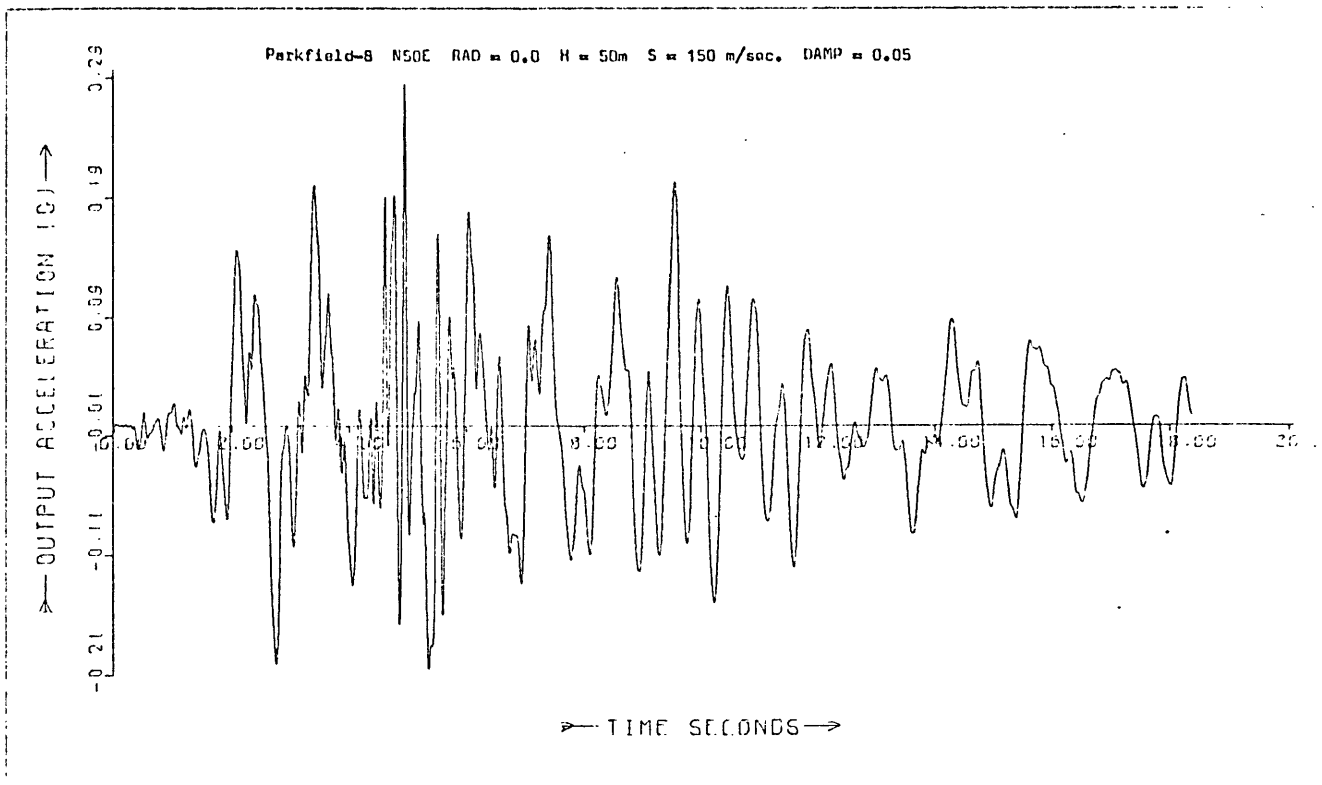


FIG.6.46aCOMPUTED GROUND SURFACE ACCELERATION TIME HISTORY AT SITE NO. 6.3o

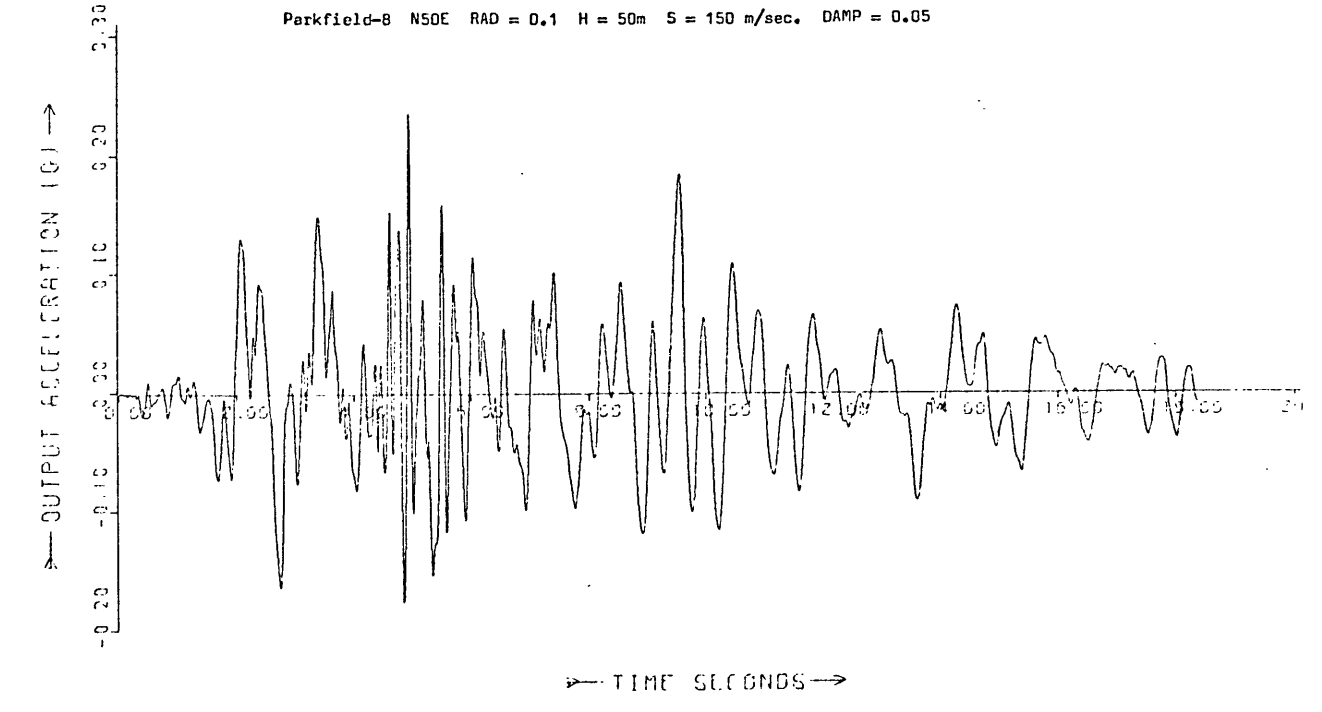


FIG. 6.47a COMPUTED GROUND SURFACE ACCELERATION TIME HISTORY AT SITE NO. 6.31

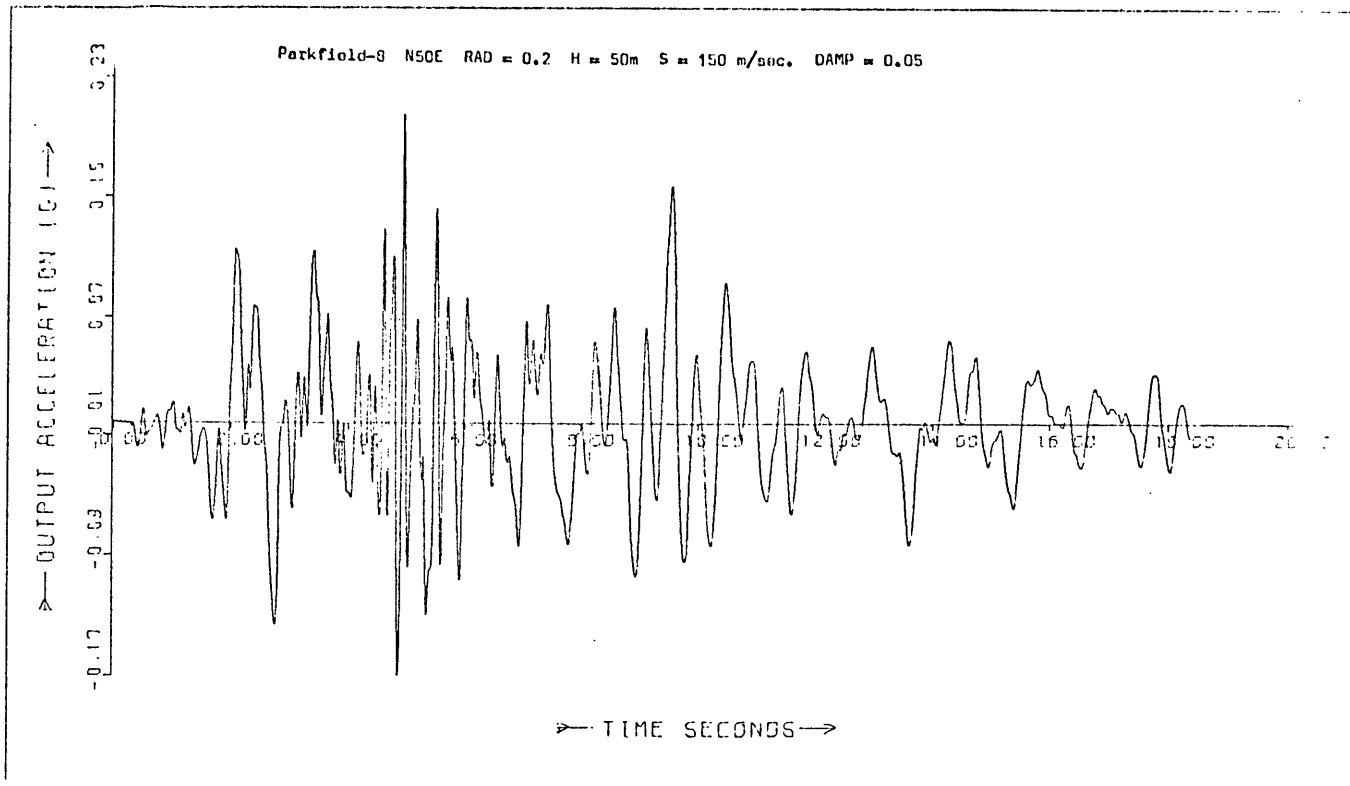


FIG. 6.48a COMPUTED GROUND SURFACE ACCELERATION TIME HISTORY AT SITE NO. 6.32

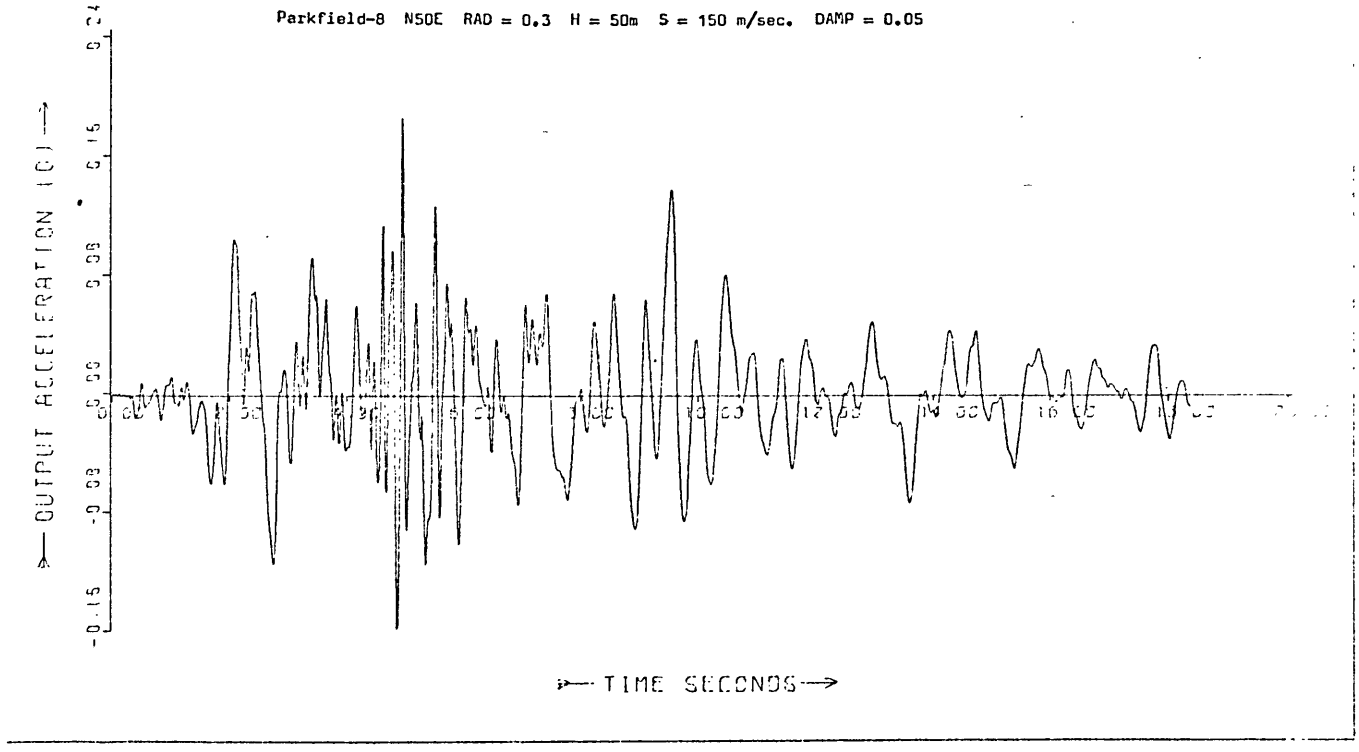


FIG. 6.49a COMPUTED GROUND SURFACE ACCELERATION TIME HISTORY AT SITE NO. 6.33

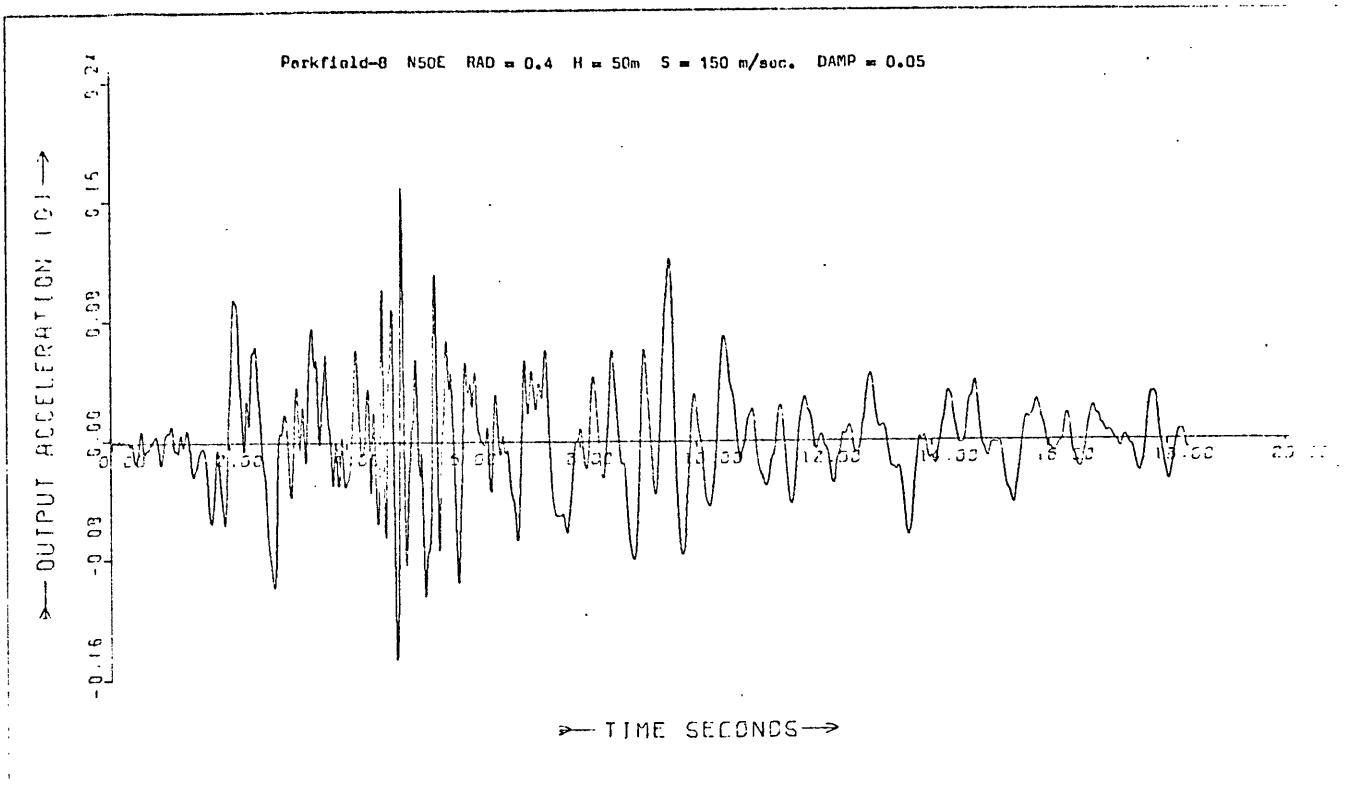


FIG.6.5a COMPUTED GROUND SURFACE ACCELERATION TIME HISTORY AT SITE NO. 6.34

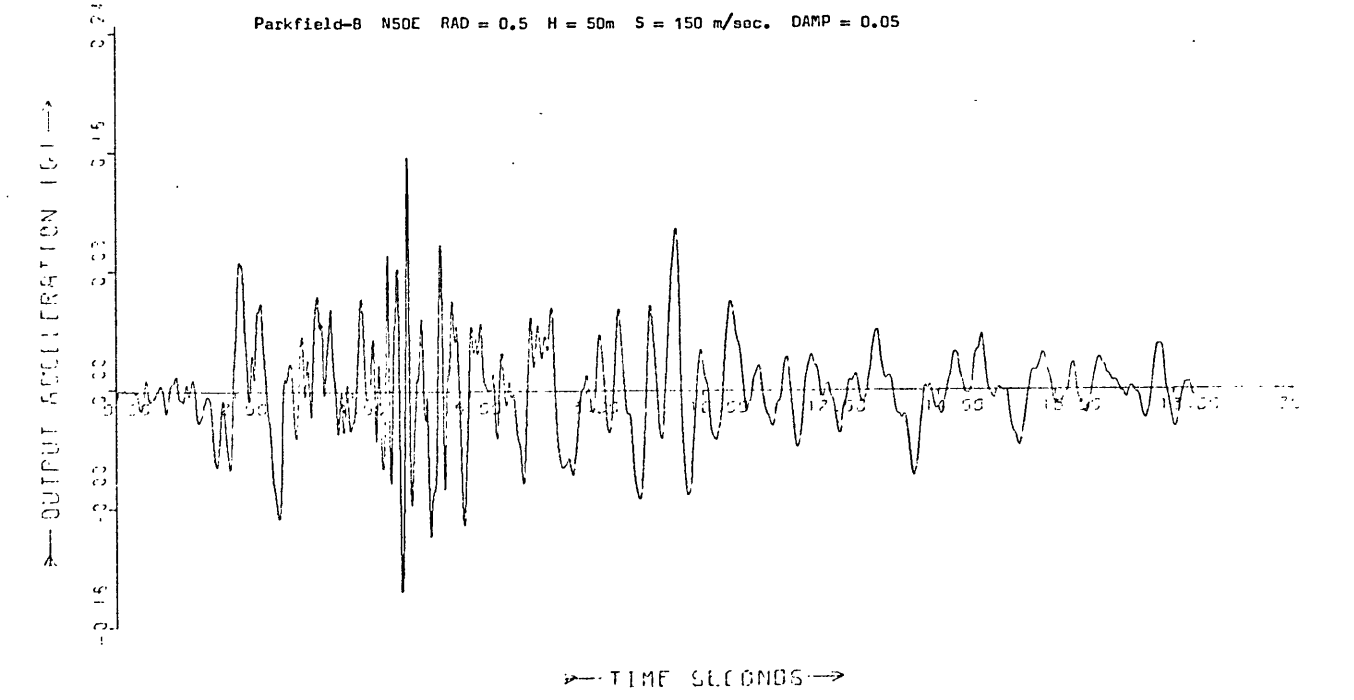


FIG.6.51a COMPUTED GROUND SURFACE ACCELERATION TIME HISTORY AT SITE NO. 6.35

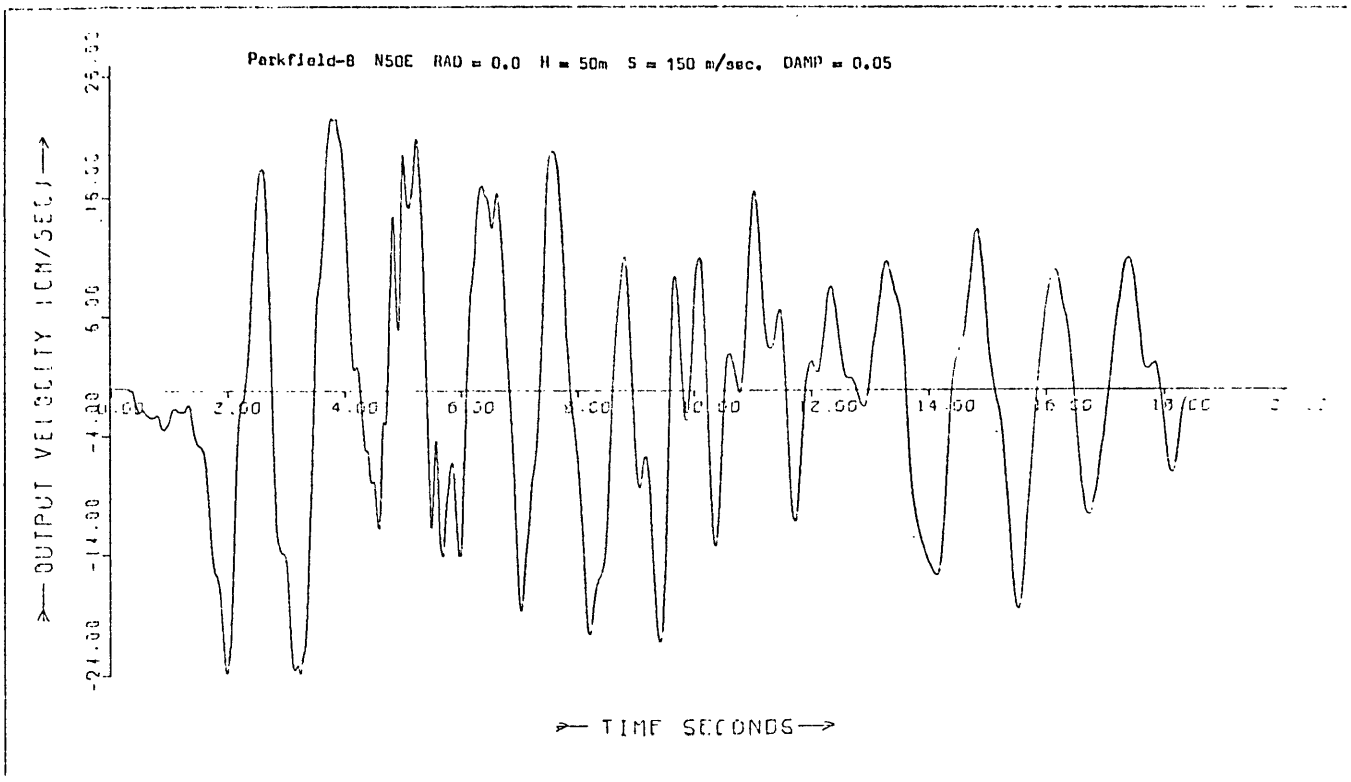


FIG.6.46b COMPUTED GROUND SURFACE VELOCITY TIME HISTORY AT SITE NO. 6.30

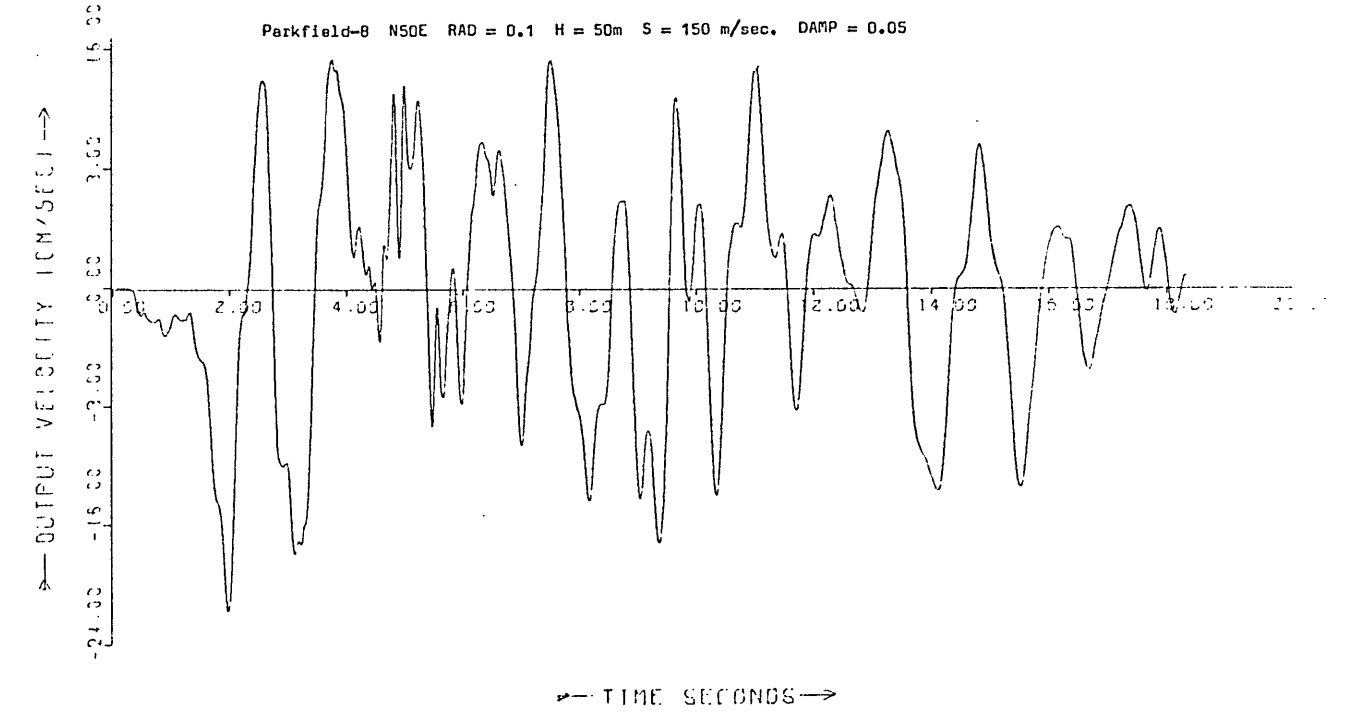


FIG. 6.47b COMPUTED GROUND SURFACE VELOCITY TIME HISTORY AT SITE NO. 6.31

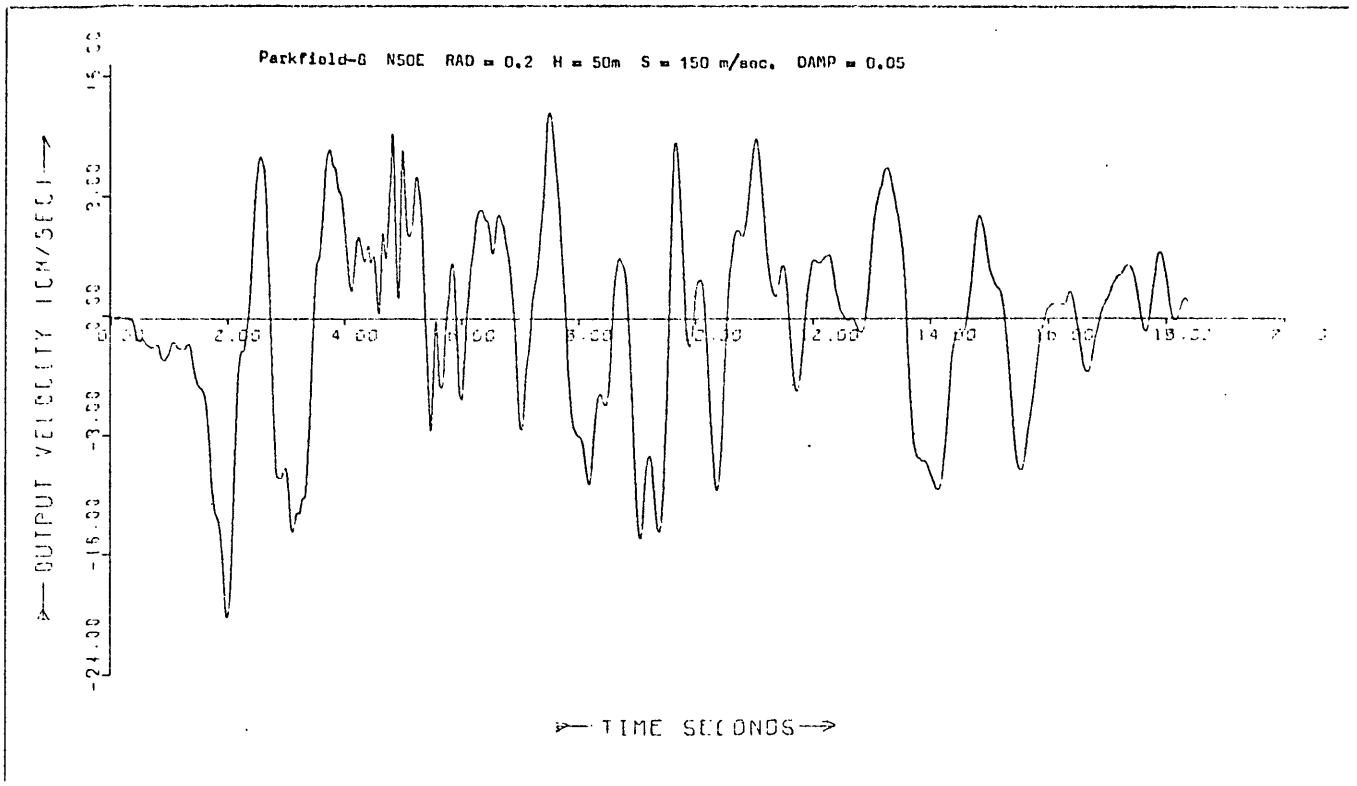


FIG. 6.48b COMPUTED GROUND SURFACE VELOCITY TIME HISTORY AT SITE NO. 3.32

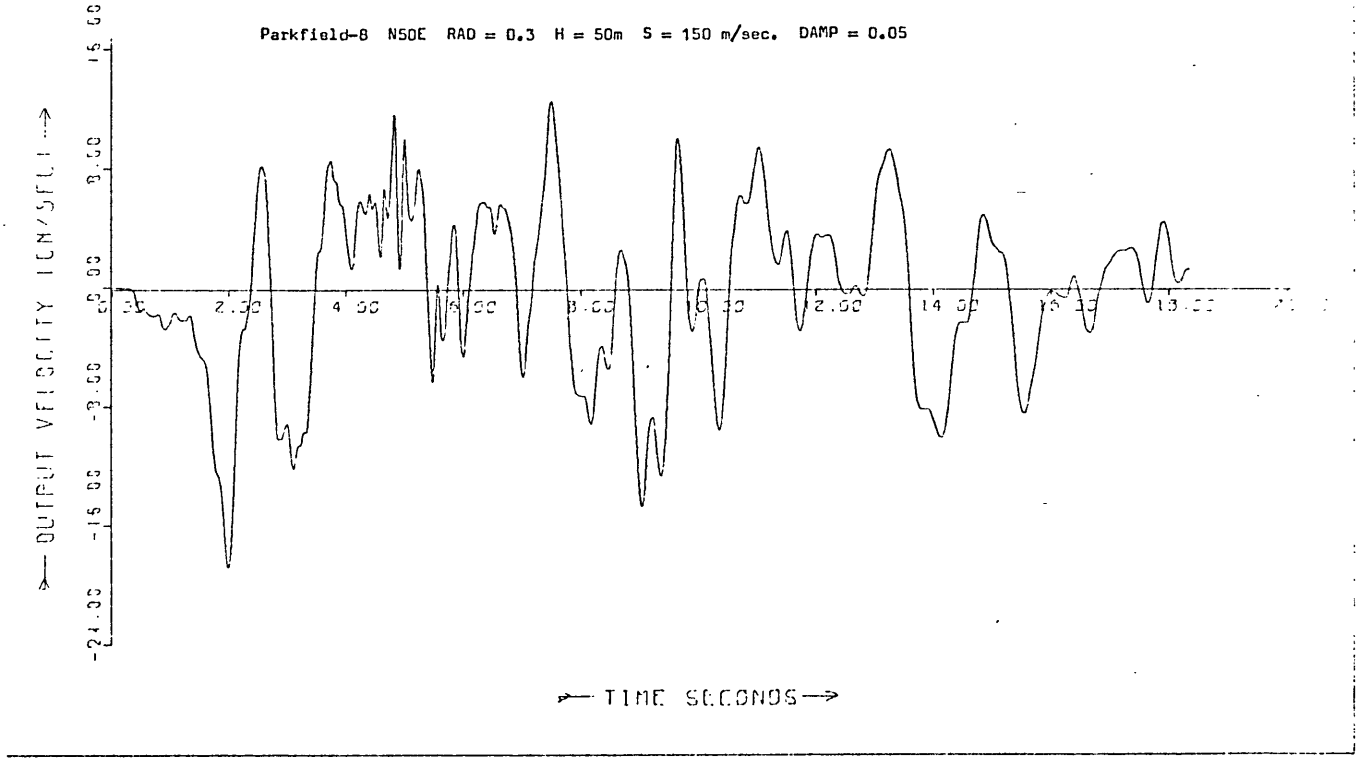


FIG. 6.49b COMPUTED GROUND SURFACE VELOCITY TIME HISTORY AT SITE NO. 3.33

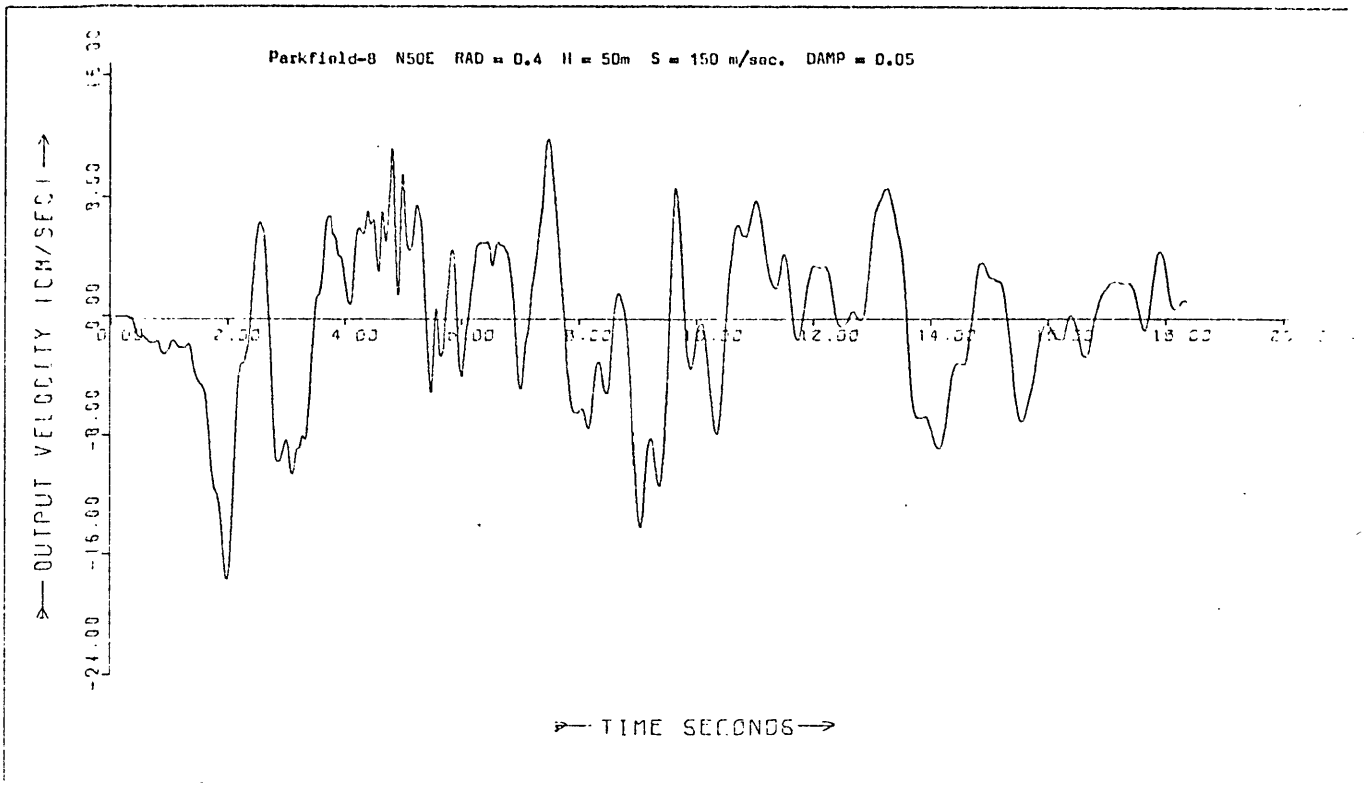


FIG.6.50b COMPUTED GROUND SURFACE VELOCITY TIME HISTORY AT SITE NO. 6.34

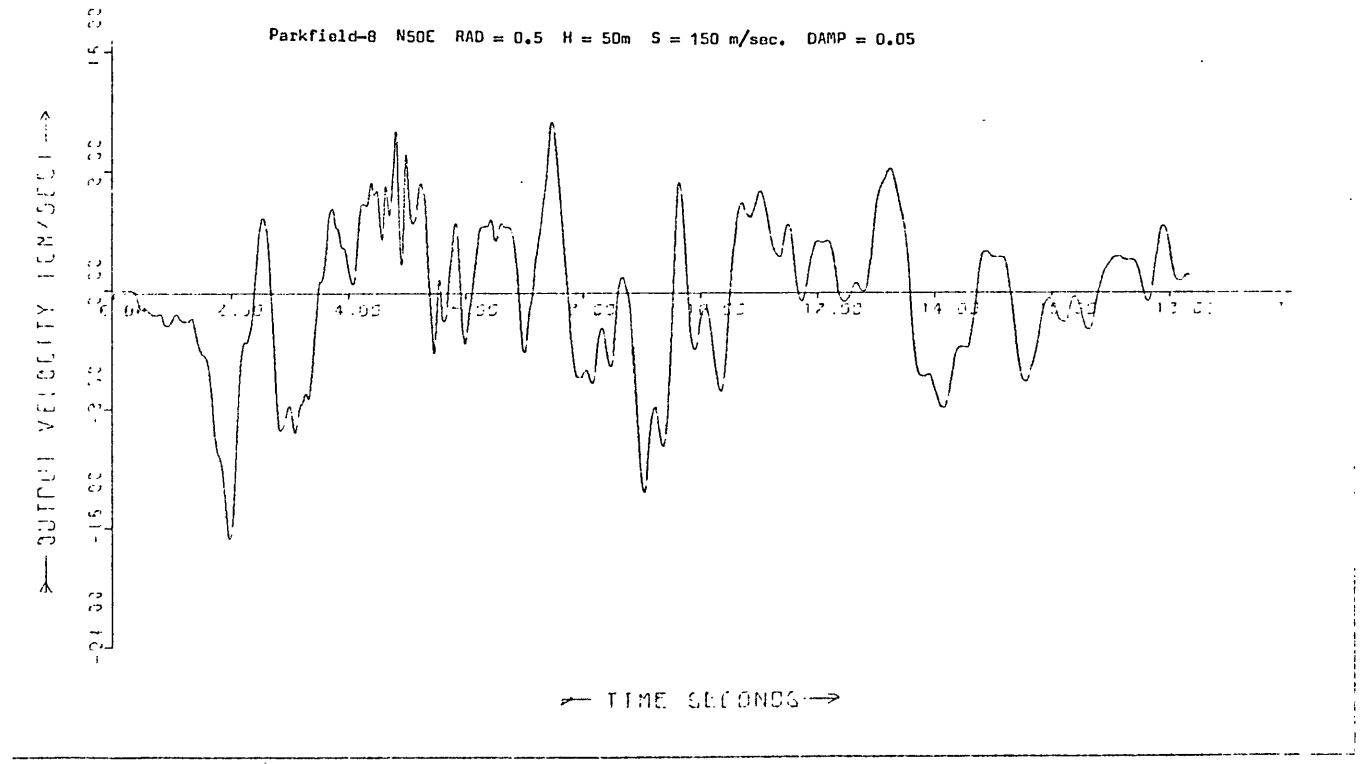


FIG. 6.51b COMPUTED GROUND SURFACE VELOCITY TIME HISTORY AT SITE NO. 6.35

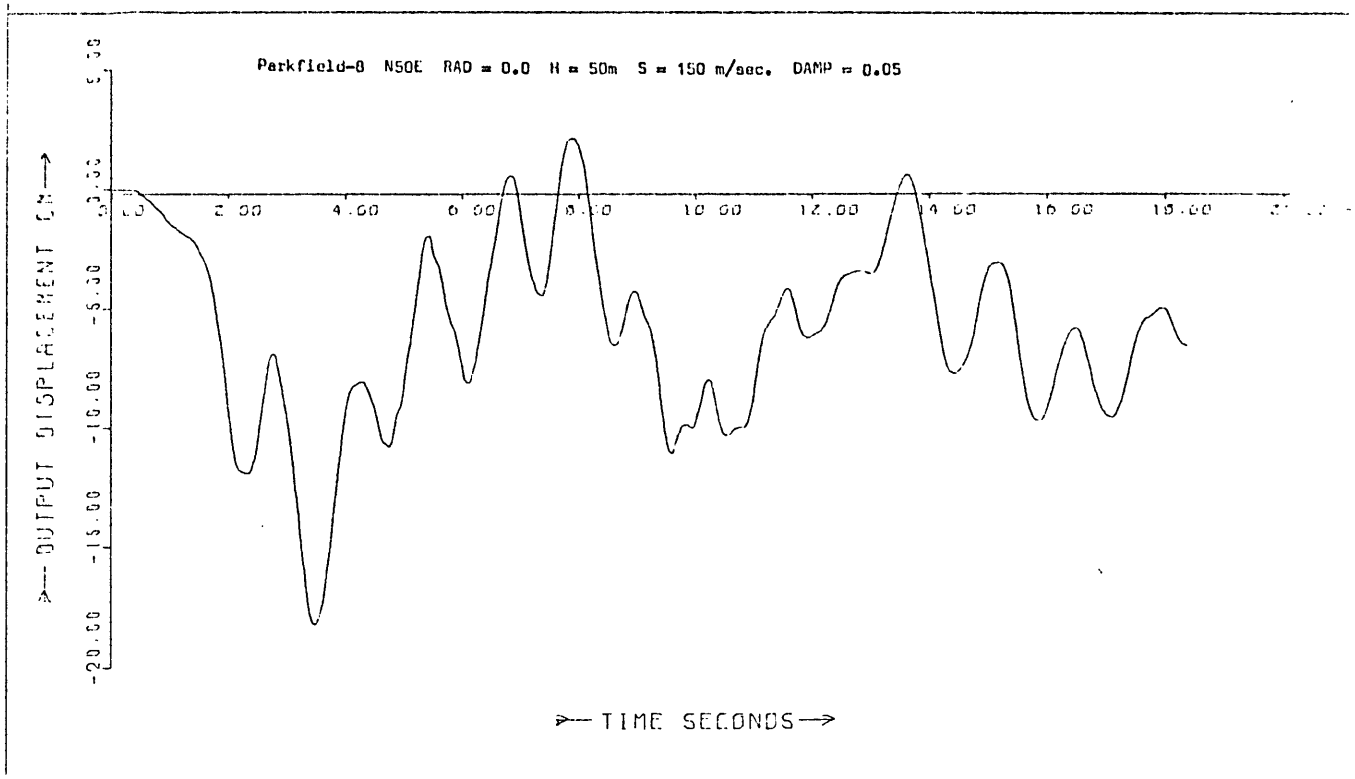


FIG. 6.46 COMPUTED GROUND SURFACE DISPLACEMENT TIME HISTORY AT SITE NO. 6.30

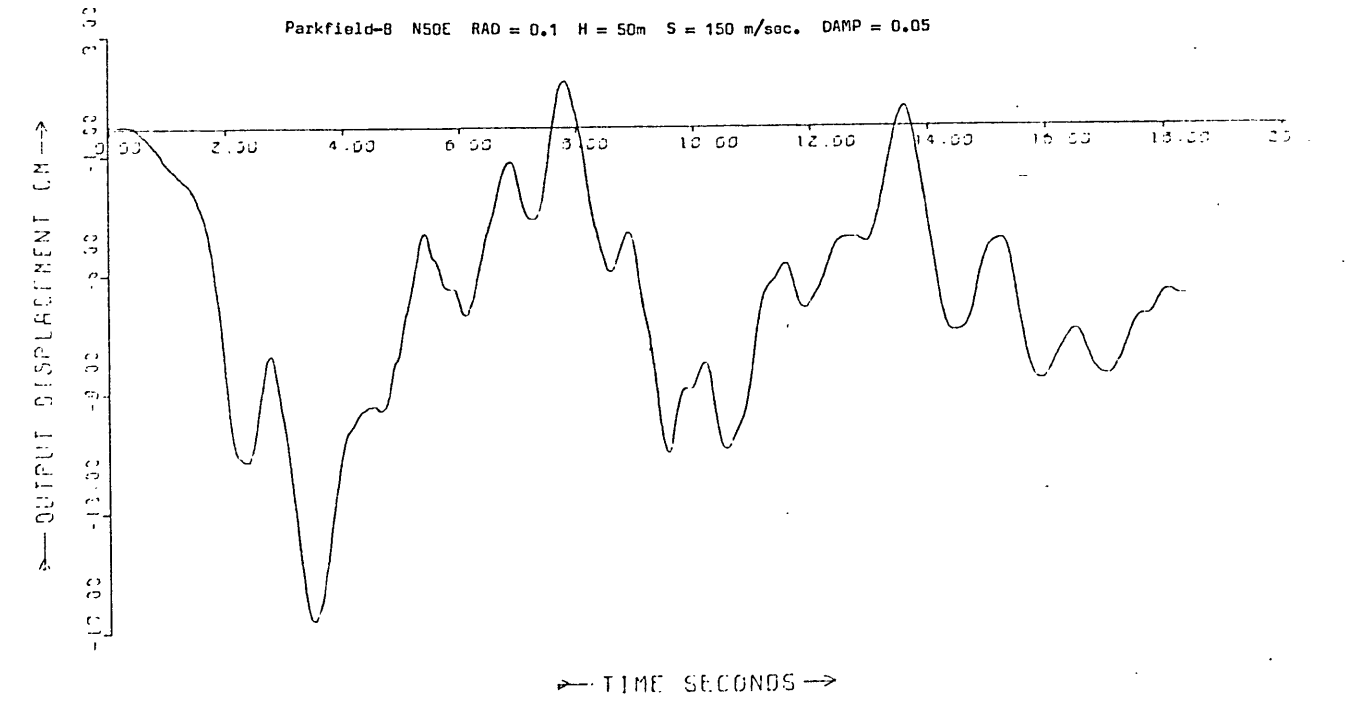


FIG. 6.47 COMPUTED GROUND SURFACE DISPLACEMENT TIME HISTORY AT SITE NO. 6.31

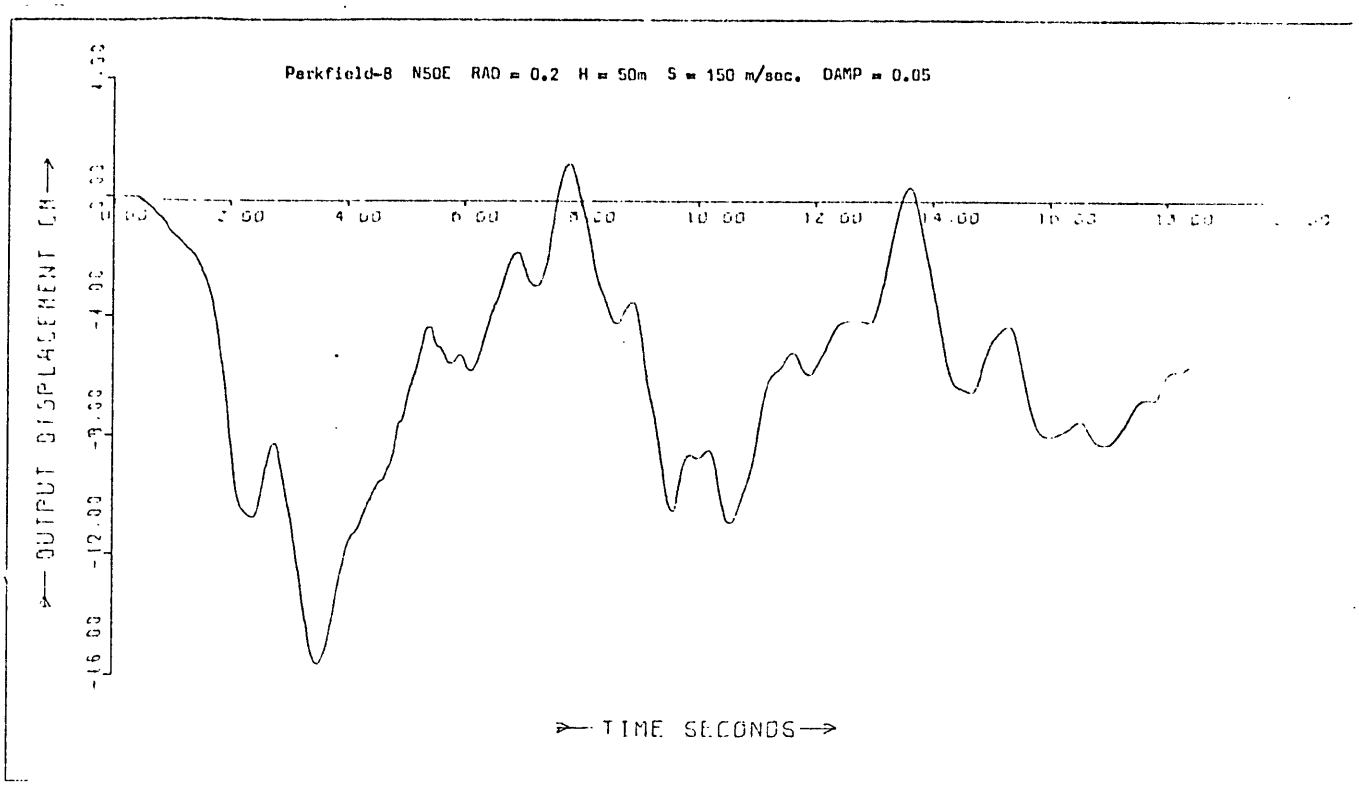


FIG. 6.48c COMPUTED GROUND SURFACE DISPLACEMENT TIME HISTORY AT SITE NO. 6.32

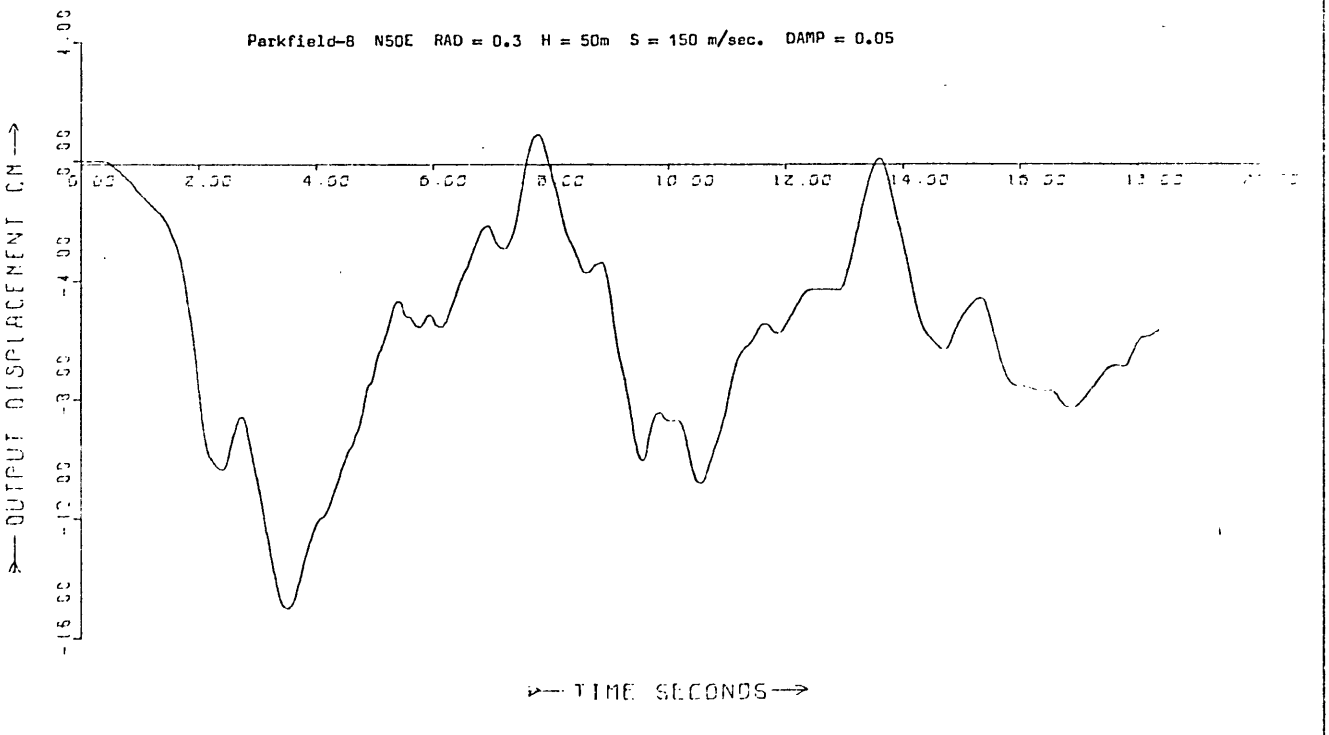


FIG. 6.49c COMPUTED GROUND SURFACE DISPLACEMENT TIME HISTORY AT SITE NO. 6.33

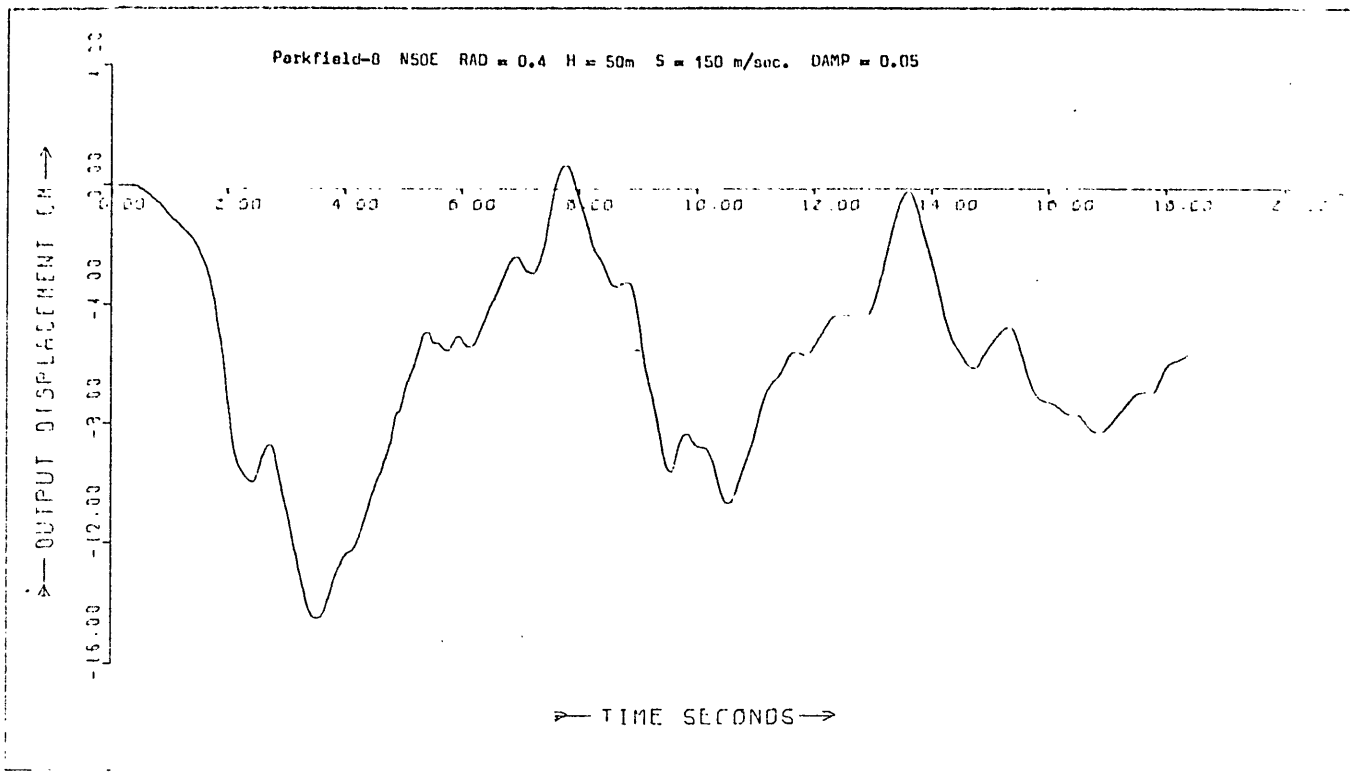


FIG.6.5oc COMPUTED GROUND SURFACE DISPLACEMENT TIME HISTORY AT SITE NO. 6.34

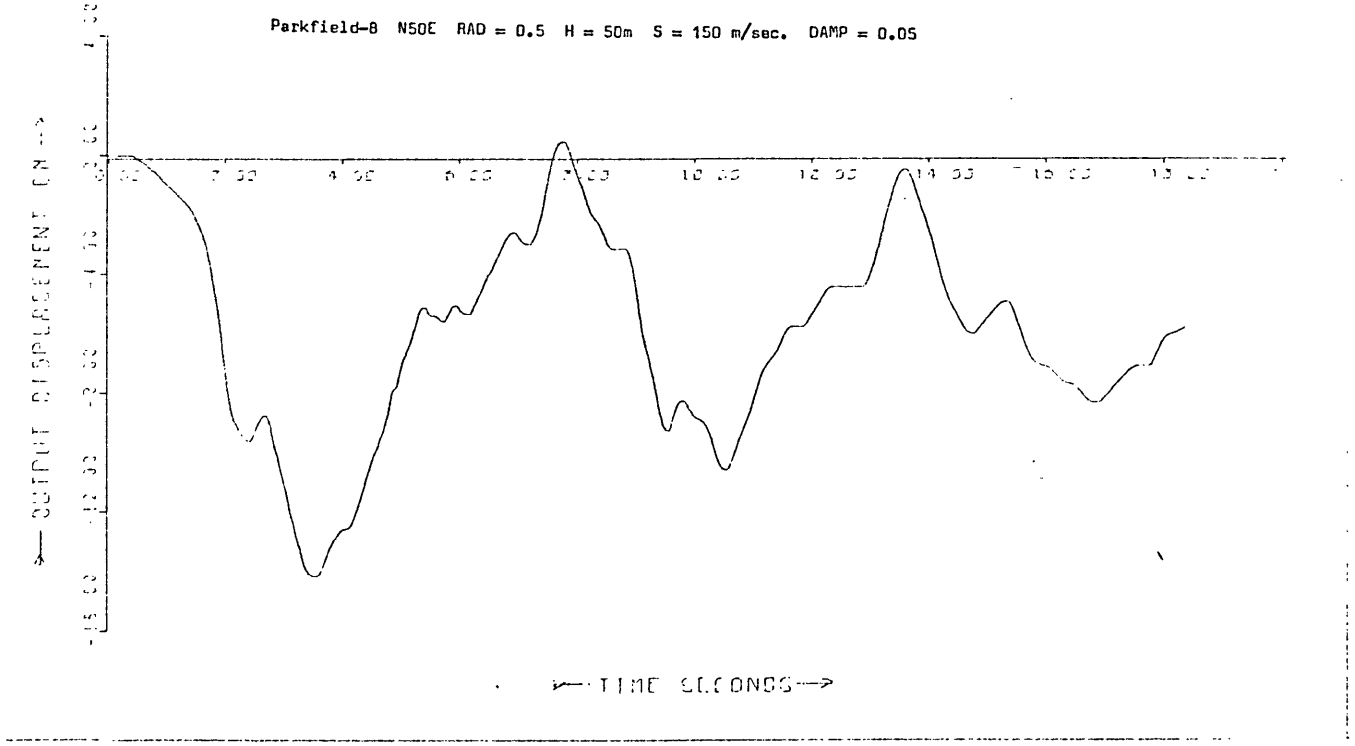


FIG.6.51c COMPUTED GROUND SURFACE DISPLACEMENT TIME HISTORY AT SITE NO. 6.35

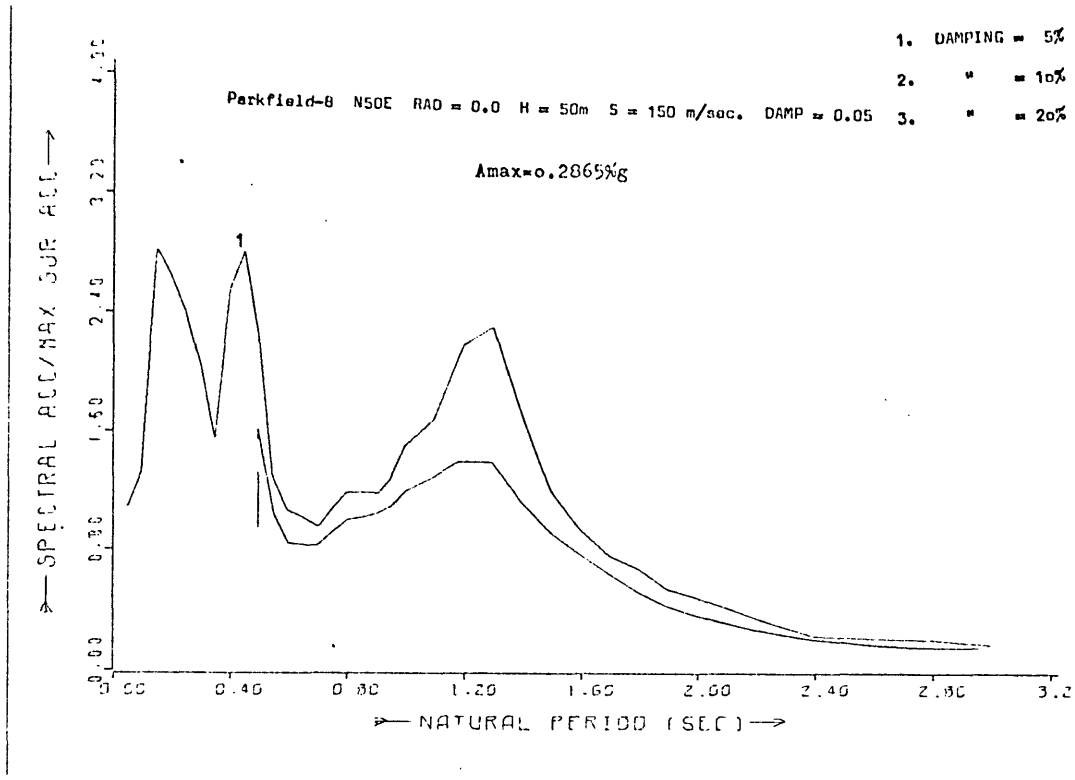


FIG.6.46d COMPUTED GROUND SURFACE ACCELERATION RESPONSE SPECTRA AT SITE NO. 6.30

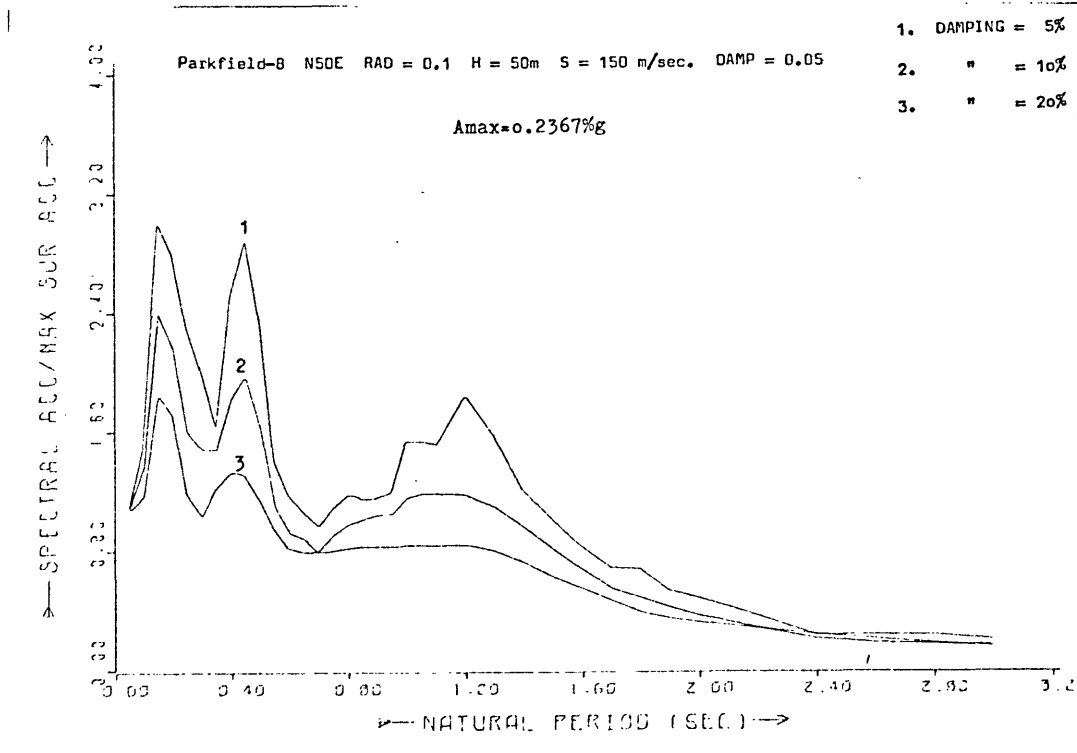


FIG.6.47d COMPUTED GROUND SURFACE ACCELERATION RESPONSE SPECTRA AT SITE NO. 6.31

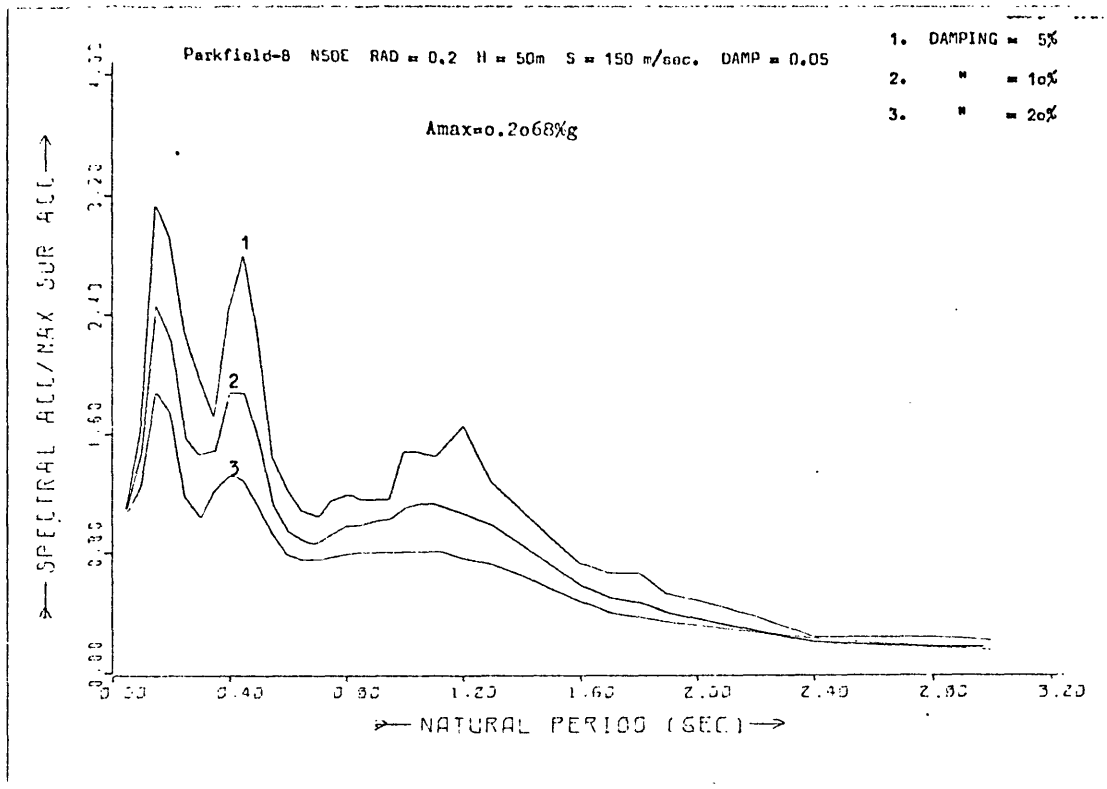


FIG.6.48d COMPUTED GROUND SURFACE ACCELERATION RESPONSE SPECTRA AT SITE NO. 6.32

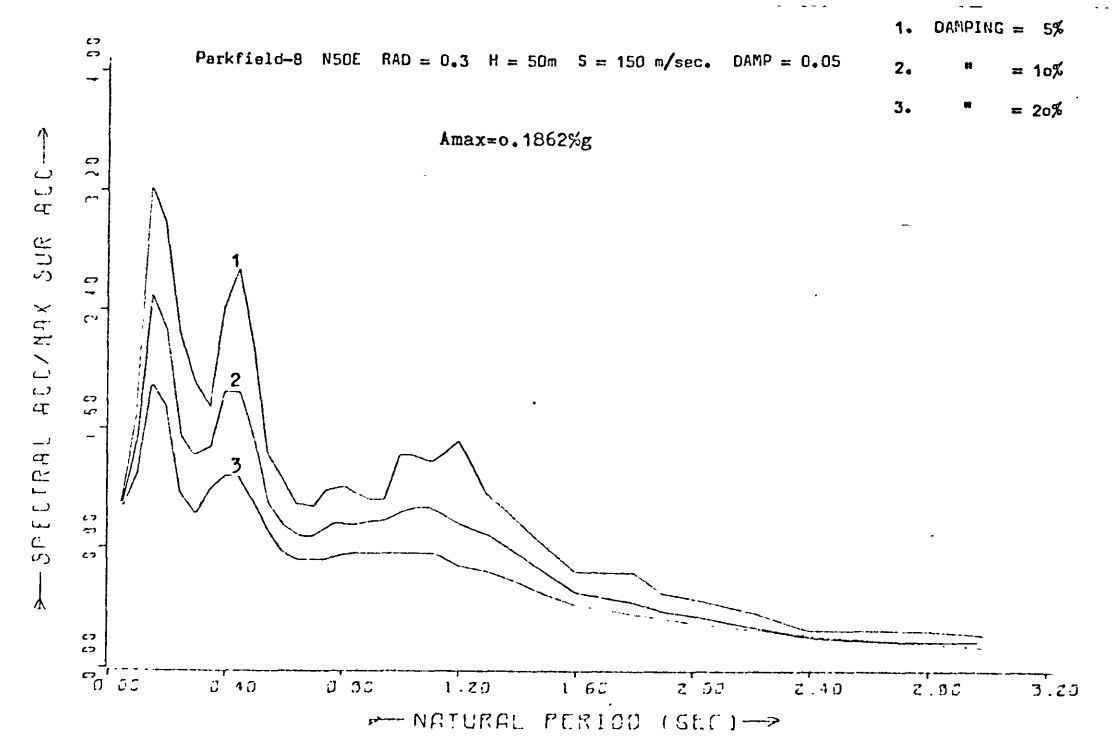


FIG. 6.49d COMPUTED GROUND SURFACE ACCELERATION RESPONSE SPECTRA AT SITE NO. 6.33

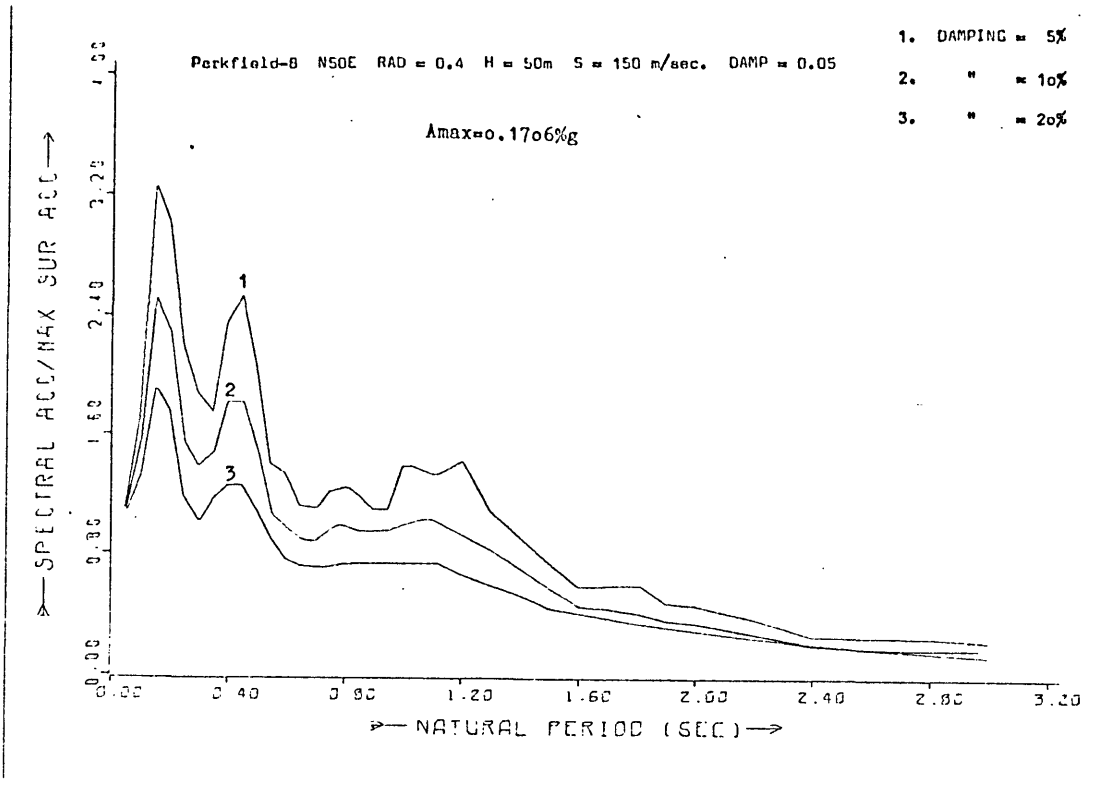


FIG. 6.5od COMPUTED GROUND SURFACE ACCELERATION RESPONSE SPECTRA AT SITE NO. 6.34

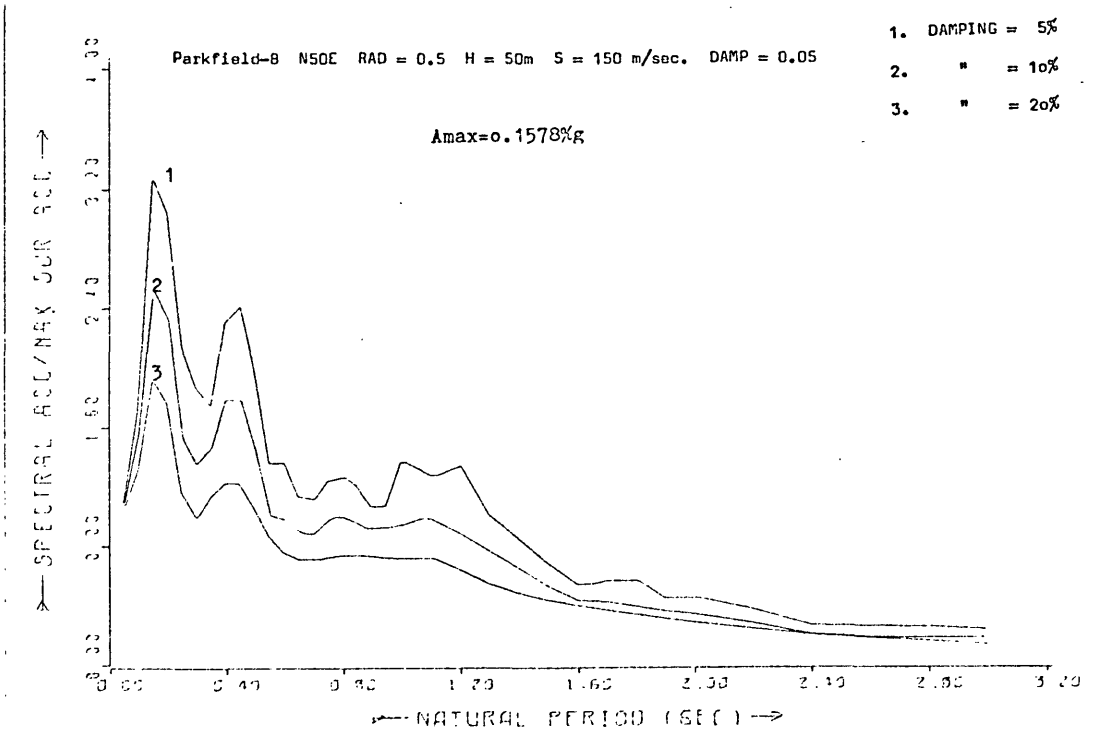


FIG.6.51d COMPUTED GROUND SURFACE ACCELERATION RESPONSE SPECTRA AT SITE NO. 6.35

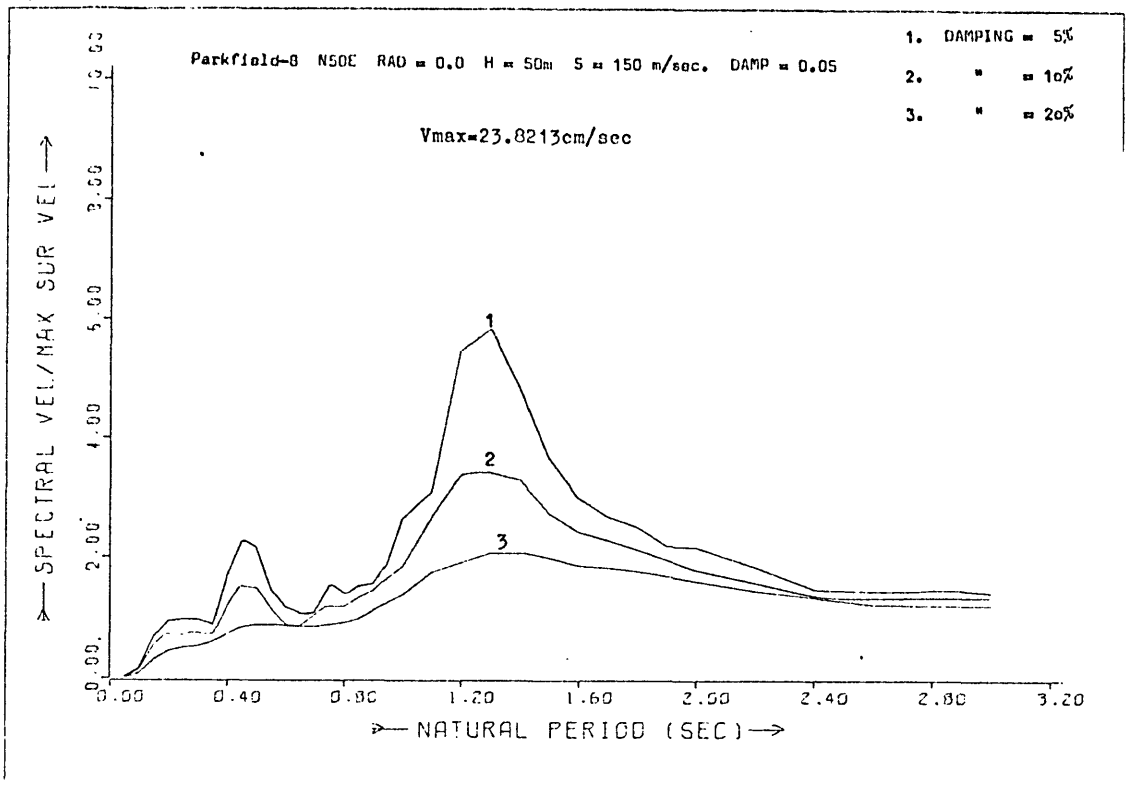


FIG.6.46e COMPUTED GROUND SURFACE VELOCITY RESPONSE SPECTRA AT SITE NO. 6.30

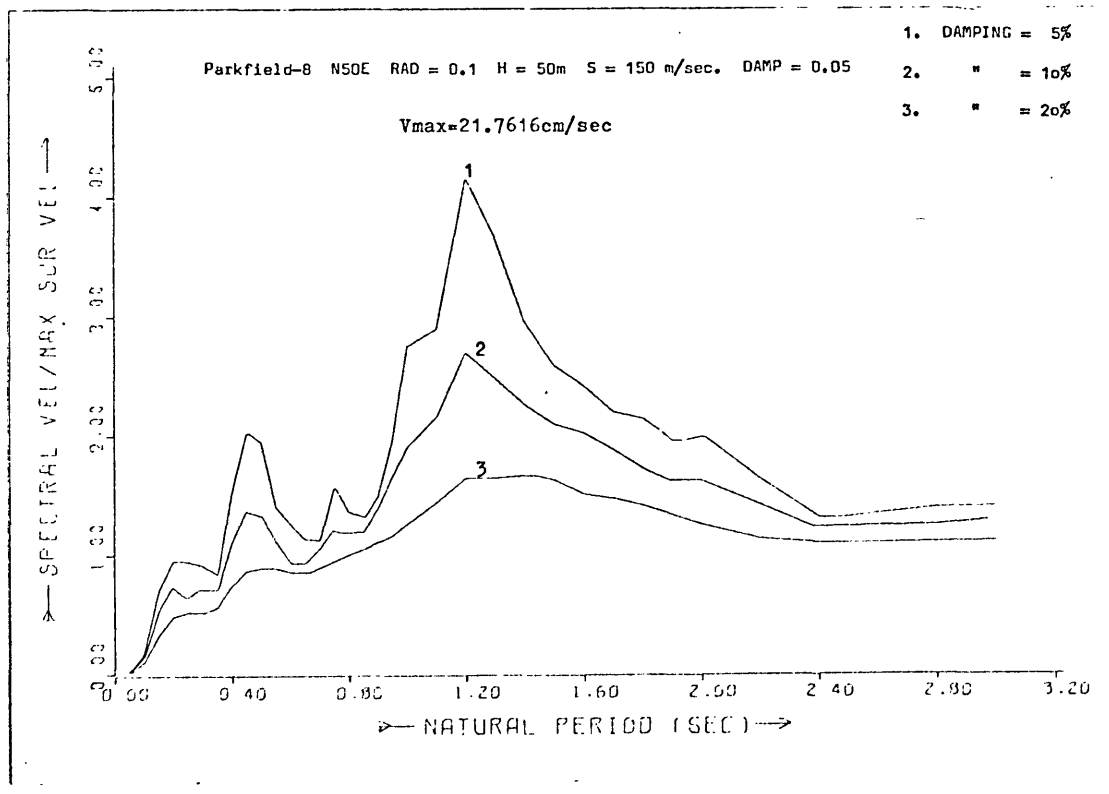


FIG.6.47e COMPUTED GROUND SURFACE VELOCITY RESPONSE SPECTRA AT SITE NO. 6.31

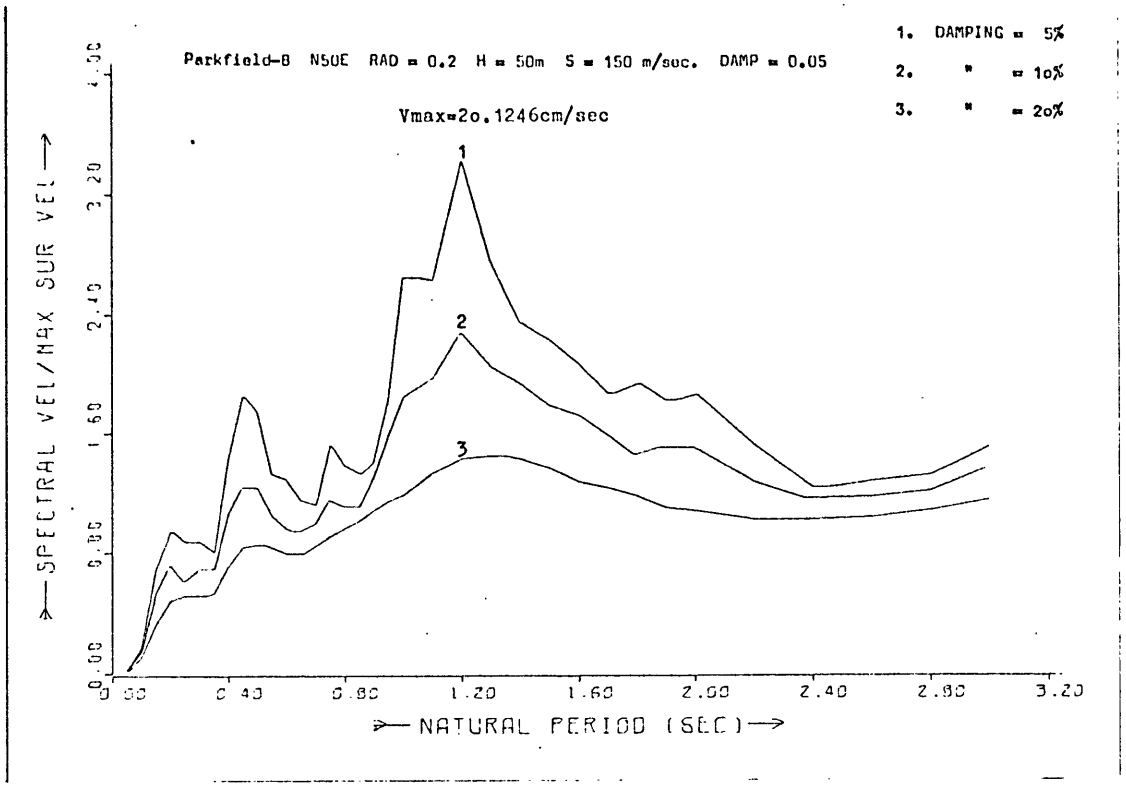


FIG. 6.48 COMPUTED GROUND SURFACE VELOCITY RESPONSE SPECTRA AT SITE NO. 6.32

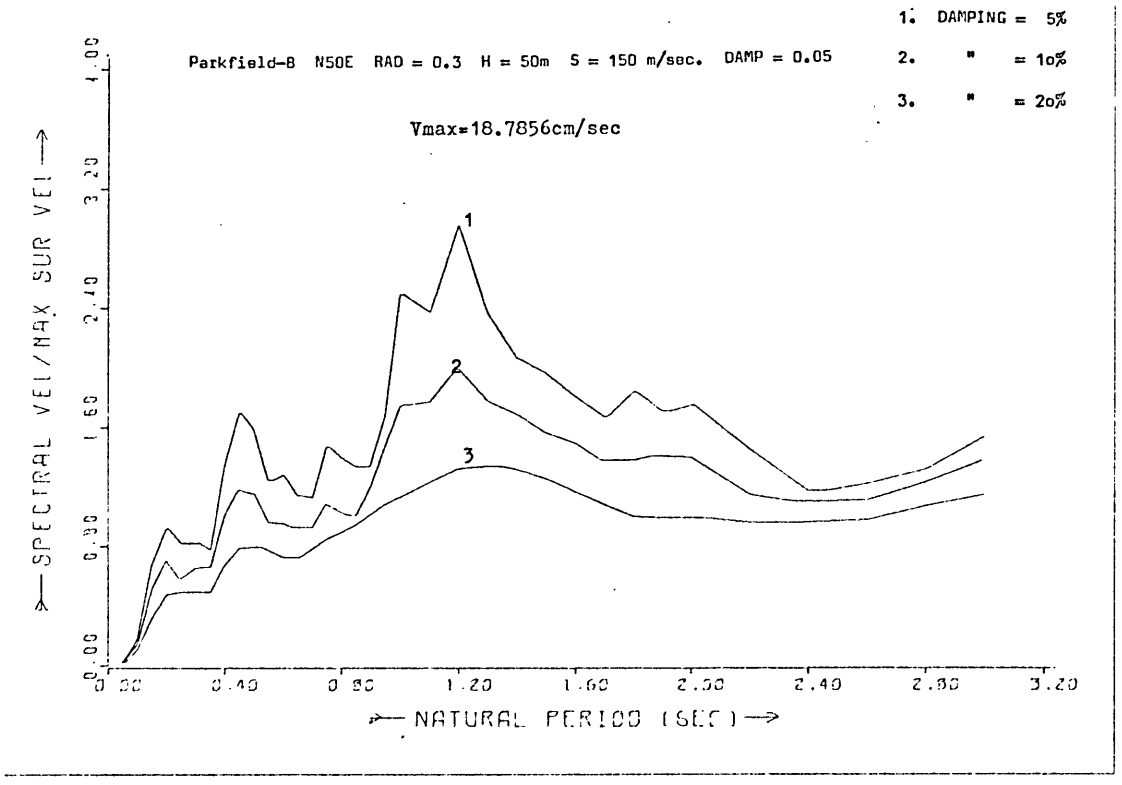


FIG.6.49 COMPUTED GROUND SURFACE VELOCITY RESPONSE SPECTRA AT SITE NO. 6.33

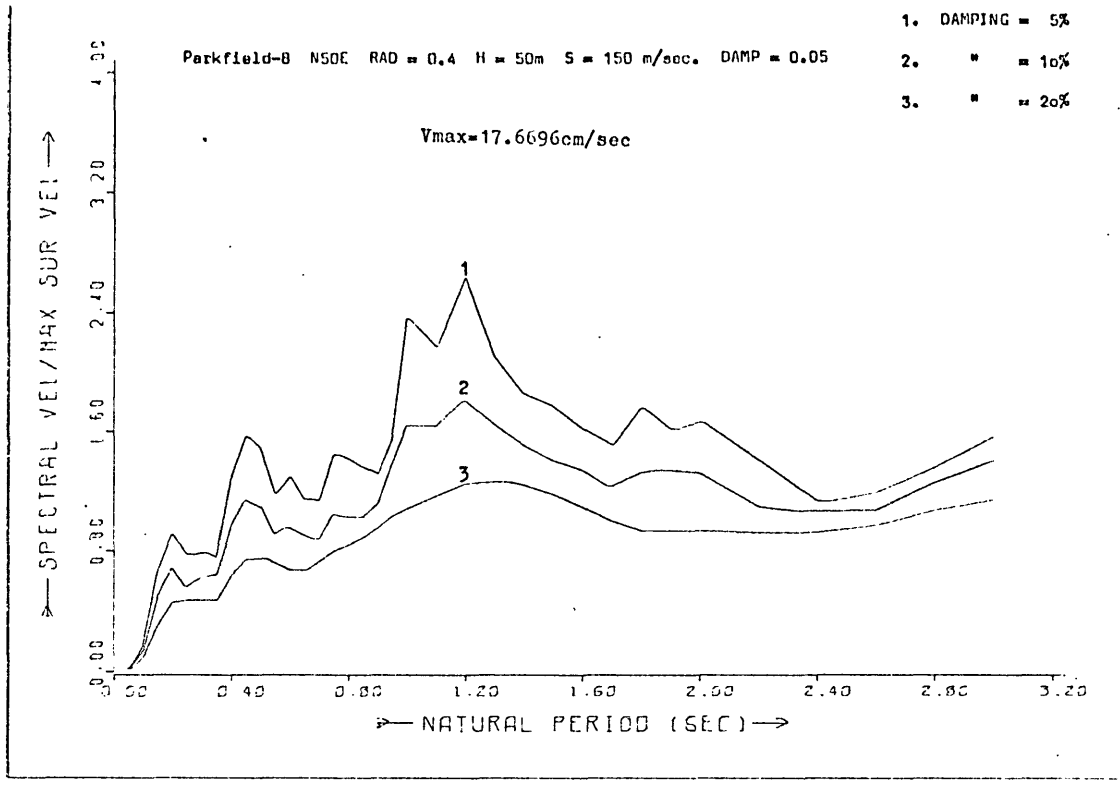


FIG.6.5oe COMPUTED GROUND SURFACE VELOCITY RESPONSE SPECTRA AT SITE NO. 6.34

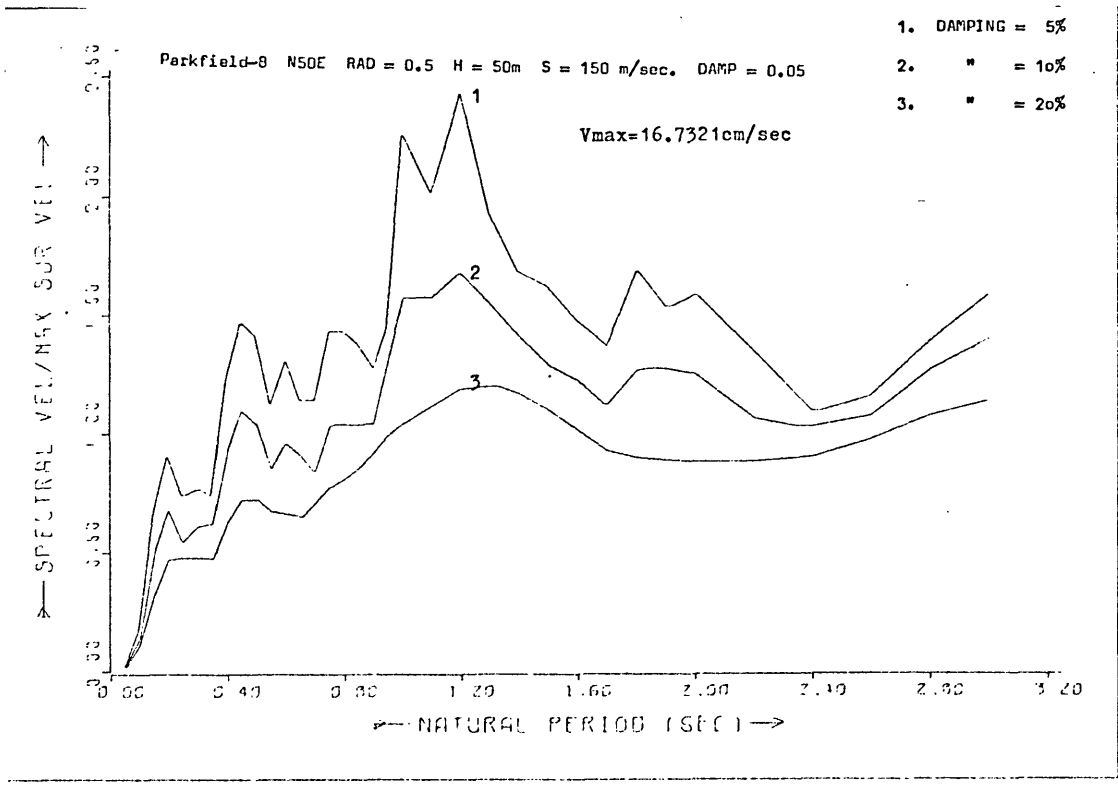


FIG 6.51e COMPUTED GROUND SURFACE VELOCITY RESPONSE SPECTRA AT SITE NO. 6.35

6.46a,b,c to 6.51a,b,c. The maximum values of these time histories and their comparison with the case when underlying bedrock is completely rigid ($S_{rock} = \infty$) are summarized in table 6.4. From table 6.4 it may be seen that maximum acceleration, velocity and displacement are 31.03%, 15.53% and 14.04% greater for a site having a completely rigid bedrock ($S_{rock} = \infty$) than a soft rock (S_{rock} = 750 m/sec), reflecting the major influence of bedrock characteristics on the developed surface motions.

Referring again to table 6.4, it is noted that maximum accelerations developed at the surface of the deposit with six different bedrock characteristics are less than those reported in tables 6.2 and 6.3, stressing the fact that under the condition that the fundamental period of the overburden is not equal to the predominant period of the bedrock motion, the condition of resonance is violated, thus reducing the effect of bedrock stiffness on computed maximum surface accelerations. It may be noted that the influence of radiation damping ratio on computed maximum surface displacements are considerably more.

To show that frequency characteristics of surface motions are affected by the stiffness of bedrock formations, figs. 6.46d to 6.51d have been included. All these figures have been summarized in fig. 6.52, which represents computed surface acceleration spectrum in normalized form. Considerable differences in frequency patterns of the motions developed on the surface of soils overlying different bedrock formations exist. Great differences in the amplitudes of spectral values are also observed. However, this behaviour is expected from the results reported in section 6.8.1.2. Considerable differences are also noticed in computed surface normalized velocity spectrum shown in figs. 6.46e to 6.51e.

The damage potential of the sites having different bedrock

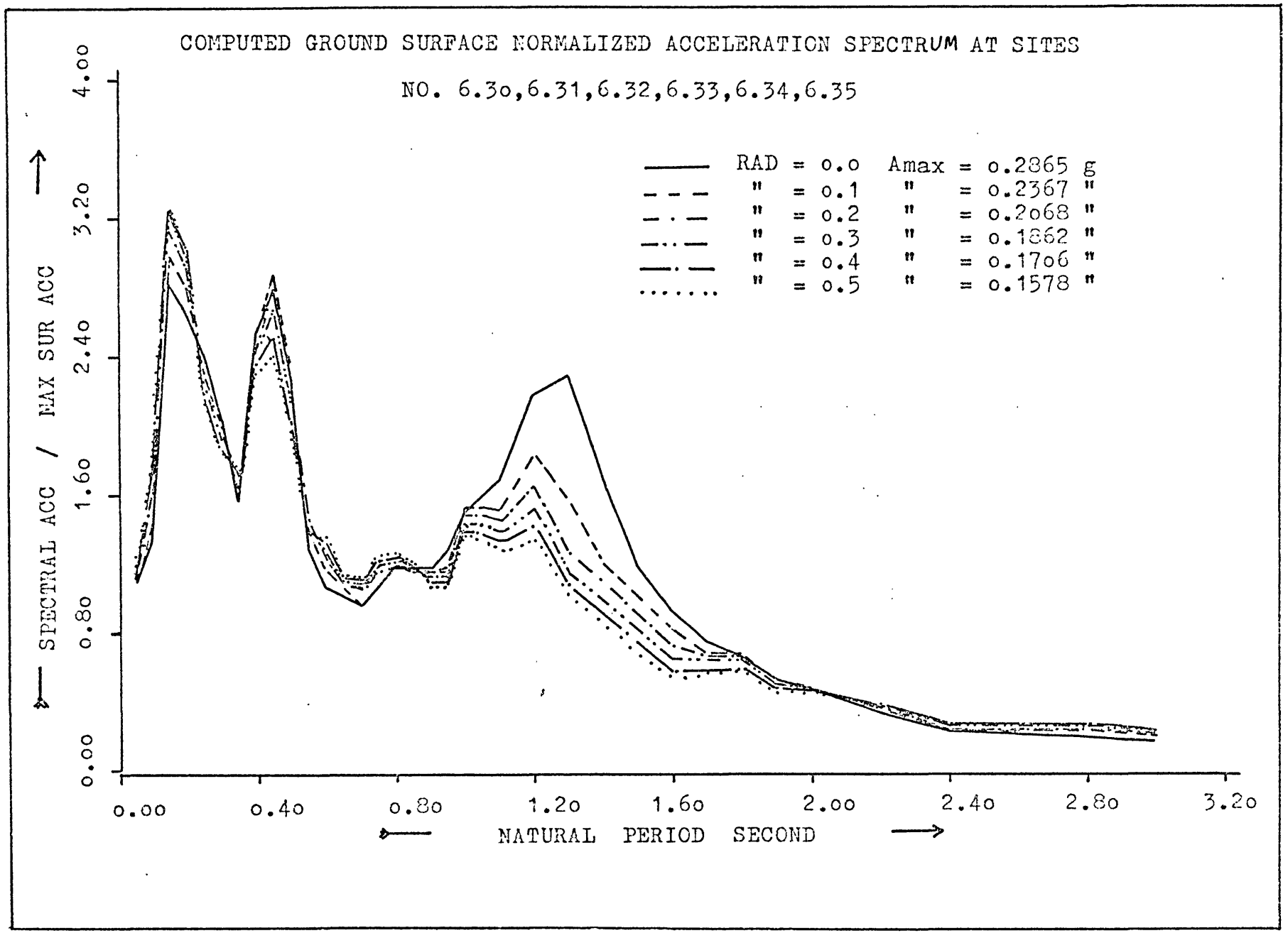

COMPUTED GROUND SURFACE NORMALIZED ACCELERATION SPECTRUM AT SITES
NO. 6.3o,6.31,6.32,6.33,6.34,6.35
RAD = o.o Amax = o.2865 g
" = o.1 " = o.2367 "
" = o.2 " = o.2o68 "
" = o.3 " = o.1862 "
" = o.4 " = o.17o6 "
" = o.5 " = o.1578 "
SPECTRAL ACC / MAX SUR ACC
0.00
0.80
1.60
2.40
3.20
4.00
0.00
0.40
0.80
1.20
1.60
2.00
2.40
2.80
3.20
NATURAL PERIOD SECOND

FIG. 6.52

DATA ON THE INFLUENCE OF BEDROCK CHARACTERISTICS ON RESPONSE OF SOIL DEPOSITS

RADIATION DAMPING RATIO	MAX. SUR. ABS. ACC.	$1 - \frac{ACC._{RAD}}{ACC._{0.0}} \times 100\%$	MAX. SUR. ABS. VEL. (cm/sec)	$1 - \frac{VEL._{RAD}}{VEL._{0.0}} \times 100\%$	MAX. SUR. ABS. DIS.	$1 - \frac{DIS._{RAD}}{DIS._{0.0}} \times 100\%$	STRENGTH $(cm/sec)^2$
0.0	0.29	00.00	23.82	0.00	18.16	0.00	965
0.1	0.24	17.24	21.76	8.65	16.60	8.59	542
0.2	0.20	31.03	20.12	15.53	15.61	14.04	381
0.3	0.19	34.48	18.78	21.16	14.95	17.67	299
0.4	0.17	41.38	17.66	25.86	14.48	20.26	250
0.5	0.16	44.83	16.73	29.76	14.13	22.19	218

TABLE 6.4

characteristics are compared in terms of strength "S" (see section 7.3.1) and are given in the last column of table 6.4. From the results, it can be concluded that the deposit underlain by infinitely rigid bedrock (RAD = 0.0) is 2.53 times more damaging than that underlain by a soft rock (RAD = 0.2).

Figs. 6.53a,b,c,d,e through 6.58a,b,c,d,e provide further comparisons of response of the soft clay shown in fig. 6.46 subjected at the bedrock level to Parkfield-5 N5W, with a predominant period of 0.3 second. The maximum values of developed accelerations, velocities and displacements and their comparison with the case when the underlying bedrock is completely rigid ($S_{rock} = \infty$) and the amount of energy available for damage at the surface of these deposits are summarized in table 6.5.

It may be noted that the sites subjected to Parkfield-5 N5W have developed greater response values, although the peak value of acceleration time history of Parkfield-5 N5W is 0.02g less than Parkfield-8 N50E. This is because the predominant period of Parkfield-5 0.3 sec. is much closer to the fundamental periods of the deposits than that of Parkfield-8 0.15 sec. The influence of radiation damping ratio on maximum surface acceleration for both cases is given in columns three of tables 6.4 and 6.5. The results clearly illustrate that radiation damping ratio has more influence on suppressing the response for the latter case than the former, indicating that radiation damping ratio is less effective in the first few higher modes of vibrations which contribute more to the developed response in the former case. Figs. 6.53d through 6.58d, which are summarized in fig. 6.59, show computed surface normalized acceleration spectrum for the latter case. From the results, it is readily apparent that at periods close to the periods of first and second modes of vibration, i.e. 1.33 sec.

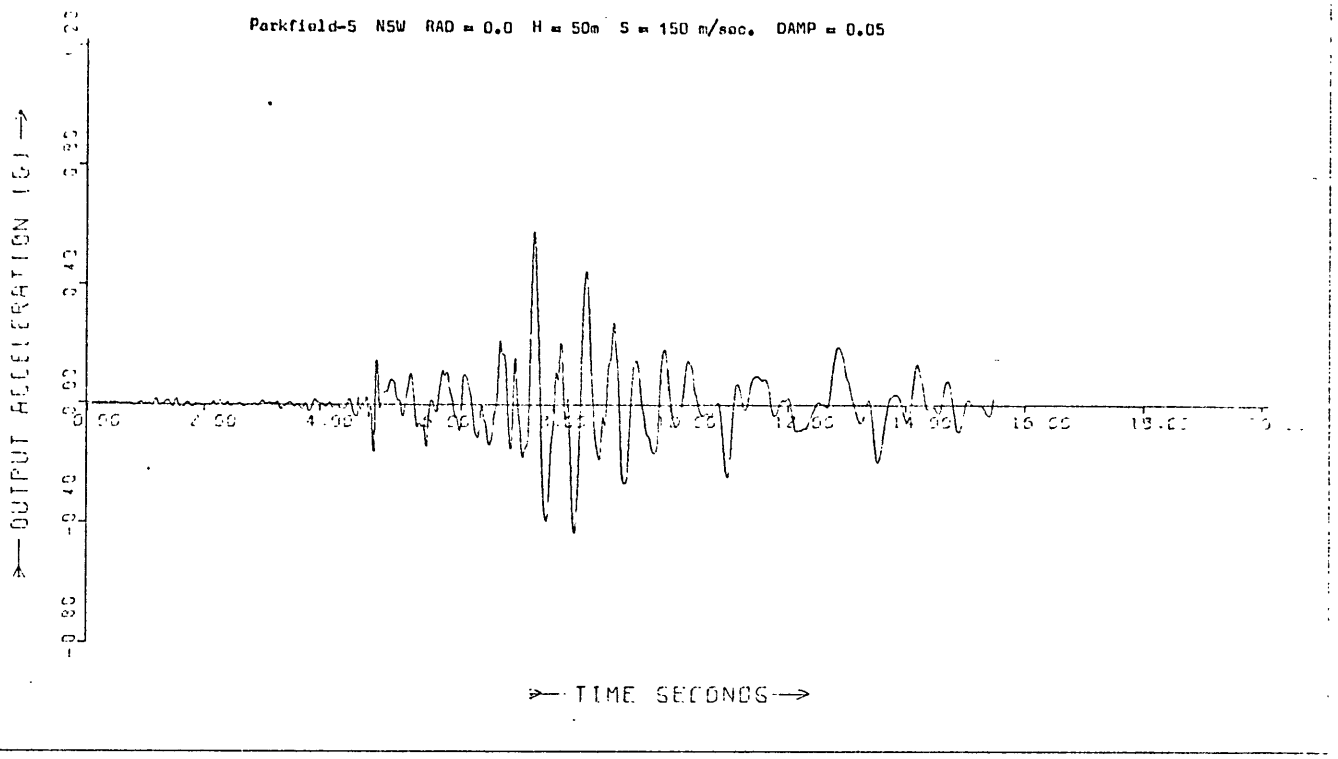


FIG.6.53a COMPUTED GROUND SURFACE ACCELERATION TIME HISTORY AT SITE NO. 6.30

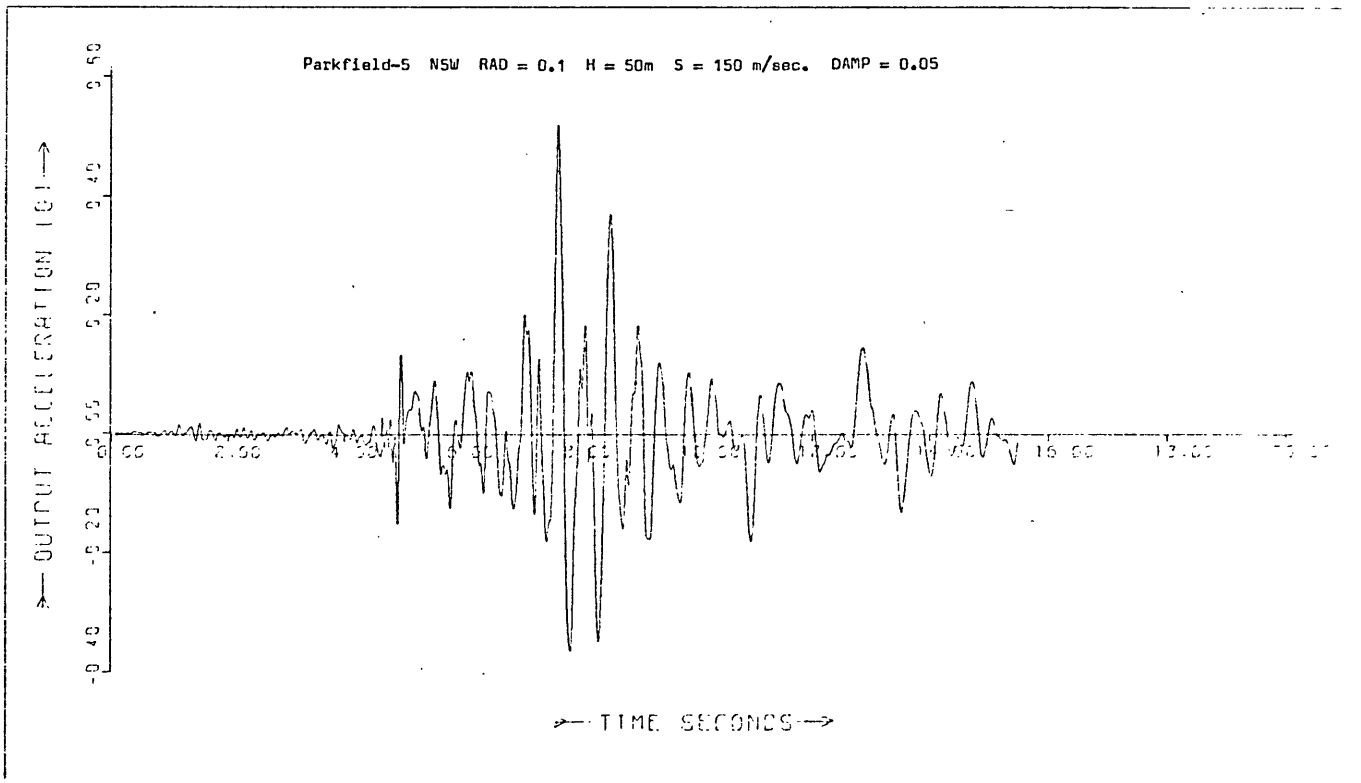


FIG.6.54a COMPUTED GROUND SURFACE ACCELERATION TIME HISTORY AT SITE NO. 6.31

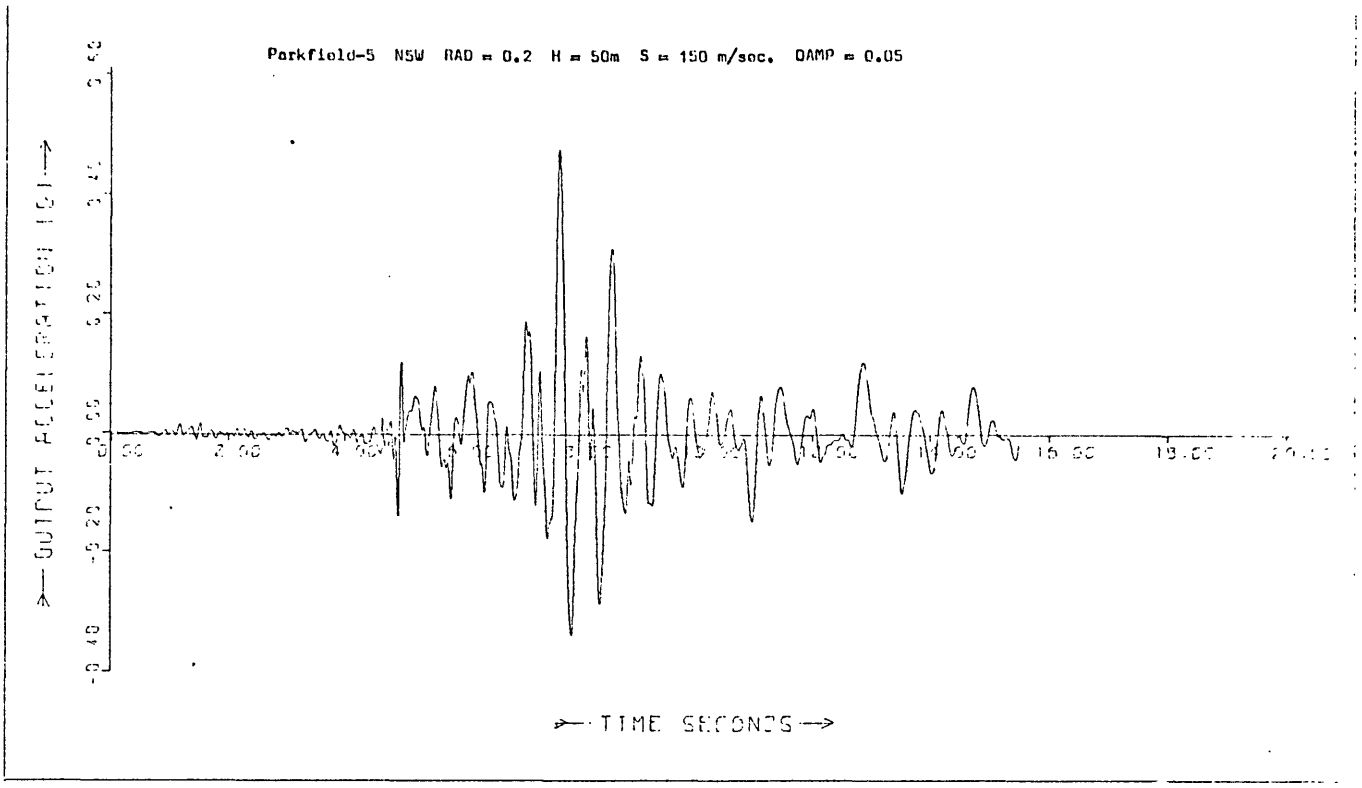


FIG.6.55a COMPUTED GROUND SURFACE ACCELERATION TIME HISTORY AT SITE NO.6. 32

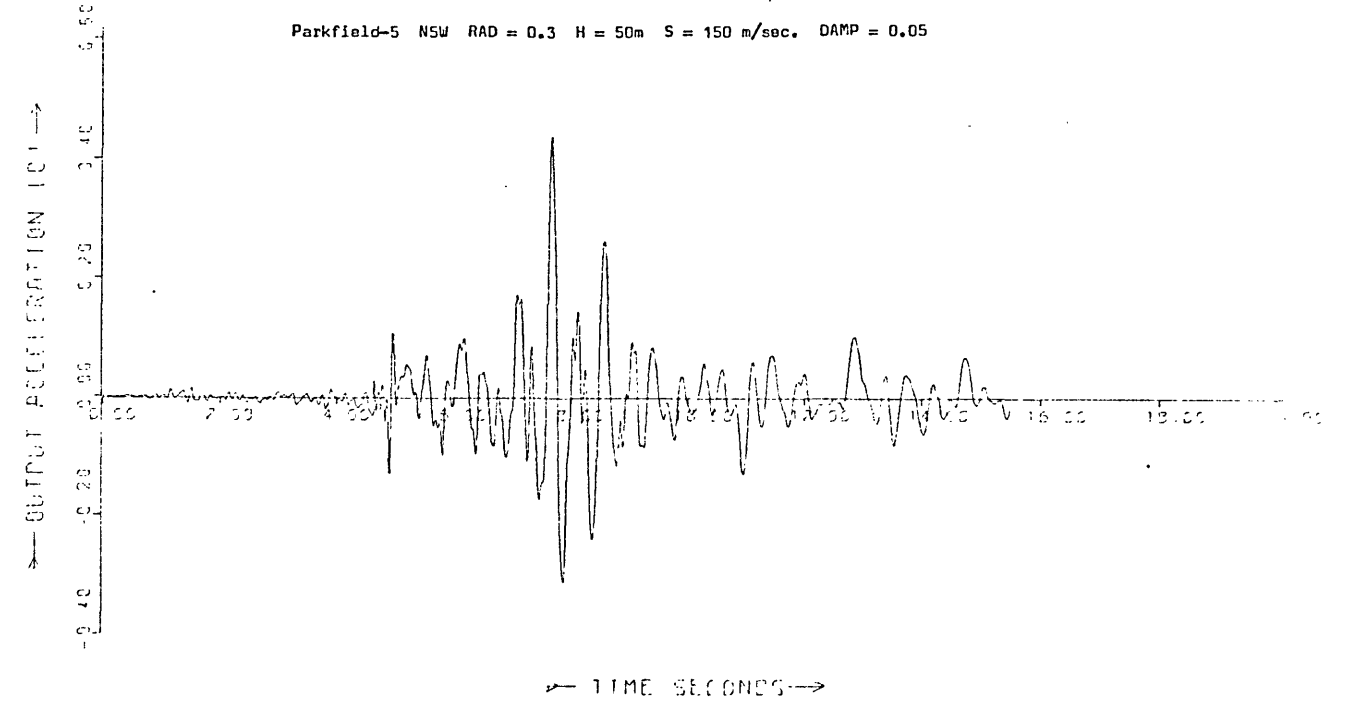


FIG. 6.56a COMPUTED GROUND SURFACE ACCELERATION TIME HISTORY AT SITE NO.6. 33

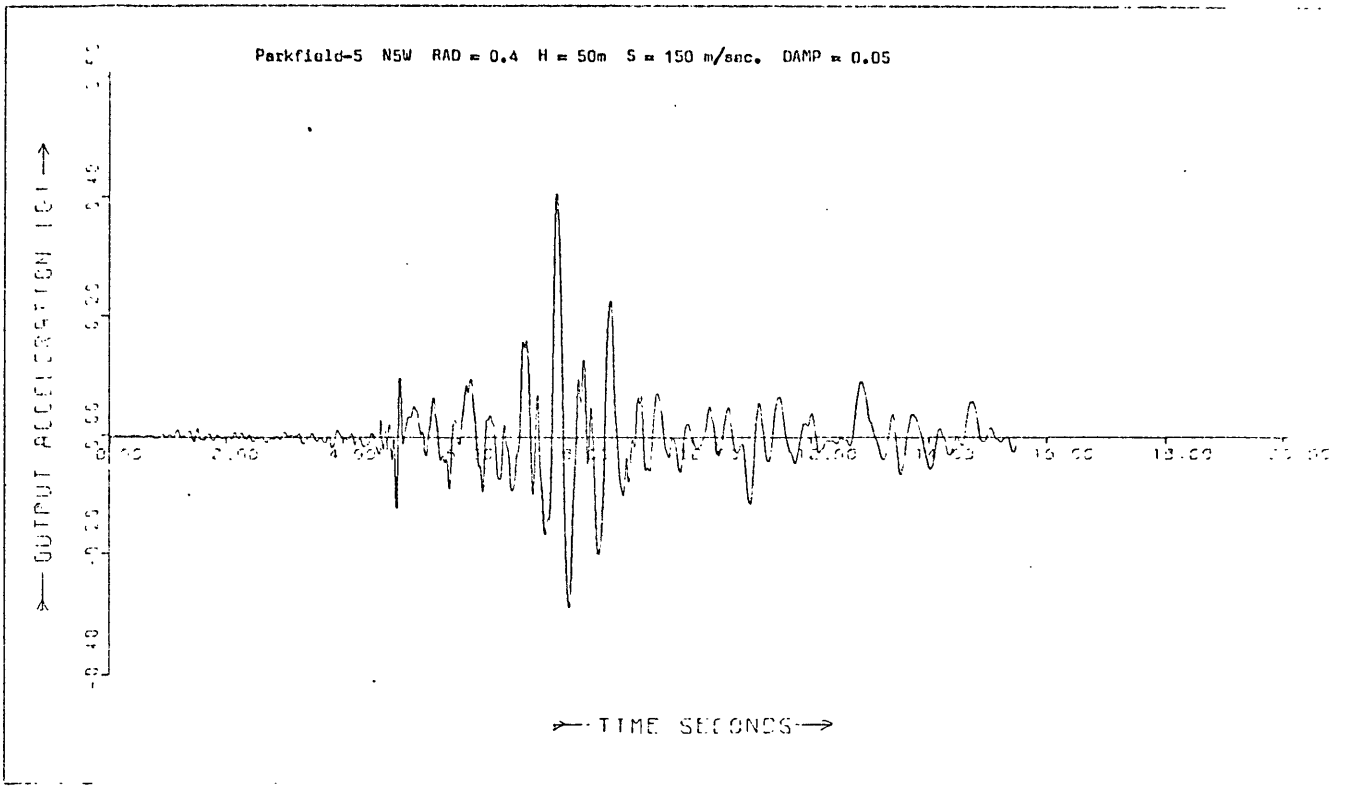


FIG. 6.57a COMPUTED GROUND SURFACE ACCELERATION TIME HISTORY AT SITE NO. 6. 34

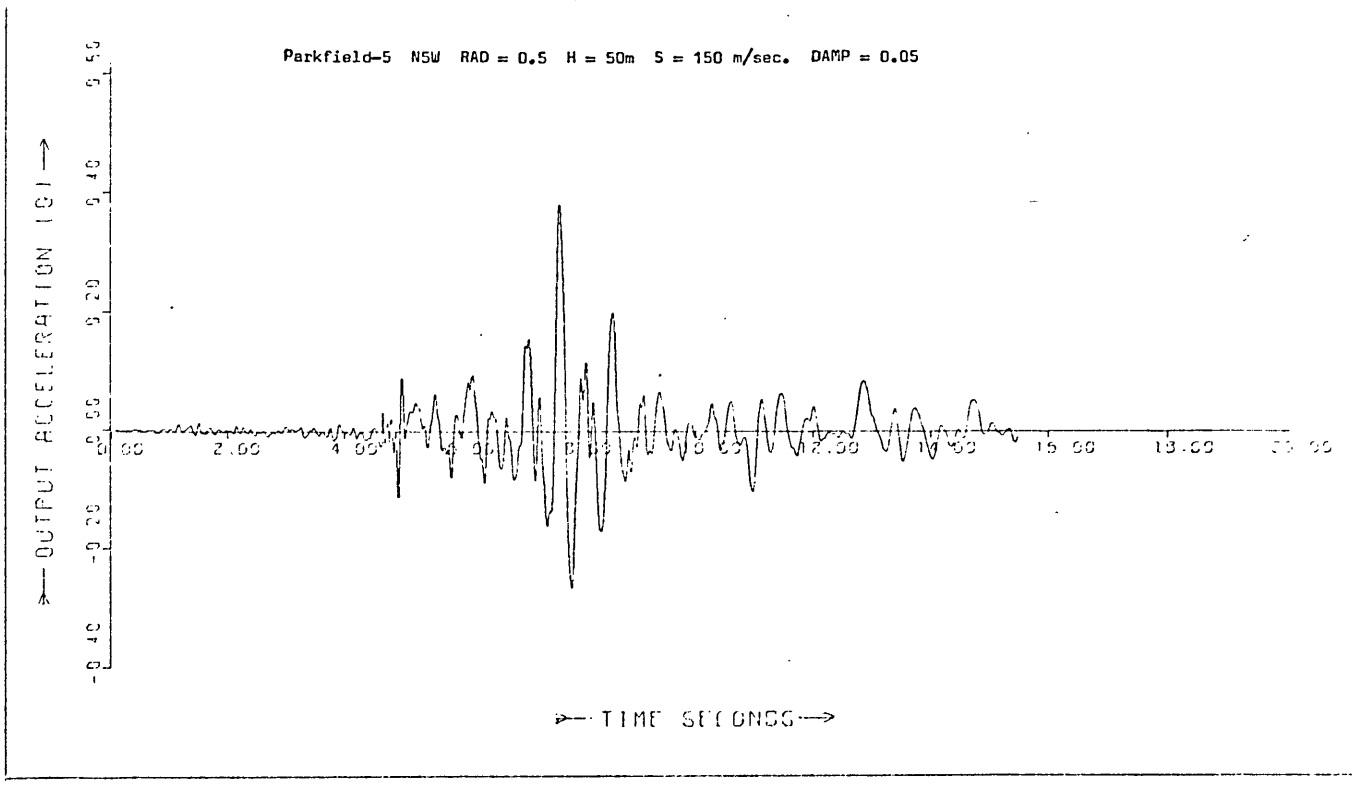


FIG.6.58a COMPUTED GROUND SURFACE VELOCITY TIME HISTORY AT SITE NO. 6.35

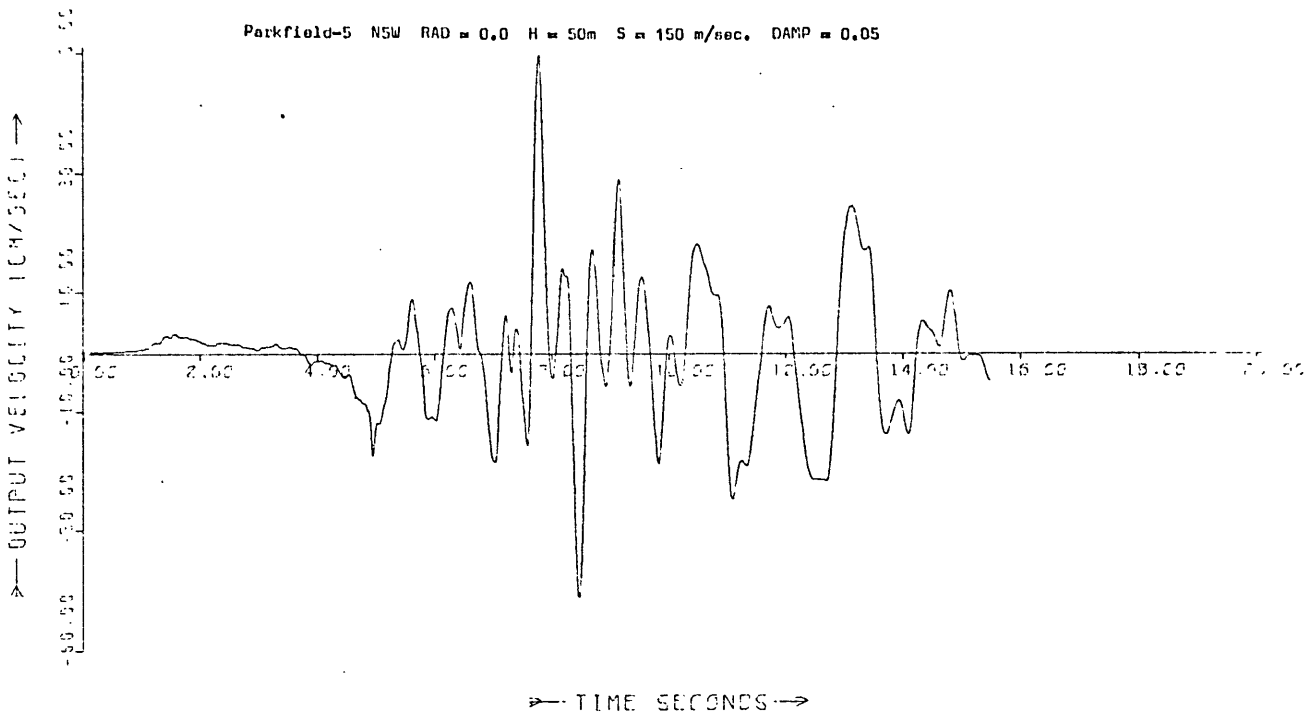


FIG. 6.53b COMPUTED GROUND SURFACE VELOCITY TIME HISTORY AT SITE NO. 6.30

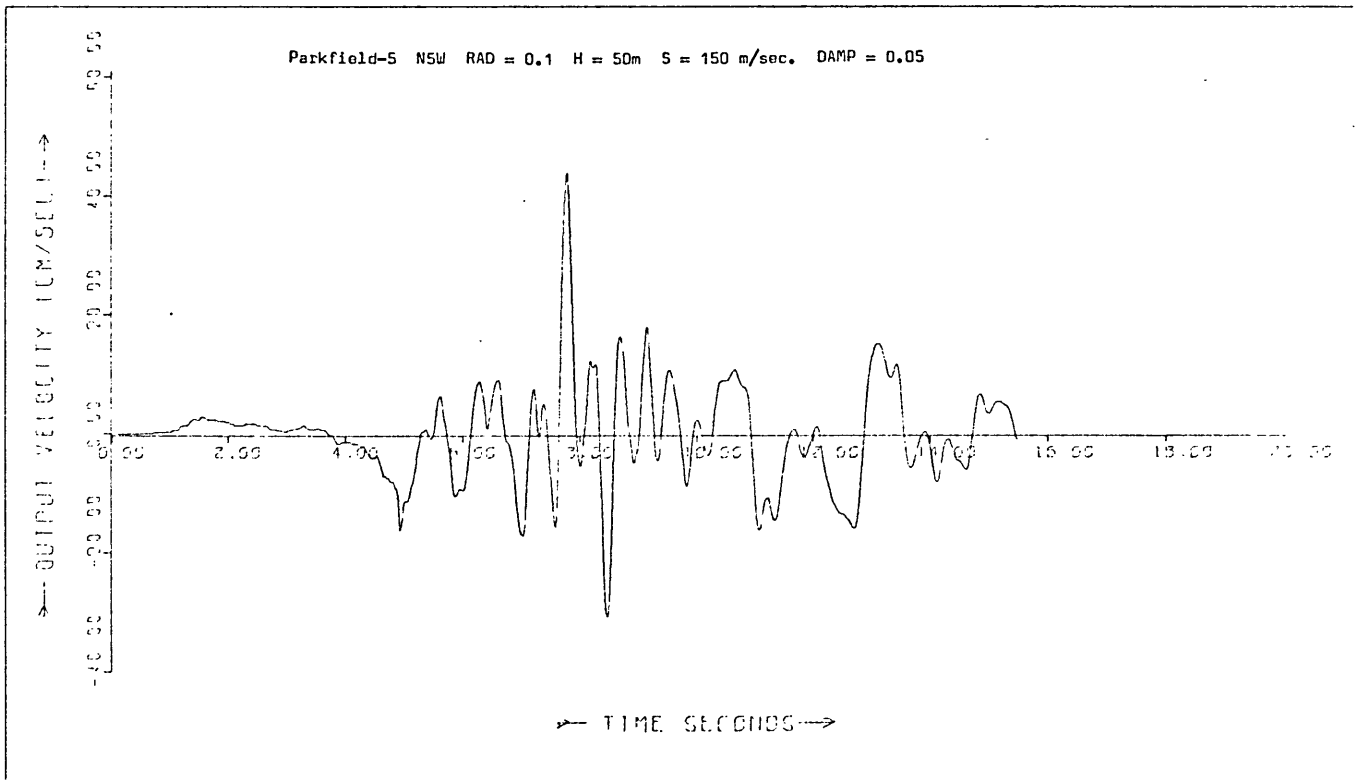


FIG.6.54b COMPUTED GROUND SURFACE VELOCITY TIME HISTORY AT SITE NO. 6.31

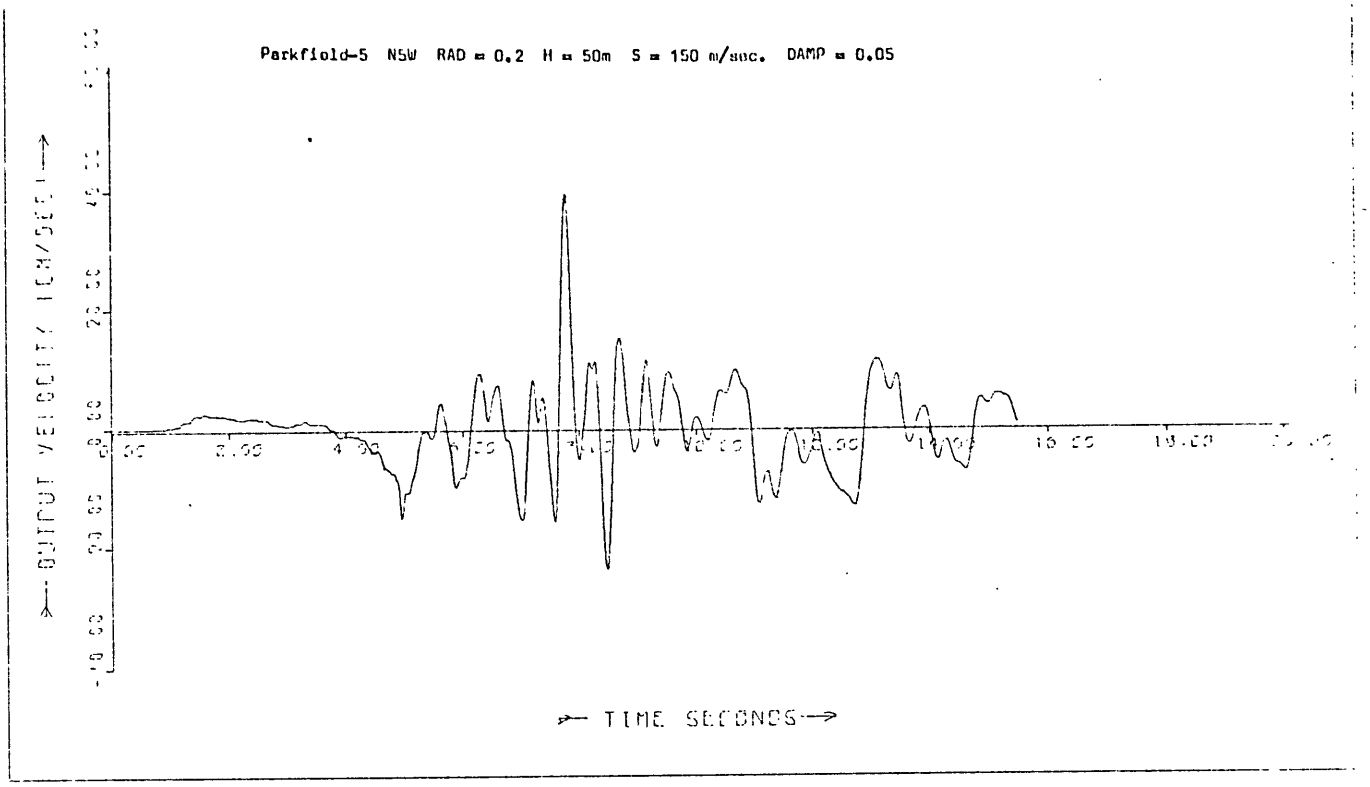


FIG. 6.55b COMPUTED GROUND SURFACE VELOCITY TIME HISTORY AT SITE NO. 6.32

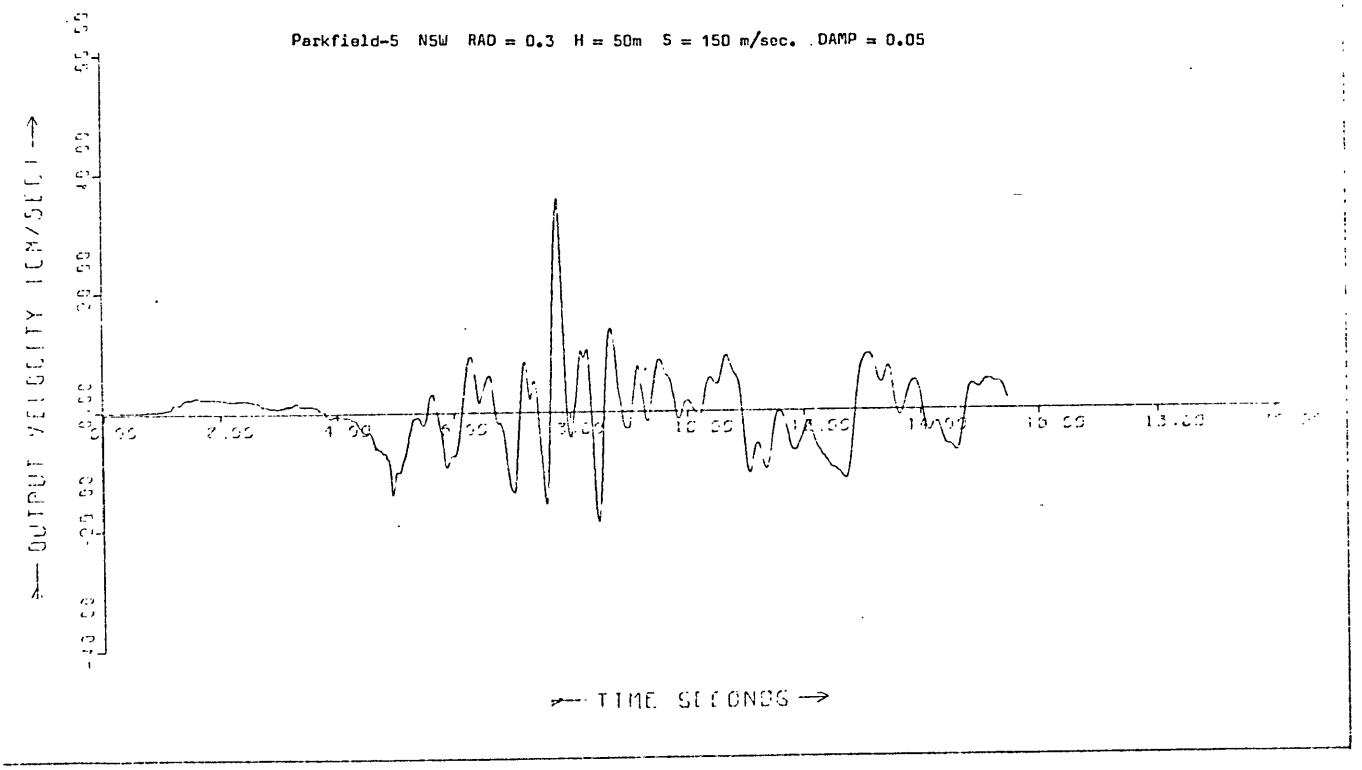


FIG.6.56b COMPUTED GROUND SURFACE VELOCITY TIME HISTORY AT SITE NO. 6.33

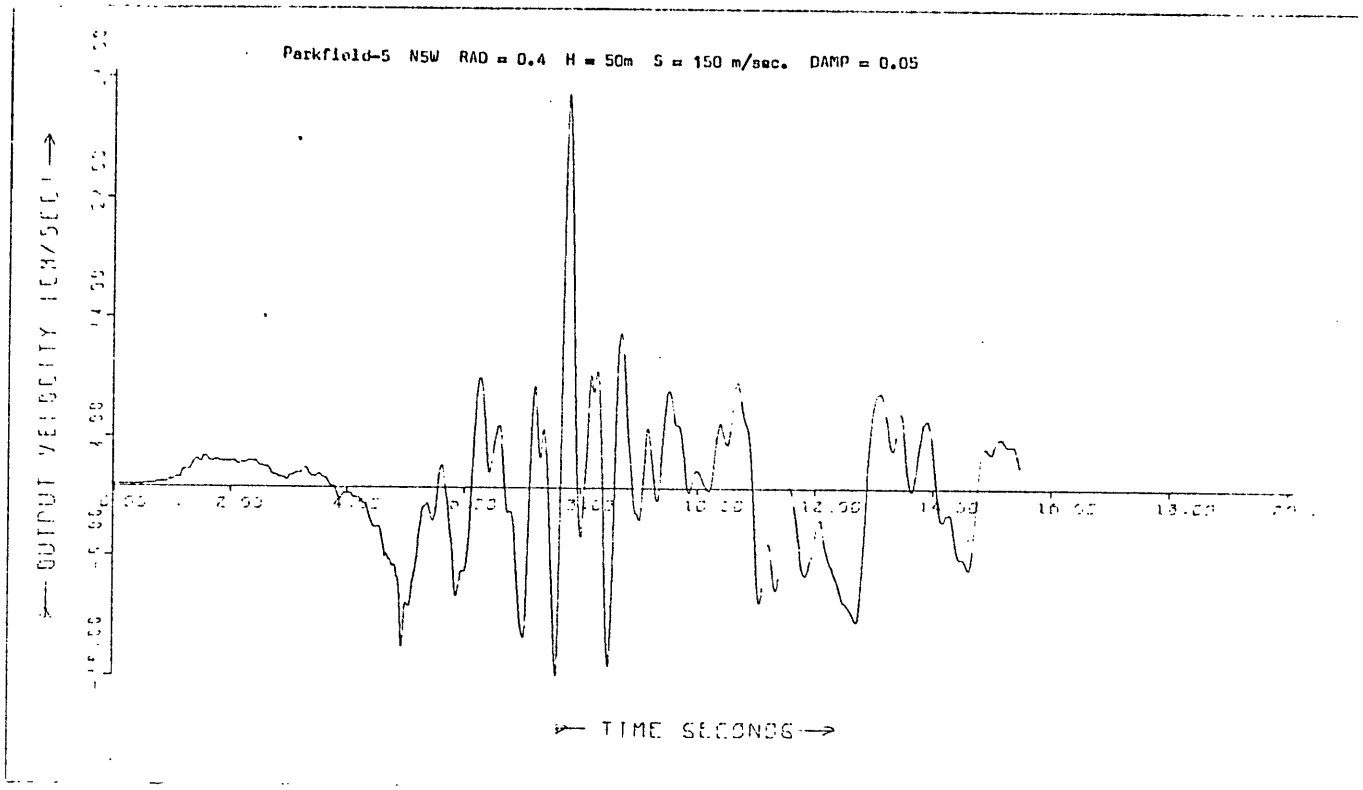


FIG 6.57b COMPUTED GROUND SURFACE VELOCITY TIME HISTORY AT SITE NO. 6.34

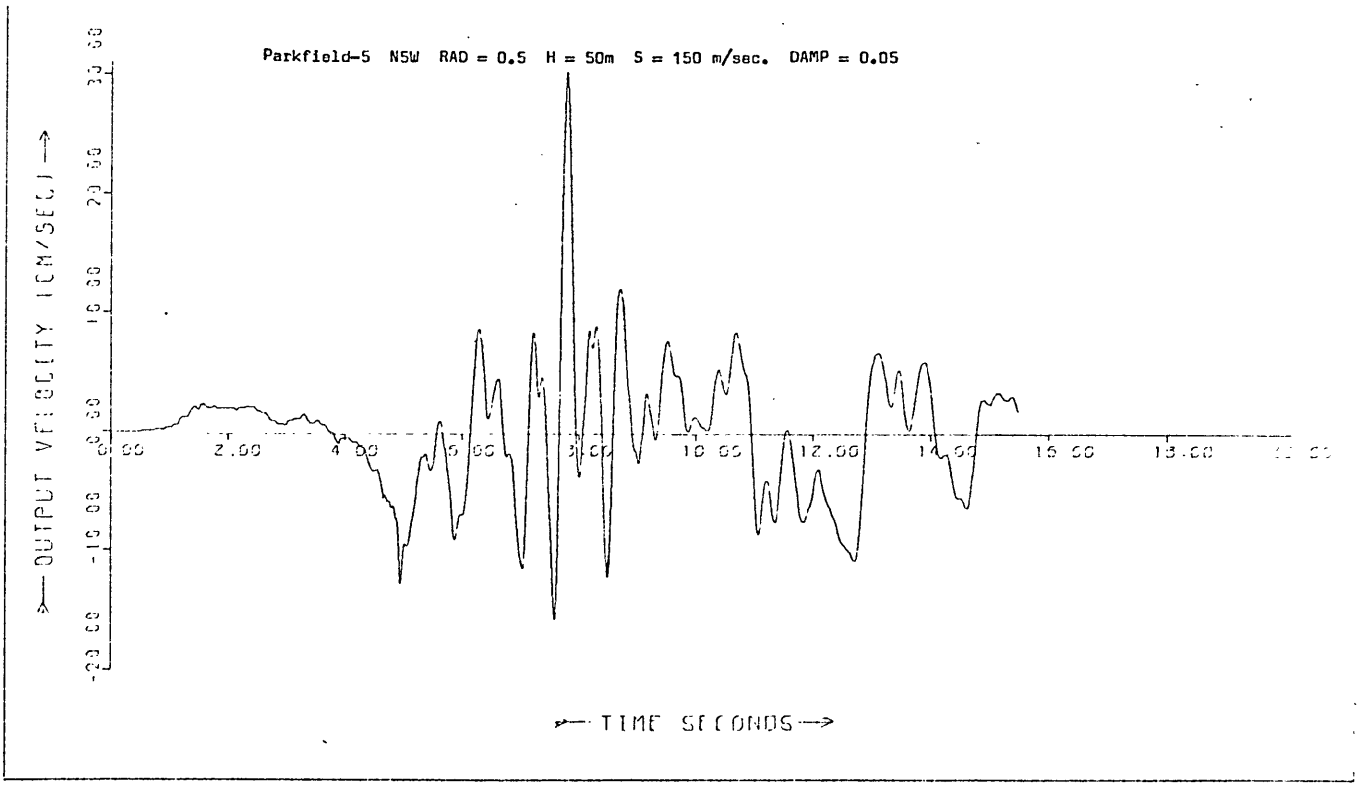


FIG.6.58b COMPUTED GROUND SURFACE VELOCITY TIME HISTORY AT SITE NO. 6.35

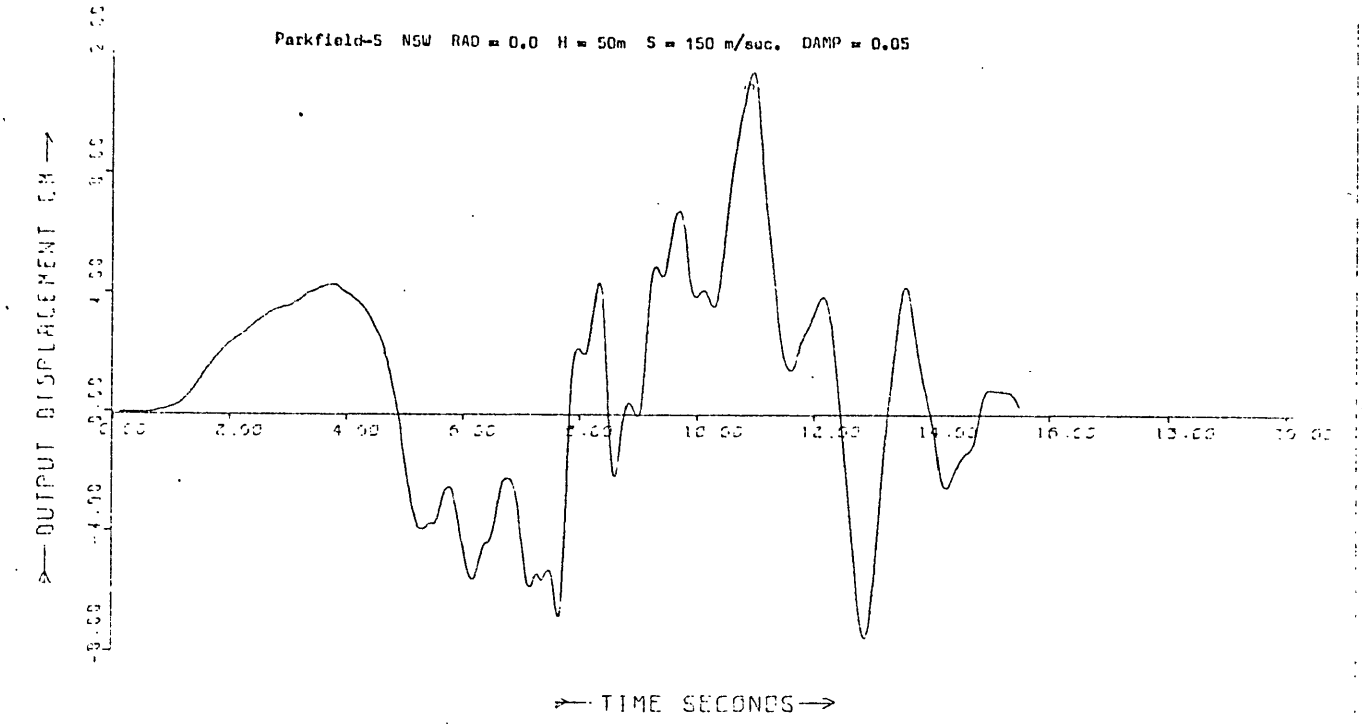


FIG 6.53c COMPUTED GROUND SURFACE DISPLACEMENT TIME HISTORY AT SITE NO. 6.30

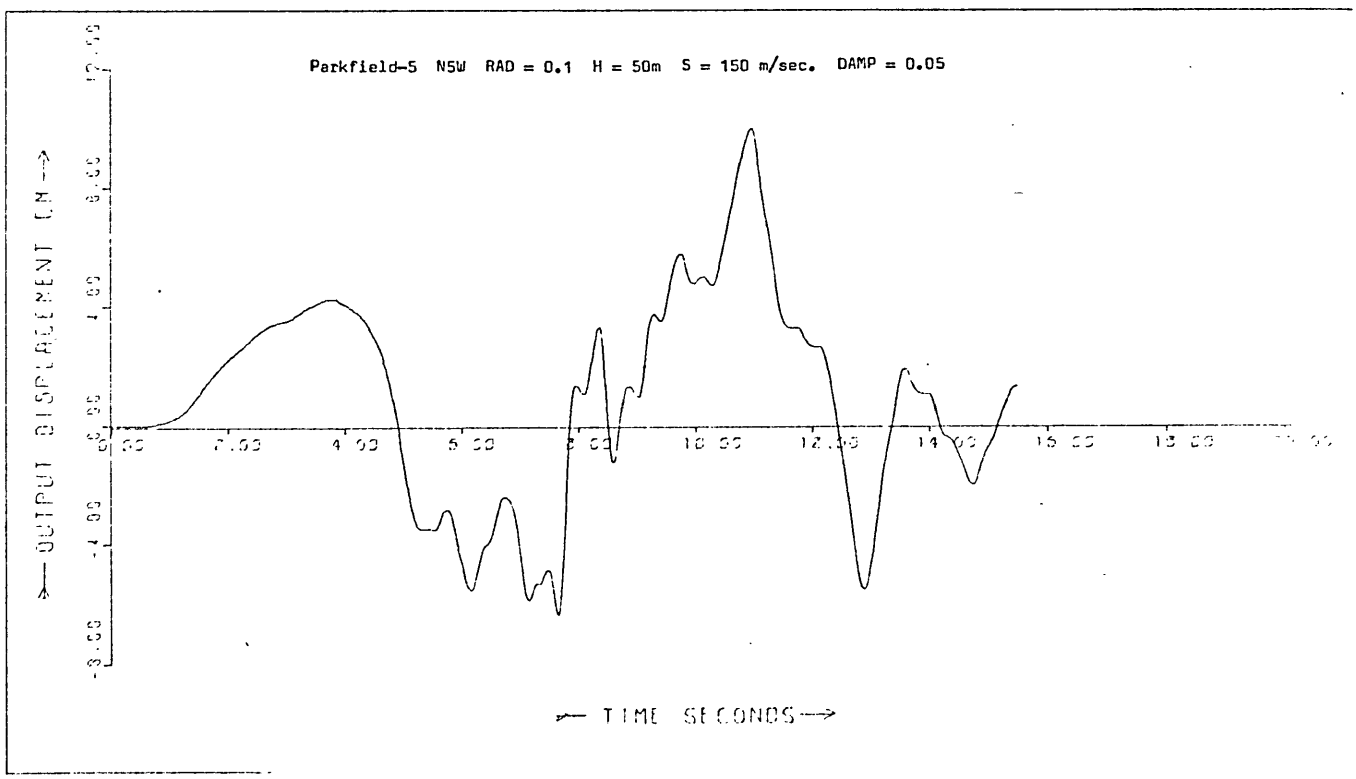


FIG.6.54c COMPUTED GROUND SURFACE DISPLACEMENT TIME HISTORY AT SITE NO. 6.31

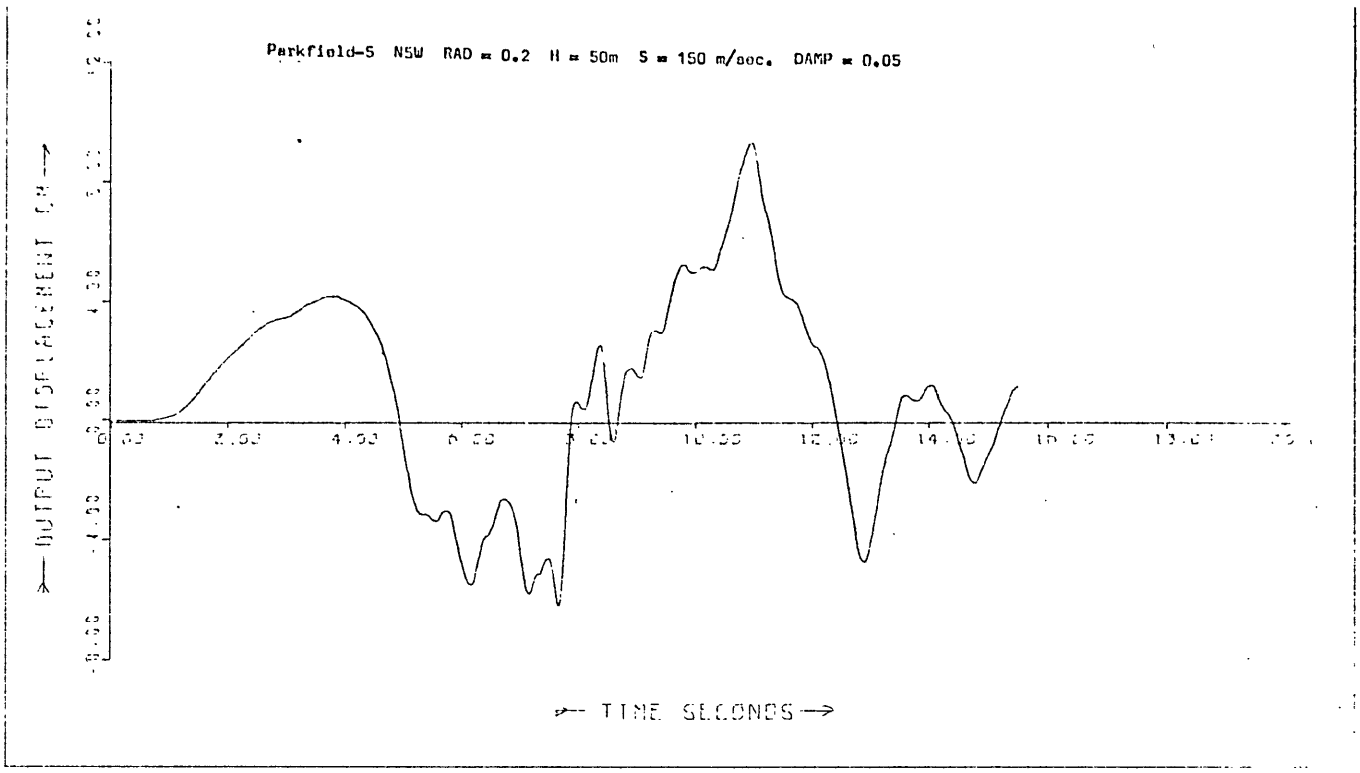


FIG 6.55c COMPUTED GROUND SURFACE DISPLACEMENT TIME HISTORY AT SITE NO. 6.32

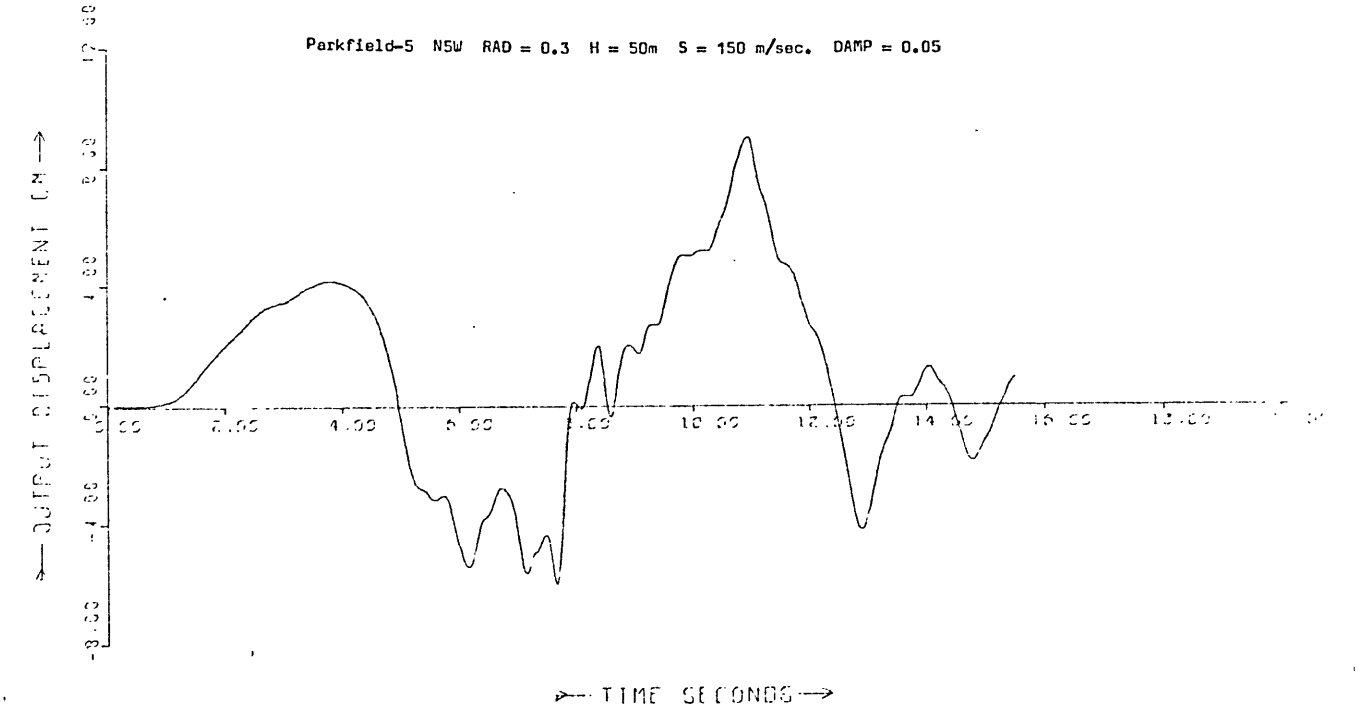


FIG 6.56c COMPUTED GROUND SURFACE DISPLACEMENT TIME HISTORY AT SITE NO. 6.33

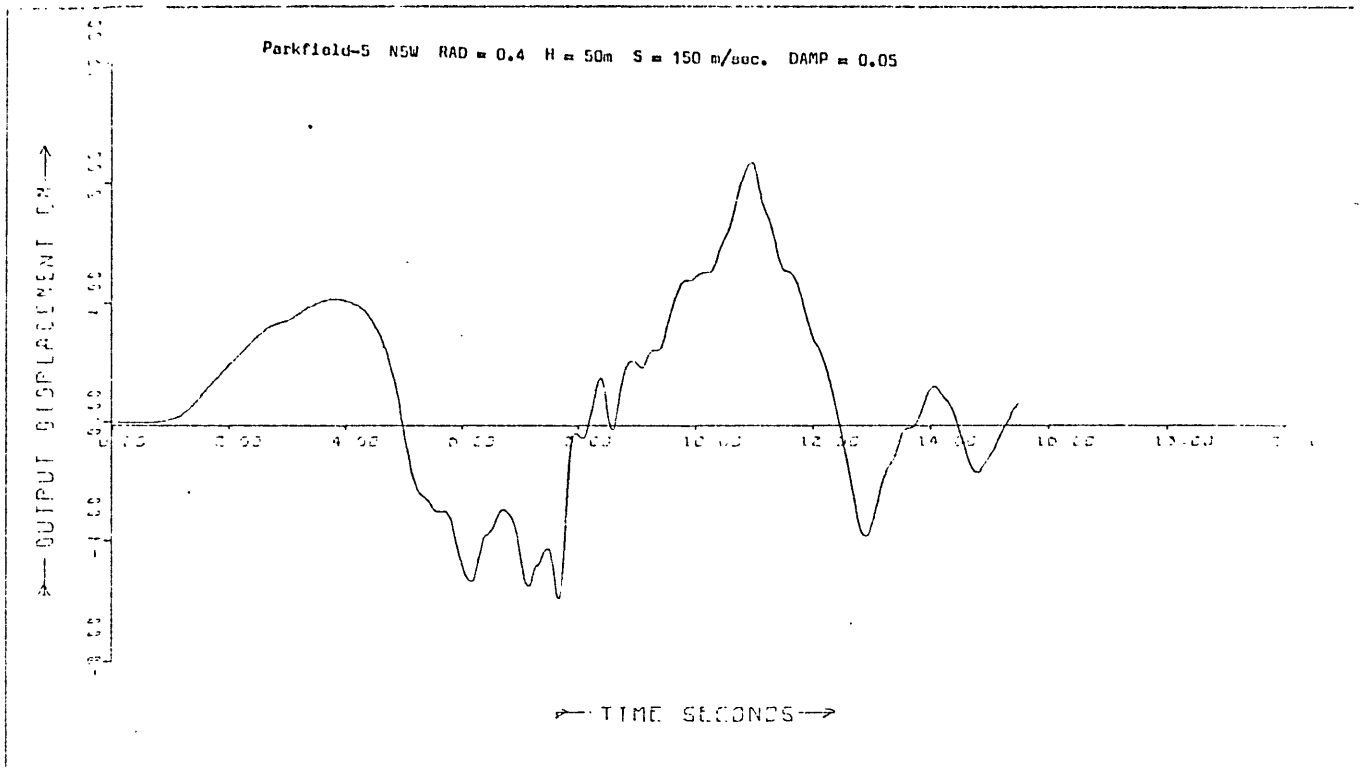


FIG. 6.57 COMPUTED GROUND SURFACE DISPLACEMENT TIME HISTORY AT SITE NO. 6.34

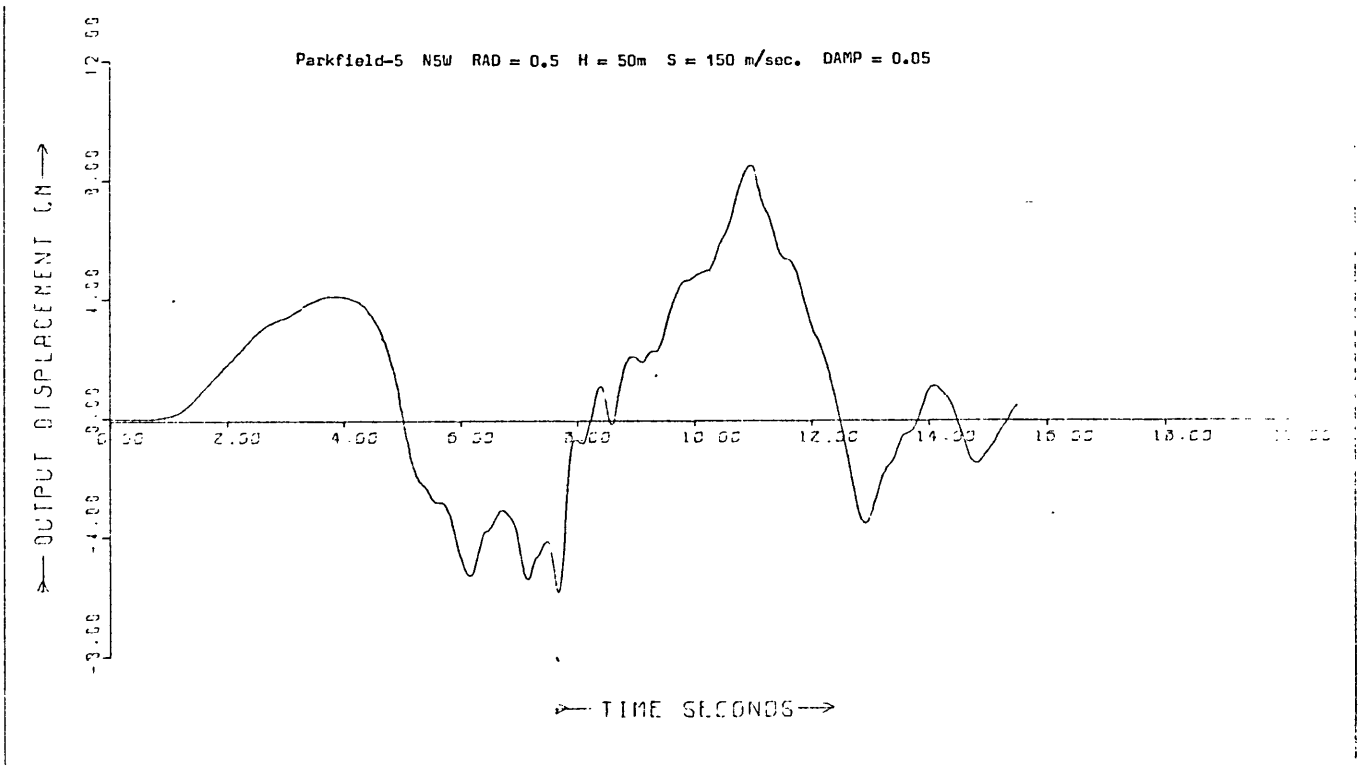


FIG. 6.58 COMPUTED GROUND SURFACE DISPLACEMENT TIME HISTORY AT SITE NO. 6.35

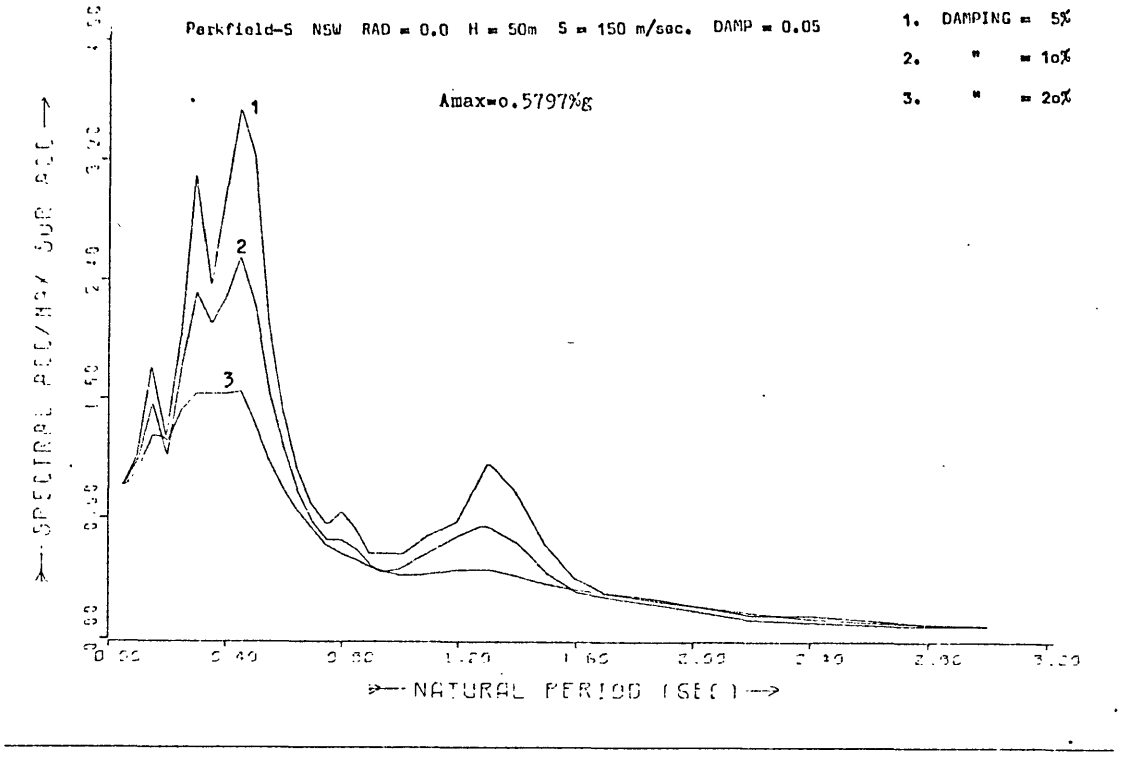


FIG. 6.53dCOMPUTED GROUND SURFACE ACCELERATION RESPONSE SPECTRA AT SITE NO. 6.3o

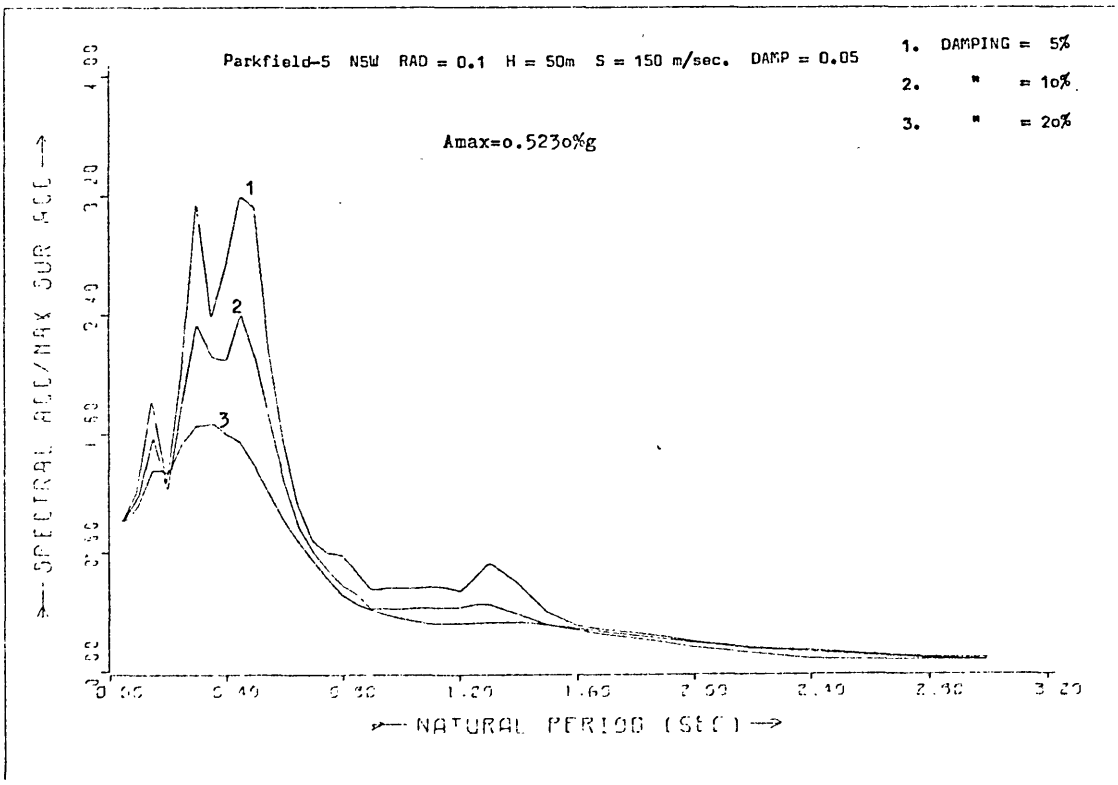


FIG. 6.54dCOMPUTED GROUND SURFACE ACCELERATION RESPONSE SPECTRA AT SITE NO. 6.31

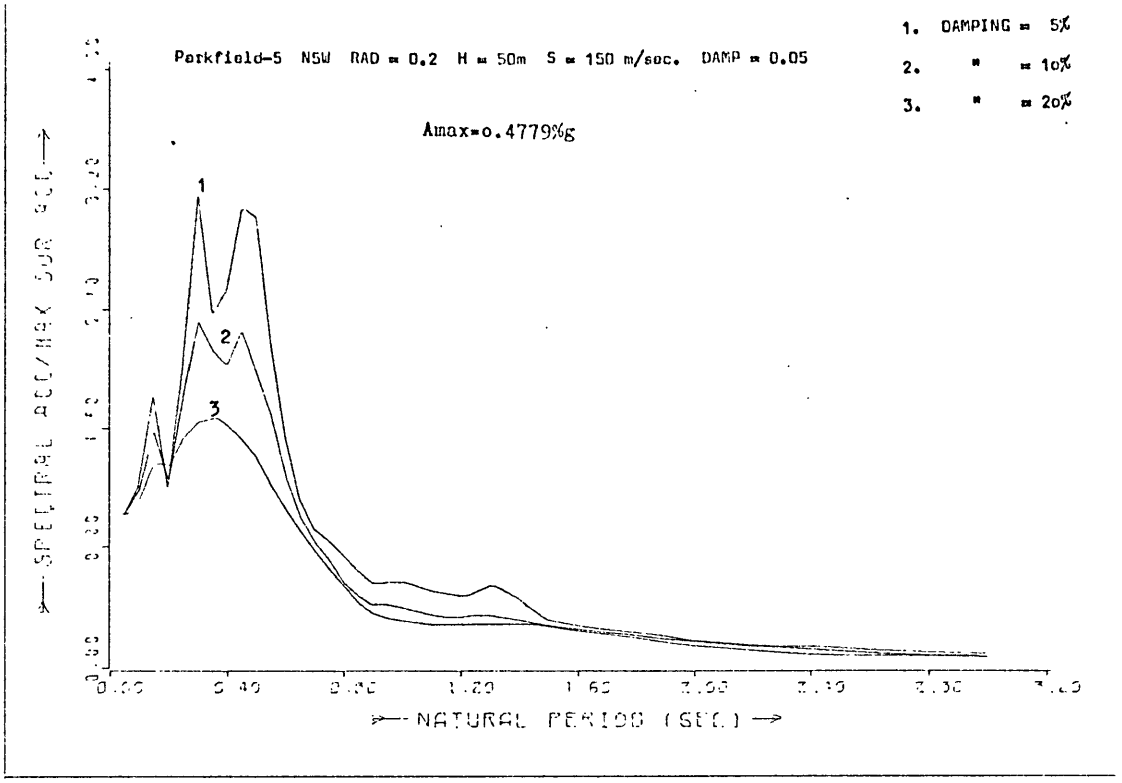


FIG.6.55d COMPUTED GROUND SURFACE ACCELERATION RESPONSE SPECTRA AT SITE NO. 6.32

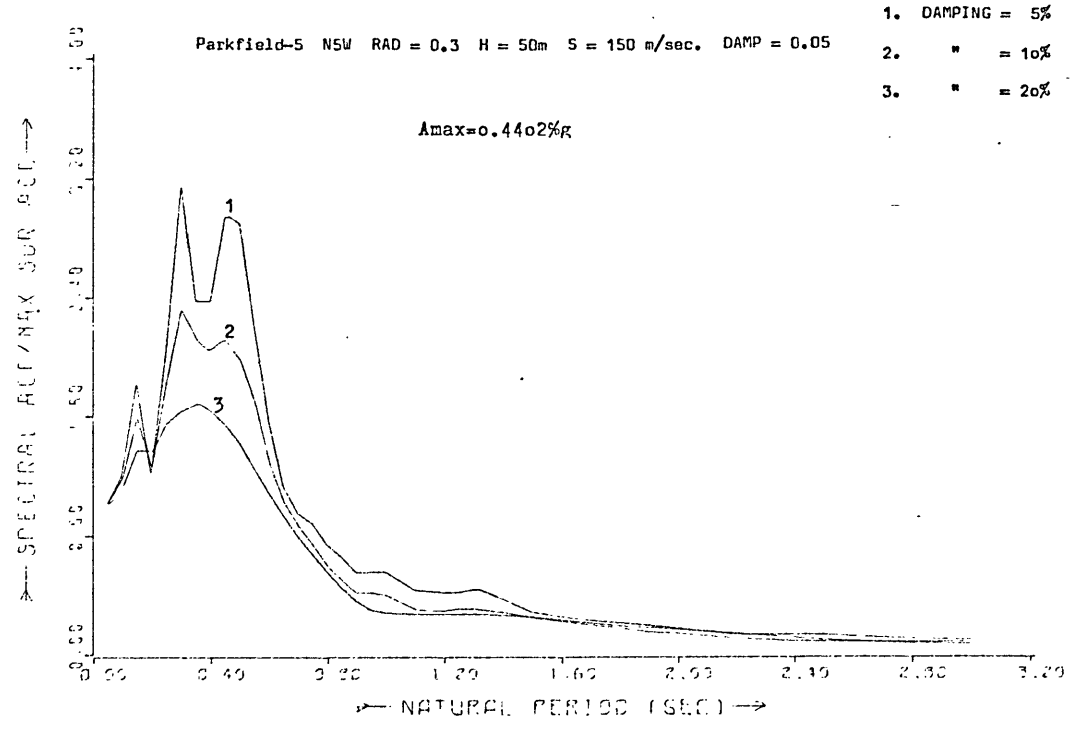


FIG.6.56d COMPUTED GROUND SURFACE ACCELERATION RESPONSE SPECTRA AT SITE NO.6.33

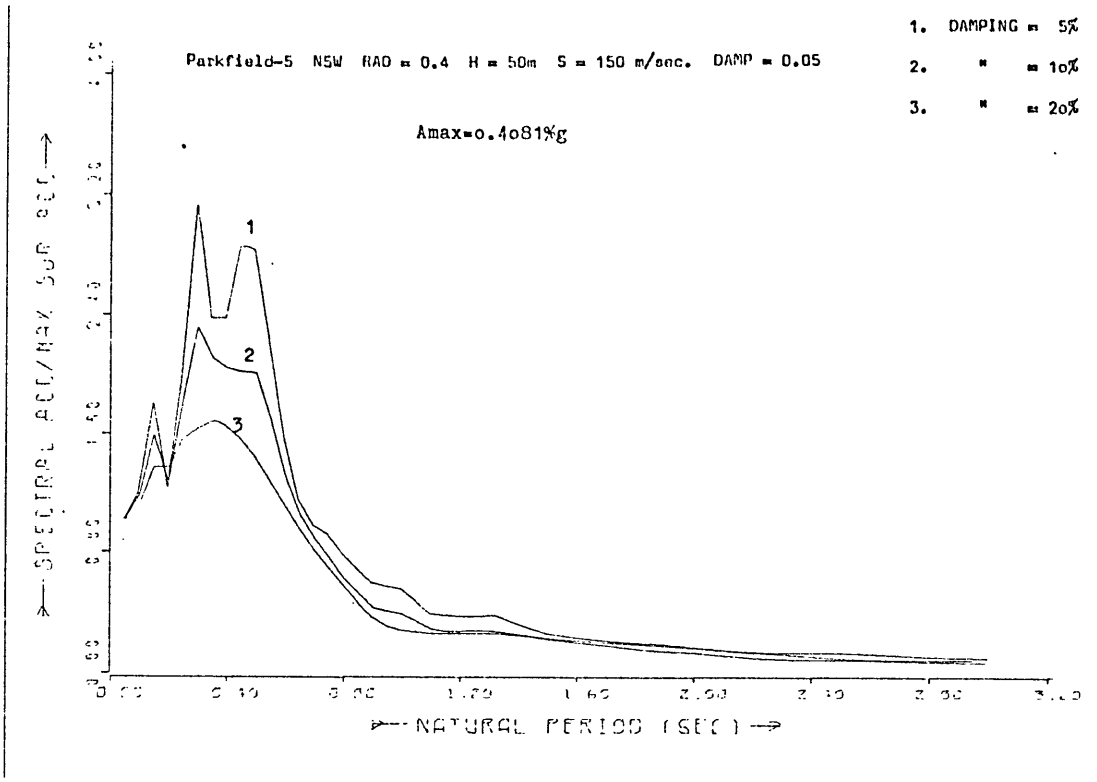


FIG.6.57dCOMPUTED GROUND SURFACE ACCELERATION RESPONSE SPECTRA AT SITE NO. 6.34

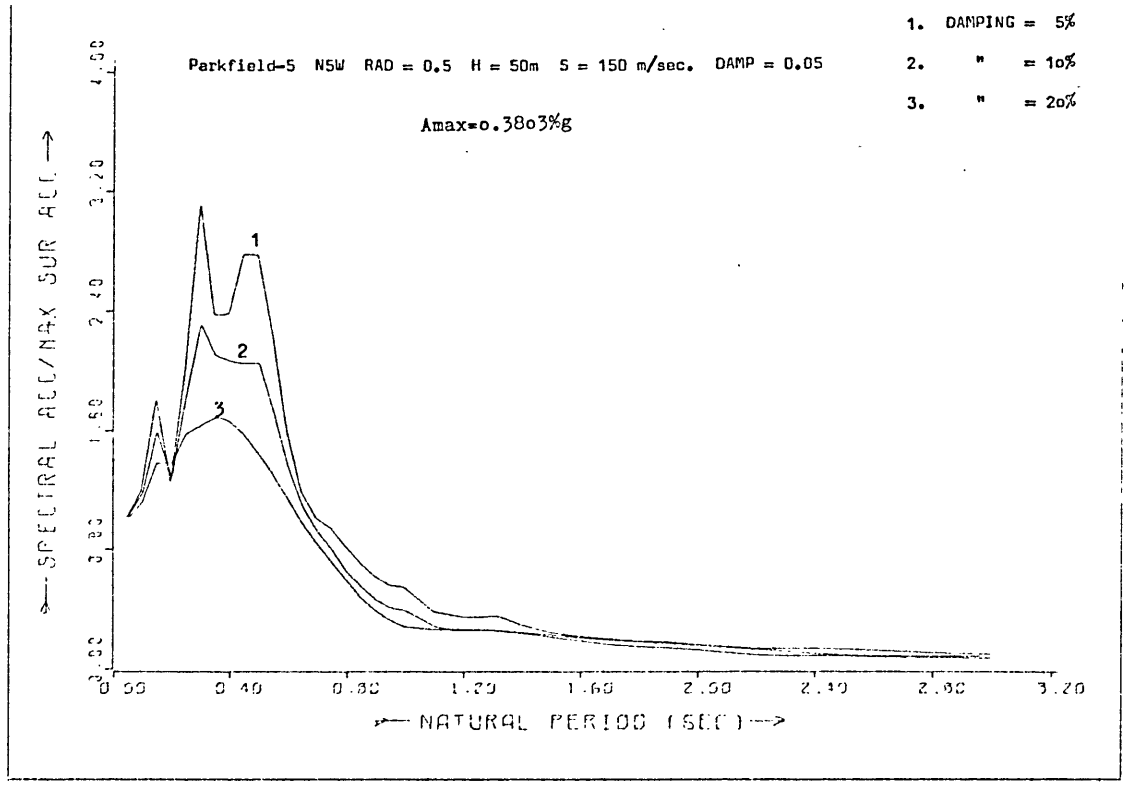


FIG.6.58dCOMPUTED GROUND SURFACE ACCELERATION RESPONSE SPECTRA AT SITE NO. 6.35

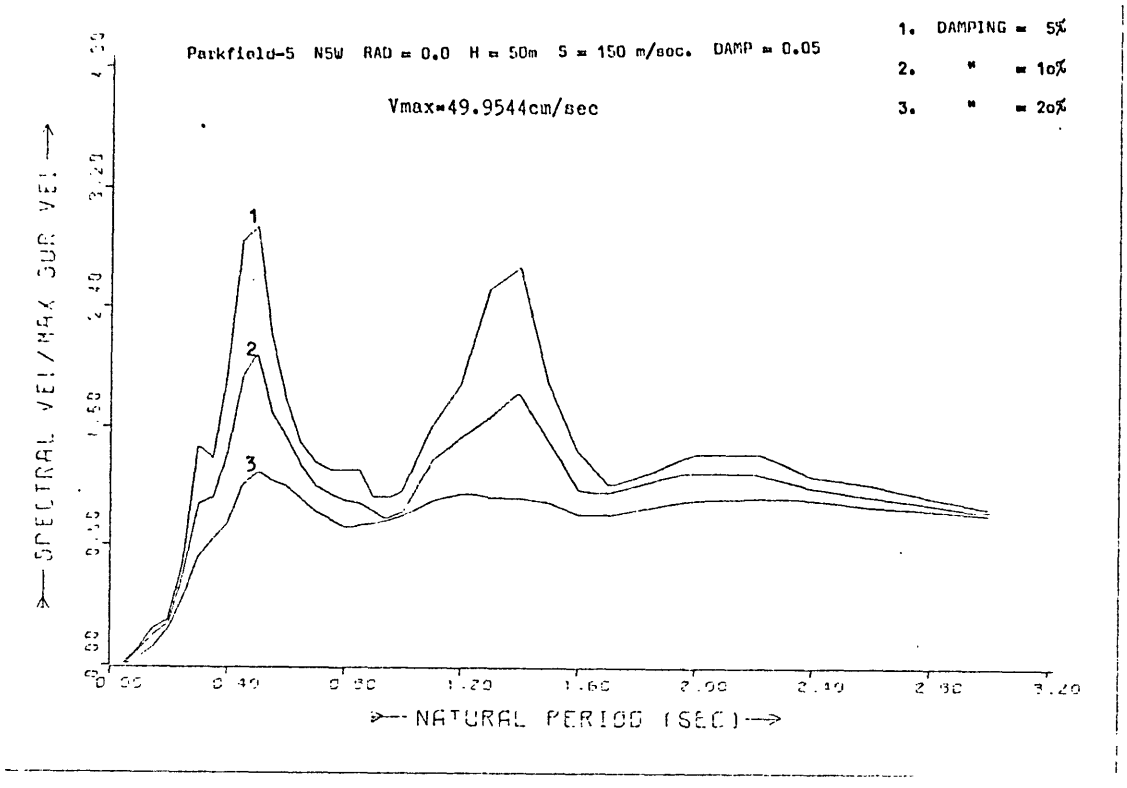


FIG.6.53eCOMPUTED GROUND SURFACE VELOCITY RESPONSE SPECTRA AT SITE NO. 6.30

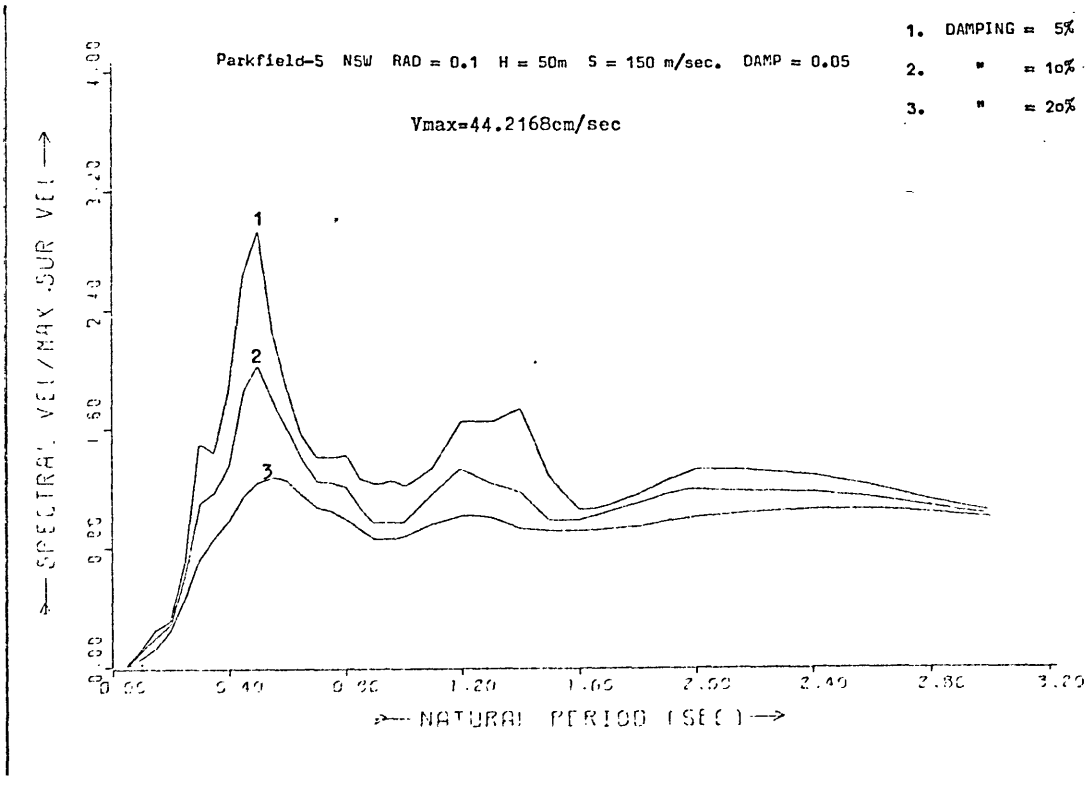


FIG.6.54eCOMPUTED GROUND SURFACE VELOCITY RESPONSE SPECTRA AT SITE NO.6.31

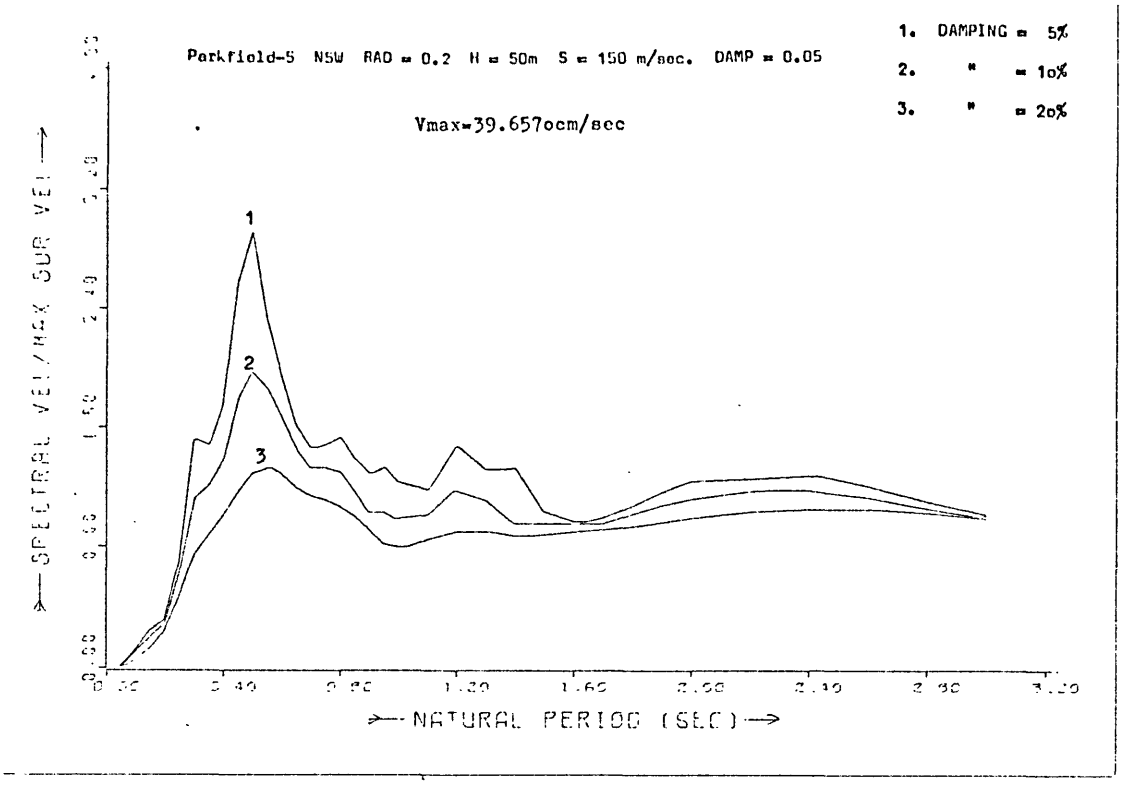


FIG.6.55e COMPUTED GROUND SURFACE VELOCITY RESPONSE SPECTRA AT SITE NO. 6.32

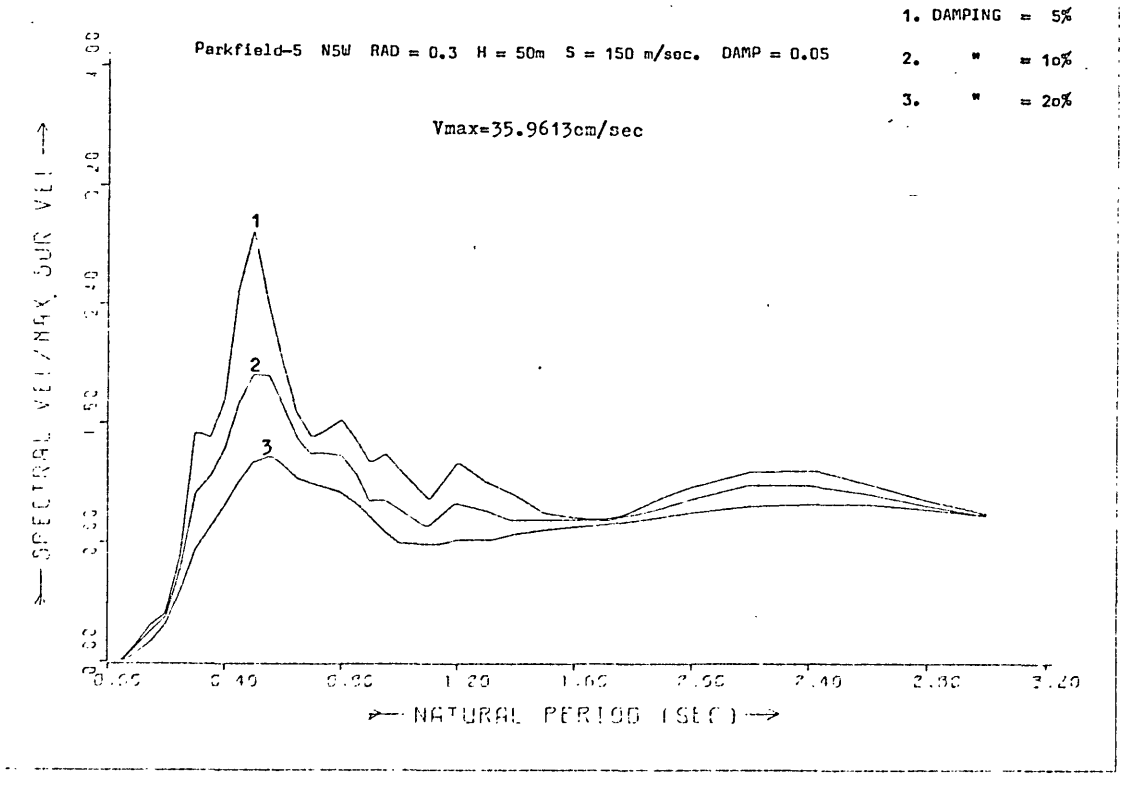


FIG.6.56e COMPUTED GROUND SURFACE VELOCITY RESPONSE SPECTRA AT SITE NO. 6.33

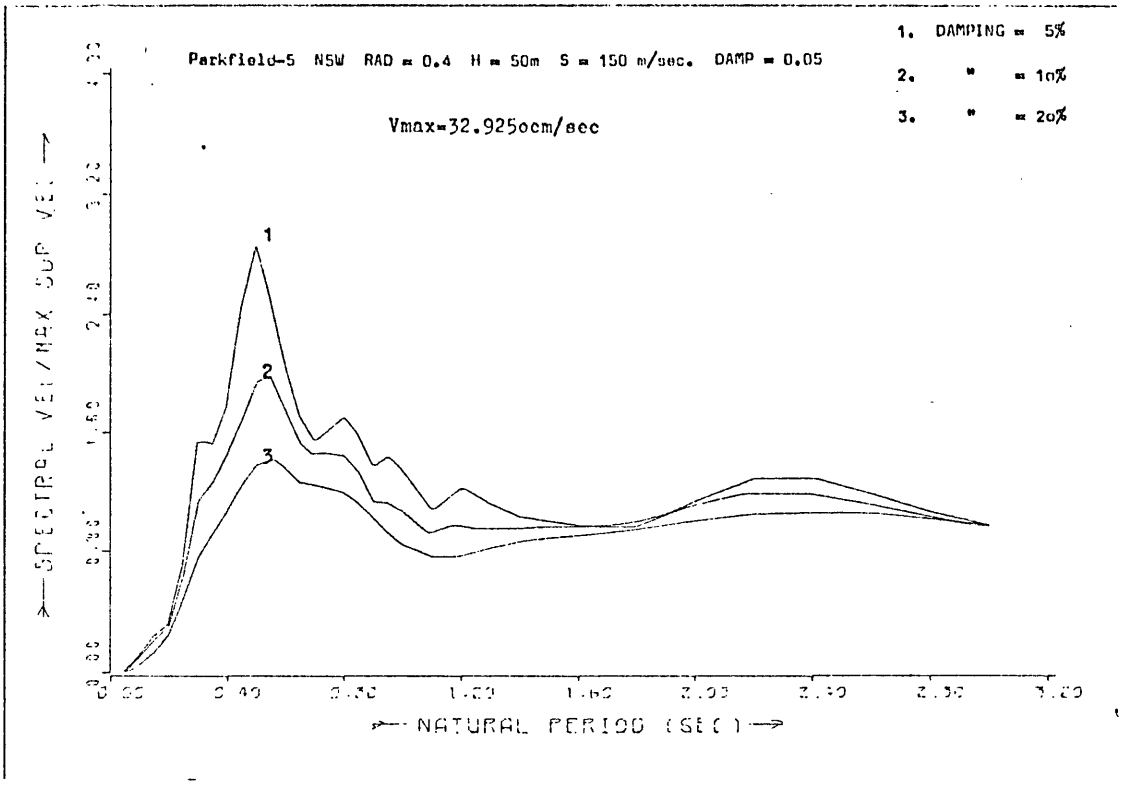


FIG.6.57e COMPUTED GROUND SURFACE VELOCITY RESPONSE SPECTRA AT SITE NO. 6. 34

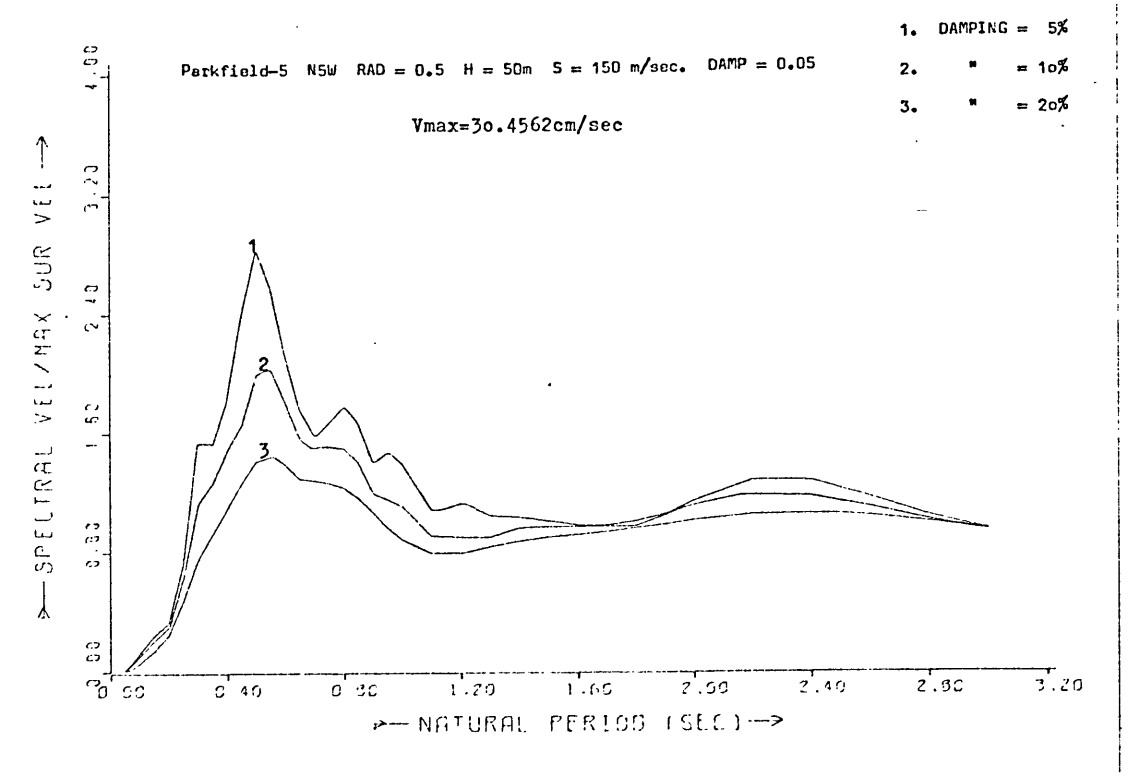


FIG.6.58e COMPUTED GROUND SURFACE VELOCITY RESPONSE SPECTRA AT SITE NO. 6.35

DATA ON THE INFLUENCE OF BEDROCK CHARACTERISTICS ON RESPONSE OF SOIL DEPOSITS

RADIATION DAMPING RATIO	MAX. SUR. ABS. ACC. (g)	$1 - \frac{ACC_{RAD}}{ACC_{0.0}} \times 100\%$	MAX. SUR. ABS. VEL. (cm/sec)	$1 - \frac{VEL_{RAD}}{VEL_{0.0}} \times 100\%$	MAX. SUR. ABS. DIS. (cm)	$1 - \frac{DIS_{RAD}}{DIS_{0.0}} \times 100\%$	STRENGTH $(cm/sec)^2$
0.0	0.58	0.00	49.95	0.00	11.44	0.00	953
0.1	0.52	10.34	44.22	11.47	10.01	12.5	542
0.2	0.48	17.24	39.66	20.60	9.38	18.00	401
0.3	0.44	24.13	35.96	28.00	9.03	21.06	325
0.4	0.40	31.03	32.92	34.09	8.78	23.25	277.44
0.5	0.38	34.48	30.45	39.03	8.58	25.0	245.35

TABLE 6.5

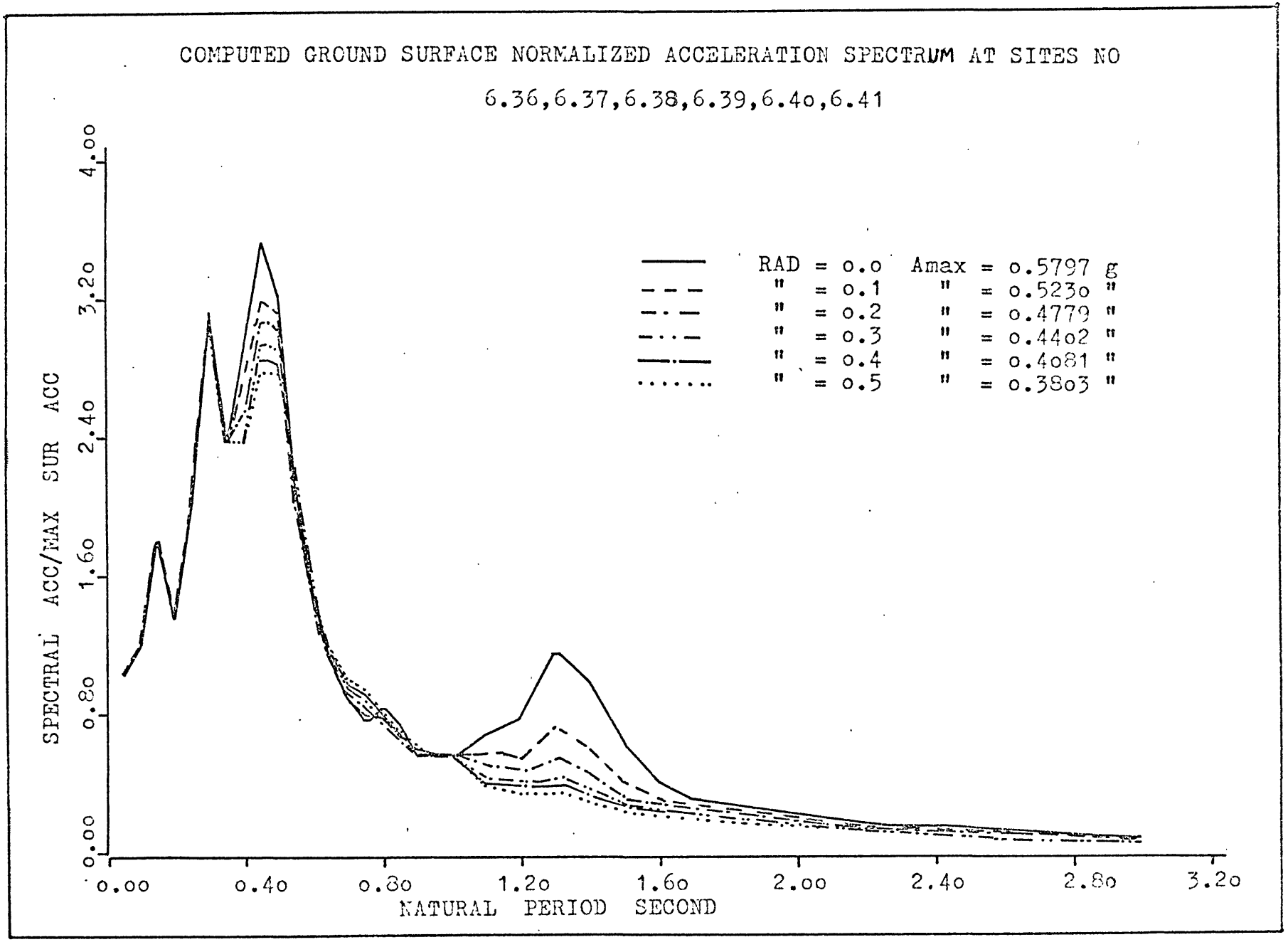

COMPUTED GROUND SURFACE NORMALIZED ACCELERATION SPECTRUM AT SITES NO
6.36,6.37,6.38,6.39,6.40,6.41
RAD = 0.0 Amax = 0.5797 g
" = 0.1 " = 0.5230 "
" = 0.2 " = 0.4779 "
" = 0.3 " = 0.4402 "
" = 0.4 " = 0.4081 "
" = 0.5 " = 0.3803 "
SPECTRAL ACC/MAX SUR ACC
0.00
0.80
1.60
2.40
3.20
4.00
0.00
0.40
0.80
1.20
1.60
2.00
2.40
2.80
3.20
NATURAL PERIOD SECOND

FIG. 6.59

and 0.44 sec., frequency characteristics of the motions vary at the six sites. Differences in the amplitudes of spectral values are observed, which are considerably great near the resonant periods of the deposit, emphasising the importance of radiation damping ratio on the developed response near the resonant periods of the overburden.

Figs. 6.53e to 6.58e, which are summarized in fig. 6.60, show normalized velocity spectrum for the deposit having different bedrock characteristics. It is apparent that energy attained by intermediate period structures will be considerably different, depending on the stiffness characteristics of bedrock formation.

CONCLUSIONS

Based on the results presented, the following conclusions are drawn:

a) The computed surface time histories of a soil deposit, in amplitude and frequency content, is influenced by radiation damping ratio. The extent of influence is considerably more on response amplitudes.

b) Strength of an earthquake motion at a given site, in terms of total energy which would be supplied to structures located on the site, is considerably dependent on the stiffness characteristics of bedrock motion.

c) The shapes of the computed surface response spectra curves are directly tied in with the deformability of bedrock formation.

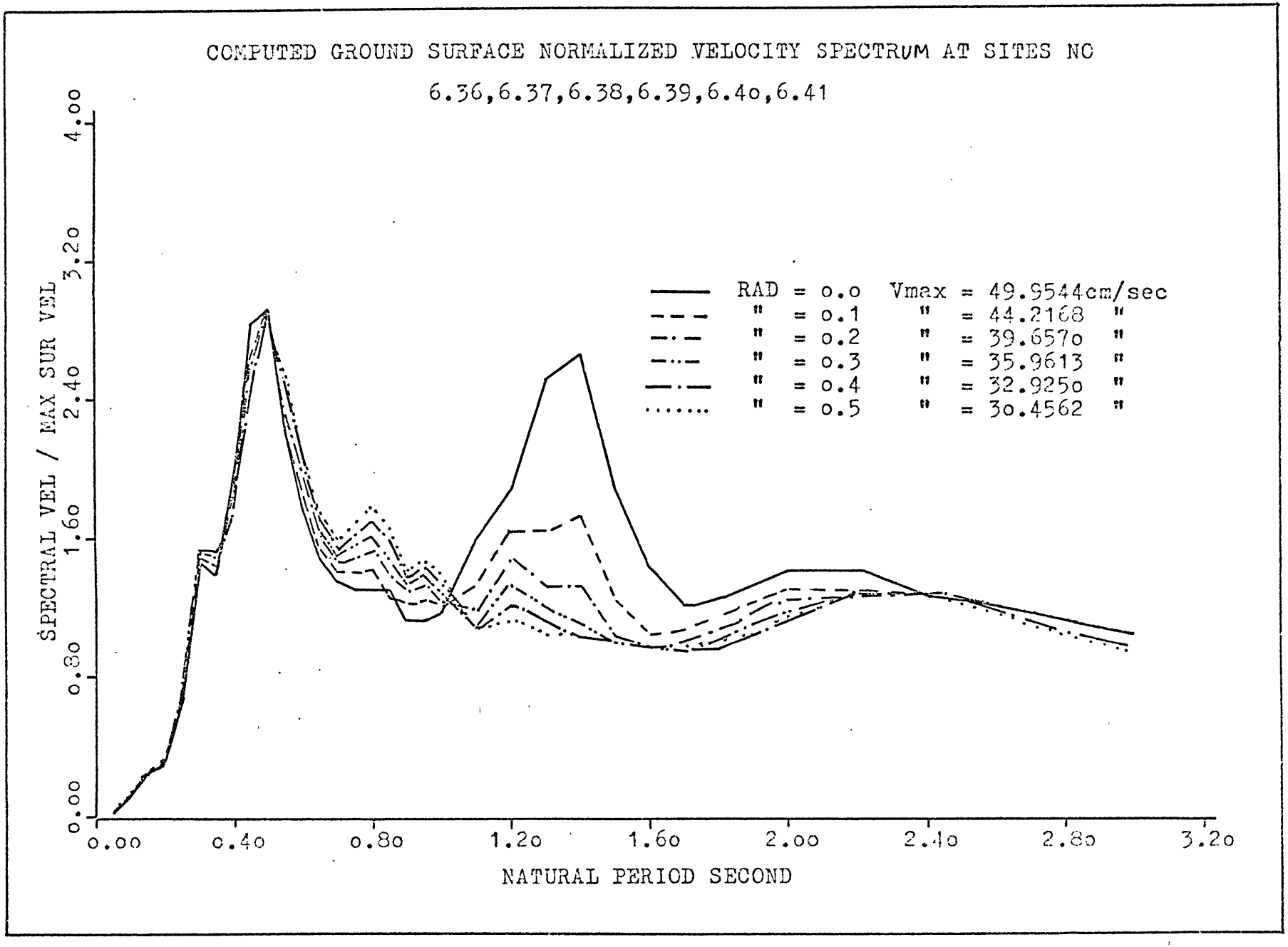

COMPUTED GROUND SURFACE NORMALIZED VELOCITY SPECTRUM AT SITES NO
6.36,6.37,6.38,6.39,6.4o,6.41
SPECTRAL VEL / MAX SUR VEL
0.00
0.80
1.60
2.40
3.20
4.00
0.00
0.40
0.80
1.20
1.60
2.00
2.40
2.80
3.20
NATURAL PERIOD SECOND
RAD = o.o Vmax = 49.9544cm/sec
" = o.1 " = 44.2168 "
" = o.2 " = 39.657o "
" = o.3 " = 35.9613 "
" = o.4 " = 32.925o "
" = o.5 " = 3o.4562 "

FIG.6.6o

DISCUSSION

The results presented in sections 6.8.2.1 and 6.8.2.2 show clearly that flexibility of bedrock formation has an important effect on the seismic response characteristics of the soil deposits. Hence conclusions drawn by Lysmer et. al., reported in section 6.8, seem inconsistent. Based on Lysmer et. al study, it is often assumed that bedrock formation is completely rigid and radiation damping effects can be neglected. The following interpretation explains the apparent inconsistency.

i) In each comparison made by Lysmer et. al. all parameters other than the amplitude of base motion and bedrock formation were kept constant. The results presented, which have formed the basis for the conclusions drawn, include the effect of the amplitude of bedrock motion and characteristics of the bedrock formation; in a strain dependent model, amplitude of bedrock motion has a considerable influence on response.

ii) As the intensity of shaking increases, rigidity of the soil decreases, hence radiation damping ratio is reduced. Under this condition it is likely that radiation damping ratio will influence the results to a lesser degree.

41

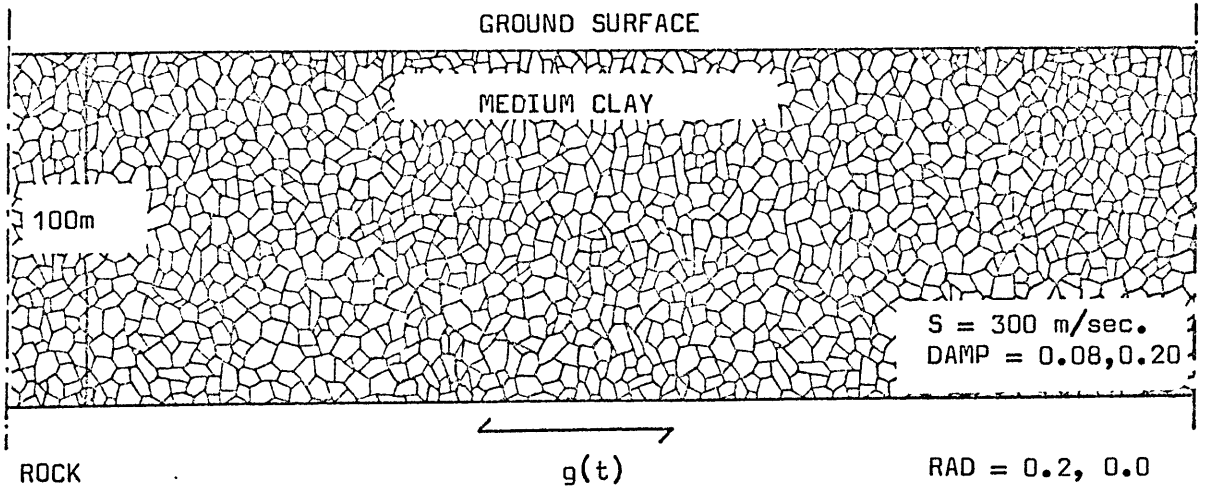
In short, it can be concluded that Lysmer et. al. conclusions are not generally true and are valid only for soil deposits with small values of radiation damping ratio, which may exhibit a softening effect during cyclic loading. The cases analysed by the authors do not include a variety of bedrock formations; three types of bedrock formations only were analysed, i.e. $S_{rock} = \infty$, 1220 and 1830 m/sec. The authors have not included any examples of deposits of soil underlain by soft rock (S_{rock} = 600 m/sec.). Therefore, the conclusions drawn may only be valid for the sites analysed

by the authors.

6.9. EVALUATION OF THE RESPONSE OF A SOIL DEPOSIT WITH FLEXIBLE BEDROCK BY MEANS OF RIGID BASE SOLUTION

Due to the cost, complexity and validity of existing mathematical models, which take into account radiation damping effects rigorously, the response of soil deposits on deformable bedrock to earthquake shocks has been evaluated by means of rigid base solutions. To account approximately for the energy transmitted to the bedrock, a certain amount of additional damping is introduced in each mode of the vibration of the rigid base solution. The work reported in this chapter sections 6.8.1.1 and 6.8.1.2 clearly illustrate that the effect of radiation damping ratio is not the same as the hysteretic damping ratio in higher modal response.

In order to check the reliability of the above approach, analyses were performed on a deposit of medium clay, shown in fig. 6.61, with fundamental period of 1.34 sec., subjected at its bedrock level to San Fernando S16E, Parkfield-8 N50E, Parkfield-5 N5W, Golden Gate N10E with predominant periods of 0.4, 0.16, 0.3 and 0.15 sec. Figs. 6.61a,b,c,d,e through 6.68a,b,c,d,e show comparison of response values developed at the surface of medium clay having an infinitely rigid base (RAD = 0.0) with hysteretic damping ratio of 0.2 and a shale type base with shear wave velocity of 1500 m/sec. The results clearly illustrate that the second approach is not acceptable. Considerable differences between frequency distribution of the two sets of calculations exist, which is clearly reflected in the normalized acceleration response spectrum shown in figs. 6.61d, 6.62d through 6.67d, 6.68d. The second model can only produce good results when first modal contribution dominates the response; this condition is less likely to be satisfied in most cases of practical interest.



RESPONSE OF HYSTERETIC DEPOSIT UNDERLAIN BY DEFORMABLE BEDROCK

SCHEMATIC SOIL PROFILE FOR SITE NO. 6.36 and 6.37

FIG. 6.61

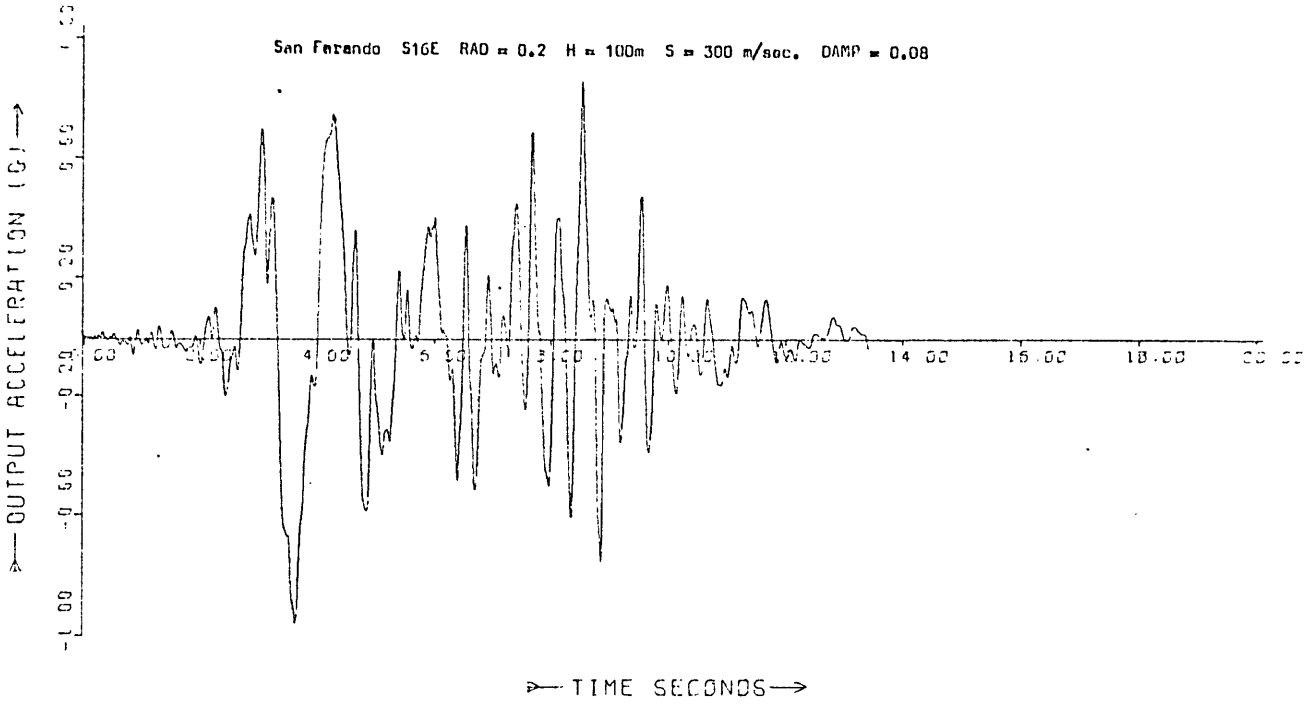


FIG. 6.61a COMPUTED GROUND SURFACE ACCELERATION TIME HISTORY AT SITE NO 6. 36

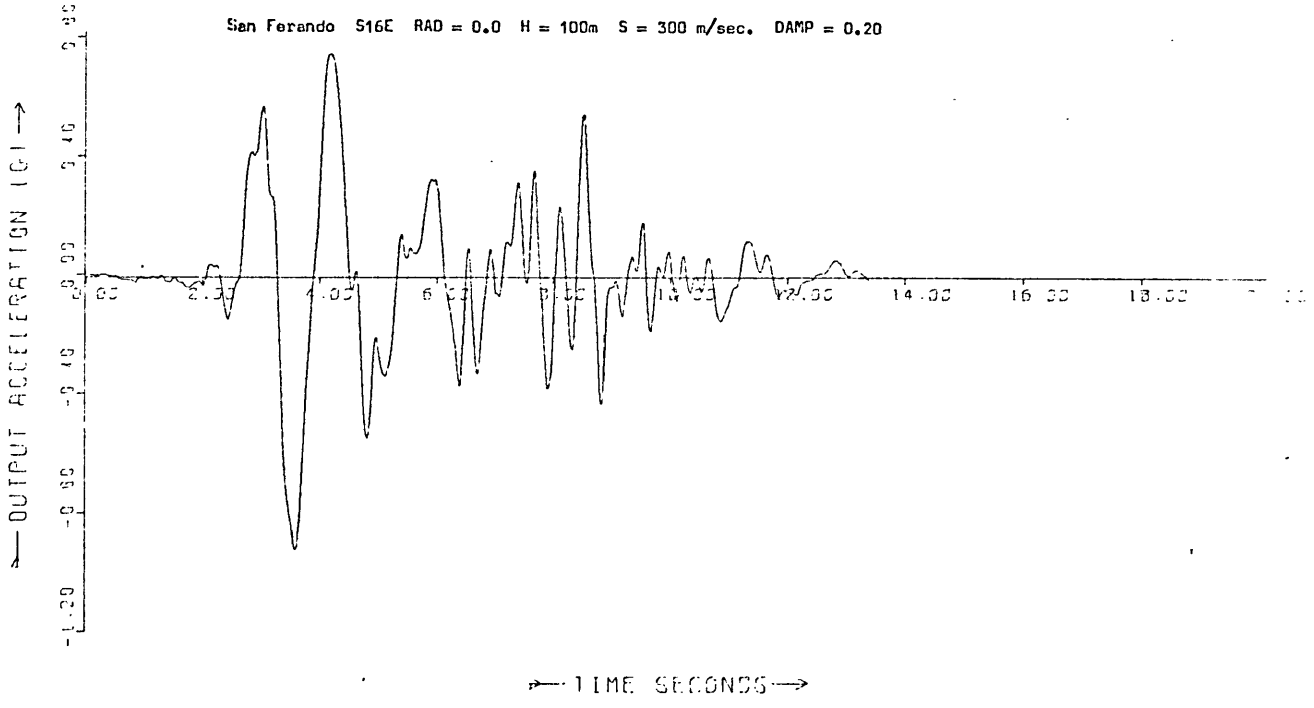


FIG. 6.62 a COMPUTED GROUND SURFACE ACCELERATION TIME HISTORY AT SITE NO 6. 37

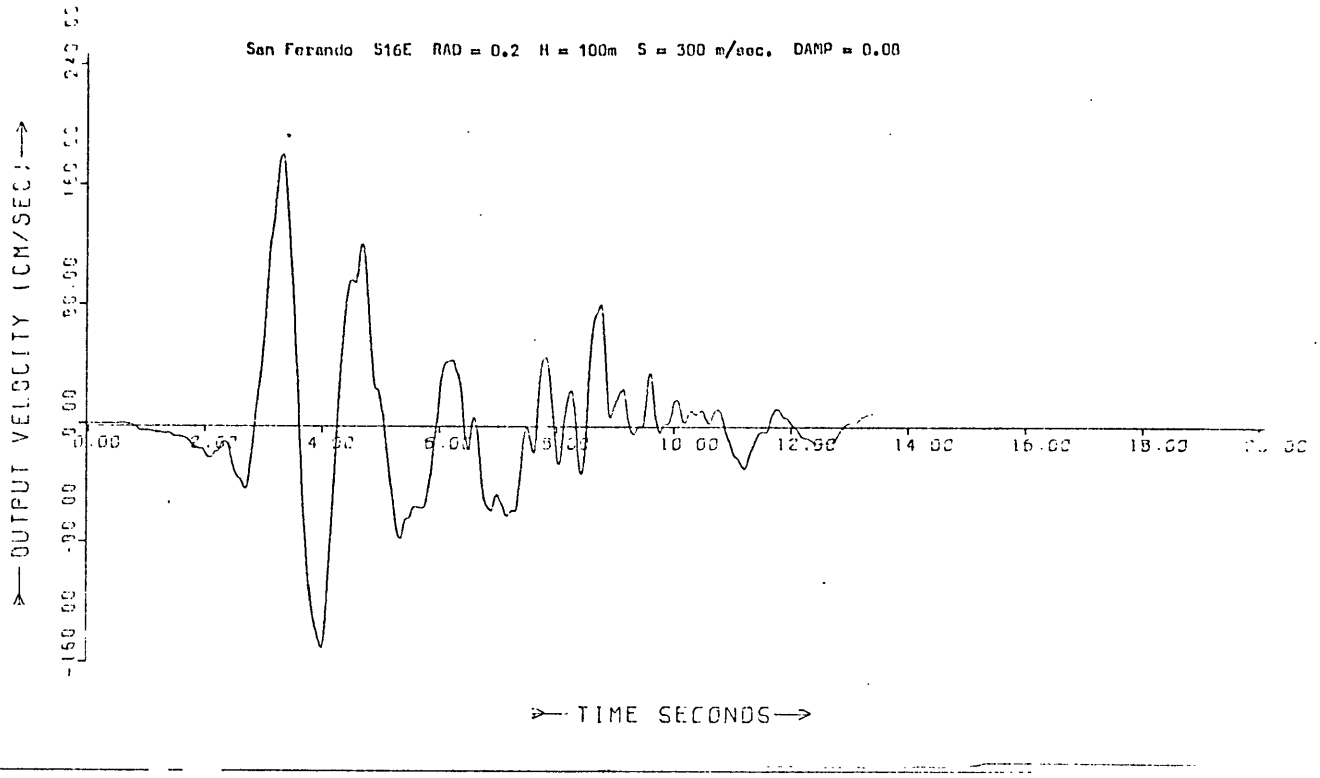


FIG. 6.61b COMPUTED GROUND SURFACE VELOCITY TIME HISTORY AT SITE NO 6.36

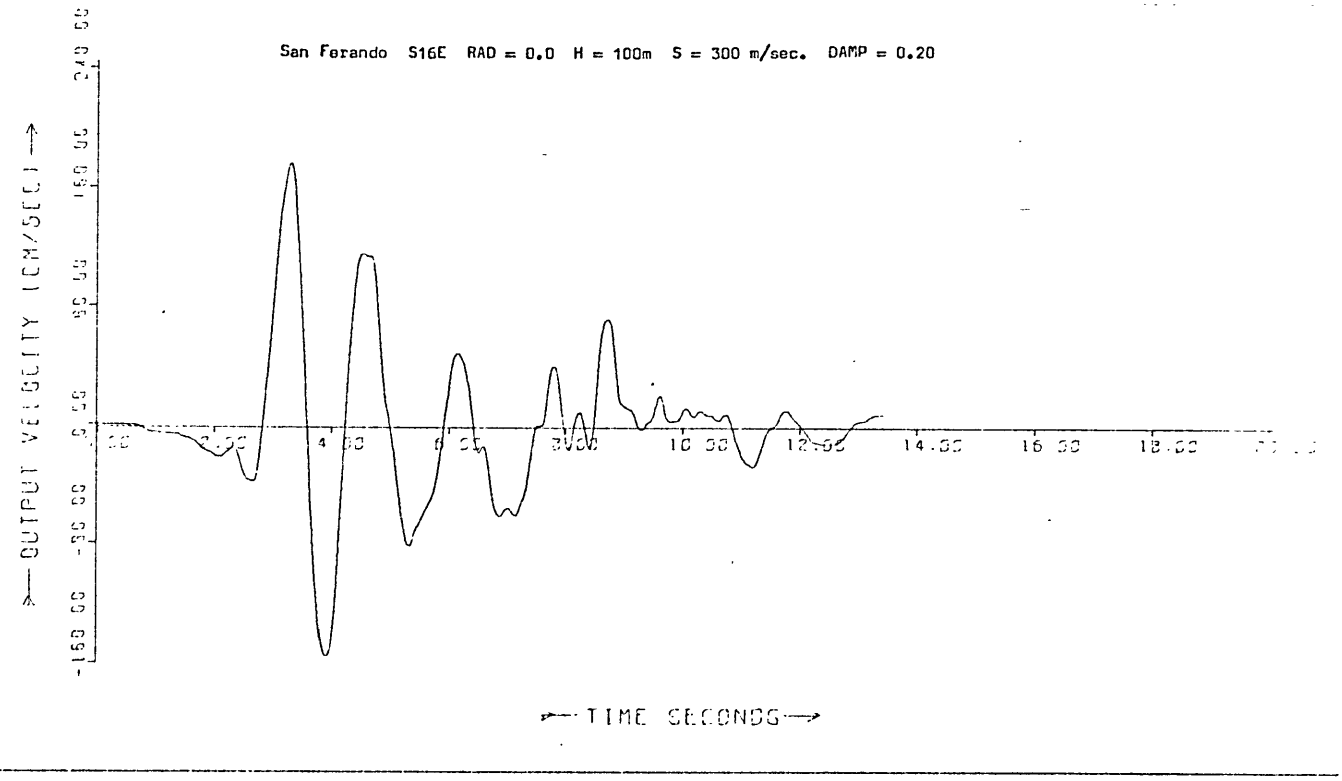


FIG.6.62b COMPUTED GROUND SURFACE VELOCITY TIME HISTORY AT SITE NO 6.37

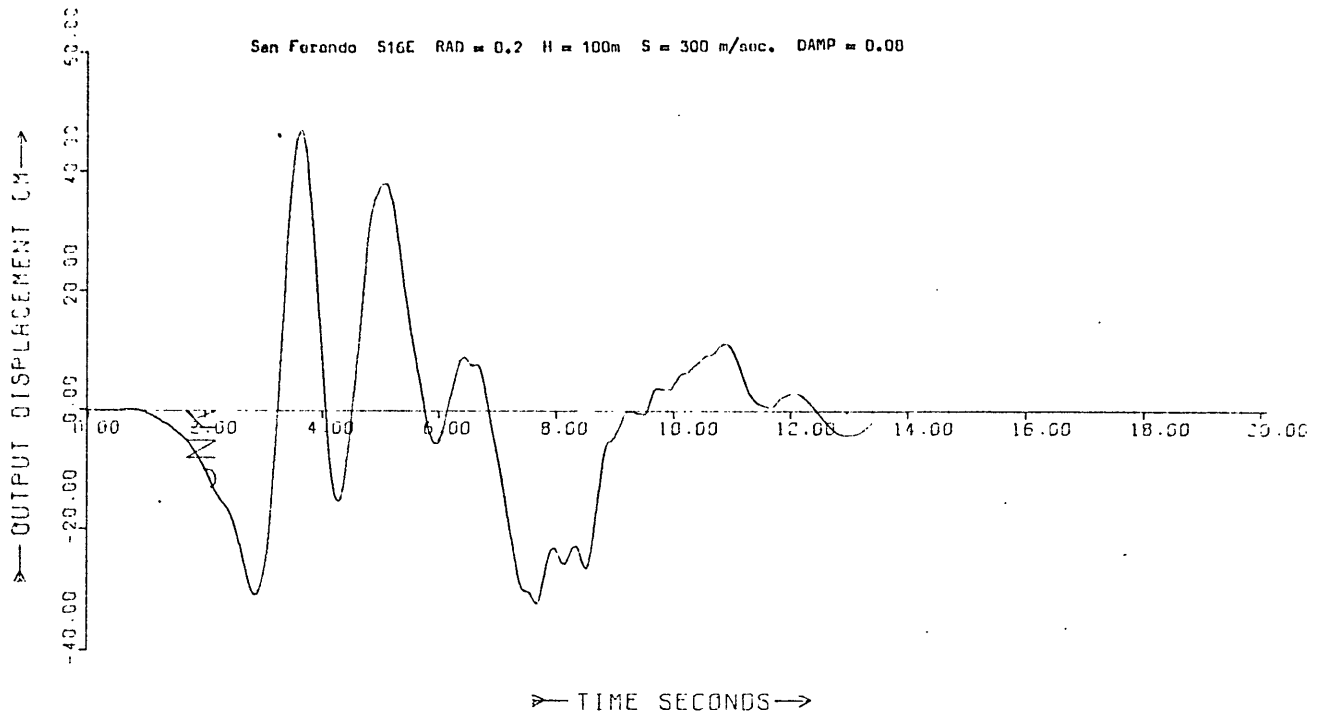


FIG.6.61c COMPUTED GROUND SURFACE DISPLACEMENT TIME HISTORY AT SITE NO 6.36

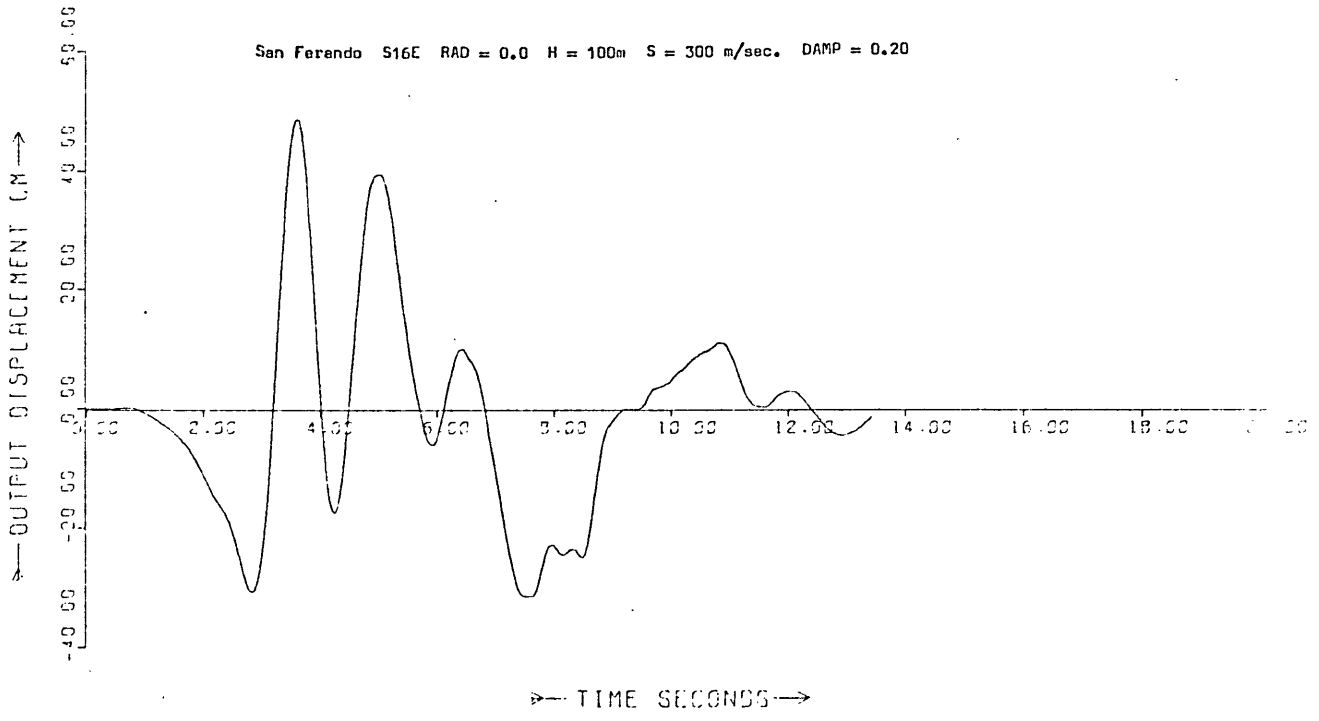


FIG. 6.62c COMPUTED GROUND SURFACE DISPLACEMENT TIME HISTORY AT SITE NO 6.37

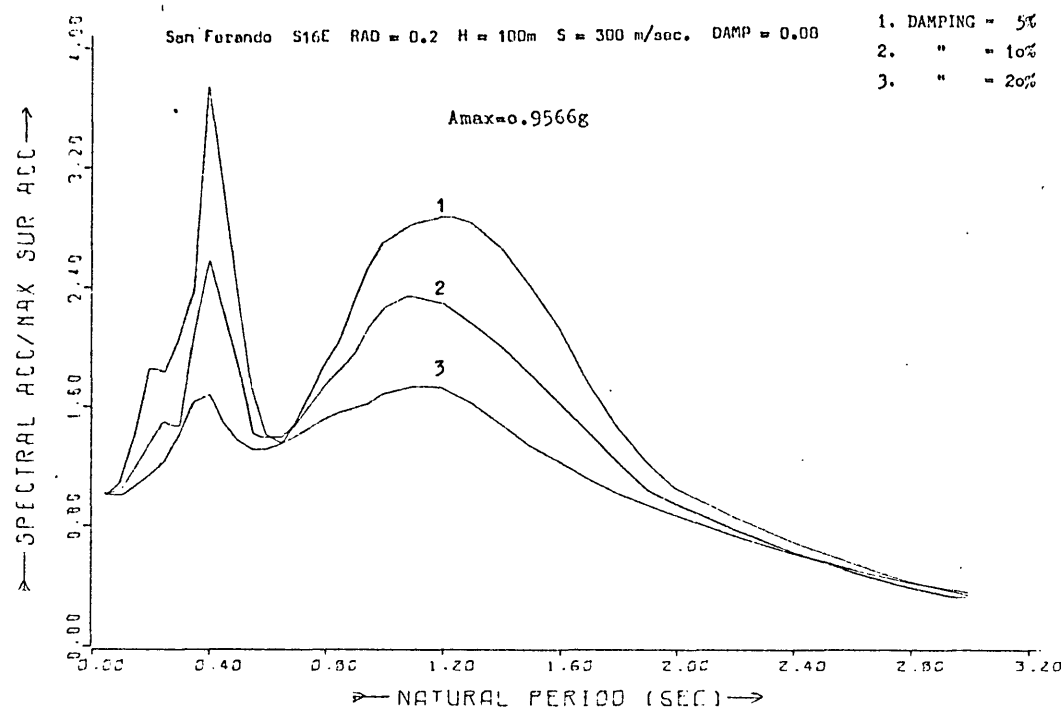


FIG. 6.61d COMPUTED GROUND SURFACE ACCELERATION RESPONSE SPECTRA AT SITE NO 6.36

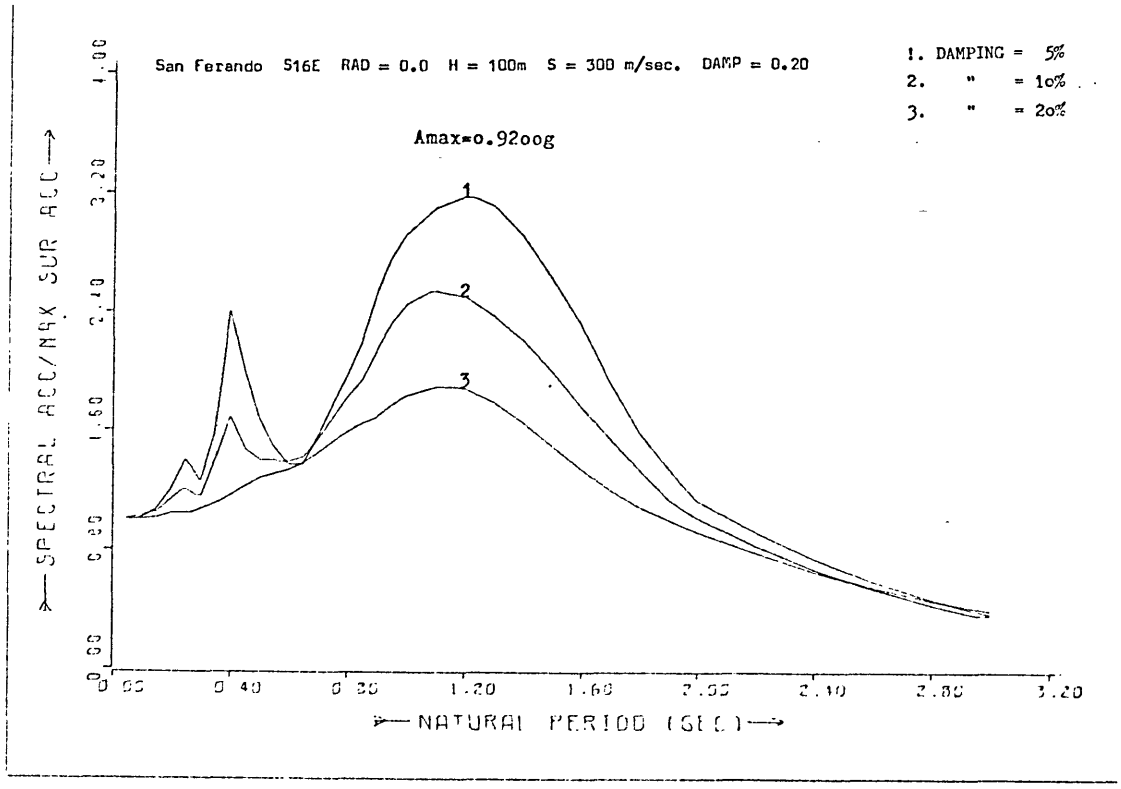


FIG. 6.62d COMPUTED GROUND SURFACE ACCELERATION RESPONSE SPECTRA AT SITE NO 6.37

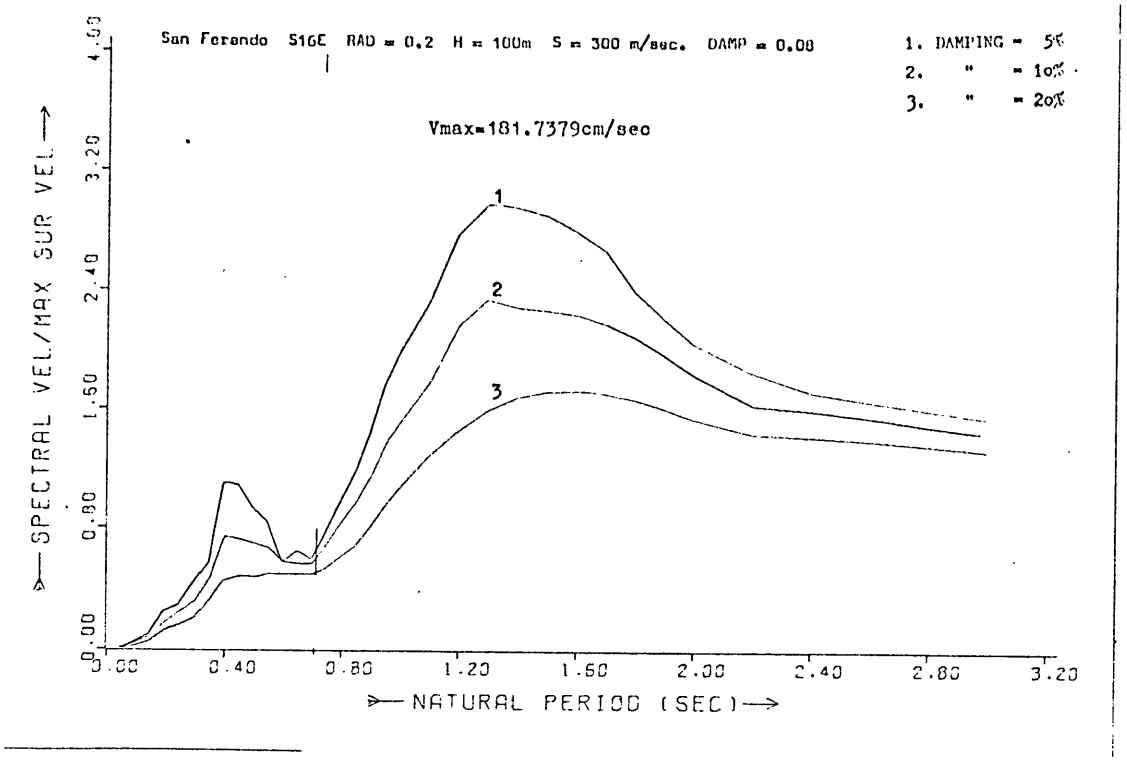


FIG. 6.61e COMPUTED GROUND SURFACE VELOCITY RESPONSE SPECTRA AT SITE NO 6.36

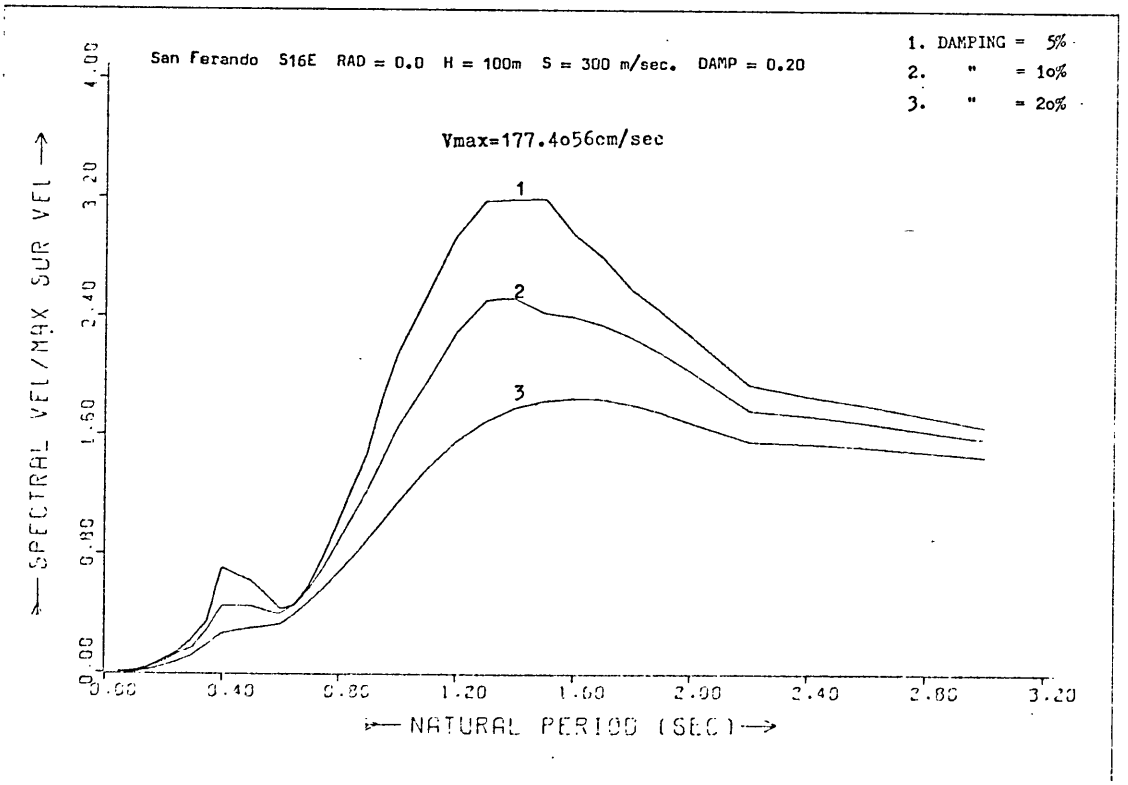


FIG. 6.62e COMPUTED GROUND SURFACE VELOCITY RESPONSE SPECTRA AT SITE NO 6.37

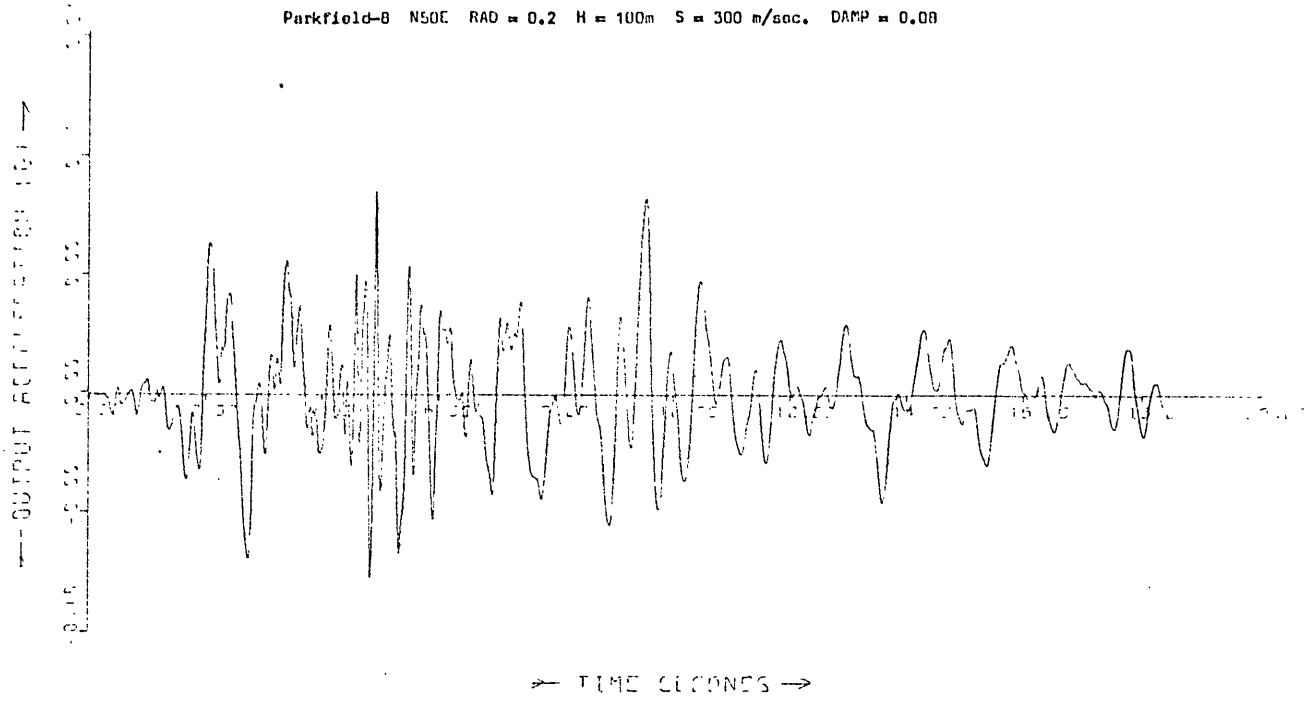


FIG. 6.63a COMPUTED GROUND SURFACE ACCELERATION TIME HISTORY AT SITE NO. 6.36

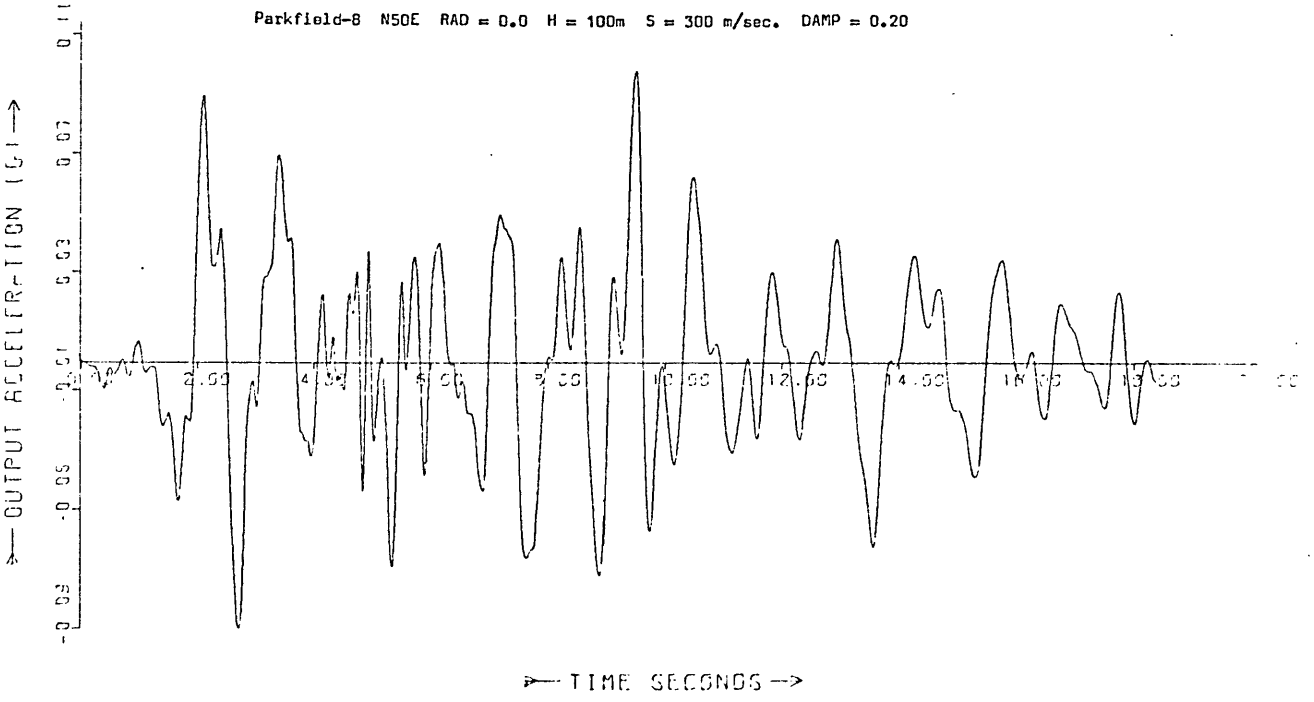


FIG. 6.64a COMPUTED GROUND SURFACE ACCELERATION TIME HISTORY AT SITE NO. 6.37

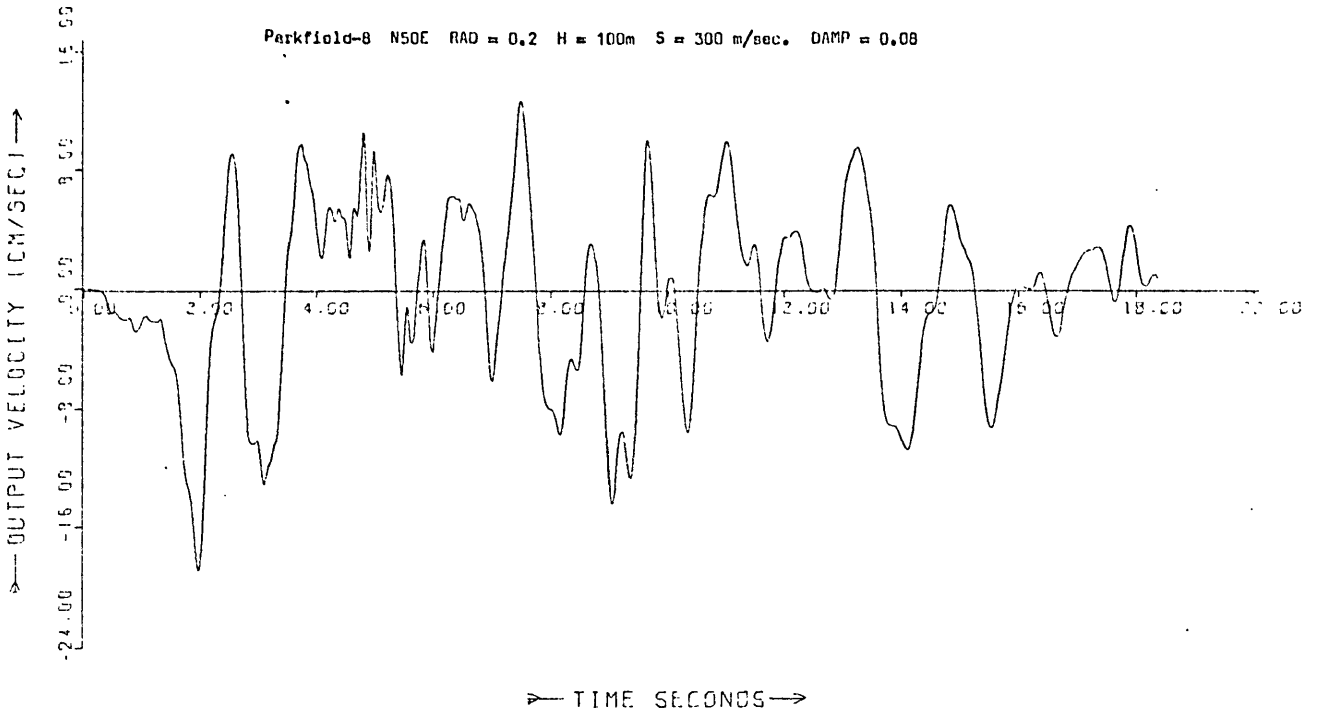


FIG.6.63b COMPUTED GROUND SURFACE VELOCITY TIME HISTORY AT SITE NO. 6.36

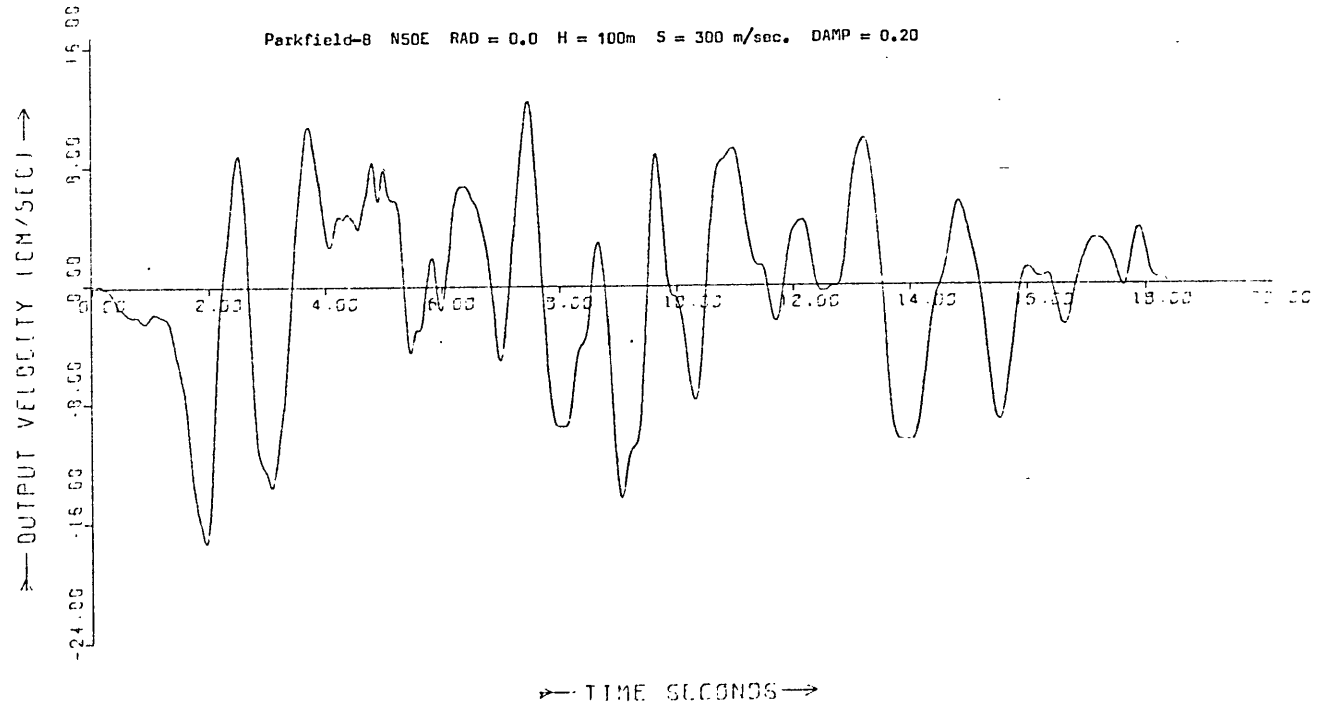


FIG.6.64b COMPUTED GROUND SURFACE VELOCITY TIME HISTORY AT SITE NO. 6.37

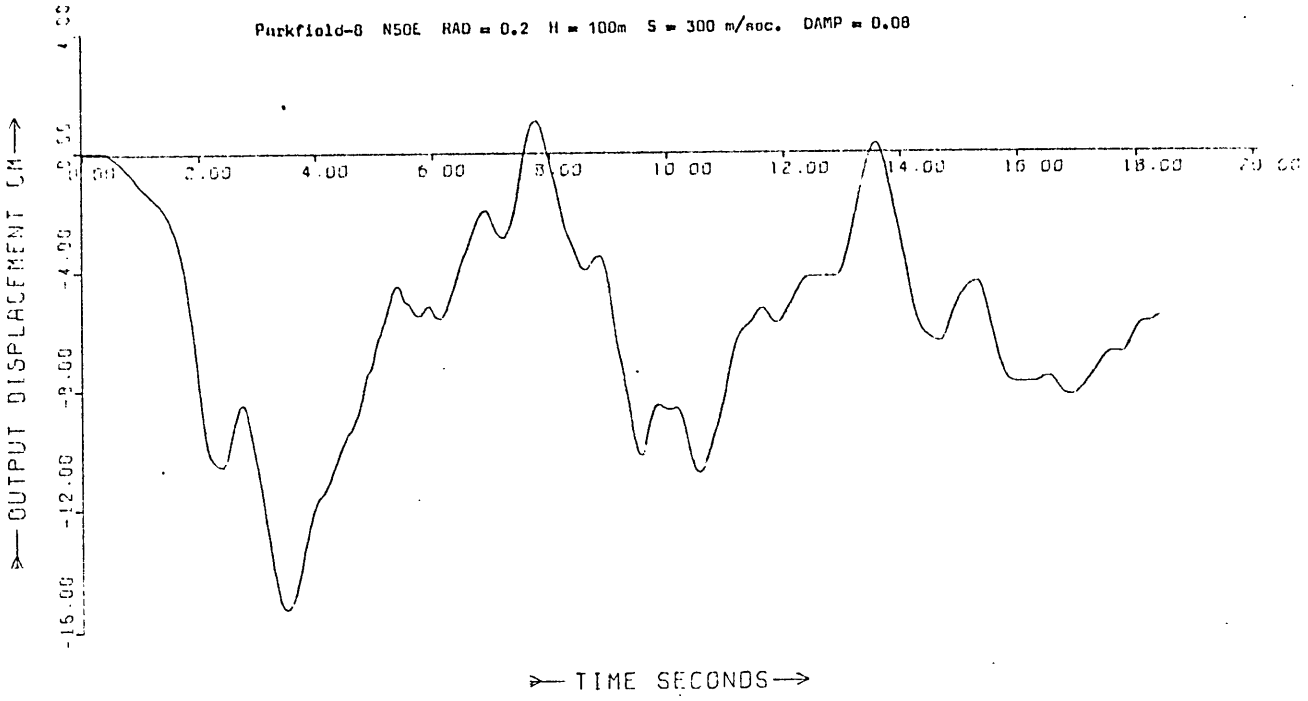


FIG.6.63COMPUTED GROUND SURFACE DISPLACEMENT TIME HISTORY AT SITE NO. 6.36

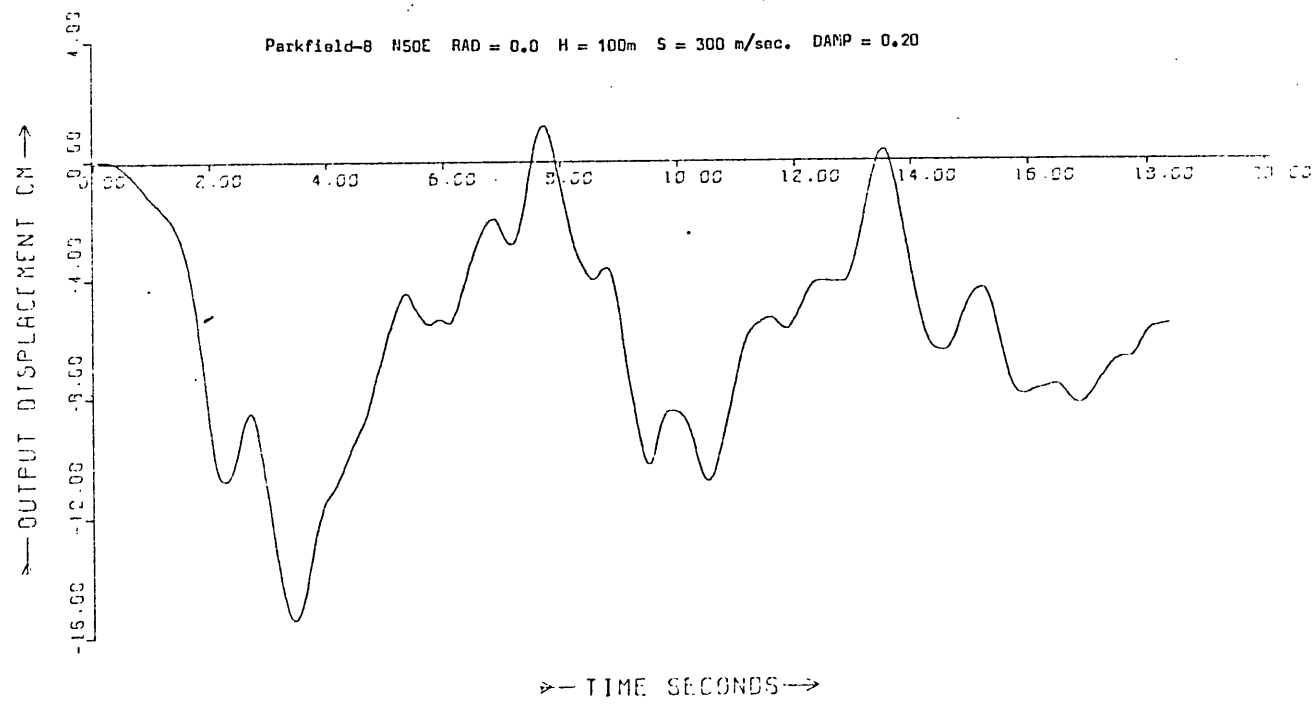


FIG. 6.64COMPUTED GROUND SURFACE DISPLACEMENT TIME HISTORY AT SITE NO. 6.37

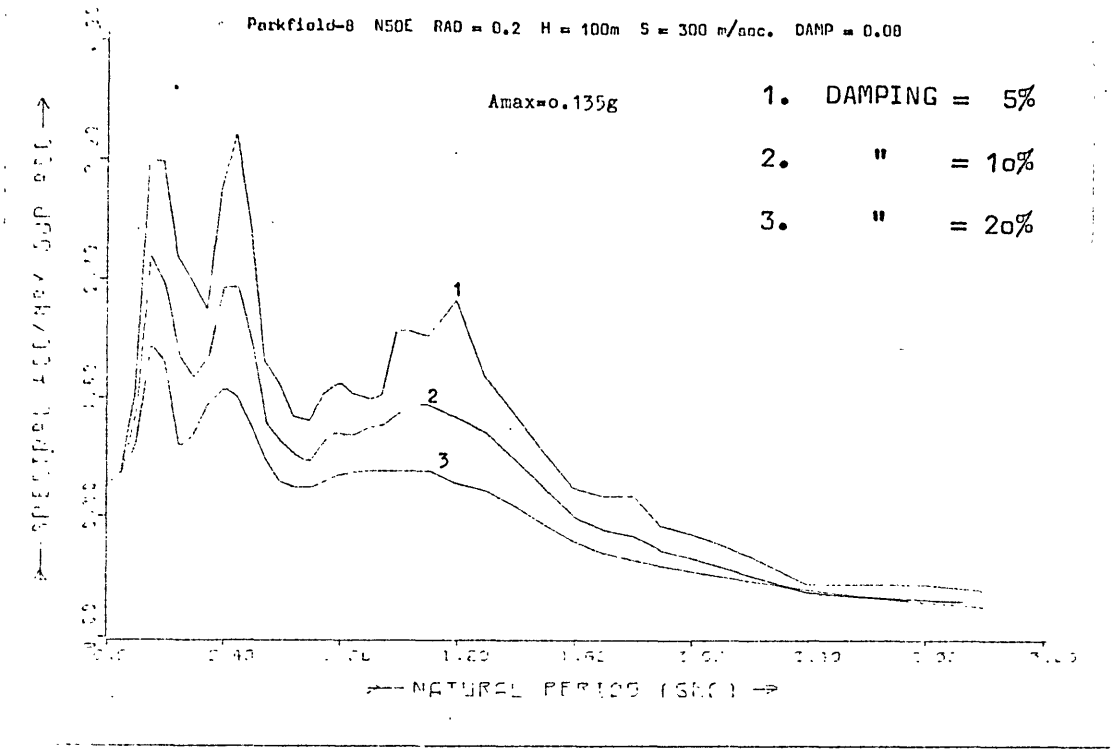


FIG.6.63d COMPUTED GROUND SURFACE ACCELERATION RESPONSE SPECTRA AT SITE NO. 6.36

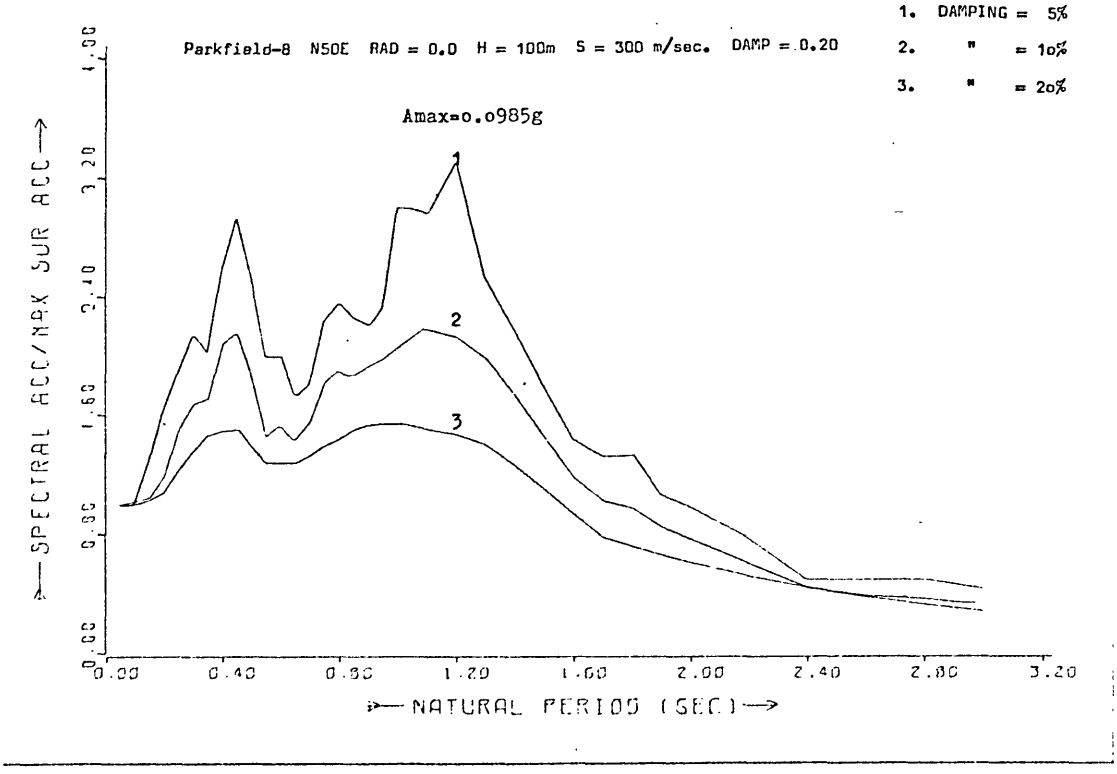


FIG. 6.64d COMPUTED GROUND SURFACE ACCELERATION RESPONSE SPECTRA AT SITE NO. 6.37

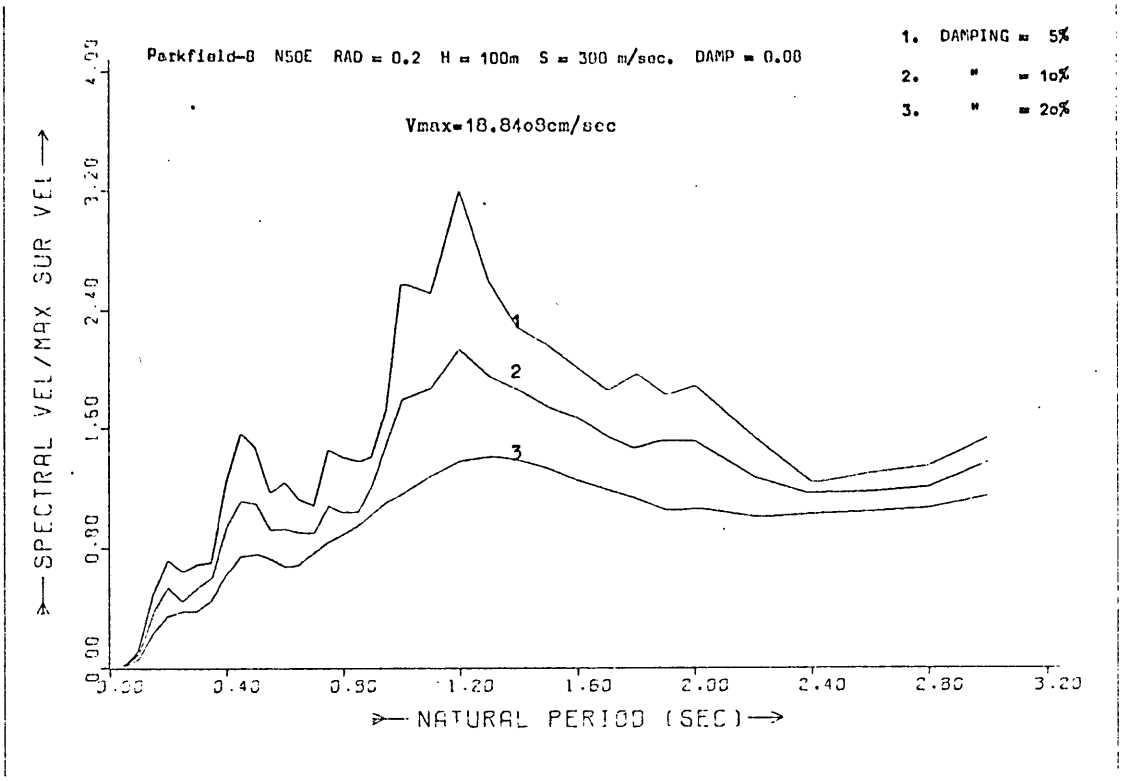


FIG.6.63eCOMPUTED GROUND SURFACE VELOCITY RESPONSE SPECTRA AT SITE NO. 6.36

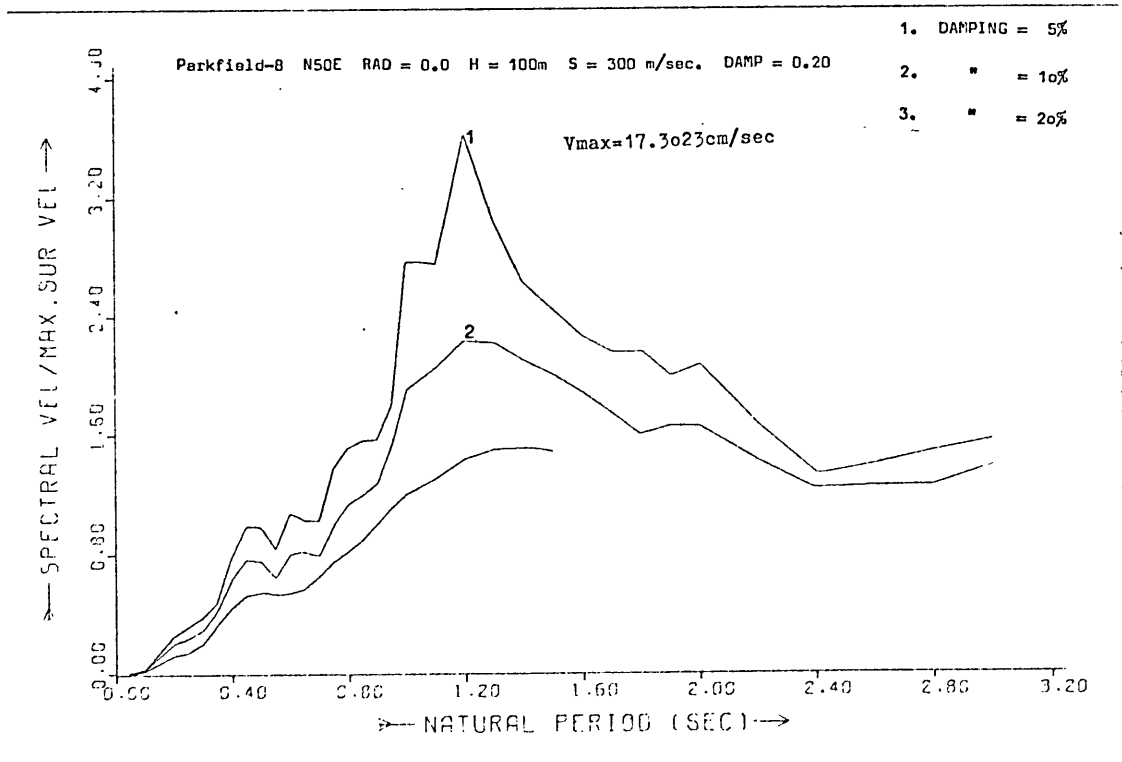


FIG.6.64eCOMPUTED GROUND SURFACE VELOCITY RESPONSE SPECTRA AT SITE NO.6.37

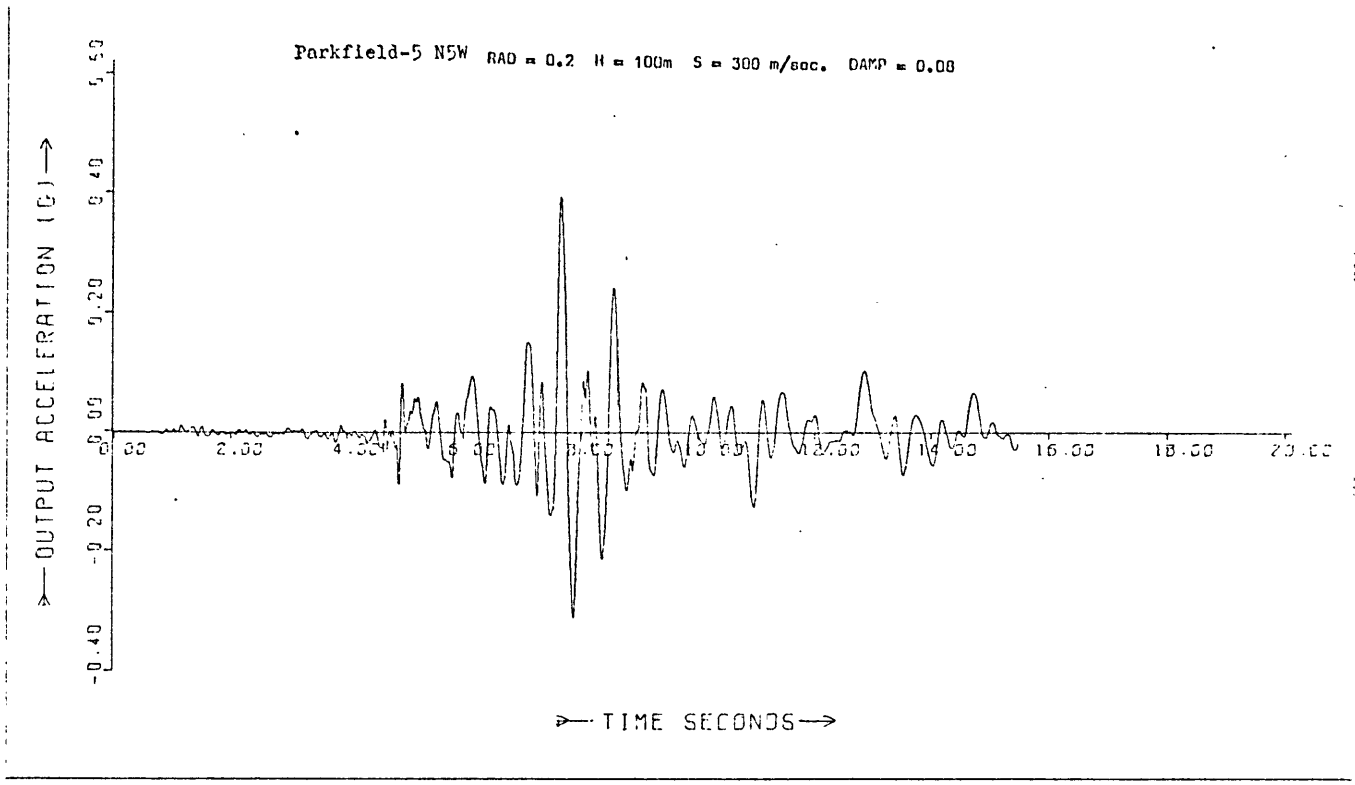


FIG. 6.65a COMPUTED GROUND SURFACE ACCELERATION TIME HISTORY AT SITE NO. 6.36

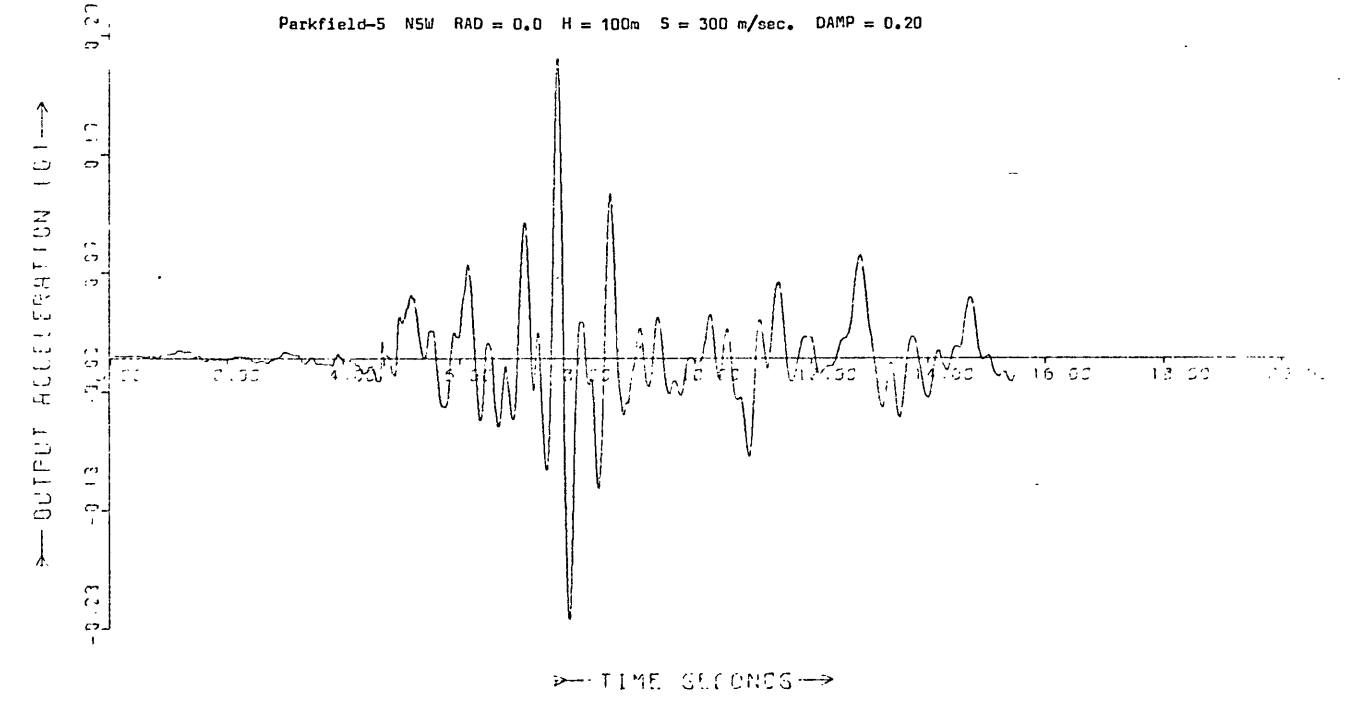


FIG. 6.66a COMPUTED GROUND SURFACE ACCELERATION TIME HISTORY AT SITE NO. 6.37

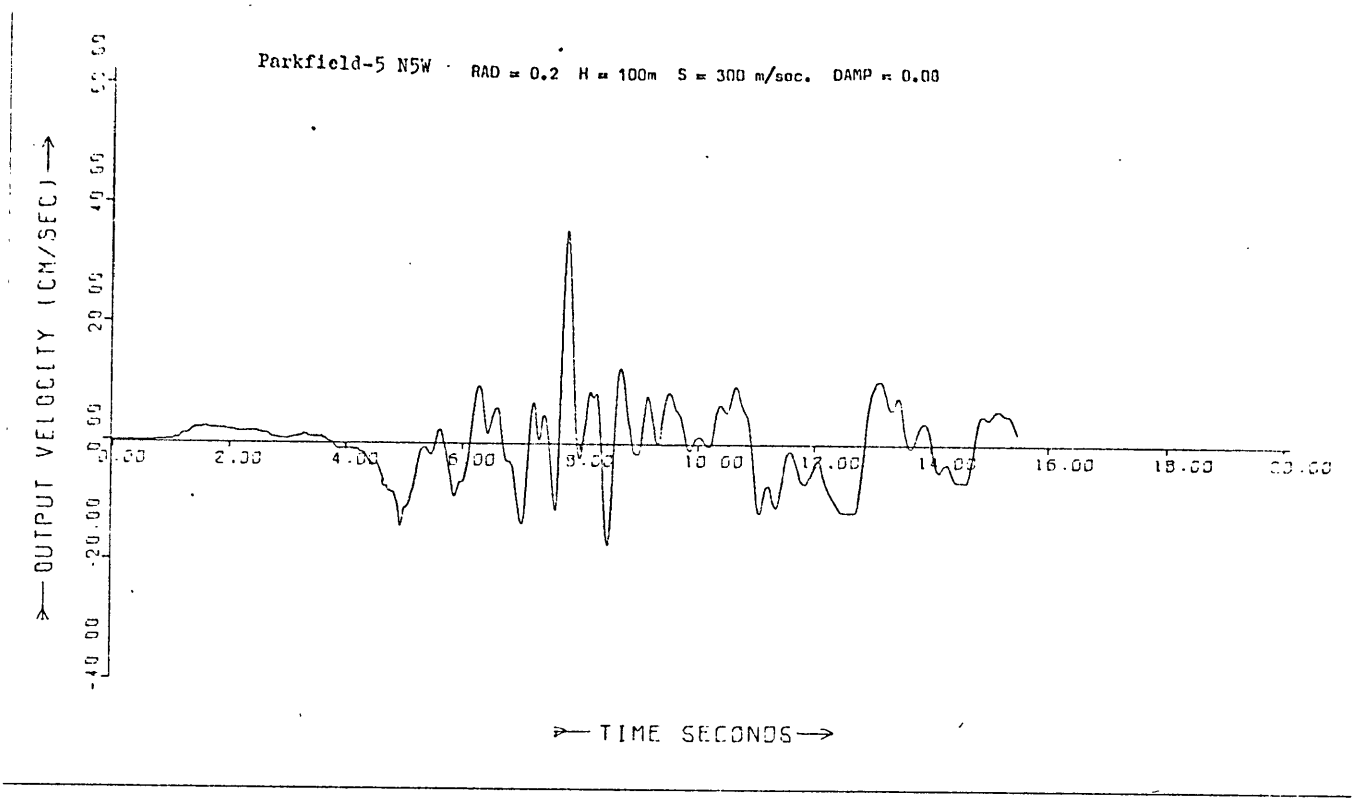


FIG.6.65b COMPUTED GROUND SURFACE VELOCITY TIME HISTORY AT SITE NO. 6.36

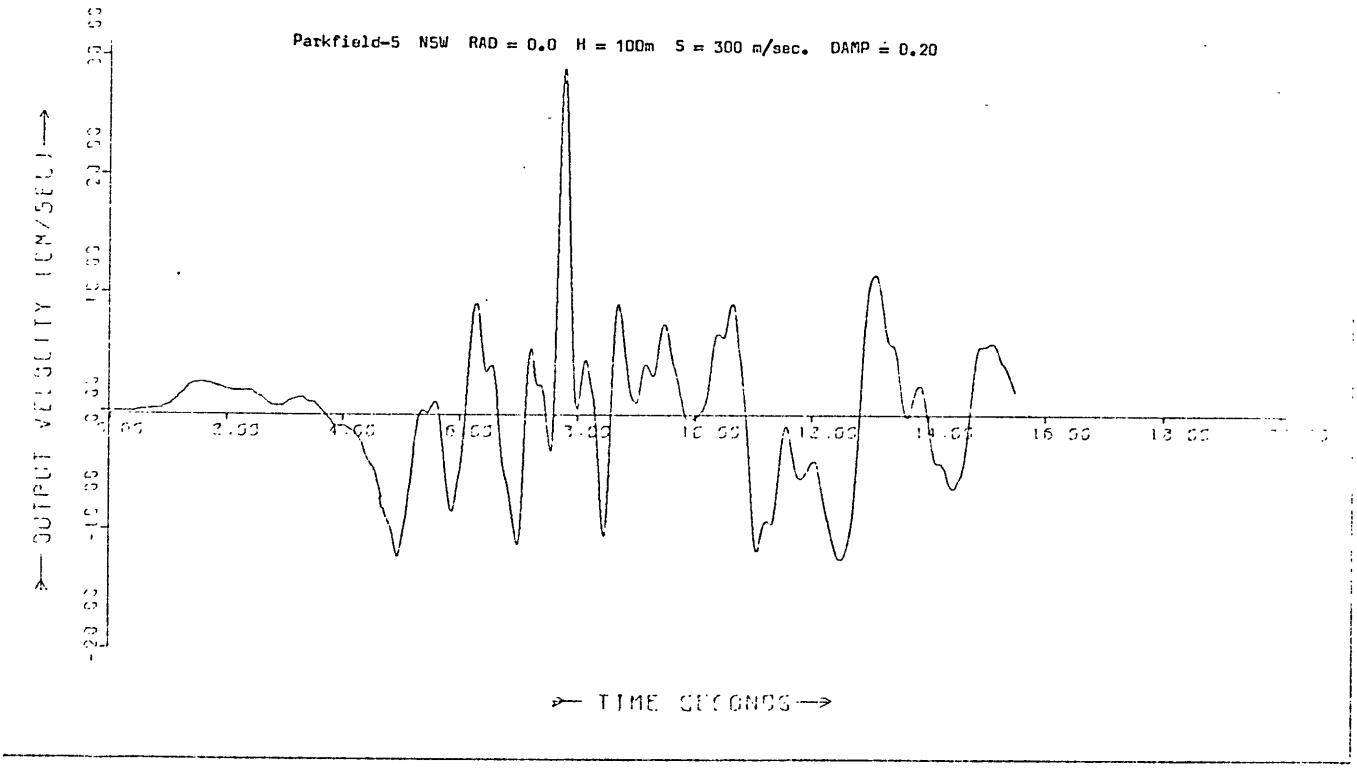


FIG.6.66b COMPUTED GROUND SURFACE VELOCITY TIME HISTORY AT SITE NO. 6.37

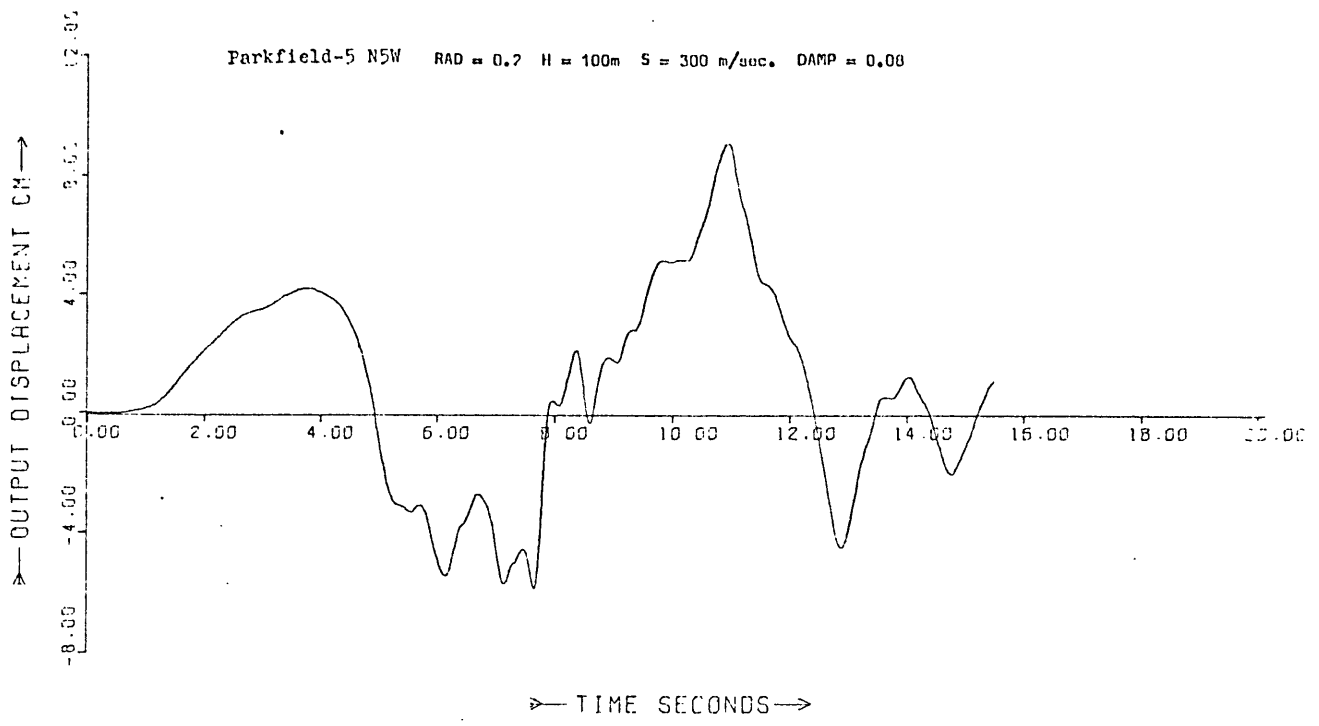


FIG.6.65c COMPUTED GROUND SURFACE DISPLACEMENT TIME HISTORY AT SITE NO. 6.36

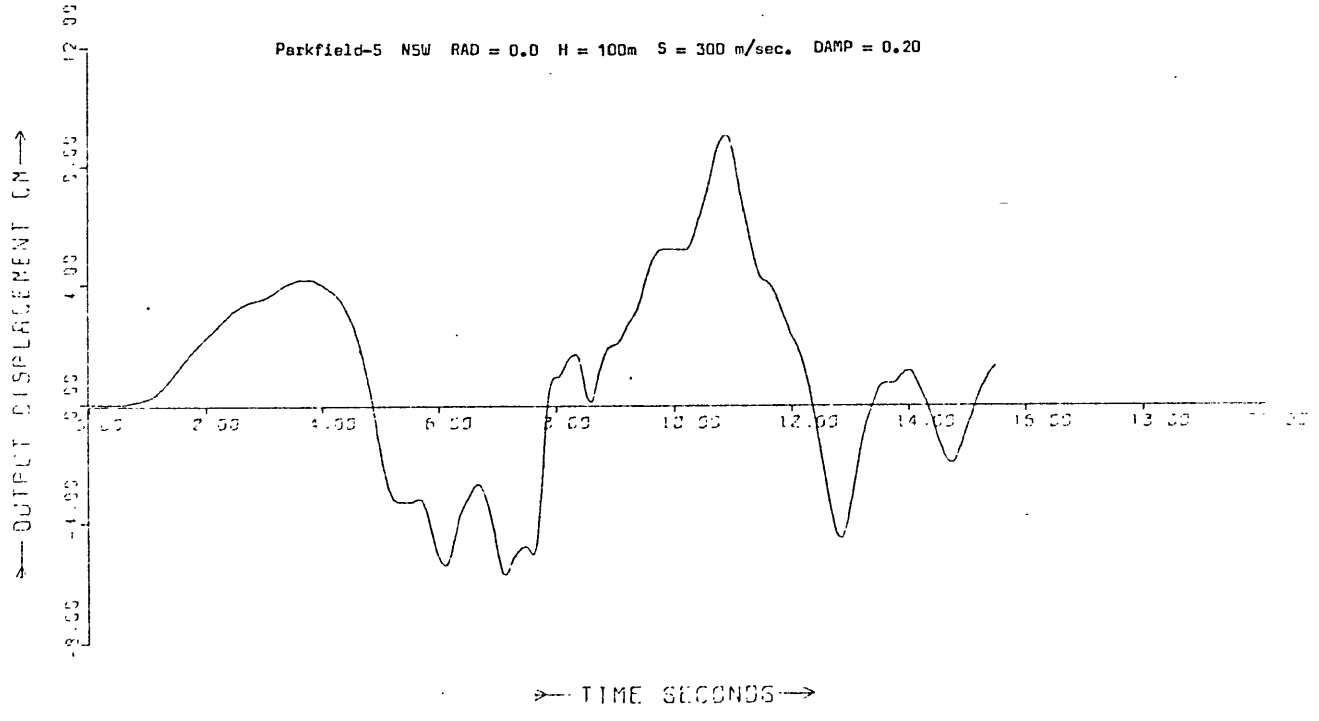


FIG.6.66c COMPUTED GROUND SURFACE DISPLACEMENT TIME HISTORY AT SITE NO. 6.37

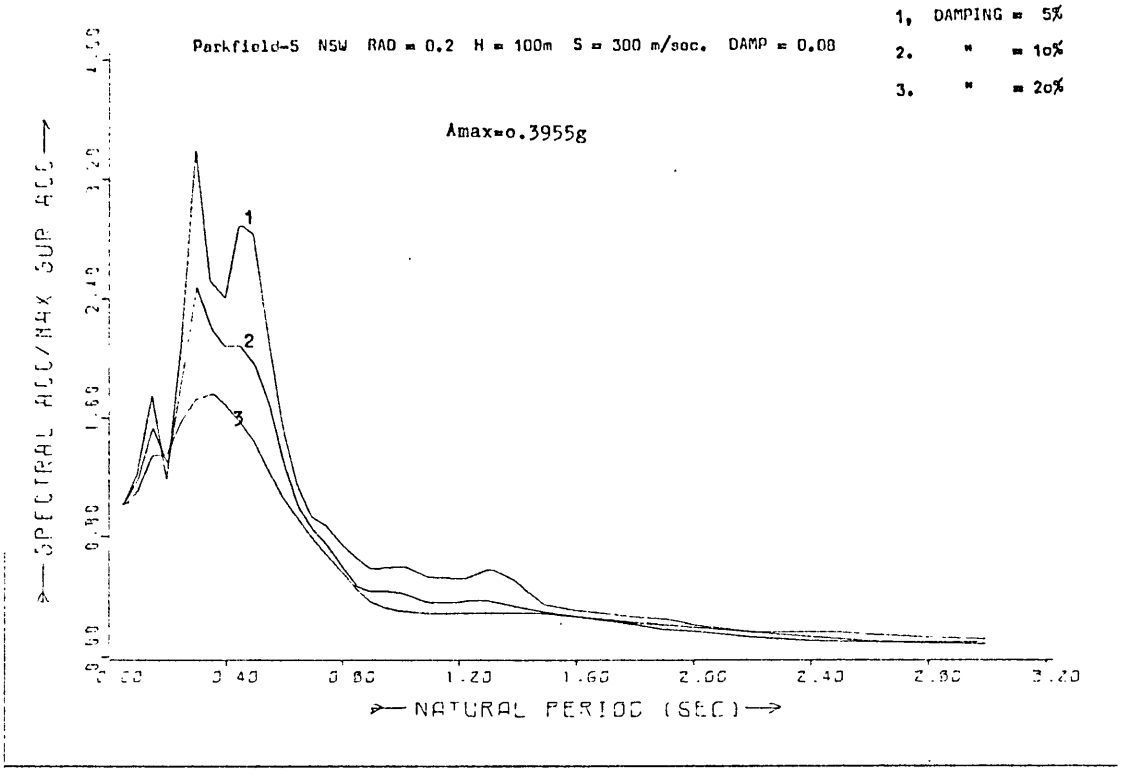


FIG. 6.65d COMPUTED GROUND SURFACE ACCELERATION RESPONSE SPECTRA AT SITE NO. 6.36

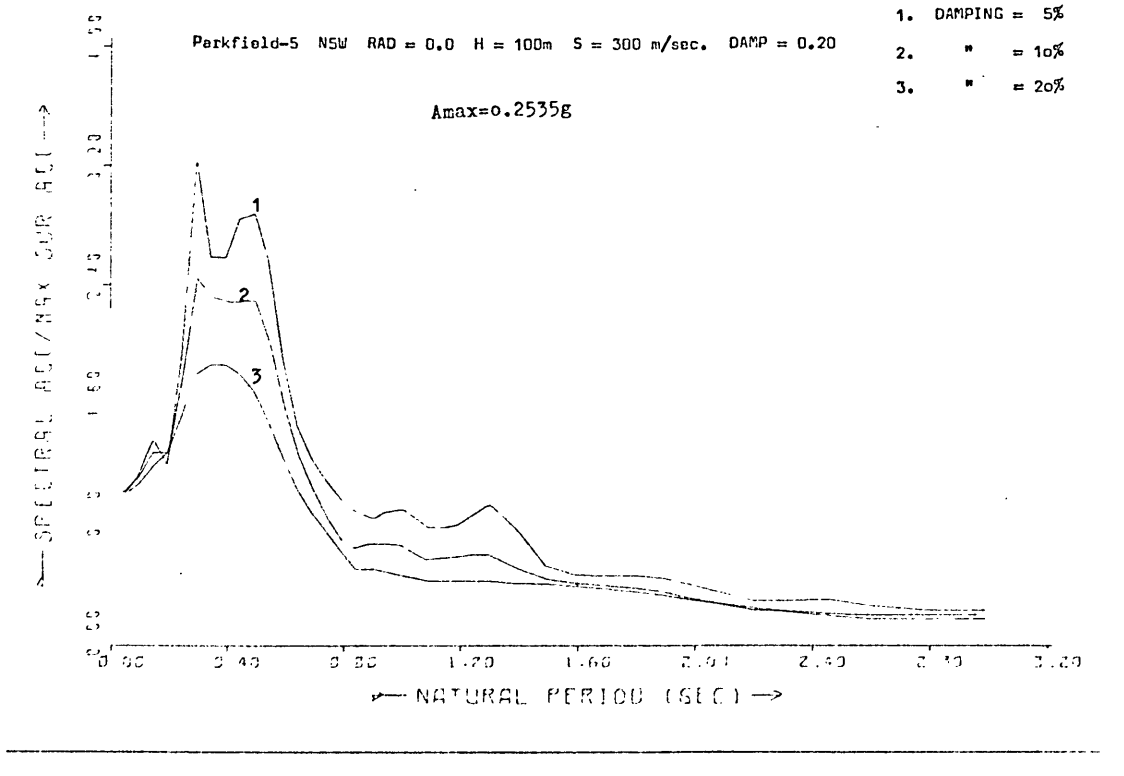


FIG.6.66d COMPUTED GROUND SURFACE ACCELERATION RESPONSE SPECTRA AT SITE NO. 6.37

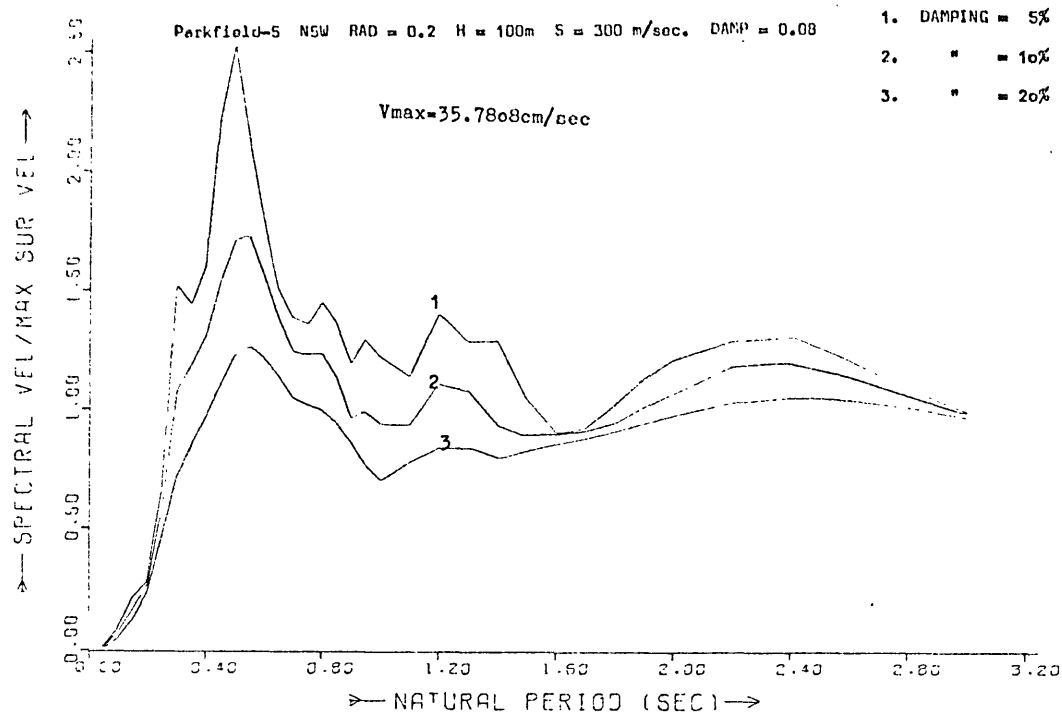


FIG.6.65 COMPUTED GROUND SURFACE VELOCITY RESPONSE SPECTRA AT SITE NO. 6.36

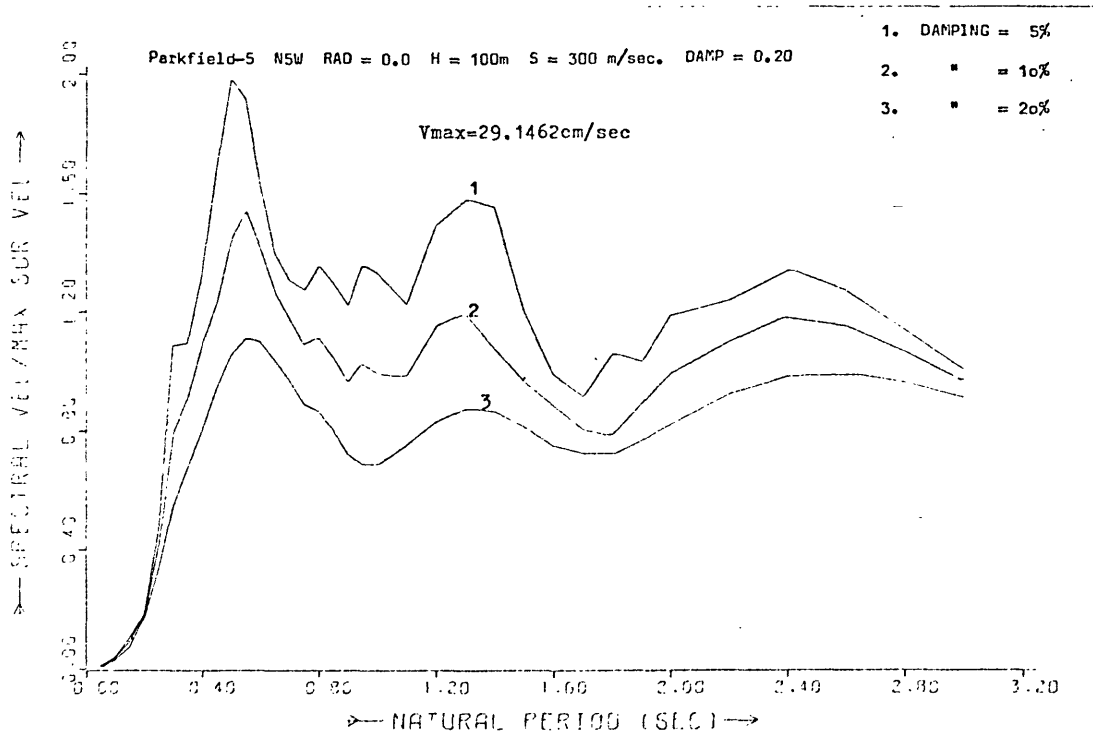


FIG.6.66 COMPUTED GROUND SURFACE VELOCITY RESPONSE SPECTRA AT SITE NO. 6.37

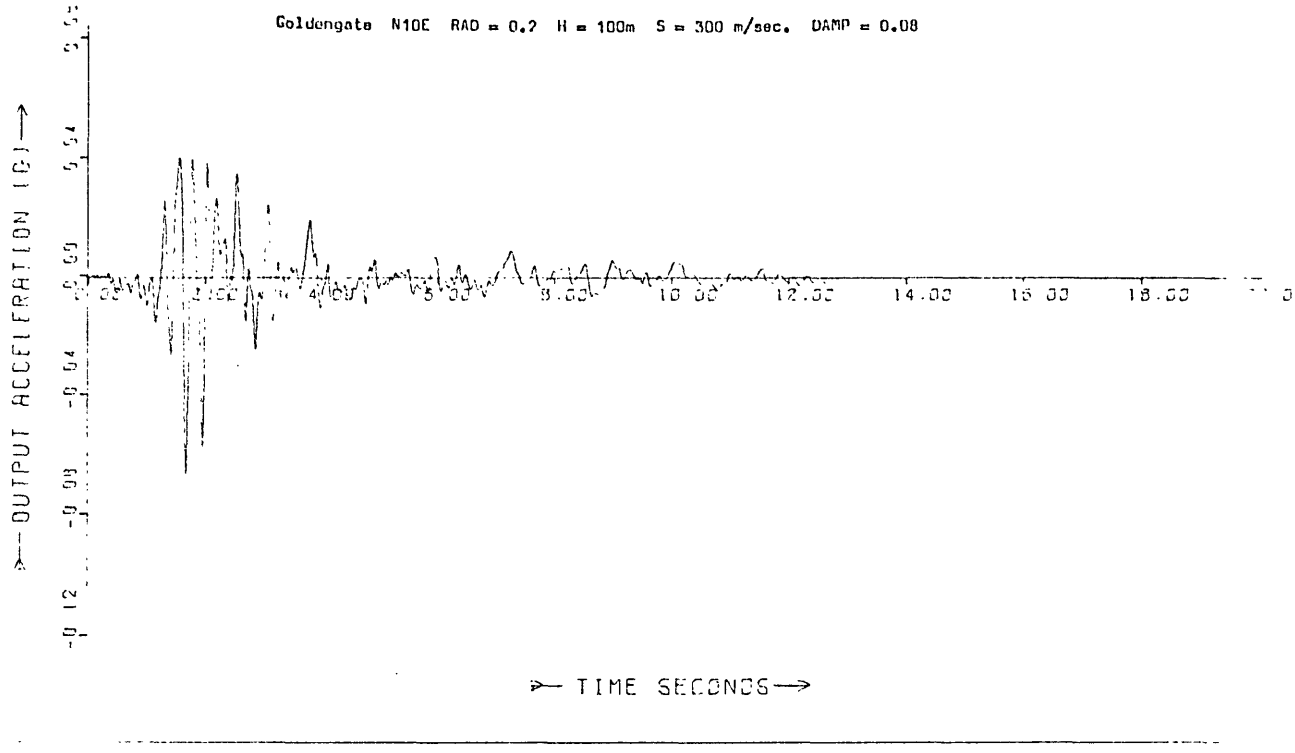


FIG.6.67a COMPUTED GROUND SURFACE ACCELERATION TIME HISTORY AT SITE NO 6.36

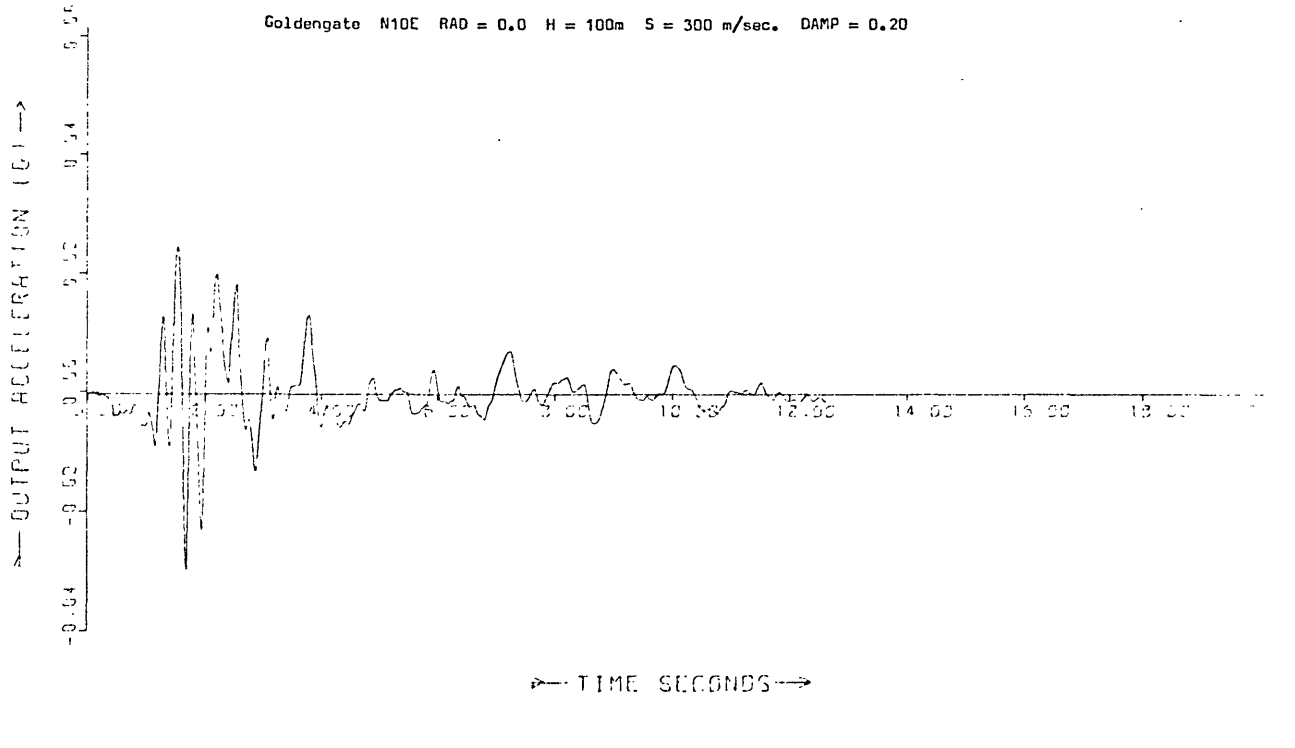


FIG.6.68a COMPUTED GROUND SURFACE ACCELERATION TIME HISTORY AT SITE NO 6.37

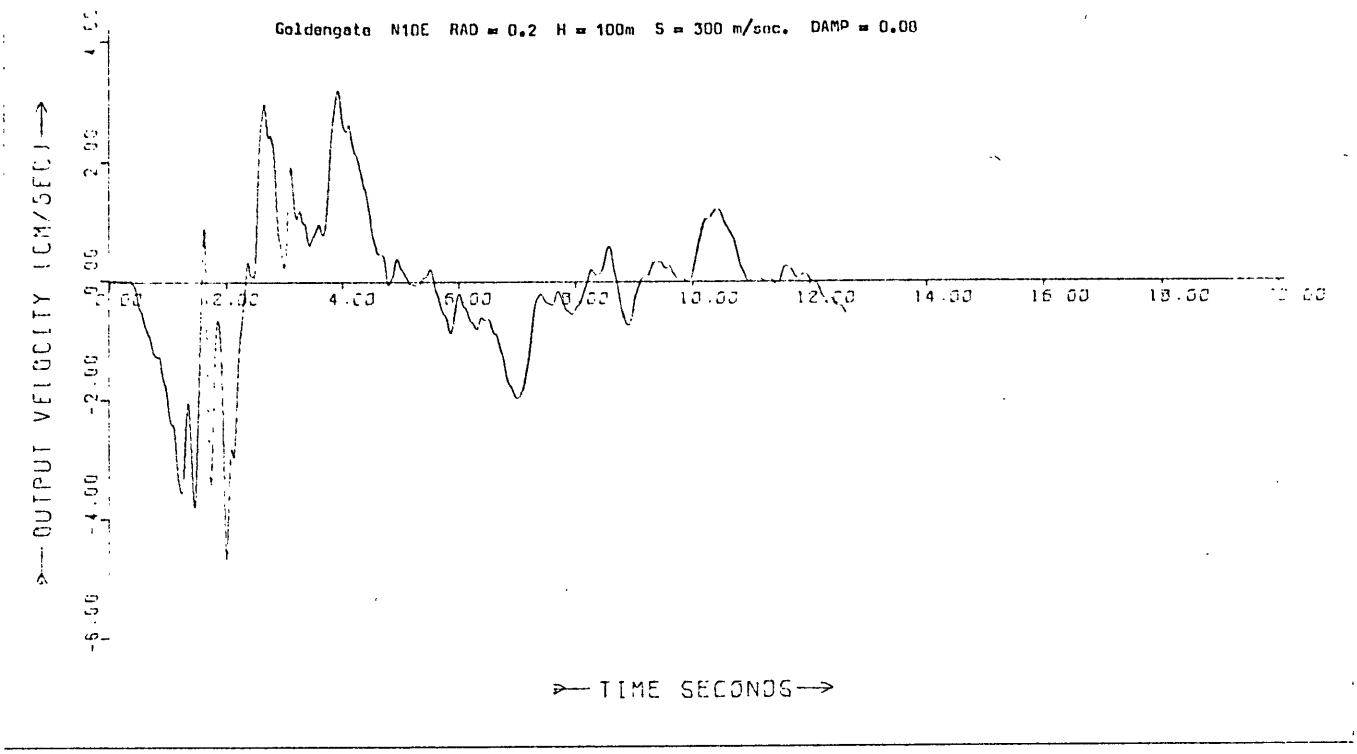


FIG 6.67b COMPUTED GROUND SURFACE VELOCITY TIME HISTORY AT SITE NO 6.36

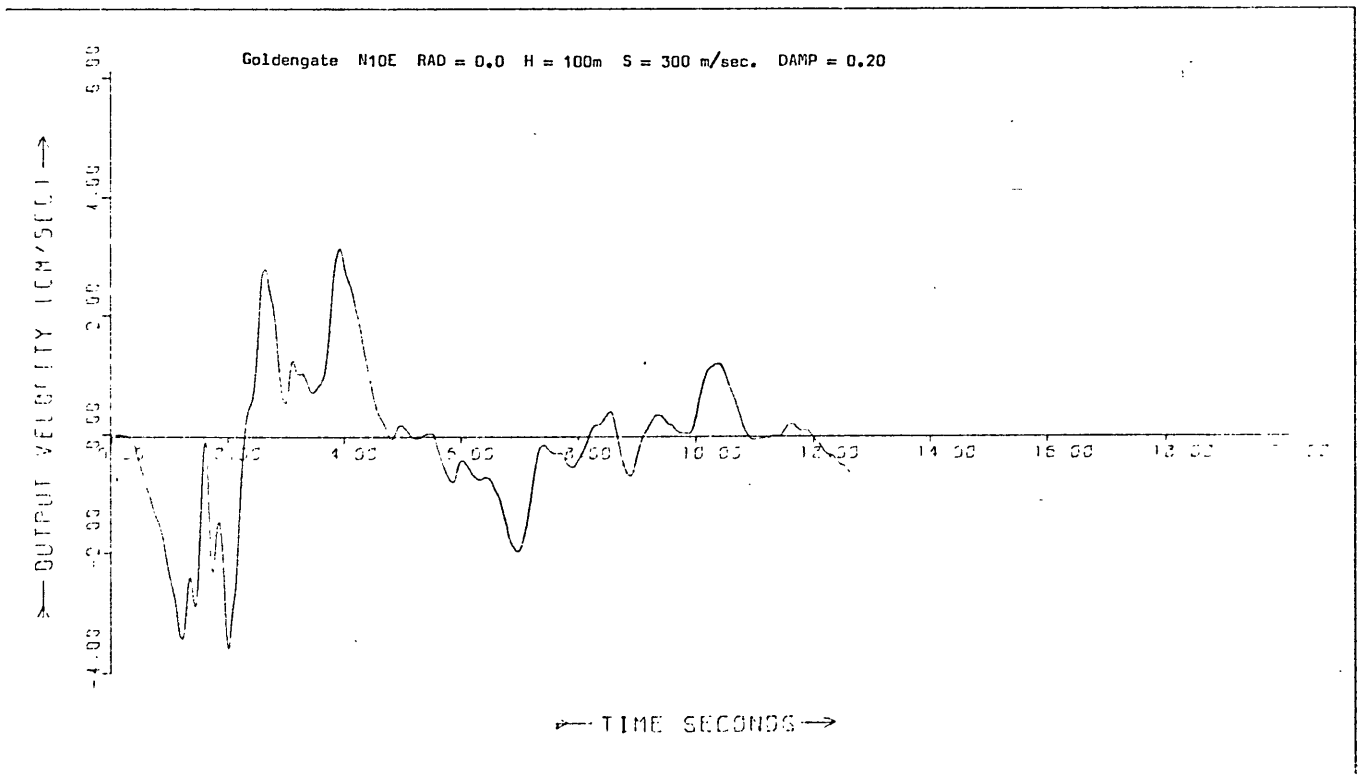


FIG. 6.68b COMPUTED GROUND SURFACE VELOCITY TIME HISTORY AT SITE NO 6.37

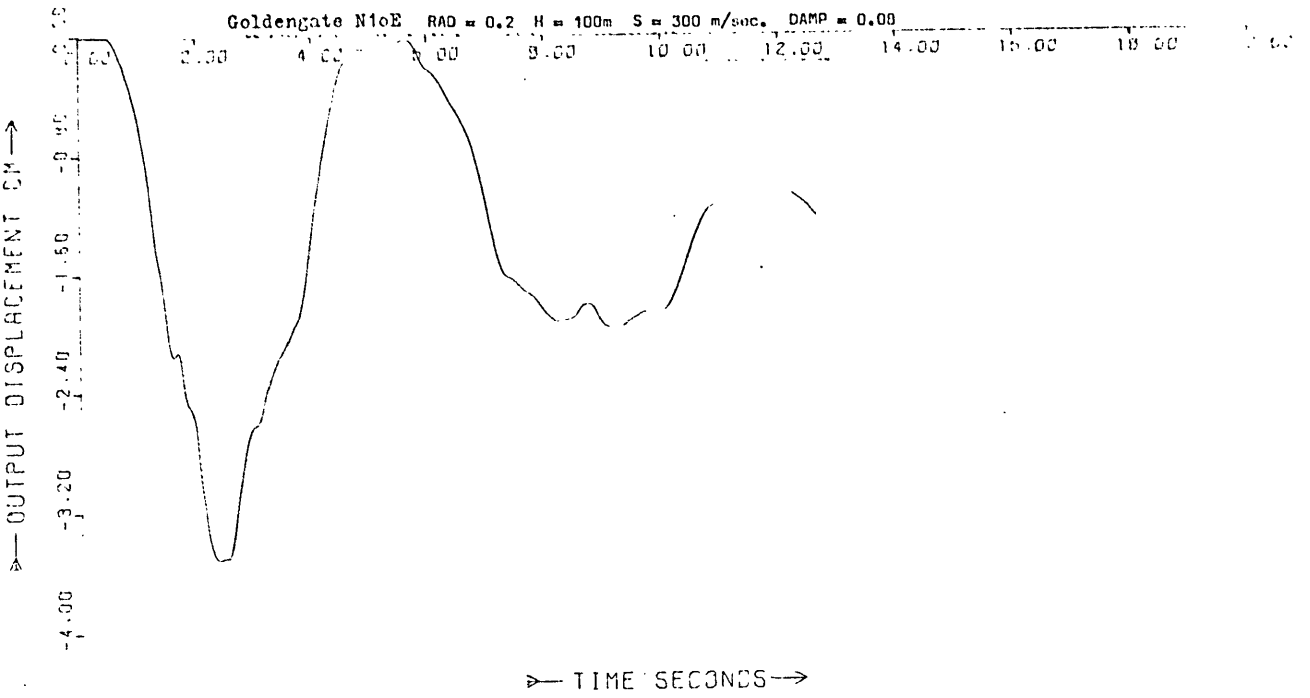


FIG.6.67c COMPUTED GROUND SURFACE DISPLACEMENT TIME HISTORY AT SITE NO 6.36

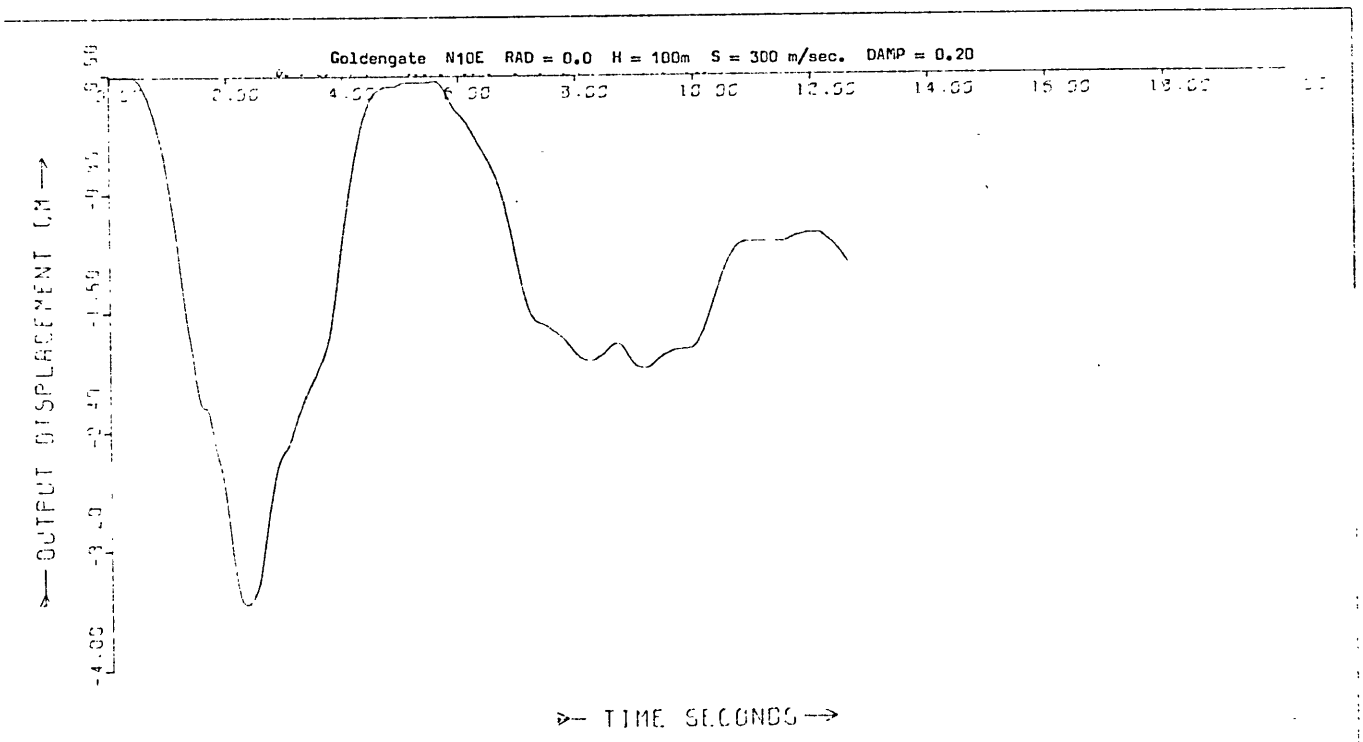


FIG.6.68c COMPUTED GROUND SURFACE DISPLACEMENT TIME HISTORY AT SITE NO 6.37

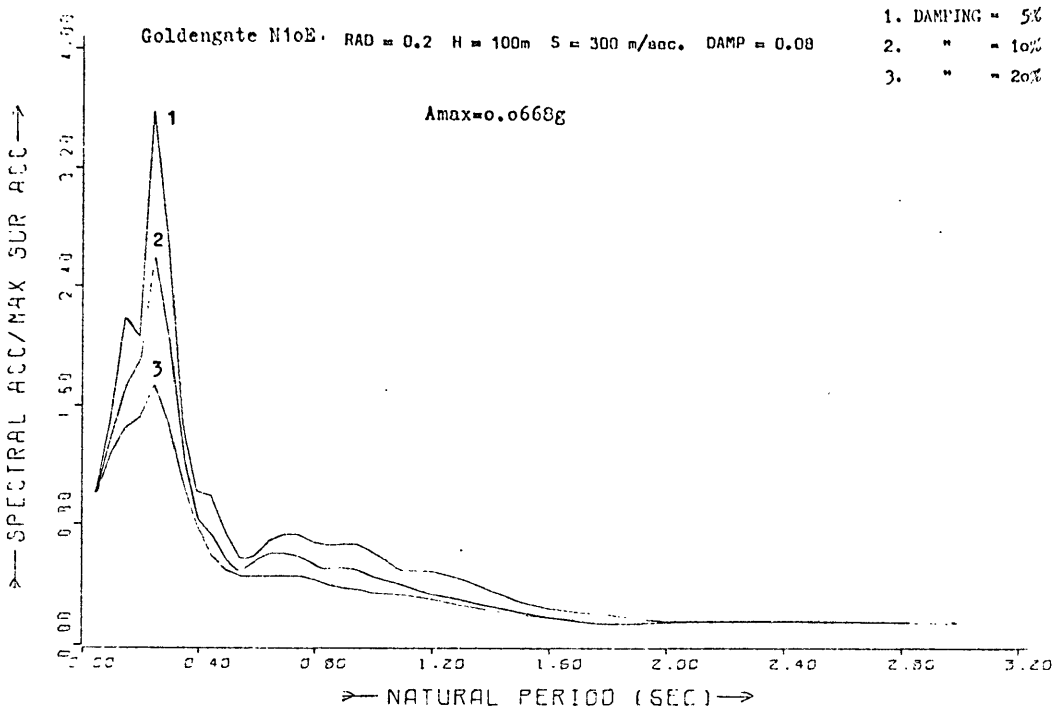


FIG.6.67d COMPUTED GROUND SURFACE ACCELERATION RESPONSE SPECTRA AT SITE NO 6.36

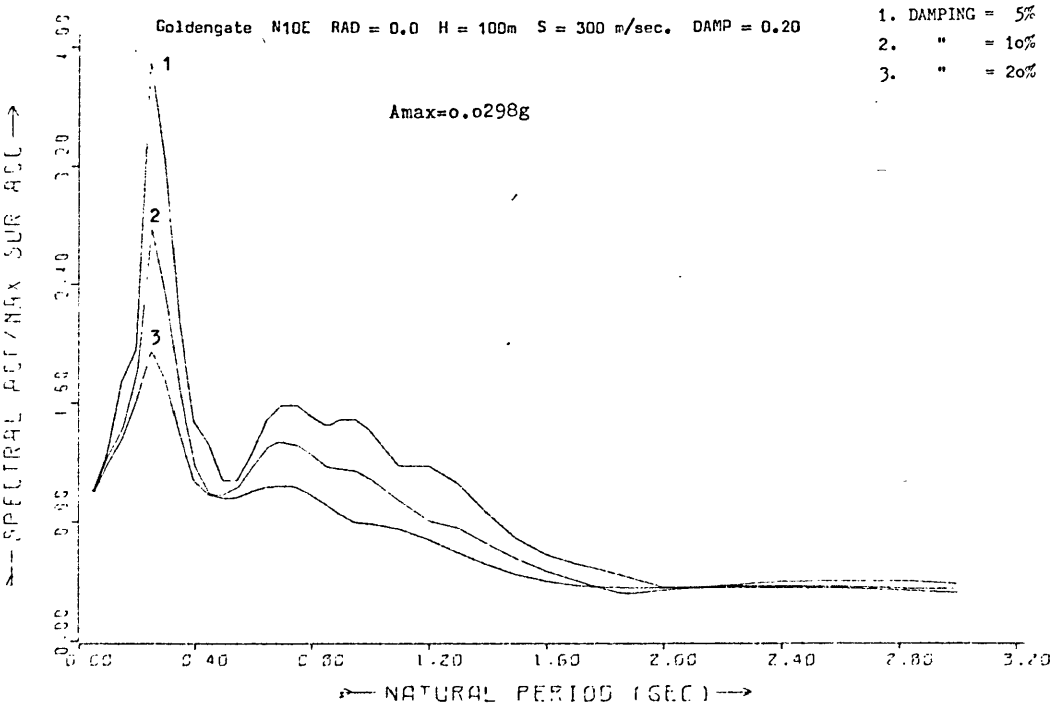


FIG.6.68d COMPUTED GROUND SURFACE ACCELERATION RESPONSE SPECTRA AT SITE NO 6.37

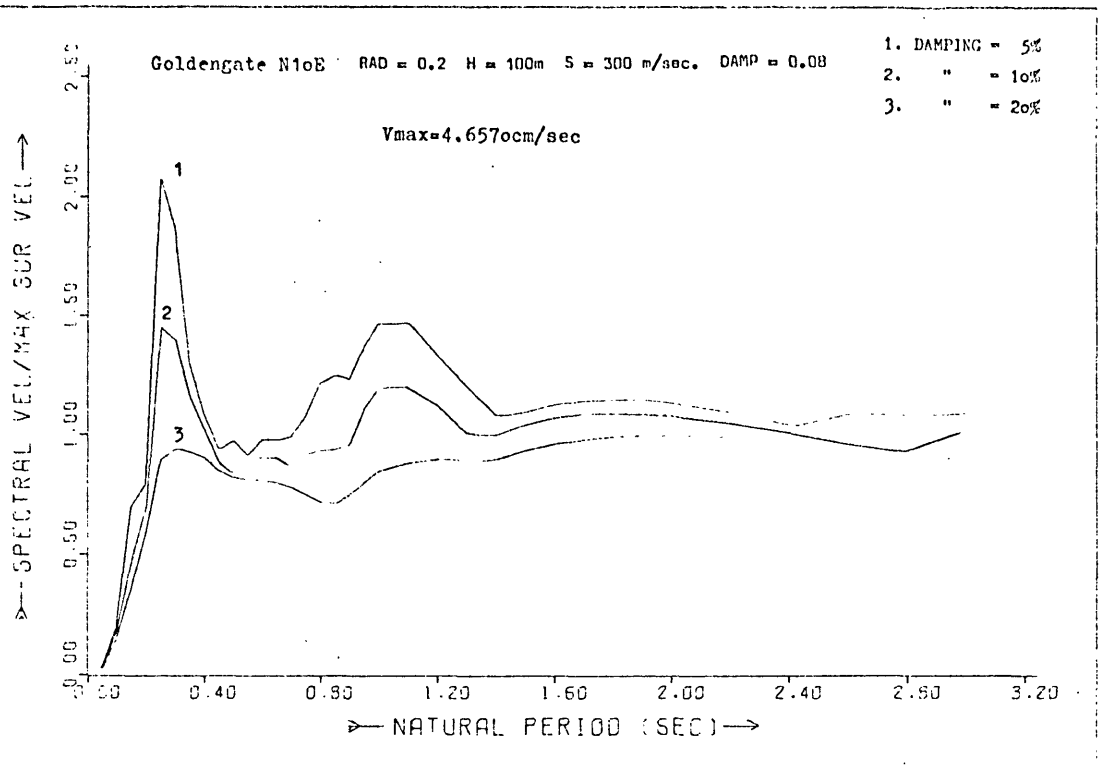


FIG.6.67e COMPUTED GROUND SURFACE VELOCITY RESPONSE SPECTRA AT SITE NO 6.36

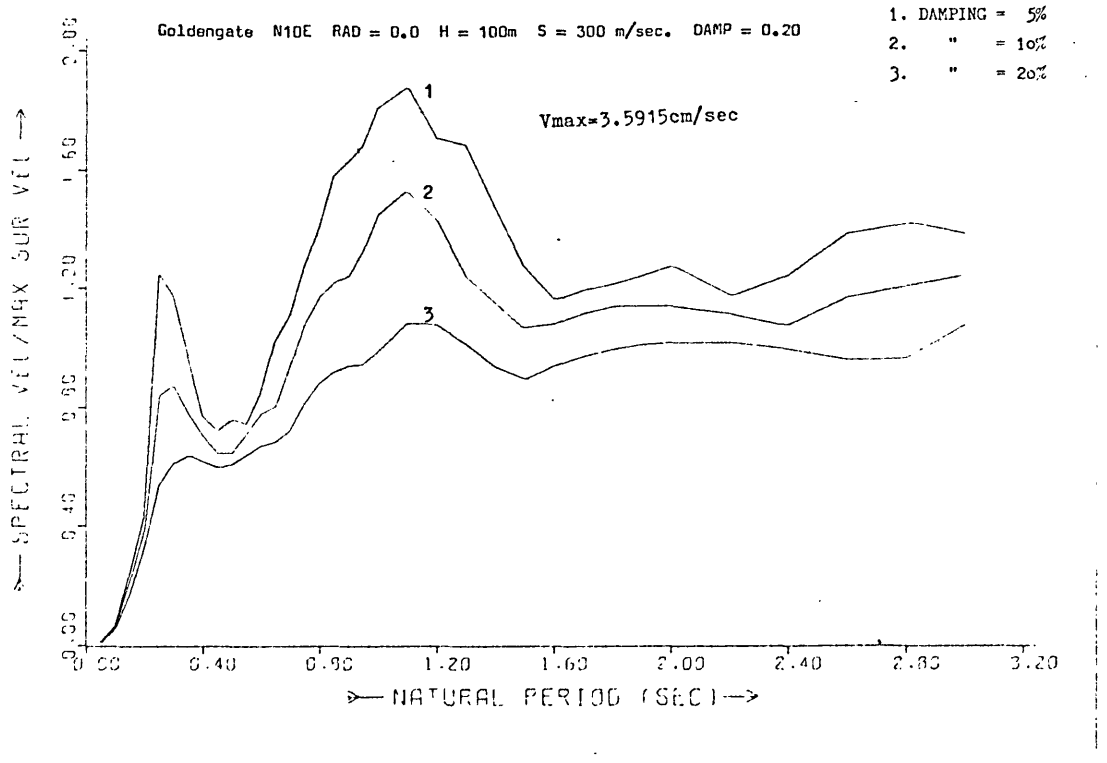


FIG. 6.68e COMPUTED GROUND SURFACE VELOCITY RESPONSE SPECTRA AT SITE NO 6.37

6.9.1. CONCLUDING REMARKS

a) Added modal damping to account for transmitted energy to the bedrock produces unacceptable results under most conditions likely to be met in practice.

b) Once more the potentiality of the proposed technique for predicting the seismic response of soil deposits has clearly become apparent.

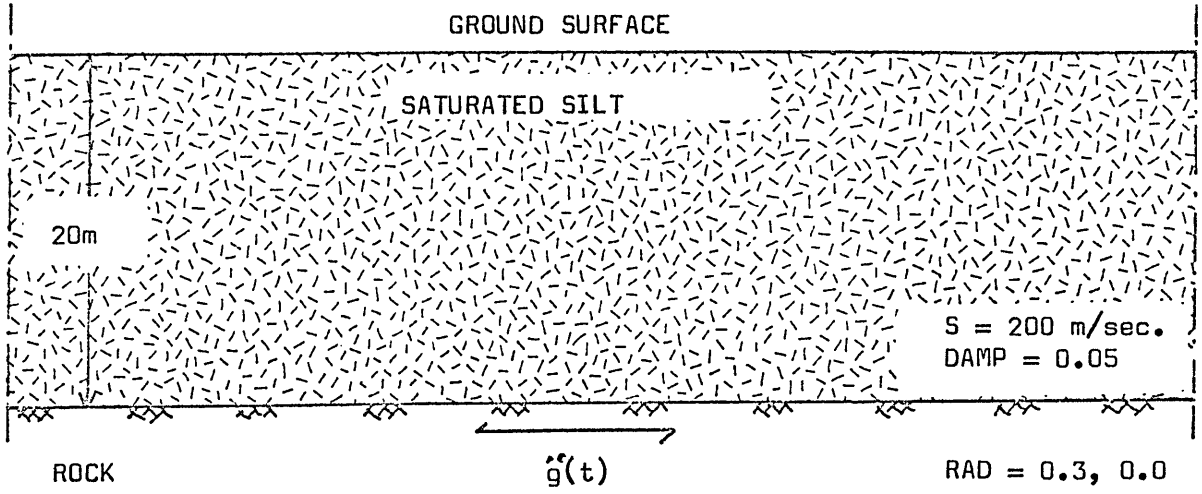
6.10. INFLUENCE OF STIFFNESS CHARACTERISTICS OF BEDROCK FORMATION ON SUBSURFACE RESPONSE OF SOIL DEPOSITS

For a variety of engineering purposes, it is desirable to estimate the response which is likely to develop at some depth in a soil deposit. It is clearly stated by Professor Ambraseys[6] that:

> Most studies of the response of soil deposit to strong motions consider an infinitely rigid bedrock which supplies the motion. It is not difficult to see that the input motion applied to bedrock level of an overburden with infinitely rigid base implies a "powerful engine" supplying an ever increasing amount of energy into an overburden that has to absorb it internally. This invariably results in an over-estimation of response in the overburden .....

This significant fact seems to have been overlooked in all subsequent investigations, perhaps partly because of the work reported by Lysmer et. al. and partly because of lack of available information on the phenomenon known as radiation damping. Since no work has been reported which supports the above facts, the following studies were performed to throw some light on the above hypothesis.

Figs. 6.69a,b,c,d,e to 6.70a,b,c,d,e show response of a 20m. deposit of saturated silt at the surface and three points, 5m, 10m, and 15m below ground surface having two different bedrock formations with shear wave velocities of infinity and 660 m/sec. The former represents a completely rigid bedrock formation and the latter a soft rock formation. In general, it is observed that the pattern of these time histories are quite dissimilar. The peaks developed on each pair have quite different amplitudes, the larger amplitude belonging to the completely rigid bedrock; these results are summarized in table 6.6.



RESPONSE OF HYSTERETIC DEPOSIT UNDERLAIN BY DEFORMABLE BEDROCK

SCHEMATIC SOIL PROFILE FOR SITE NO. 6.38 and 6.39.

FIG. 6.69

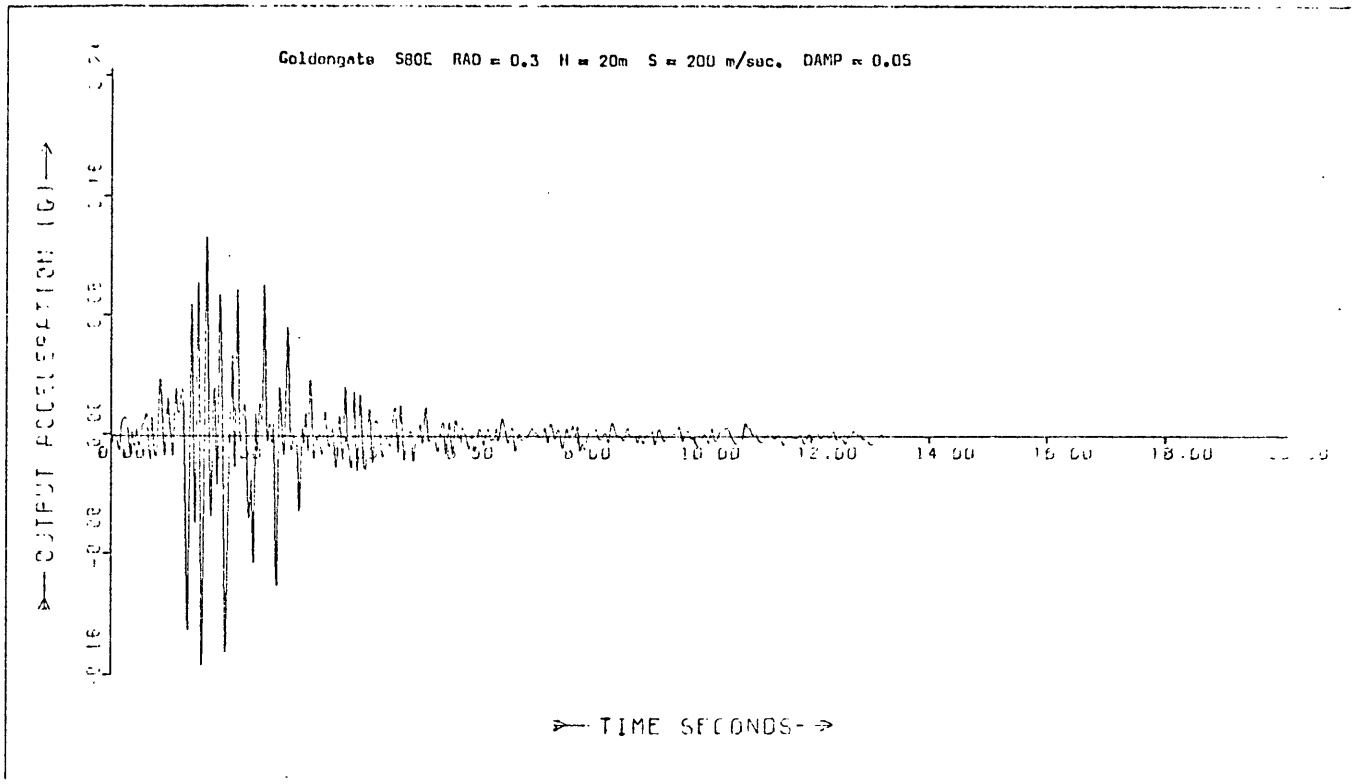


FIG.6.69a COMPUTED SURFACE ACCELERATION TIME HISTORY AT SITE NO. 6.38

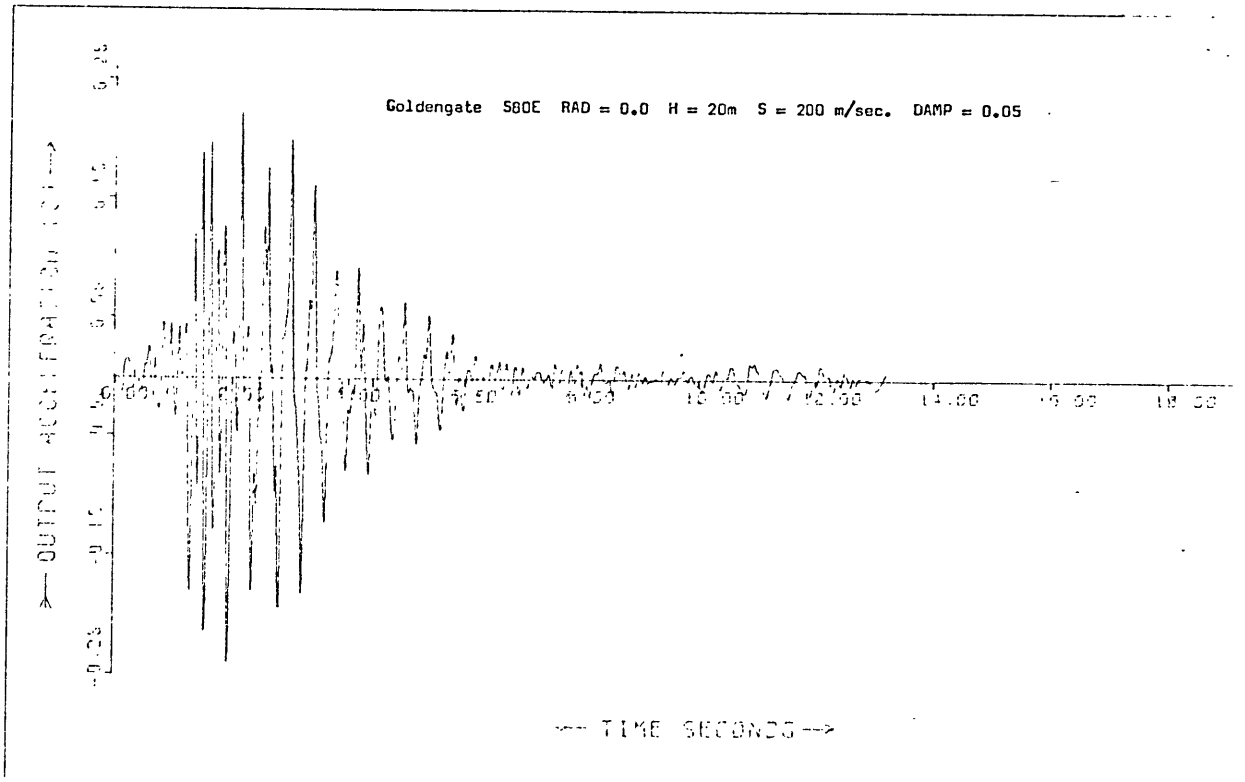


FIG.6.70a COMPUTED SURFACE ACCELERATION TIME HISTORY AT SITE NO. 6.39

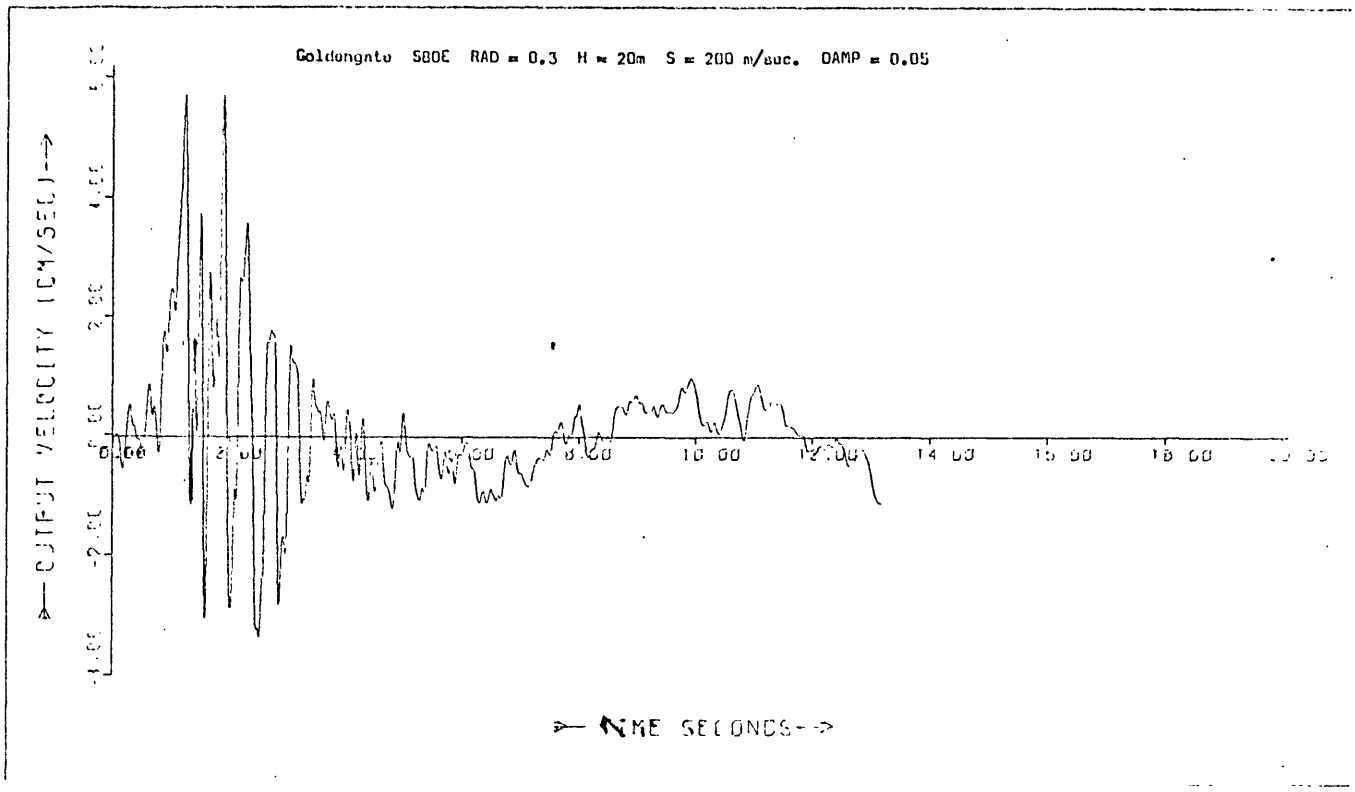


FIG6.69b COMPUTED SURFACE VELOCITY TIME HISTORY AT SITE NO. 6. 38

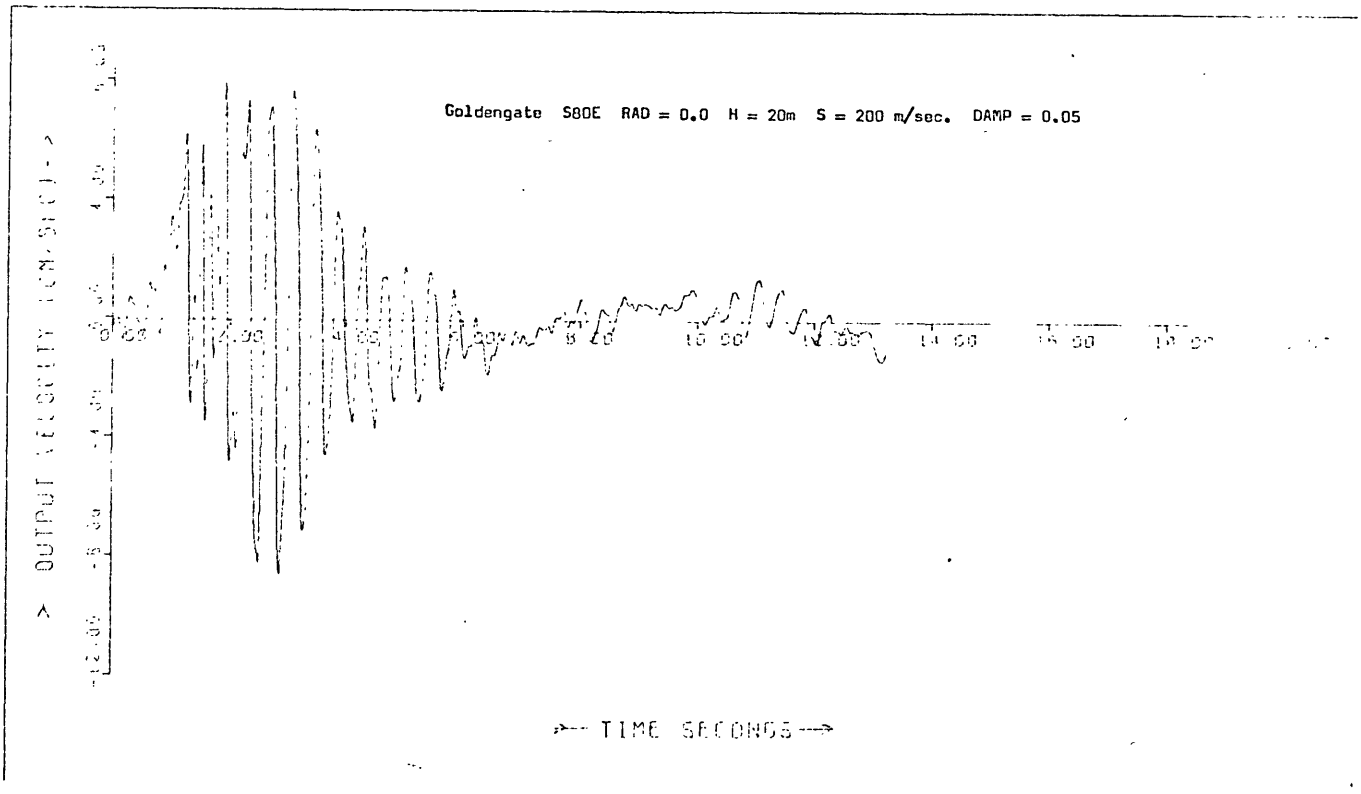


FIG.6.70bCOMPUTED SURFACE VELOCITY TIME HISTORY AT SITE NO. 6. 39

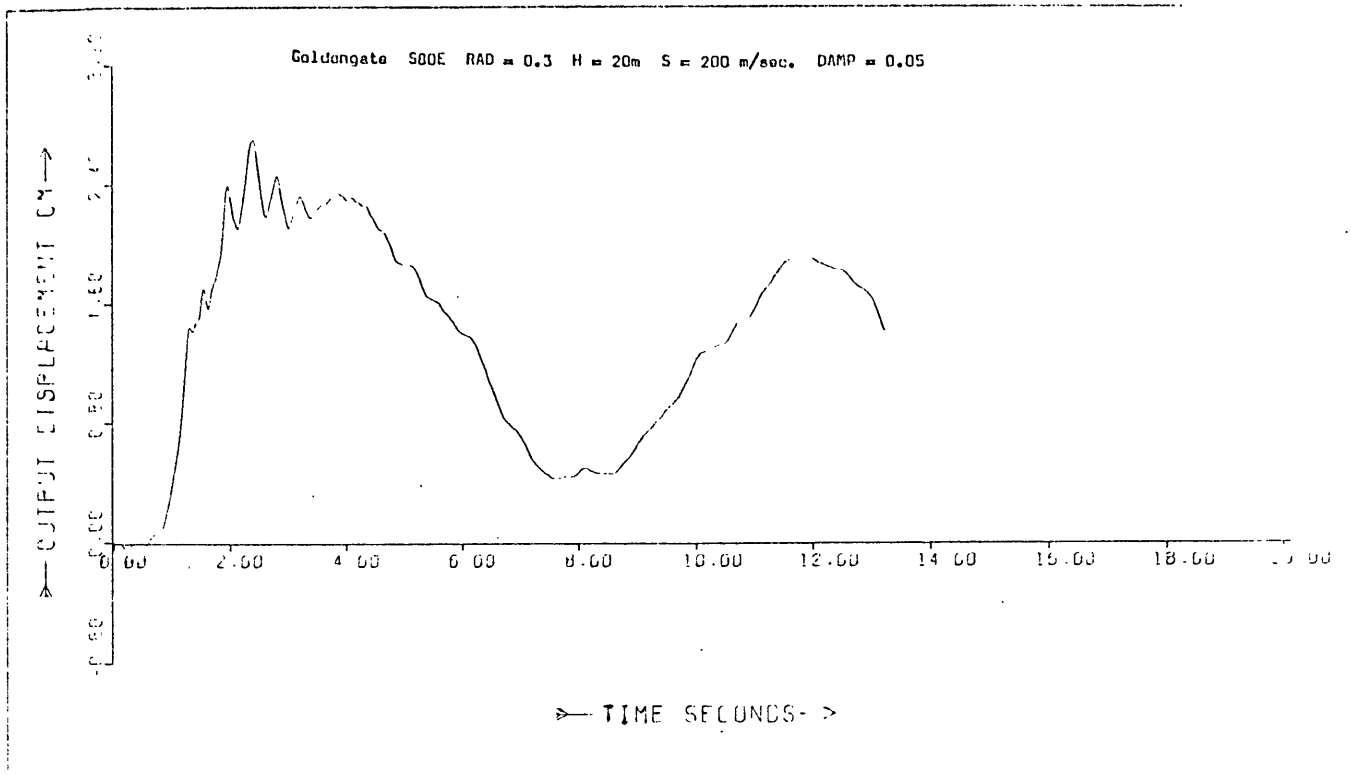


FIG 6.69c COMPUTED SURFACE DISPLACEMENT TIME HISTORY AT SITE NO. 6.38

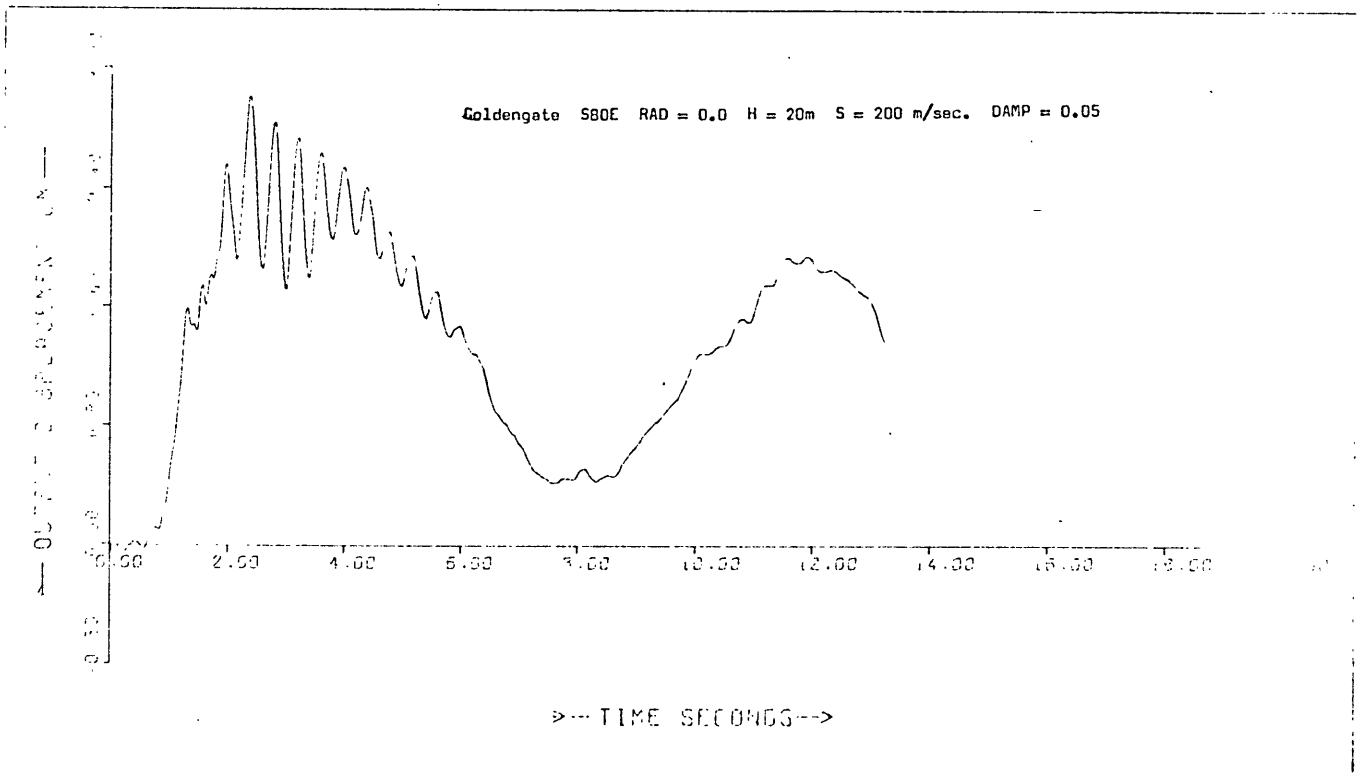


FIG 6.70c COMPUTED SURFACE DISPLACEMENT TIME HISTORY AT SITE NO. 6.39

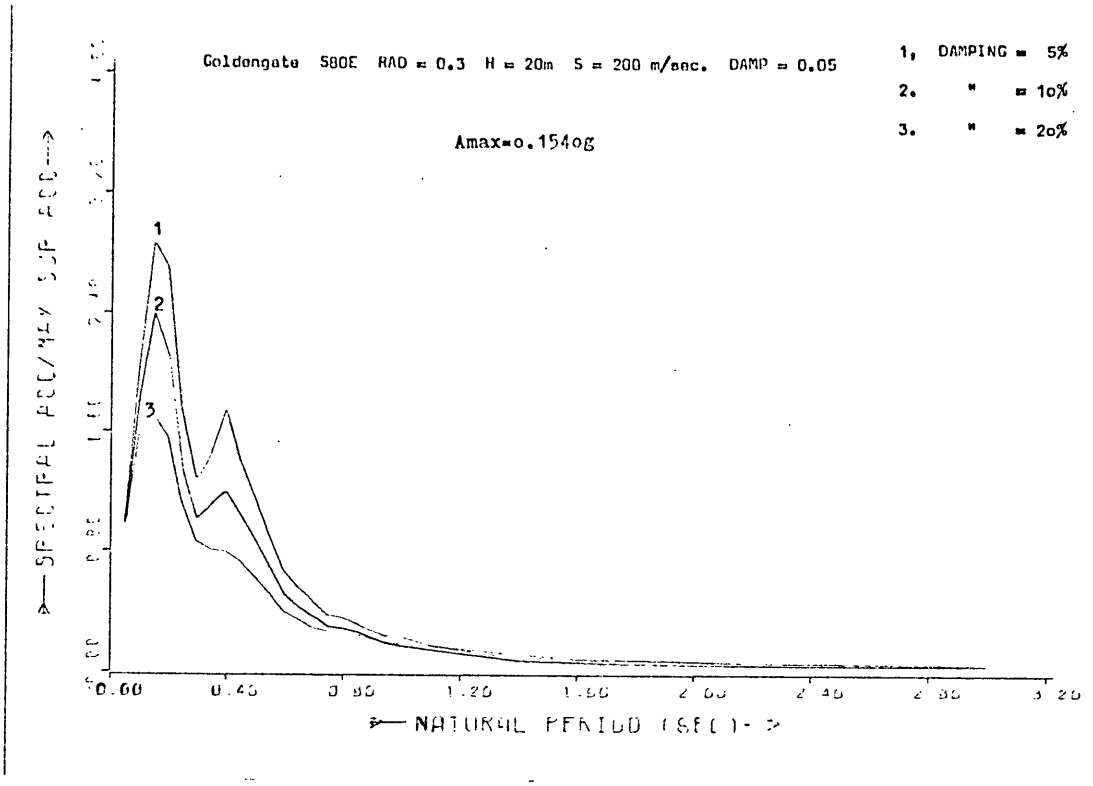


FIG6.69d COMPUTED SURFACE ACCELERATION RESPONSE SPECTRA AT SITE NO. 6. 38

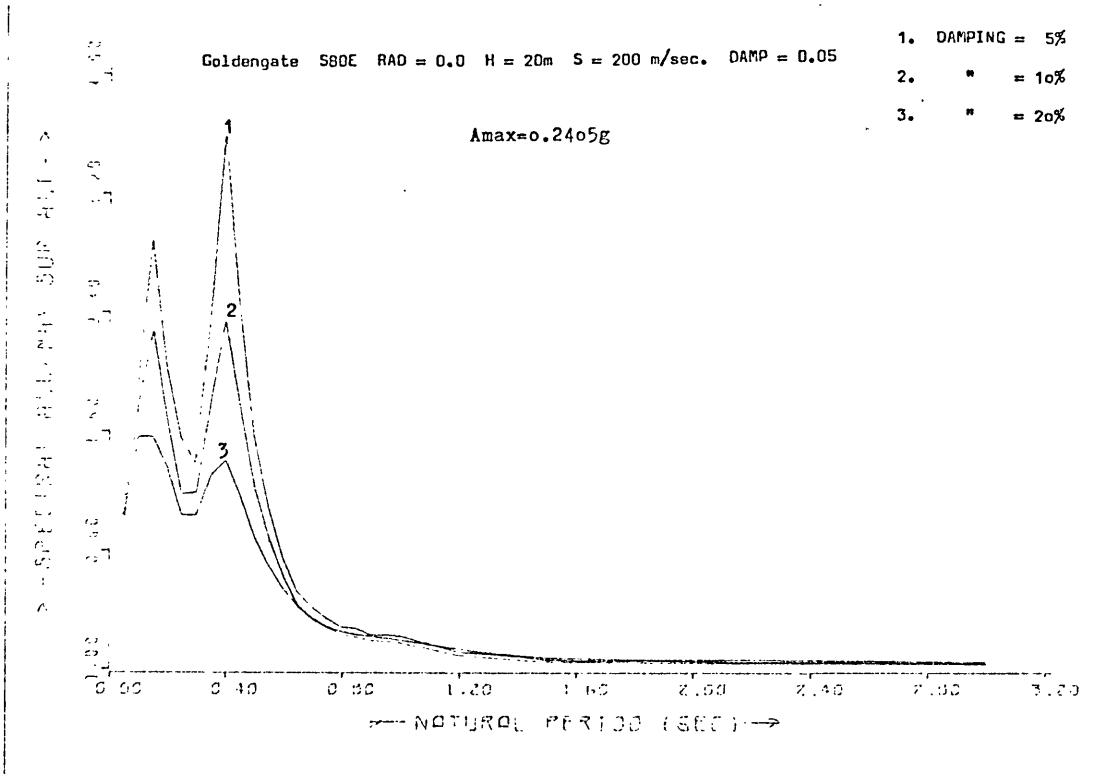


FIG6.7od COMPUTED SURFACE ACCELERATION RESPONSE SPECTRA AT SITE NO. 6. 39

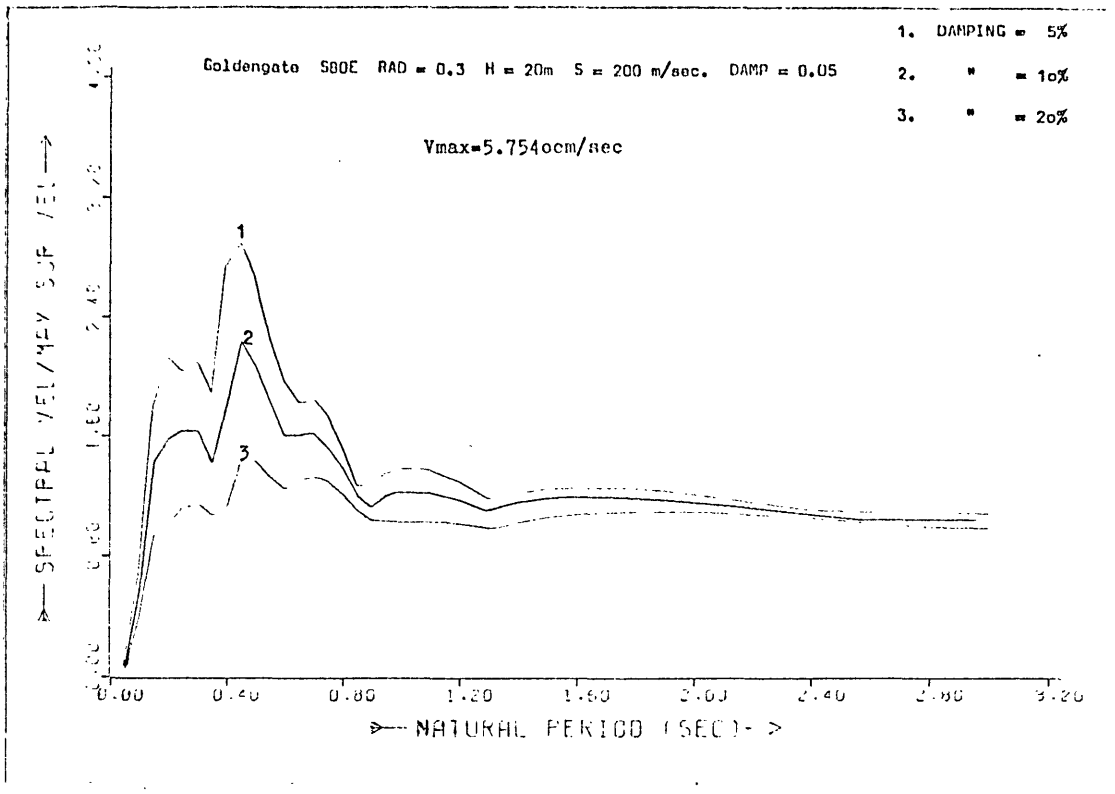


FIG.6.69eCOMPUTED SURFACE VELOCITY RESPONSE SPECTRA AT SITE NO. 6.38

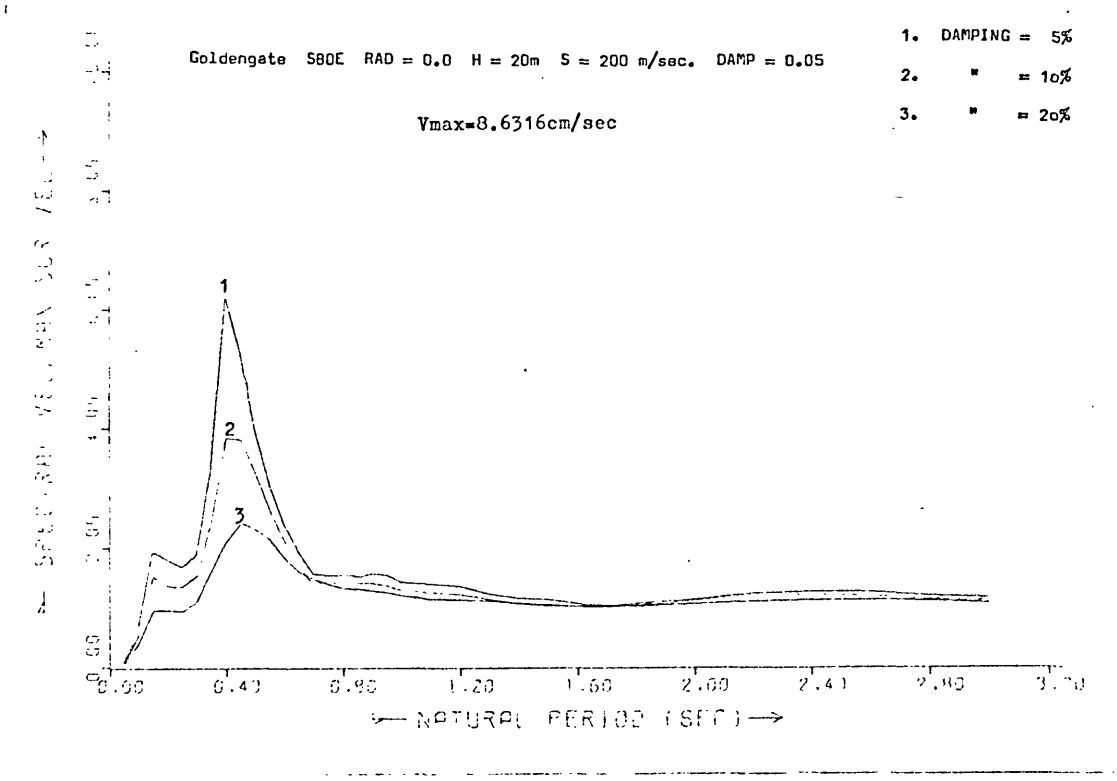


FIG.6.7oeCOMPUTED SURFACE VELOCITY RESPONSE SPECTRA AT SITE NO. 6.39

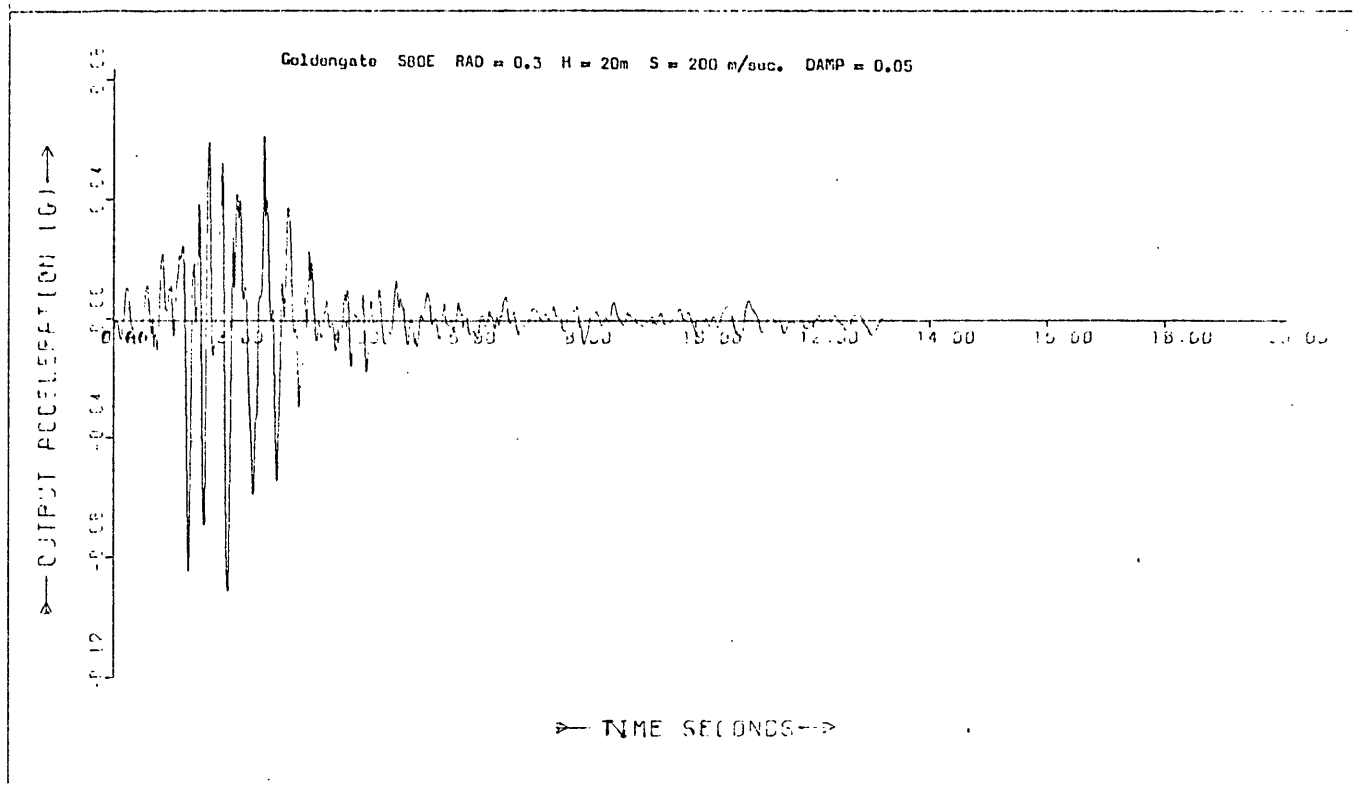


FIG.6.69a COMPUTED SUBSURFACE ACCELERATION TIME HISTORY AT SITE NO. 6.38

5m from GROUND SURFACE

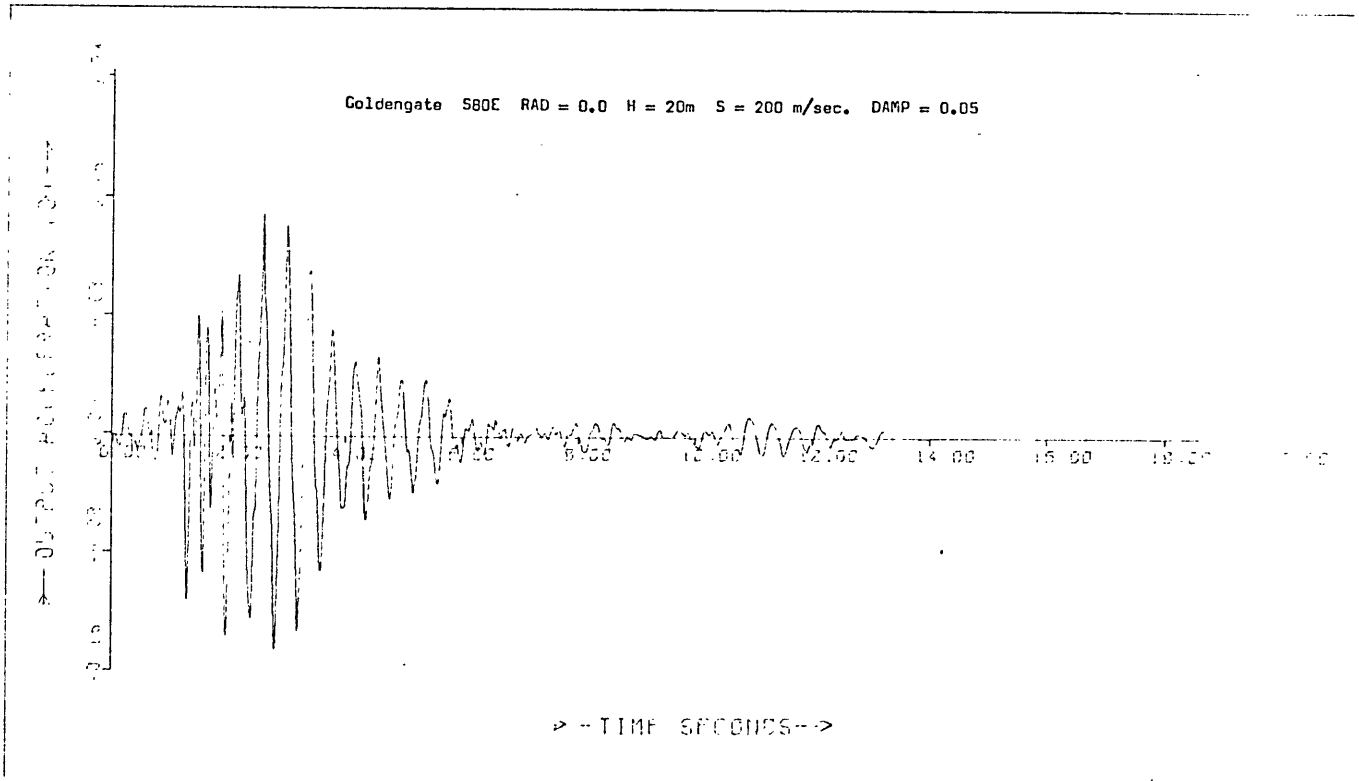


FIG.6.70b COMPUTED SUBSURFACE ACCELERATION TIME HISTORY AT SITE NO. 6.39

5m from GROUND SURFACE

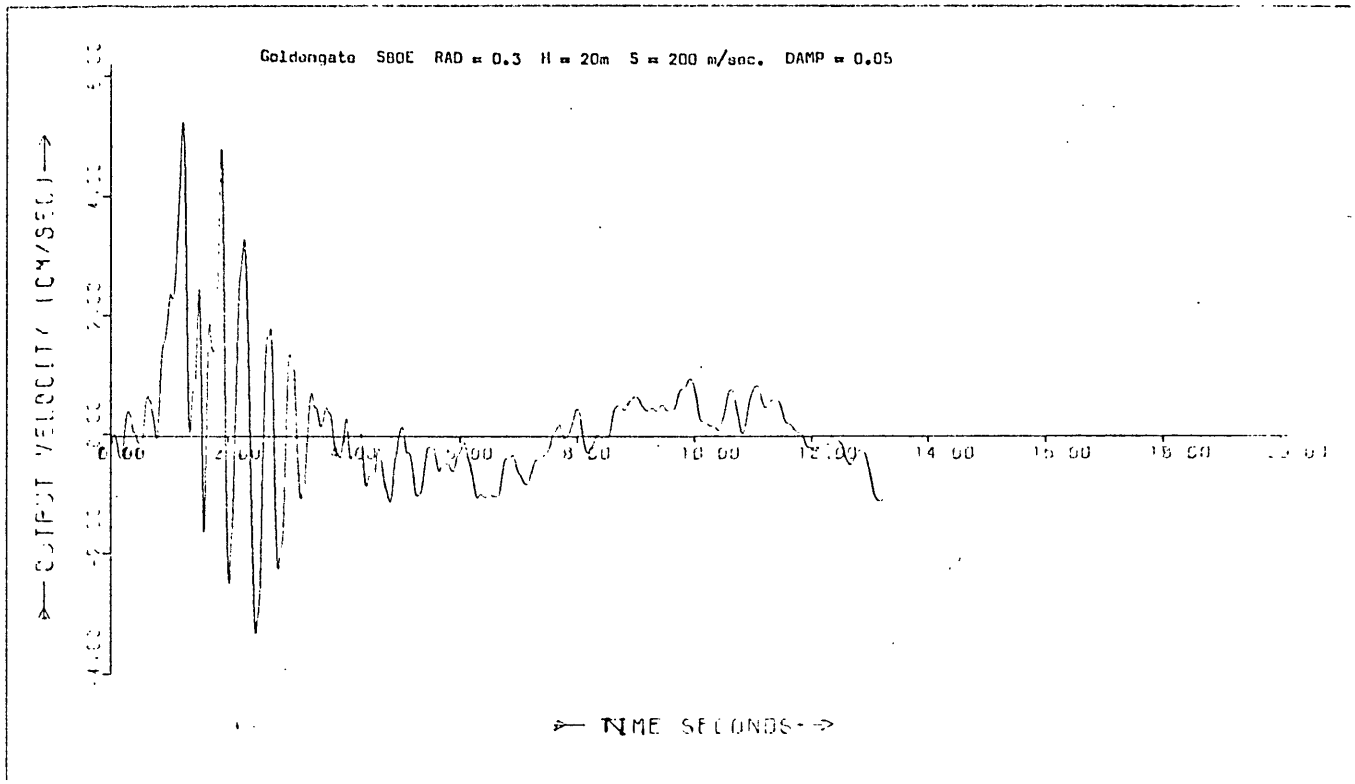


FIG 6.69b COMPUTED SUBSURFACE VELOCITY TIME HISTORY AT SITE NO. 6.38

5m from GROUND SURFACE

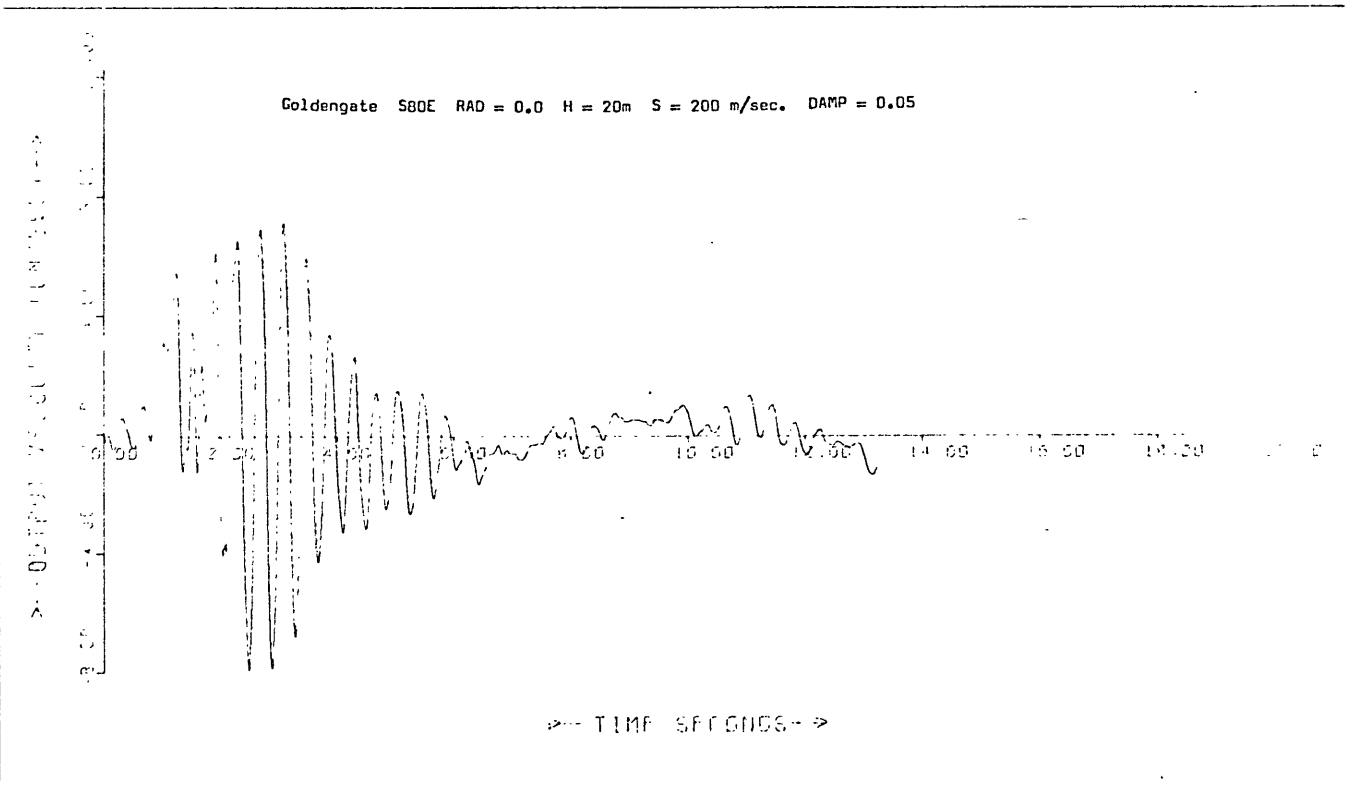


FIG 6.70b COMPUTED SUBSURFACE VELOCITY TIME HISTORY AT SITE NO. 6.39

5m from GROUND SURFACE

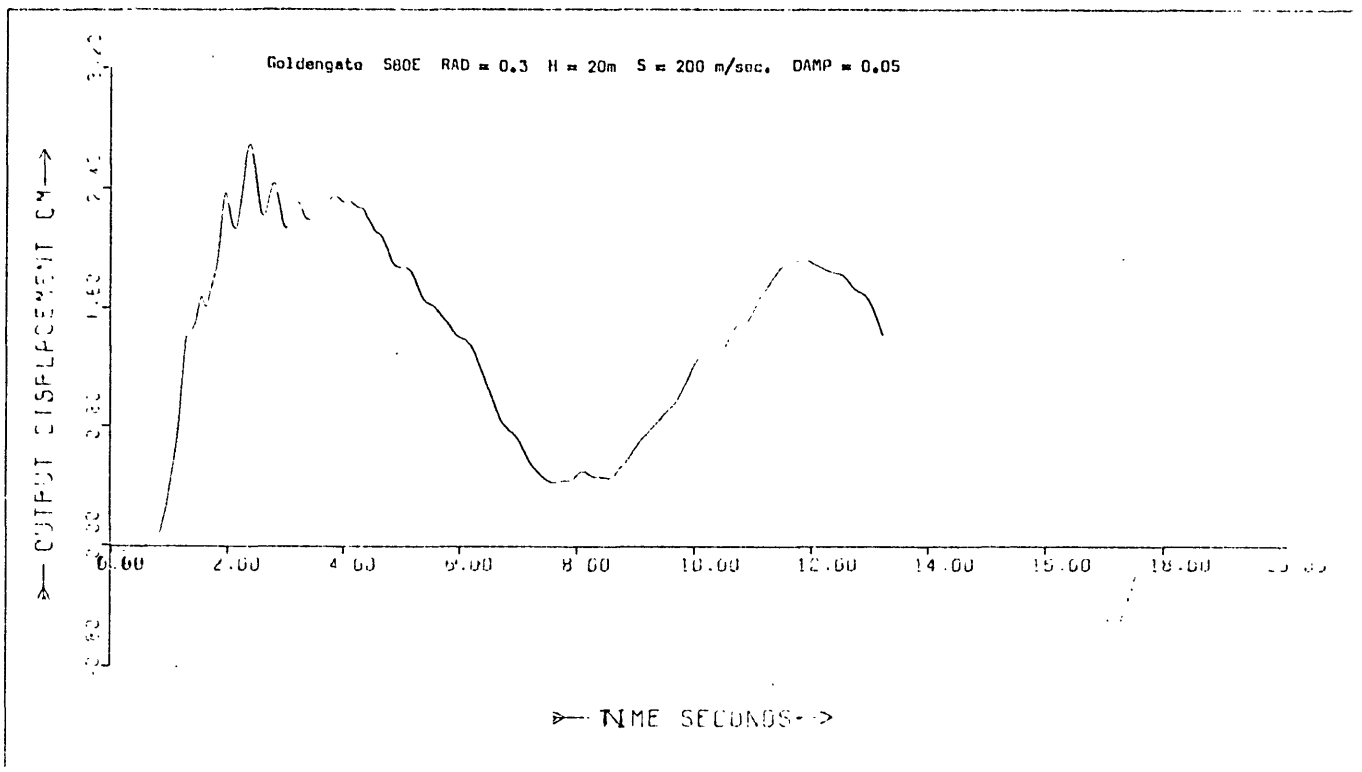


FIG.6.69cCOMPUTED SUBSURFACE DISPLACEMENT TIME HISTORY AT SITE NO.6.38

5m from GROUND SURFACE

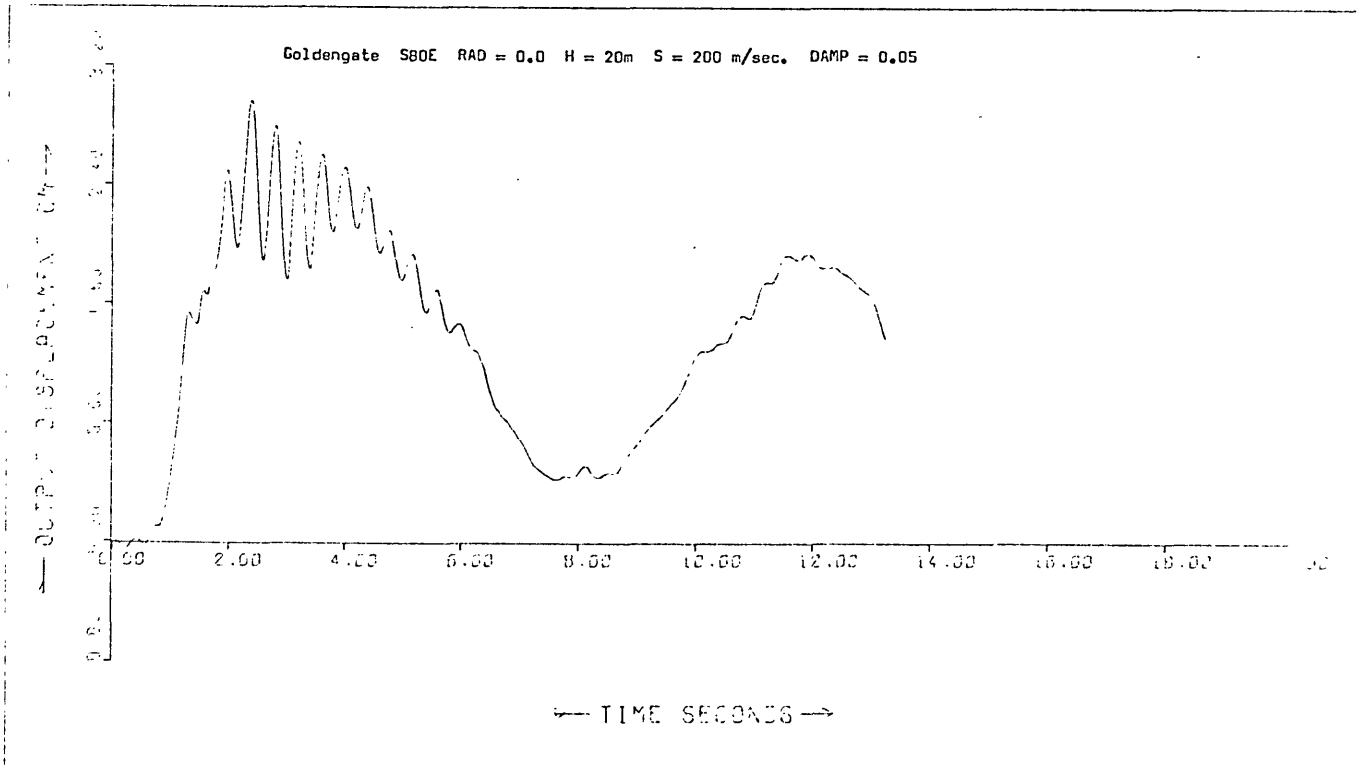


FIG.6.70cCOMPUTED SUBSURFACE DISPLACEMENT TIME HISTORY AT SITE NO.6.39

5m from GROUND SURFACE

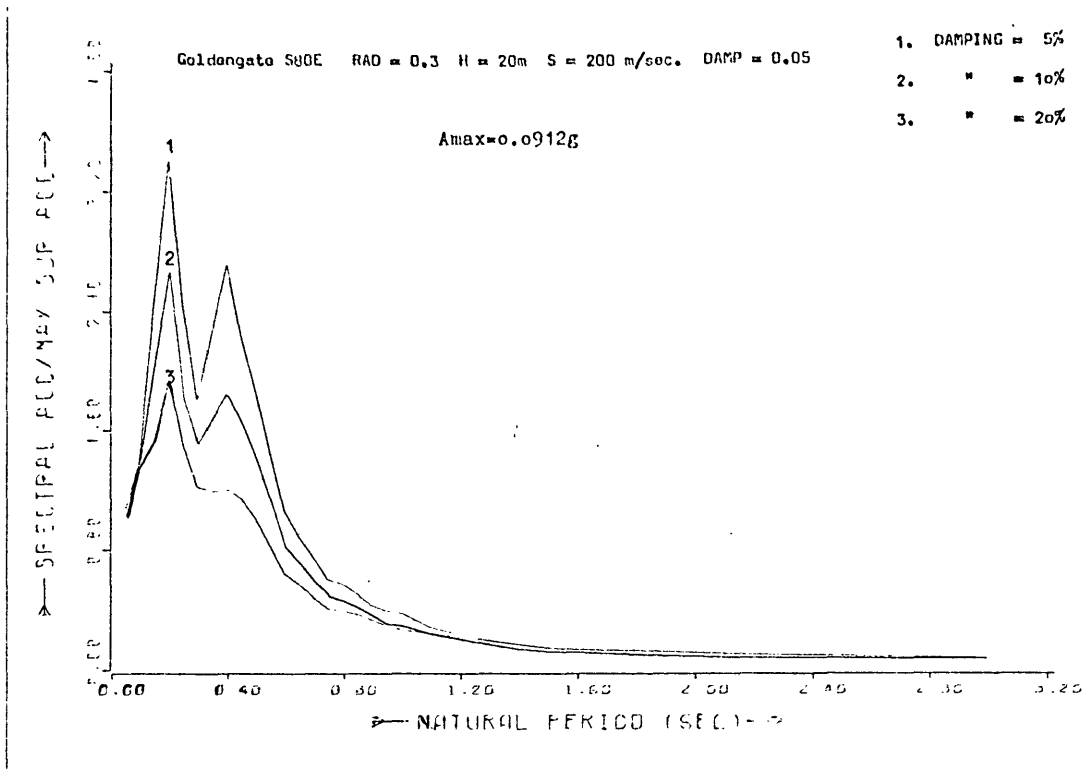


FIG6.69d COMPUTED SUBSURFACE ACCELERATION RESPONSE SPECTRA AT SITE NO. 6.38

5m from GROUND SURFACE

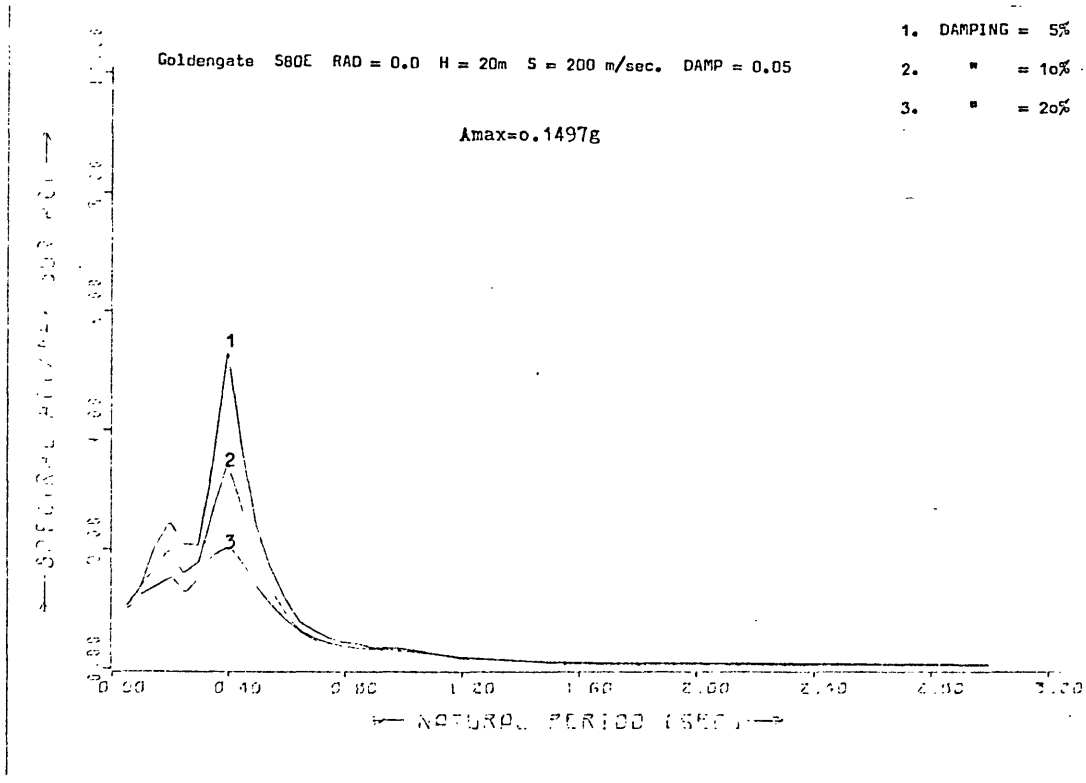


FIG.6.7odCOMPUTED SUBSURFACE ACCELERATION RESPONSE SPECTRA AT SITE NO. 6.39

5m from GROUND SURFACE

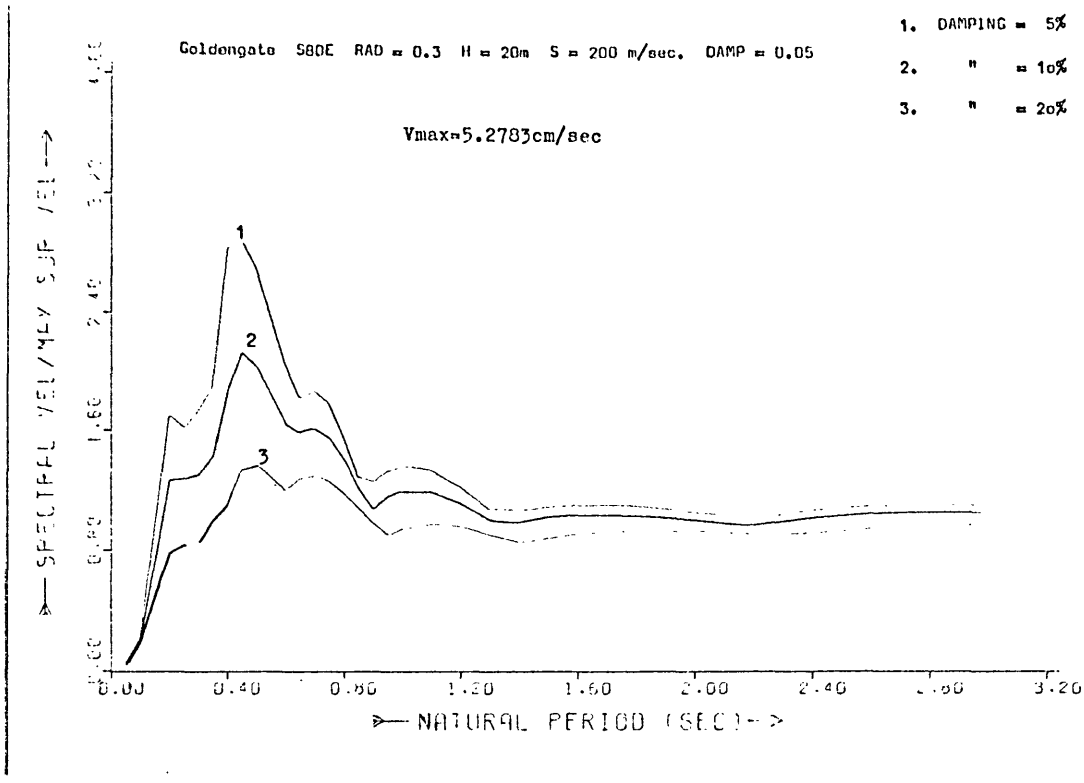


FIG 6.69e COMPUTED SUBSURFACE VELOCITY RESPONSE SPECTRA AT SITE NO 6.38

5m from GROUND SURFACE

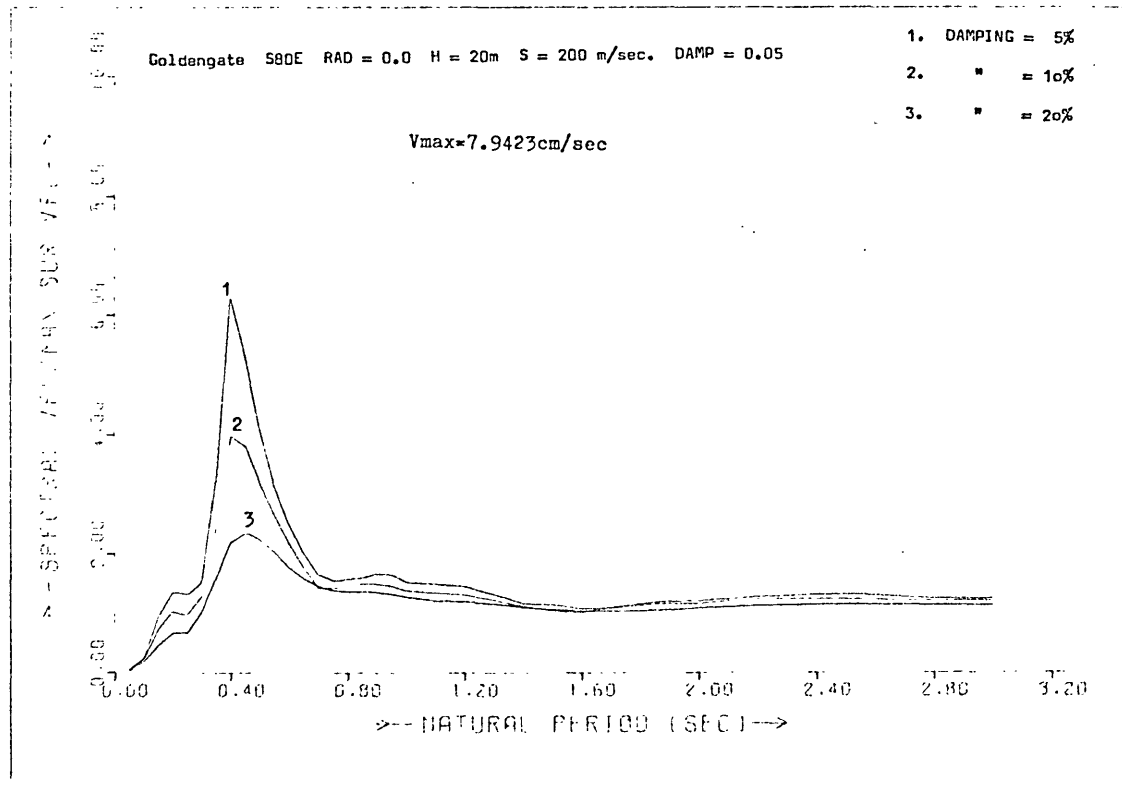


FIG.6.70e COMPUTED SUBSURFACE VELOCITY RESPONSE SPECTRA AT SITE NO. 6. 39

5m from GROUND SURFACE

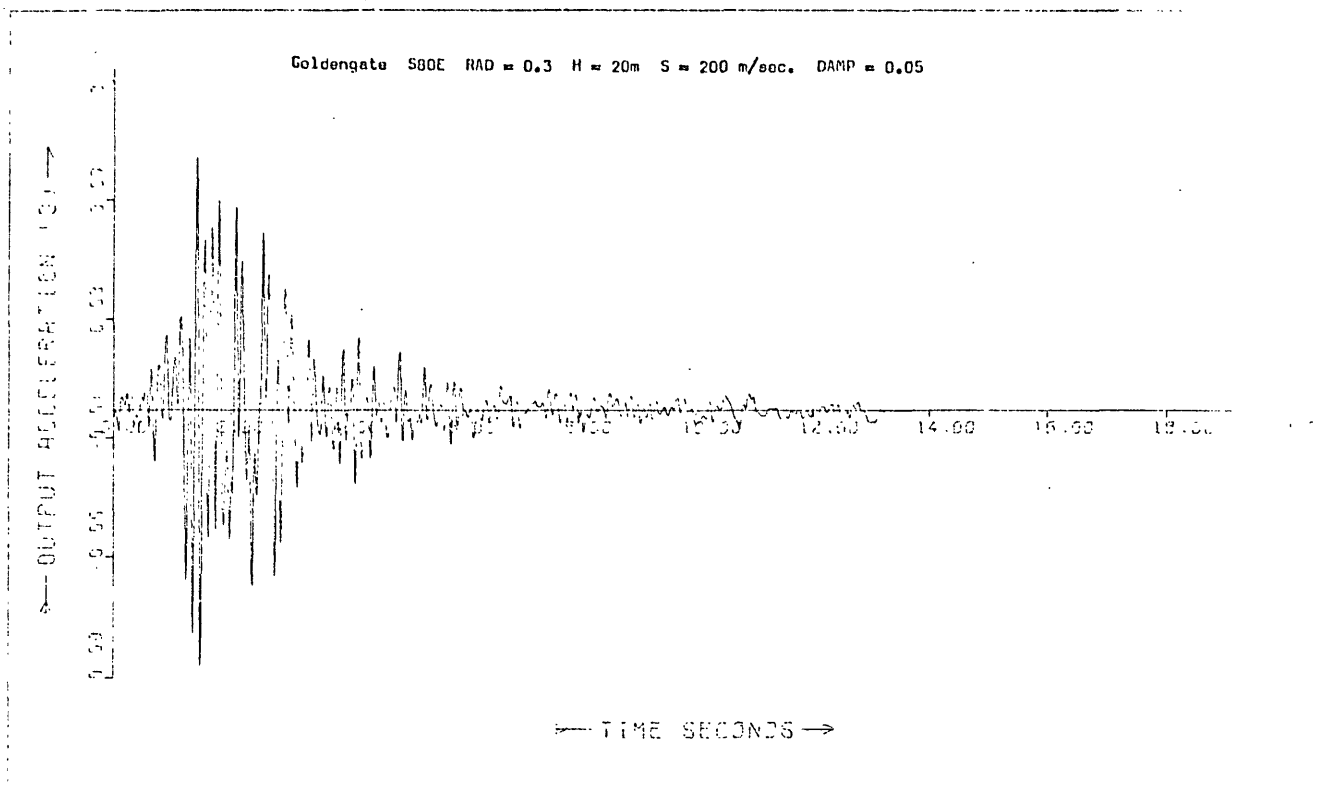


FIG6.69a COMPUTED SUBSURFACE ACCELERATION TIME HISTORY AT SITE NO. 6.38

10m from GROUND SURFACE

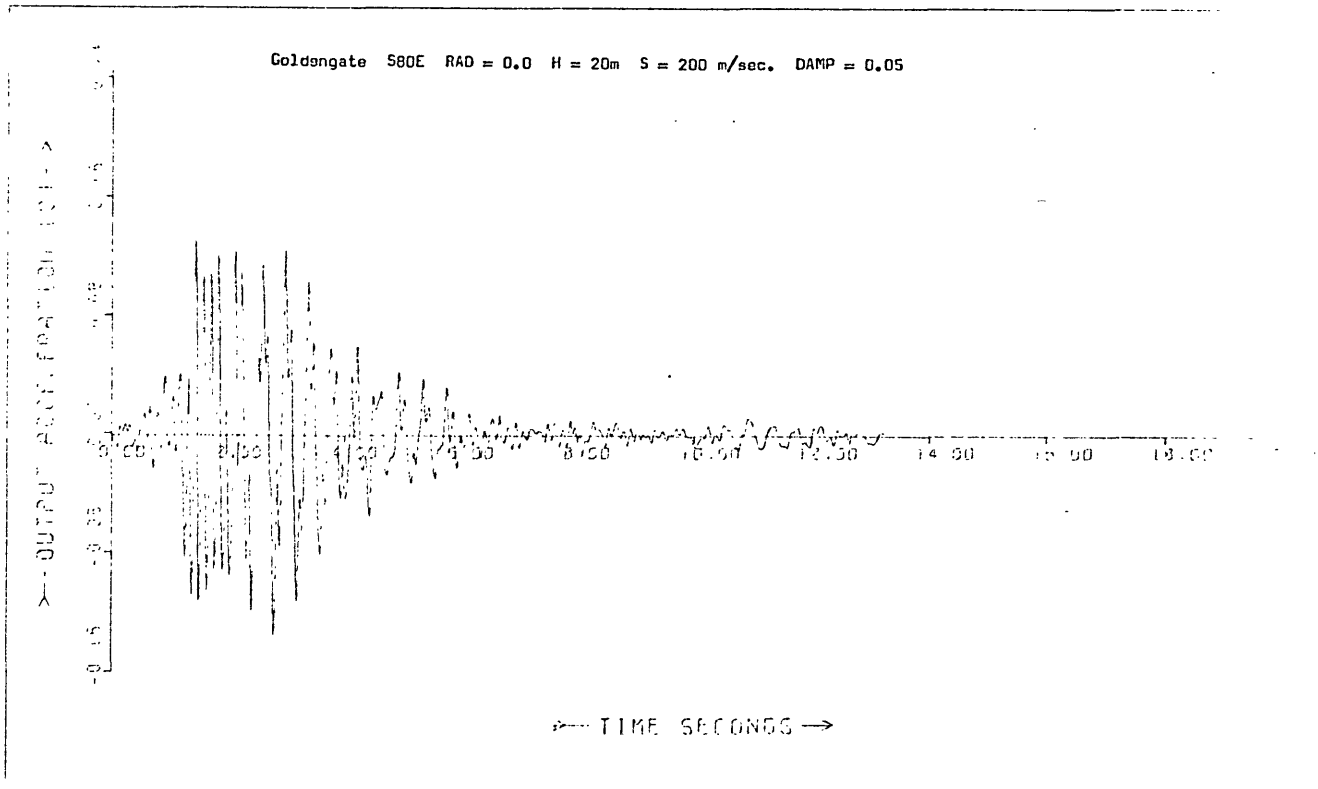


FIG. 6.70a COMPUTED SUBSURFACE ACCELERATION TIME HISTORY AT SITE NO. 6.39

10m from GROUND SURFACE

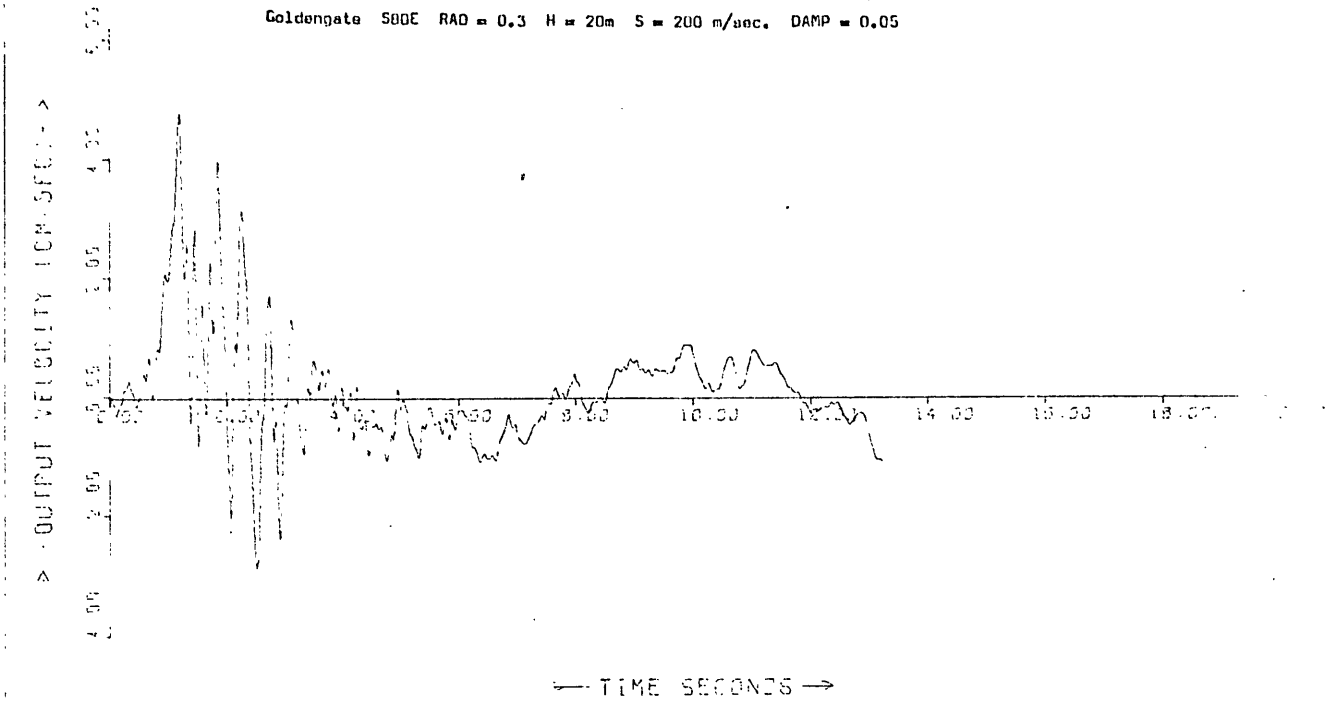


FIG6.69b COMPUTED SUBSURFACE VELOCITY TIME HISTORY AT SITE NO. 6.38

10m from GROUND SURFACE

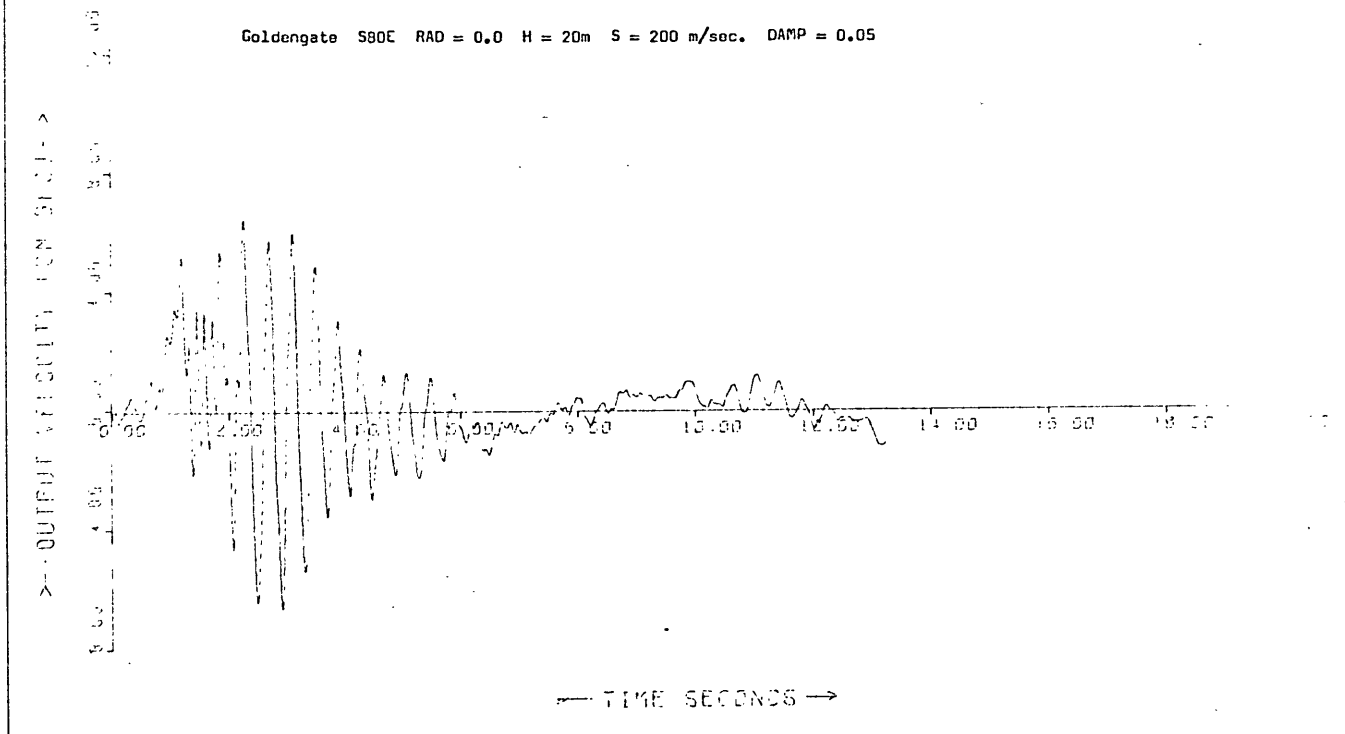


FIG.6.70bCOMPUTED SUBSURFACE VELOCITY TIME HISTORY AT SITE NO. 6.39

10m from GROUND SURFACE

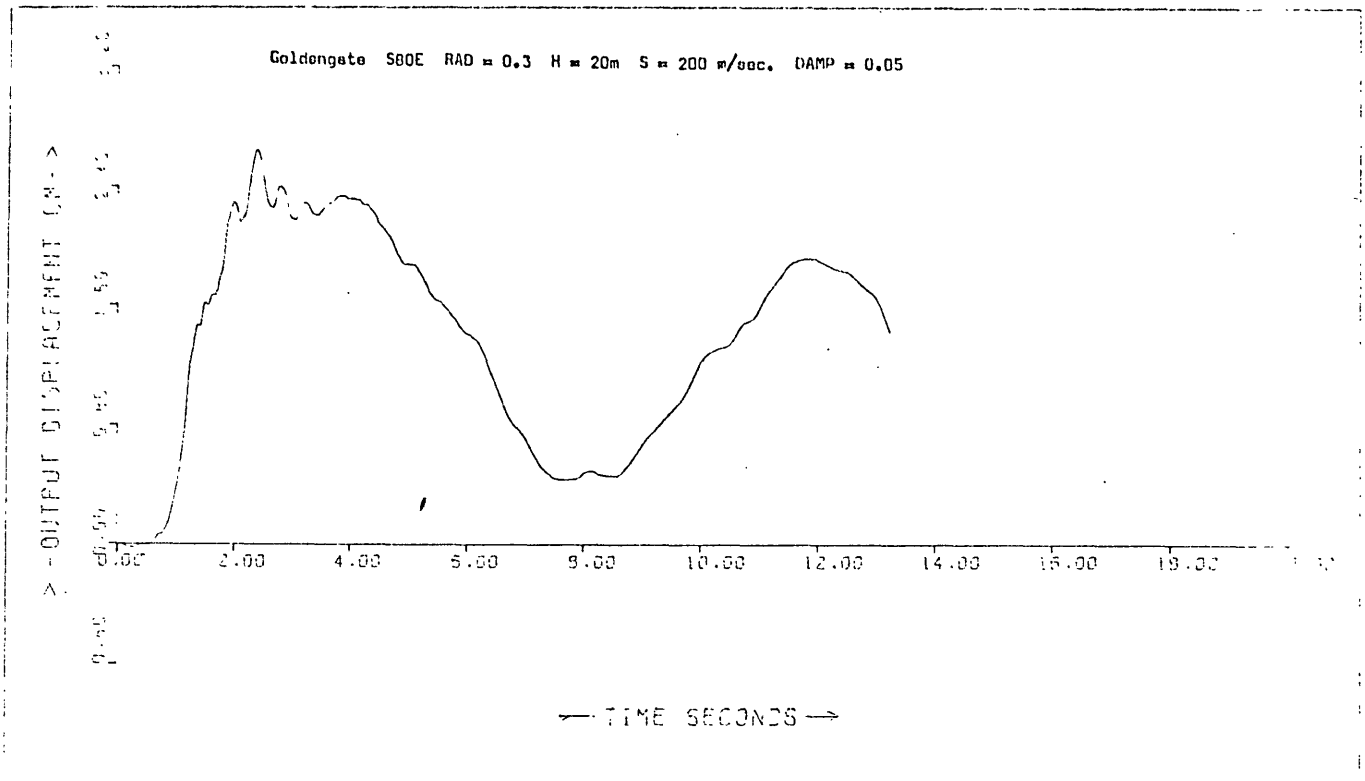


FIG.6.69c COMPUTED SUBSURFACE DISPLACEMENT TIME HISTORY AT SITE NO. 6.38

10m from GROUND SURFACE

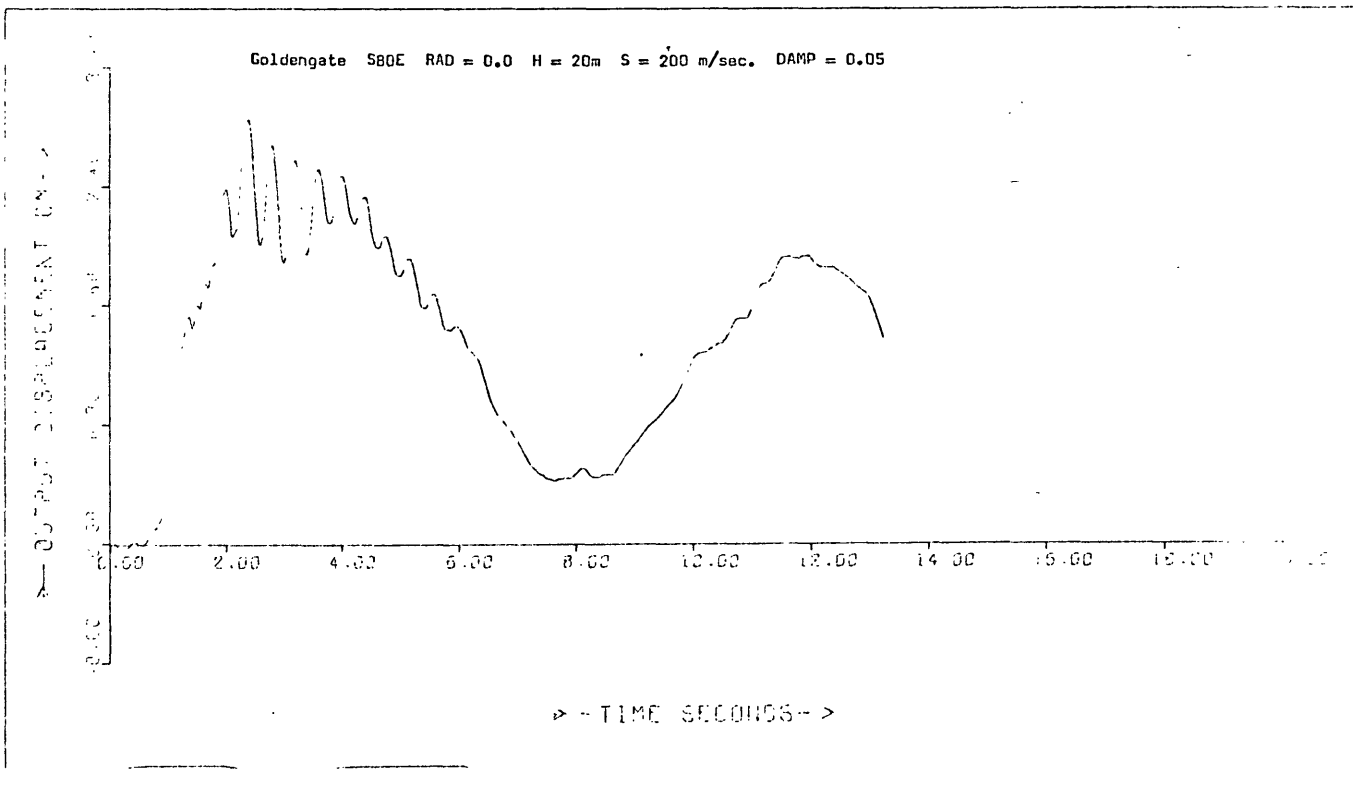


FIG.6.70c COMPUTED SUBSURFACE DISPLACEMENT TIME HISTORY AT SITE NO. 6.39

10m from GROUND SURFACE

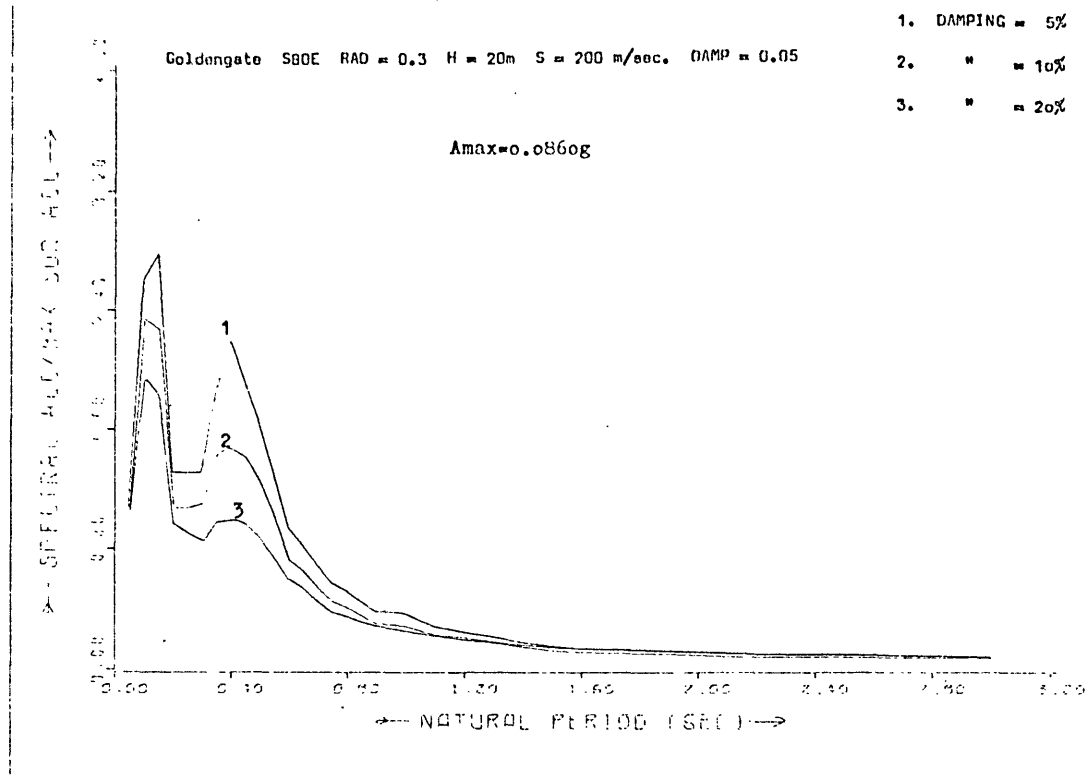


FIG.6.69d COMPUTED SUBSURFACE ACCELERATION RESPONSE SPECTRA AT SITE NO. 6.38

10m from GROUND SURFACE

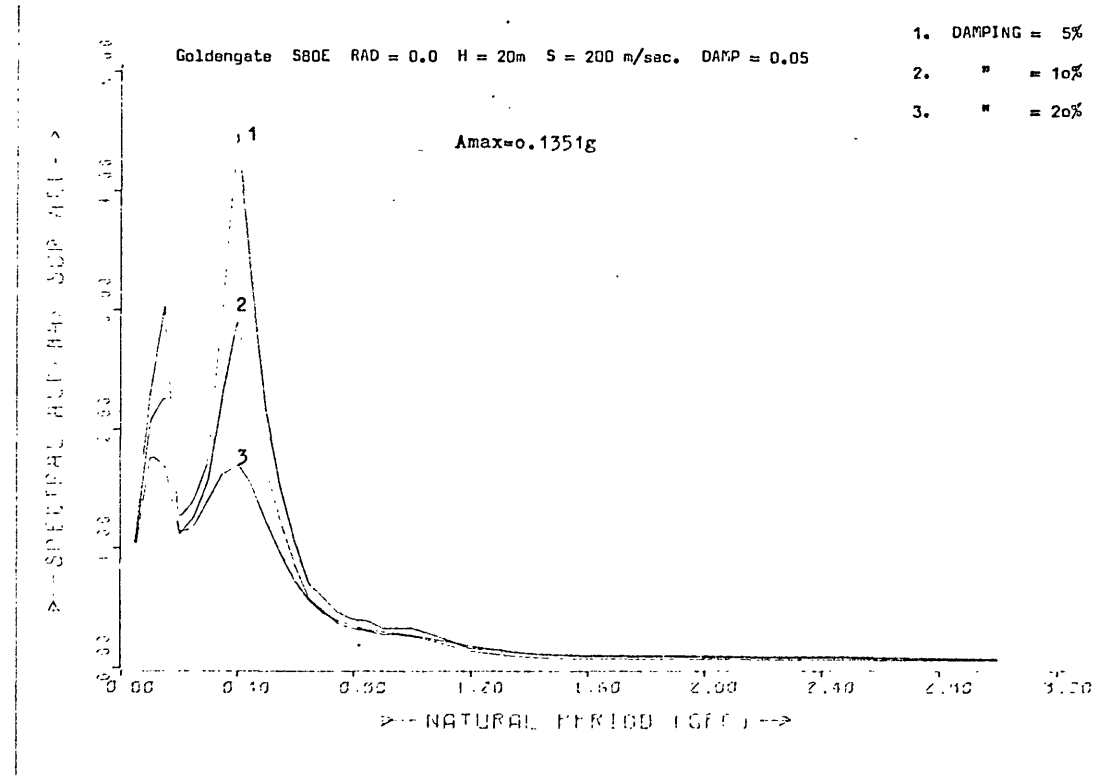


FIG.6.70dCOMPUTED SUBSURFACE ACCELERATION RESPONSE SPECTRA AT SITE NO. 6.39

10m from GROUND SURFACE

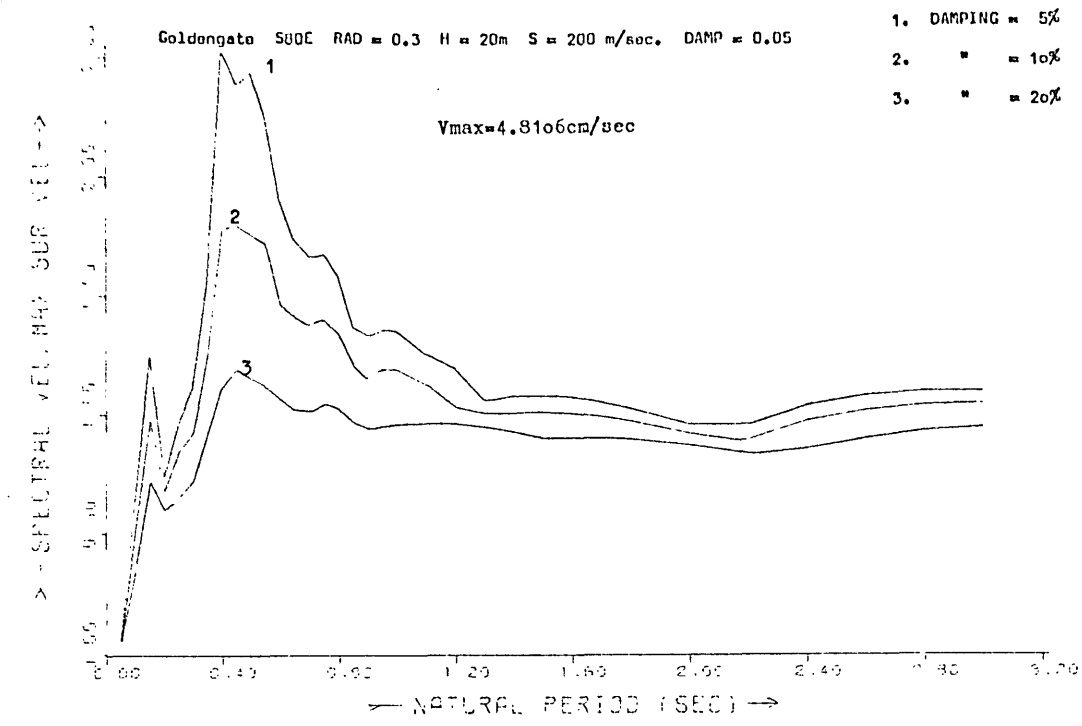


FIG.6.69eCOMPUTED SUBSURFACE VELOCITY RESPONSE SPECTRA AT SITE NO.6. 38

10m from GROUND SURFACE

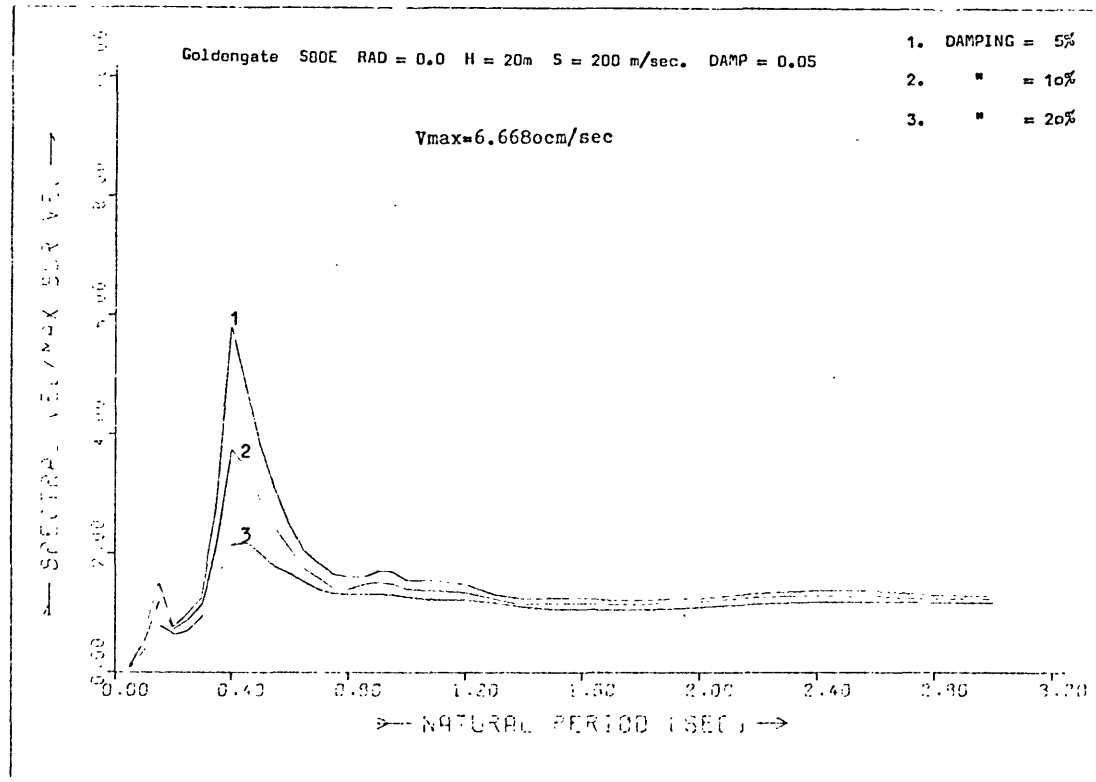


FIG.6.7oe COMPUTED SUBSURFACE VELOCITY RESPONSE SPECTRA AT SITE NO. 6. 39

10m from GROUND SURFACE

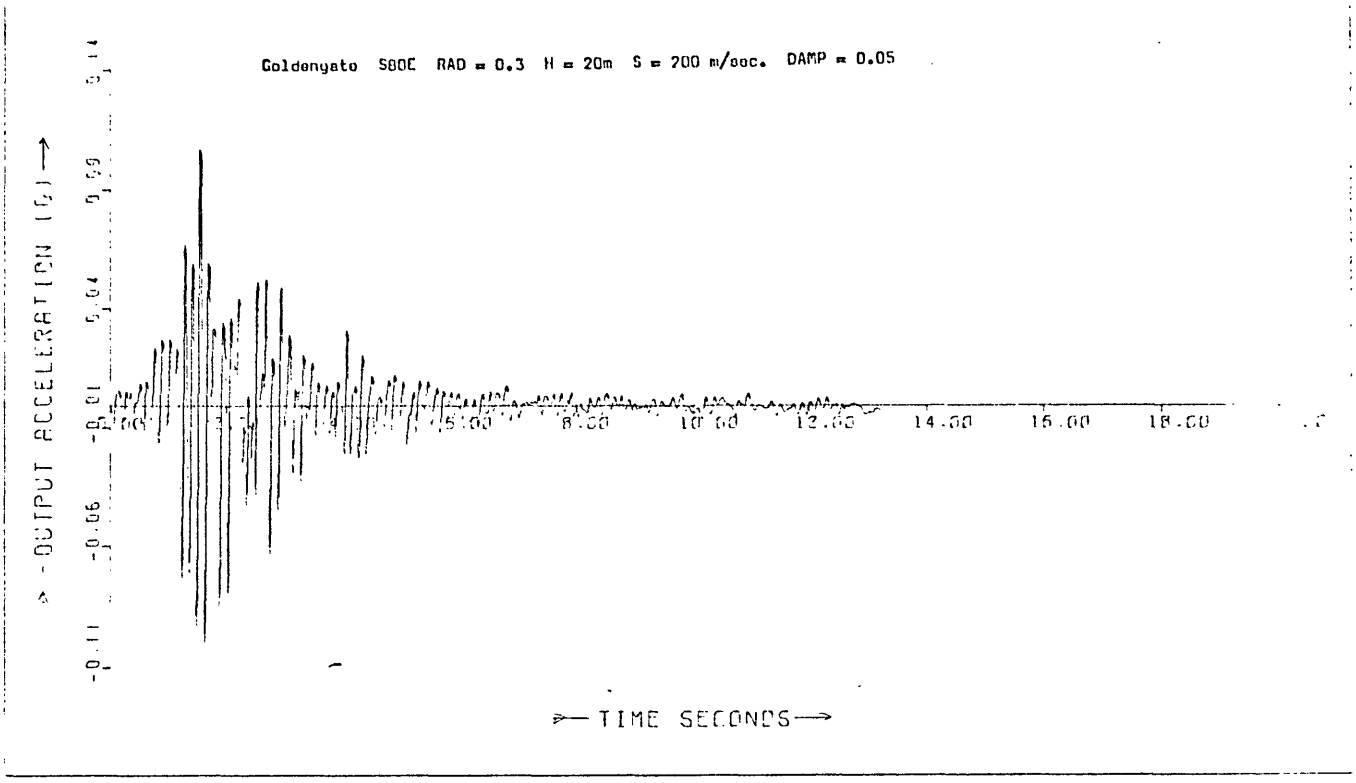


FIG.6.69a COMPUTED SUBSURFACE ACCELERATION TIME HISTORY AT SITE NO. 6.38

15m from GROUND SURFACE

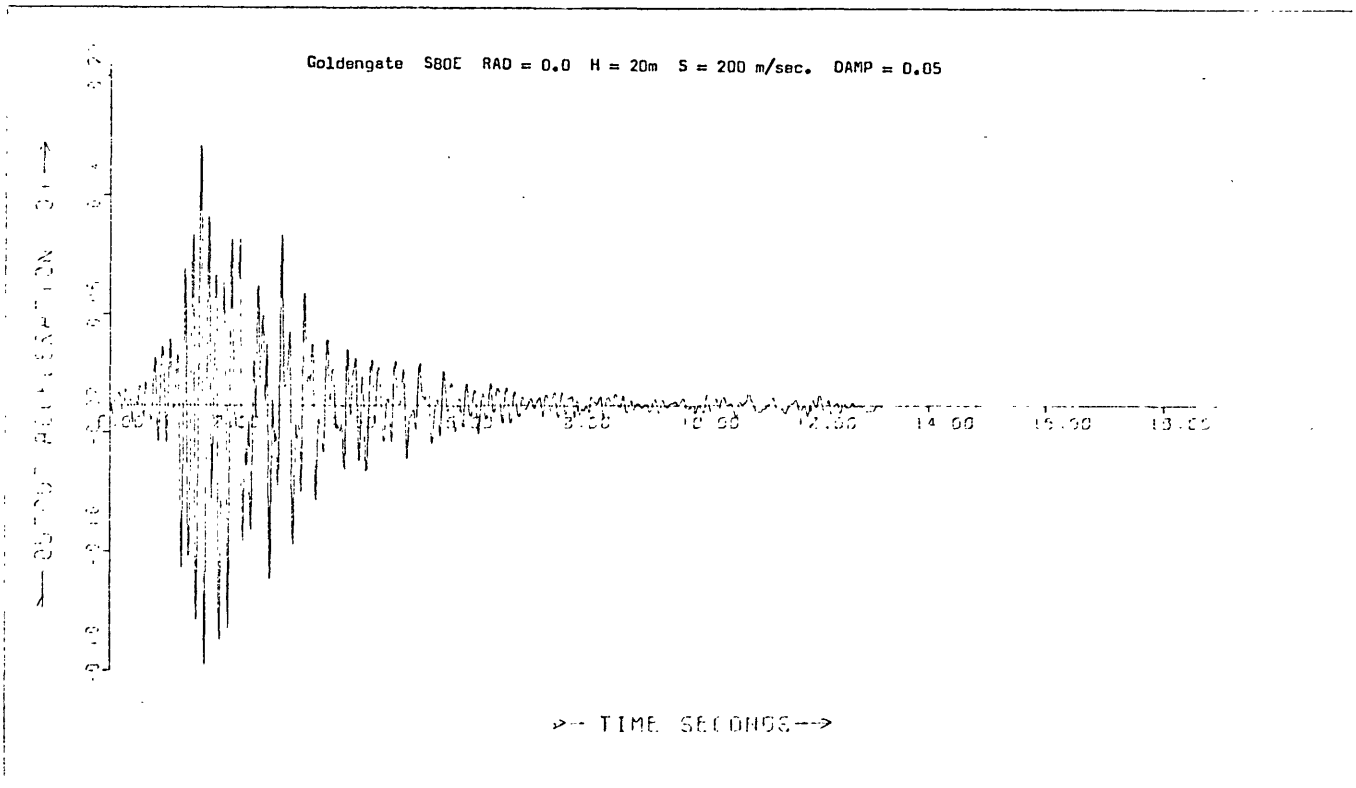


FIG.6.70a COMPUTED SUBSURFACE ACCELERATION TIME HISTORY AT SITE NO. 6.39

15m from GROUND SURFACE

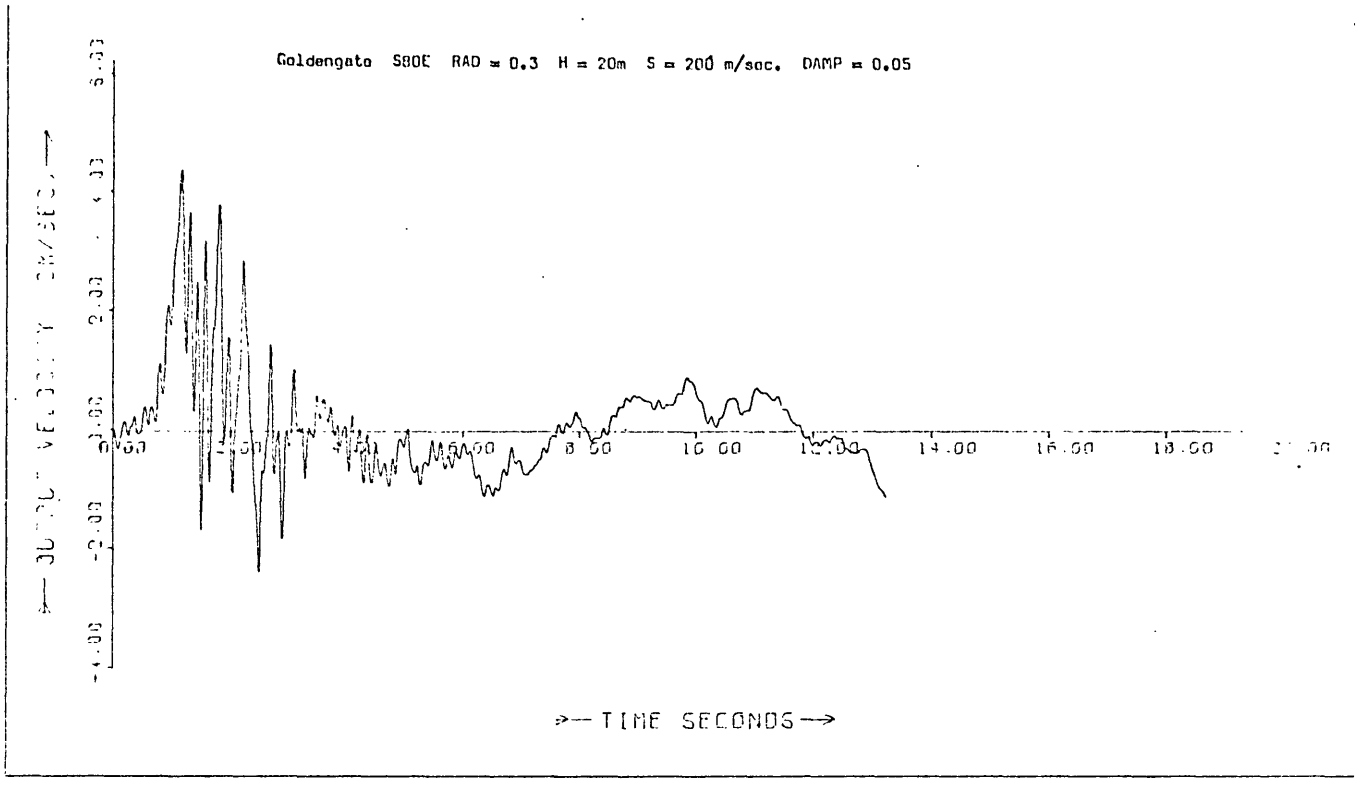


FIG. 6.69b COMPUTED SUBSURFACE VELOCITY TIME HISTORY AT SITE NO. 6. 38

15m from GROUND SURFACE

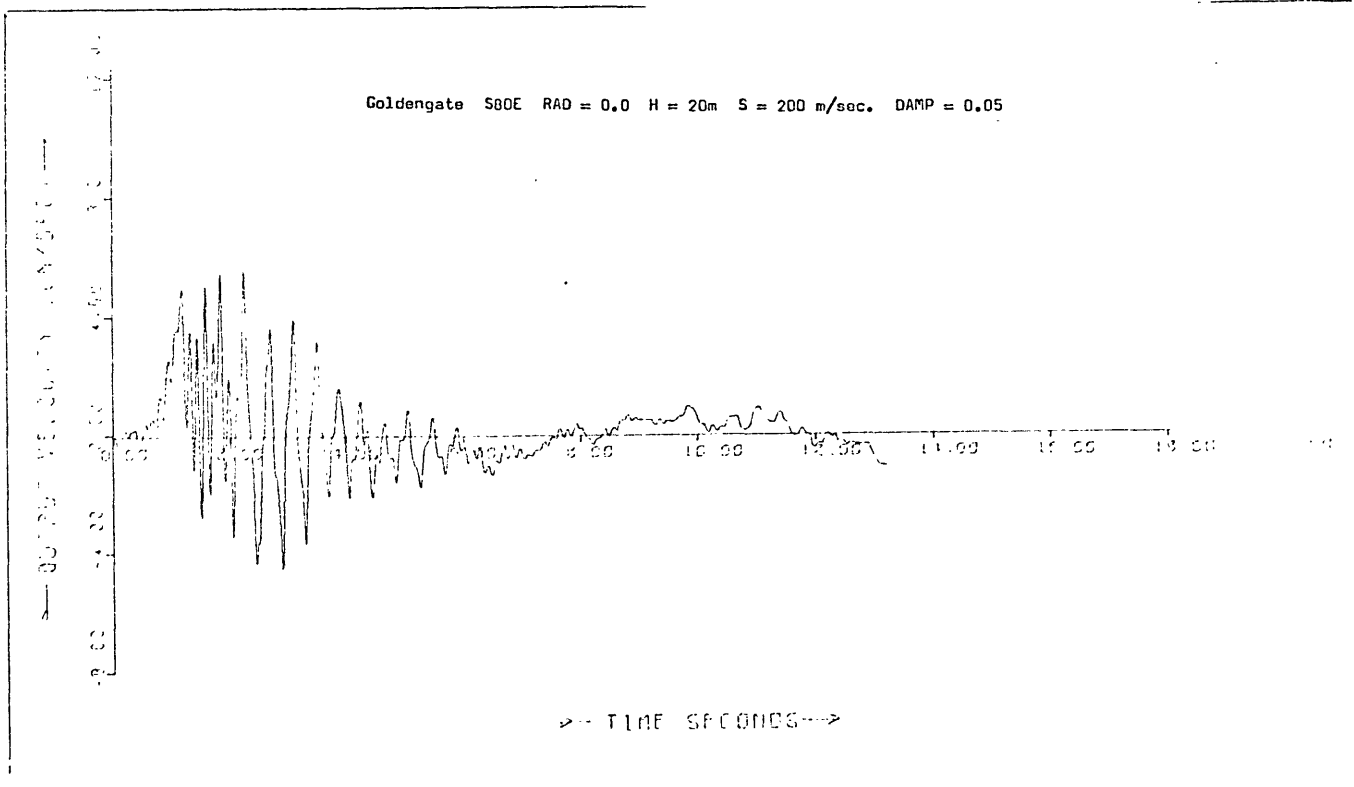


FIG. 6.70b COMPUTED SUBSURFACE VELOCITY TIME HISTORY AT SITE NO. 6. 39

15m from GROUND SURFACE

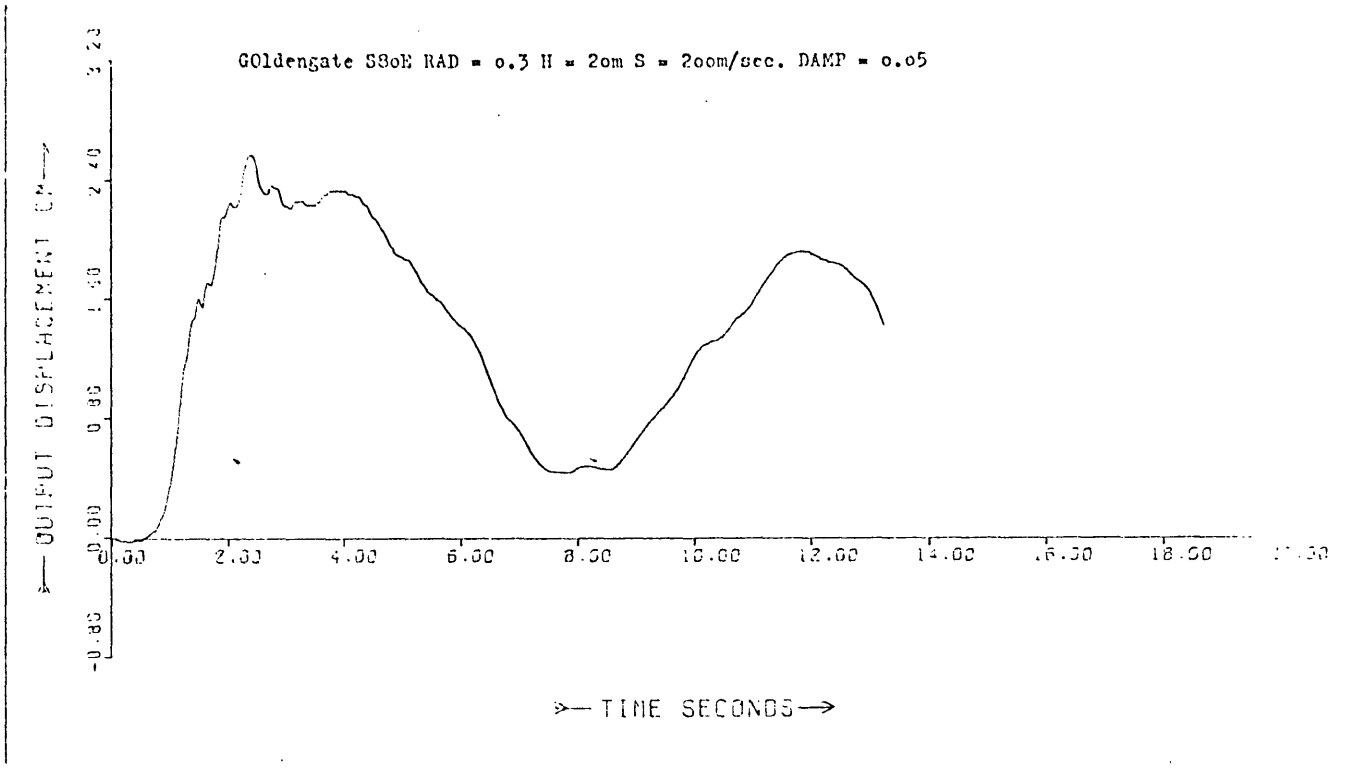


FIG. 6.69c COMPUTED SUBSURFACE DISPLACEMENT TIME HISTORY AT SITE NO.6.38

15m from GROUND SURFACE

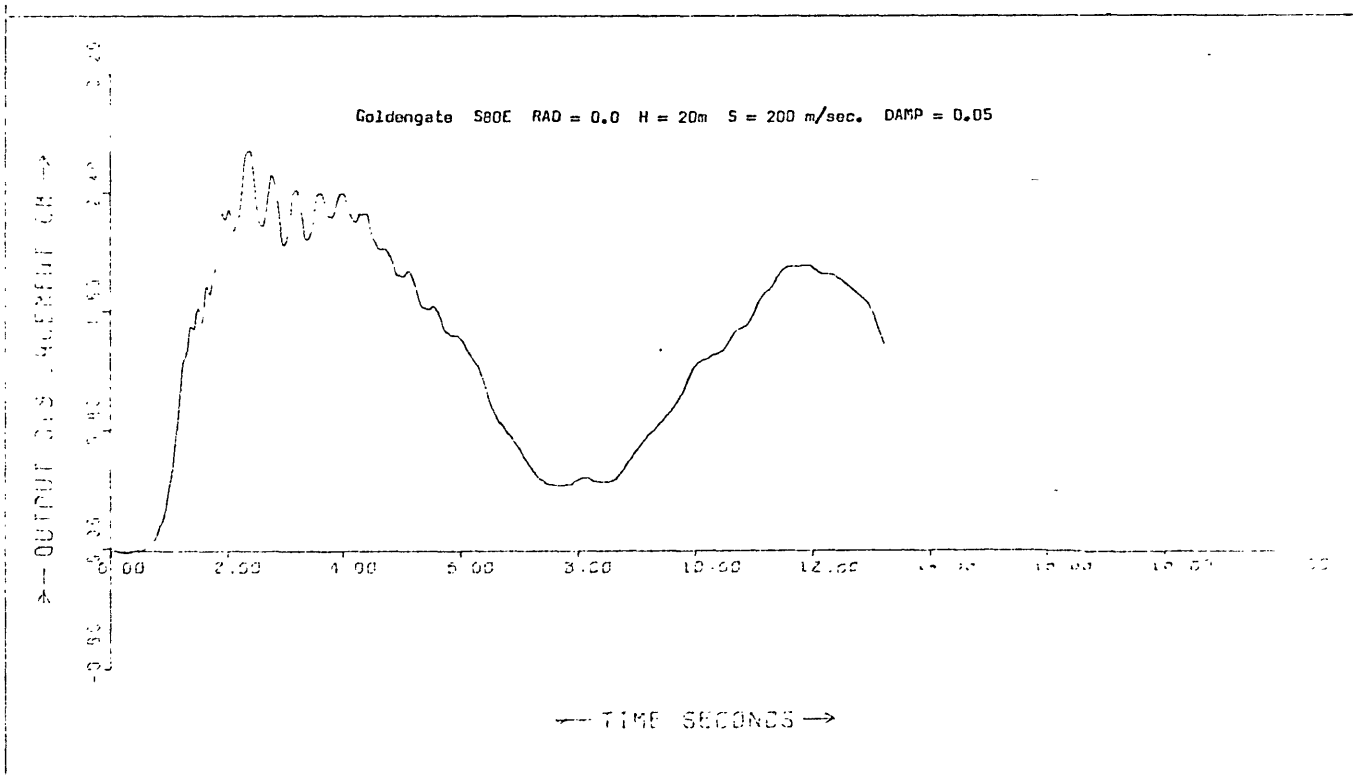


FIG6.7oc COMPUTED SUBSURFACE DISPLACEMENT TIME HISTORY AT SITE NO. 6.39

15m from GROUND SURFACE

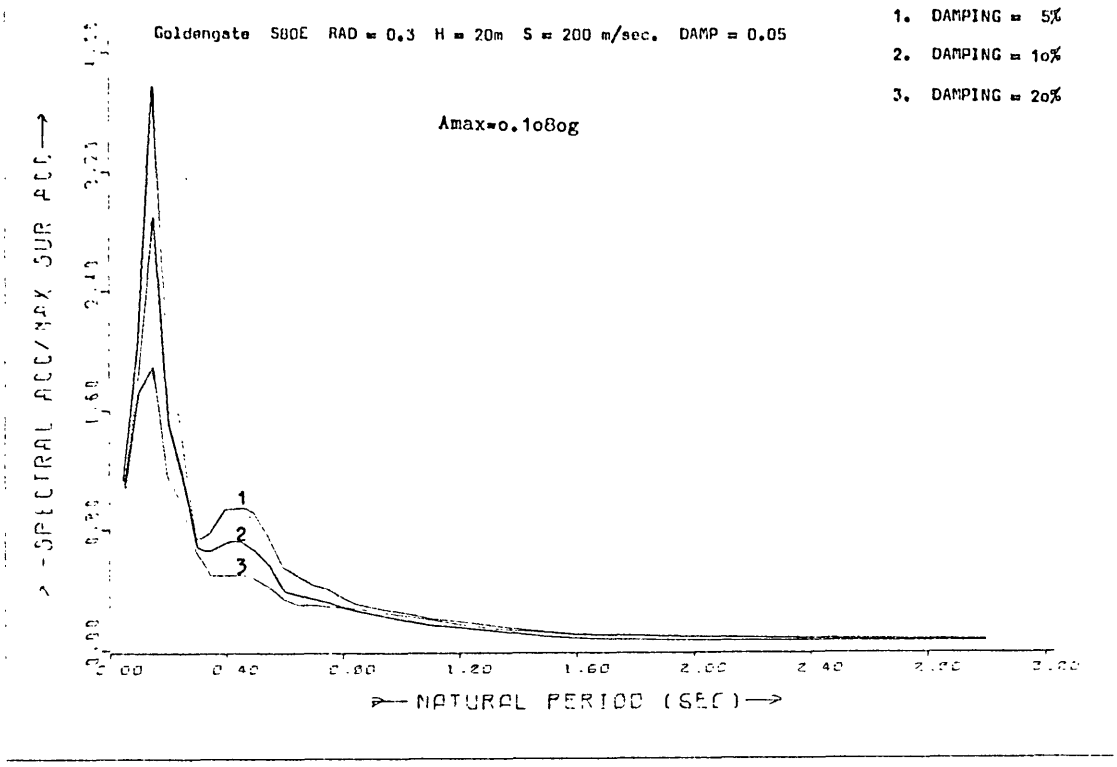


FIG.6.69d COMPUTED SUBSURFACE ACCELERATION RESPONSE SPECTRA AT SITE NO.6.38

15m from GROUND SURFACE

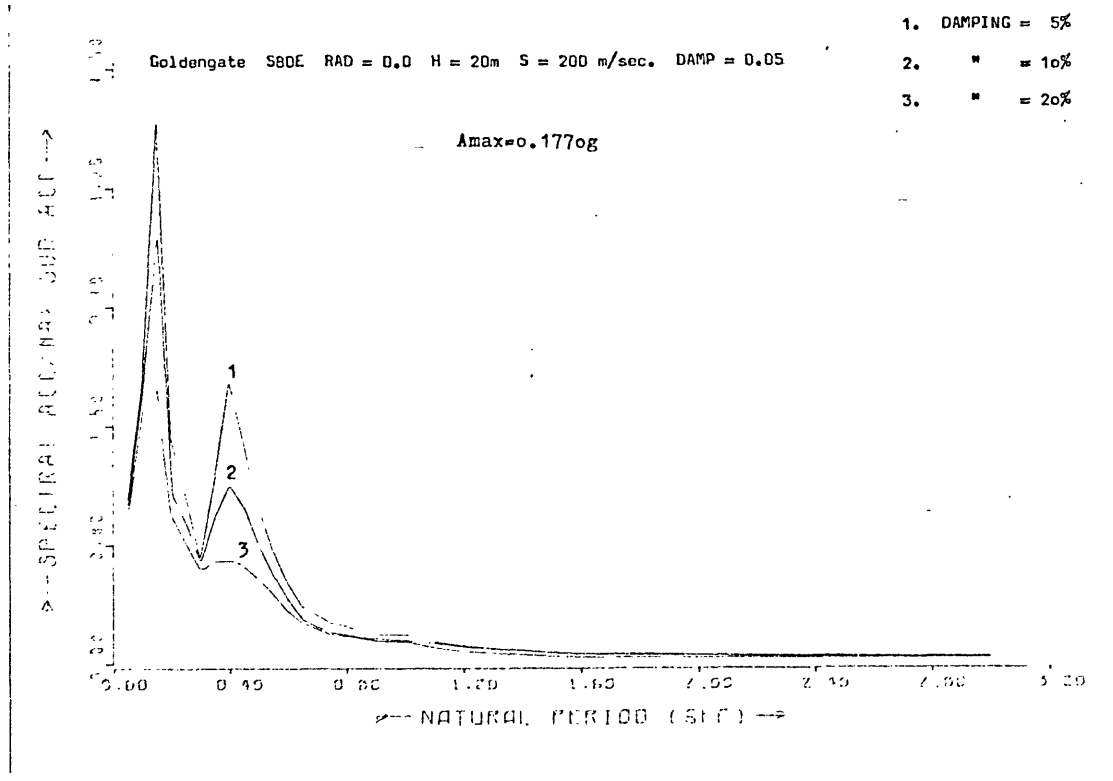


FIG.6.7od COMPUTED SUBSURFACE ACCELERATION RESPONSE SPECTRA AT SITE NO. 6.39

15m from GROUND SURFACE

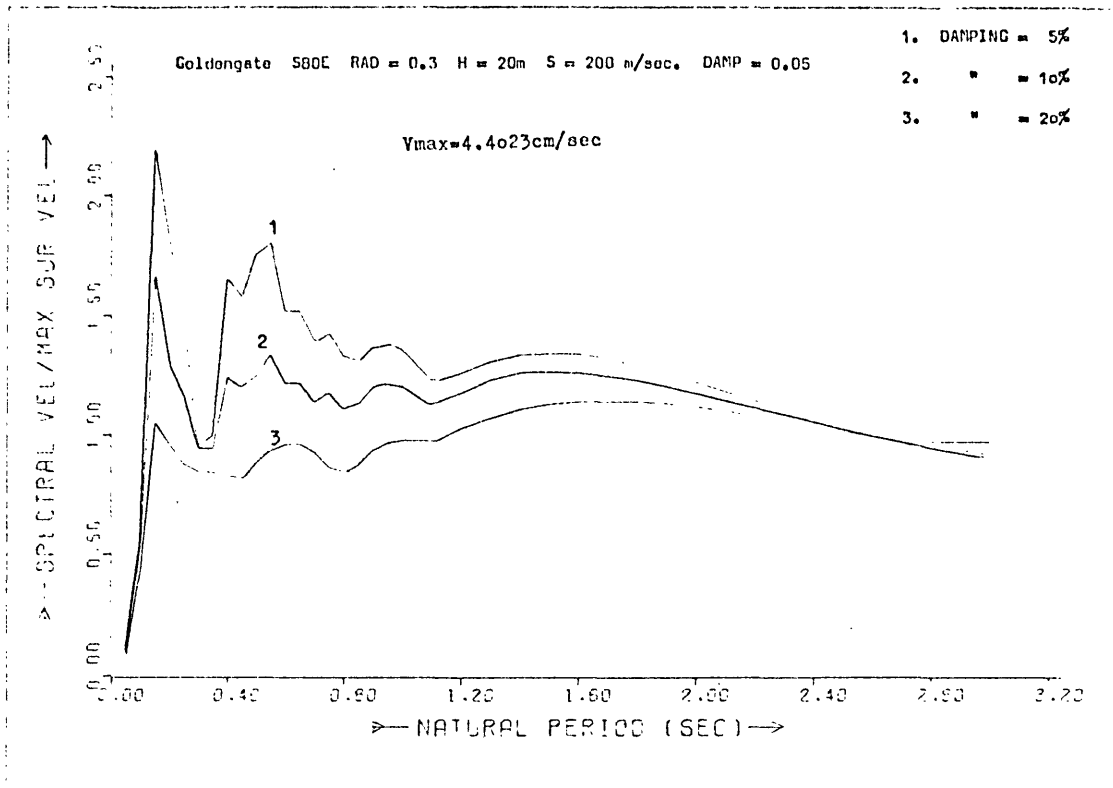


FIG 6.69e COMPUTED SUBSURFACE VELOCITY RESPONSE SPECTRA AT SITE NO. 6. 38

15m from GROUND SURFACE

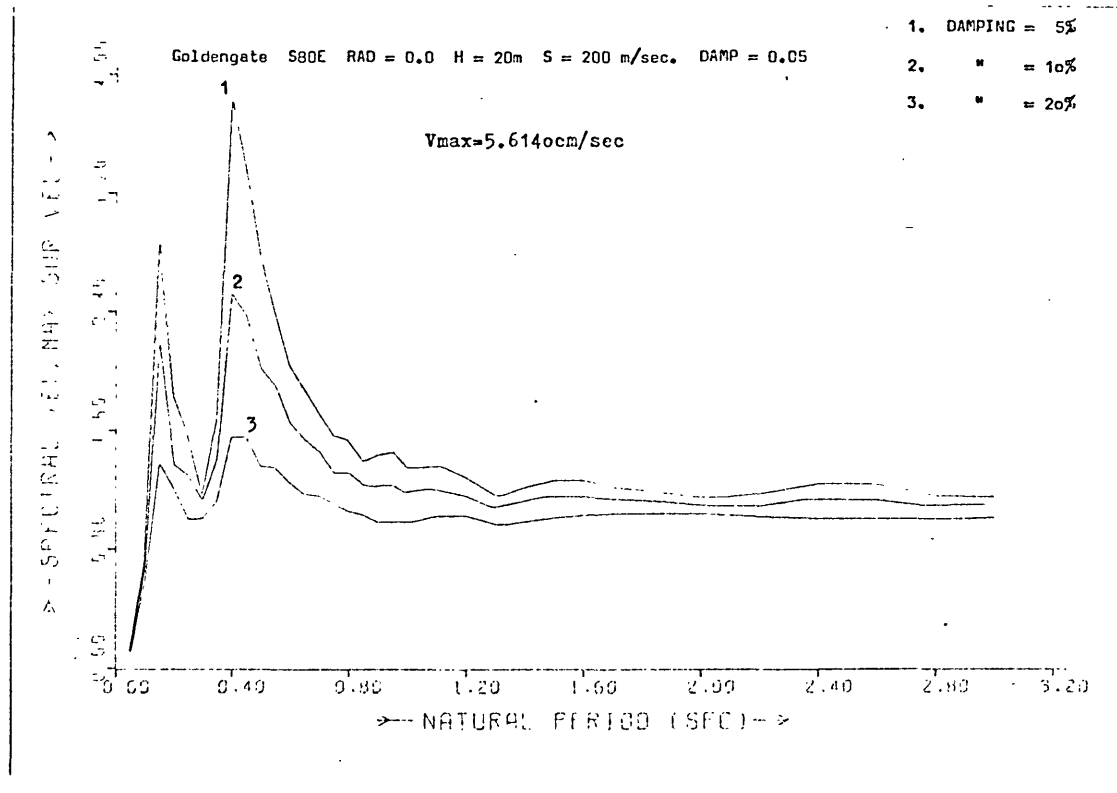


FIG 6.70e COMPUTED SUBSURFACE VELOCITY RESPONSE SPECTRA AT SITE NO. 6. 39

15m from GROUND SURFACE

DATA ON INFLUENCE OF BEDROCK CHARACTERISTICS ON SURFACE AND SUBSURFACE RESPONSE

DISTANCE FROM SURFACE (m)	MAX ABS. ACC. (g)		$1 - \frac{ACC_{RAD}}{ACC_{0.0}} \times 100$	MAX ABS. VEL. (cm/sec.)		$1 - \frac{VEL_{RAD}}{VEL_{0.0}} \times 100$	MAX. ABS. DIS. (cm)		$1 - \frac{DIS_{RAD}}{DIS_{0.0}} \times 100$
	RAD = 0.0	RAD = 0.3		RAD = 0.0	RAD = 0.3		RAD = 0.0	RAD = 0.3	
0.0	0.24	0.15	37.5%	8.63	5.75	33.41%	3.02	2.72	9.94%
5.0	0.15	0.09	40%	7.94	5.28	35.50%	2.97	2.71	8.75%
10.0	0.135	0.086	36%	6.67	4.81	27.88%	2.86	2.66	7.0%
15.0	0.18	0.11	38.9%	5.61	4.40	21.6%	2.70	2.58	4.5%

TABLE 6.6

An examination of table 6.6 shows that radiation damping ratio has a considerable effect on peak subsurface acceleration, velocity and displacement. For the rock formation having a shear wave velocity of 660 m/sec. the maximum accelerations, velocities and displacement vary from 36% to 40%, 21.6% to 33.5% and 8.75% to 4.5%, respectively, of the maximum accelerations, velocities and displacements, if the underlying rock formationwere completely rigid, and they are either less or more of the percentages of reductions computed at the surface of the deposit. The degree of influence of radiation damping ratio on subsurface response is very much dependent on the subsurface coordinates at which the response is calculated and the contribution of modal components to that point.

The frequencies of seismic motions at the specified points in the overburden are clearly reflected in the normalized acceleration spectrum shown in figs. 6.69d and 6.70d. The differences in the frequency characteristics of the computed motions are also significant.

Figs. 6.69e and 6.70eshow the velocity response spectrum obtained at the required coordinates. The observed dissimilarities of the two sets of spectrum clearly illustrate the strong influence of bedrock characteristics on computed subsurface shapes of velocity spectrum.

6.10.1. CONCLUDING REMARKS

The observations made and the data presented in this section indicate that:

a) The subsurface response of a soil deposit is highly influenced by stiffness characteristics of bedrock formation. The degree of influence is very much dependent on vibration mode shapes and the subsurface coordinate at which the

response is calculated.

b) The results of these two groups of calculations indicate that a subsurface increase in distance may increase or decrease influence of stiffness characteristics of bedrock formation on subsurface response.

c) Influence of radiation damping ratio on computed surface response may be less or more than that of subsurface response.

CHAPTER 7

INFLUENCE OF GROUND SOFTNESS, BEDROCK MOTION AND DEPTH TO BEDROCK ON GROUND RESPONSE

7.1. INTRODUCTION

It has been observed in the field that similar structures behave quite differently during earthquakes, depending upon the nature of the foundation soils. From the study of buildings and structures damaged during earthquakes, it has been observed and concluded that the vib rational characteristics of these structures are closely associated with soil conditions.

In the previous chapter, it was shown that radiation damping influences the response of foundations to seismic loading considerably. In this chapter an attempt will be made to study the manner by which response of a deposit with given bedrock characteristics is influenced by its softness, bedrock motion and depth to bedrock. A comparison between the values for the average ratio of maximum velocity/maximum acceleration and predominant period for deep cohesionless soil conditions, computed by the method developed and field recorded data from previous earthquakes, will be considered. The discussion will then be closed by means of a design example to illustrate the engineering significance of the proposed technique.

7.2. INFLUENCE OF GROUND SOFTNESS ON GROUND RESPONSE

To throw some light on the influence of ground softness on ground

response, five sites consisting of soft clay, medium clay, clay with high water content, dense sand and cemented sand, were analysed.

7.2.1. SOIL PROPERTIES FOR THE SITES

The soil depth for all sites was assumed to be 75m. It was further assumed that all the deposits were underlain by rock which had a shear wave velocity of 1500m/sec. The hysteretic damping ratio for all sites was to be uniform, equal to 0.2 and the same for each mode. The shear wave velocities for each site are shown in figs. 7.1 through 7.5. Radiation damping ratio for each site were calculated on the basis that this ratio would be roughly proportional to shear wave velocity of the overburden/shear wave velocity of its underlying rock (i.e. deviations due to density changes between the two mediums are small and for practical purposes may normally be disregarded). The damping values were assumed to be equal for all deposits. However, this might not always be the case, higher values associated with loose deposits might reduce the build-up of response considerably. Lack of quantitative data on damping values associated with each deposit does not at the present time permit one to take this effect into account.

7.2.2. BEDROCK MOTIONS FOR THIS STUDY

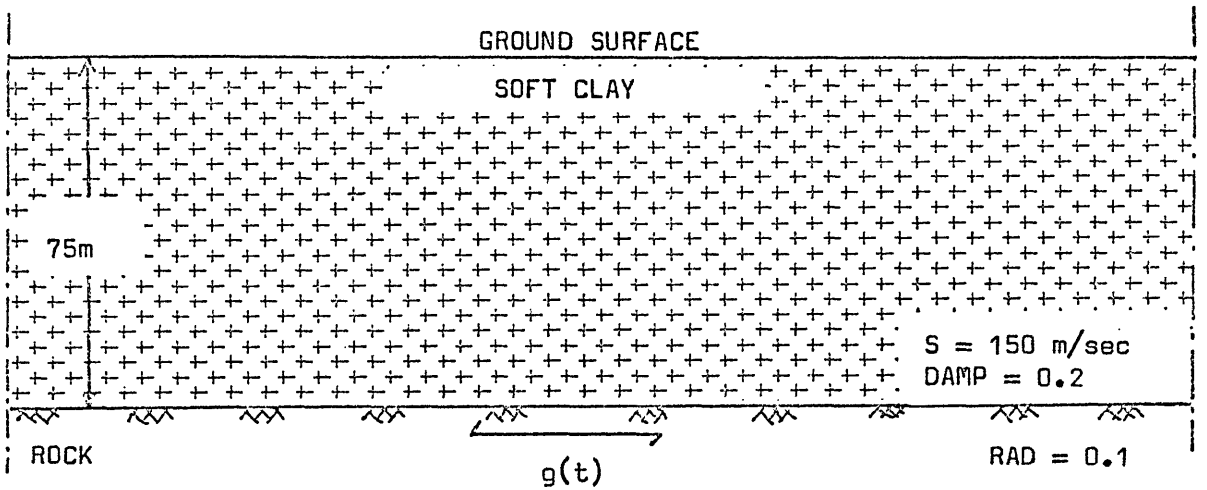
Two bedrock motions were used for this study. Parkfield-2 and Parkfield-5 with their full duration of 18.7 sec. and 15.5 sec. respectively.

7.2.3. RESULTS OF THE STUDY

Results of the calculations in terms of absolute surface acceleration, velocity and displacement, as well as acceleration,

velocity and displacement response spectra, are shown in figs. 7.1a,b,c, d, e,f through 7.5a,b,c,d,e,f.

Figs. 7.1d,e,f through 7.5d,e,f show computed surface acceleration, velocity and displacement response spectrum, for soft clay, medium clay, clay with high water content, dense sand and cemented sand subjected to Parkfield-2 at the bedrock level with a predominant period of 0.6 sec. An examination of these results shows that a decrease in softness results in a decrease in the fundamental period of the deposit and an increase in radiation damping ratio. It is observed that the response of soft clay, whose fundamental period is 2.0 sec. and is far from the predominant period of the bedrock motion - 0.6 sec., has shown the least amplitude of the peak acceleration spectral value, and cemented sand with a fundamental period of 0.66 sec. has shown the greatest; as the fundamental period of the overburden approaches the predominant period of the bedrock motion, a condition of resonance is simulated. Thus, the layer whose fundamental period is closest to the predominant period of bedrock motion develops the highest acceleration response. The three deposits, namely, medium clay, clay with high water content and dense sand with fundamental periods of 1.33, 1.0, 0.8, develop amplitudes of peak acceleration spectral values in ascending order. It may be noted that, as shown in figs. 7.1e to 7.5e, the maximum spectral velocities behave quite differently, the largest for soft clay and the smallest for clay with high water content and with an intermediate value for cemented sand. From these results, it is also observed that ratios of amplitude of the maximum spectral acceleration/peak ground acceleration and amplitude of maximum spectral velocity/peak ground velocity are approximately constant. Therefore, one expects to observe similar behaviour for maximum surface acceleration



RESPONSE OF HYSTERETIC DEPOSIT UNDERLAIN BY DEFORMABLE BEDROCK

SCHEMATIC SOIL PROFILE FOR SITE NO 7.1

FIG. 7.1

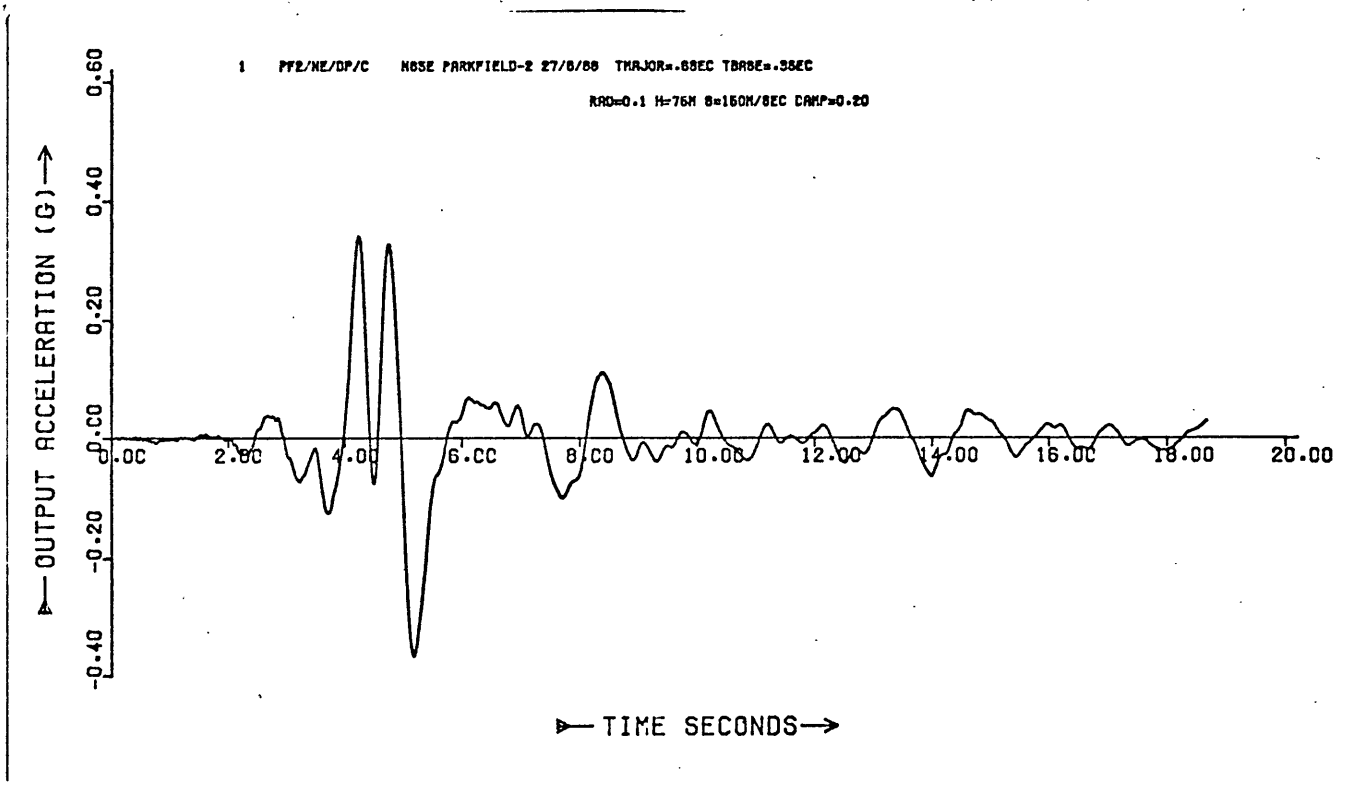


FIG.7.1a COMPUTED GROUND SURFACE ACCELERATION TIME HISTORY AT SITE NO 7.1

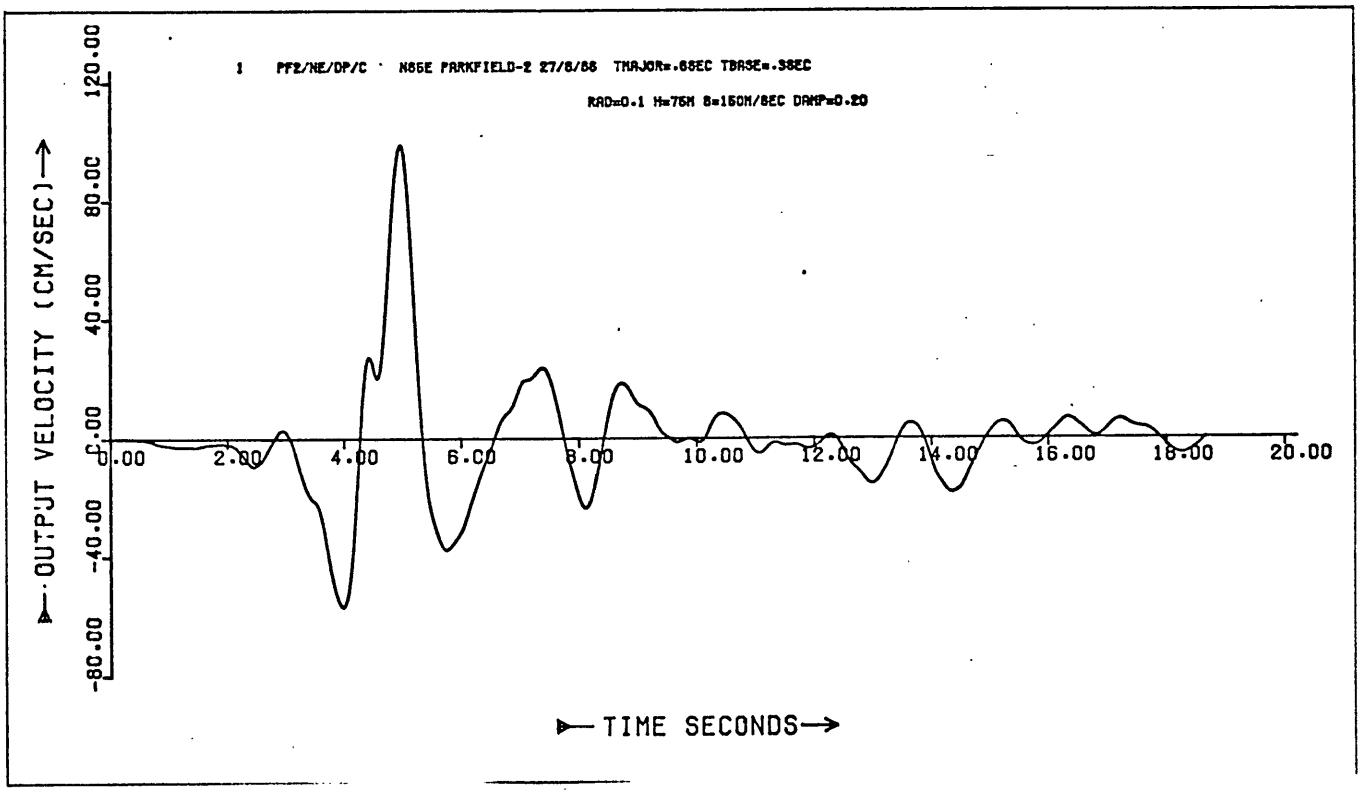


FIG.7.1b COMPUTED GROUND SURFACE VELOCITY TIME HISTORY AT SITE NO 7.1

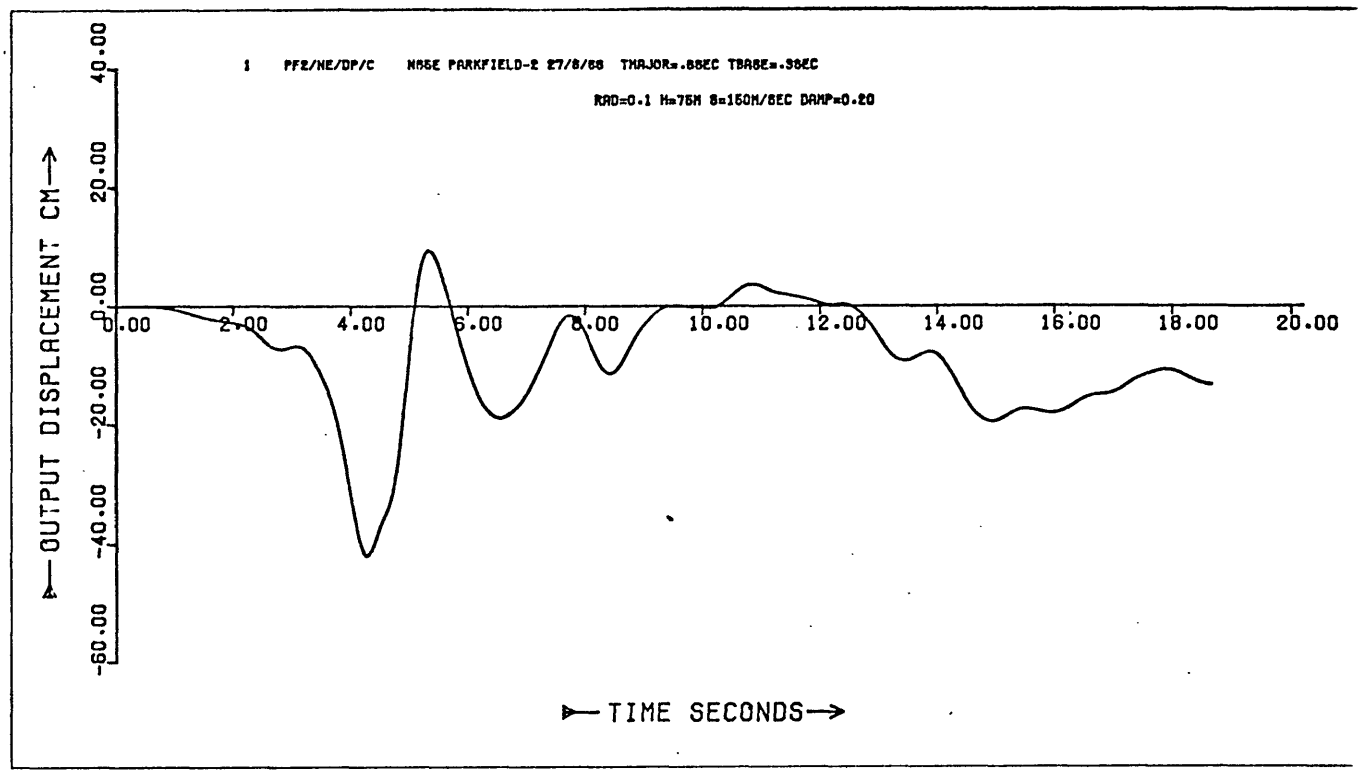


FIG.7.1c COMPUTED GROUND SURFACE DISPLACEMENT TIME HISTORY AT SITE NO 7.1

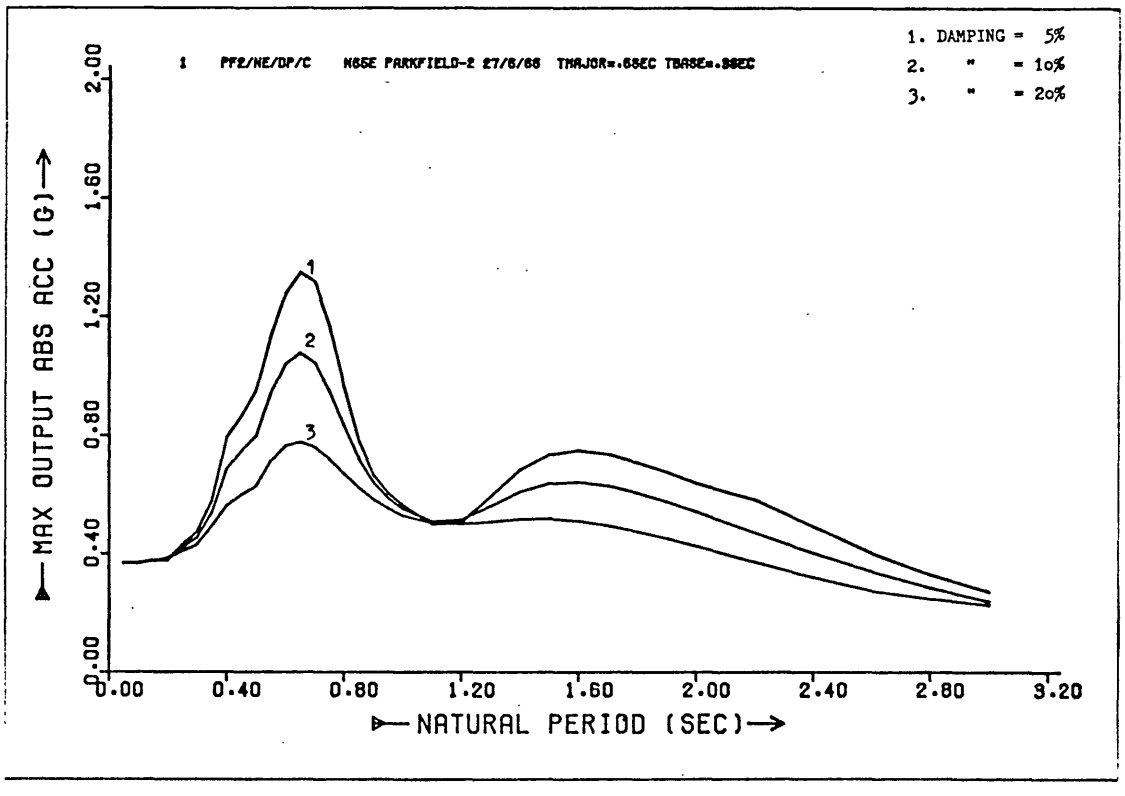


FIG.7.1d COMPUTED GROUND SURFACE ACCELERATION RESPONSE SPECTRA AT SITE NO 7.1

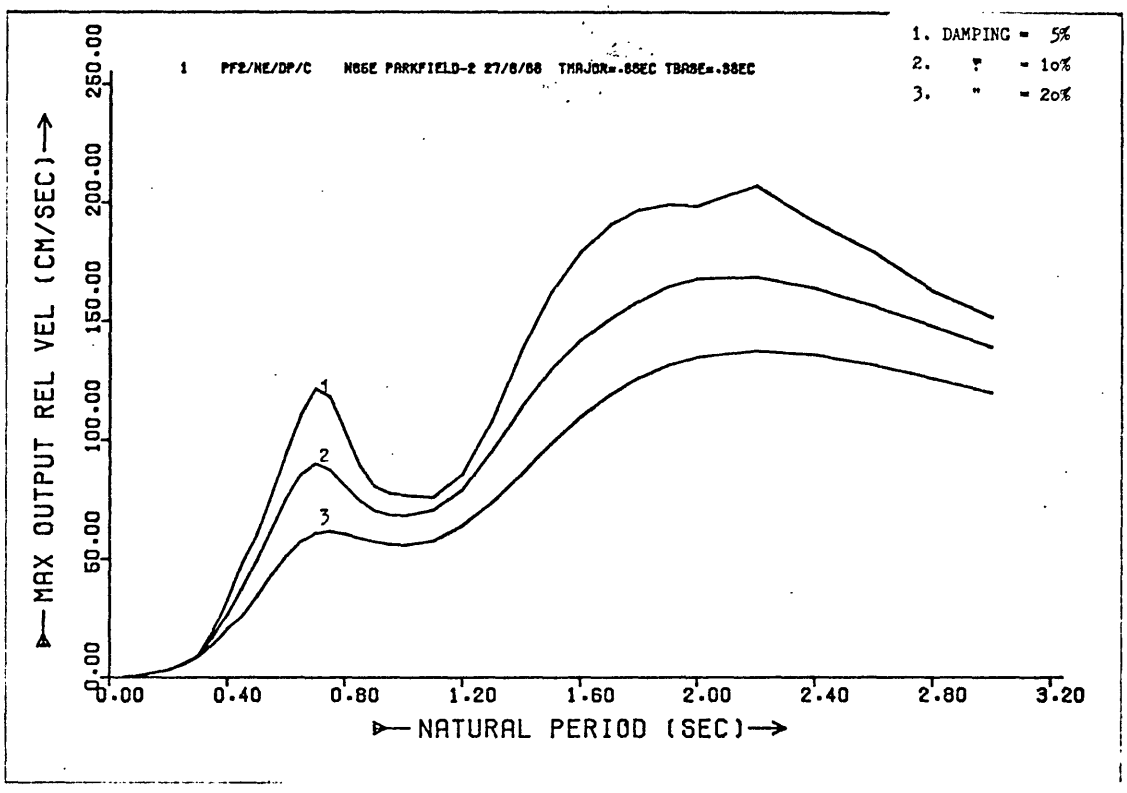


FIG. 7.1e COMPUTED GROUND SURFACE VELOCITY RESPONSE SPECTRA AT SITE NO 7.1

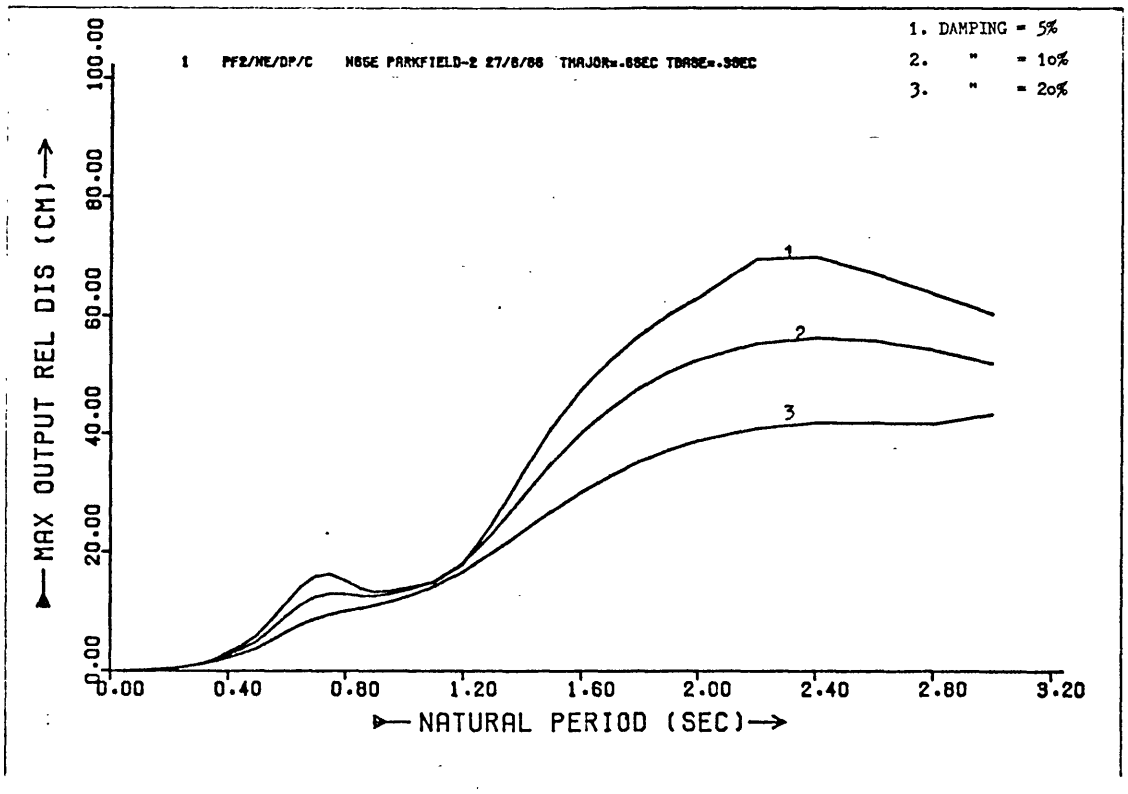
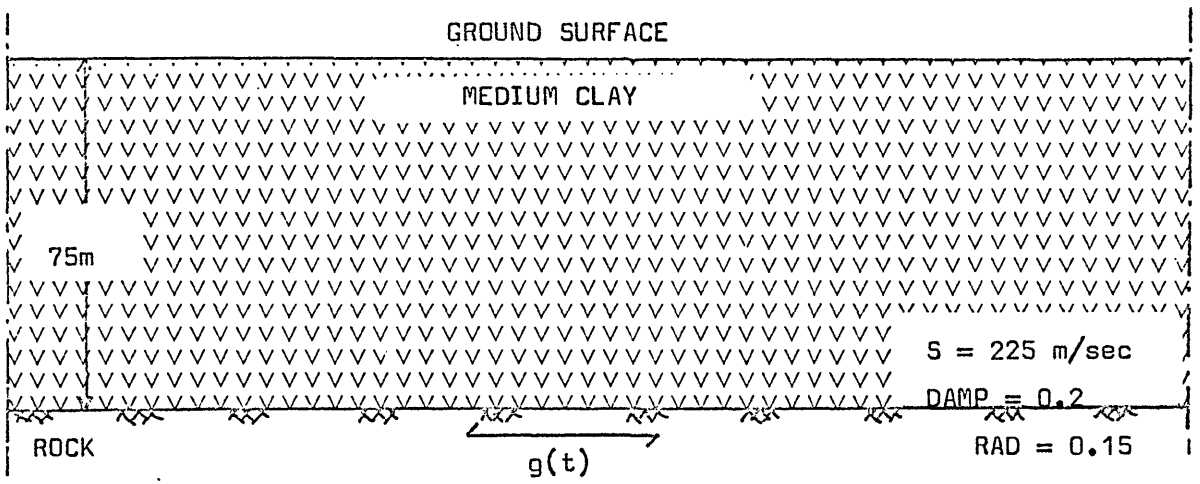


FIG. 7.1f COMPUTED GROUND SURFACE DISPLACEMENT RESPONSE SPECTRA AT SITE NO7.1



RESPONSE OF HYSTERETIC DEPOSIT UNDERLAIN BY DEFORMABLE BEDROCK

SCHEMATIC SOIL PROFILE FOR SITE NO 7.2

FIG 7.2

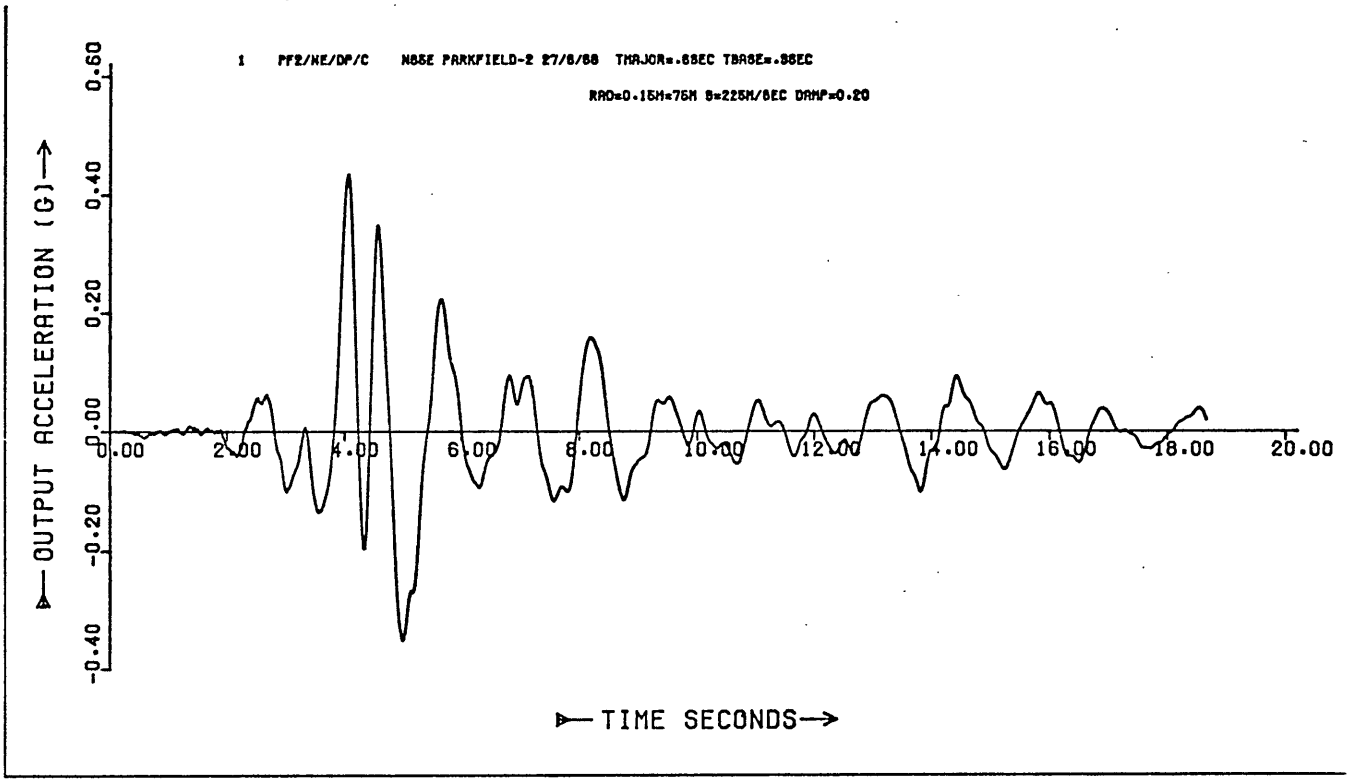


FIG.7.2a COMPUTED GROUND SURFACE ACCELERATION TIME HISTORY AT SITE NO 7.2

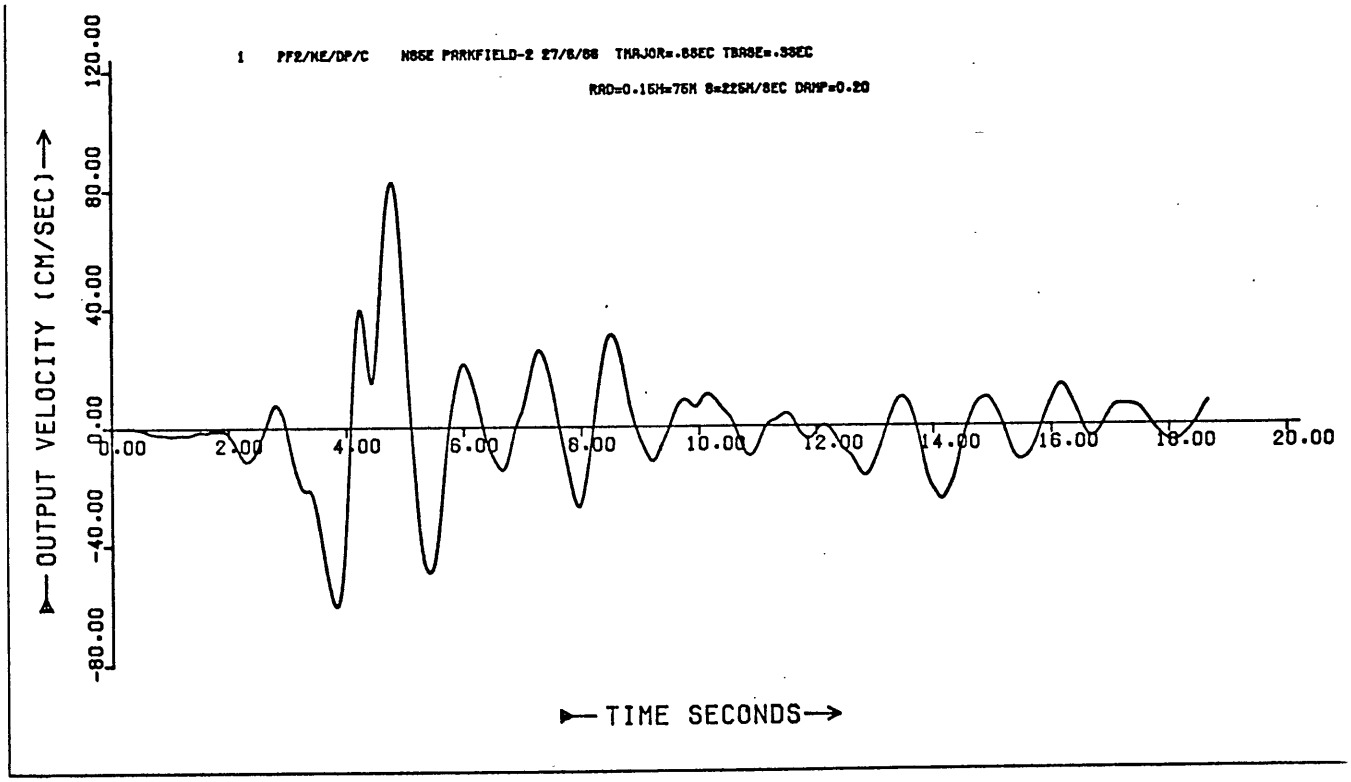


FIG. 7.2b COMPUTED GROUND SURFACE VELOCITY TIME HISTORY AT SITE NO 7.2

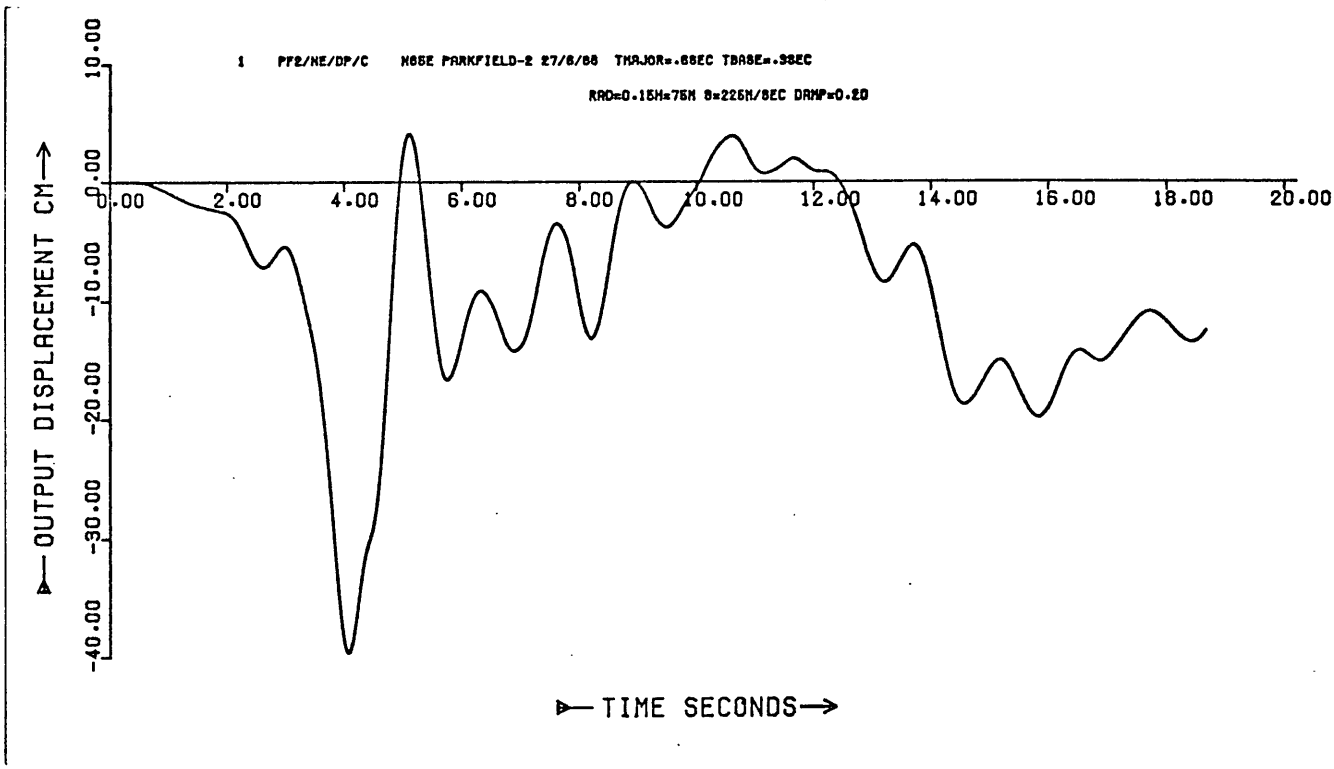


FIG. 7.2c COMPUTED GROUND SURFACE DISPLACEMENT TIME HISTORY AT SITE NO 7.2

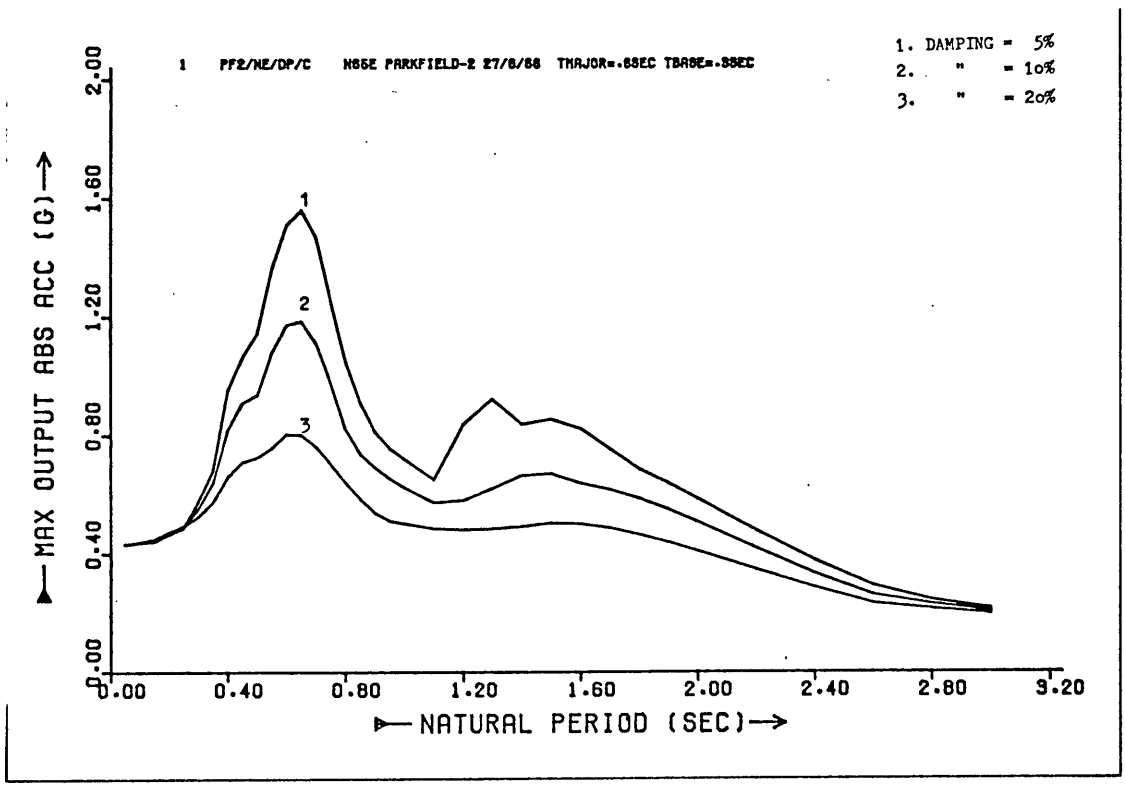


FIG. 7.2d COMPUTED GROUND SURFACE ACCELERATION RESPPONSE SPECTRA AT SITE NO 7.2

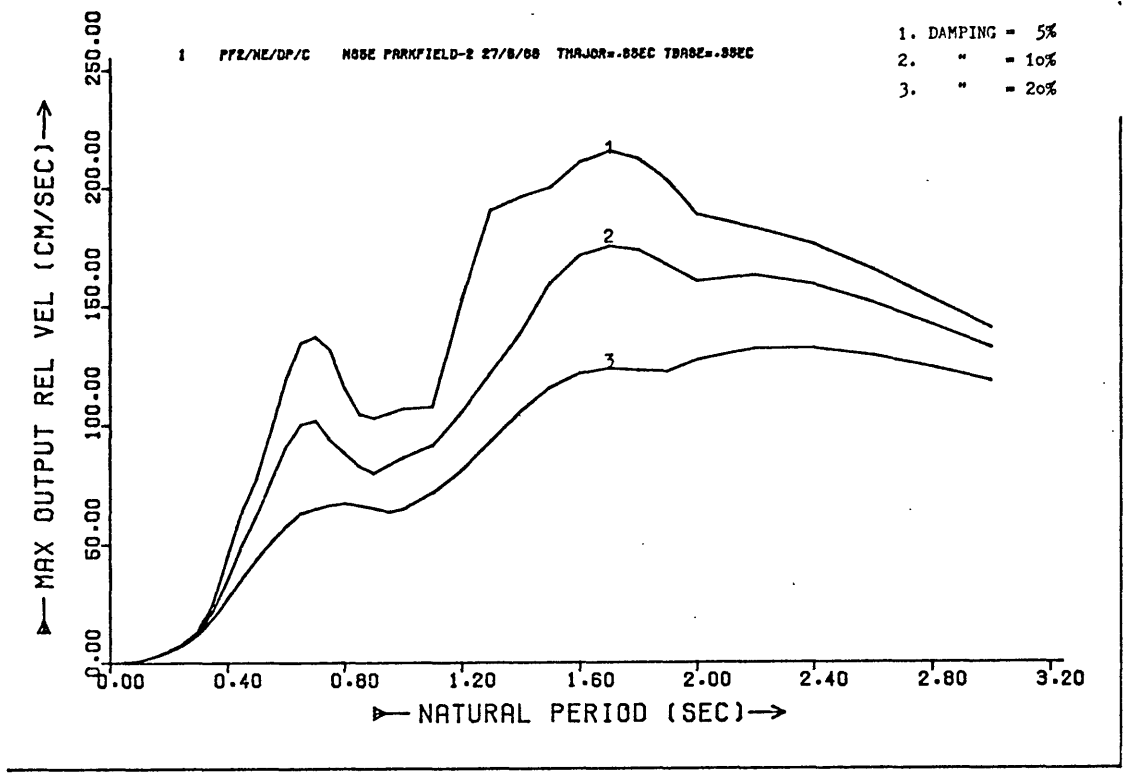


FIG. 7.2e COMPUTED GROUND SURFACE VELOCITY RESPONSE SPECTRA AT SITE NO 7.2

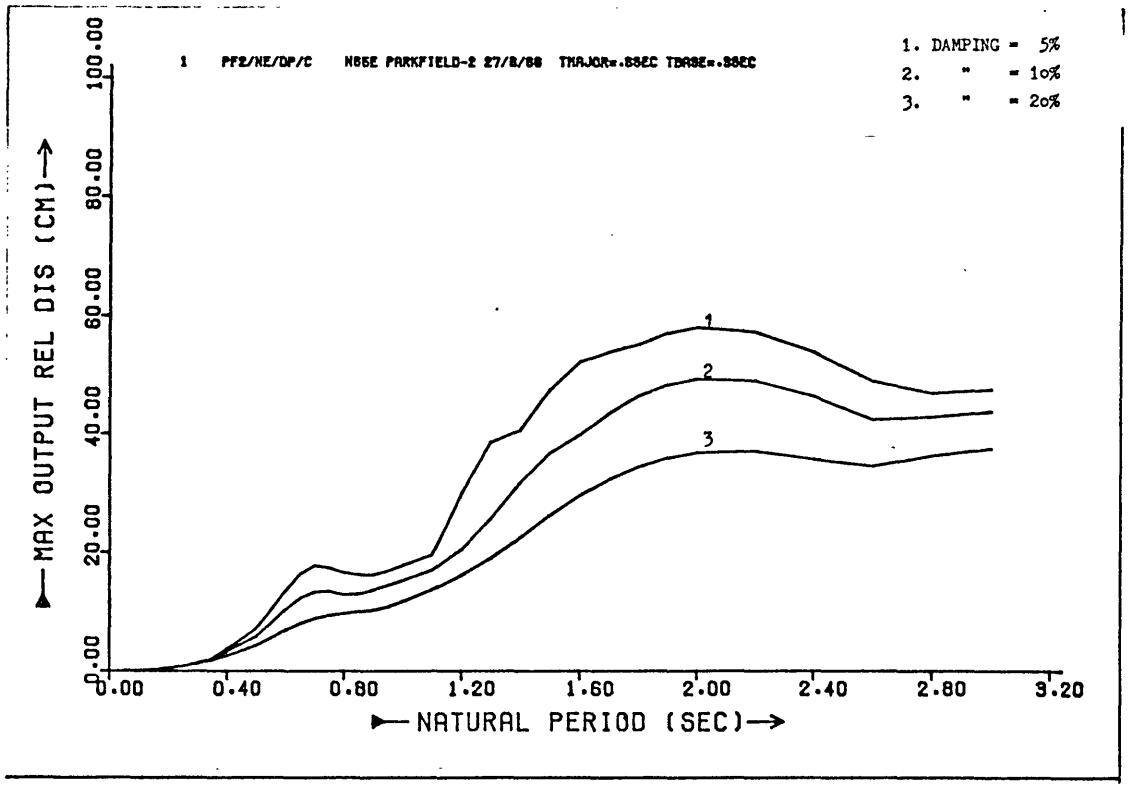
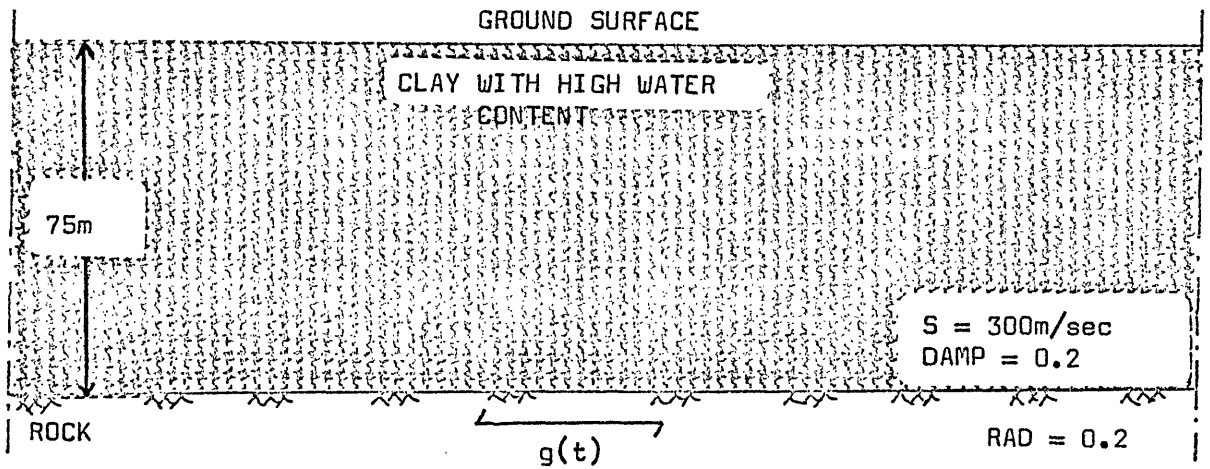


FIG. 7.2f COMPUTED GROUND SURFACE DISPLACEMENT RESPONSE SPECTRA AT SITE NO 7.2



RESPONSE OF HYSTERETIC DEPOSIT UNDERLAIN BY DEFORMABLE BEDROCK

SCHEMATIC SOIL PROFILE FOR SITE NO 7.3

FIG. 7.3

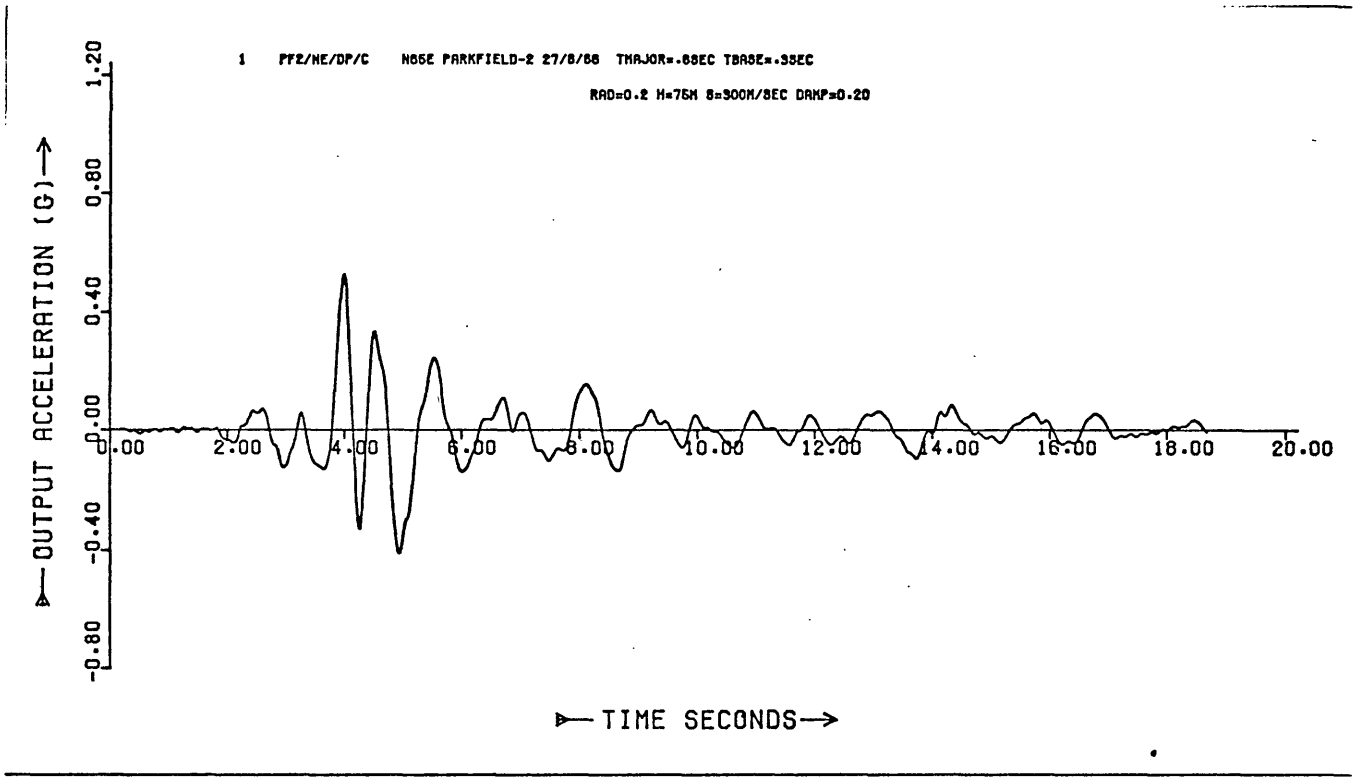


FIG.7.3a COMPUTED GROUND SURFACE ACCELERATION TIME HISTORY AT SITE NO 7.3

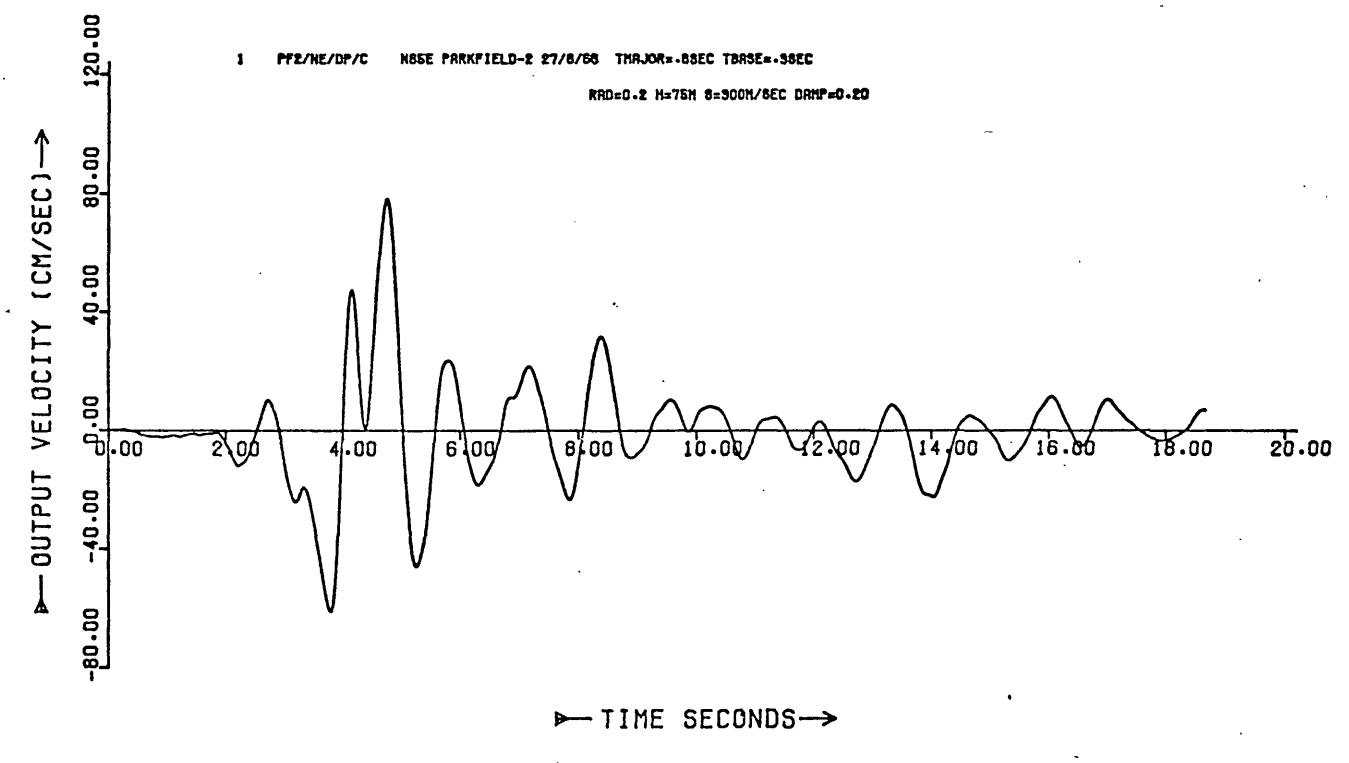


FIG.7.3b COMPUTED GROUND SURFACE VELOCITY TIME HISTORY AT SITE NO 7.3

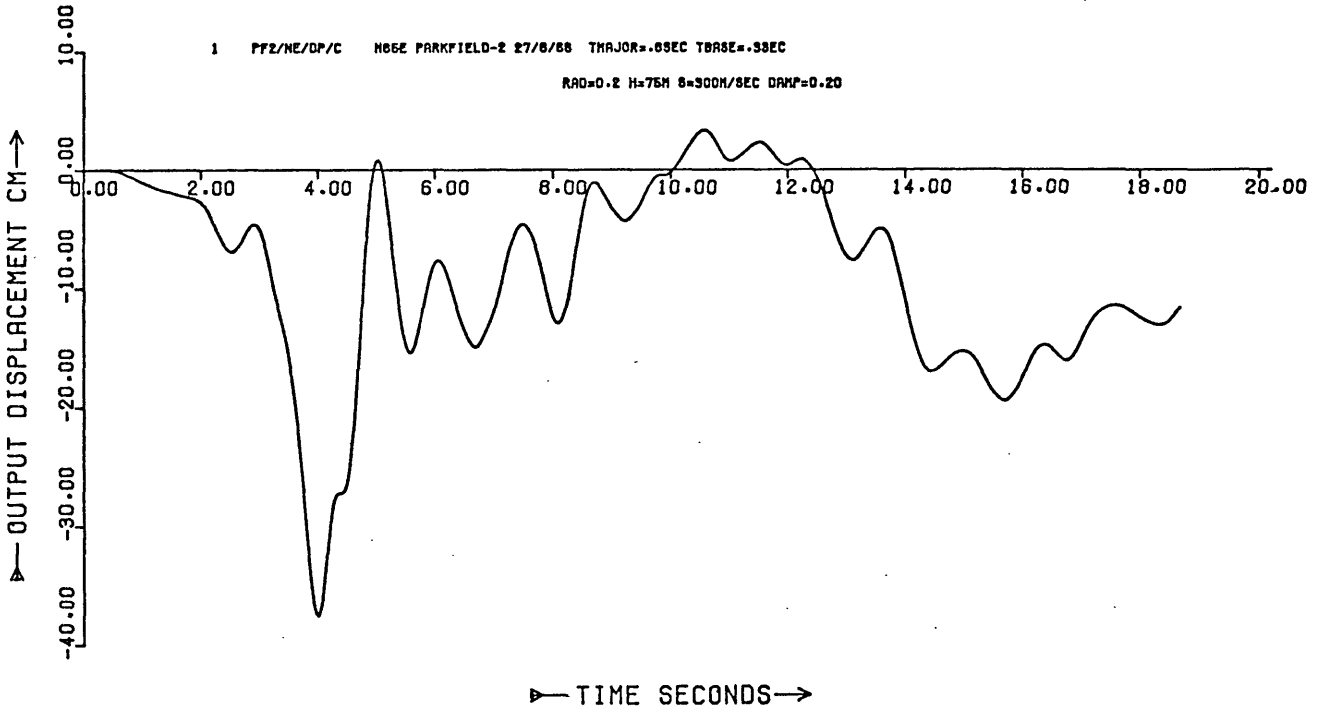


FIG. 7.3c COMPUTED GROUND SURFACE DISPLACEMENT TIME HISTORY AT SITE NO 7.3

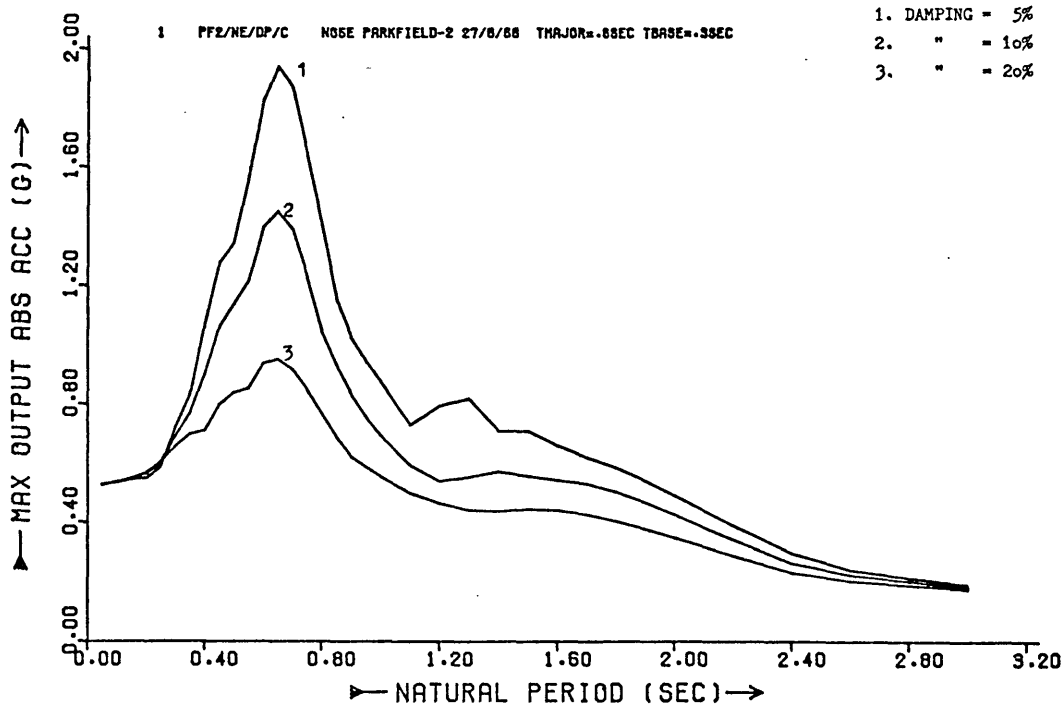


FIG. 7.3d COMPUTED GROUND SURFACE ACCELERATION RESPONSE SPECTRA AT SITE NO 7.3

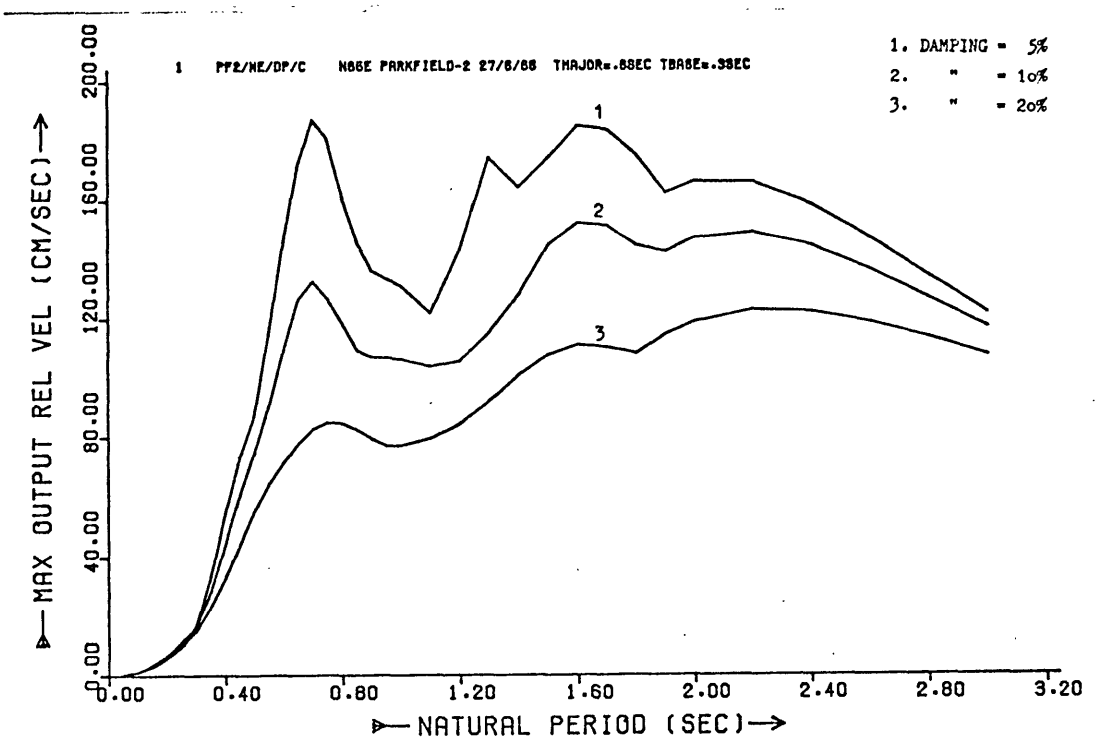


FIG. 7.3e COMPUTED GROUND SURFACE VELOCITY RESPONSE SPECTRA AT SITE NO 7.3

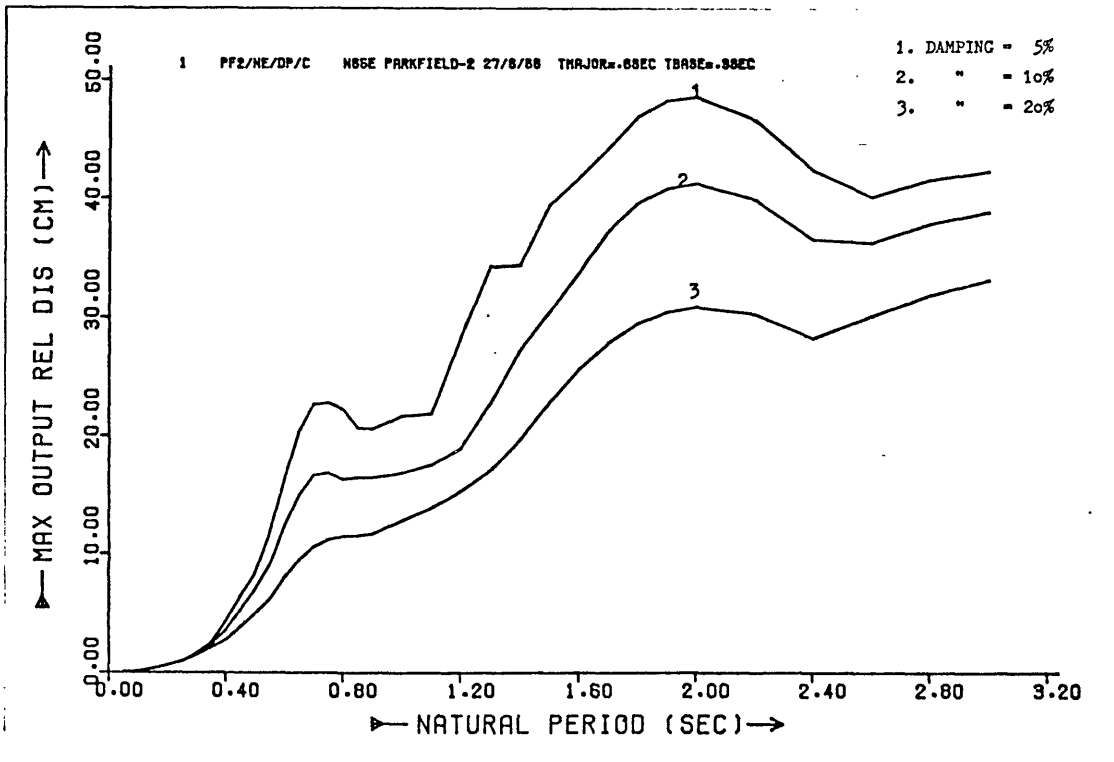
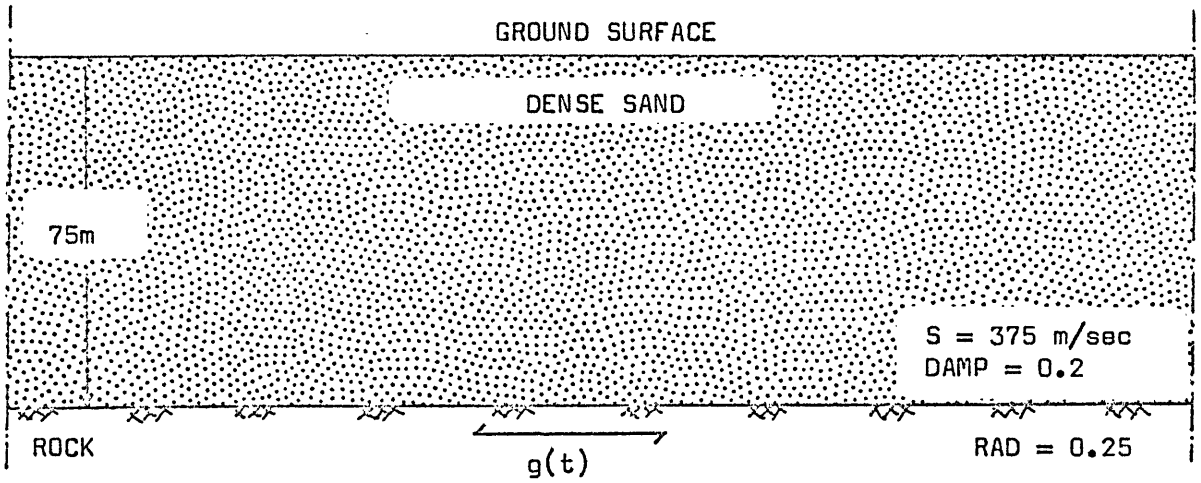


FIG. 7.3f COMPUTED GROUND SURFACE DISPLACEMENT RESPONSE SPECTRA AT SITE NO 7.3



RESPONSE OF HYSTERETIC DEPOSIT UNDERLAIN BY DEFORMABLE BEDROCK

SCHEMATIC SOIL PROFILE FOR SITE NO 7.4

FIG. 7.4

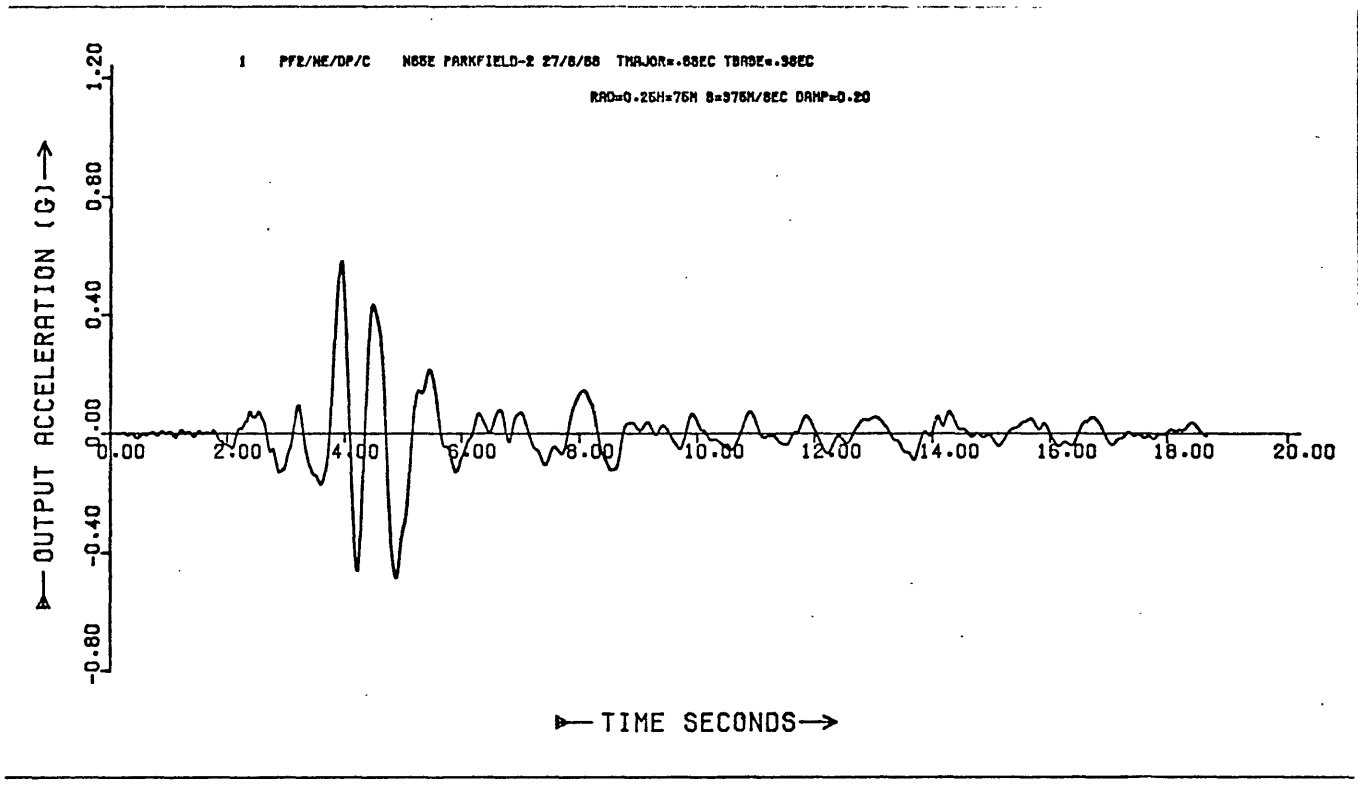


FIG. 7.4a COMPUTED GROUND SURFACE ACCELERATION TIME HISTORY AT SITE NO 7.4

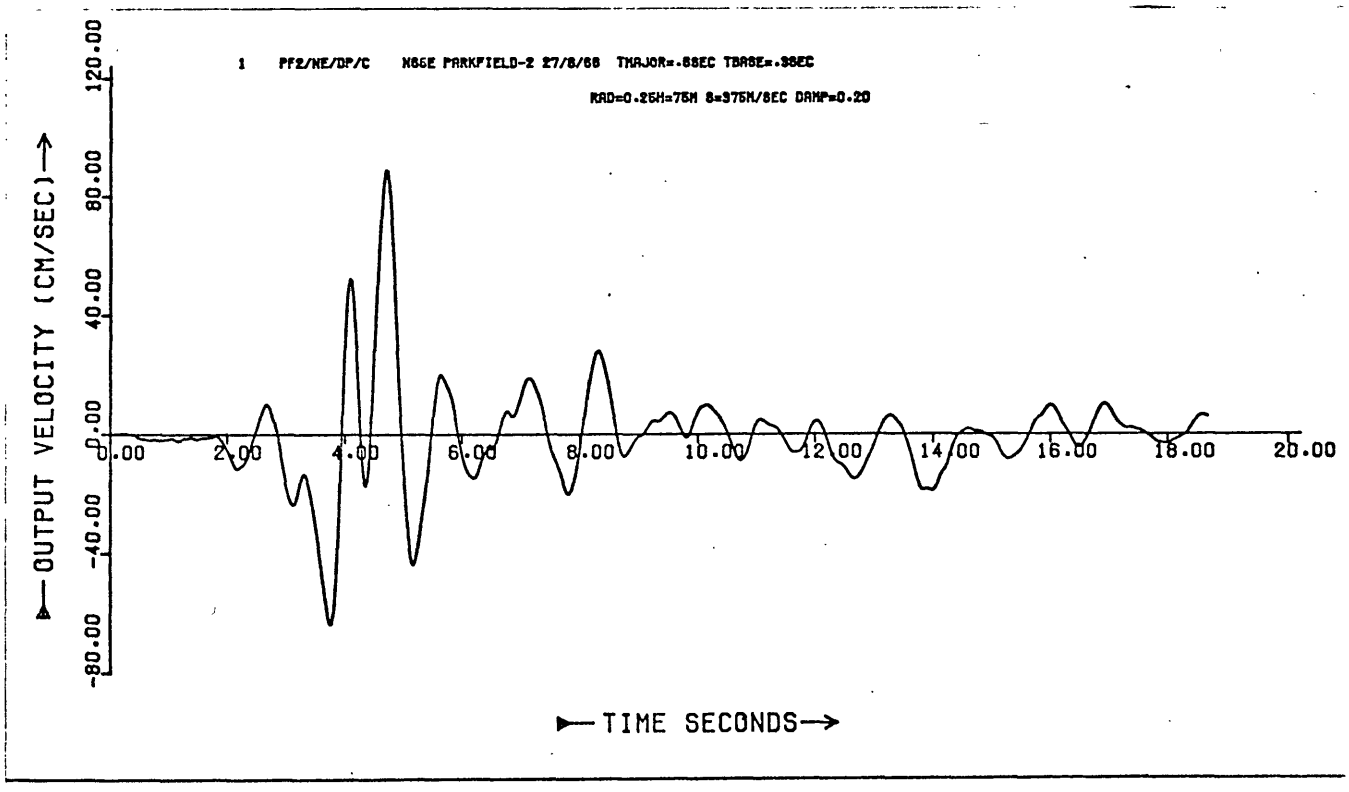


FIG. 7.4b COMPUTED GROUND SURFACE VELOCITY TIME HISTORY AT SITE NO 7.4

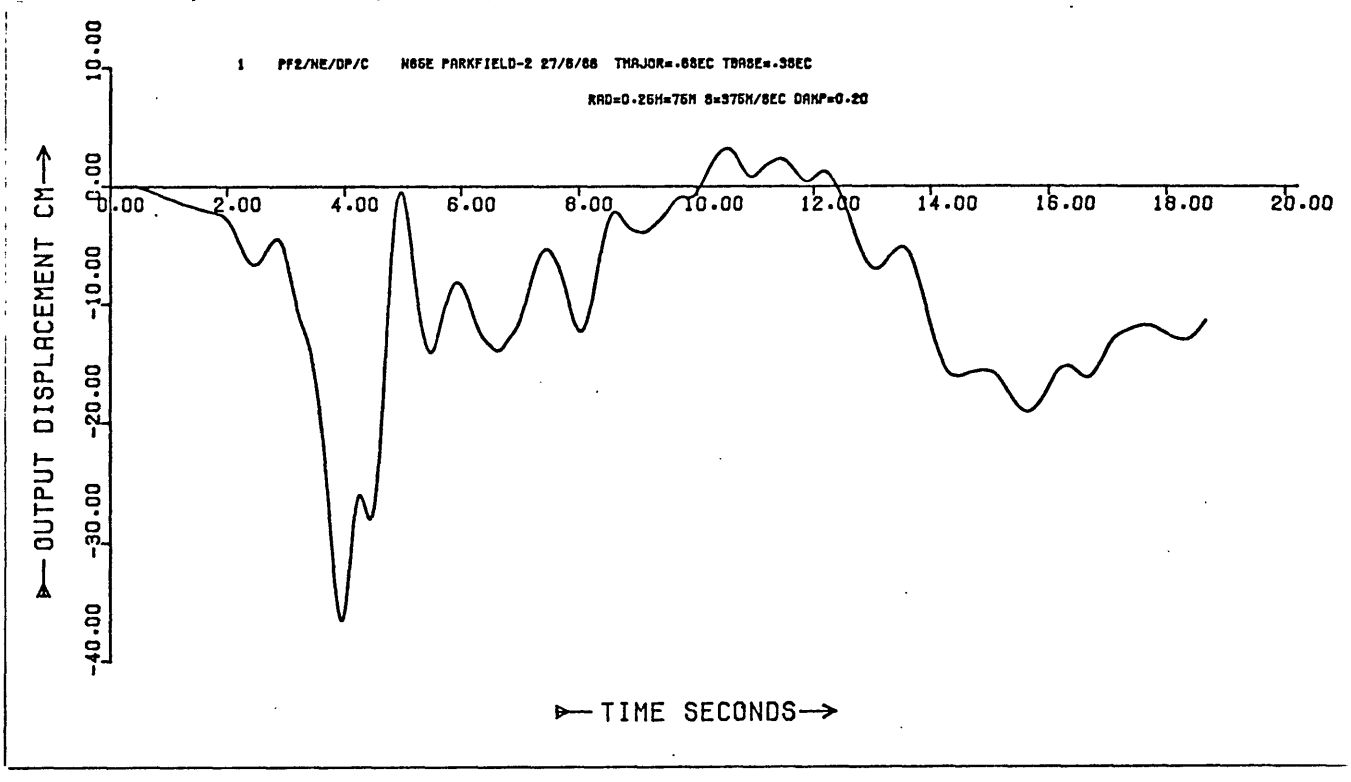


FIG. 7.4c COMPUTED GROUND SURFACE DISPLACEMENT TIME HISTORY AT SITE NO 7.4

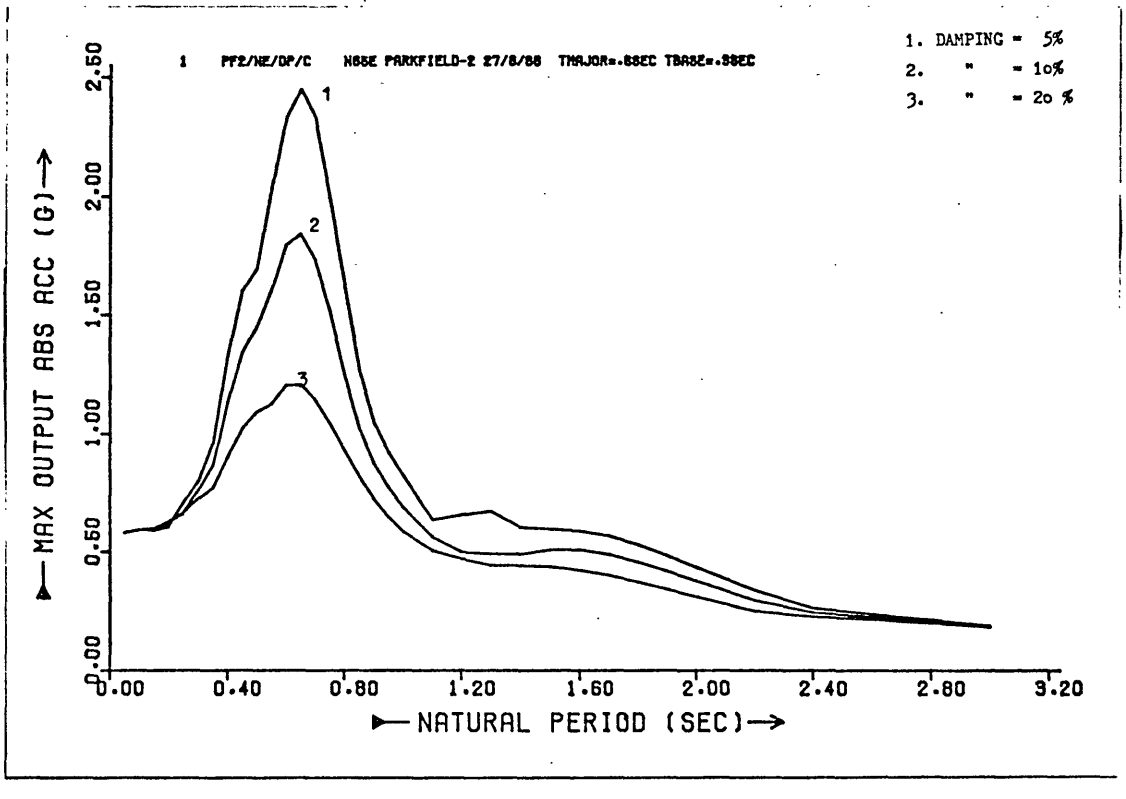


FIG. 7.4d COMPUTED GROUND SURFACE ACCELERATION RESPONSE SPECTRA AT SITE NO 7.4

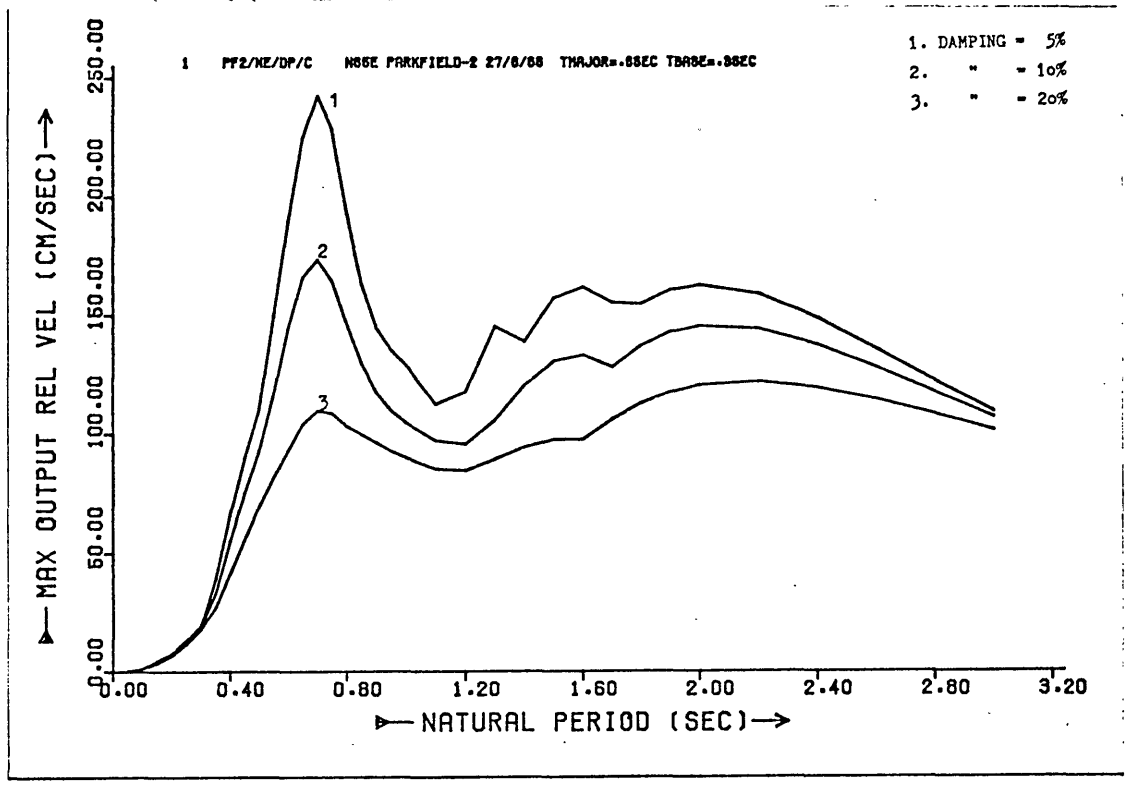


FIG. 7.4e COMPUTED GROUND SURFACE VELOCITY RESPONSE SPECTRA AT SITE NO 7.4

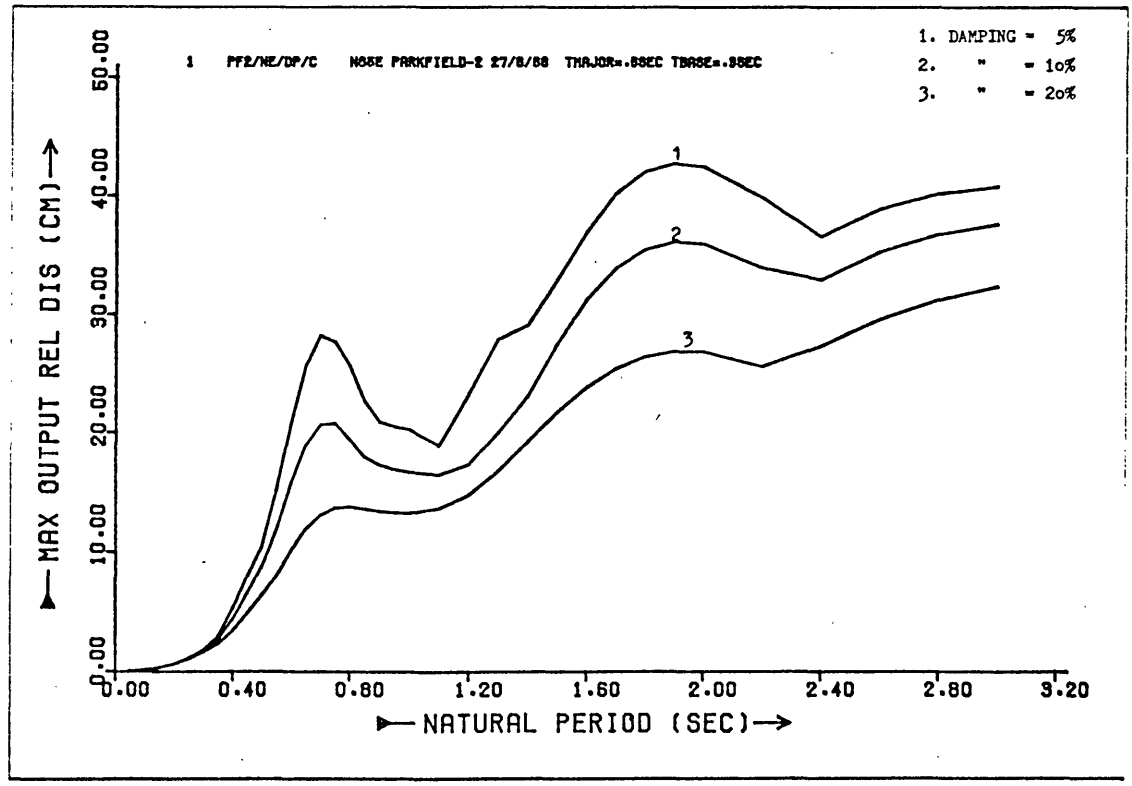
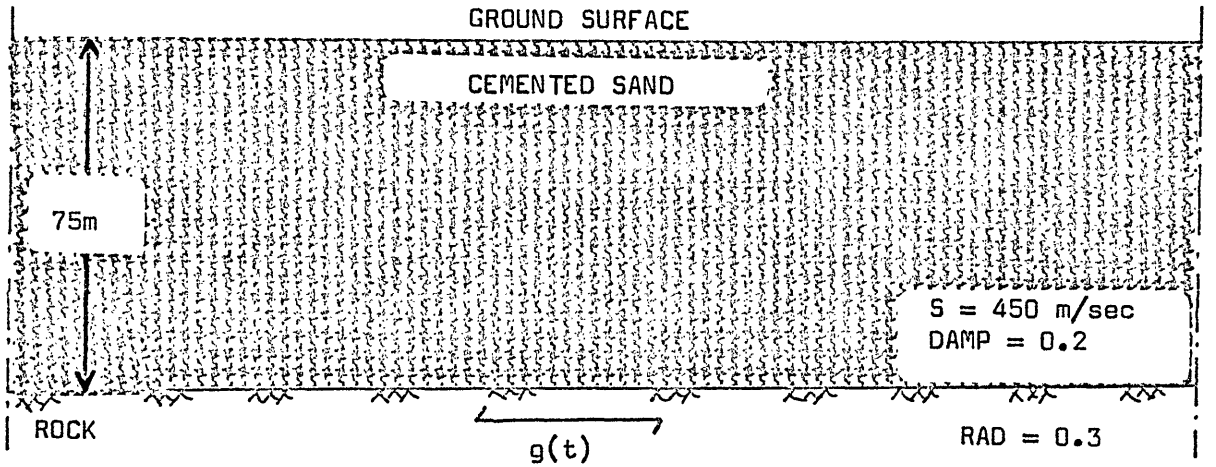


FIG. 7.4f COMPUTED GROUND SURFACE DISPLACEMENT RESPONSE SPECTRA AT SITE NO 7.4



RESPONSE OF HYSTERETIC DEPOSIT UNDERLAIN BY DEFORMABLE BEDROCK

SCHEMATIC SOIL PROFILE FOR SITE NO 7.5

FIG. 7.5

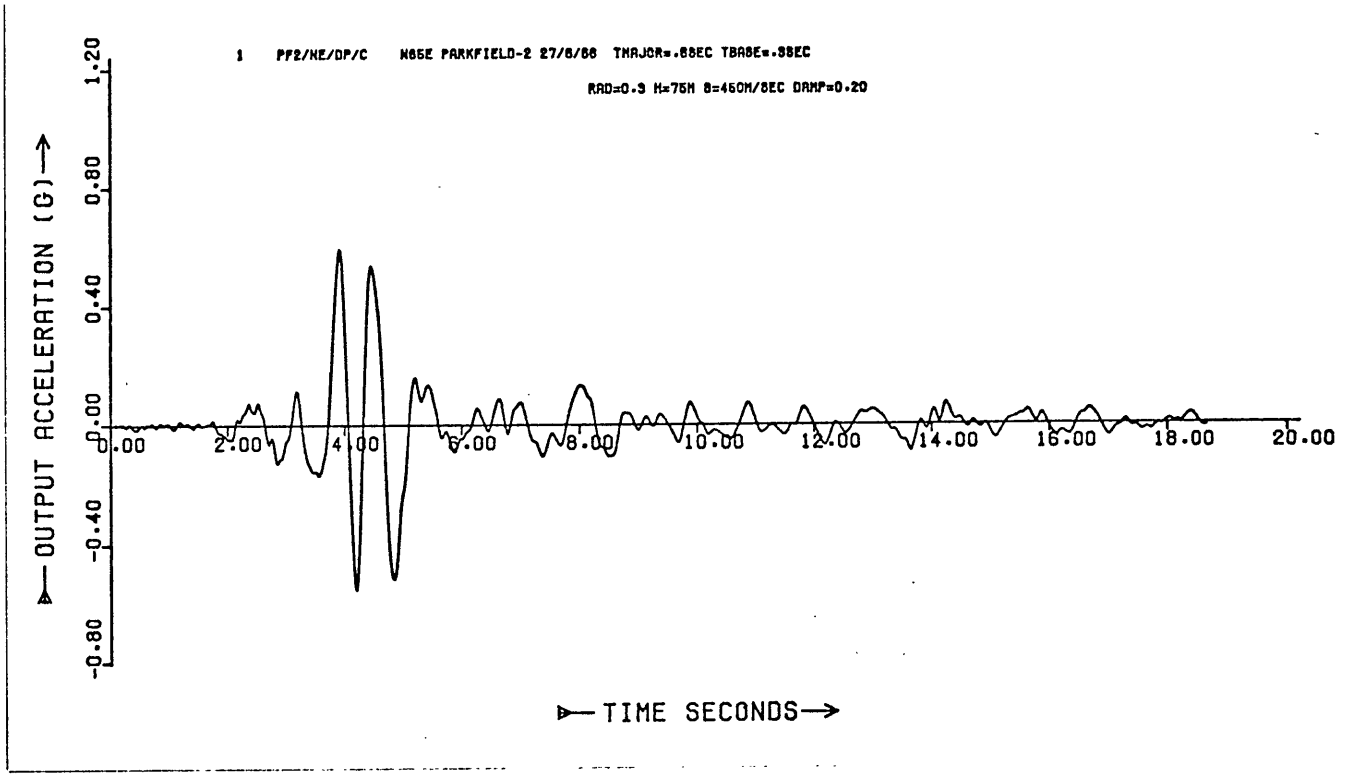


FIG.7.5a COMPUTED GROUND SURFACE ACCELERATION TIME HISTORY AT SITE NO 7.5

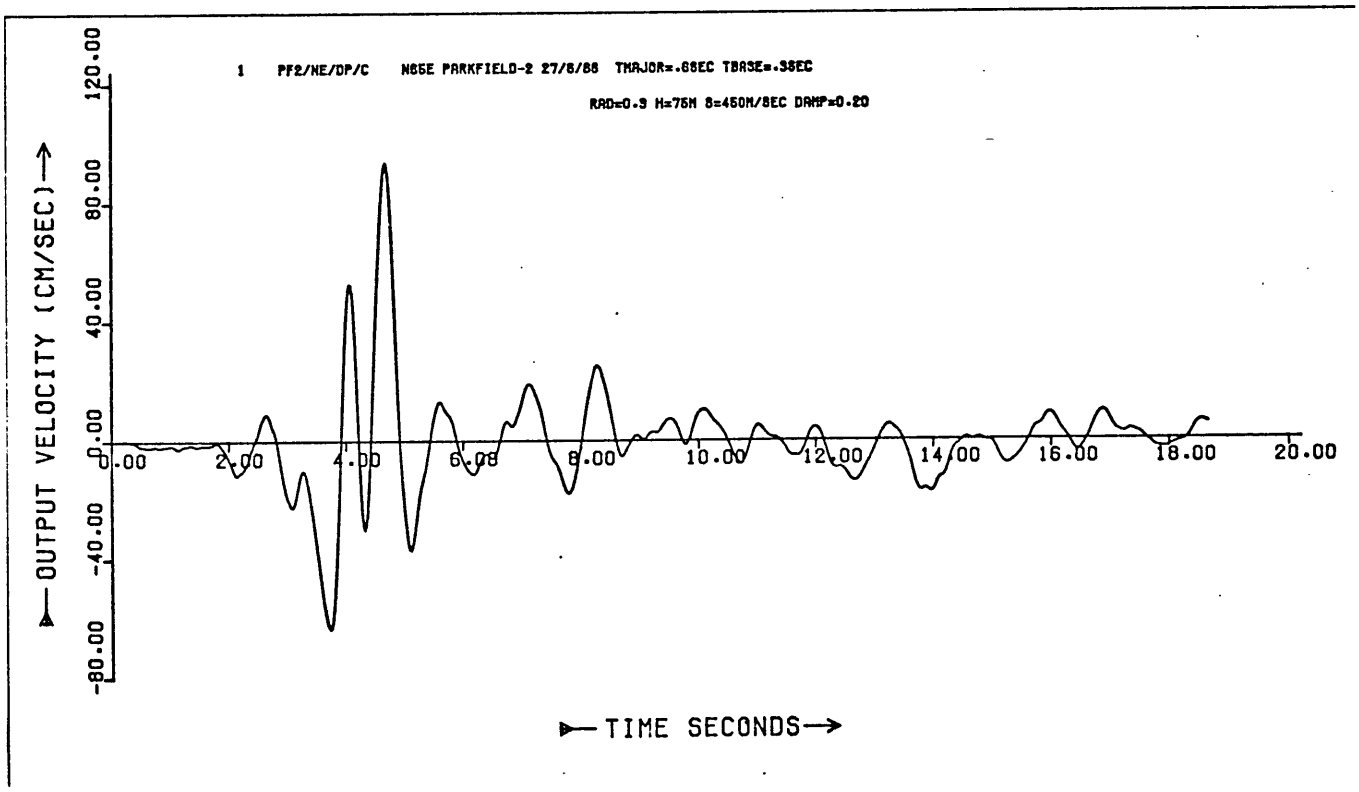


FIG.7.5b COMPUTED GROUND SURFACE VELOCITY TIME HISTORY AT SITE NO 7.5

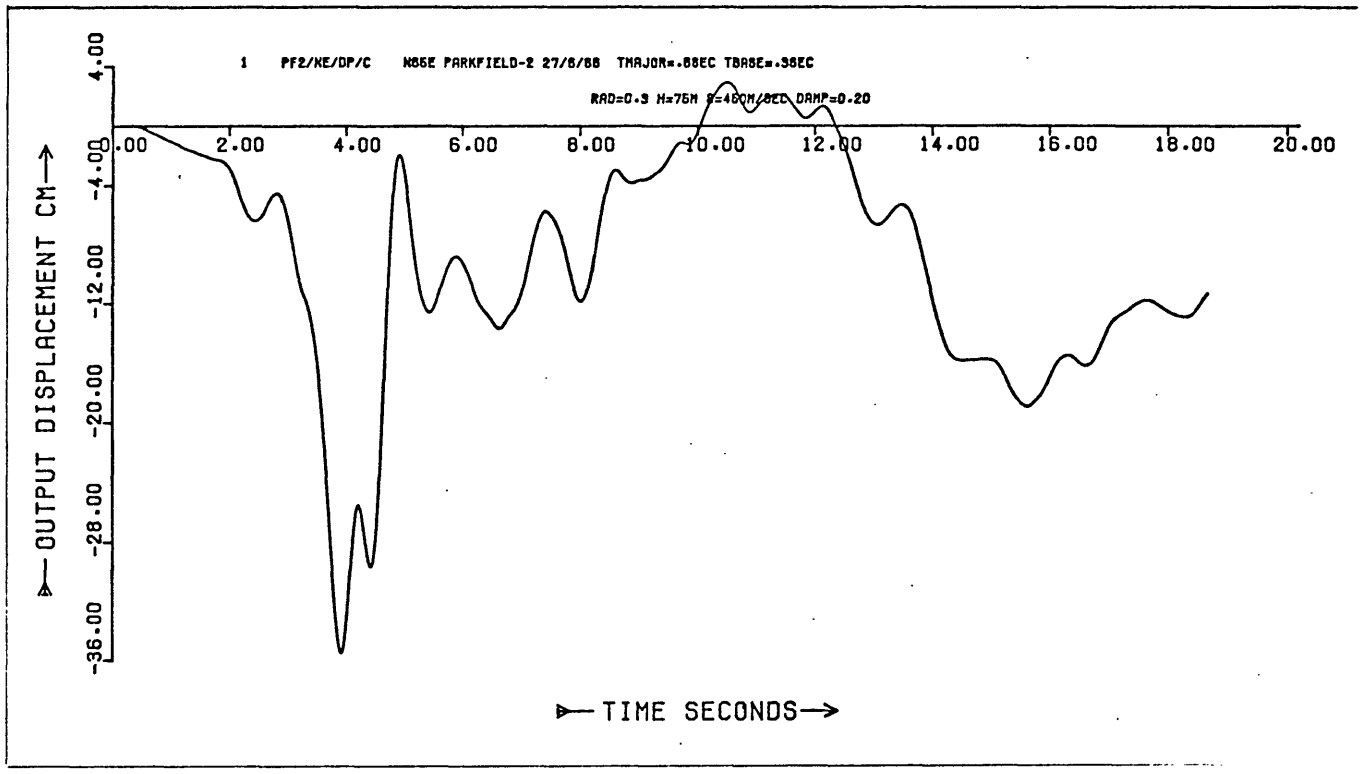


FIG.7.5c COMPUTED GROUND SURFACE DISPLACEMENT TIME HISTORY AT SITE NO 7.5

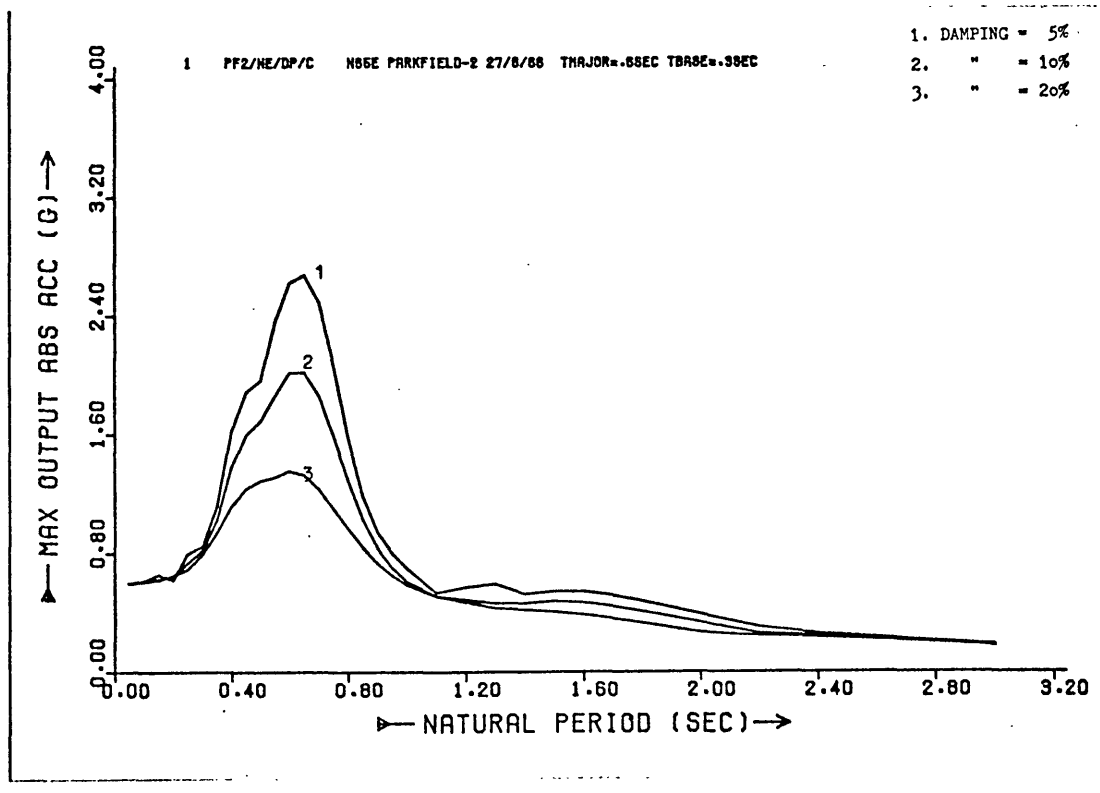


FIG.7.5d COMPUTED GROUND SURFACE ACCELERATION RESPONSE SPECTRA AT SITE NO 7.5

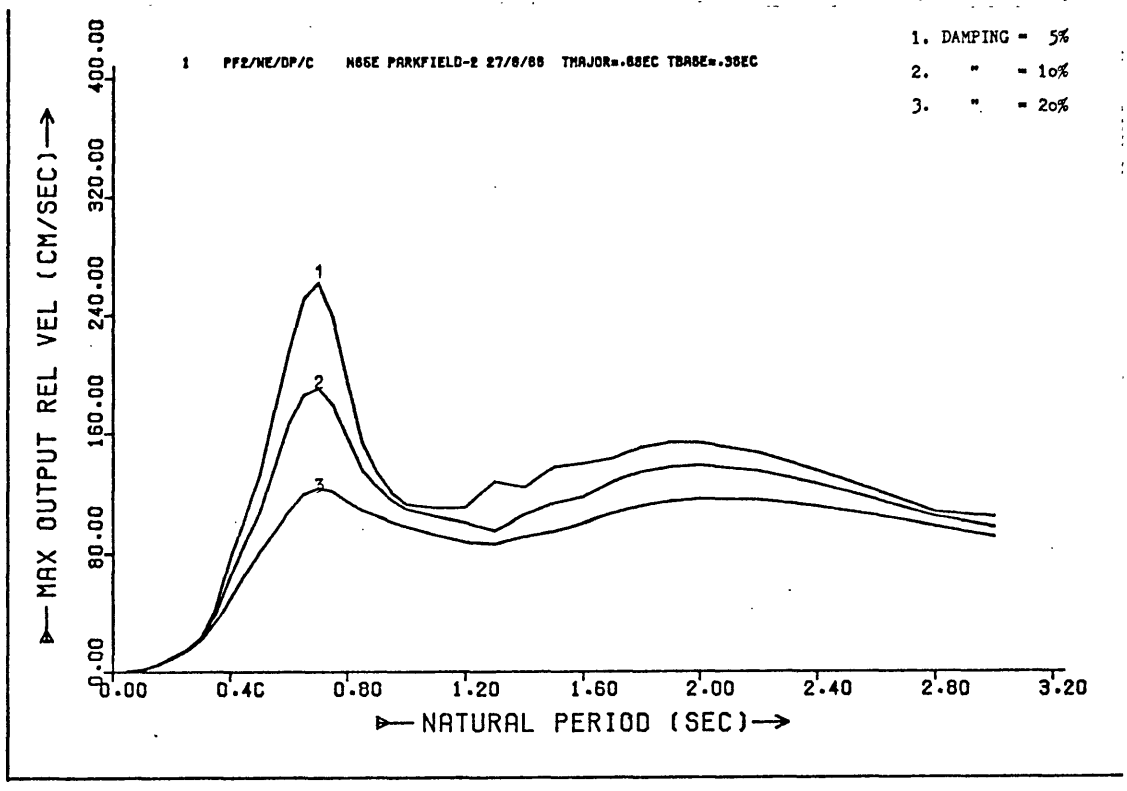


FIG.7.5e COMPUTED GROUND SURFACE VELOCITY RESPONSE SPECTRA AT SITE NO 7.5

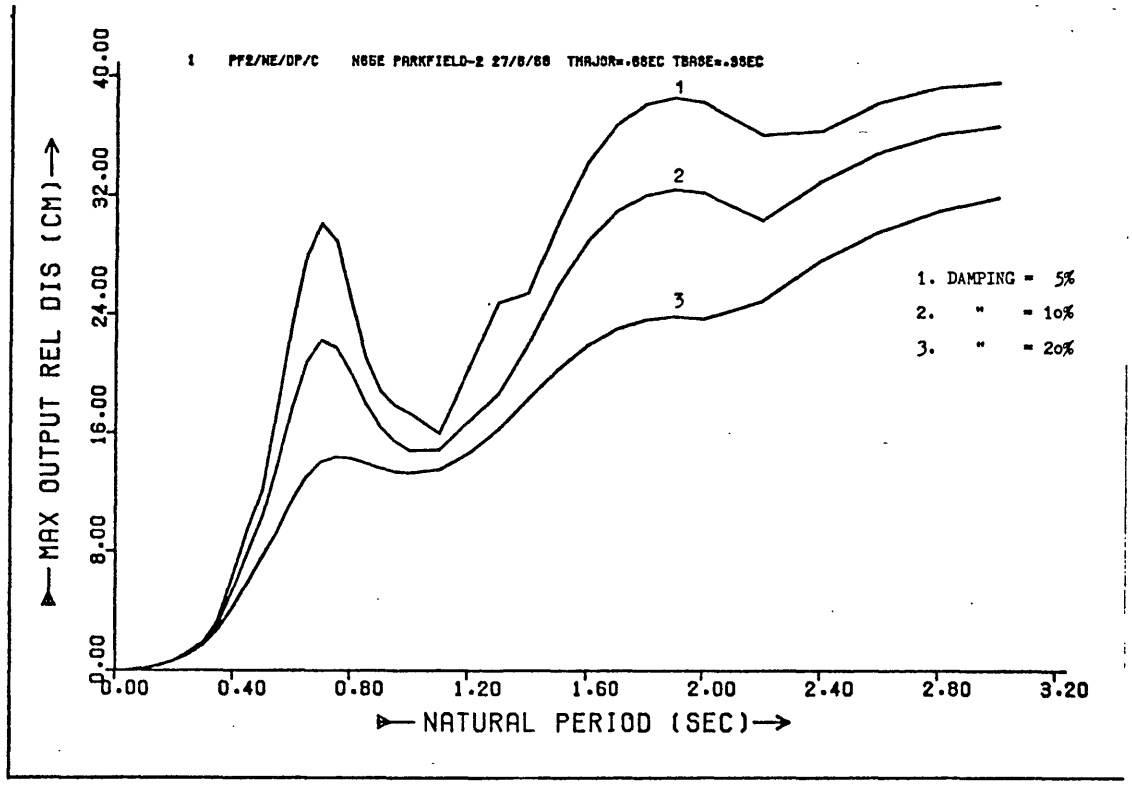


FIG. 7.5f COMPUTED GROUND SURFACE DISPLACEMENT RESPONSE SPECTRA AT SITE NO 7.5

and velocities of these sites as that exhibited by the amplitudes of maximum spectral accelerations and velocities.

Fig. 7.6 shows the influence of ground softness on maximum surface acceleration for the five sites considered. It may be seen that the maximum ground surface acceleration decreases with increasing softness. It is also very important to note that soft site does not necessarily imply higher inertia forces. Structures designed on these sites do not necessarily experience higher forces. The main cause of more damage on soft sites can be attributed to two very important factors, namely, duration of shaking and differential settlements. The former controls the numbers of cycles a structure undergoes; for example, a low structure can undergo a less number of cycles than a high structure. Recent studies by Trifunac and Brady[58], based on recorded field data, has shown that length of shaking on "soft" site is 5 to 6 seconds longer than on "intermediate" site and about 10 to 12 seconds longer than a "hard" site. The latter controls the moment capacity of structures. It is not difficult to show that in a simple portal frame, as met in ordinary 3 to 4 storey buildings, differential settlements of the order of 2-3 cm.(depending on loading conditions) at one support is enough to reduce the moment capacity at the joint opposite to the support to zero, causing complete collapse.

Fig. 7.7 shows the maximum velocities developed at the surface of the five deposits. It is noted that, for progressively harder sites, maximum ground surface velocity decreases, tending to a minimum value, and then increases as the sites become harder, a behaviour similar to amplitudes of peak spectral velocities. This is expected because, as

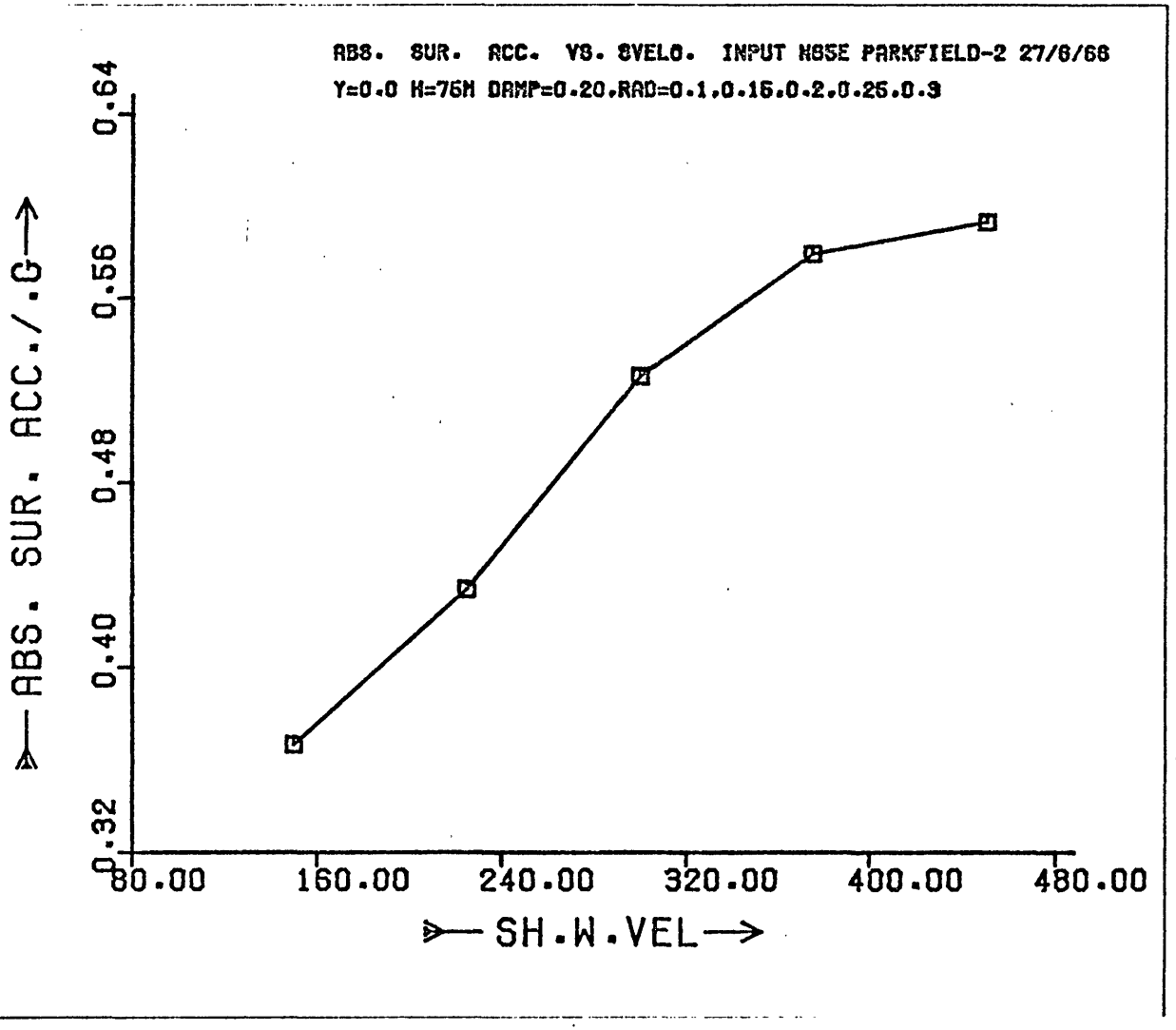
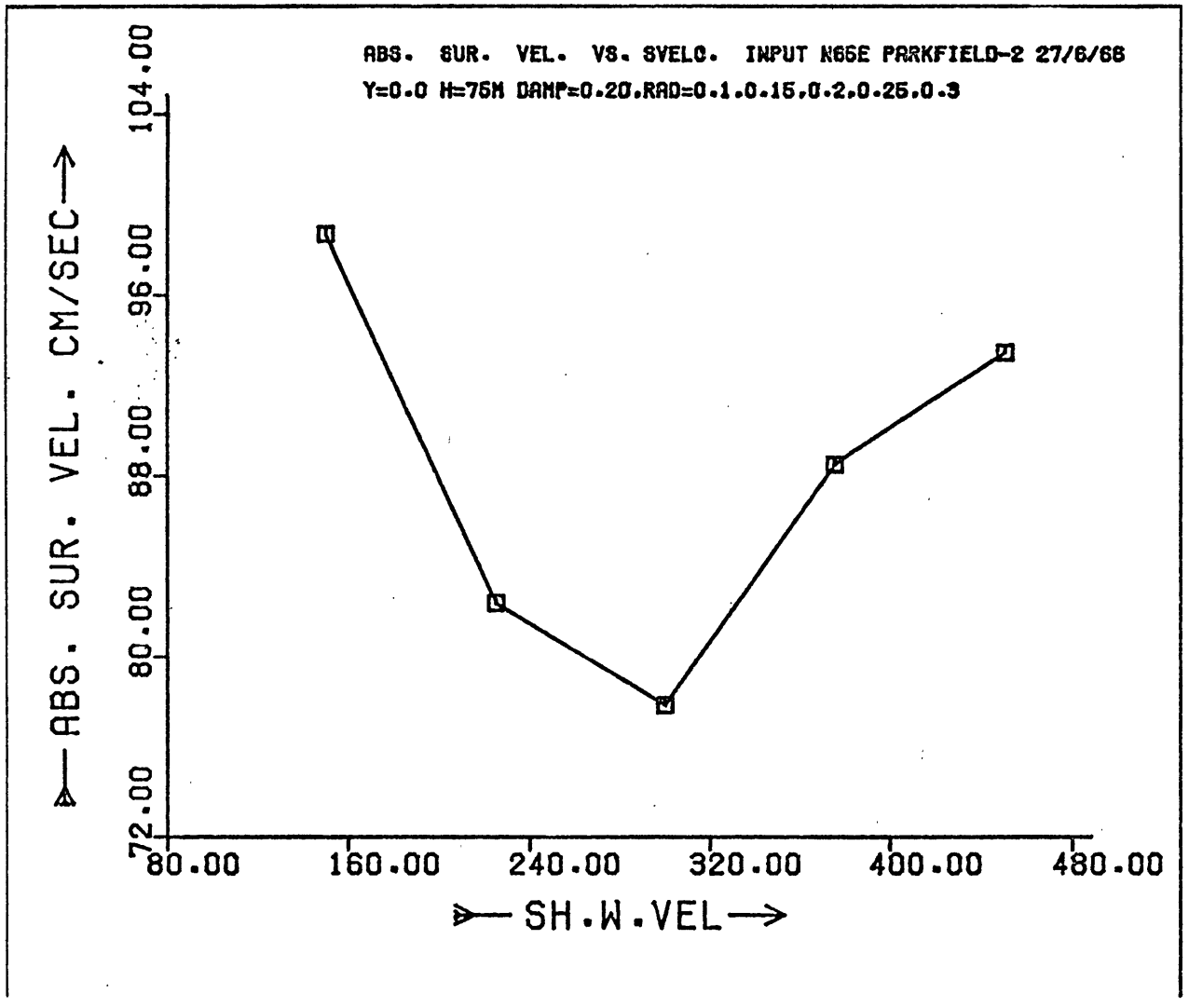


FIG.7.6

INFLUENCE OF GROUND SOFTNESS ON MAXIMUM SURFACE ACCELERATION



INFLUENCE OF GROUND SOFTNESS ON MAXIMUM SURFACE VELOCITY

FIG.7.7

mentioned earlier, the ratio of maximum spectral velocity/maximum ground velocity for the sites are roughly constant.

The influence of ground softness on maximum surface displacements is shown in fig. 7.8. The results show that a progressive increase in the softness of the deposits increases the surface displacements. This behaviour is similar to the amplitude of maximum spectral displacements for the five deposits considered. It is also noticed that the ratio of maximum spectral displacement/maximum ground displacements is also constant. In this case the average value of this ratio for 5% spectral damping is 1.56. The results also illustrate the physical realities, as frequently observed in the field and documented in the technical literature, that soft sites experience larger displacements in earthquakes.

There is little doubt that soil amplification plays an important part in the occurrence of damage at sites during earthquakes. Fig. 7.9 and 7.10 show acceleration and velocity amplification spectra for the five deposits considered. The results show that all the five deposits have amplified the bedrock motion at periods greater than 0.8 second. The soft clay with fundamental period of 2.0 seconds has shown the largest amplification at period range in between 2.15 - 2.4 seconds. Cemented sand with a fundamental period of 0.66 second has shown the greatest amplification at shorter period range 0.6 - 0.7 sec., which is due to the contribution of the first mode with a period of 0.66 second: it is strongly excited, being close to the predominant period of the bedrock motion. The amplification of soft clay may be significant for long period structures whereas that of cemented sand

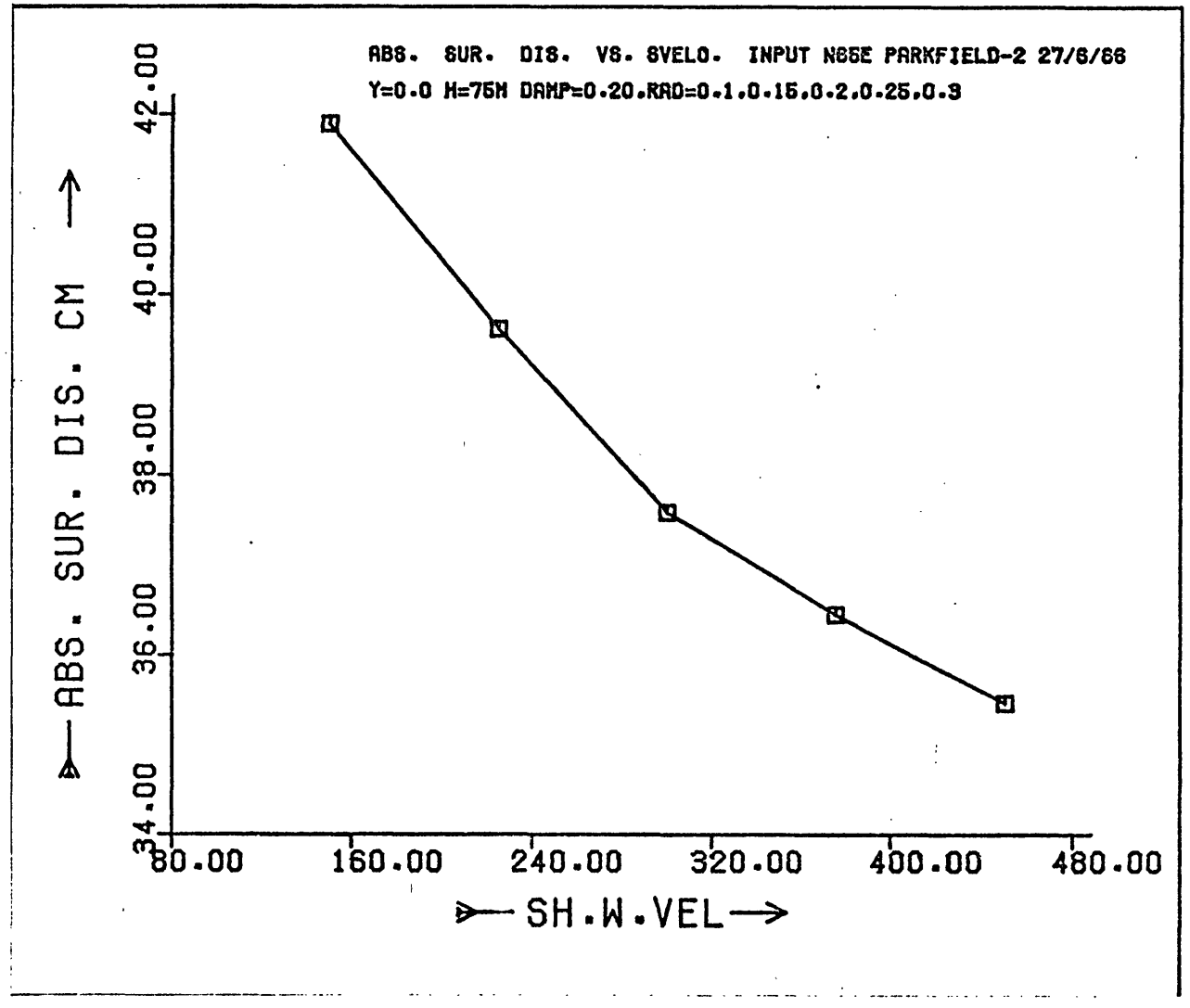


FIG.7.8

INFLUENCE OF GROUND SOFTNESS ON MAXIMUM SURFACE DISPLACEMENT

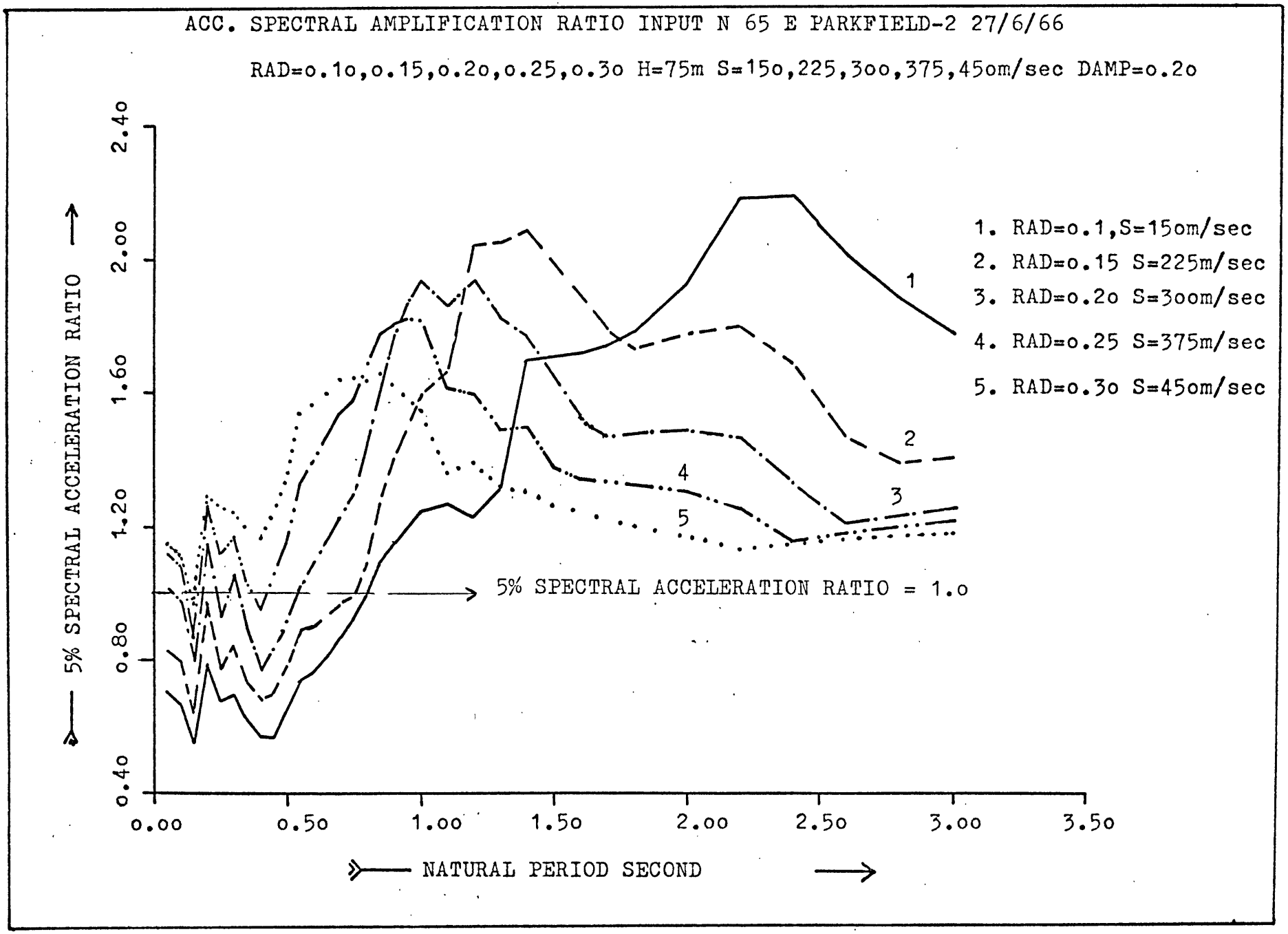

ACC. SPECTRAL AMPLIFICATION RATIO INPUT N 65 E PARKFIELD-2 27/6/66
RAD=o.1o,o.15,o.2o,o.25,o.3o H=75m S=15o,225,3oo,375,45om/sec DAMP=o.2o
5% SPECTRAL ACCELERATION RATIO
2.4o
2.oo
1.6o
1.2o
o.8o
o.4o
1. RAD=o.1,S=15om/sec
2. RAD=o.15 S=225m/sec
3. RAD=o.2o S=3oom/sec
4. RAD=o.25 S=375m/sec
5. RAD=o.3o S=45om/sec
1
2
3
4
5
5% SPECTRAL ACCELERATION RATIO = 1.o
o.oo
o.5o
1.oo
1.5o
2.oo
2.5o
3.oo
3.5o
NATURAL PERIOD SECOND

FIG.7.9

for short period structures. In general the five sites analysed illustrate that maximum amplification of overburdens with longer fundamental periods are due to the contribution of higher modes, which are strongly excited when they approach the predominant period of the bedrock motion. Comparison of the results also indicate that the effect of decreasing softness decreases the fundamental period of these deposits, thus increasing the amplification in the region of the fundamental period of these deposits. If amplification results were based on the ratio of maximum ground surface acceleration to that developed in the bedrock, one would conclude that the deposits consisting of soft clay and medium clay would have shown deamplification, whereas this is only true for a period range of less than 0.8 second.

Fig. 7.10 shows velocity amplification spectra for the five sites, showing that in the intermediate period range,i.e. 1.2 sec. to 2.0 sec., medium clay has shown the most amplification and,at large period range 2.0 to 3.0 sec.,soft clay the most. All the sites have shown deamplification at a period range of less than 1.0 second. The amplification of medium clay may be significant for intermediate period structures, indicating that energy at these periods may be large enough to push the structures into non-linear range and carry the yielding to failure. In contrast the amplification for medium clay may be significant for long period structures.

In order to illustrate that the behaviour exhibited by the five deposits is a general rule or not, table 7.1 has been included. Table 7.1 illustrates results of five more deposits of soft clay, soft to medium clay, loose gravel, sandy clay, coarse gravelwith depths to

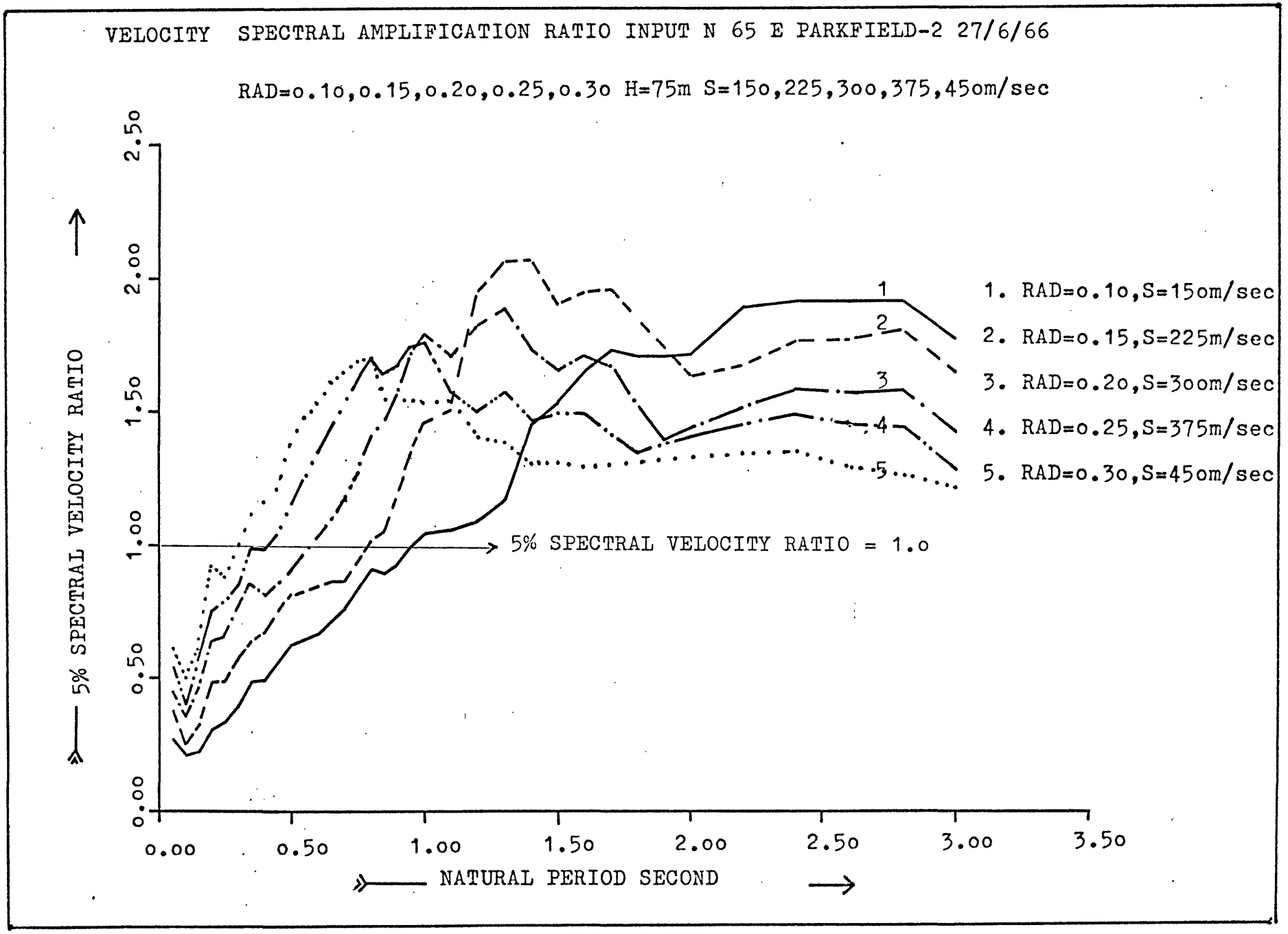

VELOCITY SPECTRAL AMPLIFICATION RATIO INPUT N 65 E PARKFIELD-2 27/6/66
RAD=o.1o,o.15,o.2o,o.25,o.3o H=75m S=15o,225,3oo,375,45om/sec
5% SPECTRAL VELOCITY RATIO
NATURAL PERIOD SECOND
0.00
0.50
1.00
1.50
2.00
2.50
3.00
3.50
5% SPECTRAL VELOCITY RATIO = 1.0
1. RAD=o.1o,S=15om/sec
2. RAD=o.15,S=225m/sec
3. RAD=o.2o,S=3oom/sec
4. RAD=o.25,S=375m/sec
5. RAD=o.3o,S=45om/sec

FIG.7.1o

BEDROCK MOTION PARKFIELD-5 N5W

DAMP=0.05, RAD=0.1,0.15,0.2,0.3,0.35, H=100m

SHEAR WAVE VELOCITY m/sec	MAX. ABS. SUR. ACC. g	MAX. ABS. SUR. VEL. cm/sec	MAX. ABS. SUR. DIS. cm	STRENGTH OF EARTH-QUAKE MOTION "S" $(cm/sec)^2$
150.0	0.41	27.83	9.37	556.08
200.0	0.45	36.65	9.89	484.61
300.0	0.48	39.66	9.38	401.62
400.0	0.45	32.48	8.81	701.58
500.0	0.63	32.5	8.36	1890

TABLE 7.1

RESULTS OF INFLUENCE OF GROUND SOFTNESS

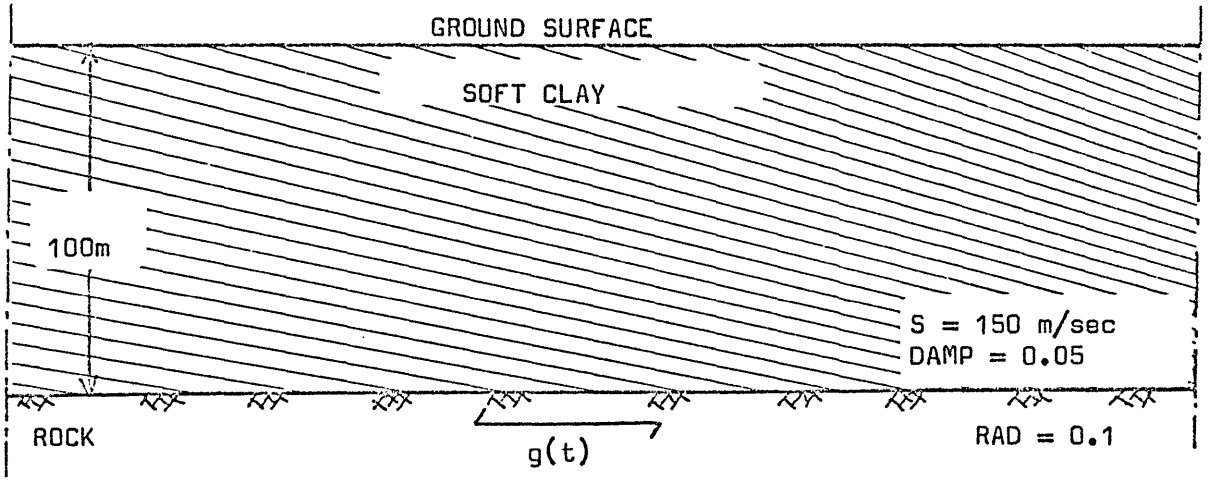
ON COMPUTED GROUND RESPONSE

bedrock level of 100m, hysteretic damping ratios of 0.05 (the same for all the deposits), subjected to Parkfield-5 NSW. The response of these sites are shown in figs. 7.11a,b,c,d,e,f through 7.15a,b,c,d,e,f.

Figs. 7.11a,b,c,d,e,f through 7.15a,b,c,d,e,f show results of the calculations in terms of ground surface acceleration, velocity and displacement time histories, as well as computed acceleration velocity and displacement spectrum in normalized form, so that the frequency characteristics of different motions is clearly reflected. The spectrum are normalized with respect to maximum ground surface acceleration, velocity and displacements (these values are marked clearly on each spectra) hence, the spectral amplitudes represent the magnification of the response of the simple structures with respect to the base motion.

Figs. 7.11d through 7.15d show normalized acceleration response spectra for the five deposits. The coarse gravel with periods in the first, second and third mode, much closer to the predominant period of the bedrock motion 0.3 second, has shown the greatest amplitude of the peak acceleration spectral value. The loose gravelhas shown the 2nd largest, because its periods at second and third mode are excited more strongly on account of these values being close to the predominant period of bedrock motion. Sandy clay and soft to medium clay have shown the same amplitudes of the peak spectral acceleration and, finally, soft clay the least.

Figs. 7.11e through 7.15e show normalized velocity response spectrum for the five deposits. The results illustrate that amplitude of peak spectral velocity is the smallest for the soft clay, then increases to a peak value for loose gravel and then remains almost



RESPONSE OF HYSTERETIC DEPOSIT UNDERLAIN BY DEFORMABLE BEDROCK

SCHEMATIC SOIL PROFILE FOR SITE NO 7.6

FIG. 7.11

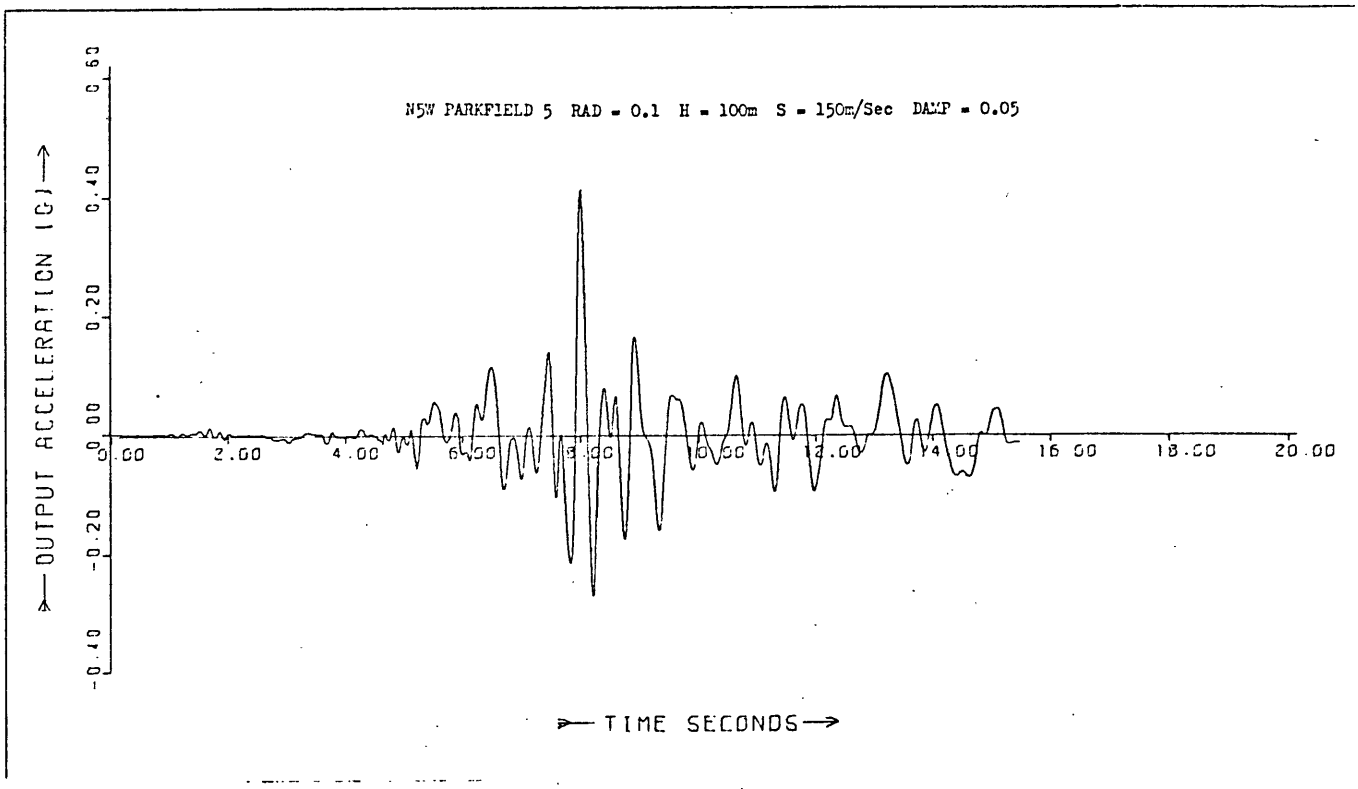


FIG. 7.11a COMPUTED GROUND SURFACE ACCELERATION TIME HISTORY AT SITE NO 7.6

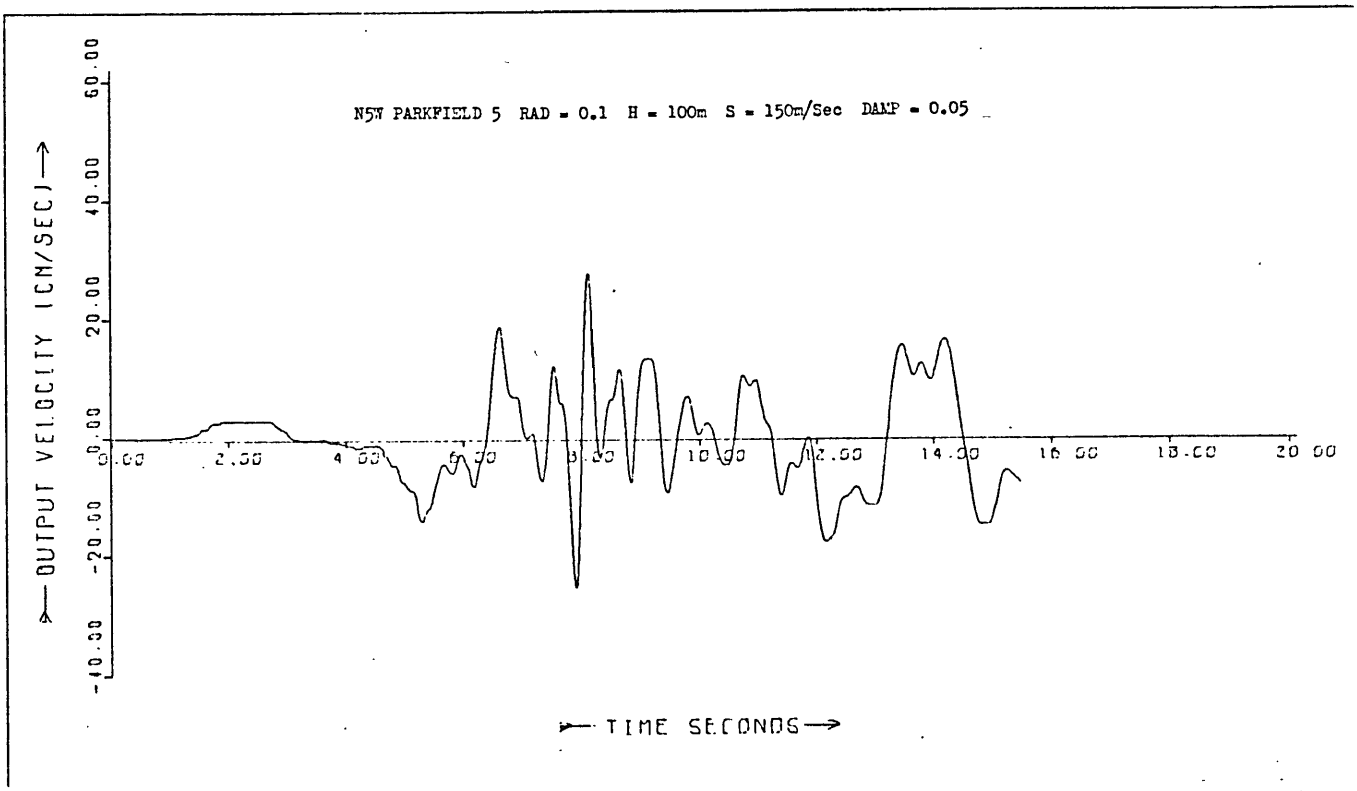


FIG.7.11b COMPUTED GROUND SURFACE VELOCITY TIME HISTORY AT SITE NO 7.6

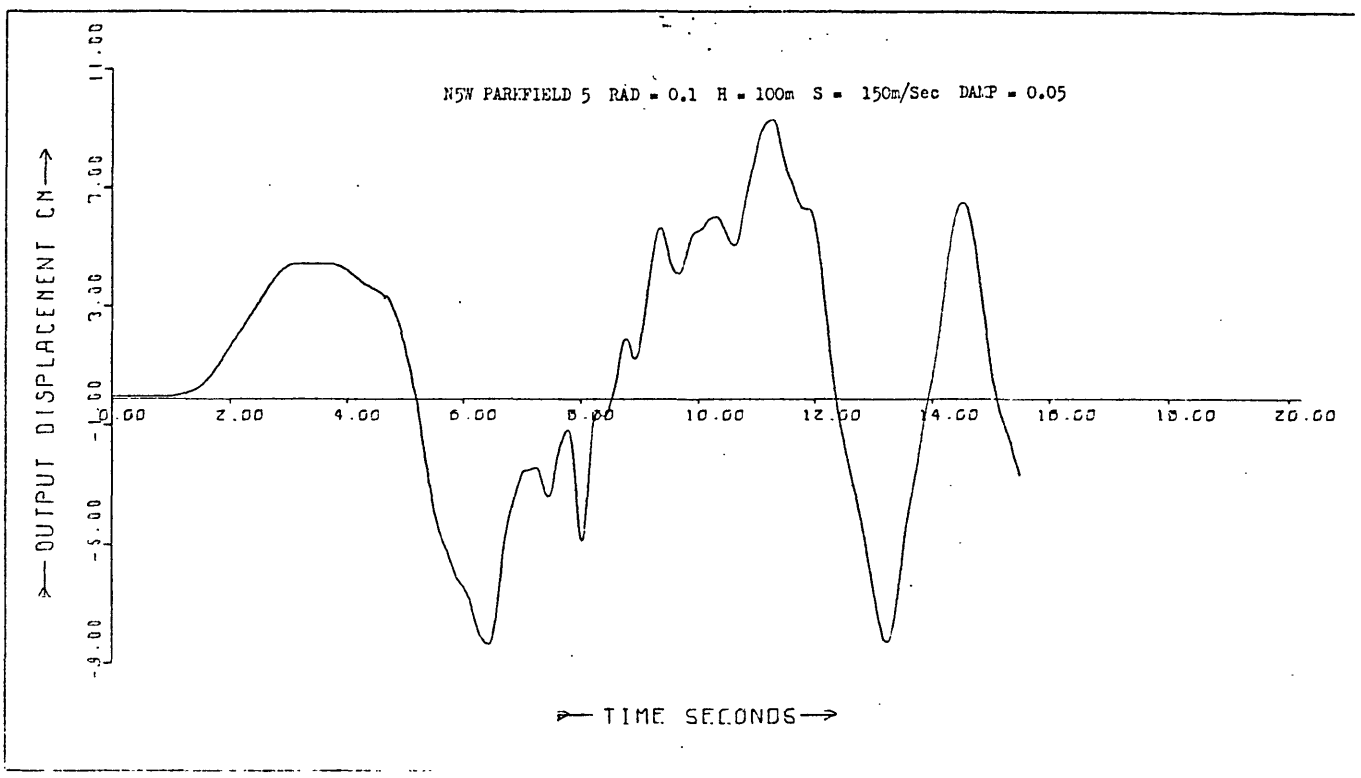


FIG.7.11c COMPUTED GROUND SURFACE DISPLACEMENT TIME HISTORY AT SITE NO 7.6

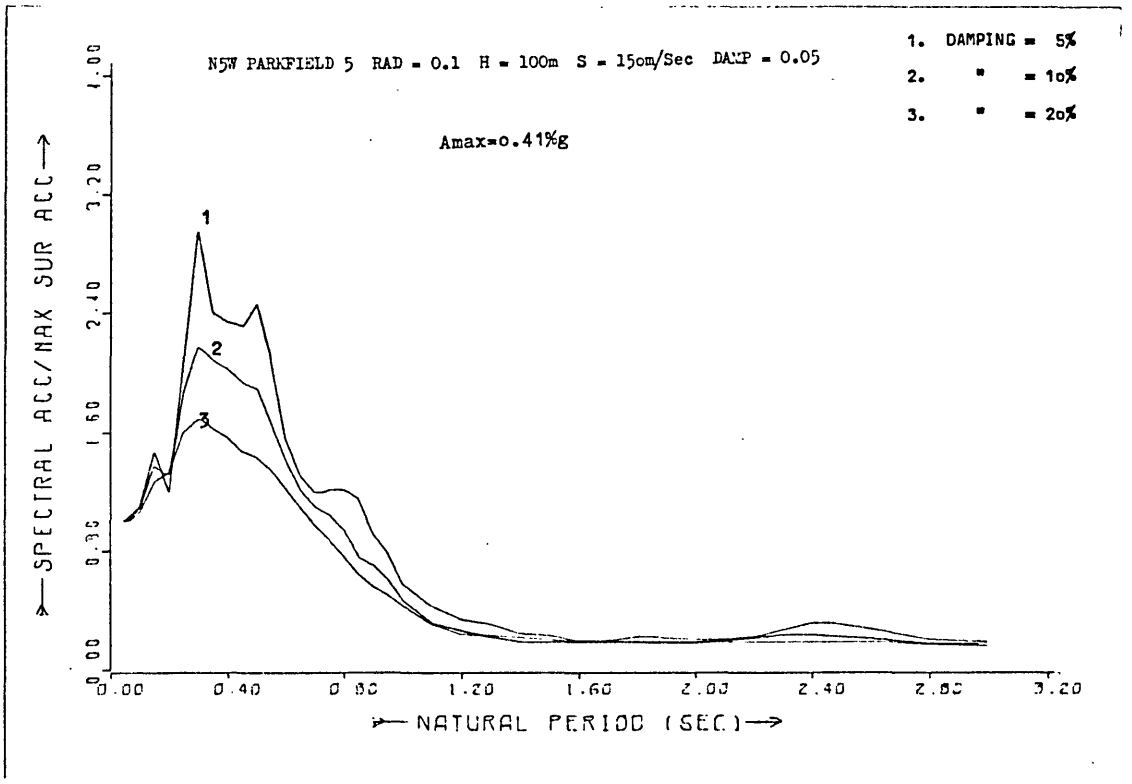


FIG.7.11d COMPUTED GROUND SURFACE ACCELERATION RESPONSE SPECTRA AT SITE NO 7.6

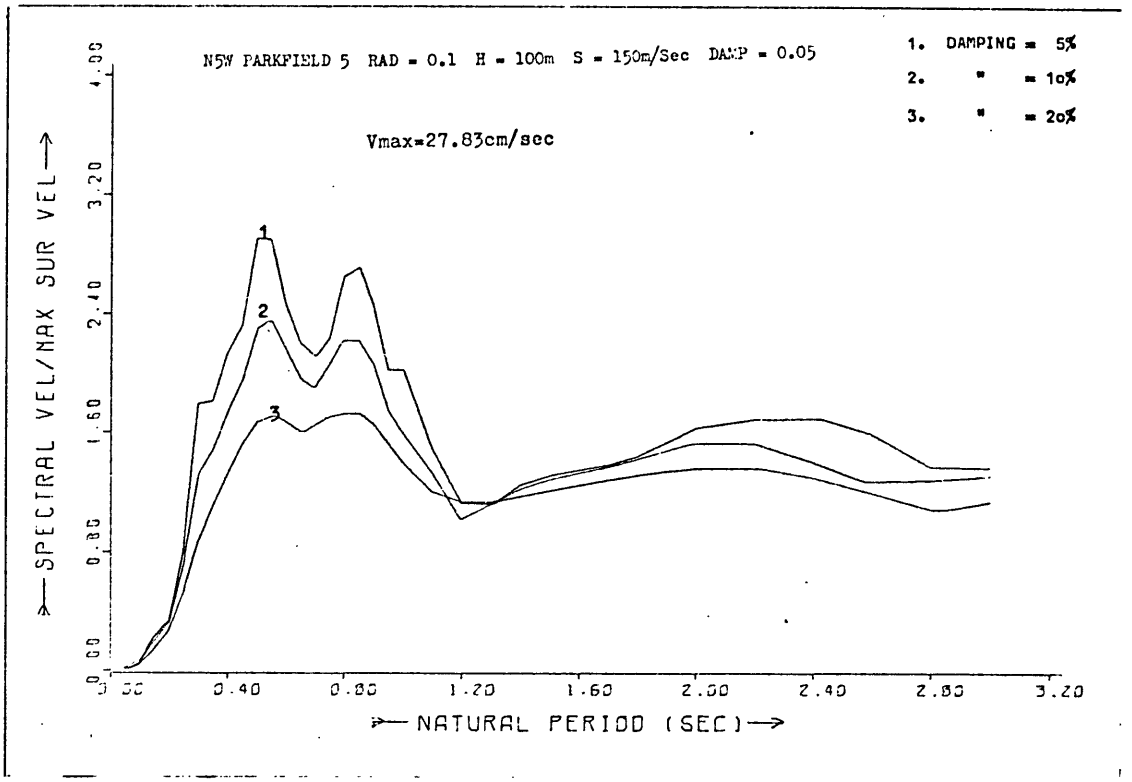


FIG.7.11e COMPUTED GROUND SURFACE VELOCITY RESPONSE SPECTRA AT SITE NO 7.6

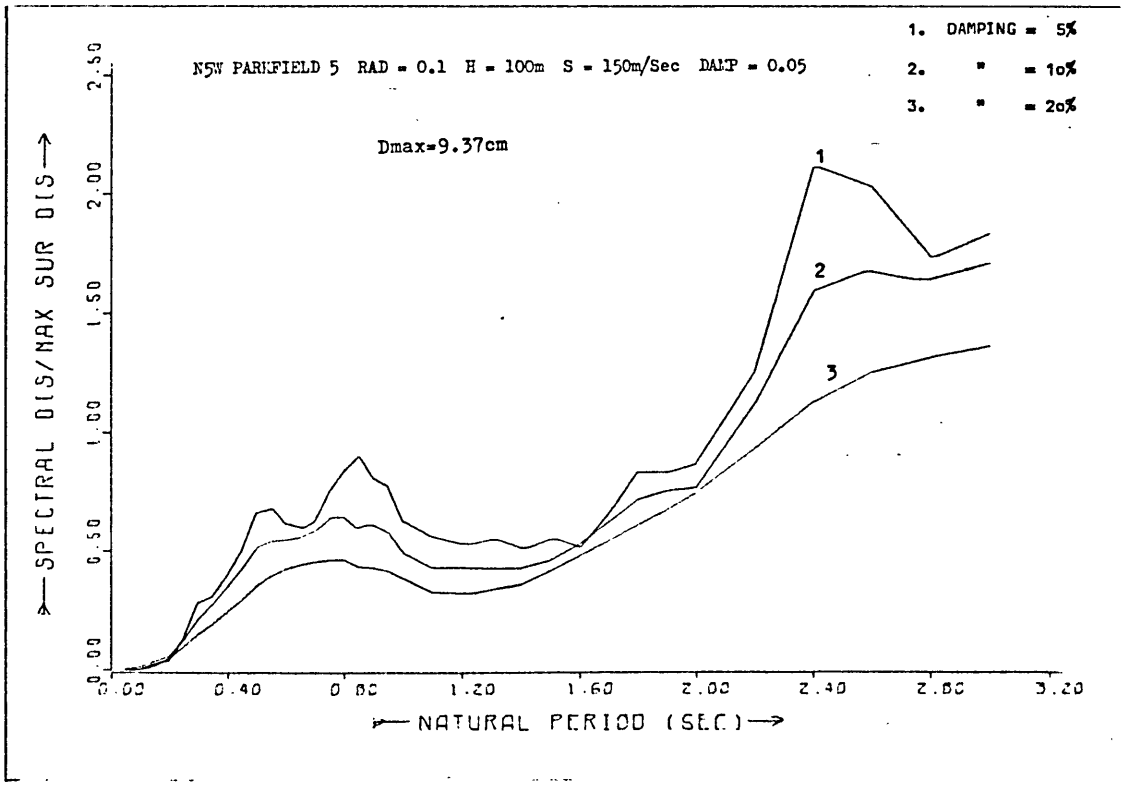
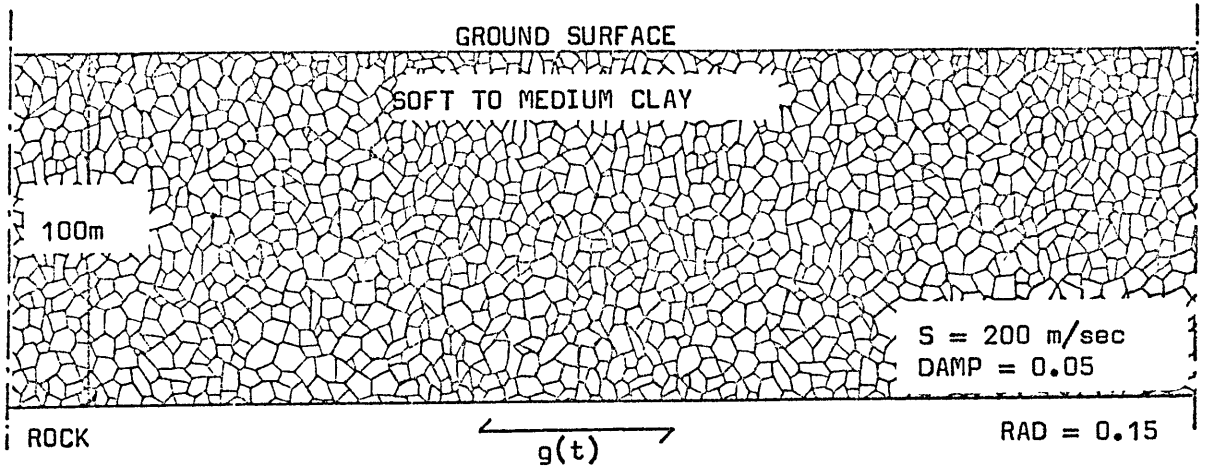


FIG.7.11f COMPUTED GROUND SURFACE DISPLACEMENT RESPONSE SPECTRA AT SITE NO 7.6



RESPONSE OF HYSTERETIC DEPOSIT UNDERLAIN BY DEFORMABLE BEDROCK

SCHEMATIC SOIL PROFILE FOR SITE NO 7.7

Fig. 7.12

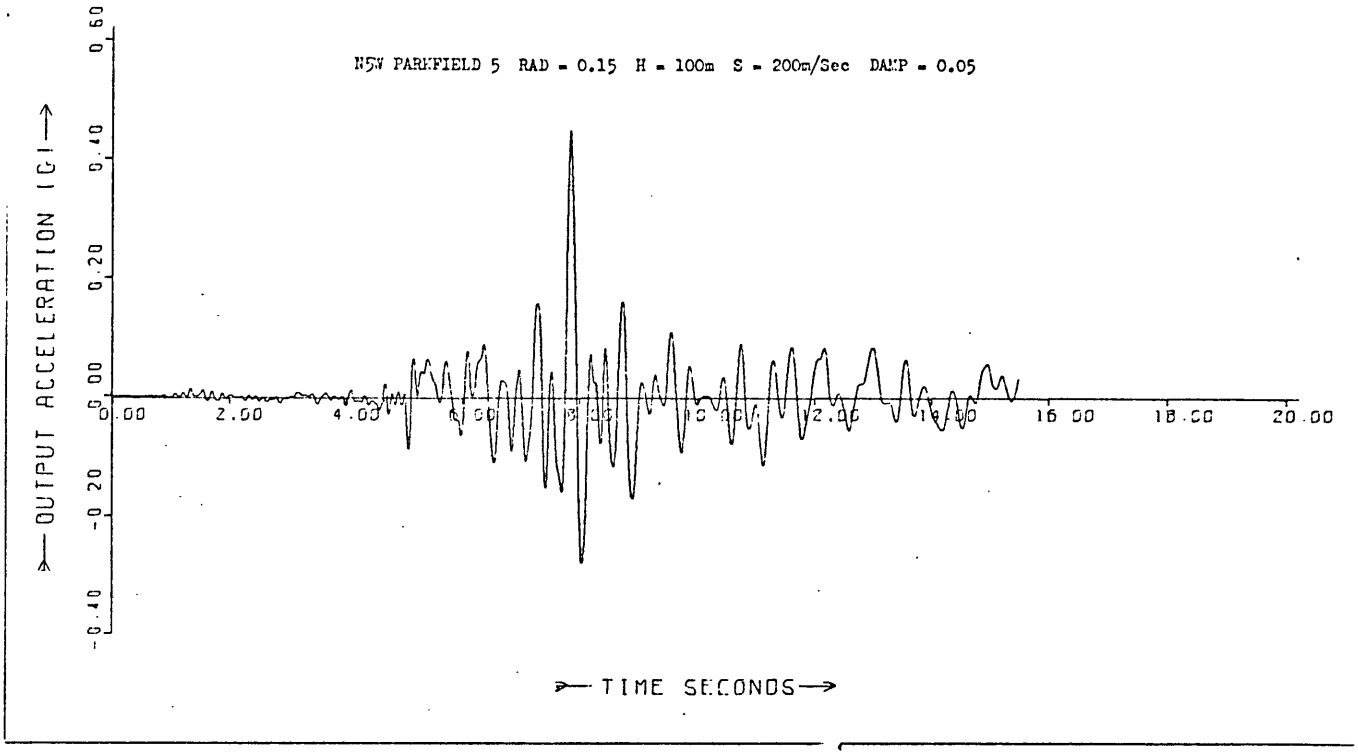


FIG7.12a COMPUTED GROUND SURFACE ACCELERATION TIME HISTORY AT SITE NO 7.7

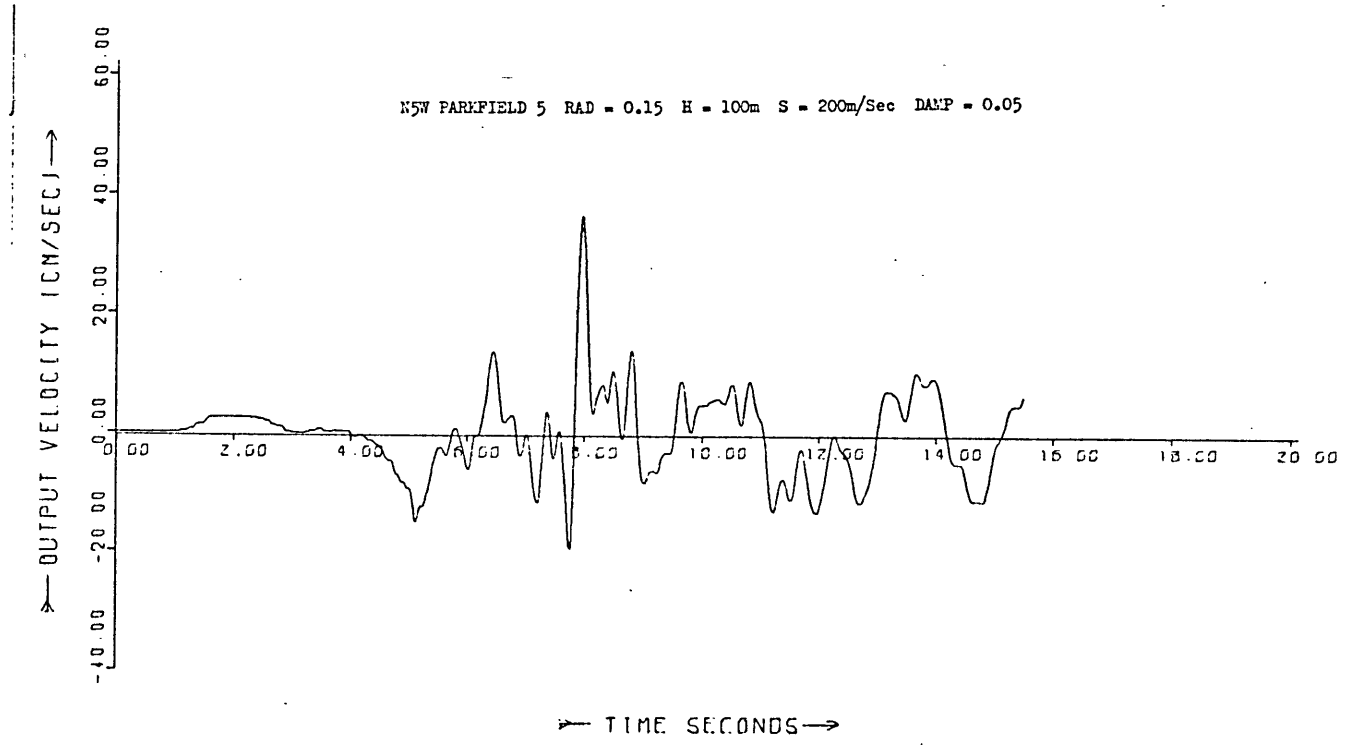


FIG. 7.12b COMPUTED GROUND SURFACE VELOCITY TIME HISTORY AT SITE NO 7.7

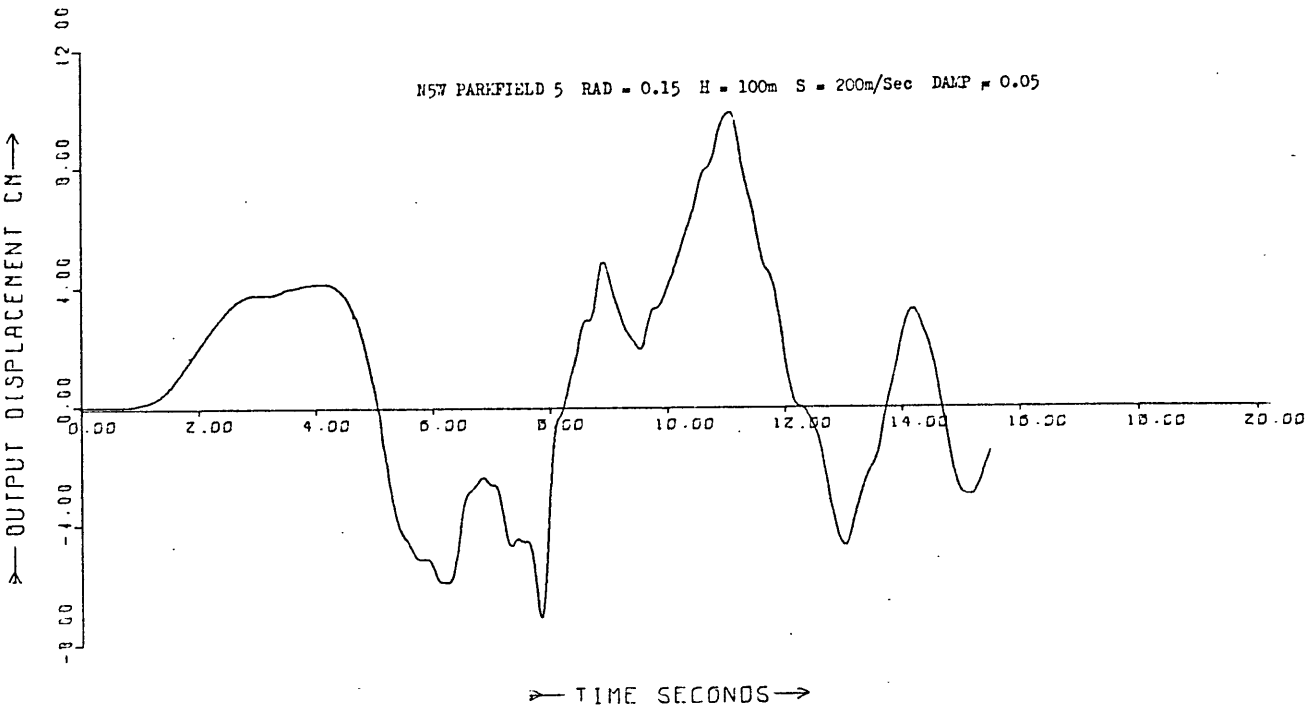


FIG 7.12c COMPUTED GROUND SURFACE DISPLACEMENT TIME HISTORY AT SITE NO 7.7

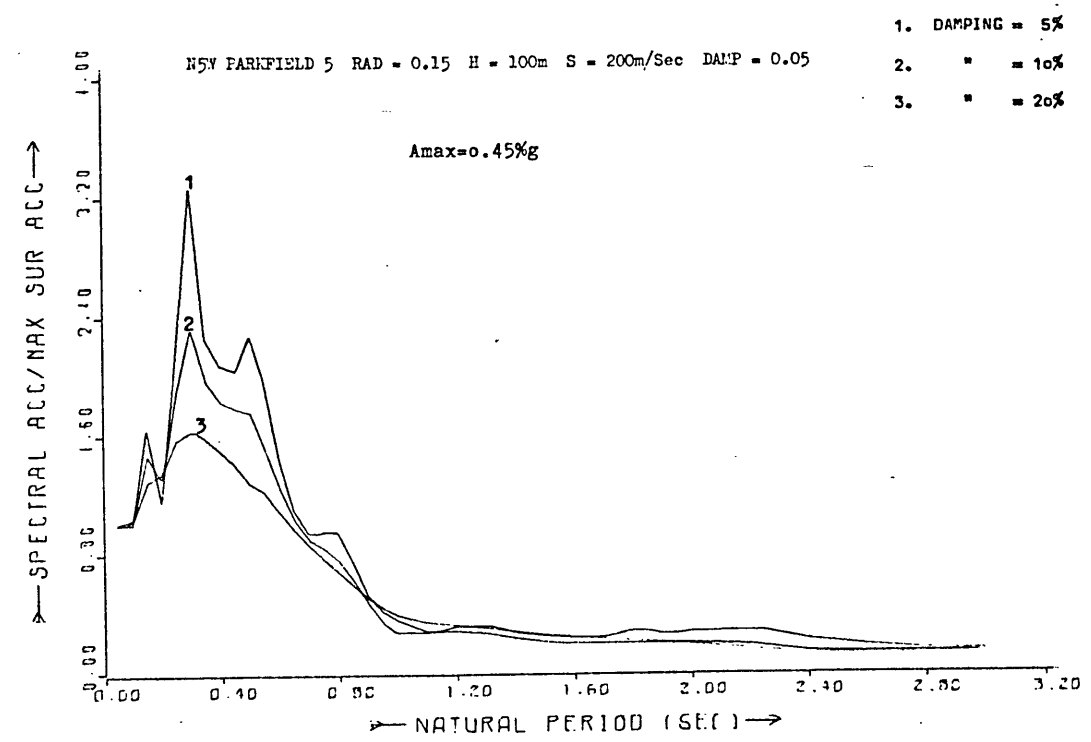


FIG 7.12d COMPUTED GROUND SURFACE ACCELERATION RESPONSE SPECTRA AT SITE NO 7.7

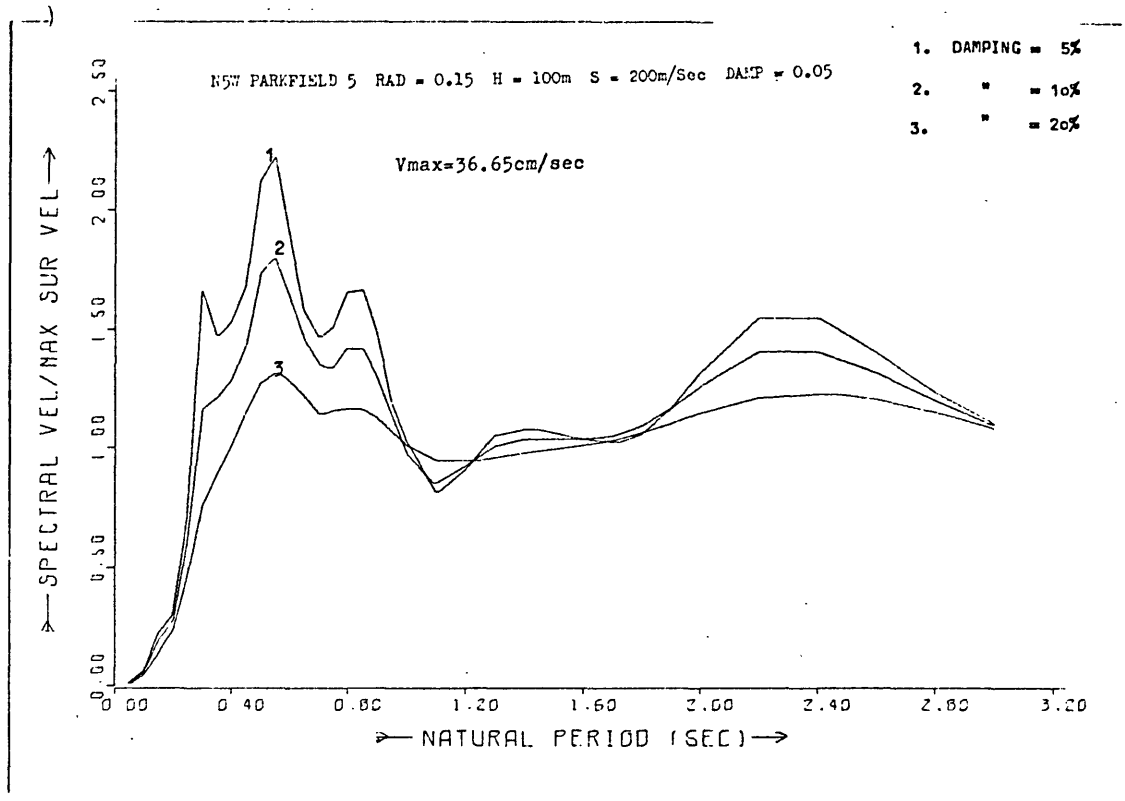


FIG. 7.12e COMPUTED GROUND SURFACE VELOCITY RESPONSE SPECTRA AT SITE NO 7.7

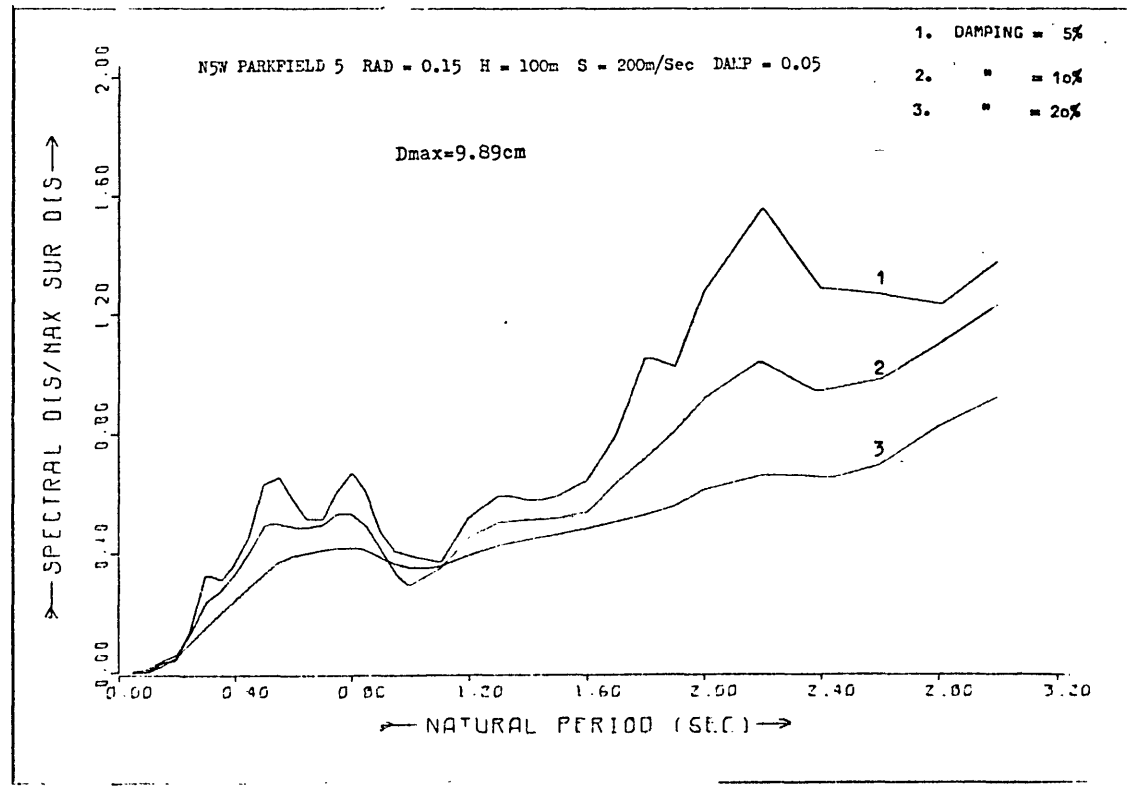
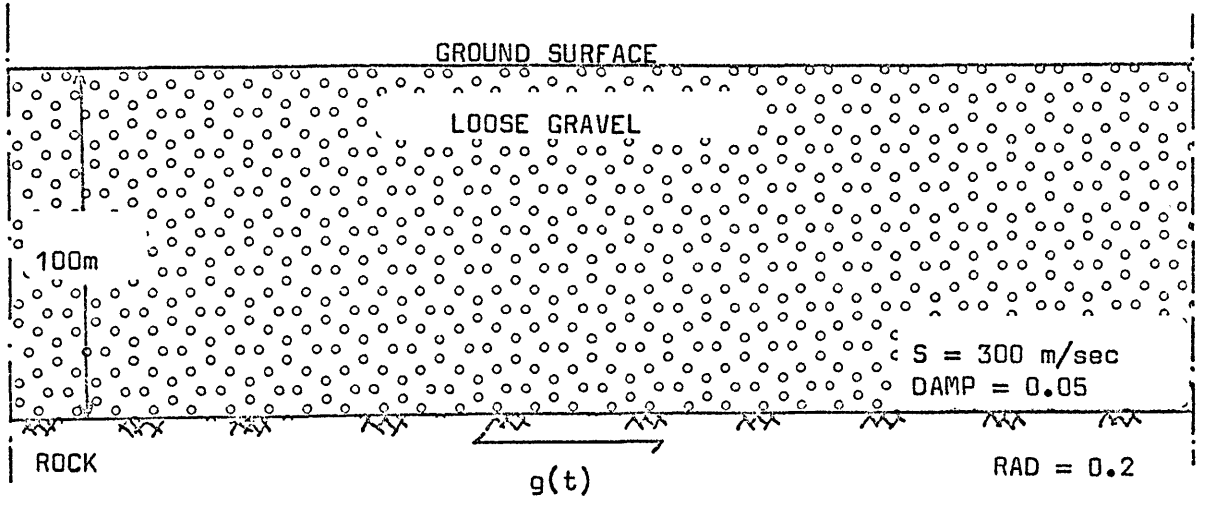


FIG. 7.12f COMPUTED GROUND SURFACE DISPLACEMENT RESPONSE SPECTRA AT SITE NO 7.7



RESPONSE OF HYSTERETIC DEPOSIT UNDERLAIN BY DEFORMABLE BEDROCK

SCHEMATIC SOIL PROFILE FOR SITE NO 7.8

FIG. 7.13

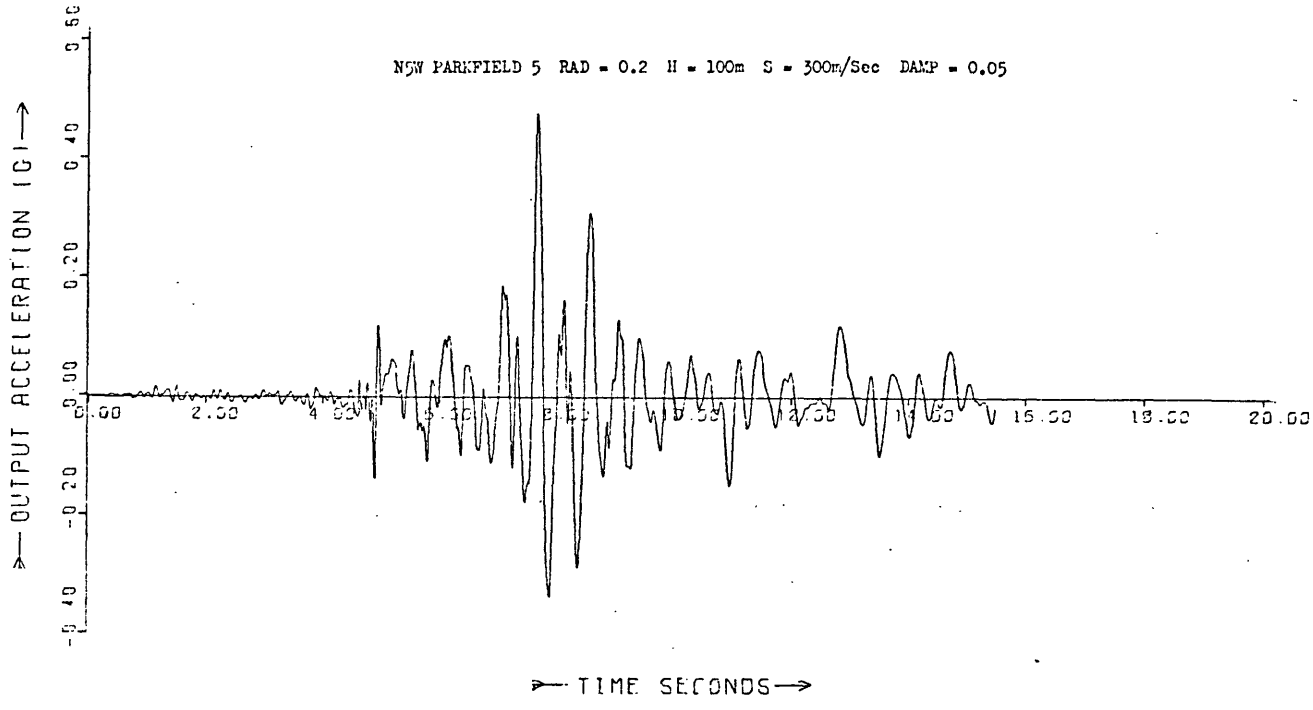


FIG. 7.13a COMPUTED GROUND SURFACE ACCELERATION TIME HISTORY AT SITE NO 7.8

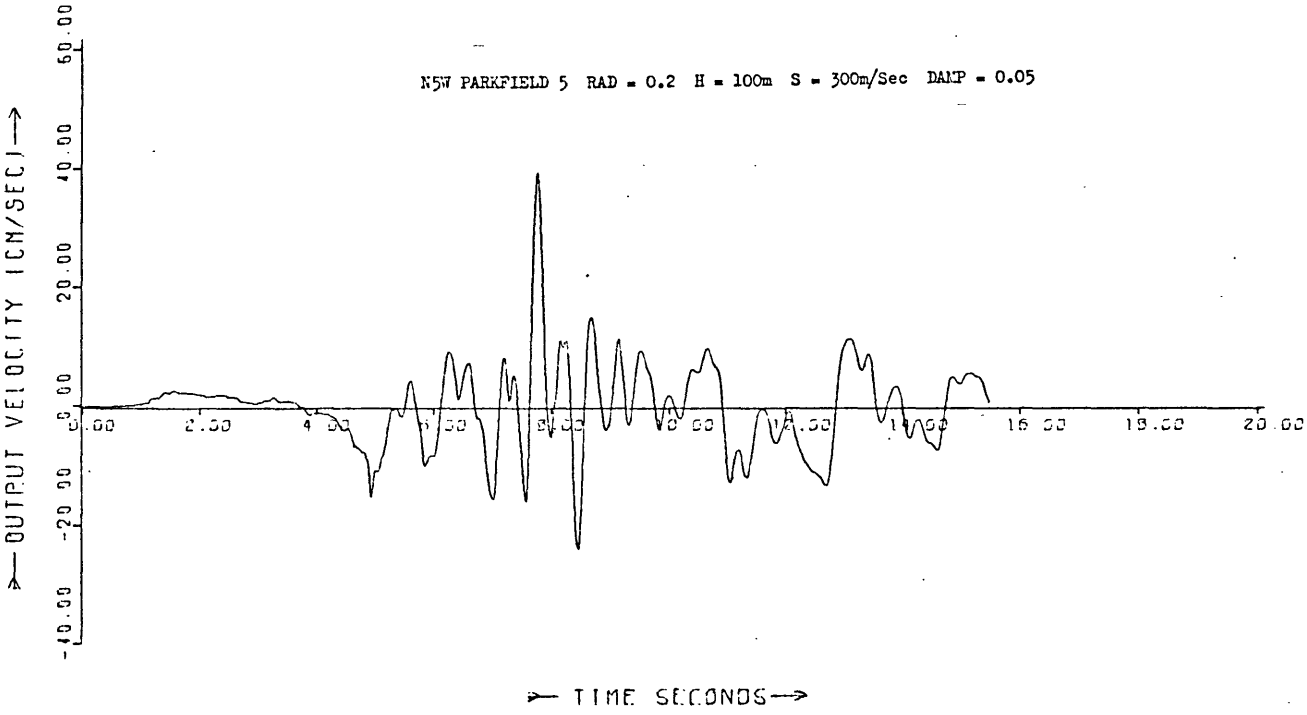


FIG. 7.13b COMPUTED GROUND SURFACE VELOCITY TIME HISTORY AT SITE NO 7.8

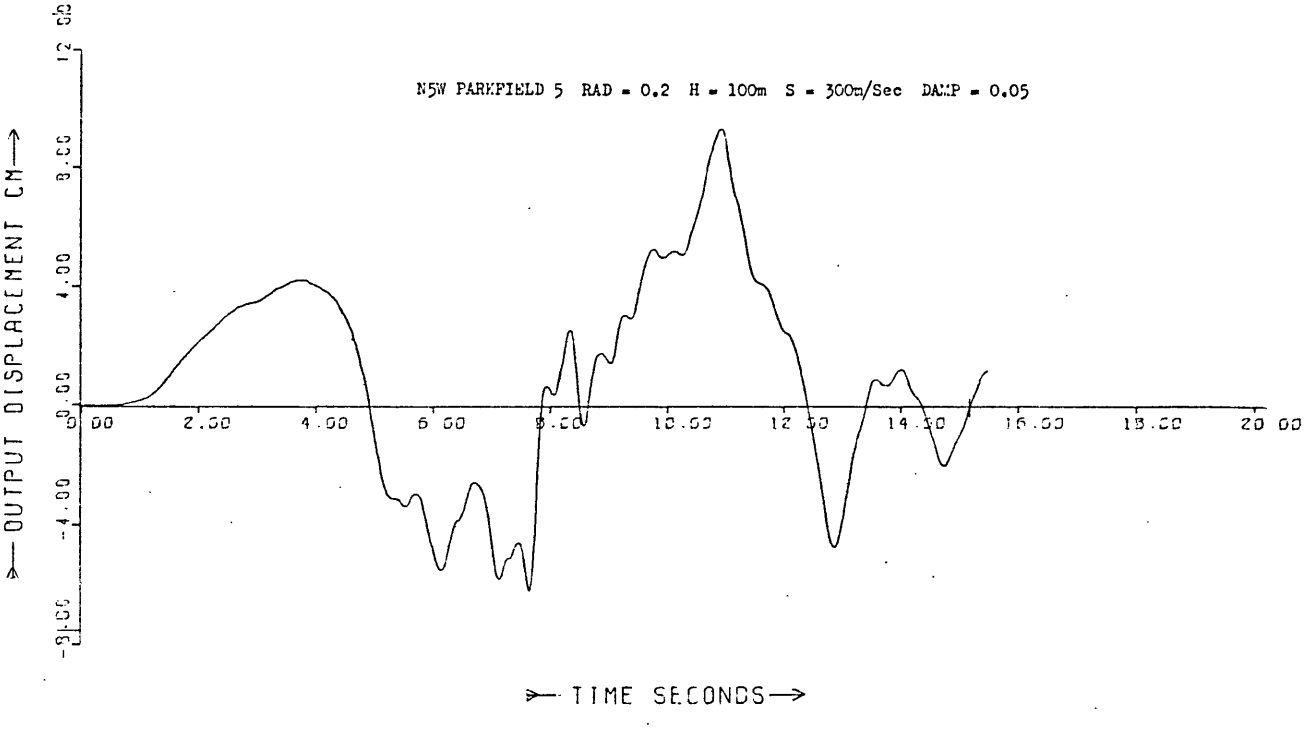


Fig 7.13c COMPUTED GROUND SURFACE DISPLACEMENT TIME HISTORY AT SITE NO 7.8

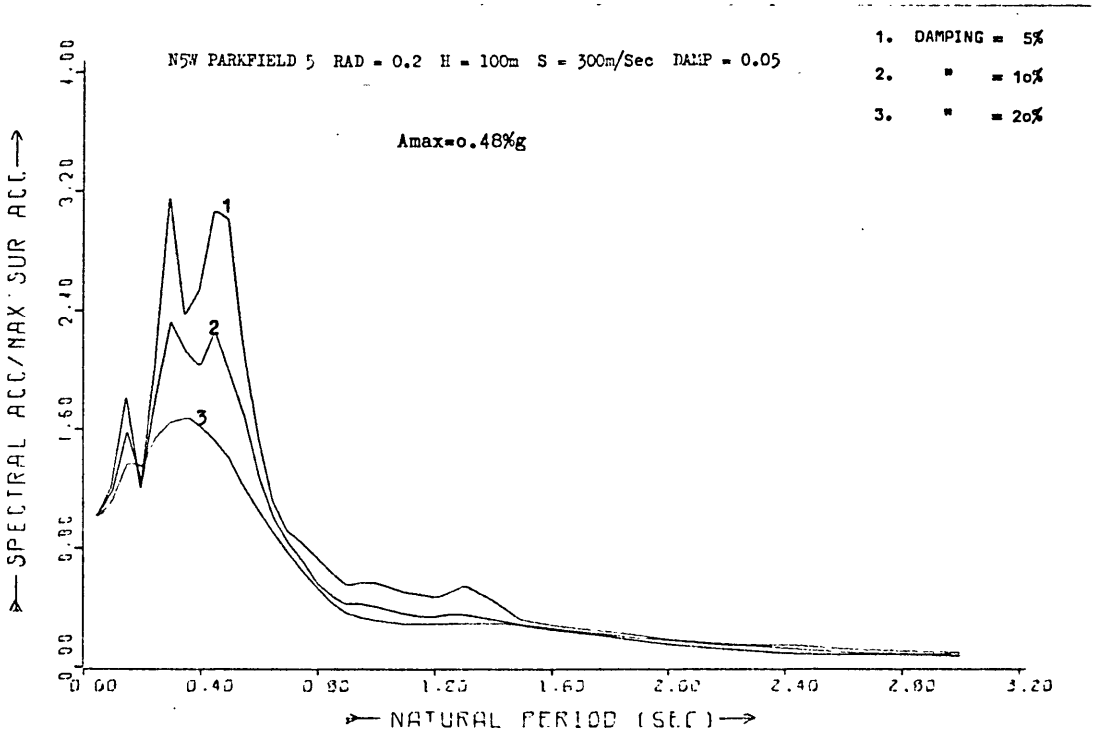


FIG.7.13d COMPUTED GROUND SURFACE ACCELERATION RESPONSE SPECTRA AT SITE NO 7.8

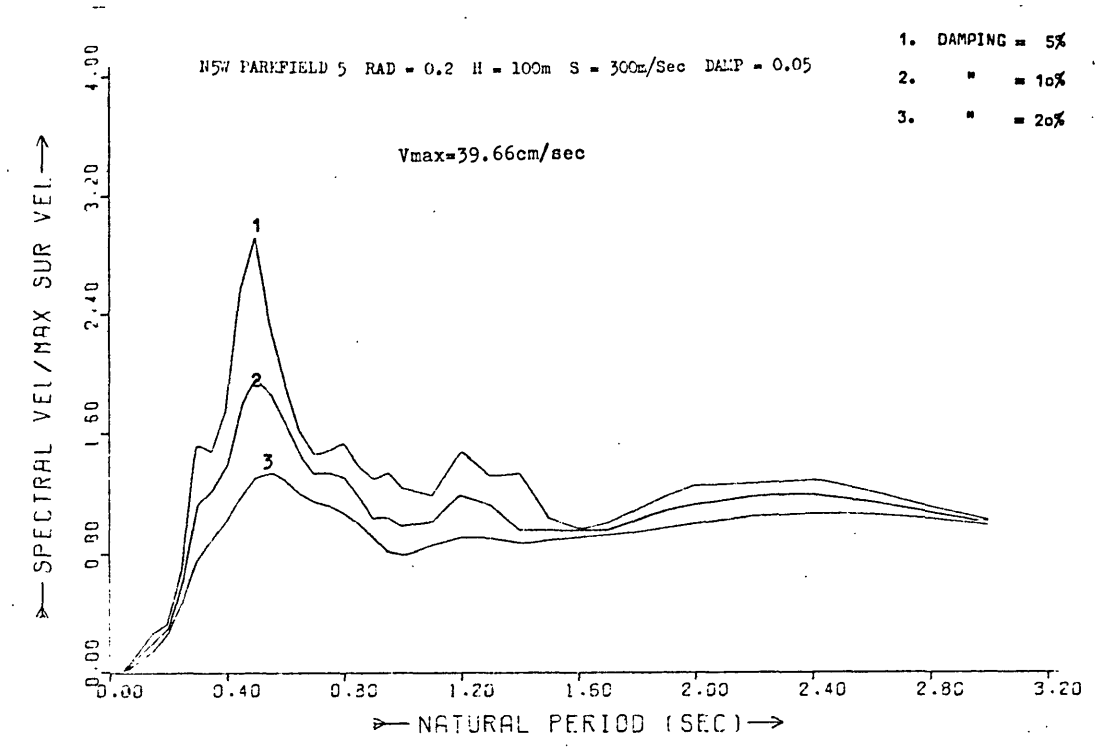


FIG.7.13e COMPUTED GROUND SURFACE VELOCITY RESPONSE SPECTRA AT SITE NO 7.8

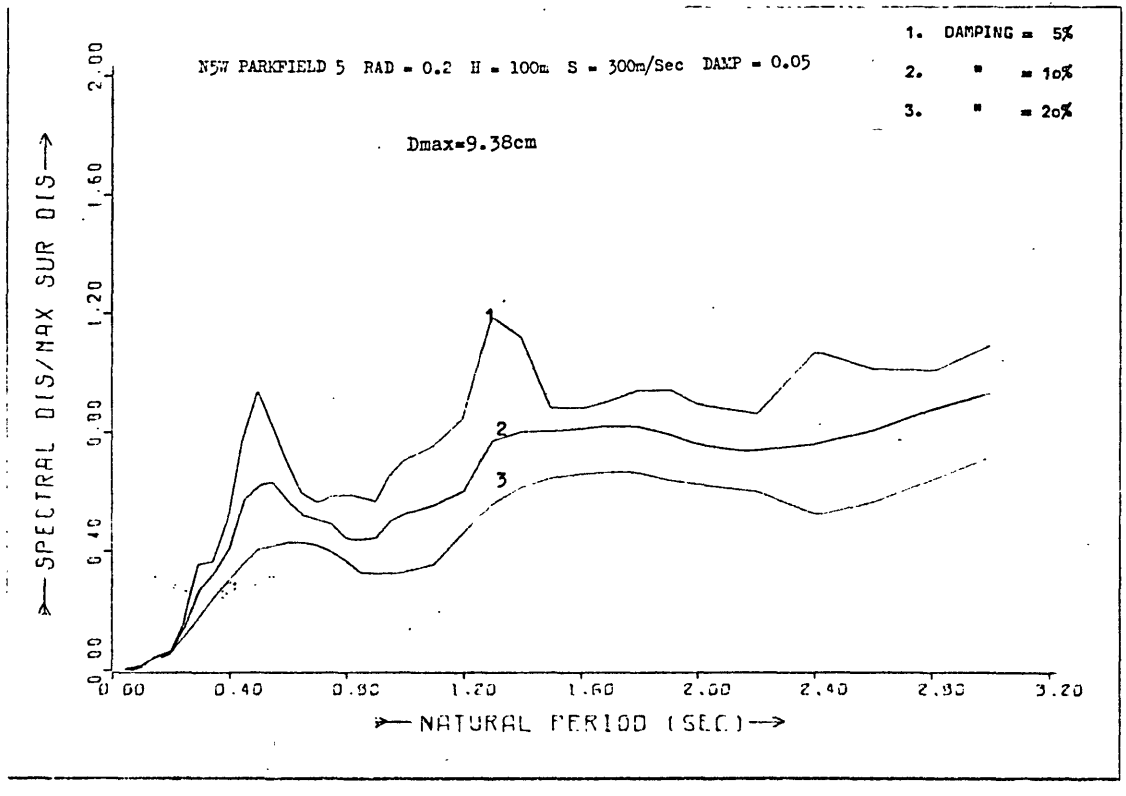
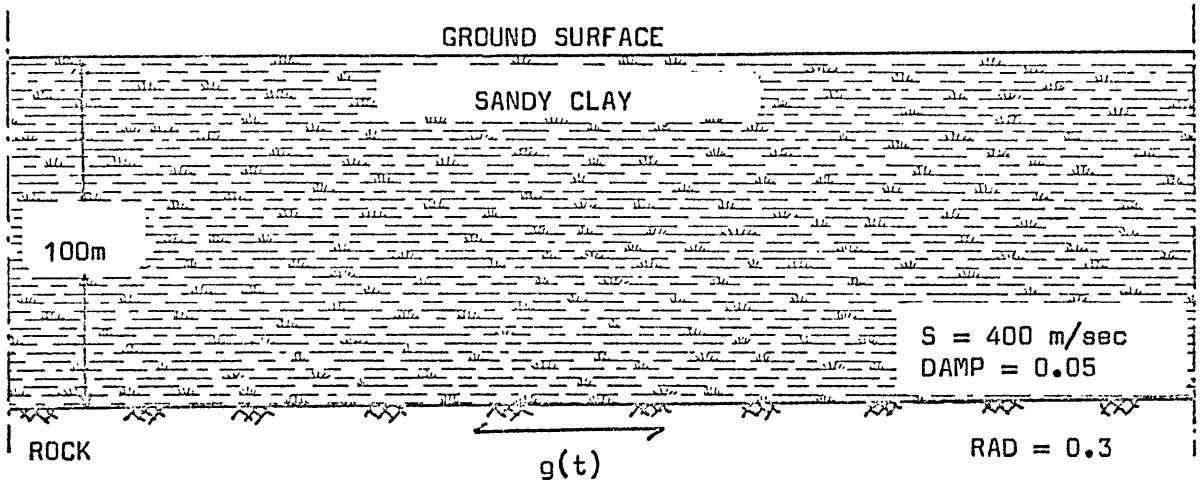


FIG.7.13f COMPUTED GROUND SURFACE DISPLACEMENT RESPONSE SPECTRA AT SITE NO 7.8



RESPONSE OF HYSTERETIC DEPOSIT UNDERLAIN BY DEFORMABLE BEDROCK

SCHEMATIC SOIL PROFILE FOR SITE NO 7.9

FIG. 7.14

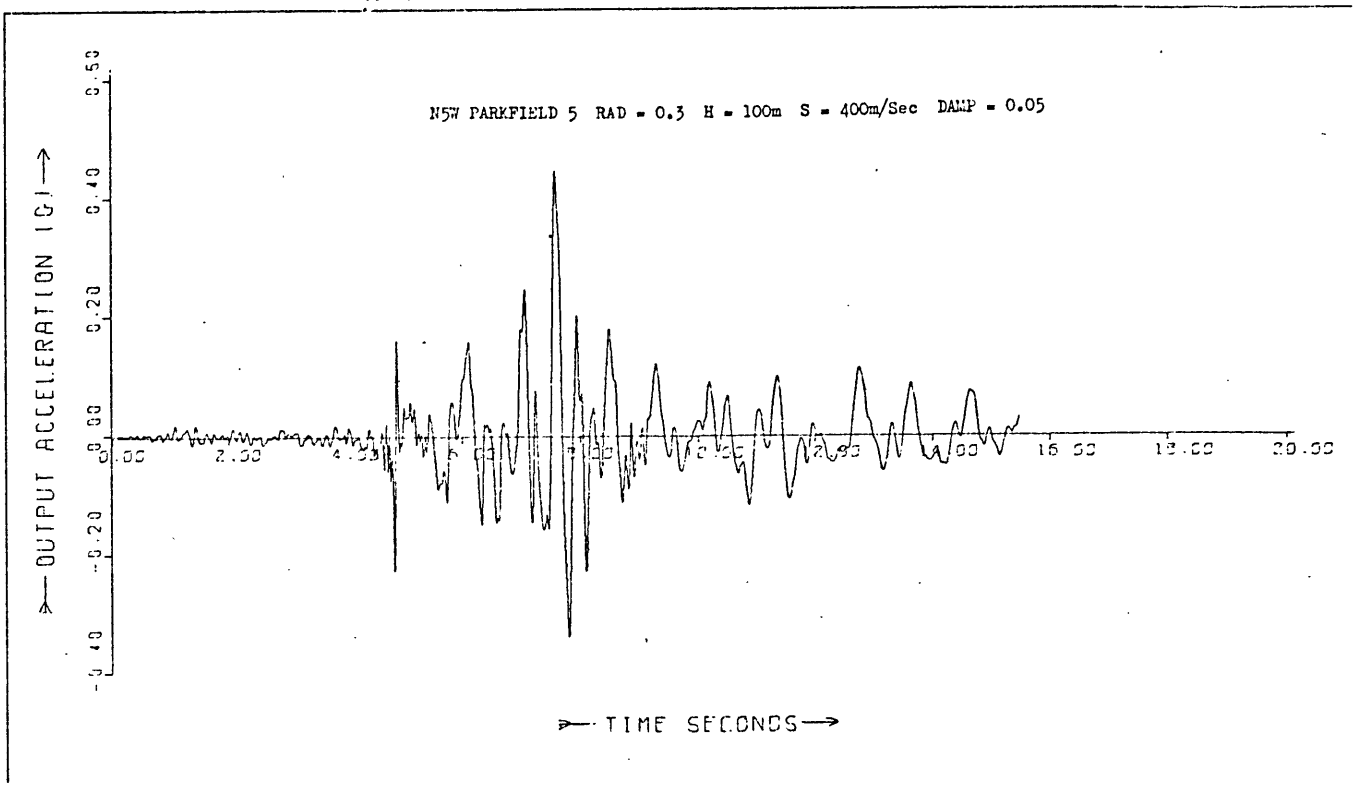


FIG.7.14a COMPUTED GROUND SURFACE ACCELERATION TIME HISTORY AT SITE NO 7.9

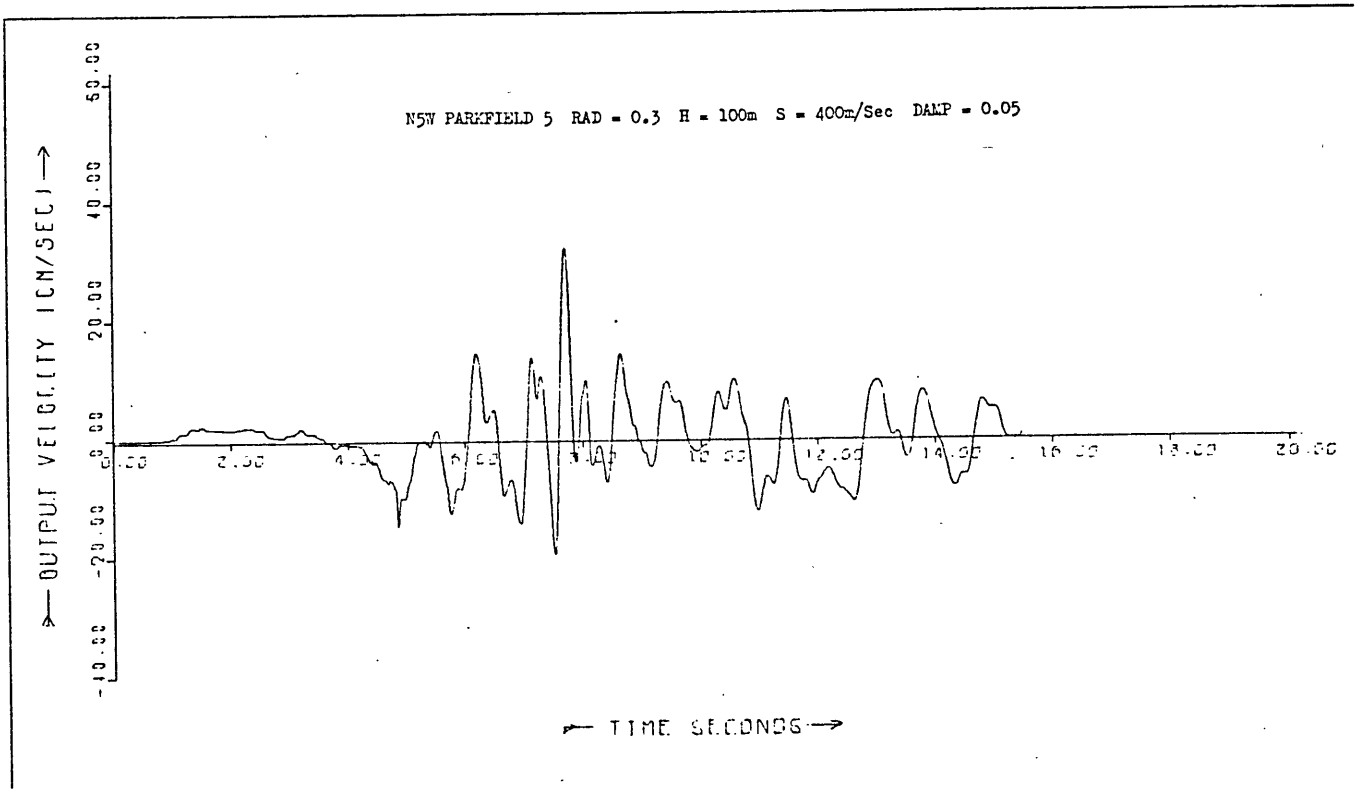


FIG.7.14b COMPUTED GROUND SURFACE VELOCITY TIME HISTORY AT SITE NO 7.9

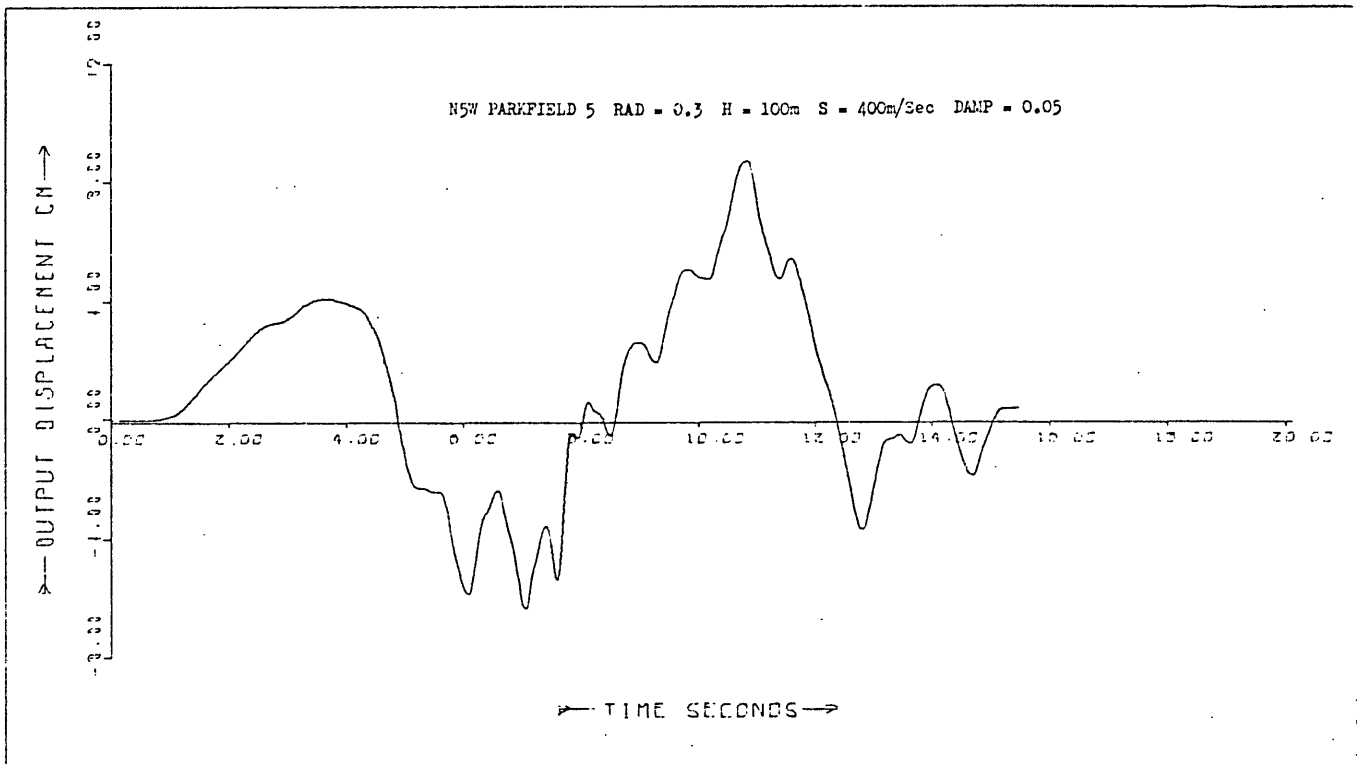


FIG.7.14c COMPUTED GROUND SURFACE DISPLACEMENT TIME HISTORY AT SITE NO 7.9

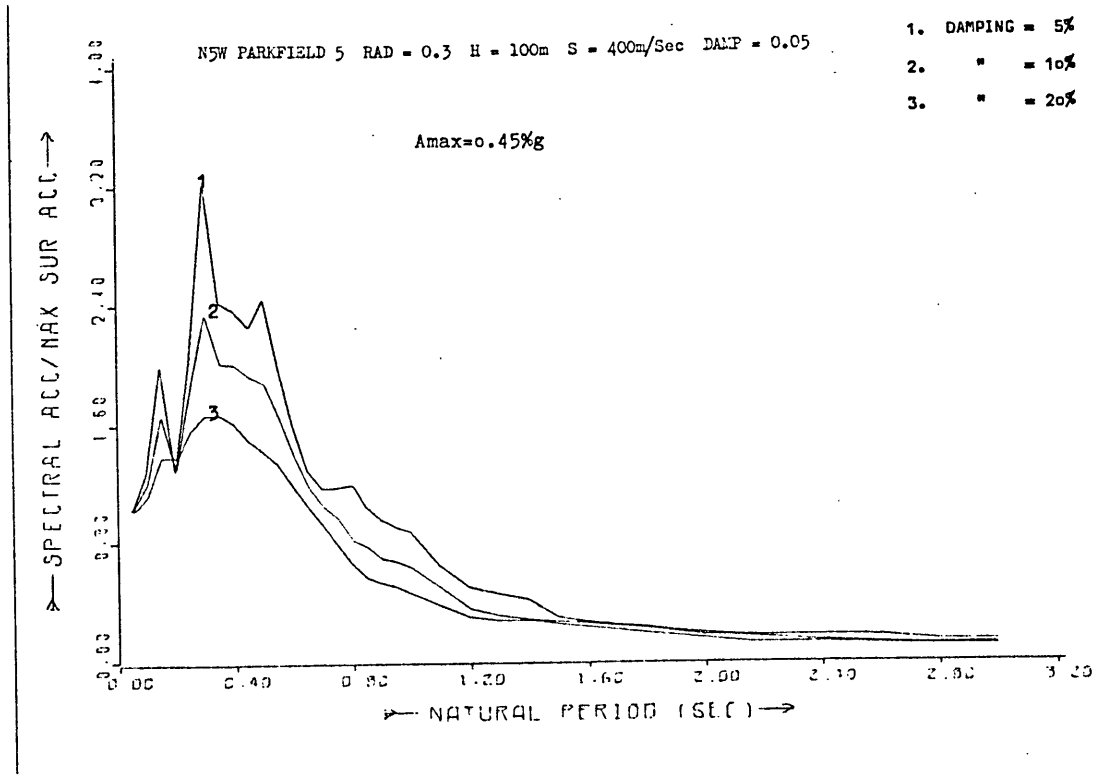


FIG.7.14d COMPUTED GROUND SURFACE ACCELERATION RESPONSE SPECTRA AT SITE NO 7.9

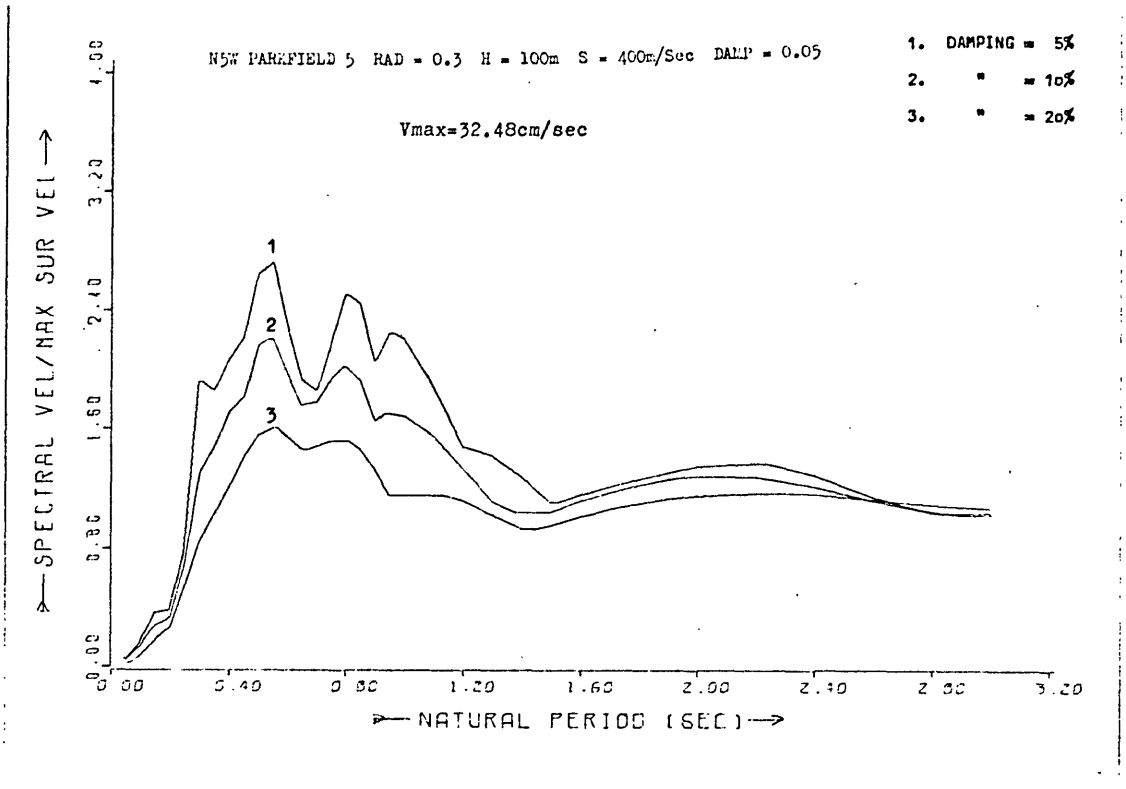


FIG.7.14e COMPUTED GROUND SURFACE VELOCITY RESPONSE SPECTRA AT SITE NO 7.9

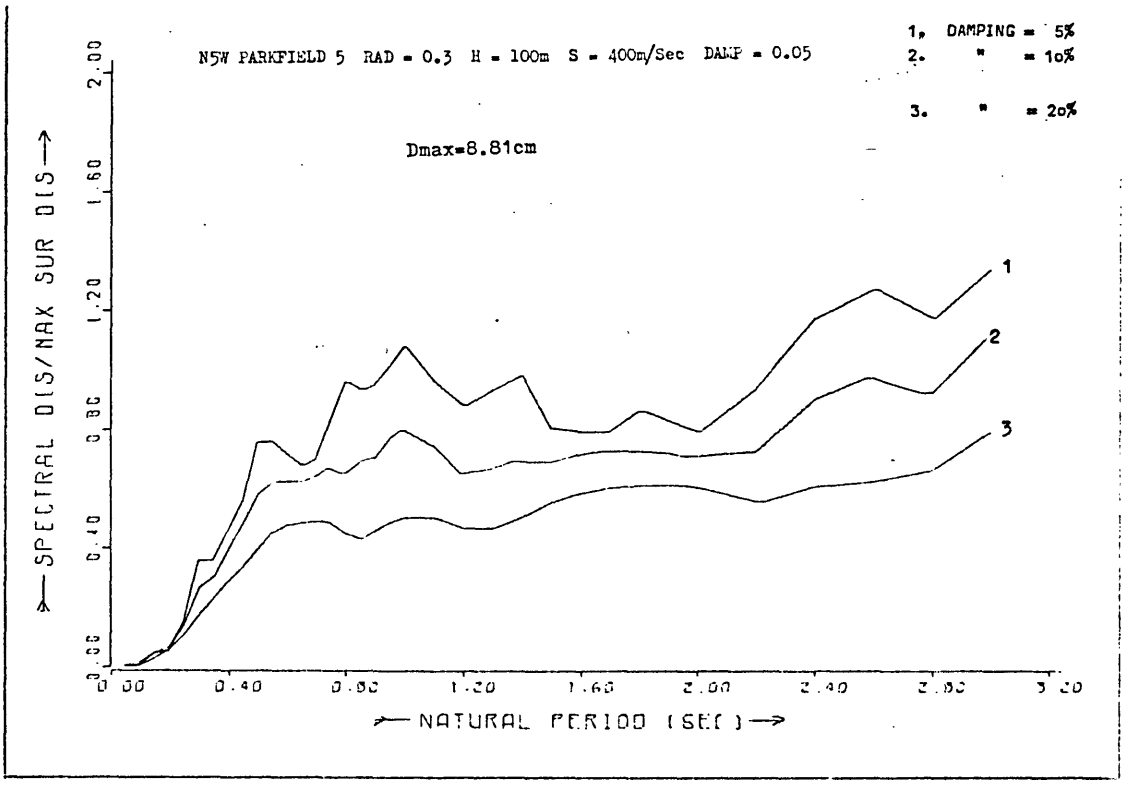
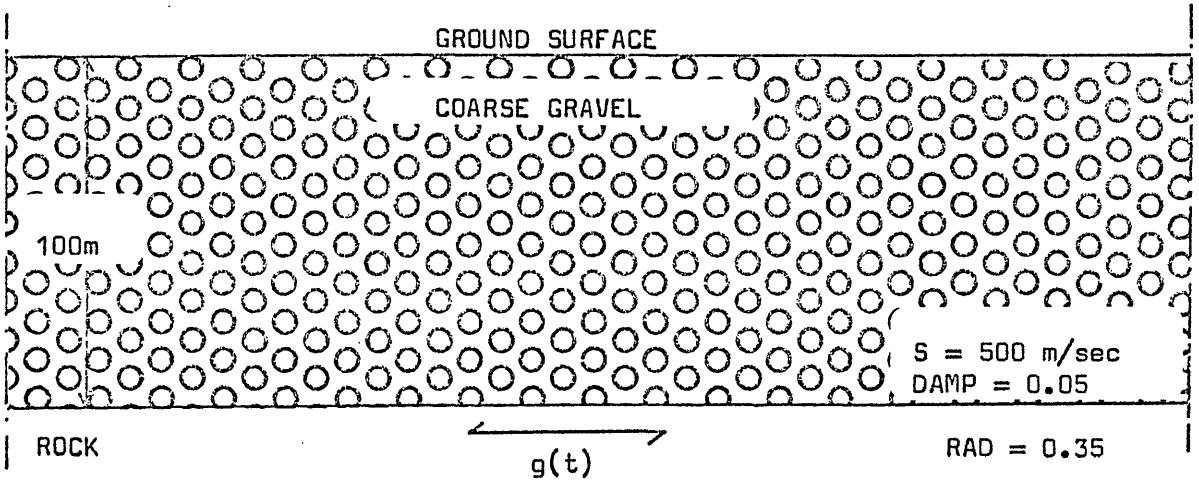


FIG.7.14f COMPUTED GROUND SURFACE DISPLACEMENT RESPONSE SPECTRA AT SITE NO 7.9



RESPONSE OF HYSTERETIC DEPOSIT UNDERLAIN BY DEFORMABLE BEDROCK

SCHEMATIC SOIL PROFILE FOR SITE NO 7.10

FIG. 7.15

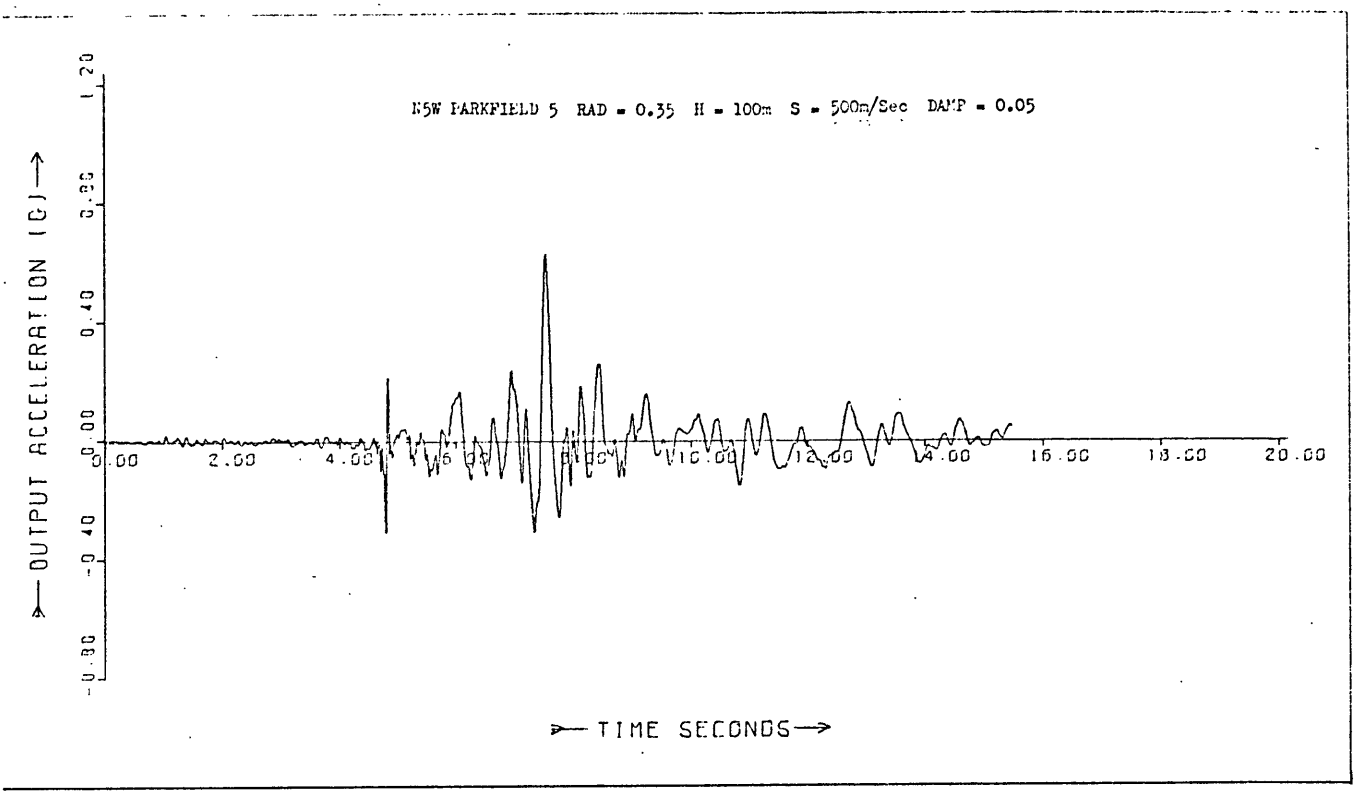


FIG.7.15a COMPUTED GROUND SURFACE ACCELERATION TIME HISTORY AT SITE NO 7.1o

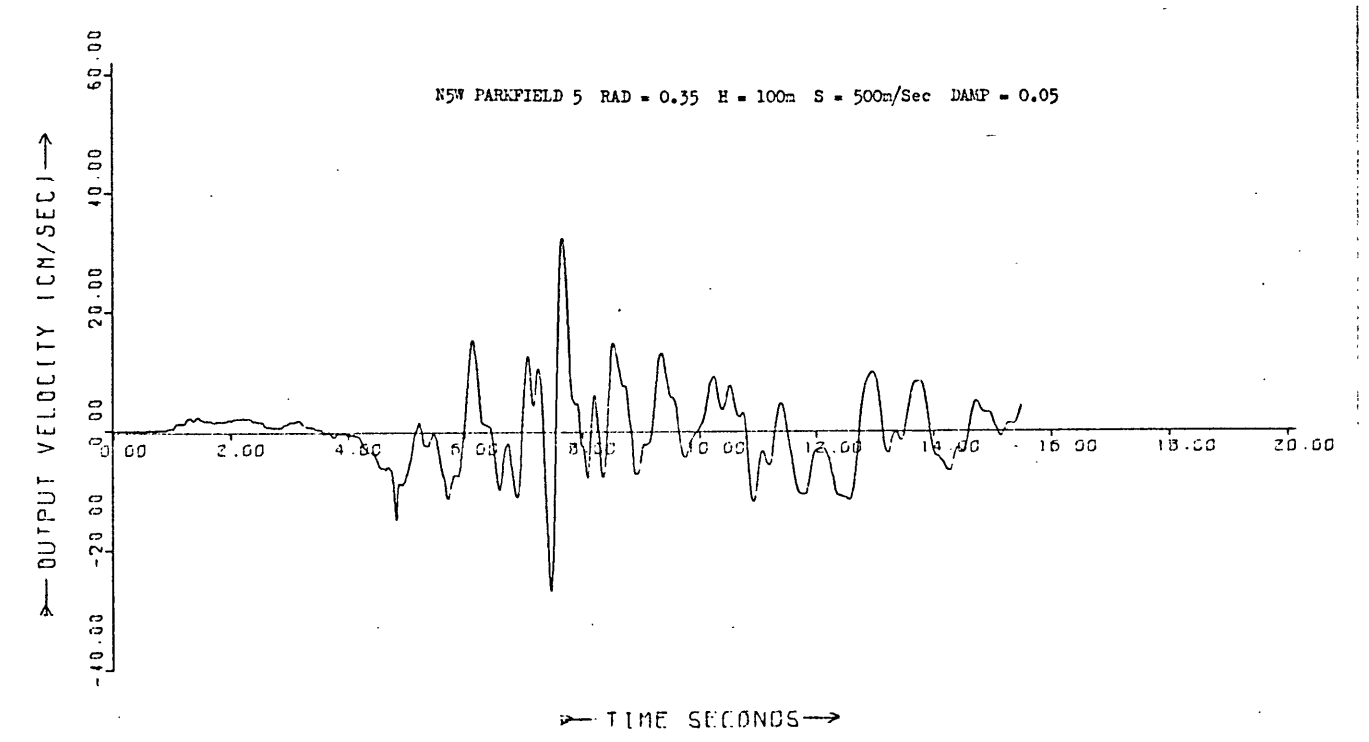


FIG.7.15b COMPUTED GROUND SURFACE VELOCITY TIME HISTORY AT SITE NO 7.1o

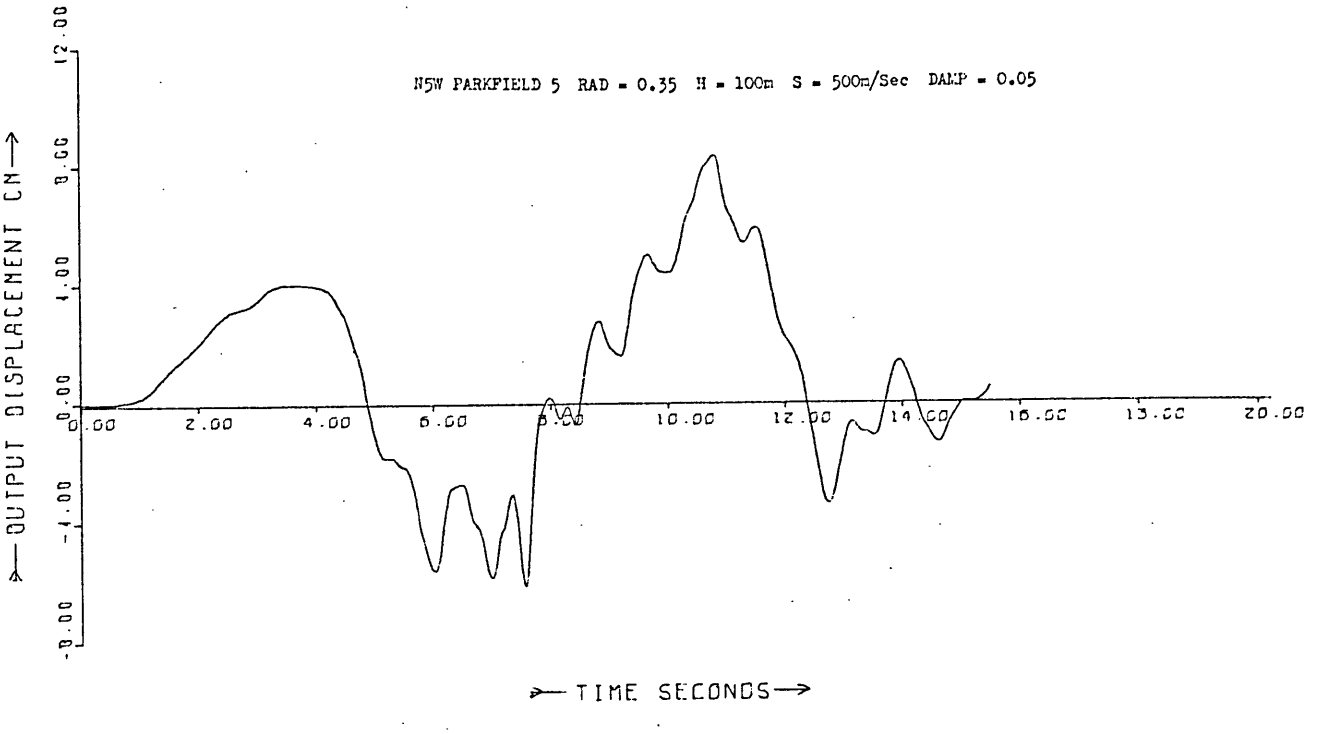


FIG.7.15c COMPUTED GROUND SURFACE DISPLACEMENT TIME HISTORY AT SITE NO 7.1o

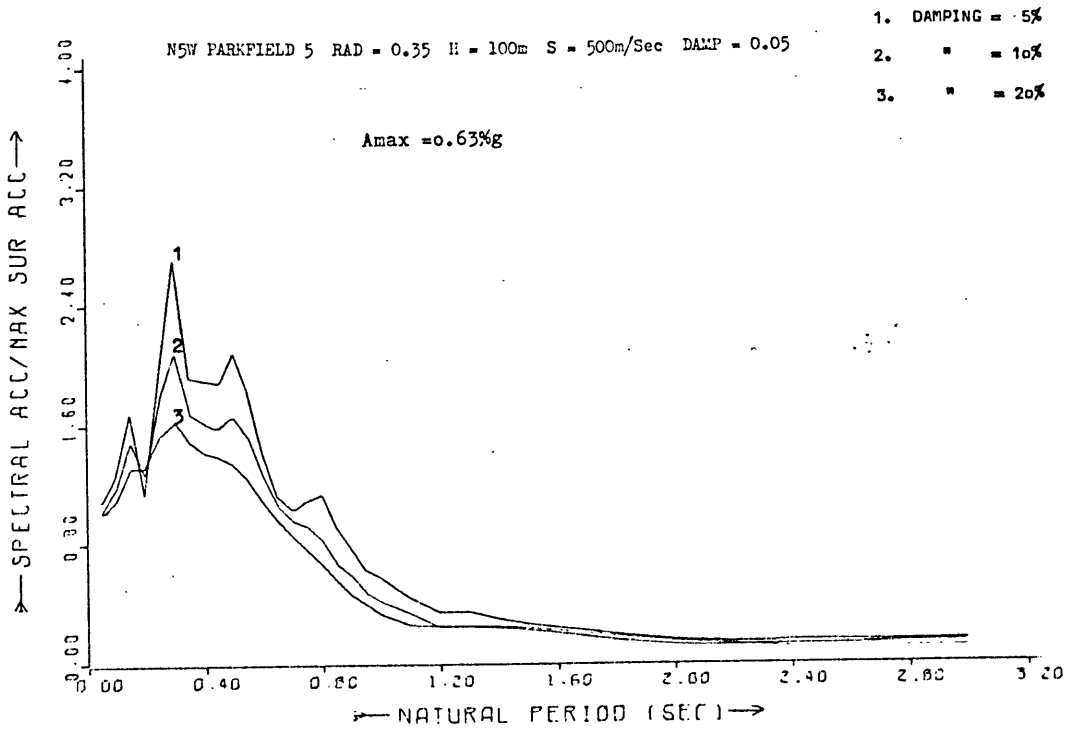


FIG.7.15d COMPUTED GROUND SURFACE ACCELERATION RESPONSE SPECTRA AT SITE NO 7.1o

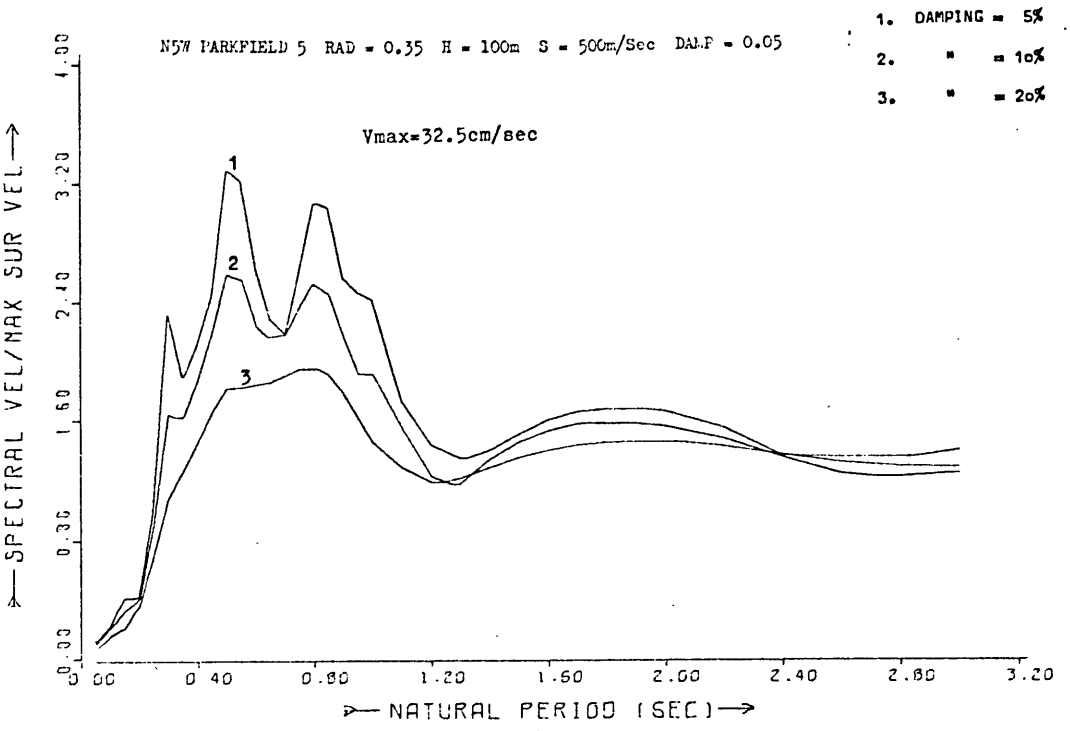


FIG.7.15e COMPUTED GROUND SURFACE VELOCITY RESPONSE SPECTRA AT SITE NO 7.1o

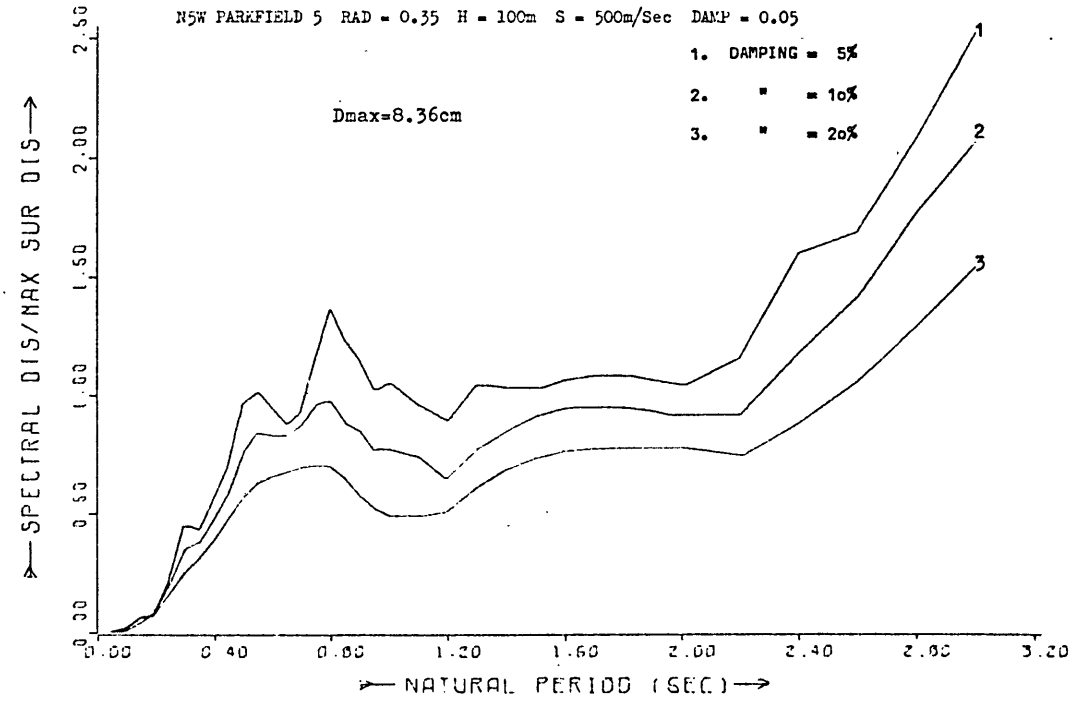


FIG.7.15f COMPUTED GROUND SURFACE DISPLACEMENT RESPONSE SPECTRA AT SITE NO 7.1o

constant as the softness decreases.

Figs. 7.11f through 7.15f illustrate normalized displacement spectrum for the deposits. The results show that amplitudes of peak spectral displacements increase to a peak value for soft to medium clay, then decrease as the softness decreases. The ratios of amplitude of the maximum spectral acceleration/peak ground surface acceleration, amplitude of the maximum spectral velocity/peak ground surface velocity and amplitude of the maximum spectral displacement/peak ground surface displacement are also almost constant.

An examination of results presented in table 7.1 shows that peak ground surface accelerations, velocities and displacements, as expected, follow the general behaviour of peak amplitude of maximum spectral accelerations, velocities and displacements. The results also illustrate that an increase in softness of the overburden does not necessarily imply a decrease in amplitude of peak ground acceleration. This is clearly illustrated by comparison of computed peak surface acceleration for sandy clay - 0.45%g with loose gravel - 0.48%g, indicating that, although loose gravel is softer than sandy clay, it has developed higher maximum surface acceleration. The results also show that soft site does not always imply large displacements; this is clearly shown by the comparison of computed maximum displacement at surface of soft clay - 9.37 cm with that of soft to medium clay - 9.89 cm, soft clay being softer than soft to medium clay.

The amplitudes of maximum acceleration and velocity have often been used to discuss the overall acceleration or velocity amplitude distribution. Figs. 7.11a,b through 7.15a,b illustrate that these

time histories are not similar, indicating that a single peak on the time histories,(either velocity or acceleration) is a very unreliable descriptor of the overall acceleration or velocity amplitude distribution. A new parameter "S" called strength of the earthquake motion, which is a measure of energy available for damage at a given site, is introduced (see section 7.3.1).

An overall examination of table 7.1 indicates that the site consisting of loose gravel with a peak ground velocity of 39.66 cm/sec., which is the greatest among the amplitudes of peak velocities of the five deposits, has shown the lowest intensity of ground shaking in terms of "S" and coarse gravel the greatest, illustrating that energy available for damage to buildings located on coarse ground is 4.7 times more than that on loose gravel. The results also emphasise the fact that it is therefore necessary to consider the whole velocity time history of ground motion.

Peak ground acceleration has often been chosen as the key descriptive parameter of the shaking. Results presented in table 7.1 indicate that two sites (soft to medium clay and sandy clay) with the same peak acceleration will have quite different damaging potential in terms of "S".

7.2.4. CONCLUDING STATEMENT

From the forgoing discussions it can be concluded that:

a) Increasing the softness of the deposit decreases the fundamental period of the deposit. This increase may increase or decrease response amplitudes.

b) Soft deposits do not necessarily imply that structures on these sites will experience higher inertia forces. The factors controlling damage on soft deposits are duration of ground shaking and reduction in moment capacity at joints of the structures due to differential settlements.

c) "Strength" may be a better measure of the destructiveness of ground motions than the amplitude of maximum acceleration or velocity.

d) In most cases (not always) soft soils underlying structures are likely to undergo large displacements during earthquakes; therefore, it is essential to design these structures for large displacements.

7.3. INVESTIGATION OF INFLUENCE OF FUNDAMENTAL PERIOD ON RESPONSE OF SOIL DEPOSITS AND A NEW MEASURE OF THE DESTRUCTIVENESS OF GROUND MOTION

It has been shown by Idriss et. al.[33] that the response of semi-infinite layers and earth banks with uniform moduli and rigid bases may be expressed as a function of the fundamental periods of the deposits and the banks. For the solution developed in this thesis (see chapter 4), due to the fact that both radiation damping ratio "RAD" and fundamental period of the deposit "T_1" are functions of shear wave velocity of the overburden, the fundamental period can not be used directly as a parameter to define the response. Role of changing 'T_1' keeping "RAD" constant is similar to that of changing depth to bedrock "H".

The response of 9 soil deposits of soft clay with hysteretic damping ratio of 0.1 and radiation damping ratio of 0.2 subjected to

E W component of Porthueneme having different depths to bedrock, ranging from 10m to 70m, were evaluated. On each deposit the corresponding fundamental period is marked and is shown in figs. 7.16 to 7.24.

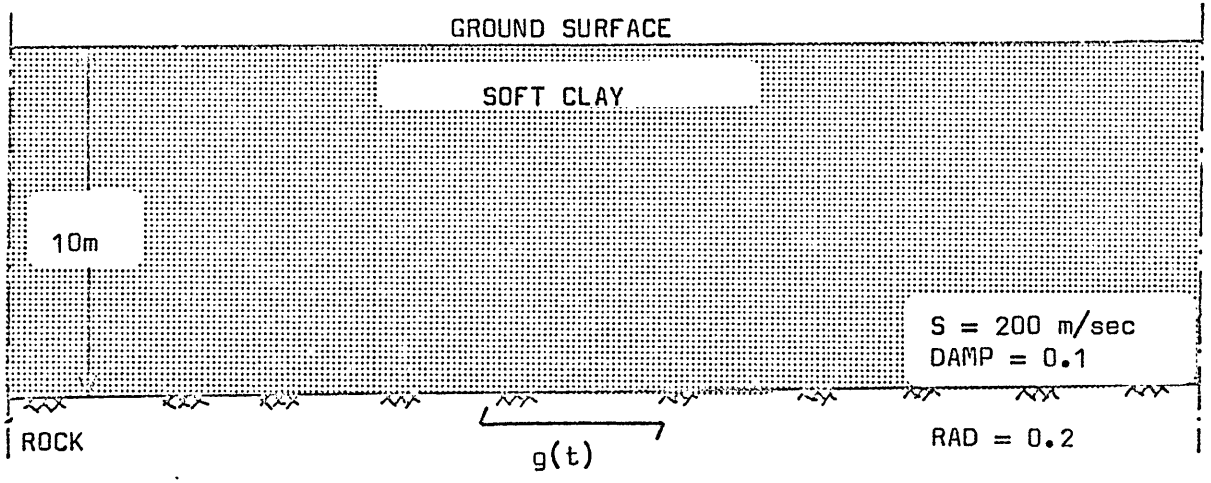
The results of the calculations in the form of acceleration, velocity and displacement time histories and acceleration, velocity and displacement response spectrum are shown in figs. 7.16a,b,c,d,e,f to 7.24a,b,c,d,e,f. It is important to note that, as expected, the response of the semi-infinite layer, whose fundamental period is 0.4 second and is close to the predominant period of the bedrock motion 0.38 second, has shown the greatest amplitude of spectral acceleration. The influence of depth to bedrock is fully investigated in section 7.7. The above cases were analysed in order to study the importance of the new parameter "Strength", which is a measure of severity of ground shaking.

7.3.1. A PARAMETER AS A MEASURE OF SEVERITY OF GROUND SHAKING

Consider an element of soil, mass "m" at the surface of an overburden. The kinetic energy which will be available for damage at time "t" while the velocity is $v(t)$ is:

$$E_{Kinetic} = \tfrac{1}{2}mv^2(t) \qquad (7.2)$$

or the total kinetic energy available to be fed into structures located on the deposit over a time interval "T_{dur}" where T_{dur} is the length of shaking is:



FUNDAMENTAL PERIOD OF THE DEPOSIT = 0.2

RESPONSE OF HYSTERETIC DEPOSIT UNDERLAIN BY DEFORMABLE BEDROCK

SCHEMATIC SOIL PROFILE FOR SITE NO 7.11

FIG. 7.16

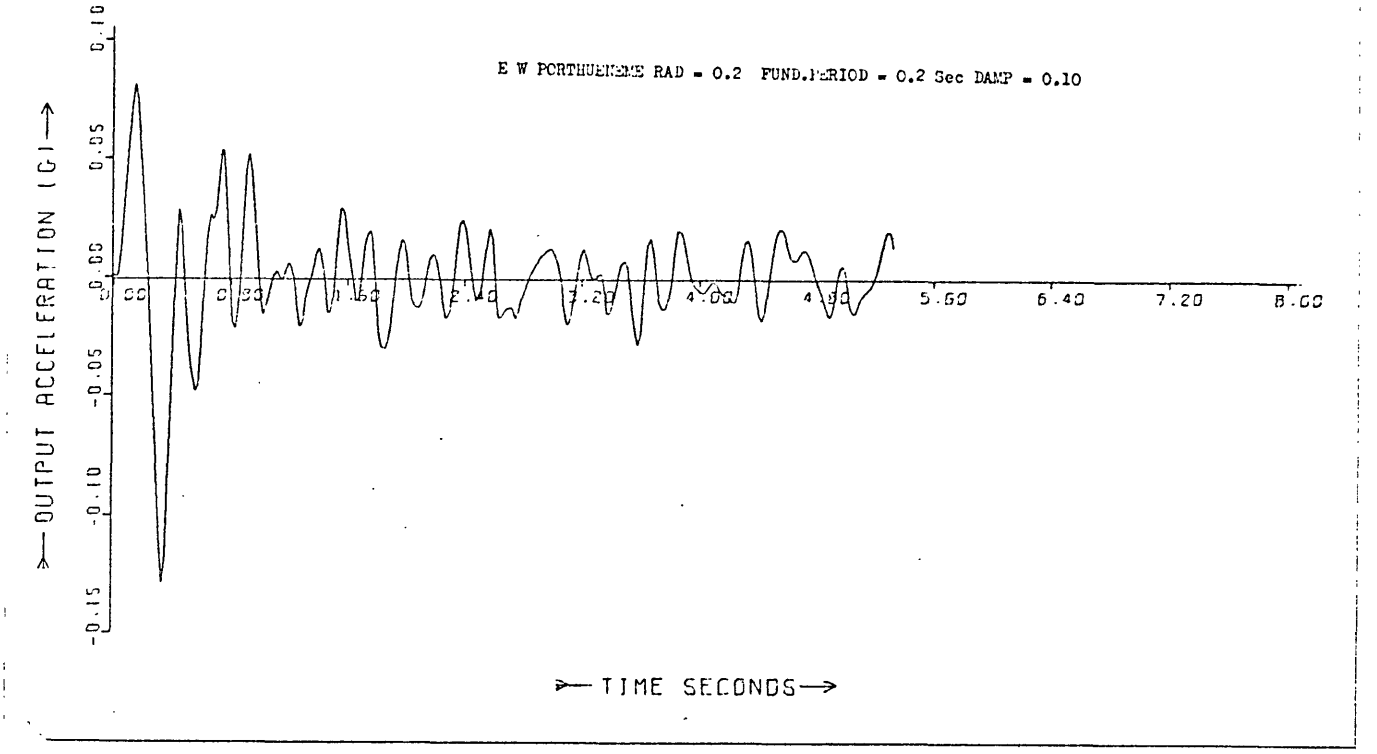


FIG. 7.16a COMPUTED GROUND SURFACE ACCELERATION TIME HISTORY AT SITE NO 7.11

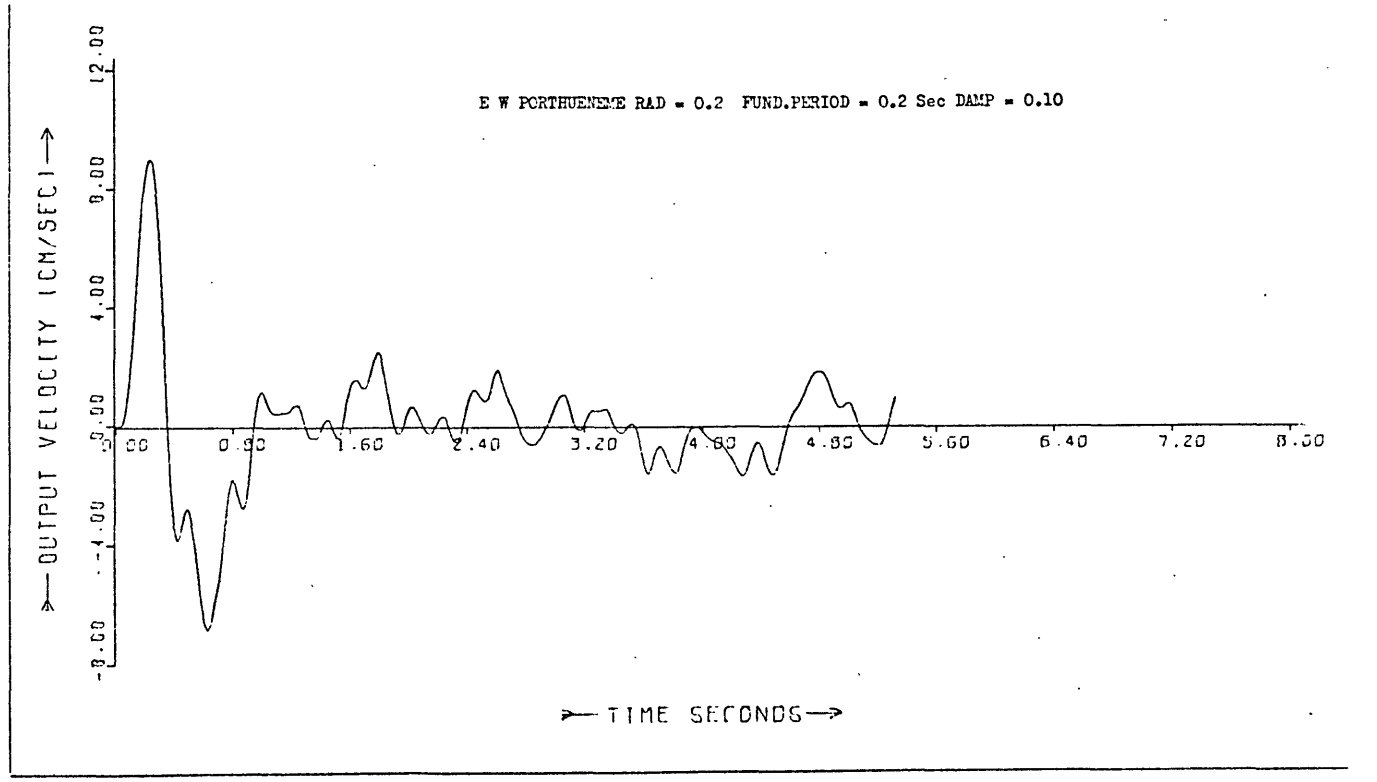


FIG. 7.16b COMPUTED GROUND SURFACE VELOCITY TIME HISTORY AT SITE NO 7.11

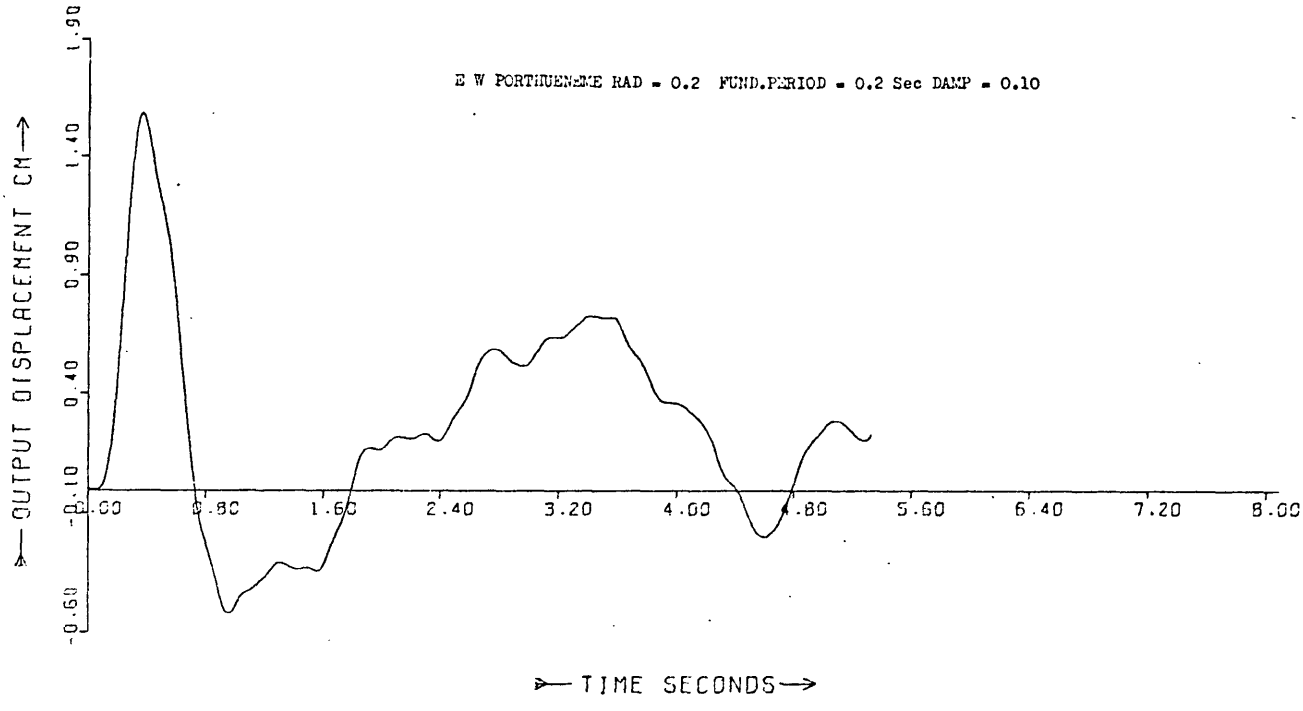


FIG.7.16c COMPUTED GROUND SURFACE DISPLACEMENT TIME HISTORY AT SITE NO 7.11

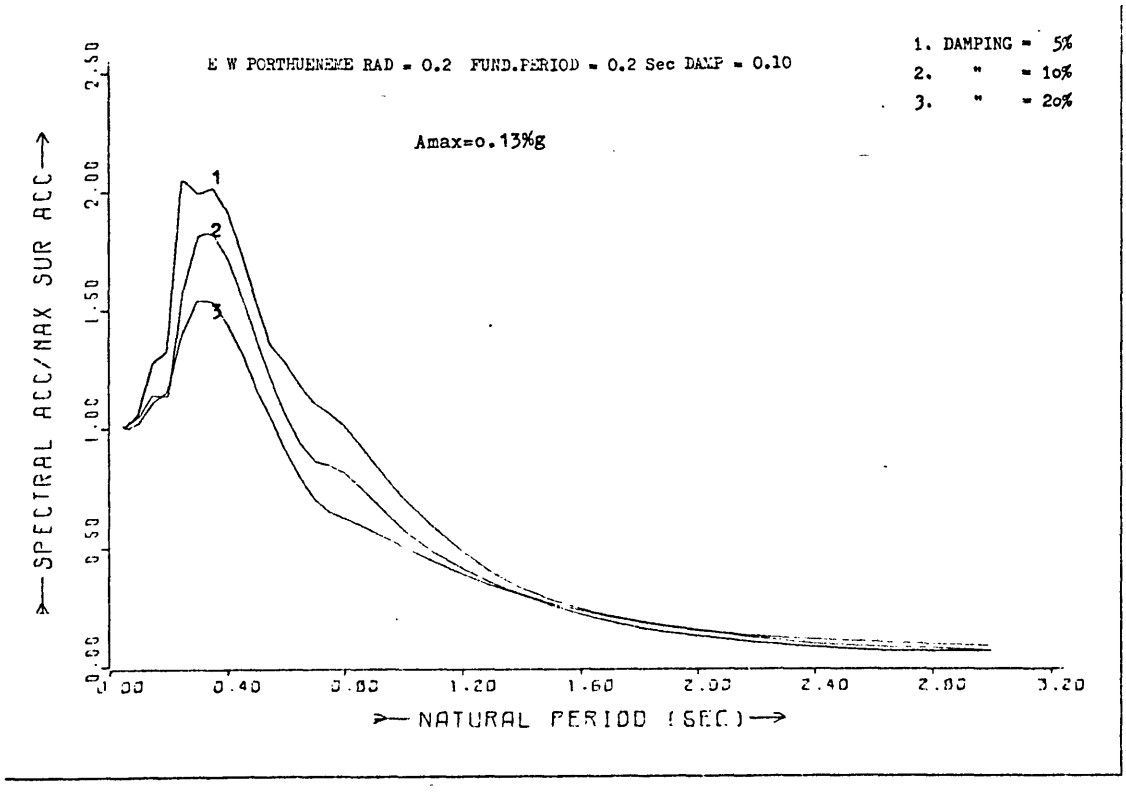


FIG.7.16d COMPUTED GROUND SURFACE ACCELERATION RESPONSE SPECTRA AT SITE NO 7.11

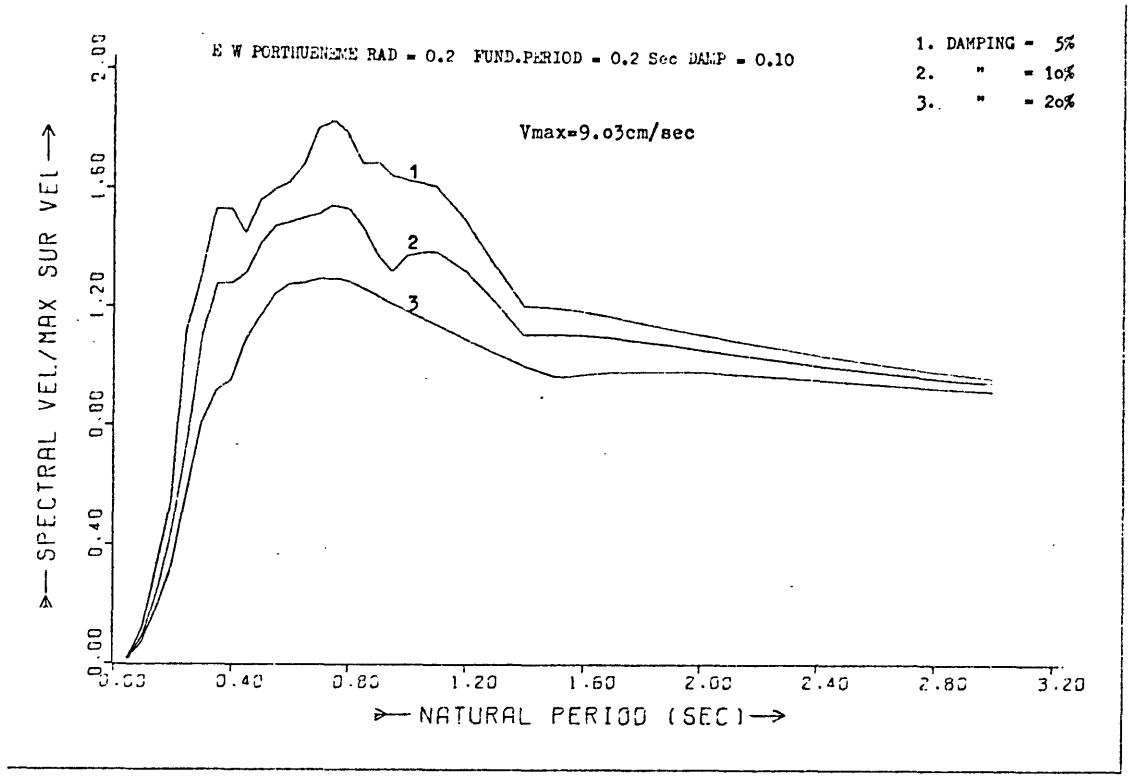


FIG. 7.16e COMPUTED GROUND SURFACE VELOCITY RESPONSE SPECTRA AT SITE NO 7.11

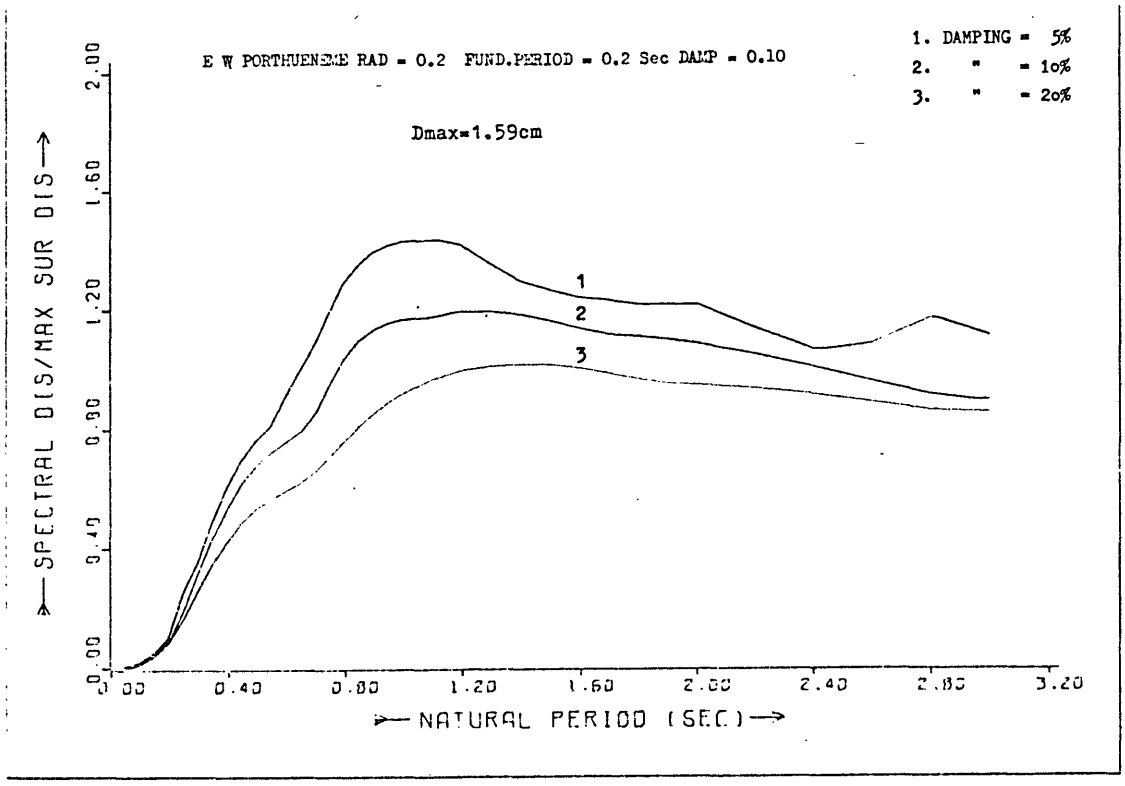
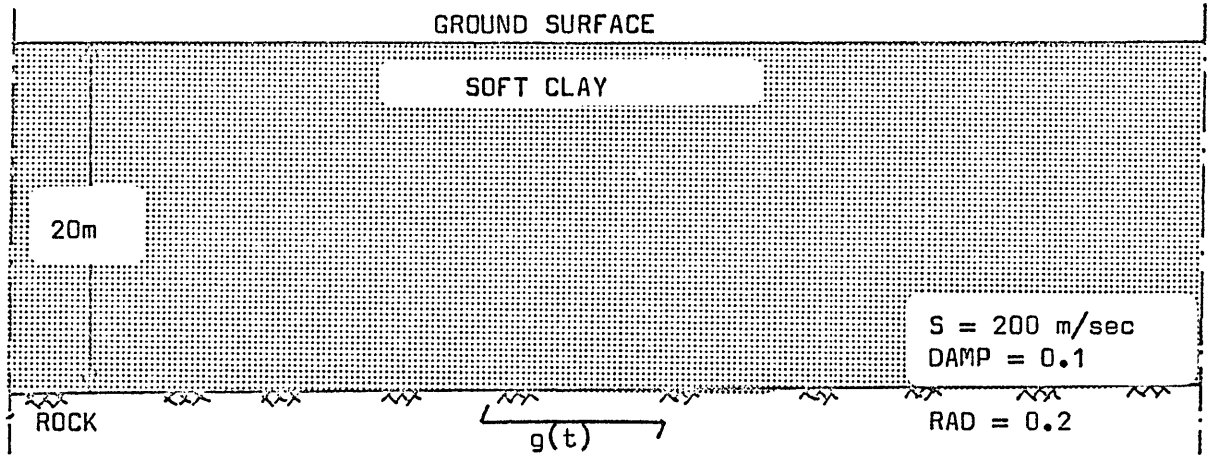


FIG 7.16f COMPUTED GROUND SURFACE DISPLACEMENT RESPONSE SPECTRA AT SITE NO 7.11



FUNDAMENTAL PERIOD OF THE DEPOSIT = 0.4

RESPONSE OF HYSTERETIC DEPOSIT UNDERLAIN BY DEFORMABLE BEDROCK

SCHEMATIC SOIL PROFILE FOR SITE NO 7.12

FIG. 7.17

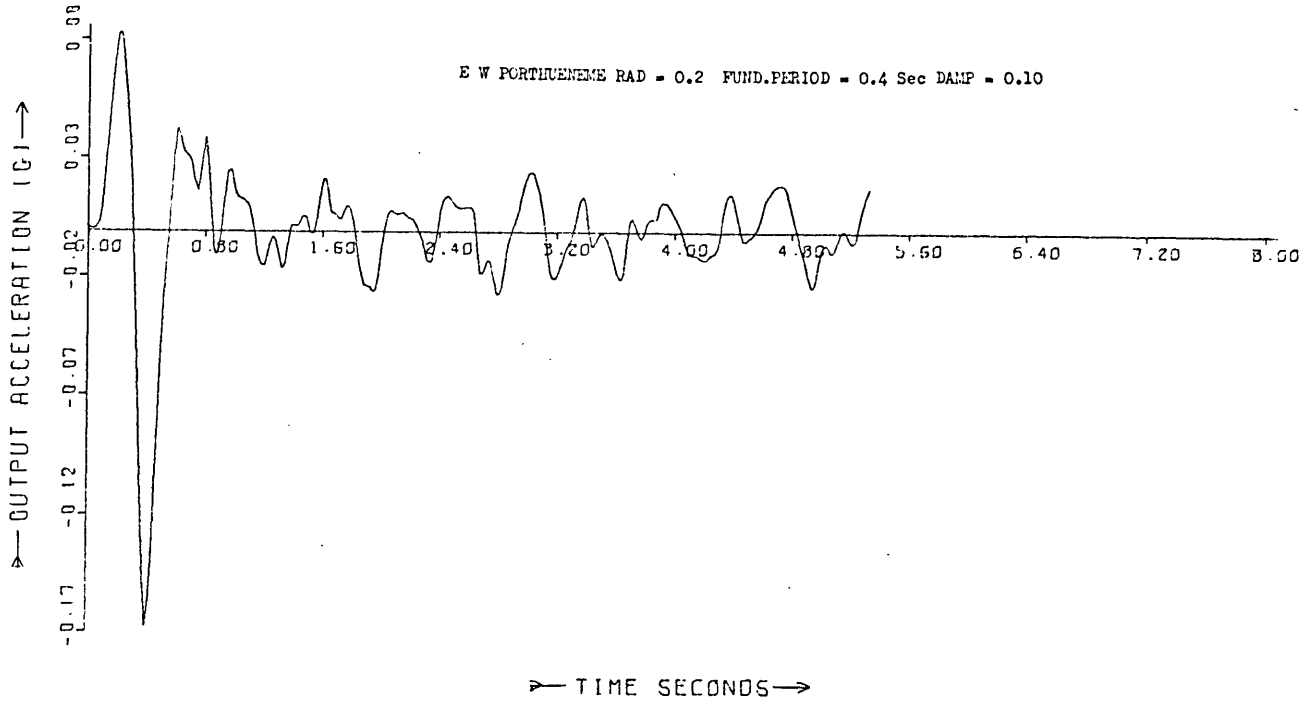


FIG.7.17a COMPUTED GROUND SURFACE ACCELERATION TIME HISTORY AT SITE NO 7.12

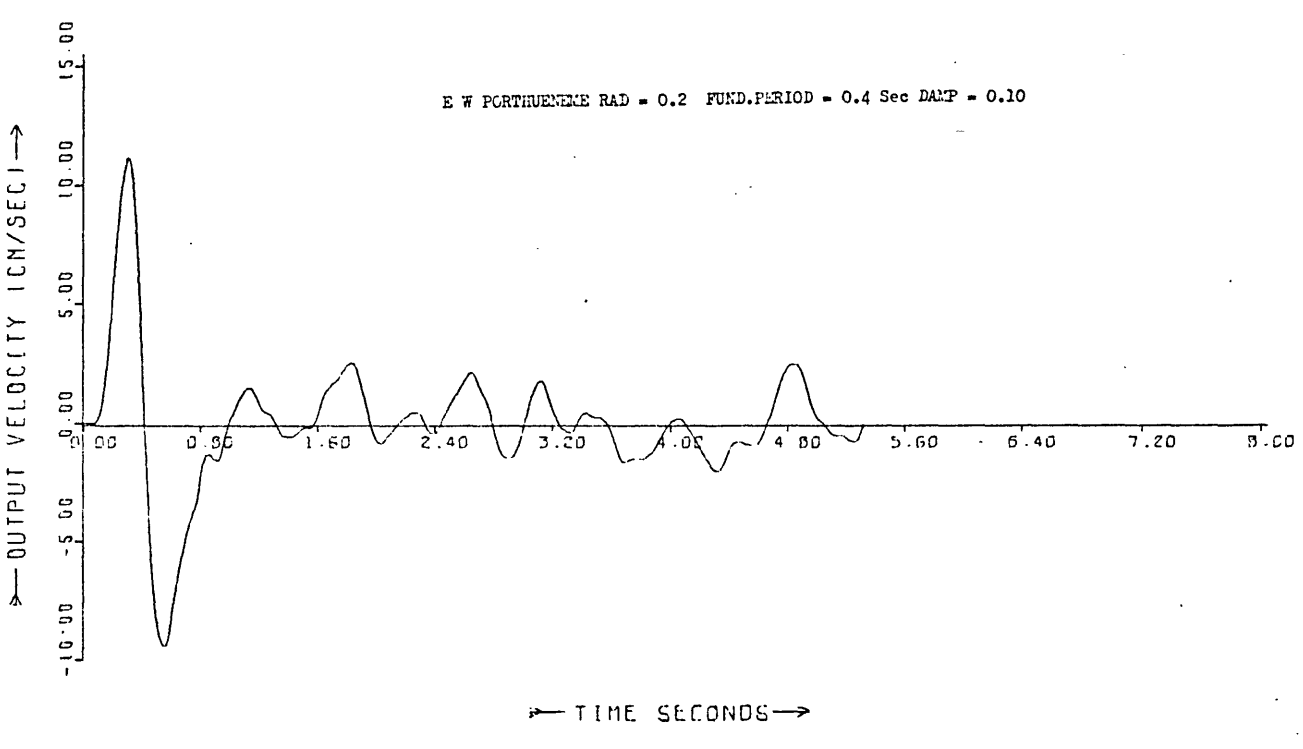


FIG.7.17b COMPUTED GROUND SURFACE VELOCITY TIME HISTORY AT SITE NO 7.12

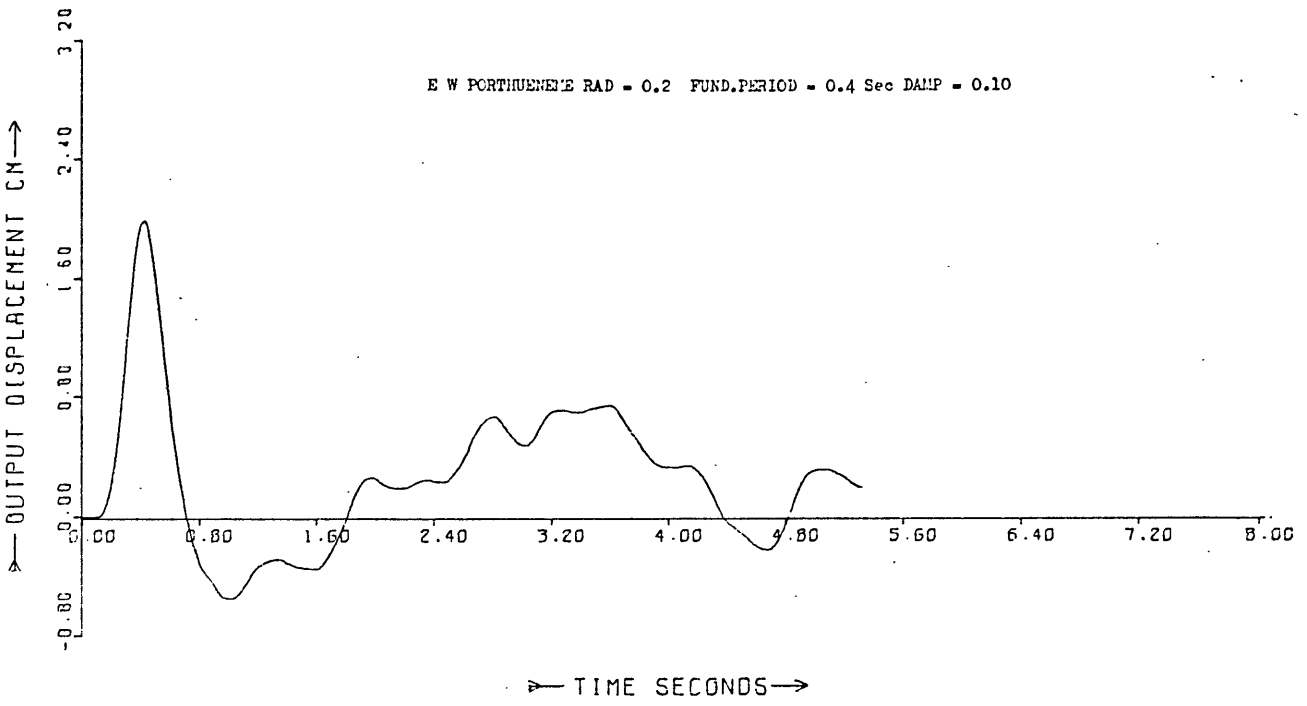


FIG.7.17c COMPUTED GROUND SURFACE DISPLACEMENT TIME HISTORY AT SITE NO 7.12

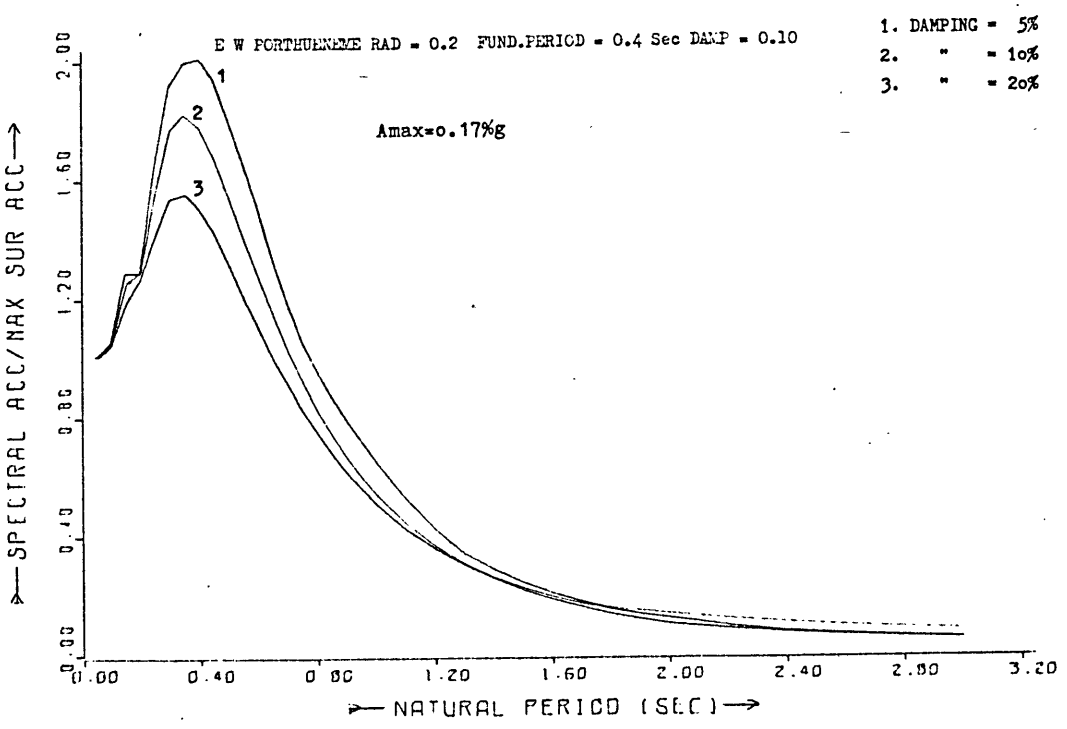


FIG.7.17d COMPUTED GROUND SURFACE ACCELERATION RESPONSE SPECTRA AT SITE NO 7.12

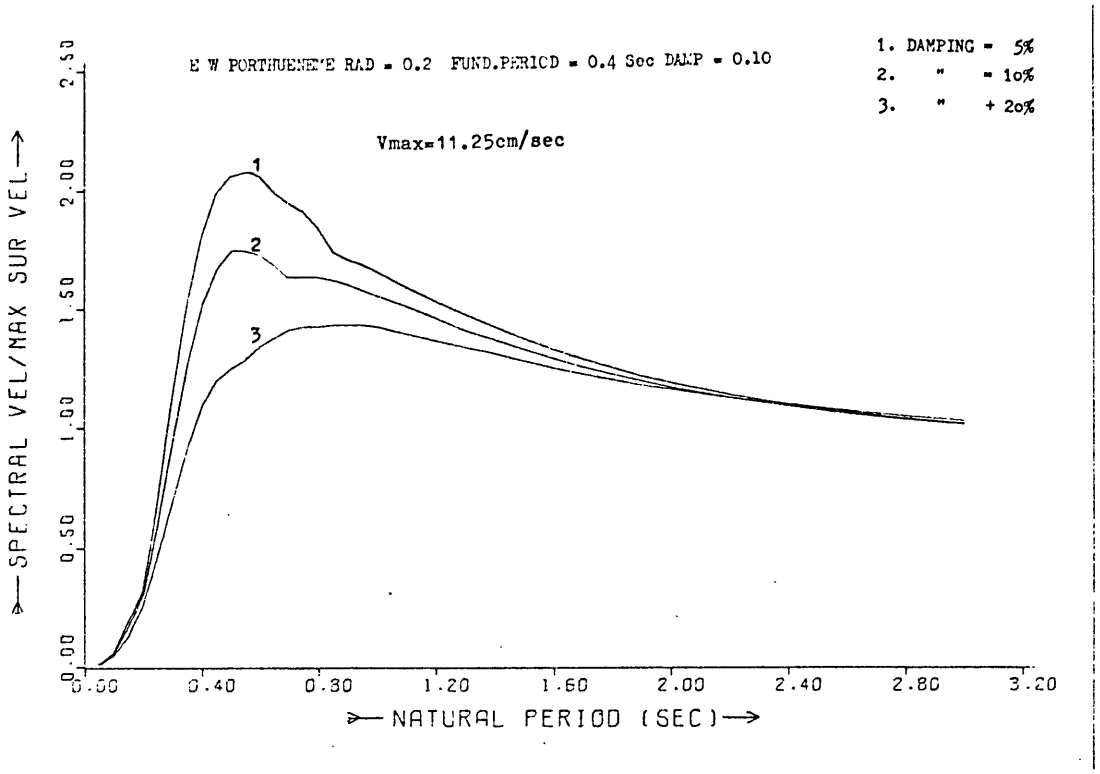


FIG 7.17e COMPUTED GROUND SURFACE VELOCITY RESPONSE SPECTRA AT SITE NO 7.12

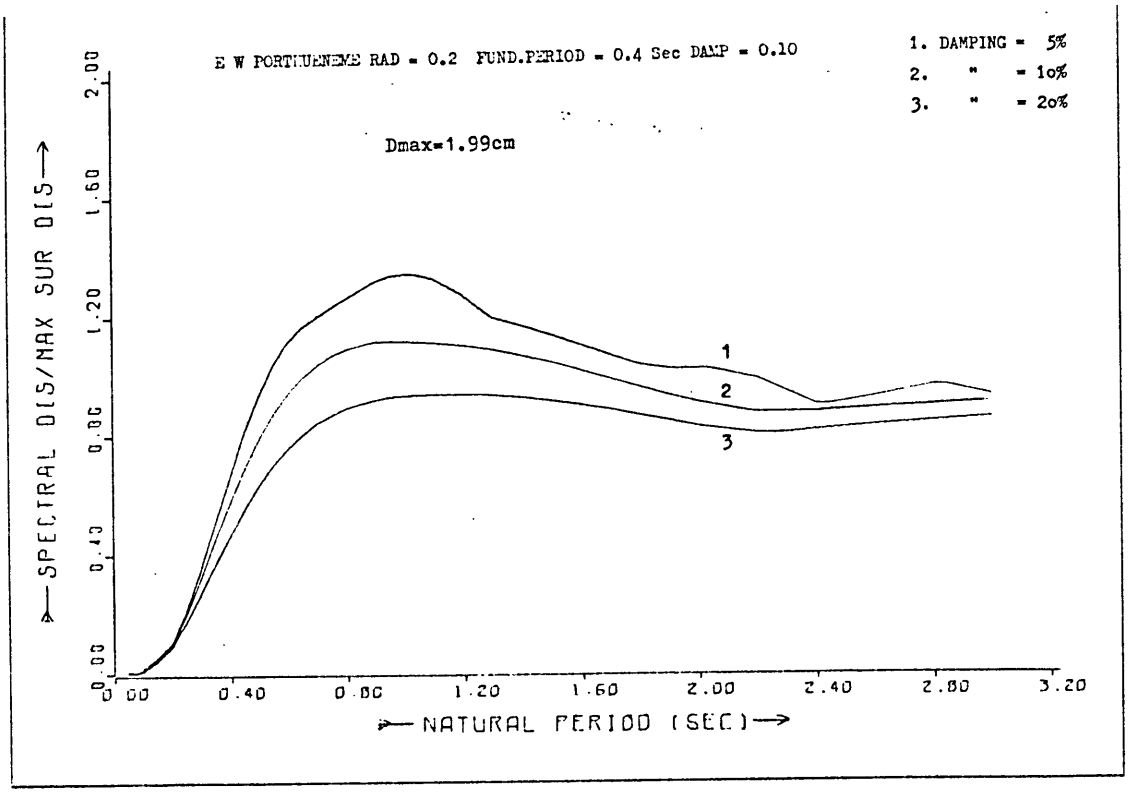
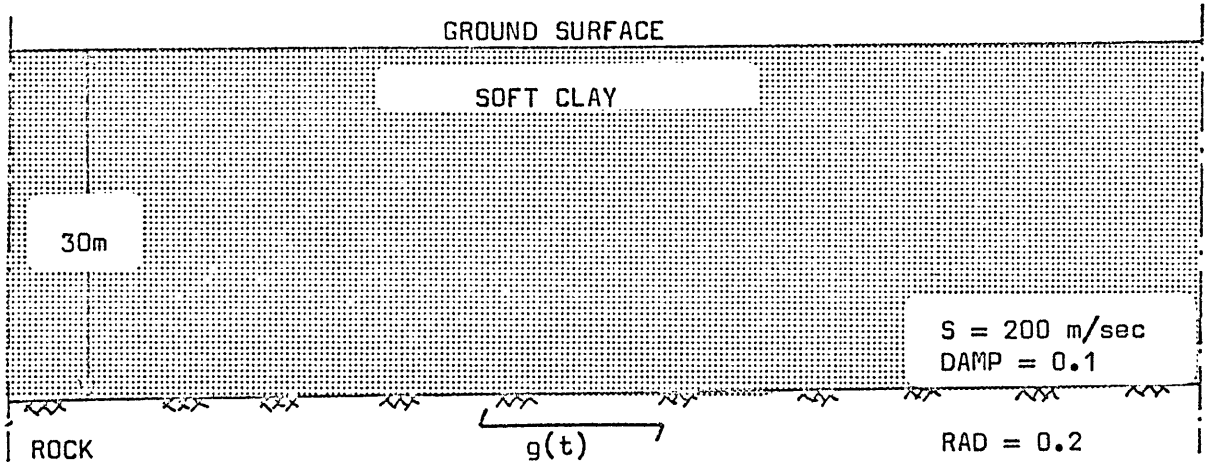


FIG. 7.17f COMPUTED GROUND SURFACE DISPLACEMENT RESPONSE SPECTRA AT SITE NO 7.12



FUNDAMENTAL PERIOD OF THE DEPOSIT = 0.6

RESPONSE OF HYSTERETIC DEPOSIT UNDERLAIN BY DEFORMABLE BEDROCK

SCHEMATIC SOIL PROFILE FOR SITE NO 7.13

FIG. 7.18

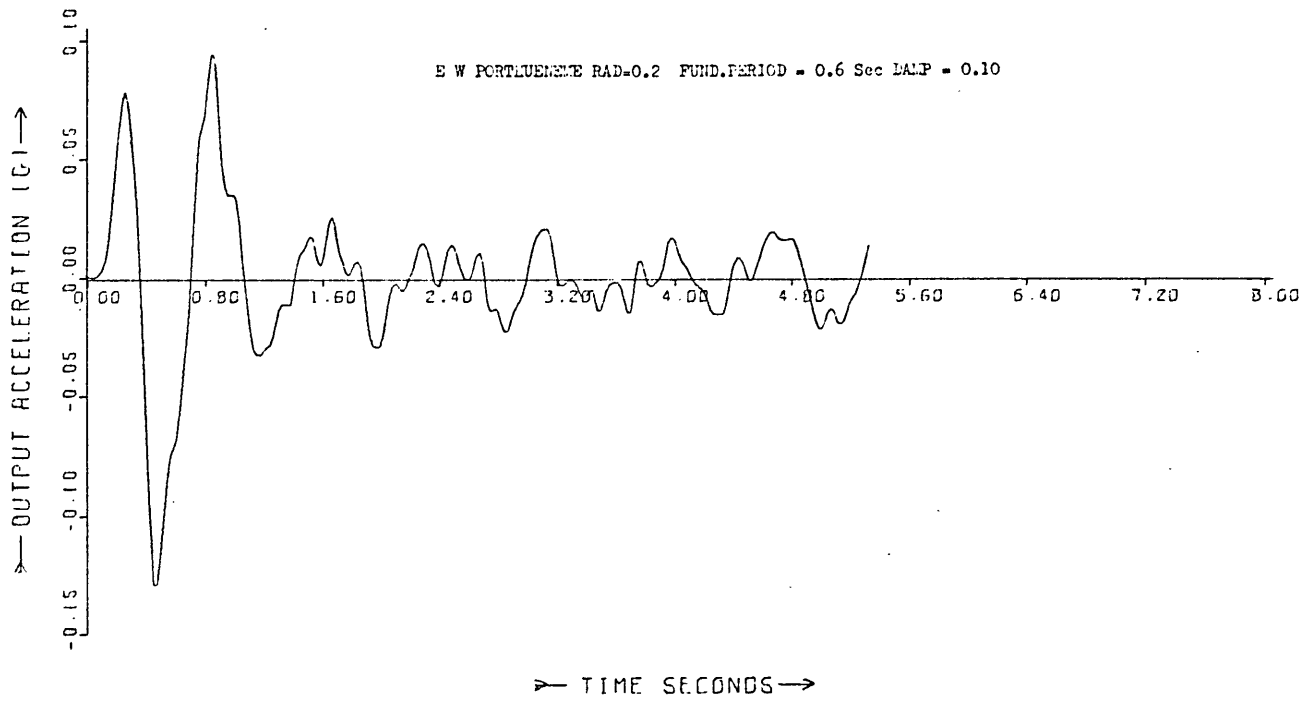


FIG. 7.18a COMPUTED GROUND SURFACE ACCELERATION TIME HISTORY AT SITE NO 7.13

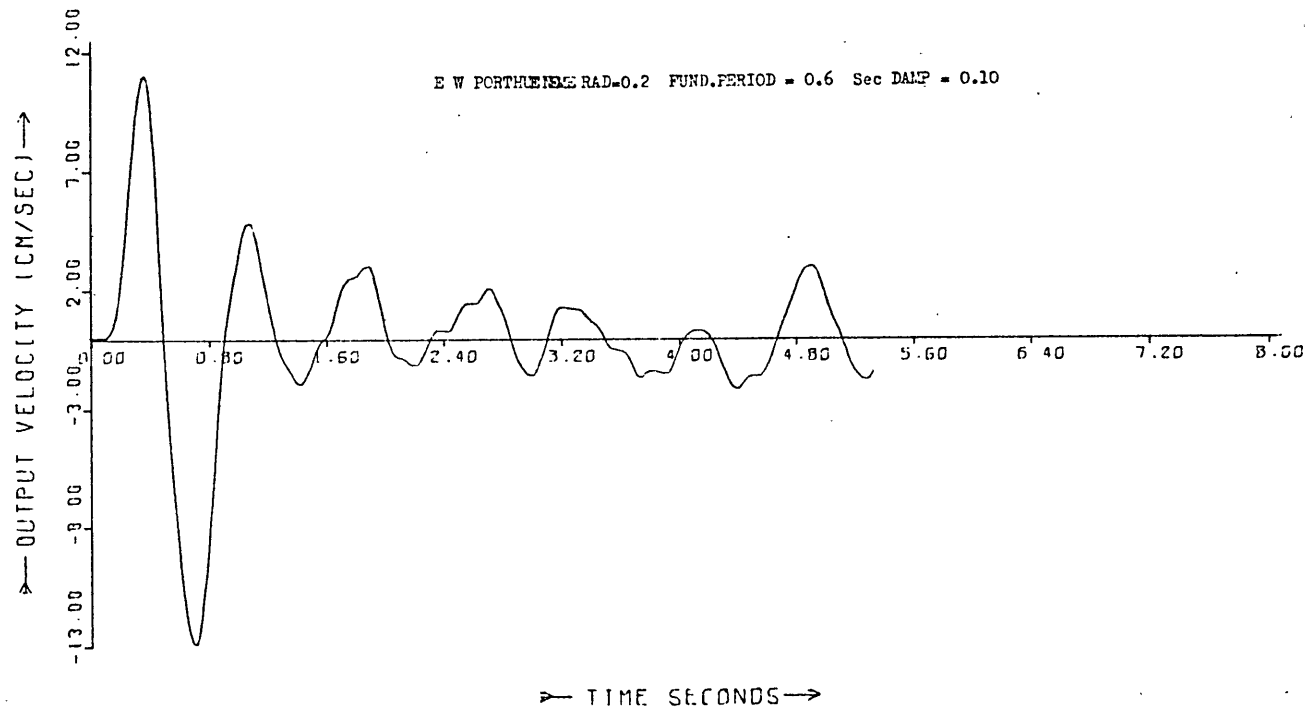


FIG. 7.18b COMPUTED GROUND SURFACE VELOCITY TIME HISTORY AT SITE NO 7.13

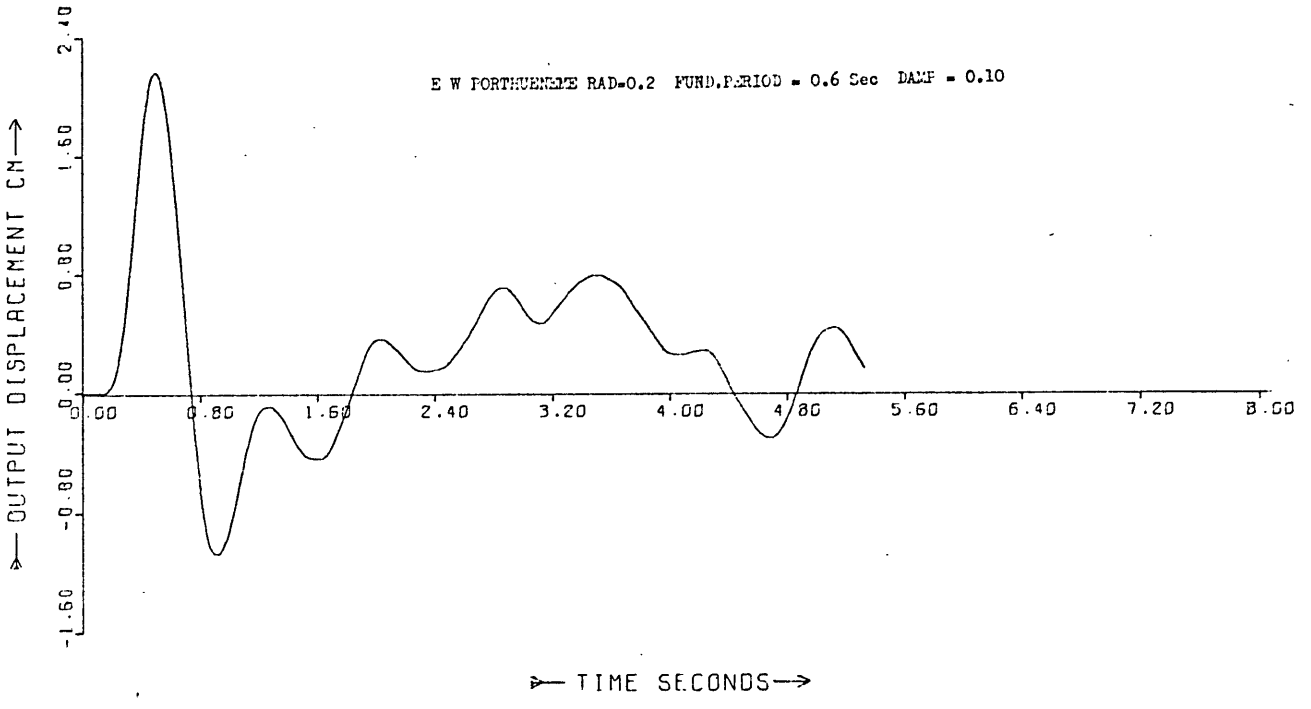


FIG. 7.18c COMPUTED GROUND SURFACE DISPLACEMENT TIME HISTORY AT SITE NO 7.13

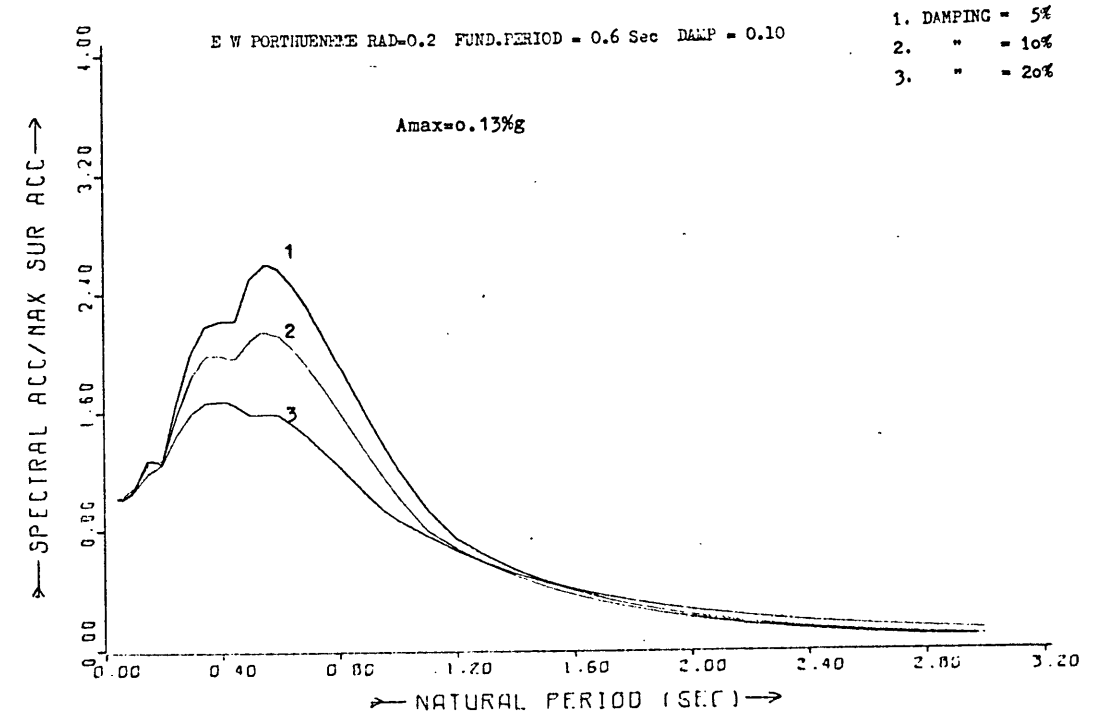


FIG. 7.18d COMPUTED GROUND SURFACE ACCELERATION RESPONSE SPECTRA AT SITE NO 7.13

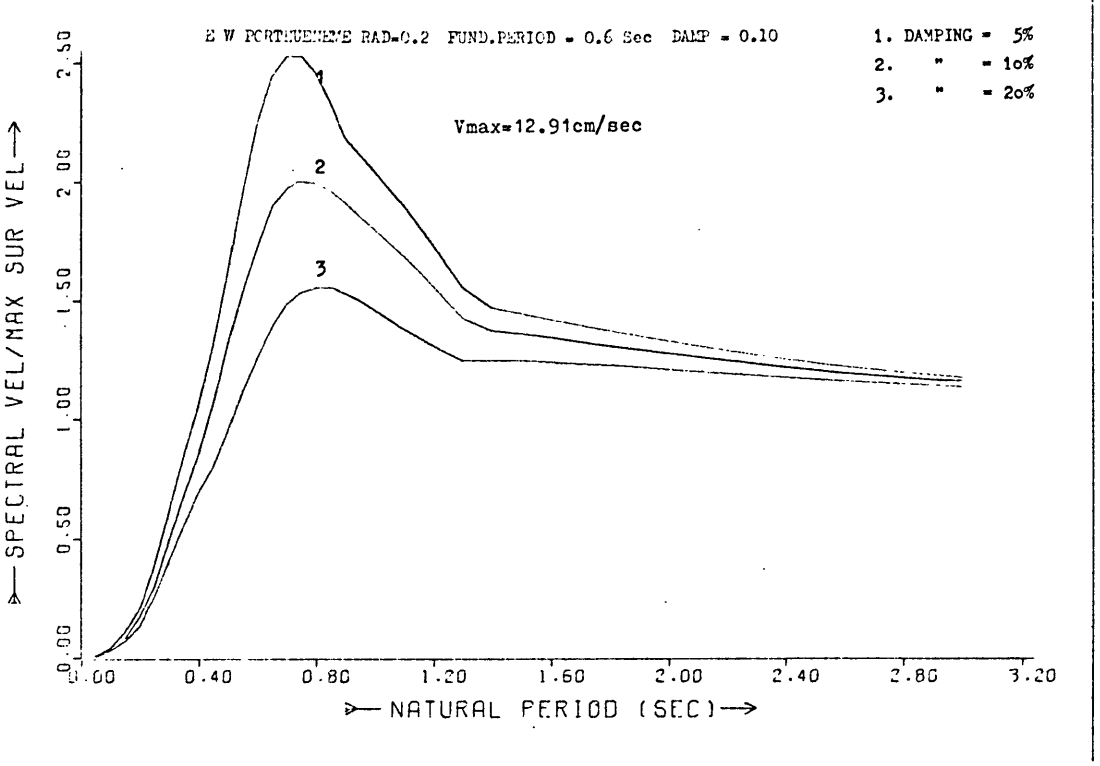


FIG. 7.18e COMPUTED GROUND SURFACE VELOCITY RESPONSE SPECTRA AT SITE NO 7.13

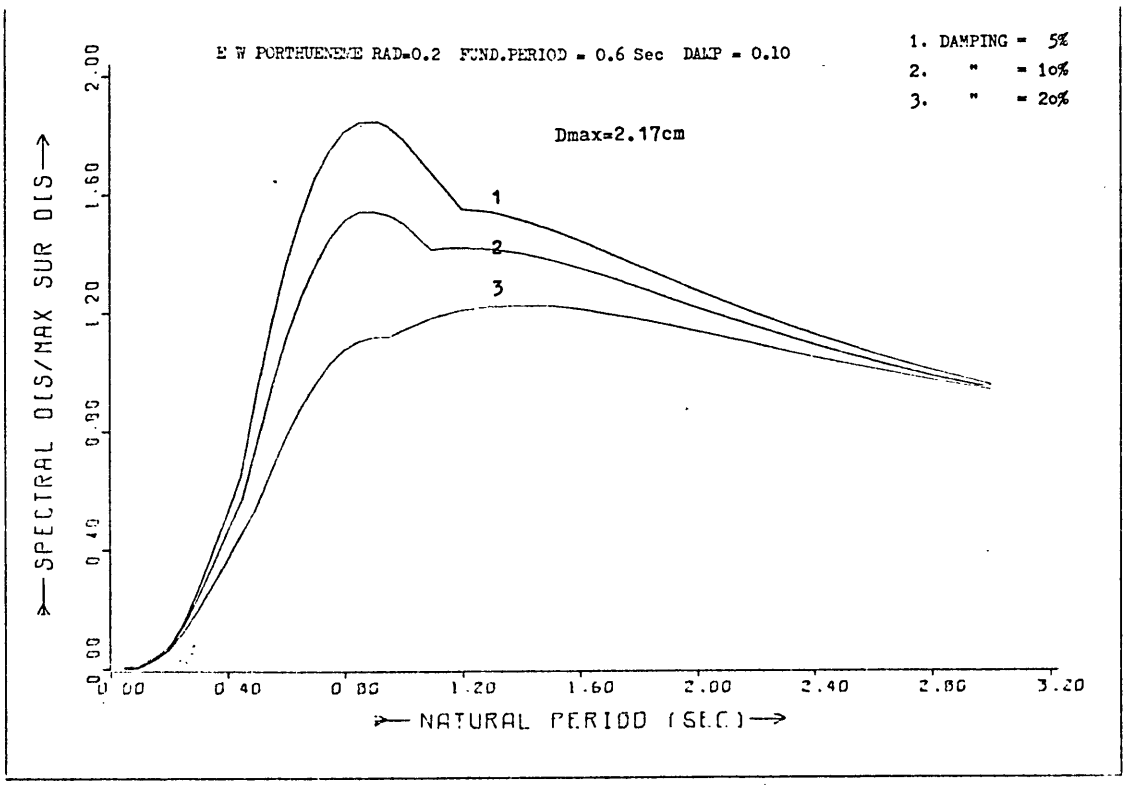
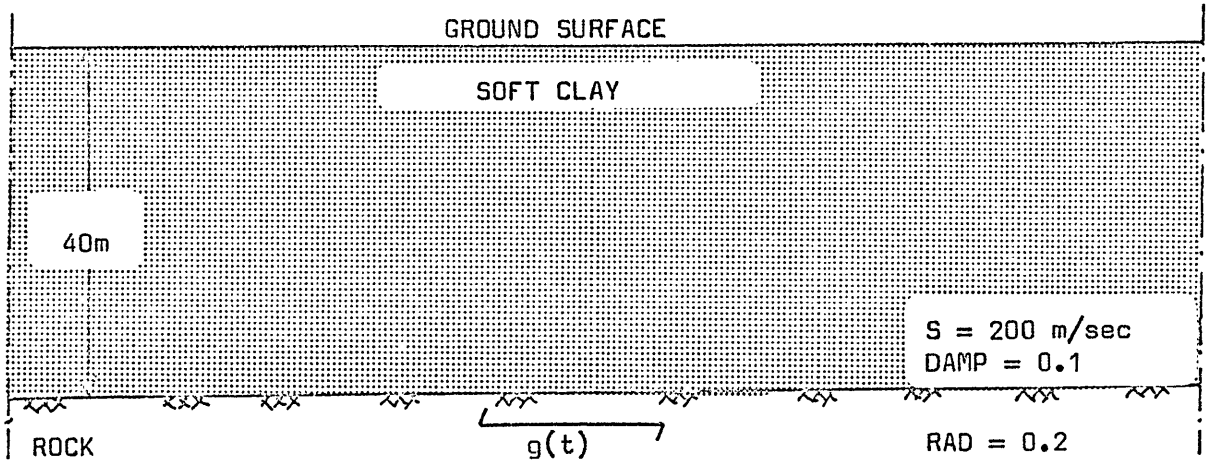


FIG.7.18f COMPUTED GROUND SURFACE DISPLACEMENT RESPONSE SPECTRA AT SITE NO7.13



FUNDAMENTAL PERIOD OF THE DEPOSIT = 0.8

RESPONSE OF HYSTERETIC DEPOSIT UNDERLAIN BY DEFORMABLE BEDROCK

SCHEMATIC SOIL PROFILE FOR SITE NO 7.14

FIG. 7.19

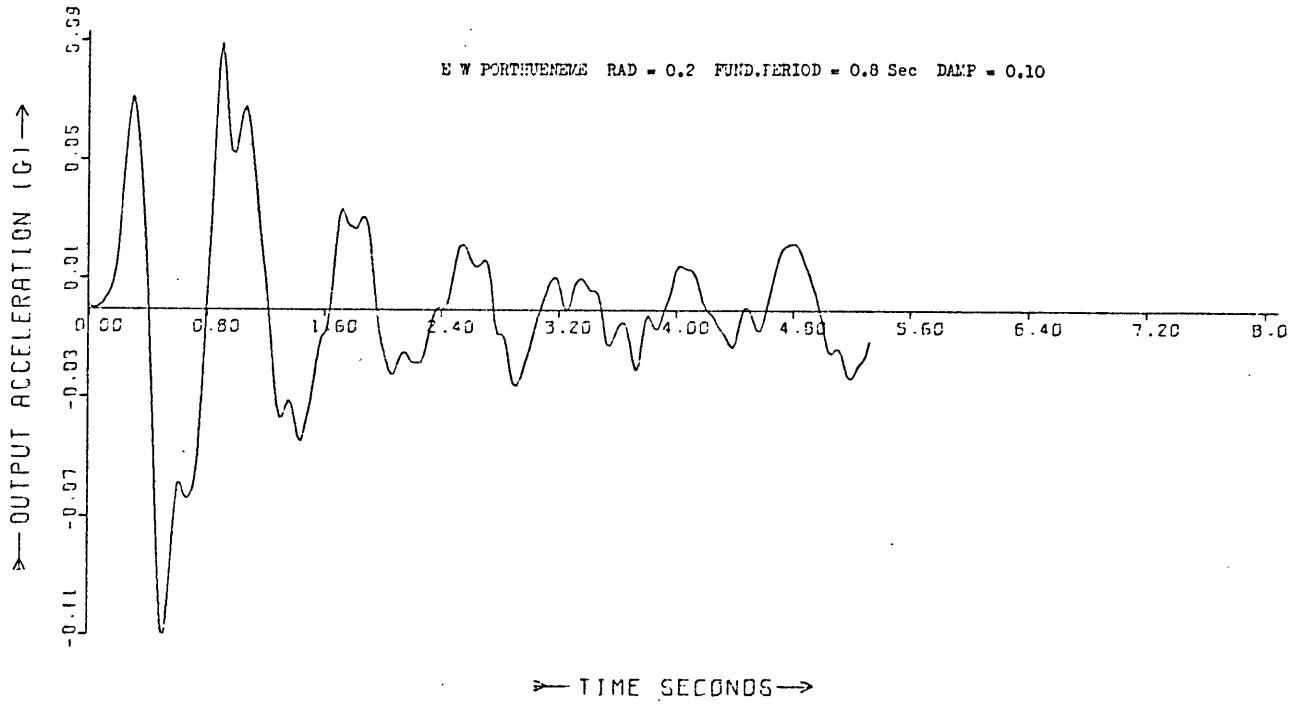


FIG. 7.19a COMPUTED GROUND SURFACE ACCELERATION TIME HISTORY AT SITE NO 7.14

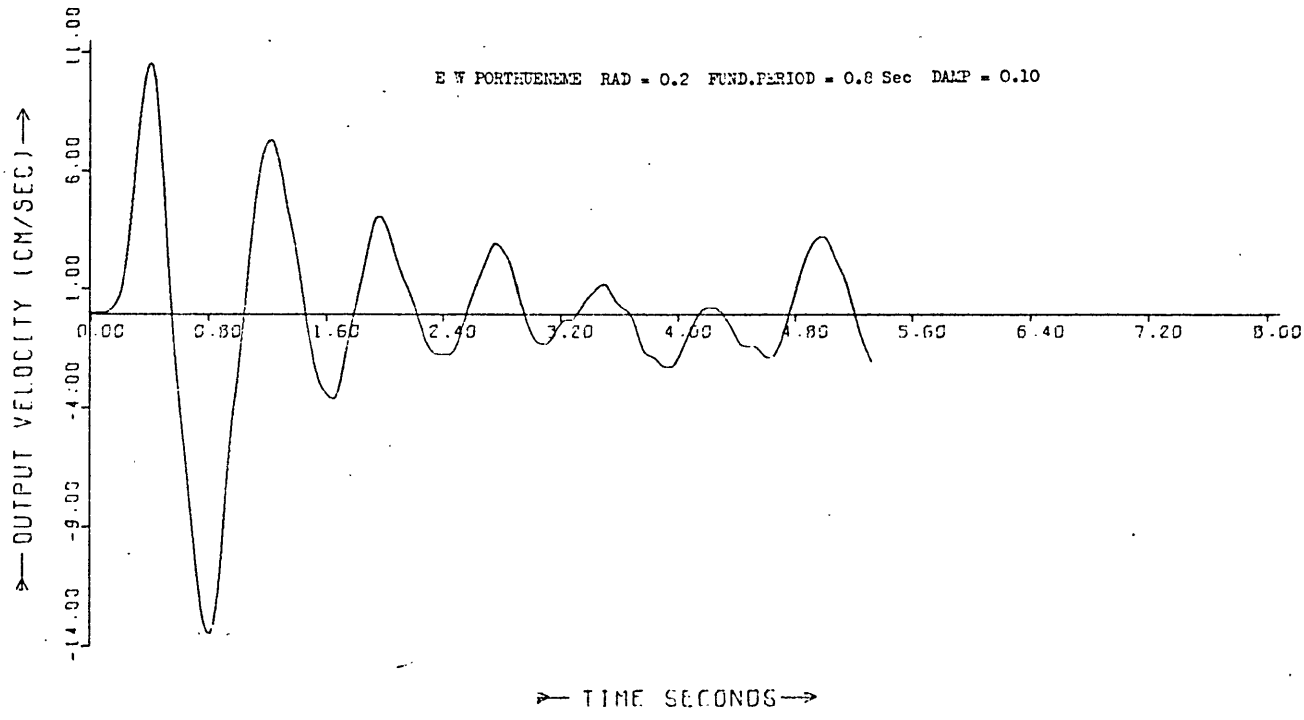


FIG. 7.19b COMPUTED GROUND SURFACE VELOCITY TIME HISTORY AT SITE NO 7.14

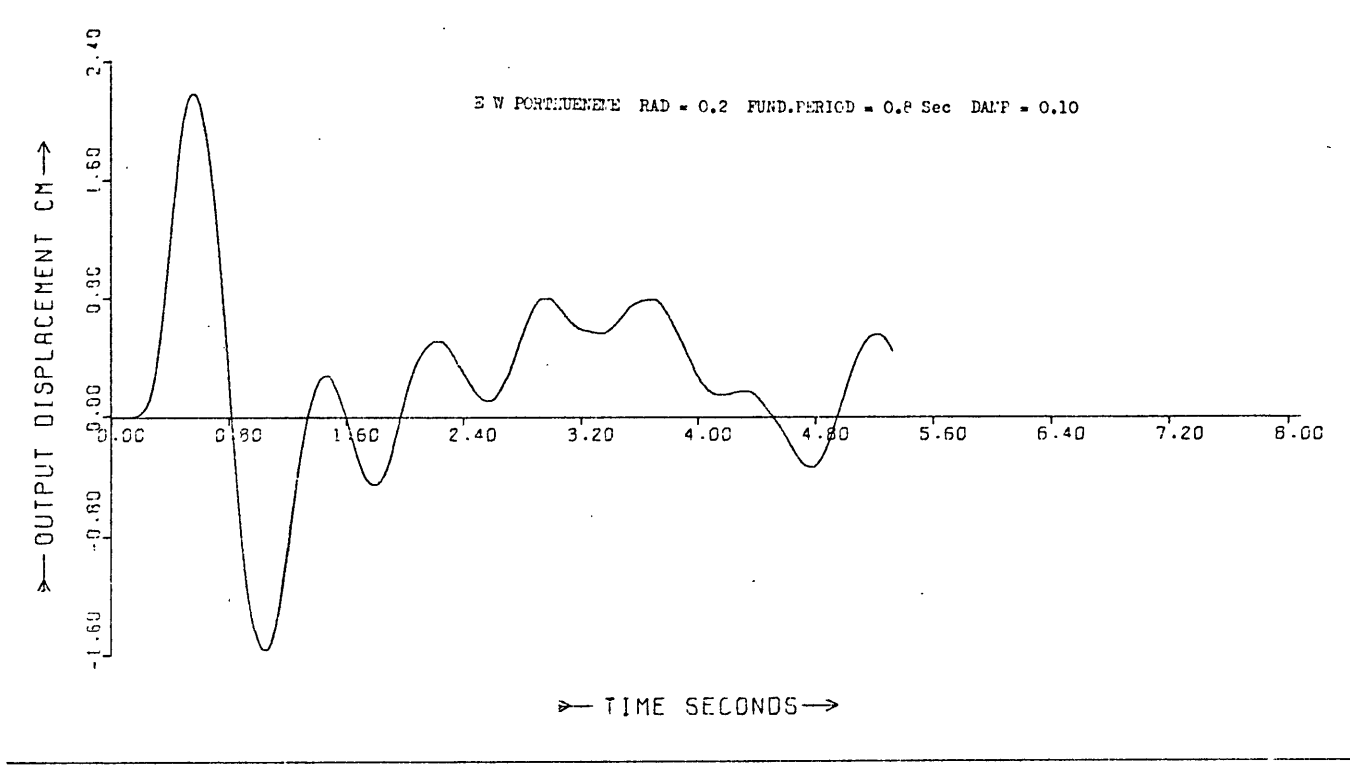


FIG. 7.19c COMPUTED GROUND SURFACE DISPLACEMENT TIME HISTORY AT SITE NO 7.14

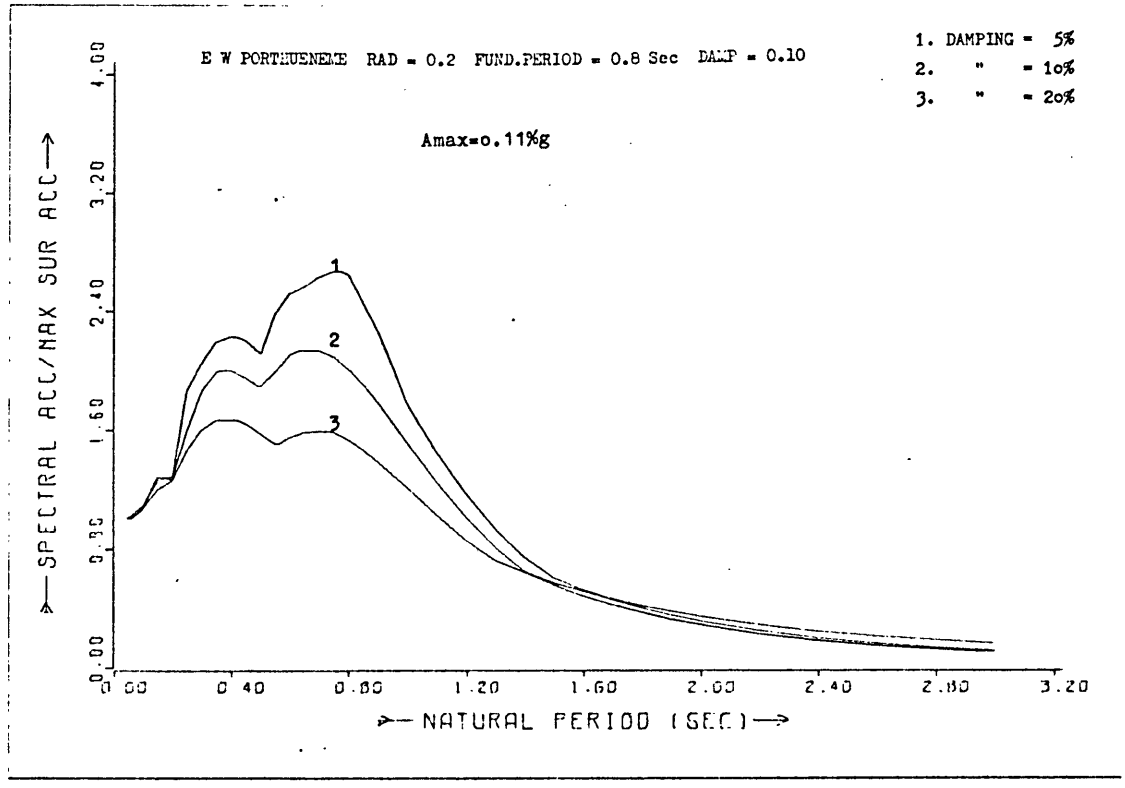


FIG. 7.19d COMPUTED GROUND SURFACE ACCELERATION RESPONSE SPECTRA AT SITE NO 7.14

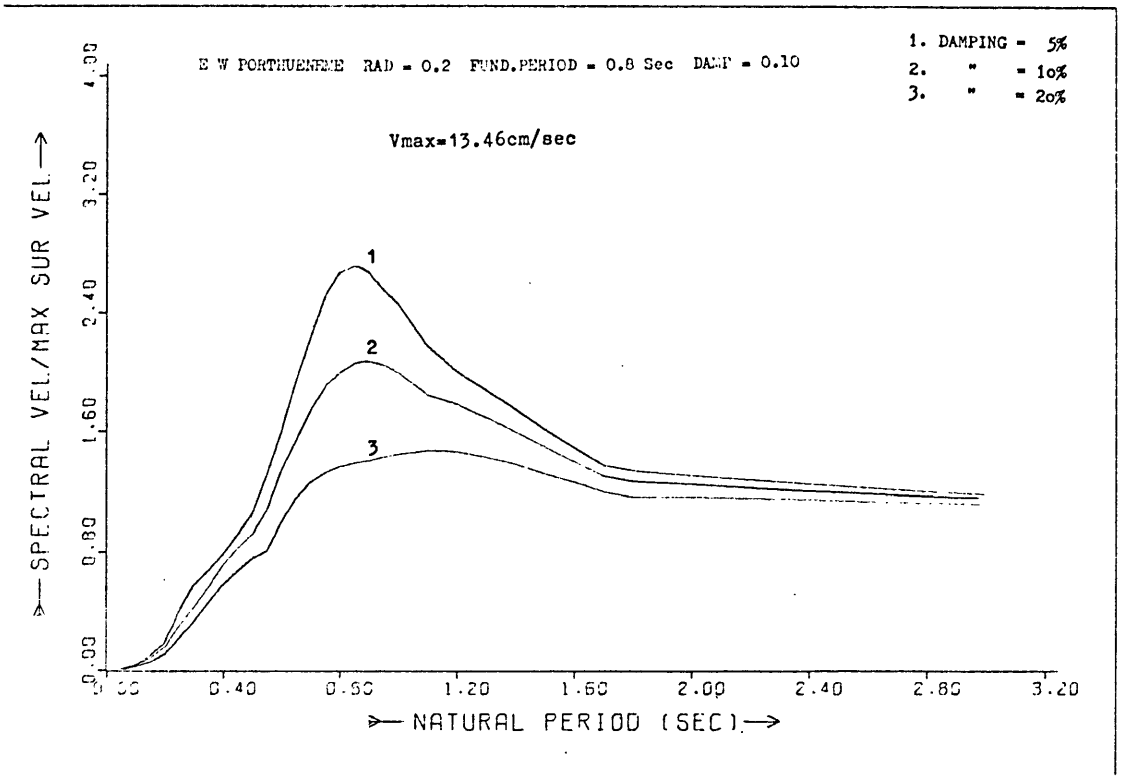


FIG. 7.19e COMPUTED GROUND SURFACE VELOCITY RESPONSE SPECTRA AT SITE NO 7.14

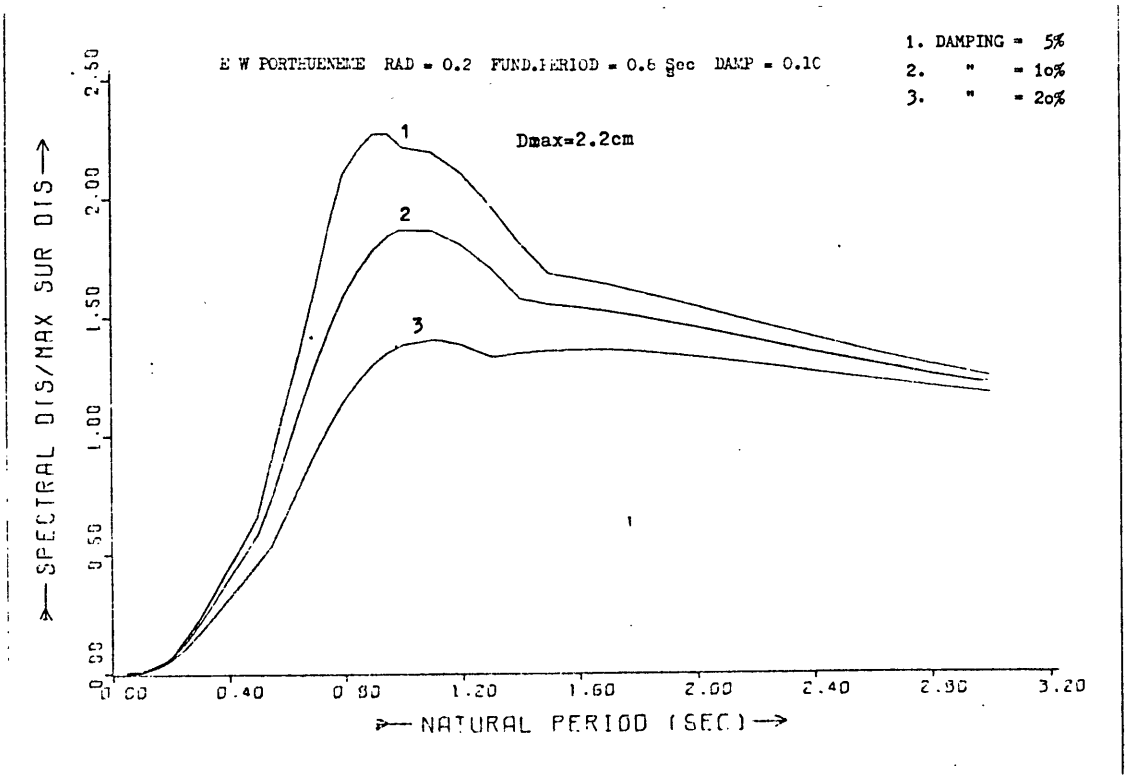
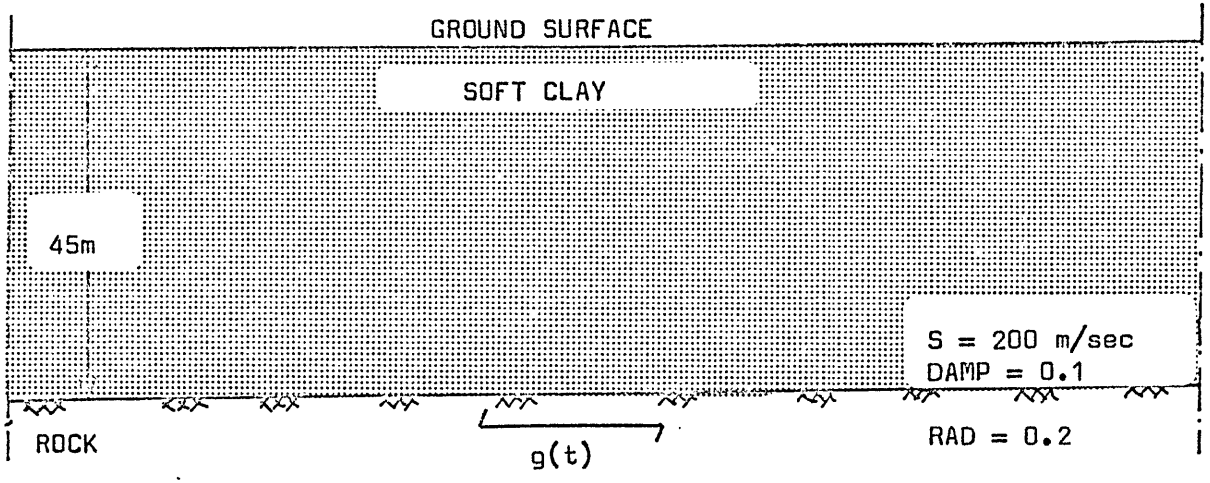


FIG.7.19f COMPUTED GROUND DISPLACEMENT RESPONSE SPECTRA AT SITE NO 7.14



FUNDAMENTAL PERIOD OF THE DEPOSIT = 0.9

RESPONSE OF HYSTERETIC DEPOSIT UNDERLAIN BY DEFORMABLE BEDROCK

SCHEMATIC SOIL PROFILE FOR SITE NO 7.15

FIG. 7.20

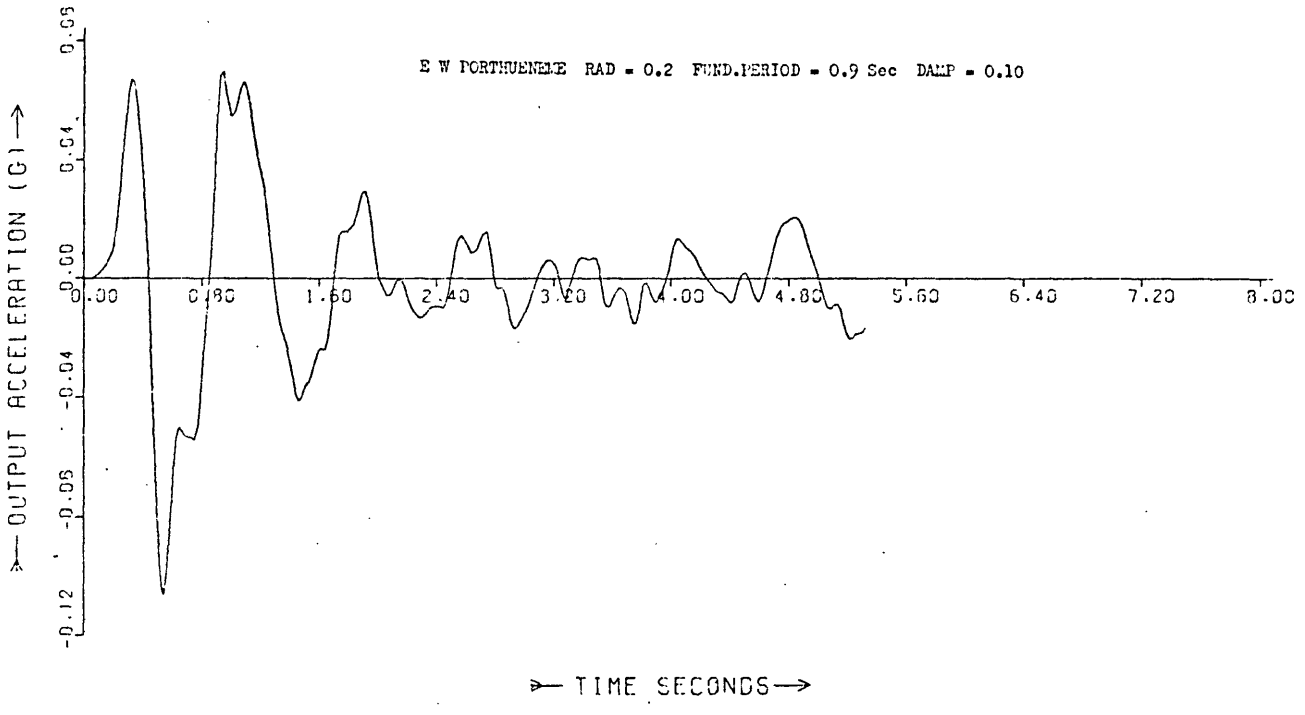


FIG.7.2oaCOMPUTED GROUND SURFACE ACCELERATION TIME HISTORY AT SITE NO 7.15

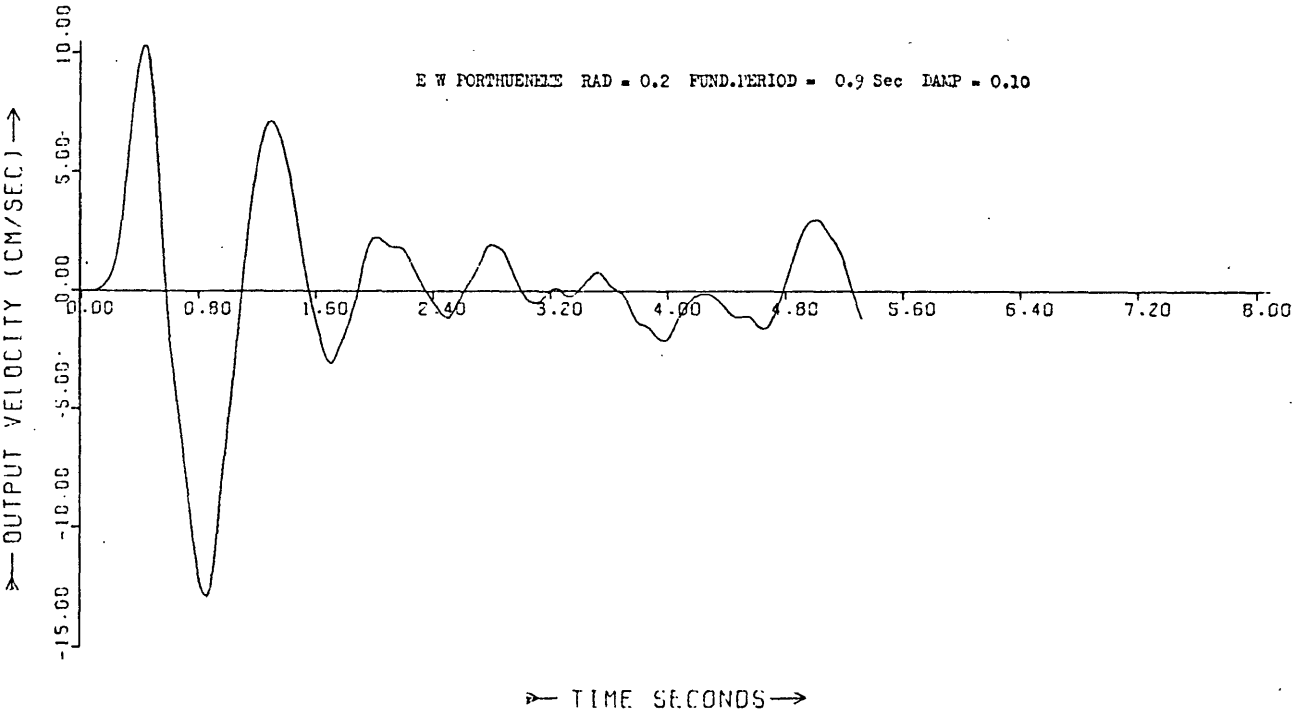


FIG.7.2obCOMPUTED GROUND SURFACE VELOCITY TIME HISTORY AT SITE NO 7.15

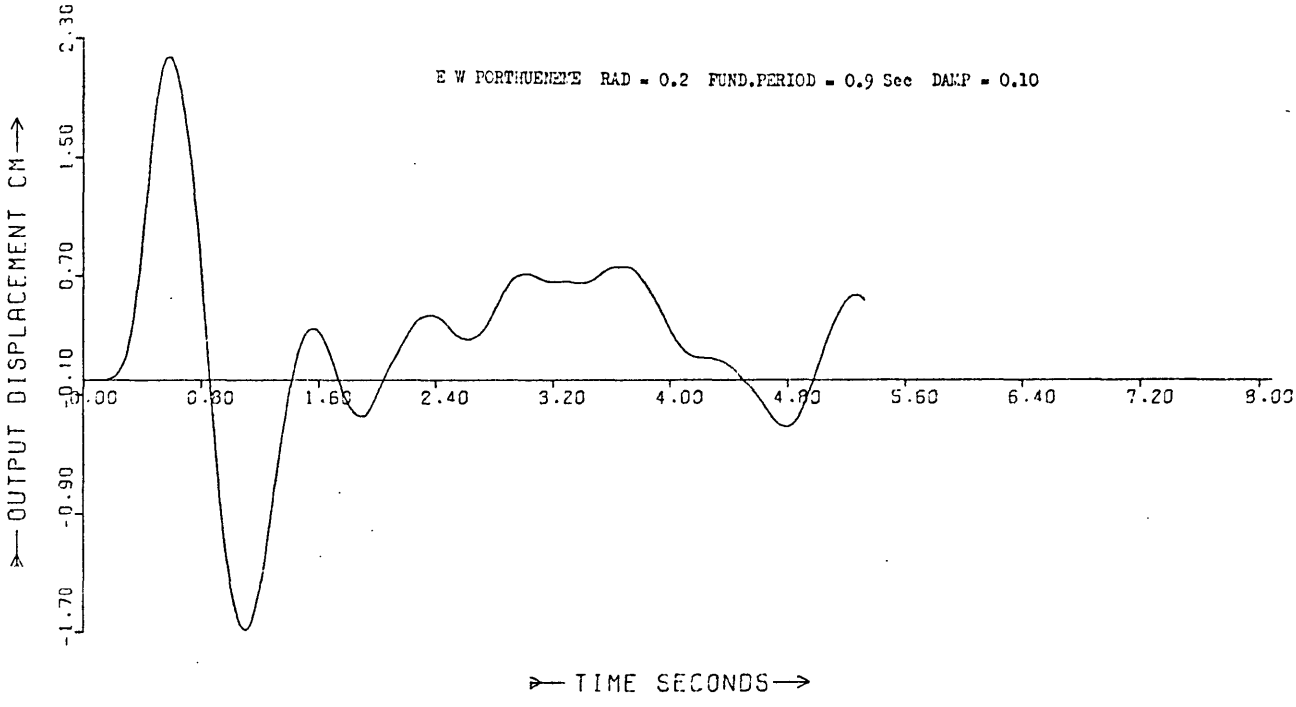


FIG 7.2oc COMPUTED GROUND SURFACE DISPLACEMENT TIME HISTORY AT SITE NO 7.15

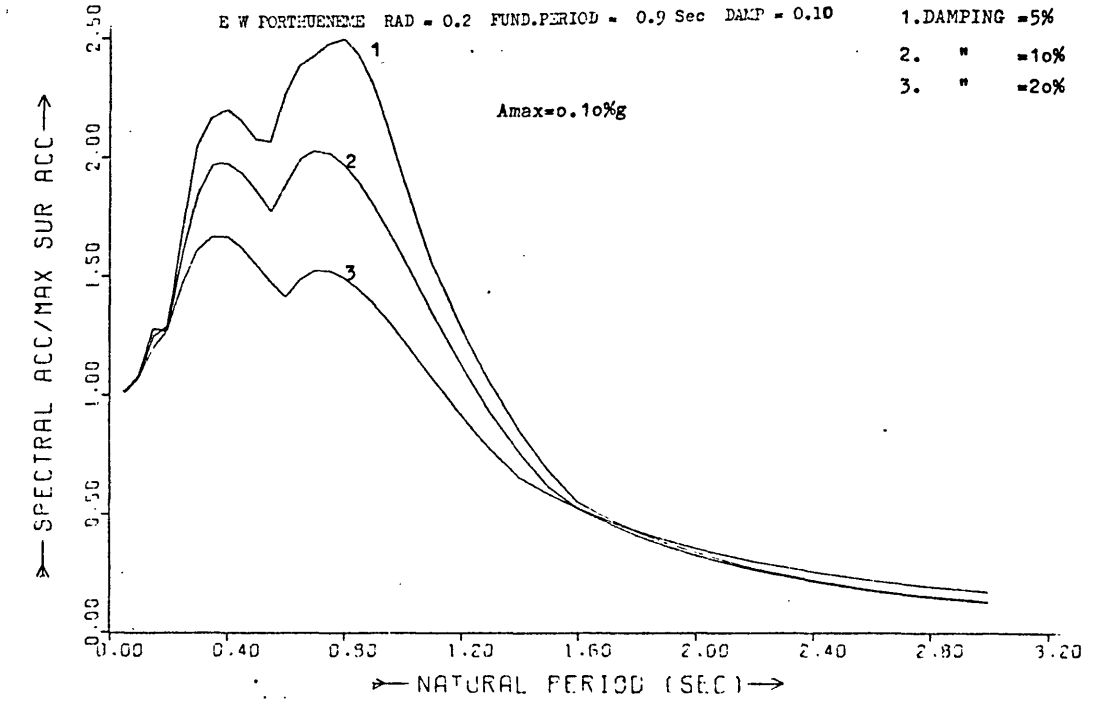


FIG7 .2od COMPUTED GROUND SURFACE ACCELERATION RESPONSE SPECTRA AT SITE NO 7.15

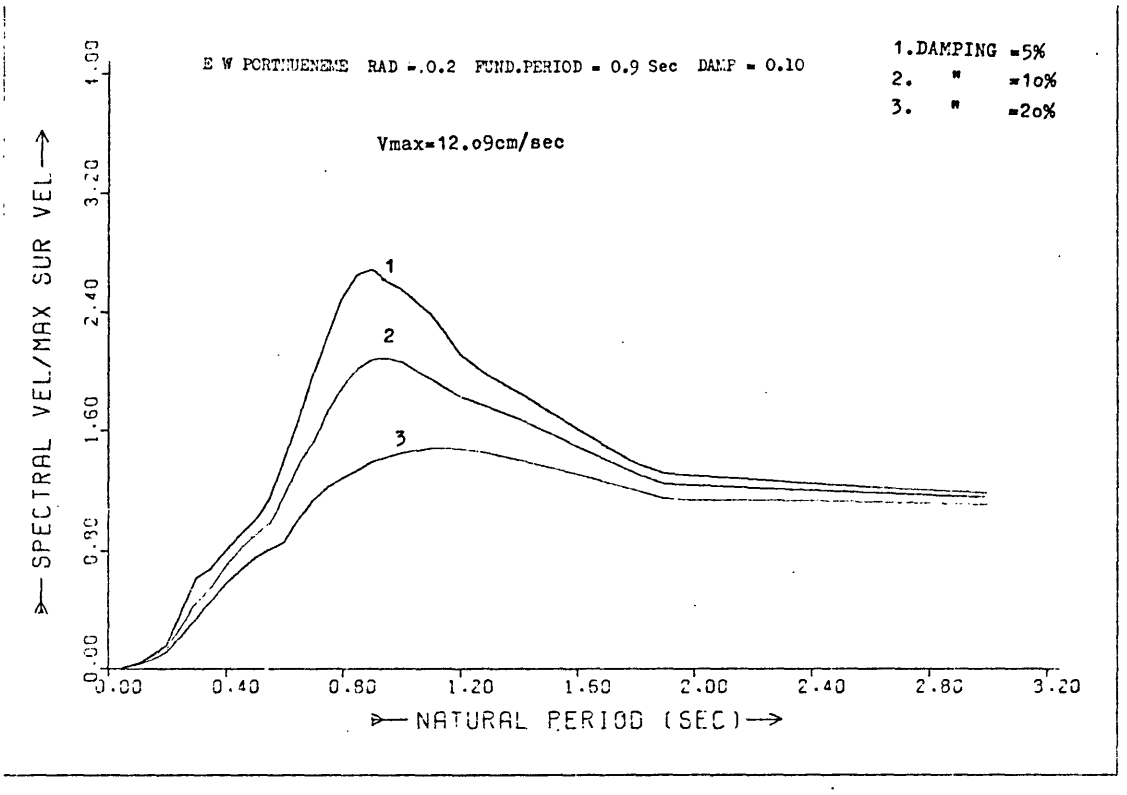


FIG 7.2oe COMPUTED GROUND SURFACE VELOCITY RESPONSE SPECTRA AT SITE NO 7.15

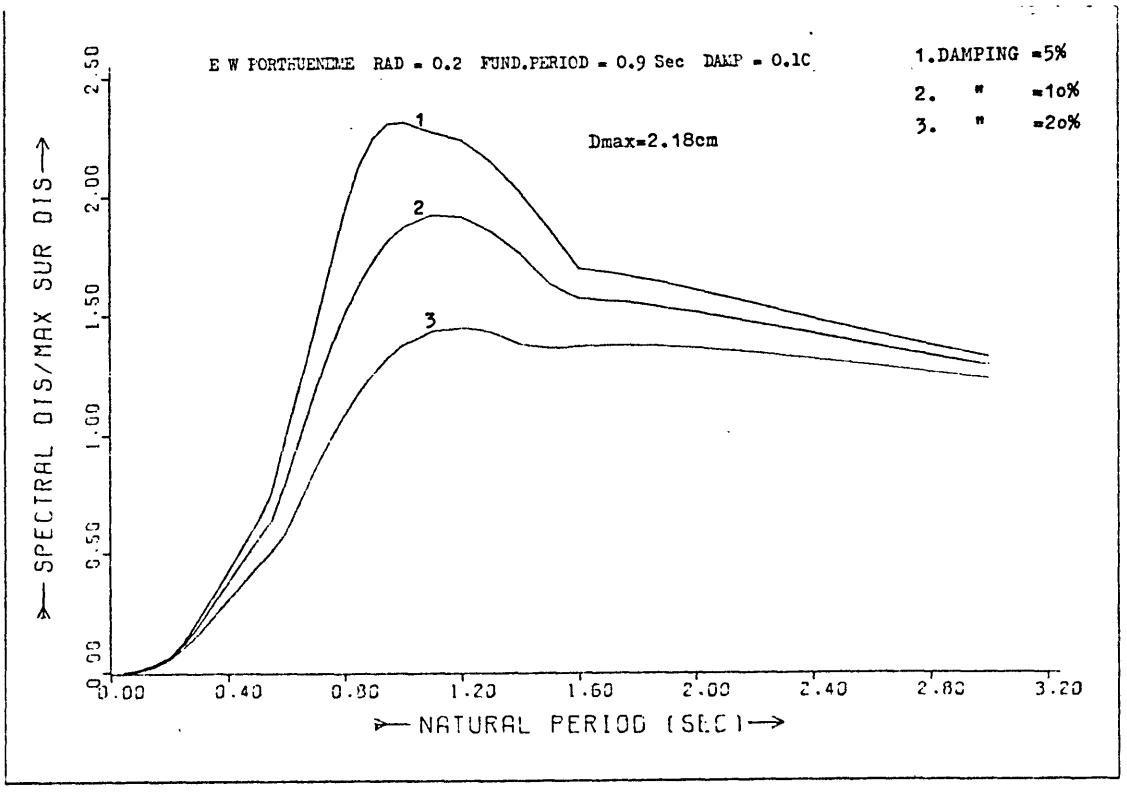
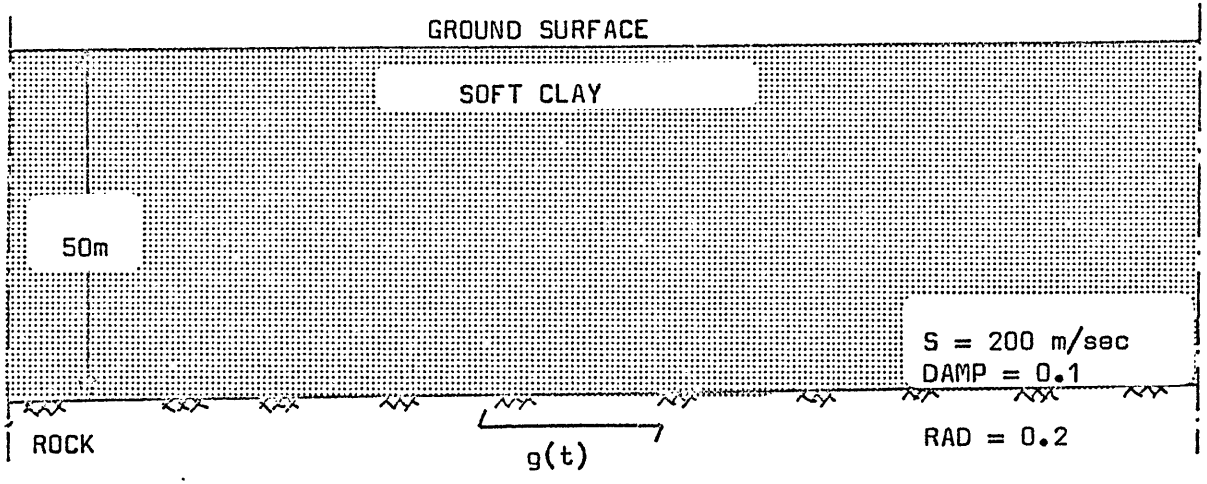


FIG. 7.2of COMPUTED GROUND SURFACE DISPLACEMENT RESPONSE SPECTRA AT SITE NO 7.15



FUNDAMENTAL PERIOD OF THE DEPOSIT = 1.0

RESPONSE OF HYSTERETIC DEPOSIT UNDERLAIN BY DEFORMABLE BEDROCK

SCHEMATIC SOIL PROFILE FOR SITE NO 7.16

FIG. 7.21

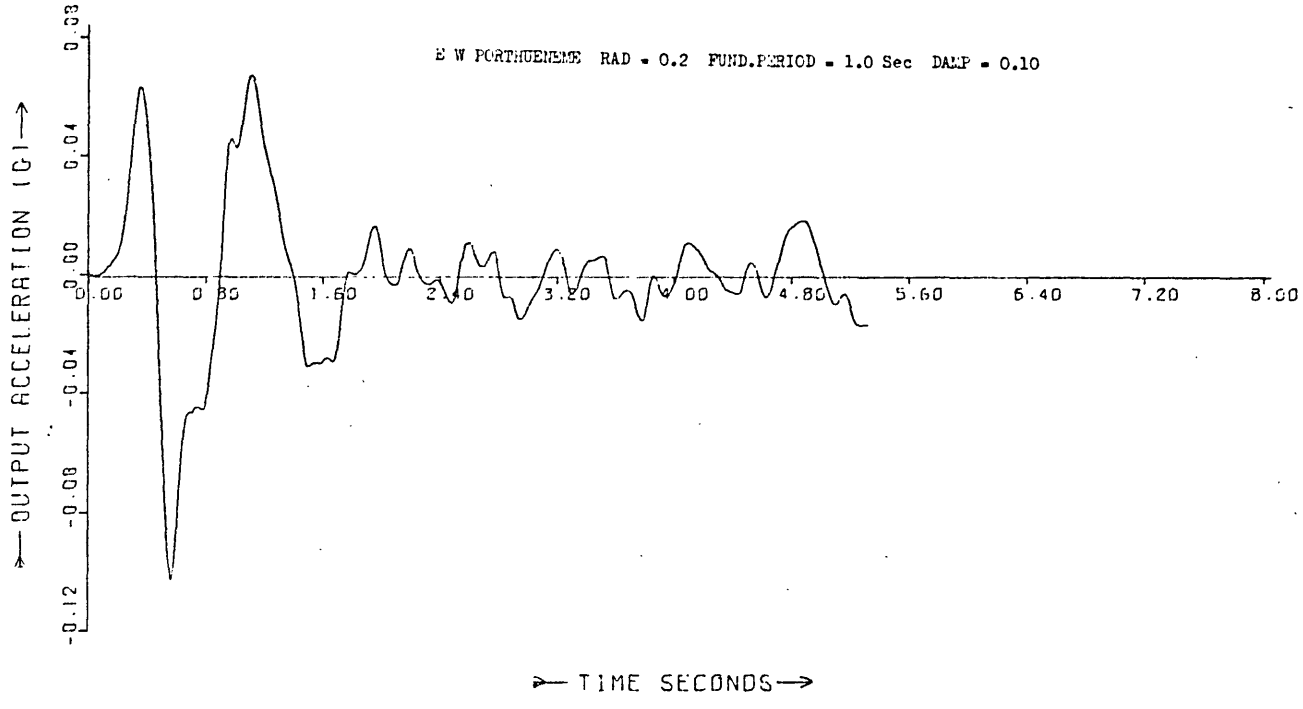


FIG.7.21a COMPUTED GROUND SURFACE ACCELERATION TIME HISTORY AT SITE NO7.16

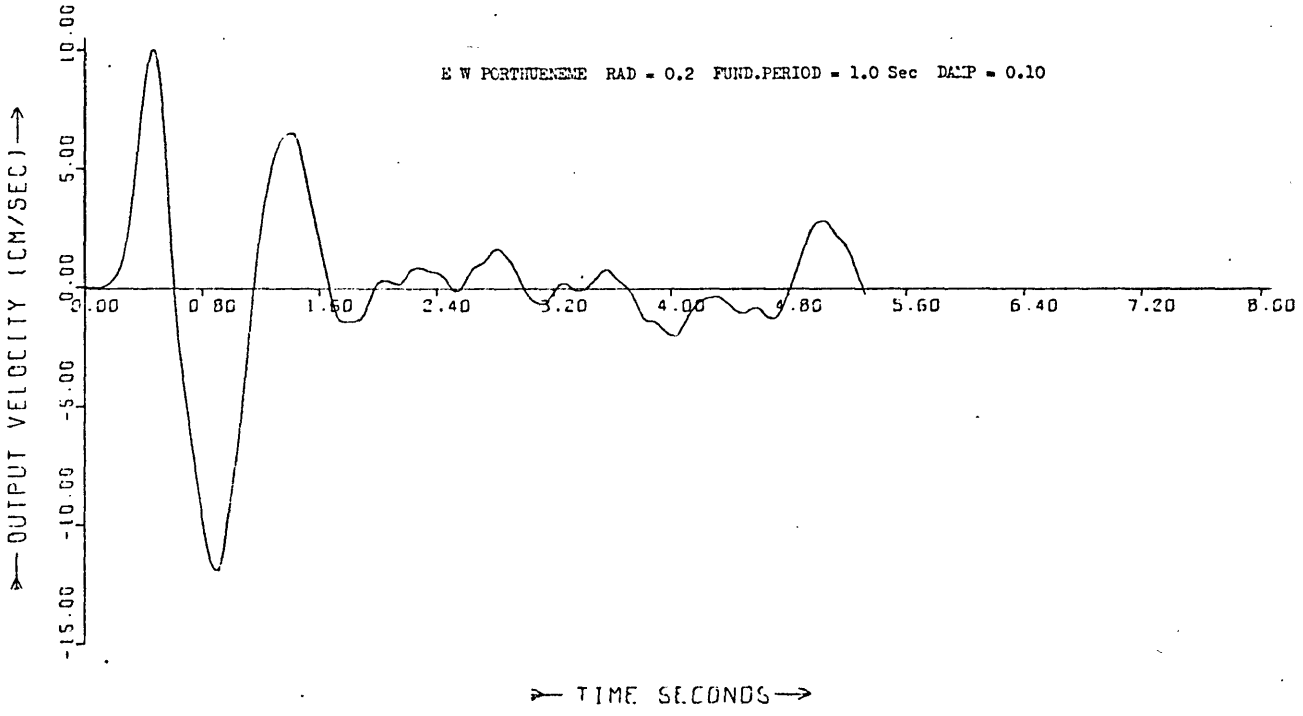


FIG.7.21b COMPUTED GROUND SURFACE VELOCITY TIME HISTORY AT SITE NO7.16

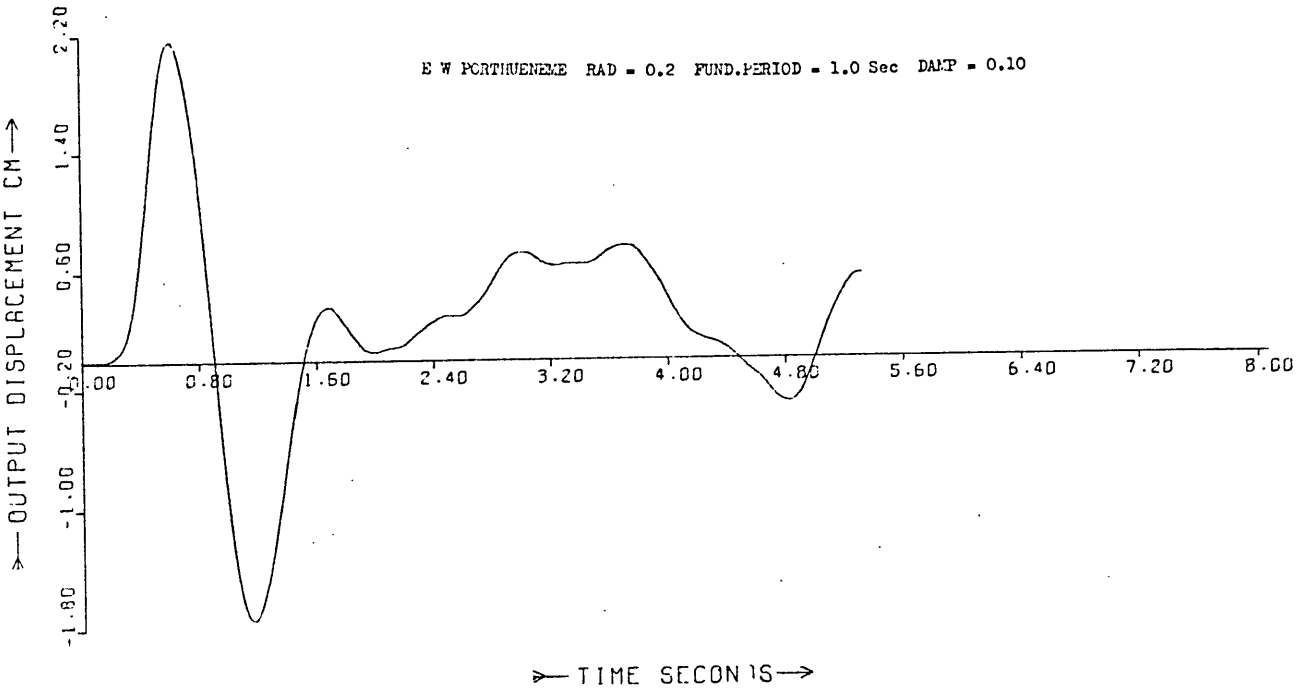


FIG.7.21cCOMPUTED GROUND SURFACE DISPLACEMENT TIME HISTORY AT SITE NO 7.16

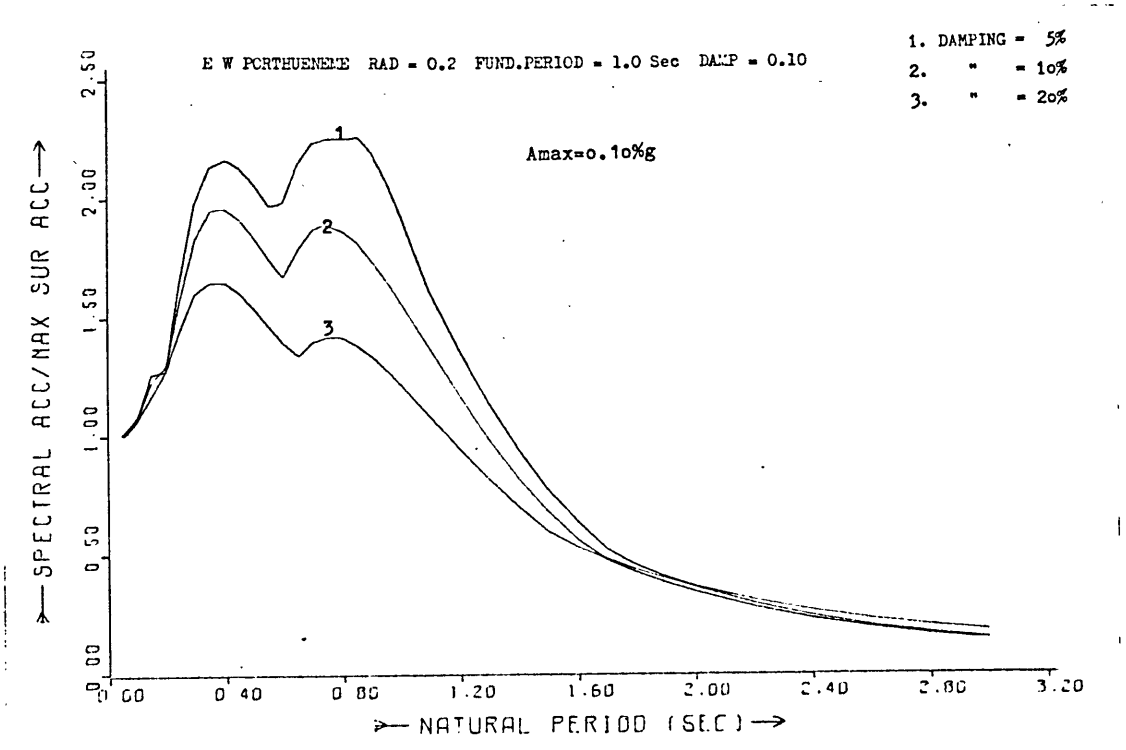


FIG.7.21dCOMPUTED GROUND SURFACE ACCELERATION RESPONSE SPECTRA AT SITE NO 7.16

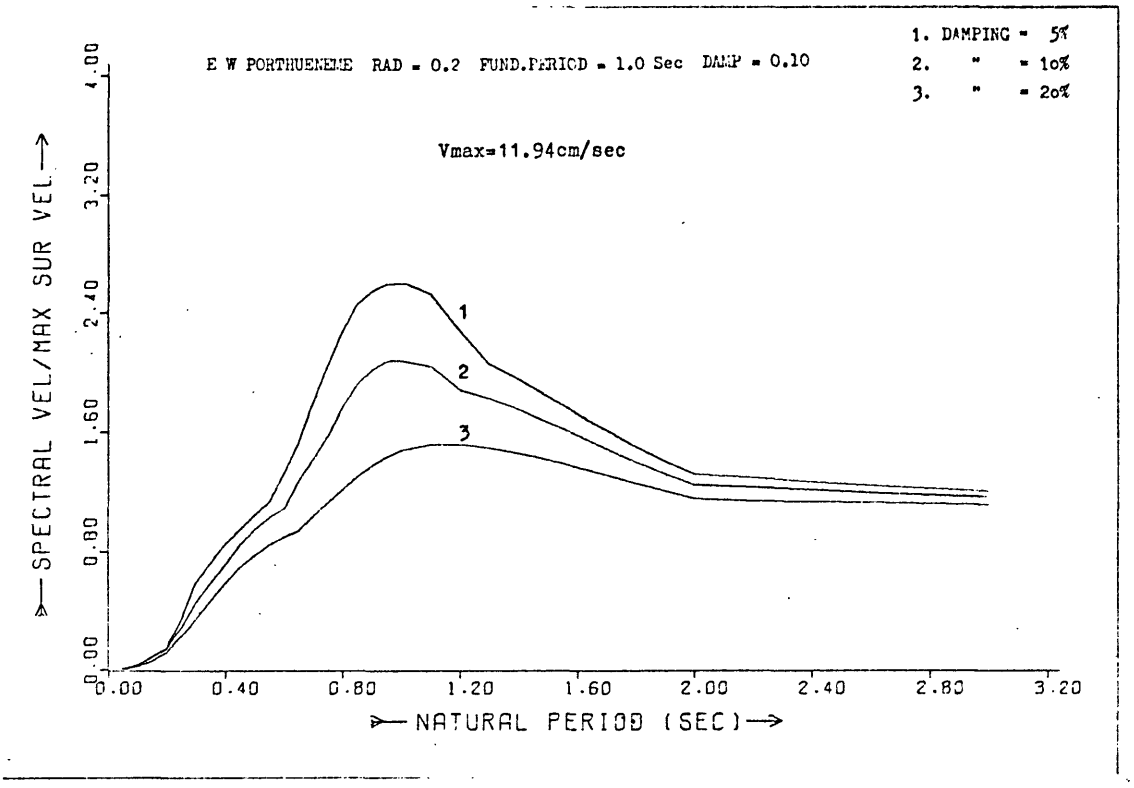


FIG.7.21e COMPUTED GROUND SURFACE VELOCITY RESPONSE SPECTRA AT SITE NO 7.16

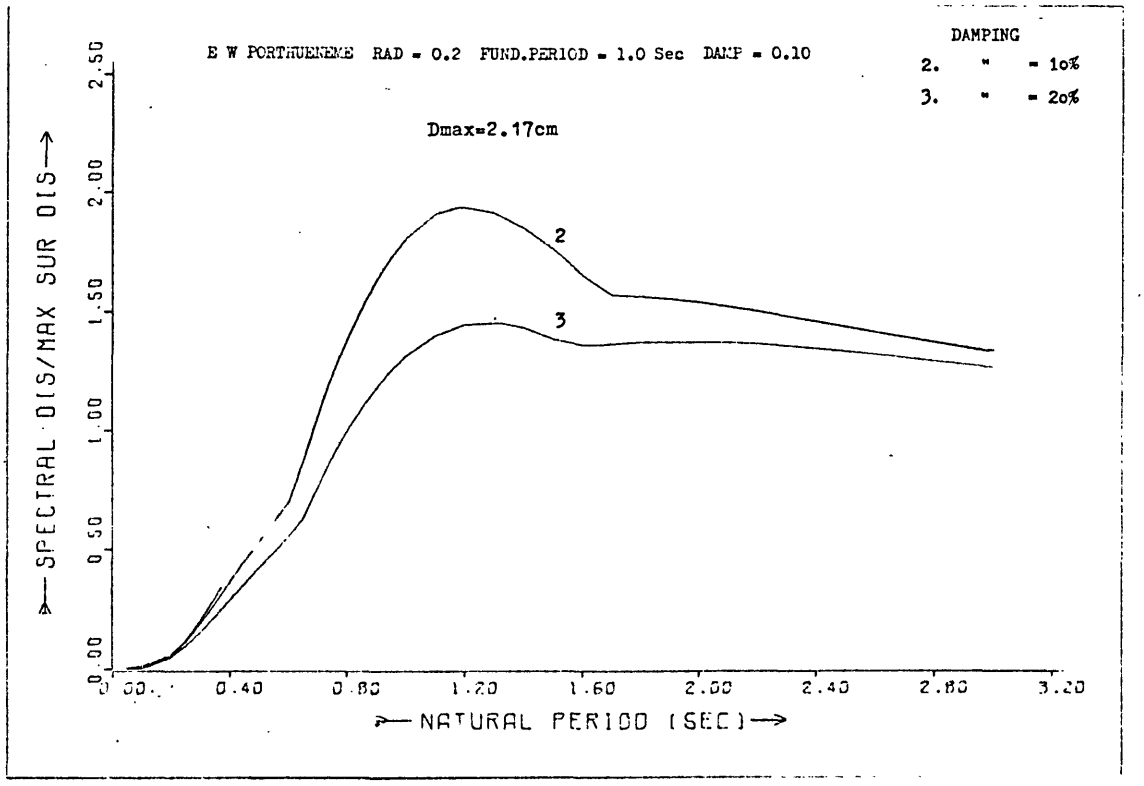
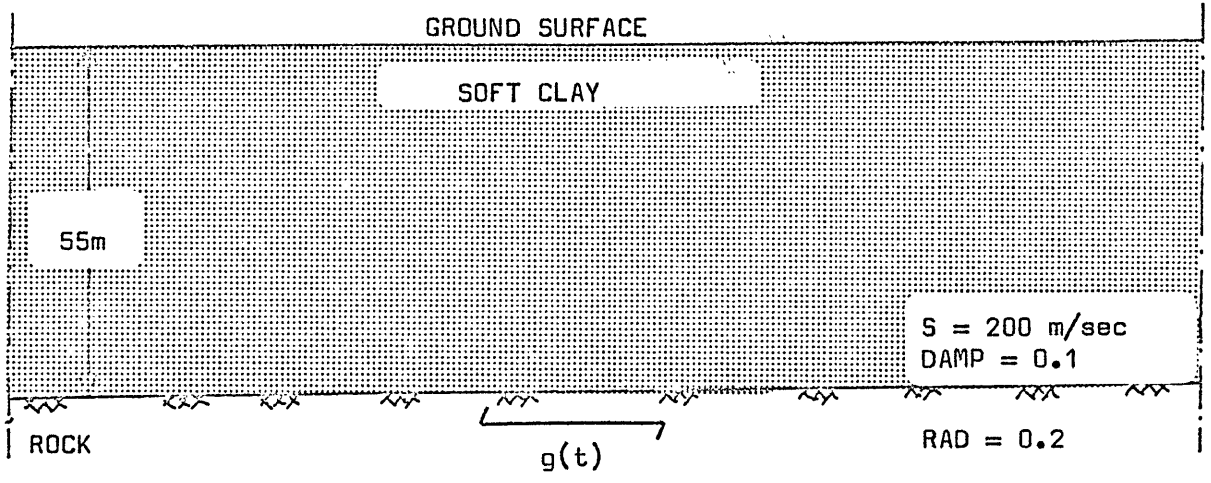


FIG.7.21f COMPUTED GROUND SURFACE DISPLACEMENT RESPONSE SPECTRA AT SITE NO 7.16



FUNDAMENTAL PERIOD OF THE DEPOSIT = 1.1

RESPONSE OF HYSTERETIC DEPOSIT UNDERLAIN BY DEFORMABLE BEDROCK

SCHEMATIC SOIL PROFILE FOR SITE NO 7.17

FIG. 7.22

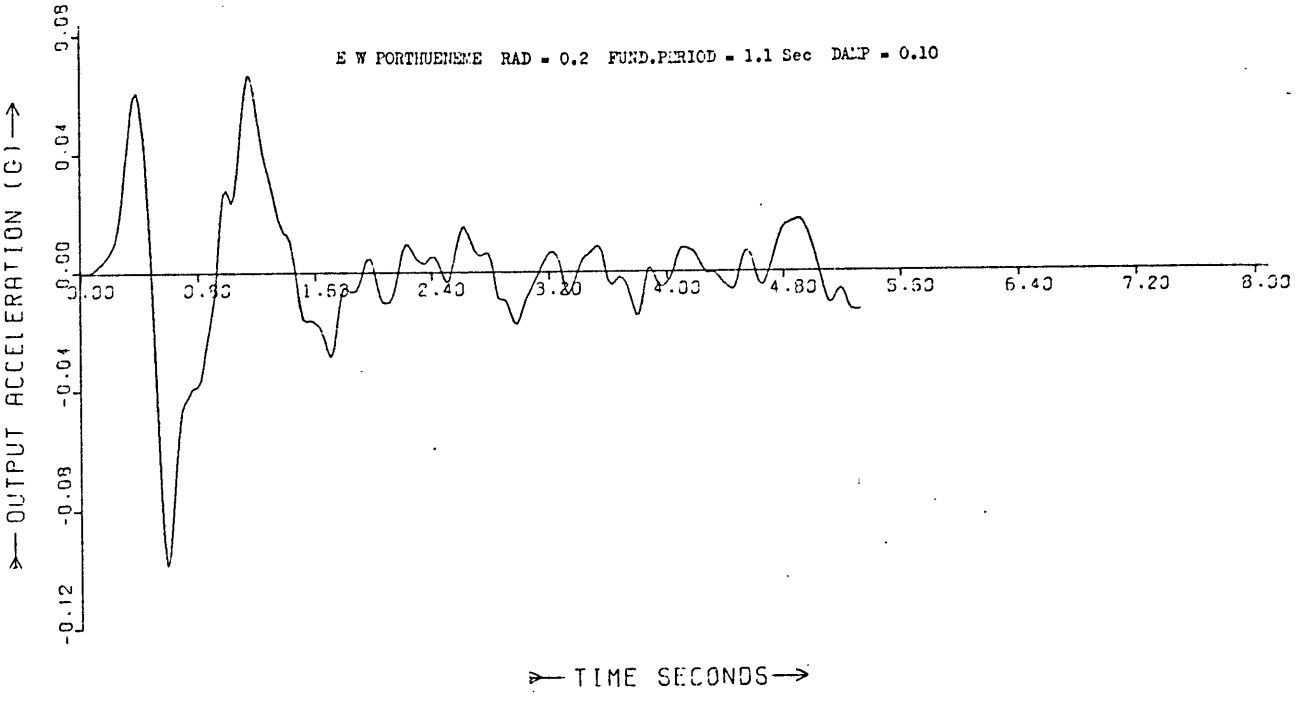


FIG.7.22a COMPUTED GROUND SURFACE ACCELERATION TIME HISTORY AT SITE NO 7.17

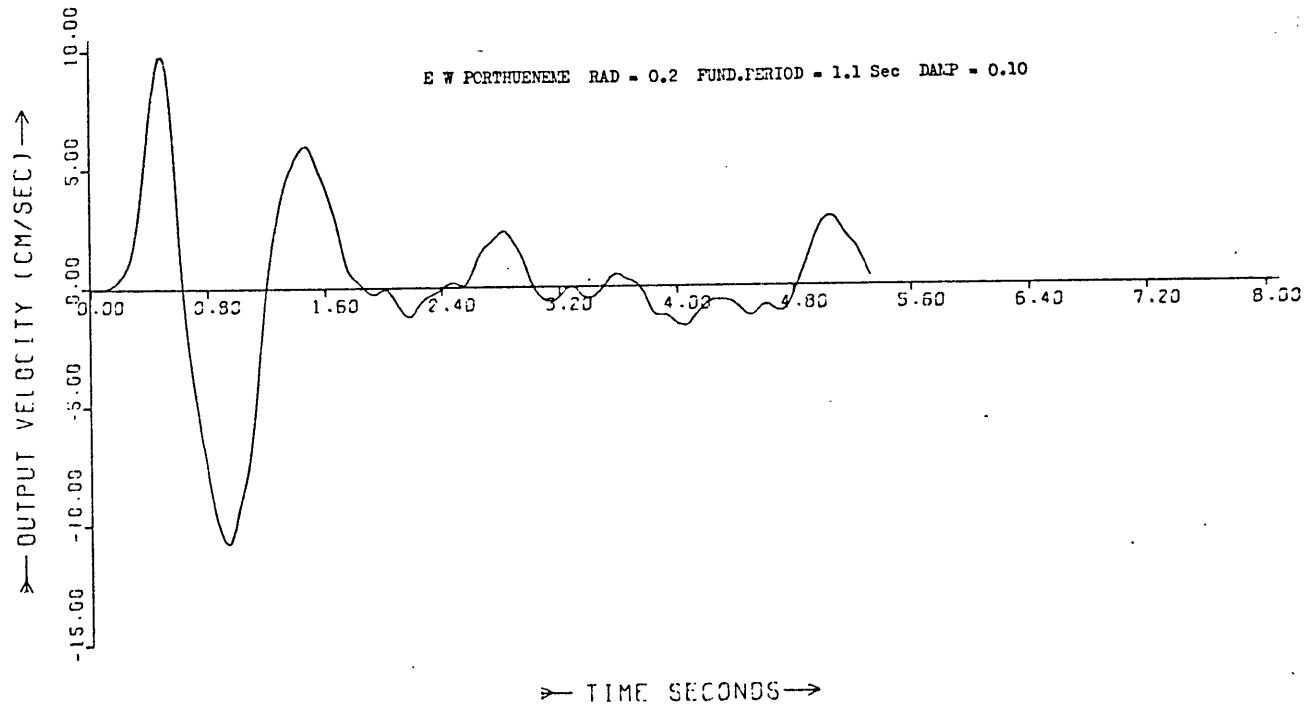


FIG. 7.22b COMPUTED GROUND SURFACE VELOCITY TIME HISTORY AT SITE NO 7.17

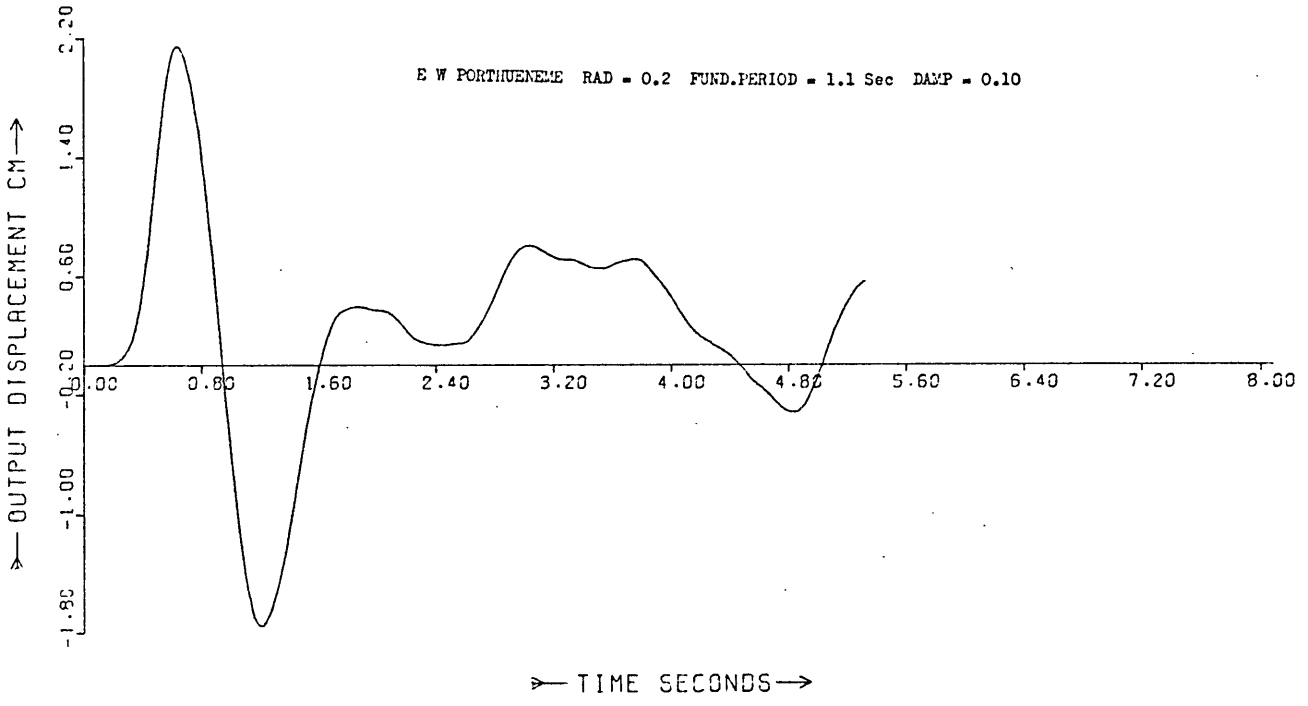


FIG. 7.22c COMPUTED GROUND SURFACE DISPLACEMENT TIME HISTORY AT SITE NO 7.17

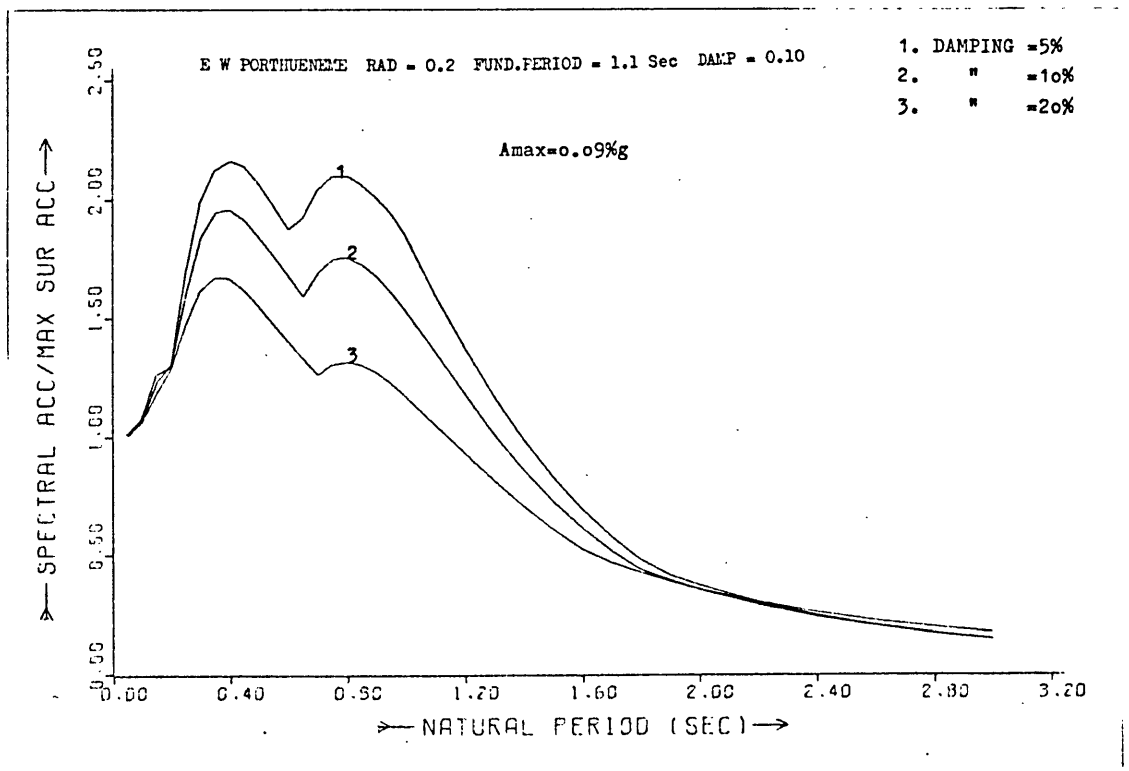


FIG.7.22d COMPUTED GROUND SURFACE ACCELERATION RESPONSE SPECTRA AT SITE NO 7.17

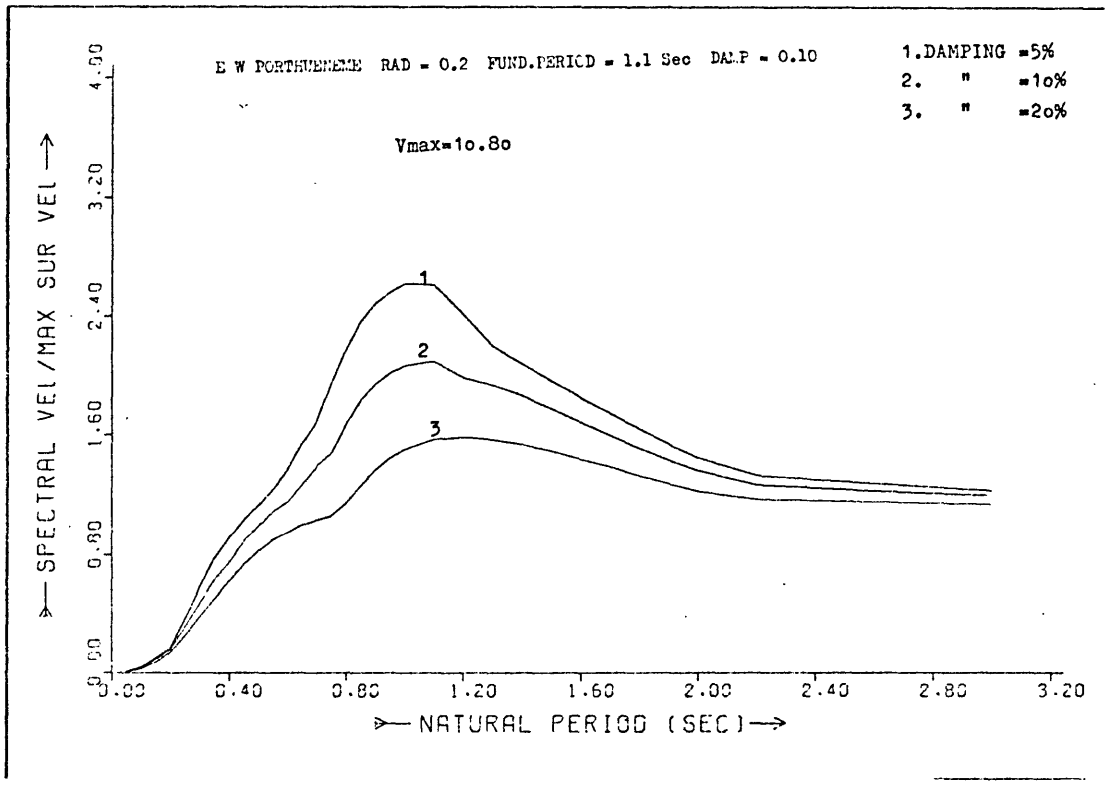


FIG.7.22e COMPUTED GROUND SURFACE VELOCITY RESPONSE SPECTRA AT SITE NO 7.17

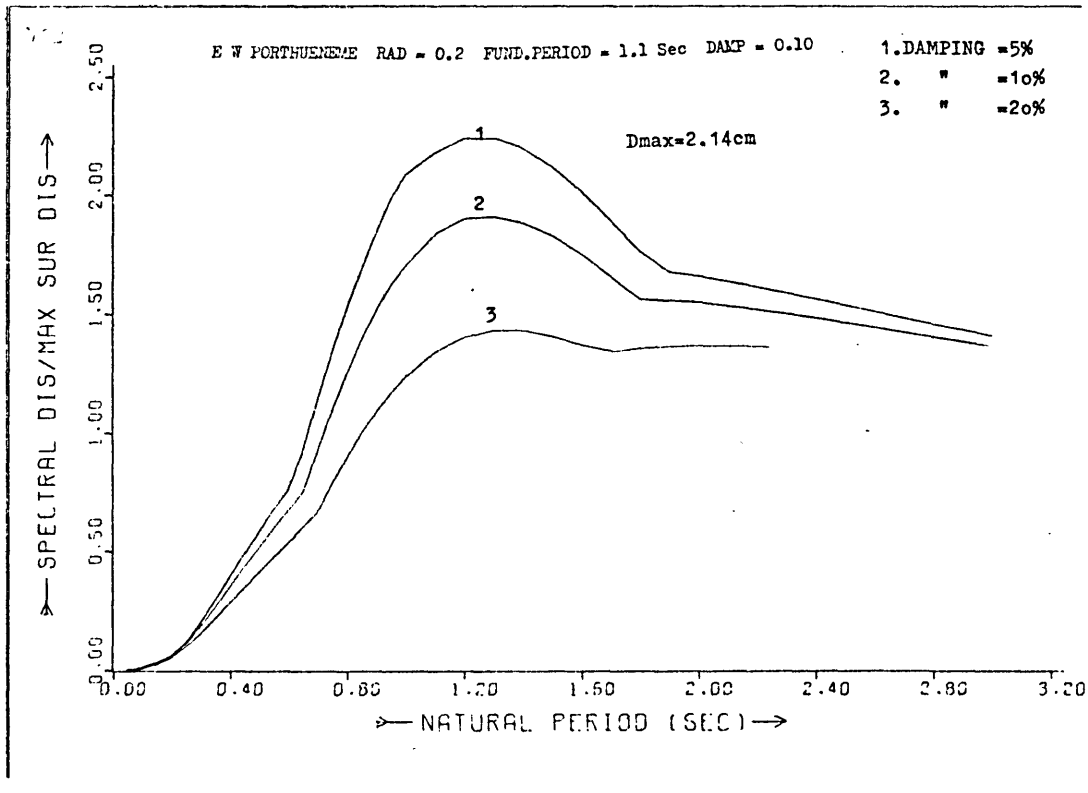
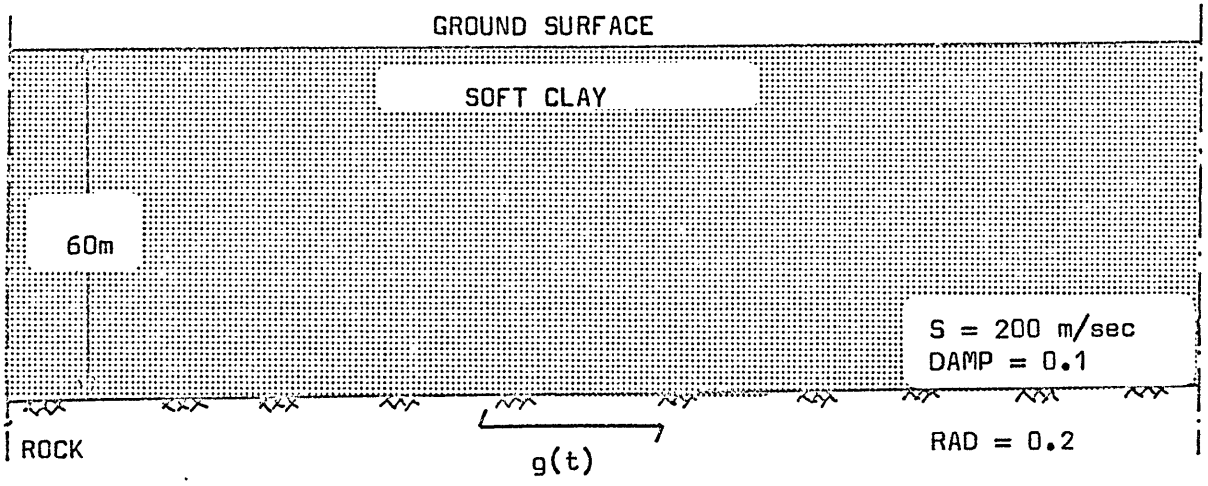


FIG.7.22f COMPUTED GROUND SURFACE DISPLACEMENT RESPONSE SPECTRA AT SITE NO 7.17



FUNDAMENTAL PERIOD OF THE DEPOSIT = 1.2

RESPONSE OF HYSTERETIC DEPOSIT UNDERLAIN BY DEFORMABLE BEDROCK

SCHEMATIC SOIL PROFILE FOR SITE NO 7.18

FIG. 7.23

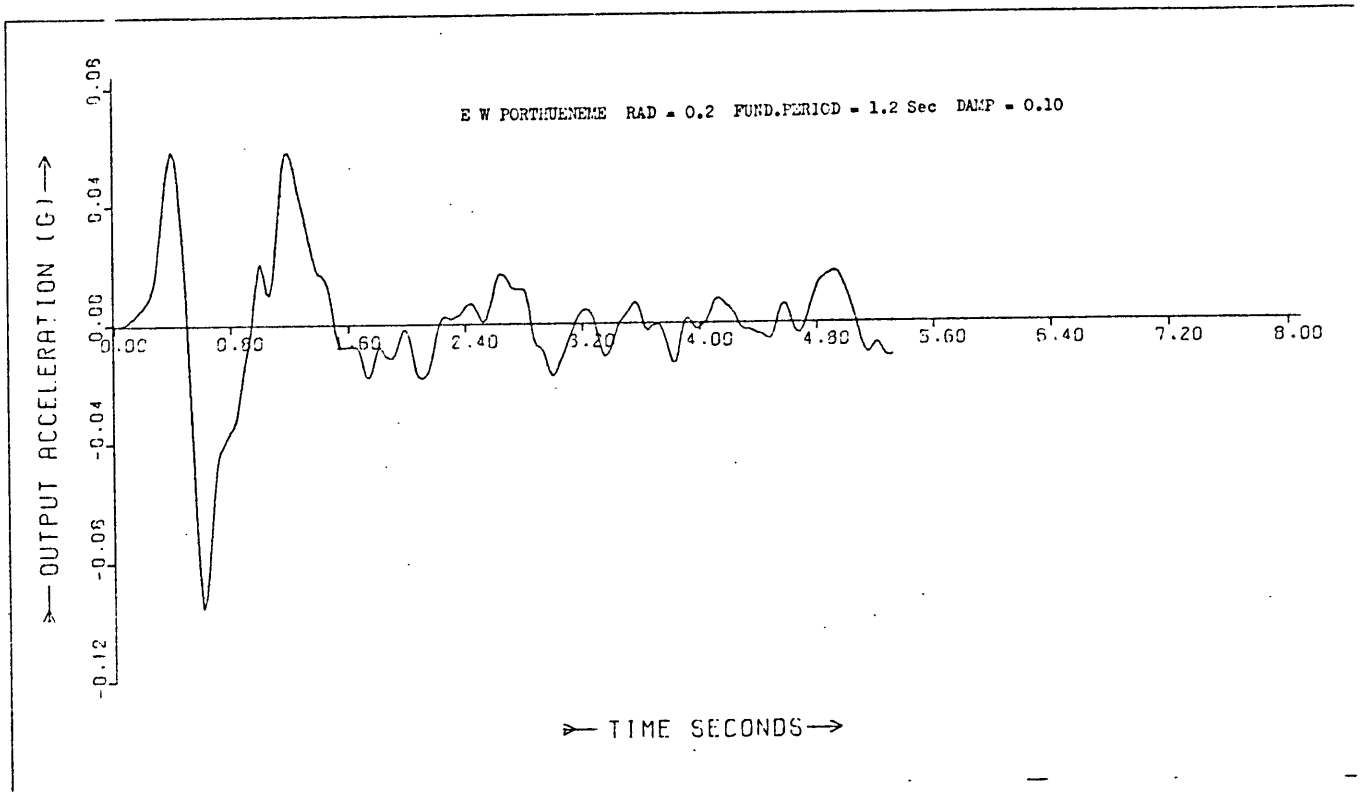


FIG. 7.23a COMPUTED GROUND SURFACE ACCELERATION TIME HISTORY AT SITE NO 7.18

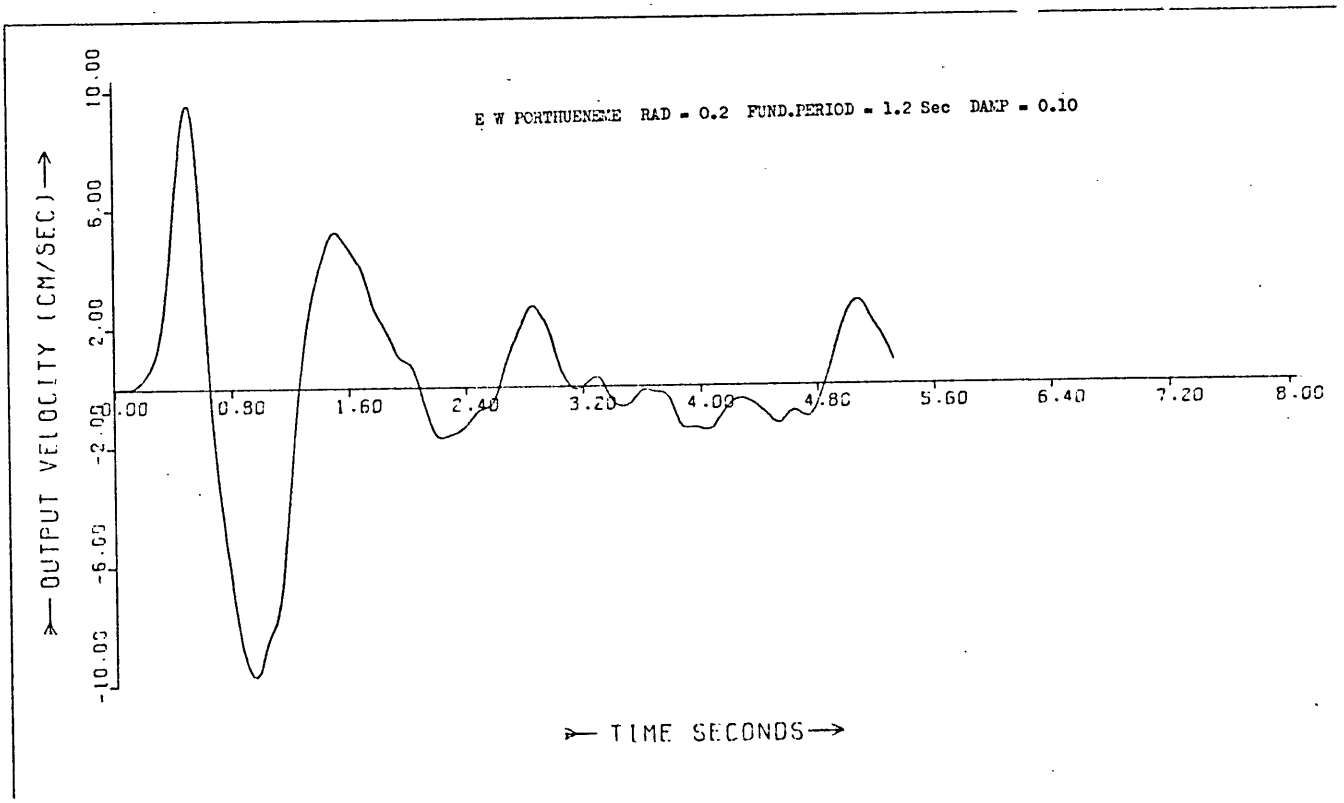


FIG. 7.23b COMPUTED GROUND SURFACE VELOCITY TIME HISTORY AT SITE NO 7.18

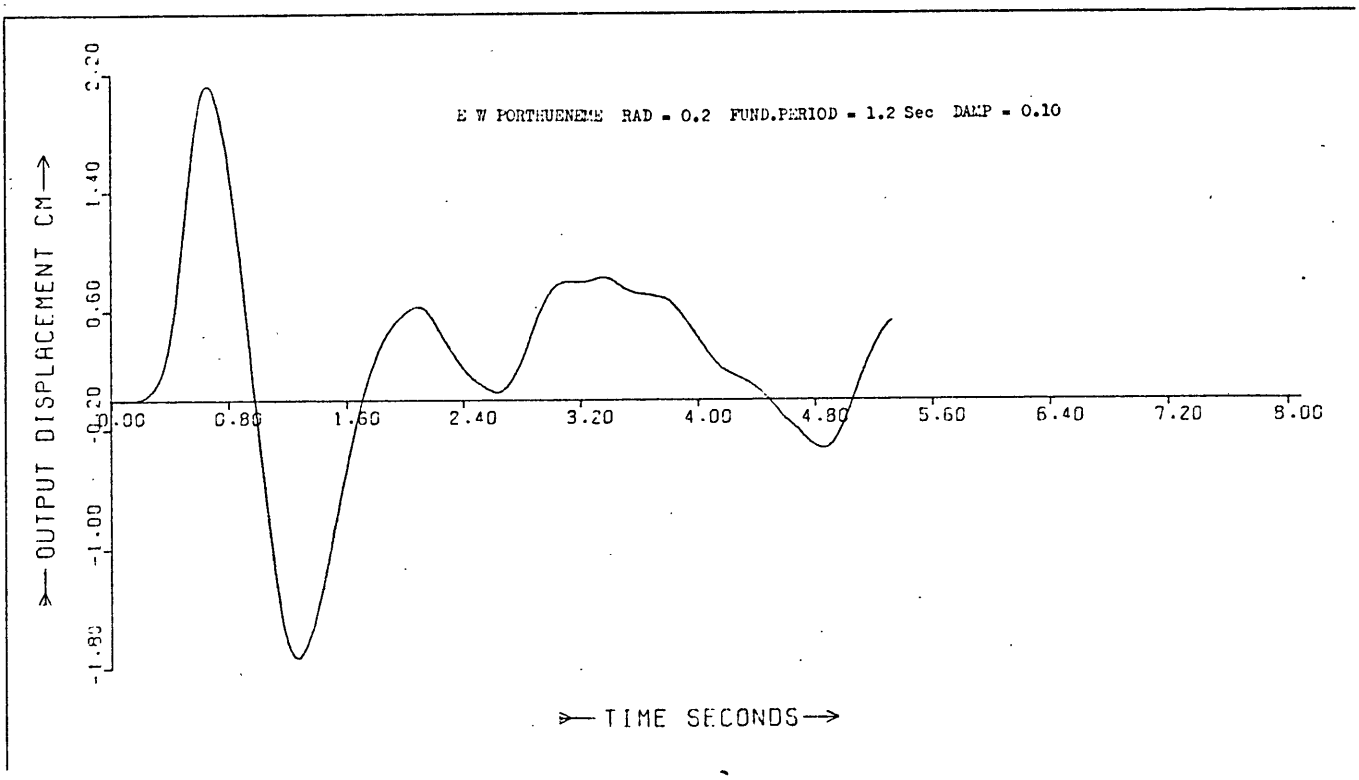


FIG 7.23c COMPUTED GROUND SURFACE DISPLACEMENT TIME HISTORY AT SITE NO 7.18

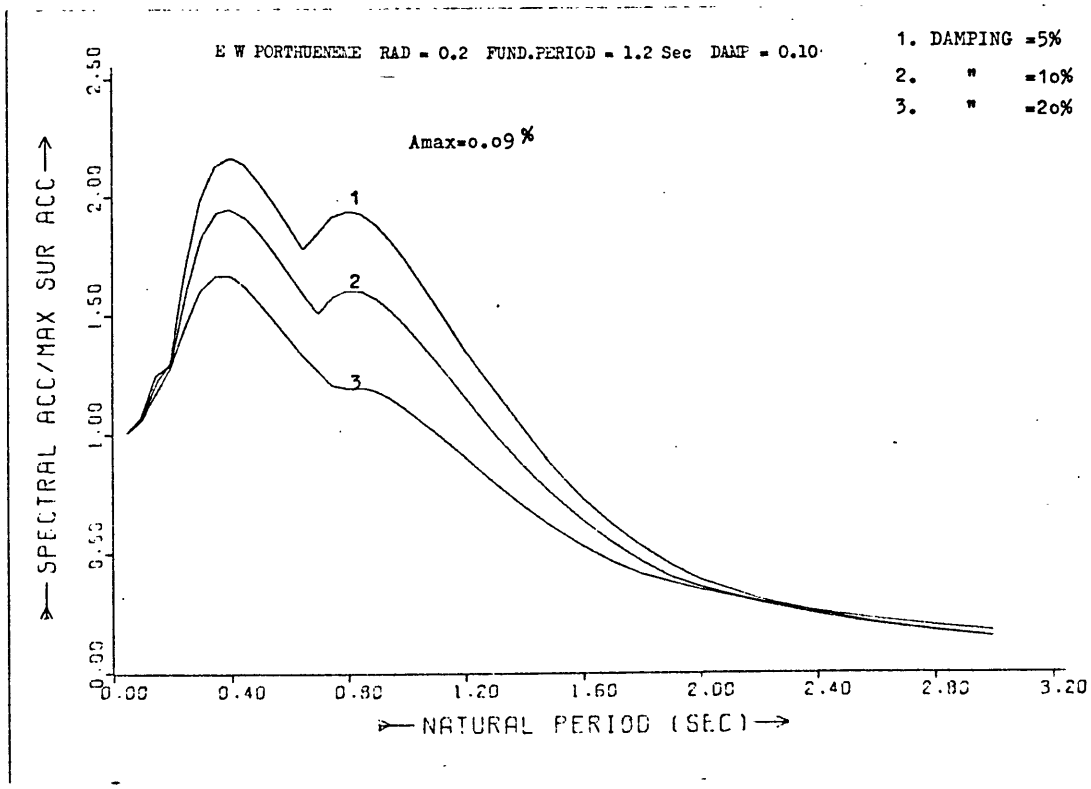


FIG.7.23d COMPUTED GROUND SURFACE ACCELERATION RESPONSE SPECTRA AT SITE NO 7.18

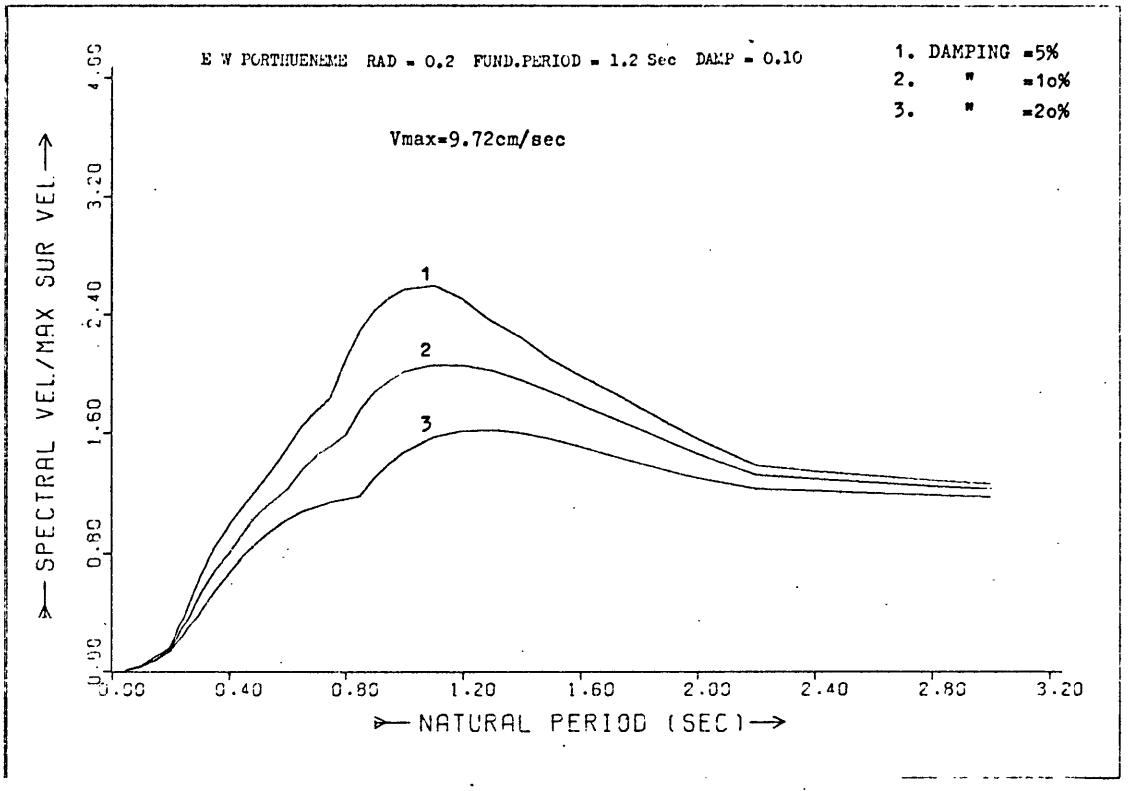


FIG.7.23e COMPUTED GROUND SURFACE VELOCITY RESPONSE SPECTRA AT SITE NO 7.18

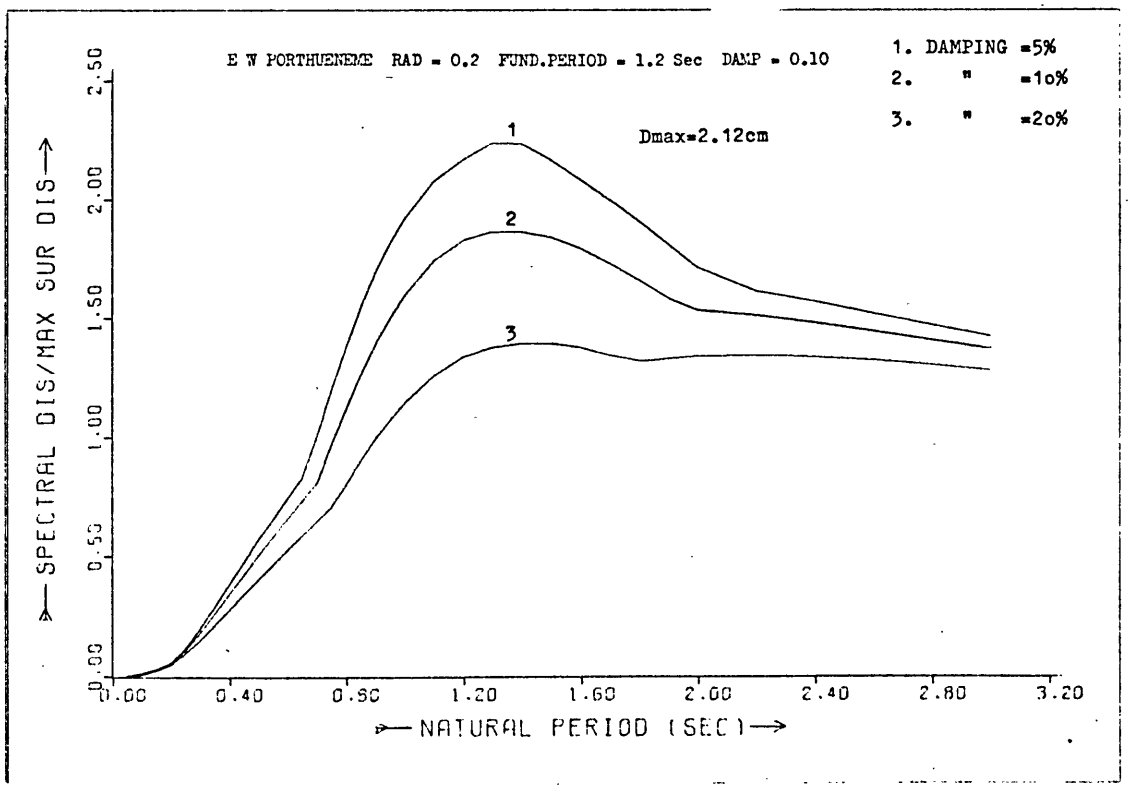
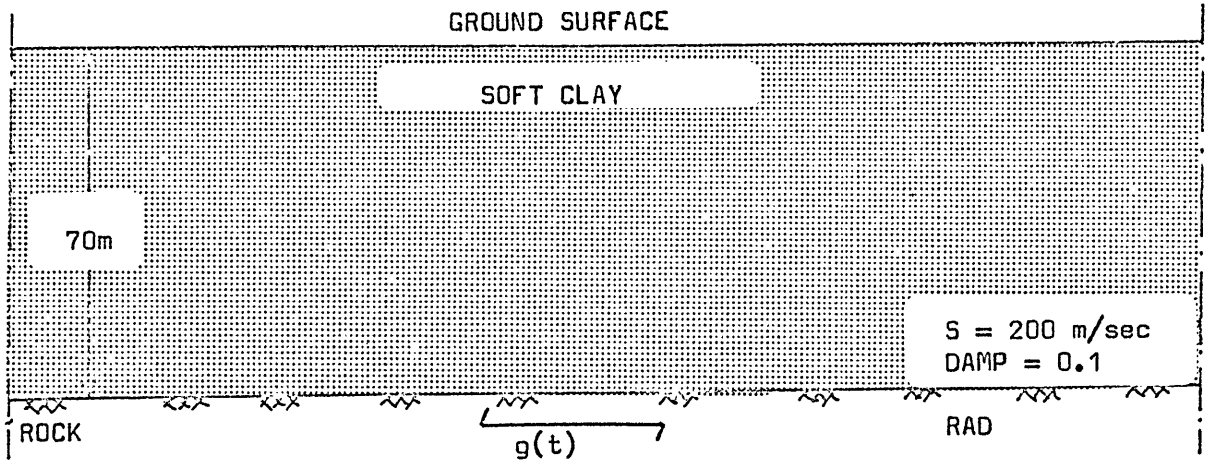


FIG. 7.23f COMPUTED GROUND SURFACE DISPLACEMENT RESPONSE SPECTRA AT SITE NO 7.18



FUNDAMENTAL PERIOD OF THE DEPOSIT = 1.4

RESPONSE OF HYSTERETIC DEPOSIT UNDERLAIN BY DEFORMABLE BEDROCK

SCHEMATIC SOIL PROFILE FOR SITE NO 7.19

FIG. 7.24

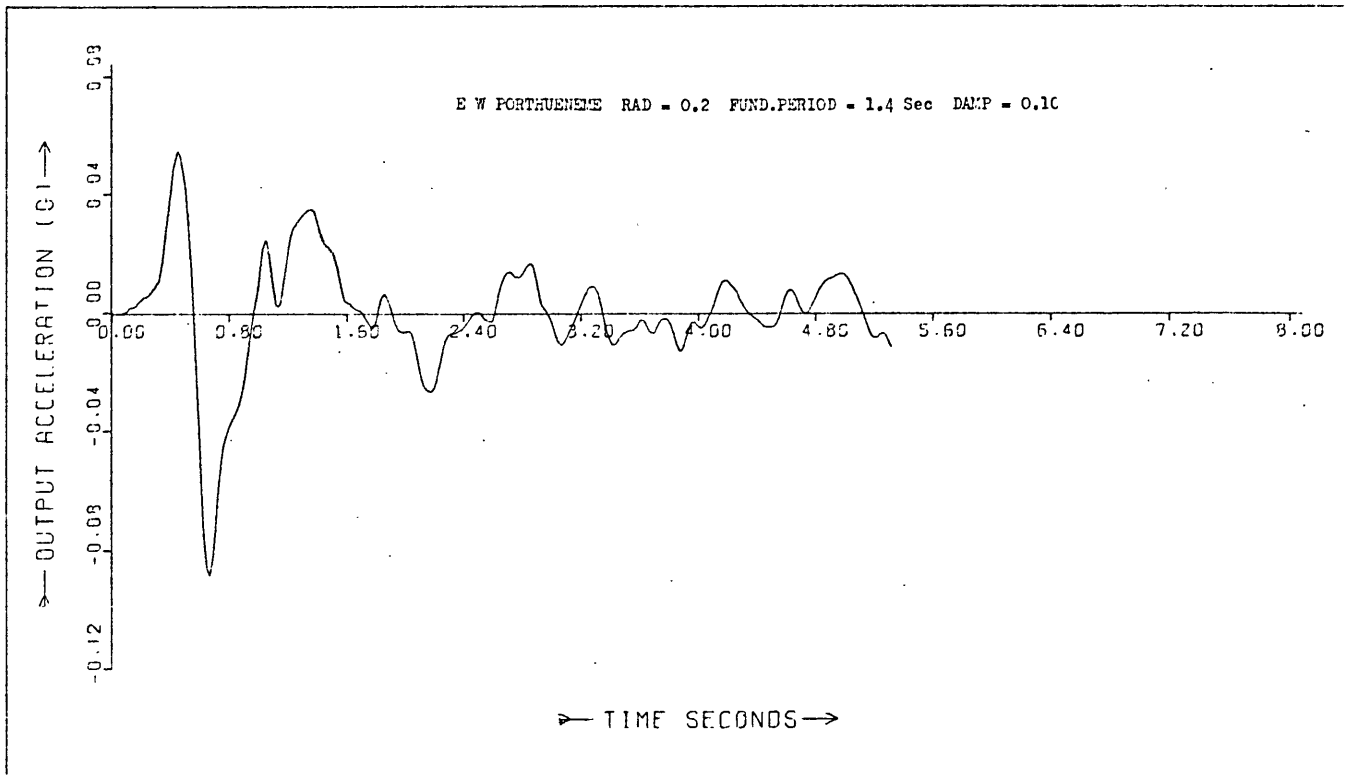


FIG7 .24a COMPUTED GROUND SURFACE ACCELERATION TIME HISTORY AT SITE NO 7.19

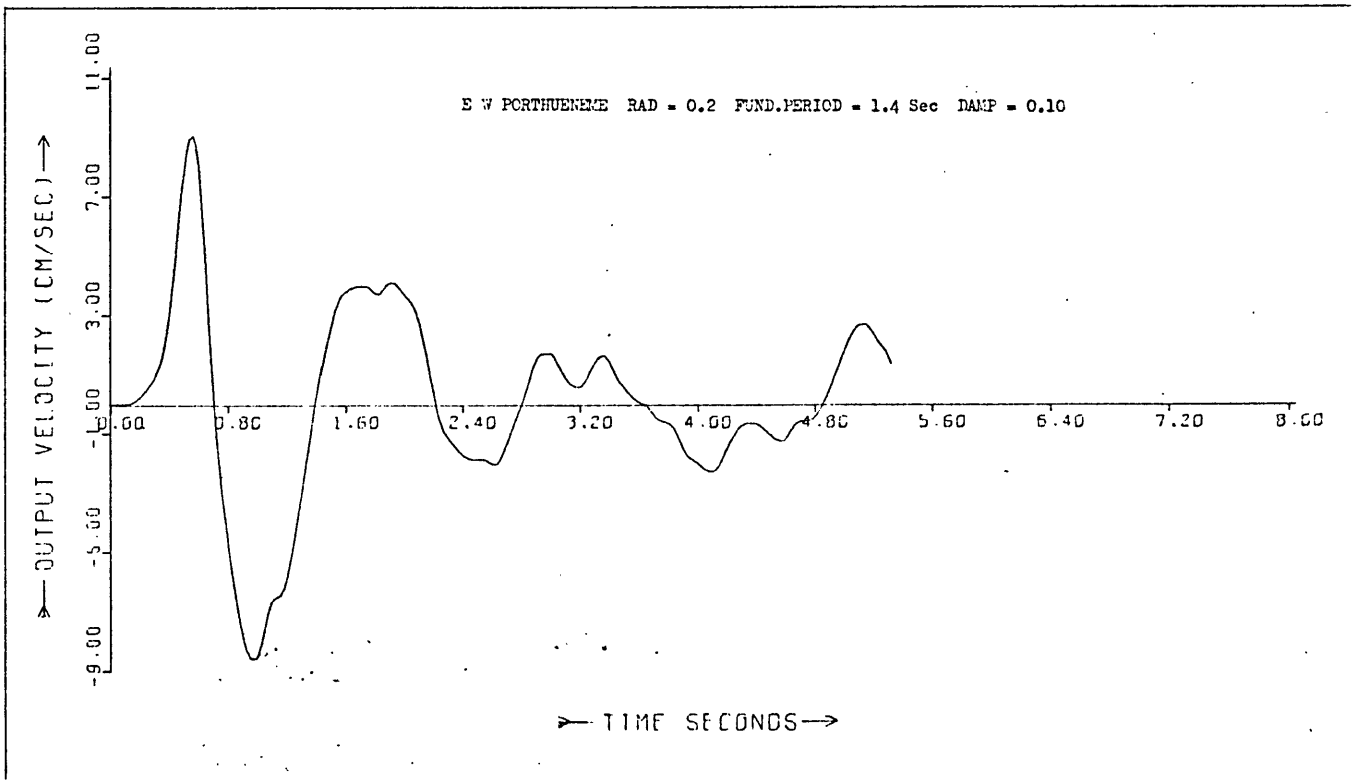


FIG. 7.24b COMPUTED GROUND SURFACE VELOCITY TIME HISTORY AT SITE NO 7.19

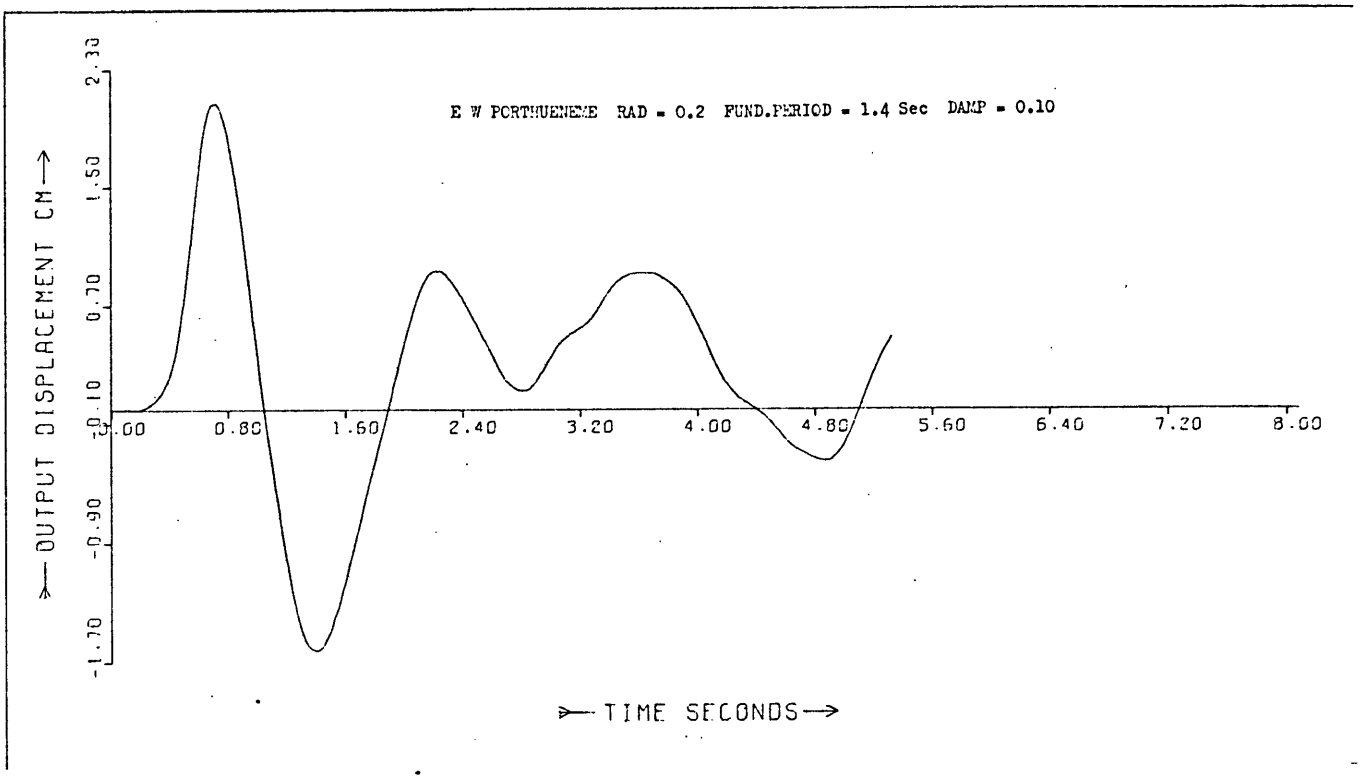


FIG7 .24c COMPUTED GROUND SURFACE DISPLACEMENT TIME HISTORY AT SITE NO 7.19

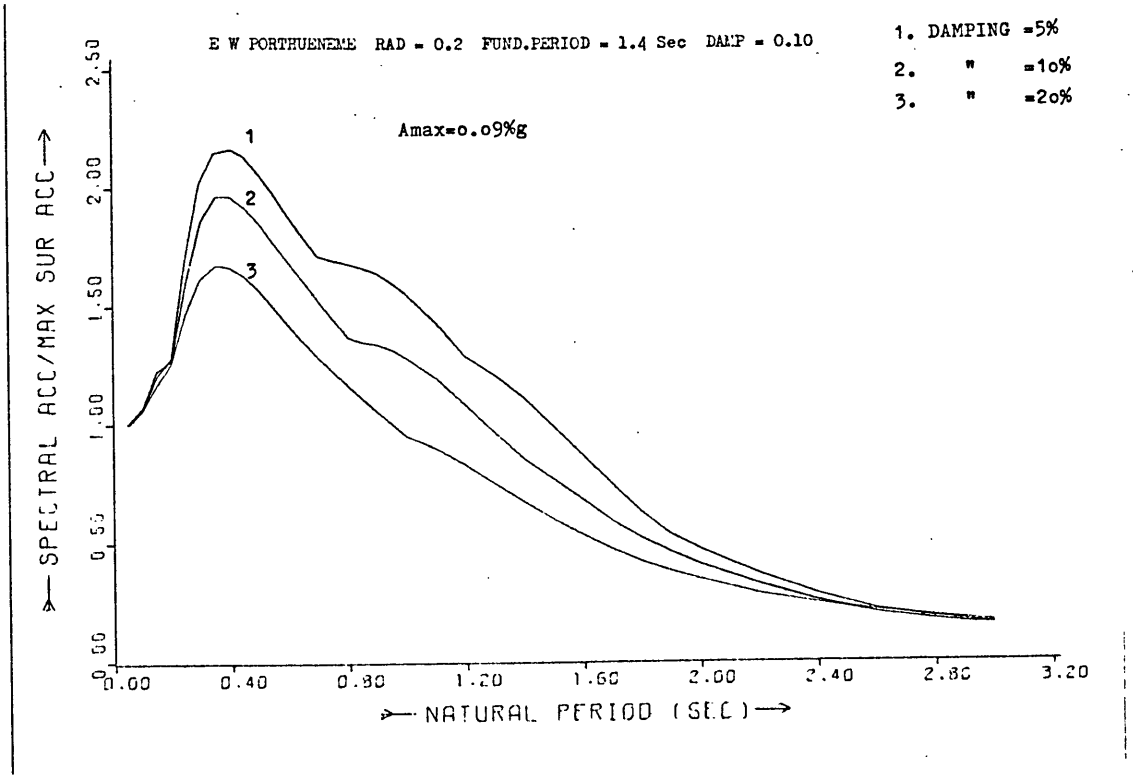


FIG7 .24d COMPUTED GROUND SURFACE ACCELERATION RESPONSE SPECTRA AT SITE NO 7.19

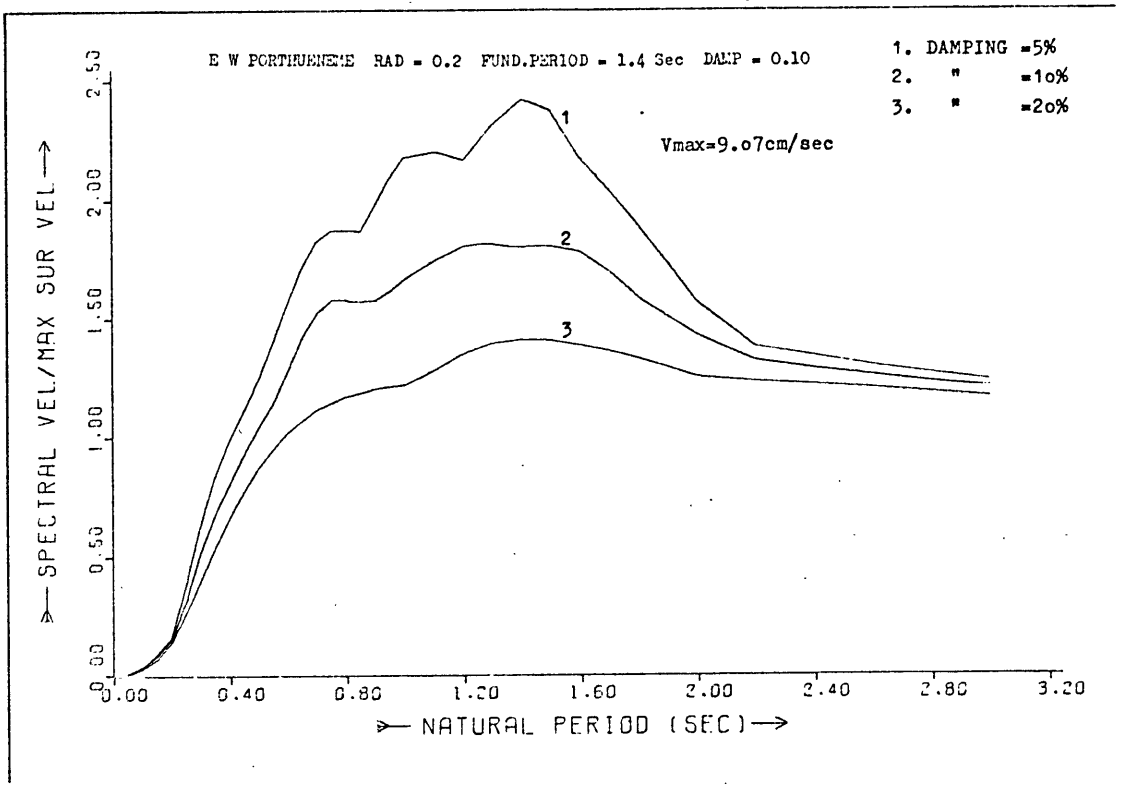


FIG. 7.24e COMPUTED GROUND SURFACE VELOCITY RESPONSE SPECTRA AT SITE NO 7.19

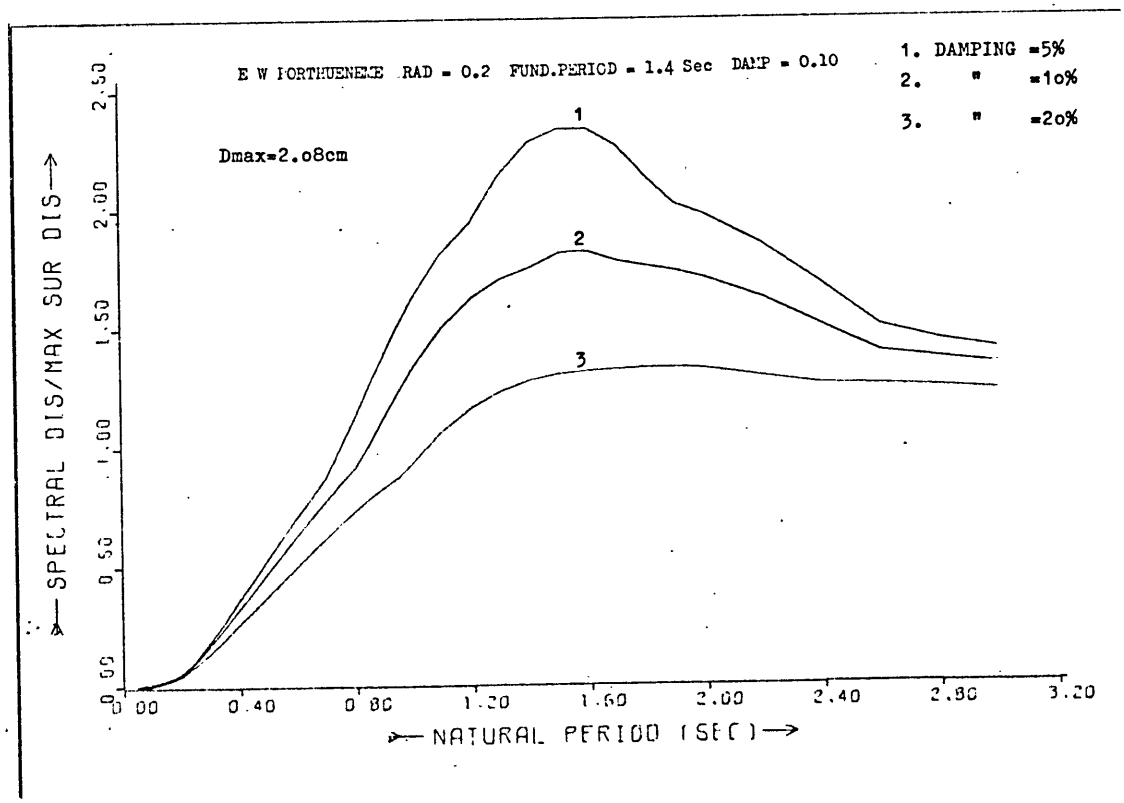


FIG.7.24f COMPUTED GROUND SURFACE DISPLACEMENT RESPONSE SPECTRA AT SITE NO 7.19

$$E_{kinetic} = 0.5.m. \sum_{t=o}^{T_{dur}} \dot{v}^2(t)\ \delta t \qquad (7.3)$$

Equation (7.3) is written as:

$$S = \frac{E_{kinetic}}{m} = o.5 \sum_{t=o}^{T_{dur}} \dot{v}^2(t)\ \delta t \qquad (7.4)$$

where "S" is the total energy available for damage per unit mass of soil. The quantity "S" is called strength of earthquake motion and is a measure of total energy which would be supplied to structures located on the site, i.e. a measure of intensity of ground shaking. The advantage of this new parameter to describe the severity of ground shaking to the "old" ones, such as Spectrum intensity defined by Housner,[31] is this: this new parameter includes duration of shaking, whereas that of Housner does not. The role played by the duration of ground shaking on structural damage is explained in section 7.8.

Fig. 7.25 shows variation of strength "S" with fundamental period of the deposits described in section 7.3. It is seen that the site with fundamental period of 0.8 second has shown the greatest strength, indicating that energy available to be fed into the structures located on this site to cause damage is the greatest; the overall distribution of amplitudes of velocities on velocity time history shown by fig. 7.19b

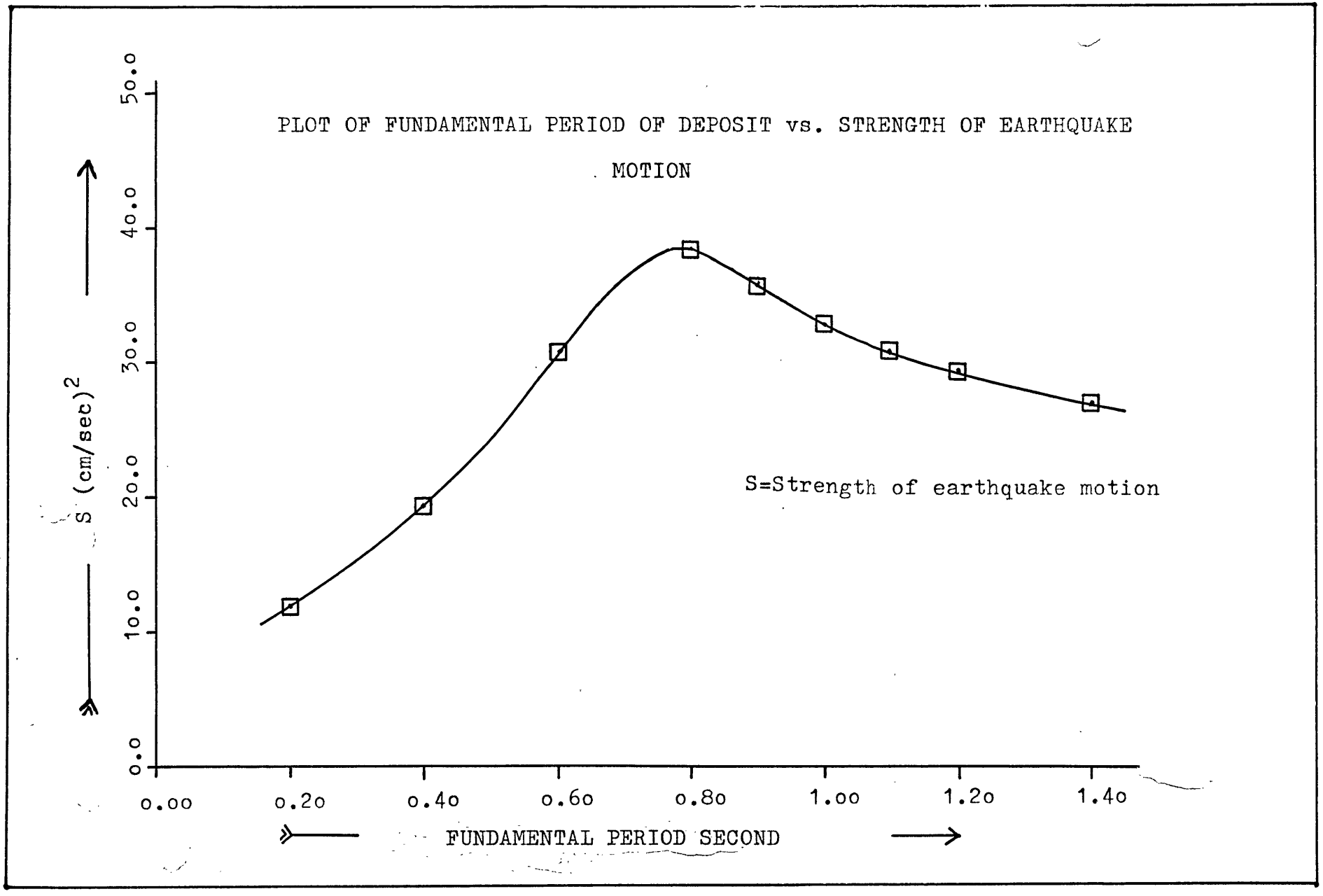

PLOT OF FUNDAMENTAL PERIOD OF DEPOSIT vs. STRENGTH OF EARTHQUAKE MOTION
S=Strength of earthquake motion
S (cm/sec)2
0.0
10.0
20.0
30.0
40.0
50.0
0.00
0.20
0.40
0.60
0.80
1.00
1.20
1.40
FUNDAMENTAL PERIOD SECOND

FIG.7.25

is the largest compared with the other eight illustrated by figs. 7.16b through 7.29b.

7.4. INFLUENCE OF BASE MOTION ON GROUND RESPONSE AND COMPARISON OF COMPUTED AND RECORDED VALUES

Response of soil deposits to earthquake motion is very much dependent on amplitude, frequency distribution and duration of bedrock motion. Variation in all these parameters would introduce variations in the computed response throughout the deposit. The effect of bedrock time history on ground response forms the objective of this section.

7.4.1. INFLUENCE OF FREQUENCY CHARACTERISTICS OF BEDROCK MOTION ON GROUND RESPONSE

In order to study the influence of frequency characteristics of seismic bedrock motion on response, two different comparisons were made between sites different only in bedrock acceleration time histories. These bedrock motions are TEMBLOR N65W and PARKFIELD-8 N40W. Both possess the same peak acceleration of 0.28%g and differ only in frequency characteristics, which is reflected through their predominant periods 0.26 and 0.2 second, respectively. It should be noted that TEMBLOR N65W and PARKFIELD-8 N40W have almost equal amplitudes throughout their duration, which is purely a matter of coincidence, and relative amplitudes of these pulses, in most cases, with respect to maximum accelerations are almost the same.

Specification of the site considered whose fundamental period is equal to 1.34 sec. is given in fig. 7.26. The computed response of this

site when subjected to the above two base motions are shown in figs. 7.26a,b,c,d,e,f through 7.27a,b,c,d,e,f. The results shown in figs. 7.26d through 7.27d indicate that the same site would have different predominant periods depending on seismic loading conditions. It is also noted that the site subjected at its base to TEMBLOR N65W with a predominant period of 0.26 second has shown greater peak amplitude of acceleration response spectra than the one subjected to PARKFIELD-8 N40W; this is because predominant period of TEMBLOR N65W - 0.26 second is much closer to the second mode period of the overburden 0.43 than that of PARKFIELD-8 with 0.2 second. The question which here arises is this; whether any changes in the frequency characteristics of bedrock motion are likely to affect damping and shear wave velocities of the overburden. This point is discussed in chapter 5. The experimental results indicate that, within the frequency range expected in earthquakes, the effects of frequency on damping and shear wave velocity are small. Therefore, the assumption made in this study that the effect of frequency characteristics of base motion is reflected through its base motion is justified.

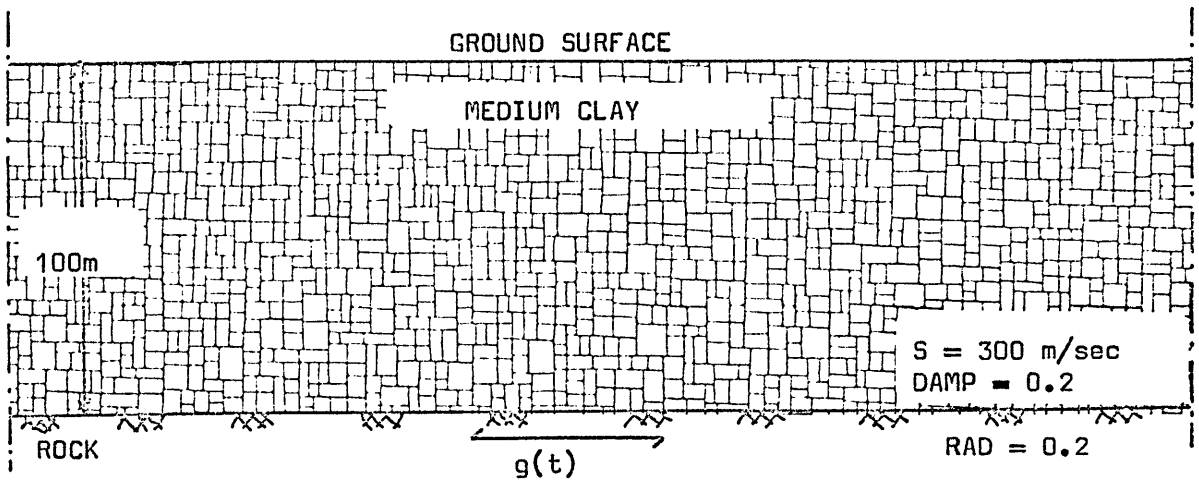
7.4.2. INFLUENCE OF AMPLITUDE OF BASE MOTION ON GROUND RESPONSE

To illustrate the influence of amplitude of base motion on computed surface response, analyses were performed on a 50m thick deposit of dense sand underlain by a bedrock five times harder in characteristics than the deposit subjected at the bedrock level to:

0.5 x N10E Goldengate

1.0 x "

1.5 x "



RESPONSE OF HYSTERETIC DEPOSIT UNDERLAIN BY DEFORMABLE BEDROCK

SCHEMATIC SOIL PROFILE FOR SITE NO 7.20

FIG. 7.26

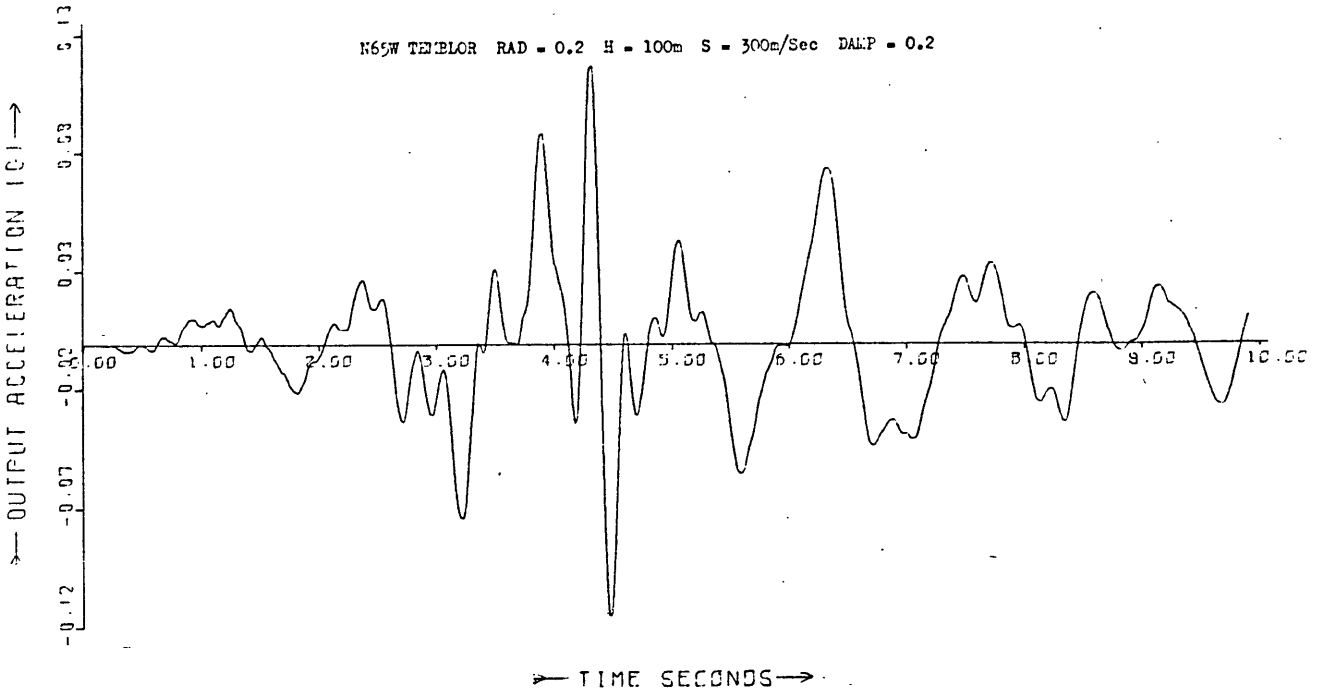


FIG.7.26a COMPUTED GROUND SURFACE ACCELERATION TIME HISTORY AT SITE NO 7.20

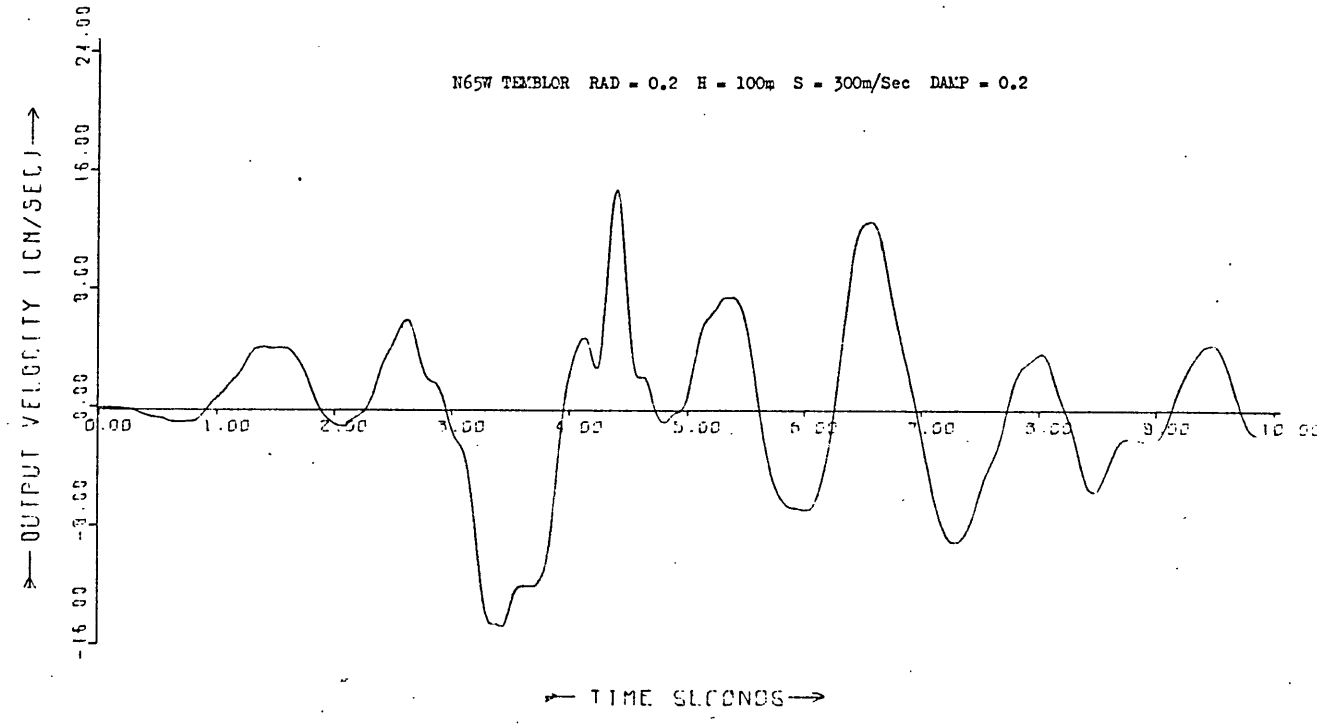


FIG. 7.26b COMPUTED GROUND SURFACE VELOCITY TIME HISTORY AT SITE NO 7.20

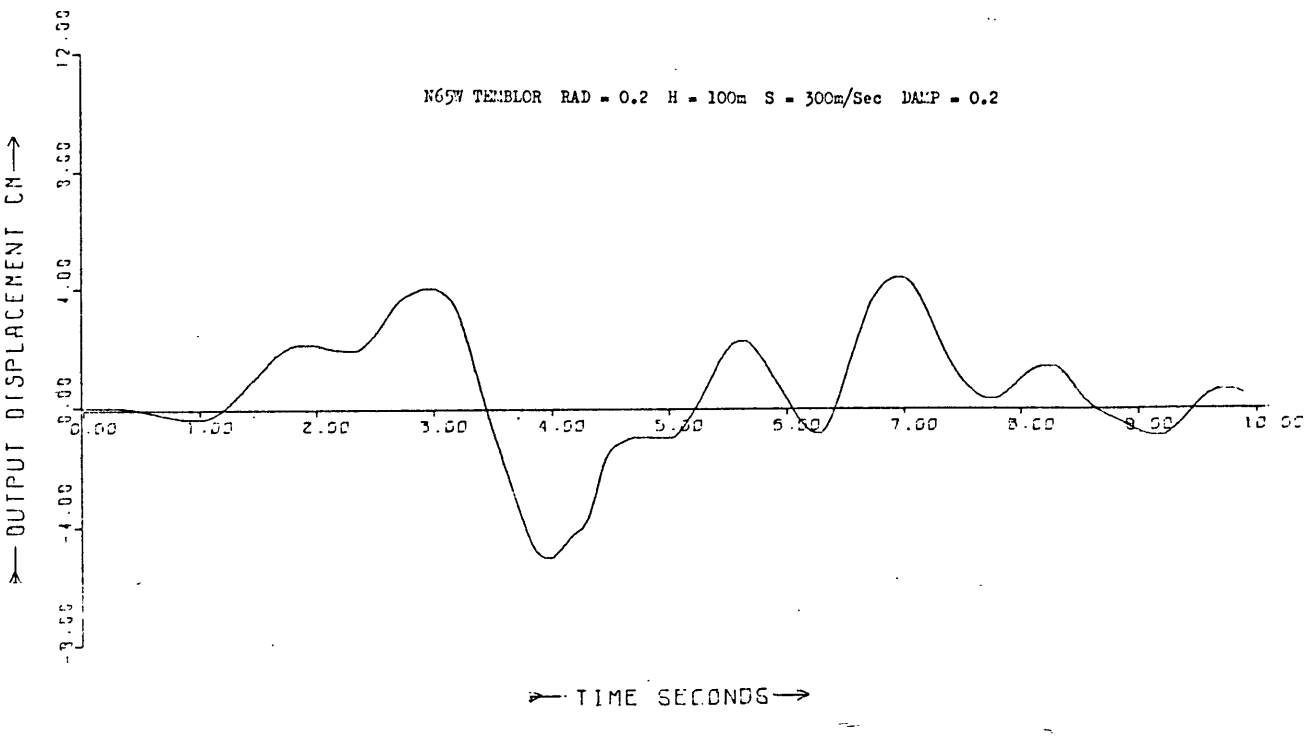


FIG.7.26c COMPUTED GROUND SURFACE DISPLACEMENT TIME HISTORY AT SITE NO 7.2

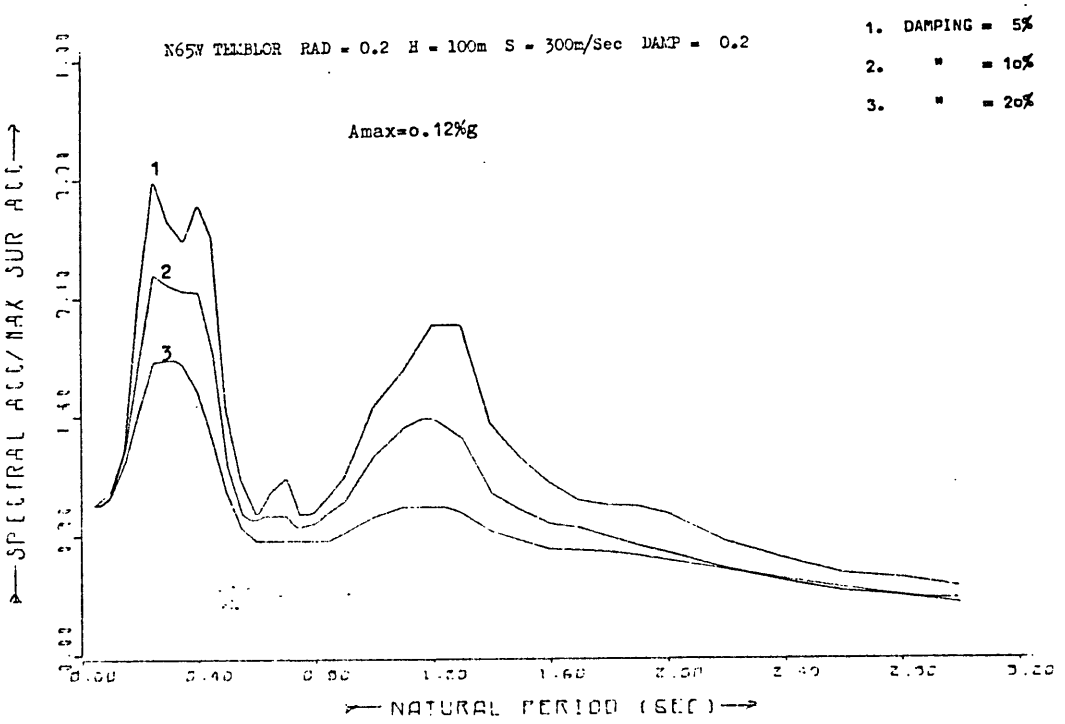


FIG.7.26d COMPUTED GROUND SURFACE ACCELERATION RESPONSE SPECTRA AT SITE NO 7.2

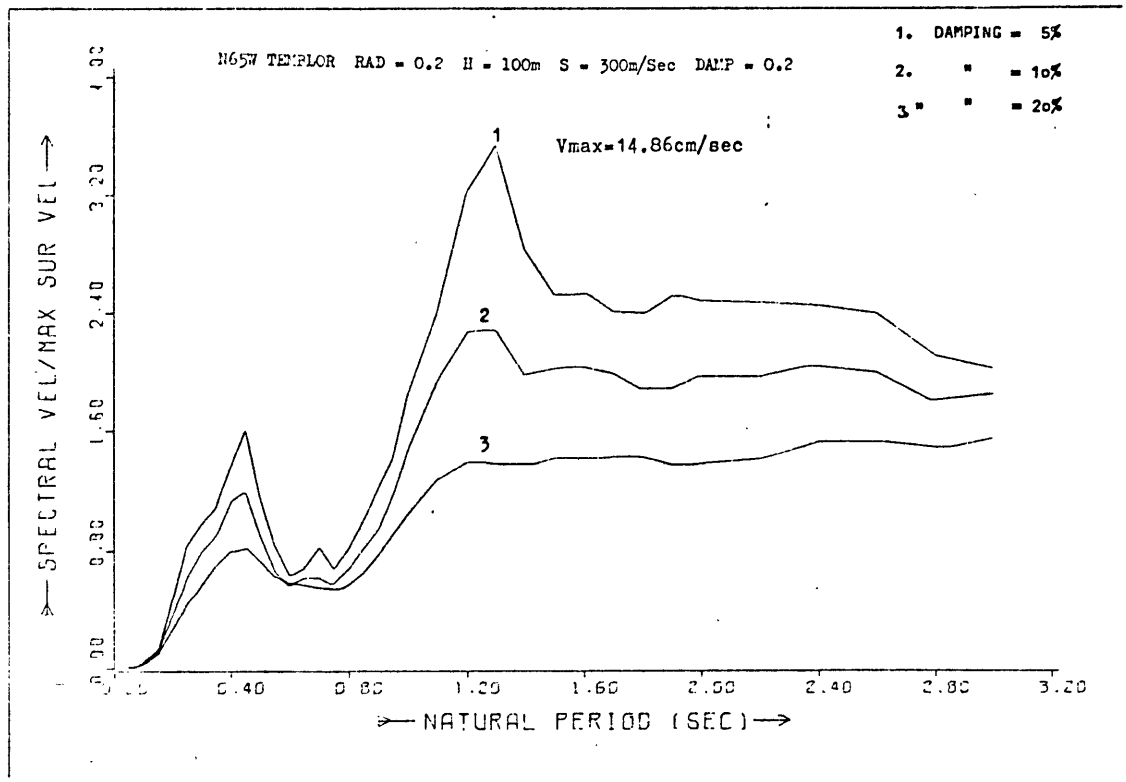


FIG. 7.26e COMPUTED GROUND SURFACE VELOCITY RESPONSE SPECTRA AT SITE NO 7.2 o

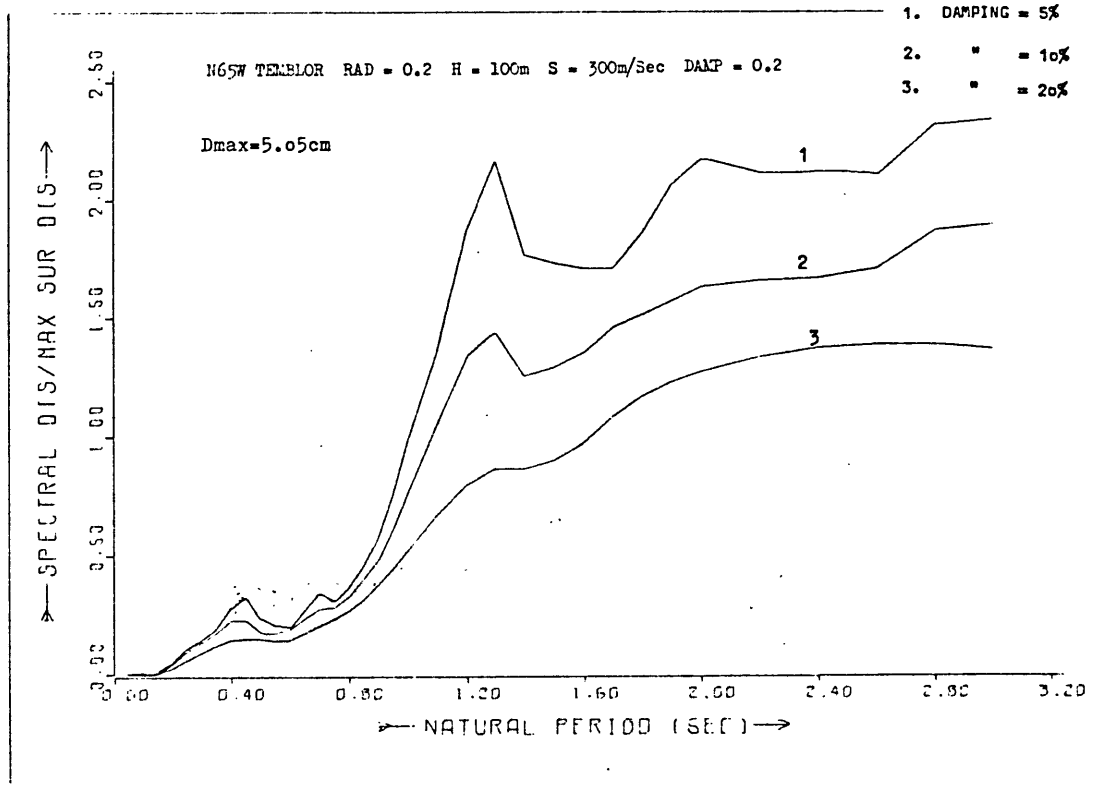


FIG.7.26f COMPUTED GROUND SURFACE DISPLACEMENT RESPONSE SPECTRA AT SITE NO 7.2o

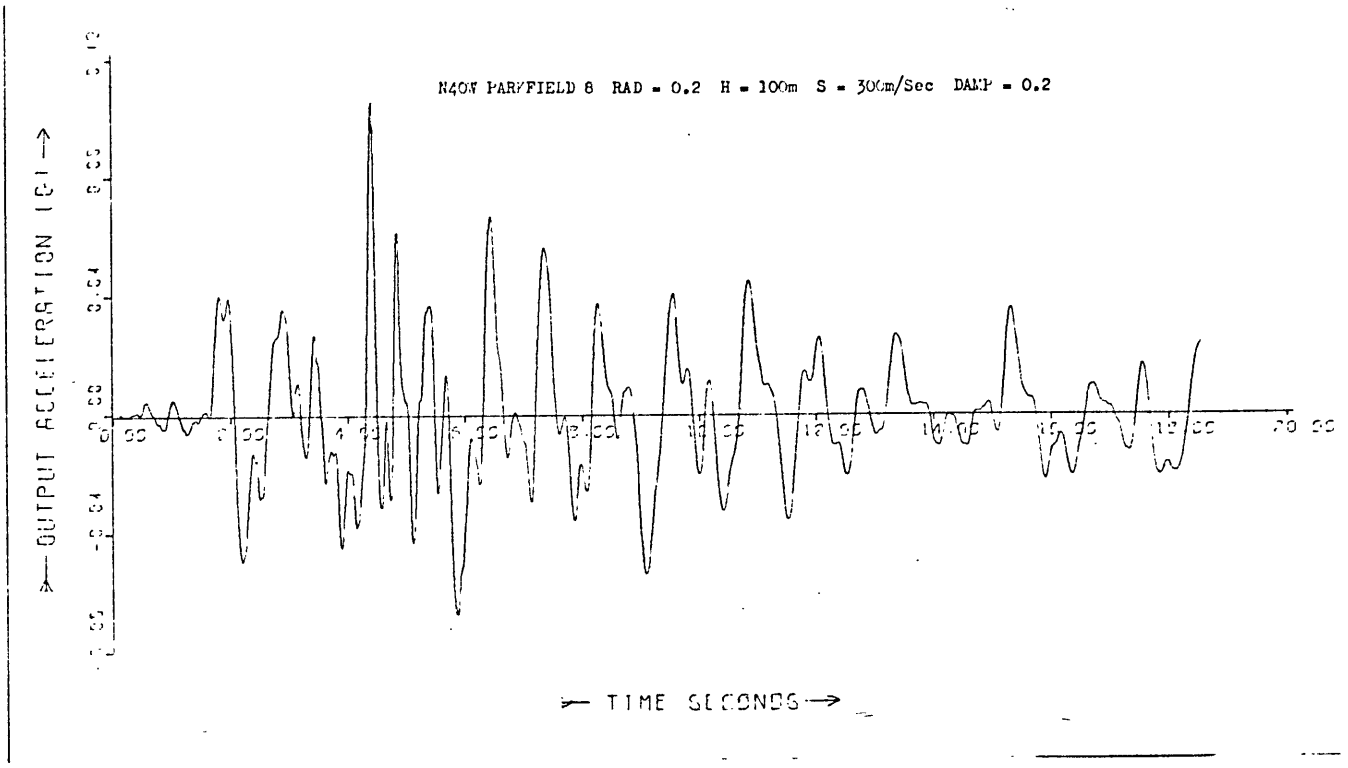


FIG7.27a COMPUTED GROUND SURFACE ACCELERATION TIME HISTORY AT SITE NO 7.2 o

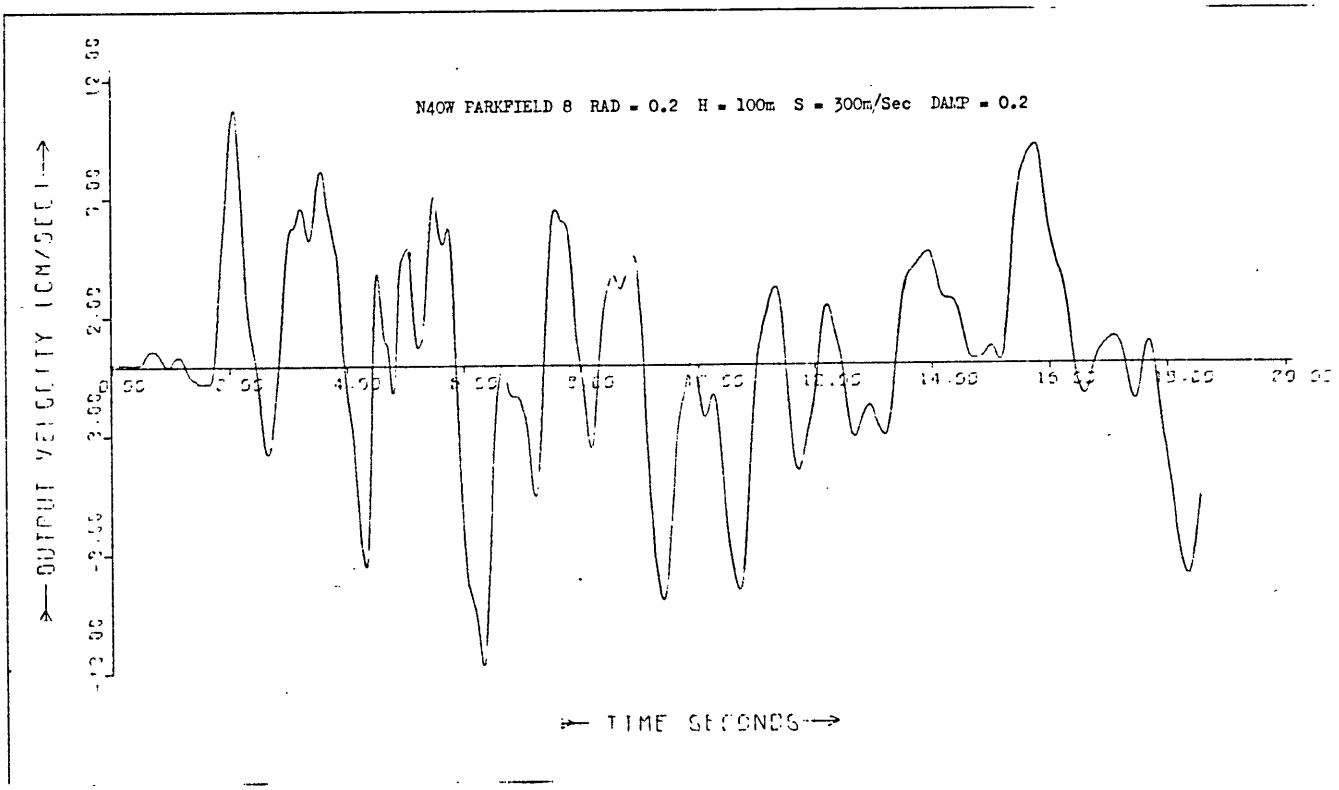


FIG.7.27b COMPUTED GROUND SURFACE VELOCITY TIME HISTORY AT SITE NO7.20

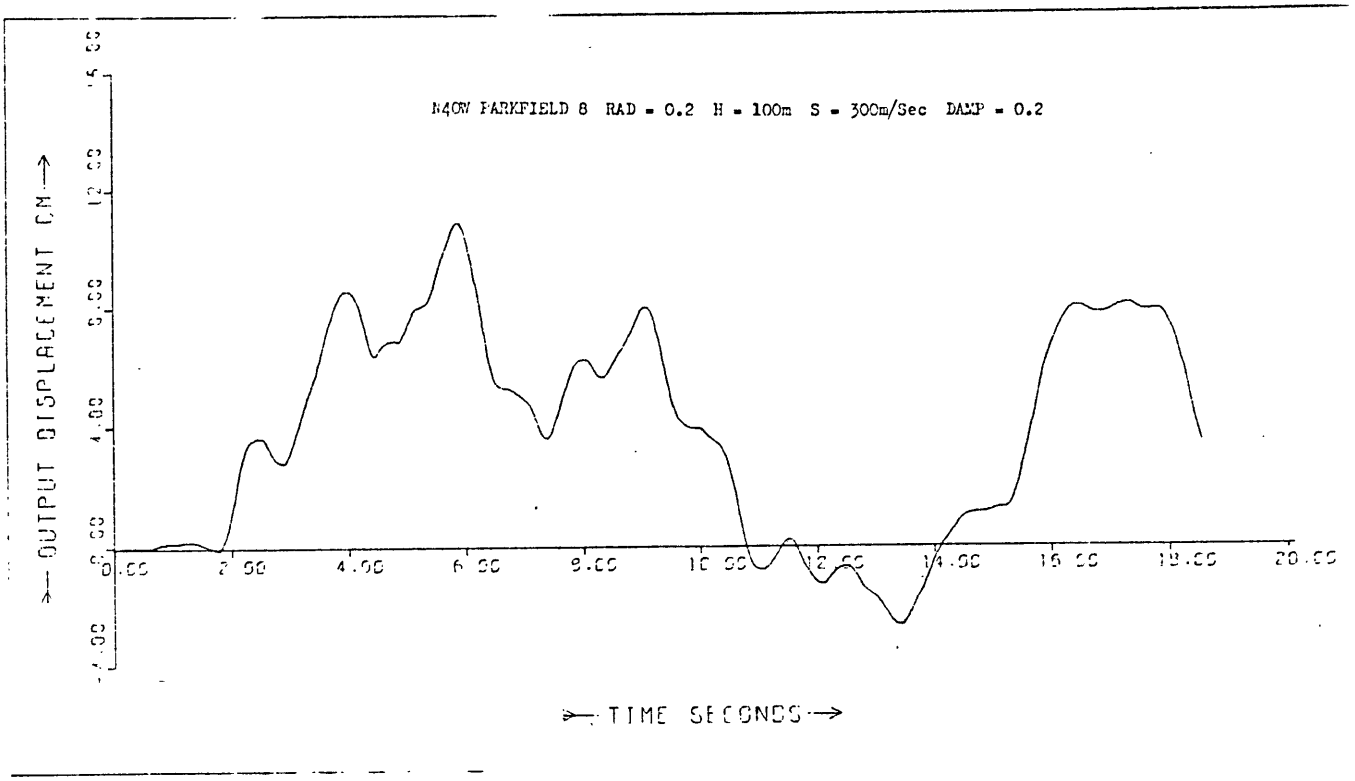


FIG.7.27c COMPUTED GROUND SURFACE DISPLACEMENT TIME HISTORY AT SITE NO 7.20

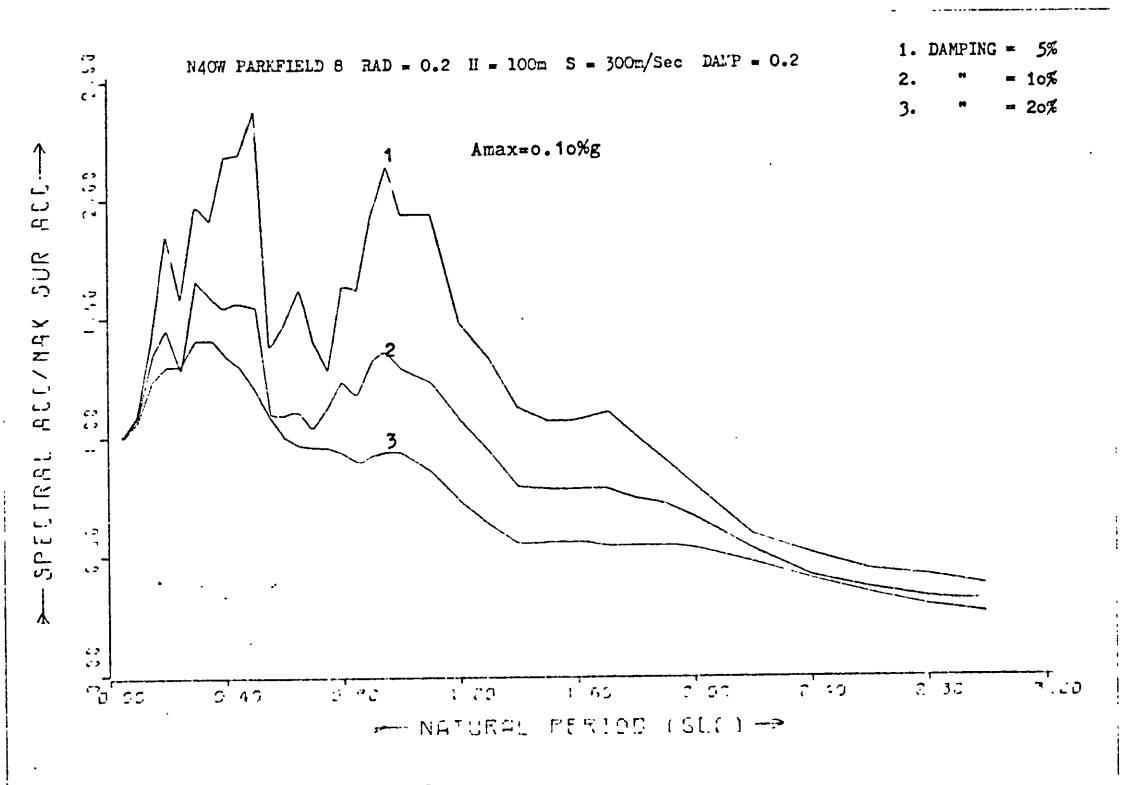


FIG.7.27d COMPUTED GROUND SURFACE ACCELERATION RESPONSE SPECTRA AT SITE NO 7.20

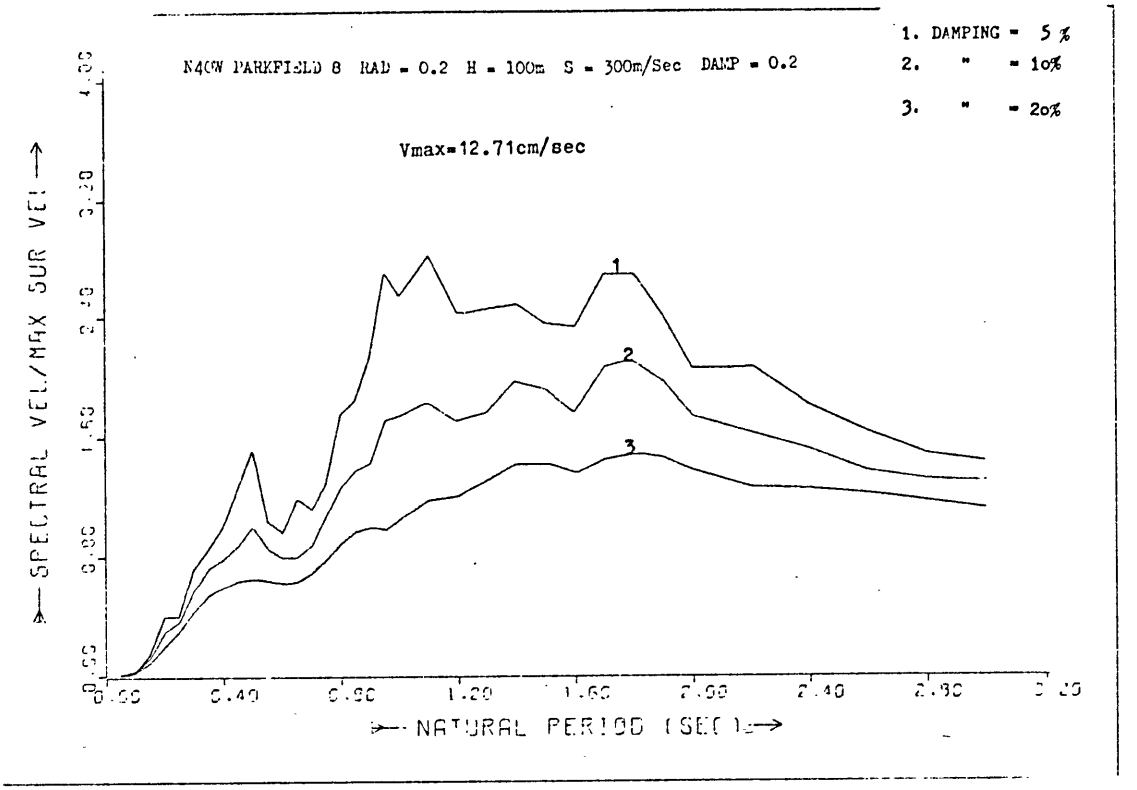


FIG 7.27e COMPUTED GROUND SURFACE VELOCITY RESPONSE SPECTRA AT SITE NO 7.20

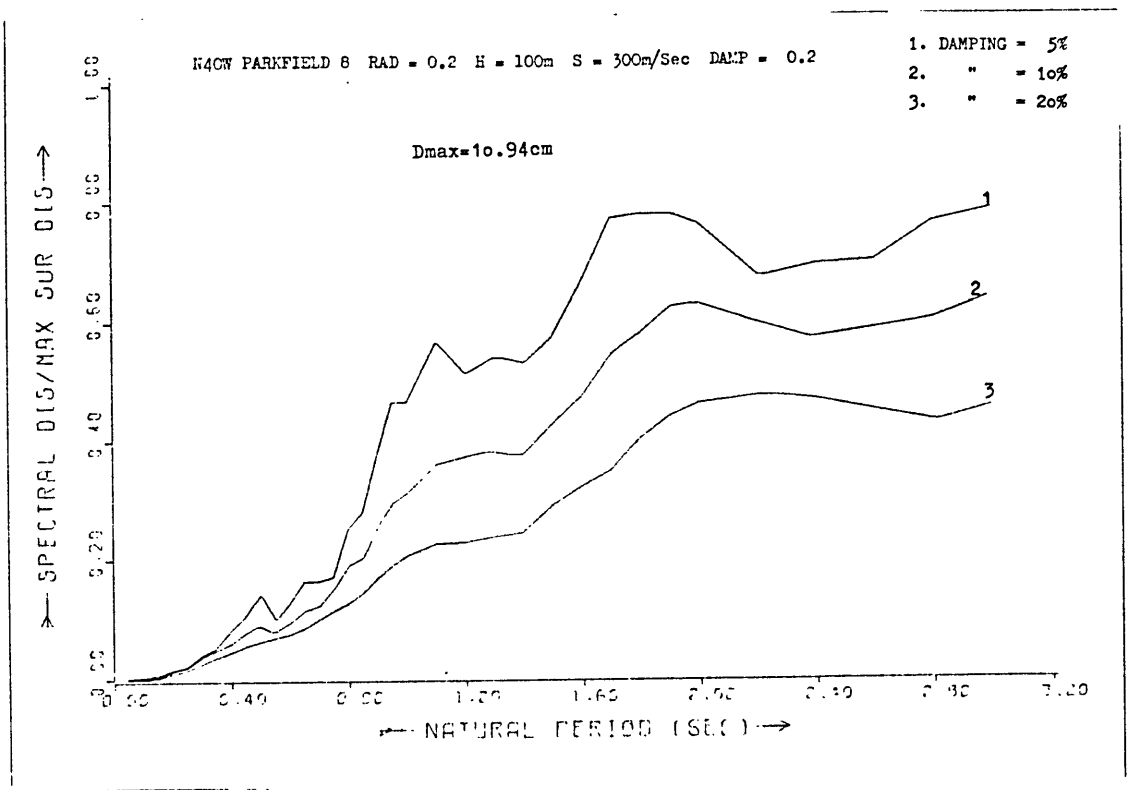


FIG 7.27f COMPUTED GROUND SURFACE DISPLACEMENT RESPONSE SPECTRA AT SITE NO 7.20

0.5 x N50E Parkfield-8

1.0 x "

1.5 x "

The hysteretic damping ratio for the deposit was assumed to be 0.02. The results of the calculations are shown in figs. 7.28a,b,c,d,e,f to 7.33a,b,c,d,e,f.

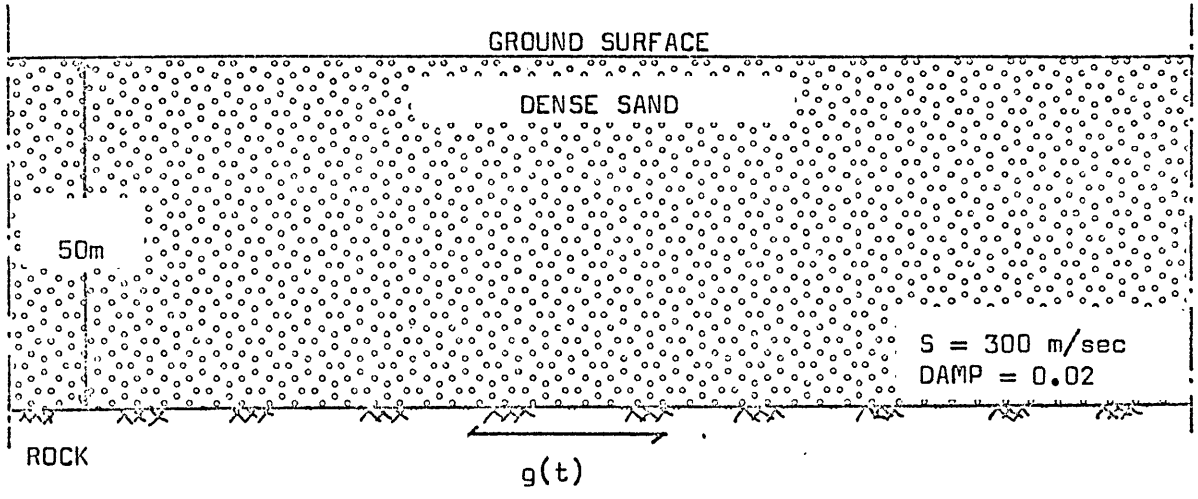
Figs. 7.28a,b,c,d,e,f through 7.33a,b,c,d,e,f show that, as expected, an increase in the amplitudes of base motions increases the computed response values by the same factor, which is expected from the developed solution given in chapter 4. The results clearly indicate that response values measured during atomic explosions or small events can be applied directly to predict performance during larger earthquakes, based on the assumption that future bedrock motions would show roughly similar frequency characteristics to those of the past bedrock motions and the deposit would not exceed its elastic limit, confirming one of Professor Ambraseys' [3] statements that: "It is worthwhile investigating the possibilities of using large nuclear explosions programs to test the full scale response of foundations ...".

7.5. CONCLUDING REMARKS

Based on the foregoing study, the following conclusions may be drawn:

a) The same site will have different predominant periods depending on character of seismic excitation at the bedrock level.

b) An increase in the amplitudes of base motion increase the computed response values by the same factor.



RESPONSE OF HYSTERETIC DEPOSIT UNDERLAIN BY DEFORMABLE BEDROCK

SCHEMATIC SOIL PROFILE FOR SITE NO 7.21

FIG. 7.28

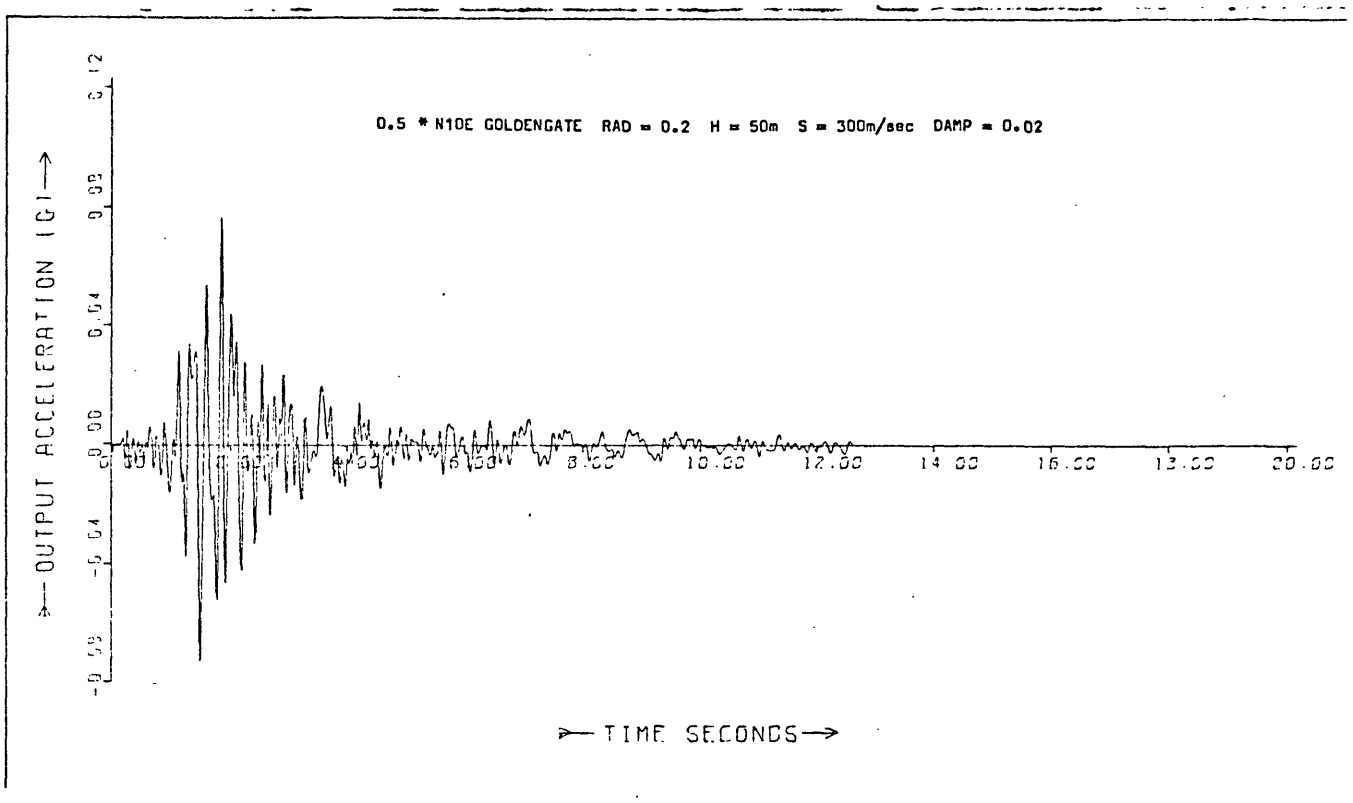


FIG7.28a COMPUTED GROUND SURFACE ACCELERATION TIME HISTORY AT SITE NO. 7.21

BEDROCK MOTION o.5 * N1oE GOLDENGATE

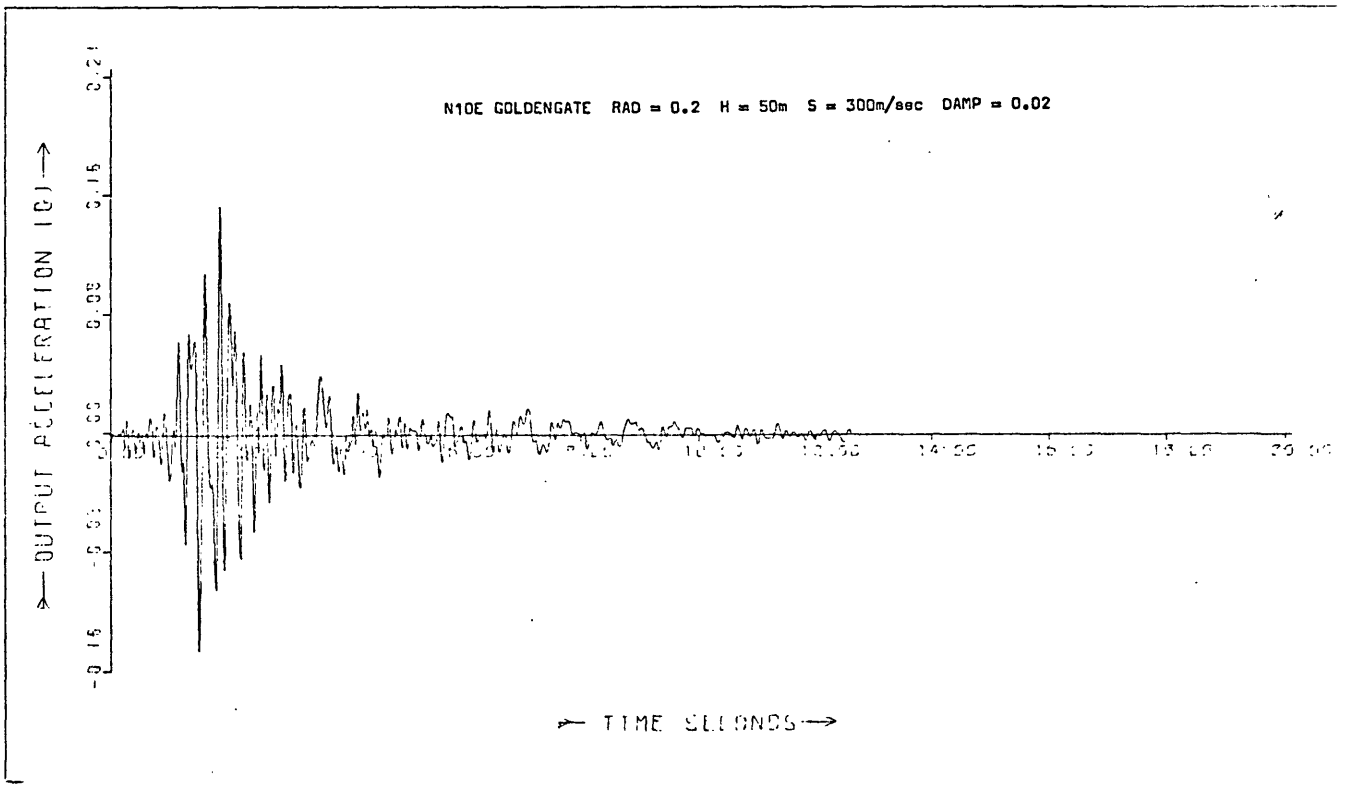


FIG.7.29aCOMPUTED GROUND SURFACE ACCELERATION TIME HISTORY AT SITE NO. 7.21

BEDROCK MOTION N1oE GOLDENGATE

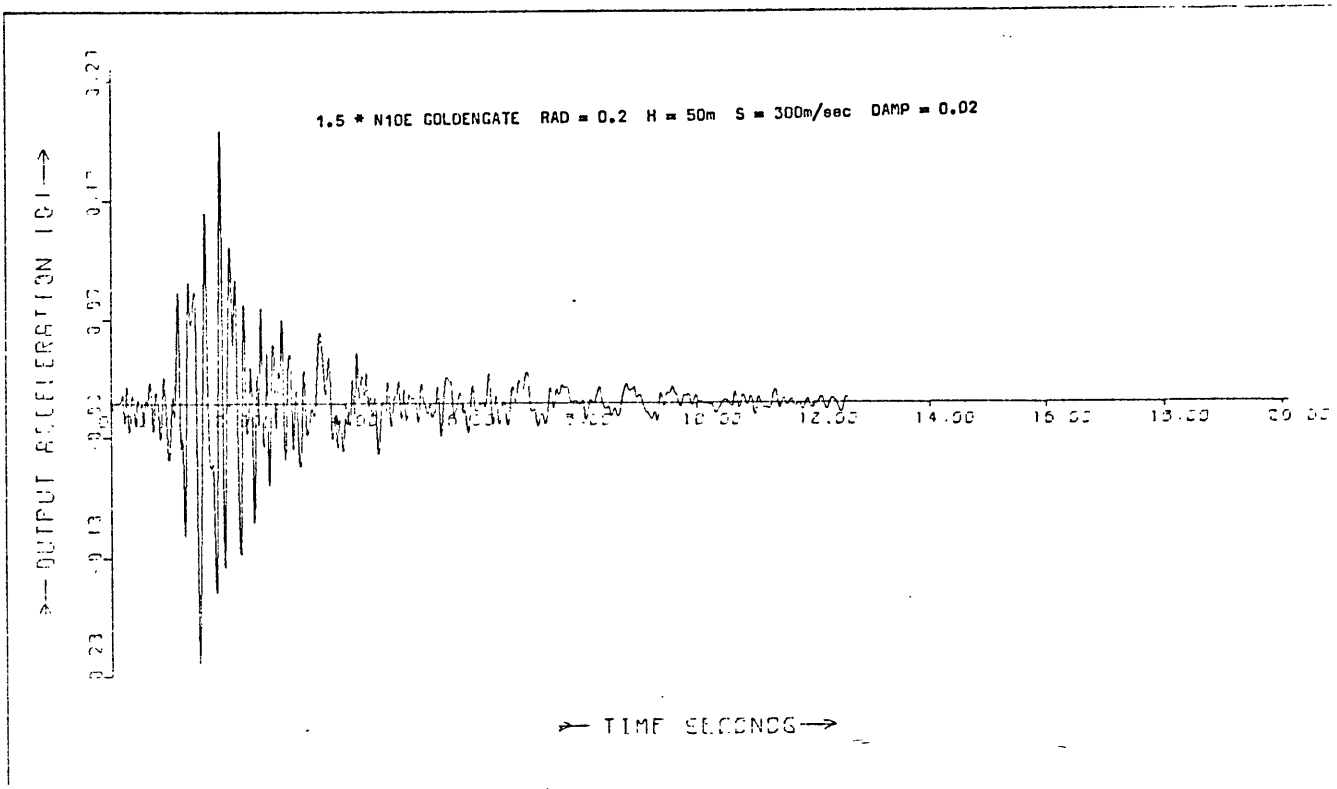


FIG 7.30a COMPUTED GROUND SURFACE ACCELERATION TIME HISTORY AT SITE NO. 7.21

BEDROCK MOTION 1.5 * N10E GOLDENGATE

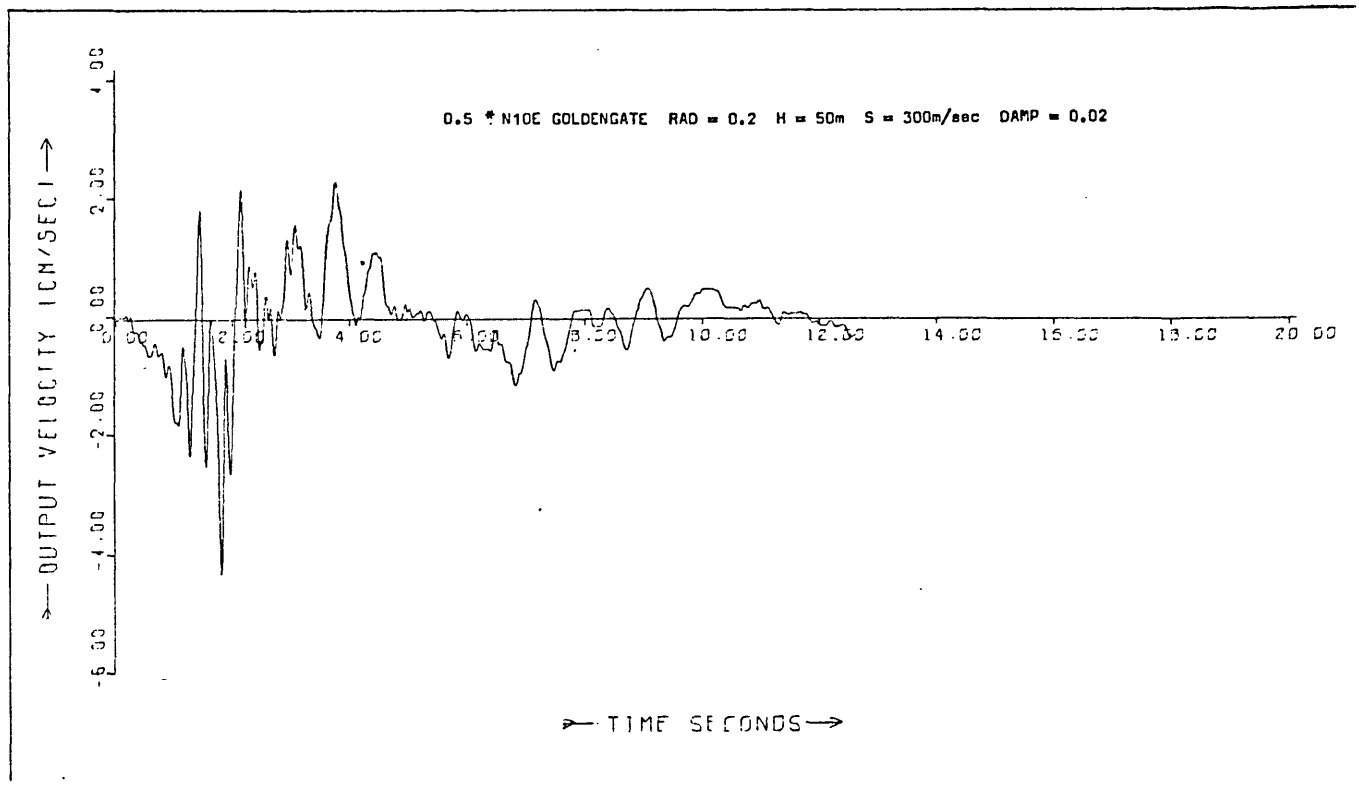


FIG. 7.28b COMPUTED GROUND SURFACE VELOCITY TIME HISTORY AT SITE NO. 7.21

BEDROCK MOTION o.5 * N1oE GOLDENGATE

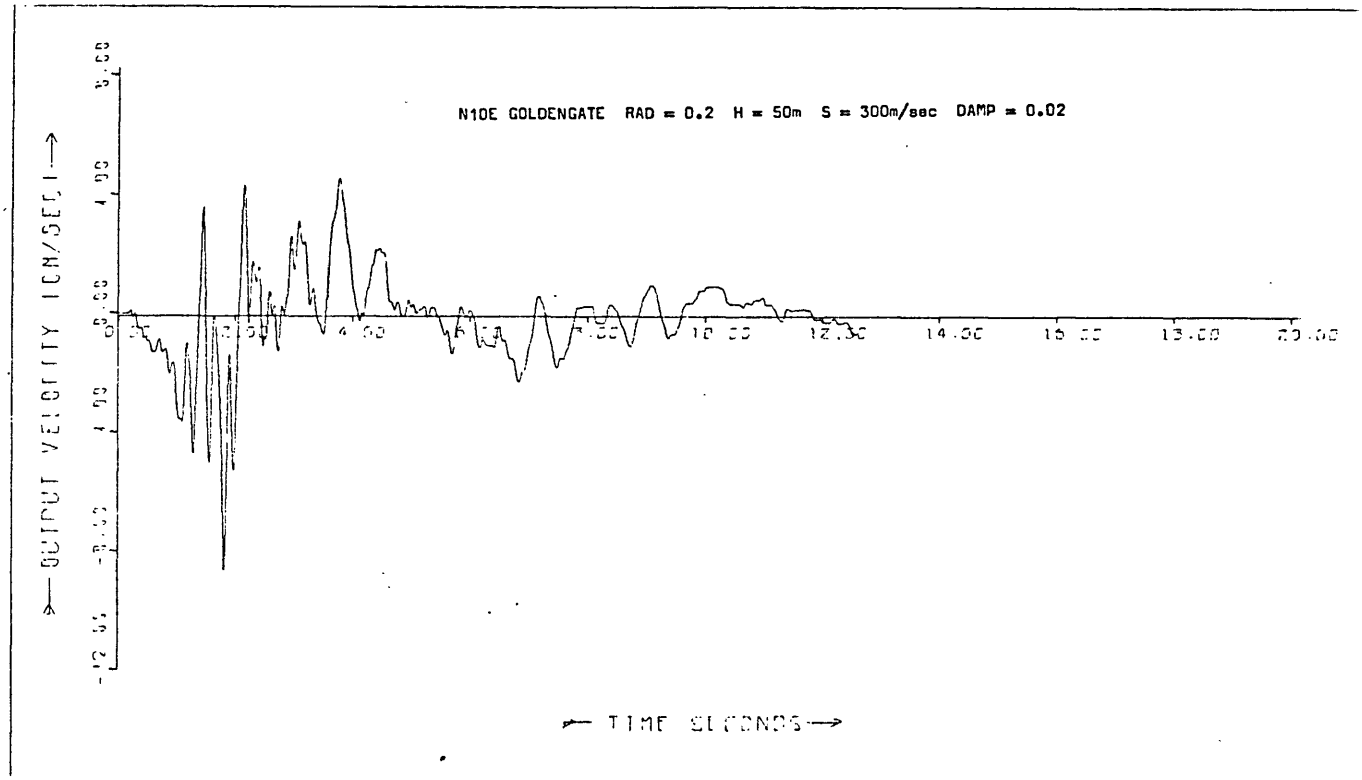


FIG. 7.29b COMPUTED GROUND SURFACE VELOCITY TIME HISTORY AT SITE NO. 7.21

BEDROCK MOTION N1oE GOLDENGATE

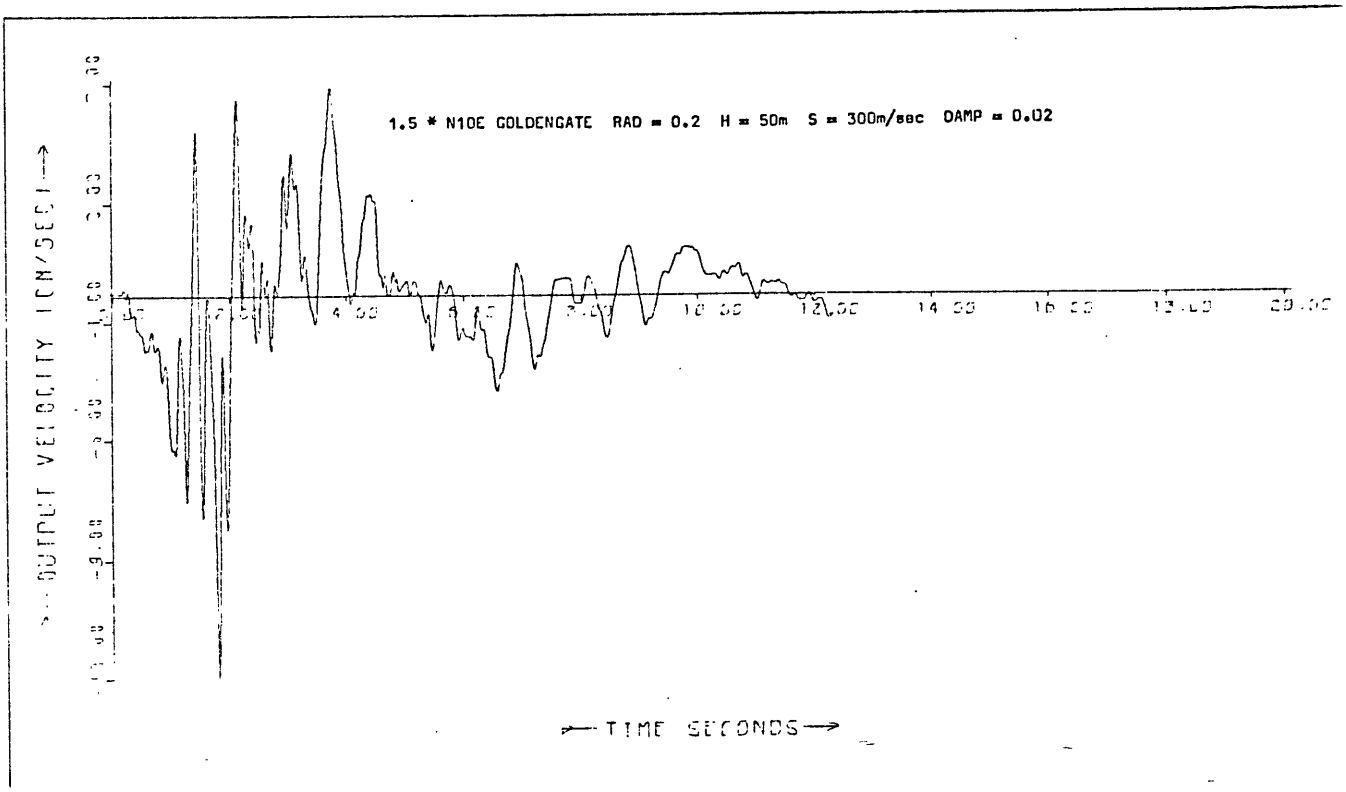


FIG7.3ob COMPUTED GROUND SURFACE VELOCITY TIME HISTORY AT SITE NO. 7.21

BEDROCK MOTION N1oE GOLDENGATE

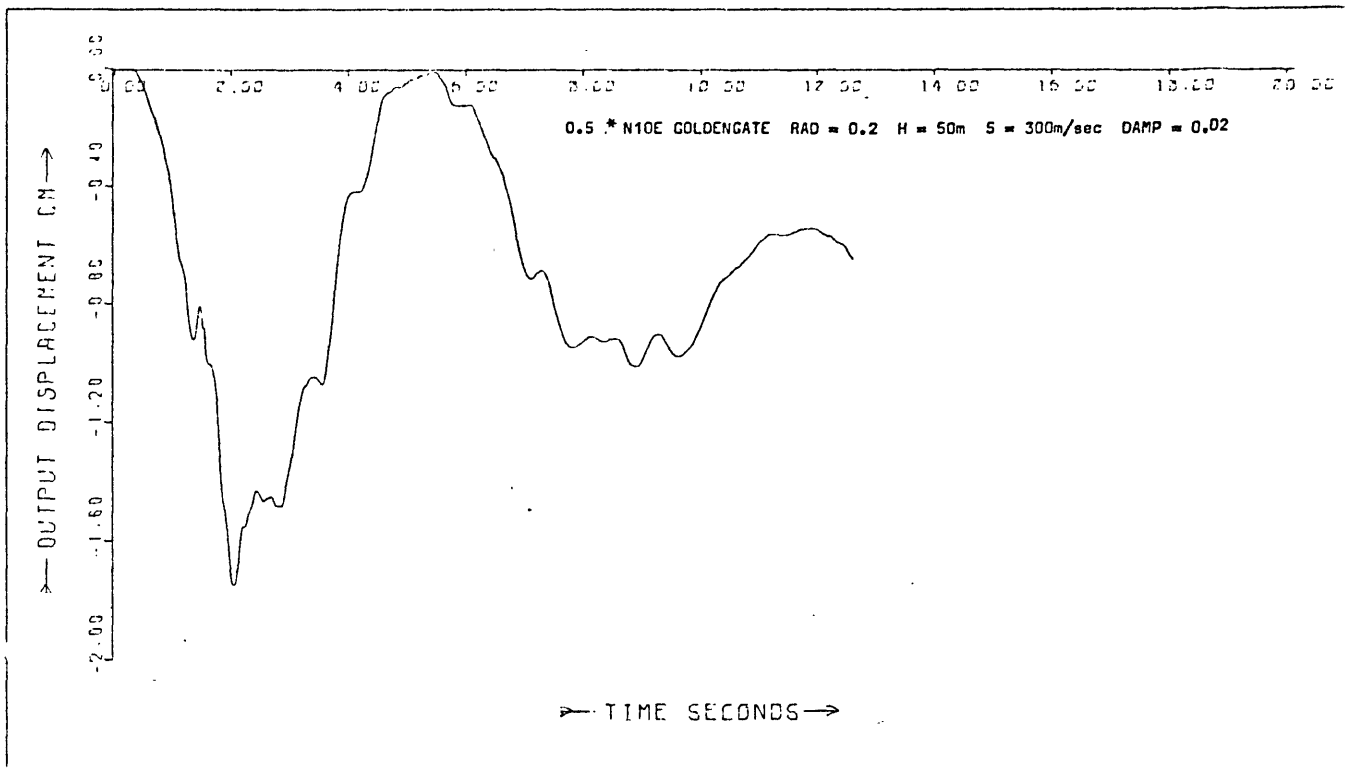


FIG.7.28cCOMPUTED GROUND SURFACE DISPLACE'ENT TIME HISTORY AT SITE NO. 7.21

BEDROCK MOTION o.5 * N1oE GOLDENGATE

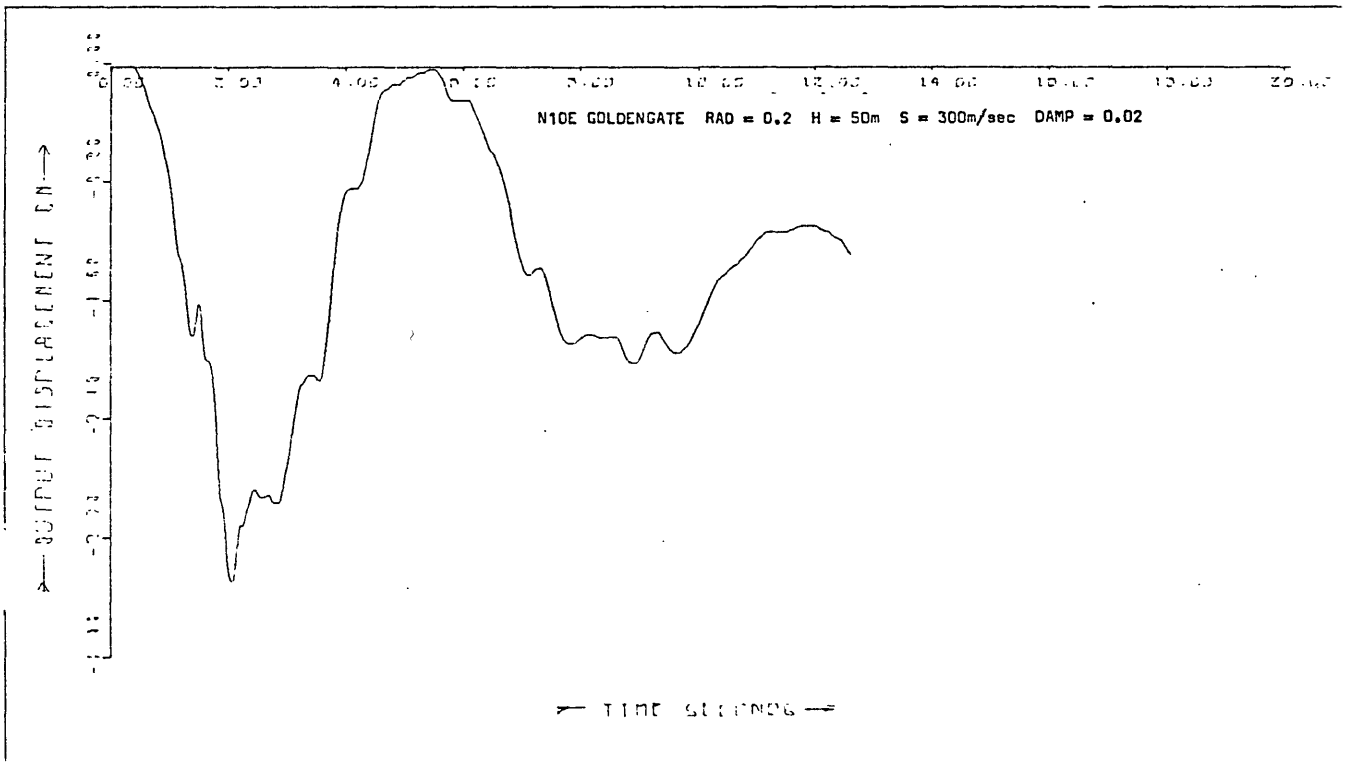


FIG.7.29cCOMPUTED GROUND SURFACE DISPLACEMENT TIME HISTORY AT SITE NO.7.21

BEDROCK MOTION N1oE GOLDENGATE

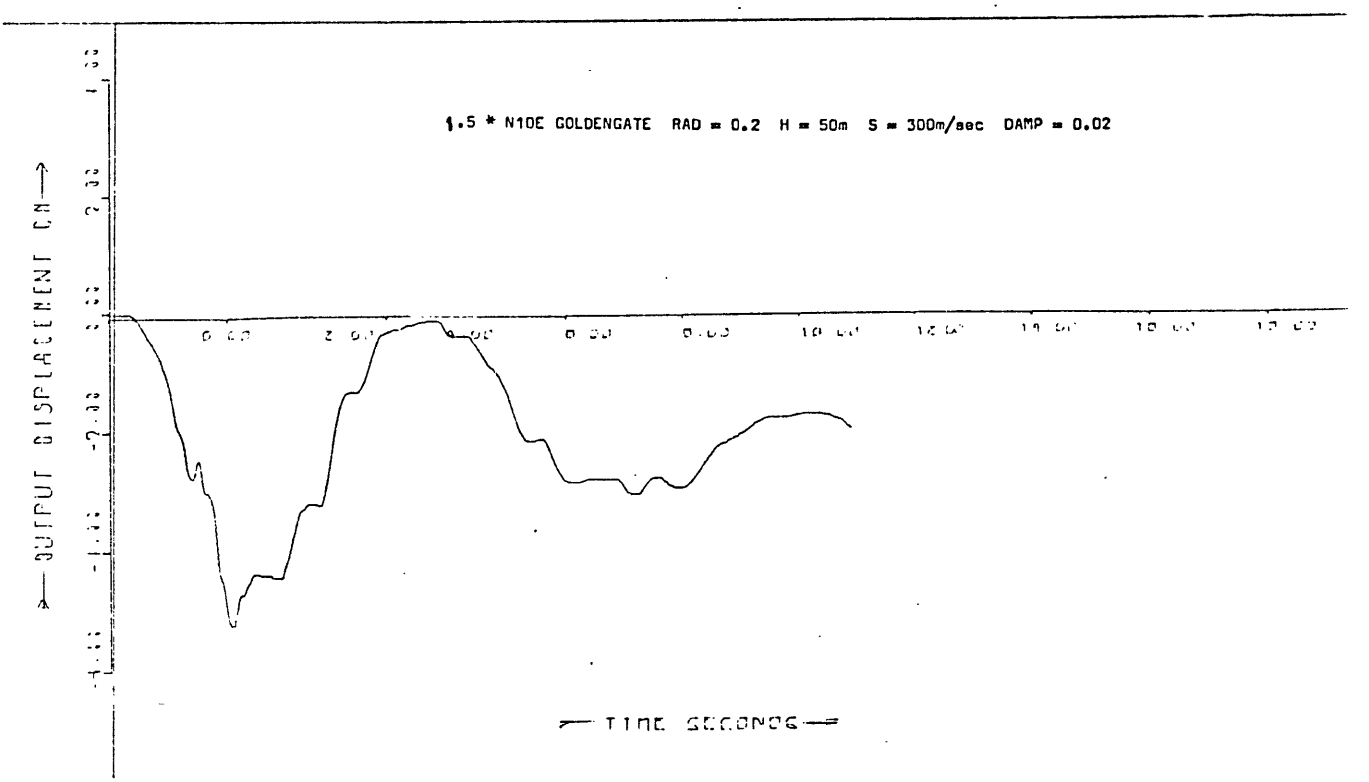


FIG 7.3oc COMPUTED GROUND SURFACE DISPLACEMENT TIME HISTORY AT SITE NO. 7.21
BEDROCK MOTION 1.5 * N1oE GOLDENGATE

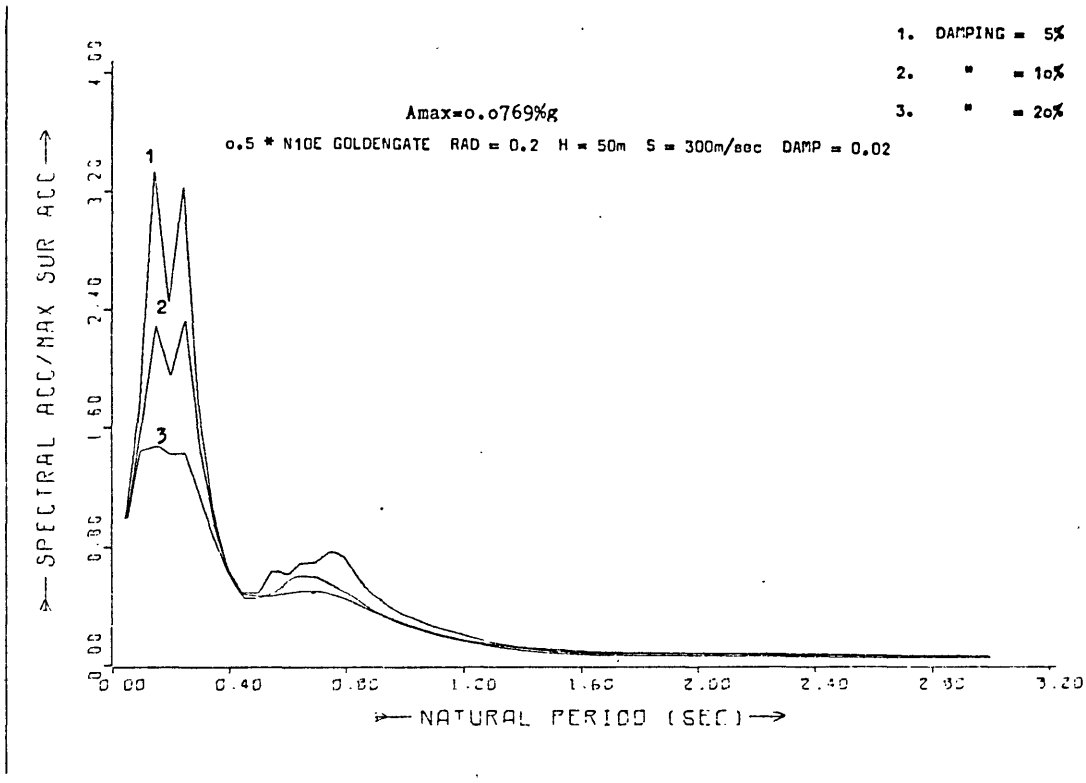


FIG.7.28d COMPUTED GROUND SURFACE ACCELERATION RESPONSE SPECTRA AT SITE NO.7.21

BEDROCK MOTION 0.5 * N10E GOLDENGATE

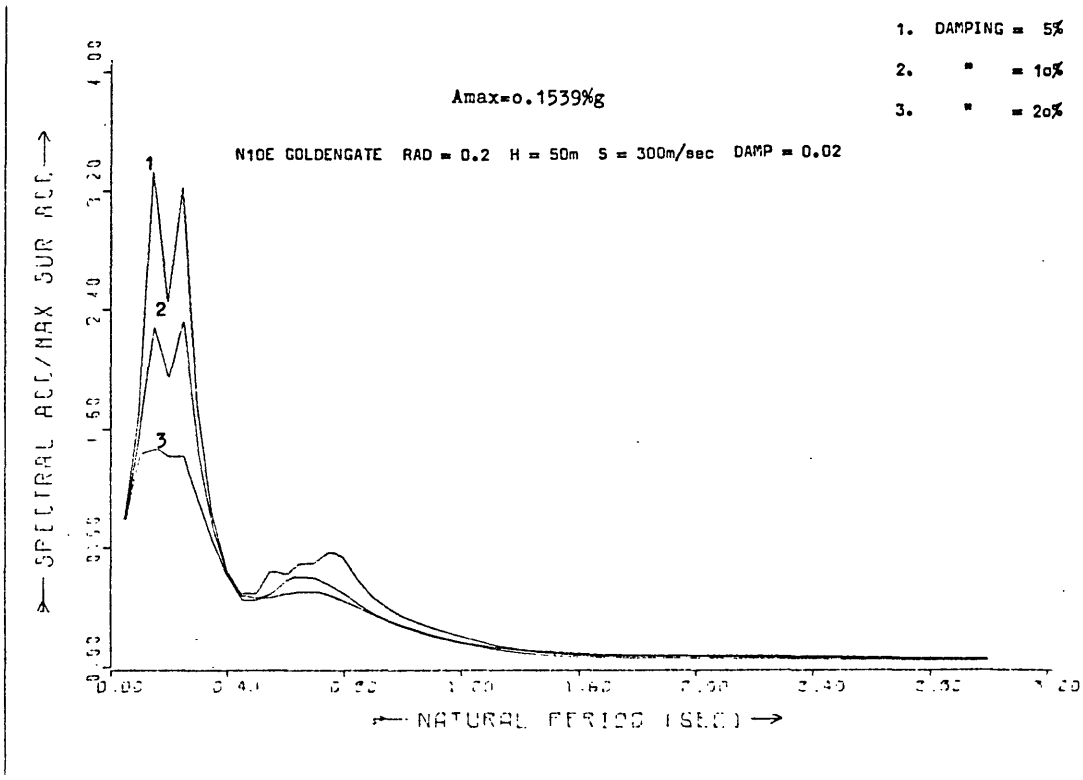


FIG.7.29d COMPUTED GROUND SURFACE ACCELERATION RESPONSE SPECTRA AT SITE NO.7.21

BEDROCK MOTION N10E GOLDENGATE

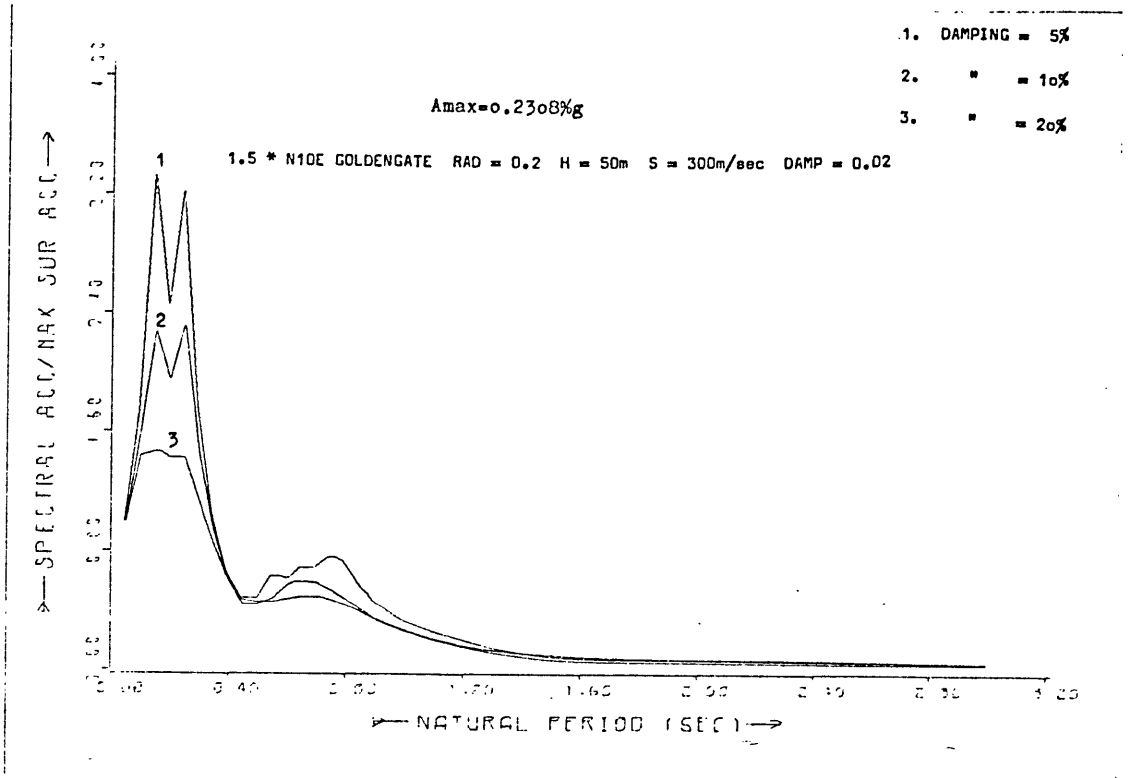


FIG 7.3od COMPUTED GROUND SURFACE ACCELERATION RESPONSE SPECTRA AT SITE NO. 7.21
BEDROCK MOTION N1oE GOLDENGATE

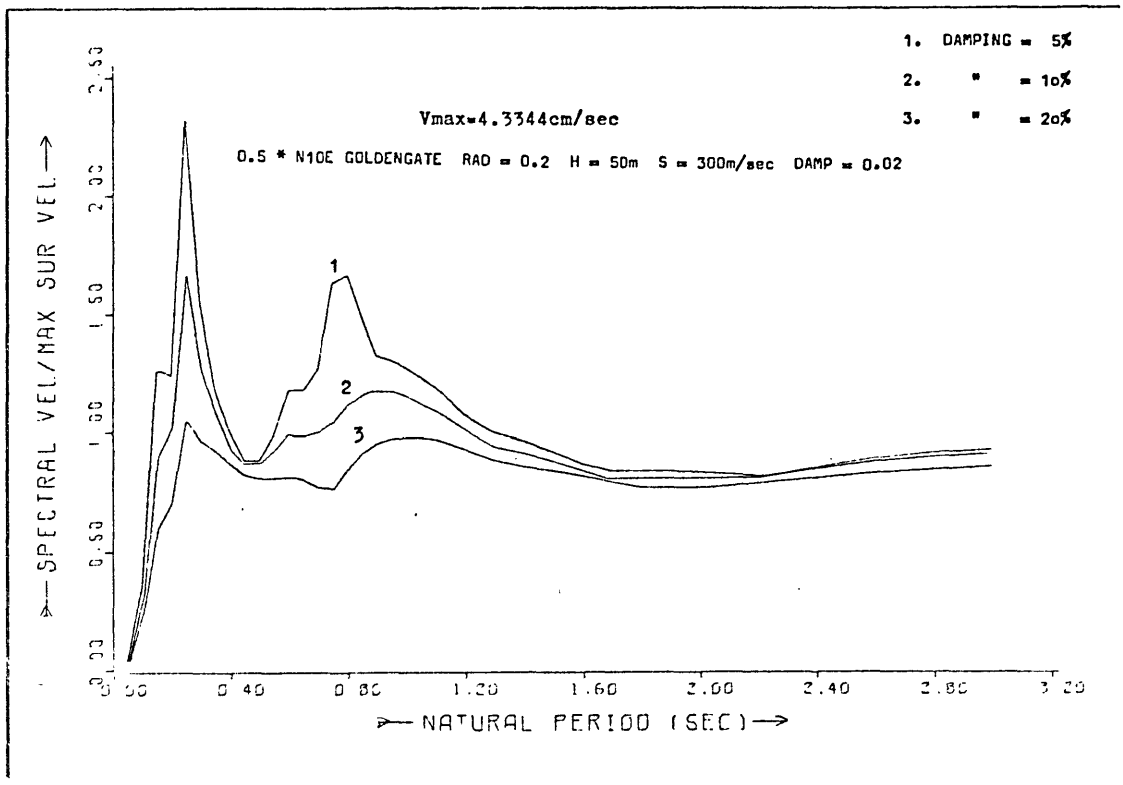


FIG 7.28e COMPUTED GROUND SURFACE VELOCITY RESPONSE SPECTRA AT SITE NO. 7.21

BEDROCK MOTION 0.5 * N10E GOLDENGATE

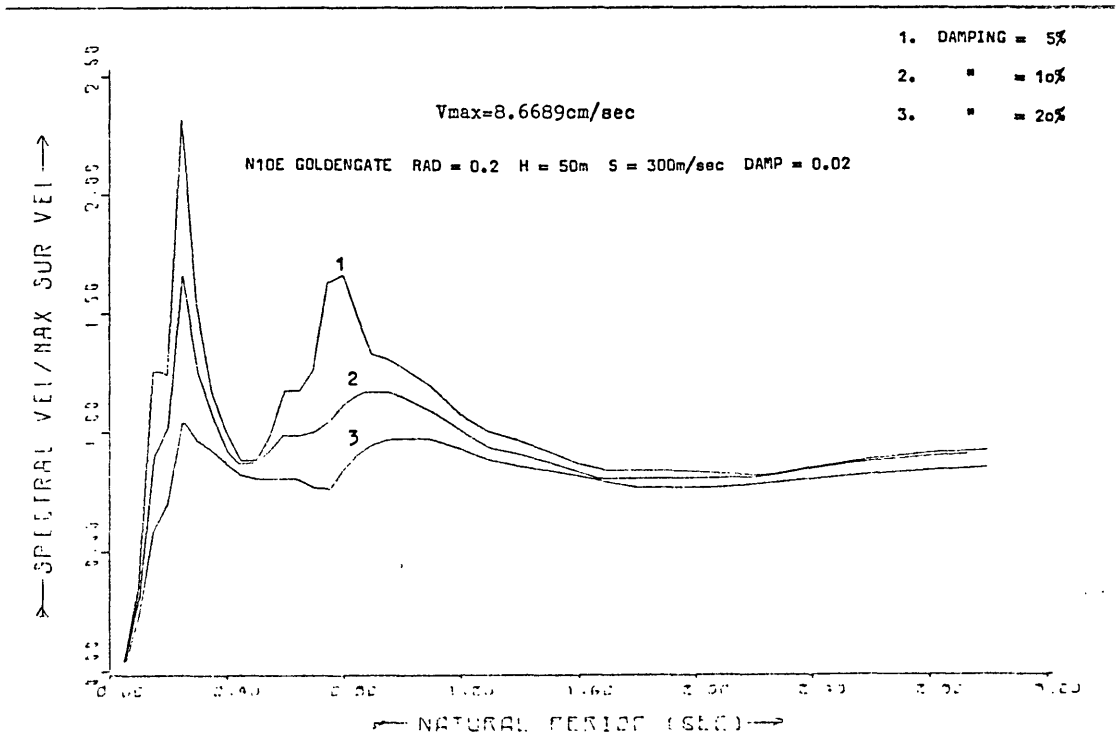


FIG. 7.29e COMPUTED GROUND SURFACE VELOCITY RESPONSE SPECTRA AT SITE NO. 7.21

BEDROCK MOTION N10E GOLDENGATE

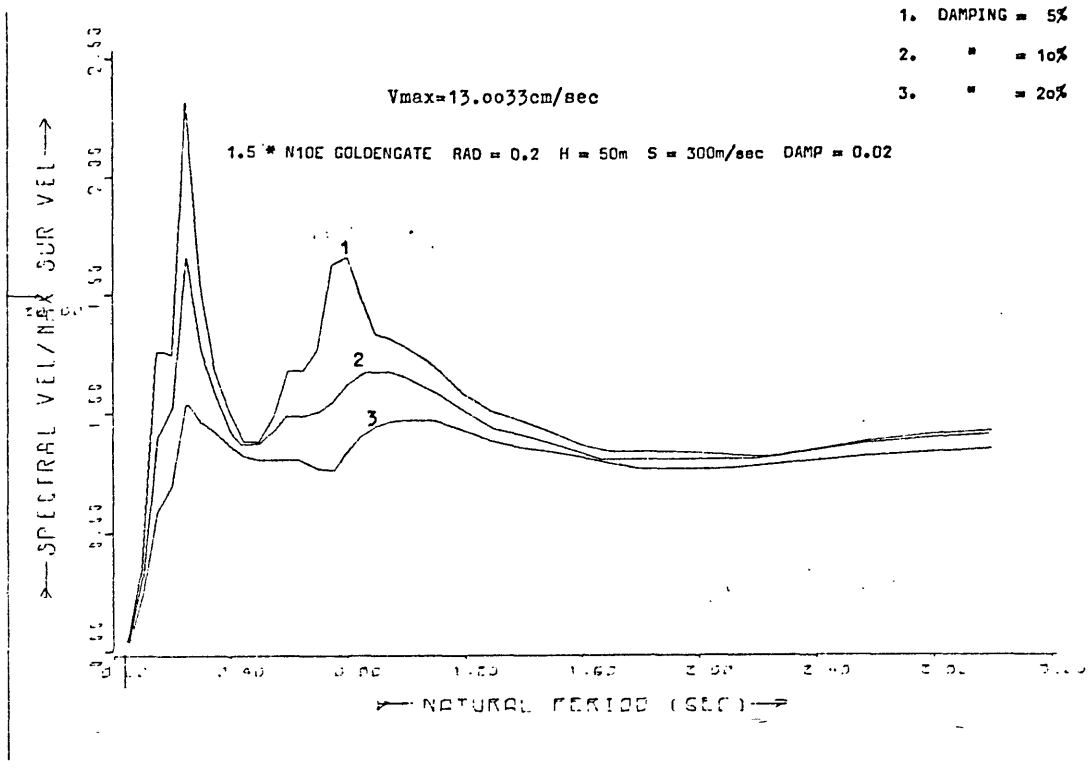


FIG.7.3oe COMPUTED GROUND SURFACE VELOCITY RESPONSE SPECTRA AT SITE NO. 7.21

BEDROCK MOTION 1.5 * N1oE GOLDENGATE

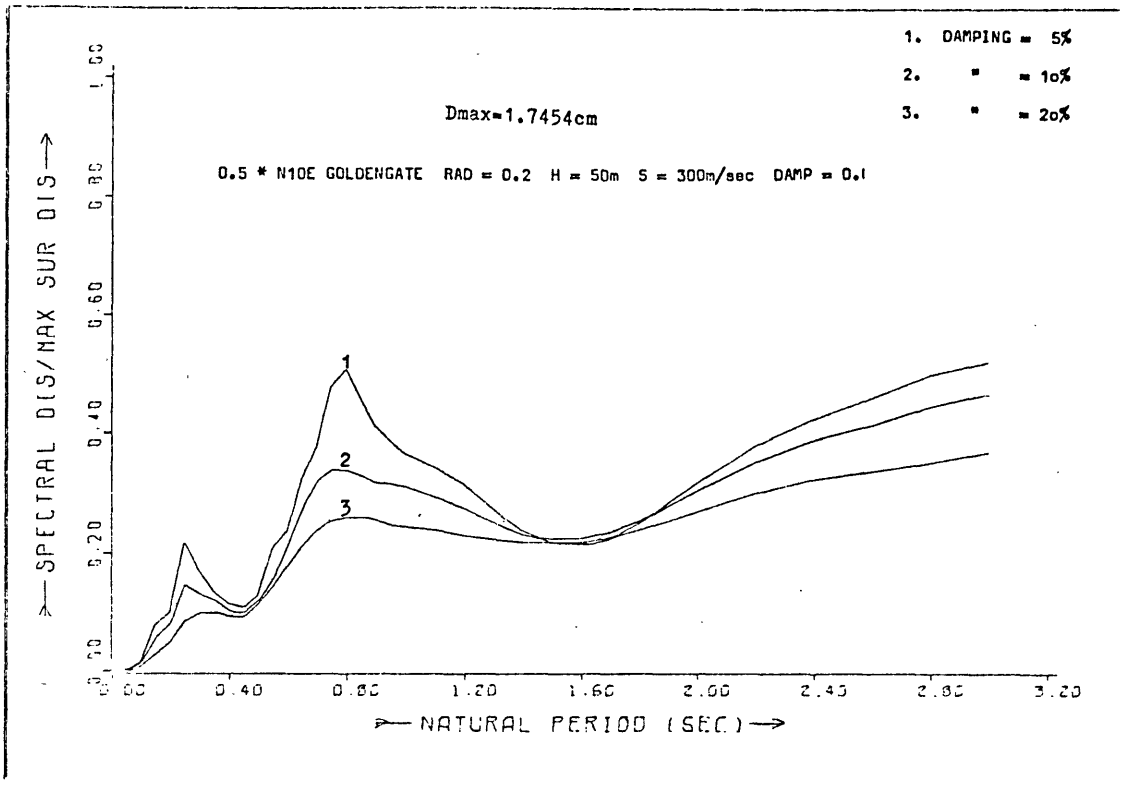


FIG.7.28f COMPUTED GROUND SURFACE DISPLACEMENT RESPONSE SPECTRA AT SITE NO.7.21

BEDROCK MOTION o.5 * N1oE GOLDENGATE

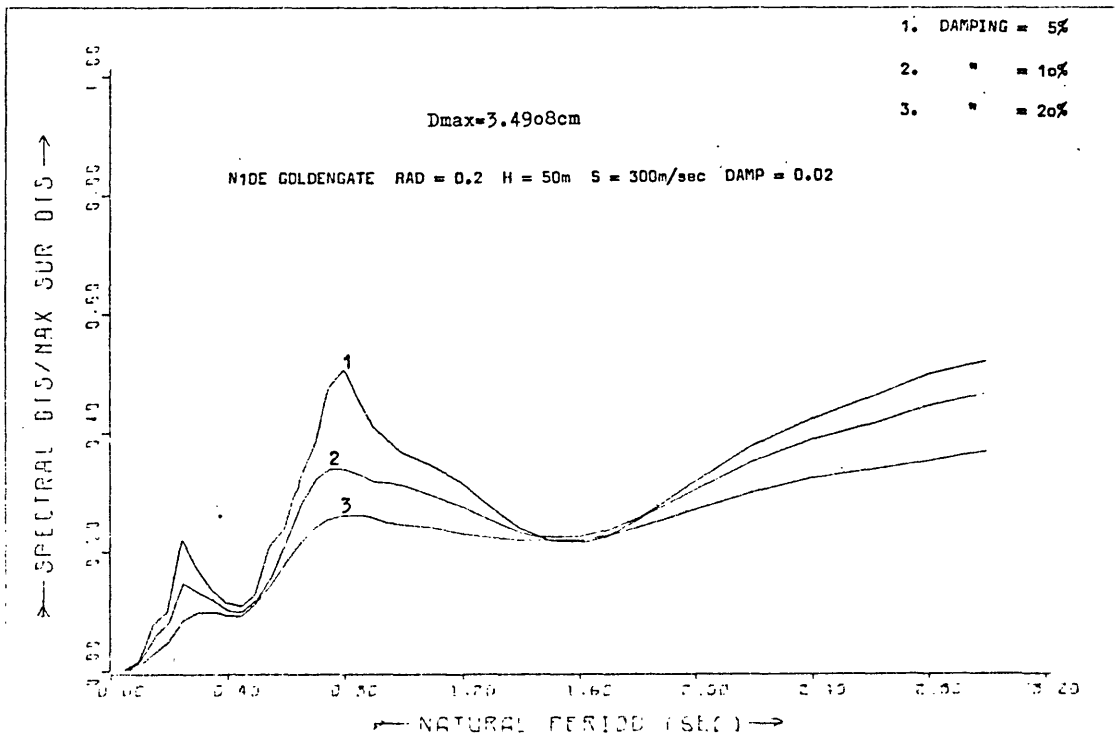


FIG.7.29fCOMPUTED GROUND SURFACE DISPLACEMENT RESPONSE SPECTRA AT SITE NO. 7.21

BEDROCK MOTION N1oE GOLDENGATE

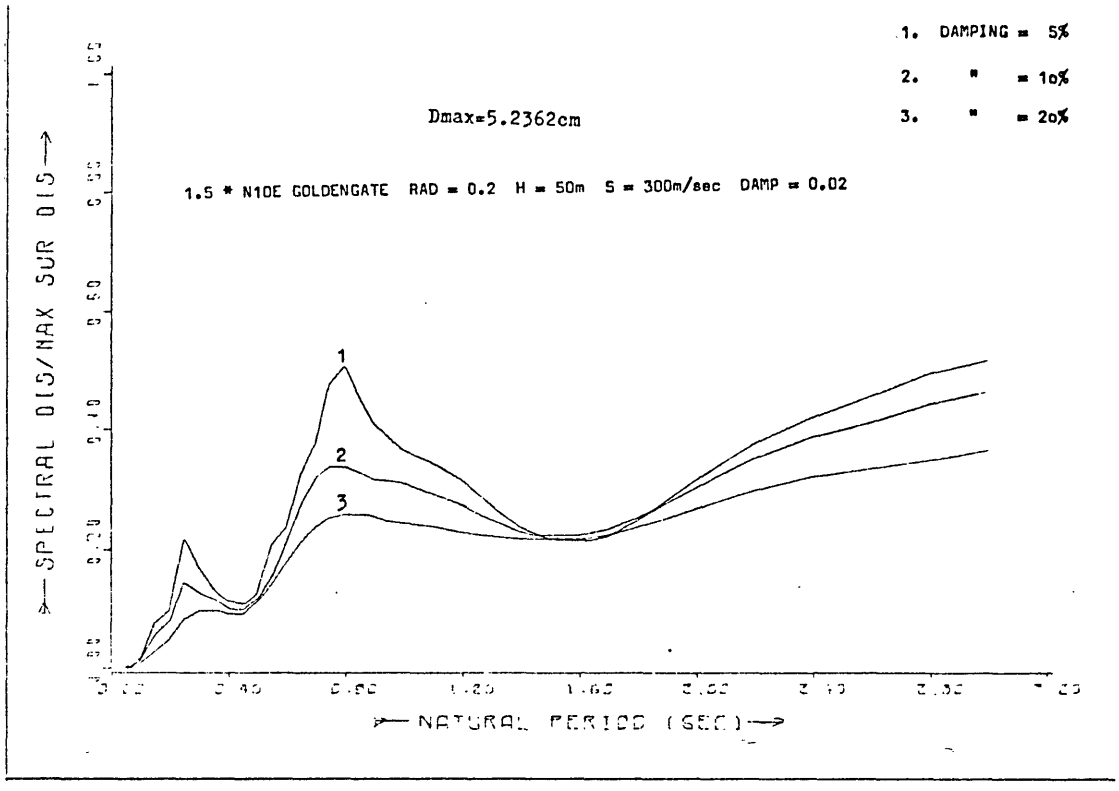


FIG.7.3of COMPUTED GROUND SURFACE DISPLACEMENT RESPONSE SPECTRA AT SITE NO. 7.21

BEDROCK MOTION N1oE GOLDENGATE

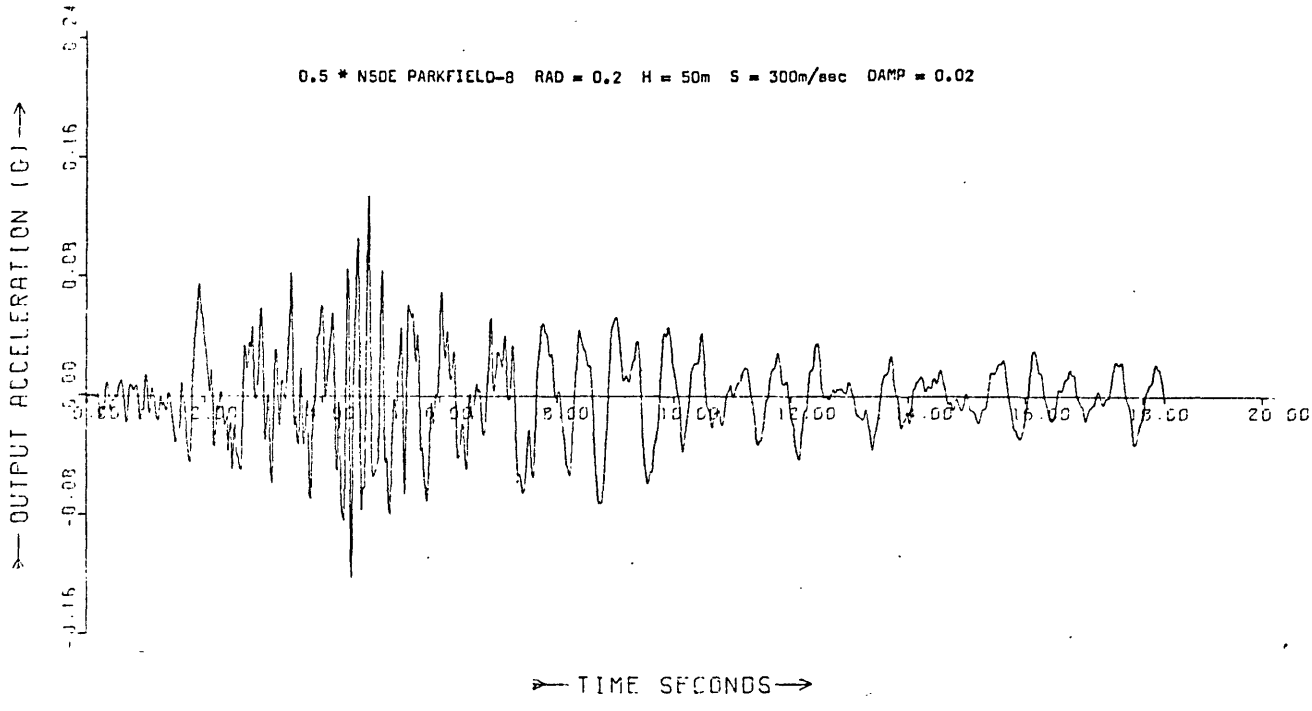


FIG7.31a COMPUTED GROUND SURFACE ACCELERATION TIME HISTORY AT SITE NO. 7.21

BEDROCK MOTION 0.5 * N50E PARKFIELD-8

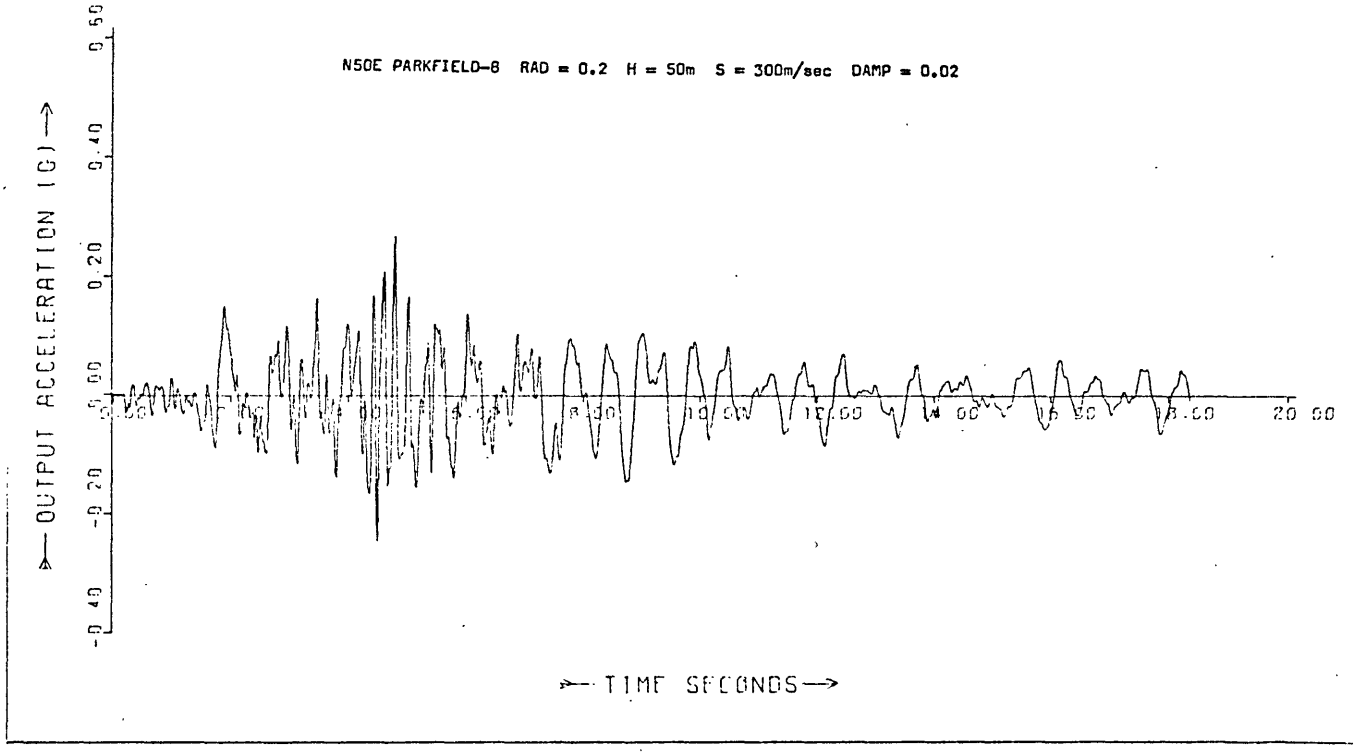


FIG.7.32a COMPUTED GROUND SURFACE ACCELERATION TIME HISTORY AT SITE NO.7.21

BEDROCK MOTION N50E PARKFIELD-8

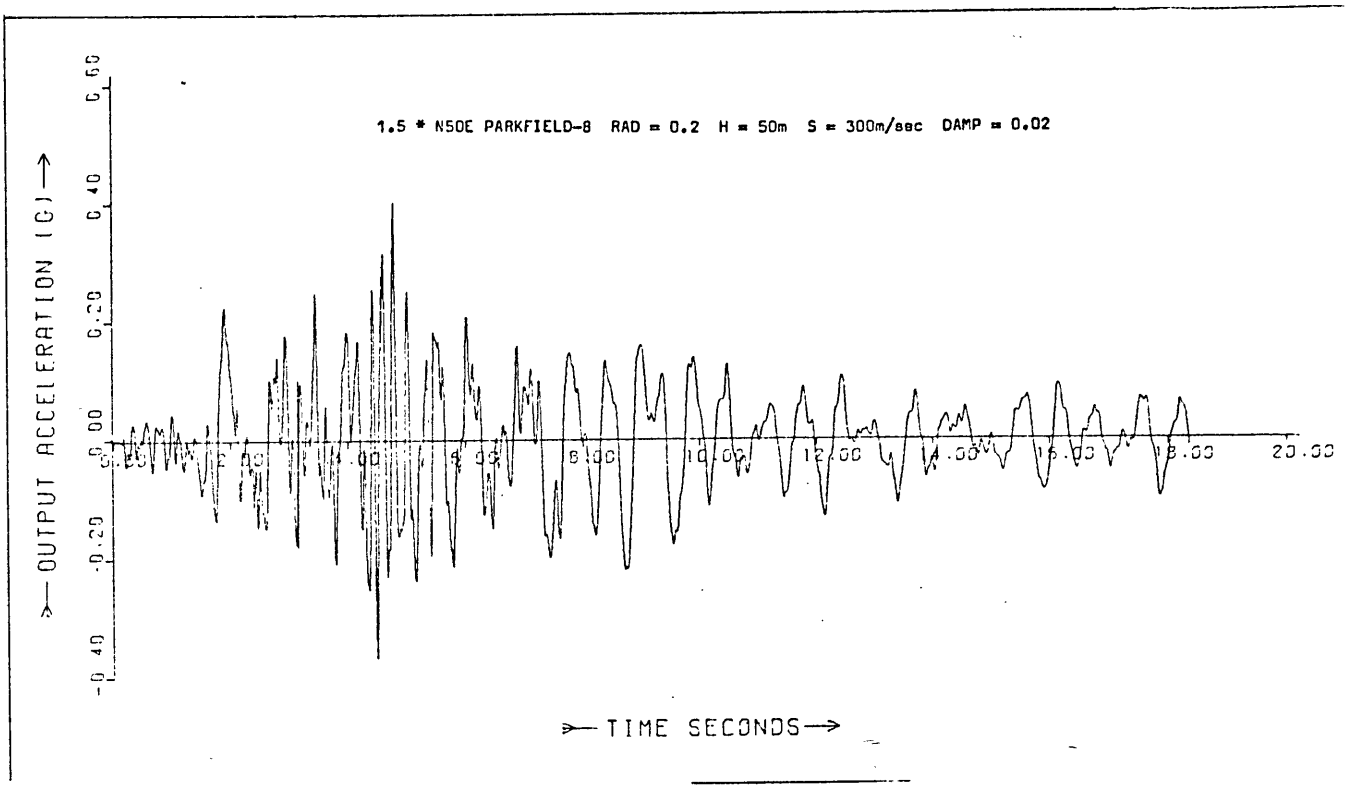


FIG7.33a COMPUTED GROUND SURFACE ACCELERATION TIME HISTORY AT SITE NO. 7.21

BEDROCK MOTION 1.5 * N50E PARKFIELD-8

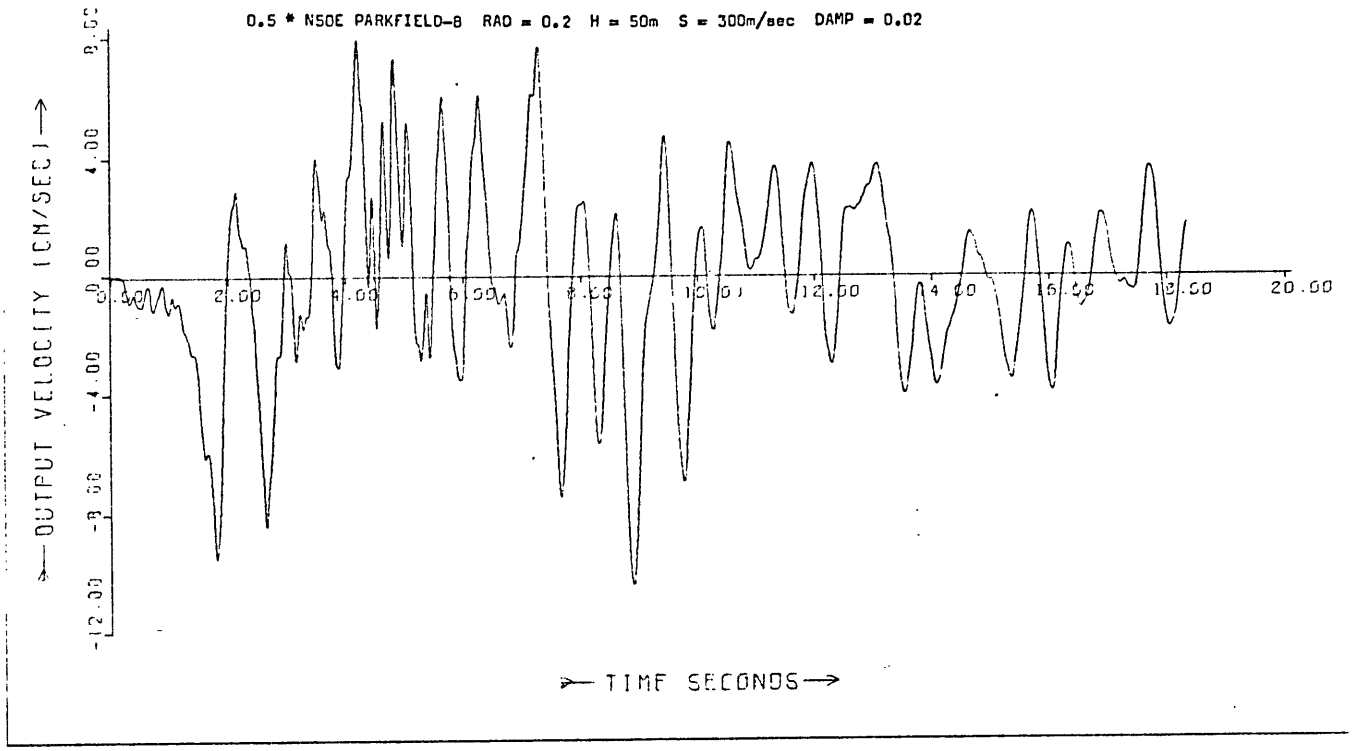


FIG. 7.31b COMPUTED GROUND SURFACE VELOCITY TIME HISTORY AT SITE NO. 7.21

BEDROCK MOTION 0.5 * N50E PARKFIELD-8

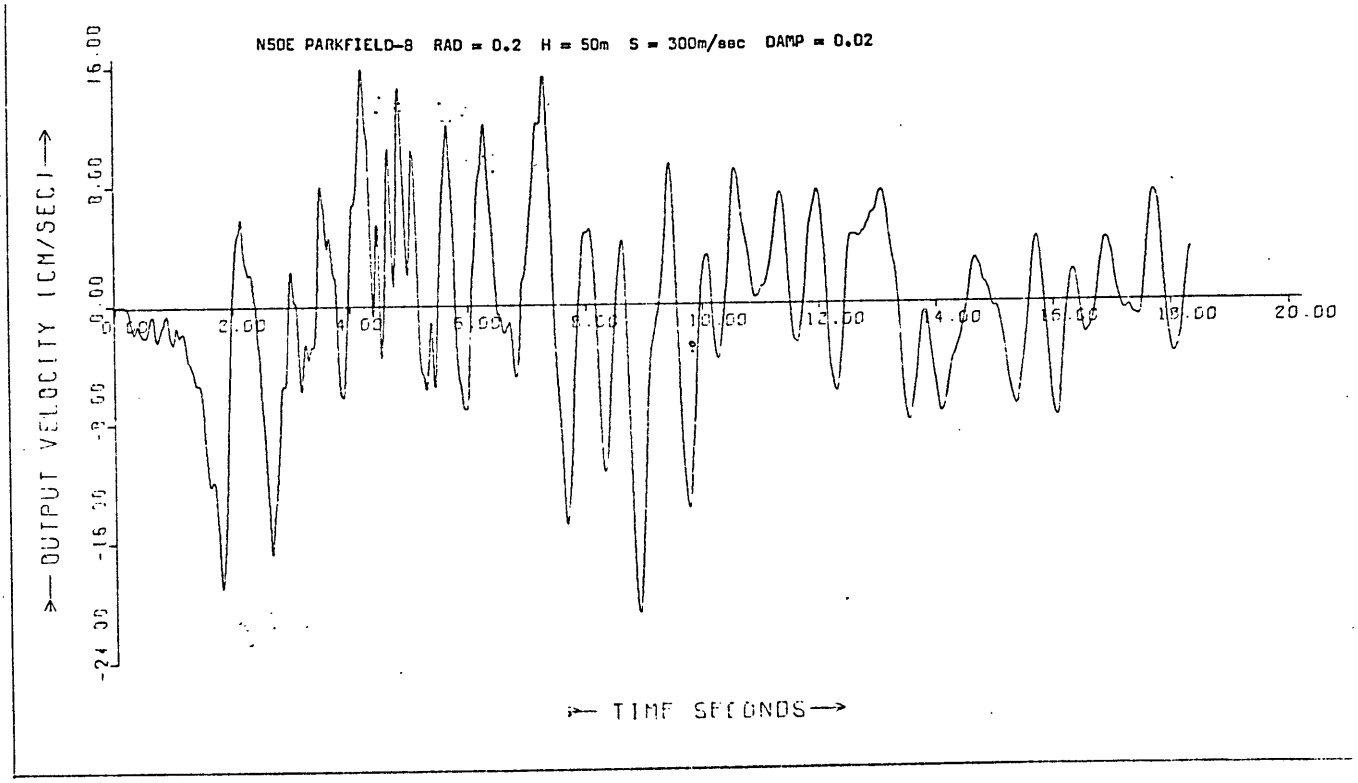


FIG.7.32b COMPUTED GROUND SURFACE VELOCITY TIME HISTORY AT SITE NO.7.21

BEDROCK MOTION N50E PARKFIELD-8

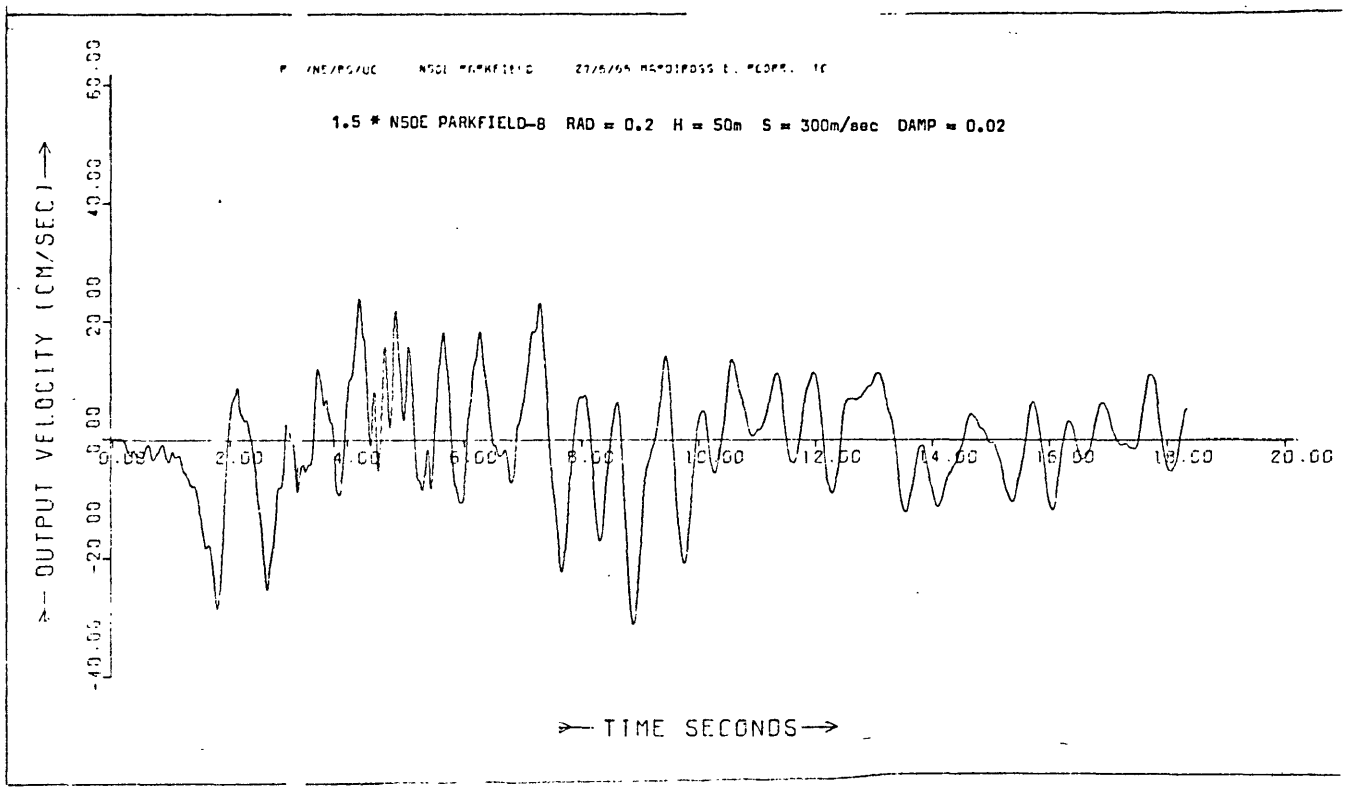


FIG.7.33b COMPUTED GROUND SURFACE VELOCITY TIME HISTORY AT SITE NO. 7.21

BEDROCK MOTION 1.5 * N50E PARKFIELD-8

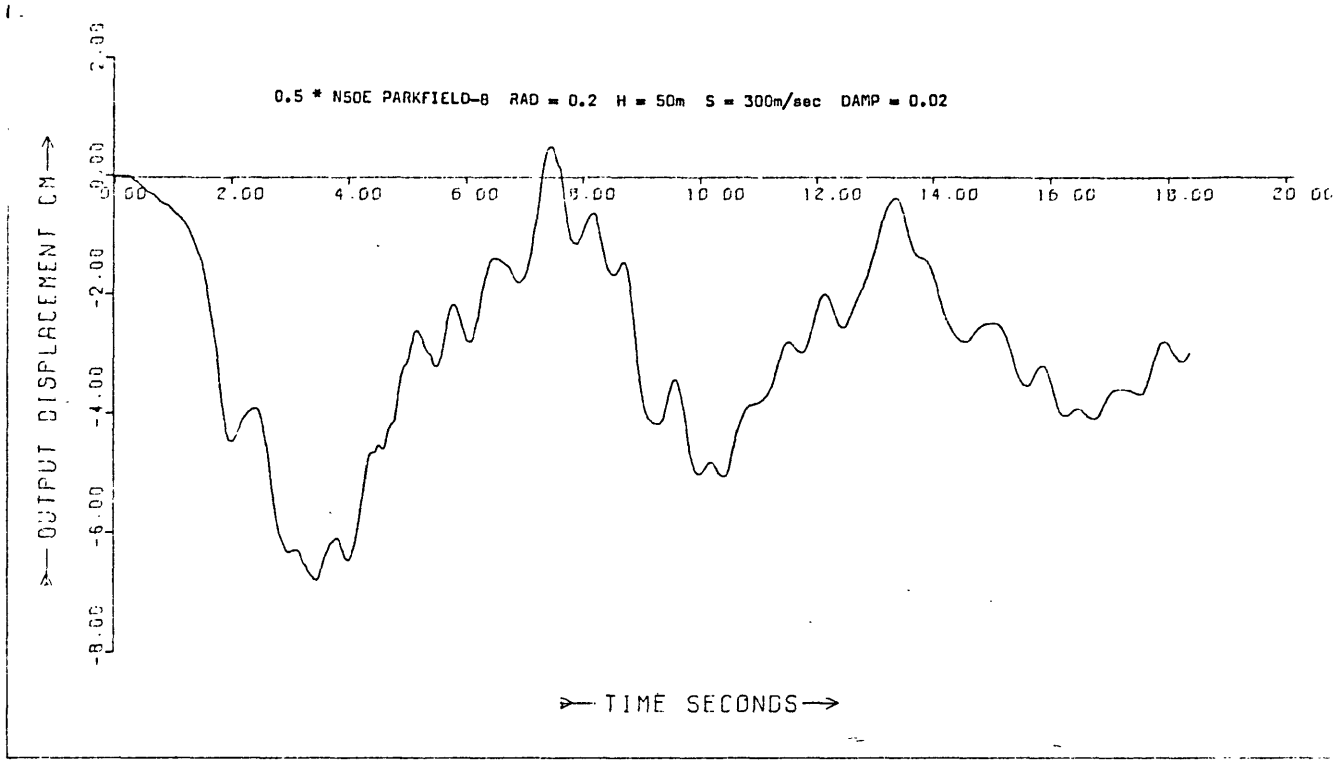


FIG. 7.31c COMPUTED GROUND SURFACE DISPLACEMENT TIME HISTORY AT SITE NO. 7.21

BEDROCK MOTION 0.5 * N50E PARKFIELD-8

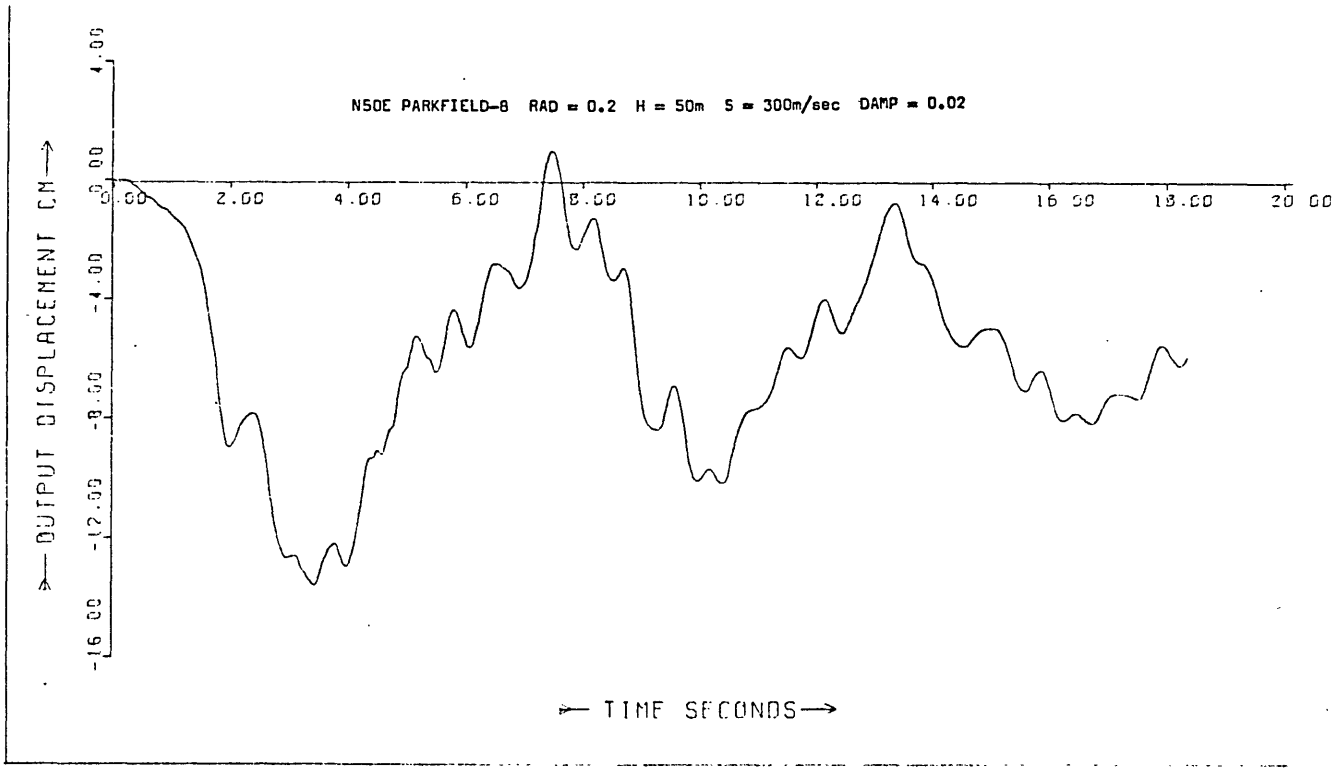


FIG.7.32c COMPUTED GROUND SURFACE DISPLACEMENT TIME HISTORY AT SITE NO.7.21

BEDROCK MOTION N50E PARKFIELD-8

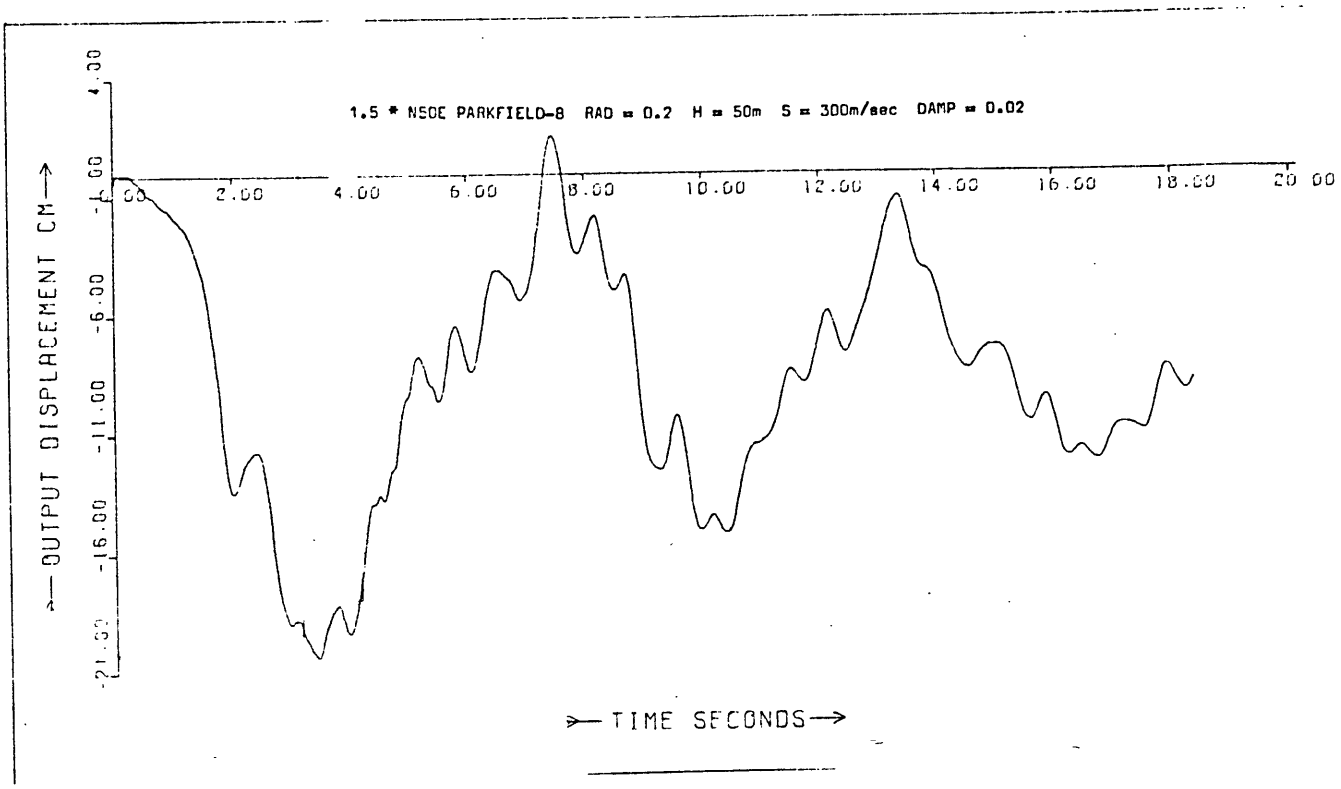


FIG.7.33COMPUTED GROUND SURFACE DISPLACEMENT TIME HISTORY AT SITE NO. 7.21
BEDROCK MOTION 1.5 * N50E PARKFIELD-8

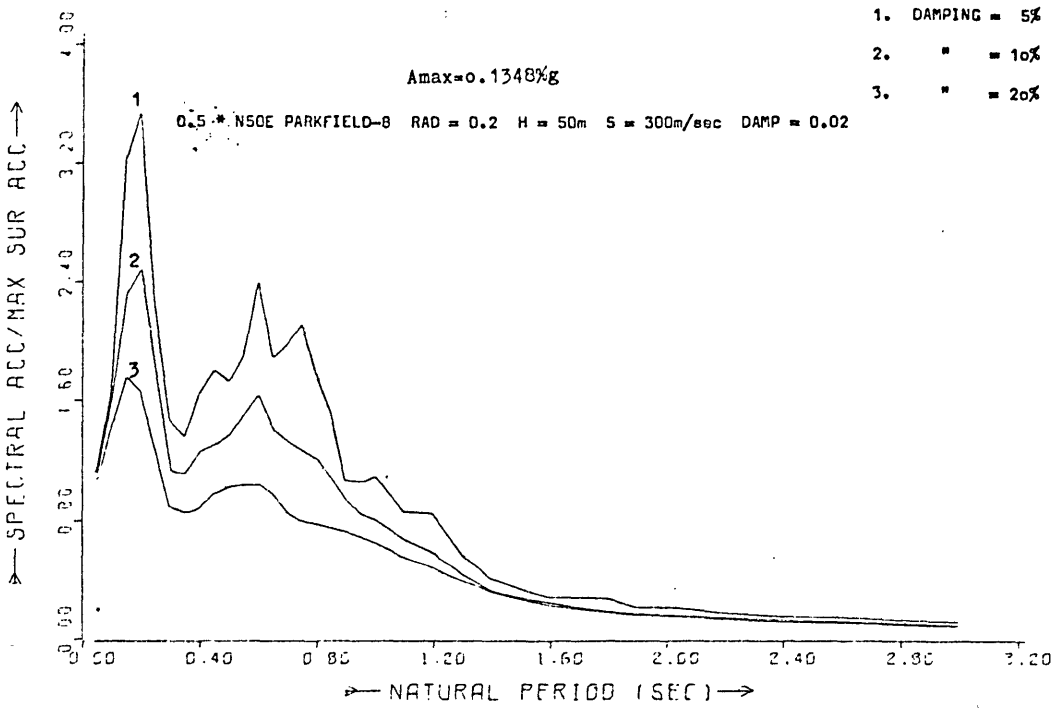


FIG. 7.31d COMPUTED GROUND SURFACE ACCELERATION RESPONSE SPECTRA AT SITE NO. 7.21

BEDROCK MOTION 0.5 * N50E PARKFIELD-8

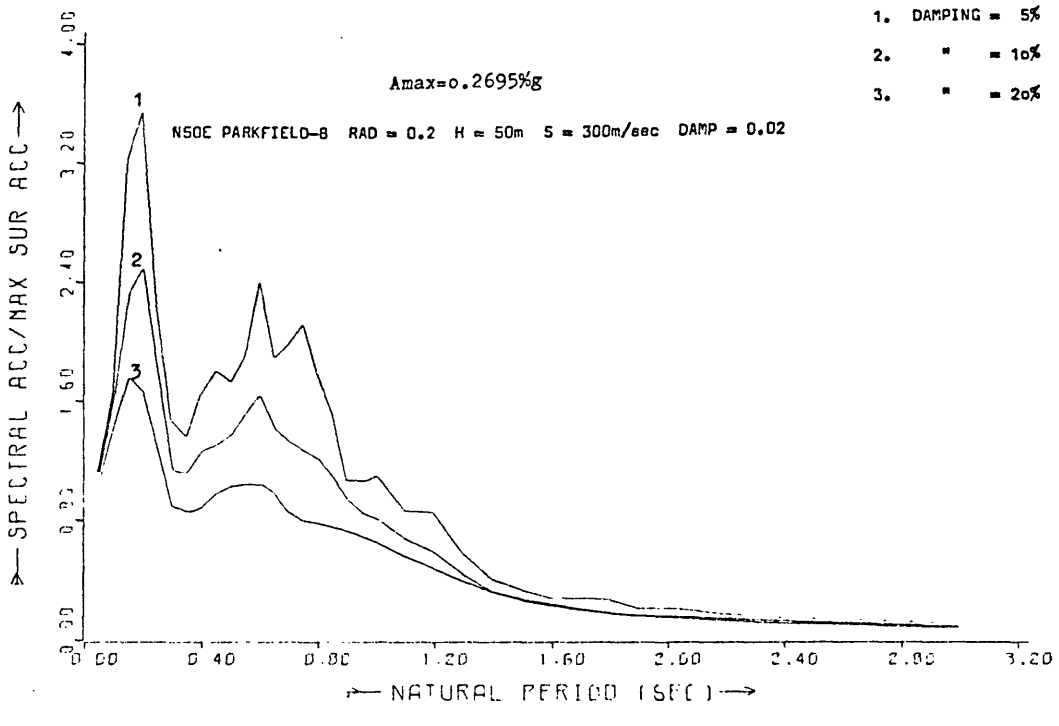


FIG.7.32d COMPUTED GROUND SURFACE ACCELERATION RESPONSE SPECTRA AT SITE NO. 7.21

BEDROCK MOTION N50E PARKFIELD-8

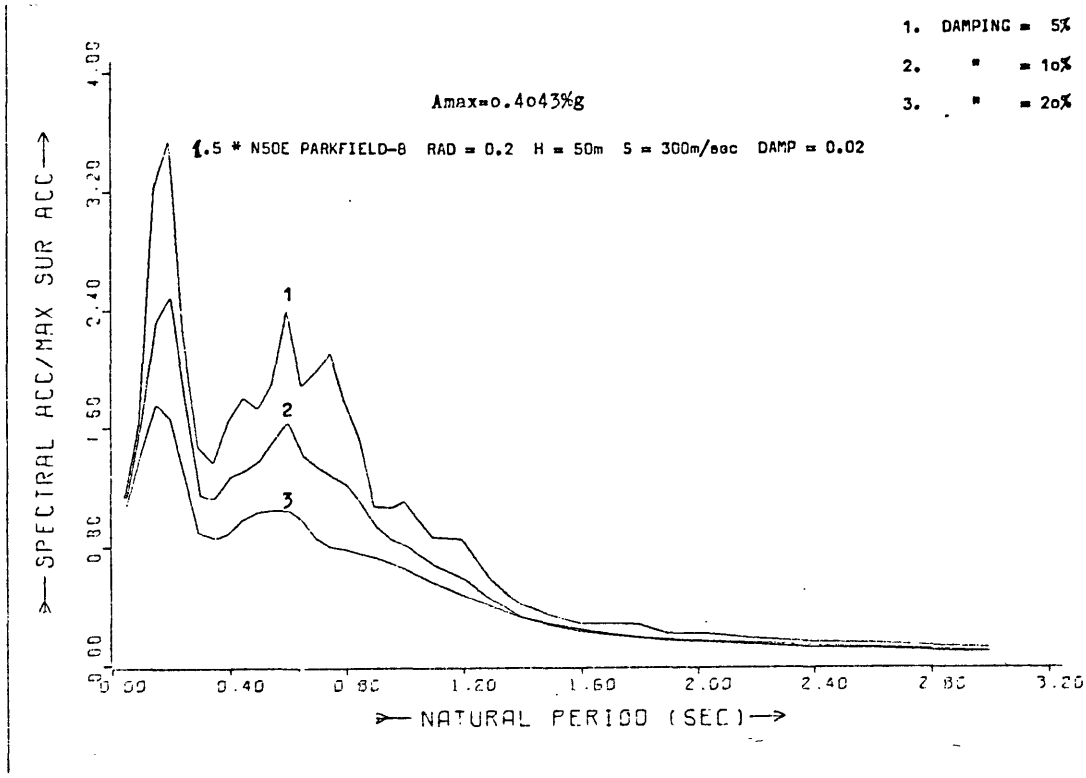


FIG.7.33dCOMPUTED GROUND SURFACE ACCELERATION RESPONSE SPECTRA AT SITE NO.7.21

BEDROCK MOTION 1.5 * N50E PARKFIELD-8

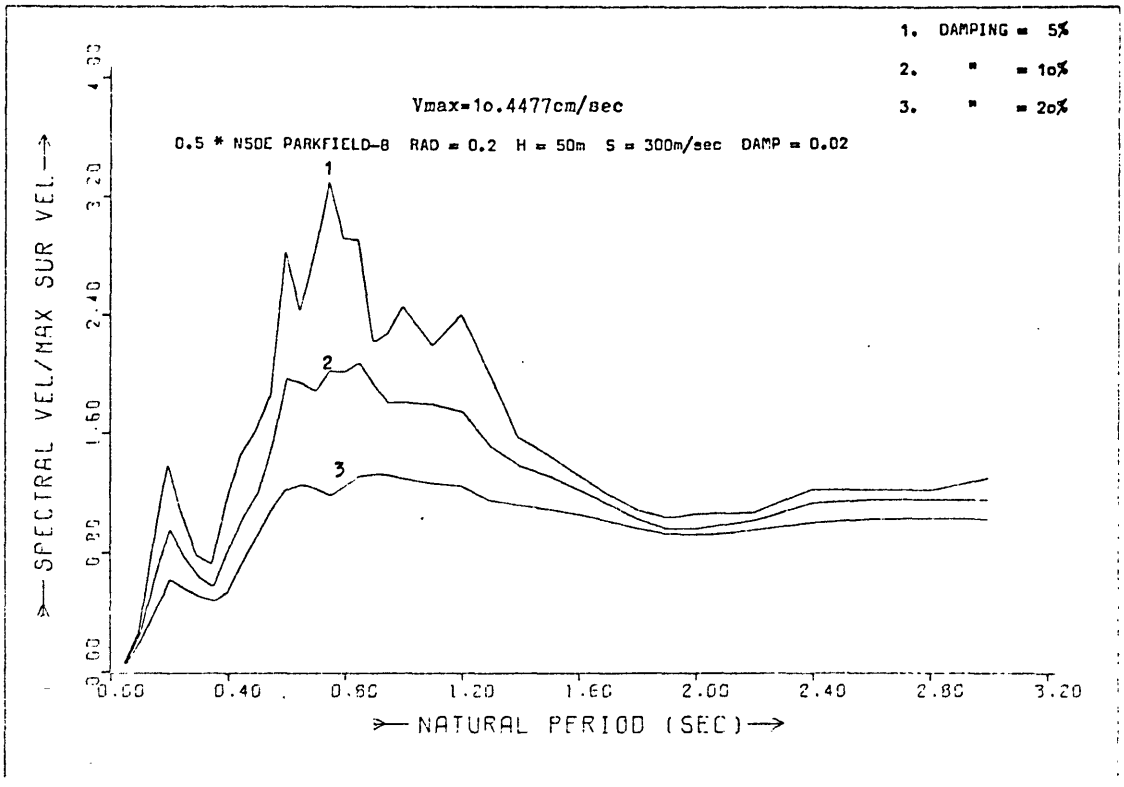


FIG.7.31e COMPUTED GROUND SURFACE VELOCITY RESPONSE SPECTRA AT SITE NO.7.21

BEDROCK MOTION 0.5 * N50E PARKFIELD-8

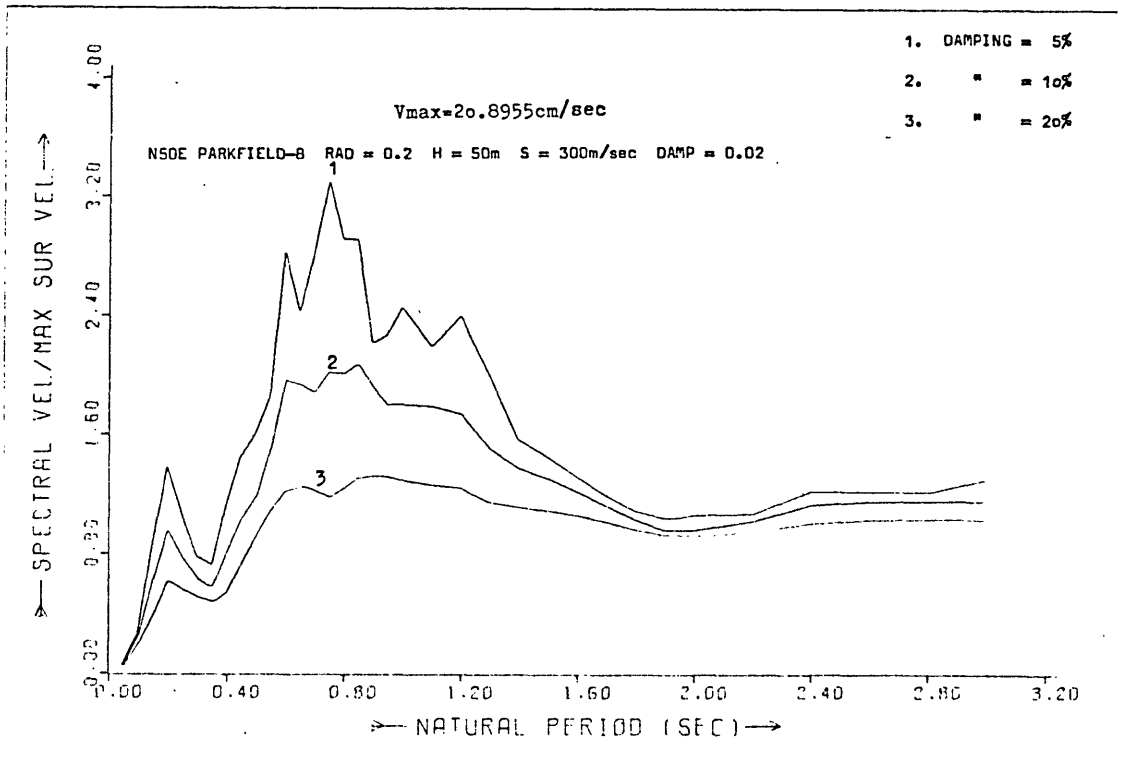


FIG.7.32e COMPUTED GROUND SURFACE VELOCITY RESPONSE SPECTRA AT SITE NO.7.21

BEDROCK MOTION N50E PARKFIELD-8

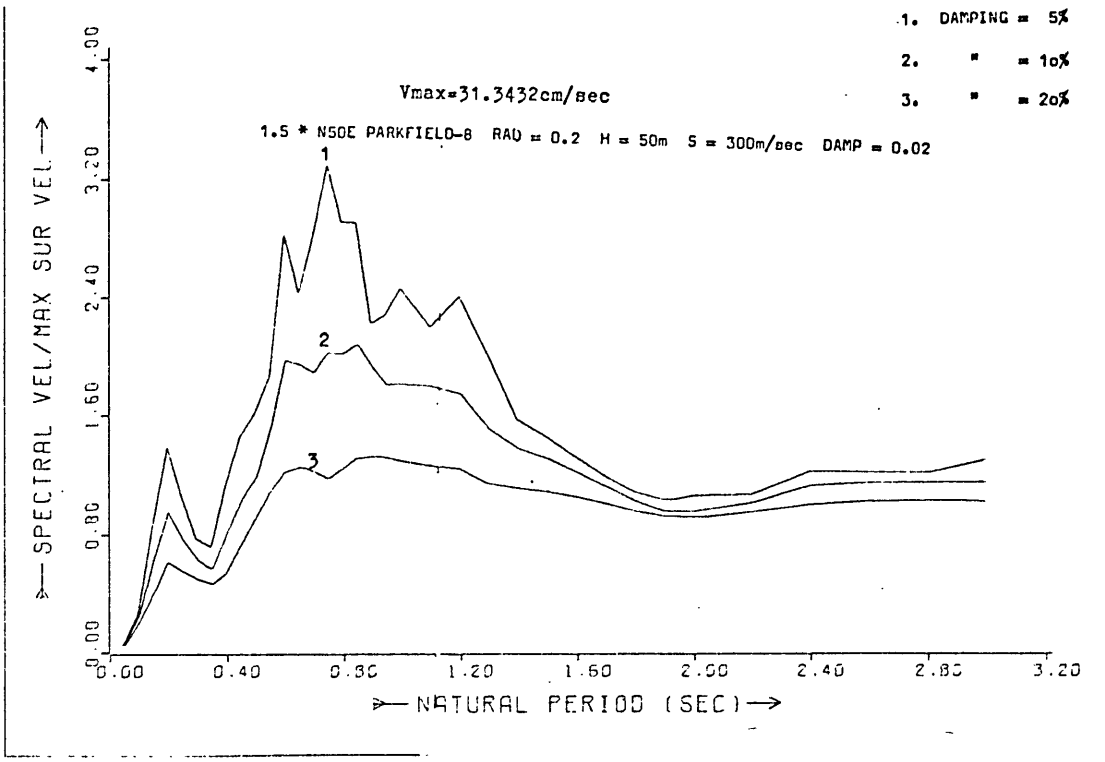


FIG.7.33eCONTOURED GROUND SURFACE VELOCITY RESPONSE SPECTRA AT SITE NO. 7.21

BEDROCK MOTION 1,5 * N50E PARKFIELD-8

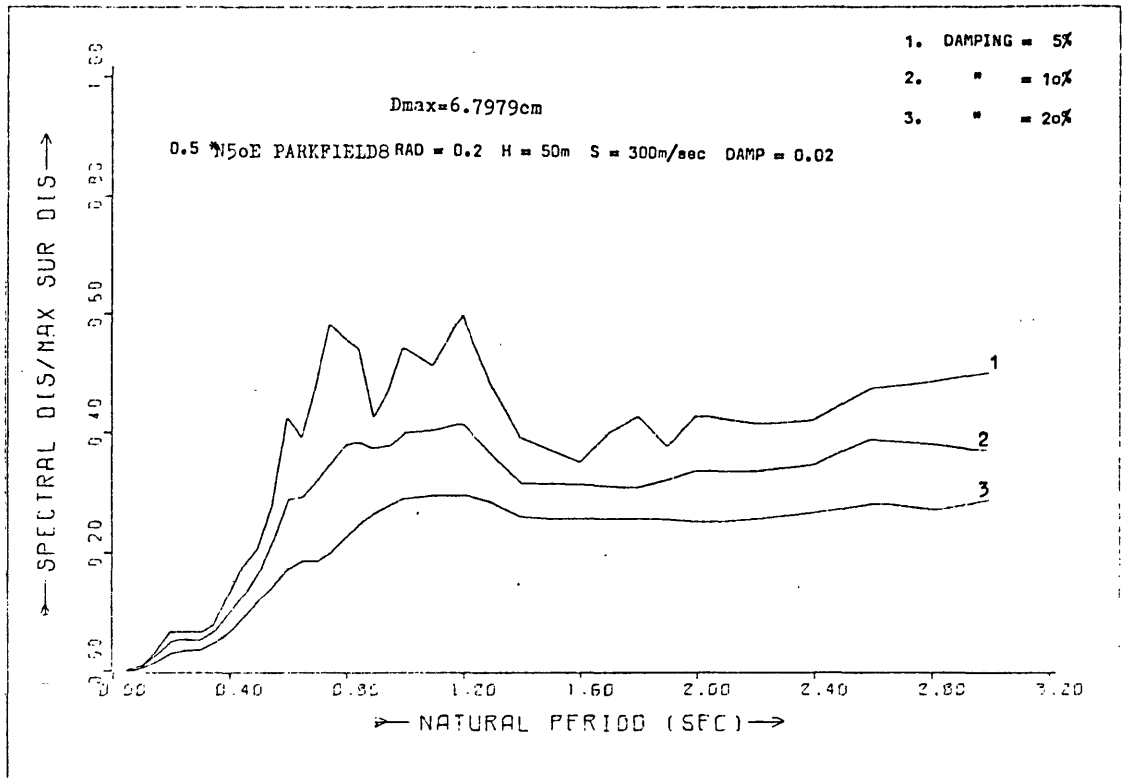


FIG.7.31f COMPUTED GROUND SURFACE DISPLACEMENT RESPONSE SPECTRA AT SITE NO. 7.21

BEDROCK MOTION 0.5 * N50E PARKFIELD-8

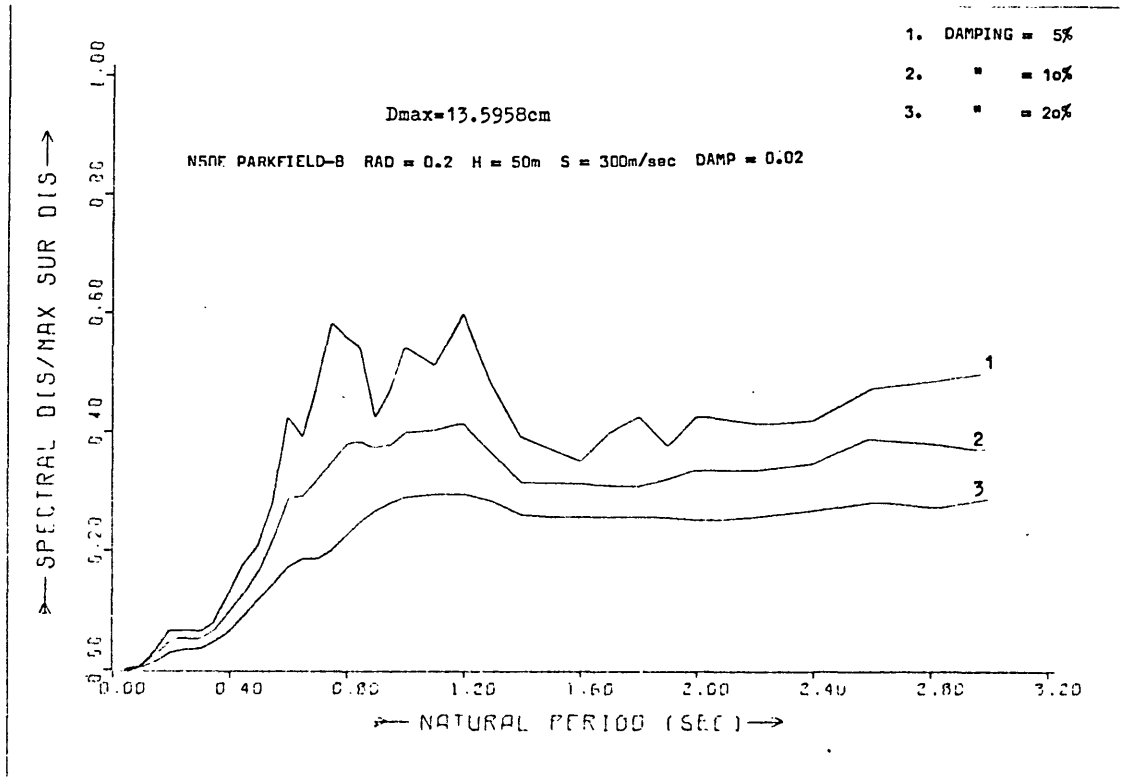


FIG.7.32f COMPUTED GROUND SURFACE DISPLACEMENT RESPONSE SPECTRA AT SITE NO. 7.21

BEDROCK MOTION N50E PARKFIELD-8

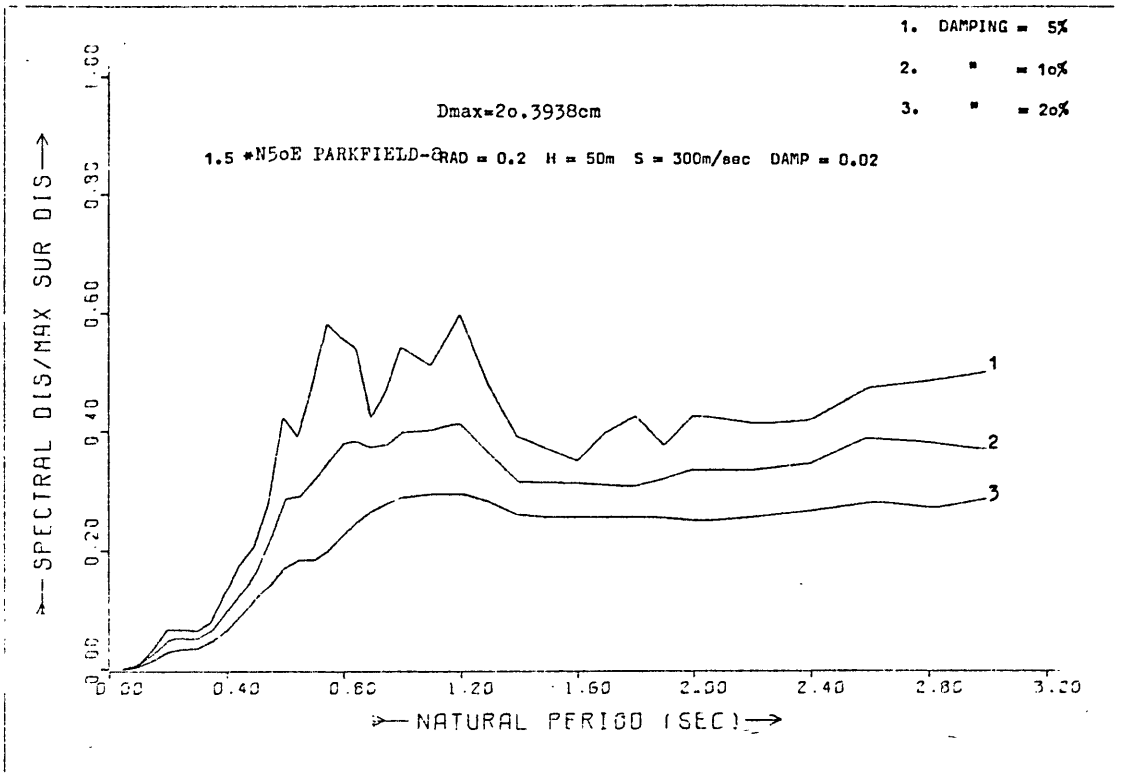


FIG. 7.33 COMPUTED GROUND SURFACE DISPLACEMENT RESPONSE SPECTRA AT SITE NO. 7.21

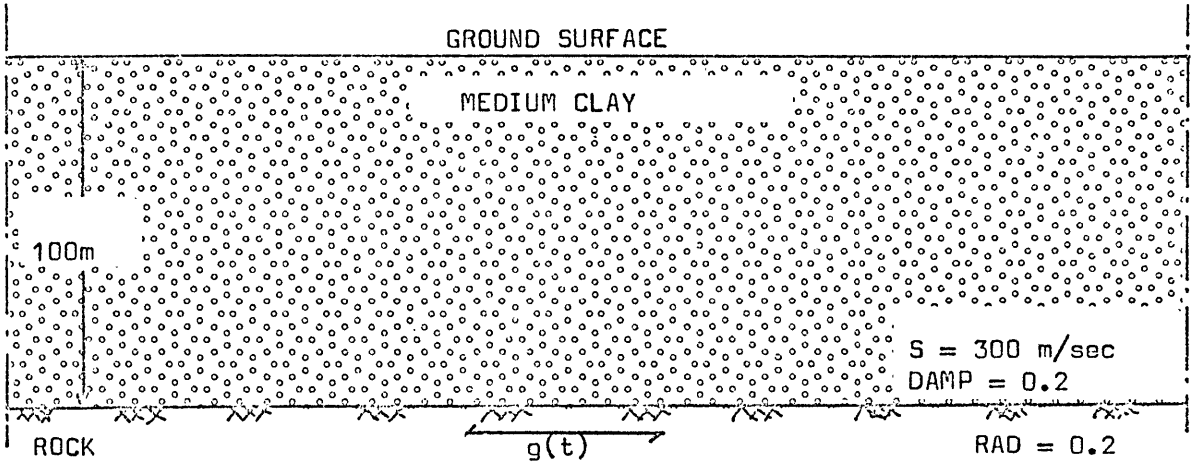
BEDROCK MOTION 1.5 * N50E PARKFIELD-8

c) Response values measured during atomic explosions or small events can be applied directly to predict performance during larger earthquakes.

7.6. COMPARISON BETWEEN RECORDED AND COMPUTED AVERAGE VALUES OF RATIO OF MAXIMUM SURFACE VELOCITY/MAXIMUM SURFACE ACCELERATION AND PREDOMINENT PERIOD FOR DEEP COHESIONLESS SOIL CONDITION

In order to check the applicability of the developed technique for predicting ground response, the new theory has been used to analyse sites of known soil conditions where ground motion has been recorded during several earthquakes. Seed, et. al.[54] published average value of ratios of maximum velocity to maximum acceleration for strong motion data recorded at several sites having deep cohesionless soil condition (where rock of shale-like or sounder in characteristics as evidenced by a shear wave velocity greater than about 760 m/sec was overlain by at least 76m of generally cohesionless soils) in California.

To determine the response of the semi-infinite layer, it is necessary to know the shear wave velocity, hysteretic damping ratio, depth to bedrock and radiation damping ratio. Those constants were determined from the description of the soil conditions at the sites given by the authors. These values are shown in fig. 7.34 and are believed to be reasonable values to approximate the constants for the soil described. However, the influence of the assumptions regarding these constants upon the ground response can easily be determined by performing parametric analysis. Such an analysis is not intended here.



RESPONSE OF HYSTERETIC DEPOSIT UNDERLAIN BY DEFORMABLE BEDROCK

SCHEMATIC SOIL PROFILE FOR SITE NO 7.22

FIG. 7.34

7.6.1. INPUT RECORDS

The following suite of thirteen records were used in the analysis:

1. S16E PACOIMA DAM
2. S74W PACOIMA DAM
3. N85E PARKFIELD-5
4. N5W PARKFIELD-5
5. N65W TEMBLOR
6. N40W PARKFIELD-8
7. S25W TEMBLOR
8. N50E PARKFIELD-8
9. E W ELCENTRO
10. S80E GOLDEN GATE
11. N10E GOLDEN GATE
12. N-S PORTHUENEME
13. E-W PORTHUENEME

Time history, response spectrum and full description of these records are shown in chapter 3.

7.6.2. RESULTS OF THE ANALYSIS

Results of the analysis in the form of computed surface acceleration and velocity time histories are shown in figs. 7.34a,b to 7.46a,b. Values of maximum acceleration and velocity computed from these time histories and the ratio of maximum ground surface velocity/maximum ground surface acceleration are summarized in table 7.2. The representative average value is approximately 58 in/sec/g. The significance of the maximum velocity/maximum acceleration ratio was noted by Newmark see Seed et al and it is interesting to note the

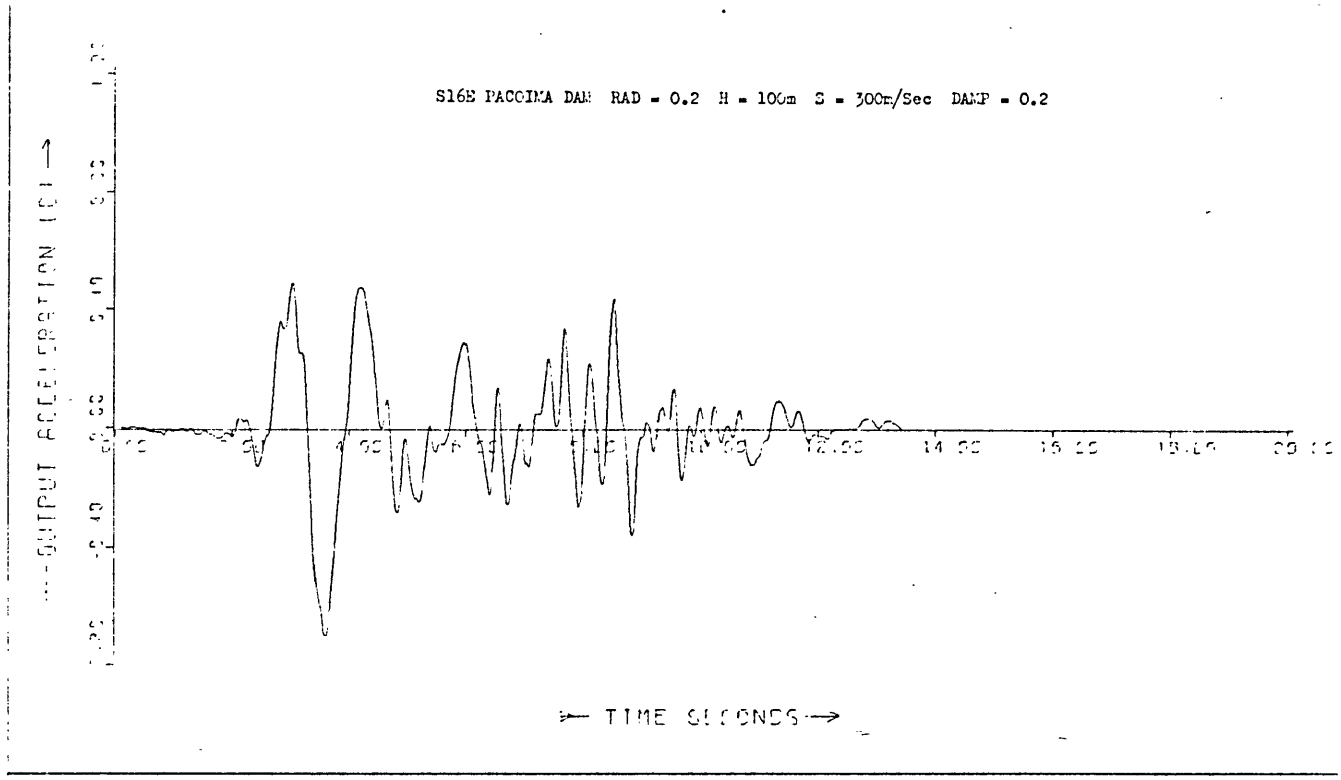


FIG7.34a COMPUTED GROUND SURFACE ACCELERATION TIME HISTORY AT SITE NO 7.22

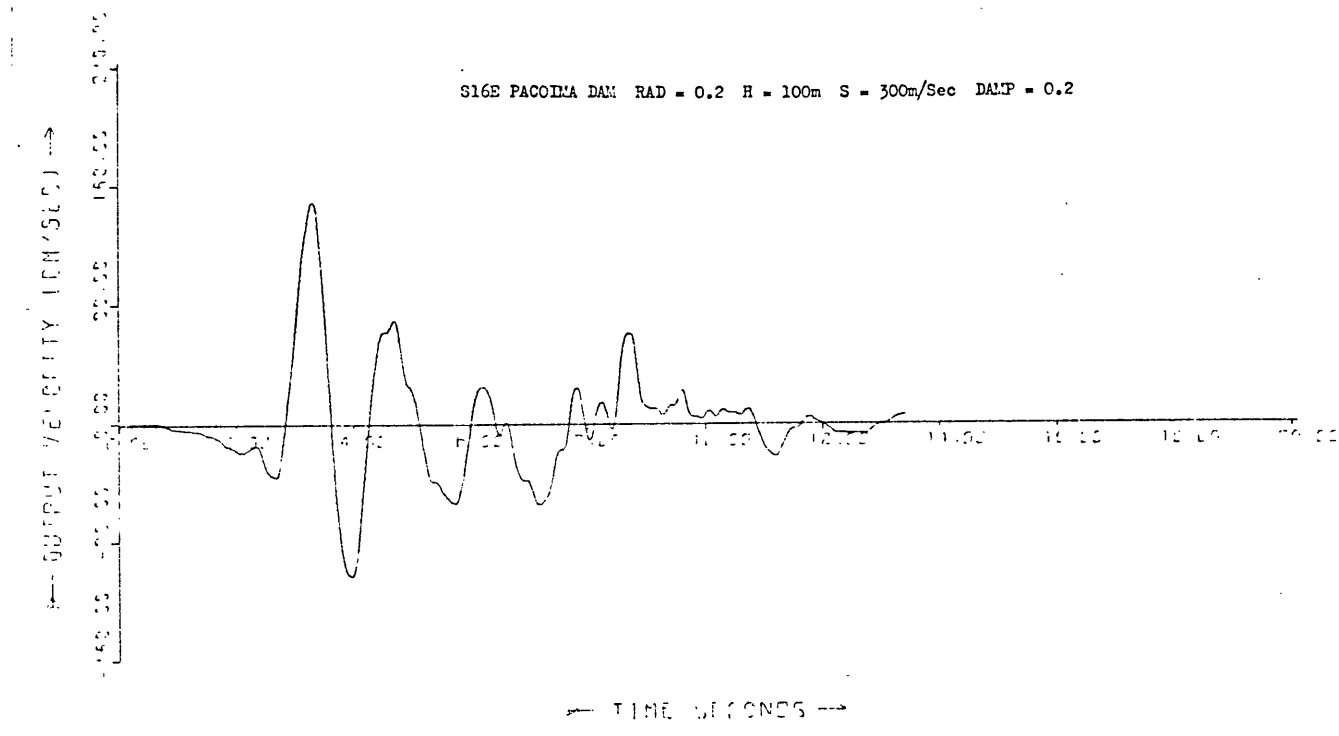


FIG.7.34b COMPUTED GROUND SURFACE VELOCITY TIME HISTORY AT SITE NO7.22

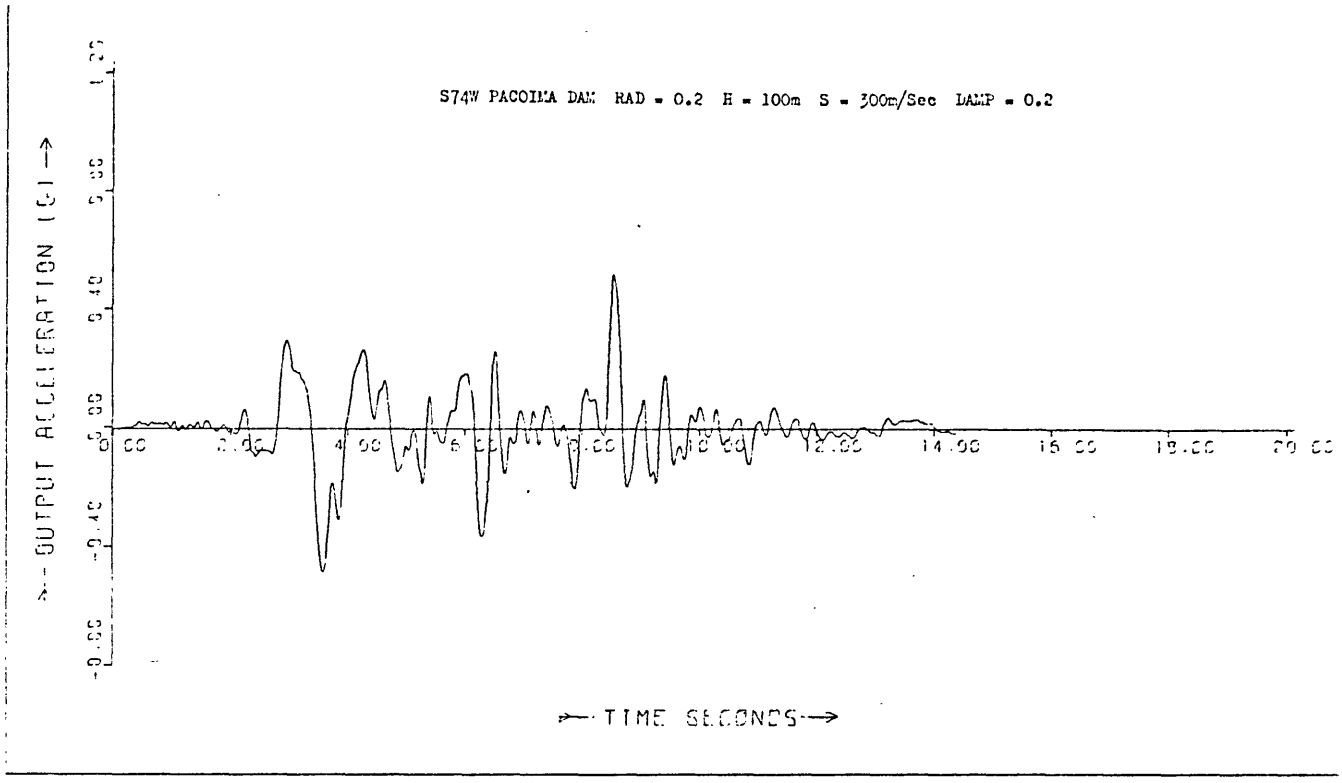


FIG.7.35a COMPUTED GROUND SURFACE ACCELERATION TIME HISTORY AT SITE NO 7.22

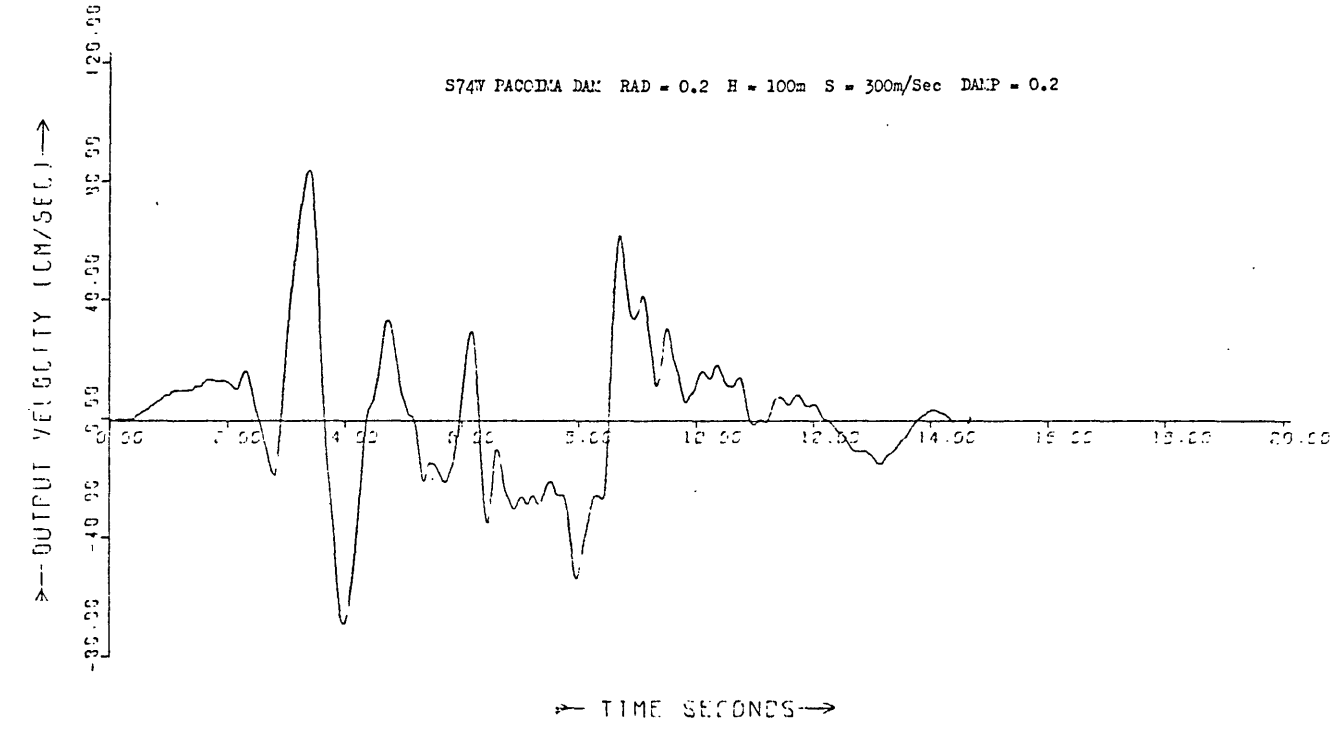


FIG.7.35b COMPUTED GROUND SURFACE VELOCITY TIME HISTORY AT SITE NO7.22

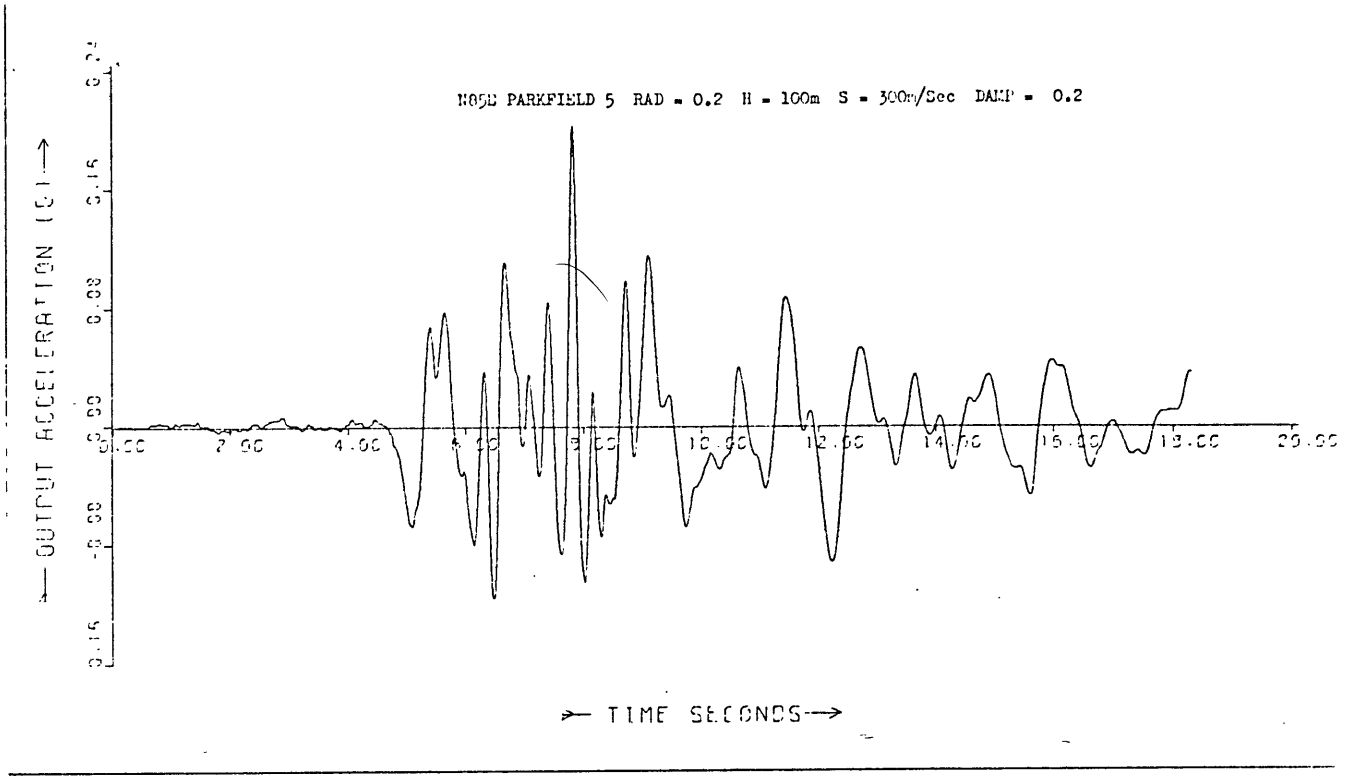


FIG. 7.36a COMPUTED GROUND SURFACE ACCELERATION TIME HISTORY AT SITE NO 7.22

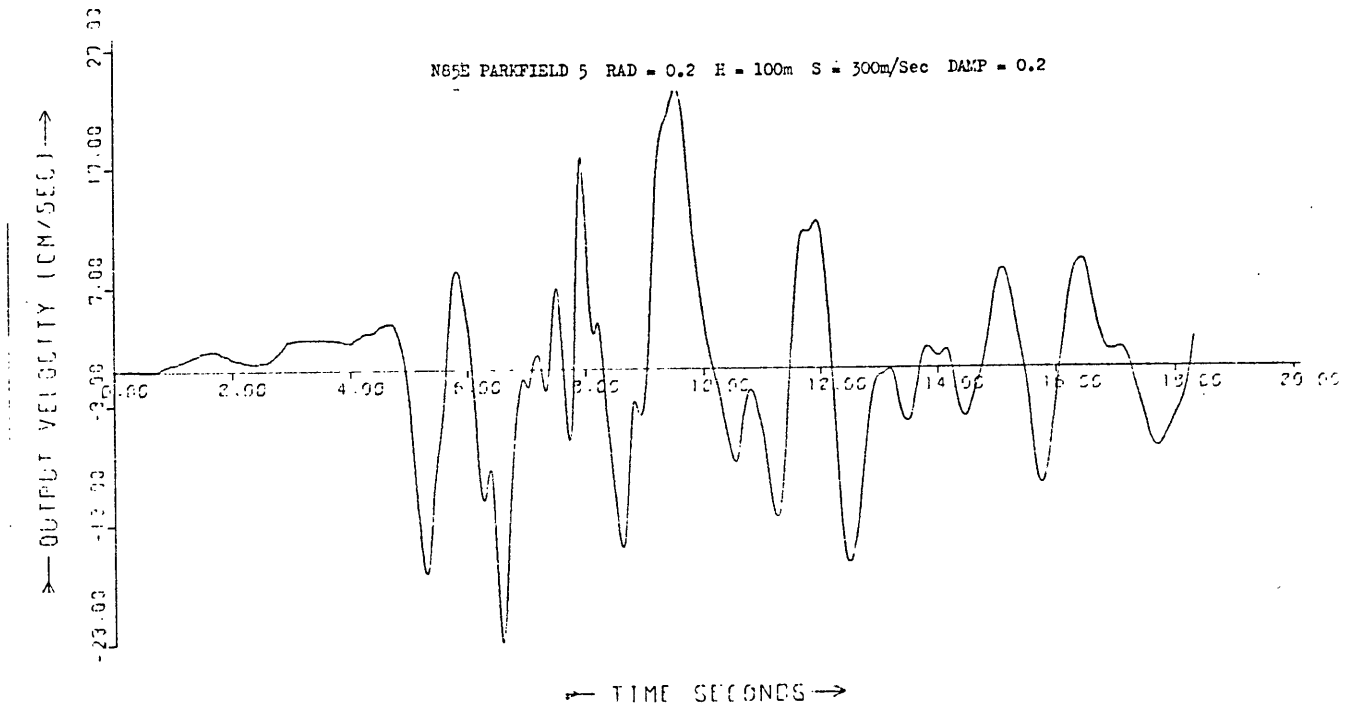


FIG. 7.36b COMPUTED GROUND SURFACE VELOCITY TIME HISTORY AT SITE NO 7.22

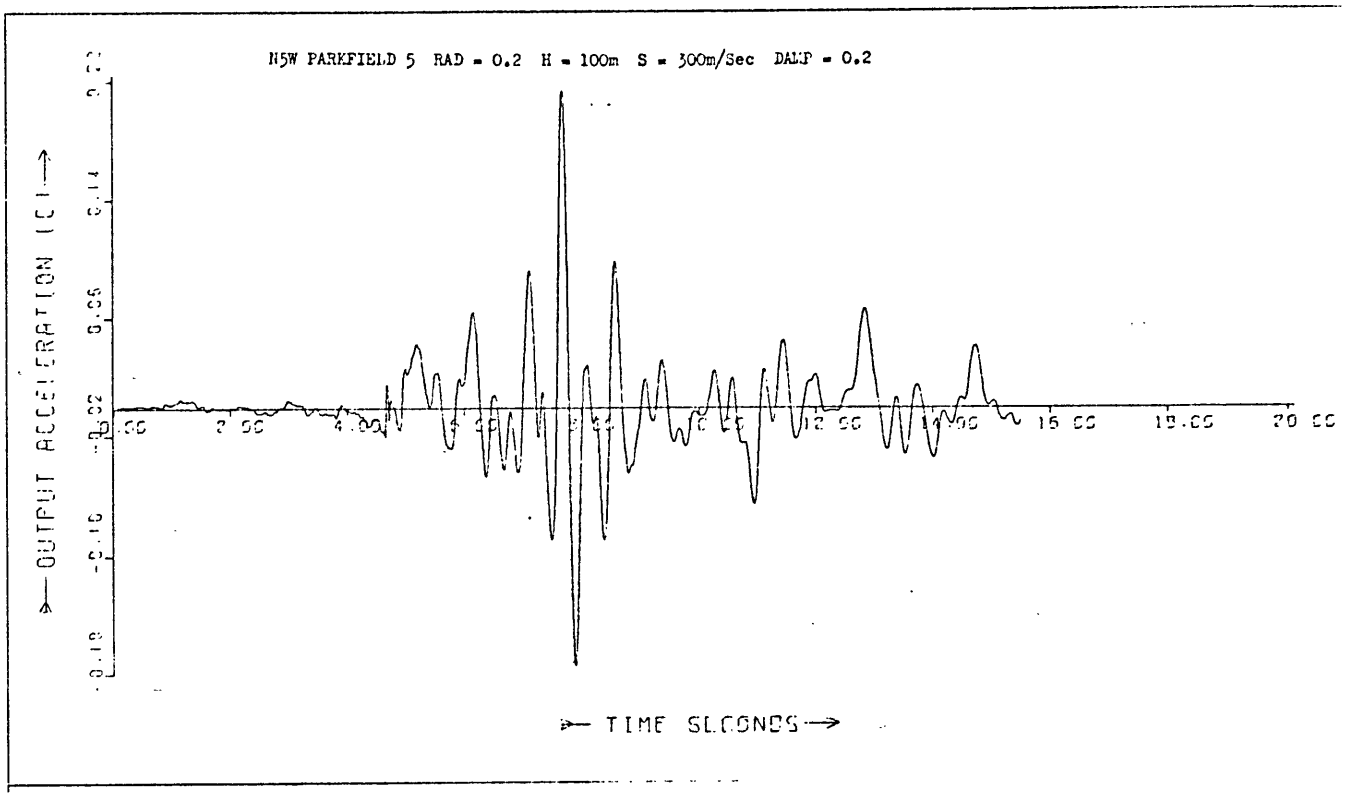


FIG. 7.37a COMPUTED GROUND SURFACE ACCELERATION TIME HISTORY AT SITE NO 7.22

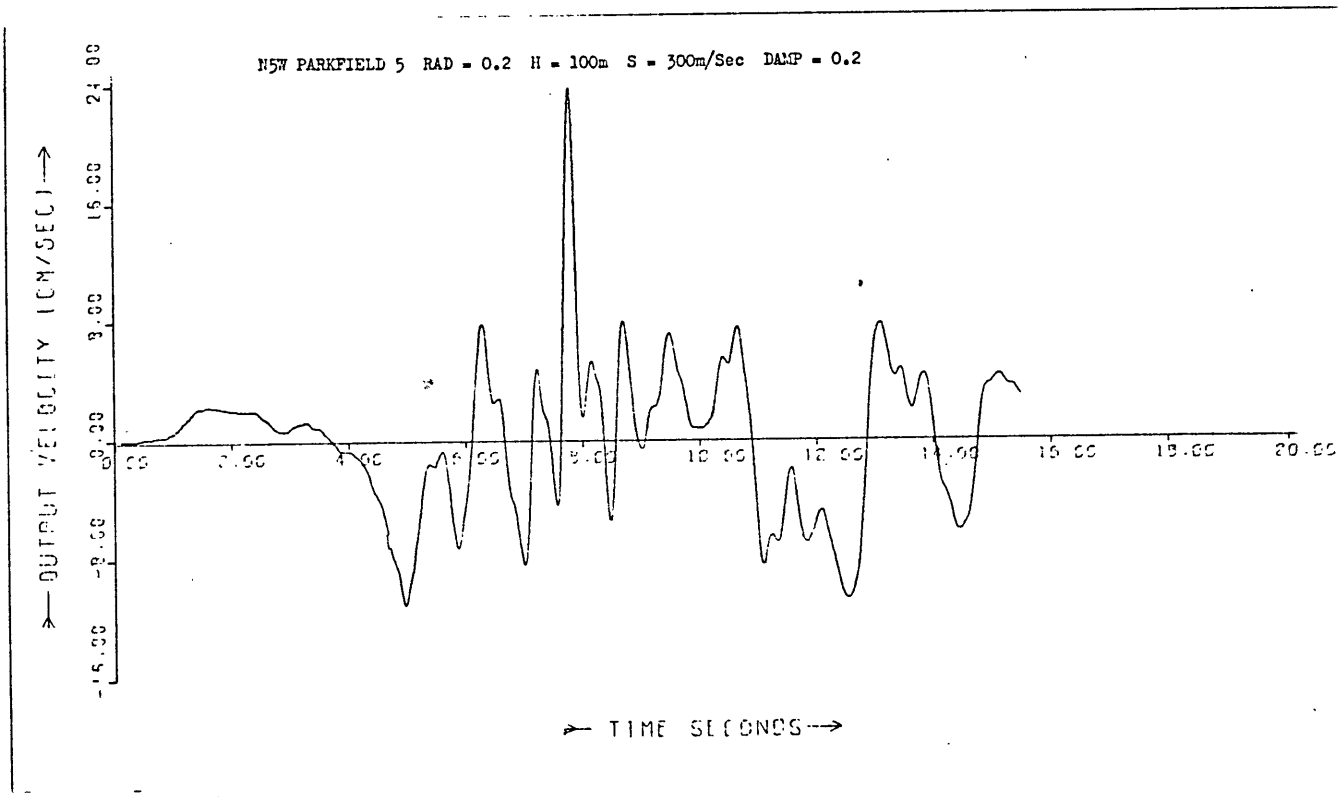


FIG. 7.37b COMPUTED GROUND SURFACE VELOCITY TIME HISTORY AT SITE NO 7.22

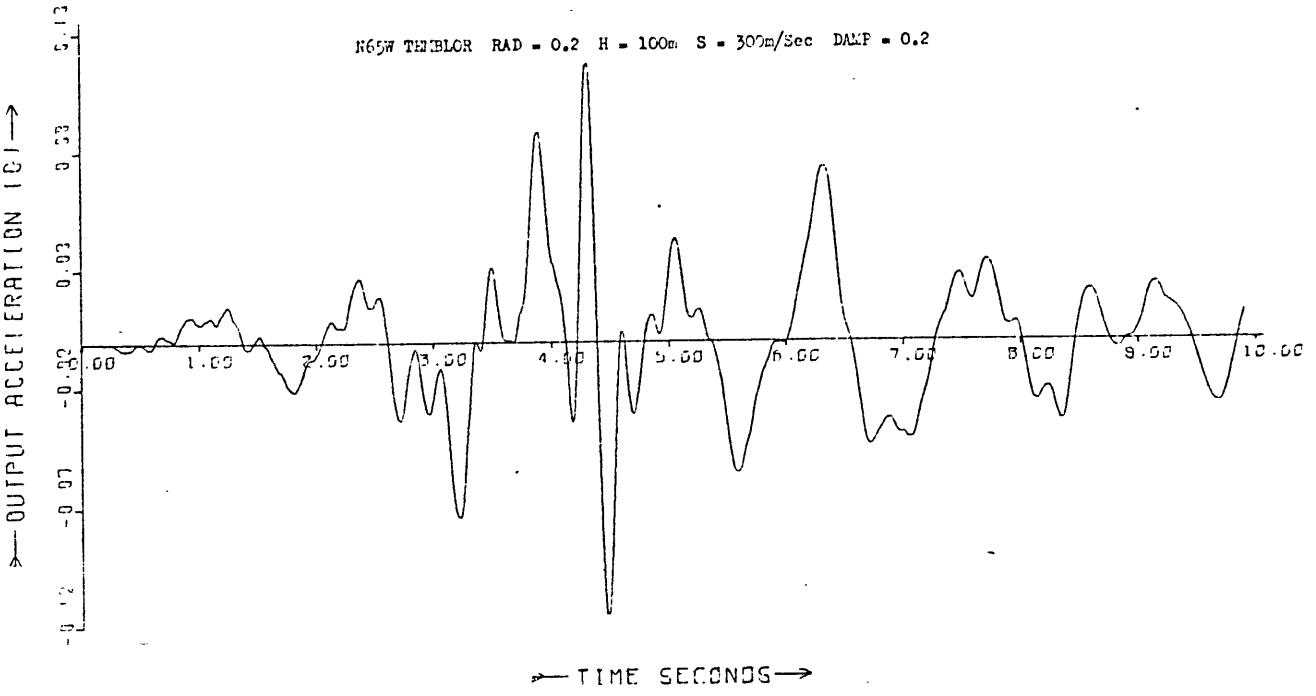


FIG.7.38a COMPUTED GROUND SURFACE ACCELERATION TIME HISTORY AT SITE NO 7.2o

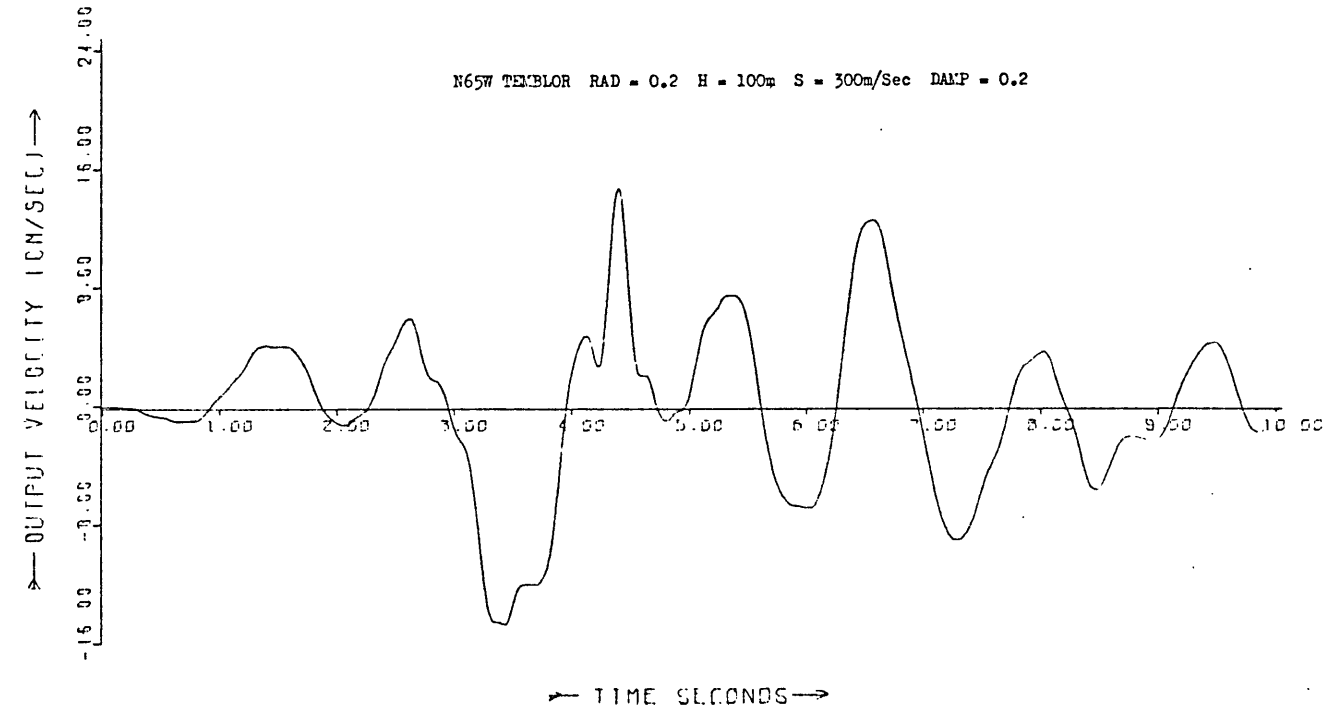


FIG. 7.38b COMPUTED GROUND SURFACE VELOCITY TIME HISTORY AT SITE NO 7.2o

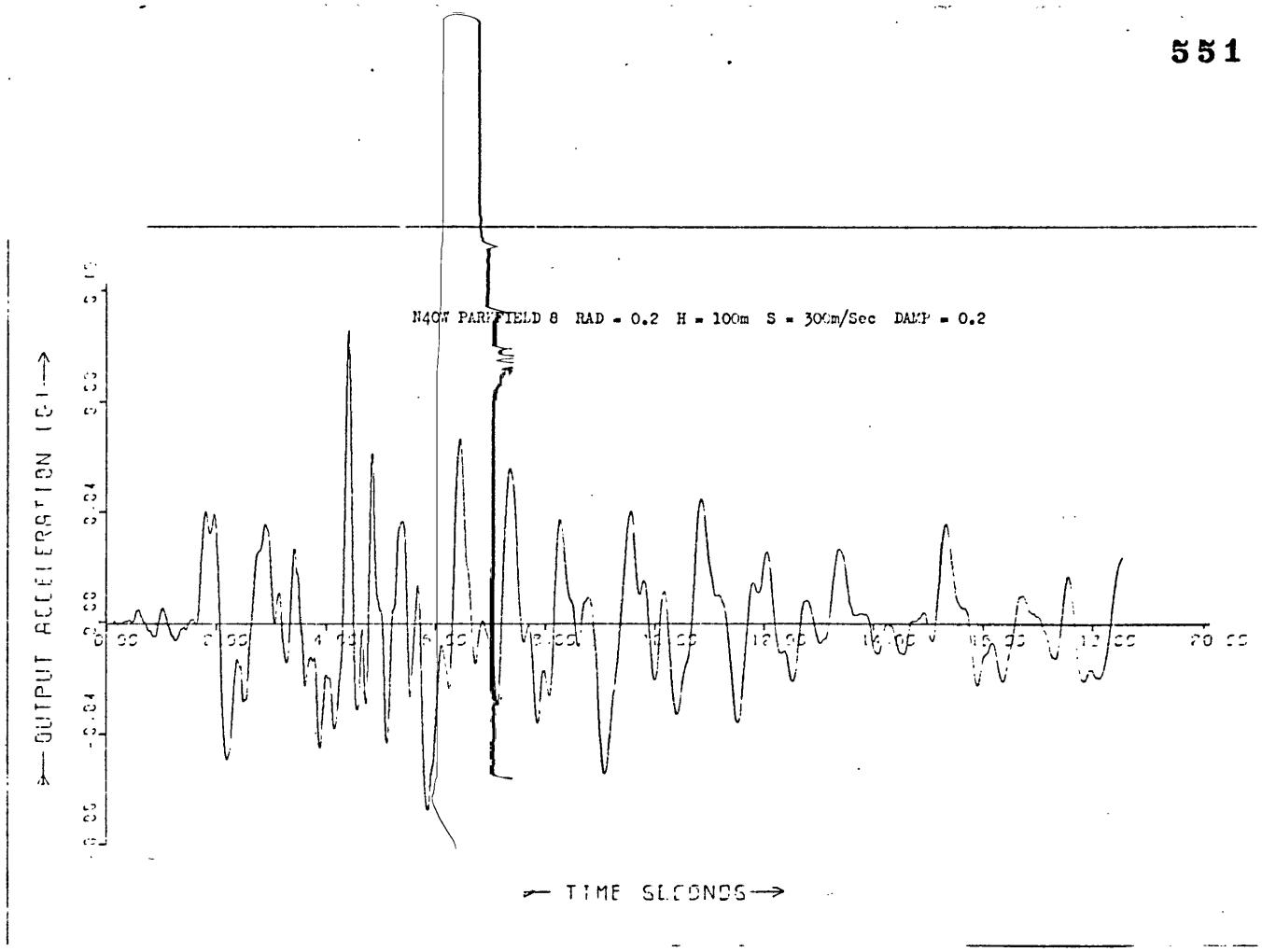


FIG7.39a COMPUTED GROUND SURFACE ACCELERATION TIME HISTORY AT SITE NO 7.2 o

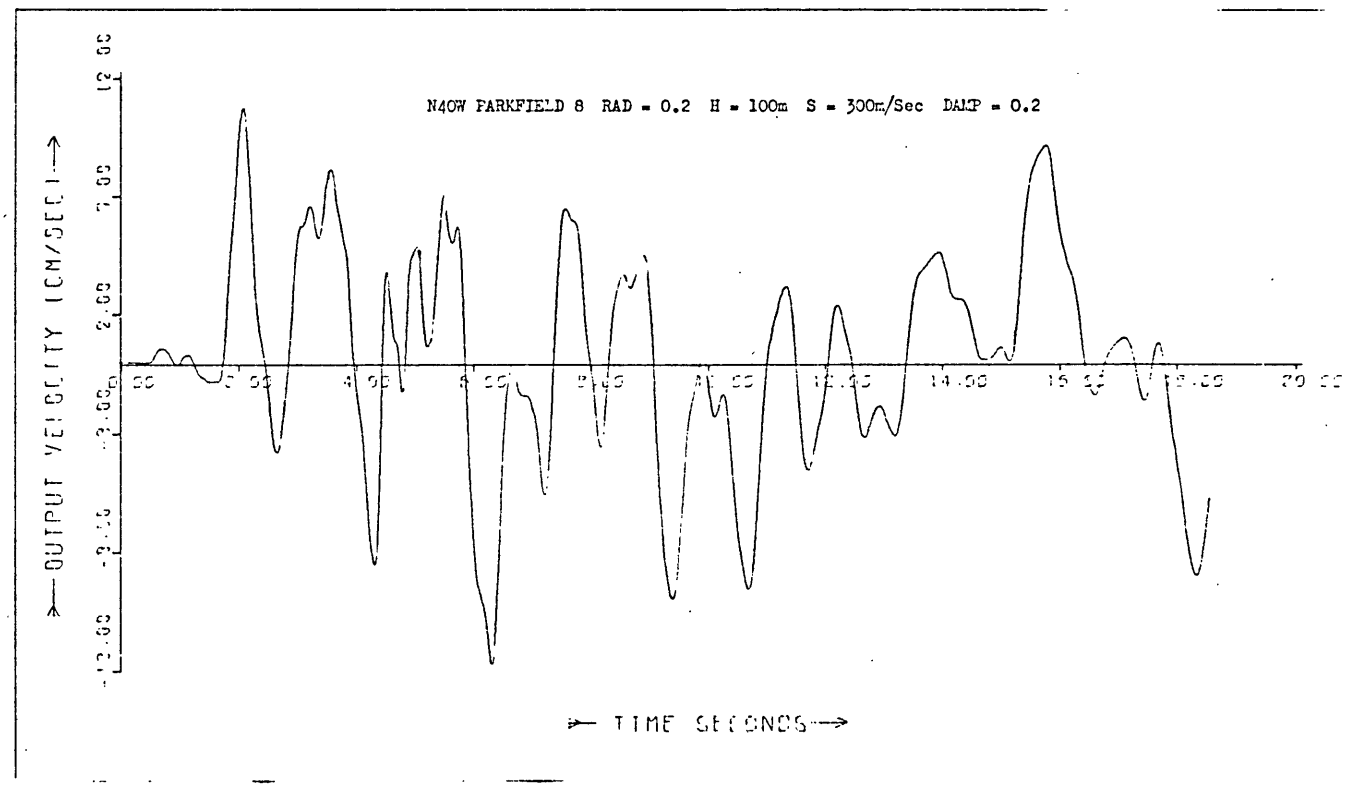


FIG.7.39b COMPUTED GROUND SURFACE VELOCITY TIME HISTORY AT SITE NO7.20

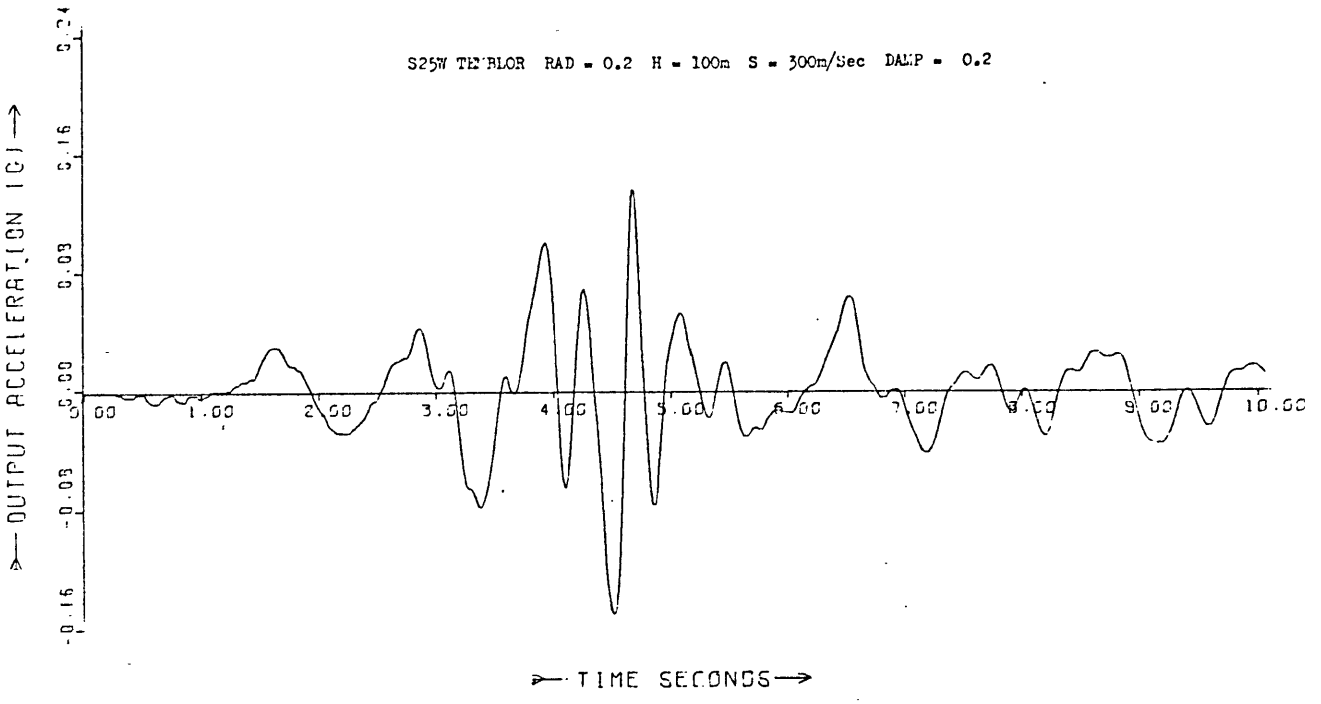


FIG.7.4oa COMPUTED GROUND SURFACE ACCELERATION TIME HISTORY AT SITE NO 7.22

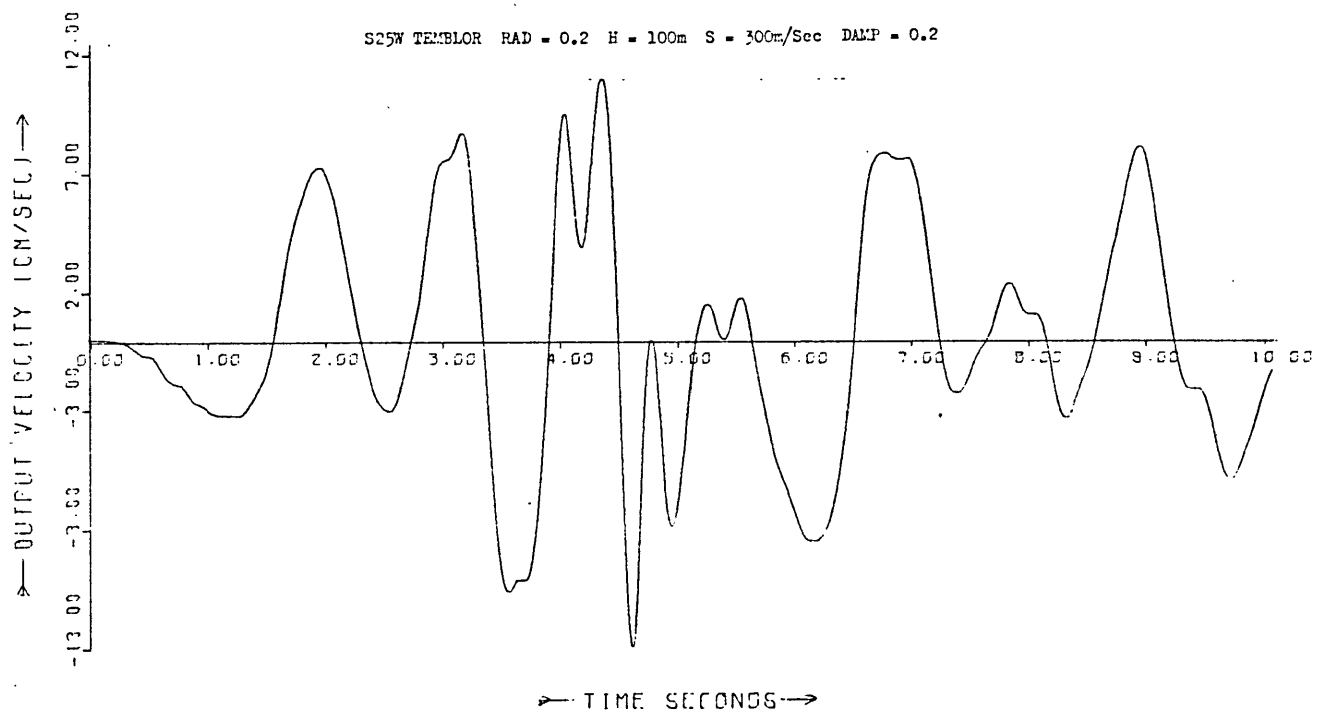


FIG.7.4ob COMPUTED GROUND SURFACE VELOCITY TIME HISTORY AT SITE NO7.22

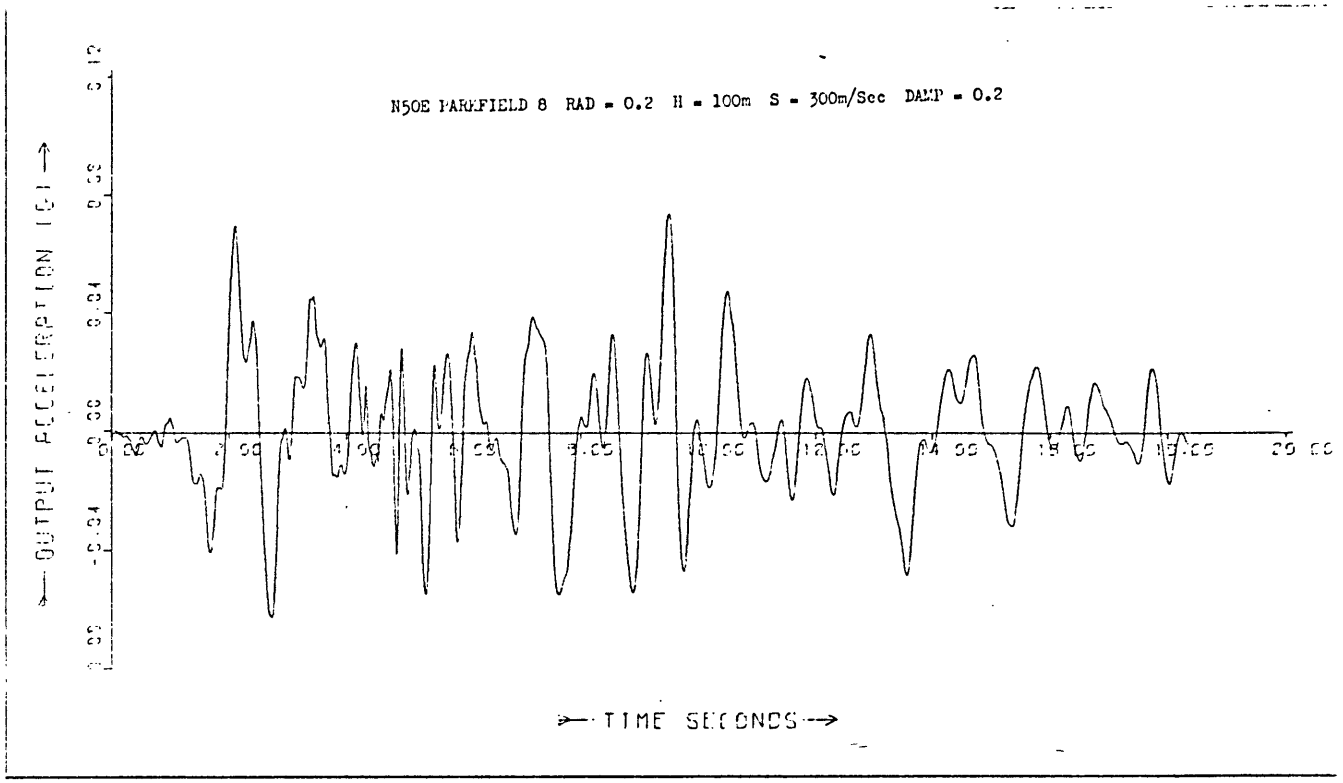


FIG 7.41a COMPUTED GROUND SURFACE ACCELERATION TIME HISTORY AT SITE NO 7.22

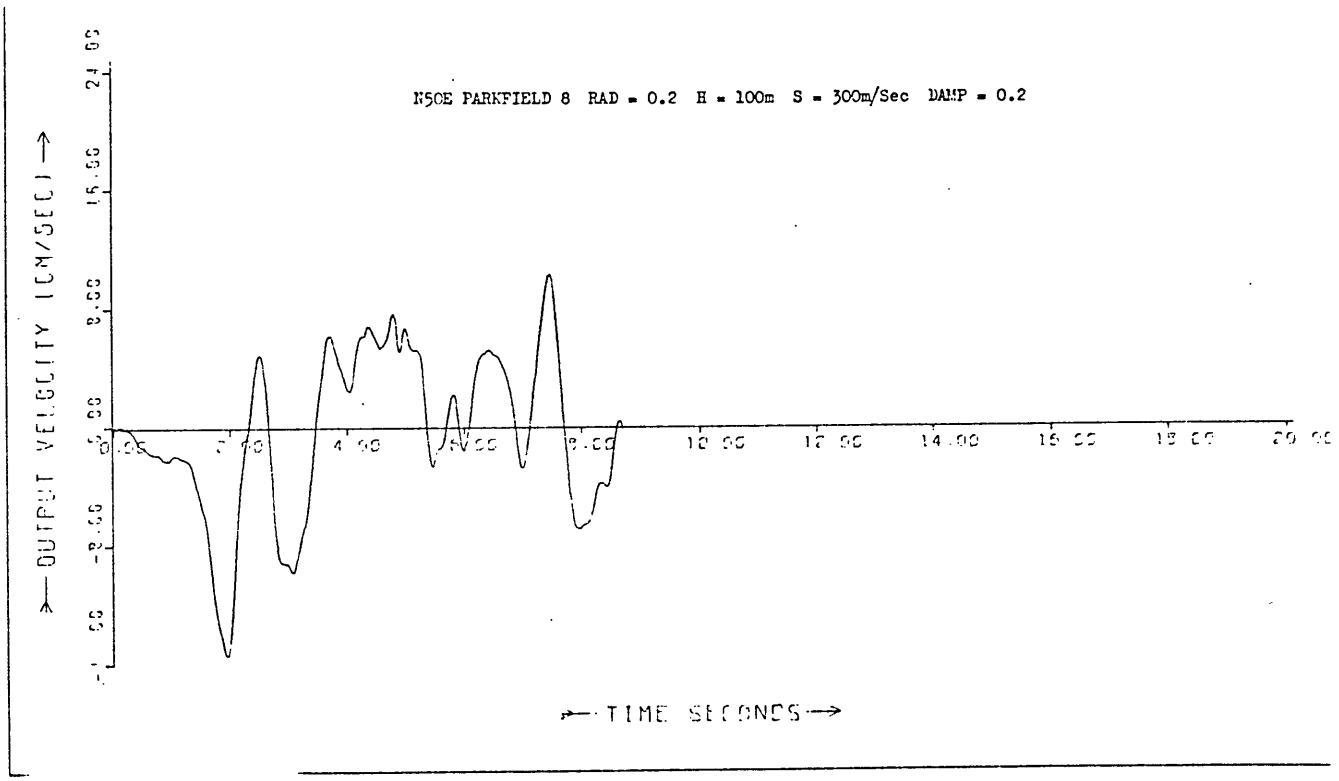


FIG7.41b COMPUTED GROUND SURFACE VELOCITY TIME HISTORY AT SITE NO 7.22

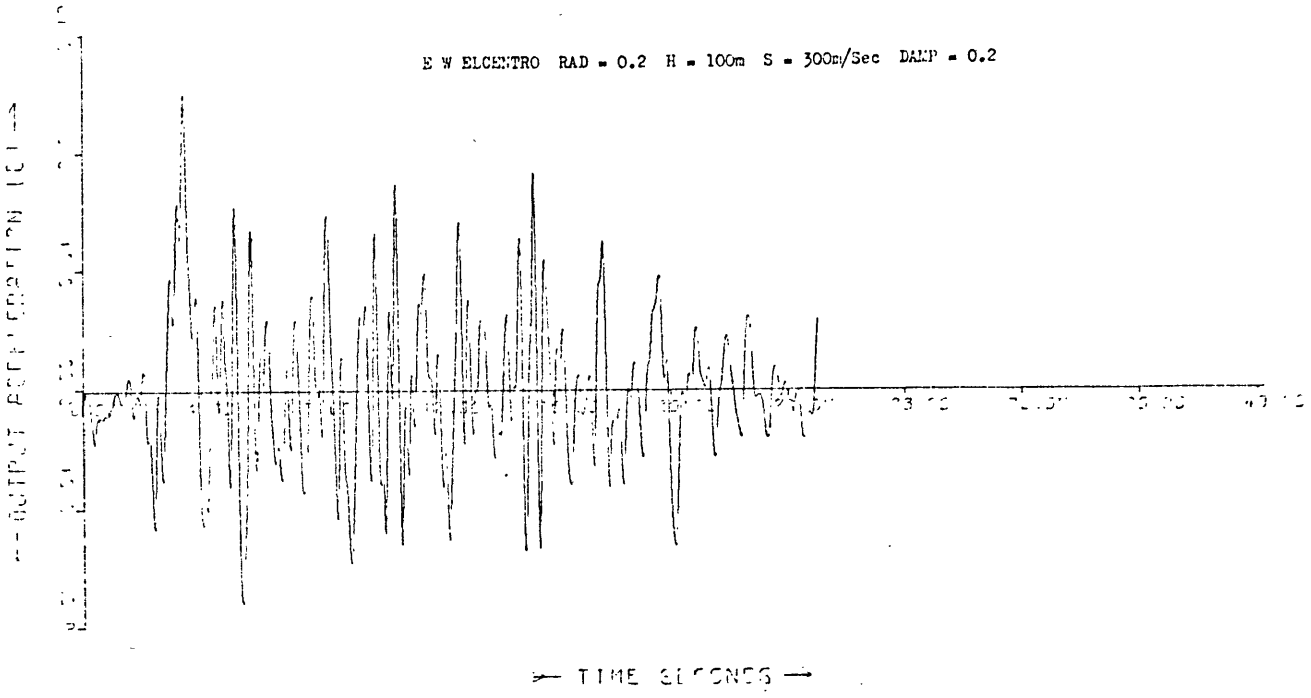


FIG.7.42a COMPUTED GROUND SURFACE ACCELERATION TIME HISTORY AT SITE NO 7.22

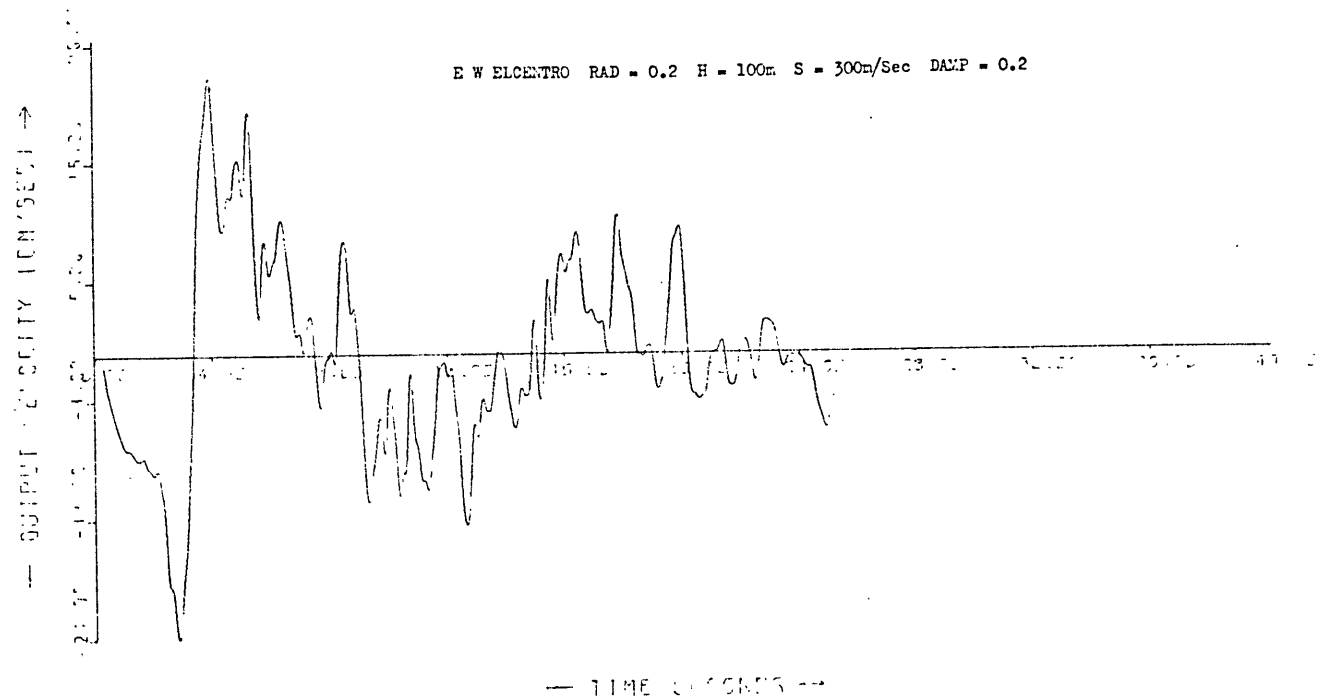


FIG. 7.42b COMPUTED GROUND SURFACE VELOCITY TIME HISTORY AT SITE NO 7.22

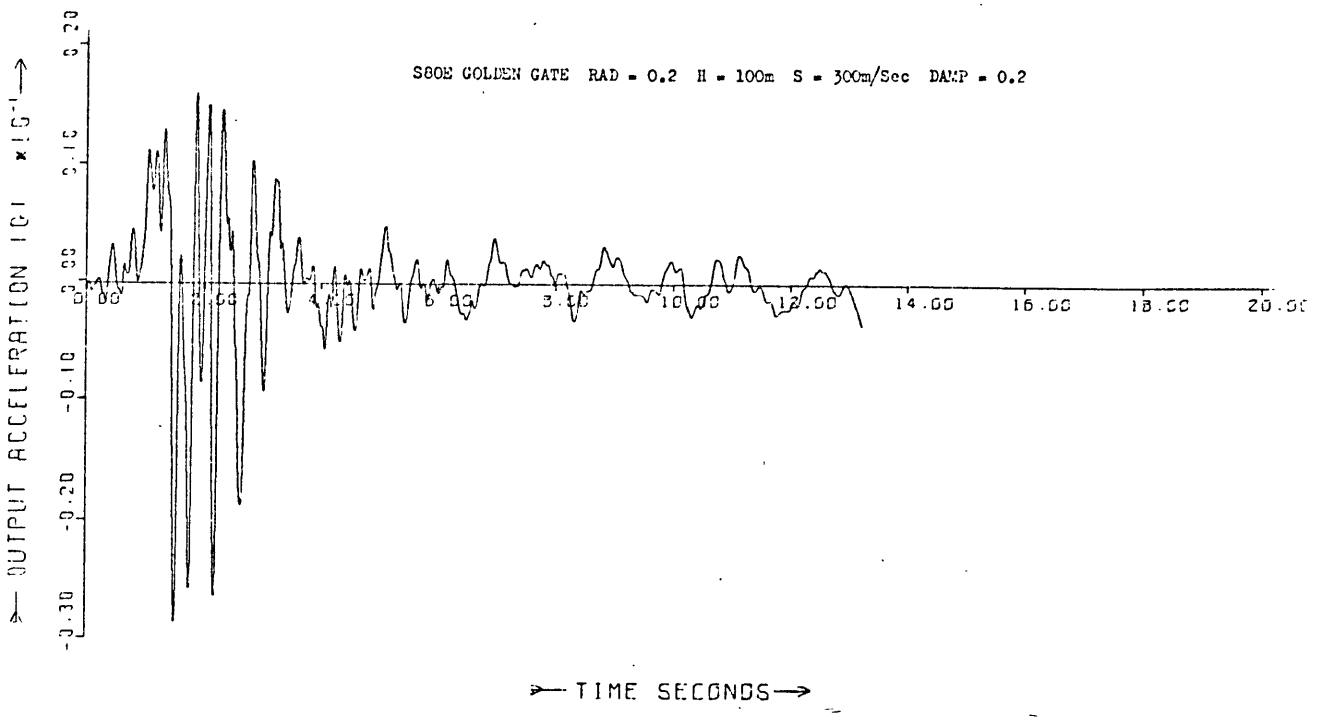


FIG.7.43a COMPUTED GROUND SURFACE ACCELERATION TIME HISTORY AT SITE NO 7.22

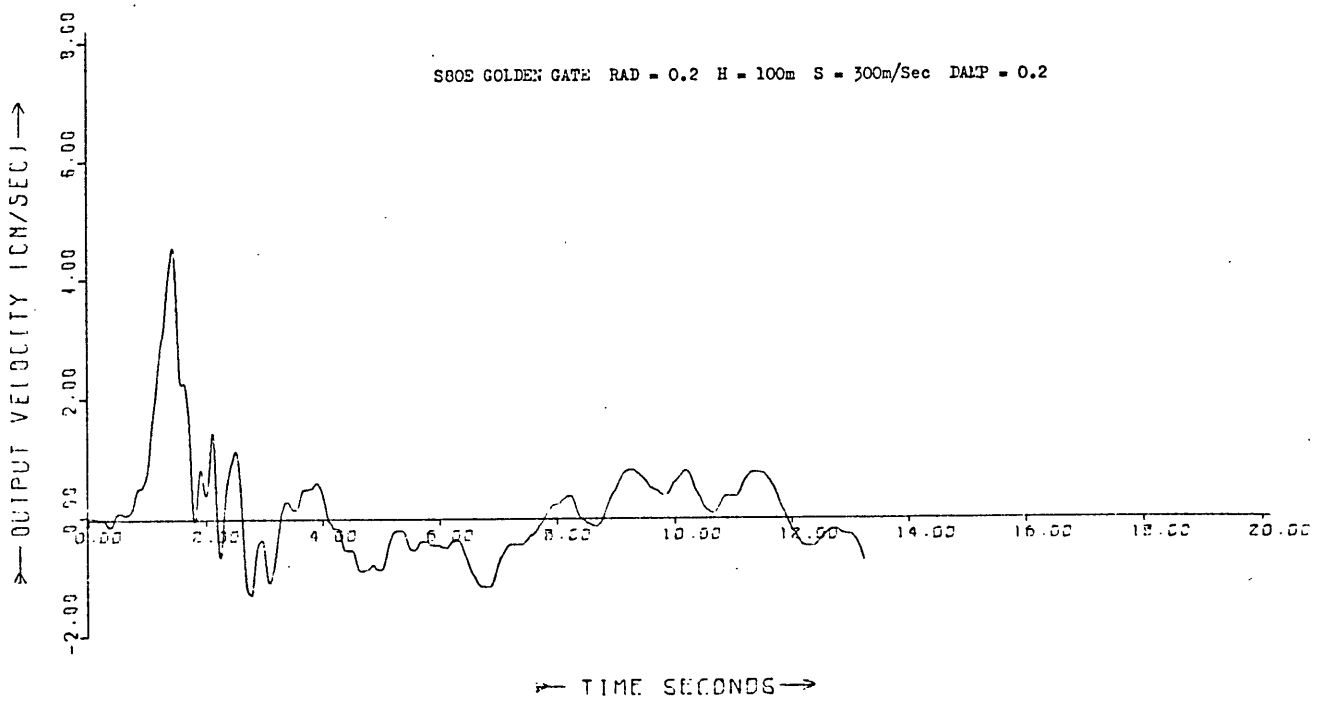


FIG.7.43b COMPUTED GROUND SURFACE VELOCITY TIME HISTORY AT SITE NO7.22

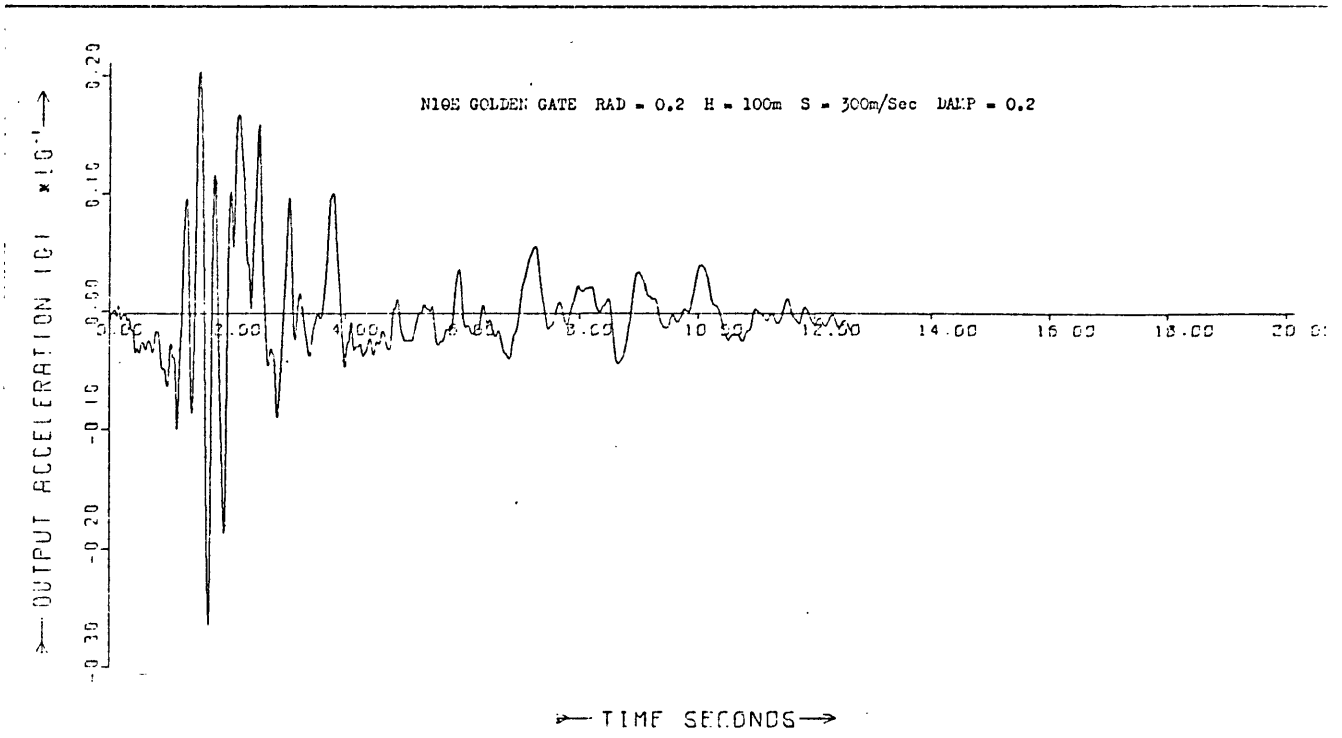


FIG.7.44a COMPUTED GROUND SURFACE ACCELERATION TIME HISTORY AT SITE NO7.22

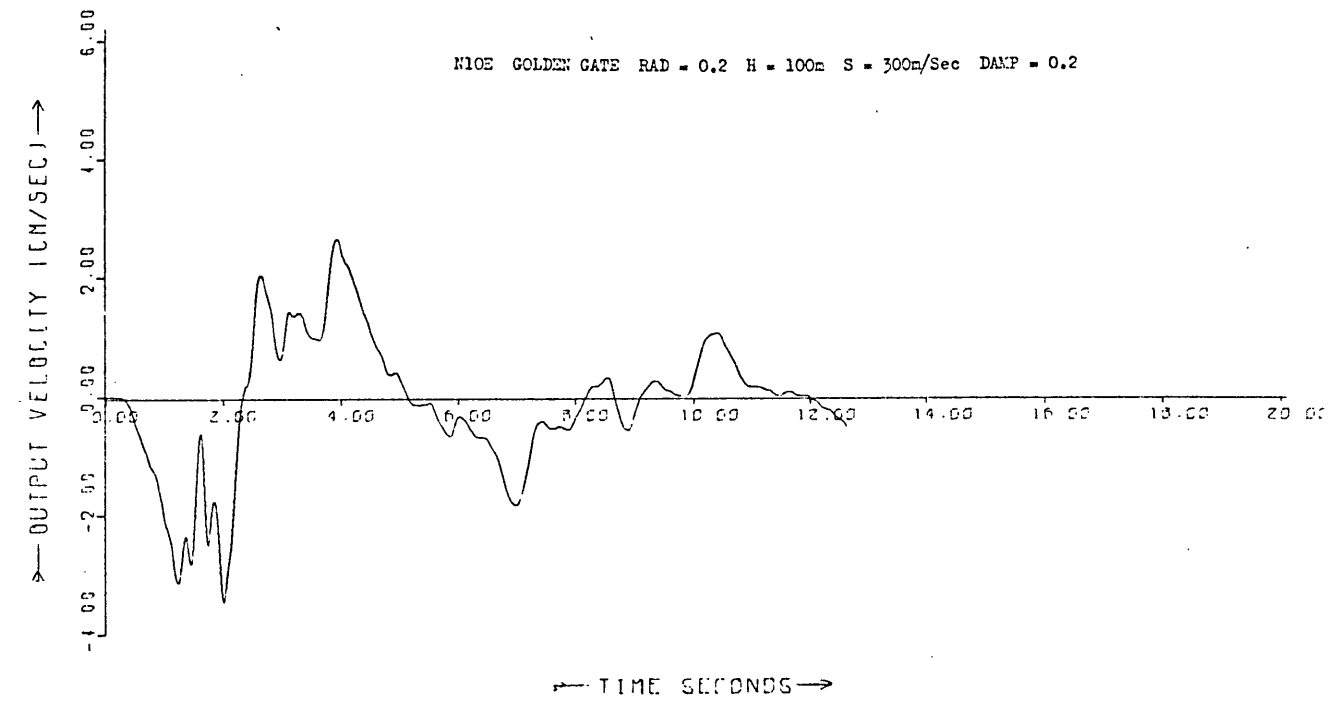


FIG.7.44b COMPUTED GROUND SURFACE VELOCITY TIME HISTORY AT SITE NO 7.22

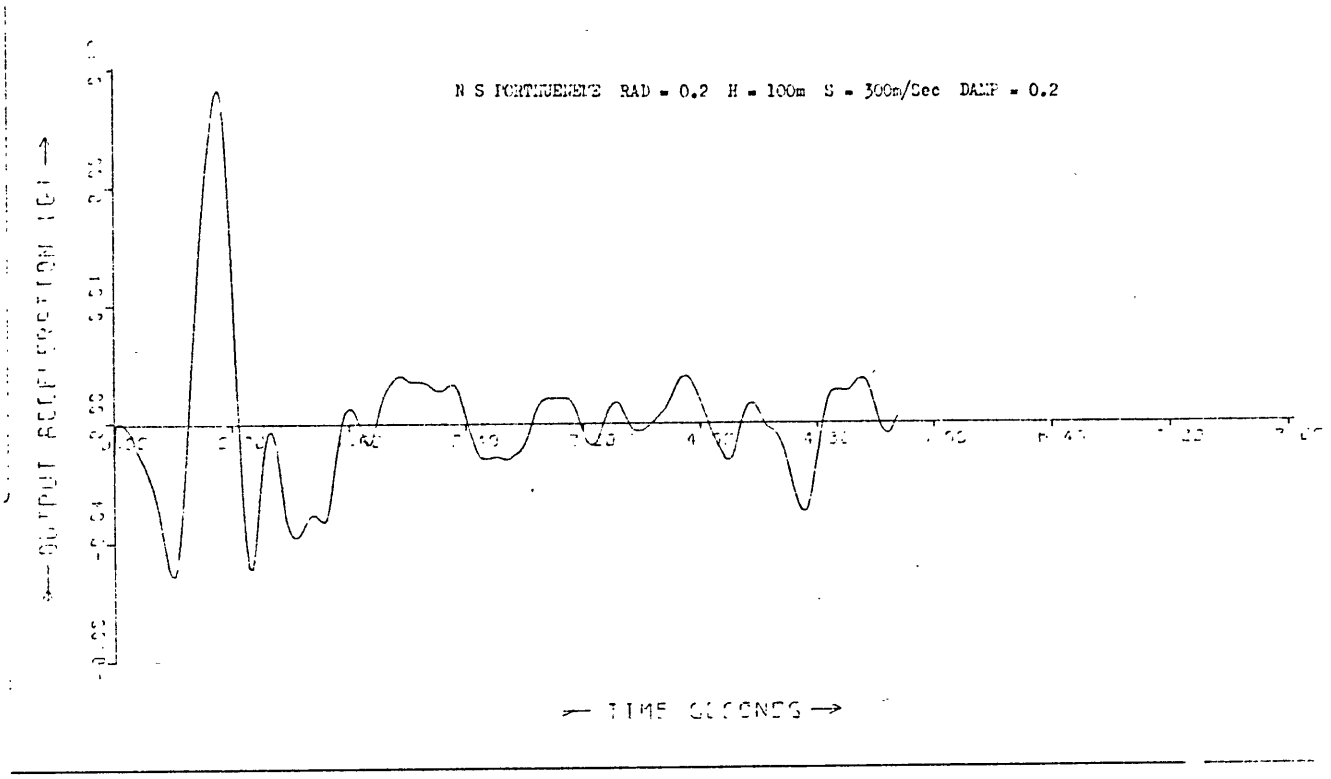


FIG.7.45a COMPUTED GROUND SURFACE ACCELERATION TIME HISTORY AT SITE NO 7.22

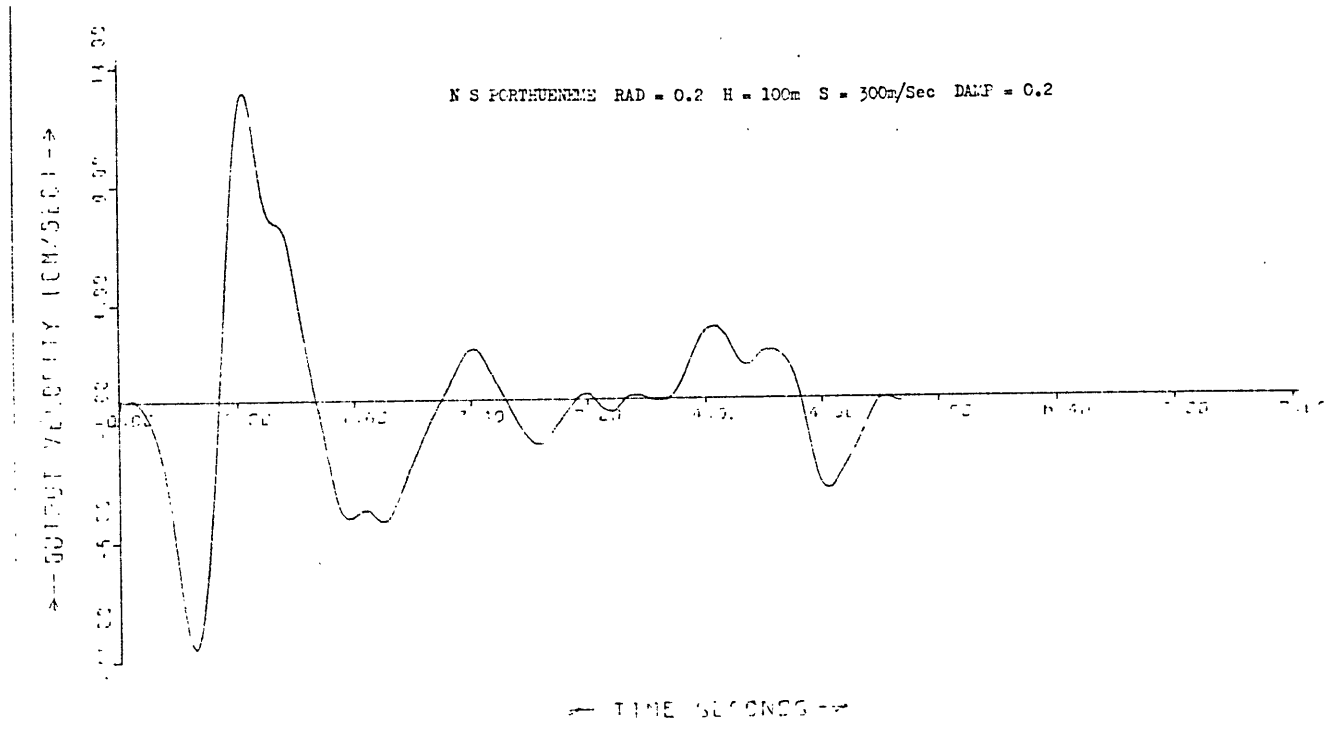


FIG.7.45b COMPUTED GROUND SURFACE VELOCITY TIME HISTORY AT SITE NO 7.22

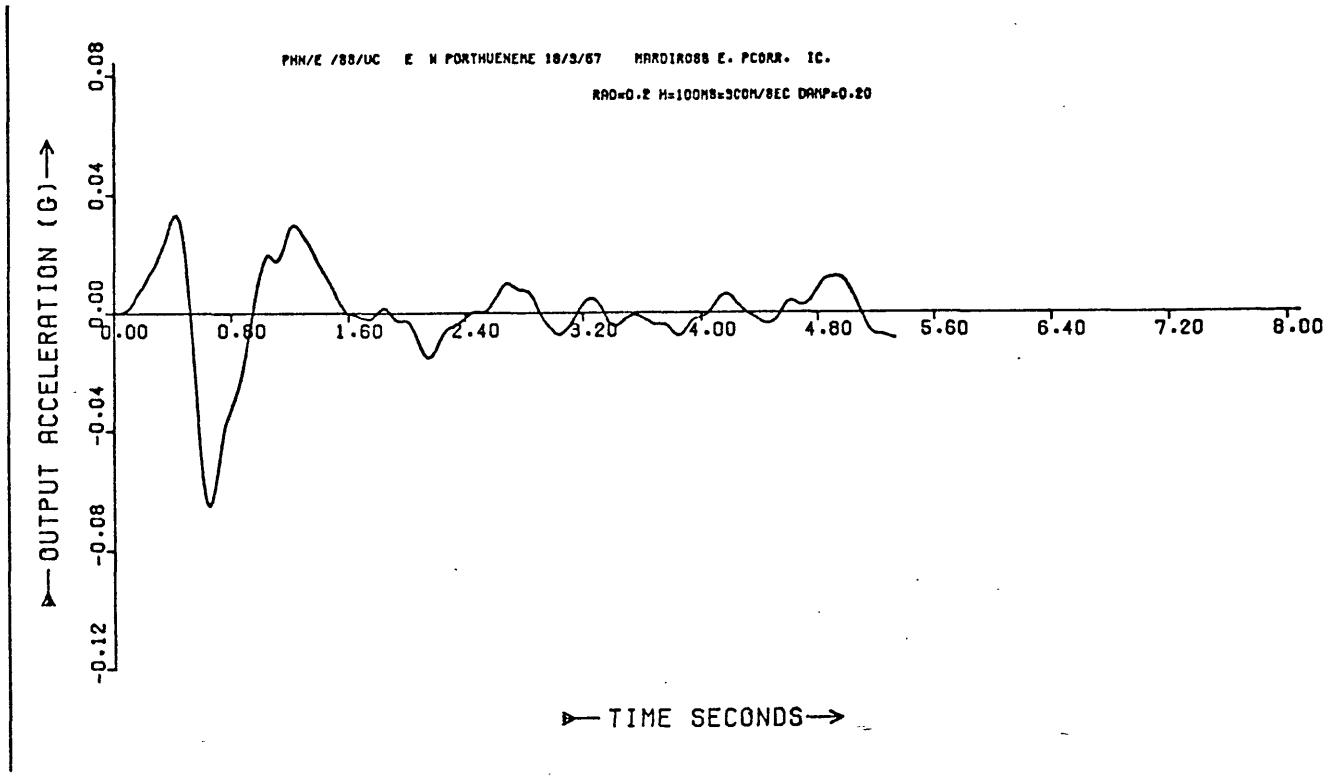


FIG.7.46a COMPUTED GROUND SURFACE ACCELERATION TIME HISTORY AT SITE NO 7.22

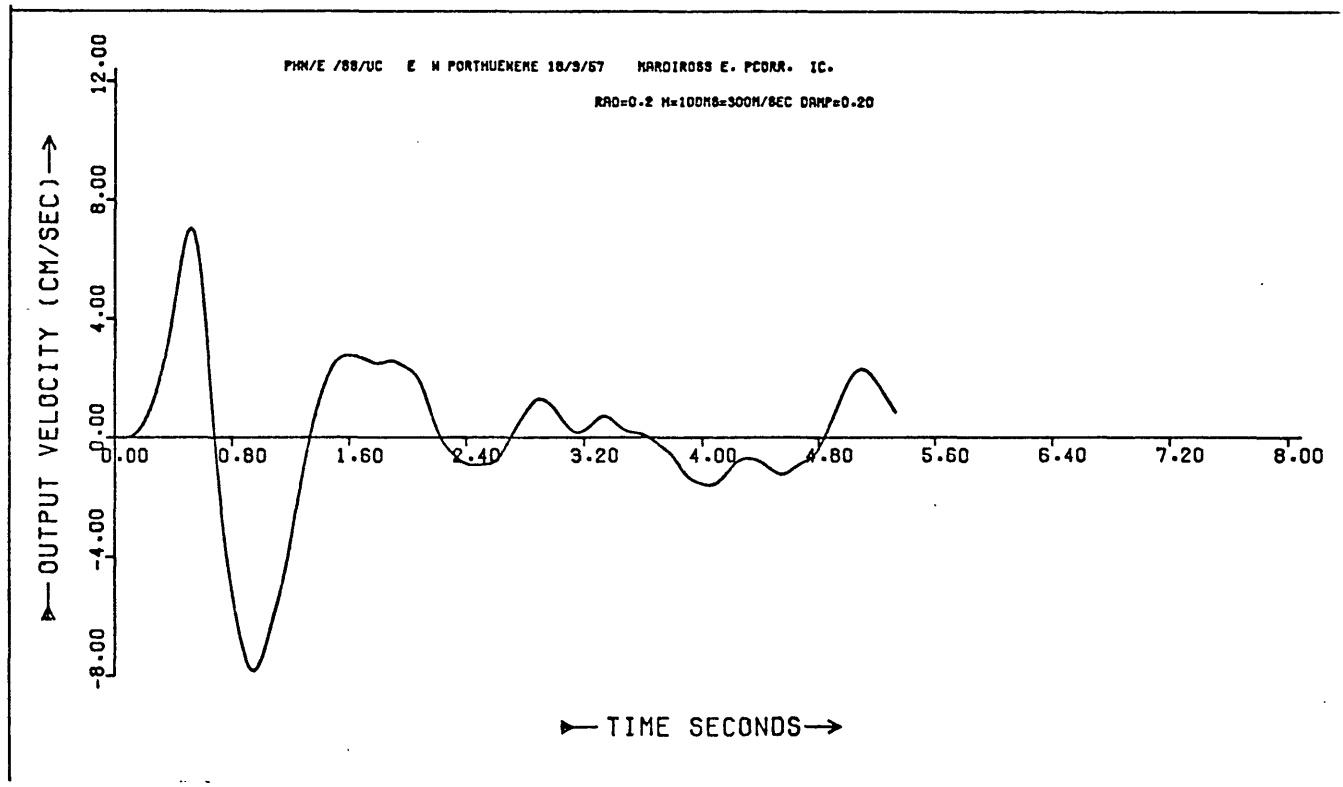


FIG.7.46b COMPUTED GROUND SURFACE VELOCITY TIME HISTORY AT SITE NO 7.22

DAMP=0.2, RAD=0.2, H=100m, S=300m/sec

BEDROCK MOTION IMPERIAL COLLEGE DATA	ACC_{max} g	VEL_{max} cm/sec	$\frac{VEL_{max}}{ACC_{max}}$ inch/sec/g
S16E SAN FERNANDO	0.702	149.83	84.02
S74W SAN FERNANDO	0.524	84.324	63.35
N85E PARKFIELD-5	0.203	23.678	45.92
N5W PARKFIELD-5	0.214	23.884	43.94
N65W TEMBLOR	0.118	14.865	49.59
N40W PARKFIELD-8	0.106	12.706	47.19
S25W TEMBLOR	0.150	12.865	33.76
N50E PARKFIELD-8	0.074	15.388	81.86
E-W ELCENTRO	0.100	23.978	94.40
S80E GOLDEN GATE	0.028	4.577	64.35
N10E GOLDEN GATE	0.026	3.450	52.24
N-S PORTHUENEME	0.113	13.004	45.30
E-W PORTHUENEME	0.065	7.819	47.35

Avg=57.94

TABLE 7.2

VALUES OF VEL_{max}/ACC_{max} FOR DEEP SOIL CONDITIONS

excellent agreement between the above value and that determined by Seed et. al [54] 55 in/sec/g.

The value of maximum velocity/maximum acceleration can be used to throw some light on the range of predominant periods of the ground motion. If the ground motion is assumed to be harmonic and peak velocity and peak acceleration develop during the same cycle of ground motion, then

$$T = 2\pi \cdot \frac{\text{maximum velocity}}{\text{maximum acceleration}} \qquad (7.5)$$

where

T = predominant period of the ground.

For the ranges of values given in table 7.2, this relationship gives the following values of periods for the peak motion

max velocity/max acceleration (in/sec/g)	period of motion (sec)
33.76 - 94.40	0.55 - 1.54

which are in excellent agreement with those determined by Seed et al, as follows:

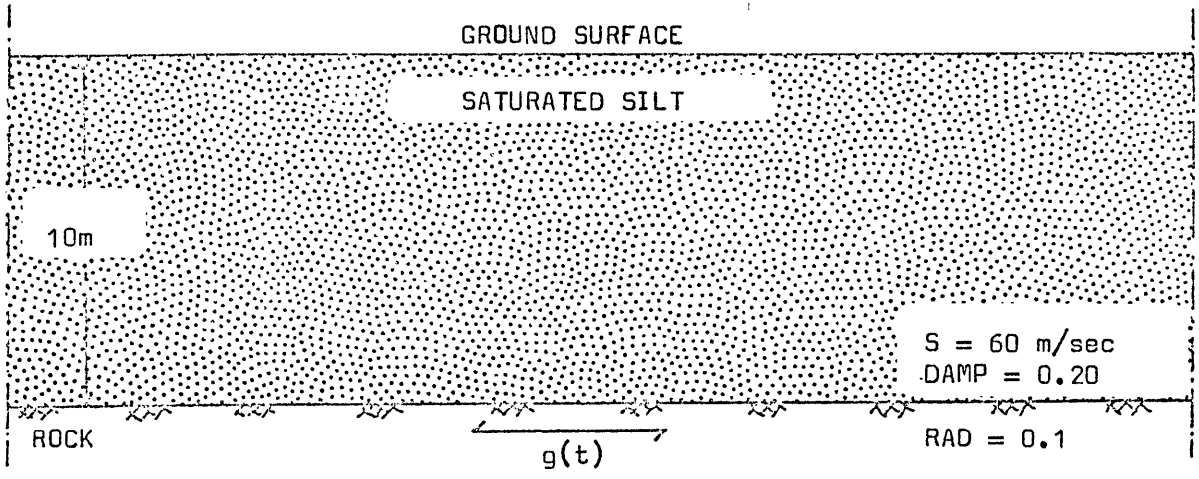
max. velocity/max. acceleration (in/sec/g)	period of motion (sec)
37 - 80	0.61 - 1.3

The degree of agreement between these results, computed from developed technique and field observations, is certainly noteworthy. The results also provide an excellent illustration of the ability of the developed analytical procedure to predict field recorded values based on a series of bedrock motion time histories recorded in the past earthquakes.

7.7. INFLUENCE OF CONFIGURATION OF DEPOSIT ON GROUND RESPONSE

The influence of configuration of deposit underlain by deformable bedrock for a semi-infinite layer can only be discussed in terms of depth to bedrock. It is of interest to study the manner by which frequency characteristics of ground motion are affected by deposits of different depth to bedrock underlain by deformable bedrock. To investigate this problem, five deposits of saturated silt, ranging in total thickness from 15m to 30m, with shear wave velocities of 60 m/sec, hysteretic damping ratio of 20% subjected at the bedrock level to Parkfield-2, were analyzed. Computed surface acceleration, velocity and displacement time histories are shown in figs. 7.47a,b,c through 7.51a,b,c and surface acceleration, velocity and displacement response spectrum are shown in figs. 7.47d,e,f to 7.51d,e,f.

Figs. 7.47d through 7.51d show that frequency characteristics of output motion and amplitude of maximum spectral acceleration changes considerably as the thickness increases. This is expected because, as fundamental periods of the deposits which range in between 0.66 sec. to 2 sec. moves away from the predominant period of base motion 0.6 sec, the condition of resonance is violated; thus the layer with fundamental period of 2 second has developed the lowest response and that of 0.66 secs.



RESPONSE OF HYSTERETIC DEPOSIT UNDERLAIN BY DEFORMABLE BEDROCK

SCHEMATIC SOIL PROFILE FOR SITE NO 7.23

FIG. 7.47

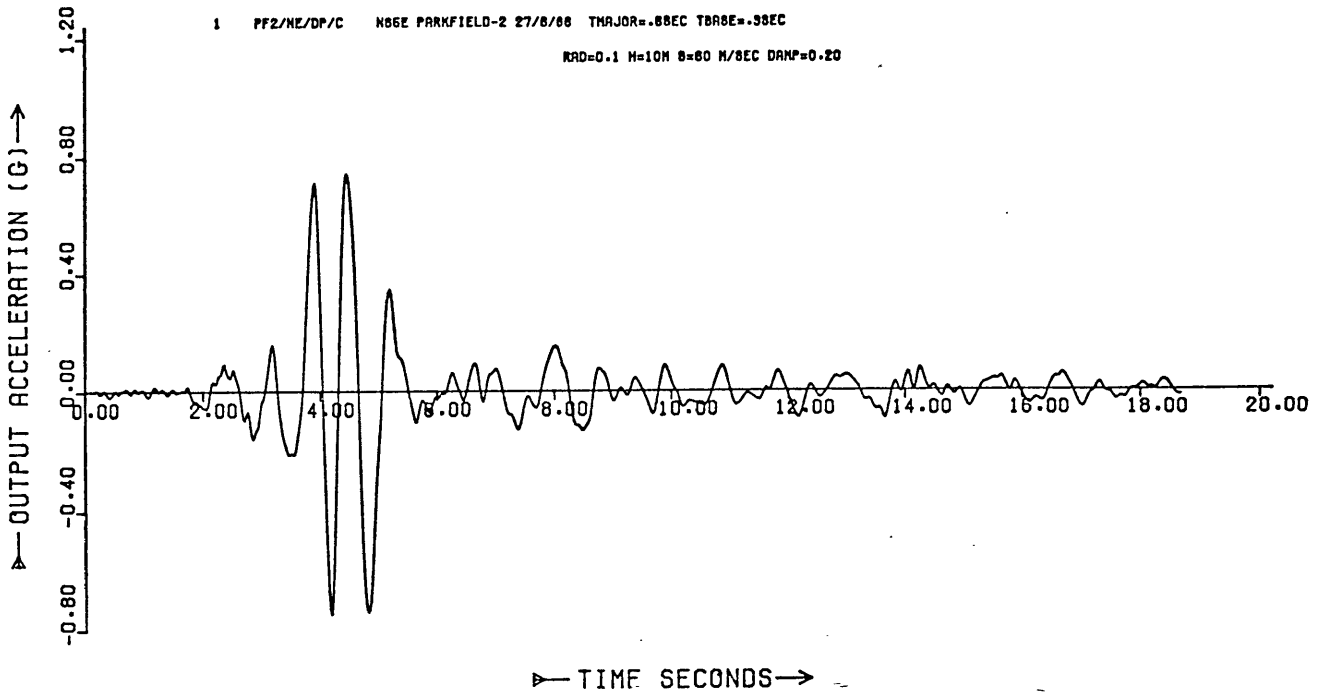


FIG.7.47a COMPUTED GROUND SURFACE ACCELERATION TIME HISTORY AT SITE NO7.23

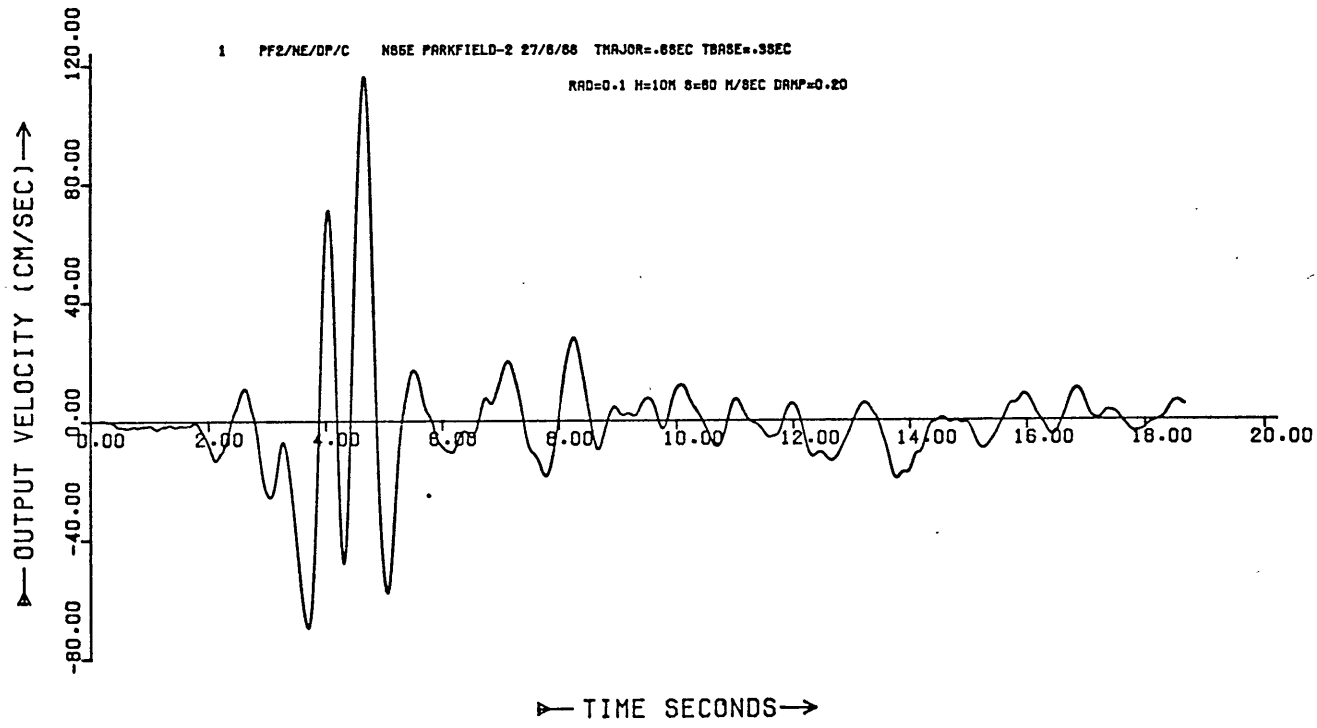


FIG.7.47b COMPUTED GROUND SURFACE VELOCITY TIME HISTORY AT SITE NO 7.23

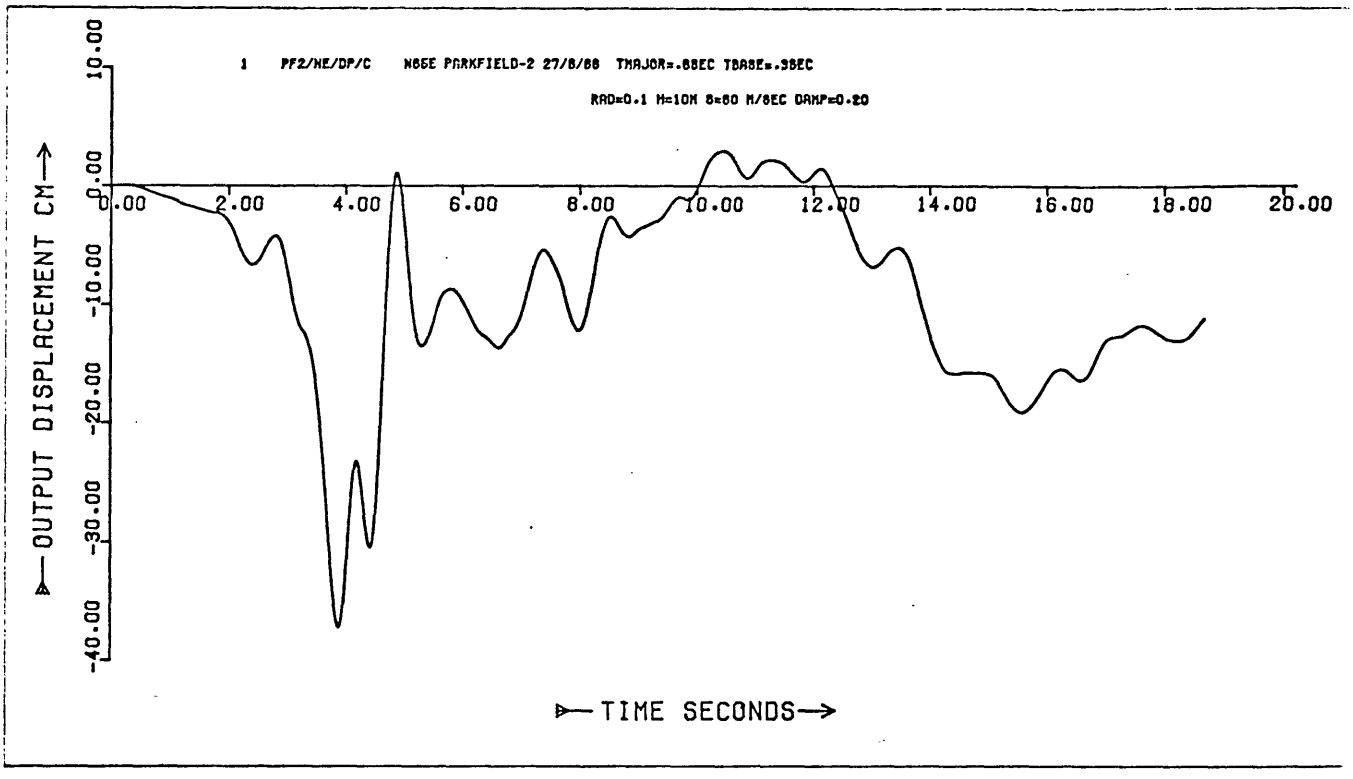


FIG.7.47c COMPUTED GROUND SURFACE DISPLACEMENT TIME HISTORY AT SITE NO 7.23

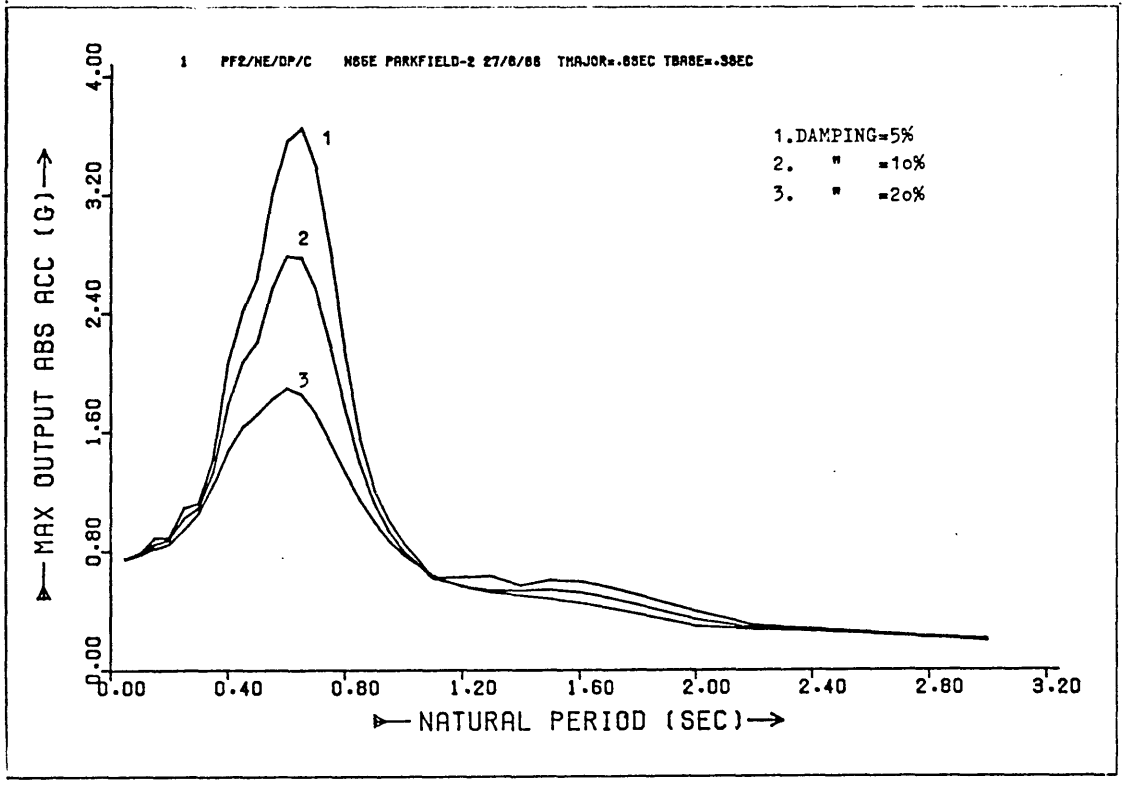


FIG.7.47d COMPUTED GROUND SURFACE ACCELERATION RESPONSE SPECTRA AT SITE NO 7.23

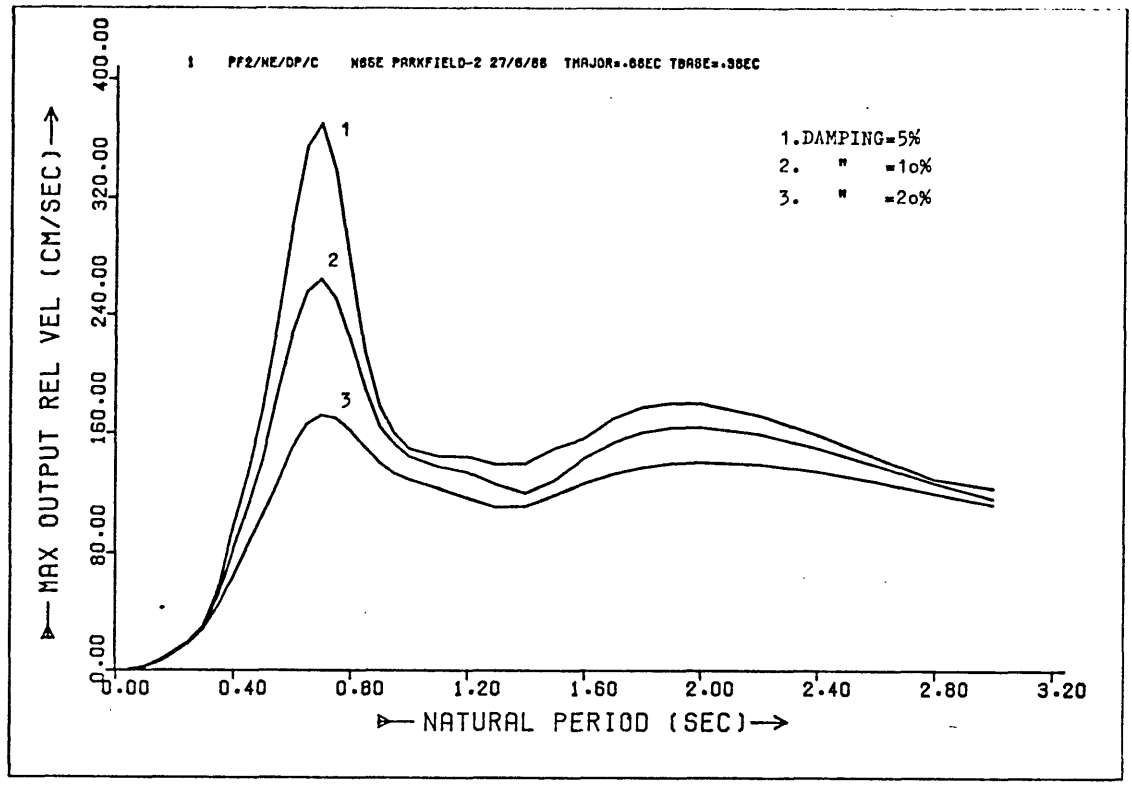


FIG.7.47e COMPUTED GROUND SURFACE VELOCITY RESPONSE SPECTRA AT SITE NO 7.23

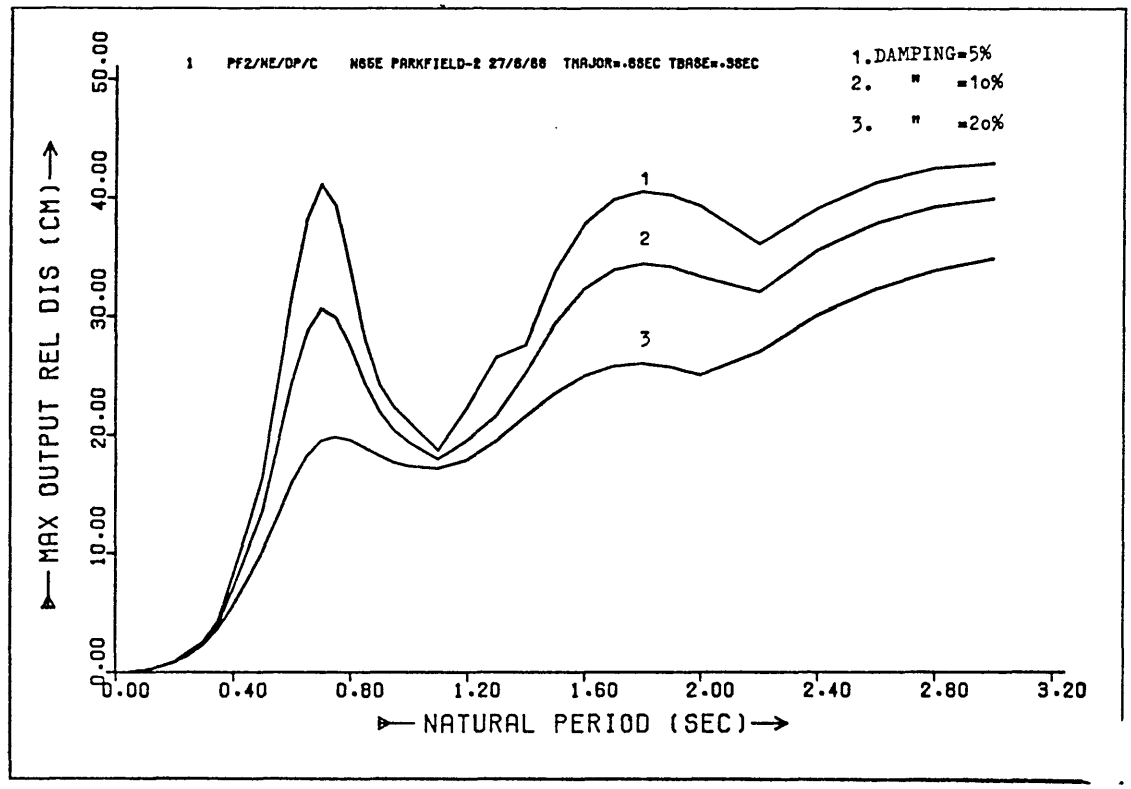
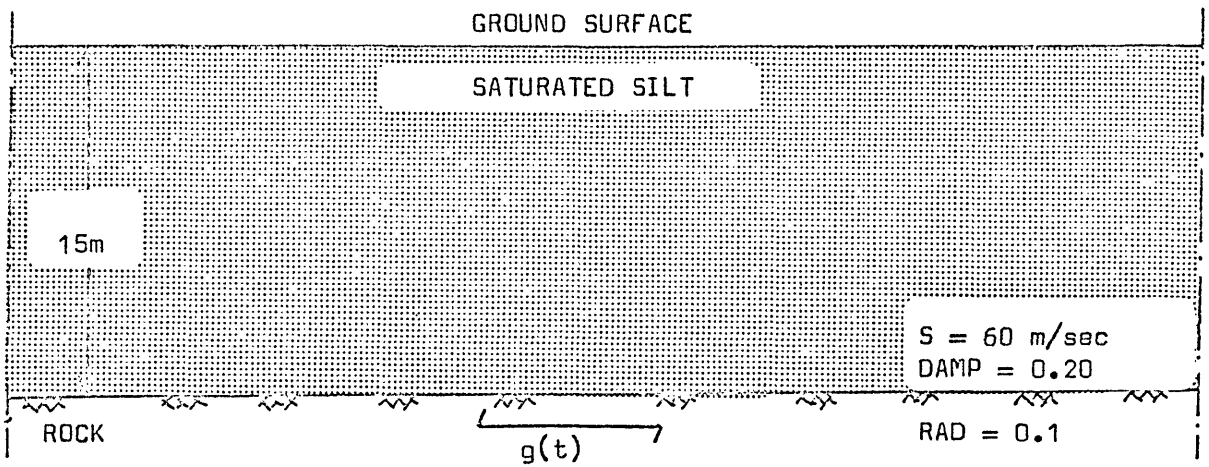


FIG.7.47f COMPUTED GROUND SURFACE DISPLACEMENT RESPONSE SPECTRA AT SITE NO 7.23



RESPONSE OF HYSTERETIC DEPOSIT UNDERLAIN BY DEFORMABLE BEDROCK

SCHEMATIC SOIL PROFILE FOR SITE NO 7.24

FIG. 7.48

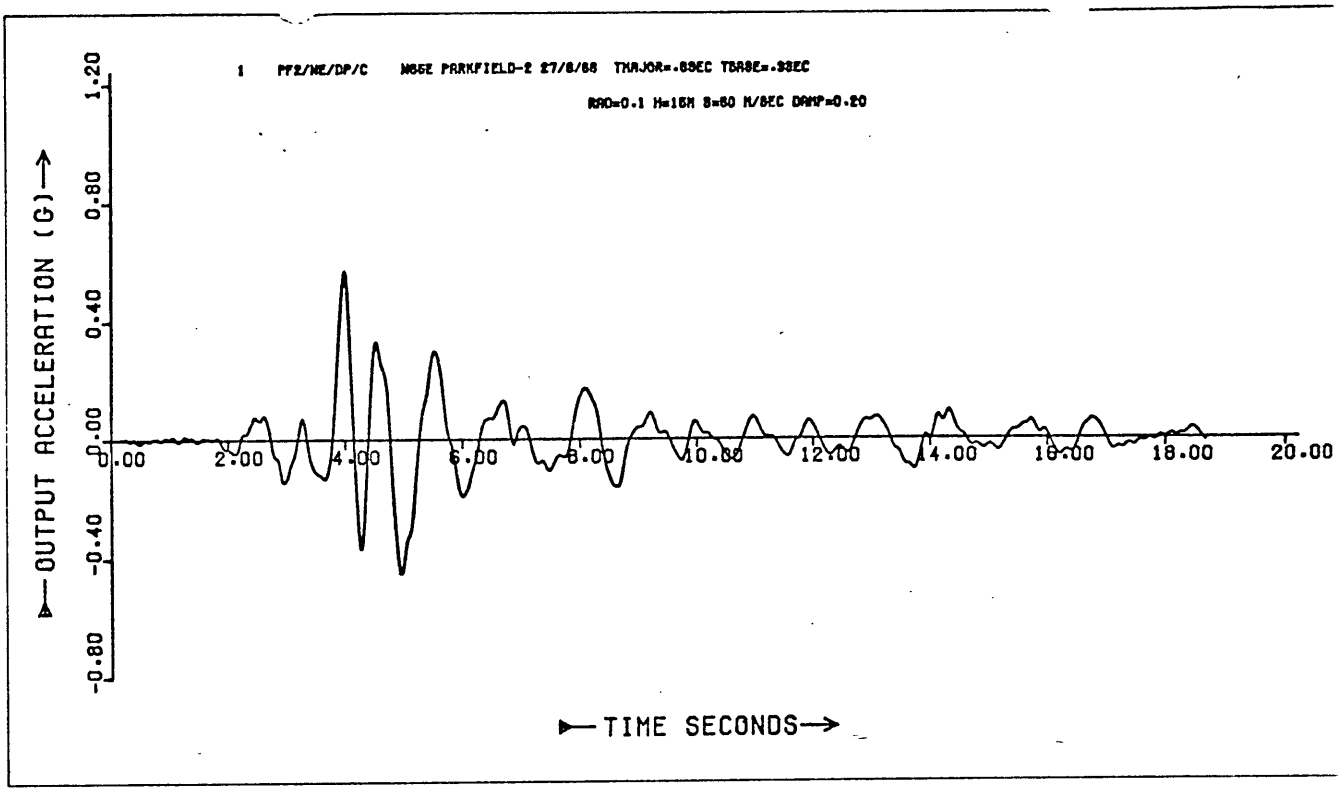


FIG. 7.48a COMPUTED GROUND SURFACE ACCELERATION TIME HISTORY AT SITE NO 7.24

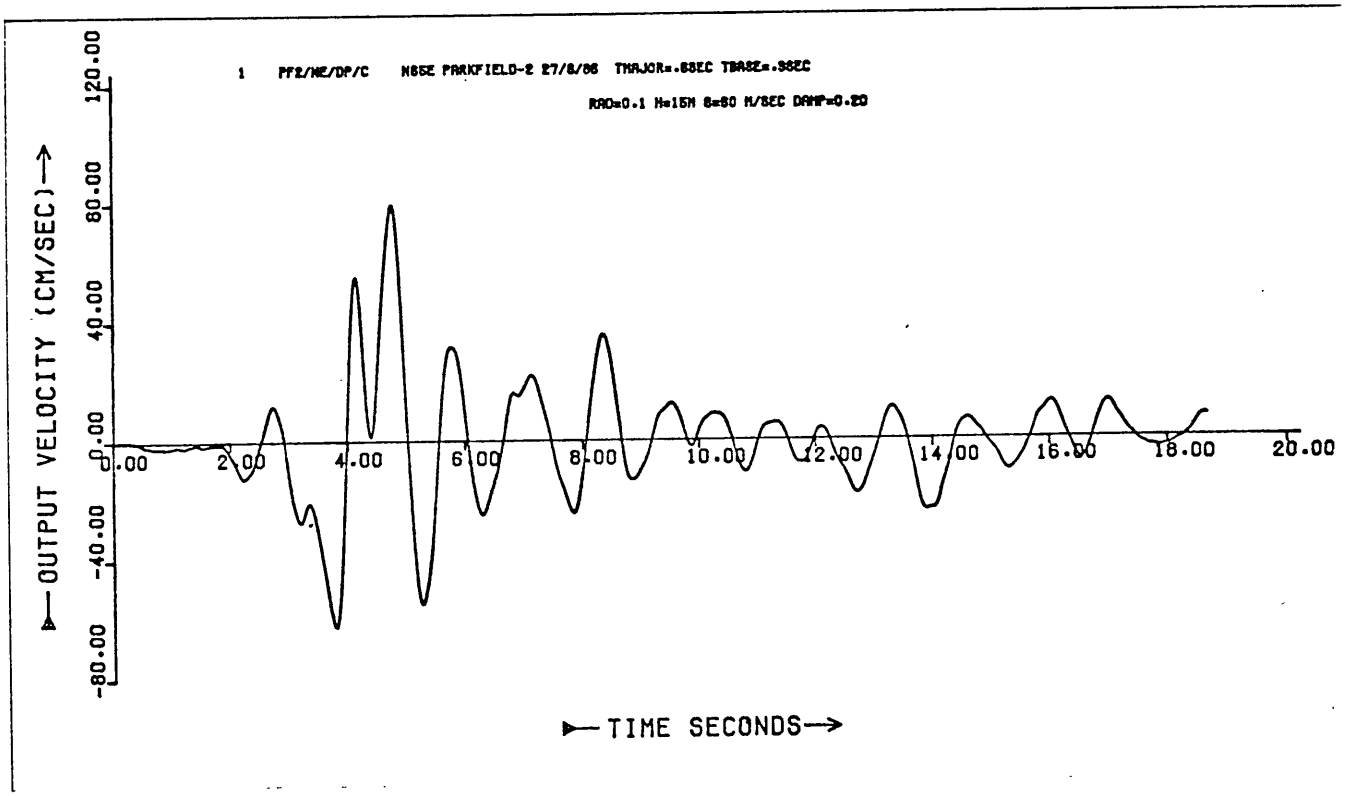


FIG. 7.48b COMPUTED GROUND SURFACE VELOCITY TIME HISTORY AT SITE NO 7.24

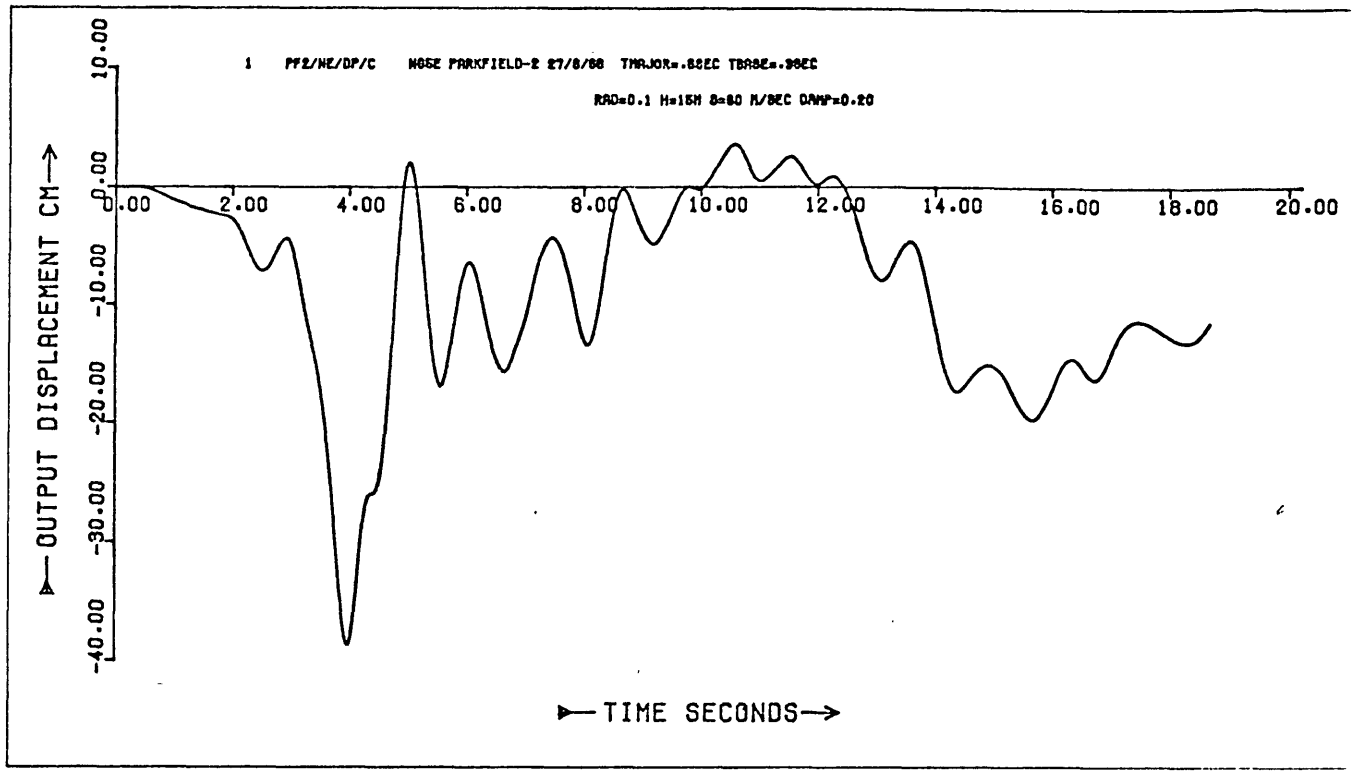


FIG.7.48c COMPUTED GROUND SURFACE DISPLACEMENT TIME HISTORY AT SITE NO 7.24

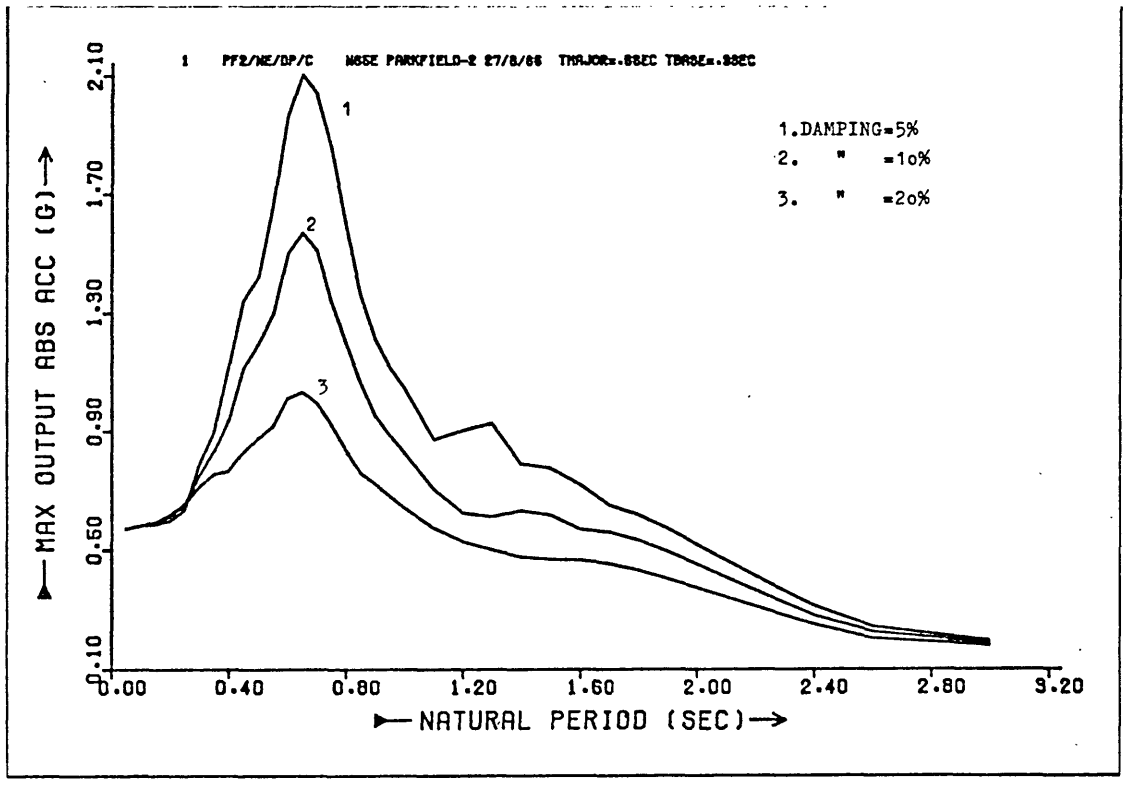


FIG. 7.48d COMPUTED GROUND SURFACE ACCELERATION RESPONSE SPECTRA AT SITE NO 7.24

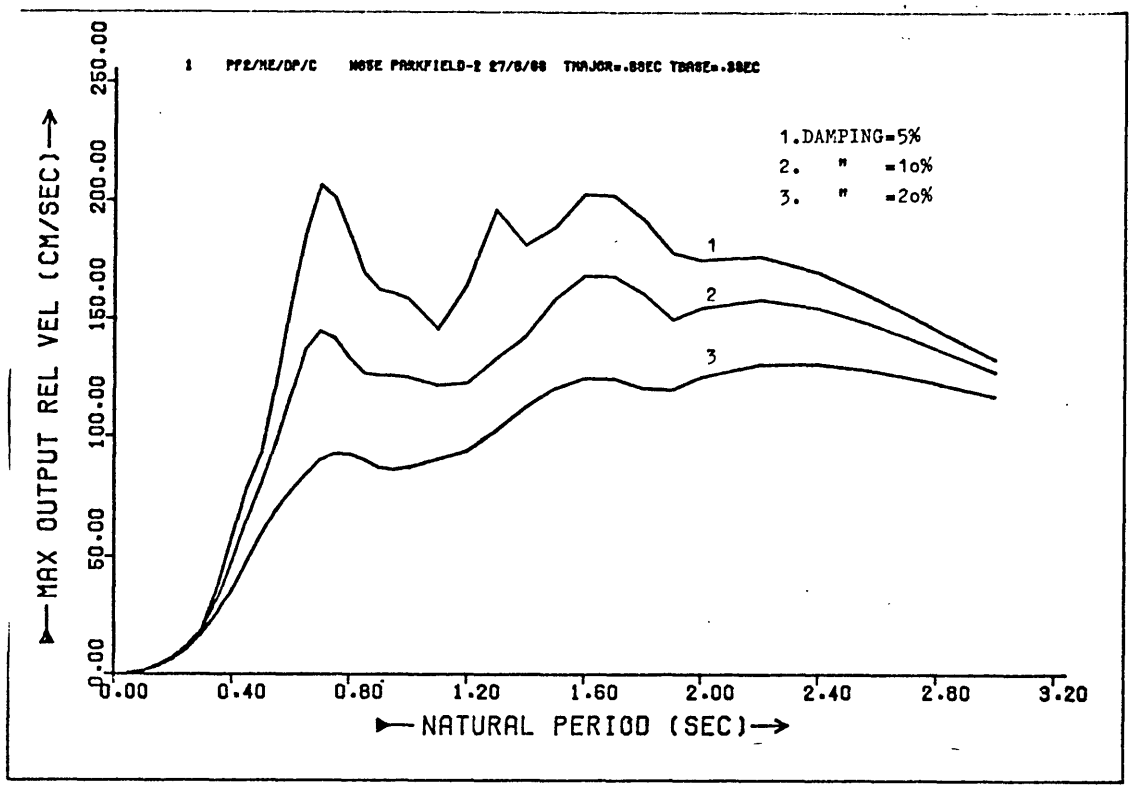


FIG.7.48e COMPUTED GROUND SURFACE VELOCITY RESPONSE SPECTRA AT SITE NO 7.24

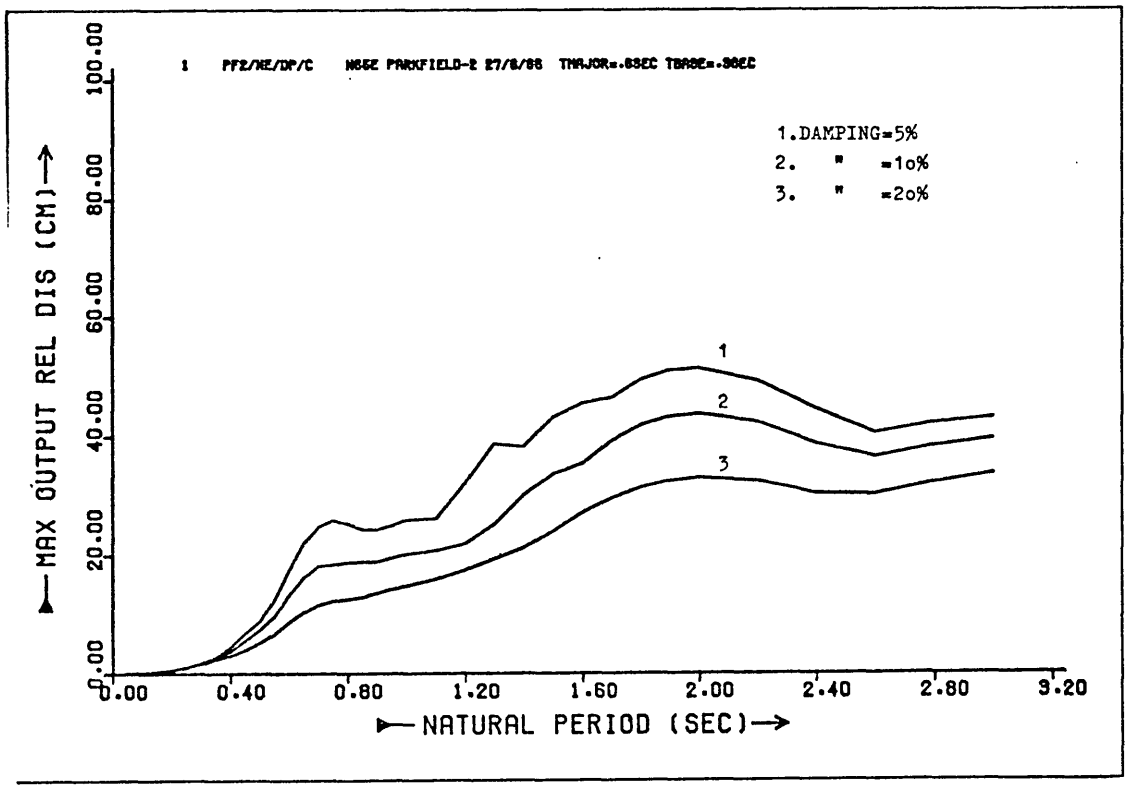
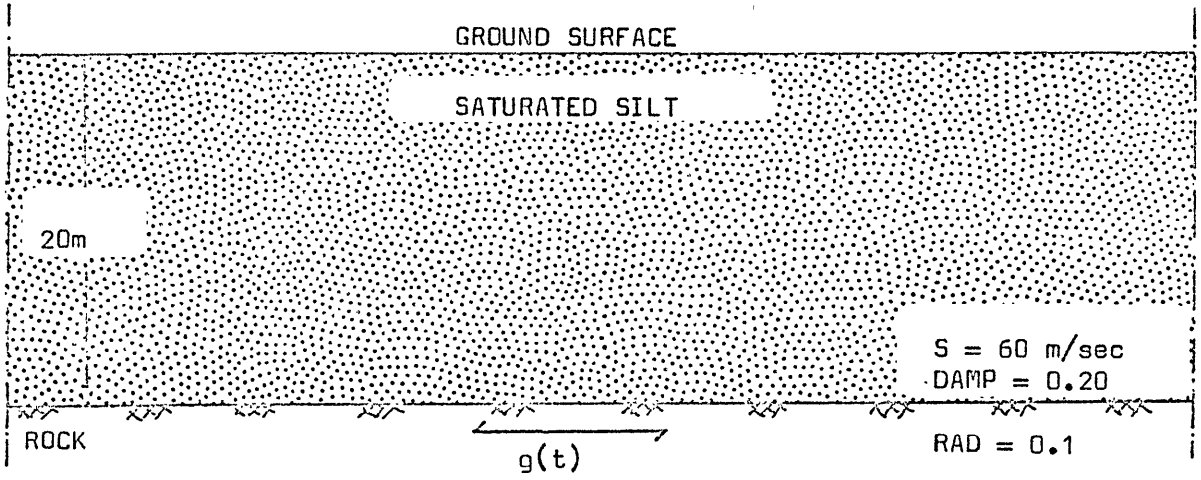


FIG.7.48f COMPUTED GROUND SURFACE DISPLACEMENT RESPONSE SPECTRA AT SITE NO 7.24



RESPONSE OF HYSTERETIC DEPOSIT UNDERLAIN BY DEFORMABLE BEDROCK

SCHEMATIC SOIL PROFILE FOR SITE NO 7.25

FIG. 7.49

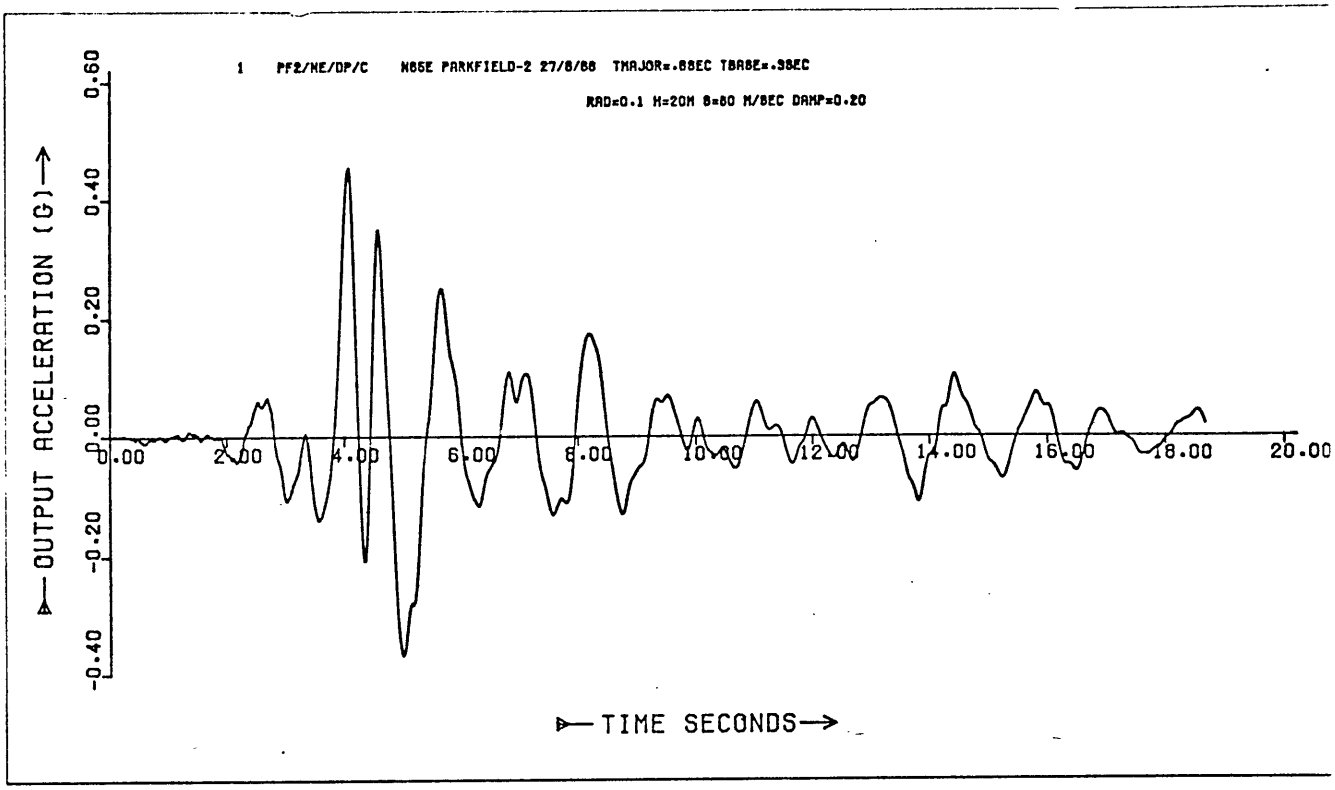


FIG. 7.49a COMPUTED GROUND SURFACE ACCELERATION TIME HISTORY AT SITE NO 7.25

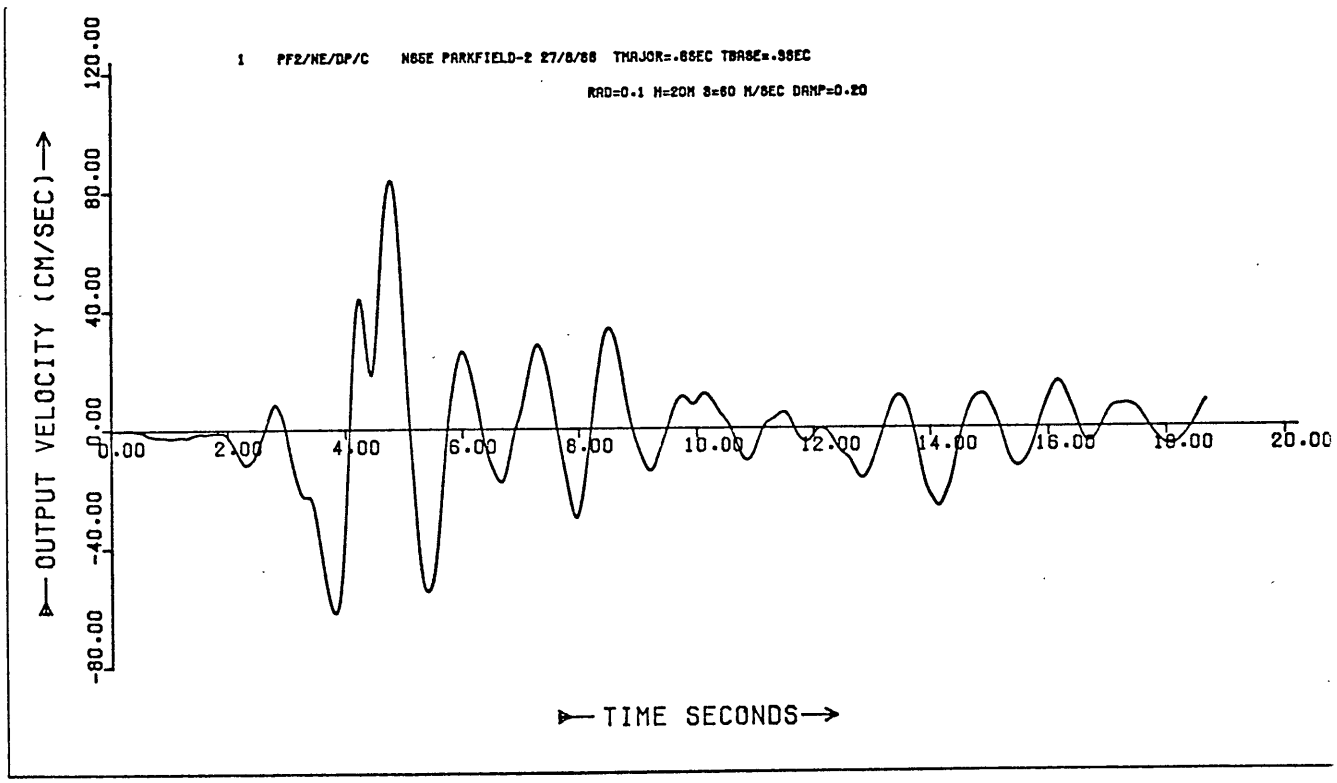


FIG.7.49b COMPUTED GROUND SURFACE VELOCITY TIME HISTORY AT SITE NO 7.25

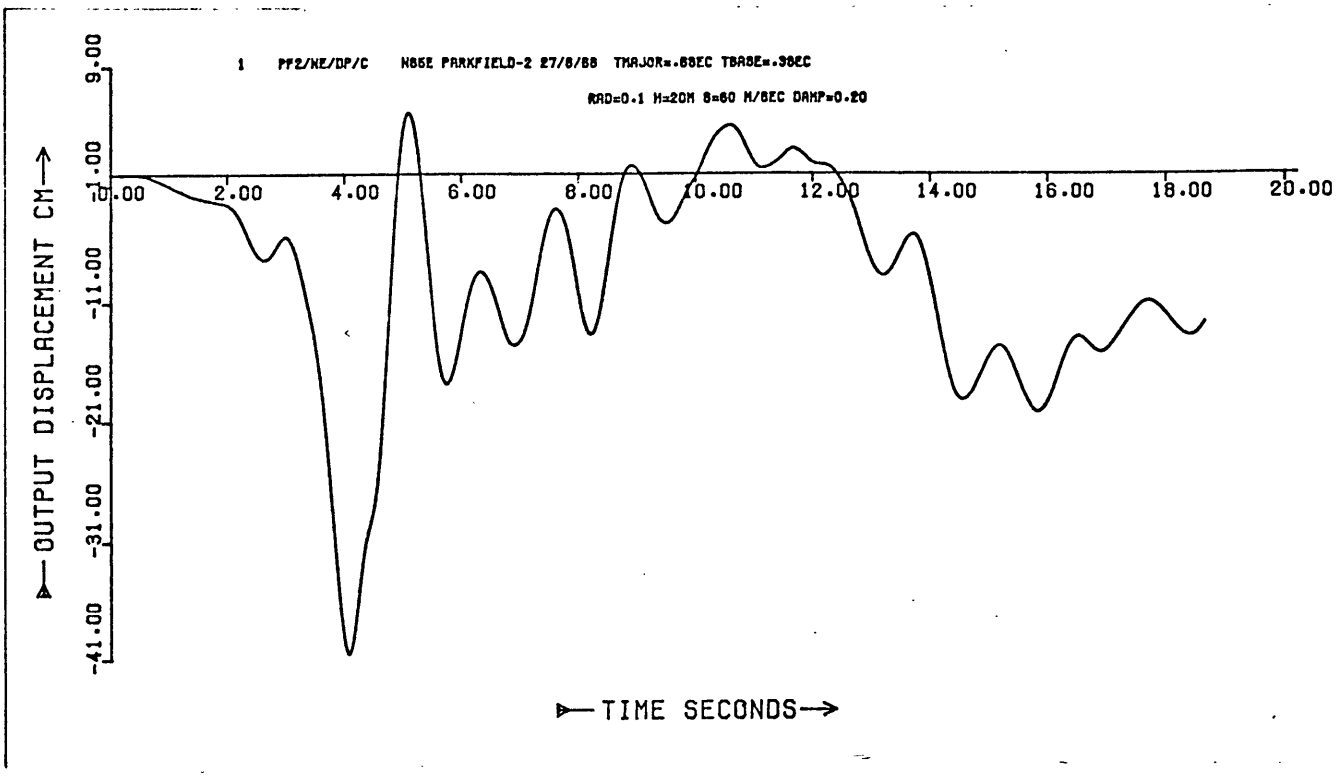


FIG.7.49c COMPUTED GROUND SURFACE DISPLACEMENT TIME HISTORY AT SITE NO 7.25

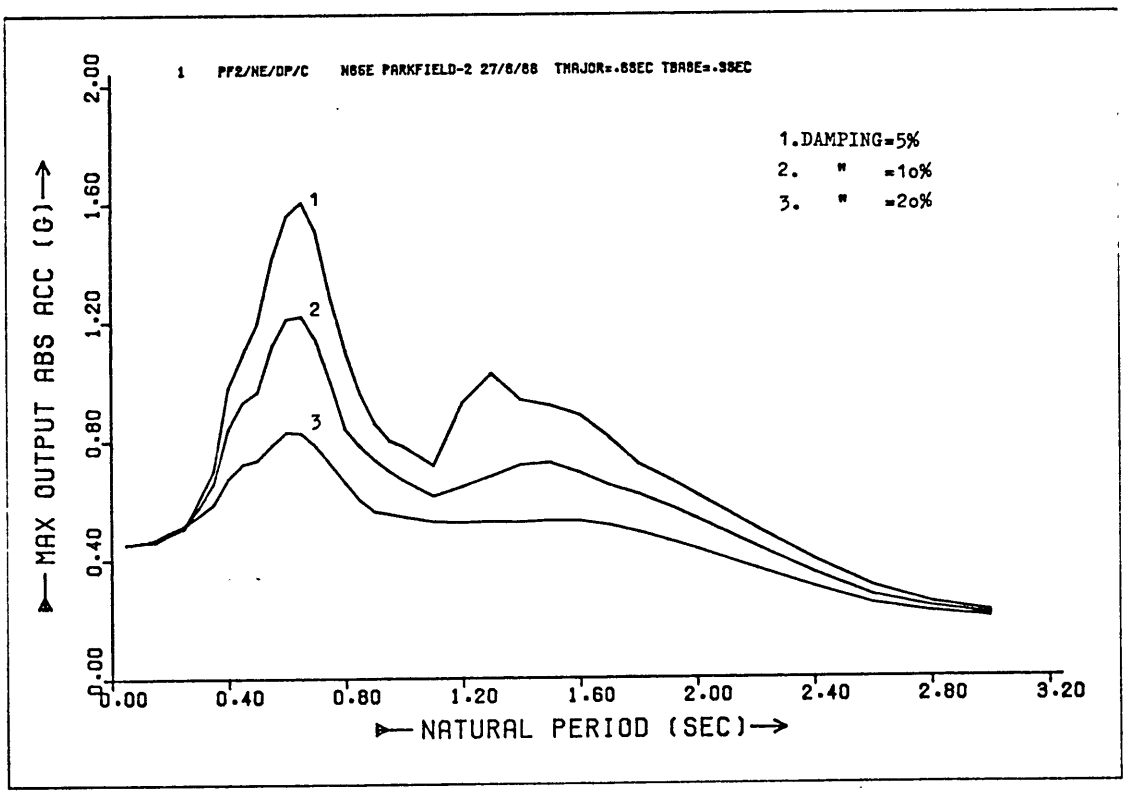


FIG.7.49d COMPUTED GROUND SURFACE ACCELERATION RESPONSE SPECTRA AT SITE NO 7.25

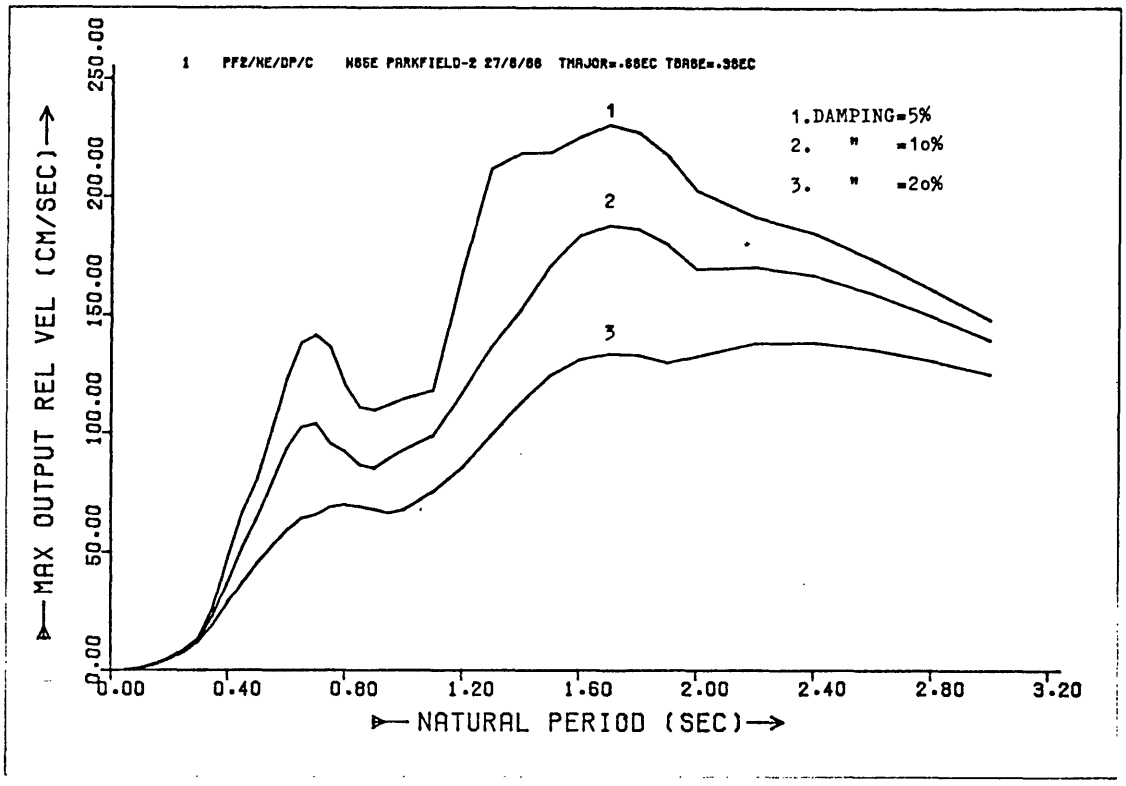


FIG. 7.49e COMPUTED GROUND SURFACE VELOCITY RESPONSE SPECTRA AT SITE NO 7.25

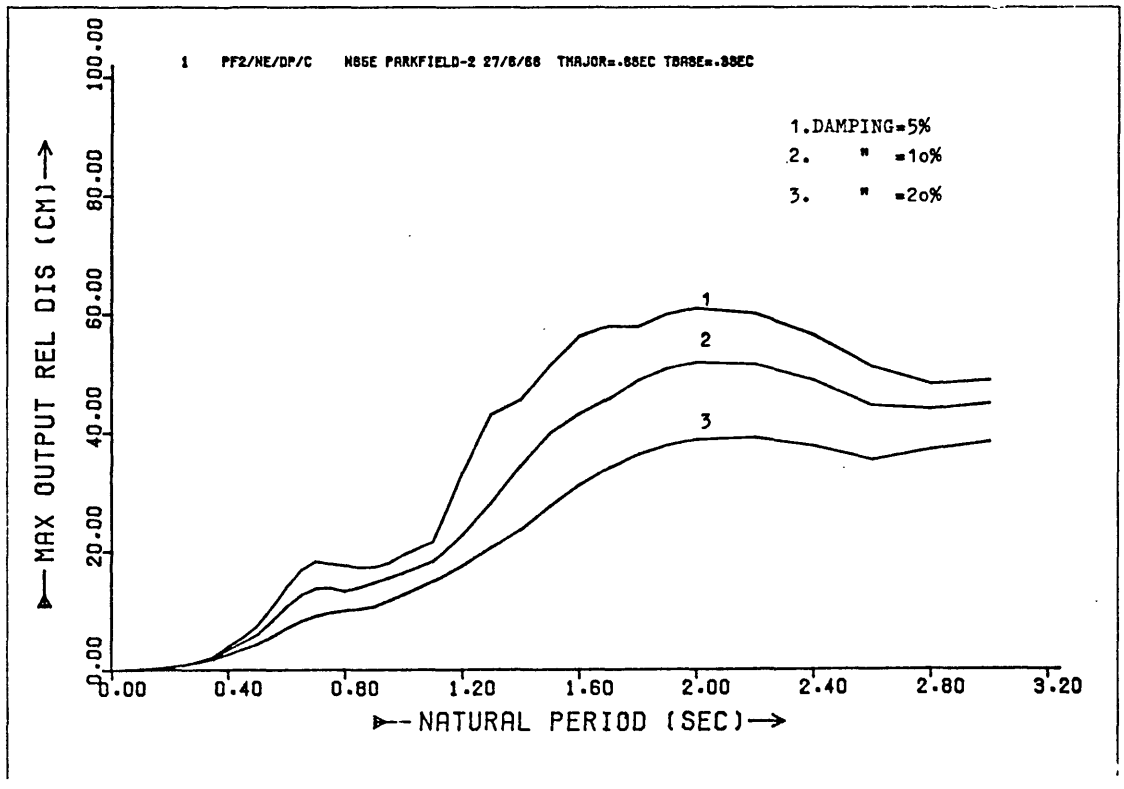
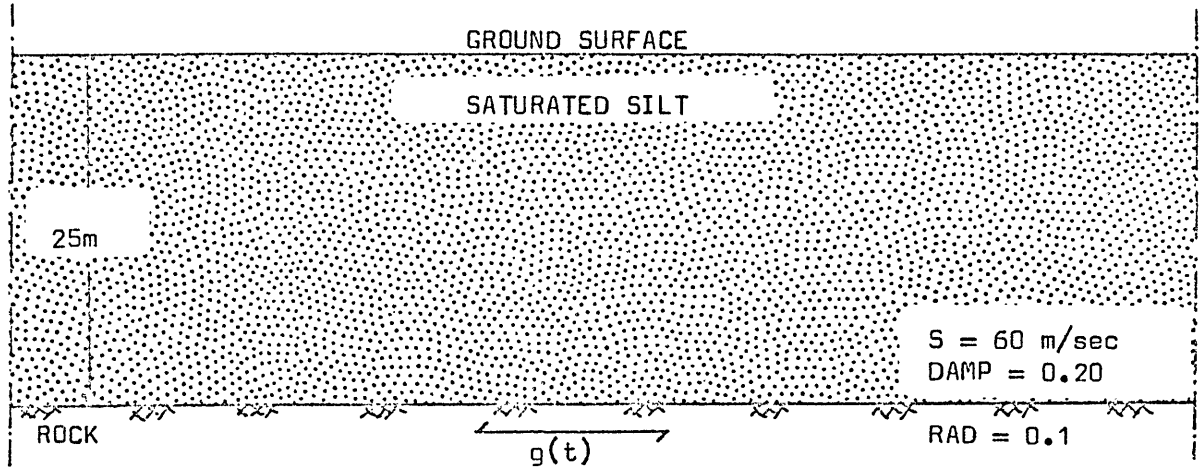


FIG. 7.49f COMPUTED GROUND SURFACE DISPLACEMENT RESPONSE SPECTRA AT SITE NO 7.25



RESPONSE OF HYSTERETIC DEPOSIT UNDERLAIN BY DEFORMABLE BEDROCK

SCHEMATIC SOIL PROFILE FOR SITE NO 7.26

FIG. 7.50

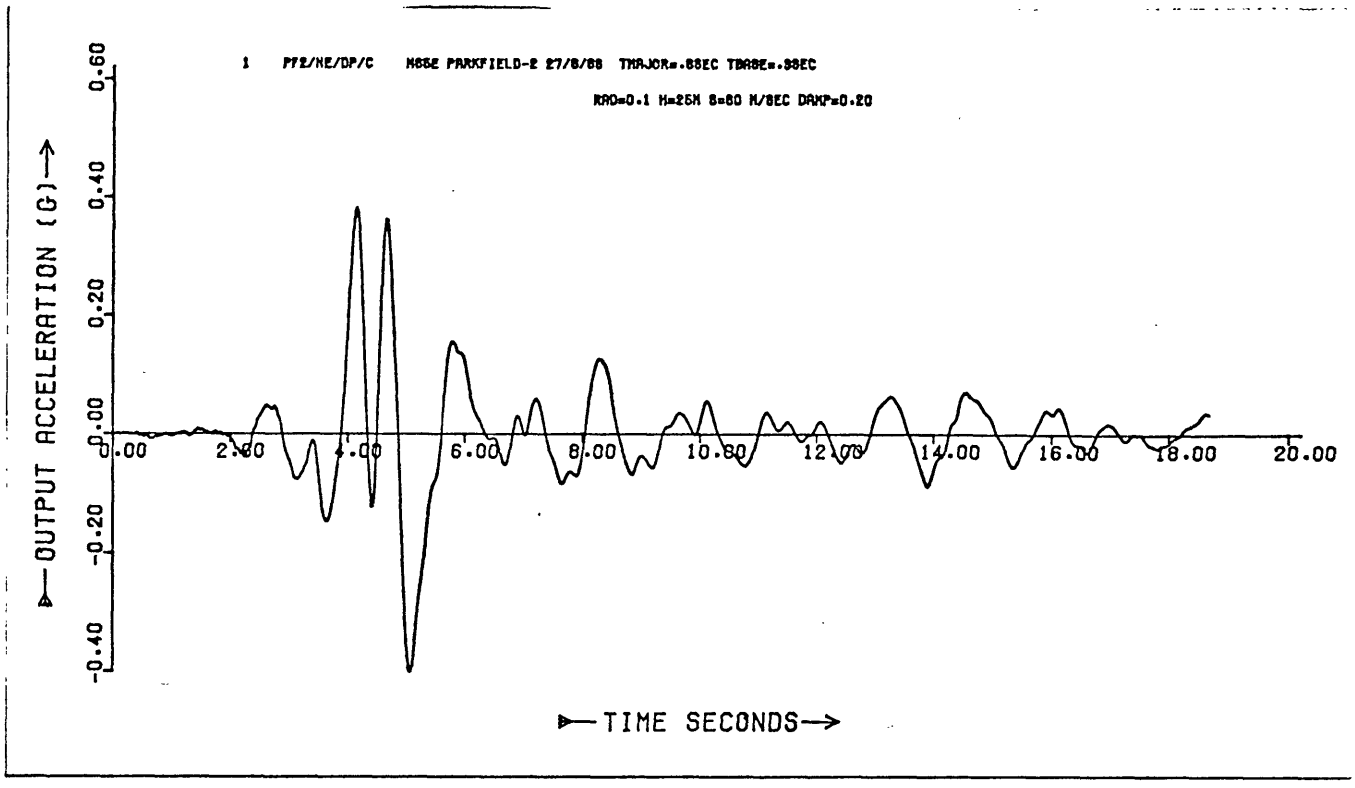


FIG. 7.5oa COMPUTED GROUND SURFACE ACCELERATION TIME HISTORY AT SITE NO 7.26

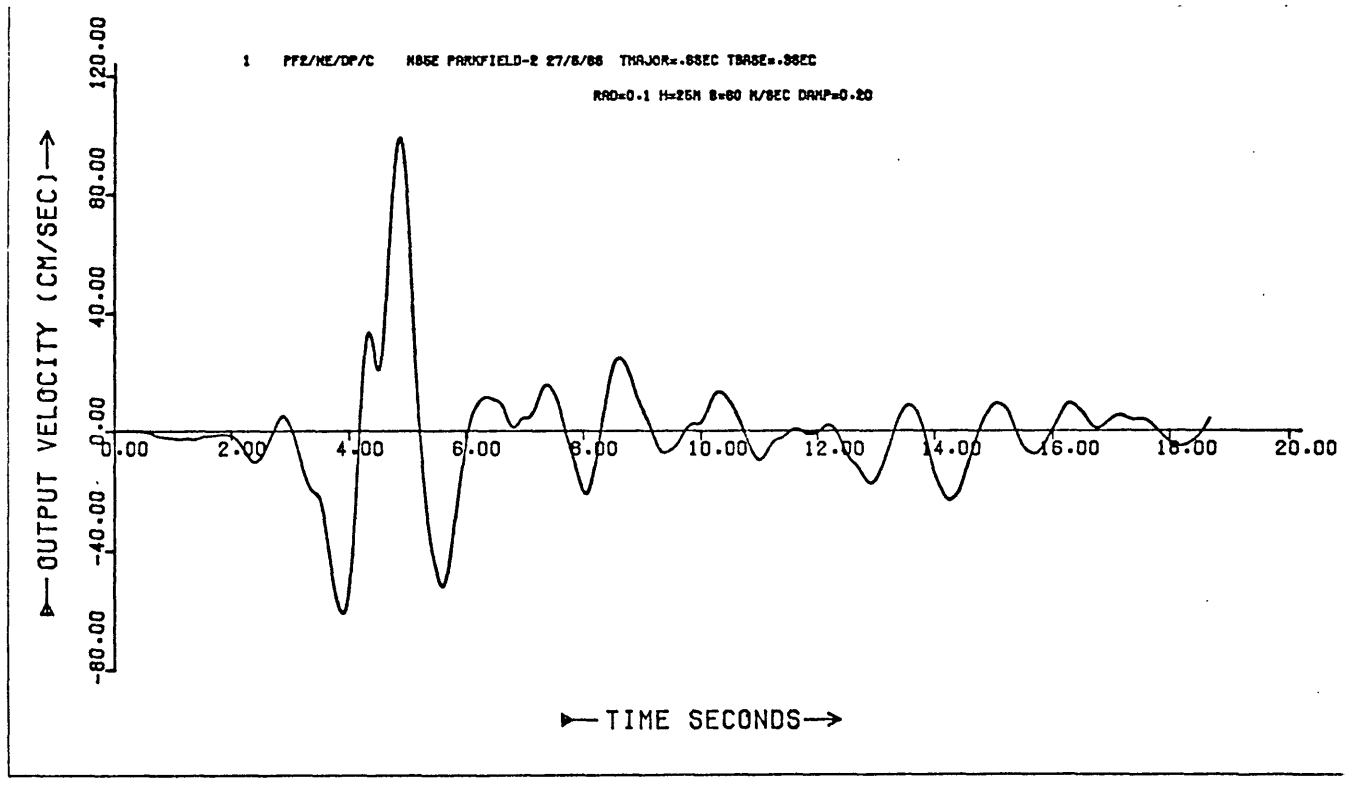


FIG. 7.5ob COMPUTED GROUND SURFACE VELOCITY TIME HISTORY AT SITE NO 7.26

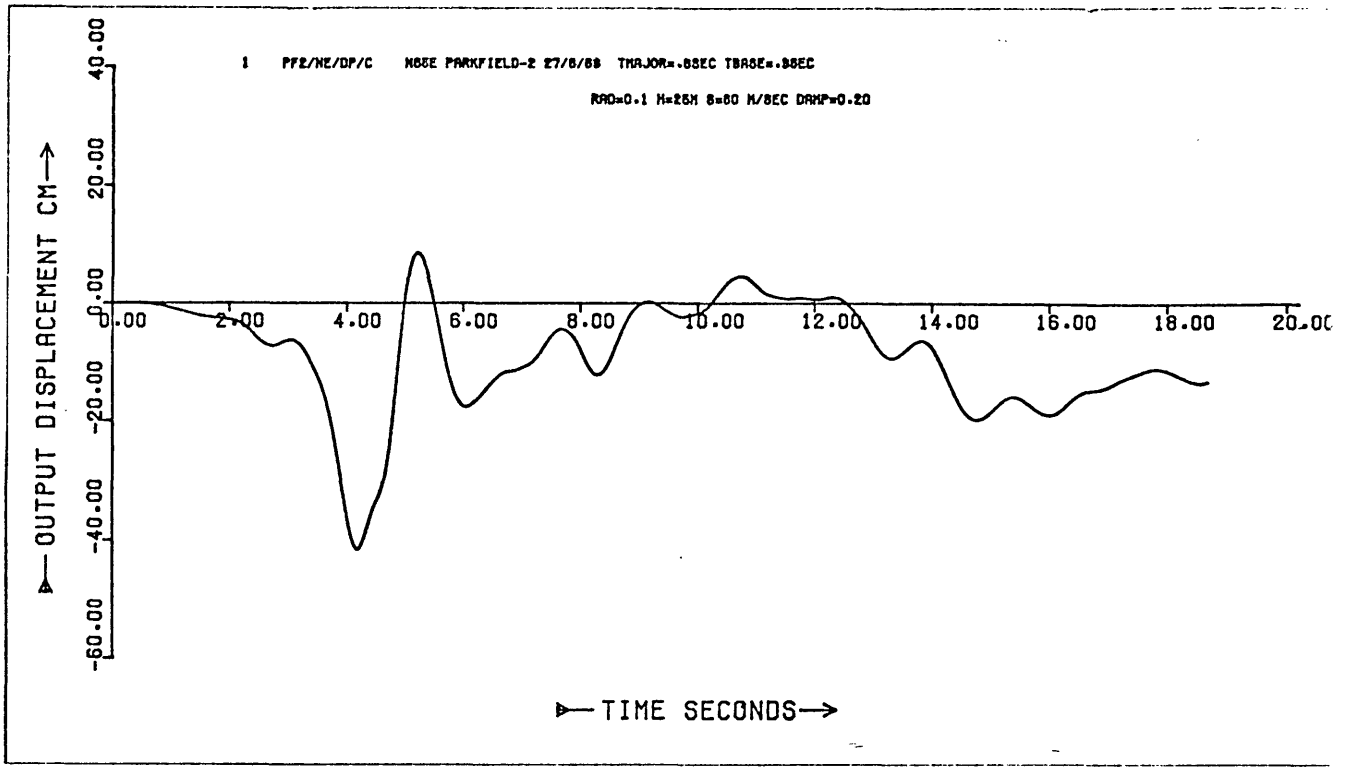


FIG.7.5oc COMPUTED GROUND SURFACE DISPLACEMENT TIME HISTORY AT SITE NO 7.27

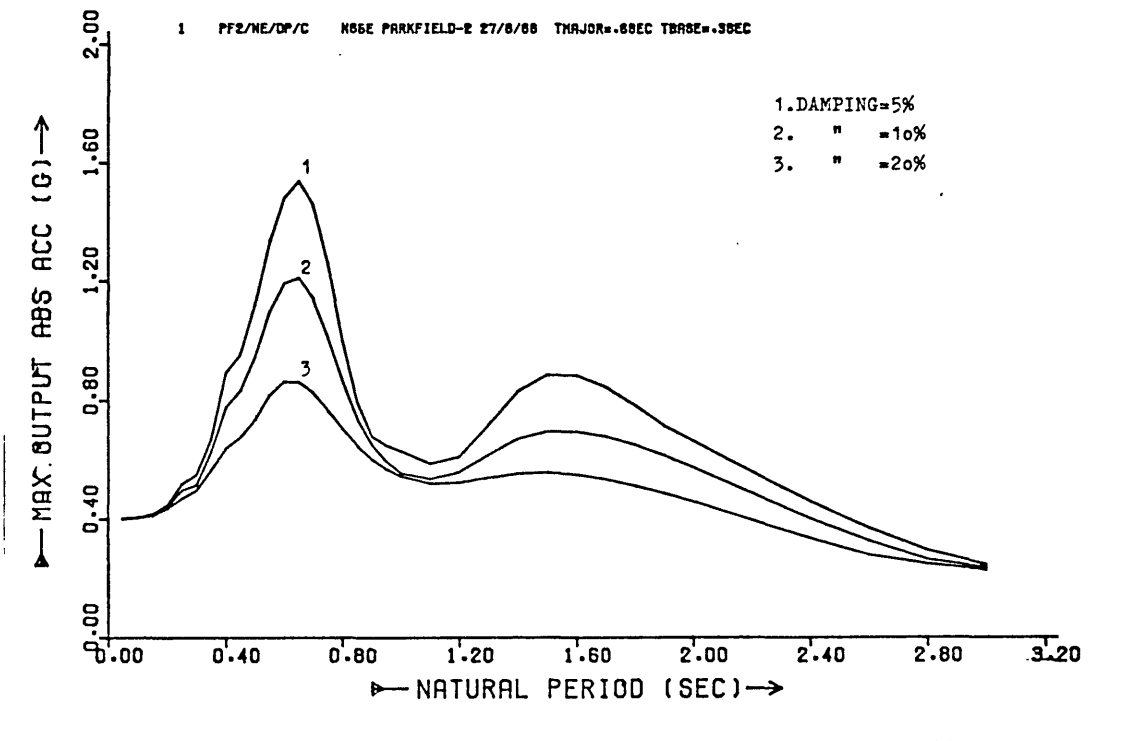


FIG7.5od COMPUTED GROUND SURFACE ACCELERATION RESPONSE SPECTRA AT SITE NO7.27

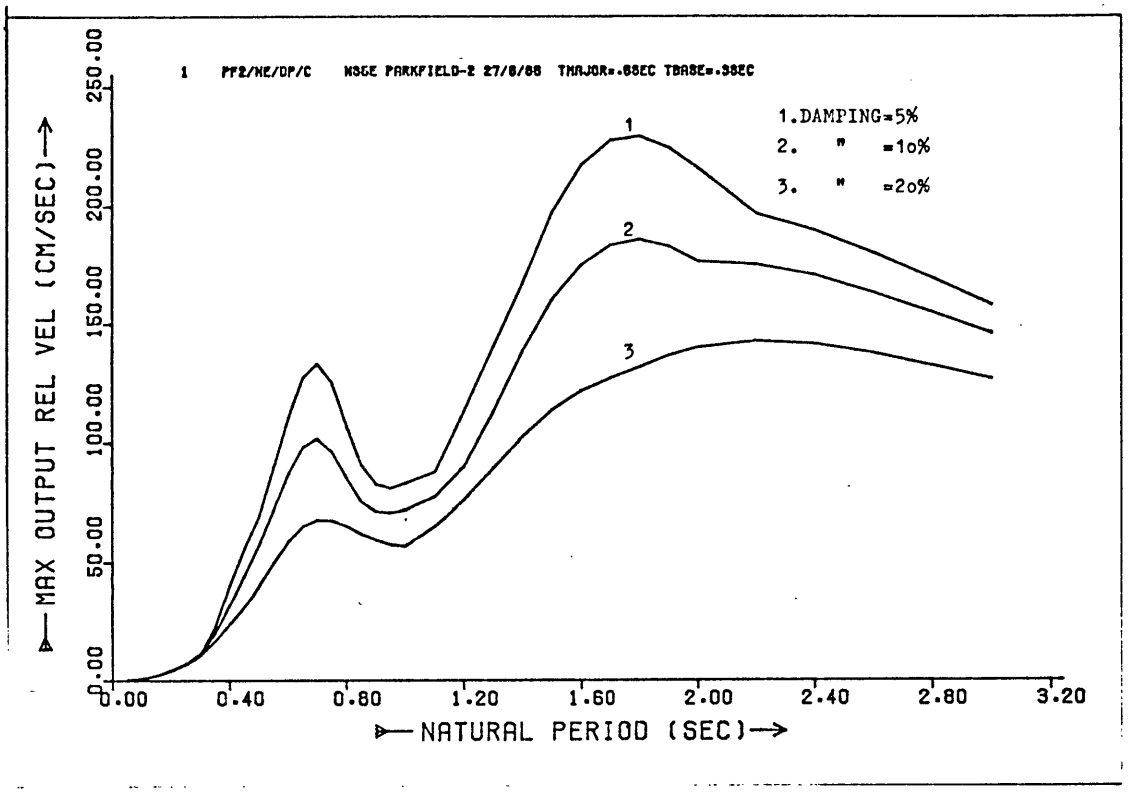


FIG7.5oe COMPUTED GROUND SURFACE VELOCITY RESPONSE SPECTRA AT SITE NO 7.27

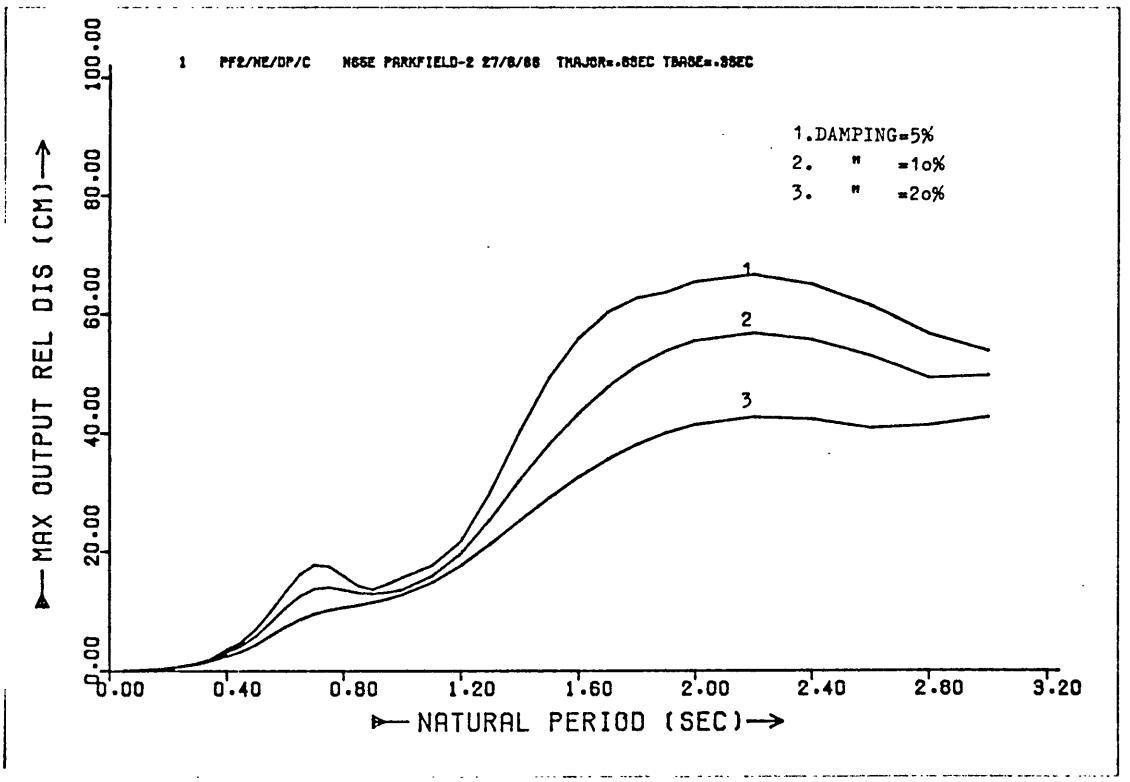
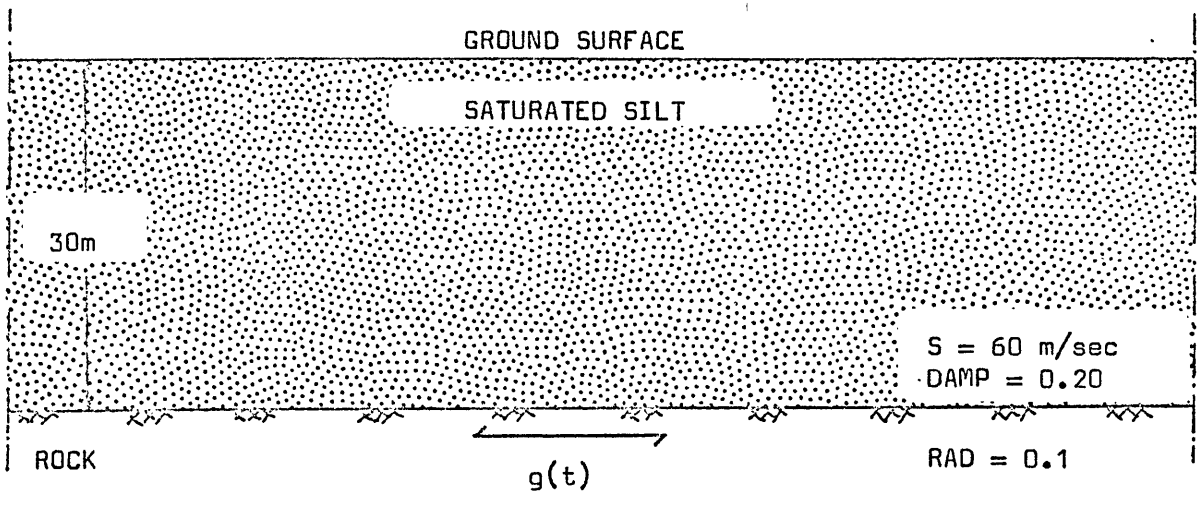


FIG.7.5of COMPUTED GROUND SURFACE DISPLACEMENT RESPONSE SPECTRA AT SITE NO 7.27



RESPONSE OF HYSTERETIC DEPOSIT UNDERLAIN BY DEFORMABLE BEDROCK

SCHEMATIC SOIL PROFILE FOR SITE NO 7.28

FIG. 7.51

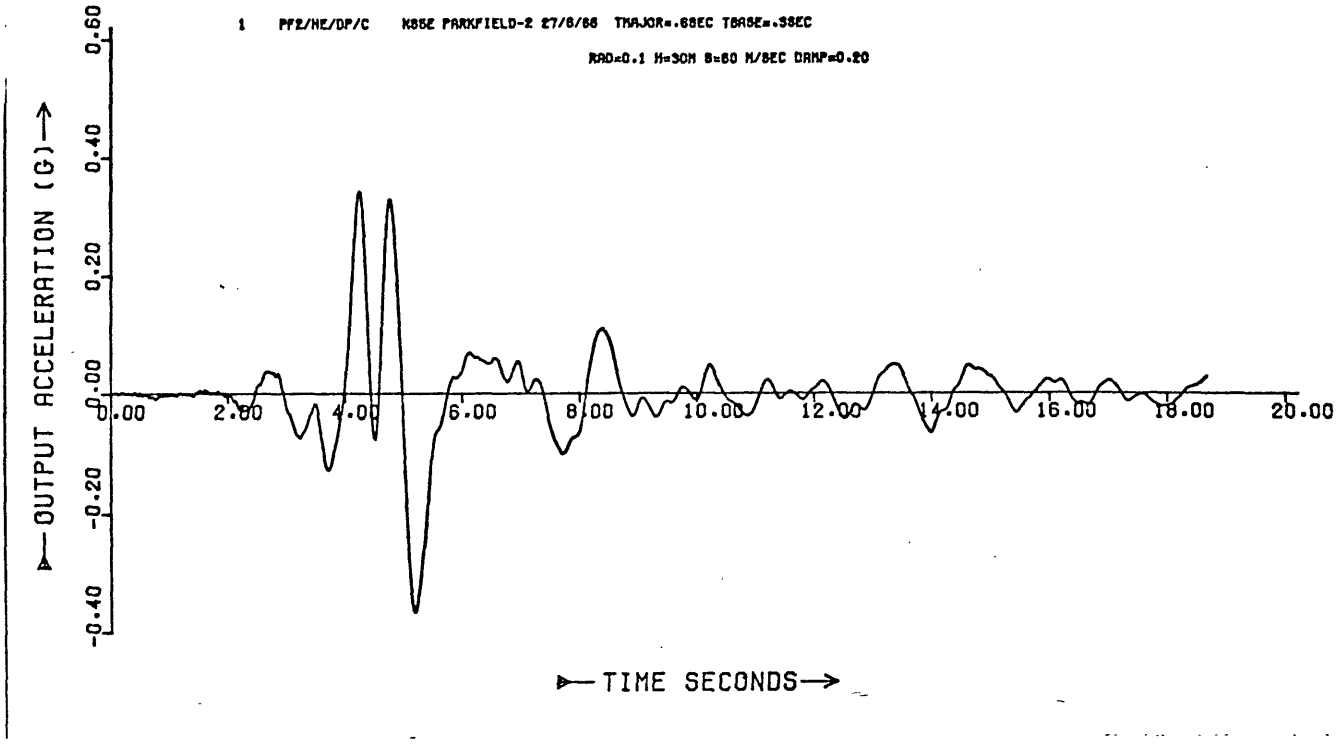


FIG7.51a COMPUTED GROUND SURFACE ACCELERATION TIME HISTORY AT SITE NO 7.28

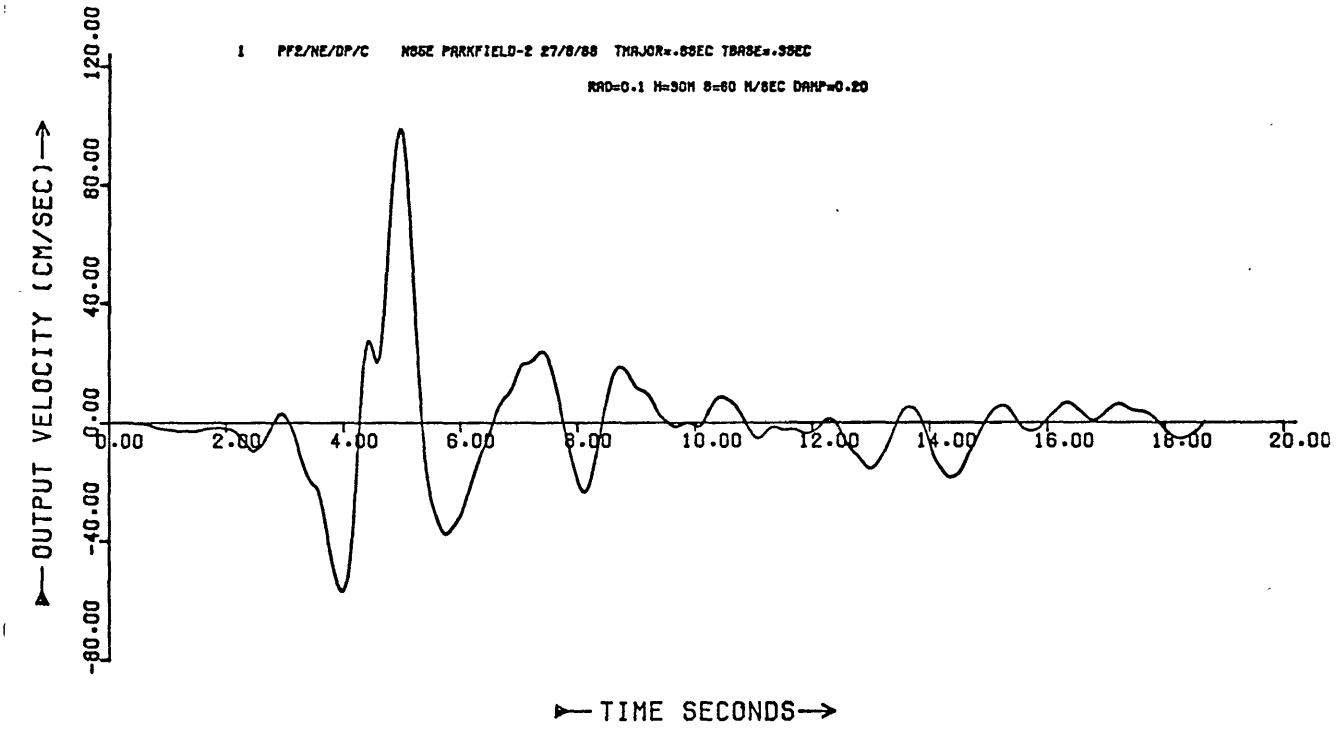


FIG.7.51b COMPUTED GROUND SURFACE VELOCITY TIME HISTORY AT SITE NO 7.28

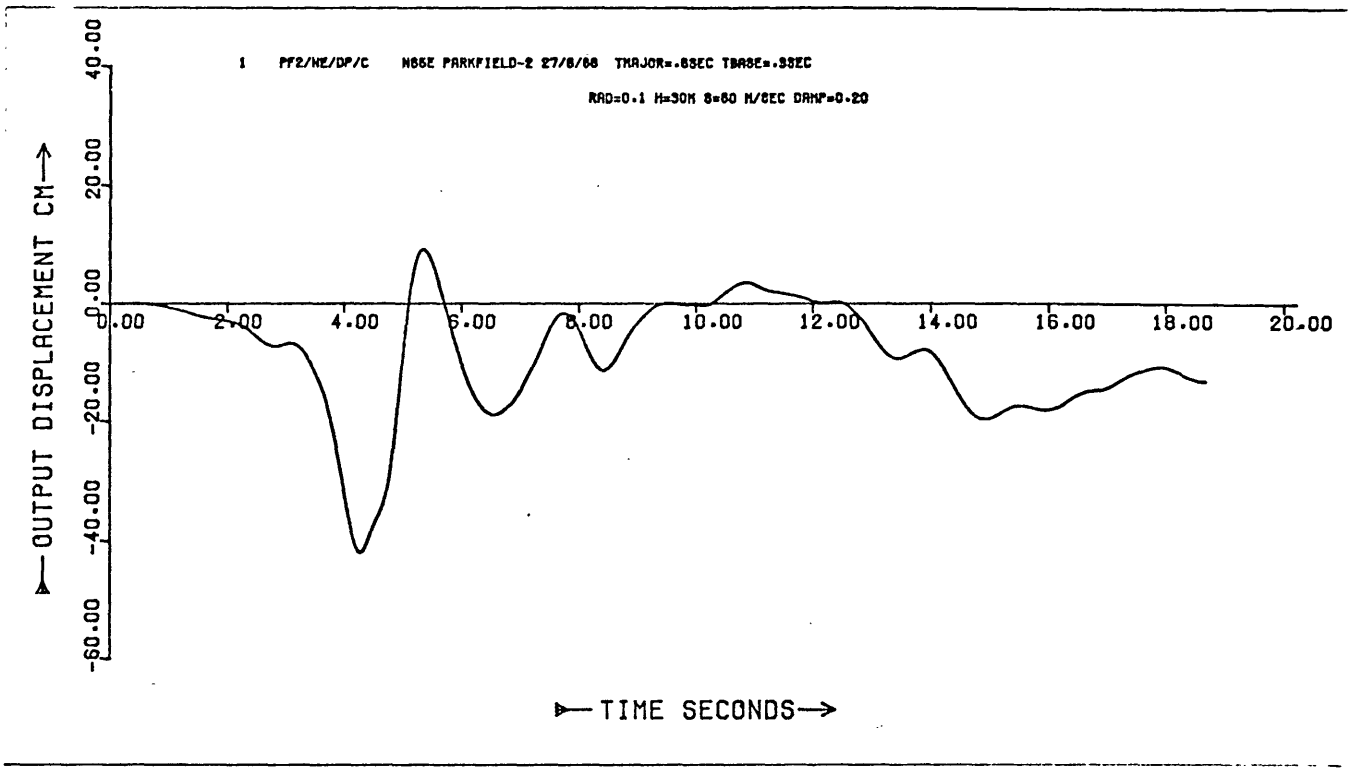


FIG.7.51cCOMPUTED GROUND SURFACE DISPLACEMENT TIME HISTORY AT SITE NO 7.28

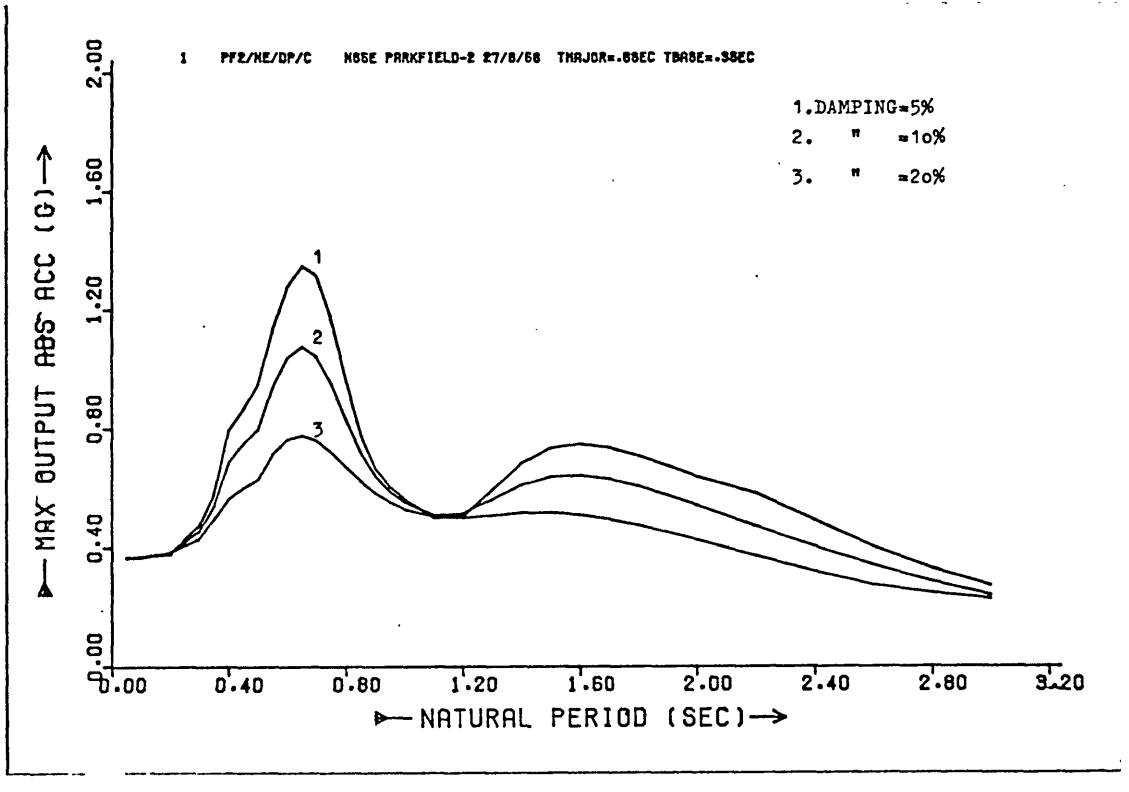


FIG7.51d COMPUTED GROUND SURFACE ACCELERATION RESPONSE SPECTRA AT SITE NO 7.28

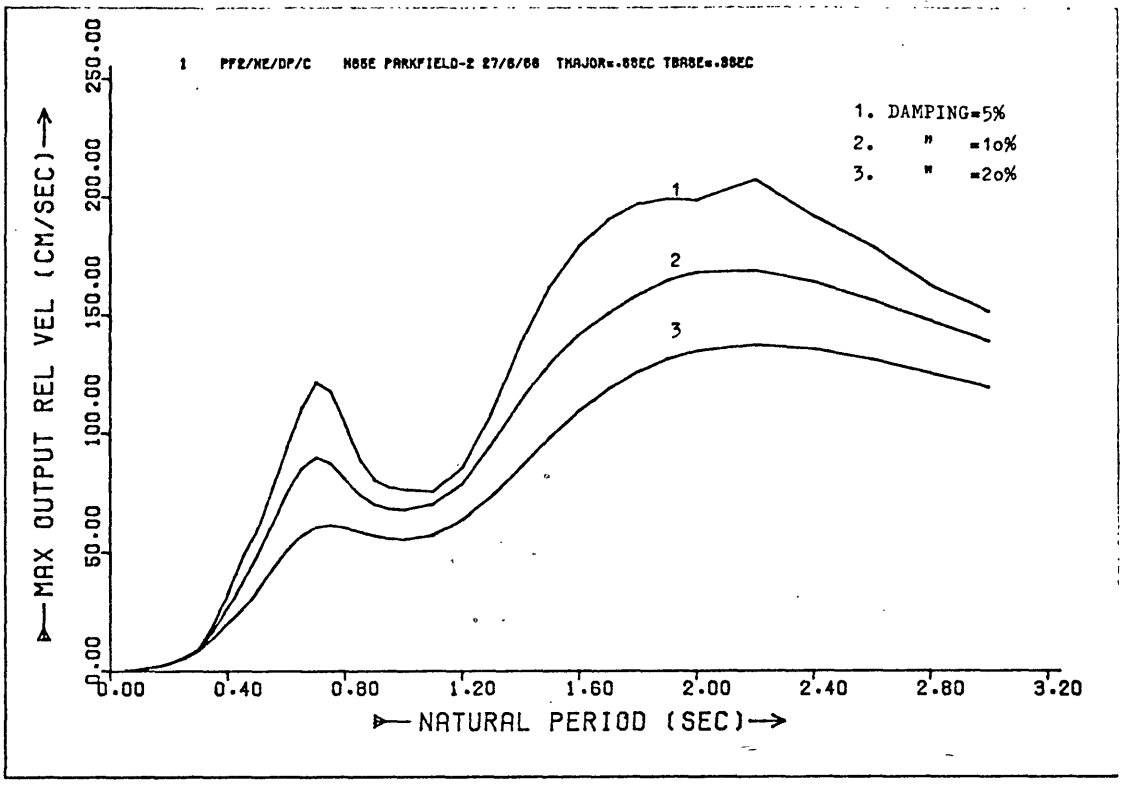


FIG.7.51e COMPUTED GROUND SURFACE VELOCITY RESPONSE SPECTRA AT SITE NO 7.28.

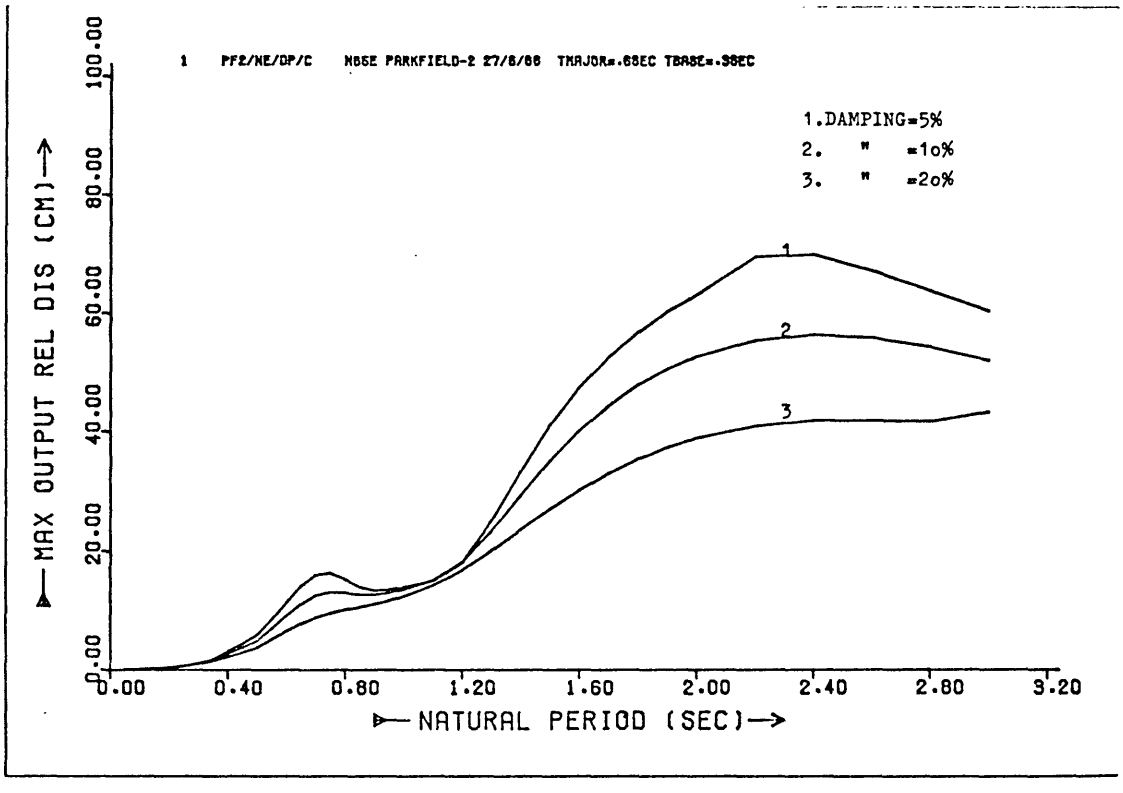


FIG7.51f COMPUTED GROUND SURFACE DISPLACEMENT RESPONSE SPECTRA AT SITE NO7.28

the highest.

Results shown in the table 7.3 indicate that an increase in the depth to bedrock of deposit may or may not cause a significant change in peak ground surface velocity and acceleration. For example, an increase in the depth to bedrock of saturated silt from 10m to 15m reduces maximum surface acceleration and velocity but increases maximum surface displacement. Increasing the depth to bedrock to 25m still reduces maximum surface acceleration but increases maximum surface velocity and displacement. A further increase to 30m does not produce significant differences in these values. An examination of results presented in table 7.3 shows that, as expected, peak ground acceleration, velocity and displacements follow roughly the general behaviour of peak amplitude of maximum spectral acceleration, velocity and displacement.

Figs. 7.52 shows surface acceleration and amplification spectrum show large amplification near the fundamental periods of these deposits. Fig. 7.53 illustrates velocity amplification spectrum for these deposits; the importance of this figure lies in the fact that multiplying co-ordinates of input spectra at each period by the ratio obtained from fig. 7.53 at corresponding period would enable one to compute output velocity spectra for all the five deposits.

7.7.1. CONCLUDING REMARKS

Based on the analysis presented in this section, the following conclusions may be reached:

a) An increase in the depth to bedrock may increase or decrease or may not change Maximum response amplitudes. An increase

BASE MOTION PARKFIELD-2 27/6/66 DAMP=0.2

RAD = 0.1, S = 60m/sec

HEIGHT OF LAYER (m)	MAX SUR ABS ACC g	MAX SUR ABS VEL cm/sec	MAX SUR ABS DIS cm
10.00	0.747	116.253	37.197
15.00	0.570	79.479	38.664
20.00	0.455	83.936	40.526
25.00	0.382	98.852	41.500
30.00	0.367	98.701	41.893

TABLE 7.3

RESULTS OF INCREASING THICKNESS OF OVERBURDEN

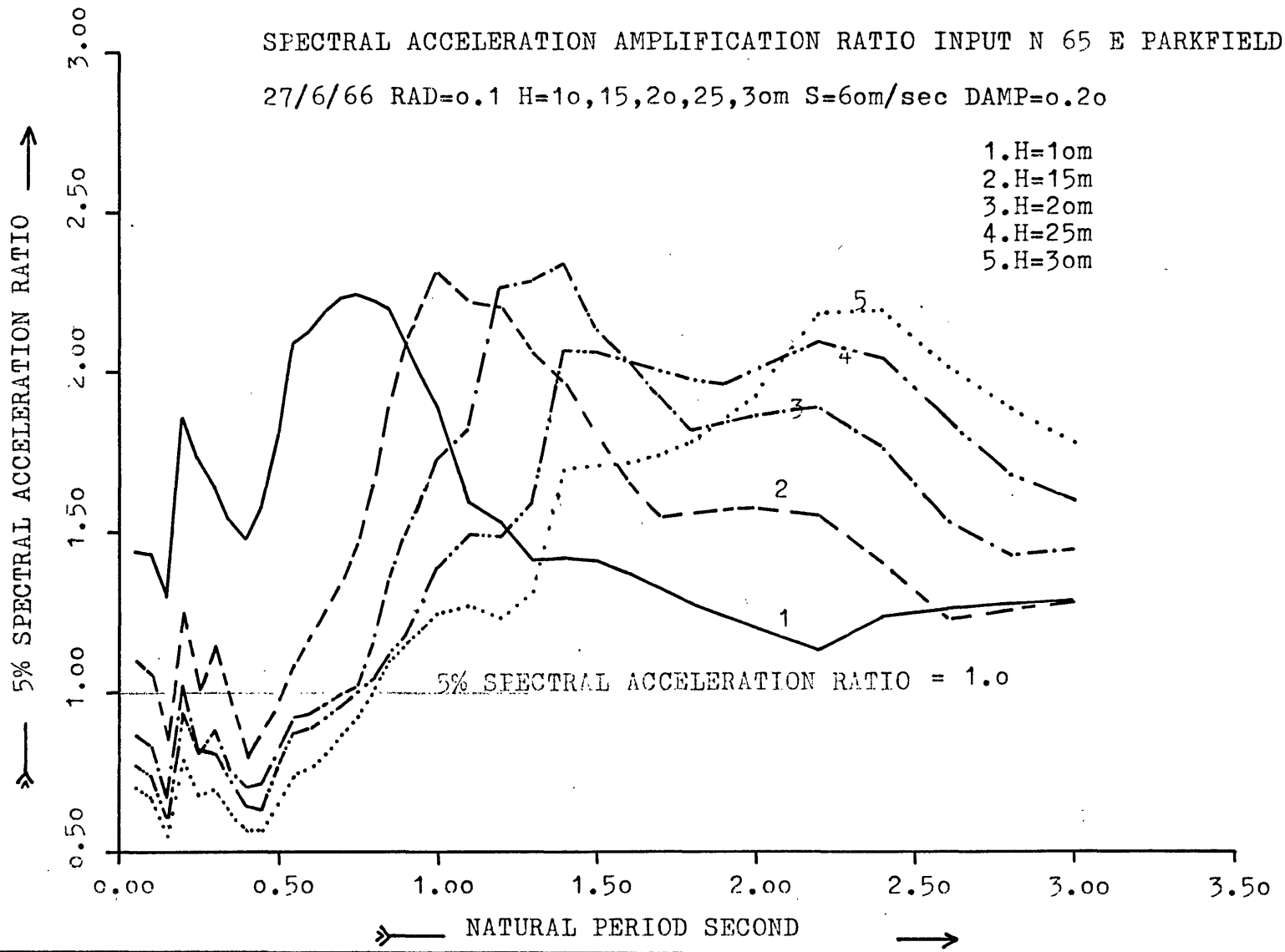

SPECTRAL ACCELERATION AMPLIFICATION RATIO INPUT N 65 E PARKFIELD-2
27/6/66 RAD=o.1 H=1o,15,2o,25,3om S=6om/sec DAMP=o.2o
1.H=1om
2.H=15m
3.H=2om
4.H=25m
5.H=3om
5% SPECTRAL ACCELERATION RATIO = 1.o
5% SPECTRAL ACCELERATION RATIO
NATURAL PERIOD SECOND
0.50
1.00
1.50
2.00
2.50
3.00
0.00
0.50
1.00
1.50
2.00
2.50
3.00
3.50

FIG.7.52

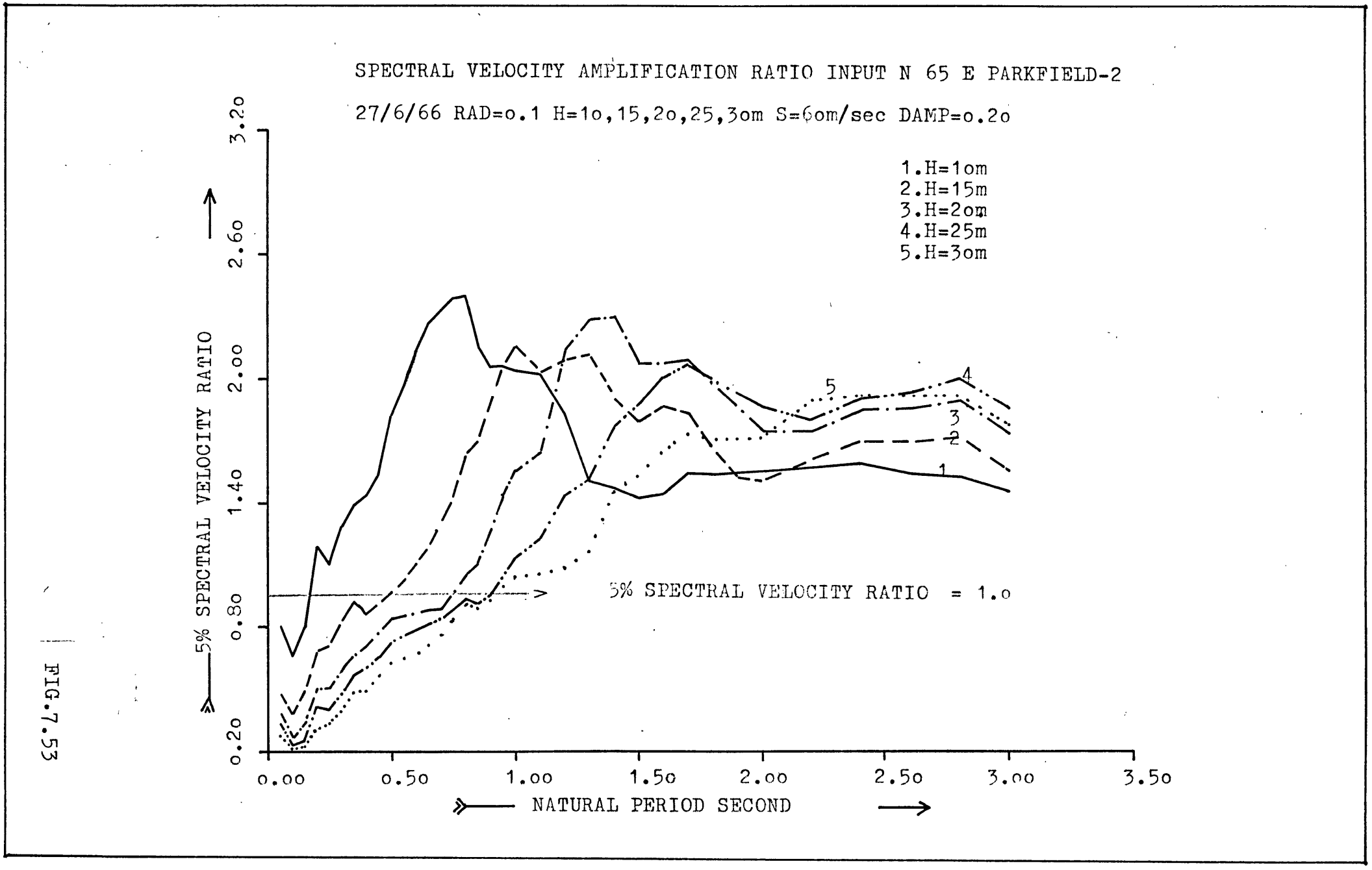

SPECTRAL VELOCITY AMPLIFICATION RATIO INPUT N 65 E PARKFIELD-2
27/6/66 RAD=o.1 H=1o,15,2o,25,3om S=6om/sec DAMP=o.2o
1.H=1om
2.H=15m
3.H=2om
4.H=25m
5.H=3om
5% SPECTRAL VELOCITY RATIO = 1.o
5% SPECTRAL VELOCITY RATIO
NATURAL PERIOD SECOND
0.20
0.8o
1.4o
2.oo
2.6o
3.2o
0.00
0.5o
1.oo
1.5o
2.oo
2.5o
3.oo
3.5o

FIG.7.53

in depth to bedrock increases fundamental period of the overburden, hence computed response is controlled by the relative values of predominant period of bedrock motion and that of fundamental period of the overburden.

b) The analysis presented here could be used to show distribution of ground response which might be expected to develop in deposits of soil extending from a shallow depth to bedrock near a mountain range to greater depths one or two Kms. away, with the same bedrock characteristics and the same bedrock motion. The waves arriving to bedrock level of an overburden one or two Km. away would propagate at different velocities, with different frequency characteristics, thus giving rise to a different bedrock motion. Since ourknowledge of spacial variation of seismic waves is limited at the present time, one cannot take this effect into account.

7.8. INFLUENCE OF DURATION OF BEDROCK MOTION ON GROUND RESPONSE

In the 1966 Parkfield earthquake it was observed that the motion near the causative fault was quite intense, but the resulting damage was very little. Many scientists working in the specialized field of Earthquake Engineering interpret the cause of less damage to be the result of duration of shaking,which was very short. Duration of shaking also controls the period at which a saturated soil deposit is under sustained pressure, thus affecting liquifiability of saturated sand deposits. Therefore, duration of base motion should also be considered.

In order to investigate the influence of the duration of bedrock shaking on ground response, two different portions of Parkfield-2 were

used as bedrock motion; first 8.5 second, which contains the region of strong shaking, and the full 18.7 sec. of the record. A comparison of response patterns of the site shown in fig. 7.54 is provided in figs. 7.54a,b,c,d,e,f to 7.55a,b,c,d,e,f which shows the response of 50m deposit of medium clay with radiation damping ratio of 0.2 and hysteretic damping ratio of 0.05 for the two bedrock motions as defined above. Figs. 7.54a,b,c to 7.55a,b,c show acceleration, velocity and displacement time histories produced along the surface of the deposit. The results clearly indicate that the longer the duration of bedrock shaking the longer the duration of computed response. It should be noted that peak ground response values are not affected when duration of bedrock motion is increased from 8.5 second to 18.7 second.

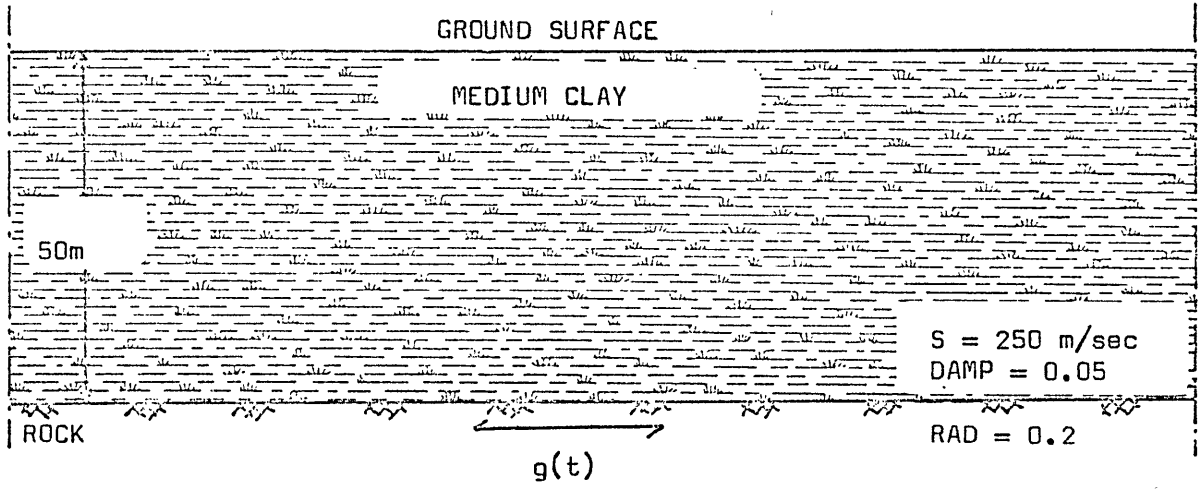
Figs. 7.54d,e to 7.55d,e show computed surface acceleration and velocity response spectrum which are identical for the two bedrock motions considered, indicating that, in the remaining 10.2 second of acceleration time history of Fig. 7.55a, pulses with appreciable amplitudes do not exist to excite the periods of the simple structure. It is the author's view that the two computed surface acceleration time histories shown in figs. 7.54a and 7.55a will have completely different damaging potential. The question here arises whether structural design can be performed using spectrum of these kinds, emphasising the need for further research along these lines.

7.8.1. CONCLUDING REMARKS

From the foregoing discussion it appears that:

a) The response of a soil deposit is strongly influenced by the value of duration of bedrock shaking.

b) Response spectra is weak in reflecting duration of ground shaking.



RESPONSE OF HYSTERETIC DEPOSIT UNDERLAIN BY DEFORMABLE BEDROCK

SCHEMATIC SOIL PROFILE FOR SITE NO 7.29

FIG. 7.54

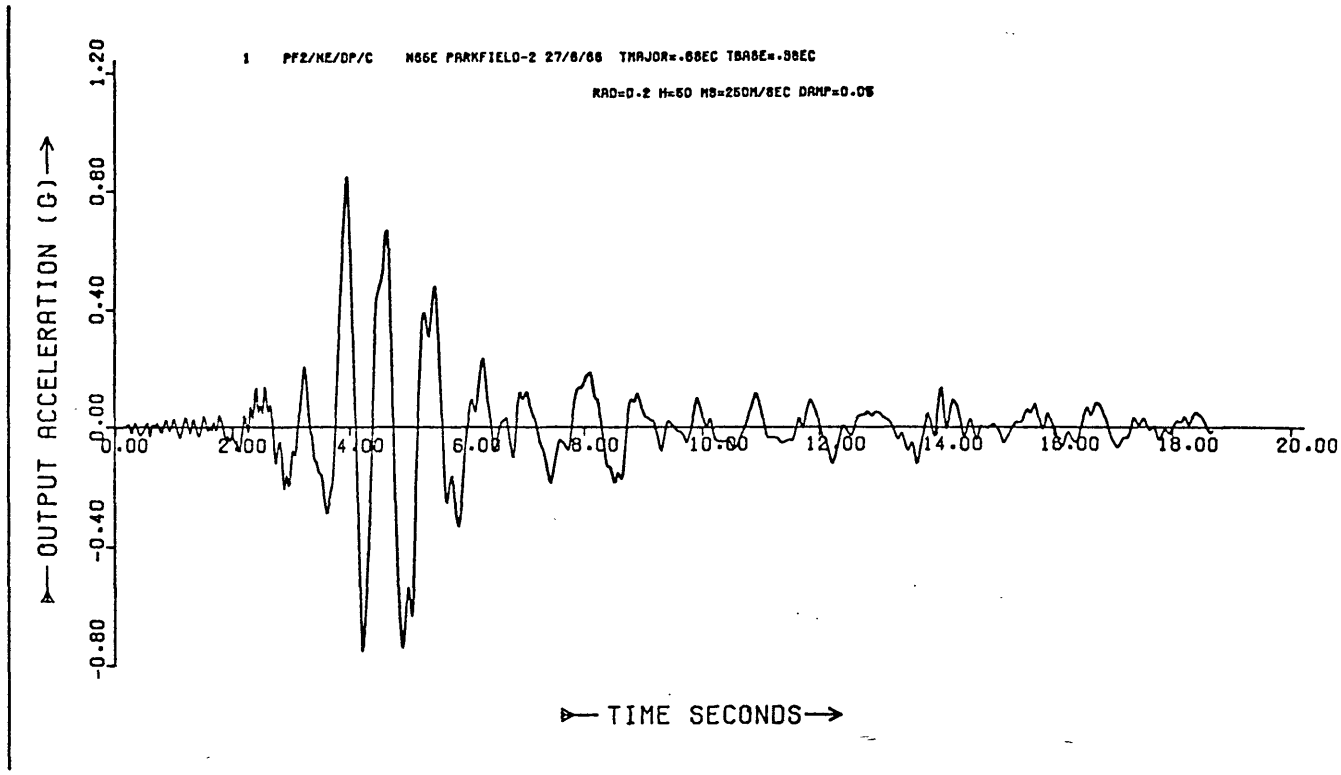


FIG.7.54a COMPUTED GROUND SURFACE ACCELERATION TIME HISTORY AT SITE NO 7.29

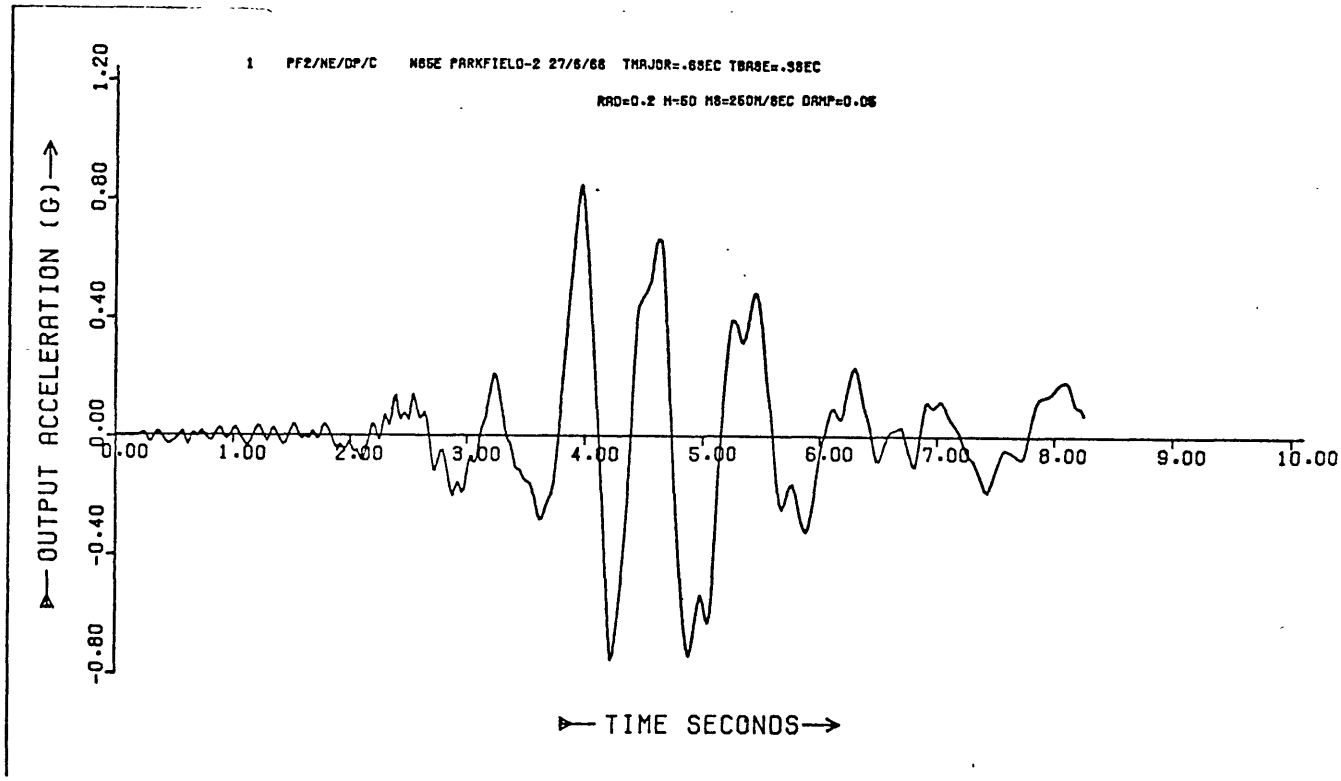


FIG.7.55a COMPUTED GROUND SURFACE ACCELERATION TIME HISTORY AT SITE NO 7.29

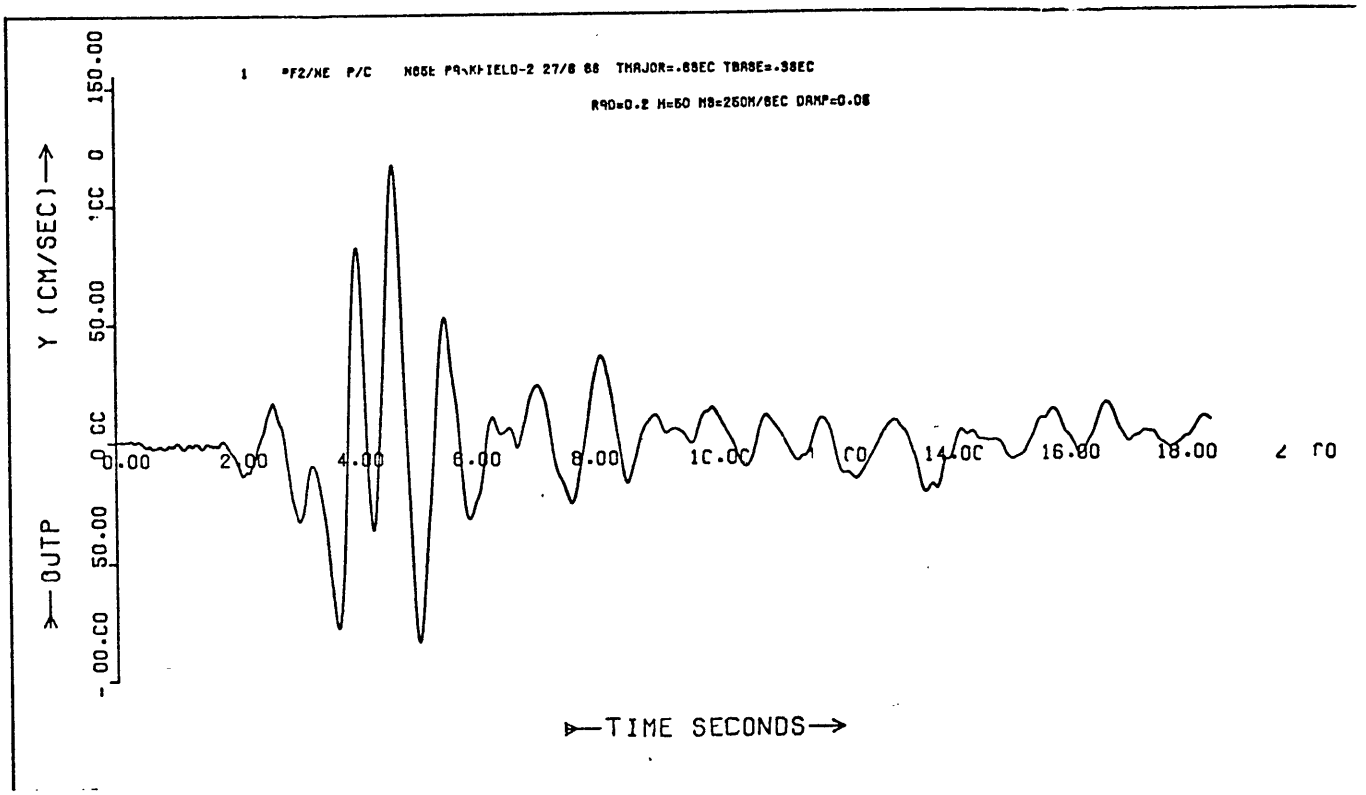


FIG.7.54b COMPUTED GROUND SURFACE VELOCITY TIME HISTORY AT SITE NO 7.29

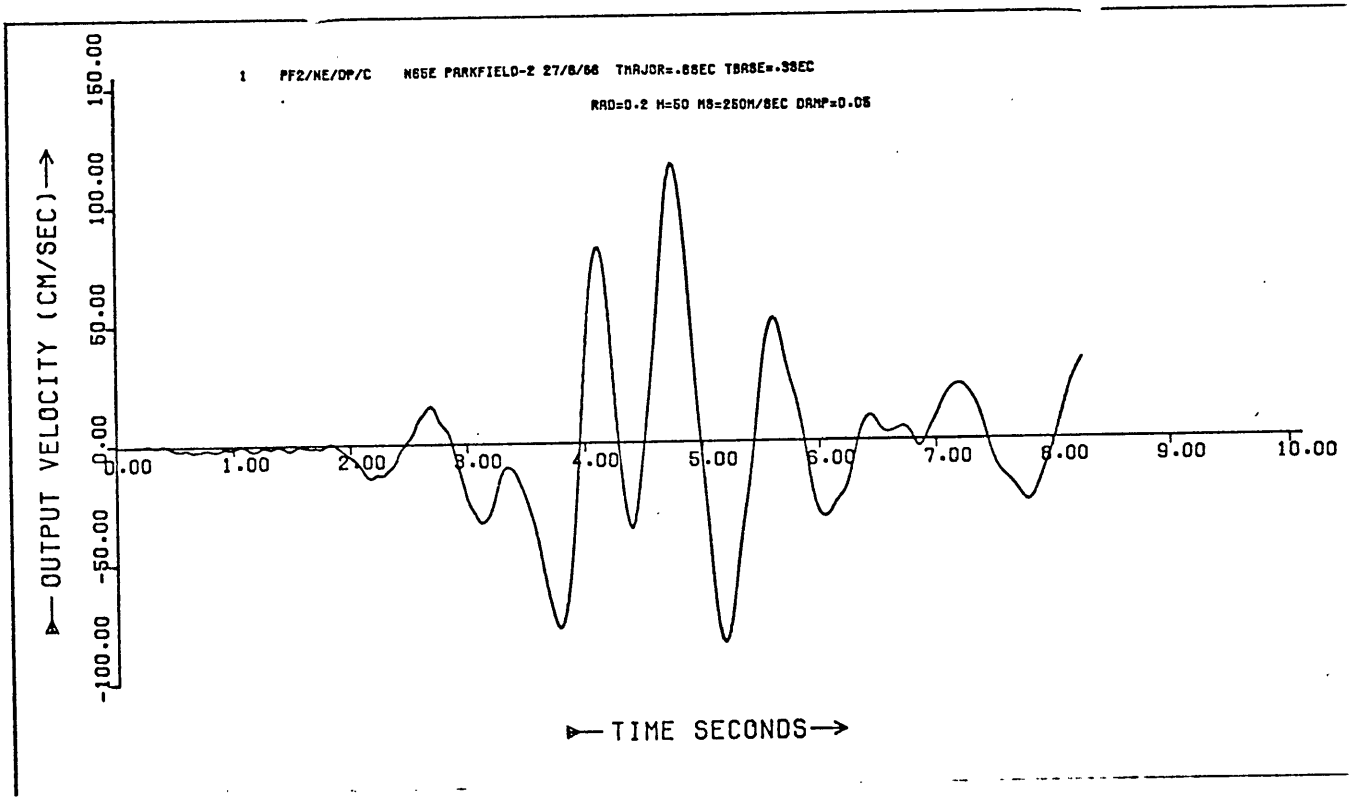


FIG.7.55b COMPUTED GROUND SURFACE VELOCITY TIME HISTORY AT SITE NO 7.29

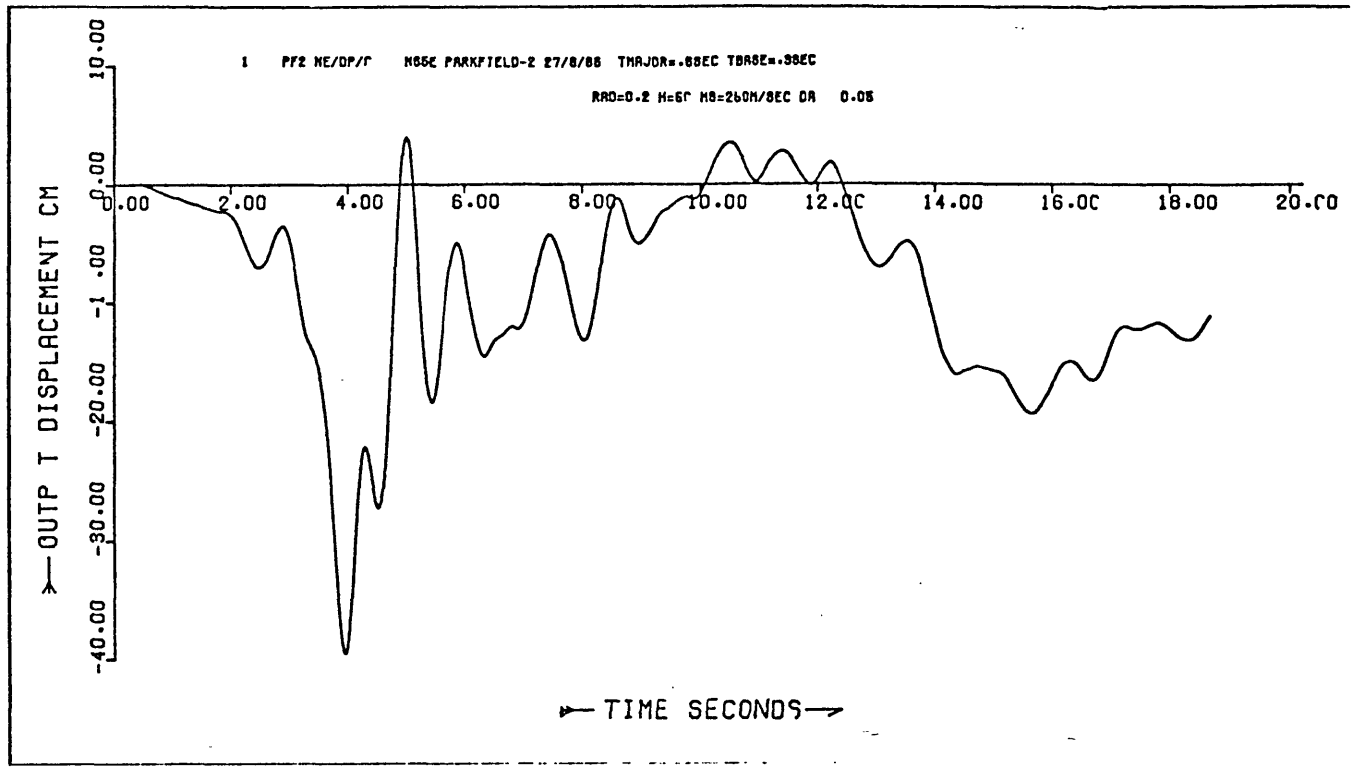


FIG7.54c COMPUTED GROUND SURFACE DISPLACEMENT TIME HISTORY AT SITE NO 7.29

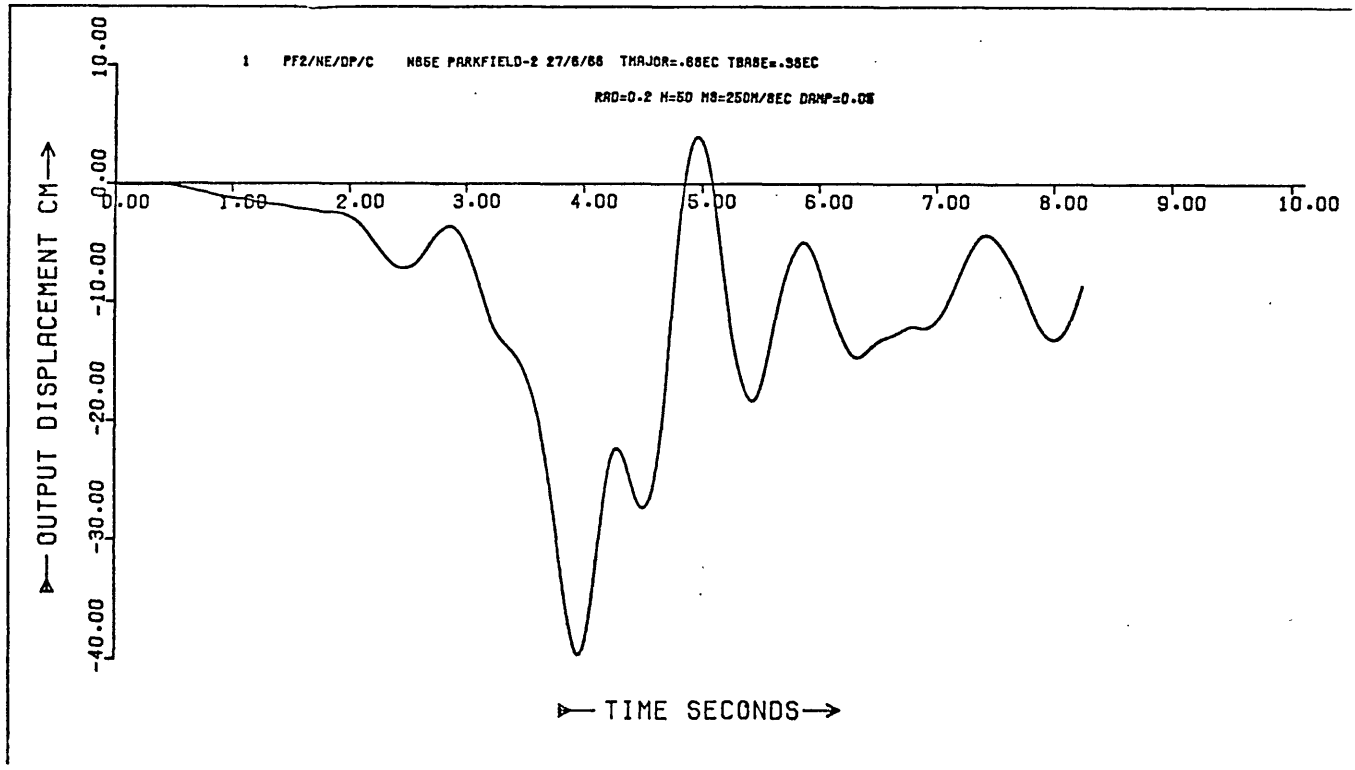


FIG.7.55c COMPUTED GROUND SURFACE DISPLACEMENT TIME HISTORY AT SITE NO 7.29

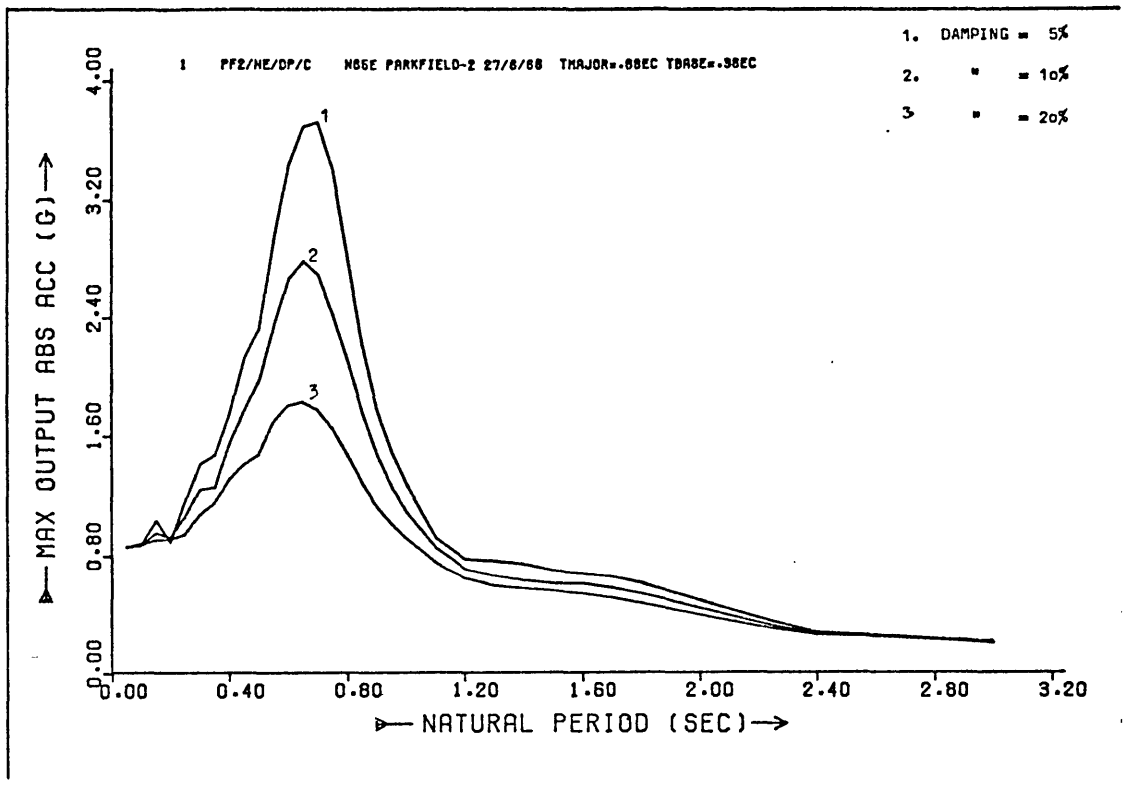


FIG.7.54d COMPUTED GROUND SURFACE ACCELERATION RESPONSE SPECTRA AT SITE NO 7.29

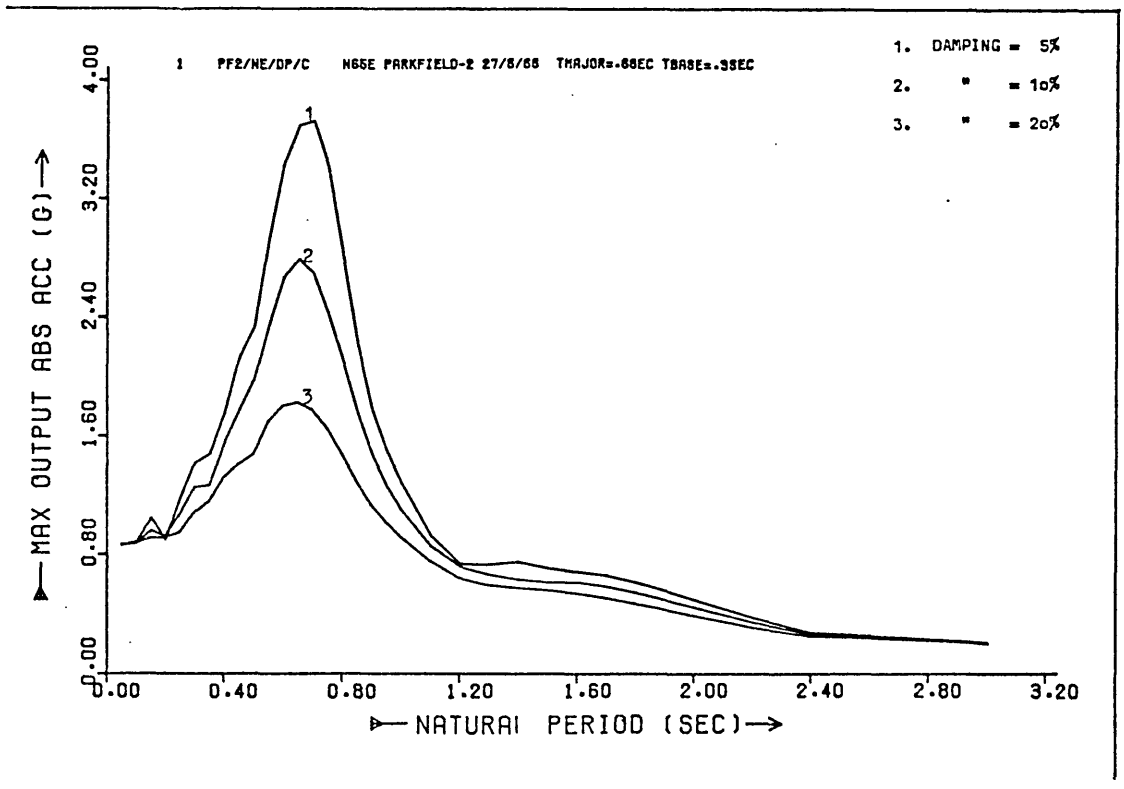


FIG 7.55d COMPUTED GROUND SURFACE ACCELERATION RESPONSE SPECTRA AT SITE NO 7.29

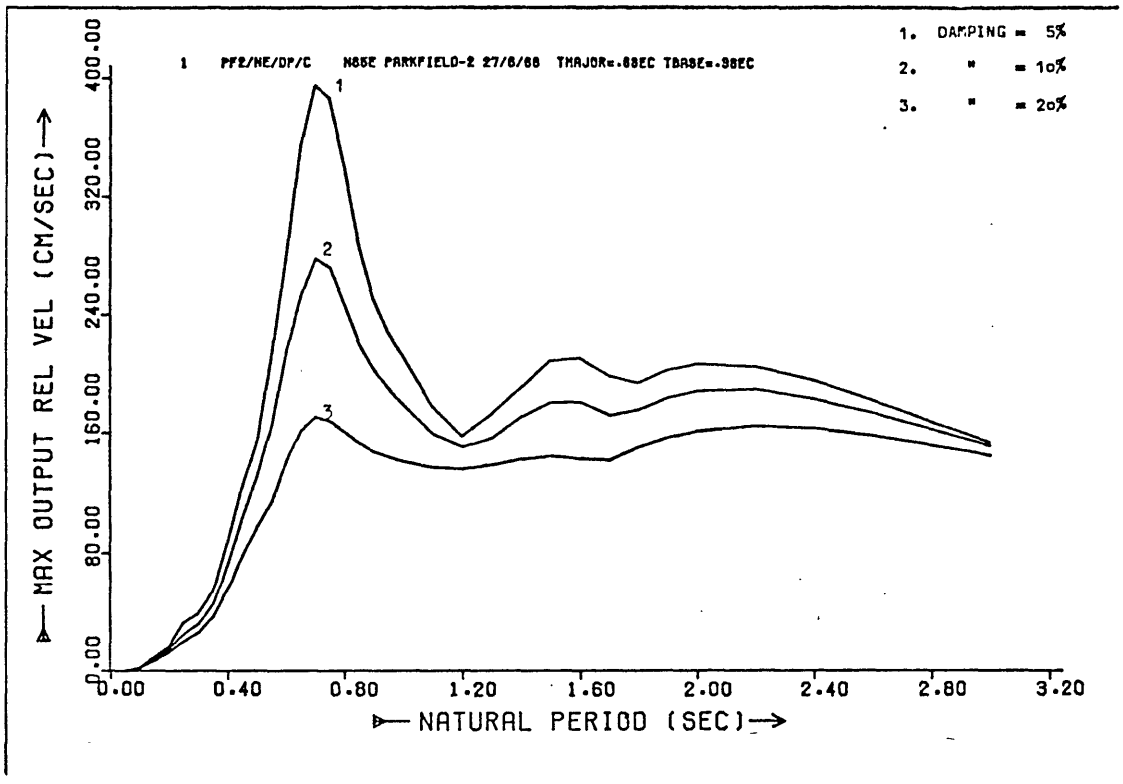


FIG.7.54e COMPUTED GROUND SURFACE VELOCITY RESPONSE SPECTRA AT SITE NO 7.29

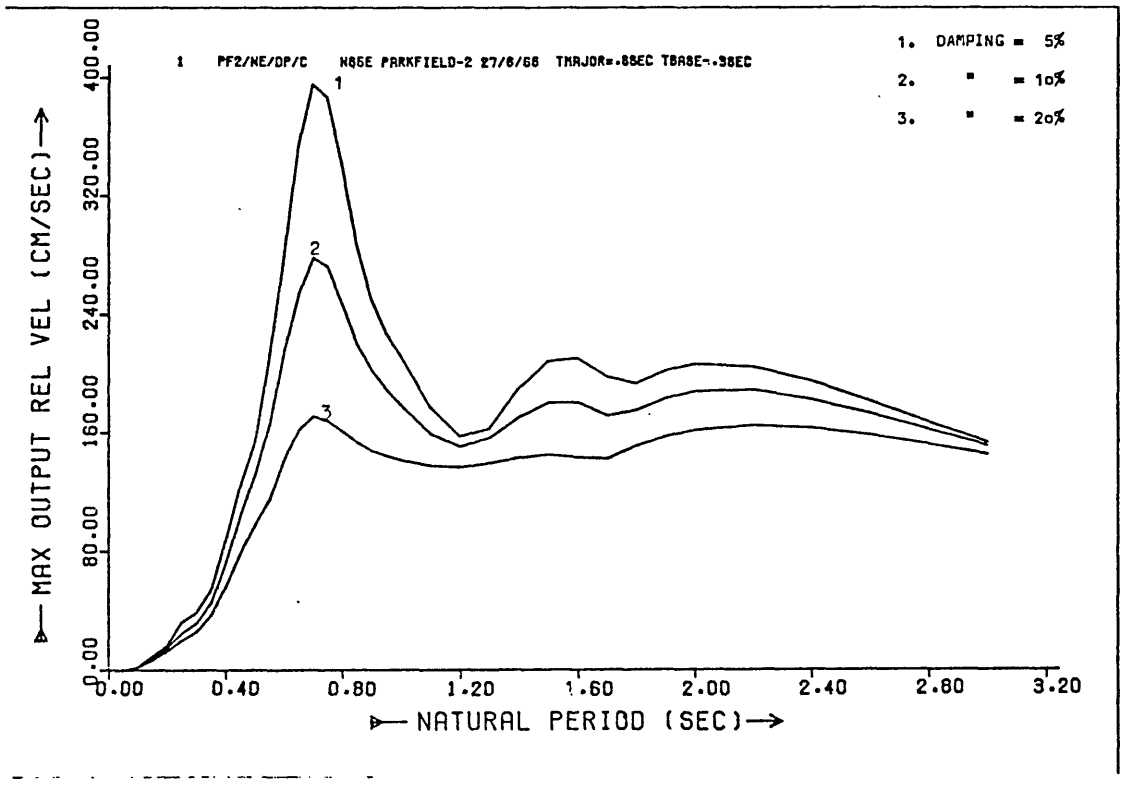


FIG.7.55e COMPUTED GROUND SURFACE VELOCITY RESPONSE SPECTRA AT SITE NO 7.29

7.9. ENGINEERING SIGNIFICANCE OF THE PROPOSED DESIGN METHOD OR SAMPLE DESIGN PROBLEM

Fixed offshore structures are designed in regions of high seismicity under sea conditions. The earthquakes occurring in the sea will develop high dynamic forces in the structure foundation system; therefore, it is important that these forces be predicted realistically for design purposes. It is the purpose of this section better to illustrate engineering significance of the proposed technique, by means of a design problem, for predicting these forces.

The site is located at the bottom of the sea which consists of 80m of loose gravel underlain by a Tuffaceous sandstone of shear wave velocity of 2500 m/sec. The pile foundation supporting the structure penetrates 10m through the loose gravel, as shown in fig. 7.56a. Bedrock motion is specified as Parkfield-2.

7.9.1. BASIC REQUIREMENTS

The basic requirements are:

i) Motion at depths of 10m below sea bottom.

ii) Site amplification.

Points (i) & (ii) are related to the topics discussed in this thesis.

7.9.1.1. MOTION AT DEPTH

Motion characteristics affecting structural response are:

a) Peak acceleration.

b) Frequency content.

c) Pulse shape.

d) Duration of shaking.

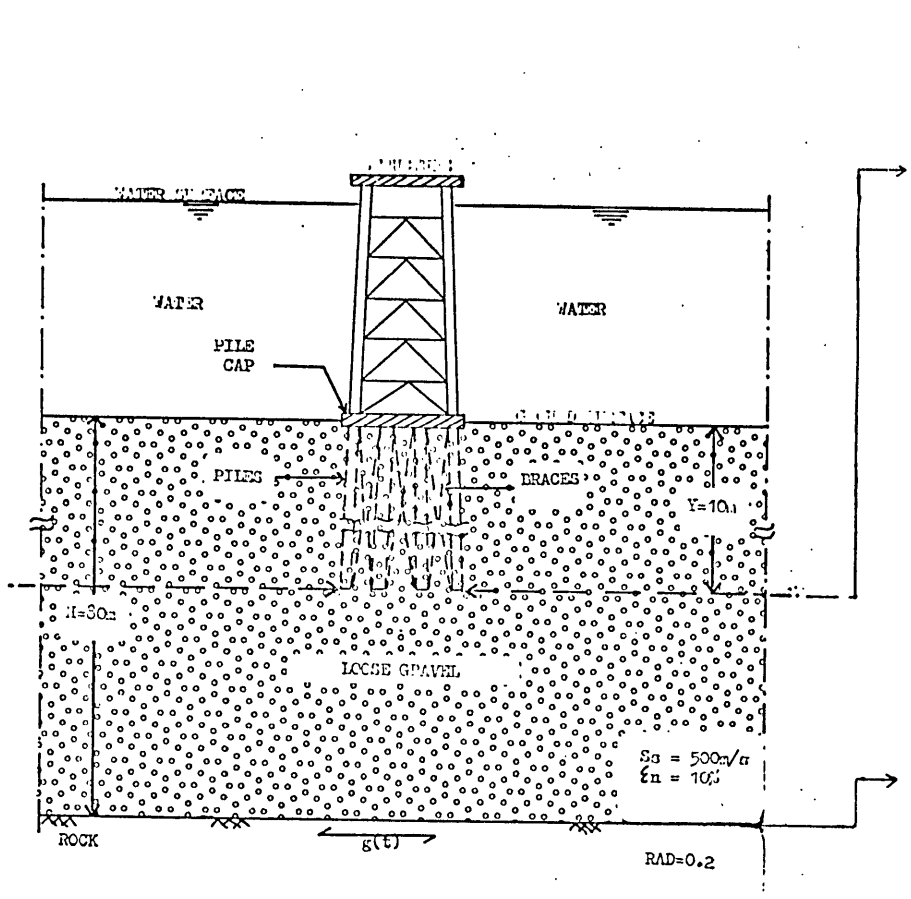
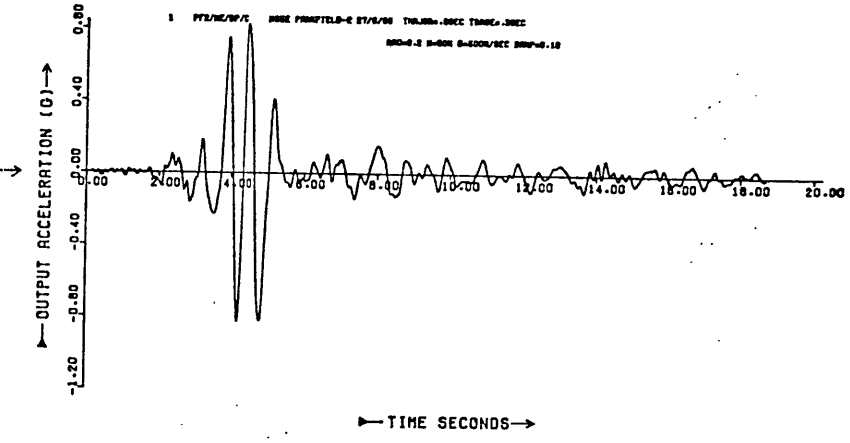
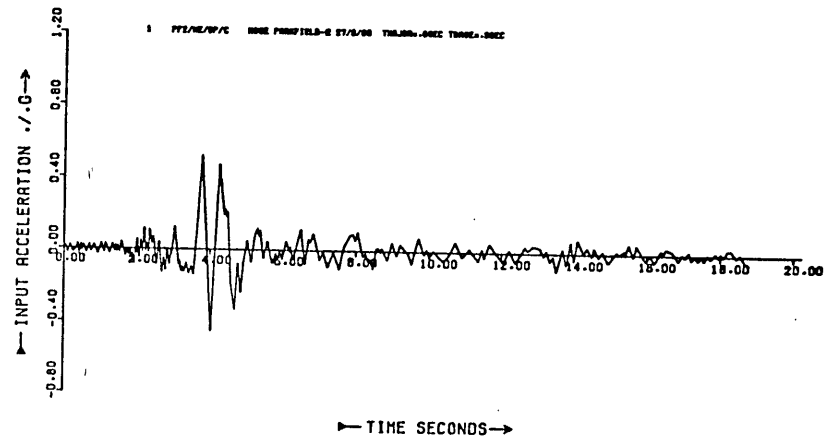


FIG.7.56a SCHEMATIC DIAGRAM OF FIXED TOWER AND ITS FOUNDATION



COMPUTED ACCELERATION TIME HISTORY AT 10m BELOW GROUND SURFACE



COMPUTED BEDROCK ACCELERATION TIME HISTORY

Peak acceleration has been chosen as the key descriptive parameter of shaking because it is related to the maximum force that the structure may undergo. Frequency content is the measure of frequencies of vibration the motion excites. Pulse shape is also important because one large pulse with relatively low frequency could push the structure into non-linear range. Duration of shaking determines the number of cycles during vibration a structure may undergo, which has a significant effect on response of yielding structures.

Figs. 7.56a,b,c show computed subsurface acceleration velocity and displacement time histories, illustrating that peak bedrock acceleration, velocity and displacement have been modified by factors of 1.56, 1.54 and 1.17, respectively. Computed subsurface acceleration time history can be used to provide answers to questions (a) , (b) & (d). However, as discussed earlier, computed velocity time history provides a better index for the design of these structures. Frequency characteristics of the motion at the base of the piles are determined from acceleration response spectra shown in fig. 7.56d.

Fig. 7.56e represents the velocity response spectra, for 5%, 10% and 20% damping, at bedrock level of the overburden and at the base of the piles. Figs. 7.56d and e were used to compute acceleration and velocity amplification spectra for 5% damping which are shown in fig. 7.56f. Acceleration amplification spectra clearly indicate that the loose gravel has amplification at all periods, large amplifications near the fundamental period of the overburden 0.64 sec., which is close to the predominant period of bedrock motion - 0.6 sec.is certainly noteworthy. Velocity amplification spectra indicates that the effect

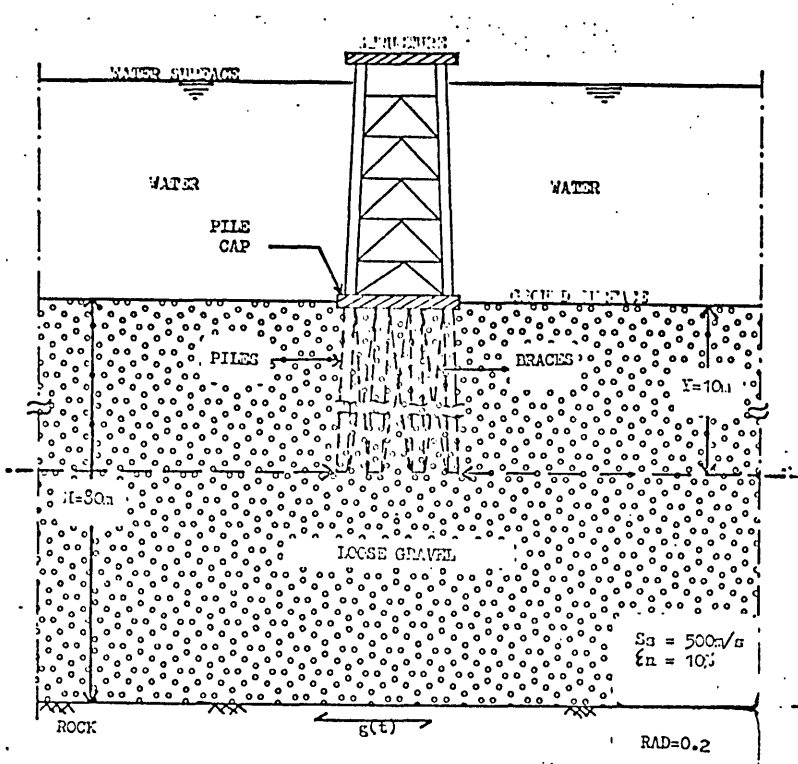
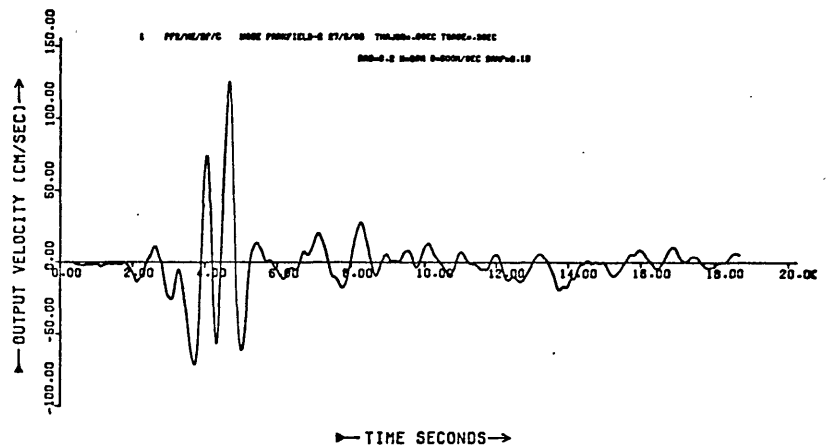
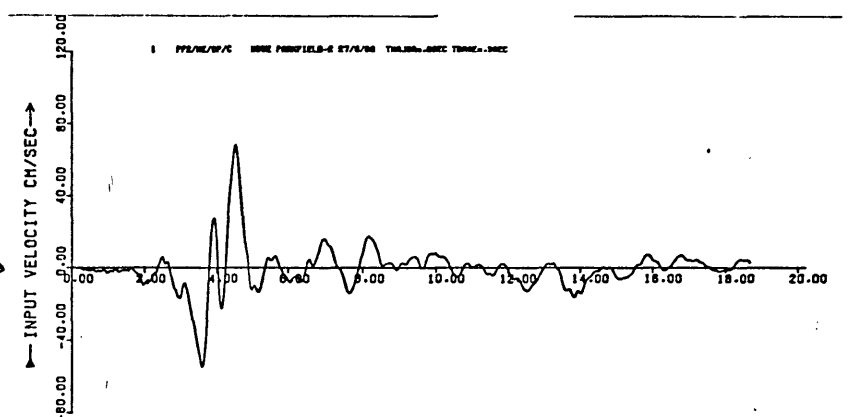


FIG.7.56b SCHEMATIC DIAGRAM OF FIXED TOWER AND ITS FOUNDATION



COMPUTED VELOCITY TIME HISTORY AT 10m BELOW GROUND SURFACE



COMPUTED BEDROCK VELOCITY TIME HISTORY

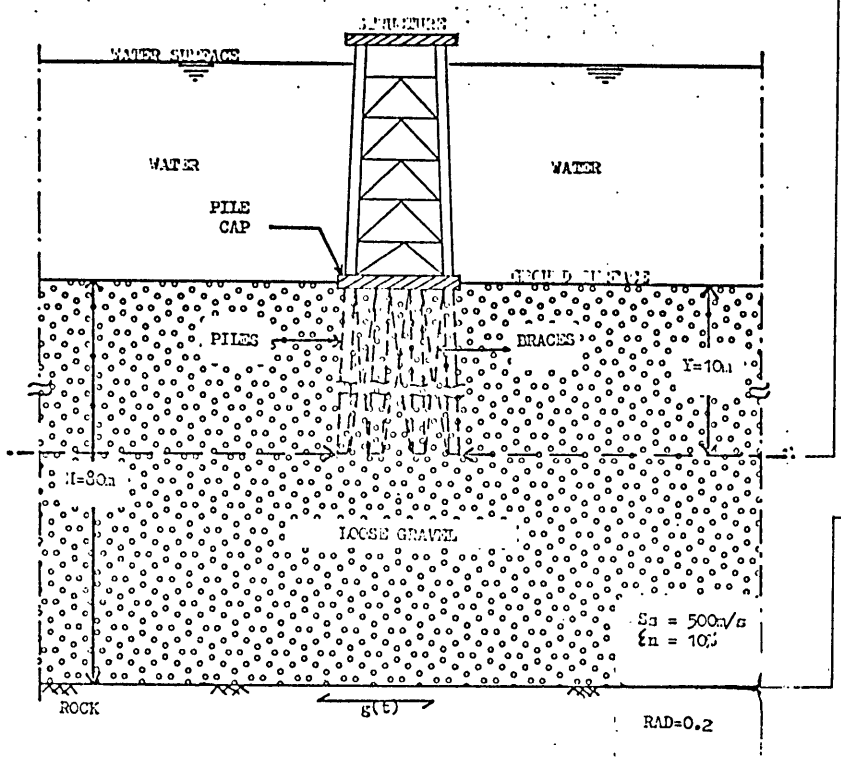
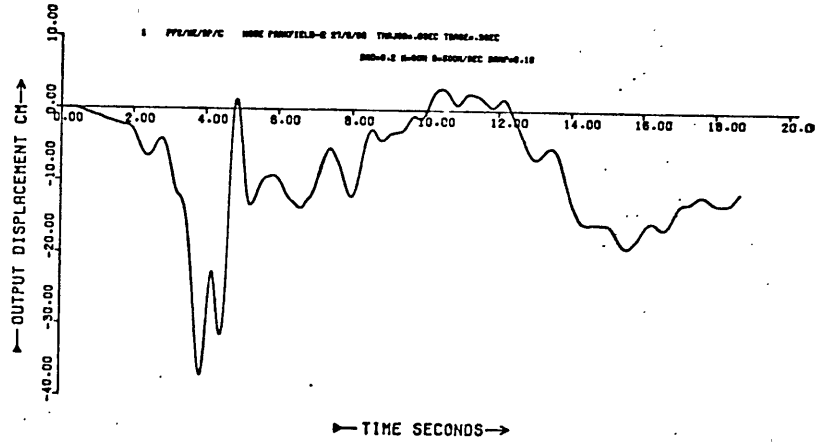
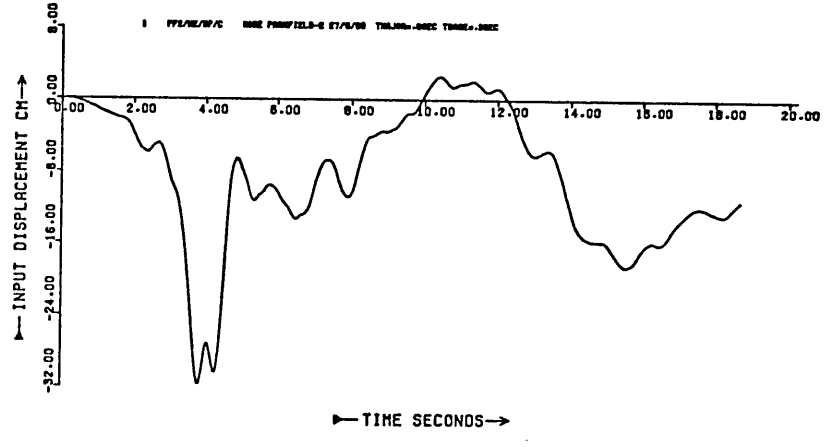


FIG.7.56c SCHEMATIC DIAGRAM OF FIXED TOWER AND ITS FOUNDATION



COMPUTED DISPLACEMENT TIME HISTORY AT 10m BELOW GROUND SURFACE



COMPUTED BEDROCK DISPLACEMENT TIME HISTORY

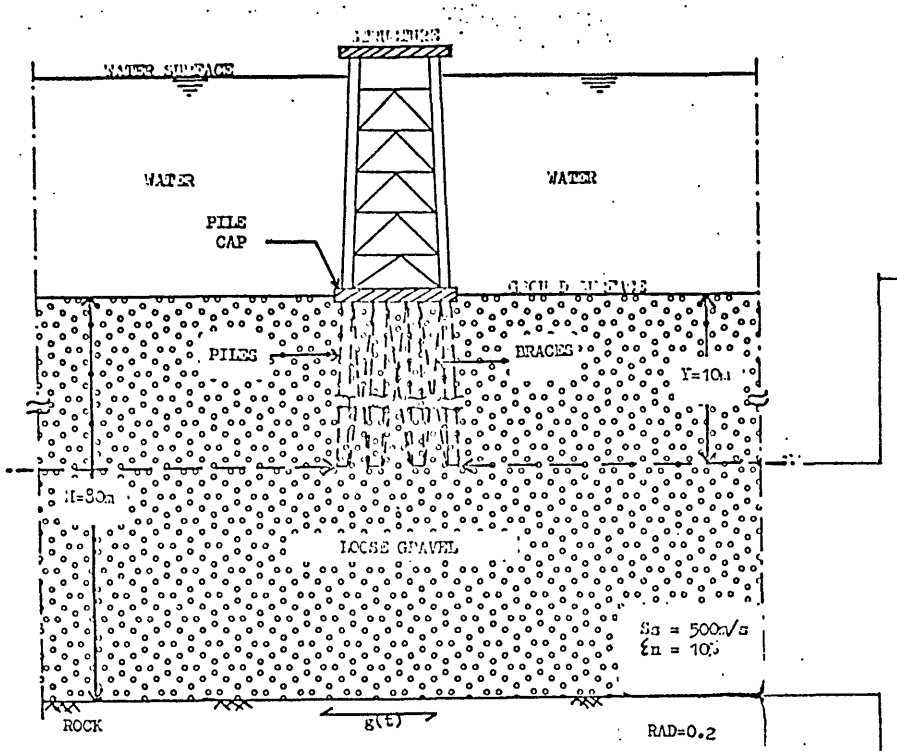
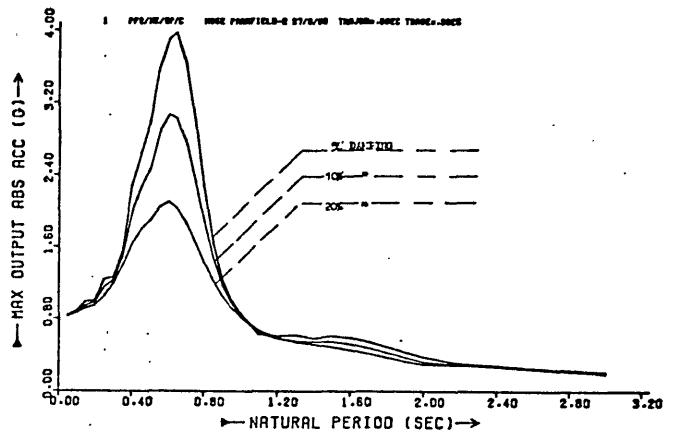
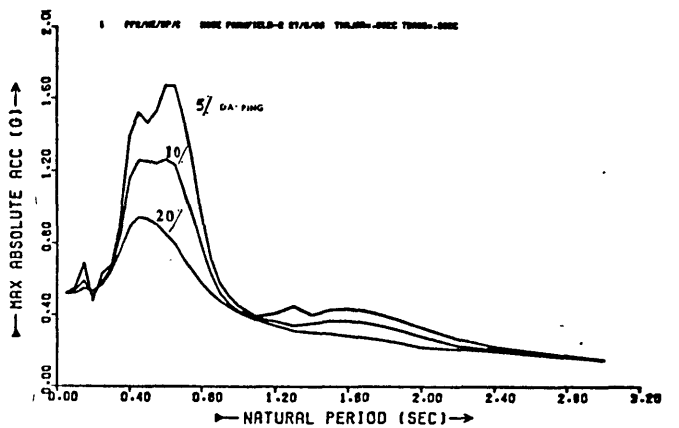


FIG.7.56d SCHEMATIC DIAGRAM OF FIXED TOWER AND ITS FOUNDATION



COMPUTED ACCELERATION RESPONSE SPECTRA AT 10m BELOW GROUND SURFACE



COMPUTED BEDROCK ACCELERATION RESPONSE SPECTRA

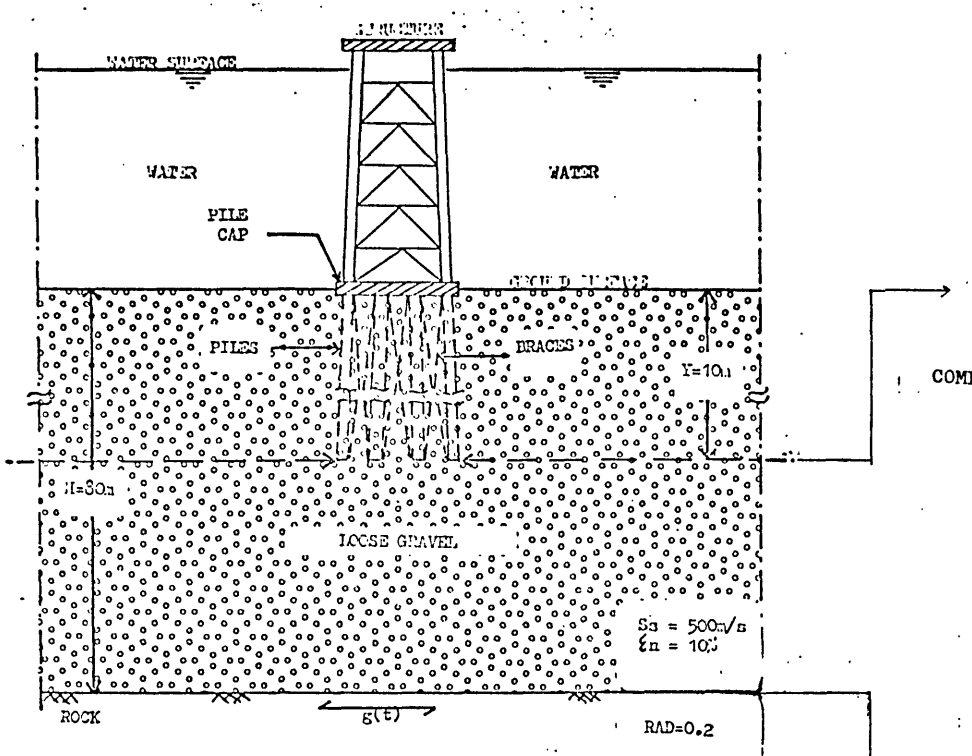
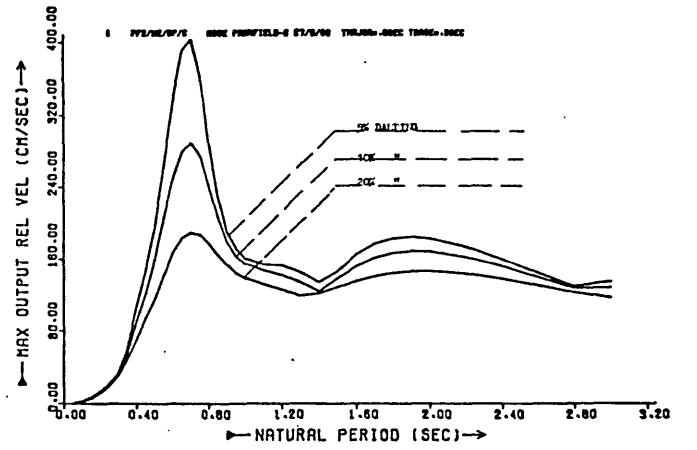
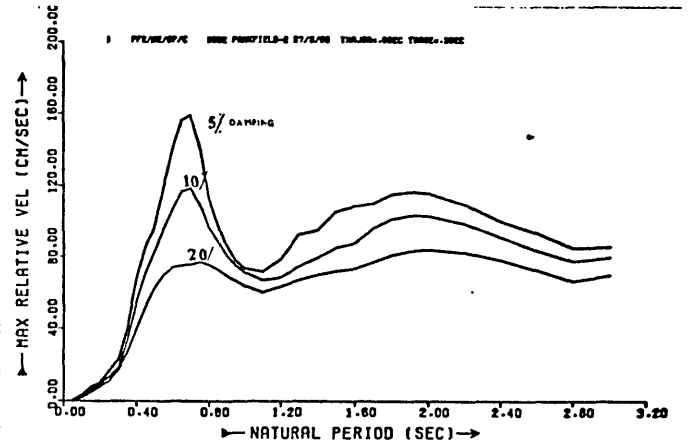


FIG.7.56e SCHEMATIC DIAGRAM OF FIXED TOWER AND ITS FOUNDATION



COMPUTED DISPLACEMENT RESPONSE SPECTRA AT 10m BELOW GROUND SURFACE



COMPUTED BEDROCK VELOCITY RESPONSE SPECTRA

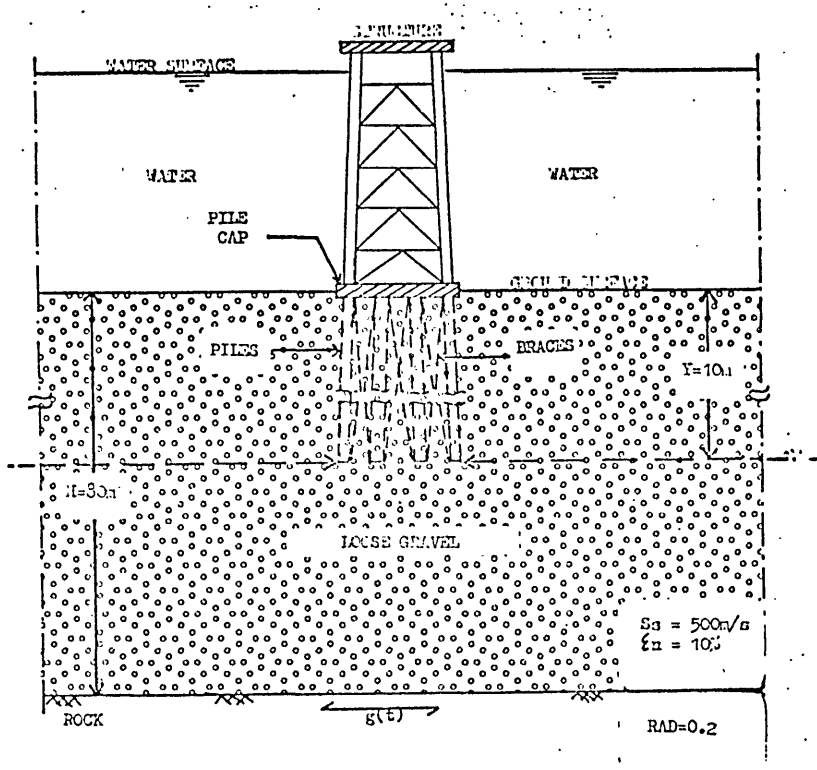
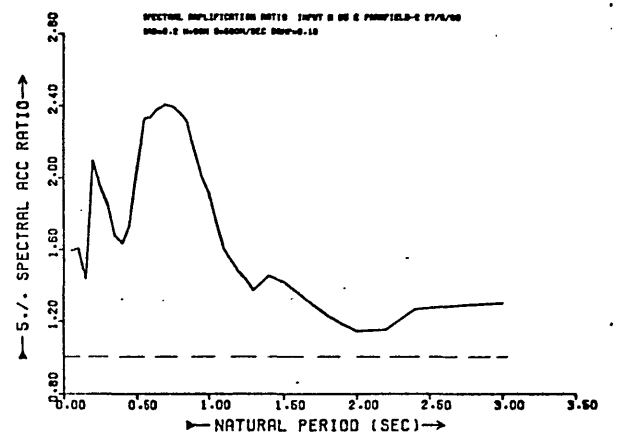
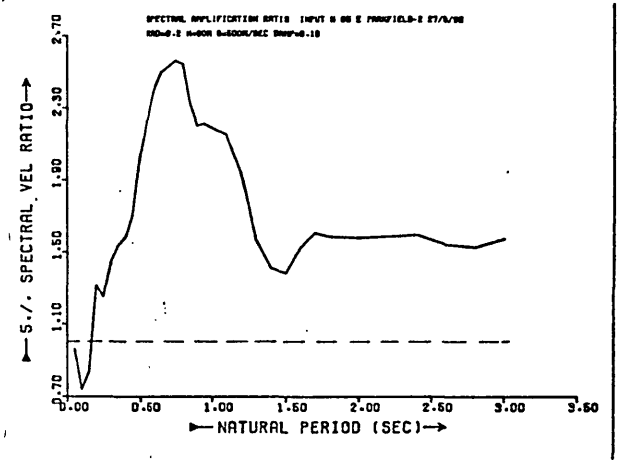


FIG.7.56f SCHEMATIC DIAGRAM OF FIXED TOWER AND ITS FOUNDATION



ACCELERATION RESPONSE SPECTRA RATIO AT 10m BELOW GROUND SURFACE



VELOCITY RESPONSE SPECTRA RATIO AT 10m BELOW GROUND SURFACE

of loose gravel was to de-amplify the motions at very low periods while amplifying them at periods greater than 0.15 second.

CHAPTER 8

PORE WATER PRESSURE DISSIPATION ASSOCIATED WITH FOUNDATION SHAKING AFTER EARTHQUAKES

8.1 INTRODUCTION

For assessing probable foundation performance under specified earthquake conditions, it is necessary to have a knowledge of redistribution of pore water pressures. These excess pore water pressures, which set up during period of shaking, play an important part in the stability of foundations. The vertical dissipation of these large pore pressures after earthquakes often causes ground water to rise up to ground surface or sometimes cover a large area, making structures tilt and settle extensively. It is the objective of this chapter to provide an analysis, which may well provide a deeper insight into the effects of pore pressure dissipation on the stability of foundations.

8.2. PREVIOUS STUDY

Housner[32] analysed the post earthquake pore water distribution in a single layer system, consisting of denser sand at the lower part and having an impervious bedrock, for two cases of initial post earthquake pore water distribution.

Ambraseys and Sqrma[4] have extended Housner's work into a two-layer system with a constant initial post earthquake excess pore water pressure in the lower layer and zero in the upper layer.

Yoshimi and Kumabara[65] have used the finite element method and have solved Ambraseys and Sarma's case for different post earthquake pore water pressure distributions.

Seed, Martin, Lysmer[55] have used a finite difference scheme and have analysed the case of a single layer system, taking into account considerations of the pore pressure redistribution which may take place during the period of the earthquake as well as the post earthquake period, and concluded that:

> "However, it is apparent that a thin layer of sand near the surface of a coarse sand or gravel deposit would serve to inhibit drainage to the part where these results would not apply."

8.3. SCOPE AND OBJECTIVE OF PRESENT STUDY

The main objectives of the present study are:

i) To provide an accurate method for analysing the post earthquake dissipation of pore water in a single layer of sand located above a weak layer of sand or an impermeable formation.

ii) To show the changes in excess pore water pressure throughout the soil profile, which occurs with time following the earthquake shaking.

8.4. ROLE OF WEAK THIN TRAPPED DEPOSIT

Upward propagation of shear waves in a deposit of sand with a thin layer of fine grained, fully saturated, loose sand, located between beds of sand deposit, will develop a condition of initial liquifaction

or liquifaction in the trapped loose deposit. The space occupied by the weak deposit will be filled with a mixture of sand and water. Migration of loose fine particles into the voids of sand just above or beneath would stop vertical drainage.

Due to the fact that the mixture of water and sand cannot transmit any shear stresses, no shear stresses would be transmitted to the layer located above the liquified layer.

8.5 THEORY

8.5.1. FORMULATION OF THE GOVERNING DIFFERENTIAL EQUATION

The differential equation governing the distribution of excess hydrostatic pressure in the deposit of sand located above the weak layer or an impermeable formation is governed by:

$$\frac{\delta u(z,t)}{\delta t} = C_v \cdot \frac{\delta^2 u(z,t)}{\delta z^2} \qquad (8.1)$$

(see appendix I for derivation of equation 8.1)

where:

C_v = coefficient of sonsolidation for vertical drainage.

z = axial coordinate

t = time

The corresponding boundary conditions are:

i) The post earthquake excess pore water pressure throughout the layer is

$$u_o \quad \text{at} \quad t=0$$

ii) The excess pore water pressure at layer surface is zero when $t > 0$

$$u(z,t)\Big|_{z=H} = 0$$

iii) The base of the layer is considered to be impervious

$$\frac{\delta u}{\delta z}(z,t)\Big|_{z=0} = 0$$

8.5.2. SOLUTION OF THE GOVERNING DIFFERENTIAL EQUATION

Solution of the governing differential equation is given in appendix J.

From appendix J, the excess pore water pressure in the deposit of sand located above the weak layer takes the form

$$u(z,t) = \frac{4u_o}{\pi} \sum_{m=1}^{\infty} \frac{(-1)^{m+1}}{(2m-1)} \cdot \left(\cos \frac{(2m-1)\pi}{2H} z\right) \cdot \exp\left(-c_v \frac{(2m-1)^2}{4H^2} \cdot \pi^2 \cdot t\right) \quad (8.2)$$

where:

H = total thickness of sand deposit located above the weak layer or impermeable formation.

8.6. SOIL PROPERTIES FOR USE IN NUMERICAL ANALYSIS

For application of the above theory to real field cases, a knowledge of coefficient of permeability and compressibility of the sand deposits is essential. Procedures for determining these characteristics and their typical values are given in chapter 5.

8.7. COMPUTER PROGRAM

The solution given by (8.2) is incorporated into a computer program named PORE PRESSURE (Pore water pressure dissipation associated with foundation shaking after earthquakes). The program determines the dissipation of excess pore water pressure with time in foundations after earthquake shaking.

The program is written in Fortran IV and has been used on CDC 6400 of Imperial College.

8.7.1. DATA PREPARATION

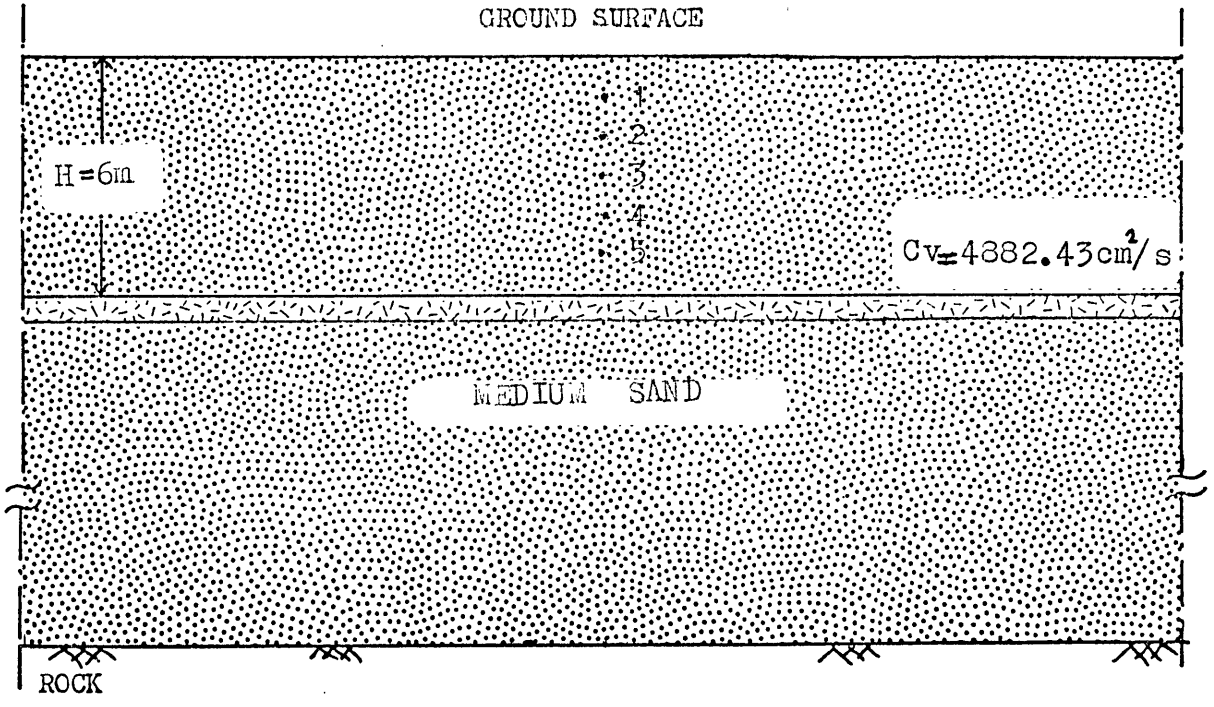
Required input data include:
time coordinates, height of the foundation or thickness above weak layer coefficient of consolidation of the sand deposit. Coordinate of the point at which excess pore water pressure is to be calculated, measured from surface of weak layer or impermeable formation.

8.7.2. OUTPUT

Information printed out includes:
Reprint of input data and ratio of excess pore water pressure to initial pore water pressure at any specified time. The program also produces a plot of these values vs. time.

8.8. NUMERICAL RESULTS

The first site which was studied consisted of a layer of medium sand six metres thick, with a C_v value of 4882.43 cm^2/sec , located above a weak layer of sand (or an impermeable formation), as shown in fig.8.10. The ground water was assumed to be at the surface of the



SCHEMATIC SOIL PROFILE FOR PORE PRESSURE DISSIPATION SITE NO. 1

FIG. 8.1D

deposit. The changes in excess pore water pressure with time at depths 1,2,3,4,5 m below ground surface in the deposit are shown in Fig.8.1.

Fig 8.1 shows the excess pore water pressure dissipates fastest at the depth of 1m below ground surface. The dissipation of excess pore water pressure becomes slower as the depth below ground surface increases. This is expected because point 1 in fig.8.1D is closer to drainage boundary (free ground surface) than point 5. This also means that a stabilization process may occur near the ground surface after about forty seconds. This was observed in the field, e.g. in the Nigata earthquake 1964, at Nigata site no instability was observed up to depths of 2-3 m below ground surface.

8.9. SENSITIVITY ANALYSIS

The factors which control the dissipation of excess pore water pressure with time at various depths in a layer of sand located above a weak layer are:

a) Height of the sand deposit located above the weak layer or impermeable formation.

b) Coefficient of consolidation of the sand deposit.

8.9.1. INVESTIGATION OF INFLUENCE OF HEIGHT OF THE DEPOSIT ON EXCESS PORE WATER PRESSURE DISSIPATION

It has been recognized by Japanese engineers[39] that the depth of sand deposit plays an important role on stability characteristics of sand deposits. To throw further light on the possible influence of height of the deposit located above weak layer or impermeable formation

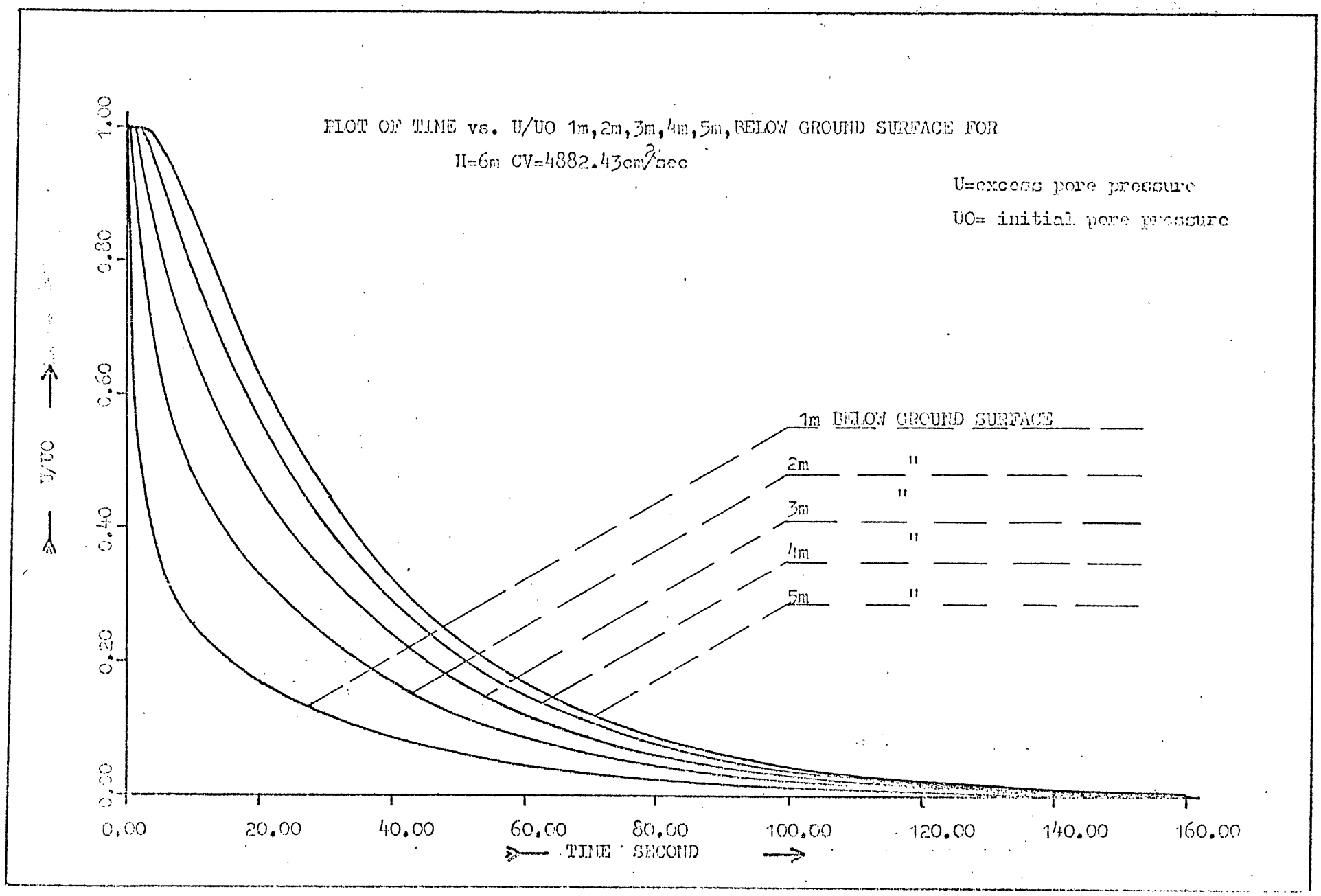
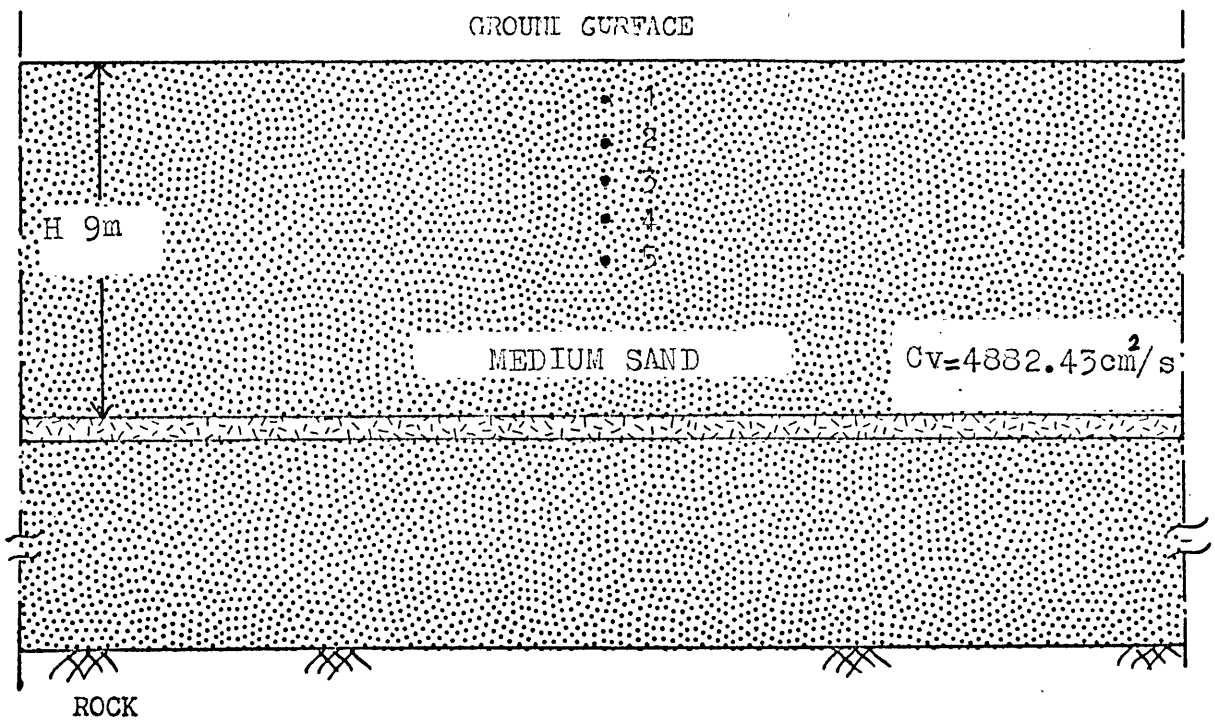

PLOT OF TIME vs. U/UO 1m,2m,3m,4m,5m,BELOW GROUND SURFACE FOR
H=6m CV=4882.43cm²/sec
U=excess pore pressure
UO= initial pore pressure
1m BELOW GROUND SURFACE
2m "
3m "
4m "
5m "
U/UO
1.00
0.80
0.60
0.40
0.20
0.00
0.00
20.00
40.00
60.00
80.00
100.00
120.00
140.00
160.00
TIME SECOND

FIG. 8.1

on dissipation of excess pore water pressure in the sand deposit, an investigation was carried out to determine the rate of change of excess pore water pressure with time in three layers of medium sand located above weak layer or impermeable formations with C_v = 4882.43 cm^2/sec and heights of 6,9,12m, respectively. The variation of excess pore pressure with time at depths 1,2,3,4,5m below ground surface are shown in figs.8.1 - 8.3. Comparisons of changes in excess pore water pressure at 1,2,3,4,5m below ground surface in the three layers over a period of 160 secs.after the earthquake are shown in figs.8.4-8.8.

Fig.8.4 shows the changes in excess pore water pressure with time at 1m below ground surface in the three layers. The excess pore water pressure dissipation is the same in the three layers up to about 16 seconds, thereafter the dissipation of excess pore water pressure in the 9m thick deposit becomes slower and equal to that of 12m thick deposit up to about 28 seconds after the earthquake. After 28 seconds the excess pore water pressure in 12m thick deposit begins to dissipate most slowly. The excess pore water pressure in the 6m thick deposit has almost reached zero at the end of 160 seconds, whereas the excess pore water pressure in the 9 and 12m thick deposits continues to dissipate. This is expected because from equation 8.2, it is apparent that the time required for a certain amount of dissipation to take place varies inversely with the square of H.

The rest of the results are presented in figs.8.5 - 8.8, which illustrate the changes in excess pore water pressure with time at depths 2,3,4,5m below ground surface in the three layers. It is apparent that the increase in height of the deposit located above a weak layer or an



SCHEMATIC SOIL PROFILE FOR PORE PRESSURE DISSIPATION SITE NO.2

FIG 8.2D

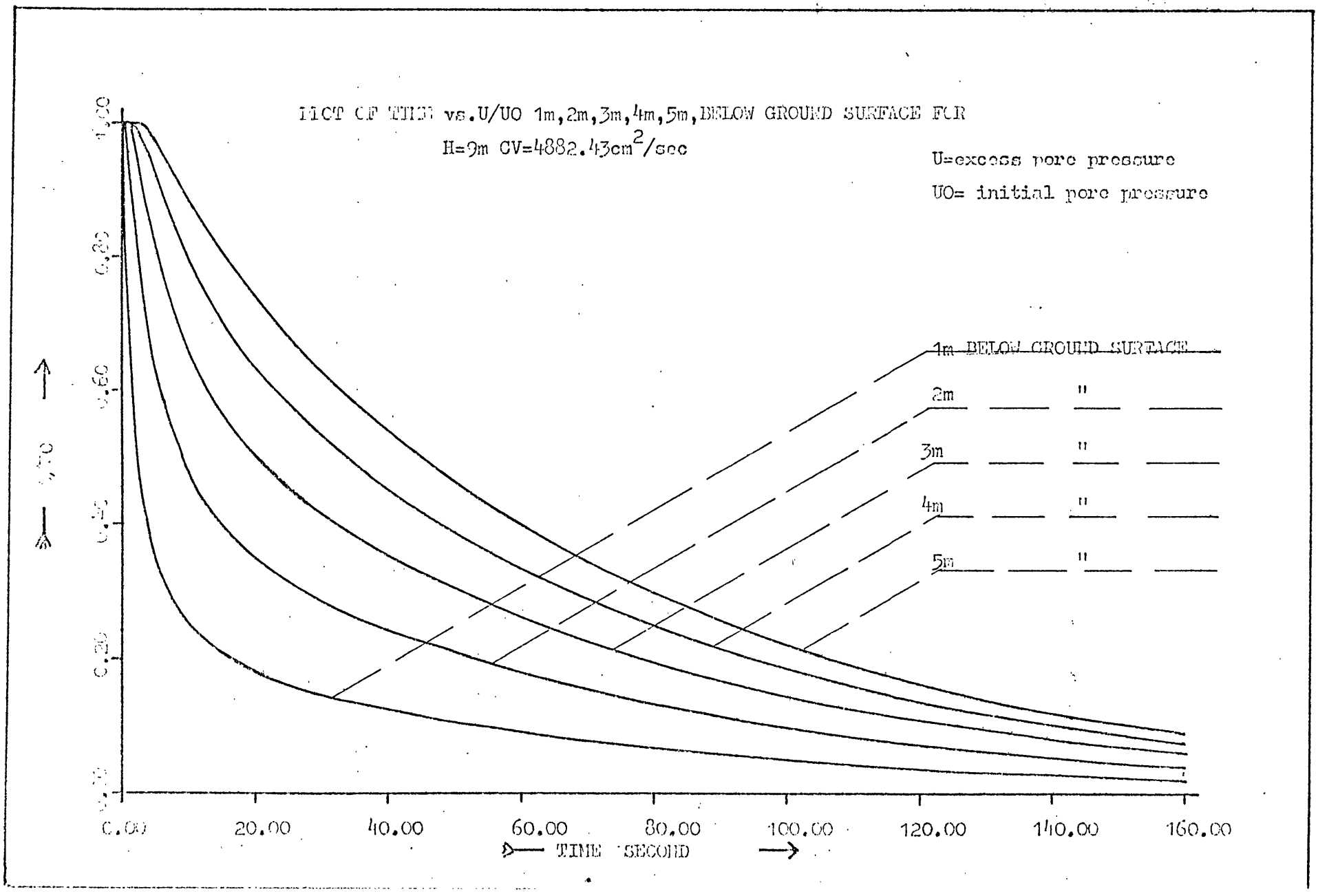
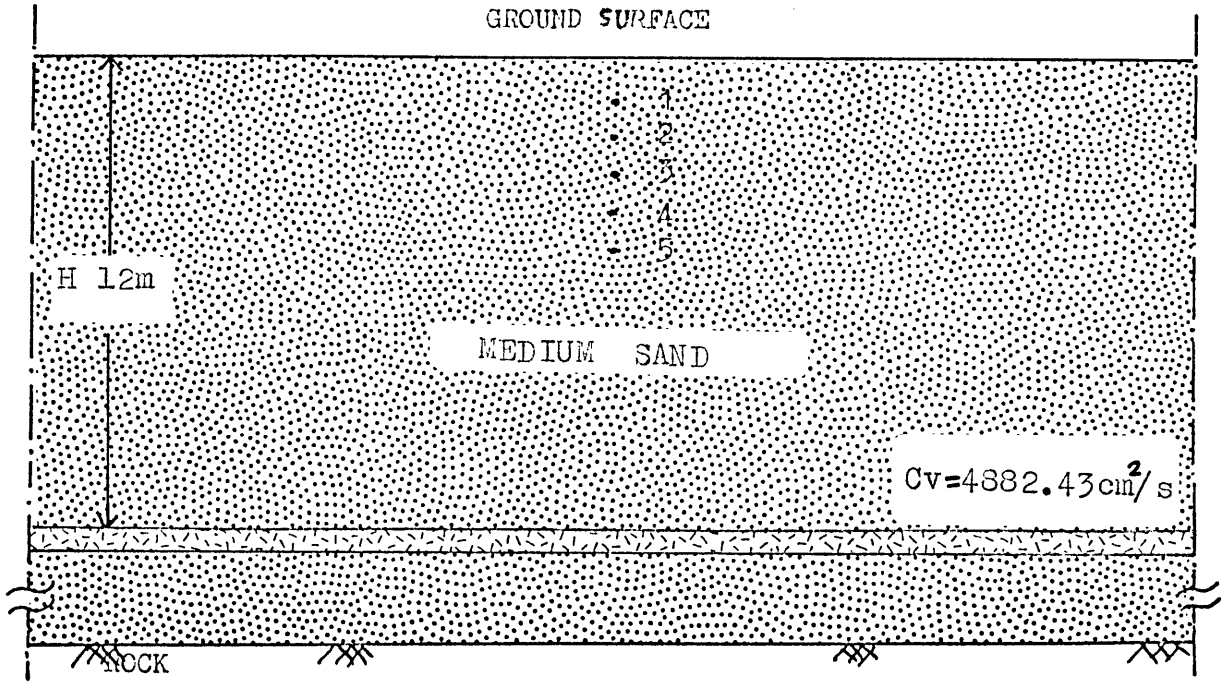

EFFECT OF TIME vs.U/UO 1m,2m,3m,4m,5m,BELOW GROUND SURFACE FOR
H=9m CV=4882.43cm²/sec
U=excess pore pressure
UO= initial pore pressure
1m BELOW GROUND SURFACE
2m " "
3m " "
4m " "
5m "
1.00
0.80
0.60
0.40
0.20
0.00
0.00
20.00
40.00
60.00
80.00
100.00
120.00
140.00
160.00
TIME SECOND

FIG. 8.2



SCHEMATIC SOIL PROFILE FOR PORE PRESSURE DISSIPATION SITE NO.3

FIG. 8.3D

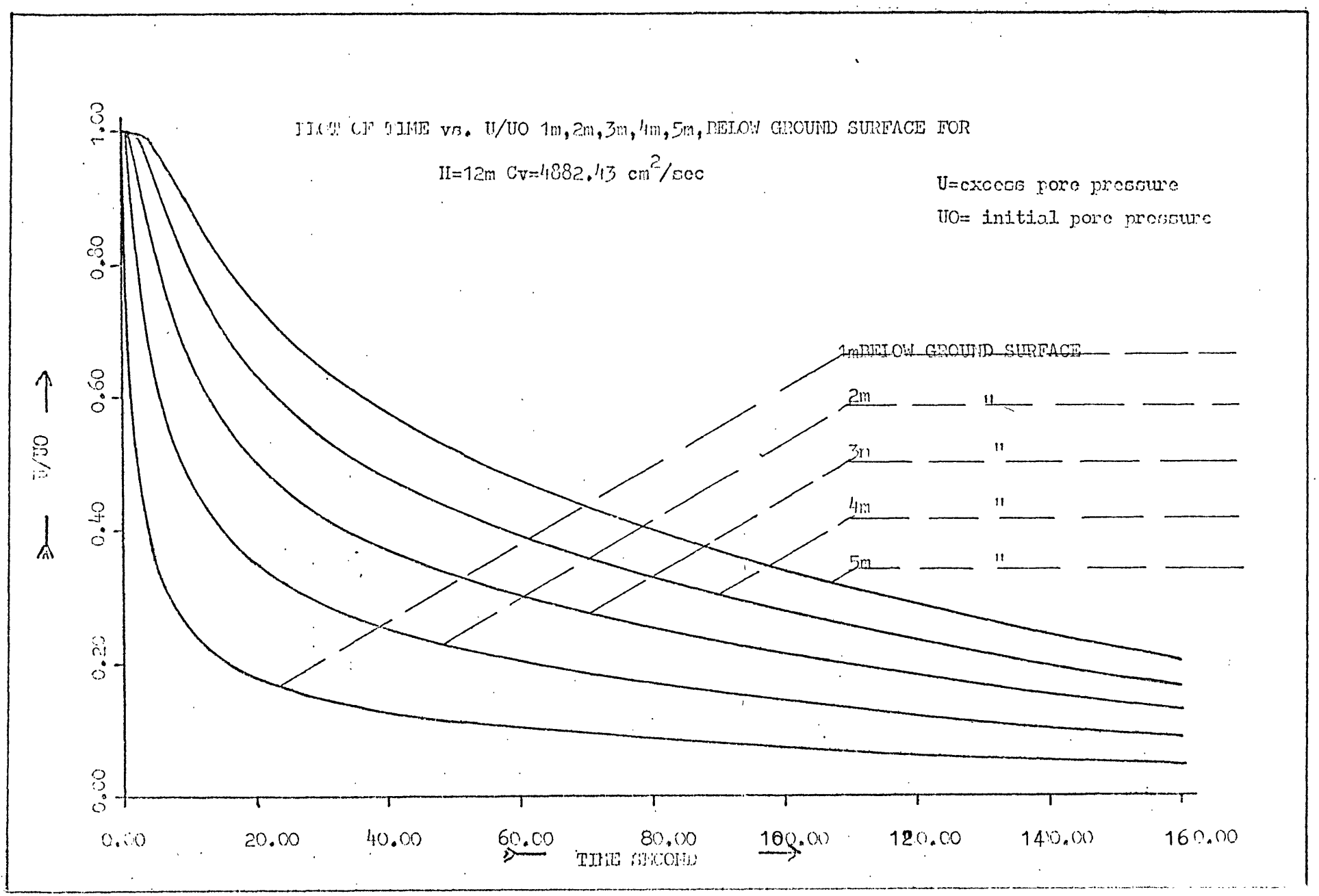

PLOT OF TIME vs. U/UO 1m,2m,3m,4m,5m,BELOW GROUND SURFACE FOR
H=12m Cv=4882.43 cm²/sec
U=excess pore pressure
UO= initial pore pressure
1mBELOW GROUND SURFACE
2m " "
3m " "
4m " "
5m " "
U/UO
1.00
0.80
0.60
0.40
0.20
0.00
0.00
20.00
40.00
60.00
80.00
100.00
120.00
140.00
160.00
TIME SECOND

FIG.8.3

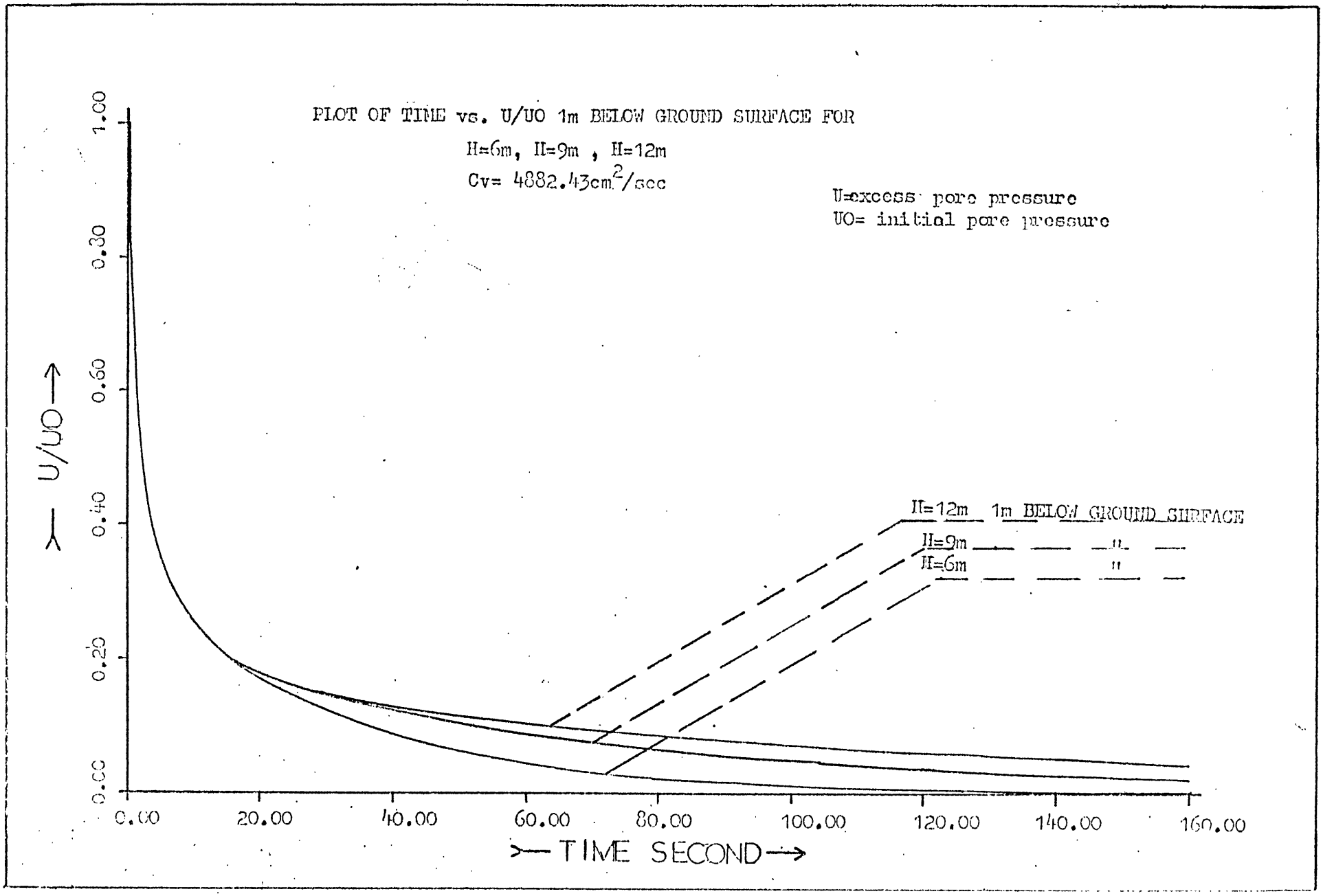

PLOT OF TIME vs. U/UO 1m BELOW GROUND SURFACE FOR
H=6m, H=9m , H=12m
Cv= 4882.43cm²/sec
U=excess pore pressure
UO= initial pore pressure
H=12m 1m BELOW GROUND SURFACE
H=9m "
H=6m "
U/UO
TIME SECOND
0.00
0.20
0.40
0.60
0.80
1.00
0.00
20.00
40.00
60.00
80.00
100.00
120.00
140.00
160.00

FIG.8.4

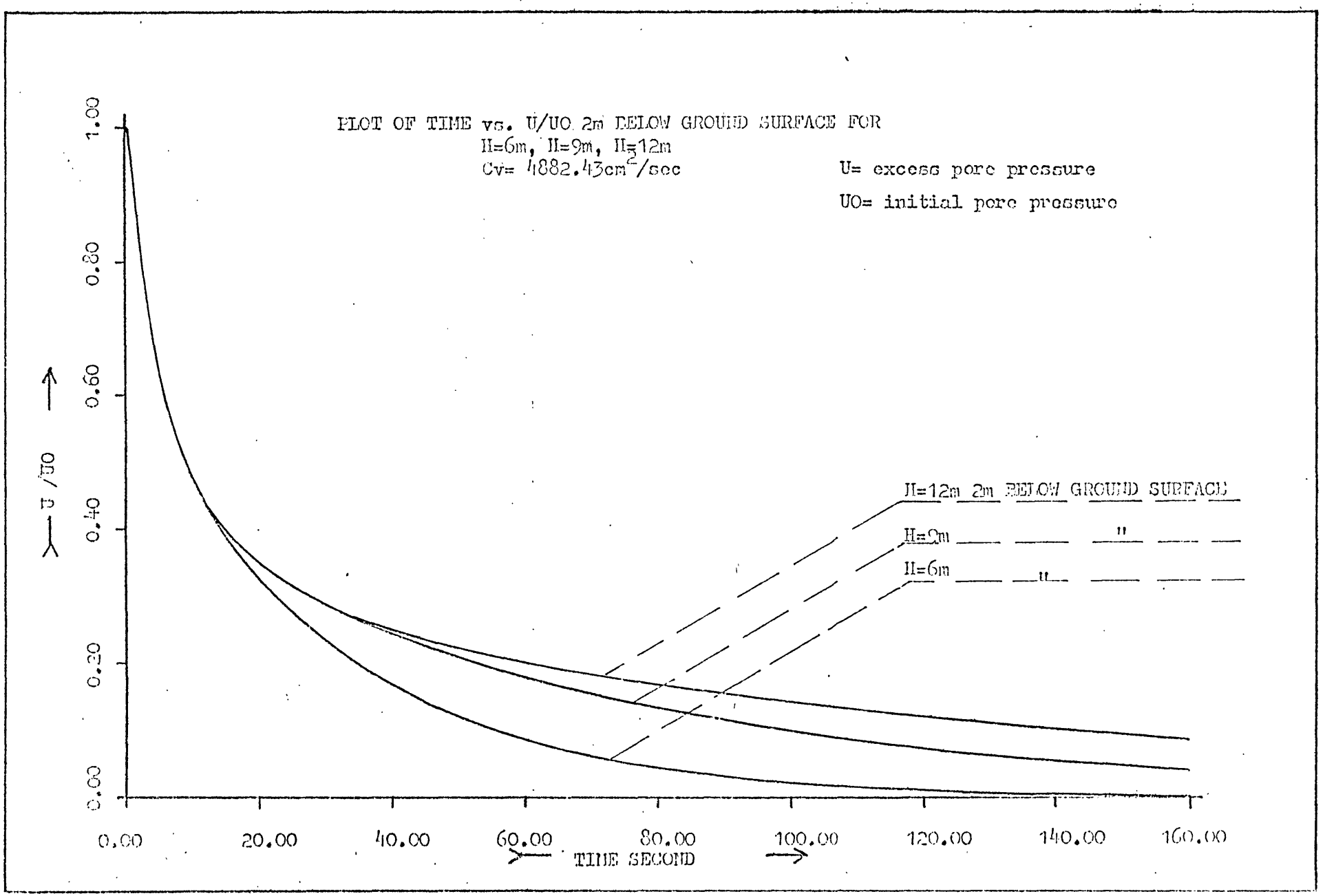

PLOT OF TIME vs. U/UO 2m BELOW GROUND SURFACE FOR
H=6m, H=9m, H=12m
Cv= 4882.43cm²/sec
U= excess pore pressure
UO= initial pore pressure
H=12m 2m BELOW GROUND SURFACE
H=9m " "
H=6m " "
U / UO
1.00
0.80
0.60
0.40
0.20
0.00
0.00
20.00
40.00
60.00
80.00
100.00
120.00
140.00
160.00
TIME SECOND

FIG.8.5

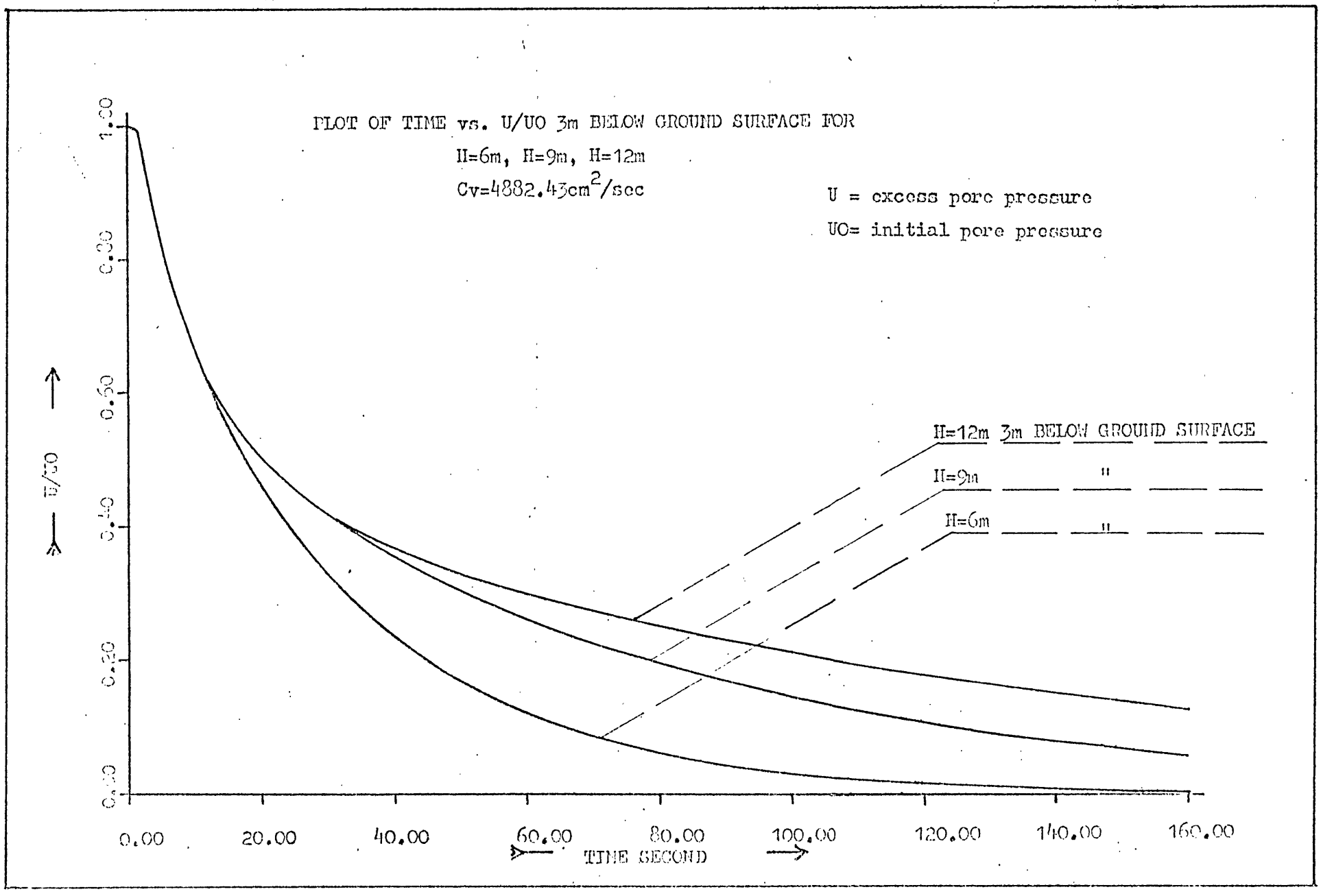

PLOT OF TIME vs. U/UO 3m BELOW GROUND SURFACE FOR
H=6m, H=9m, H=12m
Cv=4882.43cm²/sec
U = excess pore pressure
UO= initial pore pressure
H=12m 3m BELOW GROUND SURFACE
H=9m "
H=6m "
U/UO
1.00
0.80
0.60
0.40
0.20
0.00
0.00
20.00
40.00
60.00
80.00
100.00
120.00
140.00
160.00
TIME SECOND

FIG. 8.6

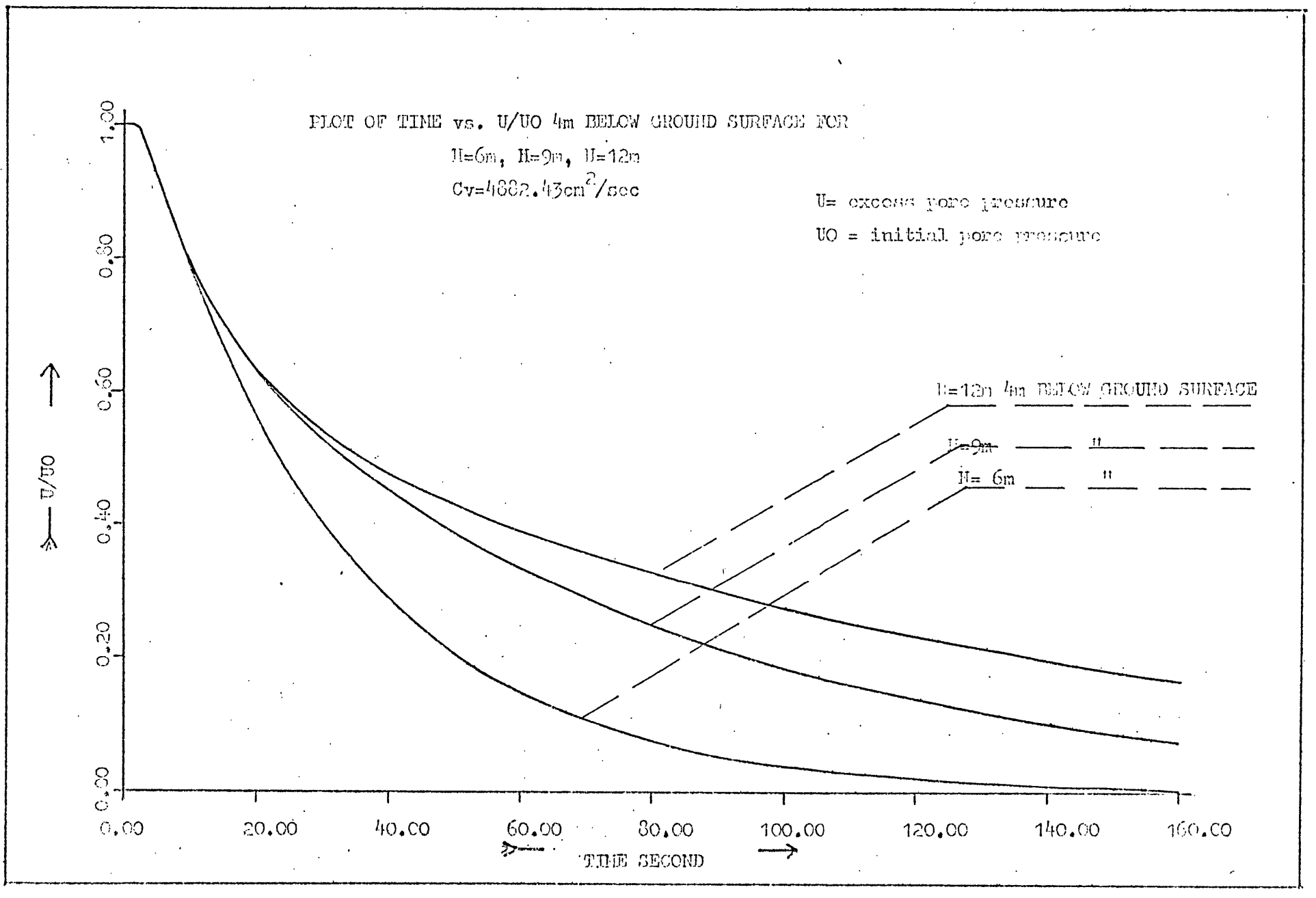

PLOT OF TIME vs. U/UO 4m BELOW GROUND SURFACE FOR
H=6m, H=9m, H=12m
Cv=4682.43cm²/sec
U= excess pore pressure
UO = initial pore pressure
H=12m 4m BELOW GROUND SURFACE
H=9m " "
H= 6m " "
U/UO
1.00
0.80
0.60
0.40
0.20
0.00
0.00
20.00
40.00
60.00
80.00
100.00
120.00
140.00
160.00
TIME SECOND

FIG.8.7

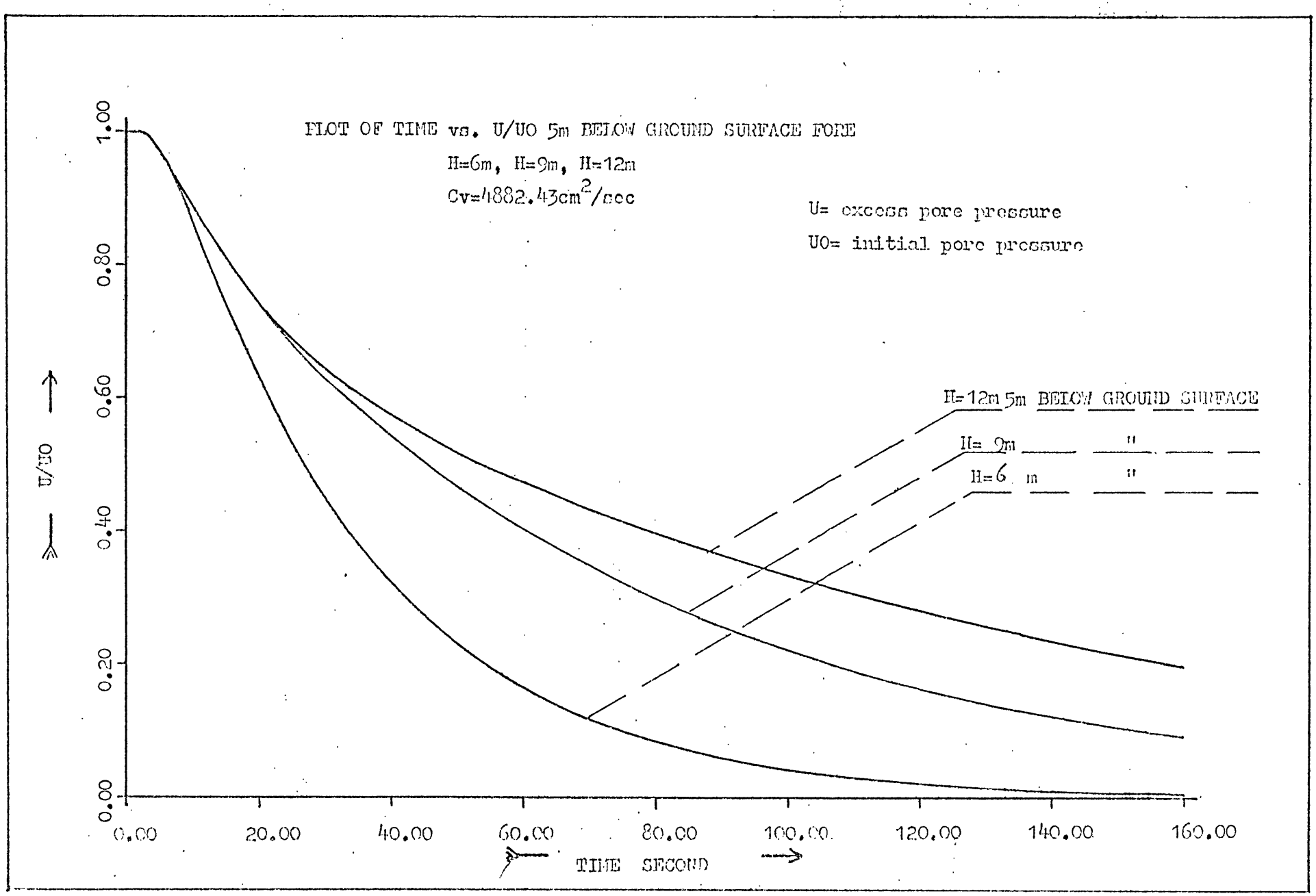

PLOT OF TIME vs. U/UO 5m BELOW GROUND SURFACE FORE
H=6m, H=9m, H=12m
Cv=4882.43cm²/sec
U= excess pore pressure
UO= initial pore pressure
H=12m 5m BELOW GROUND SURFACE
H= 9m " "
H=6 m " "
U/UO
1.00
0.80
0.60
0.40
0.20
0.00
0.00
20.00
40.00
60.00
80.00
100.00
120.00
140.00
160.00
TIME SECOND

FIG.8.8

impermeable formation has a significant effect on the excess pore water pressure dissipation with time, especially on the total time required for complete dissipation of excess pore water pressure. The effect is disadvantageous.

8.10. INVESTIGATION OF INFLUENCE OF COEFFICIENT OF CONSOLIDATION ON EXCESS PORE WATER PRESSURE DISSIPATION

To investigate the effect of coefficient of consolidation on dissipation rates, three sites similar to that explained in section 8.8 with different C_v values of 4882.43, 2441.2, 1220.61 cm^2/sec, which are typical of values for medium sand, fine sand and very fine sand, were studied. The changes in excess pore water pressure with time at depths 1,2,3,4,5m below ground surface in the deposit are shown in fig.8.9.

Fig.8.9 shows that in medium sand with twice the coefficient of consolidation of a fine sand and fine sand with twice the coefficient of consolidation of a very fine sand, the dissipation of excess pore water pressure with time is the same but twice as fast. This is expected from equation (8.2), due to the direct relationship between time and coefficient of consolidation. Figs 8.10 through 8.11 show similar behaviour for sites consisting of medium sand, fine sand and very fine sand with depths to weak layer or impermeable formation surface of 9 and 12m,respectively.

8.11. CONCLUDING REMARKS

Based on the results presented, the following conclusions are reached:

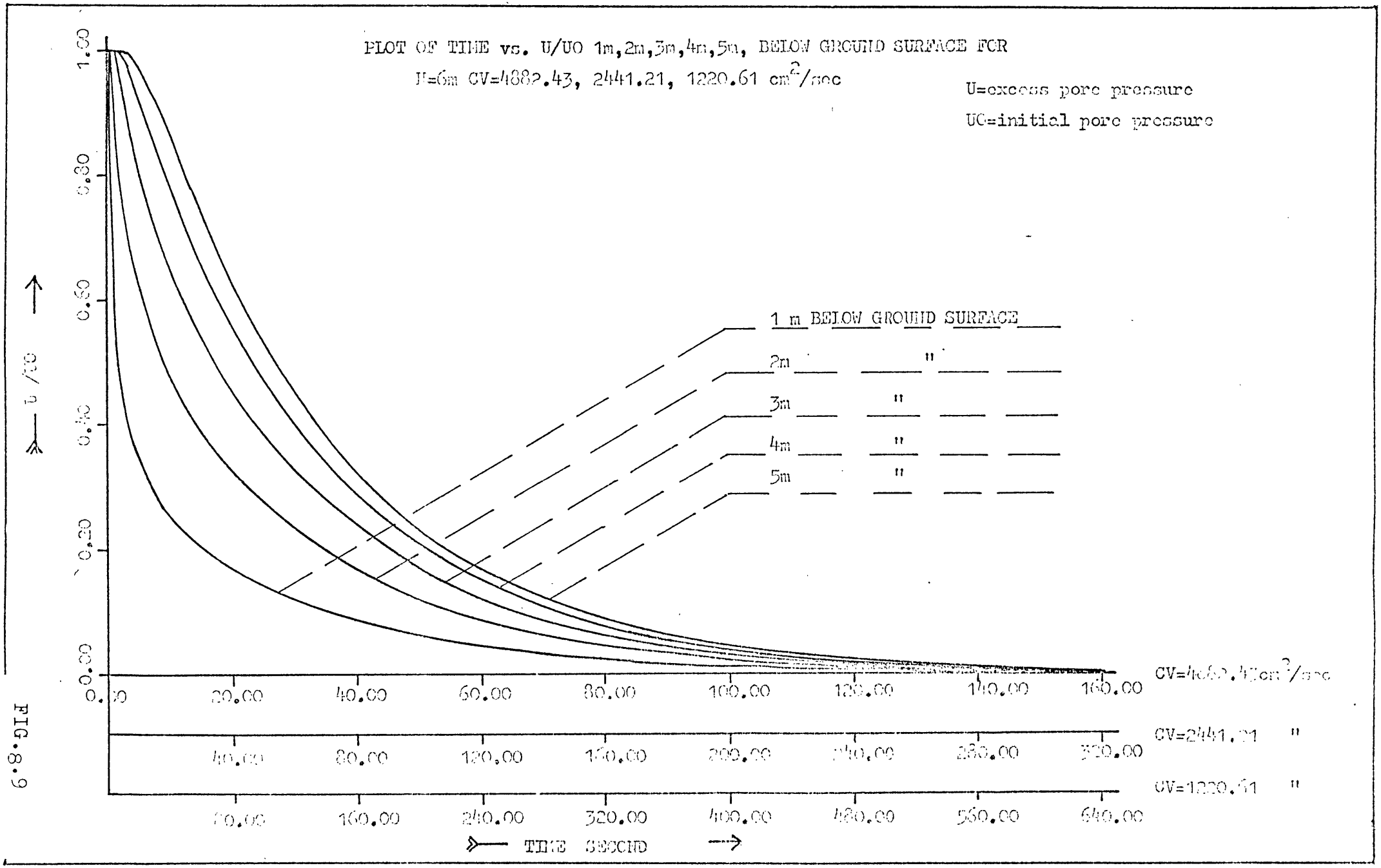

PLOT OF TIME vs. U/UO 1m,2m,3m,4m,5m, BELOW GROUND SURFACE FOR
H=6m CV=4882.43, 2441.21, 1220.61 cm²/sec
U=excess pore pressure
UO=initial pore pressure
1 m BELOW GROUND SURFACE
2m "
3m "
4m "
5m "
U/UO
1.00
0.80
0.60
0.40
0.20
0.00
0.00
20.00
40.00
60.00
80.00
100.00
120.00
140.00
160.00
CV=4882.43cm²/sec
40.00
80.00
120.00
160.00
200.00
240.00
280.00
320.00
CV=2441.21 "
80.00
160.00
240.00
320.00
400.00
480.00
560.00
640.00
CV=1220.61 "
TIME SECOND

FIG.8.9

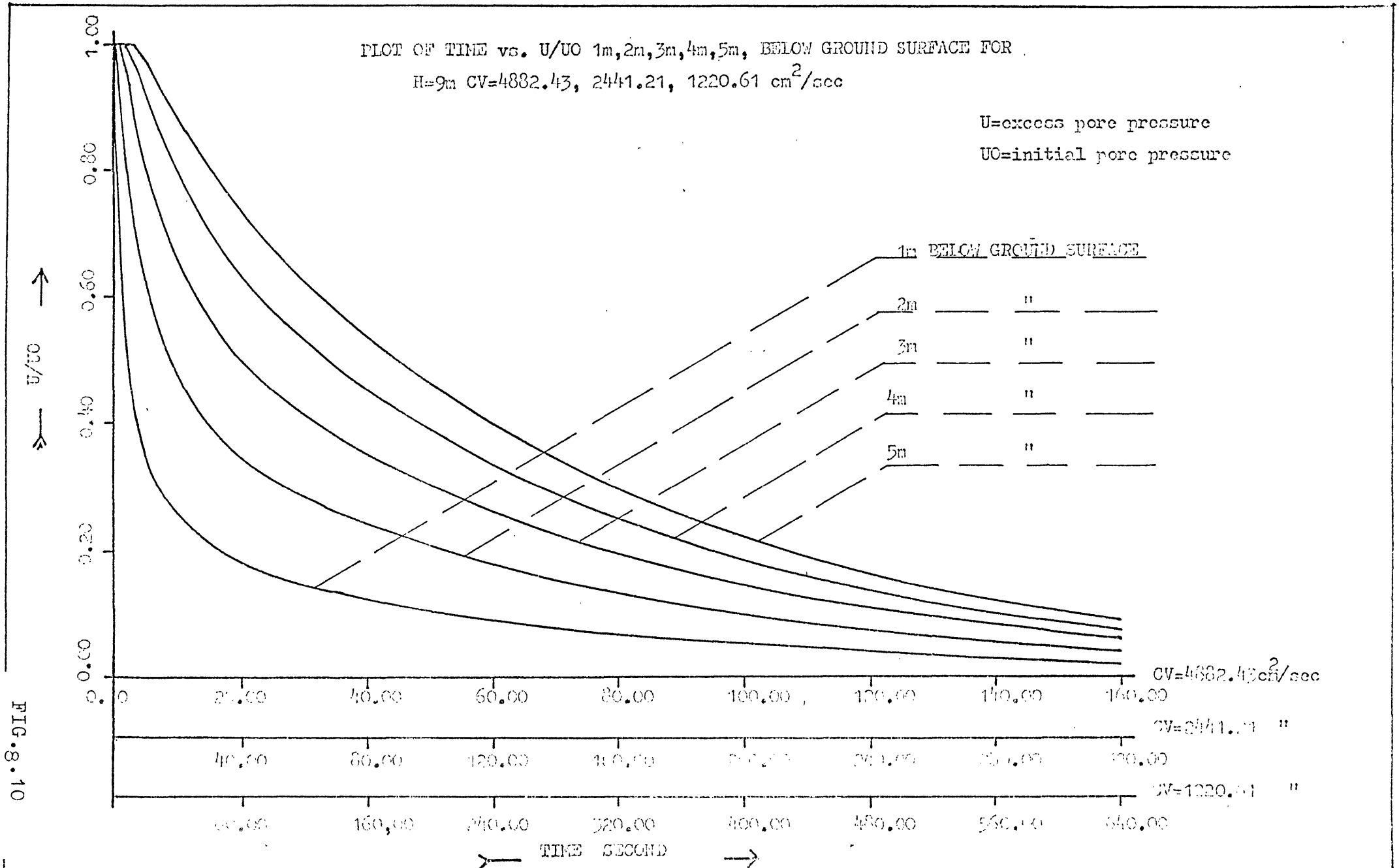

PLOT OF TIME vs. U/UO 1m,2m,3m,4m,5m, BELOW GROUND SURFACE FOR
H=9m CV=4882.43, 2441.21, 1220.61 cm²/sec
U=excess pore pressure
UO=initial pore pressure
1m BELOW GROUND SURFACE
2m " "
3m " "
4m " "
5m " "
U/UO
1.00
0.80
0.60
0.40
0.20
0.00
0.
40.00
80.00
120.00
160.00
200.00
240.00
280.00
320.00
360.00
400.00
440.00
480.00
520.00
560.00
600.00
640.00
CV=4882.43cm²/sec
CV=2441.21 "
CV=1220.61 "
TIME SECOND

FIG.8.10

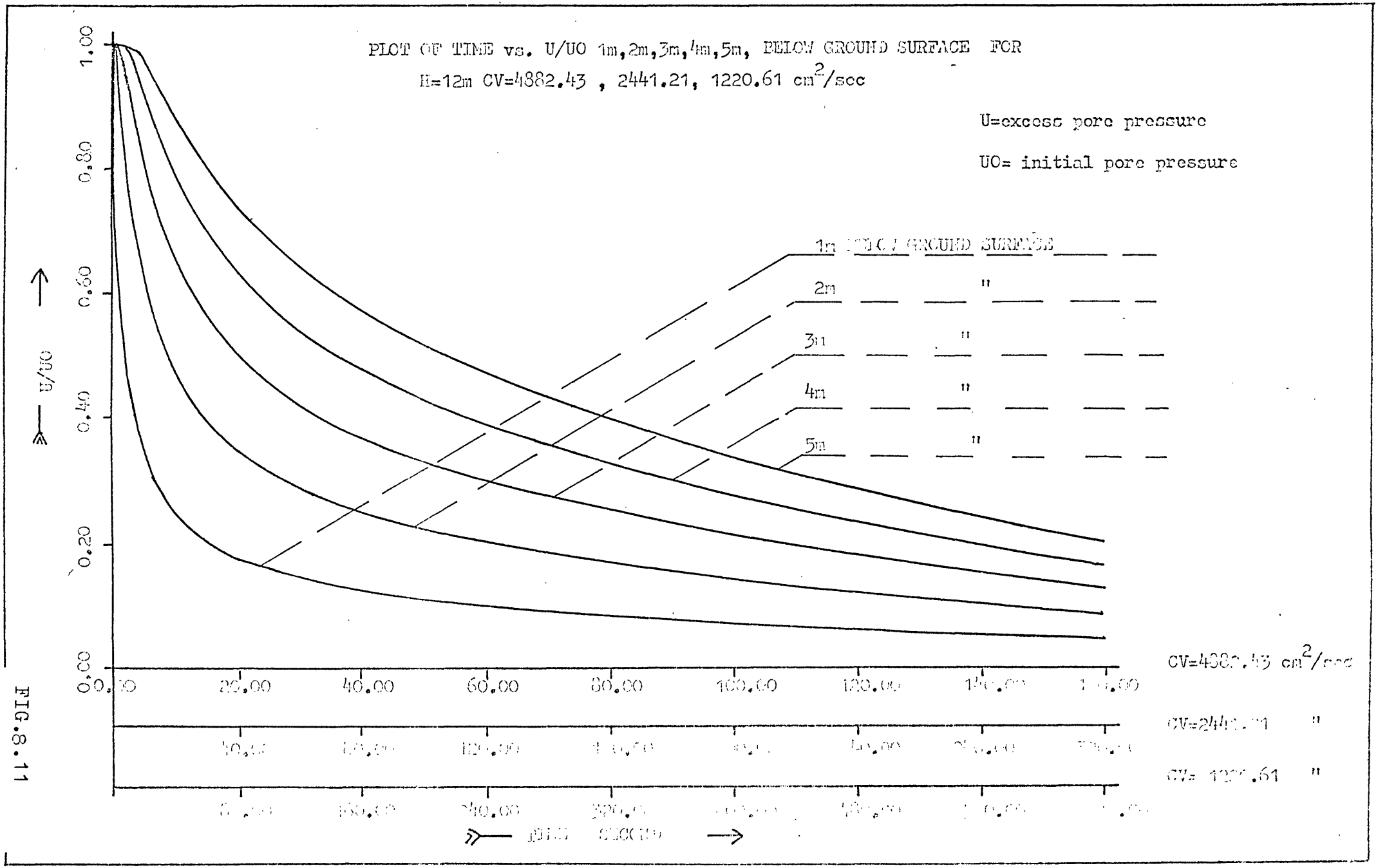

PLOT OF TIME vs. U/UO 1m,2m,3m,4m,5m, BELOW GROUND SURFACE FOR
H=12m CV=4882.43 , 2441.21, 1220.61 cm²/sec
U=excess pore pressure
UO= initial pore pressure
1m BELOW GROUND SURFACE
2m "
3m "
4m "
5m "
U/UO
1.00
0.80
0.60
0.40
0.20
0.00
20.00
40.00
60.00
80.00
CV=4882.43 cm²/sec
CV=2441.21 "
CV=1220.61 "

FIG.8.11

a) The dissipation of excess pore water pressure becomes slower as the depth below ground surface increases.

b) An increase in the thickness of the layer overlain by a weak thin layer or impermeable formation decreases the rate of dissipation of excess pore water pressure with time.

c) A decrease in the coefficient of consolidation of the deposit located above the weak layer or impermeable formation decreases the rate of dissipation of excess pore water pressure.

d) Dissipation characteristics of a deposit of sand located above a weak layer or an impermeable formation depends on both material properties of the sand deposit and depth to weak layer or impermeable formation.

CHAPTER 9

USE OF VERTICAL SAND FILTERS AS A NEW MEANS OF STABILIZING UNSTABLE SATURATED SAND DEPOSITS AGAINST EARTHQUAKES

9.1. INTRODUCTION

In the previous chapter, analysis is presented which provides some insight into the effects of vertical pore pressure dissipation in foundations after earthquakes. However, vertical drainage is not always the case, especially when thin layers of fine grained fully saturated loose sand are located in between beds of sand deposits. These layers would serve to inhibit vertical drainage to the extent that the results presented in the previous chapter would not apply. It is the objective of this chapter to study post earthquake pore pressure dissipation effects for two cases, radial drainage and three dimensional drainage associated with foundations of engineering structures.

In order to evaluate response of saturated sand deposits to seismic loading, special investigations are required to establish the susceptibility of the site to build-up of pore pressures. It is these excess pore pressures which dissipate with time after earthquakes and cause trouble. Gravels are usually considered to be safe because they do not build up much pore pressure. Loss of shear strength in saturated sand deposits, due to increase in pore pressure, would make the site

unstable; hence the ground response theory presented in the previous chapter would not apply. To remedy the situation and to eliminate one of the basic assumptions made by all the previous investigators working in this field, namely, "the site would remain stable against earthquakes", a remedial measure has been suggested here which can easily be applied to stabilize unstable saturated sand deposits.

9.2. PREVIOUS REMEDIAL MEASURES

In the past, in sites where loss of shear strength due to increase in pore pressure might occur, the following remedial measures were adopted.

9.2.1. INCREASING OVERBURDEN PRESSURE BY A PERVIOUS FILL

The idea of a beneficial effect of a surcharge was first introduced by Maslov[43] based on laboratory studies i.e. all other factors being equal, the higher the confining pressure the more cyclic shear stress is required to cause instability. Based on other types of studies, similar conclusions were drawn by Seed et. al.[51] and Ambraseys and Sarma[4]

However, as was observed in the Nigata earthquake 1967 at Nigata site, at the toes of the pervious fill, where the effect of surcharge was almost negligible, instability of a high order occurred and, as a result, the fill started to spread, causing extensive settlement to structures located on the fill.

9.2.2. DENSIFICATION OF SOIL BY MEANS OF COMPACTION PILES

Often engineering structures are designed to be supported on piles

which, during driving process, densify the soil due to two processes, vibration and displacement, finally transferring the structural load to the hard rock underlying the deposit.

However, piles do not let buildings settle but they tilt instead when the sand surrounding them becomes unstable, thus causing large settlements to structures located on them; therefore, they do not seem to be a good remedial measure.

9.2.3. DENSIFICATION OF SOIL BY MEANS OF VIBROFLOTATION

The process of vibroflotation is done by means of an equipment called "Vibroflot" which is sunk in a borehole. After starting vibroflot, the machine starts hammering the sides of the borehole. The vibroflot is then gradually raised and a continuous supply of sand is added.

As it is obvious from the technique itself, the sand near the surface of the borehole will be compacted considerably, soils far from the borehole will be affected to a lesser degree or may not be affected at all.[10] Thus this technique as carried out today does not seem to be a good remedial measure. It might have some effect if the hammering was done for a long time in very closely spaced boreholes, but this might not be economical at all.

9.3. PREVIOUS WORK

No previous work has been reported on the subject. Seed et. al. in their study which was summarized in section 8.2 have concluded:

"Improving the drainage capability of a sand deposit by

the installation of a highly pervious continuous drainage system may thus provide an effective means of stabilizing a potentially unstable deposit".

9.4. SCOPE AND OBJECTIVES OF PRESENT STUDY

The main objectives of the present study are:

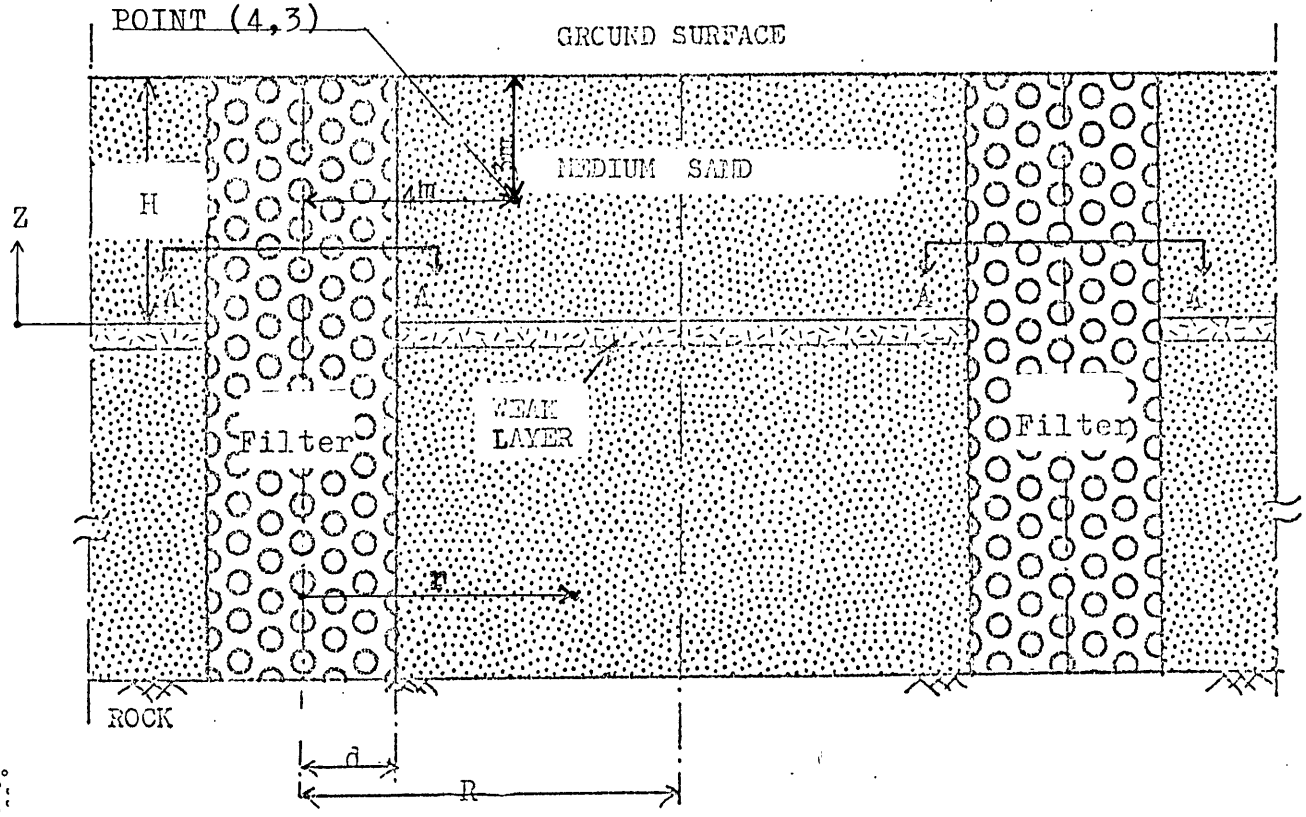
i) To provide some theory for the installation of vertical sand filters at sites considered to be unstable and possessing weak layers of trapped loose deposits or an impermeable formation at some depth below ground surface.

ii) To analyse the post earthquake redistribution of pore water pressure in a two-layer system of sand of different or similar material properties, having a weak layer of loose material trapped between beds of two deposits. The lower layer is underlain by an impervious bedrock.

iii) To throw some light on the effect of trapped weak layer on post earthquake pore water dissipation in the system shown by figs. 9.1D and 9.2D

9.5. EFFECT OF TRAPPED WEAK LAYER ON THE SYSTEM SHOWN BY FIG 9.1D

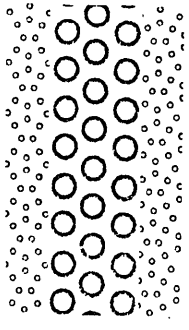
As mentioned in section 8.4, the shaking caused by the earthquake will develop a condition of initial liquifaction or liquifaction in the trapped loose deposit. Migration of loose fine particles of liquified sand into voids of the sand just beneath or above would prevent vertical drainage. There will be no dissipation of excess pore water pressure from lower layer through upper layer. The flow in the lower layer will be radial, whereas, in the upper layer, both radial and vertical.



SCHEMATIC SOIL PROFILE FOR PORE PRESSURE DISSIPATION AFTER INSTALLATION OF SAND DRAINS SITE

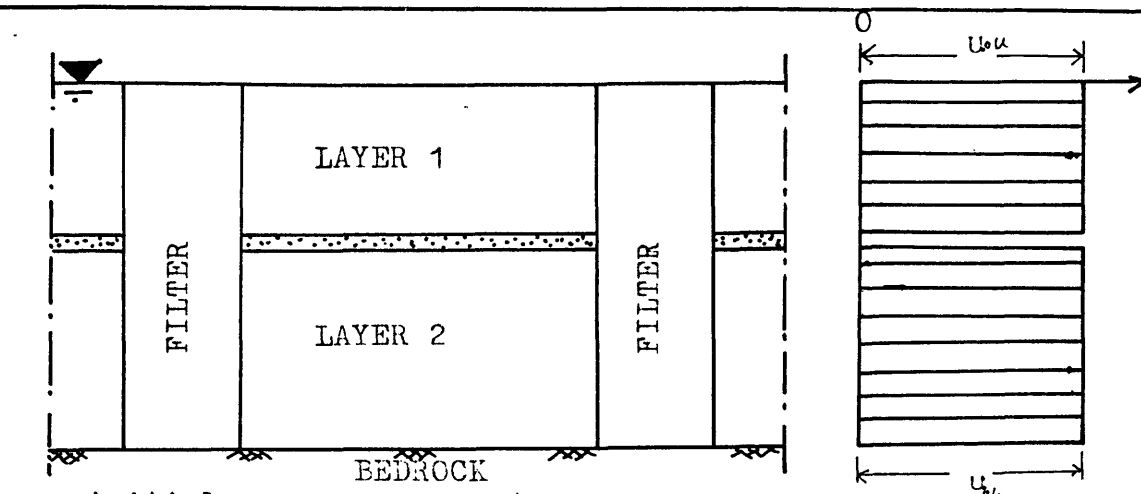
d-filter radius

R= radius of filter influence

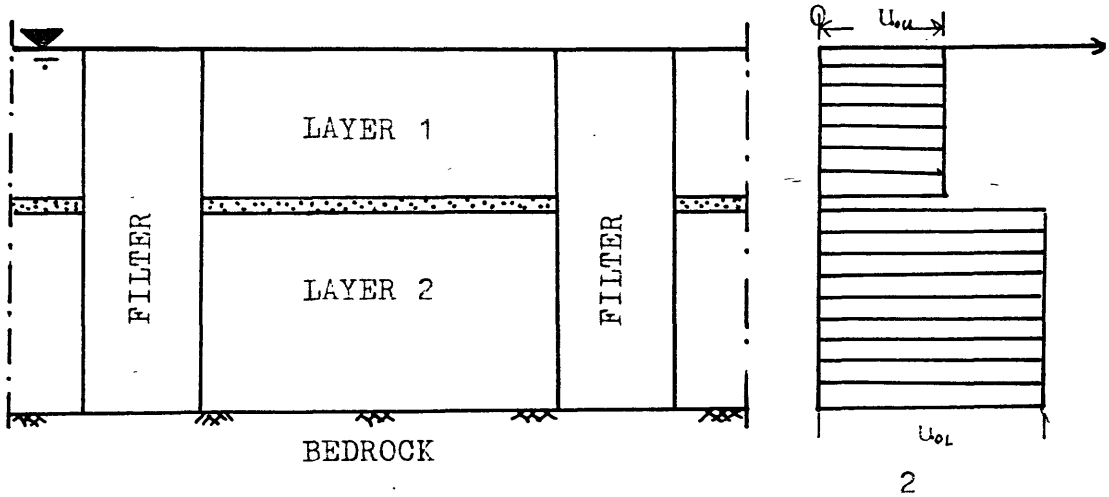


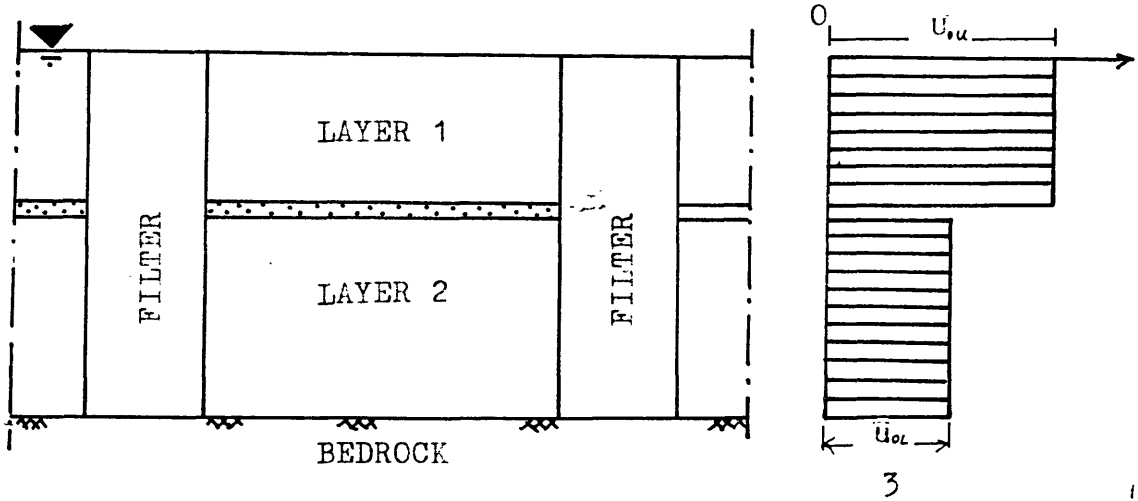
CROSS SECTION A-A

fig. 9.1D



u_{ou} = initial excess pore water pressure in the upper layer.
u_{oL} = initial excess pore water pressure in the lower layer.





INITIAL EXCESS PORE WATER PRESSURE DISTRIBUTION

fig.9.2D

As a result both layers would consolidate.

9.6. PURPOSE OF SAND FILTERS

The purpose of sand filters is to relieve the excess pore water pressure induced in the voids of the sand by the earthquake.

It is obvious that the filters would serve as supplementary outlets for the excess pore water which would squeeze out of the voids after earthquake shaking is over, thus preventing post earthquake ejection of springs of water and sand, which usually cover a large area and make structures tilt and settle extensively.

Sand filters, if functioning properly, would initiate a stabilization process and could prevent development of conditions of instability.

9.6.1. STATEMENT OF THE PROBLEM

The importance of the problem solved in this chapter lies in the fact that both cases, i.e. radial drainage as well as multi-directional drainage, are combined in one problem as shown in fig. 9.10. Either of these cases could be used separately, depending on the situations met in practice.

9.7. THEORY

9.7.1. DISSIPATION OF EXCESS PORE WATER PRESSURE AFTER EARTHQUAKE SHAKING IN THE TWO LAYER SYSTEM

The excess hydrostatic pressure set up by the earthquake will tend to dissipate after the earthquake in the upper and lower layer, according

to laws of three-and two-dimensional consolidation processes, respectively.(a diffusion process accompanying volume change).

9.7.1.1. GOVERNING DIFFERENTIAL EQUATION IN THE UPPER LAYER

The differential equation governing the distribution of excess hydrostatic pressure in the upper layer is given by

$$\frac{\delta u_c}{\delta t} = C_{h1}\left(\frac{\delta^2 u_c}{\delta \varsigma^2} + \frac{1}{\varsigma}\frac{\delta u_c}{\delta \varsigma}\right) + C_v \frac{\delta^2 u_c}{\delta z^2} \qquad (9.1)$$

where variable u (excess pore water pressure) is a function of vertical coordinate " z " radial coordinate " ς " and time "t".

C_v = coefficient of consolidation for vertical drainage.

C_h = coefficient of consolidation for horizontal drainage.

Equation (9.1) is obtained by extending the proof given in appendix I to three dimensional case and transform the resulting equation into polar coordinates by means of substitution $x = \varsigma \cos\theta$ $y = \varsigma \sin\theta$, $z = z$ assuming that $C_x = C_y = C_h$. A simple proof of this is given by [28]

It is possible to treat the differential equation (9.1) separately, considering

a) The plane radial flow equation:

$$C_{h1}\left(\frac{\delta^2 u}{\delta \varsigma^2} + \frac{1}{\varsigma}\frac{\delta u_\varsigma}{\delta \varsigma}\right) = \frac{\delta u_\varsigma}{\delta t} \qquad (9.2)$$

b) The linear vertical flow equation:

$$c_v \frac{\delta^2 u_z}{\delta z^2} = \frac{\delta u_z}{\delta t} \tag{9.3}$$

Then the excess pore water dissipation for the combined flow:

$$U_{r,z} = U_r * U_z^{50} \tag{9.4}$$

where: $\frac{u_c}{u_{ou}} = U_{r,z}$, $\frac{u}{u_{ou}} = U_r$, $\frac{u_z}{u_{ou}} = U_z$

9.7.1.2. BOUNDARY CONDITIONS FOR EQUATION 9.2

i) The post earthquake excess pore water pressure throughout the upper layer is

$$u_{ou} \quad \text{at} \quad t = 0 \quad \text{at} \quad d < \varsigma < R$$

ii) The excess pore water pressure at the filter well surface is zero

$$u(\varsigma, t)\Big|_{\varsigma = d} = 0$$

iii) No flow across the effective radius of the filter well

$$\frac{\delta u}{\delta \varsigma}(\varsigma, t)\Big|_{\varsigma = R} = 0$$

9.7.1.3. BOUNDARY CONDITIONS FOR EQUATION 9.3

The corresponding boundary conditions for equation (9.3) are given in section 8.5.1

9.7.1.4. SOLUTION OF DIFFERENTIAL EQUATION (9.2)

Solution of the differential equation (9.2) is given in appendix II.

From appendix II, the excess pore water pressure for the radial flow takes the form

$$u_s(\rho, t) = \Pi \cdot u_{cu} \sum_{n=1}^{\infty} \frac{J_0(d\alpha_n) \cdot J_1(R\alpha_n)}{J_1^2(R\alpha_n) - J_0^2(d\alpha_n)} \times$$

$$\times \left[J_0(\rho\alpha_n) \cdot Y_1(R\alpha_n) - J_1(R\alpha_n) \cdot Y_0(\rho\alpha_n) \right] \times \exp(-C_{h1} \cdot \alpha_n^2 t) \qquad (9.5)$$

where:

R = radius of filter influence

d = radius of filter.

J_0 & J_1 = Bessel functions of first kind, of zero order and first order, respectively.

Y_1, Y_0 = Bessel functions of second kind, of zero order and first order, respectively.

$\alpha_1, \alpha_2 \cdots \alpha_n$ are the roots of the following equation

$$J_0(d\alpha_n) \cdot Y_1(R\alpha_n) - J_1(R\alpha_n) \cdot Y_0(d\alpha_n) = 0 \qquad (9.6)$$

9.7.1.5. SOLUTION OF DIFFERENTIAL EQUATION (10.3)

Solution of the differential equation (9.3) is given by (8.3).

9.7.1.6. EXCESS PORE WATER DISSIPATION FOR THE COMBINED FLOW IN THE TOP LAYER

The excess pore water dissipation with time for the combined flow in the upper layer is given by combination of (9.4), (9.5) & (8.3).

$$u_1(r,z,t) = 4u_{ou} \sum_{n=1}^{\infty} \sum_{m=1}^{\infty} \frac{(-1)^{m+1}}{(2m-1)} \times \frac{J_o(d\,\alpha_n) \cdot J_1(R\,\alpha_n)}{J_1^2(R\cdot\alpha_n) - J_o^2(d\,\alpha_n)} \times$$

$$\times \left[\left[J_o(r\cdot\alpha_n).Y_1(R\cdot\alpha_n) - J_1(R\cdot\alpha_n).Y_o(r\cdot\alpha_n) \right] \times \cos\left(\frac{(2m-1)\,\Pi\,.Z}{2H}\right) \right] \times$$

$$\times \exp\left(-C_{h1}.\alpha_n^2 t - \frac{C_v.\,\Pi^2.(2m-1)^2}{4H^2}\, t \right) \qquad (9.7)$$

where α_n are the roots of equation (9.6), other symbols are as previously defined.

9.7.2. GOVERNING DIFFERENTIAL EQUATION IN THE LOWER LAYER

The differential equation governing the distribution of excess pore water pressure in the lower layer is given by

$$C_{h2}\left(\frac{\delta^2 u_r}{\delta r^2} + \frac{1}{r}\frac{\delta u_r}{\delta r} \right) = \frac{\delta u_r}{\delta t} \qquad (9.8)$$

similar to (9.2) except C_{h1} is replaced by C_{h2} where C_{h2} = coefficient of consolidation for the lower layer for horizontal drainage. The reason for this is explained in section 9.5

9.7.2.1. BOUNDARY CONDITIONS FOR EQUATION (10.8)

Boundary conditions for equation (9.8) are the same as those given in section 9.7.1.2. except u_{ou} replaced by u_{oL} which is the post earthquake excess pore water pressure throughout the lower layer

9.7.2.2. SOLUTION OF DIFFERENTIAL EQUATION (9.8)

Solution of differential equation (9.8) which gives the excess pore water pressure in the lower layer takes the form

$$u_2(\xi, t) = \Pi \cdot u_{oL} \sum_{n=1}^{\infty} \frac{J_o(d\,\alpha_n) \cdot J_1(R\,\alpha_n)}{J_1^2(R\,\alpha_n) - J_o^2(d\,\alpha_n)} \times$$

$$\times \left[J_o(\xi\,\alpha_n) \cdot (R\,\alpha_n) - J_1(R\,\alpha_n) \cdot {}_o(\xi\,\alpha_n) \right] \times \exp -C_{h2} \cdot \alpha_n^2 t) \qquad (9.9)$$

where:

$\alpha_1, \alpha_2, \ldots \alpha_n$ are the roots of equation (9.6) other symbols are as previously defined.

9.8. COMPUTER PROGRAM

Solutions given by 9.7 & 9.9 were incorporated into a computer program named FILTER (use of vertical sand filters as a new means of stabilizing unstable saturated sand deposits against earthquakes.) This program consists of a main program and two subroutine (RADFL1) & (VERTF2). The program is developed for installation of vertical sand filters in areas where instability is likely to occur and the proposed site possesses a weak layer or an impermeable formation at some depth

below ground surface. The purpose of the program is to compute the ratio of excess pore water pressure to initial pore water pressure at any point in the two layer system shown in fig.9.10 for known field and laboratory data of sands in combination with general filter specifications.

Output from the program includes input data, excess pore water pressure over initial pore water pressure, along with their time of occurrence, both for three-dimensional drainage in the upper layer and two-dimensional drainage in the lower layer.

The program is coded in FORTRAN IV and has been used on CDC 6400 computer of Imperial College.

9.9. INFLUENCE OF SAND FILTERS ON POST EARTHQUAKE DISSIPATION OF EXCESS PORE WATER PRESSURE

To investigate the influence of vertical sand filters on distribution of excess pore water pressure following earthquake, three sites of medium sand 30m thick with $C_v = C_h$ values of 4882.43 cm^2/sec, each having a weak layer located 12,9,6m below ground surface, as shown in fig.9.10, were chosen. The ground water was assumed to be at the surface of the deposit.

The post earthquake changes in excess pore water pressure, with time at depths 3,4,5m below ground surface, a distance of 2,3,4m from filter axis, over a period of 160 secs.after earthquake excitation, for the three sites, before and after installation of vertical sand filters, are shown in figs.9.1 through 9.9.

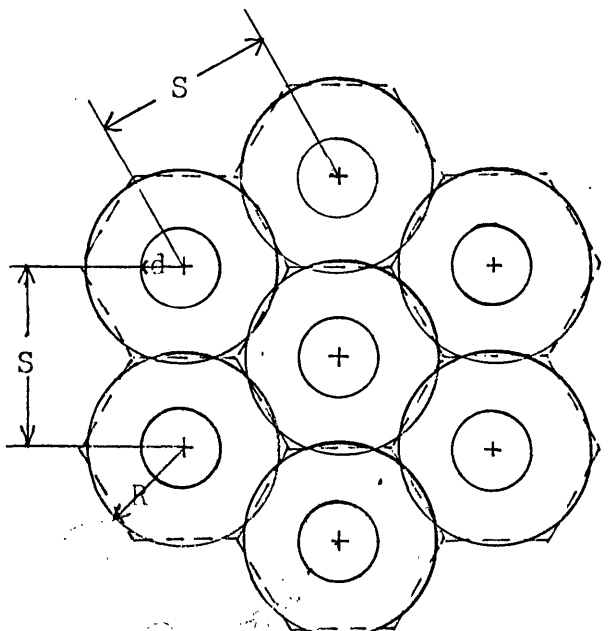
Filters were assumed to have been constructed in a triangular pattern as shown in fig.9.3D, with full penetration throughout the depth of the two layers. Fig.9.1 shows the changes in excess pore water pressure with time, before and after installation of sand filters at coordinates (2,3),(3,3),(4,3) in the first site described above. Installation of sand filters causes 80% of the total excess pore water pressure generated during earthquake shaking at point (4,3) to dissipate in the first 29 seconds, whereas the normal time for 80% dissipation would have been 110 secs. This also means that a stablization process will take place after 29 seconds. Thus reducing upward flow of water to the ground surface which can cause extensive damage to structures, by creating a "quick" condition at the surface of the deposit.

Figs.9.2 - 9.3 show similar results for depths below ground surface of 4 and 5m. These results indicate that installation of sand filters has much more beneficial effect on dissipation of excess pore water pressure at greater depths below ground surface, because the distance the excess pore water has to flow in order to escape is reduced considerably. Hence the time of dissipation is reduced considerably.

Figs.9.4 through 9.9 show similar behaviour for second and third sites with depth to weak layer surface of 9 and 6m, respectively.

Fig.9.10 shows radial dissipation of excess pore water pressure in the lower layer over a period of 160 seconds after earthquake at distances of 2,3,4m from filter axis. The excess pore water pressure dissipates fastest at the distance of 2m from filter axis. The dissipation of excess pore water pressure becomes slower as the distance from filter axis increases. This is expected because points (2, z) are

LAYOUT OF SAND FILTERS

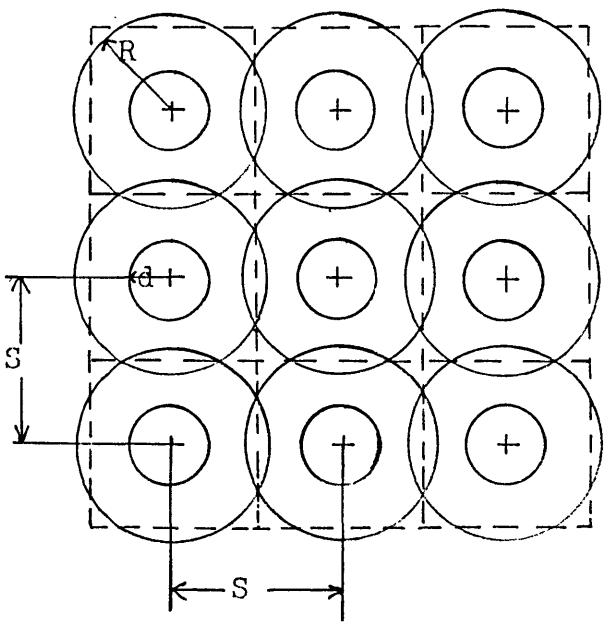


TRIANGULAR PATTERN

R = 0.525 * S

R = effective radius of filters.

S = spacing of filters.



SQUARE PATTERN

R = 0.564 * S

fig. 9.3D

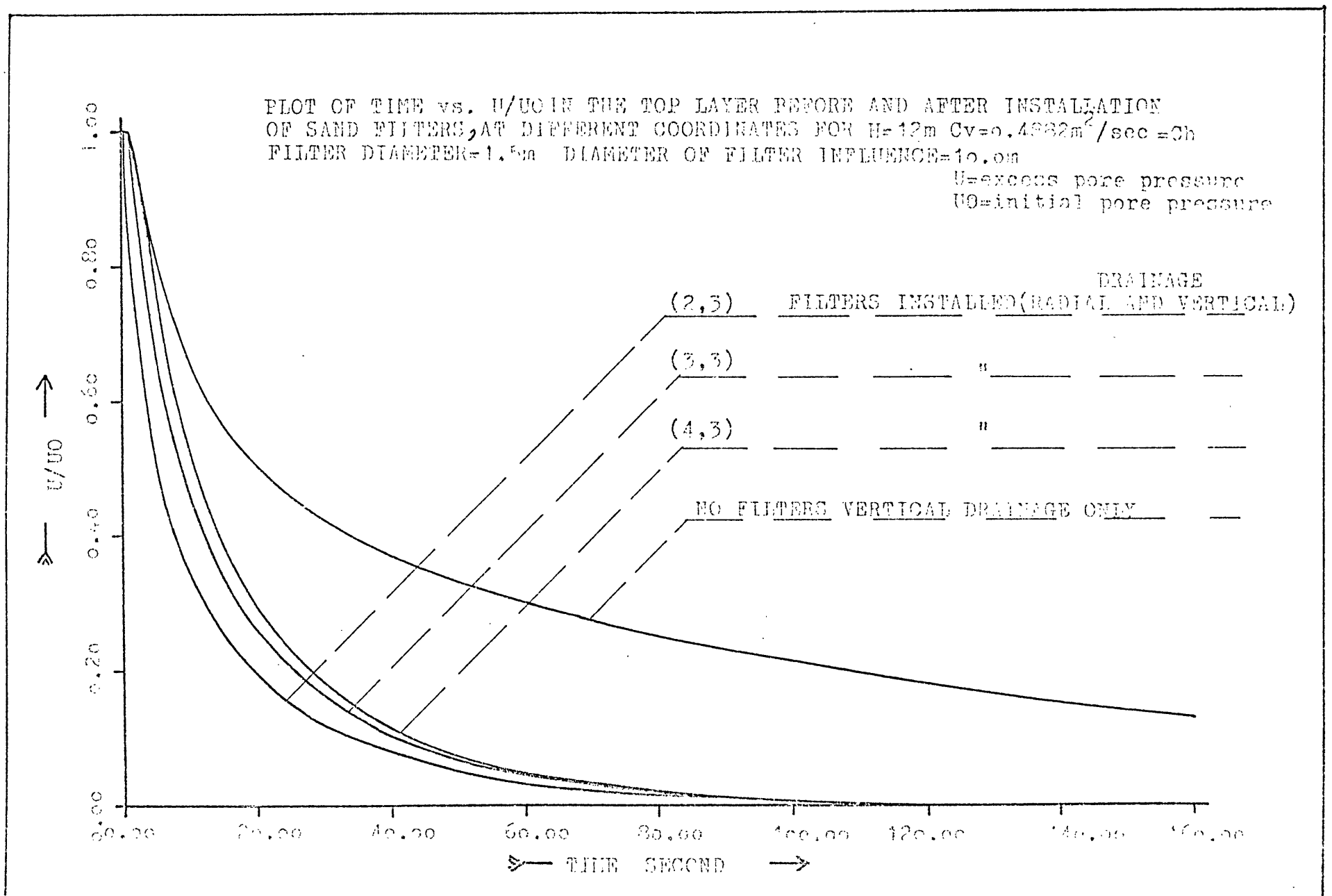

PLOT OF TIME vs. U/UO IN THE TOP LAYER BEFORE AND AFTER INSTALLATION
OF SAND FILTERS, AT DIFFERENT COORDINATES FOR H=12m Cv=0.4982m²/sec =Ch
FILTER DIAMETER=1.5m DIAMETER OF FILTER INFLUENCE=10.0m
U=excess pore pressure
UO=initial pore pressure
DRAINAGE
(2,3) FILTERS INSTALLED(RADIAL AND VERTICAL)
(3,3) " "
(4,3) " "
NO FILTERS VERTICAL DRAINAGE ONLY
U/UO
1.00
0.80
0.60
0.40
0.20
0.00
TIME SECOND

Fig. 9.4

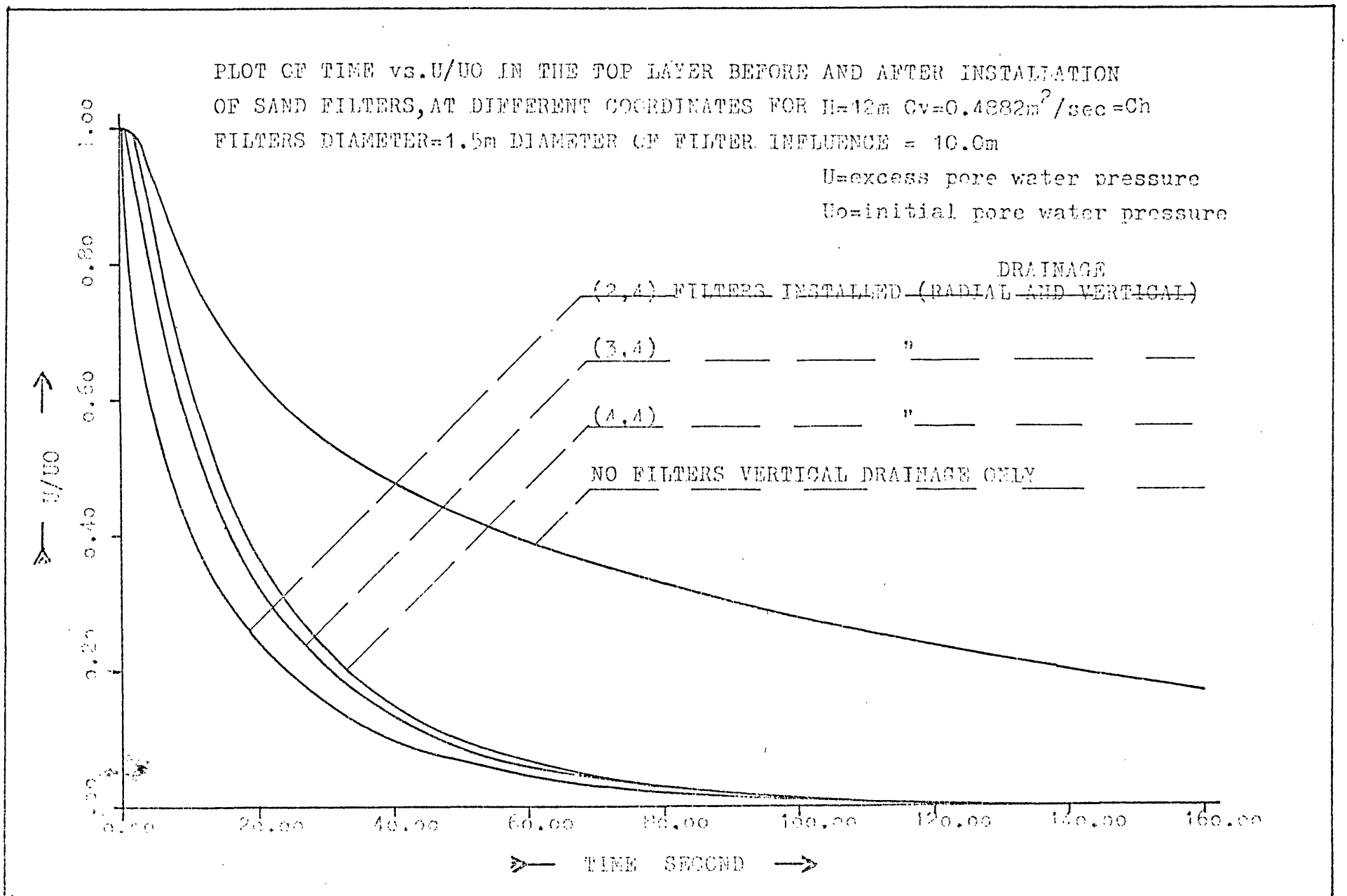

PLOT OF TIME vs.U/UO IN THE TOP LAYER BEFORE AND AFTER INSTALLATION
OF SAND FILTERS, AT DIFFERENT COORDINATES FOR H=12m Cv=0.4882m²/sec =Ch
FILTERS DIAMETER=1.5m DIAMETER OF FILTER INFLUENCE = 10.0m
U=excess pore water pressure
Uo=initial pore water pressure
DRAINAGE
(2,4) FILTERS INSTALLED (RADIAL AND VERTICAL)
(3,4) " "
(4,4) " "
NO FILTERS VERTICAL DRAINAGE ONLY
U/Uo
1.00
0.80
0.60
0.40
0.20
0.00
20.00
40.00
60.00
80.00
100.00
120.00
140.00
160.00
TIME SECOND

Fig. 9.2

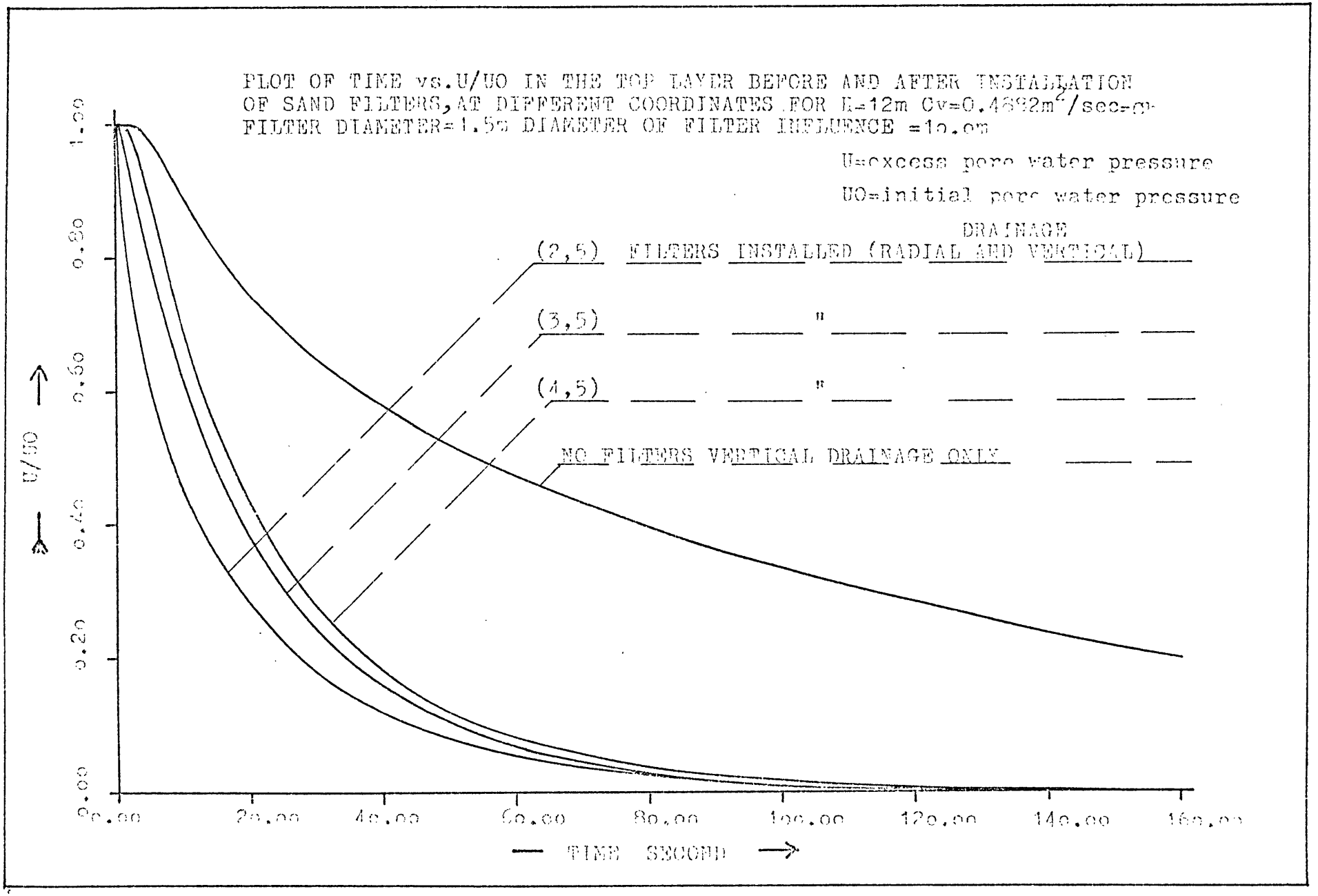

PLOT OF TIME vs.U/UO IN THE TOP LAYER BEFORE AND AFTER INSTALLATION
OF SAND FILTERS, AT DIFFERENT COORDINATES FOR R=12m Cv=0.46?2m²/sec=C
FILTER DIAMETER=1.5m DIAMETER OF FILTER INFLUENCE =1?.?m
U=excess pore water pressure
UO=initial pore water pressure
DRAINAGE
(2,5) FILTERS INSTALLED (RADIAL AND VERTICAL)
(3,5) " "
(4,5) " "
NO FILTERS VERTICAL DRAINAGE ONLY
U/UO
1.00
0.80
0.60
0.40
0.20
0.00
20.00
40.00
60.00
80.00
100.00
120.00
140.00
160.00
TIME SECOND

Fig. 9.3

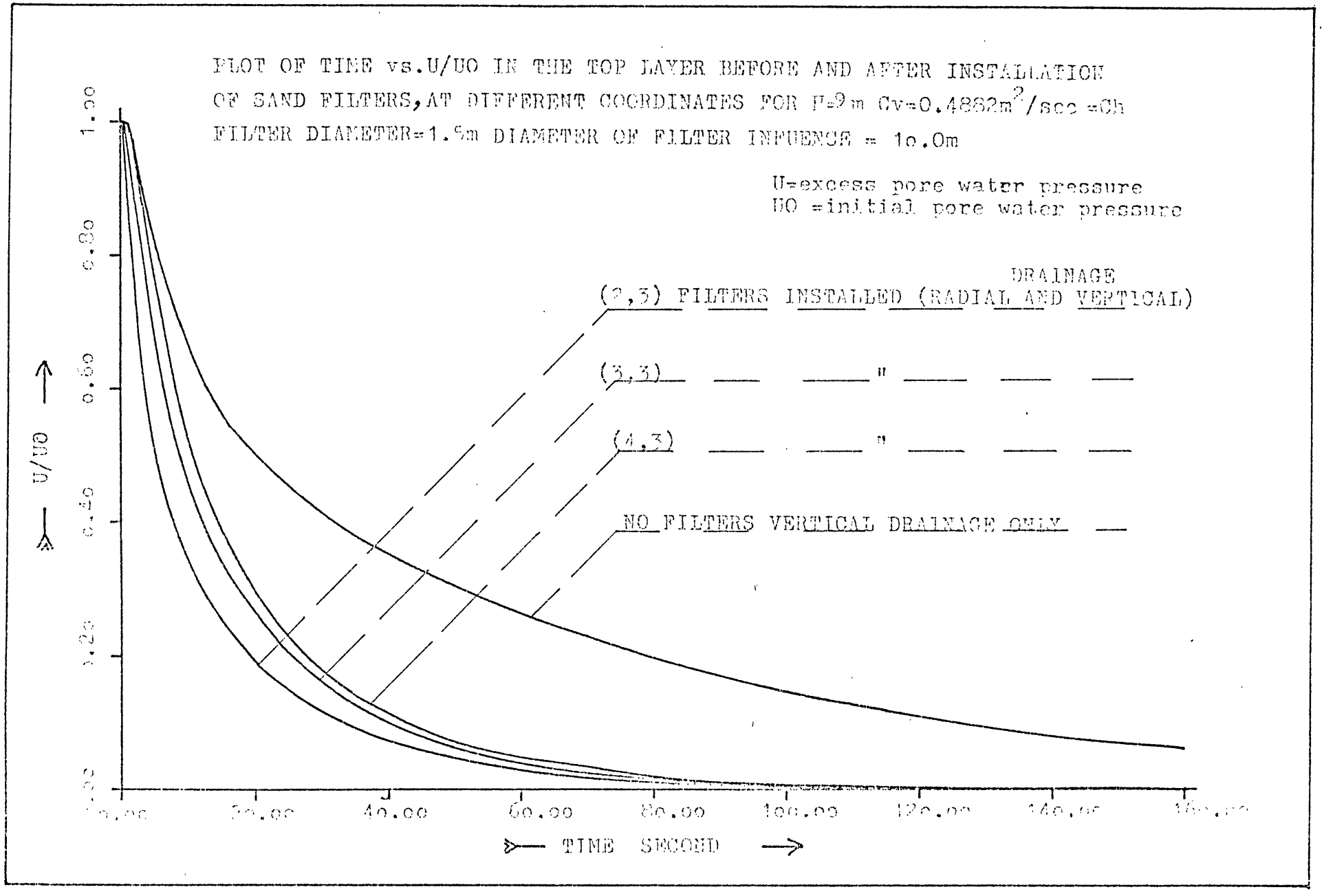

PLOT OF TIME vs.U/UO IN THE TOP LAYER BEFORE AND AFTER INSTALLATION
OF SAND FILTERS, AT DIFFERENT COORDINATES FOR r=9m Cv=0.4882m²/sec =Ch
FILTER DIAMETER=1.5m DIAMETER OF FILTER INFLUENCE = 10.0m
U=excess pore water pressure
UO =initial pore water pressure
DRAINAGE
(2,3) FILTERS INSTALLED (RADIAL AND VERTICAL)
(3,3) " "
(4,3) " "
NO FILTERS VERTICAL DRAINAGE ONLY
U/Uo
1.00
0.80
0.60
0.40
0.20
40.00
60.00
80.00
100.00
TIME SECOND

Fig. 9.4

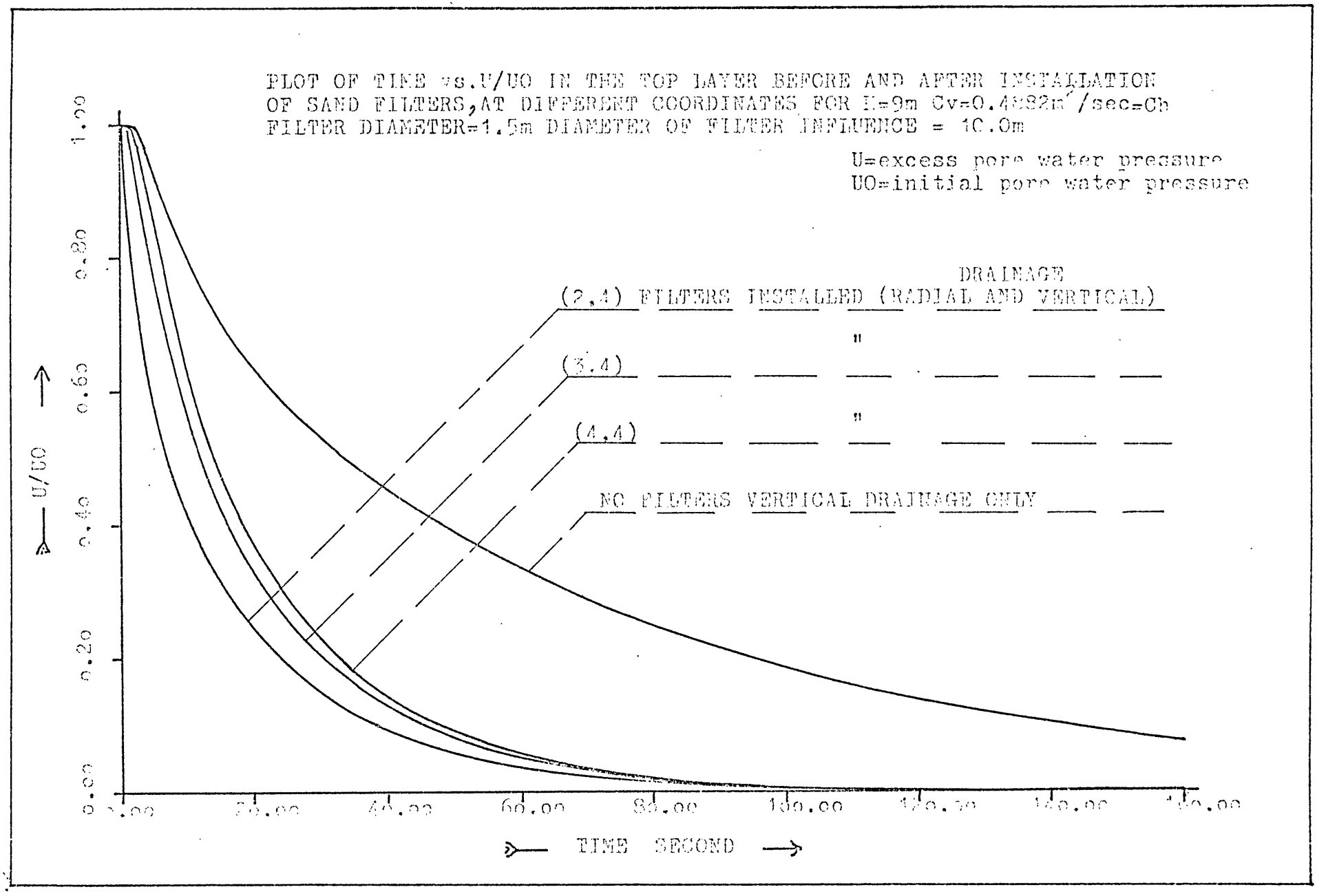

PLOT OF TIME vs.U/UO IN THE TOP LAYER BEFORE AND AFTER INSTALLATION
OF SAND FILTERS, AT DIFFERENT COORDINATES FOR H=9m Cv=0.4
FILTER DIAMETER=1.5m DIAMETER OF FILTER INFLUENCE = 10.0m
U=excess pore water pressure
UO=initial pore water pressure
DRAINAGE
(2,4) FILTERS INSTALLED (RADIAL AND VERTICAL)
"
(3,4)
"
(4,4)
NO FILTERS VERTICAL DRAINAGE ONLY
U/UO
1.00
0.80
0.60
0.40
0.20
0.00
20.00
40.00
60.00
80.00
100.00
120.00
140.00
160.00
TIME SECOND

Fig. 9.5

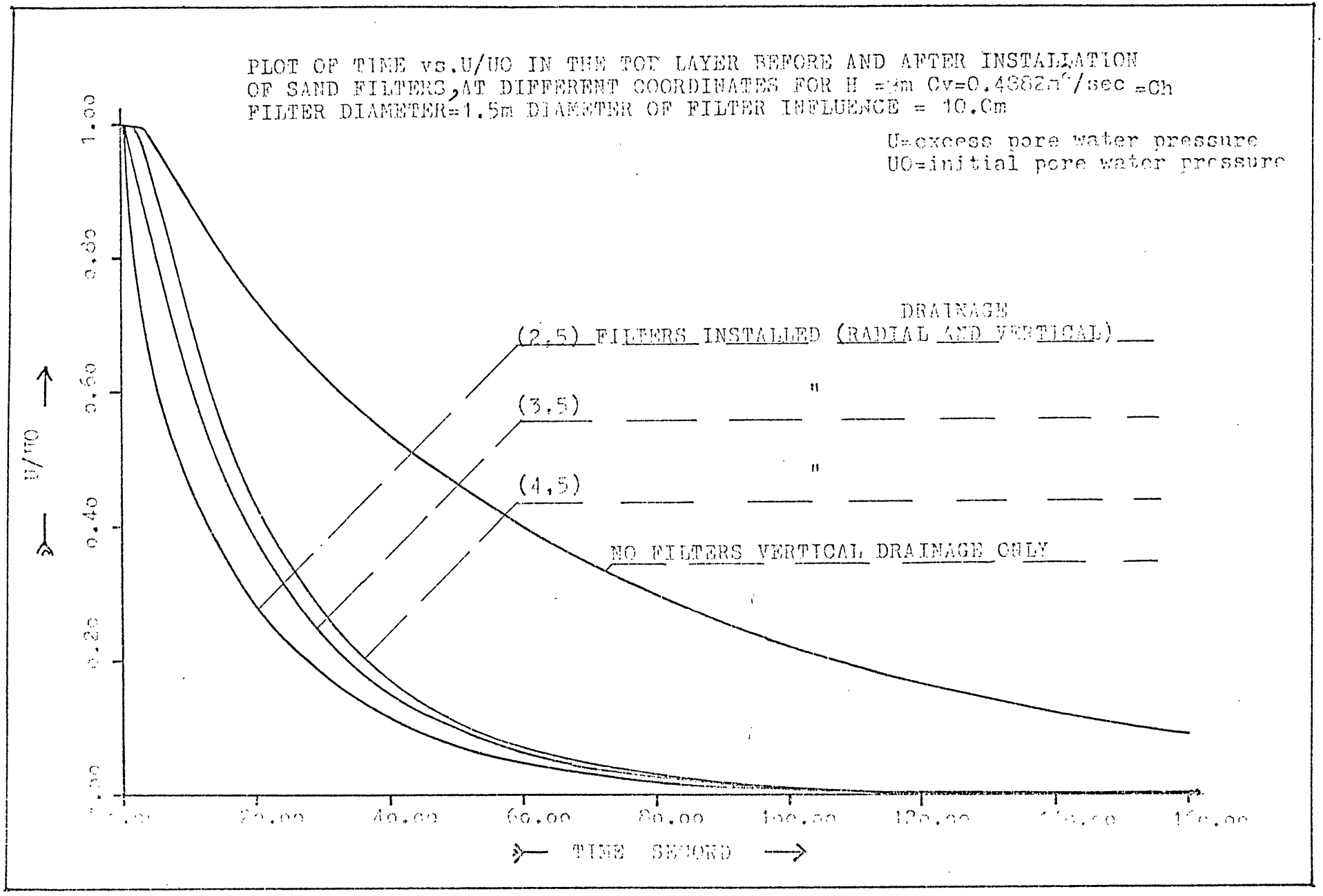

PLOT OF TIME vs.U/UO IN THE TOT LAYER BEFORE AND AFTER INSTALLATION
OF SAND FILTERS,AT DIFFERENT COORDINATES FOR H =4m Cv=0.4382m²/sec =Ch
FILTER DIAMETER=1.5m DIAMETER OF FILTER INFLUENCE = 10.0m
U=excess pore water pressure
UO=initial pore water pressure
DRAINAGE
(2,5) FILTERS INSTALLED (RADIAL AND VERTICAL)
"
(3,5)
"
(4,5)
NO FILTERS VERTICAL DRAINAGE ONLY
U/UO
1.00
0.80
0.60
0.40
0.20
0.00
20.00
40.00
60.00
80.00
100.00
120.00
160.00
TIME SECOND

Fig. 9.6

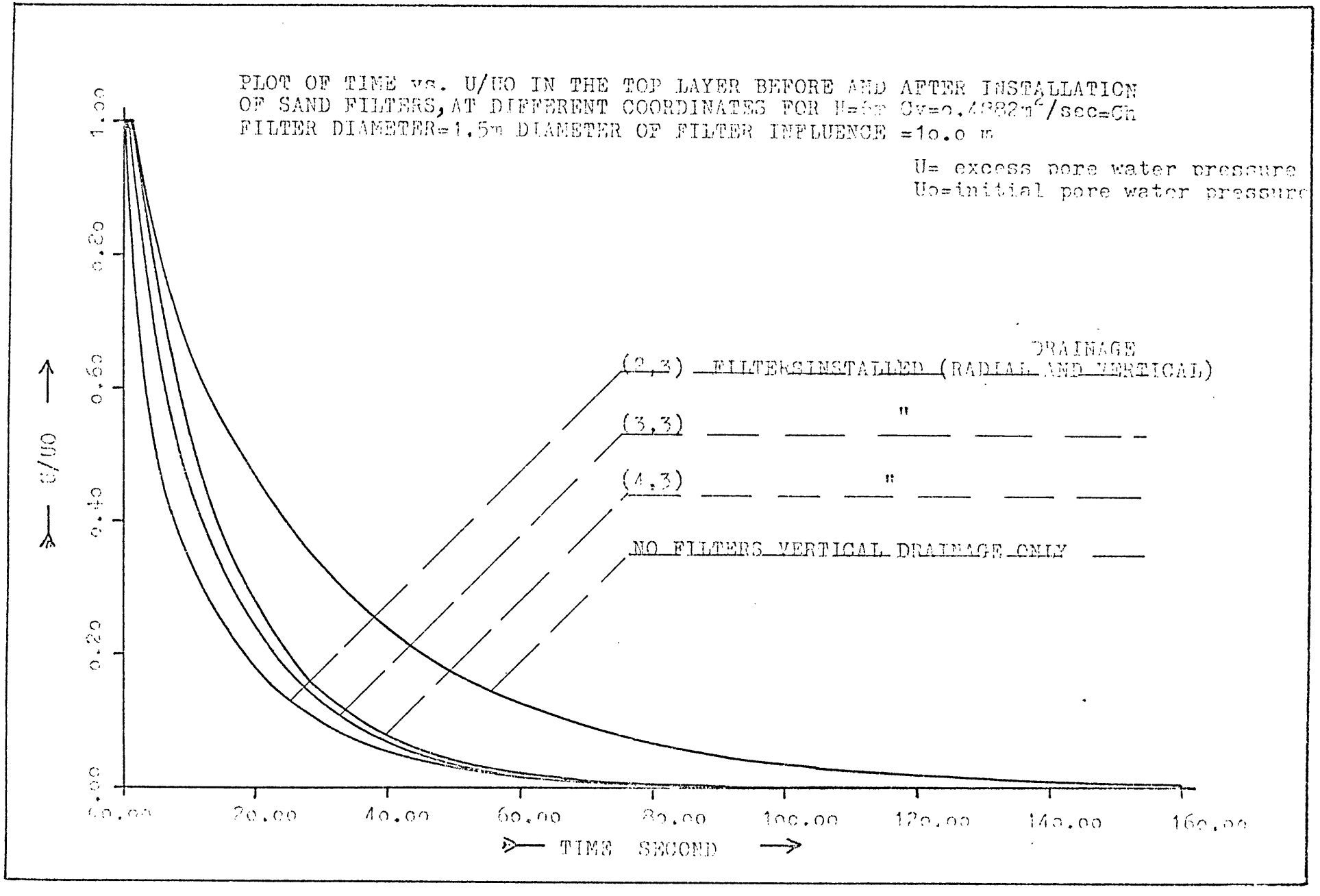

PLOT OF TIME VS. U/UO IN THE TOP LAYER BEFORE AND AFTER INSTALLATION
OF SAND FILTERS, AT DIFFERENT COORDINATES FOR H=6m Cv=0.4382m²/sec=Ch
FILTER DIAMETER=1.5m DIAMETER OF FILTER INFLUENCE =10.0 m
U= excess pore water pressure
Uo=initial pore water pressure
(2,3) FILTERSINSTALLED (RADIAL AND VERTICAL) DRAINAGE
(3,3) " "
(4,3) " "
NO FILTERS VERTICAL DRAINAGE ONLY
U/Uo
1.00
0.80
0.60
0.40
0.20
0.00
20.00
40.00
60.00
80.00
100.00
120.00
140.00
160.00
TIME SECOND

Fig. 9.7

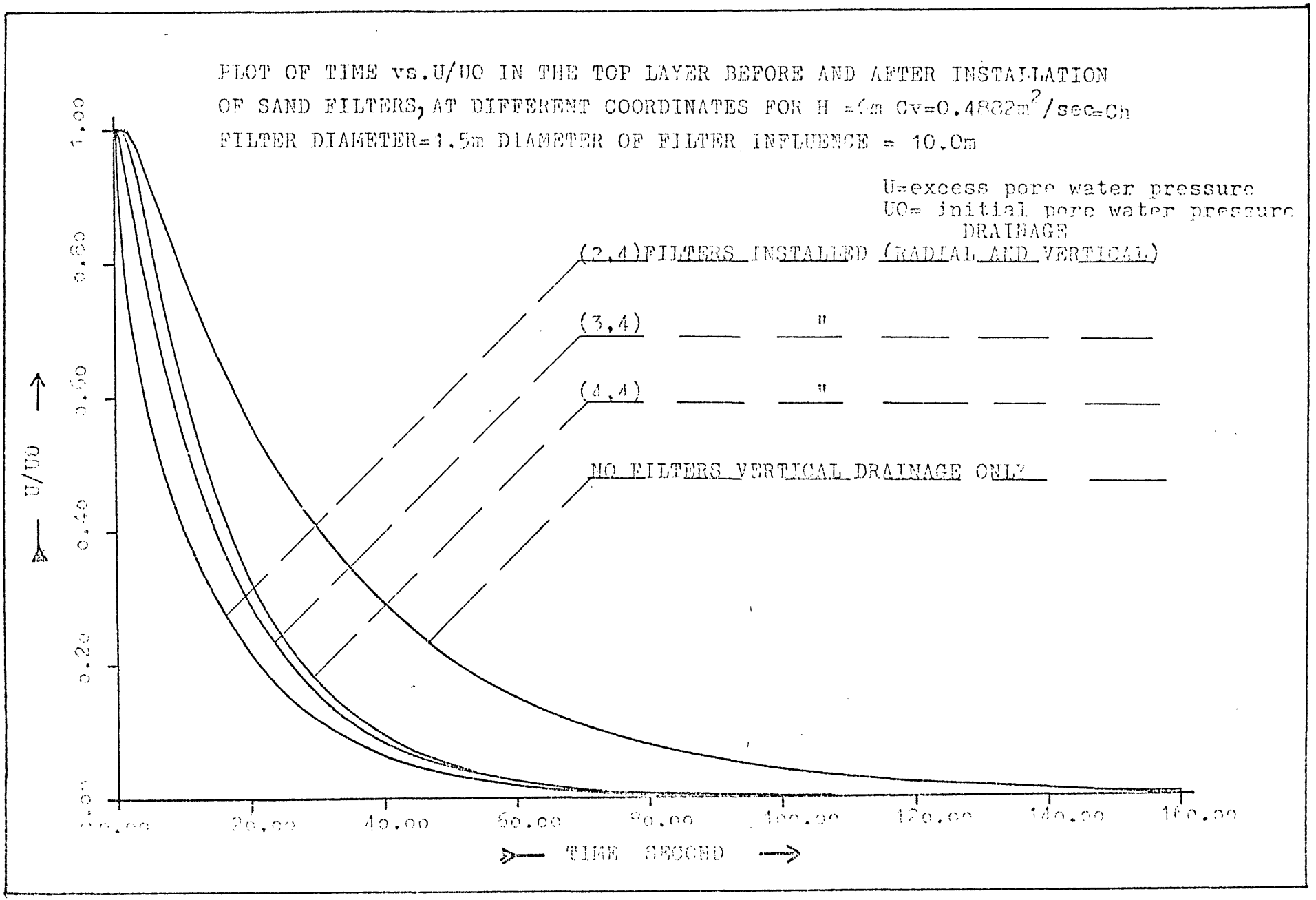

PLOT OF TIME vs.U/UO IN THE TOP LAYER BEFORE AND AFTER INSTALLATION
OF SAND FILTERS, AT DIFFERENT COORDINATES FOR H =6m Cv=0.4802m²/sec=Ch
FILTER DIAMETER=1.5m DIAMETER OF FILTER INFLUENCE = 10.0m
U=excess pore water pressure
UO= initial pore water pressure
DRAINAGE
(2,4)FILTERS INSTALLED (RADIAL AND VERTICAL)
(3,4) " "
(4,4) " "
NO FILTERS VERTICAL DRAINAGE ONLY
U/UO
1.00
0.80
0.60
0.40
0.20
20.00
40.00
60.00
120.00
140.00
160.00
TIME SECOND

Fig. 9.8

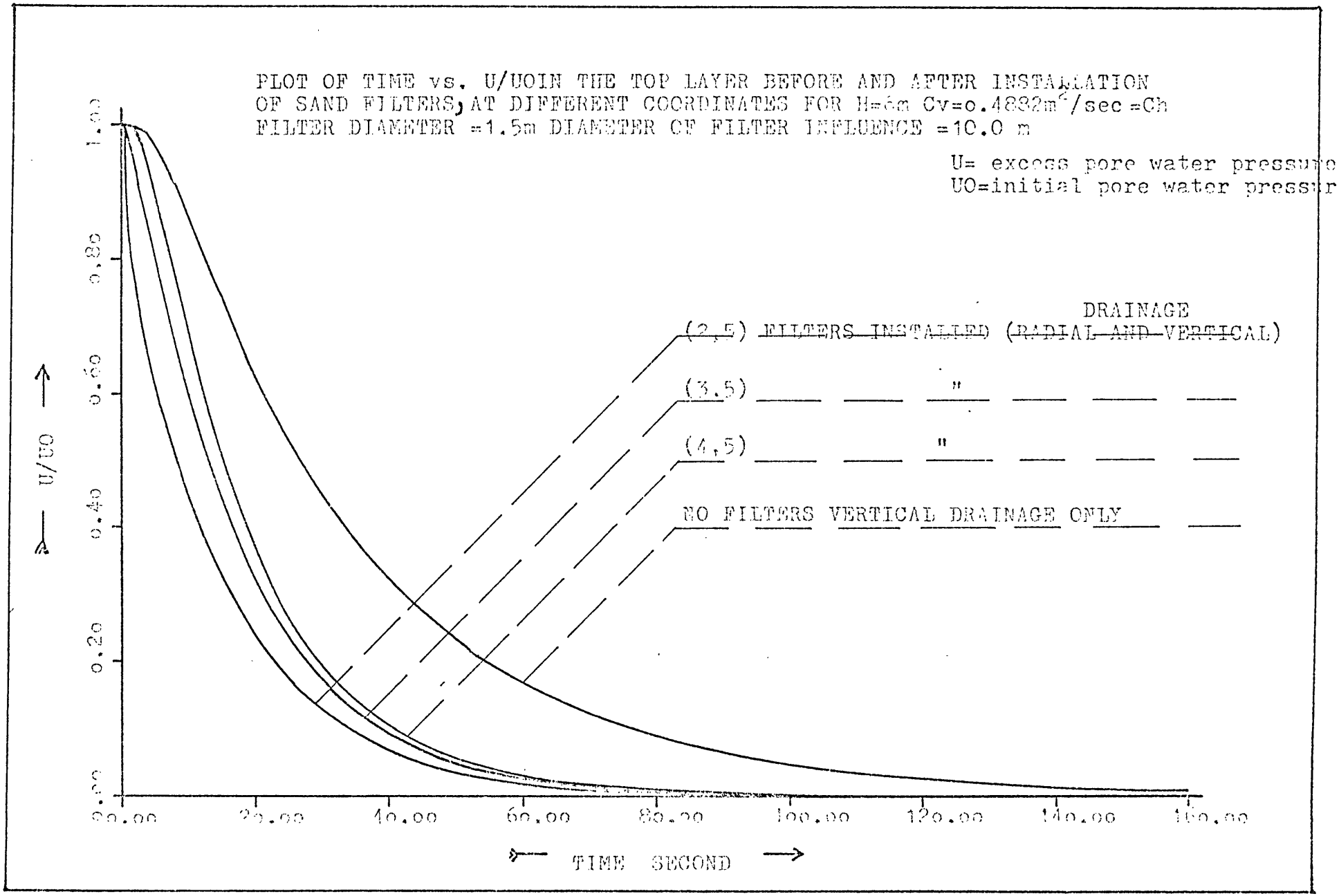

PLOT OF TIME vs. U/UOIN THE TOP LAYER BEFORE AND AFTER INSTALLATION
OF SAND FILTERS, AT DIFFERENT COORDINATES FOR H=6m Cv=o.4882m²/sec =Ch
FILTER DIAMETER =1.5m DIAMETER OF FILTER INFLUENCE =10.0 m
U= excess pore water pressure
UO=initial pore water pressure
DRAINAGE
(2,5) FILTERS INSTALLED (RADIAL AND VERTICAL)
(3,5) " "
(4,5) " "
NO FILTERS VERTICAL DRAINAGE ONLY
U/UO
0.80
0.60
0.40
0.20
20.00
40.00
60.00
80.00
100.00
120.00
140.00
TIME SECOND

Fig. 9.9

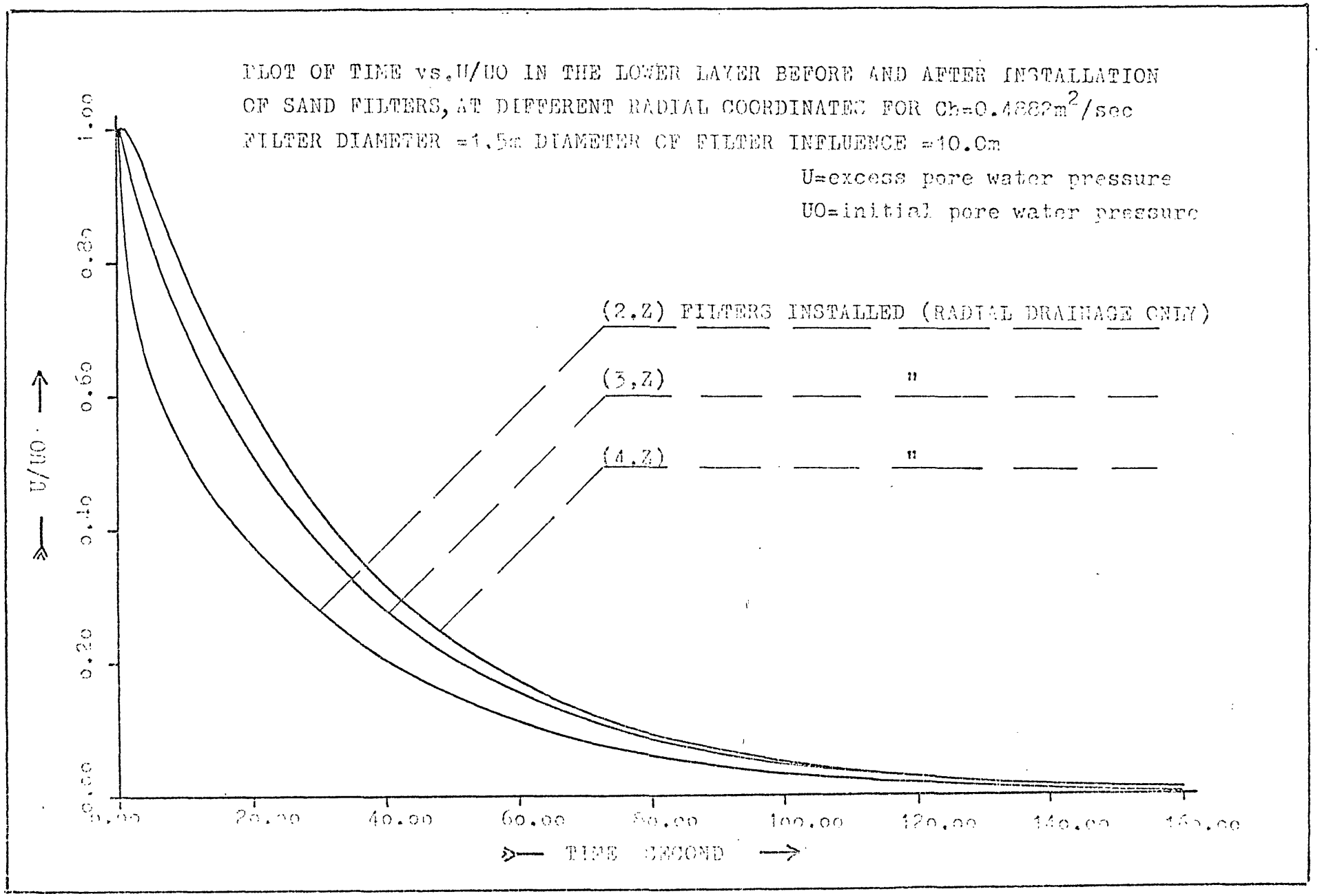

PLOT OF TIME vs.U/UO IN THE LOWER LAYER BEFORE AND AFTER INSTALLATION
OF SAND FILTERS, AT DIFFERENT RADIAL COORDINATES FOR Ch=0.4882m²/sec
FILTER DIAMETER =1.5m DIAMETER OF FILTER INFLUENCE =10.0m
U=excess pore water pressure
UO=initial pore water pressure
(2,Z) FILTERS INSTALLED (RADIAL DRAINAGE ONLY)
(3,Z) " "
(4,Z) " "
U/UO
1.00
0.80
0.60
0.40
0.20
0.00
20.00
40.00
60.00
100.00
120.00
TIME SECOND

Fig. 9.10

closer to drainage boundary than points (4,z).

9.10. INFLUENCE OF LAYOUT AND SPACING OF SAND FILTERS ON DISSIPATION OF EXCESS PORE WATER PRESSURE

9.10.1. LAYOUT OF SAND FILTERS

Layout of sand filters must be in such a way as to provide radial symmetry; therefore, filters may be spaced in square or triangular patterns, as shown in fig.9.3D. The effective radius of each filter is the radius of the circle equal in area to the area served by each filter. If the filters are spaced in:

a) triangular patterns

$$R = 0.525.S \qquad (10.10)$$

b) square patterns

$$R = 0.564.S \qquad (10.11)$$

where R = effective radius of filters.

S = spacing of filters.

9.10.2. SPACING OF SAND FILTERS

Three of the most significant factors determining spacing of sand filters are:

a. To prevent any shear slides during earthquakes as well as during construction of sand filters.

b. To shorten the route of excape of excess pore water as much as possible.

c. To achieve a certain per cent of dissipation of total excess pore water at a specified time after earthquake.

To investigate the effect of filter spacing on dissipation of excess pore water pressure, a site similar to that described in section 9.9, with different diameters of filter influence,i.e. 14.0, 12.0, 10.0m,was studied. Comparison of changes in excess pore water pressure, with time at different coordinate systems in the top layer for three-dimensional flow, are shown in figs. 9.11 through 9.19. and for the lower layer for radial flow in figs. 9.20 through 9.22.

Fig.9.11 shows the changes in excess pore water pressure with time for the three cases considered in the upper layer at a distance of 2m from filter axis and 3m below ground surface,i.e. (2,3), over a post earthquake period of 160 seconds. The dissipation of excess pore water pressure with time is the same for the three diameters of filter influence up to about 8 secs; thereafter, it differs, fastest for the 10m diameter of filter influence and slowest for the 14m. This is expected because from equation (10.7) it is apparent that some time must elapse before the effect of reduction of drainage path becomes apparent.

Figs. 9.12 through 9.19 show similar comparisons for different coordinates. It is noticed that in the three cases considered spacing of the filters are 9.25, 11.45, 13.33m, respectively, (calculated from equation 9.10) which are considerably greater than the total depth of the upper layer. This explains why a decrease in influence of filter diameter has a nominal effect on dissipation rate. To direct most of

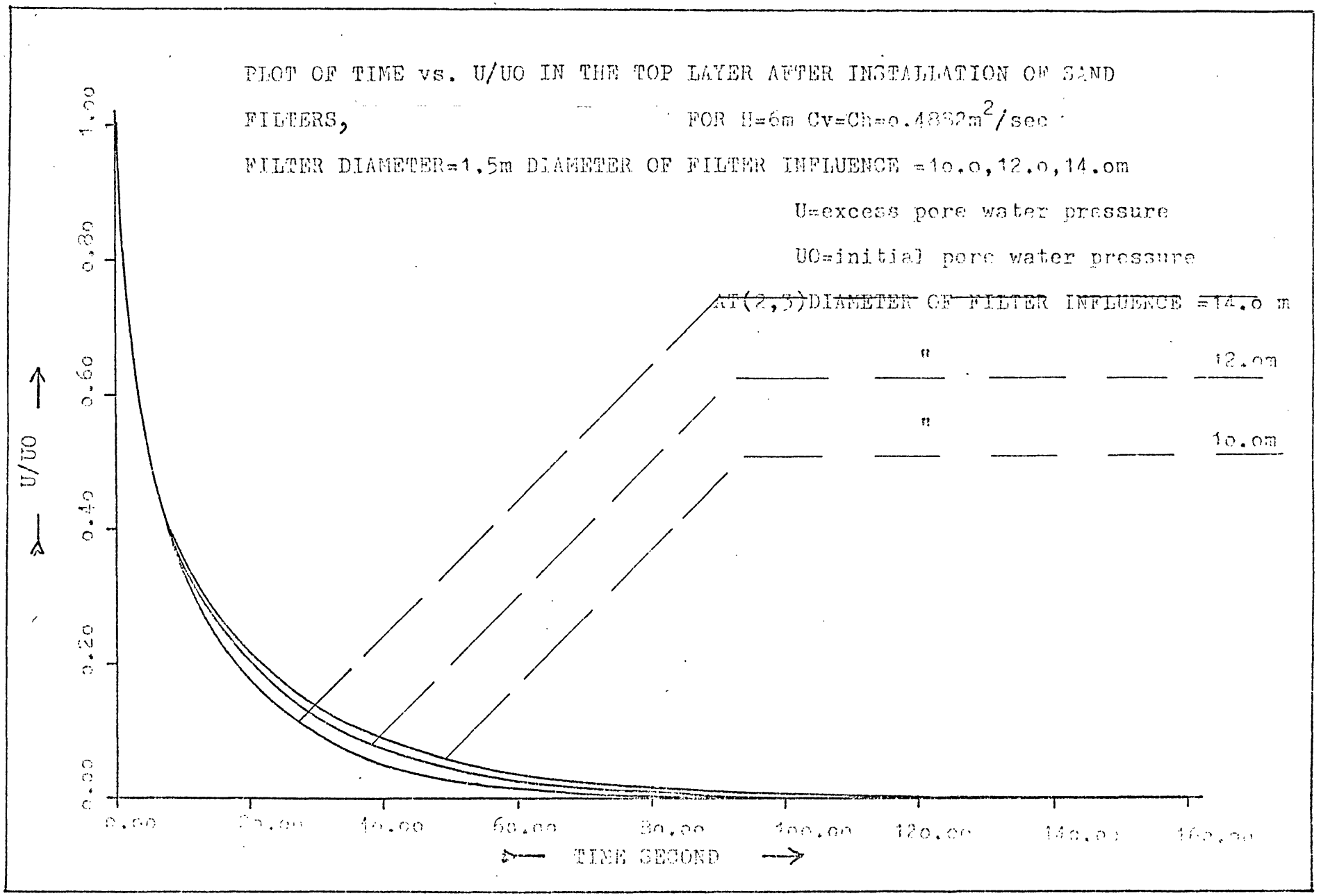

PLOT OF TIME vs. U/UO IN THE TOP LAYER AFTER INSTALLATION OF SAND
FILTERS,
FOR H=6m Cv=Ch=0.4892m²/sec
FILTER DIAMETER=1.5m DIAMETER OF FILTER INFLUENCE =10.0,12.0,14.0m
U=excess pore water pressure
UO=initial pore water pressure
AT(2,3)DIAMETER OF FILTER INFLUENCE =14.0 m
" 12.0m
" 10.0m
U/UO
1.00
0.80
0.60
0.40
0.20
0.00
0.00
10.00
60.00
100.00
120.00
TIME SECOND

Fig. 9.11

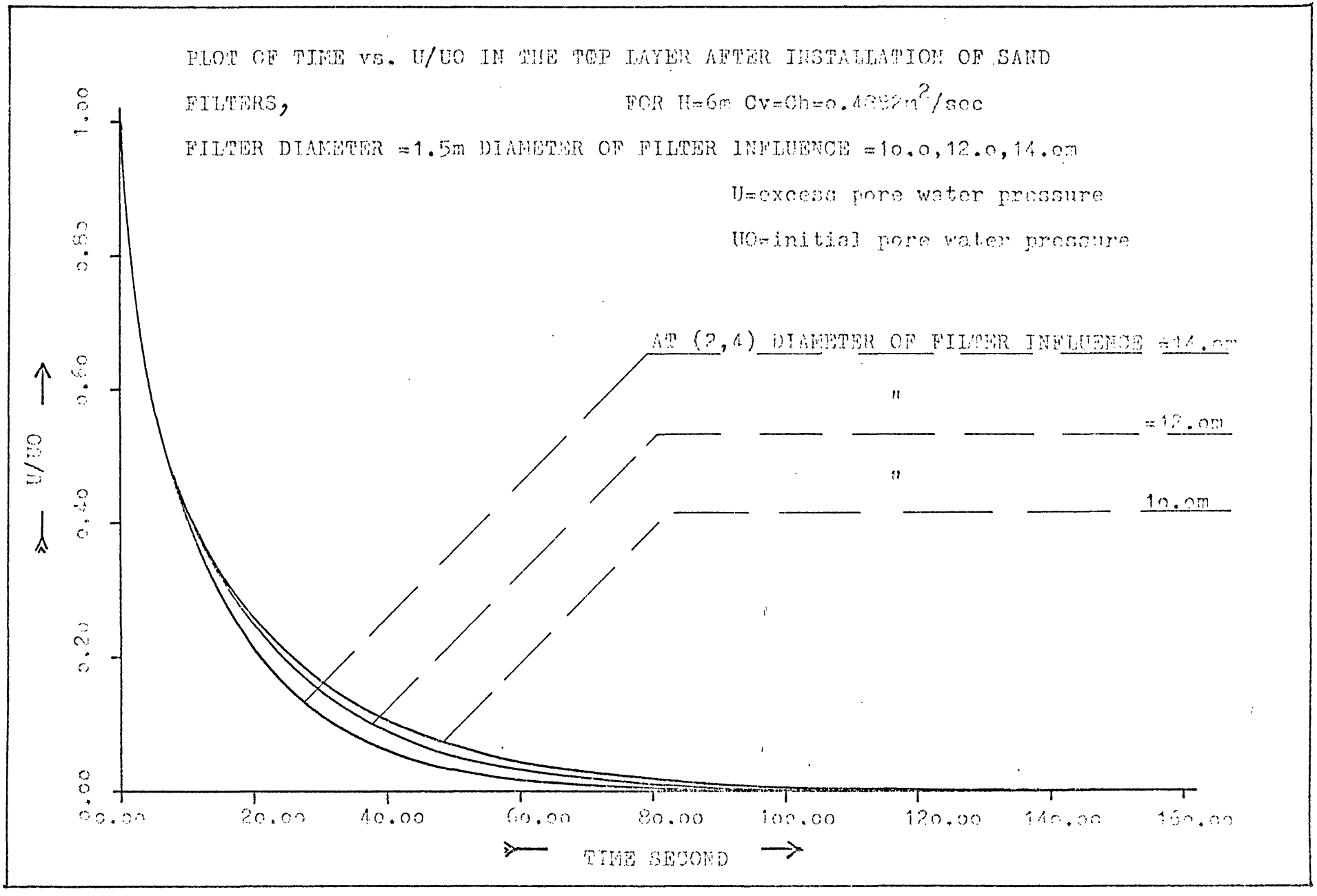

PLOT OF TIME vs. U/UO IN THE TOP LAYER AFTER INSTALLATION OF SAND
FILTERS,
FOR H=6m Cv=Ch=o.4[illegible]m²/sec
FILTER DIAMETER =1.5m DIAMETER OF FILTER INFLUENCE =1o.o,12.o,14.om
U=excess pore water pressure
UO=initial pore water pressure
AT (2,4) DIAMETER OF FILTER INFLUENCE =14.om
"
=12.om
"
1o.om
U/UO
TIME SECOND
1.oo
o.8o
o.6o
o.4o
o.2o
o.oo
2o.oo
4o.oo
6o.oo
8o.oo
1oo.oo
12o.oo
14o.oo

Fig. 9.12

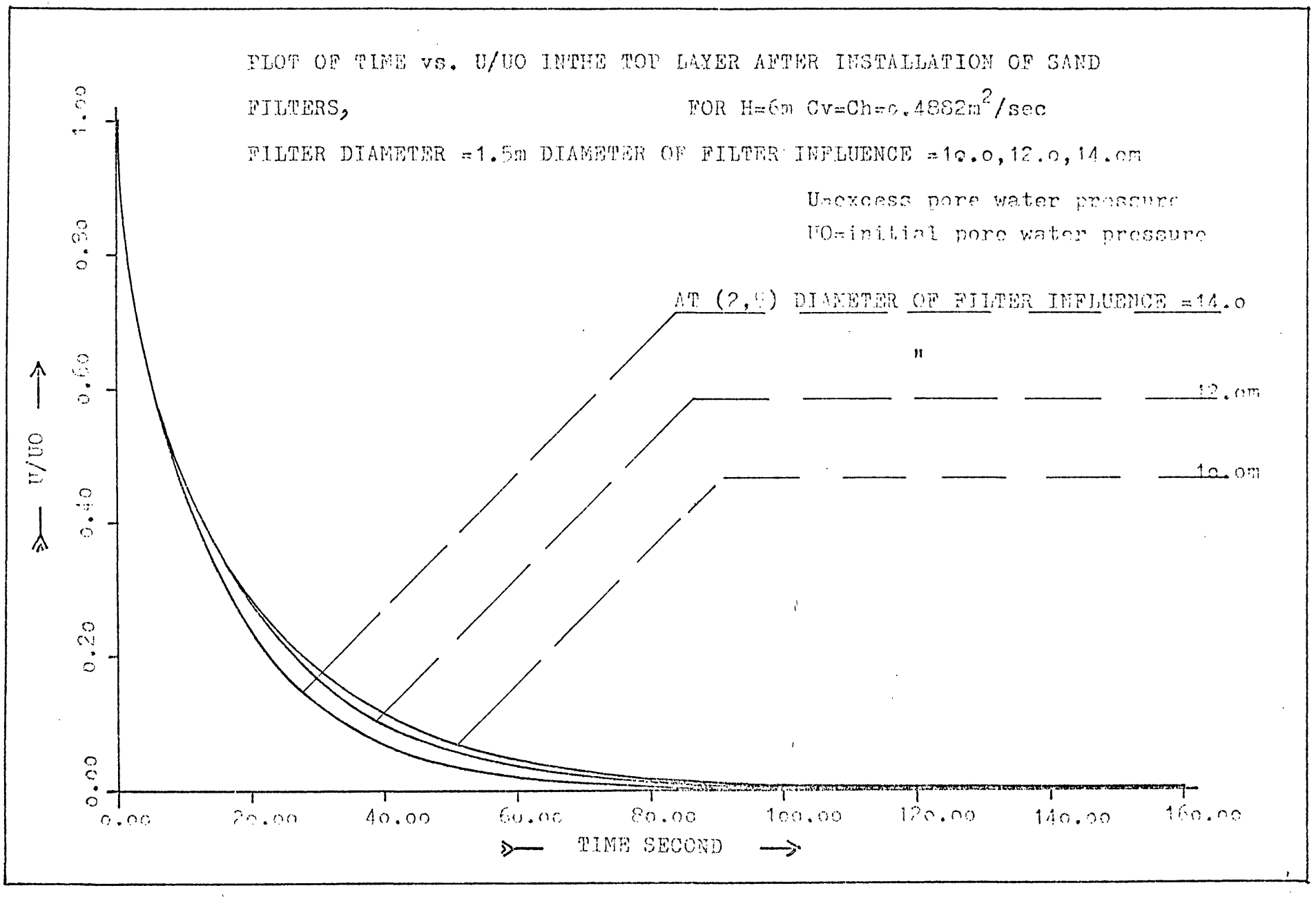

PLOT OF TIME vs. U/UO INTHE TOP LAYER AFTER INSTALLATION OF SAND
FILTERS, FOR H=6m Cv=Ch=0.4882m²/sec
FILTER DIAMETER =1.5m DIAMETER OF FILTER INFLUENCE =10.0,12.0,14.0m
U=excess pore water pressure
UO=initial pore water pressure
AT (2,5) DIAMETER OF FILTER INFLUENCE =14.0
"
12.0m
10.0m
U/UO
1.00
0.80
0.60
0.40
0.20
0.00
0.00
20.00
40.00
60.00
80.00
100.00
120.00
140.00
160.00
TIME SECOND

Fig. 9.13

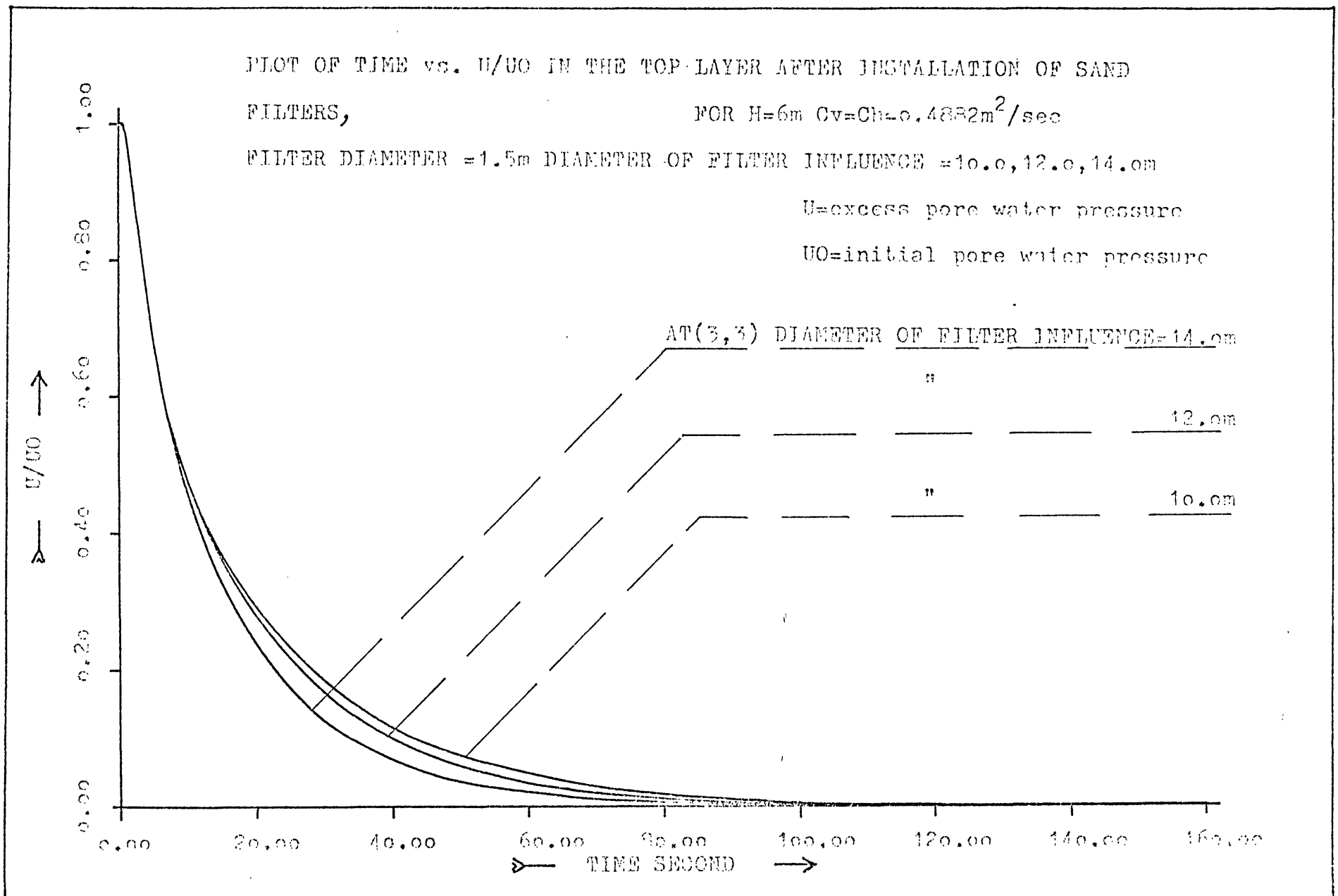

PLOT OF TIME vs. U/UO IN THE TOP LAYER AFTER INSTALLATION OF SAND FILTERS,
FOR H=6m Cv=Ch=0.4882m²/sec
FILTER DIAMETER =1.5m DIAMETER OF FILTER INFLUENCE =10.0,12.0,14.0m
U=excess pore water pressure
UO=initial pore water pressure
AT(3,3) DIAMETER OF FILTER INFLUENCE=14.0m
"
12.0m
"
10.0m
U/UO
1.00
0.80
0.60
0.40
0.20
0.00
0.00
20.00
40.00
60.00
80.00
100.00
120.00
140.00
160.00
TIME SECOND

Fig. 9.14

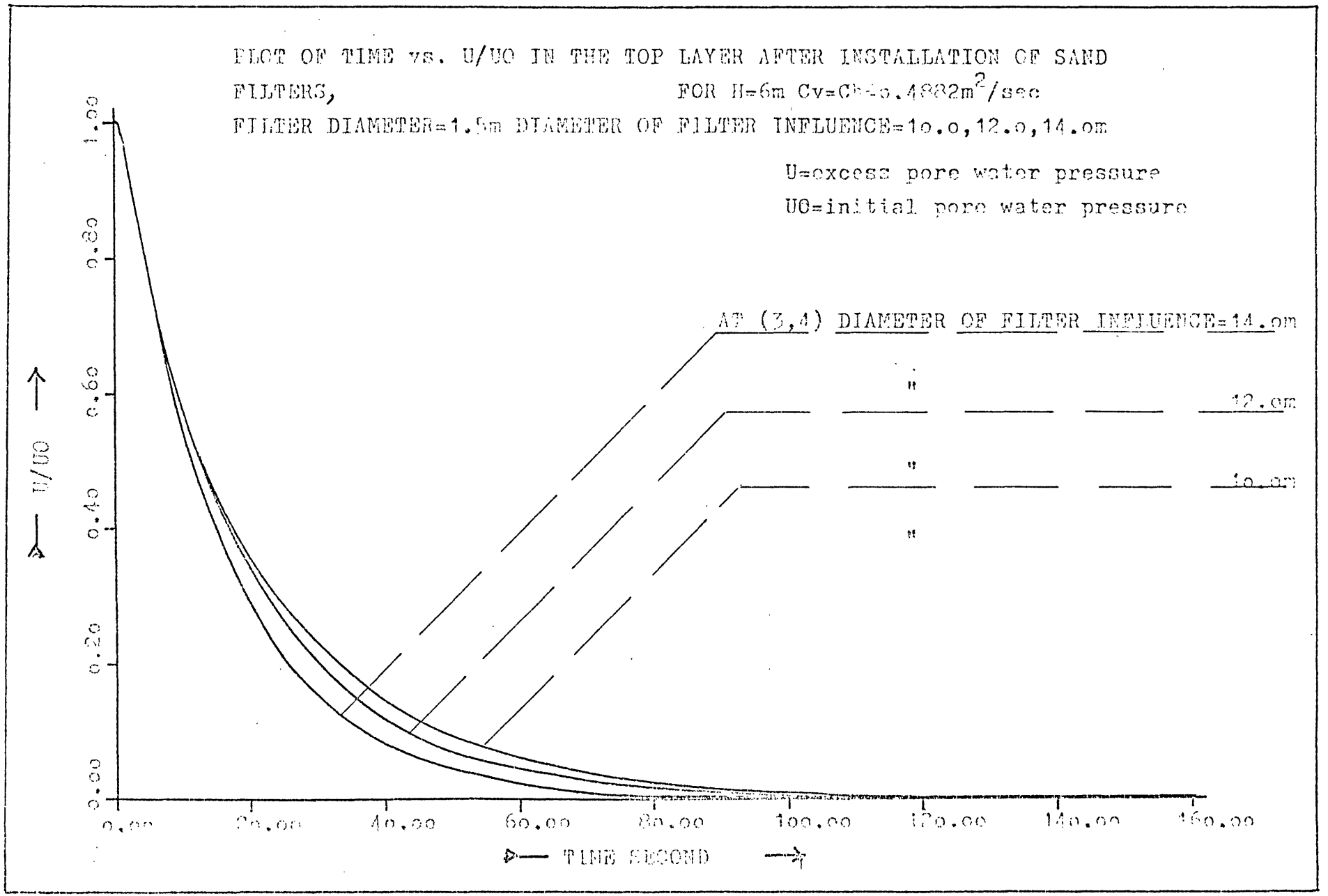

PLOT OF TIME vs. U/UO IN THE TOP LAYER AFTER INSTALLATION OF SAND FILTERS,
FOR H=6m Cv=Ch=0.4882m²/sec
FILTER DIAMETER=1.5m DIAMETER OF FILTER INFLUENCE=10.0,12.0,14.0m
U=excess pore water pressure
UO=initial pore water pressure
AT (3,4) DIAMETER OF FILTER INFLUENCE=14.0m
"
12.0m
"
10.0m
"
U/UO
1.00
0.80
0.60
0.40
0.20
0.00
0.00
20.00
40.00
60.00
80.00
100.00
120.00
140.00
160.00
TIME SECOND

Fig.9.15

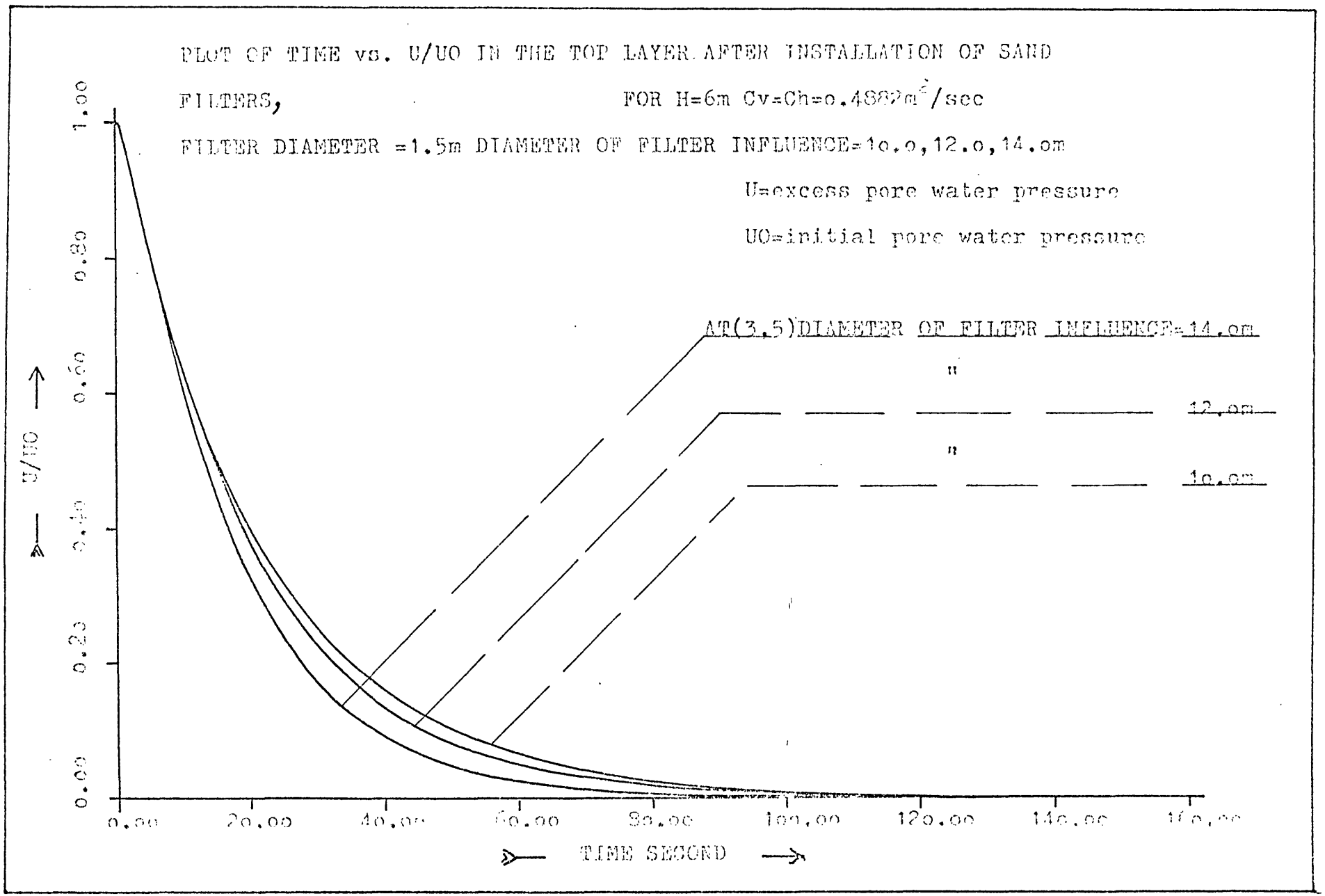

PLOT OF TIME vs. U/UO IN THE TOP LAYER AFTER INSTALLATION OF SAND
FILTERS,
FOR H=6m Cv=Ch=o.4882m²/sec
FILTER DIAMETER =1.5m DIAMETER OF FILTER INFLUENCE=1o.o,12.o,14.om
U=excess pore water pressure
UO=initial pore water pressure
AT(3.5)DIAMETER OF FILTER INFLUENCE=14.om
"
12.om
"
1o.om
U/UO
1.oo
o.8o
o.6o
o.4o
o.2o
o.oo
2o.oo
4o.oo
6o.oo
8o.oo
1oo.oo
12o.oo
14o.oo
TIME SECOND

Fig. 9.16

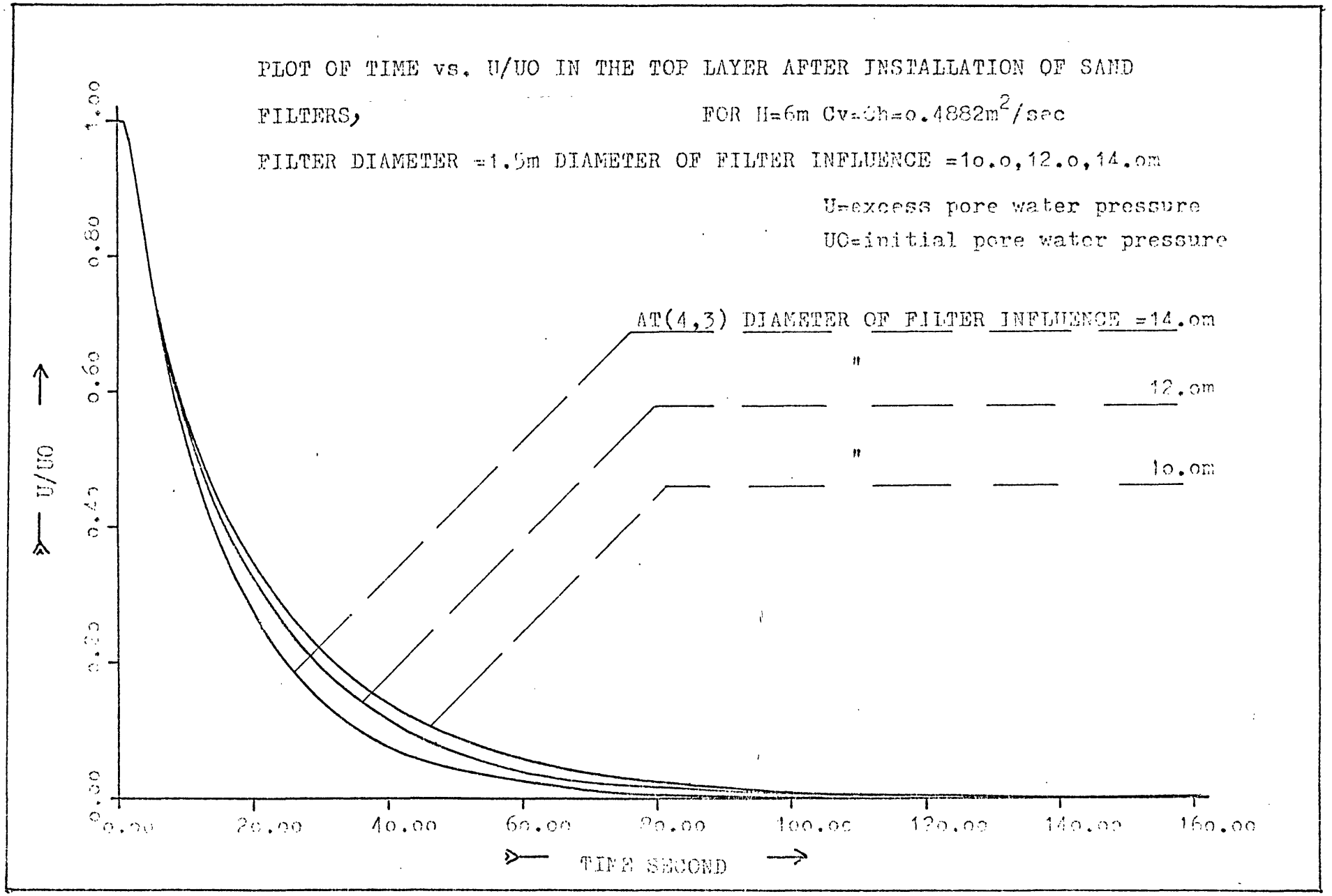

PLOT OF TIME vs. U/UO IN THE TOP LAYER AFTER INSTALLATION OF SAND FILTERS,
FOR H=6m Cv=Ch=o.4882m²/sec
FILTER DIAMETER =1.5m DIAMETER OF FILTER INFLUENCE =1o.o,12.o,14.om
U=excess pore water pressure
UO=initial pore water pressure
AT(4,3) DIAMETER OF FILTER INFLUENCE =14.om
"
12.om
"
1o.om
U/UO
TIME SECOND
1.00
0.80
0.60
0.40
0.20
0.00
2o.oo
4o.oo
6o.oo
8o.oo
1oo.oo
12o.oo
14o.oo
16o.oo

Fig. 9.17

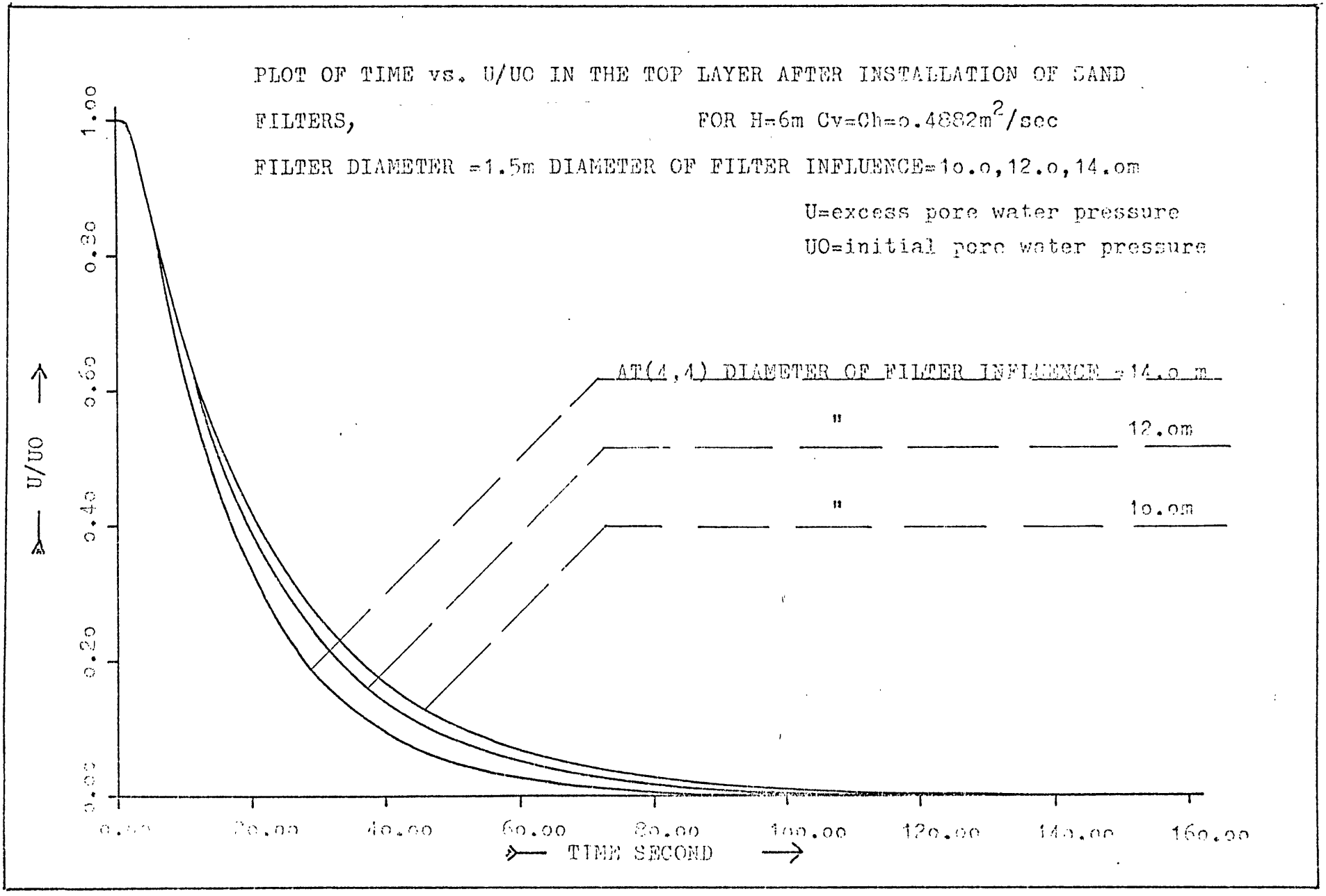

PLOT OF TIME vs. U/UO IN THE TOP LAYER AFTER INSTALLATION OF SAND FILTERS,
FOR H=6m Cv=Ch=o.4882m²/sec
FILTER DIAMETER =1.5m DIAMETER OF FILTER INFLUENCE=1o.o,12.o,14.om
U=excess pore water pressure
UO=initial pore water pressure
AT(4,4) DIAMETER OF FILTER INFLUENCE =14.o m
"
12.om
"
1o.om
U/UO
1.oo
o.8o
o.6o
o.4o
o.2o
4o.oo
6o.oo
8o.oo
1oo.oo
12o.oo
16o.oo
TIME SECOND

Fig. 9.18

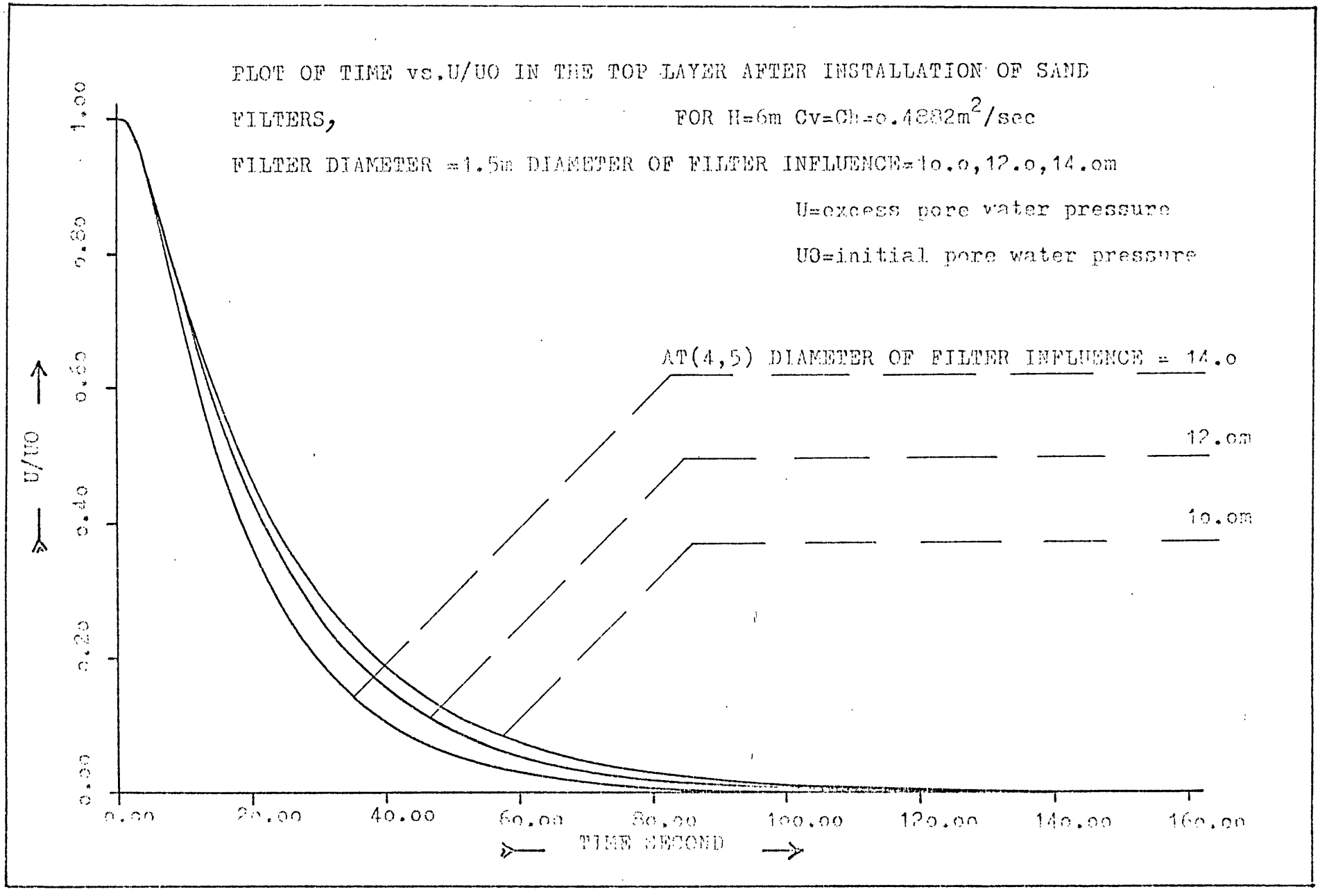

PLOT OF TIME vs.U/UO IN THE TOP LAYER AFTER INSTALLATION OF SAND
FILTERS,
FOR H=6m Cv=Ch=0.4882m2/sec
FILTER DIAMETER =1.5m DIAMETER OF FILTER INFLUENCE=10.0,12.0,14.0m
U=excess pore water pressure
UO=initial pore water pressure
AT(4,5) DIAMETER OF FILTER INFLUENCE = 14.0
12.0m
10.0m
U/UO
1.00
0.80
0.60
0.40
0.20
0.00
0.00
20.00
40.00
60.00
80.00
100.00
120.00
140.00
160.00
TIME SECOND

Fig. 9.19

the flow towards sand filters, spacing of the filters must be much less than the total height of the deposit located above weak layer.

Figs.9.20 through 9.22 show comparisons of pore pressure redistribution for radial drainage towards sand filters in the lower layer over a period of 160 seconds after earthquake excitation at distances of 2,3,4m from filter axis, for the three cases considered.

Fig.9.20 shows the first of these comparisons at a distance of 2m from filter axis. The dissipation of excess pore water pressure with time is the same for the three diameters of filter influence up to about 9 seconds, thereafter fastest for the 10m diameter of filter influence and slowest for the 14m. The excess pore water pressure for the 10m diameter of filter influence has almost reached zero at the end of 160 seconds, whereas the excess pore water pressure for the 14m diameter of filter influence continues to dissipate.

Figs.9.21 - 9.22 show similar comparisons for the rest of the coordinates considered. It is noticed that the rate of dissipation of excess pore water pressure decreases as the drainage path increases.

9.11. INFLUENCE OF DIAMETER OF SAND FILTERS ON DISSIPATION CHARACTERISTICS OF EXCESS PORE PRESSURE

Two of the most important factors determining the diameter of sand filters are:

a. The filters must be wide enough to drain away the expelled water after the earthquake excitation and remain functional during and after earthquake.

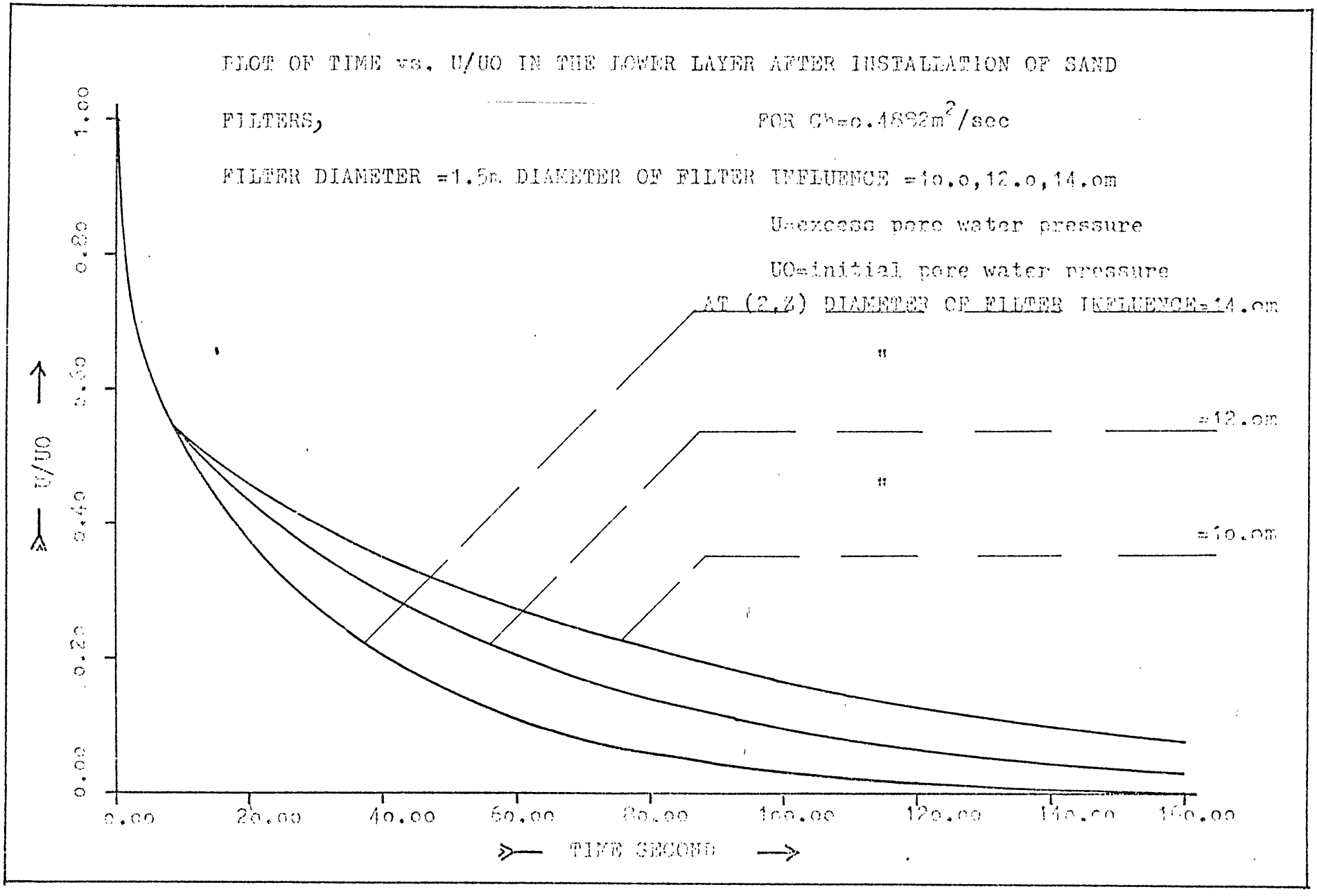

PLOT OF TIME vs. U/UO IN THE LOWER LAYER AFTER INSTALLATION OF SAND
FILTERS,
FOR Ch=0.4892m²/sec
FILTER DIAMETER =1.5m. DIAMETER OF FILTER INFLUENCE =10.0,12.0,14.0m
U=excess pore water pressure
UO=initial pore water pressure
AT (2,Z) DIAMETER OF FILTER INFLUENCE=14.0m
"
=12.0m
"
=10.0m
U/UO
1.00
0.80
0.60
0.40
0.20
0.00
0.00
20.00
40.00
60.00
80.00
100.00
120.00
140.00
160.00
TIME SECOND

Fig. 9.20

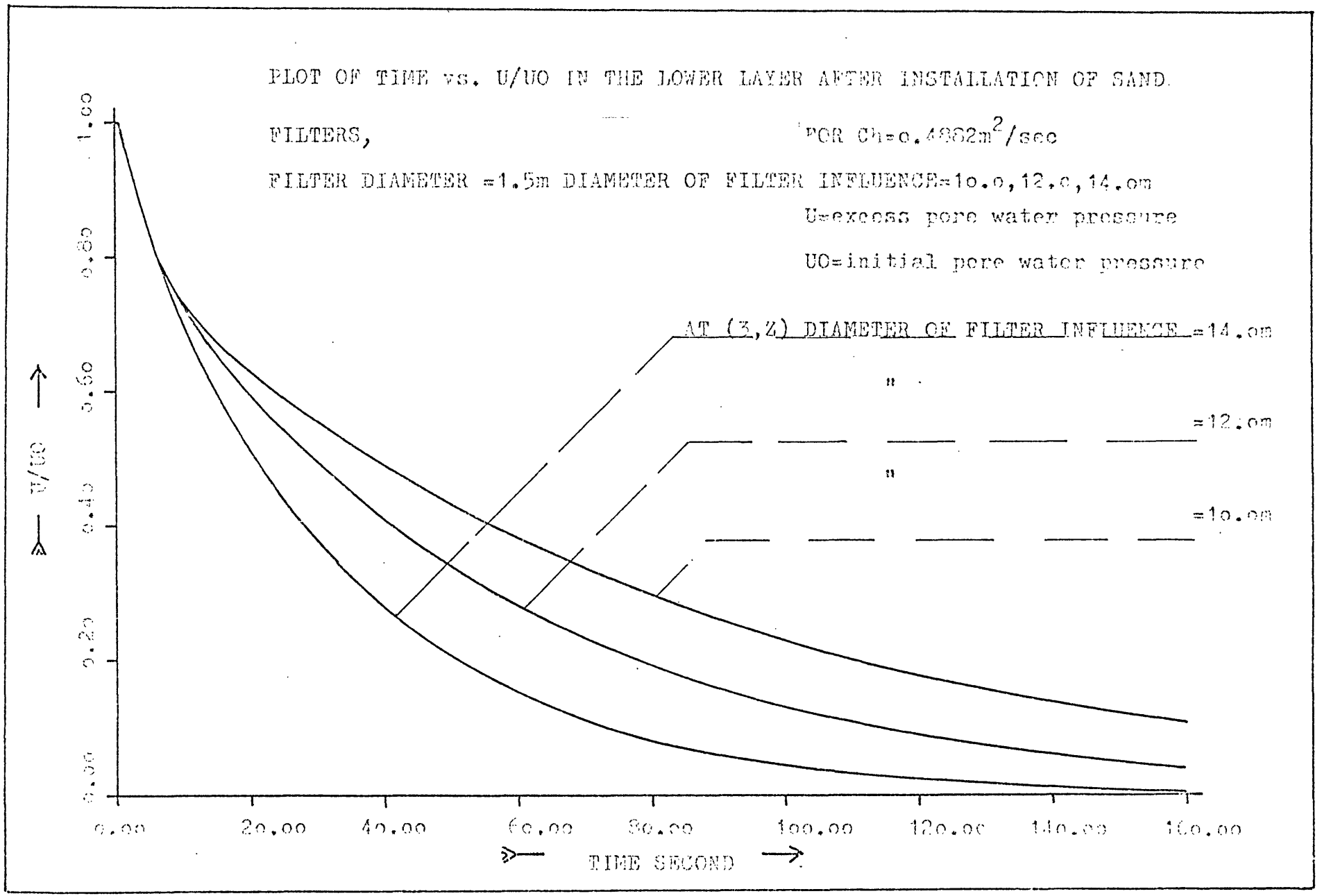

PLOT OF TIME vs. U/UO IN THE LOWER LAYER AFTER INSTALLATION OF SAND.
FILTERS,
FOR Ch=0.4862m²/sec
FILTER DIAMETER =1.5m DIAMETER OF FILTER INFLUENCE=10.0,12.0,14.0m
U=excess pore water pressure
UO=initial pore water pressure
AT (3,Z) DIAMETER OF FILTER INFLUENCE =14.0m
=12.0m
=10.0m
U/UO
1.00
0.80
0.60
0.40
0.20
0.00
20.00
40.00
60.00
80.00
100.00
120.00
140.00
160.00
TIME SECOND

Fig. 9.21

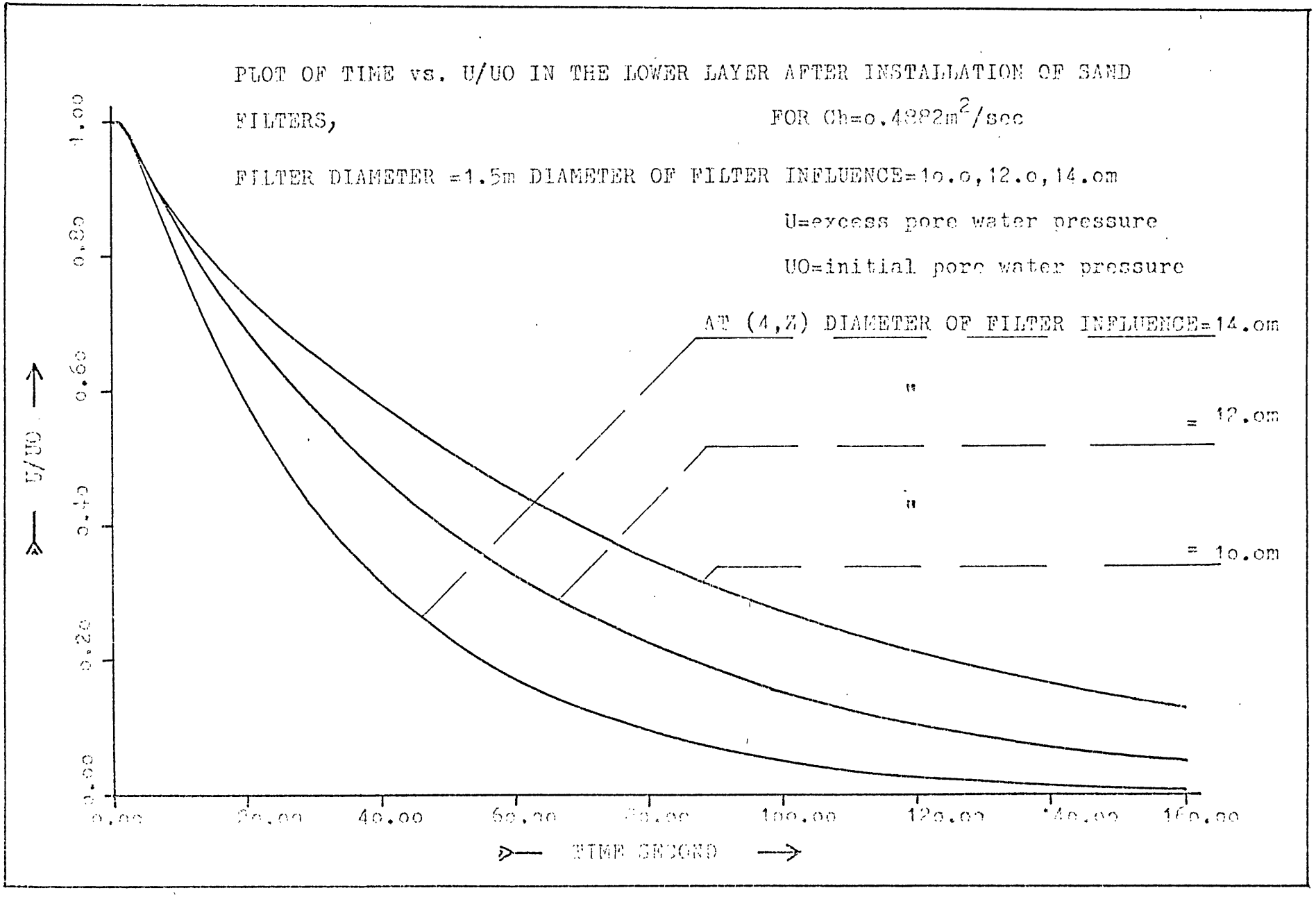

PLOT OF TIME vs. U/UO IN THE LOWER LAYER AFTER INSTALLATION OF SAND FILTERS,
FOR Ch=o.4882m²/sec
FILTER DIAMETER =1.5m DIAMETER OF FILTER INFLUENCE=1o.o,12.o,14.om
U=excess pore water pressure
UO=initial pore water pressure
AT (4,Z) DIAMETER OF FILTER INFLUENCE=14.om
"
= 12.om
"
= 1o.om
U/UO
TIME SECOND

Fig. 9.22

b. To be drilled easily and economically in practice.

The amount of maximum displacement induced just below the weak layer by an earthquake may be computed by the ground response analysis given in chapters 4 & 5, based upon a knowledge of the bedrock motion time history. It is obvious that the earthquake will develop a condition of initial liquifaction or liquifaction in the trapped loose deposit, and no shear stresses would be transmitted to the layer located above the liquified layer, consequently initiating extensive settlements in the overlying deposit. It may well be justified to base the size of the diameters of filters on the maximum calculated displacements on top of the lower layer, thus ignoring the effect of the layer located above the weak zone. (This situation is similar to a multi-degree freedom system in which one of the springs near the top of the system is replaced by a weak spring. The motion developed just below the weak spring will not be affected by the motion of masses connected to the weak spring after failure of the weak spring). The structures located on top of the top layer should be placed on deep piles which would penetrate through the lower layer a considerable distance, or possibly the whole depth. Cross-bracings should be introduced into the piles, in order to prevent piles from bending when the soil adjacent to the piles settles extensively during and after earthquake shaking.

To investigate the influence of diameter of sand filters on the dissipation rate of excess pore water pressure, a site similar to that described in section 9.9 with different diameters of sand filters of 1.5, 2.0, 2.5 and 3.0m was studied (with present time drilling tools all these four sizes can be drilled easily and economically up to any

depth required). Comparisons of variation of excess pore water pressure with time at different coordinates in the system over a post earthquake period of 160 seconds in the lower and upper layer are shown in figs.9.23 through 9.34. Tables 9.1 and 9.2 illustrate the results for 80% dissipation of excess pore water pressure.

It is apparent that the diameter of filters are of importance. As evident from results of table 9.1 and 9.2, doubling of diameter of filters causes a decrease in 80% dissipation time, roughly by a factor of 1.5 to 2.0 in the upper layer and 2.0 to 4.0 in the lower layer. This is expected because the drainage path is decreased, hence the rate of flow should increase. It is also apparent from figs.9.23 through 9.34 that an increase in filter diameter affects dissipation rates throughout the whole period.

9.12. INFLUENCE OF HORIZONTAL COEFFICIENT OF CONSOLIDATION ON DISSIPATION CHARACTERISTICS OF EXCESS PORE PRESSURE

It has been generally recognized by soil Engineers that the coefficient of consolidation in horizontal direction is greater than that in vertical direction. This is because the permeability of soil in horizontal direction is usually considerably greater than that in vertical direction. This ratio is normally $1 < \frac{C_h}{C_v} < 2.$[17] To throw some light on the manner the excess pore water dissipation in the two layers may be influenced by this fact, a site similar to that described in section 9.9 was studied.

The results of these studies for upper layer are represented in figs.9.35 through 9.43, which show the relationship between excess pore

COORDINATE OF EACH POINT	TIME (SECONDS) FOR 80% DISSIPATION OF EXCESS PORE WATER PRESSURE			
	FILTER DIAMETER 3.0m	FILTER DIAMETER 2.5m	FILTER DIAMETER 2.0m	FILTER DIAMETER 1.5m
(2,3)	6.4	10.4	14.4	18.4
(2,4)	7.6	12.8	17.6	21.6
(2,5)	8.8	13.6	18.8	24.0
(3,3)	14.4	17.6	20.0	23.2
(3,4)	16.8	20.0	23.2	26.4
(3,5)	18.0	21.6	24.8	28.4
(4,3)	17.6	20.0	22.8	25.6
(4,4)	20.0	22.4	26.0	28.8
(4,5)	20.8	24.0	27.0	30.4

TABLE 9.1

EFFECT OF FILTER DIAMETER ON THE DISSIPATION RATE IN THE TOP LAYER

DISTANCE FROM FILTER AXIS m	TIME (SECOND) FOR 80% DISSIPATION OF EXCESS PORE WATER PRESSURE			
	FILTER DIAMETER 3.0m	FILTER DIAMETER 2.5m	FILTER DIAMETER 2.0m	FILTER DIAMETER 1.5m
2	10.4	20.0	29.6	42.4
3	24.8	32.0	40.0	52.0
4	29.6	36.0	44.8	56.8

TABLE 9.2

EFFECT OF FILTER DIAMETER ON THE DISSIPATION RATE IN THE LOWER LAYER

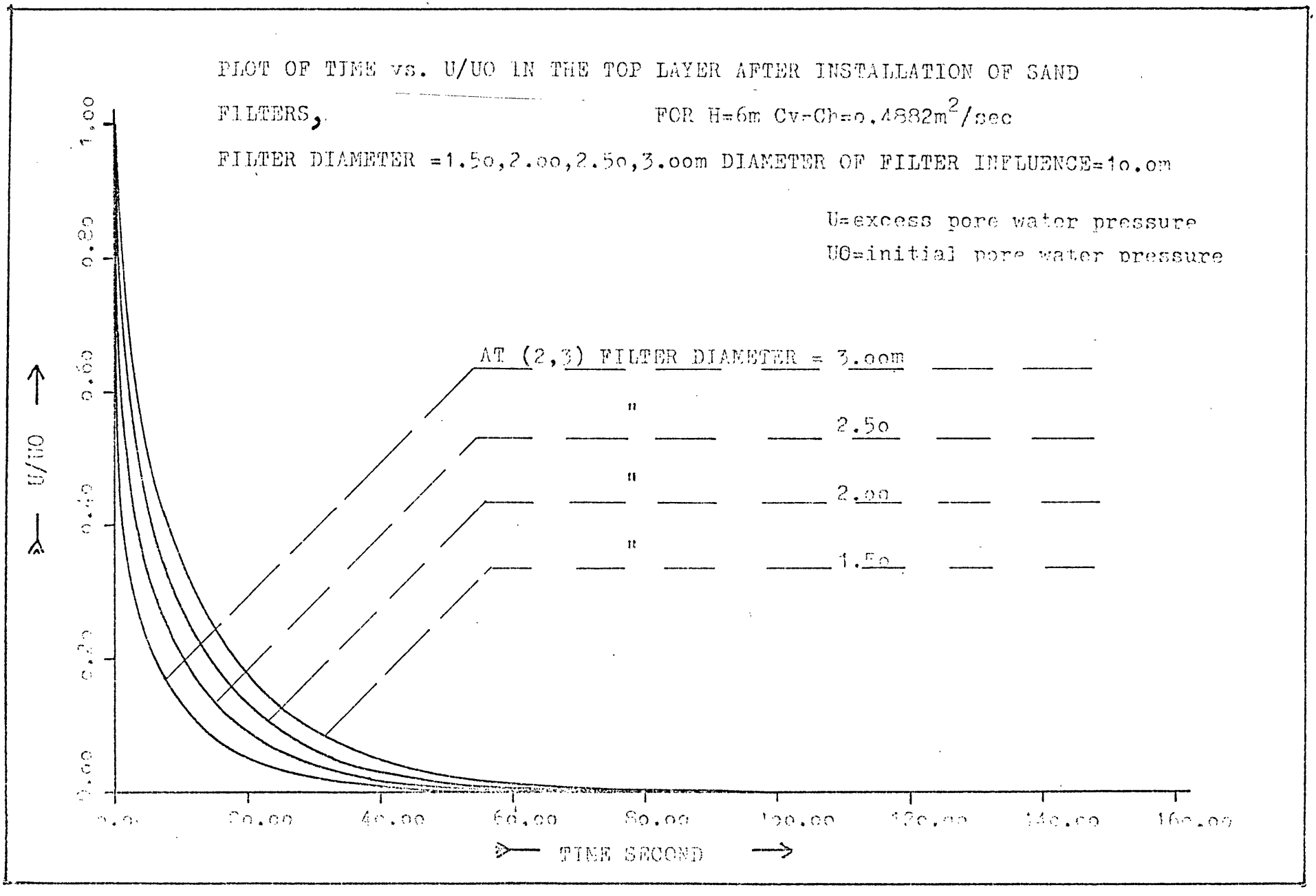

PLOT OF TIME vs. U/UO IN THE TOP LAYER AFTER INSTALLATION OF SAND FILTERS,
FOR H=6m Cv=Ch=0.4882m²/sec
FILTER DIAMETER =1.5o,2.oo,2.5o,3.oom DIAMETER OF FILTER INFLUENCE=1o.om
U=excess pore water pressure
UO=initial pore water pressure
AT (2,3) FILTER DIAMETER = 3.oom
" 2.5o
" 2.oo
" 1.5o
U/UO
1.oo
0.8o
0.6o
0.4o
0.2o
0.oo
2o.oo
4o.oo
6o.oo
8o.oo
12o.oo
14o.oo
16o.oo
TIME SECOND

Fig. 9.23

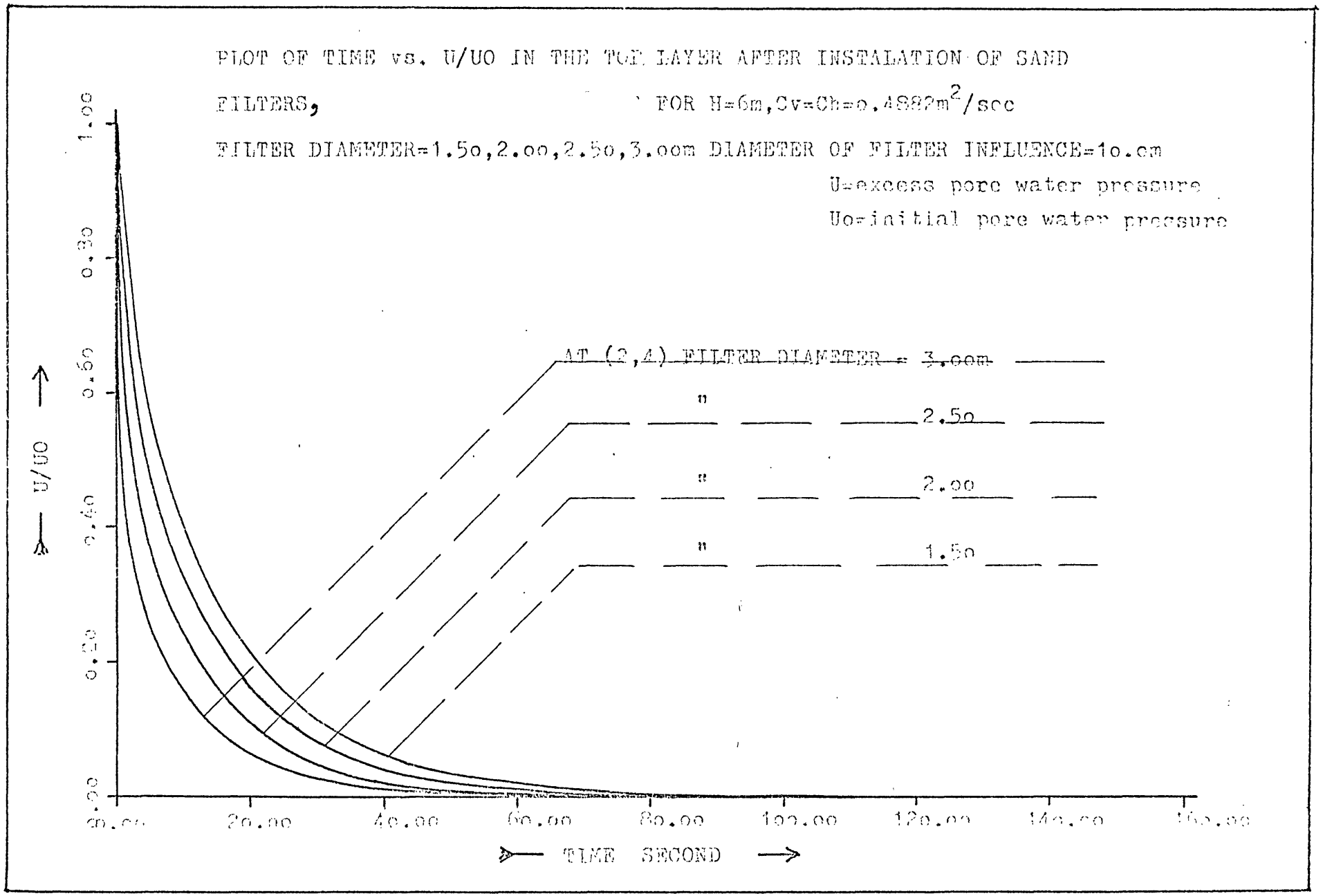

PLOT OF TIME vs. U/UO IN THE TOE LAYER AFTER INSTALATION OF SAND
FILTERS, FOR H=6m,Cv=Ch=0.4882m²/sec
FILTER DIAMETER=1.5o,2.oo,2.5o,3.oom DIAMETER OF FILTER INFLUENCE=1o.cm
U=excess pore water pressure
Uo=initial pore water pressure
AT (2,4) FILTER DIAMETER = 3.oom
"
2.5o
"
2.oo
"
1.5o
U/UO
1.oo
0.8o
0.6o
0.4o
0.2o
0.oo
2o.oo
4o.oo
6o.oo
8o.oo
12o.oo
TIME SECOND

Fig.9.24

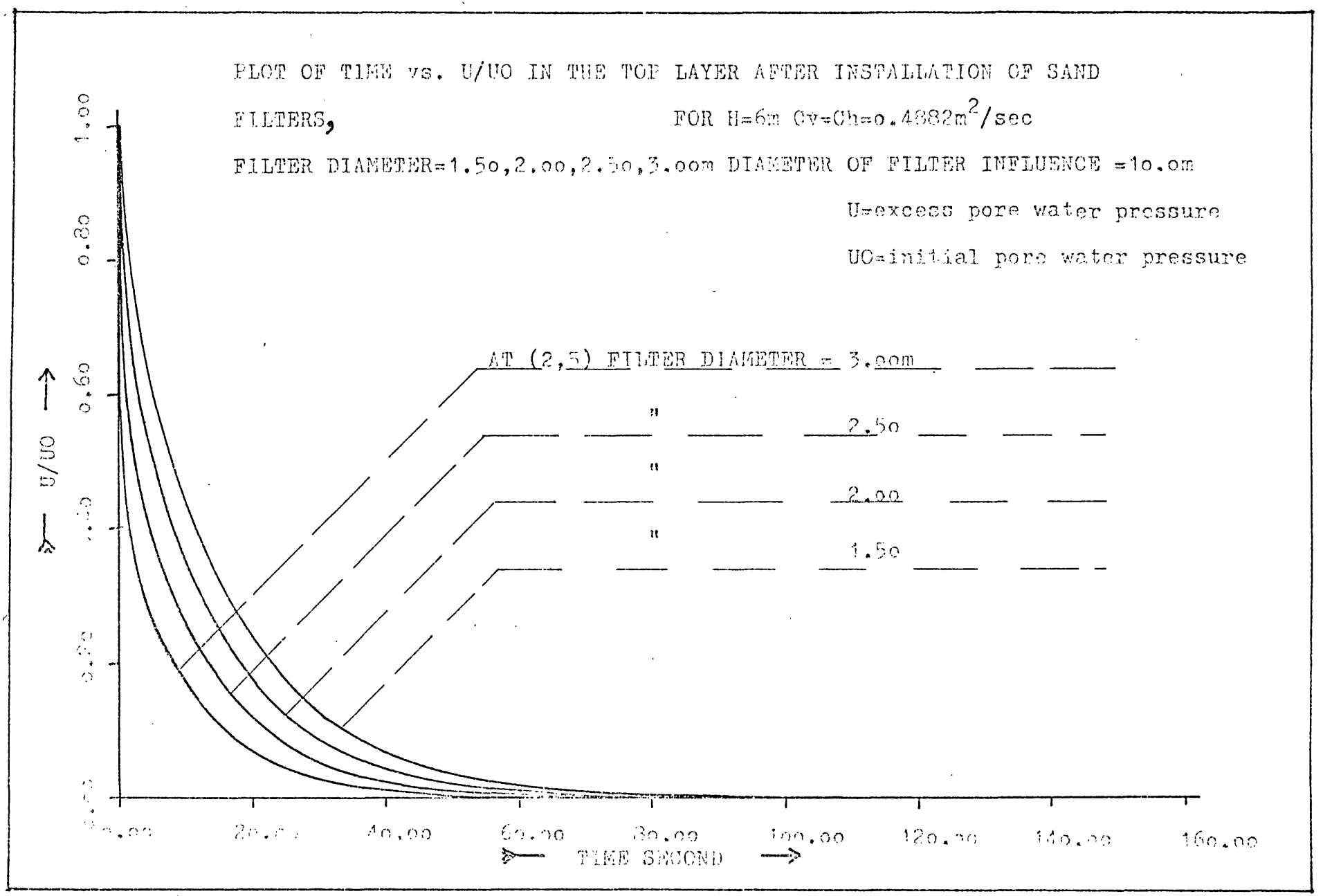

PLOT OF TIME vs. U/UO IN THE TOP LAYER AFTER INSTALLATION OF SAND
FILTERS, FOR H=6m Cv=Ch=0.4682m²/sec
FILTER DIAMETER=1.5o,2.oo,2.5o,3.oom DIAMETER OF FILTER INFLUENCE =1o.om
U=excess pore water pressure
UO=initial pore water pressure
AT (2,5) FILTER DIAMETER = 3.oom
" 2.5o
" 2.oo
" 1.5o
U/UO
1.oo
o.8o
o.6o
TIME SECOND
16o.oo

Fig. 9.25

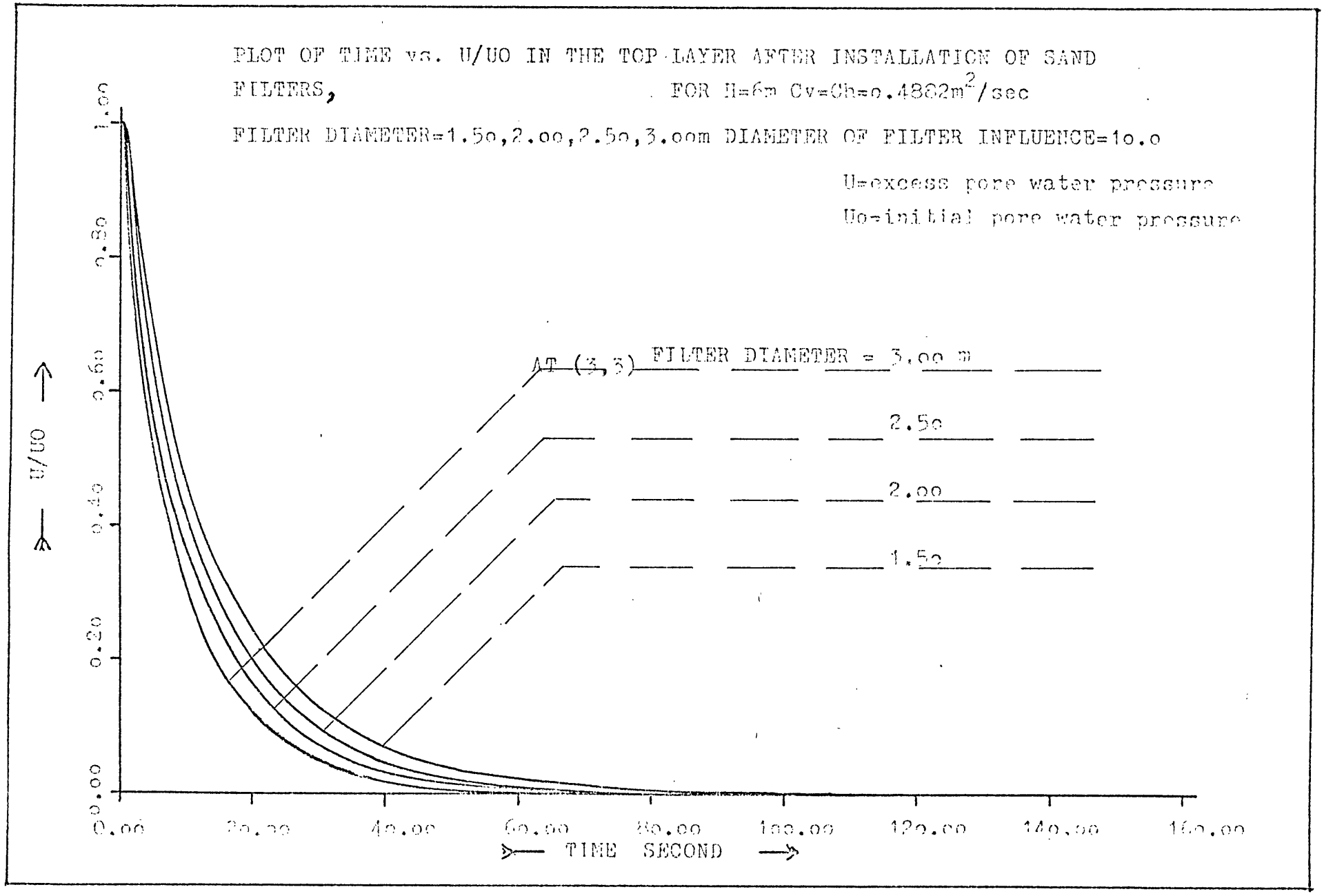

PLOT OF TIME vs. U/UO IN THE TOP LAYER AFTER INSTALLATION OF SAND FILTERS,
FOR H=6m Cv=Ch=0.4882m²/sec
FILTER DIAMETER=1.5o,2.oo,2.5o,3.oom DIAMETER OF FILTER INFLUENCE=1o.o
U=excess pore water pressure
Uo=initial pore water pressure
AT (3,3) FILTER DIAMETER = 3.oo m
2.5o
2.oo
1.5o
U/UO
TIME SECOND
0.00
0.20
0.40
0.60
0.80
1.00
0.00
20.00
40.00
60.00
80.00
100.00
120.00
140.00
160.00

Fig. 9.26

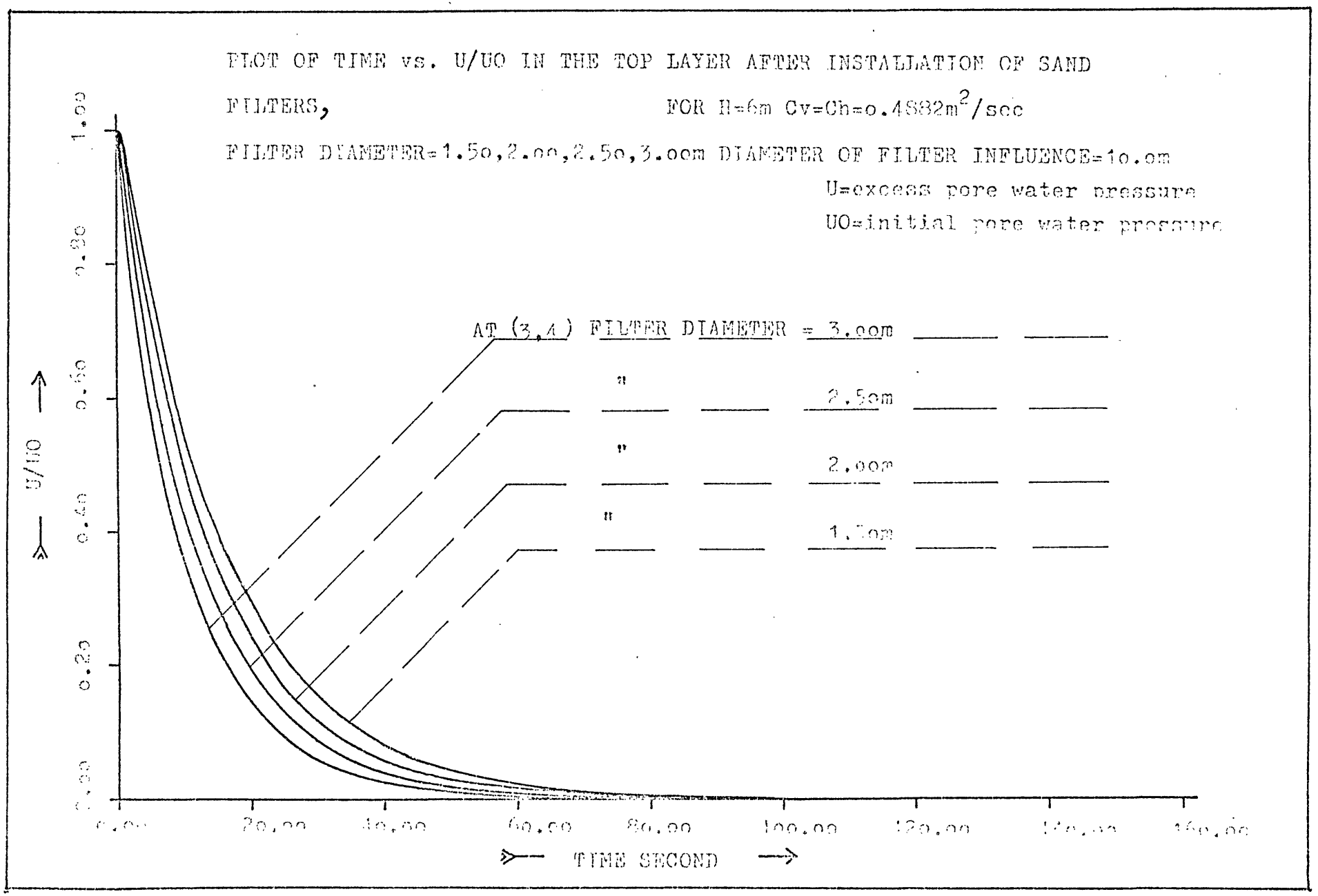

PLOT OF TIME vs. U/UO IN THE TOP LAYER AFTER INSTALLATION OF SAND FILTERS,
FOR H=6m Cv=Ch=o.4882m²/sec
FILTER DIAMETER=1.5o,2.oo,2.5o,3.oom DIAMETER OF FILTER INFLUENCE=1o.om
U=excess pore water pressure
UO=initial pore water pressure
AT (3,4) FILTER DIAMETER = 3.oom
"
2.5om
"
2.oom
"
1.5om
U/UO
0.20
0.40
0.60
0.80
1.00
20.00
40.00
60.00
80.00
100.00
120.00
TIME SECOND

Fig. 9.27

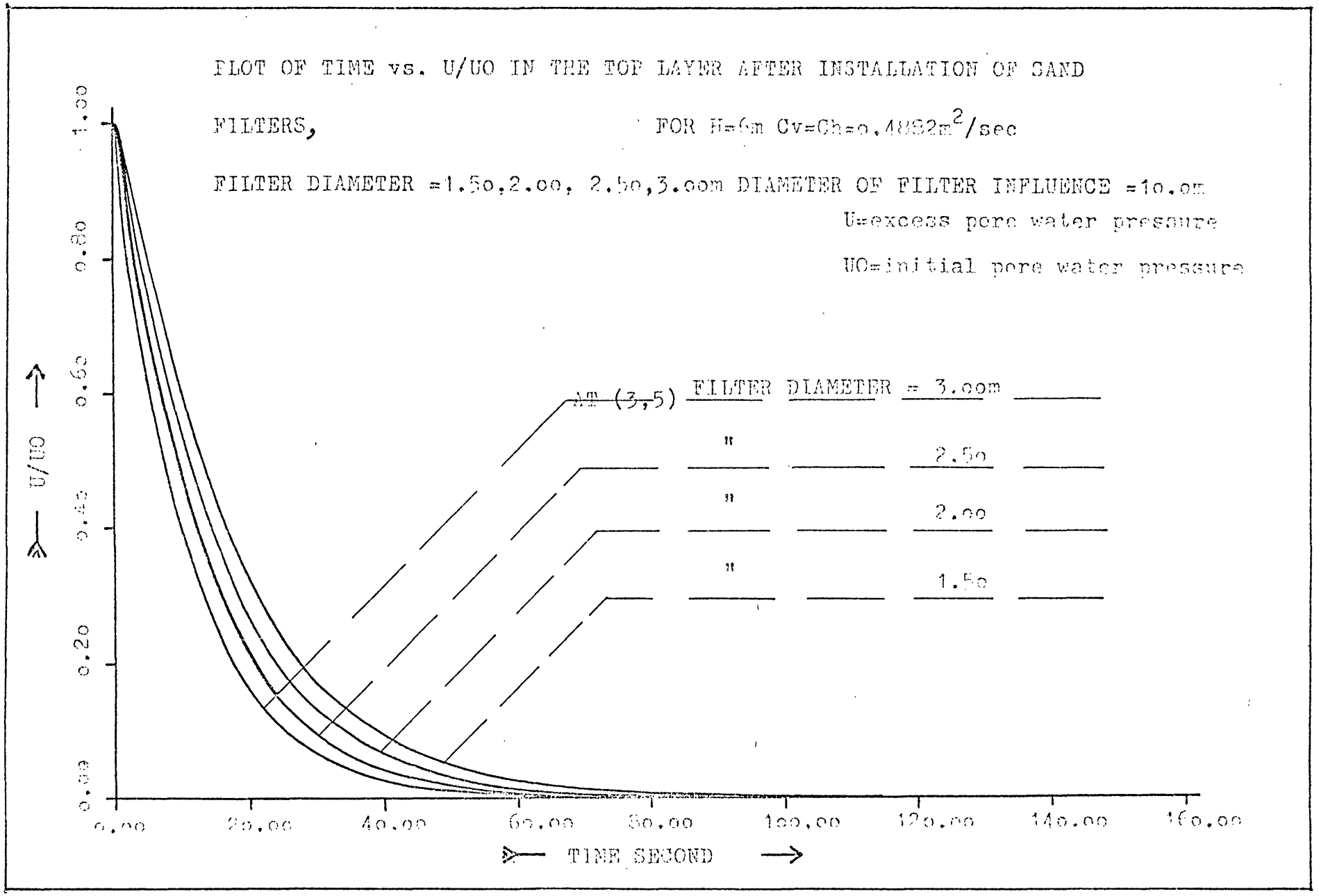

PLOT OF TIME vs. U/UO IN THE TOP LAYER AFTER INSTALLATION OF SAND
FILTERS, FOR H=6m Cv=Ch=0.4852m²/sec
FILTER DIAMETER =1.5o,2.oo, 2.5o,3.oom DIAMETER OF FILTER INFLUENCE =1o.om
U=excess pore water pressure
UO=initial pore water pressure
FILTER DIAMETER = 3.oom
"
2.5o
"
2.oo
"
1.5o
U/UO
TIME SECOND
1.oo
o.8o
o.6o
o.4o
o.2o
o.oo
2o.oo
4o.oo
6o.oo
8o.oo
1oo.oo
12o.oo
14o.oo
16o.oo

Fig. 9.28

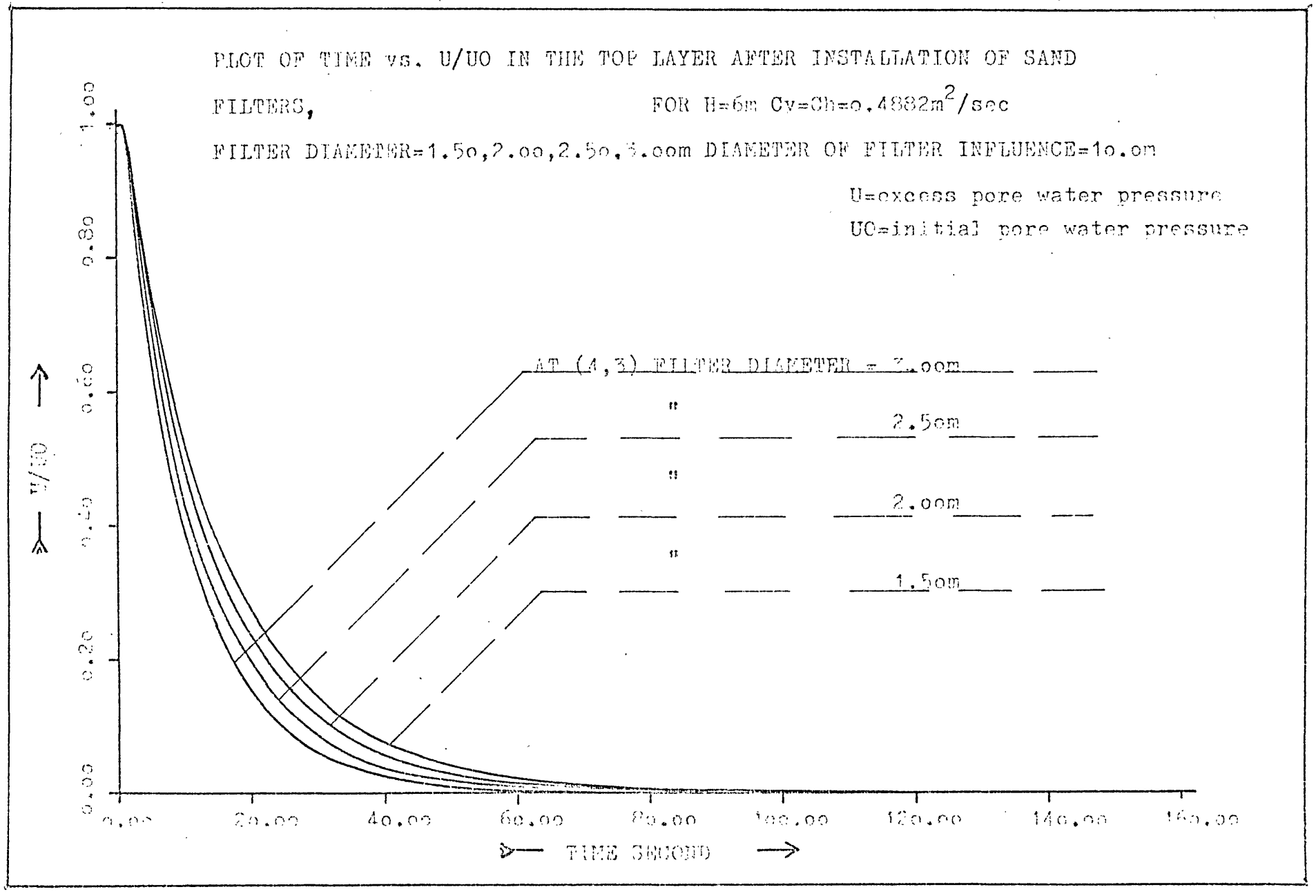

PLOT OF TIME vs. U/UO IN THE TOP LAYER AFTER INSTALLATION OF SAND
FILTERS, FOR H=6m Cv=Ch=0.4882m2/sec
FILTER DIAMETER=1.50,2.00,2.50,3.00m DIAMETER OF FILTER INFLUENCE=10.0m
U=excess pore water pressure
UO=initial pore water pressure
AT (4,3) FILTER DIAMETER = 3.00m
" 2.50m
" 2.00m
" 1.50m
U/UO
TIME SECOND
1.00
0.80
0.60
0.40
0.20
0.00
20.00
40.00
60.00
80.00
100.00
120.00
140.00
160.00

Fig. 9.29

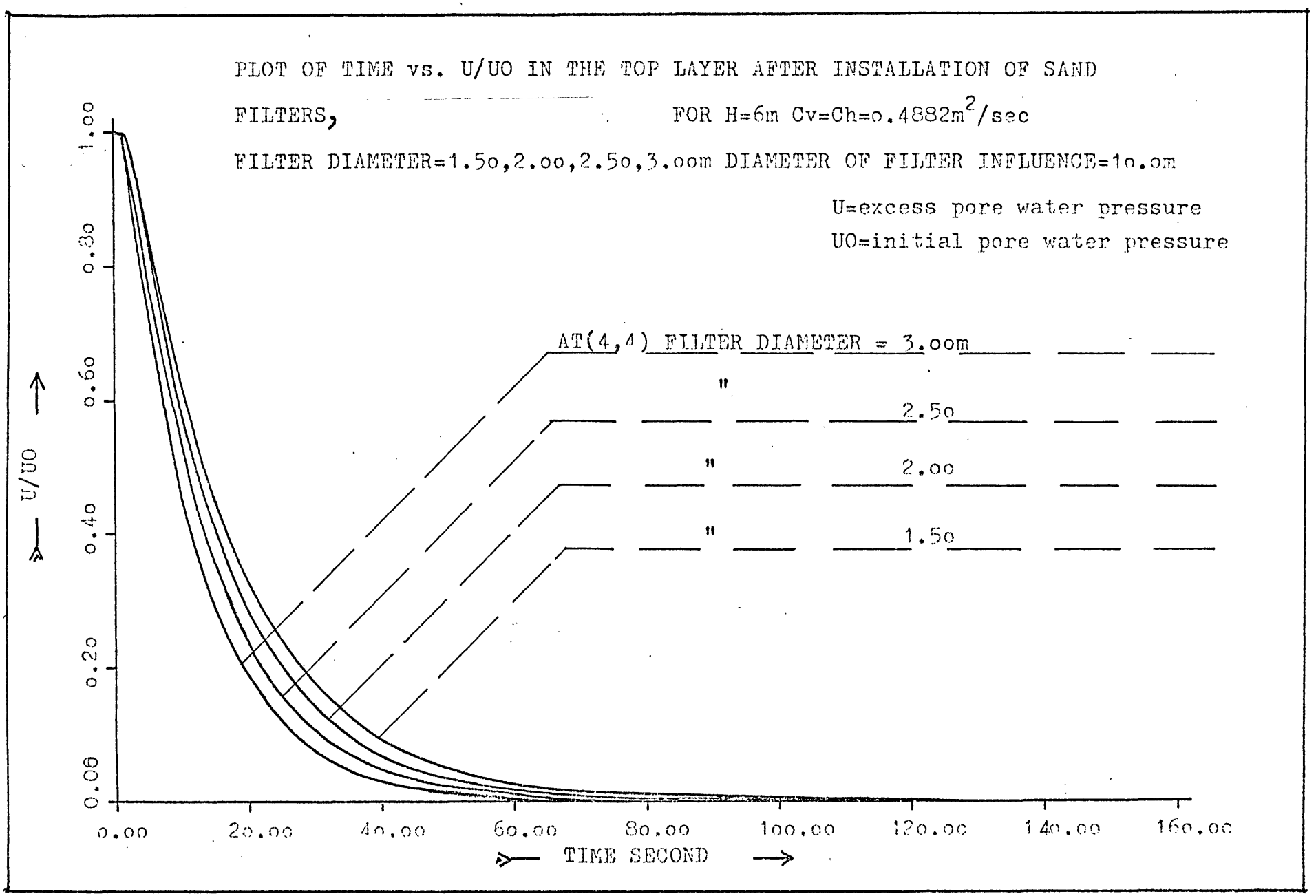

PLOT OF TIME vs. U/UO IN THE TOP LAYER AFTER INSTALLATION OF SAND FILTERS,
FOR H=6m Cv=Ch=o.4882m²/sec
FILTER DIAMETER=1.5o,2.oo,2.5o,3.oom DIAMETER OF FILTER INFLUENCE=1o.om
U=excess pore water pressure
UO=initial pore water pressure
AT(4,4) FILTER DIAMETER = 3.oom
" 2.5o
" 2.oo
" 1.5o
u/uo
1.oo
o.8o
o.6o
o.4o
o.2o
o.oo
o.oo
2o.oo
4o.oo
6o.oo
8o.oo
1oo.oo
12o.oo
14o.oo
16o.oo
TIME SECOND

Fig. 9.3o

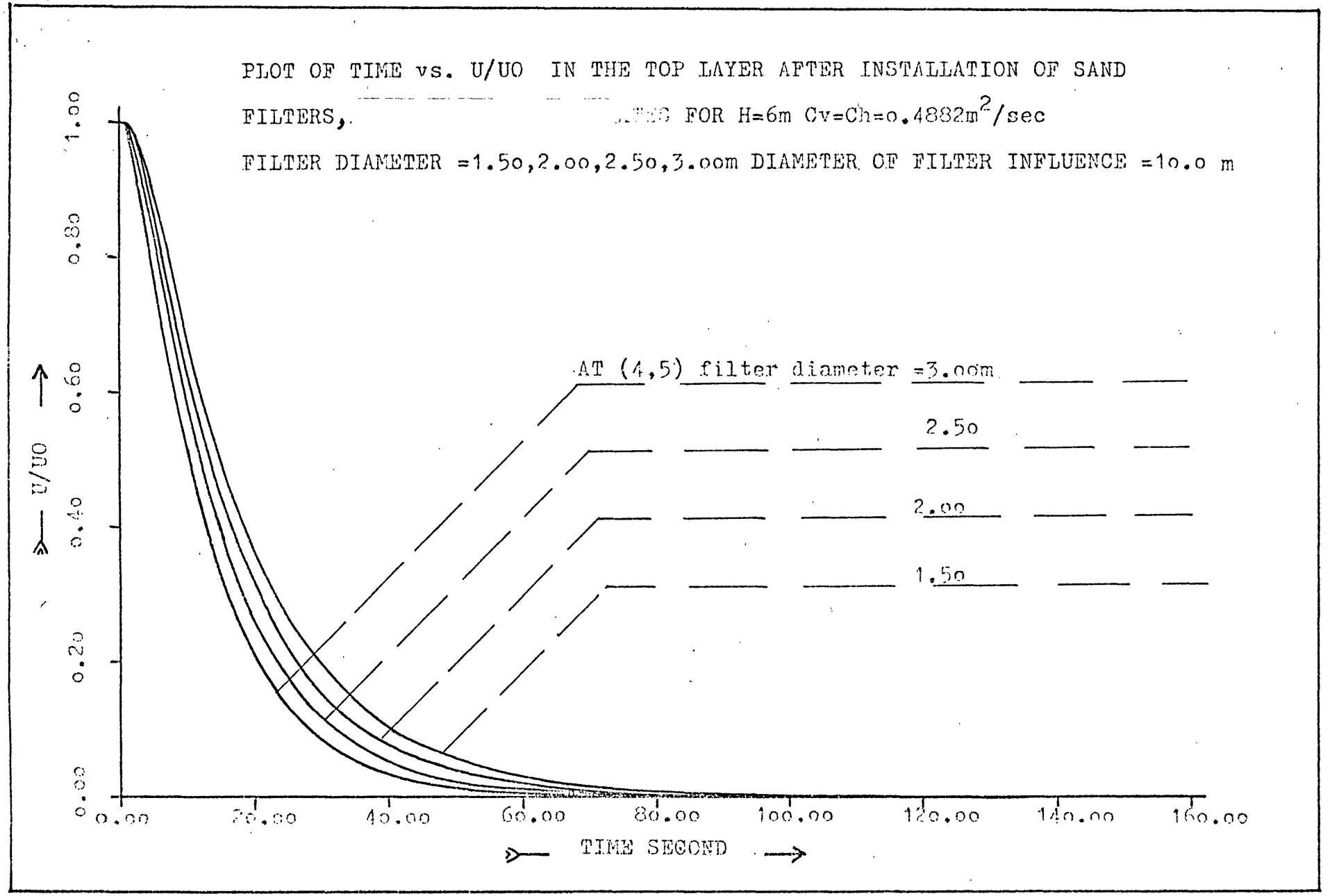

PLOT OF TIME vs. U/UO IN THE TOP LAYER AFTER INSTALLATION OF SAND
FILTERS, FOR H=6m Cv=Ch=o.4882m2/sec
FILTER DIAMETER =1.5o,2.oo,2.5o,3.oom DIAMETER OF FILTER INFLUENCE =1o.o m
AT (4,5) filter diameter =3.oom
2.5o
2.oo
1.5o
U/UO
TIME SECOND
0.00
0.20
0.40
0.60
0.80
1.00
0.00
20.00
40.00
60.00
80.00
100.00
120.00
140.00
160.00

Fig. 9.31

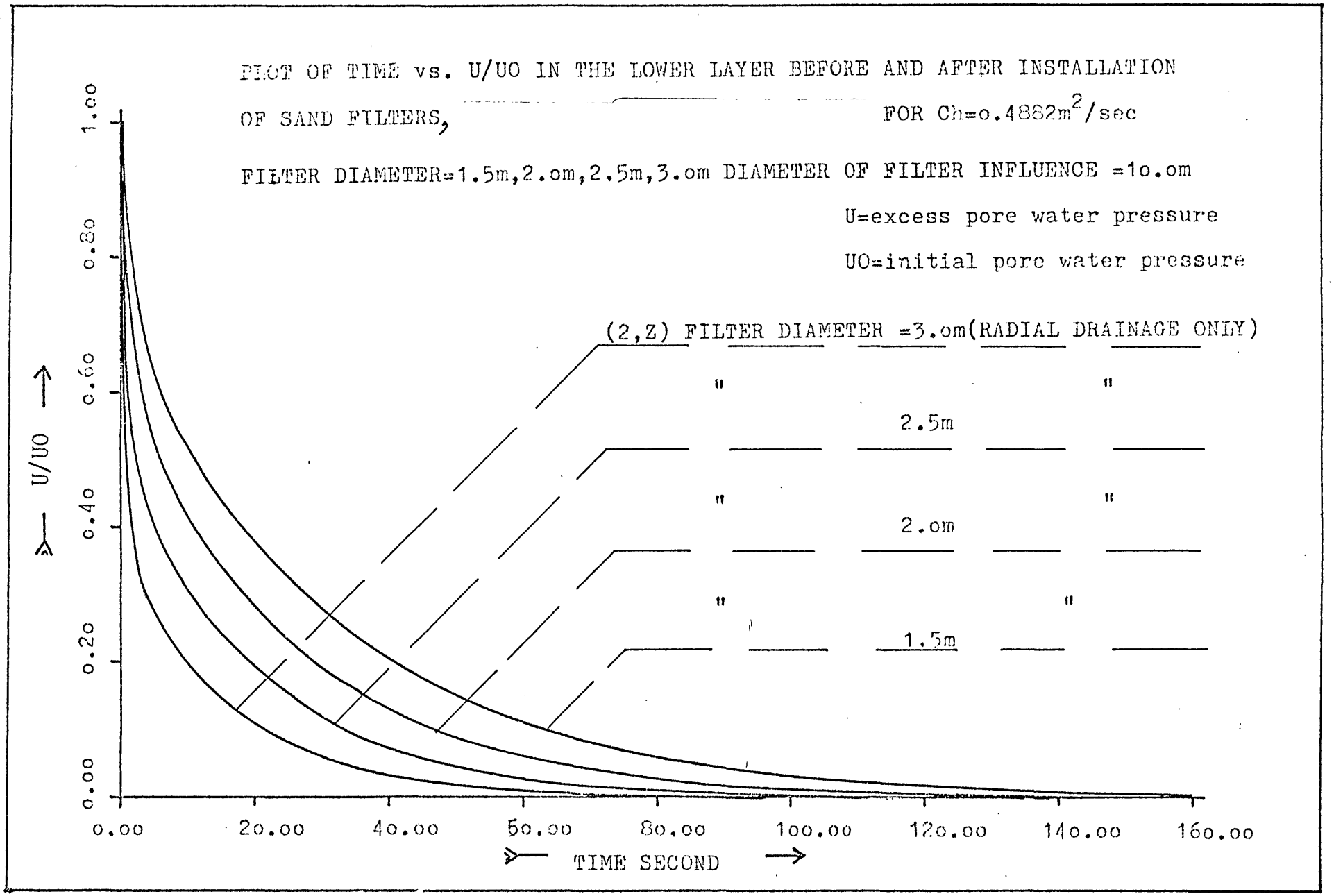

PLOT OF TIME vs. U/UO IN THE LOWER LAYER BEFORE AND AFTER INSTALLATION
OF SAND FILTERS, FOR Ch=o.4882m²/sec
FILTER DIAMETER=1.5m,2.om,2.5m,3.om DIAMETER OF FILTER INFLUENCE =1o.om
U=excess pore water pressure
UO=initial pore water pressure
(2,Z) FILTER DIAMETER =3.om(RADIAL DRAINAGE ONLY)
"
"
2.5m
"
"
2.om
"
"
1.5m
U/UO
1.oo
o.8o
o.6o
o.4o
o.2o
o.oo
0.00
2o.oo
4o.oo
6o.oo
8o.oo
1oo.oo
12o.oo
14o.oo
16o.oo
TIME SECOND

Fig. 9.32

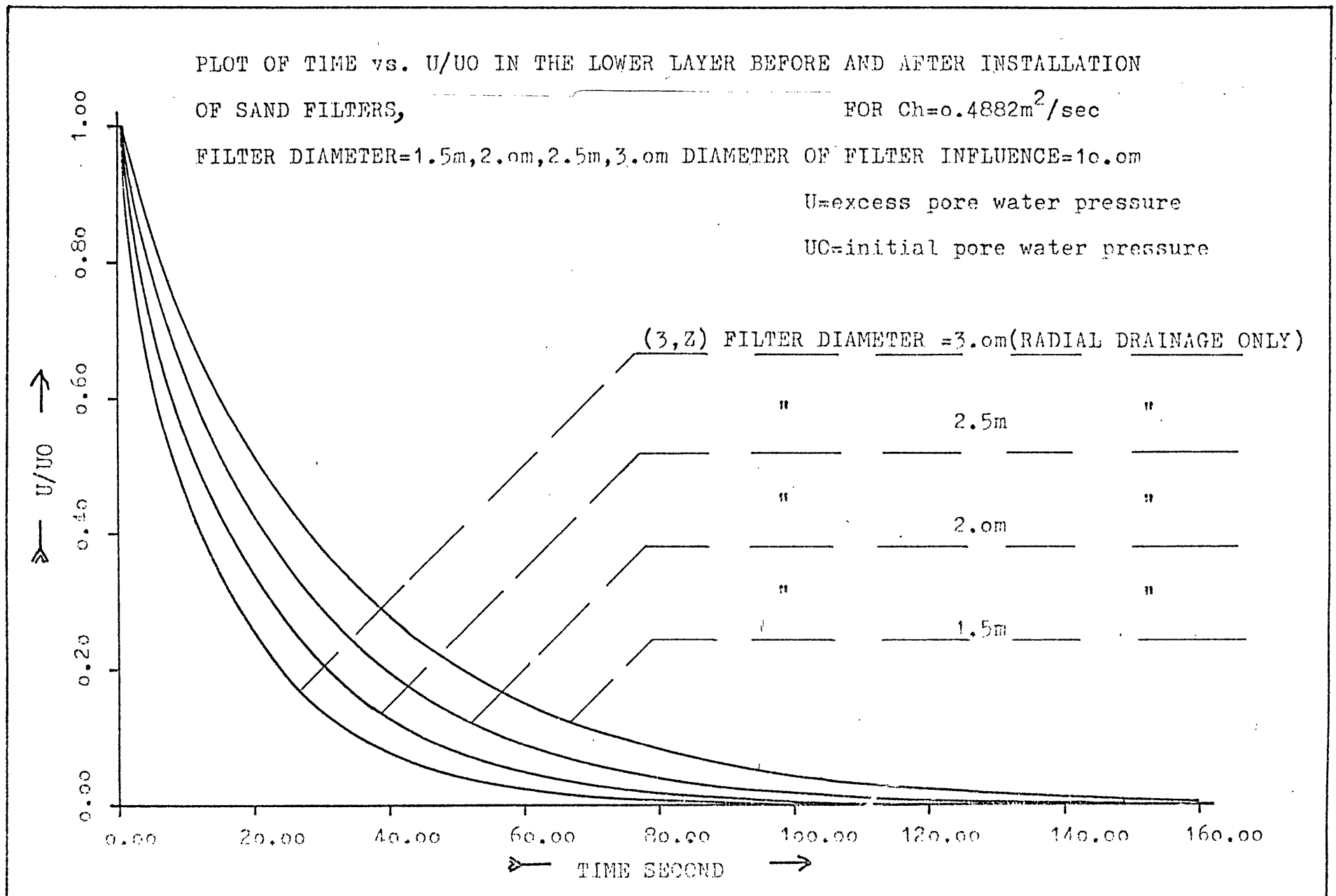

PLOT OF TIME vs. U/UO IN THE LOWER LAYER BEFORE AND AFTER INSTALLATION
OF SAND FILTERS, FOR Ch=o.4882m2/sec
FILTER DIAMETER=1.5m,2.om,2.5m,3.om DIAMETER OF FILTER INFLUENCE=1o.om
U=excess pore water pressure
UC=initial pore water pressure
(3,Z) FILTER DIAMETER =3.om(RADIAL DRAINAGE ONLY)
" 2.5m "
" 2.om "
" 1.5m "
U/UO
1.oo
o.8o
o.6o
o.4o
o.2o
o.oo
o.oo
2o.oo
4o.oo
6o.oo
8o.oo
1oo.oo
12o.oo
14o.oo
16o.oo
TIME SECOND

Fig. 9.33

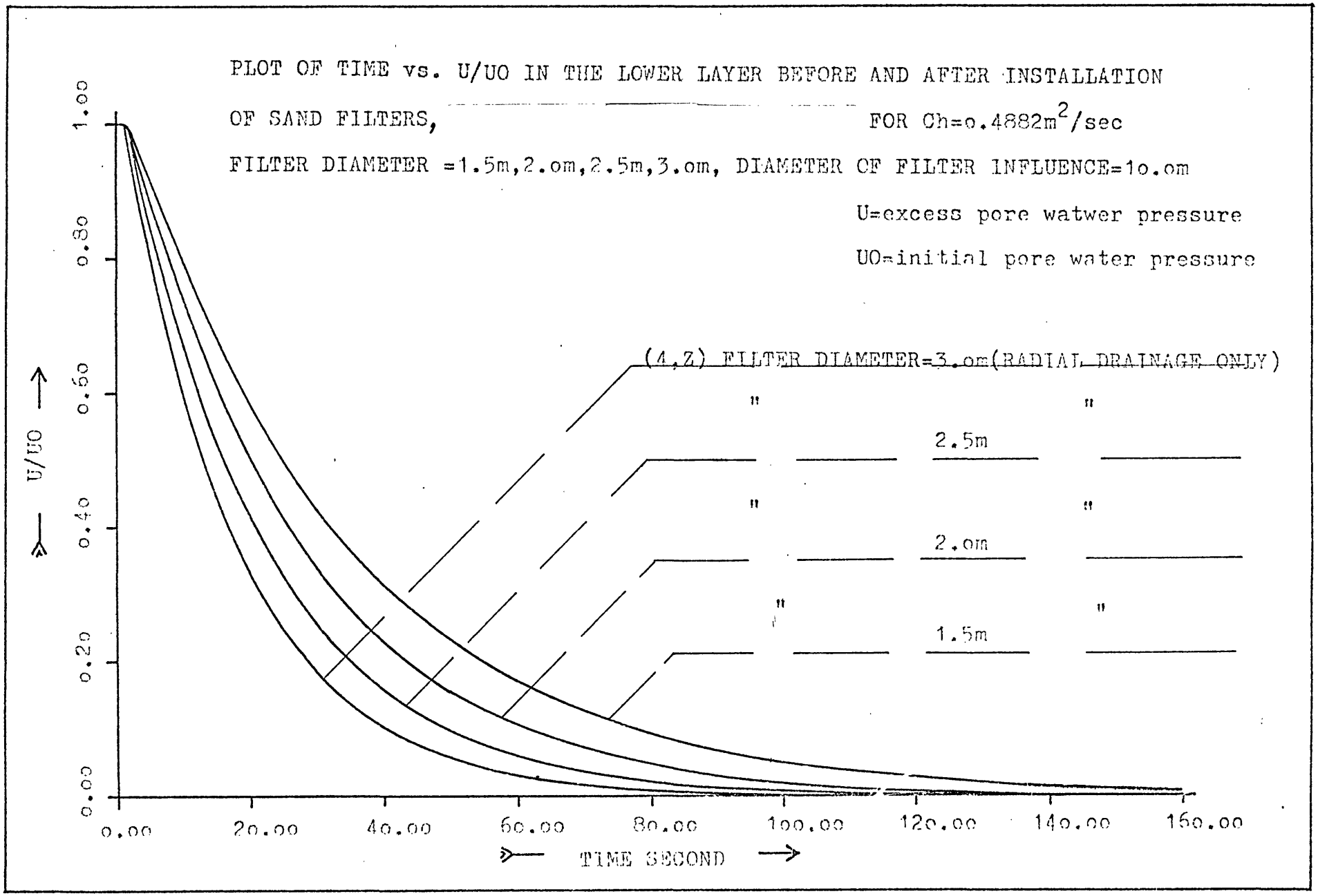

PLOT OF TIME vs. U/UO IN THE LOWER LAYER BEFORE AND AFTER INSTALLATION
OF SAND FILTERS, FOR Ch=o.4882m²/sec
FILTER DIAMETER =1.5m,2.om,2.5m,3.om, DIAMETER OF FILTER INFLUENCE=1o.om
U=excess pore watwer pressure
UO=initial pore water pressure
(4,Z) FILTER DIAMETER=3.om(RADIAL DRAINAGE ONLY)
"
"
2.5m
"
"
2.om
"
"
1.5m
U/UO
1.oo
o.8o
o.6o
o.4o
o.2o
o.oo
o.oo
2o.oo
4o.oo
6o.oo
8o.oo
1oo.oo
12o.oo
14o.oo
16o.oo
TIME SECOND

Fig. 9.34

water pressure and time for $C_h = C_v$, $C_h = 1.5C_v$ and $C_h = 2C_v$. All these figures compare the results which would have been obtained if the sand filters were absent. The results for the lower layer are shown in figs.9.44 - 9.46.

Fig.9.35 through 9.46 demonstrate the pronounced effects of C_h on the dissipation rates in the lower and upper layer. The effect is more in the lower layer than in the upper layer. This is because in the lower layer the excess pore water can only dissipate in a radial direction.

9.13. DESIGN OF VERTICAL SAND FILTERS AND METHODS OF INSTALLATION

A detailed design of vertical sand filters is beyond the purpose of this chapter. A few general remarks are only made here. It is desired to keep sand filters functional during the whole life of the structure under which the vertical sand filters are to be installed; therefore, careful design of these filters is required. Filters must be graded and have sufficient conductivity to provide relatively free drainage; piping and intrusion of native sand should be prevented. They must not get clogged over a long period of time.

A review of modern drilling machinery which can be used for installation of vertical sand filters is given by [64] with special design of drilling bucket to fit the soil type it is today possible to keep smearing effect to a minimum.

9.14. DESIGN PROCEDURE AND DESIGN EXAMPLE

Based on the studies done in this chapter, the following steps are

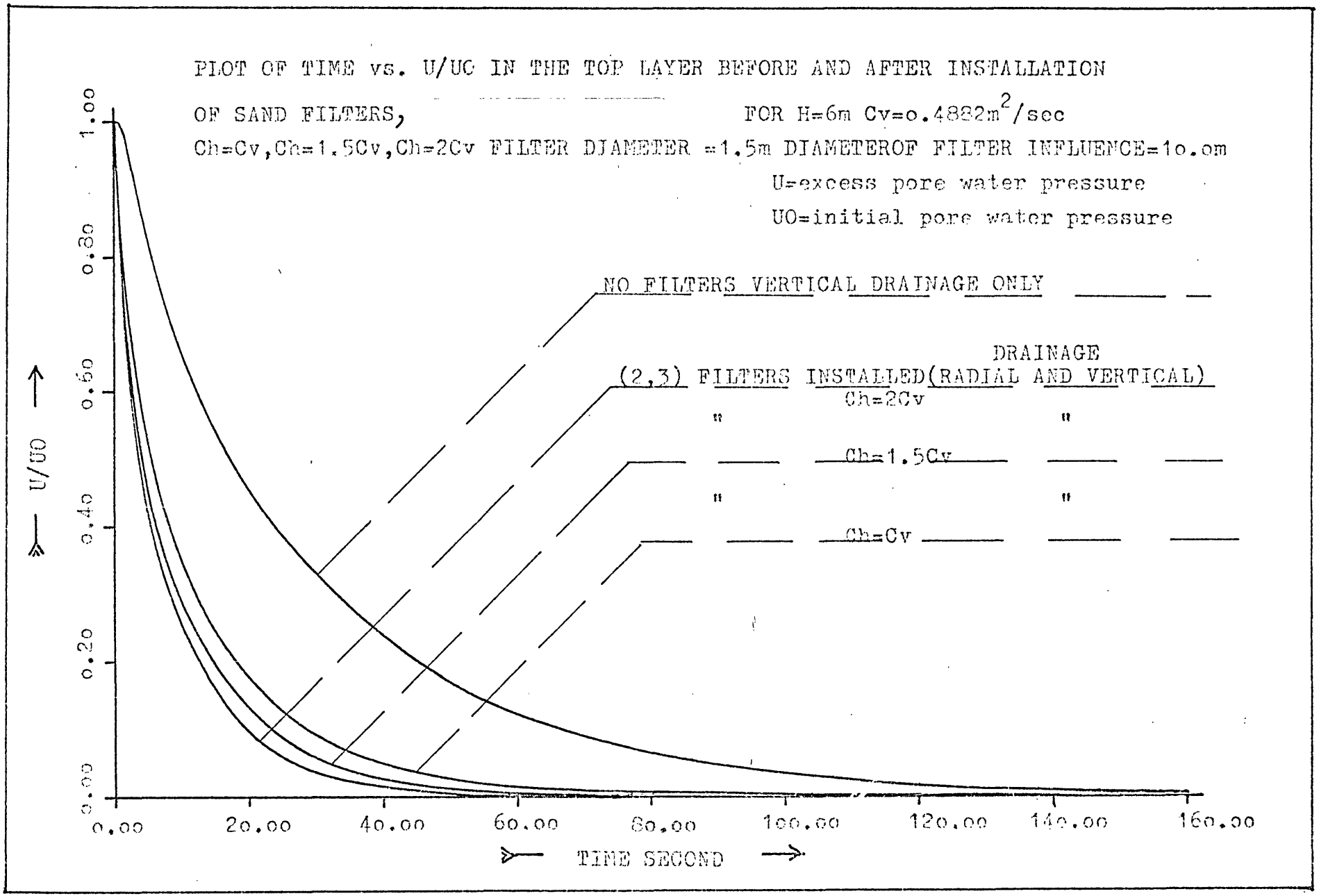

PLOT OF TIME vs. U/UO IN THE TOP LAYER BEFORE AND AFTER INSTALLATION
OF SAND FILTERS, FOR H=6m Cv=o.4882m²/sec
Ch=Cv,Ch=1.5Cv,Ch=2Cv FILTER DIAMETER =1.5m DIAMETEROF FILTER INFLUENCE=1o.om
U=excess pore water pressure
UO=initial pore water pressure
NO FILTERS VERTICAL DRAINAGE ONLY
DRAINAGE
(2,3) FILTERS INSTALLED(RADIAL AND VERTICAL)
Ch=2Cv
"
"
Ch=1.5Cv
"
"
Ch=Cv
U/UO
1.00
o.8o
o.6o
o.4o
o.2o
o.oo
o.oo
2o.oo
4o.oo
6o.oo
8o.oo
1oo.oo
12o.oo
14o.oo
16o.oo
TIME SECOND

Fig. 9.35

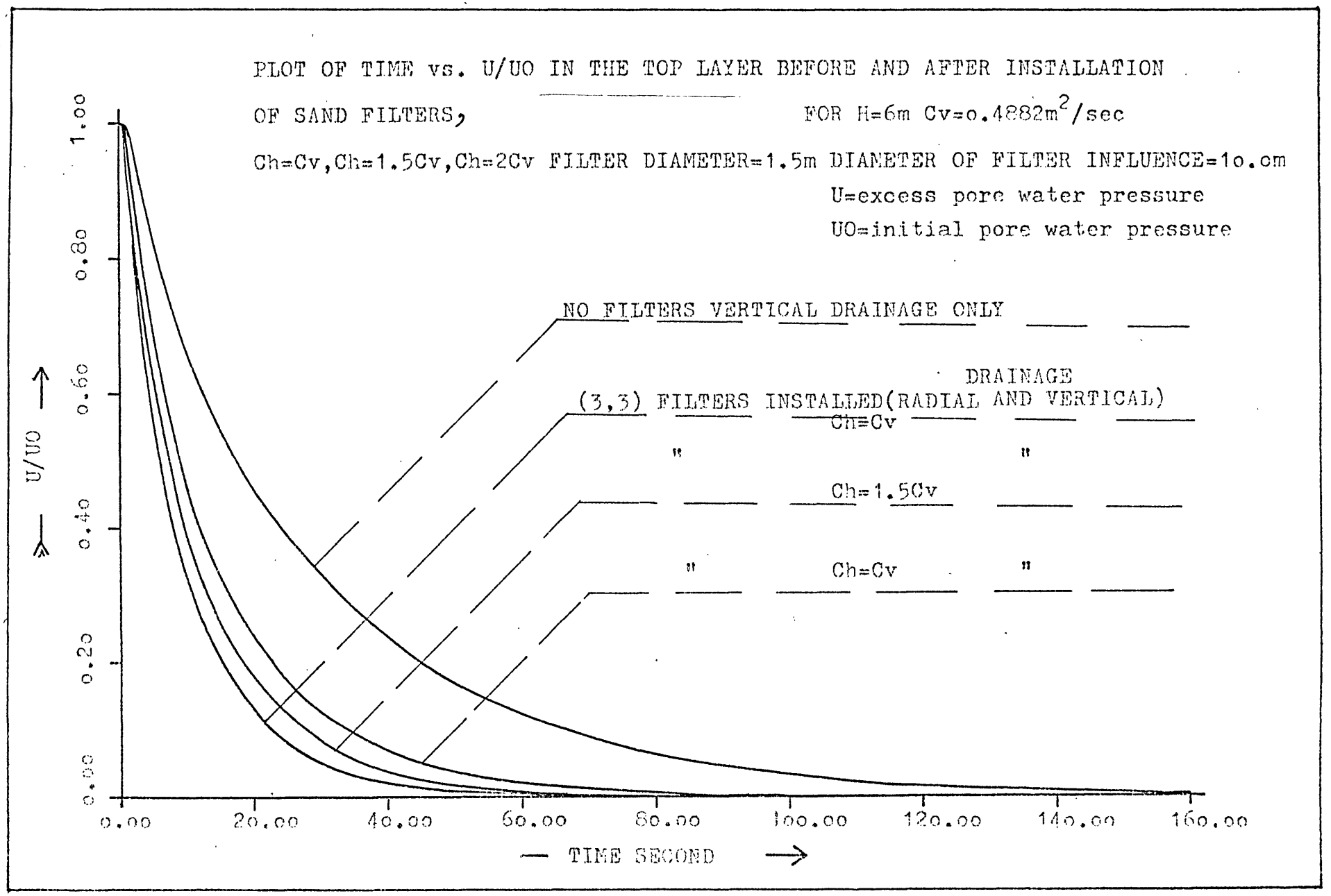

PLOT OF TIME vs. U/UO IN THE TOP LAYER BEFORE AND AFTER INSTALLATION
OF SAND FILTERS,
FOR H=6m Cv=o.4882m²/sec
Ch=Cv,Ch=1.5Cv,Ch=2Cv FILTER DIAMETER=1.5m DIANETER OF FILTER INFLUENCE=1o.cm
U=excess pore water pressure
UO=initial pore water pressure
NO FILTERS VERTICAL DRAINAGE ONLY
(3,3) FILTERS INSTALLED(RADIAL AND VERTICAL) DRAINAGE
Ch=Cv
"
"
Ch=1.5Cv
"
Ch=Cv
"
U/UO
1.00
o.8o
o.6o
o.4o
o.2o
o.oo
0.00
2o.oo
4o.oo
6o.oo
8o.oo
1oo.oo
12o.oo
14o.oo
16o.oo
TIME SECOND

Fig. 9.36

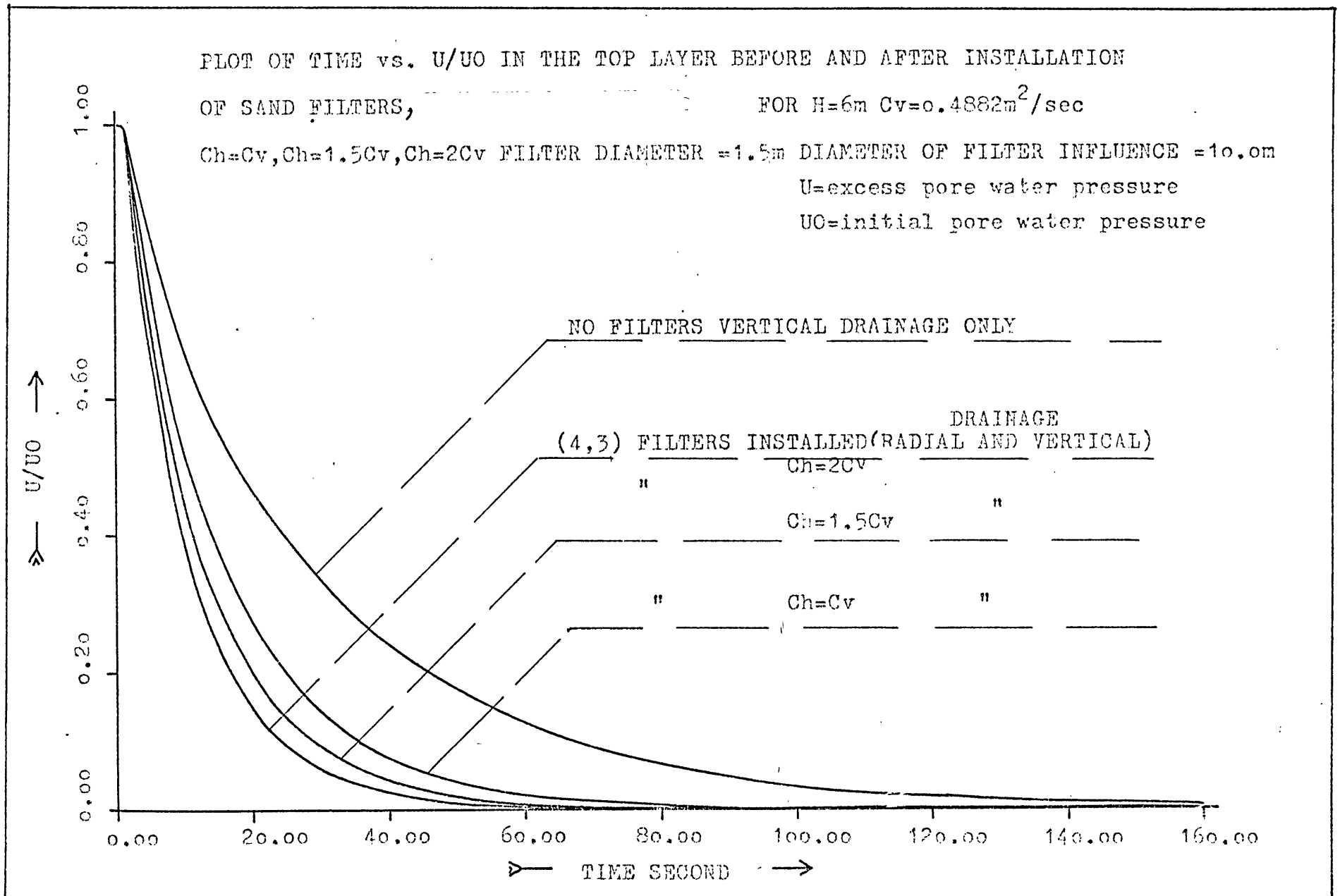

PLOT OF TIME vs. U/UO IN THE TOP LAYER BEFORE AND AFTER INSTALLATION
OF SAND FILTERS, FOR H=6m Cv=o.4882m²/sec
Ch=Cv,Ch=1.5Cv,Ch=2Cv FILTER DIAMETER =1.5m DIAMETER OF FILTER INFLUENCE =1o.om
U=excess pore water pressure
UO=initial pore water pressure
NO FILTERS VERTICAL DRAINAGE ONLY
(4,3) FILTERS INSTALLED(RADIAL AND VERTICAL) DRAINAGE
Ch=2Cv
"
Ch=1.5Cv
"
"
Ch=Cv
"
U/UO
1.00
0.80
0.60
0.40
0.20
0.00
0.00
20.00
40.00
60.00
80.00
100.00
120.00
140.00
160.00
TIME SECOND

Fig. 9.37

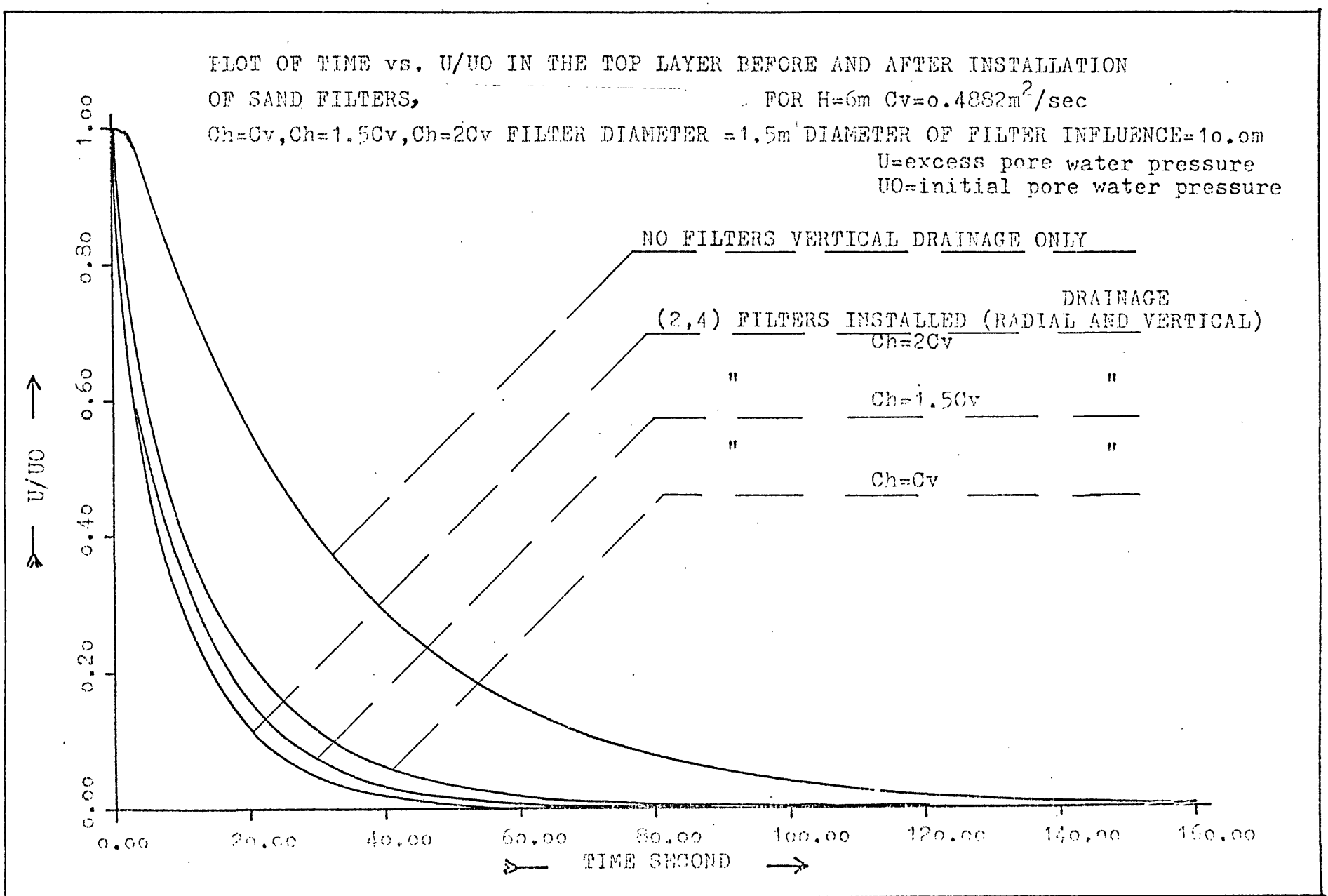

PLOT OF TIME vs. U/UO IN THE TOP LAYER BEFORE AND AFTER INSTALLATION
OF SAND FILTERS, FOR H=6m Cv=o.4882m²/sec
Ch=Cv,Ch=1.5Cv,Ch=2Cv FILTER DIAMETER =1.5m DIAMETER OF FILTER INFLUENCE=1o.om
U=excess pore water pressure
UO=initial pore water pressure
NO FILTERS VERTICAL DRAINAGE ONLY
(2,4) FILTERS INSTALLED (RADIAL AND VERTICAL) DRAINAGE
Ch=2Cv
"
Ch=1.5Cv
"
Ch=Cv
U/UO
1.00
0.80
0.60
0.40
0.20
0.00
0.00
20.00
40.00
60.00
80.00
100.00
120.00
140.00
160.00
TIME SECOND

Fig. 9.38

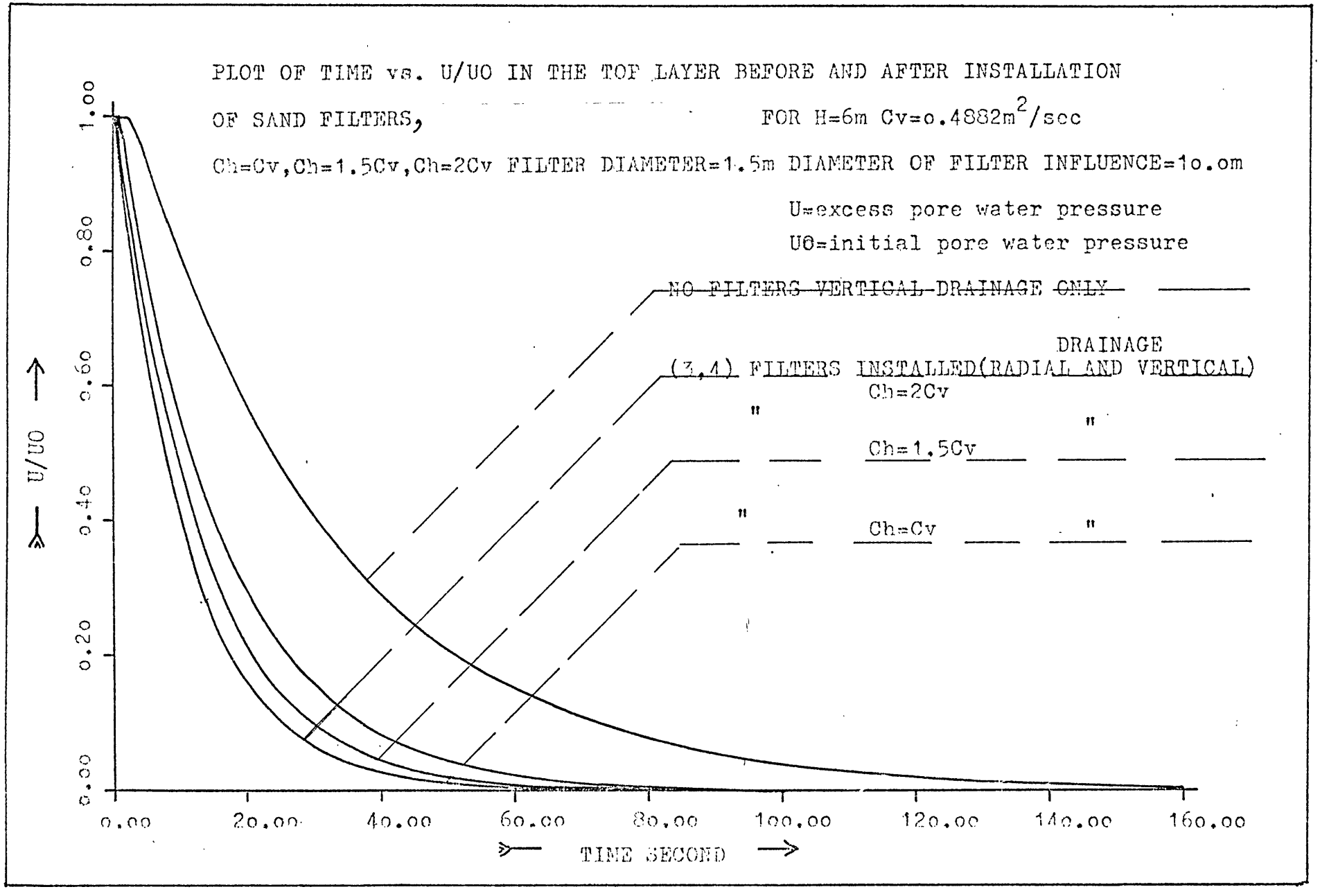

PLOT OF TIME vs. U/UO IN THE TOP LAYER BEFORE AND AFTER INSTALLATION
OF SAND FILTERS, FOR H=6m Cv=o.4882m²/sec
Ch=Cv,Ch=1.5Cv,Ch=2Cv FILTER DIAMETER=1.5m DIAMETER OF FILTER INFLUENCE=1o.om
U=excess pore water pressure
UO=initial pore water pressure
NO FILTERS VERTICAL DRAINAGE ONLY
(3,4) FILTERS INSTALLED(RADIAL AND VERTICAL) DRAINAGE
Ch=2Cv
"
"
Ch=1.5Cv
"
Ch=Cv
"
U/UO
1.00
o.8o
o.6o
o.4o
o.2o
o.oo
0.00
2o.oo
4o.oo
6o.oo
8o.oo
1oo.oo
12o.oo
14o.oo
16o.oo
TIME SECOND

Fig. 9.39

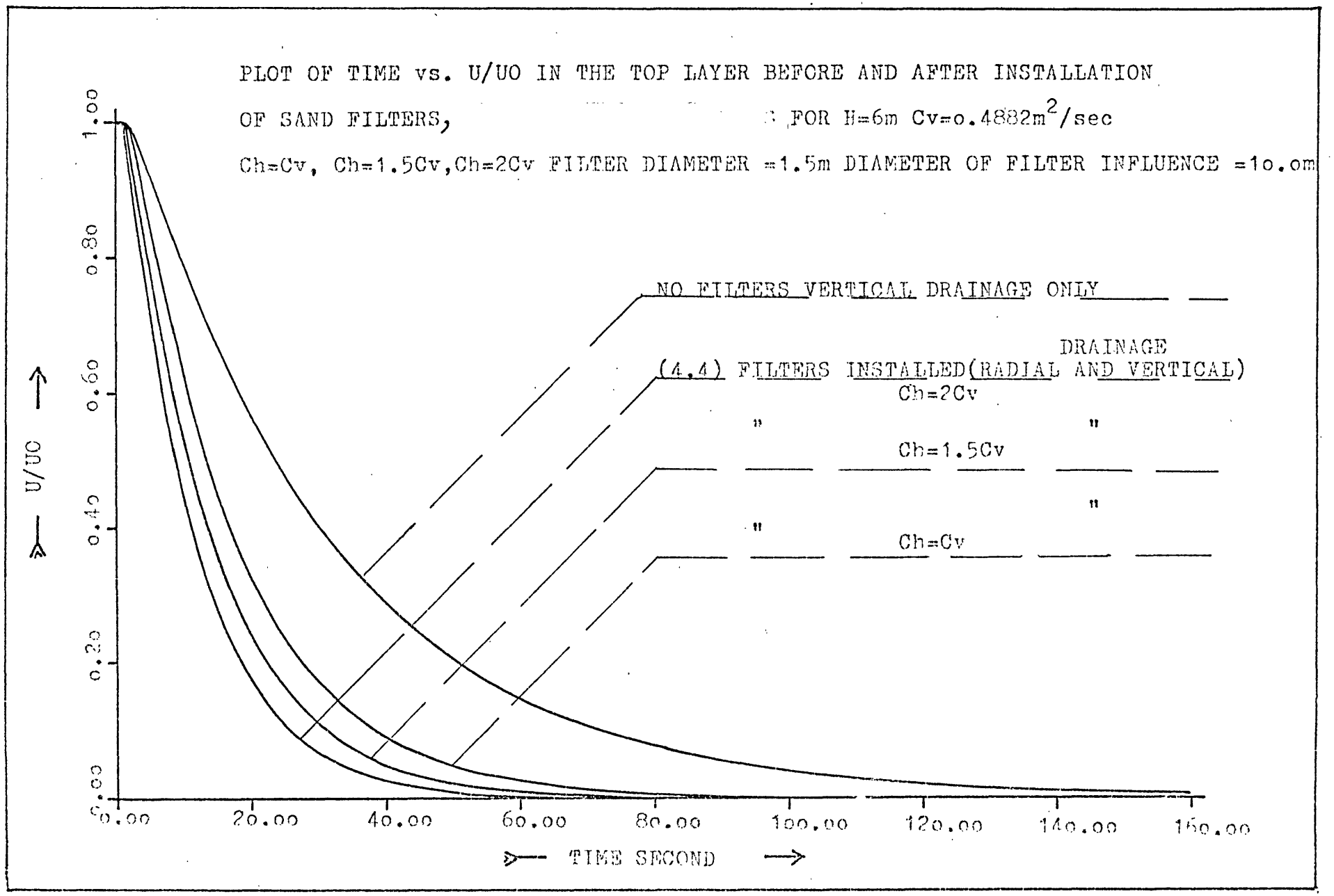

PLOT OF TIME vs. U/UO IN THE TOP LAYER BEFORE AND AFTER INSTALLATION
OF SAND FILTERS, FOR H=6m Cv=o.4882m2/sec
Ch=Cv, Ch=1.5Cv,Ch=2Cv FILTER DIAMETER =1.5m DIAMETER OF FILTER INFLUENCE =1o.om
NO FILTERS VERTICAL DRAINAGE ONLY
(4.4) FILTERS INSTALLED(RADIAL AND VERTICAL) DRAINAGE
Ch=2Cv
"
Ch=1.5Cv
"
"
Ch=Cv
U/UO
1.00
0.80
0.60
0.40
0.20
0.00
0.00
20.00
40.00
60.00
80.00
100.00
120.00
140.00
160.00
TIME SECOND

Fig. 9.4o

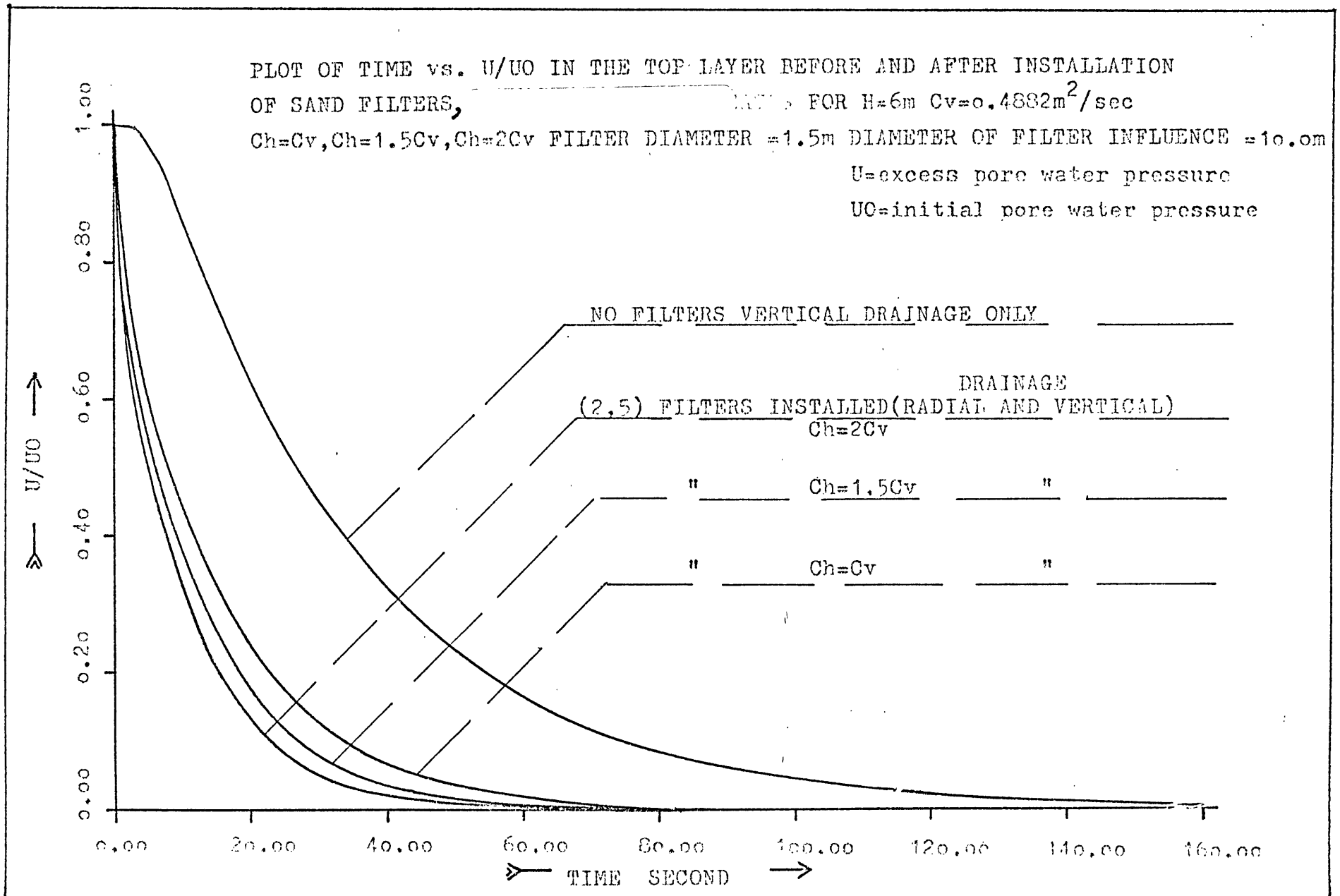

PLOT OF TIME vs. U/UO IN THE TOP LAYER BEFORE AND AFTER INSTALLATION
OF SAND FILTERS, FOR H=6m Cv=o.4882m²/sec
Ch=Cv,Ch=1.5Cv,Ch=2Cv FILTER DIAMETER =1.5m DIAMETER OF FILTER INFLUENCE =1o.om
U=excess pore water pressure
UO=initial pore water pressure
NO FILTERS VERTICAL DRAINAGE ONLY
(2,5) FILTERS INSTALLED(RADIAL AND VERTICAL) DRAINAGE
Ch=2Cv
" Ch=1.5Cv "
" Ch=Cv "
U/UO
1.00
0.80
0.60
0.40
0.20
0.00
0.00
20.00
40.00
60.00
80.00
100.00
120.00
140.00
160.00
TIME SECOND

Fig. 9.41

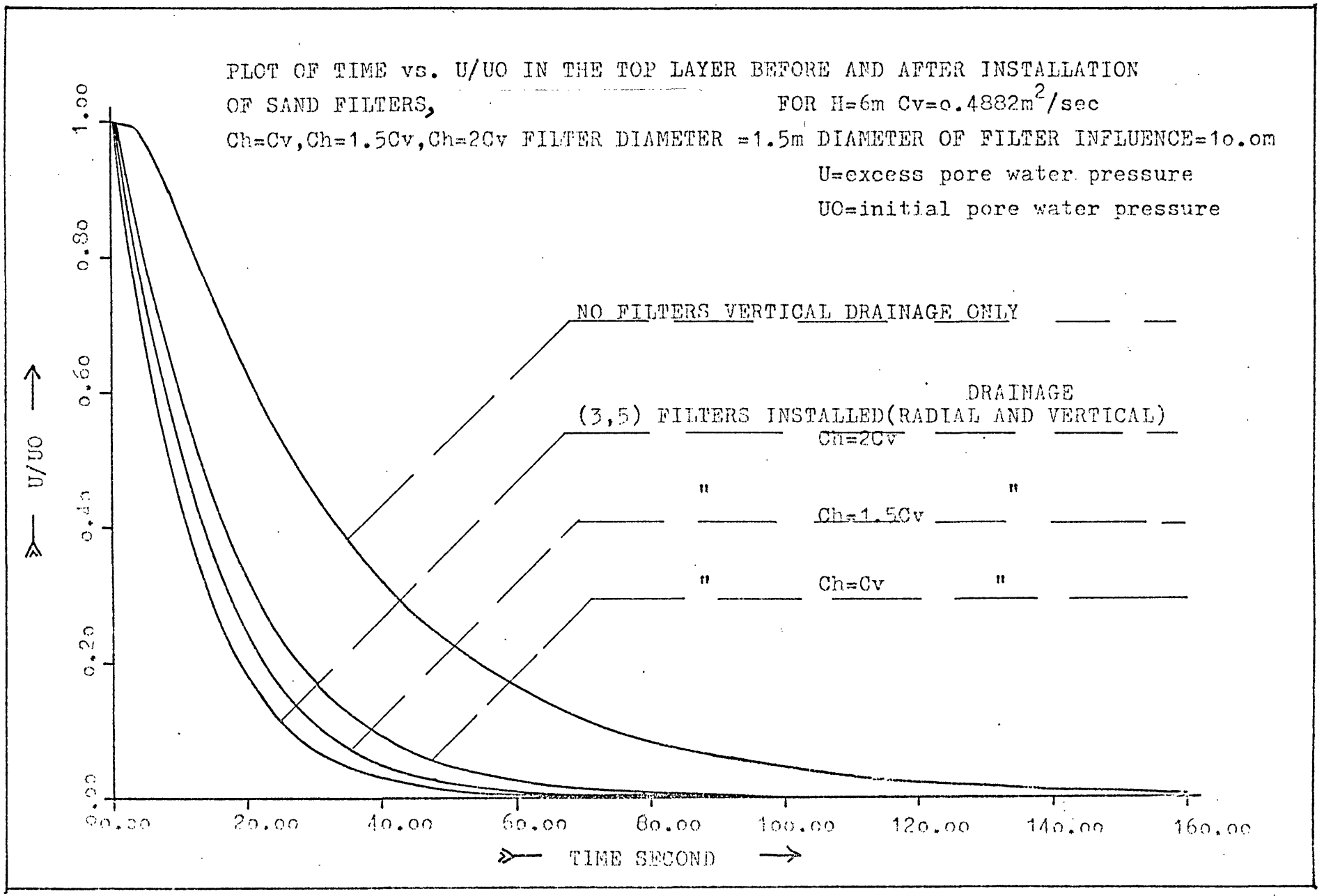

PLOT OF TIME vs. U/UO IN THE TOP LAYER BEFORE AND AFTER INSTALLATION
OF SAND FILTERS, FOR H=6m Cv=o.4882m²/sec
Ch=Cv,Ch=1.5Cv,Ch=2Cv FILTER DIAMETER =1.5m DIAMETER OF FILTER INFLUENCE=1o.om
U=excess pore water pressure
UO=initial pore water pressure
NO FILTERS VERTICAL DRAINAGE ONLY
(3,5) FILTERS INSTALLED(RADIAL AND VERTICAL) DRAINAGE
Ch=2Cv
"
Ch=1.5Cv
"
Ch=Cv
"
U/UO
1.00
0.80
0.60
0.40
0.20
0.00
20.00
40.00
60.00
80.00
100.00
120.00
140.00
160.00
TIME SECOND

Fig. 9.42

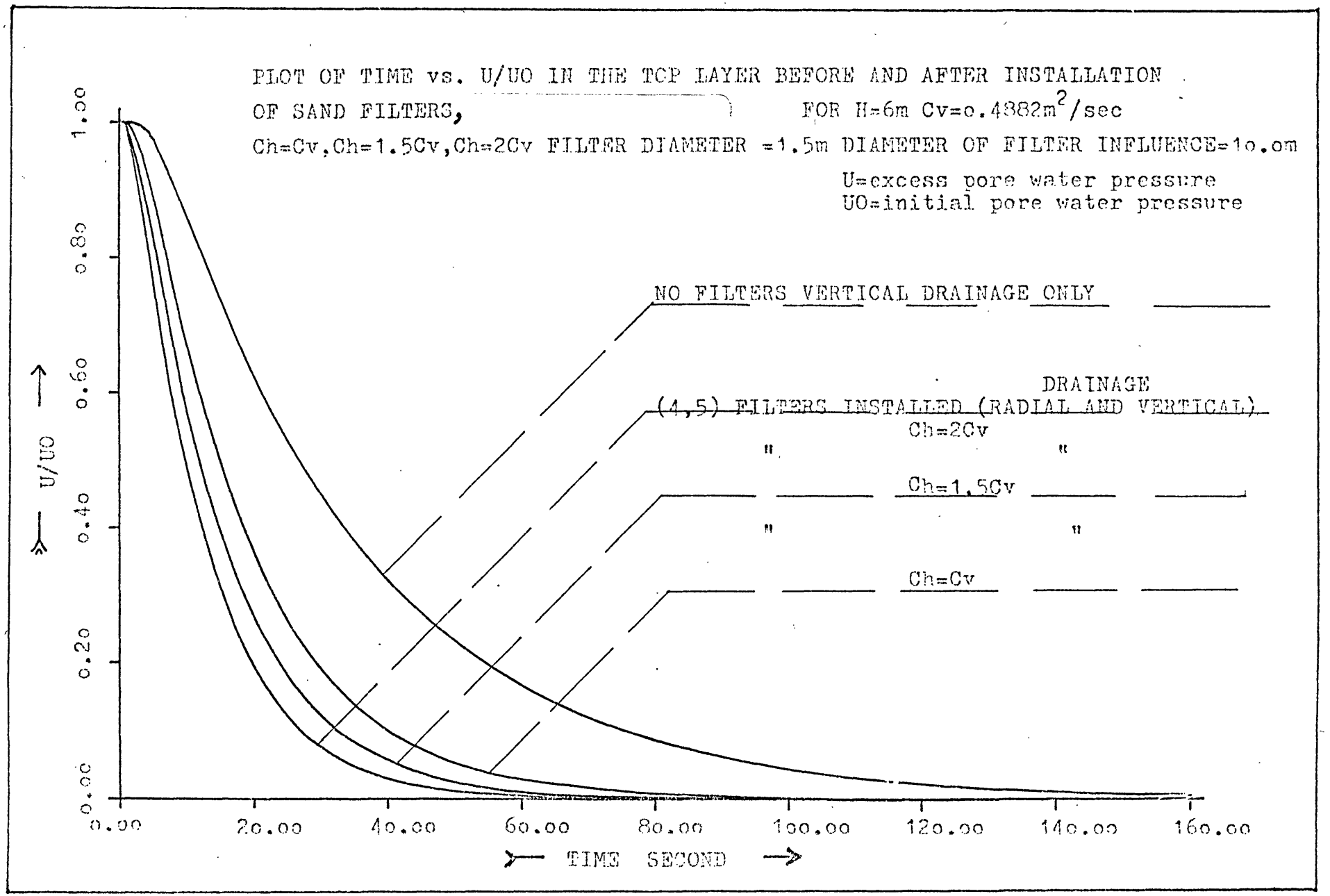

PLOT OF TIME vs. U/UO IN THE TOP LAYER BEFORE AND AFTER INSTALLATION
OF SAND FILTERS, FOR H=6m Cv=o.4882m²/sec
Ch=Cv, Ch=1.5Cv, Ch=2Cv FILTER DIAMETER =1.5m DIAMETER OF FILTER INFLUENCE=1o.om
U=excess pore water pressure
UO=initial pore water pressure
NO FILTERS VERTICAL DRAINAGE ONLY
DRAINAGE
(4,5) FILTERS INSTALLED (RADIAL AND VERTICAL)
Ch=2Cv
"
"
Ch=1.5Cv
"
"
Ch=Cv
U/UO
1.oo
o.8o
o.6o
o.4o
o.2o
o.oo
o.oo
2o.oo
4o.oo
6o.oo
8o.oo
1oo.oo
12o.oo
14o.oo
16o.oo
TIME SECOND

Fig. 9.43

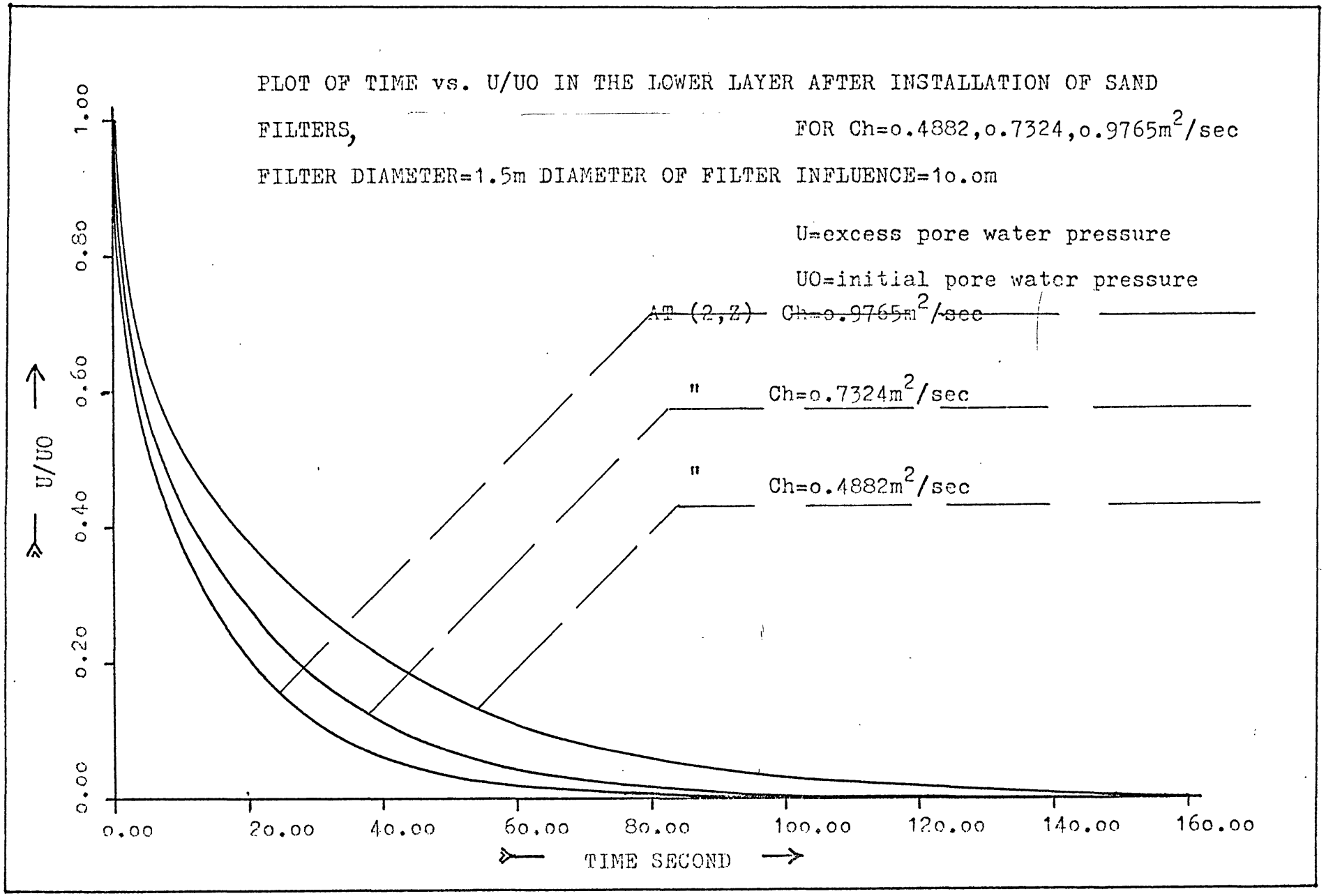

PLOT OF TIME vs. U/UO IN THE LOWER LAYER AFTER INSTALLATION OF SAND FILTERS,
FOR Ch=o.4882,o.7324,o.9765m²/sec
FILTER DIAMETER=1.5m DIAMETER OF FILTER INFLUENCE=1o.om
U=excess pore water pressure
UO=initial pore water pressure
AT (2,Z) Ch=o.9765m²/sec
" Ch=o.7324m²/sec
" Ch=o.4882m²/sec
U/UO
1.00
o.8o
o.6o
o.4o
o.2o
o.oo
o.oo
2o.oo
4o.oo
6o.oo
8o.oo
1oo.oo
12o.oo
14o.oo
16o.oo
TIME SECOND

Fig. 9.44

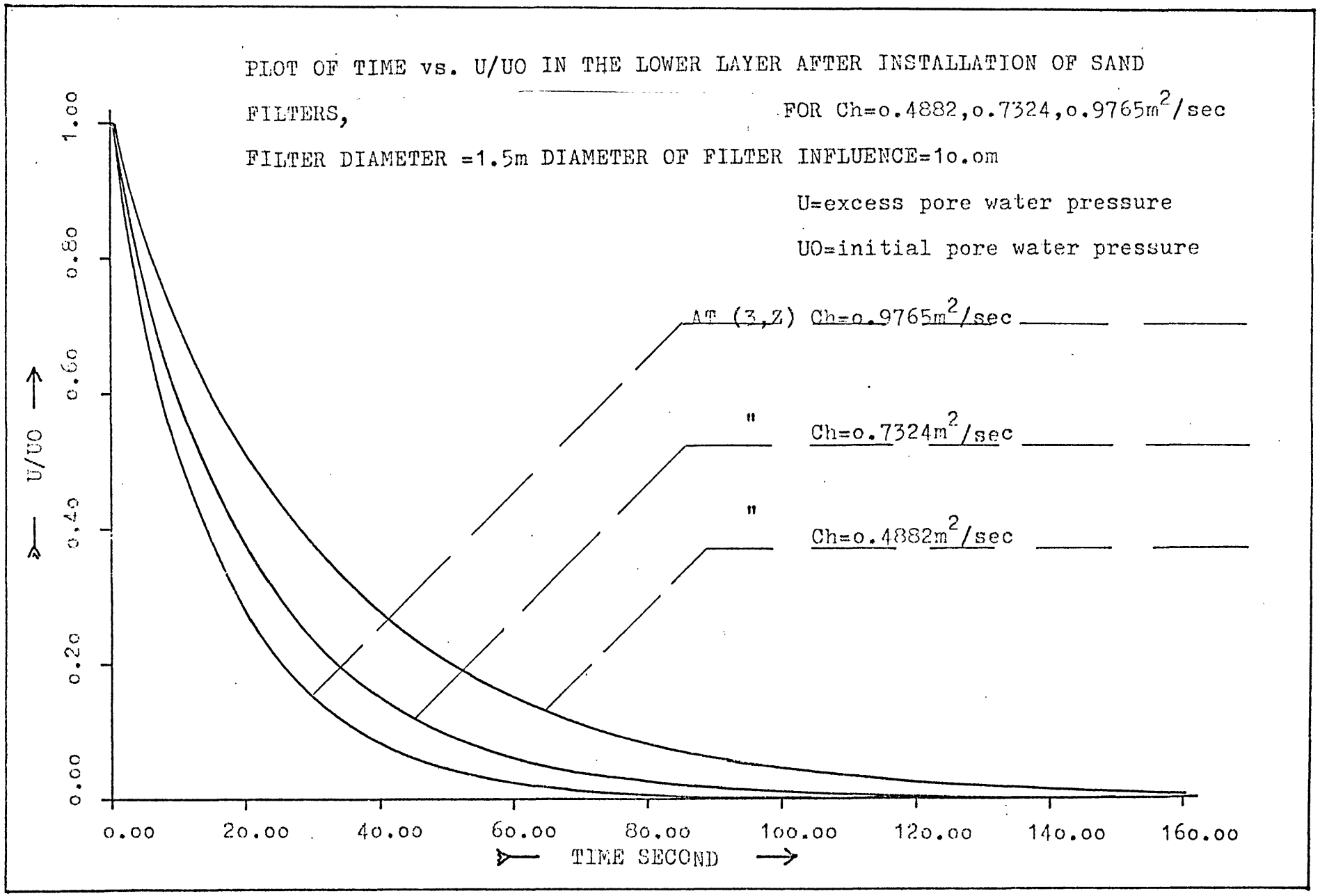

PLOT OF TIME vs. U/UO IN THE LOWER LAYER AFTER INSTALLATION OF SAND FILTERS,
FOR Ch=o.4882,o.7324,o.9765m²/sec
FILTER DIAMETER =1.5m DIAMETER OF FILTER INFLUENCE=1o.om
U=excess pore water pressure
UO=initial pore water pressure
AT (3,Z) Ch=o.9765m²/sec
" Ch=o.7324m²/sec
" Ch=o.4882m²/sec
U/UO
1.00
o.8o
o.6o
o.4o
o.2o
o.oo
o.oo
2o.oo
4o.oo
6o.oo
8o.oo
1oo.oo
12o.oo
14o.oo
16o.oo
TIME SECOND

Fig.9.45

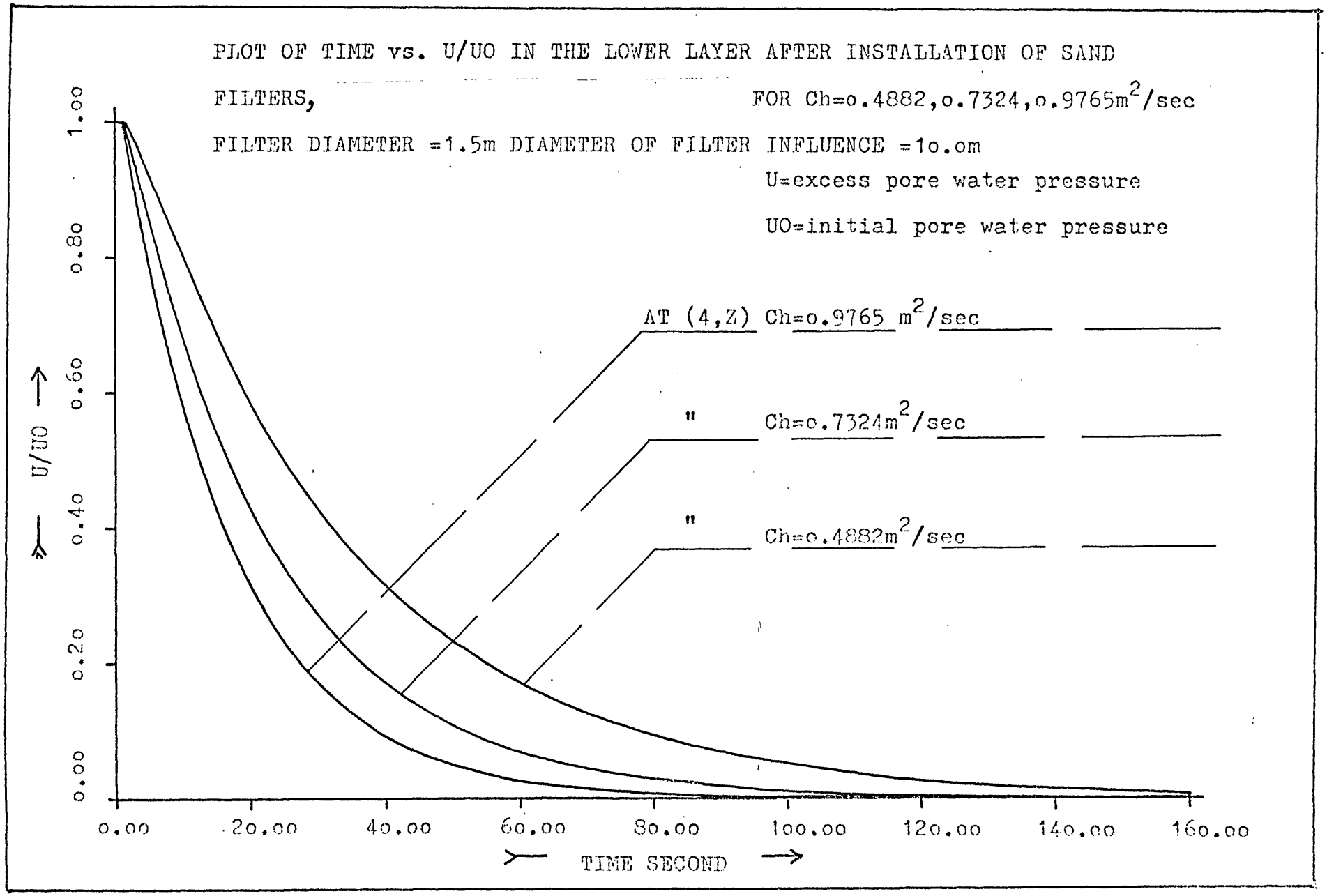

PLOT OF TIME vs. U/UO IN THE LOWER LAYER AFTER INSTALLATION OF SAND FILTERS,
FOR Ch=o.4882,o.7324,o.9765m²/sec
FILTER DIAMETER =1.5m DIAMETER OF FILTER INFLUENCE =1o.om
U=excess pore water pressure
UO=initial pore water pressure
AT (4,Z) Ch=o.9765 m²/sec
" Ch=o.7324m²/sec
" Ch=o.4882m²/sec
U/UO
TIME SECOND
0.00
0.20
0.40
0.60
0.80
1.00
0.00
20.00
40.00
60.00
80.00
100.00
120.00
140.00
160.00

Fig. 9.46

recommended for the installation of vertical sand filters.

a) Estimation of bedrock motion at a given site.

b) Determination of soil and bedrock properties.

c) Calculation of maximum displacement on top of the lower layer, using the computer program named "EARTHQUAKE". (given in chapter 5).

d) Based on this result, determine size of diameter of sand filters, allowing for smearing.

e) Use "FILTER" and calculate dissipation rates of excess pore water pressure at different coordinates in the upper and lower layers over a post earthquake period of time; for different spacings of sand filters, choose the spacing which gives the maximum dissipation over a minimum period of time. (It is more economical to install more filters with required diameters than a few with very large diameters).

*f) Estimate post earthquake initial excess pore water pressure in the two layer system.

*g) Design the graded filter and outlet blanket.

*h) Do foundation stability analysis. (During earthquake).

9.14.1. CASE STUDY

9.14.1.1. EFFECT OF INSTALLATION OF VERTICAL SAND FILTERS AT NIGATA SITE

The aim of this analysis is to investigate the effect of installation of vertical sand filters on post earthquake excess pore water

---

* Outside the scope of this study.

dissipation at Nigata site following 1964 Nigata earthquake.

The site analysed consisted of 30m of medium sand underlain by an impermeable base having a weak layer located 6m below ground surface, possessing uniform soil properties throughout with C_v = 0.4882 m^2/sec , $C_h = 2C_v$, which are typical values for medium sand. A minor difference between this site and Nigata site exists,i.e. here the ground water was assumed to be at the surface, whereas at Nigata site it was located 1.5 - 2.0m below ground surface.

Filters were assumed to have been constructed in a triangular pattern, with full penetration through the depth of the two layers. Further, it was assumed that steps (a) to (d) in section 9.14 gave filter diameter of 1.5m.

"FILTER" was run with diameter of filter influence of 10m. The dissipation of excess pore water pressure at a critical point (4,5) in the upper layer and throughout the lower layer a distance of 4m from filter axis over a post earthquake period of 160 seconds was calculated.

"PORE PRESSURE" was run and the dissipation rate of excess pore water pressure over the same period of time before installation of sand filters was calculated. The results are shown in figs. 9.43 and 9.46.

These results, which have been discussed extensively throughout this chapter, clearly indicate that instability would not have developed at Nigata site following magnitude 7.5 earthquake of 1964 if the developed remedial measure had been adopted. The excess pore water pressure developed by the earthquake at Nigata site would have dissipated very rapidly, thus creating a stabilization process and preventing

development of instability.

9.15. CONCLUDING REMARKS

The following conclusions can be drawn from this study:

a) Installation of vertical sand filters has a considerable beneficial effect on dissipation time of excess pore water pressure.

b) The dissipation time of excess pore water pressure for radial flow is directly proportional to (radius of filter/radius of filter influence)^2.

c) An increase in the coefficient of consolidation in horizontal direction increases the dissipation rate of excess pore water pressure.

d) No instability would have developed at Nigata site if the developed remedial measure had been adopted.

CHAPTER 10

SUMMARY OF NEW DEVELOPMENTS, MAIN CONCLUSIONS OF PRESENT INVESTIGATION AND SUGGESTIONS FOR FUTURE RESEARCH

10.1. SUMMARY OF NEW DEVELOPMENTS

The major new developments and information that were obtained as a result of this investigation may be summarized as follows:

i) A method for seismic response analysis of semi-infinite soil deposits on deformable bedrock formation is developed. The proposed method offers a substantial advance to the present knowledge.

ii) A computer program was written which provides an effective means of determining seismic response of soil deposits on deformable bedrock.

iii) Thirty-nine examples are given in which the effect of deformability of bedrock formation on computed surface and subsurface response has been investigated. The examples include idealized and real sites and sites where deformability of the bedrock is maximized.

iv) A solid explanation of radiation damping phenomenon and its utilization in design has been given.

v) A new parameter as a measure of severity of ground shaking has been proposed and the influence of bedrock characteristics on this

parameter has been investigated.

vi) The reasons for opposing conclusions having been reached by Laysmer et al and Papastamatiou have been considered.

vii) Ten examples are given in which the influence of ground softness on ground response is investigated.

viii) Ratios of maximum spectral acceleration/maximum ground acceleration, maximum spectral velocity/maximum ground velocity and maximum spectral displacement/maximum ground displacement are shown to be roughly constant.

ix) The influence of duration of bedrock motion on ground response has been investigated. It has been shown that response spectra is weak in reflecting the duration of ground shaking.

x) Comparisons between field recorded and theoretically computed average values of ratio of maximum surface velocity/maximum surface acceleration and computed values of predominant period for deep cohesionless soil conditions have been made.

xi) To show the engineering significance of the proposed method, a detailed design (only the aspects of the problem related to the topic) of a fixed offshore structure has been proposed.

xii) A critical review of all the work which has been published in the last two decades on the subject has been presented.

xiii) A state-of-the-art on the character of bedrock motion is discussed. Based on existing field data, it has been

confirmed that very close to the causative fault during the San Fernando earthquake of 1971 the bedrock maximum acceleration and velocity may have exceeded 200%g and 160cm/sec., respectively. Bedrock attenuation laws in the near-field of the earthquake have been developed.

xiv) A new definition for duration of motion is proposed.

xv) A closed form solution for expressing the rate of pore pressure dissipation after earthquake excitation is developed. The theory could be used in evaluation of effects of pore pressure dissipation on the stability of the saturated sand deposits.

xvi) Closed form solutions for expressing the rate of pore pressure dissipation after earthquake excitation for radial drainage effects towards vertical sand filters as a means of stabilizing potentially unstable deposits and three dimensional drainage associated with foundations of a variety of structures are developed.

Besides the above new developments, independent investigations were carried out on the influence of depth to bedrock, frequency characteristics and amplitude of bedrock motion, etc., on ground response, which could provide useful guidance for the practising engineers. Independent investigations were also carried out on correction of bedrock motions and computation of corresponding response spectra.

10.2. MAIN CONCLUSIONS OF PRESENT INVESTIGATION

From the research reported, the following conclusions can be drawn:

(a) The behaviour of soil deposits during earthquakes is a function of soil properties, bedrock motion, depth to bedrock as well as physical properties of the underlying bedrock formation.

(b) The results illustrate clearly that the deformability of the bedrock formation has an important effect on the seismic response characteristics of the soil deposits. Consequently, the usual assumption that the overburden rests on an infinitely rigid bedrock formation should be discarded.

(c) The influence of bedrock formation on response was studied in terms of radiation damping ratio. It was shown that the radiation damping ratio in most cases influences frequency characteristics and amplitudes of motions. A higher radiation damping ratio was found, in general, to develop a smaller response with completely different frequency characteristics. The frequency characteristics of the motions was found to be unaffected only under the special condition that the fundamental period of the deposit is equal to the predominent period of the bedrock motion (first mode of vibrations dominating the response). Under this condition, the influence of bedrock formation characteristics on computed response is maximized and amplitudes of motions are affected considerably. It was only under this special

condition that equivalence between the radiation and hysteretic damping ratios could be established.

(d) The strength of an earthquake at a given site in terms of total energy, which would be transferred from ground to structures, is highly dependent on the stiffness characteristics of bedrock formation, emphasising the need to determine stiffness characteristics of bedrock formation in planning investigation programs of soil and rock conditions.

(e) The subsurface response of a soil deposit was demonstrated to be highly influenced by stiffness characteristics of bedrock formation. The degree of influence may be less or more than that of surface response. This is strong evidence that critical re-examination and re-appraisal of present day techniques, for prediction of liquifaction potentials of saturated sand deposits and estimation of subsurface response to be used for a variety of engineering purposes, are required.

(f) The maximum values of the accelerations or velocities or response spectrumare often employed in seismic design of structures located at the surface of a soil deposit. Based on the information developed, it is reasonable to conclude that neither amplitude of maximum acceleration nor velocity or acceleration response spectra are suitable parameters for earthquake resistant design of engineering structures. Instead, the use of the new measure of destructiveness of ground motion "S" (strength) o; the whole of the velocity

time history is proposed. "S" is a better measure for the destructiveness of an earthquake motion than the Housner's spectral intensity.

(g) The results of the theoretical studies conducted to determine the influence of ground softness on ground response have led to the conclusion that soft deposits do not necessarily imply that structures on these sites will experience higher inertia forces. The factors controlling damage on soft deposits are length of ground shaking and reduction in moment capacity at joints of the structure due to differential settlements. In most cases (not always), soft soils underlying structures are likely to undergo large displacements during earthquakes; therefore, it is often essential to design these structures for large horizontal displacements.

(h) Due to the fact that both the radiation damping ratio and the fundamental period of the deposit are functions of shear wave velocity of the overburden, this implies that the fundamental period of a soil deposit on deformable bedrock cannot be used directly as a parameter to define the response.

(i) The same site exhibits different surface ground response when different bedrock motions with the same maximum acceleration are used.

(j) From the results of the theoretical studies conducted to determine the influence of duration of bedrock motion on ground response clearly, it may be reasonable to conclude

that the response of a soil deposit is strongly influenced by the duration of bedrock motion. One very important disadvantage of the response spectra is its preclusion of duration of shaking.

(k) From the investigation of amplitude of base motion on ground response, it may be concluded that an increase in the amplitude of base motion increases the computed response values by the same factor, emphasising the fact that response values measured during atomic explosions or small quakes can be applied directly to predict performance during relatively larger quakes, based on the assumption that future bedrock motions would show roughly similar frequency characteristics to those of the past bedrock motions and the soil deposit does not exceed its elastic limit.

(L) The satisfactory agreement between the results predicted by the developed procedure and those computed from data recorded during previous earthquakes is proof that the developed procedure and the computer program written have some validity in Engineering Seismology and provide an effective means of predicting response of soil deposits during earthquakes to any given bedrock motion and material properties of the soil deposit. The proposed method is very economical as regards computational time and size of computers required.

(M) The present study also includes an investigation into the variation of pore pressure with time in deposits of saturated sands after the end of the excitation. It was realized that

it was very important to study this aspect of the problem; it has a great significance in terms of loss of bearing capacity of shallow footings and stability of soil deposits. Instalations of vertical sand filters considerably increases the dissipation rate of excess pore water pressures, thus creating a stabilization process and preventing development of any instability.

(N) It is believed that the research work reported in this thesis has thrown some light on the nature of behaviour of soil deposits on deformable bedrock formation during earthquakes. While considerable simplifying assumptions regarding configuration of deposit, material properties, etc., have been made, it is believed that such studies are invaluable in practical design problems and give food for thought to practising design engineers.

10.3. SUGGESTIONS FOR FUTURE RESEARCH

Lastly, arises the question of suggestions for future research. Future research along the following lines is desirable:

(a) Extension of present work to two-dimensional analysis and comparison of the results with the one-dimensional case.

(b) Instrumentation of selected sites (with different bedrock formation stiffness characteristics) and measurement of bedrock motions and motions at different depths as well as ground surface and correlation of these results with theoretical results.

(c) Further research is also required in determining dynamic material properties of soils, both in laboratory and in the field.

(d) Analytical studies should be continued to predict the extent and type of faulting in future earthquakes, so that simple mathematical models, starting at the source, could be used to calculate bedrock motion at nearby sites.

CHAPTER II

THE RECOMMENDED APPROACH FOR ASSESSMENT OF SEISMIC DESIGN SPECTRA: ACCOUNTING FOR THE LOCAL SITE CONDITIONS

11.1. INTRODUCTION

Assessment of ground motion characteristics of the design earthquake for sites threatened by seismic ground motion is a major issue in dynamic analysis of engineering structures. The El Centro 1940 accelogram has been widely used by earthquake engineers as a seismic design motion for earthquake proof design in many countries where strong ground motion data are not available. Comparison of the latest recorded data in many countries with the El Centro record show considerable differences, both in frequency characteristics and amplitudes of the motion.

The new method of analysis which will be presented in this chapter is based on a combination of approaches two and three discussed in chapter 3 in order to arrive at the bedrock motion. The major new features introduced are:

a) Use of scaling factor to scale the time coordinates of the bedrock motion.

b) Use of maximum bedrock velocity as a criterion for prediction of bedrock motion.

c) Computation of surface motion from the estimated bedrock motions, using the theory developed in chapter 4.

11.2. BASIC INFORMATION

As a first step, the site soil and bedrock conditions must be determined and the potential earthquake magnitude established. Additional information, such as the predominant period of bedrock motion, duration of bedrock shaking and maximum velocity at the bedrock surface, is also necessary.

11.2.1. THE POTENTIAL EARTHQUAKE MAGNITUDE

To start with, the design earthquake magnitude can be determined by the following two methods:

(a) Assuming that during the lifetime of the structure there will be a major event (Say M = 6.5) in the area.

(b) Use of past experience, i.e. a thorough review of both the seismicity and the geology of the area.

Approach (b) is very important but not enough. Gaps during the observation period are often the reason for such maps to cause seismological surprises. Therefore, potentiality of the future earthquake must be taken into account.

11.2.2. PREDOMINANT PERIOD OF THE BEDROCK MOTION

Predominant periods of the bedrock motions, using data from stations on or near granitic rock, are related to Magnitude by Gutenberg and Richter[25] by the equation:

$$\log T_{pb} = -1.1 + 0.1M \qquad (11.1)$$

where M is Richter magnitude and T_{pb} is predominant period of the bedrock. (11.1) is only valid for epicentral distances $\lesssim$ 50km.

The assessment of the predominant period of the bedrock motion may be carried out with the aid of Gutenburg-Richter formula, supplimented by data from small earthquakes or strong explosions. The results obtained from strong explosions, though not very good, will provide some idea.

11.2.3. PREDICTION OF MAXIMUM BEDROCK VELOCITY

The next stage of the method requires the estimation of maximum bedrock velocity at the bedrock formation of the proposed site. Amplitude of maximum bedrock velocity is chosen because it is less sensitive to effects, such as fracture propagation, as the fault ruptures.

The assessment of maximum bedrock velocity at a given epicentral distance can be done by means of a local attenuation equation. In the absence of one, the following attenuation equation can be used to describe the variation of expected maximum velocity with earthquake magnitude and epicentral distance:

$$v = 32\, e^{M}/(R + 25)^{1.7} \qquad (11.2)$$

where v is the maximum velocity in cm/sec. on hard ground or weathered rock, M is the Richter magnitude of the earthquake and R is the epicentral distance in kilometres (on the basis of the American events)[40]. The values obtained for v for a given M and R should be checked against other similar formulae; attenuation of peak velocity is not only highly dependent on the area, but also on the location of the proposed site w.r.t. the epicentre of potential earthquake. The two points A and B shown in fig.11.1, although possessing the same epicentral distance,

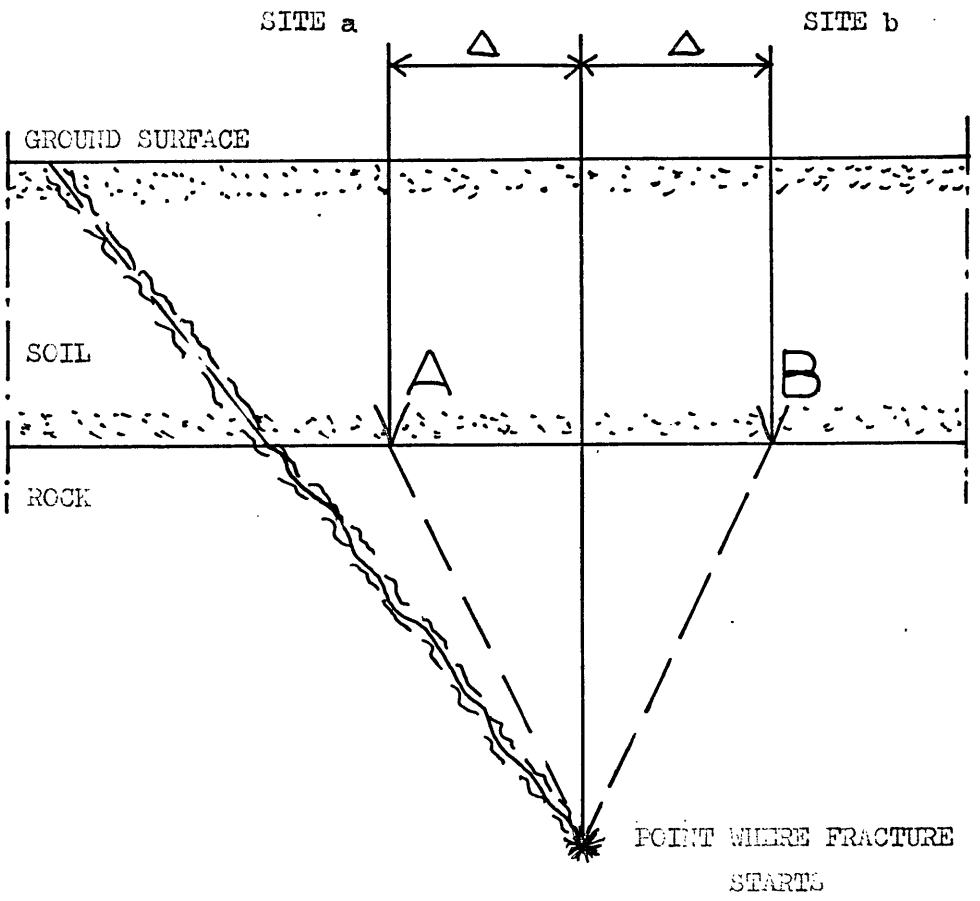


FIG. 11.1 LOCATION OF PROPOSED SITE W.R.T. THE EPICENTRE OF POTENTIAL EARTHQUAKE.

will have different arrival patterns, therefore - different motions.

11.2.4. ASSESSMENT OF DURATION OF BEDROCK MOTION

Finally, calculate the duration of bedrock motion for the design earthquake using equation in section 3.2.1.

11.3 METHOD OF ANALYSIS

The general method of analysis for assessment of the surface motion characteristics involves the following four steps:

(a) Choose a number of existing strong motion records with different frequency characteristics. Try to include records made under similar conditions to yours, if possible.

(b) Multiply the time and acceleration coordinates of the chosen records by the following factors, respectively:

$$t_f \qquad (11.3)$$

$$A_f \qquad (11.4)$$

where t_f is the time factor by which the time coordinate of the chosen accelerogram should be multiplied to give the new required predominant period. t_f is obtained by computer runs using "SPECTRA" given in section 3.1.3. Figs. 11.2 and 11.3 present the results of the analysis for Golden Gate S80E adjusted by t_f values of 2 and 3 to give new predominent periods of 0.25 and 0.4 seconds, respectively. The value of A_f is determined from the relation:

$$A_f^* = \frac{2\pi}{T_{pb}} \cdot \frac{V_b}{A_s} \qquad (11.5)$$

---

* This is a first approximation to A_f. Its true value is obtained by trial and error.

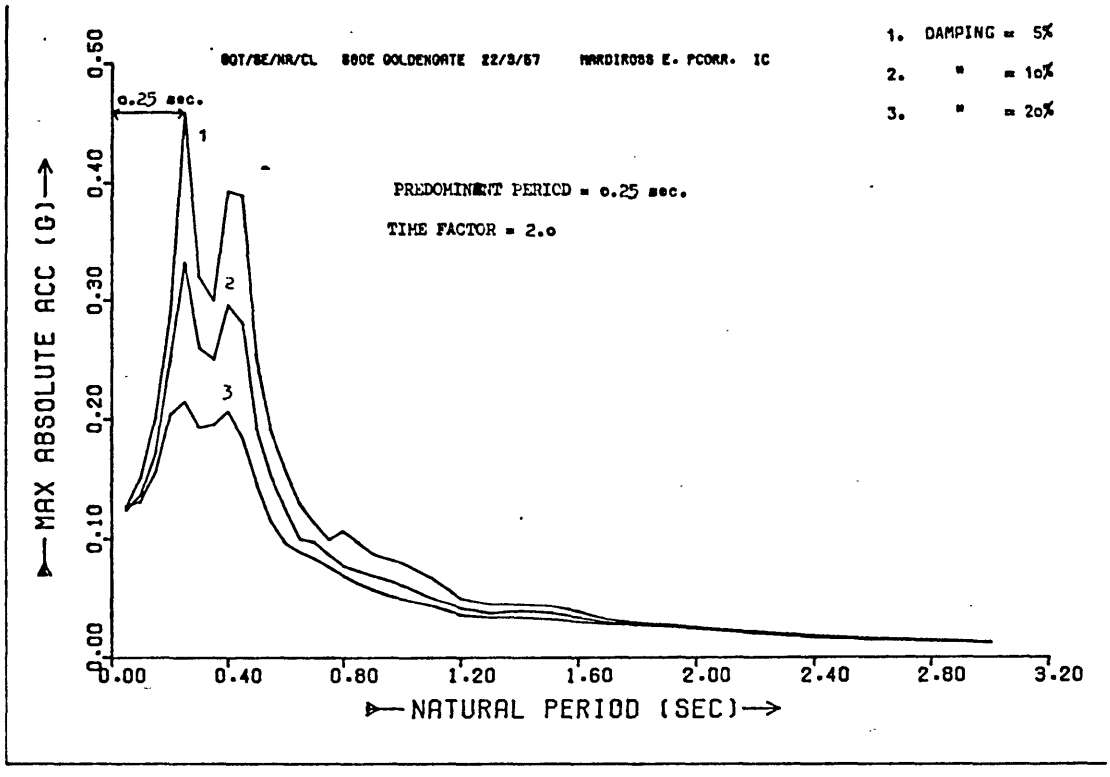


FIG. 11.2 COMPUTED ACCELERATION RESPONSE SPECTRA FOR TIME FACTOR = 2.0

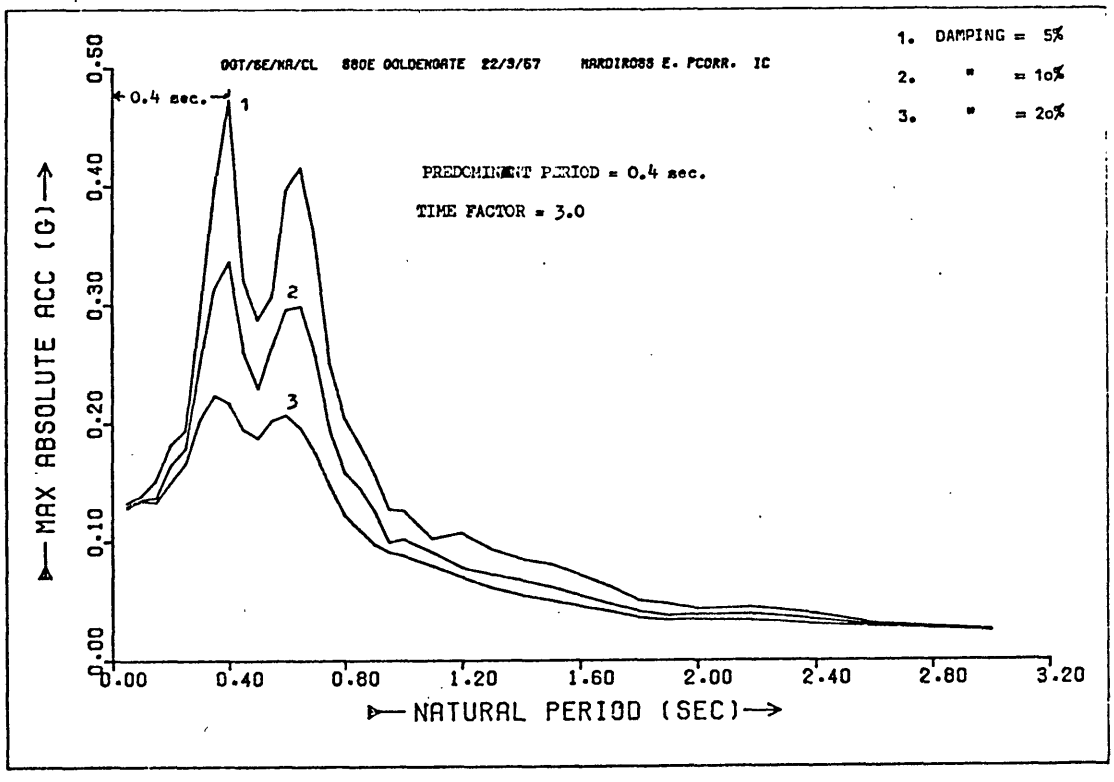


FIG.11.3 COMPUTED ACCELERATION RESPONSE SPECTRA FOR TIME FACTOR = 3.0

where V_b is the maximum estimated bedrock velocity, A_y is the peak acceleration of the chosen accelogram, T_{pb} is the predominant period of the adjusted accelogram.

(c) Adjust the duration of shaking of the strong portion of the records to the value calculated for the design earthquake.

(d) Use the computer program "EARTHQUAKE" to evaluate the effect of local soil conditions upon the bedrock motion, employing the dynamic properties of soil and bedrock.

11.4. DESIGN SPECTRUM OR TIME HISTORIES AND SEISMIC MICROZONING

With the four steps discussed in section 11.3 one can calculate design spectrum. It is important to examine the validity of the proposed method of analysis for a building site in a highly seismic region. It is assumed that an earthquake of magnitude 6.9 is likely to occur at an epicentral distance of 40km. (with a focal depth $\ll$ 20km) from a proposed building site, marked "A" shown in fig. 11.4, underlain by 40m of medium sand with shear wave velocity of 300 m/sec. followed by a very deep formation of shale with shear wave velocity of 800 m/sec. Densities of the medium sand and the shale are 2000 kg/m^3 and 2100 kg/m^3, respectively. Hysteretic damping ratios of the sand was assumed to be 0.02. Calculate the following:

a) Design velocity and acceleration response spectrum or Design time histories.

b) Strength of the potential earthquake motion "S" (see 7.3.1) at the proposed site.

c) Suggest procedures for seismic microzoning of the region.

In the light of the previous discussion regarding the method of

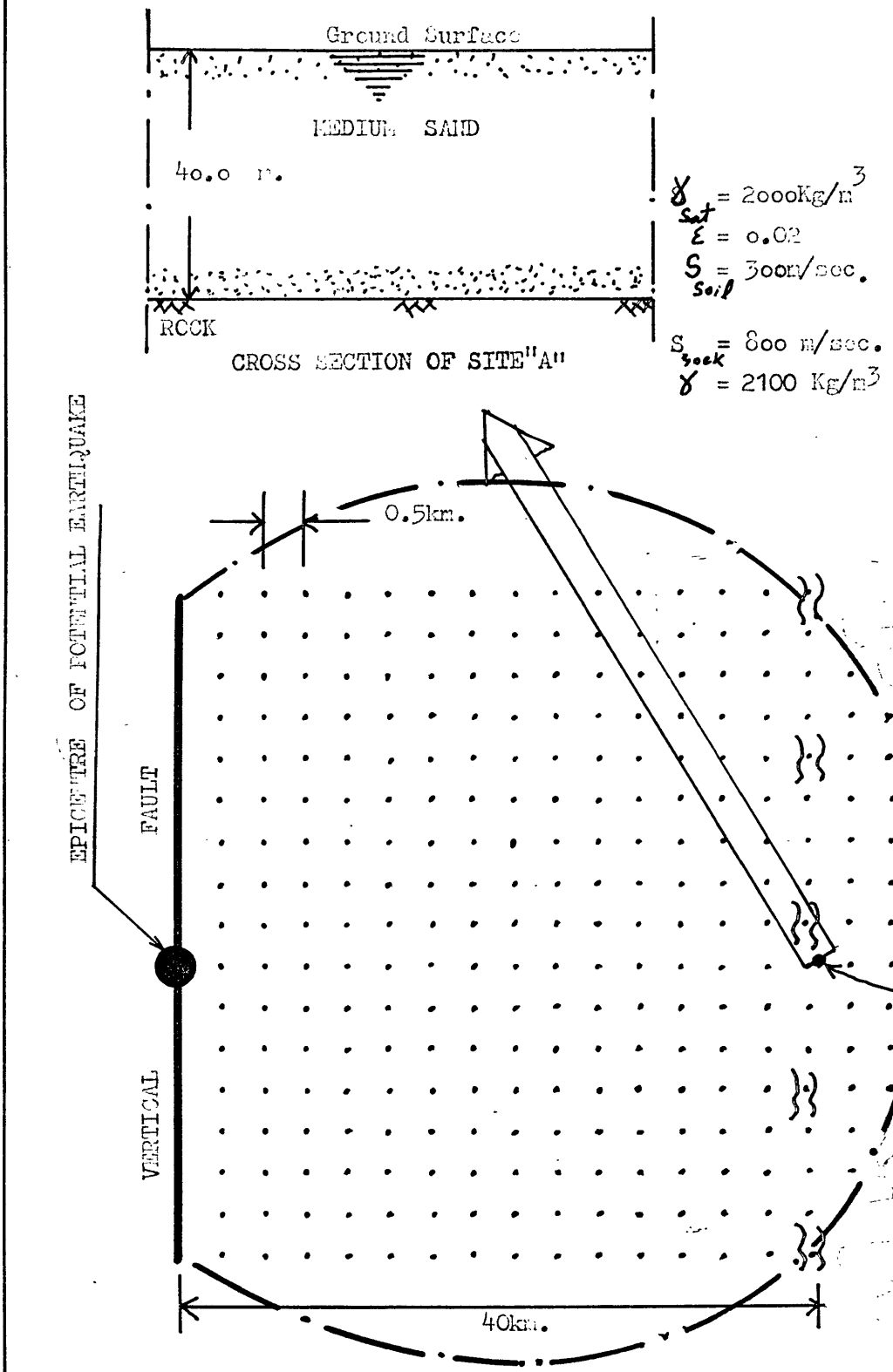


FIG. 11.4 SELECTED AREA FOR SEISMIC MICROZONING

analysis, there are three parameters to be computed. Computed values of these parameters for M = 6.9 and epicentral distance R = 40km. are the design values of maximum bedrock velocity equal to 30 cm/sec., predominant period of bedrock motion equal to 0.4 sec. and duration of bedrock shaking equal to 14.0 sec. The next step in arriving at response spectrum or time histories is to select a number of accelograms from "rock sample" or "hard ground" and adjust these motions by appropriate values calculated from 11.3 and 11.4.

The velocity and acceleration design spectrum and the design time histories for site A, based on two bedrock motions, i.e. Golden Gate S80E and San Fernando S16E* adjusted by t_f = 3.0, A_f = 2.056 and t_f = 1.0, A_f = 0.280 having accounted for the potential changes, which may result from variations in local soil conditions using "EARTHQUAKE", are presented in figs. 15-16 a,b,c,d .Obviously, the more bedrock motions are included the more ground surface spectrum and time histories will be obtained. Therefore, one should design for all the calculated spectrum, in this case too. It is much more meaningful to base the design on the characteristics of the individual spectrum rather than on the characteristics of an overall average.

The computed values of the more useful parameter "S" defined in section 7.3.1, which is a measure of the total energy which would be supplied to structures located at site A, are 890 and 510 $(cm/sec)^2$.

It is important to note that the predicted design parameters given

---

* This accelogram as available in the Dept. of Civil Eng. of Imperial College possess duration of shaking slightly below 14.0 sec.

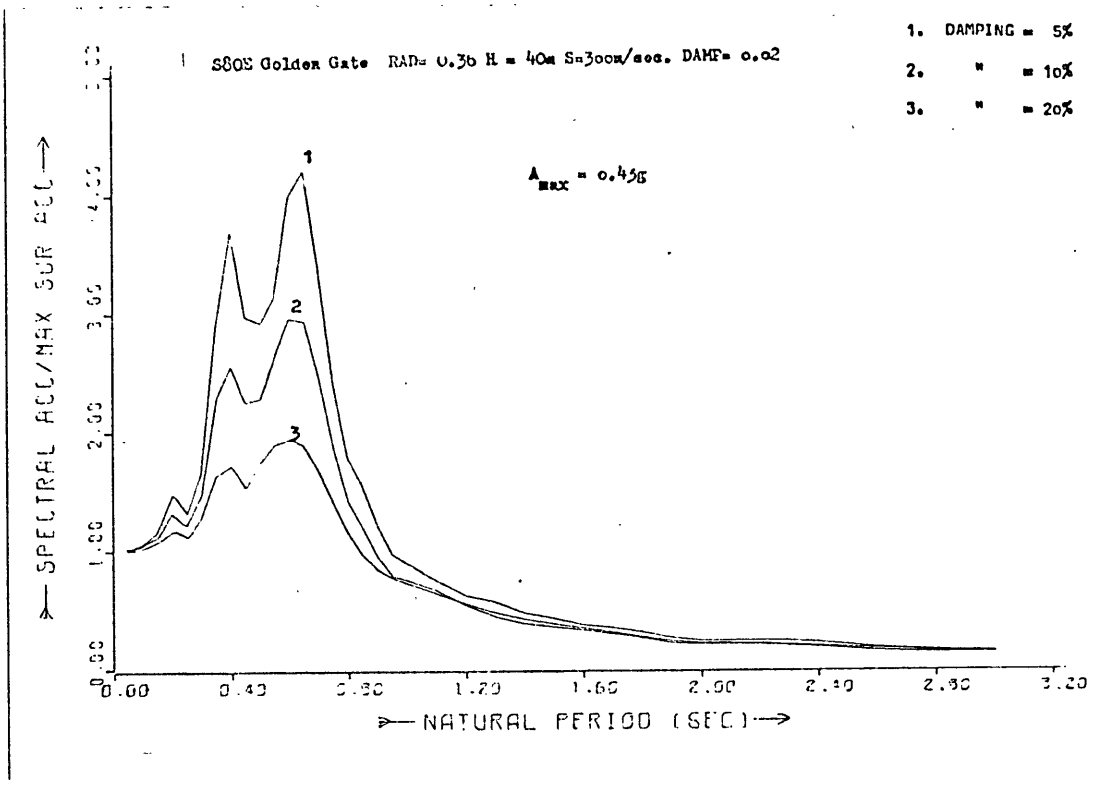


FIG.11.5a COMPUTED GROUND SURFACE ACCELERATION RESPONSE SPECTRA AT SITE A.

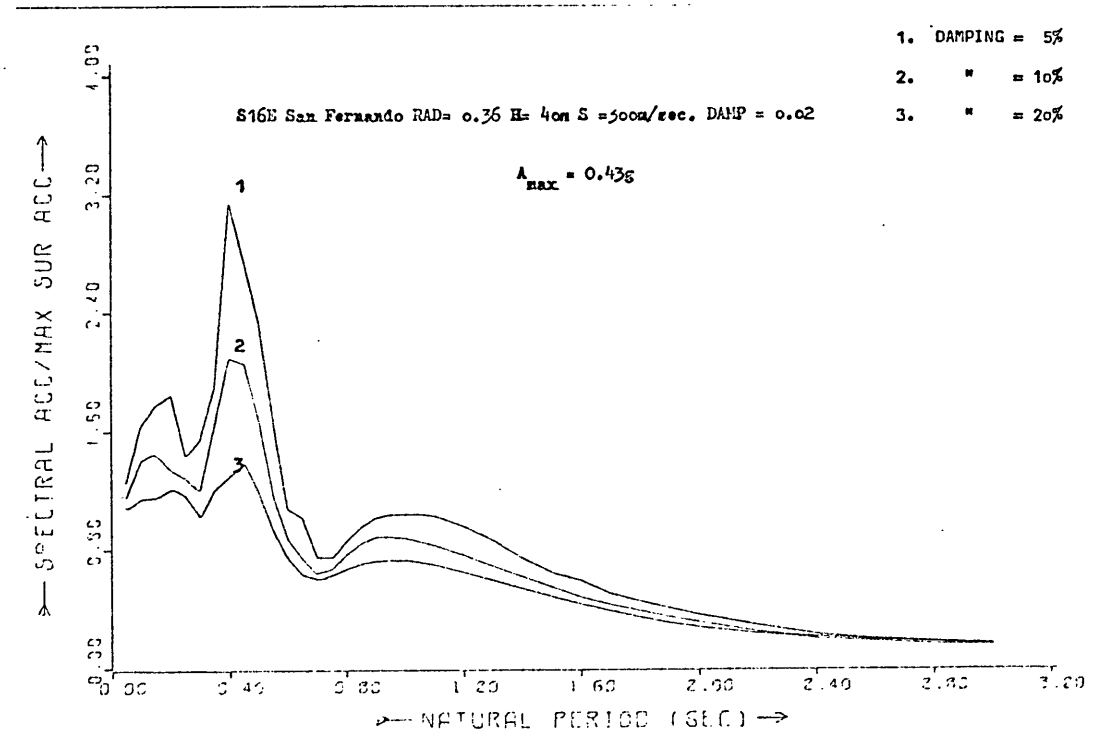


FIG.11.6a COMPUTED GROUND SURFACE ACCELERATION RESPONSE SPECTRA AT SITE A.

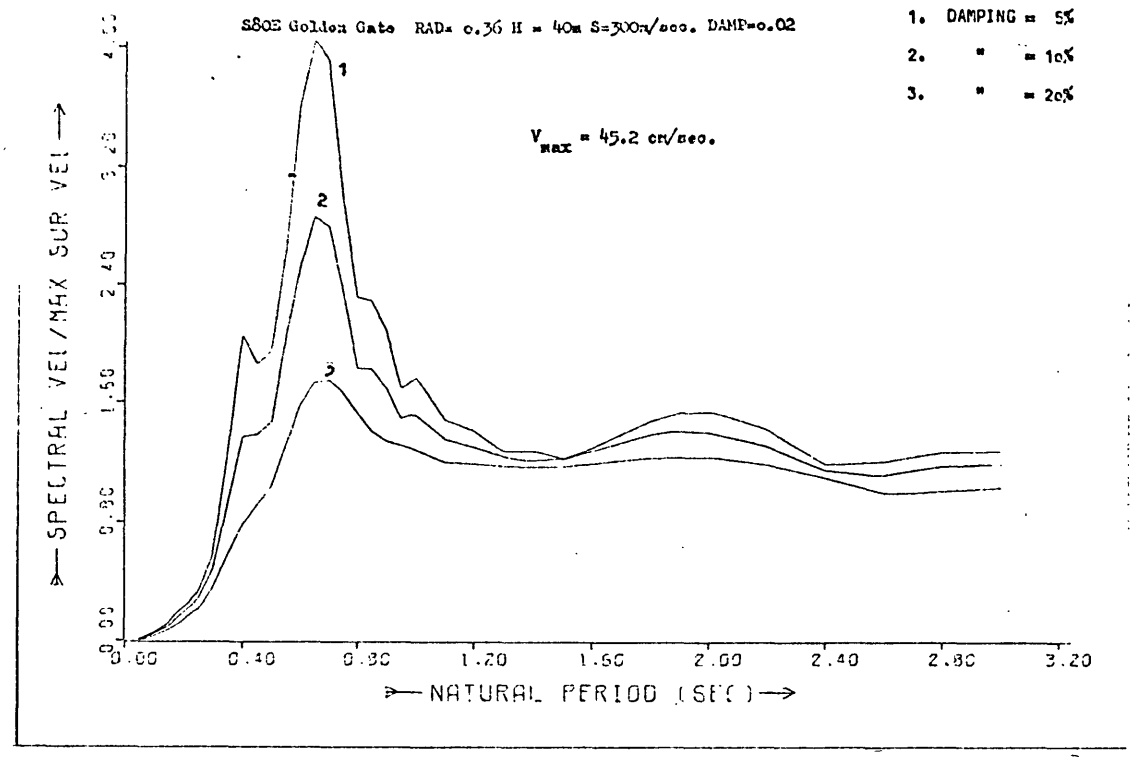


FIG.11.5b COMPUTED GROUND SURFACE VELOCITY RESPONSE SPECTRA AT SITE A.

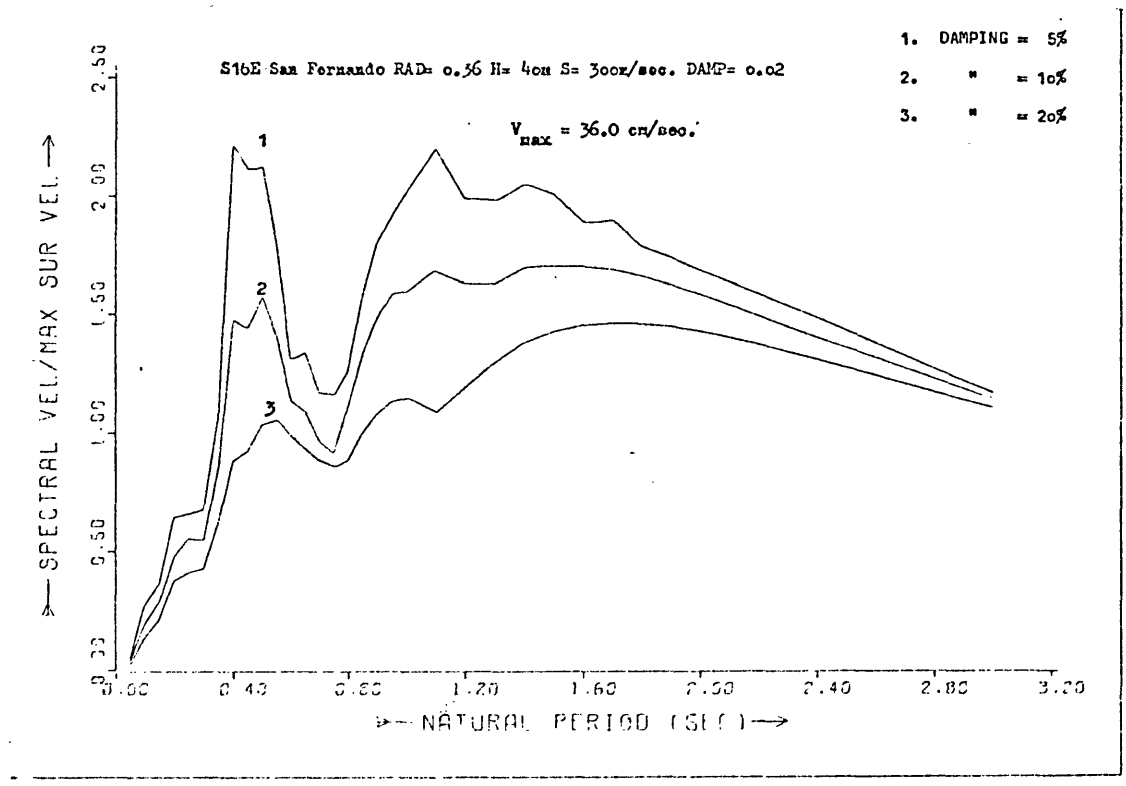


FIG.11.6b COMPUTED GROUND SURFACE VELOCITY RESPONSE SPECTRA AT SITE A.

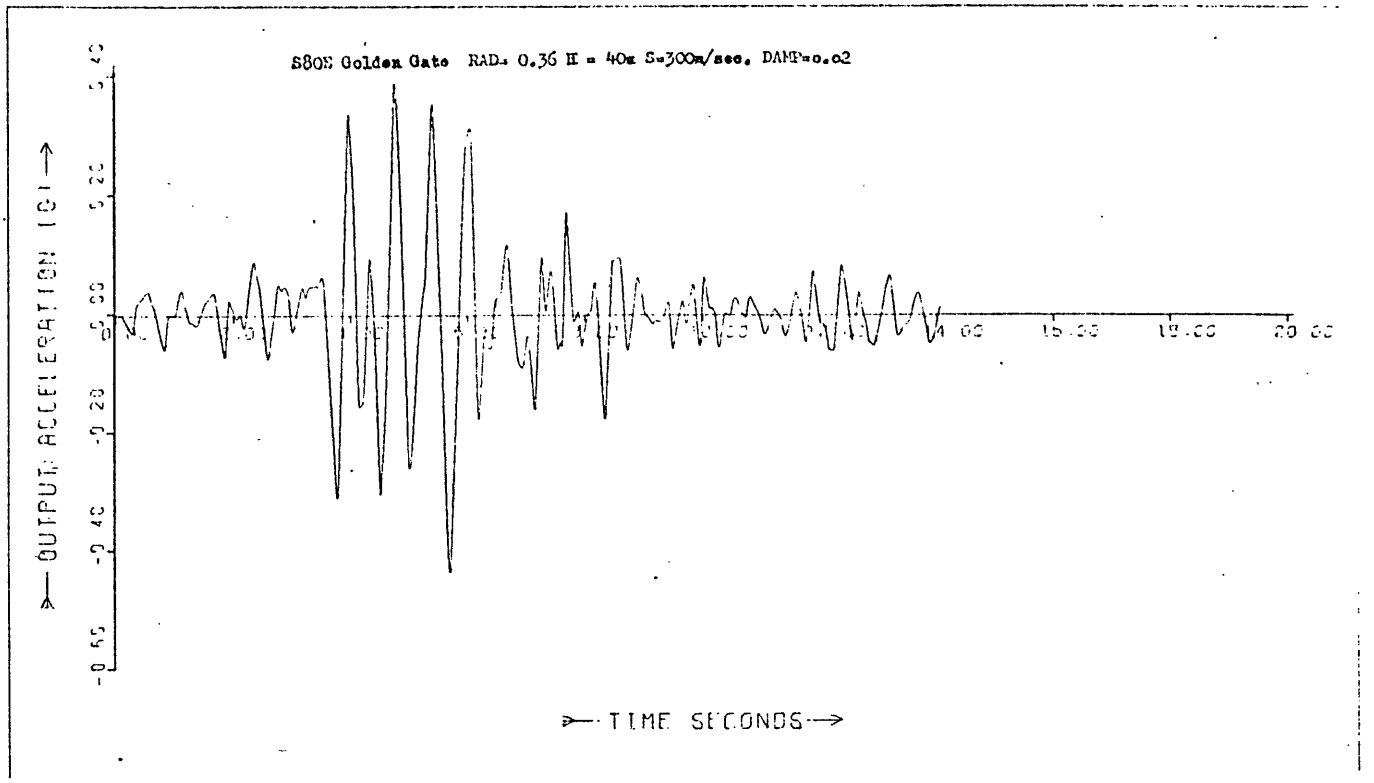


FIG.11.5c COMPUTED GROUND SURFACE ACCELERATION TIME HISTORY AT SITE A.

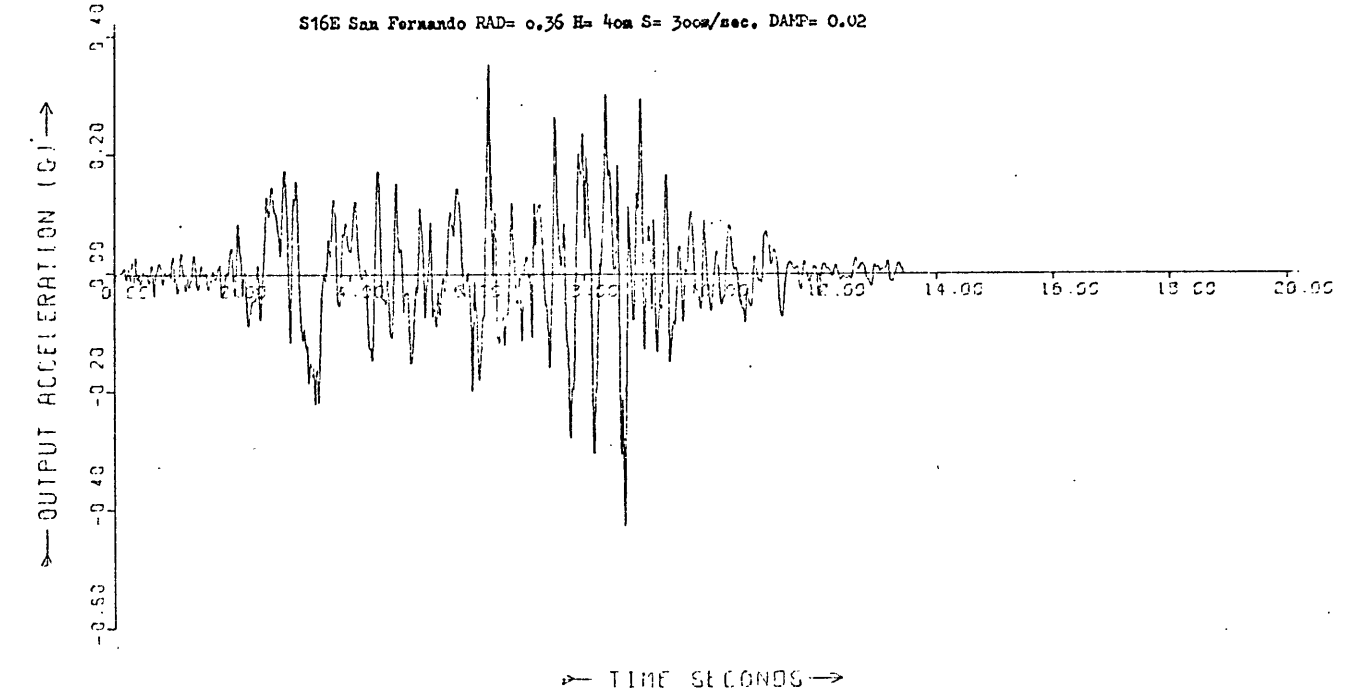


FIG.11.6c COMPUTED GROUND SURFACE ACCELERATION TIME HISTORY AT SITE A.

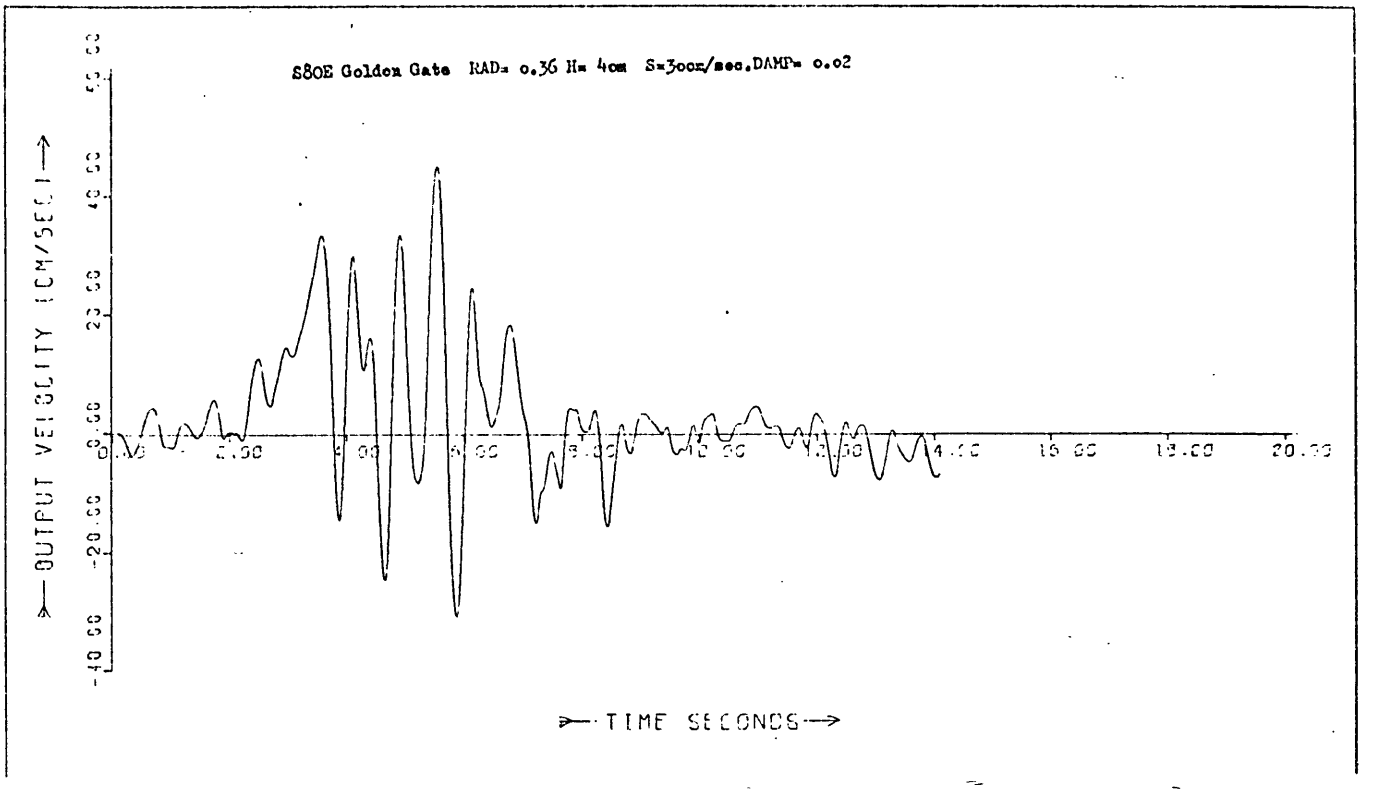


FIG.11.5d COMPUTED GROUND SURFACE VELOCITY TIME HISTORY AT SITE A.

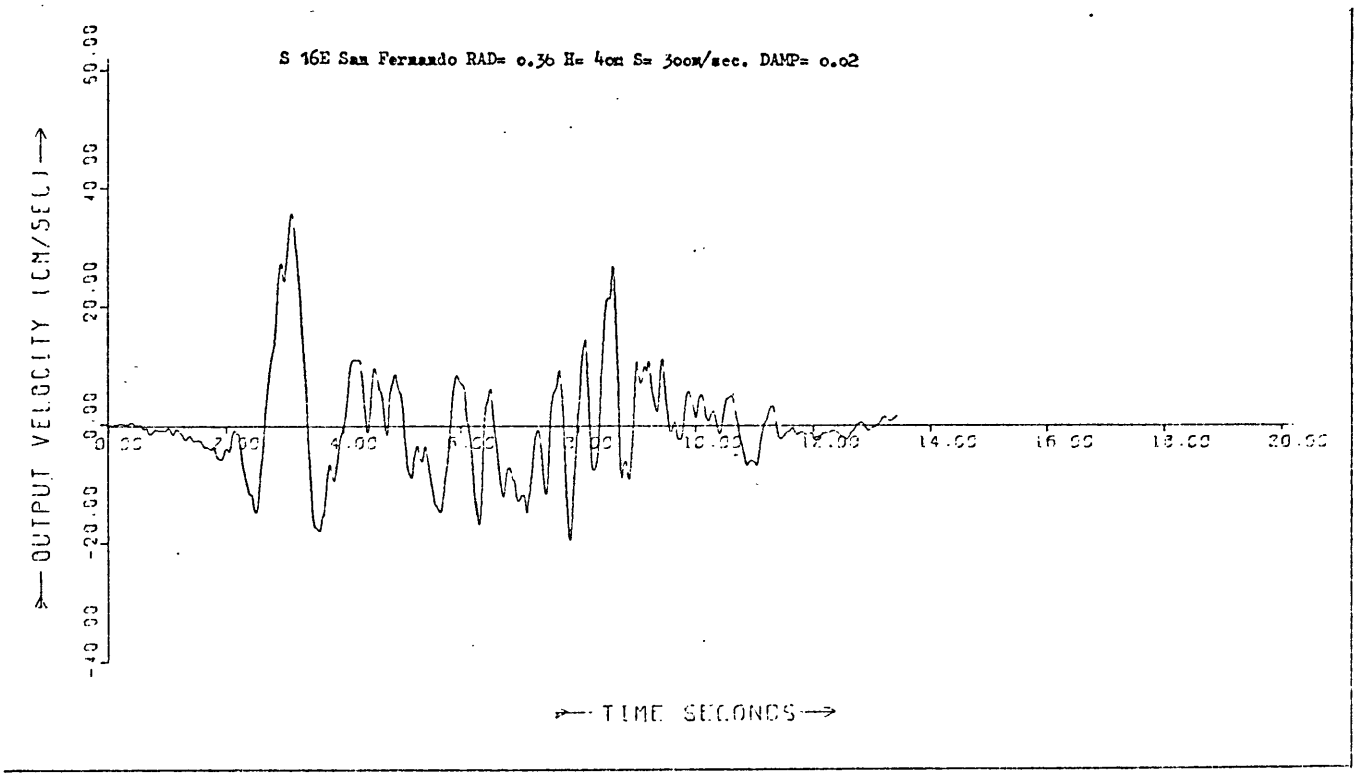


FIG. 11.6d COMPUTED GROUND SURFACE VELOCITY TIME HISTORY AT SITE A.

in this section, as well as the computed acceleration and velocity time histories, could be used for seismic microzonation of the region for several design magnitudes and epicentral or source distances. The capability of the method used for seismic microzonation purposes permits the expected values of the design parameters to be calculated exactly on each grid point shown in fig. 11.4.. Variations in design earthquake magnitude and epicentral or source distance on calculated design parameters could easily be assessed and the errors associated with such variations computed.

11.5. EVALUATION OF EFFECTS OF POST EARTHQUAKE RATES OF PORE PRESSURE DISSIPATION

No seismic microzonation or prediction of design data for earthquake proof design is complete without computing the rates of dissipation of pore pressure in different coordinates of the deposit underlying the proposed building site following the earthquake. For such purposes the analysis presented in chapter 8 may be used. The dissipation rates of these excess pore water pressures, especially at greater depths, could be considerably increased by the installation of vertical sand filters (see chapter 9) at the proposed building site, thus reducing the post earthquake risk of extensive settlement and tilt of the buildings to be constructed at the site.

11.6. CONCLUSIONS

Based on the study reported in this chapter it may be concluded that:

(a) The new method of analysis presented in this chapter provides

a useful means of calculating the design spectrum, the design motion time histories and the strength of the design earthquake at a particular site in many seismic parts of the world where no strong-motion data is available.

(b) The main features of the bedrock motion should not be estimated from Modified Mercalli (MMI), defined in 1931 or Medvedev Sponheuer and Karnik (MSK) defined in 1964, intensity scales. These scales are not only objective scales but are designed for non-specialist designed buildings. Do not consider tall structures, prefabricated structures and long distance effect, etc. Approximate correlations of maximum bedrock velocity, duration of bedrock shaking and predominant period of bedrock motion with MMI or MSK would, therefore, only provide very rough estimates under certain conditions and be completely misleading under others. Instead the approach (a) in section 11.2.1. is proposed.

c) The recommendations made and the new method of analysis presented would result in a considerable amount of savings in the total cost of the proposed projects. In particular, the new method allows a clear demonstration of the importance of taking into account the influence of local soil conditions on potential seismic motions.

APPENDICES

APPENDIX A: EVALUATION OF INPUT DISPLACEMENT 723

APPENDIX B: EVALUATION OF RESPONSE SPECTRA 726

APPENDIX C: EVALUATION OF GOVERNING WAVE EQUATION IN ONE DIMENSIONAL SYSTEM 732

APPENDIX D: TRANSMITTING BOUNDARY CONDITION..... 736

APPENDIX E: THE LEGITIMATE USE OF THE CONVOLUTION THEOREM..... 742

APPENDIX F: CONTOUR OF INTEGRATION 746

APPENDIX G: ROOTS OF THE TRANSCENDENTAL EQUATION GIVEN BY EQUATION 4.3E 749

APPENDIX H: EVALUATION OF INTEGRALS DESCRIBED IN SECTION 4.4.2 754

APPENDIX I: DERIVATION OF BASIC EQUATION GIVEN BY 8.1 761

APPENDIX J: SOLUTION OF DIFFERENTIAL EQUATION GIVEN BY 8.1 767

APPENDIX K: SOLUTION OF DIFFERENTIAL EQUATION GIVEN BY 9.2 772

APPENDIX A

EVALUATION OF INPUT DISPLACEMENT

APPENDIX A

EVALUATION OF INPUT DISPLACEMENT

To obtain bedrock displacements, equation (H .7) was integrated once more.

$$g_o(\tau) = \frac{E_i}{6}(\tau - t_{i-1})^3 + \frac{F_i}{2}(\tau - t_{i-1})^2 + D_i(\tau - t_{i-1}) + G_i \qquad (A.1)$$

where:

from (H .5) $$E_i = \frac{\ddot{g}_{oi}(\tau) - \ddot{g}_{o\,i-1}(\tau)}{t_i - t_{i-1}} \qquad (A.2)$$

from (H.6) $$F_i = \ddot{g}_{o(i-1)}(\tau) \qquad (A.3)$$

from (H.8) $$D_i = \dot{g}_{o(i-1)}(\tau) \qquad (A.4)$$

Imposing initial conditions i.e. at $\tau = t_{i-1}$, $g_o(\tau) = g_{o\,i-1}(\tau)$ on (A.1) we have:

$$G_i = g_{o\,i-1}(\tau) \qquad (A.5)$$

Also $$g_o(\tau)\Big|_{\tau=0} = 0 \quad (IX.6) \quad \& \quad \dot{g}_o(\tau)\Big|_{\tau=0} = 0 \qquad (A.7)$$

Therefore, the record was integrated step by step and ground displacement at any time was calculated.

APPENDIX B

EVALUATION OF RESPONSE SPECTRA

APPENDIX B

EVALUATION OF RESPONSE SPECTRA

This appendix describes the method of evaluation of response spectra, as defined in chapter 6. Equations of motion of the simple oscillator shown in fig B .1 is as follows:

$$M(\ddot{u}(t) + \ddot{g}_o(t)) + c\dot{u}(t) + Ku(t) = 0 \qquad (B.1)$$

notations are defined in fig B .1. Writing (B .1) in the form:

$$\ddot{u}(t) + \frac{C}{M}\dot{u}(t) + \frac{K}{M}u(t) = -\ddot{g}_o(t) \qquad (B.2)$$

calling $\omega_n = \sqrt{\frac{K}{M}}$ (B .3) $\frac{C}{M} = 2 \cdot \xi_n \cdot \omega_n$ (B .4)

(B .2) becomes:

$$\ddot{u}(t) + 2 \cdot \xi_n \cdot \omega_n \cdot \dot{u}(t) + \omega_n^2 u(t) = -\ddot{g}_o(t) \qquad (B.5)$$

Taking Laplace transform of both sides of (B .5)

$$p^2\bar{u}(p) + 2 \cdot \xi_n \cdot \omega_n \cdot p\bar{u}(p) + \omega_n^2\bar{u}(p) = -\overline{\ddot{g}_o}(p) \qquad (B.6)$$

where:

$$\overline{\ddot{g}_o}(p) = \int_o^\infty \ddot{g}_o(t).\ e^{-pt}dt \qquad (B.7)$$

M=Mass

C=viscous damping coefficient

K=spring constant

u(t)=relative displacement of mass M

$g_o(t)$=input displacement

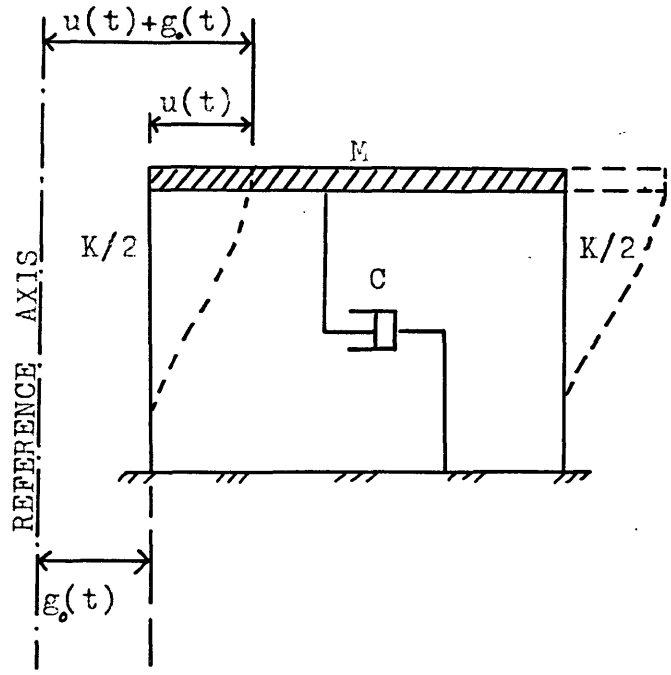


FIG. B .1 SINGLE DEGREE OF DYNAMIC SYSTEM

from (B .6)

$$\bar{u}(p) = -\frac{1}{(p^2 + 2\cdot\xi_n\,\omega_n p + \omega_n^2)} \cdot \bar{\ddot{g}}_o(p) \qquad (\text{B .8})$$

To use convolution integral we call

$$G(t) = \mathcal{L}^{-1}\left[\bar{\ddot{g}}_o(p)\right] = \ddot{g}_o(t) \qquad (\text{B .9})$$

$$F(t) = \mathcal{L}^{-1}\left[-\frac{1}{(p^2 + 2\cdot\xi_n\cdot\omega_n p + \omega_n^2)}\right] \qquad (\text{B .10})$$

From standard Laplace transform tables (B .10) becomes

$$F(t) = -\frac{1}{\omega_n\sqrt{1-\xi_n^2}} \cdot e^{-\xi_n\omega_n t}.\sin\omega_n\sqrt{1-\xi_n^2}\,t \qquad (\text{B .11})$$

But

$$\mathcal{L}^{-1}\left[G(t).F(t)\right] = \int_0^t G(\tau).F(t-\tau)\,d\tau \qquad (\text{B .12})$$

$$\left|u(t)\right|_{max} = \left| -\frac{1}{\omega_n\sqrt{1-\xi_n^2}} \int_o^t \ddot{g}_o(\tau).\ e^{-\xi_n \omega_n (t-\tau)} \sin \omega_n\sqrt{1-\xi_n^2}(t-\tau)d\tau \right|_{max}$$

(B .13)

differentiating (B .13) w.r.t. "t"

$$\left|\dot{u}(t)\right|_{max} = \left| \frac{\xi_n}{\sqrt{1-\xi_n^2}} \int_o^t \ddot{g}_o(\tau).\ -e^{\xi_n \omega_n (t-\tau)} \sin \omega_n\sqrt{1-\xi_n^2}(t-\tau)d\tau - \right.$$

$$\left. - \int_o^t \ddot{g}_o(\tau).\ e^{-\xi_n \omega_n (t-\tau)} \cos \omega_n\sqrt{1-\xi_n^2}(t-\tau)d\tau \right|_{max}$$

(B .14)

differentiating (B .14) once more w.r.t. "t"

$$\left|\ddot{u}(t) + \ddot{g}_o(t)\right|_{max} = \left| \frac{\omega_n(1-2\xi_n^2)}{\sqrt{1-\xi_n^2}} \int_o^t \ddot{g}_o(\tau).\ e^{-\xi_n \omega_n (t-\tau)} \sin \omega_n\sqrt{1-\xi_n^2}(t-\tau)d\tau \right.$$

$$\left. + 2\xi_n \omega_n \int_o^t \ddot{g}_o(\tau).\ -e^{\xi_n \omega_n (t-\tau)} \cos \omega_n\sqrt{1-\xi_n^2}(t-\tau)d\tau \right|_{max}$$

(B .15)

equations (B .13), (B .14) , (B .15) are respectively the displacement velocity and acceleration spectrum values. A plot of these values for various natural periods known as response spectra were made. The computational work was done using Imperial College CDC 6400 computer at ICCC.

APPENDIX C

EVALUATION OF GOVERNING WAVE EQUATION

IN ONE DIMENSIONAL SYSTEM

APPENDIX C

EVALUATION OF GOVERNING WAVE EQUATION

Consider the free vibration of an element of soil, thickness "dy" with unit cross-sectional area at a depth "y" in an elastic layer shown in fig (C.1). Let the ground acceleration at the base of layer be $\ddot{g}_o(t)$. Calling the relative elastic displacement due to shear $u(y,t)$, the shearing force at the depth "y" on the top face of the element is:

$$-G. \frac{\delta u}{\delta y}(y,t) * \overbrace{1*1}^{\text{area}} \qquad (C.1)$$

The shear force on the element a distance "dy" is given by

$$G \left[\frac{\delta^2 u(y,t)}{\delta y^2} dy + \frac{\delta u}{\delta y}(y,t) \right] * \overbrace{1 * 1}^{\text{area}} \qquad (C.2)$$

The inertia force of the elementary volume 1x1xdy is given by

$$\overbrace{\rho * 1 * 1 * dy}^{\text{mass}} \left[\frac{\delta^2 u(y,t)}{\delta t^2} + \ddot{g}_o(t) \right] \qquad (C.3)$$

For equilibrium of the element

$$(C.1) + (C.2) = (C.3)$$

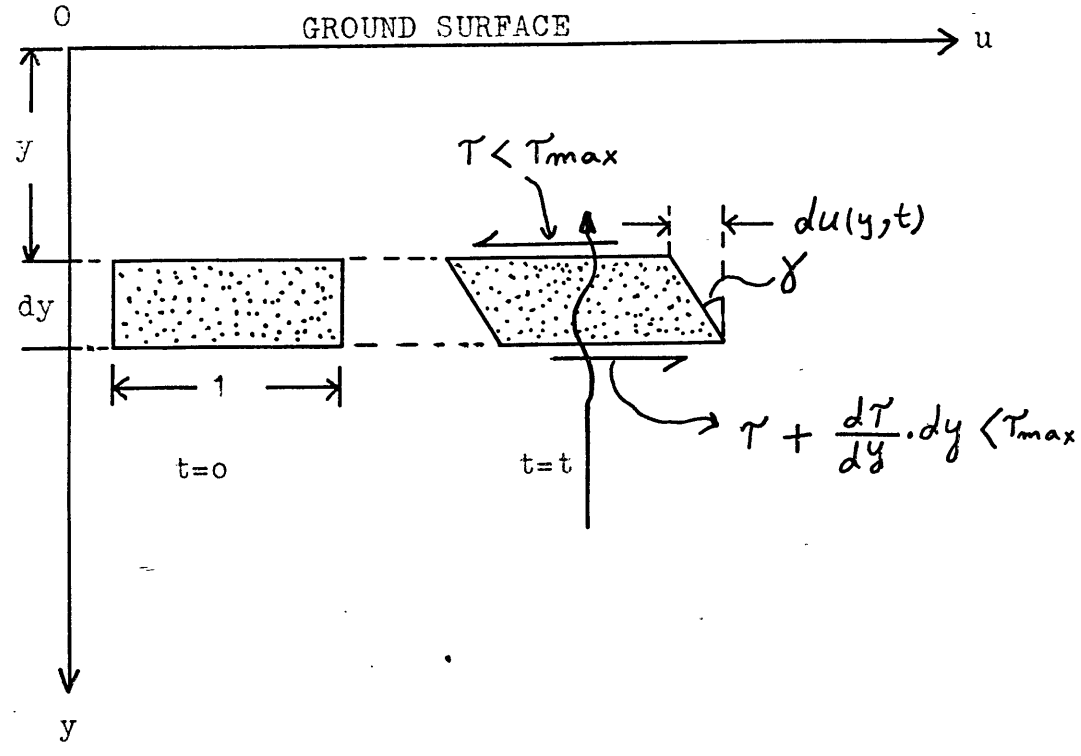


FIG. C.1 SHEAR FORCES ON AN ELEMENTARY VOLUME 1*1*dy LOCATED AT A DEPTH y IN AN ELASTIC LAYER

$$G.\frac{\delta^2 u}{\delta y^2}(y,t) = \rho.\left[\frac{\delta^2 u(y,t)}{\delta t^2} + \ddot{g}_o(t)\right] \qquad (C.4)$$

Calling

$$u_{abs}(y,t) = u(y,t) + g_o(t) \qquad (C.5)$$

Combining (C.5) & (C.6)

$$\rho.\frac{\delta^2 u_{abs}}{\delta t^2}(y,t) = G.\frac{\delta^2 u_{abs}}{\delta y^2}(y,t) \qquad (C.6)$$

Including viscous damping in (C.6) we have

$$\rho.\frac{\delta^2 u_{abs}}{\delta t^2}(y,t) = G.\frac{\delta^2 u_{abs}}{\delta y^2}(y,t) + C1.\frac{\delta^2}{\delta y^2}\left(\frac{\delta u_{abs}}{\delta t}(y,t)\right) \qquad (C.7)$$

where:

ρ = mass density of the layer.

G = shear modulus of the layer.

C1 = coefficient of viscosity in shear of the layer.

$g_o(t)$ = input displacement at the base of the layer.

APPENDIX D

TRANSMITTING BOUNDARY CONDITION

APPENDIX D.

TRANSMITTING BOUNDARY CONDITION

The passage of a shear wave in a small element of soil and rock at the boundary of Fig(D.1) is shown in fig (D.2). Considering an incident wave with unit wave front area, the shear strain at the boundary is given by:

$$\gamma = \frac{du_{abs}}{dy} \qquad (D.1)$$

Equation (D.1) can be written as

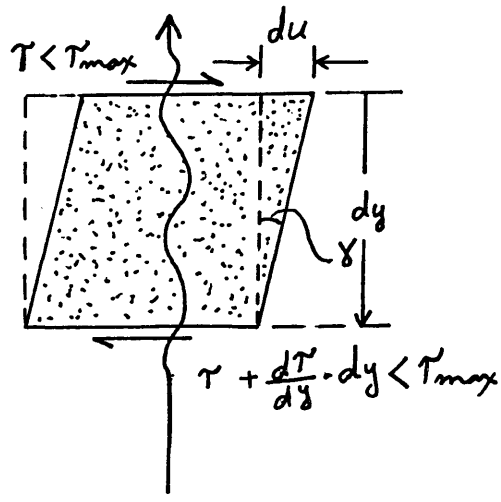
$$\gamma = \frac{du_{abs}}{dt} \times \frac{dt}{dy} \qquad (D.2)$$

$$\frac{du_{abs}}{dt} = \dot{u}_{abs} \text{ (particle velocity)} \qquad (\ .3)$$

$$\frac{dy}{dt} = S \text{ (shear wave velocity)} \qquad (D.4)$$

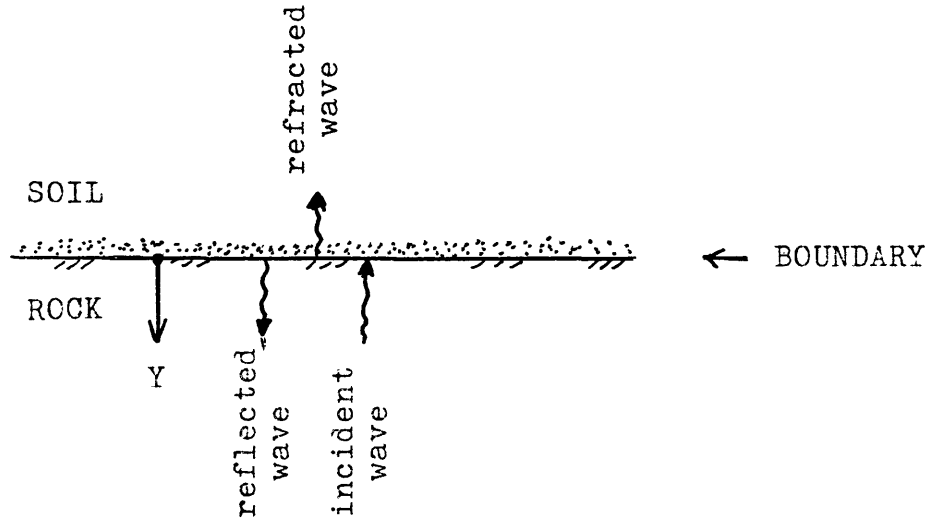
Combining (D.2), (D.3) & (D.4)

$$\gamma = \dot{u}_{abs}/S \qquad (D.5)$$



STRESS INCREMENT CAUSED BY A VERTICALLY TRAVELLING SHEAR WAVE

(a)



(b)

SCHEMATIC DIAGRAM OF OVERBURDUN AND BEDROCK INTERFACE . FOR CLARITY THE PATH OF THE WAVES WAS SLIGHTLY DISPLACED

FIG. D.1

Also stress τ on the element is

$$\tau = \rho . s^2 . \gamma \qquad (D.6)$$

Combining (D .5) & (D .6)

$$\underline{\tau = \rho . s . \dot{u}_{abs}} \qquad (D.7)$$

Let u_{inc} be an arbitrary function in the form

$$u_{\substack{inc \\ abs}} = g_o(t + \frac{y}{s_{rock}}) \qquad (D.8)$$

therefore

$$\frac{d}{dt} u_{\substack{inc \\ abs}} = \dot{u}_{\substack{inc \\ abs}} = \dot{g}_o(t + \frac{y}{s_{rock}}) \qquad (D.9)$$

By continuity of velocity at the boundary

$$\underline{\dot{u}_{\substack{inc \\ abs}} - \dot{u}_{\substack{ref \\ abs}} = \dot{u}_{\substack{trans \\ abs}}} \qquad (D .10)$$

By continuity of stress at the boundary

$$\tau_{inc} + \tau_{ref} = \tau_{trans} \qquad (D.11)$$

Combining (D.7) with (D .11), dividing both sides of resulting equation by $S_{rock} \cdot \rho_{rock}$ and calling $\frac{S_{soil.\ soil}}{S_{rock.\ rock}} = RAD$ (D.12)

equation (D .11) becomes

$$\begin{cases} \overset{\circ}{u}_{\substack{inc \\ abs}} + \overset{\circ}{u}_{\substack{ref \\ abs}} = RAD \cdot \overset{\cdot}{u}_{\substack{trans \\ abs}} & (D.13) \\ \overset{\cdot}{u}_{\substack{inc \\ abs}} - \overset{\circ}{u}_{\substack{ref \\ abs}} = \overset{\circ}{u}_{\substack{trans \\ abs}} & (D.14) \end{cases}$$

Eliminating $u_{\substack{ref \\ abs}}$ in (D.13) & (D .14)

$$\frac{\overset{\cdot}{u}_{\substack{trans \\ abs}}}{\overset{\cdot}{u}_{\substack{inc \\ abs}}} = \frac{2}{(1 + RAD)} \qquad (D.15)$$

Combining (D .8) & (D .15)

$$\hat{u}_{\substack{trans \\ abs}} = \frac{2}{(1 + RAD)} \cdot \hat{g}_o\left(t + \frac{y}{S_{rock}}\right) \qquad (D.16)$$

At the boundary $y = 0$ (D.16) becomes

$$\left(2\hat{g}_o(t) - \hat{u}_{\substack{trans \\ abs}}\right) = RAD \cdot \hat{u}_{\substack{trans \\ abs}} \qquad (D.17)$$

from (D .7)

$$\hat{u}_{\substack{trans \\ abs}} = S_{soil} \cdot du_{\substack{trans \\ abs}} / dy \qquad (D.18)$$

Combining (D .17) & (D .18)

$$\frac{1}{S_{soil}} \cdot \left(2\hat{g}_o(t) - \hat{u}_{\substack{trans \\ abs}}\right) = RAD \cdot \frac{du_{\substack{trans \\ abs}}}{dy} \qquad (D.19)$$

APPENDIX E

THE LEGITIMATE USE OF THE CONVOLUTION THEOREM

APPENDIX E

THE LEGITIMATE USE OF THE CONVOLUTION THEOREM

The legitimate use of the convolution theorem requires the absolute existence of the absolute value of Laplace integrals of the functions G(t) and F(t). Laplace integral of G(t) is the following:

$$\int_0^\infty e^{-pt} G(t)\,dt \qquad (E.1)$$

$$\left| \int_0^\infty e^{-pt}.G(t)\,dt \right| \leqslant \int_0^\infty e^{-\text{Real part of } p.t} |G(t)|\,dt \qquad (E.2)$$

For (E.2) to exist absolutely the following must exist i.e.

$$\int_0^\infty e^{-\text{Real part of } p.t} |G(t)|\,dt \qquad (E.2)a$$

from (5.18) $$G(t) = \dot{g}_0(t) \qquad (E.3)$$

we must show that

$$\int_0^\infty \left| \dot{g}_0(t) \right| \cdot e^{-\text{Real part of } p.t} dt \qquad (E.4)$$

exists.

Calling $$P = \gamma + i p_2 \qquad (E.5)$$

$$\int_0^\infty \left| \dot{g}_0(t) \right| . e^{-\gamma t} dt \qquad (E.6)$$

since $\dot{g}_0(t)$ is a continuous function of t

$$\ll A. \int_0^\infty e^{-\gamma t} dt \qquad (E.7)$$

$$= A/\gamma \qquad \therefore \text{exists absolutely} \qquad (E.8)$$

Since F(t) is bounded, as before it can be shown that

$$\int_0^\infty e^{-(\text{Real part of } P).t} \left| F(t) \right| dt \qquad (E.9)$$

$$= B/\gamma \qquad \therefore \text{exists absolutely.}$$

Therefore, it can be concluded that Laplace integrals of F(t) & G(t) exist absolutely.

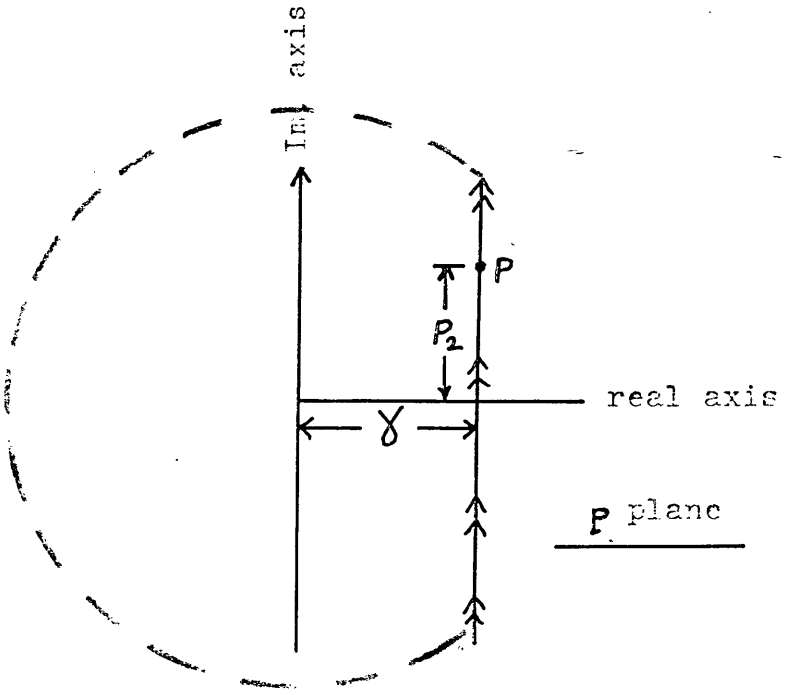
APPENDIX F

CONTOUR OF INTEGRATION

APPENDIX F

CONTOUR OF INTEGRATION

It is the objective of this appendix to show that the contour of integration is in the form given by fig 4.3 i.e. with real part of " P " which is " γ " greater than zero ($\gamma > 0$).



The final solution of (4.19) given by (4.59) is bounded i.e. has a definite value at a given time "t". Therefore, absolute value of Laplace Integral of u(y,t) should exist. Laplace integral of u(y,t) is the following:

$$\int_0^\infty e^{-Pt}\, u(y,t)dt$$

OR

$$\left| \int_0^{\infty} e^{-Pt} u(y,t)dt \right| \leqslant \int_0^{\infty} e^{-\text{Real part of } P \cdot t} |u(y,t)| \, dt \qquad (F.1)$$

For (F .1) to exist absolutely the following must exist i.e.

$$\int_0^{\infty} e^{-\text{Real part of } P \cdot t} |u(y,t)| \, dt \qquad (F.2)$$

$$P = \gamma + i P_2 \qquad (F.3)$$

$$\int_0^{\infty} e^{-\gamma t} |u(y,t)| \, dt \leqslant \beta \int_0^{\infty} e^{-\gamma t} dt \qquad (F.4)$$

where β is a constant.

$$\leqslant \beta \left[-\frac{1}{\gamma} \cdot e^{-\gamma t} \right]_0^{\infty} \qquad (F.5)$$

For (F .5) to exist $\gamma > 0$ i.e. real part of P given by (F .3) should be positive. Therefore, the contour of integration is in the form as shown in this appendix.

APPENDIX G

ROOTS OF THE TRANSCENDENTAL EQUATION GIVEN BY EQUATION 4.38

APPENDIX G

ROOTS OF THE TRANSCENDENTAL EQUATION GIVEN BY EQUATION 4.38

The transcendental equation whose roots are of interest is as follows:

$$\coth RH = -RAD \qquad (G.1)$$

where from (4.32)

$$R = \frac{M}{\sqrt{S^2 + CM}} \qquad (G.2)$$

In terms of exponentials (G.1) becomes:

$$\frac{e^{(\frac{M}{\sqrt{S^2+CM}})H} - e^{-(\frac{M}{\sqrt{S^2+CM}})H}}{e^{(\frac{M}{\sqrt{S^2+CM}})H} + e^{-(\frac{M}{\sqrt{S^2+CM}})H}} = -RAD \qquad (G.3)$$

OR

$$e^{2(\frac{M}{\sqrt{S^2+CM}})H} = -1. \frac{1 - RAD}{1 + RAD} \qquad (G.4)$$

Since $S_{soil} \cdot \rho_{soil}$ is always less than $S_{rock} \cdot \rho_{rock}$ therefore value

of $$RAD = \frac{S_{soil} \cdot \rho_{soil}}{S_{rock} \cdot \rho_{rock}} < 1$$

Equation (G.4) can be written as:

$$e^{2\left(\frac{M}{\sqrt{S^2 + CM}}\right)H} = e^{(-\lambda \Pi \pm 2 \Pi n \lambda)} \cdot \frac{1 - RAD}{1 + RAD} \qquad (G.5)$$

Taking logarithms of both sides

$$\left(\frac{M}{\sqrt{S^2 + CM}}\right)H = -\frac{1}{2}\log_e\left(\frac{1 + RAD}{1 - RAD}\right) \pm \lambda\left(n\Pi \mp \frac{\Pi}{2}\right) \qquad (G.6)$$

calling

$$K = \frac{1}{2}\log_e \frac{1 + RAD}{1 - RAD} \; ; \; a_n = n\Pi - \frac{\Pi}{2} \text{ where } n = 1,2,3,\ldots$$

equation (G.6) becomes:

$$\left(\frac{M_n}{\sqrt{S^2 + CM_n}}\right)H = -K \pm \lambda a_n \qquad (G.7)$$

solving for M_n from (G.7) we obtain

$$M_n = \omega_n(- L_n \pm \lambda F_n) \qquad (G.8)$$

where:

$$L_n = \xi_n + \frac{K}{a_n} E_n - \frac{\xi_n K^2}{a_n^2} - D_n \qquad (G.9)$$

$$F_n = \frac{K}{a_n} D_n + E_n - \frac{2\,\xi_n K}{a_n} \qquad (G.10)$$

$$E_n = \left[\frac{d_n + \sqrt{d_n^2 + f_n^2}}{2}\right]^{\frac{1}{2}} \qquad (G.11)$$

$$D_n = \left[\frac{-d_n + \sqrt{d_n^2 + f_n^2}}{2}\right]^{\frac{1}{2}} \qquad (G.12)$$

$$d_n = 1 - \xi_n^2 + \frac{\xi_n^2 K^2}{a_n} \qquad (G.13)$$

$$f_n = 2\,\frac{\xi_n^2 K}{a_n} \qquad (G.14)$$

$$\xi_n = \frac{C1.\ \omega_n}{2G} \qquad (G.15)$$

$$G = \rho . S^2 \qquad (G.16)$$

$$\omega_n = a_n . \frac{S}{H} \qquad (G.17)$$

notice here ξ_n given by (G.15) is the hysteretic damping ratio. For choosing the correct signs of M_n values, two special cases were solved namely RAD = 0, $\xi_n \neq 0$ and RAD $\neq$ 0, $\xi_n = 0$. The correct signs for M_n values were picked up by comparing the above M_n values with the corresponding M_n values of the two special cases.

APPENDIX H

EVALUATION OF INTEGRALS DESCRIBED IN SECTION 4.4.2

APPENDIX H

EVALUATION OF INTEGRALS DESCRIBED IN SECTION 4.4.2

A new scheme is presented in this appendix for evaluation of the following integrals:

$$S_{dnc}(t) = \int_0^t \dot{g}_o(\tau).e^{-\omega_n \zeta_n (t-\tau)} \cos \omega_n F_n (t-\tau) d\tau \qquad (H.1)$$

$$S_{dns}(t) = \int_0^t \dot{g}_o(\tau).e^{-\omega_n \zeta_n (t-\tau)} \sin \omega_n F_n (t-\tau) d\tau \qquad (H.2)$$

First we evaluate (H.1). Expanding $\cos \omega_n F_n (t-\tau)$ and rearranging (H.1) we have:

$$S_{dnc}(t) = e^{-\omega_n \zeta_n t} \left[\cos \omega_n F_n t \int_0^t \dot{g}_o(\tau).e^{\omega_n \zeta_n \tau}.\cos \omega_n F_n \tau d\tau + \right.$$

$$+ \sin \omega_n F_n t \left[\int_0^t \dot{g}_0(\tau) . e^{\omega_n b_n \tau} \sin \omega_n F_n \tau \, d\tau \right] \qquad (H.3)$$

In a corrected acceleration record the ground acceleration $\ddot{g}_0(\tau)$ in a small interval of time $t_{i-1} \leqslant \tau \leqslant t_i$ is assumed to be a linear function of time given by:

$$\ddot{g}_0(\tau) = E_i (\tau - t_{i-1}) + F_i \qquad (H.4)$$

where

$$E_i = \frac{\ddot{g}_{0i}(\tau) - \ddot{g}_{0\,i-1}(\tau)}{t_i - t_{i-1}} \qquad (\overline{VII}.5) \qquad F_i = \ddot{g}_{0(i-1)}(\tau) \qquad (H.6)$$

are constants for the interval in between t_i & t_{i-1}

Integrating (H.4) we have:

$$\dot{g}_0(\tau) = \frac{E_i}{2} (\tau - t_{i-1})^2 + F_i (\tau - t_{i-1}) + D_i \qquad (H.7)$$

Imposing initial conditions i.e. at $\tau = t_{i-1}$, $\dot{g}_0(\tau) = \dot{g}_{0\,i-1}(\tau)$ on (H.7) we have:

$$D_i = \dot{g}_{0\,i-1}(\tau) \qquad (H.8)$$

combining (H .3) and (H .7)

$$\int_0^t \dot{g}_o(\tau).e^{\omega_n \zeta_n \tau}.\cos\omega_n F_n \tau \, d\tau = \frac{E_i}{2}\int_0^t \tau^2.e^{\omega_n \zeta_n \tau}\cos\omega_n F_n \tau \, d\tau +$$

$$+ (F_i - E_i.t_{i-1})\int_0^t \tau.e^{\omega_n \zeta_n \tau}.\cos\omega_n F_n \tau \, d\tau +$$

$$+ \left(\frac{E_i}{2} t_{i-1}^2 - F_i.t_{i-1} + D_i\right)\int_0^t e^{\omega_n \zeta_n \tau}.\cos\omega_n F_n \tau \, d\tau \quad (H.9)$$

$$\int_0^t \dot{g}_o(\tau).e^{\omega_n \zeta_n \tau}.\sin\omega_n F_n \tau \, d\tau = \frac{E_i}{2}\int_0^t \tau^2.e^{\omega_n \zeta_n \tau}.\sin\omega_n F_n \tau \, d\tau +$$

$$+ (F_i - E_i.t_{i-1})\int_0^t \tau.e^{\omega_n \zeta_n \tau}.\sin\omega_n F_n \tau \, d\tau +$$

$$+ \left(\frac{E_i}{2} t_{i-1}^2 - F_i\, t_{i-1} + D_i\right)\int_0^t e^{\omega_n \zeta_n \tau}.\sin\omega_n F_n \tau \, d\tau \quad (H.10)$$

calling $a = \omega_n \zeta_n$ (H.11) $b = \omega_n F_n$ (H.12)

where: $a = a_n$ and $b = b_n$

$$\int \tau^2 . e^{a\tau} \sin b\tau \, d\tau = \frac{e^{a\tau}}{a^2 + b^2} \left\{ \left[a\tau^2 - \frac{2(a^2-b^2)}{a^2+b^2}\tau + \frac{2a(a^2-3b^2)}{(a^2 + b^2)^2} \right] \sin b\tau - \right.$$

$$\left. - \left[b\tau^2 - \frac{4ab}{a^2+b^2}\tau + \frac{2b(3a^2-b^2)}{(a^2 + b^2)^2} \right] \cos b\tau \right\} \qquad (H.13)$$

$$\int \tau^2 . e^{a\tau} \cos b\tau \, d\tau = \frac{e^{a\tau}}{a^2 + b^2} \left\{ \left[a\tau^2 - \frac{2(a^2-b^2)}{a^2+b^2}\tau + \frac{2a(a^2-3b^2)}{(a^2 + b^2)^2} \right] \cos b\tau + \right.$$

$$\left. + \left[b\tau^2 - \frac{4ab}{a^2 + b^2}\tau + \frac{2b(3a^2- b^2)}{(a^2+ b^2)^2} \right] \sin b\tau \right\} \qquad (H.14)$$

$$\int \tau . e^{a\tau} . \sin b\tau \, d\tau = \frac{e^{a\tau}}{a^2+ b^2} \left[\left(a\tau - \frac{a^2- b^2}{a^2+ b^2} \right) \sin b\tau - \right.$$

$$\left. -\left(b\tau - \frac{2ab}{a^2+ b^2} \right) \cos b\tau \right] \qquad (H.15)$$

$$\int \tau . e^{a\tau} . \cos b\tau \, d\tau = \frac{e^{a\tau}}{a^2+ b^2} \left[\left(a\tau - \frac{a^2- b^2}{a^2+ b^2} \right) \cos b\tau + \right.$$

$$\left. + \left(b\tau - \frac{2ab}{a^2+ b^2} \right) \sin b\tau \right] \qquad (H.16)$$

$$\int e^{a\tau}.\sin b\tau\, d\tau = \frac{e^{a\tau}(a\sin b\tau - b\cos b\tau)}{a^2 + b^2} \qquad (H .17)$$

$$\int e^{a\tau}.\cos b\tau\, d\tau = \frac{e^{a\tau}(a\cos b\tau + b\sin b\tau)}{a^2 + b^2} \qquad (H .18)$$

Equations (H .9) - (H .18) give the complete solution for $S_{dnc}(t)$ of (H .3) for the interval zero to "t". For the interval "t" to (t + dt) equation (H .3) was rewritten in the following form:

$$S_{dnc}(t + dt) =$$

$$= e^{-a(t+dt)} \left\{ \cos b(t+dt) \left[\int_0^t \dot{g}_o(\tau).e^{a\tau}.\cos b\tau\, d\tau + \int_t^{t+dt} \dot{g}_o(\tau).e^{a\tau}\cos b\tau\, d\tau \right] + \right.$$

$$\left. + \sin b(t+dt) \left[\int_0^t \dot{g}_o(\tau).e^{a\tau}\sin b\tau\, d\tau + \int_t^{t+dt} \dot{g}_o(\tau).e^{a\tau}.\cos b\tau\, d\tau \right] \right\} \qquad (H.19)$$

To evaluate (H .2) $\sin b(t-\tau)$ was expanded and equation (H .2) was written in the following form:

$$S_{dns}(t) = e^{-at} \left[\sin bt \int_0^t \dot{g}_o(\tau).e^{a\tau}\cos b\tau\, d\tau - \right.$$

$$- \cos bt \int_0^t \dot{g}_o(\tau).e^{a\tau}.\sin b\tau \, d\tau \Big] \qquad (H.20)$$

combining (H .9) - (H.18) give the complete solution for $S_{dns}(t)$ of (H ,2) for the interval zero to "t". For the interval "t" to (t + dt) equation (H .20) was rewritten in the following form:

$$S_{dns}(t + dt) =$$

$$= e^{-a(t+dt)} \Bigg\{ \sin b(t+dt) \Bigg[\int_0^t \dot{g}_o(\tau).e^{a\tau}.\cos b\tau \, d\tau + \int_t^{t+dt} \dot{g}_o(\tau).e^{a\tau}.\cos b\tau \, d\tau -$$

$$- \cos b(t+dt) \Bigg[\int_0^t \dot{g}_o(\tau).e^{a\tau}\cos b\tau \, d\tau + \int_t^{t+dt} \dot{g}_o(\tau).e^{a\tau}\cos b\tau \, d\tau \Bigg] \Bigg\} \qquad (H .21)$$

The computational work was done using Imperial College CDC 6400 computer at ICCC.

APPENDIX I

DERIVATION OF BASIC EQUATION GIVEN BY 8.1

APPENDIX I

DERIVATION OF BASIC EQUATION GIVEN BY S.1

Consider an element of sand having dimensions 1x1xdz within a sand deposit located above a weak layer or an impermeable formation of thickness "H", as shown in fig. I.1, through which water is flowing in the z-direction.

The following assumptions are made:

i) After the earthquake, a diffusion process accompanied with volume change in the soil element will be involved.

ii) Darcy's law is valid.

iii) The soil is homogeneous and fully saturated.

iv) The boundaries of the element do not change with time (the process is entirely one-dimensional).

v) The coefficient of permeability (K) and the coefficient of volume compressibility (m_v) remain constant throughout the process.

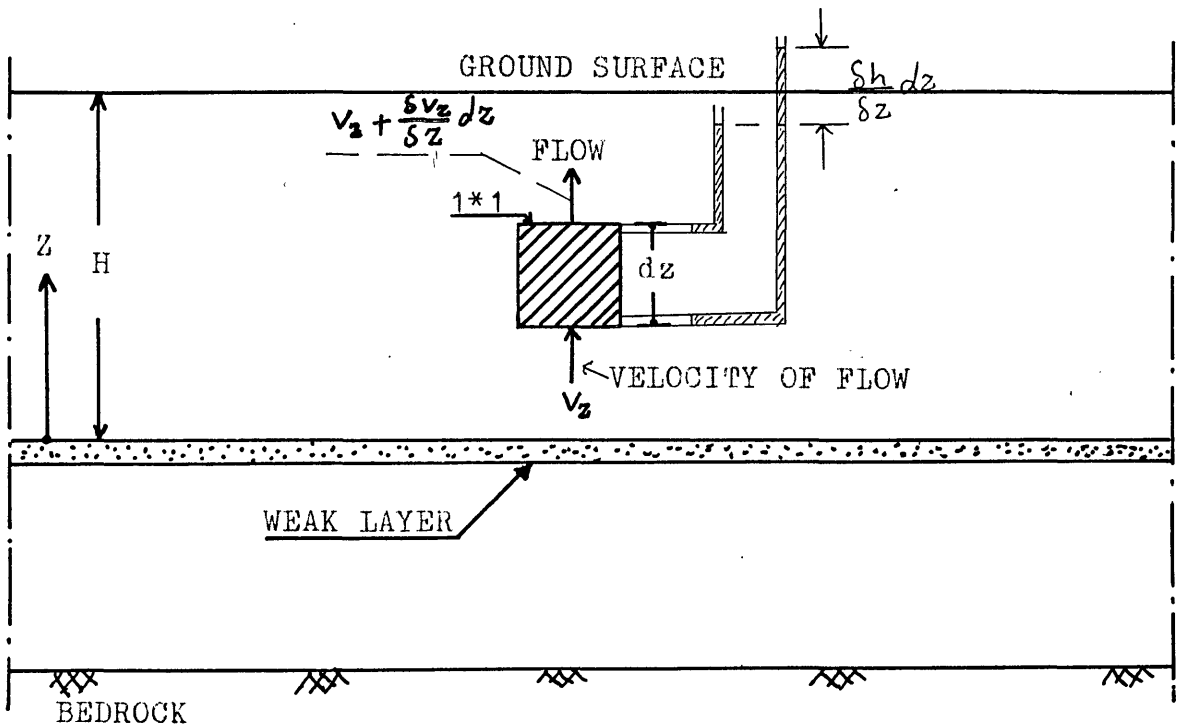
vi) The water and solid particles are incompressible.

vii) A unique and linear relationship between void ratio and effective stress is assumed.

By continuity principle:

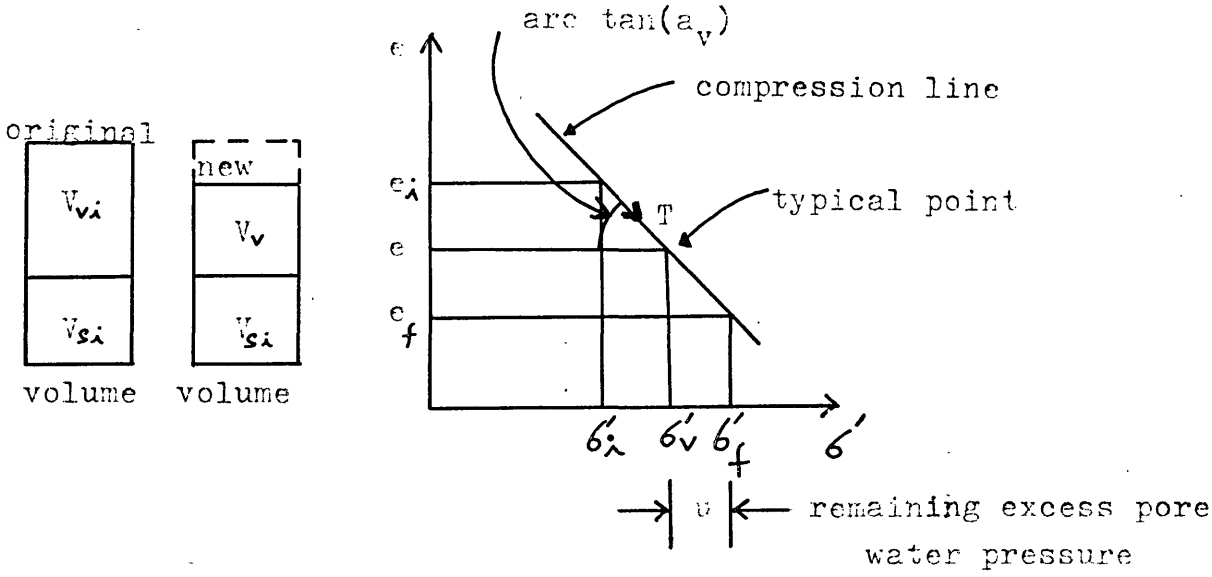
Rate of change of volume = net decrease in quantity

of the element of water in the element



ELEMENT WITHIN A SAND DEPOSIT LOCATED ABOVE A WEAK LAYER

Fig.I.1



calling:

V_{v_i} = volume of voids initially

V_{s_i} = volume of solids initially

V_v = volume of voids at a typical point T

* ε_v = new volume/original volume = $\dfrac{V_v + V_{s_i}}{V_{v_i} + V_{s_i}}$

$$= \frac{1 + e}{1 + e_i} \quad \text{where} \quad e = \frac{V_v}{V_{s_i}} \; ; \quad e_i = \frac{V_{v_i}}{V_{s_i}}$$

e = void ratio at point T

e_i = initial void ratio

From definition * we can write the following:

$$\text{Rate of change of volume of the element} = \frac{d(\text{volume})}{dt} = \begin{pmatrix}\text{original}\\ \text{volume}\\ (1\text{x}1\text{x}dz)\end{pmatrix} \cdot \frac{d\varepsilon_v}{dt}$$

$$= \frac{1}{1 + e_i} \cdot \frac{\delta e}{\delta t} \cdot dz$$

$$= \overbrace{\frac{1}{1 + e_i} \times \frac{\delta e}{\delta \sigma'_v}}^{m_v} \cdot \frac{\delta \sigma'_v}{\delta t} \cdot dz \qquad (I.1)$$

$a_v = -\frac{\delta e}{\delta \sigma'_v}$: coefficient of compressibility

$m_v = \frac{1}{1 + e_i} \cdot a_v$: coefficient of volume compressibility

By the principal of effective stress

$$\sigma'_v = \sigma_v - u \qquad (I.2)$$

where:

σ'_v = effective vertical stress.

σ_v = total vertical stress.

u = excess pore water pressure.

differentiating both sides of (I.2) w.r.t "t"

$$\frac{\delta \sigma'_v}{\delta t} = \frac{\delta \sigma_v}{\delta t} - \frac{\delta u}{\delta t} \qquad (I.3)$$

There is no change in total vertical stress, therefore

$$\frac{\delta \sigma_v}{\delta t} = 0$$

or I.3 can be written as

$$\frac{\delta \sigma'}{\delta t} = - \frac{\delta u}{\delta t} \qquad (I.4)$$

combining (I.1) & (I.4)

Rate of change of volume of the element $= - m_v \cdot \frac{\delta u}{\delta t} \cdot dz$ (I.5)

Net decrease in quantity of water in the element $= \frac{\delta V_z}{\delta z} \times dz \times 1 \times 1$ (I.6)

By Darcy's law

$$V_z = K \cdot i = -K \cdot \frac{\delta h}{\delta z} = - \frac{K}{\gamma_w} \cdot \frac{\delta u}{\delta z} \qquad (I.7)$$

where γ_w = density of water

i = hydraulic gradient

K = coefficient of permeability

V_z = velocity of flow

combining (I.6) & (I.7)

Rate of change of volume of the element $= - \frac{K}{\gamma_w} \cdot \frac{\delta^2 u}{\delta z^2} \cdot dz$ (I.8)

equating (I.8) & (I.5)

$$\frac{\delta u}{\delta t} = \frac{K}{\gamma_w \cdot m_v} \cdot \frac{\delta^2 u}{\delta z^2} \qquad (I.9)$$

where $C_v = \frac{K}{\gamma_w \cdot m_v}$ is called coefficient of consolidation $(L^2 T^{-1})$

Therefore (I.9) becomes

$$\frac{\delta u}{\delta t} = C_v \cdot \frac{\delta^2 u}{\delta z^2}$$

APPENDIX J

SOLUTION OF DIFFERENTIAL EQUATION GIVEN BY 8.1

APPENDIX J

SOLUTION OF DIFFERENTIAL EQUATION GIVEN BY (8.1)

As shown in appendix I, the differential equation governing the distribution of excess hydrostatic pressure in the deposit of sand located above a weak layer or an impermeable formation is governed by:

$$\frac{\delta u(z,t)}{\delta t} = C_v . \frac{\delta^2 u(z,t)}{\delta z^2} \qquad (J.1)$$

The boundary conditions as given in section (8.5.1) are

$$u(z,0) = u_o \qquad \text{at} \quad t = 0 \qquad (J.2)$$

$$u(z,t)\Big|_{z=H} = 0 \qquad (J.3) \qquad \frac{\delta u(z,t)}{\delta z}\Big|_{z=o} = 0 \qquad (J.4)$$

The Laplace transform ofeequation (I.1) is

$$\frac{d^2\bar{u}(z,p)}{dz^2} - \frac{p}{C_v}\,\bar{u}(z,p) = -\frac{u_o}{C_v} \qquad (J.5)$$

where: $\bar{u}(z,p) = \int_o^\infty u(z,t).e^{-pt}dt$ is the Laplace transform of the excess pore water pressure.

The general solution of (J.5) is

$$\bar{u}(z, p) = A \cosh \lambda z + B \sinh \lambda z + \frac{u_o}{p} \qquad (J.6)$$

where $\lambda^2 = \frac{p}{c_v}$, A and B are constants to be evaluated from boundary conditions (J.4) & (J.3)

$$\bar{u}(z, p) = \frac{u_o}{p}\left[1 - \frac{\cosh \lambda z}{\cosh \lambda H}\right] \qquad (J.7)$$

Therefore, by the Inversion Theorem

$$u(z,t) = \frac{u_o}{2\pi i} \int_{\gamma - i\infty}^{\gamma + i\infty} \frac{e^{pt}}{p} \cdot \left[1 - \frac{\cosh(z.(p/c_v)^{\frac{1}{2}})}{\cosh(H.(p/c_v)^{\frac{1}{2}})}\right] dp \qquad (J.8)$$

The integrand of (J.8) is a single-valued* function of p with poles at $p = 0$, and at the roots of $\cosh(H.(p/c_v)^{\frac{1}{2}}) = 0$

---

* Since

$$\frac{\cosh\,(z(p/c_v)^{\frac{1}{2}})}{\cosh(H(p/c_v)^{\frac{1}{2}})} = \frac{1 + \frac{z^2}{2!}.\frac{p}{c_v} + \frac{z^4}{4!}(p/c_v)^2 + \ldots}{1 + \frac{H^2}{2!}.\frac{p}{c_v} + \frac{H^4}{4!}(p/c_v)^2 + \ldots}$$

and this contains only integral powers of p

i.e at the roots of $\cos \lambda (H(P/C_v)^{\frac{1}{2}}) = 0$, whose roots are

$$P = -\frac{\pi^2 . C_v}{4H^2} (2m - 1)^2 \qquad \text{where } m = 1,2,3 \ldots m$$

Evaluating the residue at $P = 0$ we have

$$\left[e^{Pt} . \left[1 - \frac{\cosh (z.(P/C_v)^{\frac{1}{2}})}{\cosh(H.(P/C_v)^{\frac{1}{2}})} \right] \right]_{P=o} = 0 \qquad (J.9)$$

The residue at $P = -\frac{\pi^2 . C_v}{4H^2} (2m - 1)^2$ are found from

$$\left[\frac{-e^{Pt} . \cosh(z.(P/C_v)^{\frac{1}{2}}}{P . \frac{d}{dP}\left[\cosh(H(P/C_v)^{\frac{1}{2}})\right]} \right] P = -\frac{\pi^2 . C_v}{4H^2} (2m-1)^2 \qquad (J.10)$$

we find that the denominator of the above expression becomes

$$\left[P \frac{d}{dP}\left[\cosh(H(P/C_v)^{\frac{1}{2}})\right] \right] P = -\frac{\pi^2 C_v}{4H^2} (2m-1)^2 = -\frac{\pi}{4} . (2m-1) \sin\left(\frac{2m-1}{2}\right)\pi \qquad (J.11)$$

The final solution, which equals the sum of all the residues, can now

be written as:

$$u(z,t) = \frac{4u_o}{\Pi} \sum_{m=1}^{\infty} \frac{(-1)^{m+1}}{(2m-1)} .(\cos \frac{(2m-1)\Pi}{2H} z). \exp(-C_v \frac{(2m-1)^2}{4H^2}.\Pi^2.t) \qquad (J.12)$$

A few remarks on this solution seem appropriate:

i) It is noticed that the above solution satisfies boundary conditions given by (J.3) & (J .4)

ii) Boundary condition (J.1) was tested numerically by taking 40 terms in the series and calculating the ratio of $\frac{u}{u_o}(z,t)$ at t=0 for the site given by fig 8.1D. A value very close to one was obtained.

iii) The above solution gave slow convergence in the neighbourhood of very small values of "t". The series has, therefore, been evaluated with 40 terms for all the results given in section 8.8 - 8.10.

iv) The solution gives a realistic picture of physical realities.

APPENDIX K

SOLUTION OF DIFFERENTIAL EQUATION GIVEN BY 9.2

APPENDIX K

SOLUTION OF DIFFERENTIAL EQUATION GIVEN BY (9.2)

The governing differential equation relating excess pore water pressure, radial position on time is given by

$$\frac{\delta u}{\delta t}(\varsigma,t) = C_h\left(\frac{\delta^2 u}{\delta \varsigma^2}(\varsigma,t) + \frac{1}{\varsigma}\frac{\delta u}{\delta \varsigma}(\varsigma,t)\right) \qquad (K.1)$$

The boundary conditions as given in section (9.7.1.2) are

$$u(\varsigma,0) = u_{oi} \quad \text{at} \quad d < \varsigma < R \qquad (K.2)$$

$$u(\varsigma,t)\Big|_{s=d} = 0 \qquad (K.3) \qquad \frac{\delta u}{\delta \varsigma}(\varsigma,t)\Big|_{\varsigma=R} = 0 \qquad (K.4)$$

The Laplace transform of equation (K.1) is

$$\frac{d^2\bar{u}}{d\varsigma^2}(\varsigma,P) + \frac{1}{\varsigma}\frac{d\bar{u}}{d\varsigma}(\varsigma,P) - \frac{P}{C_h}\bar{u}(\varsigma,P) = -\frac{u_o}{C_h} \qquad (K.5)$$

where: $\bar{u}(\varsigma,P) = \int_0^\infty u(\varsigma,t).e^{-Pt}\,dt$ is the Laplace transform of the excess pore water pressure and $C = C_h$

The general solution of (K .5) is

$$\bar{u}(\varsigma, P) = AI_o((P/C)^{\frac{1}{2}}\varsigma) + BK_o((P/C)^{\frac{1}{2}}\varsigma) + \frac{u_o t}{P} \qquad (K.6)$$

Imposing boundary condition (K .4) i.e. $\frac{\delta \bar{u}(\varsigma, P)}{\delta \varsigma}\Big|_{\varsigma=R}$ and (K .3) i.e. $\bar{u}(\varsigma, P)\Big|_{\varsigma=d} = 0$ on (K .6) and solving for A and B we finally have:

$$\bar{u}(\varsigma, P) = \frac{u_o}{P}\left[1 - \frac{I_o((P/C)^{\frac{1}{2}}\varsigma).K_1((P/C)^{\frac{1}{2}}R) + I_1((P/C)^{\frac{1}{2}}R).K_o((P/C)^{\frac{1}{2}}\varsigma)}{I_o((P/C)^{\frac{1}{2}}d).K_1((P/C)^{\frac{1}{2}}R) + I_1((P/C)^{\frac{1}{2}}R).K_o((P/C)^{\frac{1}{2}}d)}\right] \qquad (K.7)$$

Therefore, by the Inversion theorem

$$u(\varsigma,P) = \frac{u_o t}{2\pi i}\int_{\gamma-i\infty}^{\gamma+i\infty}\frac{e^{Pt}}{P}\left\{1 - \frac{I_o((P/C)^{\frac{1}{2}}\varsigma).K_1((P/C)^{\frac{1}{2}}R)+I_1((P/C)^{\frac{1}{2}}R).K_o((P/C)^{\frac{1}{2}}\varsigma)}{I_o((P/C)^{\frac{1}{2}}d).K_1((P/C)^{\frac{1}{2}}R)+I_1((P/C)^{\frac{1}{2}}R).K_o((P/C)^{\frac{1}{2}}d)}\right\}dP \qquad (K.8)$$

The integrand of (K .8) is a single valued function of P. Since

$I_o(0) = 1$ and $I_1(0) = 0$ and $\lim_{P\to o} \dfrac{K_o((P/C)^{\frac{1}{2}} s)}{K_1((P/C)^{\frac{1}{2}} R)} = 0$ the residue at $P = 0$ is zero. To find the zeros of the denominator put $P = -C\alpha^2$, then it becomes

$$I_o(i\alpha d).K_1(i\alpha R) + I_1(i\alpha R).K_o(i\alpha d) =$$

$$= J_o(d\alpha).\left\{-\tfrac{1}{2}\pi(J_1(R\alpha) - iy_1(R\alpha)\right\} + iJ_1(R\alpha)\left\{-\tfrac{1}{2}\pi i(J_o(d\alpha) - iy_o(d\alpha))\right\} =$$

$$= \frac{\pi}{2}.i.\left\{J_o(d\alpha).y_1(R\alpha) - J_1(R\alpha).y_o(d\alpha)\right\} \qquad (K.9)$$

Let $\alpha_1, \alpha_2, \ldots$ be the roots of the equation (K.10) all are real[1]

$$J_o(d\alpha).y_1(R\alpha) - J_1(R\alpha).y_o(d\alpha) = 0 \qquad (K.10)$$

Then the rest of the poles of the integrand of (K.8) are $P = -C\alpha_1^2$, $-C\alpha_K^2 \ldots -C\alpha_n^2$. For the residue at the pole $P = -C\alpha_K^2$ where $\alpha = \alpha_K$ is a zero of (K.9)

$$\frac{d}{d\alpha}\left[J_o(d\alpha).y_1(R\alpha) - J_1(R\alpha).y_o(d\alpha)\right]_{P=-C\alpha_K^2} =$$

$$= \frac{2}{\pi\alpha_K}\left[\frac{J_o^2(d\alpha_K) - J_1^2(R\alpha_K)}{J_o(d\alpha_K) \cdot J_1(R\alpha_K)}\right]$$

so the residue at the pole $P = -C\alpha_K^2$ is

$$\Pi \times \frac{J_o(d\alpha_K).J_1(R\alpha_K)}{J_1^2(R\alpha_K) - J_o^2(d\alpha_K)} X \left[J_o(\varsigma\alpha_K).y_1(R\alpha_K) - J_1(R\alpha_K).y_o(\varsigma\alpha_K) \right] . e^{-\alpha_K^2 t}$$

with this result the solution becomes

$$u(\varsigma, t) = \Pi . u_{o_L} \sum_{n=1}^{\infty} \frac{J_o(d\alpha_n) . J_1(R\alpha_n)}{J_1^2(R\alpha_n) - J_o^2(d\alpha_n)} X$$

$$X \left[J_o(\varsigma\alpha_n).y_1(R\alpha_n) - J_1(R\alpha_n).y_o(\varsigma\alpha_n) \right] X \exp(-C_h.\alpha_n^2.t)$$

All the symbols are defined in section 9.7.1.3.

A few remarks to this solution seem appropriate:

i) As expected this solution satisfies the boundary condition given by (K .3).

ii) Numerical results given by figs 9.1, 9.20 through 9.22 and 9.44 through 9.46 indicated that boundary condition (K.2) is also satisfied.

iii) The solution gives realistic pictures of physical realities.

iv) Throughout this study it was found that the solution gave very fast convergence, therefore, the series were evaluated using

only 15 terms.

v) Roots of equation (K .10) were found by means of a computer program developed by the author, based on half interval method described by [8]. The first five values obtained from the computer program were checked against the known values given by [1].

REFERENCES

1. Abramowitz, M. and Stegun, I.M., "Handbook of Mathematical Functions", Dover Pub., (1965)

2. Ambraseys, N.N., "The Seismic Stability of Earth Dams," Ph.D. Thesis, University of London, (1958)

3. ---- "Summary Report of Session A-5", Proc. 4th Int. Conf. on Earthquake Engineering, Vol.1, pp. 116-120, (1969)

4. ---- and Sarma, S.K., "Liquifaction of Soil Induced by Earthquake", Bull. Seism. Soc. Am., No.2, pp. 651-664, (1969)

5. ---- "Lectures on Soil Dynamics", presented at Imperial College London, winter term, (1973)

6. ---- "Dynamic and Response of Foundation Materials in Epicentral Regions of strong Earthquakes", Proc. 5th World Conference on Earthquake Engineering, Rome, 1, CXXVI - CXLVIII, (1973)

7. Aramaki, G. and Koga, K., "An Experimental Study of the Characteristics of the Subgrade Reaction in the Poor Subsoil", Preprints of the Sixth World (1976)

8. Arden, B.W. and Astill, K.N., "Numerical Algorithms: and Applications", Addison Wesley Ltd., (1970)

9. Benioff, M.A., "The Physical Evaluation of Seismic Destructiveness", Bull. Seism. Soc. Am., 24, pp.398 - 403, (1934)

10. Bishop, A.W., discussion of Dynamic Compaction "Ground Treatment by Deep Compaction", Institution of Civil Engineers, London, pp.138-140, (1976)

11. Bogdanoff, J.L., Goldberg, J.E. and Bernard, M.C., "Response of a Simple Structure to Random Earthquake-Type Disturbance", Bull. Seismol. Soc. Am., 51, pp.293-310 (1961)

12. Bolt, B.A., "Elastic Waves in the Vicinity of the Earthquake Source", Earthquake Engineering, ed. Weigel, R.L., Prentice Hall, (1970)

13. Chen, T.F. and William, B.J., "Multi-Linear Analysis for Ground Motion Studies of a Layered System", U.S. Geological Survey, California, (1974)

14. Clough, R.W., "Earthquake Analysis by Response Spectrum Superposition", Bull. Seism. Soc. Am., 52, No.3, July, (1962)

15. Clough, R.W. and Penyien, J., "Dynamics of Structures", McGraw-Hill, London, (1975)

16. Costantino, C.J., Miller, C.A. and Lufrano, L.A. "Mesh Size Criteria For Soil Amplification Studies", Transactions of the 3rd International Conf. on Structural Mechanics in Reactor Technology, vol.4, part K, pp.K213, 1-12, (1975)

17. Craig, R.F., "Soil Mechanics", Van Nortrand Reinhold Ltd., (1976)

18. Dobry, R., Idriss, I.M., Chang, C.Y. and Ng, E., "Influence of Magnitude, Site Conditions and Distance on Significant Duration of Earthquakes", preprints of the Sixth World Conf. on Earthquake Eng., New Delhi, Theme 2, paper No,23, (1976)

19. Doelsch, D., "Guide to the Application of the Laplace and Z-Transforms", William Clowes and Sons Ltd., (1971)

20. Dowrick, D.J., "Earthquake Resistant Design", John Wiley and Sons, (1977)

21. Dezfulian, H. and Seed, H.B., "Seismic Response of Soil Deposits Underlain by Sloping Rock Boundaries", Research Report, Geotechnical Eng., University of California, Berkeley, June, (1969)

22. ---- "Response of Nonuniform Soil Deposits to Traveling Seismic Waves", Research Report, Geotechnical Eng., University of California, Berkeley, (1969)

23. Finn, W.D.L., "Dynamics of Soils and Soil Structures", preprints of the Sixth World Conference on Earthquake Eng. New Delhi, Theme Report on Topic 6, (1976)

24. Goldberg, J.E., Bogdanoff, J.L. and Sharpe, D.R., "The Response of Simple Nonlinear System to Random Disturbance of the Earthquake Type", Bull. Seism. Soc. Am., 54, pp.263-276, (1964)

25. Gutenberg, B. and Richter, C., "Earthquake Magnitude, Intensity, Energy and Acceleration", Bull. Seism. Soc. Am., 46, pp.105-146, (1956)

26. Hall, W.J., Newmark, N.M. and Hendron, A.J., "Classification, Engineering Properties and Field Exploration of Soils, Intact Rock and In situ Rock Masses", U.S. Atomic Energy Commission, Washington, (1975)

27. Hardin, B.O. and V.P. Drnevich, "Shear Modulus and Damping in Soils: Measurements and Parameter Effects", Journal of the Geotechnical Engineering Division, ASCE, SM6, pp.603-624, (1972)

28. Heading, J., "Mathematical Methods in Science and Engineering", 2nd. Edition, Edward Arnold Ltd., (1970)

29. Heading, J., "Ordinary Differential Equations", Unwin Brothers Ltd., (1976)

30. Herrera, I. and Rosenblueth, E., "Response Spectra on Stratified Soil", Proc. 3rd. World Conf. on Earthquake Eng., Vol.I, New Zealand, pp.1-41, (1965)

31. Housner, G.W., "Intensity of Ground Motion During Strong Earthquakes", Calif. Inst. of Technology, Earthquake Research Lab., Aug., (1952)

32. ——— "The Mechanism of Sand Blows," Bull. Seism. Soc. Am., 48, No.1, pp.151-161, (1958)

33. Idriss, I.M. and Seed, H.B., "Response of Earth Banks During Earthquakes", Journal of Soil Mechanics and Foundations Division, ASCE 93, No. SM3, May, pp.61-82, (1967)

34. ——— "Seismic Response of Horizontal Soil Layers", Journal of the Soil Mechanics and Foundations Division, ASCE, 94, No. SM4, July, pp.1003-1031, (1968)

35. Imasaki, T., Unpublished test results, Ground Vibration Section, Earthquake Research Institute, Ministry of Construction, Japan, (1976)

36. Kanai, K., "The Effect of Solid Viscosity of Surface Layer on the Earthquake Movements", Bull, Tokyo Univ., Earthquake Research Inst., Vol.28, pp.31-35, (1950)

37. ——— "Relation Between the Nature of Surface Layer and the Amplitude of Earthquake Motion", Part I to IV, Bull., Tokyo Univ., Earthquake Research Inst., (I) vol. 30, pp31-37, (II) vol.31, pp.219-226, (III) vol.31, pp.276-279, (IV) vol.34, pp.167-183, (1952),(1953), (1953) and (1956)

38. Kiefer, J., "Influence of Soil Conditions on Ground Response During Earthquakes", Research Report, University of California, Berkeley, (1968)

39. Kishida, H. , "Characteristics of Liquified Sands During Mino-Omari, Tohnankai and Fukin Earthquakes", Soils and Foundations, vol.9, No.1, (1969)

40. Lominitz, C. and Rosenblueth, E., "Seismic Risk and Engineering Decisions", Elsenier, (1976)

41. Lysmer, J., Seed, H.B. and Schnabel, P.B., "Influence of Base Rock Characteristics on Ground Response", Research Report No. EERC 70-7, University of California, Berkeley, (1970)

42. Mal, A.K. and Duke, C.M., "Transfer Functions For Surface Wave", preprints of the Sixth World Conference on Earthquake Engineering, New Delhi, Theme 6, paper No. 49, (1976)

43. Maslov, N.N., "Questions of Seismic Stability of Submerged Sandy Foundations and Structures", Proc., 4th. Int. Conf. on Soil Mechanics and Foundation Eng., London, England, (1957)

44. Matthiesen, R.B., Duke, C.M., Leeds, D.J. and Frasen, J.C. "Site Characteristics of Southern California Strong-Motion Earthquake Stations", part I & II, Dept. of Eng., Univ. of California, Los Angeles, Calif. Report No.64-15, (1964)

45. Newmark, N. and Rosenblueth, E., "Fundamentals of Earthquake Engineering", Prentice-Hall, (1971)

46. Papastamatiou, D., "Ground Movements and Response of Earth Structures to Strong Earthquakes", Ph.D. thesis, University of London, (1970)

47. Penzien, J., Scheffey, C.F. and Parmelec, R.A. "Seismic Analysis of Bridges on Long Piles", Journal of the Engineering Mechanics Division, ASCE, 90, No. EM3, June, pp.223-254, (1964)

48. Rosset, J.M. and Whitman, R.V., "Theoretical Background for Amplification Studies", M.I.T., Research Report No. R69-15, Dept of Civil Eng., (1969)

49. Savage, J.C., "Radiation from a Realistic Model of Faulting", Bull. of Seism. Soc. of Am. 56 pp.577-592, (1966)

50. Scott, R.F., "Principles of Soil Mechanics", Addison-Wesley Ltd., (1963)

51. Seed, H.B. and Idriss, I.M., "Analysis of Soil Liquifaction, Nigata Earthquake", Journal of Soil Mechanics and Foundations Division, ASCE, 93, pp.93-108, (1967)

52. Seed, H.B., Idriss, I.M. and Kiefer, F.W., "Characteristics of Rock Motions During Earthquakes", Journal of Soil Mechanics and Foundations Division, ASCE, 95, No. SM5, Sept. pp.1199-1218, (1969)

53. Seed, H.B. and Idriss, I.M., "Soil Moduli and Damping Factors for Dynamic Response Analysis", Research Report No. EERC 70-10, University of California, Berkeley, (1970)

54. Seed, H.B., Murarka, R., Lysmer, J. and Idriss, I.M., "Relationships of Maximum Acceleration, Maximum Velocity, Distance From Source, and Local Site Conditions for Moderately Strong Earthquakes", Bull. Seism. Soc. Am. 66, No.4, pp.1323-1342, (1976)

55. Seed, H.B., Martin, P.P. and Lysmer, J., "Pore Water Pressure Change During Soil Liquifaction", Journal of the Geotechnical Engineering Division, ASCE, 102, GT4, pp.323-346, (1976)

56. Seed, H.B., Murarka, R., Lysmer, J. and Idriss, I.M., "Relationship of Maximum Acceleration, Maximum Velocity, Distance From Source, and Local Site Conditions For Moderately Strong Earthquakes", Bull. Seism. Soc. Am. 66, pp.1323-1342, (1976)

57. Streeter, V.L., Wylie, E.B. and Richart, F.E., "Soil Motion Computations By Characteristics Method", Journal of the Geotechnical Engineering Division, ASCE 100, GT3, March, (1974)

58. Trifunac, M.D. and Brady, A.G., "A study on the Duration of Strong Earthquake Ground Motion", Bull. Seism. Soc. Am., 65, No.3, pp.581-626, (1975)

59. Tsai, N.C., "Influence of Local Geology on Earthquake Ground Motion", Ph.D., thesis, California Inst. of Tech., (1969)

60. Tsai, N. and Housner, G., "Calculation of Surface Motion of a Layered Half-Space", Bull. Seism. Soc. Am., 60, pp.1625-1651, (1970)

61. Whitman, R.V. and Richart, F.E., "Design Procedures for Dynamically Loaded Foundations", Journal of Soil Mechanics and Foundations Division, Proc. ASCE, 93, No. SM6, Nov. pp.169, (1967)

62. Whitman, R.V., "Stress-Strain Behaviour of Soil During Dynamic Loading", Seminar De Ingenieria Sismo-Resistant, Vol.II, Universidad de Los Andes, Bogata, (1972)

63. ——— "Effect of Local Soil Conditions Upon Earthquake Ground Motions", Seminar De Ingenieria Sismo-Resistente Vol.II, Universidad de Los Andes, Botata, (1972)

64. Woodward, R.J., Gardner, W.S. and Greer, D.M., "Drilled Pier Foundations", McGraw-Hill Book Company, London, (1972)

65. Yoshimi, Y. and Kumabara, F., "Effect of Subsurface Liquifaction on Strength of Surface Soil," Soils and Foundations, Vol.13, No.2, June, (1973)